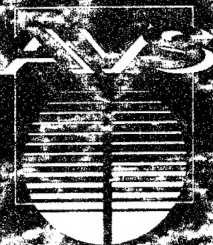


TECHNICAL SESSIONS • AVS SHORT COURSE PROGRAM • EQUIPMENT EXHIBIT

# AMERICAN VACUUM SOCIETY



## *41st National Symposium*

NANO 3: THIRD INTERNATIONAL CONFERENCE  
ON NANOMETER-SCALE SCIENCE & TECHNOLOGY

*Colorado Convention Center  
Denver, Colorado  
October 24-28, 1994*

FINAL PROGRAM

199 10630 164

## TABLE OF CONTENTS

5K Run Information.....	4
1994 Program Committee.....	9
1994 Short Course Information.....	113
1994 Technical Program At A Glance ...378-Inside Back Cover	
Abstracts.....	114-356
Author Index.....	357-374
AVEM Annual Seminar.....	32
AVS Awards Reception.....	11
AVS Fellows.....	18
Albert Nerken Award.....	14
Gaede-Langmuir Award.....	12
Graduate Research Awards.....	18
John A. Thornton Memorial Award & Lecture.....	16
JVST Shop Note Award.....	17
Nellie Yeoh Whetten Award.....	17
Peter Mark Memorial Award.....	16
The Medard W. Welch Award.....	12
AVS Officers and Directors.....	8
AVS Past Awardees.....	10
Business and Committee Meetings.....	34
CALENDAR OF EVENTS.....	36-112
Author and Titles	
Daily Other Events	
Short Courses	
Technical Sessions	
Monday morning, Oct. 24.....	36
Monday afternoon, Oct. 24.....	42
Tuesday morning, Oct. 25.....	52
Tuesday afternoon, Oct. 25.....	60
Wednesday morning, Oct. 26.....	72
Wednesday afternoon, Oct. 26.....	80
Thursday morning, Oct. 27.....	90
Thursday afternoon, Oct. 27.....	98
Friday morning, Oct. 28.....	108
Division Awards.....	19
Equipment Exhibition.....	2
Exhibit Programs.....	331-356
Floor Plans (Convention Center).....	7
Floor Plans (Hotel).....	6
Focus Areas.....	29
Future Meetings.....	377
Greetings.....	3
Map of City Hotels.....	5
Plenary Lecture.....	31
Program Overview.....	22
Special and Evening Sessions.....	33
Symposium Information.....	2
Technical Sessions Number Key.....	35
Topical Conferences.....	28
Travel Information.....	4
Tutorial Information.....	115

## SYMPOSIUM LOCATION

Colorado Convention Center  
700 14th Street  
Denver, CO 80202  
303/640-8000

## SYMPOSIUM REGISTRATION HOURS

Sun. 3:00 p.m. to 8:00 p.m.	Wed. 7:30 a.m. to 5:00 p.m.
Mon. 7:00 a.m. to 5:00 p.m.	Thurs. 7:30 a.m. to 5:00 p.m.
Tues. 7:30 a.m. to 6:00 p.m.	Fri. 8:00 a.m. to 12 Noon

## SHORT COURSE REGISTRATION HOURS

Sun. 7:30 a.m. to 1:30 p.m.	Mon. 7:00 a.m. to 5:00 p.m.
(TUTORIAL Radisson Hotel)	
Sun. 8:00 a.m. to 8:30 a.m.	Tu.-Th. 7:30 a.m. to 5:00 p.m.
(1 course Radisson Hotel)	
Sun. 4:00 p.m. to 7:00 p.m.	Fri. 7:30 a.m. to 12 Noon

## SYMPOSIUM REGISTRATION FEES

	Pre-registration (Pre-Paid)	Registration at the door
Member	\$235.00	\$275.00
Non-Member	\$295.00	\$335.00
One day	\$125.00	\$125.00
*Student Member	\$ 25.00	\$ 25.00
*Student Non-Member	\$ 35.00	\$ 35.00
NANO 3 Reception	\$ 15.00	\$ 15.00
NANO 3 Proceedings	\$ 30.00	\$ 30.00

AVS tax ID Number: 04-2392373

\*A bonafide full time university student must present student I.D. Part-time students and postdoctoral fellows do not qualify for a student rate.

The PROCEEDINGS from this Symposium will be published in the May/June issue of JVST. Active AVS Members in 1995 will receive the PROCEEDINGS.

## EXHIBIT SHOW HOURS

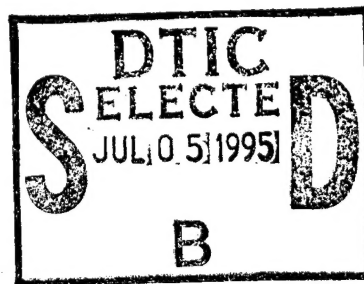
Tuesday, October 25.	11:00 a.m. to 6:00 p.m.
Wednesday, October 26.	10:00 a.m. to 5:00 p.m.
Thursday, October 27.	10:00 a.m. to 3:00 p.m.

## OFFICE LOCATIONS AND PHONE NUMBERS

Symposium Registration	Lobby Area	—303/446-4230
Short Course Registration	C 111	—303/446-4231
Message Board	Lobby Area	
Local Arrangements	A 214	—303/446-4232
Headquarters		
Education Center	Lobby Area	
Companions' Headquarters	Silver Room (H)	
Companions' Registration	Lobby Area	
(S.Mo,Tu Only)		
AVS Employment Center	Lobby Area	
JVST Editorial Office	212	
Presenters Preview Room	113	
Publicity/Press Room	210	—303/446-4233



REPORT DOCUMENTATION PAGE			Form Approved OMB No. 0704-0188	
<small>Public reporting burden for this collection of information is estimated to average 1 hour per response, including the time for reviewing instructions, searching existing data sources, gathering and maintaining the data needed, and completing and reviewing the collection of information. Send comments regarding this burden estimate or any other aspect of this collection of information, including suggestions for reducing this burden, to Washington Headquarters Services, Directorate for Information Operations and Reports, 1215 Jefferson Davis Highway, Suite 1204, Arlington, VA 22202-4302, and to the Office of Management and Budget, Paperwork Reduction Project (0704-0188), Washington, DC 20503.</small>				
1. AGENCY USE ONLY (Leave blank)		2. REPORT DATE Apr 95	3. REPORT TYPE AND DATES COVERED Final 26 Sep 94 - 25 Dec 94	
4. TITLE AND SUBTITLE NANO 3: Third International Conference on Nanometer-Scale + Technology			5. FUNDING NUMBERS  DAAH04-94-G-0423	
6. AUTHOR(S) Richard Colton Christie Marrian				
7. PERFORMING ORGANIZATION NAME(S) AND ADDRESS(ES) American Vacuum Society 120 Wall Street New York, New York 10005			8. PERFORMING ORGANIZATION REPORT NUMBER	
9. SPONSORING/MONITORING AGENCY NAME(S) AND ADDRESS(ES) U.S. Army Research Office P.O. Box 12211 Research Triangle Park, NC 27709-2211			10. SPONSORING/MONITORING AGENCY REPORT NUMBER  ARO 33589.1-PH-CF	
11. SUPPLEMENTARY NOTES The views, opinions and/or findings contained in this report are those of the author(s) and should not be construed as an official Department of the Army position, policy, or decision, unless so designated by other documentation.				
12a. DISTRIBUTION/AVAILABILITY STATEMENT  Approved for public release; distribution unlimited.			12b. DISTRIBUTION CODE	
13. ABSTRACT (Maximum 200 words)  Papers presented at the 41st National Symposium and NANO 3: Third International Conference on Nanometer-Scale-Science & Technology at Colorado Convention Center, Denver, Colorado, October 24-28 1994.				
14. SUBJECT TERMS			15. NUMBER OF PAGES	
			16. PRICE CODE	
17. SECURITY CLASSIFICATION OF REPORT UNCLASSIFIED	18. SECURITY CLASSIFICATION OF THIS PAGE UNCLASSIFIED	19. SECURITY CLASSIFICATION OF ABSTRACT UNCLASSIFIED	20. LIMITATION OF ABSTRACT  UL	



# Greetings

Welcome to Denver! On behalf of the Program Committee we are pleased to present this Program for the 41st National Symposium of the American Vacuum Society. The Symposium, comprising technical sessions of the Society's eight divisions, three Topical Conferences, the short course program, and the Equipment Exhibition, is being held in the Colorado Convention Center. Many of the business functions are held in the headquarters hotel, the Radisson, located a few blocks from the Convention Center.

Both the Convention Center and the Radisson are located in the heart of downtown Denver, ideally situated to take advantage of the many cultural, historic, dining, and shopping attractions of the city. We think you will find Denver a convenient and exciting city to hold the AVS National Symposium.

Equally exciting is the technical program that we have assembled for this year. Ninety-two technical sessions and eighteen poster sessions make this the largest technical program yet offered by the AVS. Approximately one thousand papers selected from over 1300 abstracts are included in the meeting. In the tradition of the AVS, each Division offers a broad range of topical material and a selection of invited speakers representing the best current work in their fields.

There is always a large overlap of interest among division programs, and this year we are attempting a new means of coordinating these interdisciplinary interests. We have identified four Focus Areas within the program. These represent either major new topical areas that are being introduced to the program, or areas of where a common thread of inter-

est runs through a number of divisions. We have scheduled Focus Area sessions in a sequential fashion through the week.

The four Focus Areas for this meeting are 1) Si-Based Optoelectronics; 2) Sensors, in-situ Diagnostics, and Process Control; 3) Nanostructure Fabrication and Atomic Scale Manipulation of Surfaces; 4) Surface Contamination and Control.

Focus Area sessions are highlighted in the Program at a Glance and also in the "Calendar of Events."

Three Topical Conferences are also featured at this year's meeting. NANO 3, the Third International Conference on Nanometer-Scale Science and Technology is being sponsored by the Nanometer-Scale Science and Technology Division. This program is designed to provide a forum for the science and technology of phenomena in many diverse fields which are apparent on the nanometer scale. NANO 3 also offers a special plenary session on Monday morning, and a Monday evening reception for NANO 3 attendees. Two additional topical conferences are making repeat appearances after their enthusiastic reception at last year's meeting. The Manufacturing Science and Technology Topical Conference continues our efforts to provide the research community with perspective and familiarity with manufacturing issues that present opportunities for research and to highlight AVS research that delivers or promises substantial relevance to manufacturing. The conference is again co-sponsored by the IEEE. The Biomaterials Interfaces Topical Conference provides a forum

where biotechnologists and interface scientists can share their perspective views on the research and development opportunities with biomaterials.

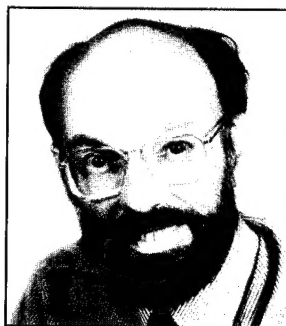
Monday at 12:45 p.m. features the Plenary Address for this year's meeting. Our speaker is Dr. John Armstrong, Vice President, Science and Technology of IBM (retired). Dr. Armstrong's address titled, "The Role of Research in the Technological Balance of Power," examines the needs and directions of science and technology in an increasingly international economy and what contributions research can make in this new economic environment.

Wednesday evening occasions the annual AVS Awards Assembly and Reception. All Symposium registrants are welcome to attend and congratulate this year's AVS award winners.

As always, the Manufacturers Exhibit is a major part of the AVS Symposium. The Exhibit is held Tuesday through Thursday in the Convention Center. A special poster session on New Vacuum Products is scheduled for Wednesday at 5:00 p.m. in Ballroom 4 of the Convention Center.

The Convention Center is also the site of the Short Course Program. These courses run concurrently with the AVS Symposium.

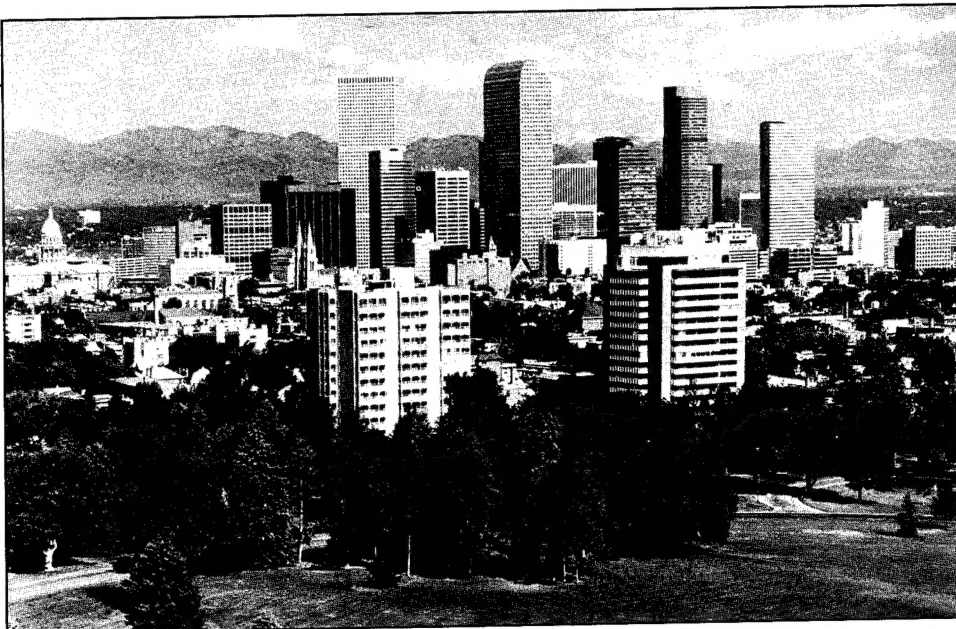
The Local Arrangements Committee, chaired by Pete Sheldon will be available to assist you throughout the week. For our traveling companions, a full and interesting Companions Program is available to take advantage of the plentiful and unusual entertainment, recreational, and cultural activities available in the Denver area.



Thomas M. Mayer  
Program Chair



Ellen B. Stechel  
Program Vice Chair



*The snow-capped Rockies form an attractive backdrop to Denver, the Mile High City.  
Credit: Denver Metro Convention & Visitors Bureau*

## General Information

### INTRODUCTORY MEMBERSHIP OFFER

If you have paid the \$295 or \$335 non-member registration fee, we invite you to apply for membership through our Introductory Membership Invitation. Non-members who apply and are accepted for AVS membership during the Symposium may have \$60 of their non-member registration fee transferred and credited to their 1995 membership dues. Membership application forms are available at the registration desk and the Education Center.

Completed applications must be submitted to the Education Center staff for processing during **THE WEEK OF THE SYMPOSIUM ONLY**.

### TRANSPORTATION INFORMATION

**16th STREET SHUTTLE SERVICE** - Getting around Denver is easy and convenient. Once downtown, you will find the shuttles on the 16th Street Mall to be free as well as fast, running between the Lower Downtown Historic District in the northwest and Civic Center Park and the State Capitol in the southeast approximately every 90 seconds.

Most of the hotels listed above are located within one or two blocks of the 16th Street Shuttle. The stop for the Convention Center is California and 16th, which is only two blocks from the Convention Center.

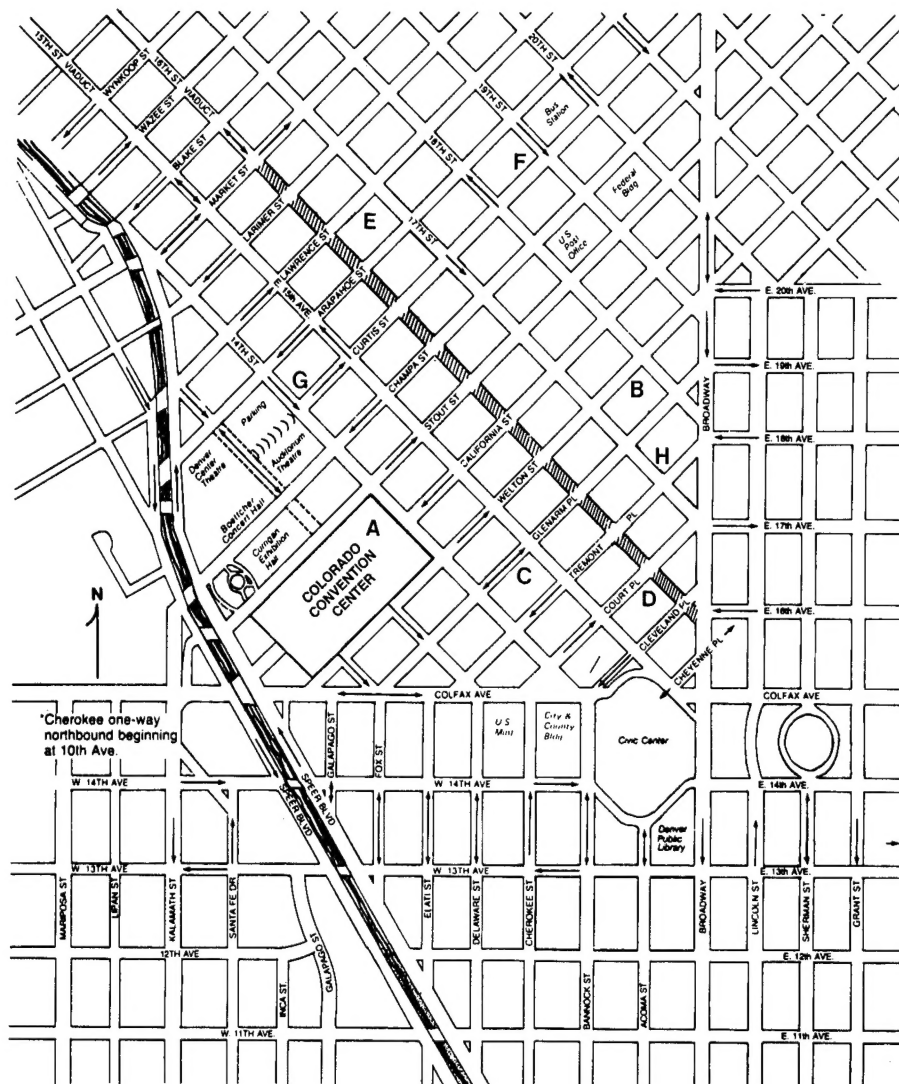
### FOURTEENTH AVS RUN

The Fourteenth Annual AVS Run will be held on Wednesday, October 26th. A map identifying the starting point will be provided at the race registration desk. The race site will be along the Platte River.

The run donation is \$15.00 US (late fee after October 3). This includes a high-quality, commemorative tee-shirt, race numbers, awards (in many age categories) and post-race refreshments. All runners, competitive or a bit less serious, are invited to participate.

The **CORPORATE DIVISION RACE** will again be held. Each team needs at least three members, all working for the same organization. Contact the race director to register teams.

- A) Colorado Convention Center
- B) Hyatt Regency Denver
- C) Holiday Inn Downtown
- D) Radisson Hotel (Headquarters)
- E) Westin Hotel
- F) Embassy Suites Hotel
- G) Executive Tower Inn
- H) The Comfort Inn



# DENVER

## CREDITS:

Program Editor – Angela Mulligan  
Abstract Editor – Lynn Pizzo

## Cover Image:

Domain structure of a two dimensional Ag-Cu alloy,  
Courtesy of Bob Hwang, Sandia National Labs  
Livermore, CA

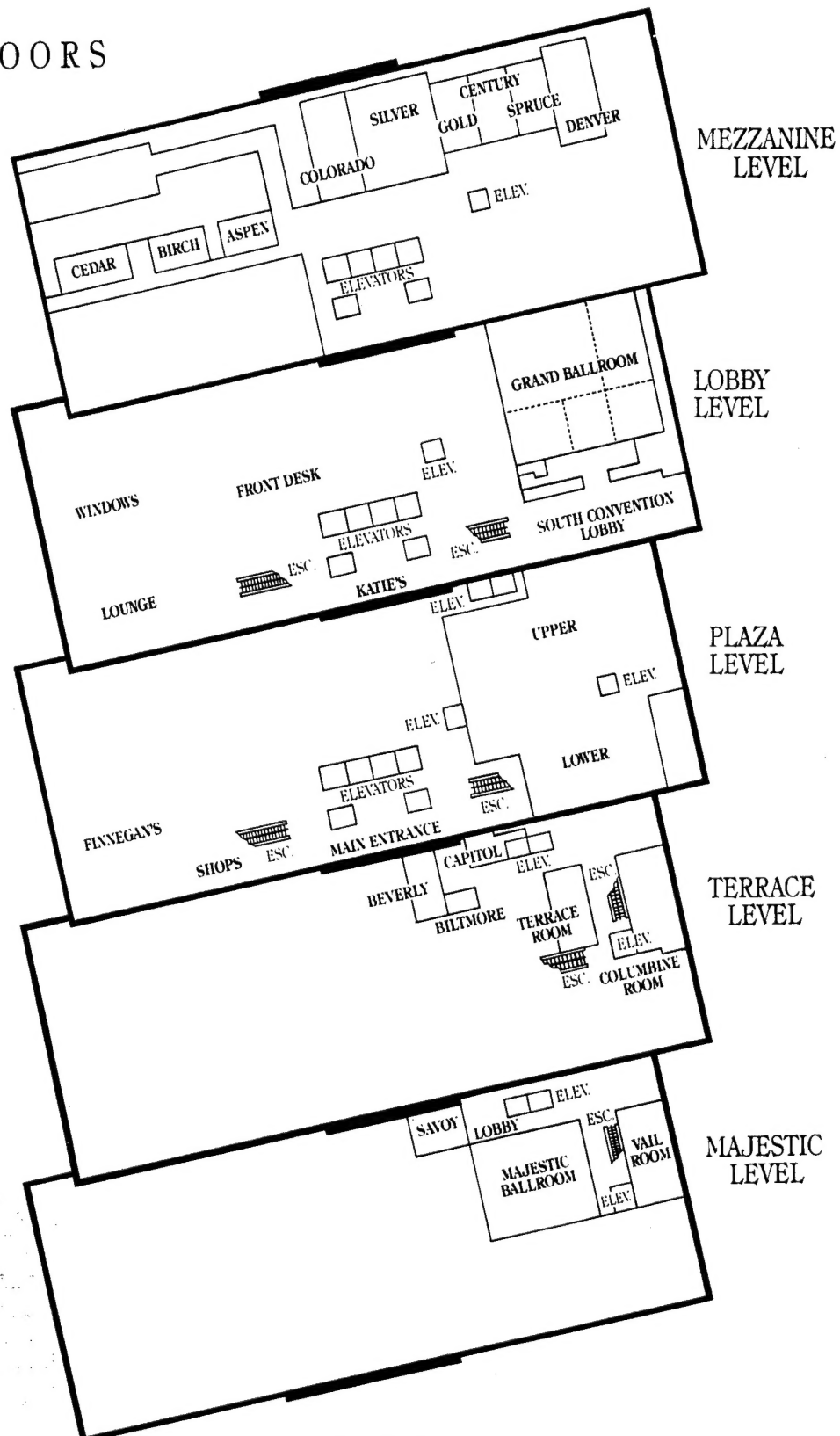
5

<b>Accession For</b>	
NTIS GRA&I	<input checked="" type="checkbox"/>
DTIC TAB	<input type="checkbox"/>
Unannounced	<input type="checkbox"/>
Justification	
By	
Distribution/	
Availability Codes	
Dist	Avail and/or Special
A-1	

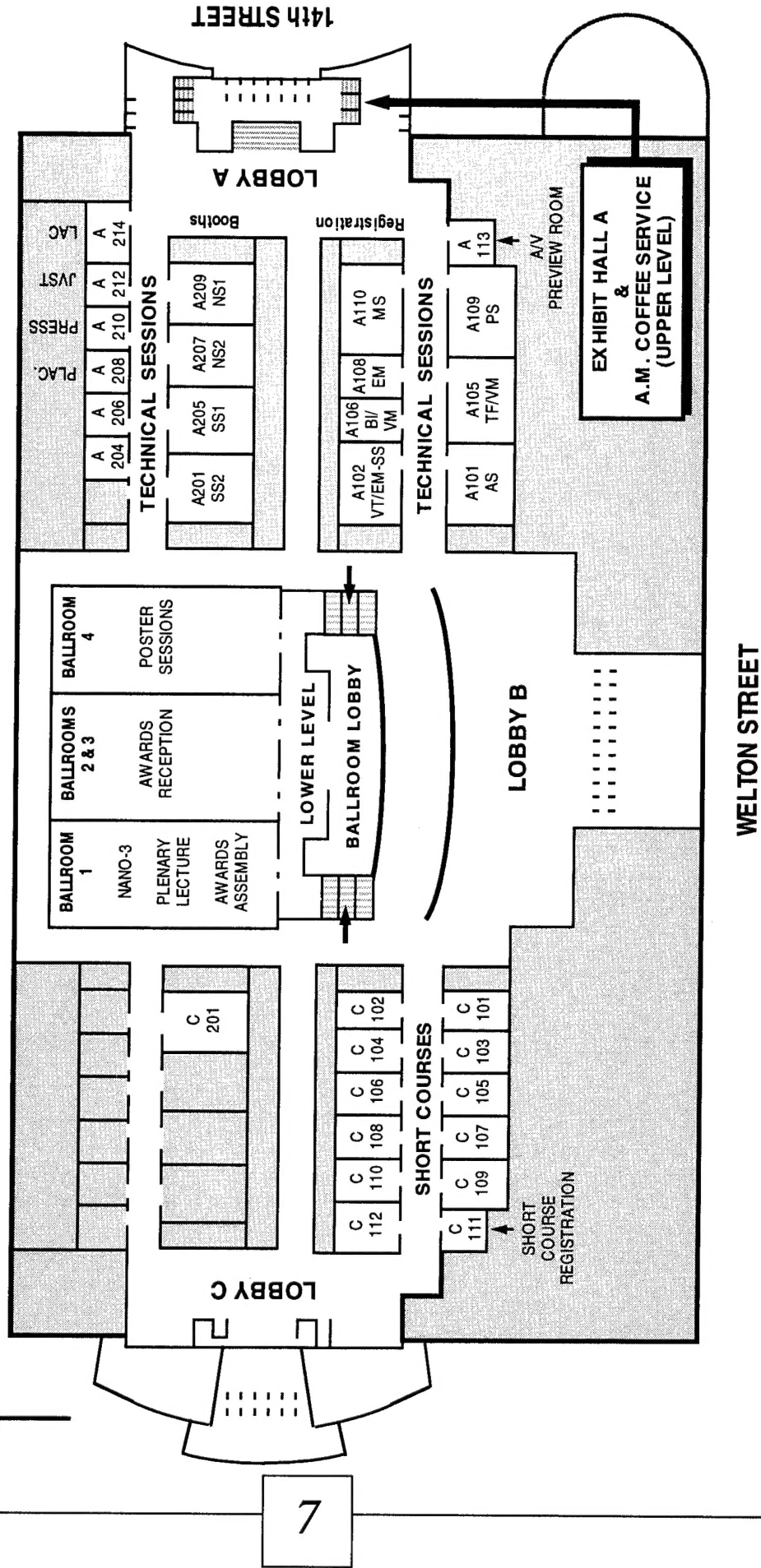
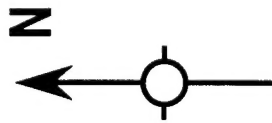


# RADISSON HOTEL

## 5 FLOORS



# COLORADO CONVENTION CENTER



# 1994 OFFICERS AND DIRECTORS

## President

John R. Noonan  
Argonne National Laboratory  
Bldg. 378T Room #130  
9700 S. Cass Avenue  
Argonne, IL 60439  
Tel: 708/252-9254  
Fax: 708/252-5948

## President-Elect

John H. Weaver  
University of Minnesota  
Dept. of Chem Engrg & Matls Sci  
151 Amundson Hall  
Minneapolis, MN 55455  
Tel: 612/625-6548  
Fax: 612/625-6043

William D. Westwood, Secretary  
Bell-Northern Research Ltd.

N. Rey Whetten, Technical Director,  
Treasurer

H. Frederick Dylla,  
Immediate Past President, CEBAF

Bruce D. Sartwell  
US Naval Research Laboratory

James S. Solomon  
University of Dayton

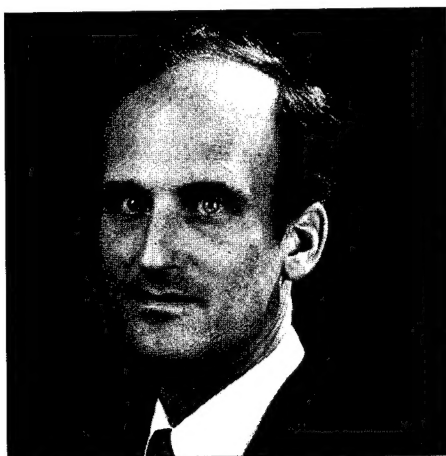
Roger L. Stockbauer  
Louisiana State University

Eric M. Stuve  
University of Washington

Patricia A. Thiel  
Iowa State University

Christine B. Whitman  
CVC Products Inc.

## 1994 LOCAL ARRANGEMENTS COMMITTEE



Peter Sheldon, Chair  
National Renewable Energy Lab.



Lawrence Kazmerski, Vice Chair  
National Renewable Energy Lab.

Grant Armstrong, MKS Instruments  
Food Services Coordinator

Sally Asher, NREL  
Audio-Visual Coordinator

Tom Christensen, Univ of Colorado  
Registration Coordinator, Local

Lucy Czanderna,  
Companions Program Coordinator, Local

Tim Gessert, NREL  
Poster Session, Asst Coordinator

Phyllis Greene  
Registration Coordinator

Doug Jones, Omega Analytical Services  
Treasurer

Deirdre Lavalley, MKS Instruments  
Exhibit/Publicity Coordinator

Mona Lilien, Granville Phillips  
Food Services Asst Coordinator

Art Nelson, NREL  
Science Educators Coordinator

David Niles, NREL  
Facilities Coordinator

Roland Pitts, NREL  
Facilities Coordinator

Jim Sites, Colorado State University  
Poster Session Coordinator

Bernie Smilak, Quivas Group  
Short Course Coordinator

Virginia Whetten  
Companions Program Coordinator

# 1994 PROGRAM COMMITTEE

Thomas M. Mayer, Chair  
Sandia National Labs, MS 0344  
Albuquerque, NM 87185-0344  
Tel: 505/844-0770  
Fax: 505/844-5470

Ellen B. Stechel, Vice Chair  
Sandia National Labs, MS 0345  
Albuquerque, NM 87185-0345  
Tel: 505/844-2436  
Fax: 505/844-5459

N. Rey Whetten, AVS Technical Dir  
American Vacuum Society  
120 Wall Street, 32nd Floor  
New York, NY 10005  
Tel: 212/248-0328  
Fax: 212/248-0245

Marion Churchill, Meetings Manager  
American Vacuum Society  
120 Wall Street, 32nd Floor  
New York, NY 10005  
Tel: 212/248-0327  
Fax: 212/248-0245

Lynn Pizzo, Conference Secretary  
Xerox Webster Research Center  
800 Phillips Road, 0114-41D  
Webster, NY 14580  
Tel: 716/422-4978  
Fax: 716/242-8928

## Applied Surface Science Division

J.T. GRANT, CHAIR  
University of Dayton  
A.W. Czanderna, NREL  
G.D. Davis, Martin Marietta Lab  
R.W. Linton, Univ of North Carolina  
G.C. Nelson, Sandia National Lab  
A.L. Testoni, Digital Equipment Corp.

## Electronic Matls & Processing Div

F.A. HOULE, CHAIR  
IBM Almaden Research Center  
F.G. Celii, Texas Instruments  
S.M. George, Univ of Colorado  
H.P. Gillis, Georgia Inst of Tech  
I.P. Herman, Columbia University  
P.H. Holloway, Univ of Florida  
G. Lucovsky, North Carolina State Univ  
P. Mooney, IBM  
M. Olmstead, Univ of Washington

## Nanometer-Scale Science and Technology/NANO 3

R.J. COLTON, CHAIR NST  
Naval Research Lab  
R. Hamers, Univ of Wisconsin  
M. Reed, Yale University  
C. Teague, NIST

## NANO 3

C.R.K. MARRIAN, CHAIR  
Naval Research Lab  
H. Ahmed, Cambridge University, UK  
C.L. Bai, Chinese Academy of Sciences, China  
J.A. Dagata, NIST  
M.-H. Hara, RIKEN, Japan  
Y. Kuk, Seoul National Univ., Korea  
H. Launois, CNRS, France  
S.M. Prokes, Naval Research Lab  
J.P. Rabe, Max-Planck Inst, Germany  
D. Rugar, IBM Almaden Research Center  
H. Tokumoto, Natl Inst for Advanced Res, Japan

## Plasma Science & Technology Div

J.L. CECCHI, CHAIR  
University of New Mexico  
M. Barnes, LAM Research  
L. Ephrath Cecchi, Sandia National Labs  
D. Denton, Univ of Wisconsin  
S.M. Gorbalkin, Oak Ridge National Lab  
R.A. Gottscho, AT&T Bell Labs  
D.B. Graves, Univ of California, Berkeley  
W.L. Hsu, Sandia National Labs  
H.-G. Kim, University of Rochester  
M.J. Kushner, University of Illinois  
T.C. Lee, AT&T Bell Labs  
M. Nakamura, Fujitsu Ltd  
S. Pang, University of Michigan  
J.L. Shohet, University of Wisconsin  
S. Tachi, Hitachi, Ltd

## Surface Science Division

J.C. HEMMINGER, CHAIR  
Univ of California, Irvine  
E. Carter, Univ of California, Los Angeles  
S. Chiang, IBM  
J. Cowin, Battelle Pacific Northwest Labs  
L.H. Dubois, ARPA  
T. Engel, University of Washington  
G. Fisher, General Motors Research Lab  
J.E. Reutt-Robey, Univ of Maryland  
P. Thiel, Iowa State University  
B. Tonner, Univ of Wisconsin  
M.J. Weaver, Purdue University  
D. Zehner, Oak Ridge National Labs

## Thin Film Division

B.P. HICHTA, CHAIR  
Optical Coatings Lab Inc  
C. Aita, Univ of Wisconsin, Milwaukee  
S. Barnett, Northwestern University  
D. Chatterjee, Eastman Kodak Co  
D. Glocker, Kodak VCER Lab/CTD/MRE  
R.A. Hoffman, Alcoa Tech Center  
W.L. Hsu, Sandia National Labs  
R. Messier, Pennsylvania State Univ  
D. Pappas, Gillette Co  
F.O. Sequeda, Azotic Coatings Tech  
J.H. Thomas, III, 3M

## Vacuum Metallurgy Division

I.G. PETROV, CHAIR  
University of Illinois  
D. CARMICHAEL, CO-CHAIR  
Vacuum Technology Inc.  
C.R. Parent, Gillette Co  
S. Rohde, Univ of Nebraska  
B. Sartwell, US Naval Res Lab  
J.E. Sundgren, Linkoping Univ  
M-S Wong, Northwestern Univ

## Vacuum Technology Division

N.T. PEACOCK, CHAIR  
HPS Div of MKS Instruments  
M. Benapfl, Lawrence Livermore Nat Lab  
H.F. Dylla, CEBAF  
L. Hinkle, MKS Instruments  
J.K.G. Panitz, Sandia National Labs  
J.L. Provo, Martin Marietta  
J.W. Weed, Sandia National Labs

## Topical Conference:

### Manufacturing Sci & Technology

G.W. RUBLOFF, CO-CHAIR  
North Carolina State University  
M. LIEHR, CO-CHAIR  
IBM T.J. Watson Research Center  
C. Brundle, IBM  
A. Diebold, Sematech  
F.R. Dill, IBM  
L. Ephrath Cecchi, Sandia National Labs  
J. Grant, Univ of Dayton  
I. Herman, Columbia University  
J. McVittie, Stanford University  
N. Peacock, HPS Div of MKS Instr  
M. Kushner, Univ of Illinois  
C. Sorenson, SEMI/Sematech  
C. Spanos, Univ of California, Berkeley  
A. Strojwas, Carnegie Mellon University  
A. Testoni, Digital Equipment Corp  
K. Uram, LAM Research  
C. Whitman, CVC Products Inc.

## Topical Conference:

### Biomaterial Interfaces

J.J. HICKMAN, CO-CHAIR  
SAIC  
B.D. RATNER, CO-CHAIR  
University of Washington



# AMERICAN VACUUM SOCIETY AWARD WINNERS

## MEDARD W. WELCH AWARD

1970	Erwin W. Mueller	1978	Georg H. Hass	1988	Peter Sigmund
1971	Gottfried K. Wehner	1979	Gert Ehrlich	1989	Robert Gomer
1972	Kenneth C.D. Hickman	1981	Harrison E. Farnsworth	1990	Jerry M. Woodall
1973	Lawrence A. Harris	1983	H.H. Wieder	1991	Max Lagally
1974	Homer D. Hagstrum	1984	William S. Spicer	1992	Ernst Bauer
1975	Paul A. Redhead	1985	Theodore E. Madey	1993	George Comsa
1976	Leslie Holland	1986	Harald Ibach	1994	John T. Yates, Jr.
1977	Charles B. Duke	1987	Mark J. Cardillo		

## GAEDE-LANGMUIR AWARD

1978	Pierre V. Auger	1986	Rointan F. Bunshah	1992	Russell D. Young
1980	Daniel Alpert	1986	Alfred Y. Cho	1994	Robert J. Celotta
1982	Alfred H. Sommer	1988	John R. Arthur, Jr.	1994	Daniel T. Pierce
1984	Alfred Benninghoven	1990	Francois M. d'Heurle		

## ALBERT NERKEN AWARD

1985	John L. Vossen	1989	Charles D. Wagner	1992	Paolo della Porta
1986	Donald J. Santeler	1989	Martin P. Seah	1993	John O'Hanlon
1987	Marsbed Hablanian	1990	J. Peter Hobson	1994	Hajime Ishimaru
1988	Stanley L. Milora	1991	Harold R. Kaufman		

## PETER MARK AWARD

1980	Christopher R. Brundle	1985	Franz J. Himpsel	1990	Stephen M. Rossnagel
1981	Lawrence L. Kazmerski	1986	Richard A. Gottscho	1991	William J. Kaiser
1982	Charles M. Magee	1987	Raymond T. Tung	1993	Robert Hamers
1983	D. James Chadi	1988	Jerry D. Tersoff	1994	Marjorie Olmstead
1984	Barbara J. Garrison	1989	Randall M. Feenstra		

## HONORARY MEMBERSHIP

1967	Daniel Alpert	1992	Marsbed Hablanian	1970	Paul A. Redhead
1955	A.S.D. Barrett	1989	Nancy L. Hammond	1992	Donald Santeler
1981	Leonard C. Beavis	1983	J. Peter Hobson	1985	Kai Siegbahn
1983	Daniel G. Bills	1981	Dorothy M. Hoffman	1988	Jack H. Singleton
1975	Rointan F. Bunshah	1986	Manfred S. Kaminsky	1989	John L. Vossen
1991	John Coburn	1956	Rudy A. Koehler	1980	Gottfried K. Wehner
1963	Benjamin B. Dayton	1978	James M. Lafferty	1958	Medard W. Welch
1985	Richard A. Denton	1975	William J. Lange	1981	N. Rey Whetten
1982	Charles B. Duke	1965	Wilfred G. Matheson	1984	J. Roger Young
1981	Maurice H. Francombe	1968	Luther E. Preuss		
1955	Kenneth C.D. Hickman	1991	J. Lyn Provo		

## JOHN THORNTON MEMORIAL AWARD

1989	Eric Kay	1992	Thomas R. Anthony	1994	David Hoffman
1990	Maurice Francombe	1993	John W. Coburn		
1991	Joseph E. Greene	1993	Harold F. Winters		

## NELLIE YEOH WHETTEN AWARD

1990	Jani C. Ingram	1992	Hope Michelson	1994	Monica Katiyar
1991	Lucia Markert	1993	Laura Tedder		

## RUSSELL AND SIGURD VARIAN FELLOW AWARD

1984	Kenneth T.Y. Kung (Massachusetts Institute of Technology)
1985	Anne L. Testoni (Northwestern University)
1986	Jingguang G. Chen (University of Pittsburgh)
1987	Joanne R. Levine (Northwestern University)
1988	Christopher E. Aumann (University of Wisconsin)
1989	Brian S. Swartzentruber (University of Wisconsin)
1990	Guangquan Lu (University of California, San Diego)
1991	Michael Flatte (University of California, Santa Barbara)
1992	Rex Ramsier (University of Pittsburgh)
1993	Daniel Kelly (University of California, Santa Barbara)

THE AMERICAN VACUUM SOCIETY

cordially invites you

to attend

the Awards Assembly

on

Wednesday, October 26, 1994

in

Ballroom 1

Colorado Convention Center

at 6:45 p.m.

followed by the

Awards Reception

# AVS AWARDS TO BE PRESENTED AT THE 41ST NATIONAL SYMPOSIUM

## AWARDS ASSEMBLY & RECEPTION

The American Vacuum Society Awards Assembly and Reception will be held on Wednesday, October 26, 1994 at 6:45 p.m. in Ballroom 1 of the Colorado Convention Center. The Medard W. Welch Award will be presented to John T. Yates, Jr. The Gaede-Langmuir Award will be presented to Robert J. Celotta and Daniel T. Pierce. The Albert Nerken Award will be presented to Hajime Ishimaru. The John A. Thornton Memorial Award will be presented to David W. Hoffman, and the Peter Mark Award will be presented to Marjorie Olmstead. The newly elected Fellows as well as the Graduate Research Awards for 1994 will be presented. The winners of the award for the best Shop Notes published in the *Journal of Vacuum Science and Technology* will be announced. The Awards Reception will immediately follow the Awards Assembly.

## MEDARD W. WELCH AWARD

The Medard W. Welch Award was established in 1969 to commemorate the pioneering efforts of M.W. Welch in founding and supporting the American Vacuum Society. It is presented to recognize and encourage outstanding research in the fields of interest to the American Vacuum Society. The award consists of a medal and a cash prize.



**JOHN T. YATES, JR.**

**Dr. John T. Yates, Jr.,** University of Pittsburgh, *"for the development and use of modern measurement methods to provide insights into the behavior of chemisorbed species on metal and semiconductor surfaces."*

John T. Yates, Jr. received his B.S. degree from Juniata College and his Ph.D in physical chemistry from MIT. Following a three-years' term as Assistant Professor at Anitoch College, he joined the National Bureau of Standards, first as a NRC Postdoctoral Research Fellow and then, from 1965 until 1982, as a member of its scientific staff. His research is in the fields of surface chemistry and physics, including both the structure and spectroscopy of surface species, the dynamics of surface processes, and the development of new methods for research in surface chemistry.

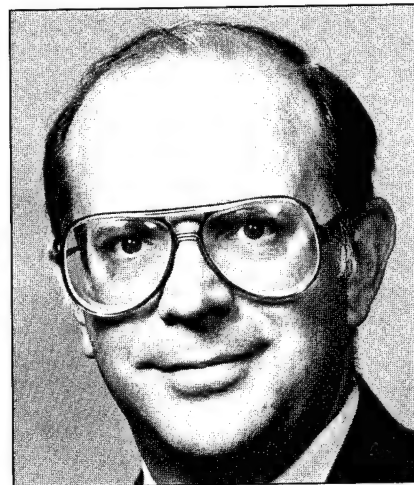
Dr. Yates was Senior Visiting Scholar at the University of East Anglia, Norwalk, in 1970-1971, and Sherman Fairchild Distinguished Scholar at Caltech in 1977-1978.

Professor Yates joined the University of Pittsburgh in 1982 as the first R.K. Mellon Professor of Chemistry and as the Director of the new University of Pittsburgh Surface Science Center. He has established the Surface Science Center and has created a strong research program there. Here, working with students and postdoctoral staff, his influence actively extends over a wide range of research projects. He is also active in undergraduate and graduate teaching. In addition, he maintains close relationships with a number of surface science research programs in academic, government, and industrial research laboratories throughout the world, as well as serving on the editorial boards of five journals and two book series in surface science and catalysis. He is a member of the Program Selection Committee of the Gordon Research Conference. He is a coeditor of the ACS journal, *Langmuir*. He has been active in AVS and ACS affairs for the last 20 years, including being a past member of the AVS Board of Directors and Trustees, past Chairman of

the Surface Science Division of the AVS (for the second time), and the past chairman of the ACS Division of Colloid and Surface Chemistry. He has organized a number of symposia for the ACS National Meetings, APS National Meetings and for Gordon Research Conferences. He is the co-author of a book entitled "The Surface Scientists Guide to Organometallic Chemistry," ACS, 1987. He is the coeditor of two books, "Vibrational Spectroscopy of Molecules on Surfaces," Plenum, 1987 and "Chemical Perspectives of Microelectronic Materials," Materials Research Society 1989.

## GAEDE-LANGMUIR AWARD

The Gaede-Langmuir Award was established in 1977 by an endowing grant from Dr. Kenneth C.D. Hickman. It is presented biennially to recognize and encourage outstanding discoveries and inventions in the sciences and technologies of interest to the American Vacuum Society. The award consists of an inscribed plaque, certificate and cash prize.



**ROBERT J. CELOTTA**

**Dr. Robert J. Celotta,** NIST, *"for their innovative development of advanced, spin-polarized electron beam technology and their scientific contributions to atomic, surface, and microstructure physics."*

Robert Celotta received his B.S. degree in Physics from the City College of New York in 1964 and went on to get his Ph.D. in Physics at New York University in 1969. His research career actually started while he was an undergraduate working part time as a Research Assistant at IBM Watson Labs (at Columbia University) on the construction of high current cyclotron conceived by L.H. Thomas. His graduate work at NYU included atomic beam determinations of tensor polarizabilities and electron-atom collision cross sections under the supervision of Ben Bederson, currently the Editor-in-Chief at APS. Celotta then accepted a Postdoc with Jan Hall at the Joint Institute of Laboratory Astrophysics in Boulder Colorado to establish a new way to accurately determine molecular electron affinities via laser photodetachment spectrometry.

In 1971, Celotta joined the Electron Physics Group at NIST (then the National Bureau of Standards) and led an effort in monochromatic electron scattering from gases, primarily determining oscillator strengths over a very wide spectral range and exploring negative ion resonance phenomena. Then, in 1975, Dan Pierce, fresh from participating in the discovery at ETH in Zurich that GaAs could be made to emit spin polarized electrons, joined Bob Celotta on the staff of the Electron Physics Group. Thus began a period of scientific collaboration and friendship that continues to the present day. They shared the conviction that a great deal could be learned about atoms and surfaces if the electron spin parameter could be controlled and measured much more effectively than had been to date. Together with their colleagues, Pierce and Celotta set out to develop the first low energy GaAs spin polarized electron gun. This electron gun produced beams similar in current and other characteristics to conventional electron guns, yet the spin direction of the electron beam could be modulated while the current remained constant. This allows the spin dependent part of any subsequent electron interaction to be determined. The source was first used to study the spin-orbit effect in spin polarized LEED and then observed spin splittings in electron surface states. But, by 1979, they realized that surface magnetism was the most exciting application the new spin polarization techniques and they had made their first

observation of a surface hysteresis curve by using polarized electron diffraction. In the years immediately following, they proposed the transverse magnetization configuration for spin-dependent photoemission, observed the effect of electron polarization on elastic and inelastic electron scattering from ferromagnets, observed the spin and energy of secondary electrons from ferromagnets, utilized the detection of polarized electrons in scanning electron microscopy (SEMPA) to provide images of magnetic domains, made spin polarized, inverse photoemission measurements, determined the temperature dependence of surface magnetization, and developed two new types of spin polarization detectors. Starting in the early 1980's, Celotta also led a project at NIST to measure the interactions between polarized electrons and spin polarized atom beams, in some cases making such complete scattering measurements that quantum phases and amplitudes were obtainable instead of less complete cross section information.

Currently, Celotta and his colleagues use polarization techniques in, for example, SEMPA studies of exchange coupling between magnetic layers using nanofabrication methods to produce wedge shaped crystal structures of accurate dimensions and precise structure. He is also interested in the possibility of a spin-dependent tunneling probe of magnetic structure.

Most recently, Celotta and colleagues have demonstrated that laser fields can be used to focus neutral atomic beams to form nanostructures on surfaces.

Polarized electron experiments are notoriously complex and much of the work mentioned above could not have been done without the collaborative efforts of many highly talented scientists, including former and present members of the NIST Electron Physics Group, and the highly supportive environment provided by NIST.

Robert Celotta is an author of more than 200 publications, is the Editor-in-Chief of *Methods of Experimental Physics*, and is a holder of three patents ranging from polarization detection to nanolithography. He has received the Distinguished Young Scientist Award from the Maryland Academy of Sciences, two IR-100 awards, the Federal Laboratory Consortium Award for Excellence in Technology Transfer, the Outstanding and Distinguished Career in Science Award of the Washington

Academy of Sciences and, from NIST, the Silver Medal and Gold Medal Awards, the E.U. Condon Award, and the W.P. Slichter Award. He is a NIST Fellow, a Fellow of the American Physical Society and is the Leader of the NIST Electron Physics Group.



**DANIEL T. PIERCE**

**Dr. Daniel T. Pierce, NIST, "for their innovative development of advanced, spin-polarized electron beam technology and their scientific contributions to atomic, surface, and microstructure physics".**

Daniel Pierce received his B.S. degree in Physics from Stanford University in 1962. After two years teaching physics at Tri-Chandra College in Kathmandu, Nepal with the U.S. Peace Corps, he returned to Wesleyan University in Connecticut where he received an M.A. in Physics in 1966. He received his Ph.D in Applied Physics from Stanford University in 1970, for work involving photoemission measurements of the electronic structure of Ni above and below the Curie temperature and calculations of the corresponding energy distribution curves from an interpolated band structure. He remained with Prof. W.E. Spicer at Sanford for a year as a postdoctoral researcher to study amorphous semiconductors and help develop plans for the Stanford Synchrotron Radiation Laboratory.

In 1971, Dr. Pierce joined the group of



Prof. H.C. Siegmann at the Eidgenössische Technische Hochschule (ETH) in Zurich to investigate magnetic materials using spin-polarized photoemission. He took part in studies of the spin-dependent electronic structure of magnetic transition metals and magnetic insulators and ferrites such as  $\text{EuO}$  and  $\text{Fe}_3\text{O}_4$ . He shared in the discovery that electrons photoemitted from negative electron affinity GaAs with circularly polarized light are highly spin polarized. This result is the basis of the GaAs spin-polarized electron source that is the most widely used source of spin-polarized electrons for investigations in atomic, solid state, and high energy physics.

Dr. Pierce joined the NIST (National Institute of Standards and Technology, formerly National Bureau of Standards) in 1975. Pierce and R.J. Celotta, with whom he shares this award, and colleagues at NIST developed the GaAs spin-polarized electron source for low-energy applications. Polarized electron scattering was used to investigate symmetry relations in low energy electron diffraction from surfaces, where the spin dependence arises from the spin-orbit interaction. The spin dependence measured for surface resonance scattering in low-energy Rydberg states has led to a better model of the surface potential barrier in  $\text{W}(100)$ .

Recognizing the power of spin polarized electrons for studying surface magnetism, Pierce, Celotta, and their collaborators carried out the first polarized low energy electron diffraction measurements from a magnetic material, the  $\text{Ni}(110)$  surface. The results showed the size of the spin dependent scattering due to the exchange interaction and indicated the sensitivity of surface magnetism to adsorbates. These measurements established a new, sensitive means to measure the degree of surface magnetic order. Polarized electron scattering from ferromagnetic glasses confirmed the theoretical predictions that the temperature dependence of the surface magnetization at low temperatures should have the same power law of the bulk, but found a larger prefactor than predicted which can be explained by a reduced exchange coupling of the surface to the bulk.

The GaAs polarized electron source at NIST was used to make the first spin polarized inverse photoemission measurements demonstrating that information can

be obtained about the spin dependent electronic structure of the unfilled states in a ferromagnet. This information, complementary to that from spin polarized photoemission, is of particular interest because the 3d holes play a key role in transition metal magnetism. Spin polarized inverse photoemission measurements revealed how chemisorption induces changes in surface magnetism.

Energy- and spin-resolved secondary electron measurements carried out at NIST showed that a ferromagnetic metal yields an abundance of highly polarized secondary electrons. This made clear the possibility of measuring the polarization of secondary electrons generated in a scanning electron microscope to achieve high resolution imaging of surface magnetization. The technique, which has come to be known as scanning electron microscopy with polarization analysis or SEMPA, has been used to investigate a variety of fundamental and technologically important aspects of magnetic microstructure including the influence of the surface on domain wall microstructure, domains in Ni-Fe memory elements and thin film recording media, and the oscillatory exchange coupling of two magnetic layers through a nonmagnetic spacer layer. Dr. Pierce's present research interests include the application of SEMPA to surface and thin film magnetism, the characterization and understanding of thin film growth using the STM, and the achievement of spin dependent magnetic contrast in STM measurements.

Dr. Pierce has authored or co-authored 150 publications including several book chapters and review articles. He has three joint patents which include GaAs polarized electron source and two types of spin analyzer. He has shared in two IR-100 Awards, the Department of Commerce Silver and Gold Medals, the NIST E.U. Condon and William P. Slichter Awards, and the Washington Academy of Science Distinguished Achievement Award. Dr. Pierce wishes to acknowledge the supportive research environment he has benefited from at Stanford, ETH and NIST, and the fruitful collaborations he has enjoyed throughout his career with many talented colleagues from these and other laboratories. Pierce is a NIST Fellow and a Fellow of the American Physical Society.

## ALBERT NERKEN AWARD

The Albert Nerken Award was established in 1984 by Veeco Instruments, Inc. in recognition of its founder, Albert Nerken, as a founding member of the American Vacuum Society, his early work in the field of high vacuum and leak detection, and his contributions to the commercial development of the instrumentation. It is presented to recognize outstanding contributions to the solution of technological problems in areas of interest to the American Vacuum Society. The award consists of a cash prize and a certificate.



**HAJIME ISHIMARU**

**Dr. Hajime Ishimaru**, National Laboratory for High-Energy Physics, Japan, *"for his unique contributions to the development and characterization of aluminum alloys for use in ultra-high vacuum environments."*

Hajime Ishimaru was born in 1940 in Sapporo, Japan and graduated high school in Sapporo. He received a B.S. degree in physics from Hokkaido University in 1963 and an M.S. in nuclear physics from Tohoku University in 1965. In 1970, he received the SciDr in plasma physics from Nagoya University where his research was in energy-mass analysis for highly ionized steady state plasma. Dr. Ishimaru received the EngDr from Tokyo University in 1980, working in the areas of vacuum feedthroughs-coaxial, multi-pin/coaxial

multi-pin complex vacuum feedthroughs in ultrahigh vacuum and cryogenic.

From 1969 to 1972, he worked at the Tokyo University as Research Associate on diagnosis of the plasma and molecular beam. In 1972, Dr. Ishimaru joined the National Laboratory for High Energy Physics in Tsukuba, Japan. He currently heads the TRISTAN Vacuum Group, an aluminum constructed electron-position collider beam storage ring and the B Factory under construction. He directed the construction of the beam transport line of the proton linear accelerator, beam monitoring and operation of the proton synchrotron, development of the all aluminum alloy vacuum system, and construction of TRISTAN  $e^+e^-$  large storage accelerator. As Professor, he also manages the research of Ph.D Graduate students for Accelerator Science, The Graduate University for Advanced Studies in Japan.

A major contribution of Dr. Ishimaru was in aluminum vacuum technology where he pioneered the development of all aluminum ultrahigh vacuum materials, components, and systems for vacuum in the low  $10^{-23}$  Torr region. In 1977, he discovered the residual radioactivity in aluminum decays with half-life as short as 15 hours and the first to have experimental data on the decay of the residual radioactivity of vacuum material. He then embarked upon developing techniques for surface treatment of aluminum. Initially, EX-mirrored finished was developed by enclosing the working portion of a lathe in a larger vacuum chamber under a controlled atmosphere of oxygen and argon gases. A diamond tipped tool was used to cut the inner surface of high purity aluminum producing a new oxide layer of less than 30 Å thick. Other surface treatments developed were EX-extrusion, EX-process, and EX-GBB process. Outgassing rates for these surface treatments after a 24 hour bakeout at 150°C was in the low  $10^{-14}$  Torr L/s  $cm^2$ . Dr. Ishimaru developed special welding techniques for aluminum by TIG for flanges, fittings, vacuum vessels, and electron beam welding for feedthroughs and bellows for very small weld seams.

To complete this new aluminum tech-

nology, Ishimaru has developed an all aluminum conflat flange, titanium carbide coated knife-edge together with a re-usable aluminum gaskets and high strength aluminum nuts and bolts. He developed an aluminum single structure bellows for connecting to the beam line chamber for baking and adsorption of mechanical distortions and for the tolerance against "melt-down" by the particle beam. Other developments included aluminum metal seal right angle valves, double metal-seal gate valves, optical windows, feedthroughs, manipulators, non-water cooling vacuum furnace, and a portal vacuum suitcase using very light weight aluminum alloy honeycombed panels. Also, a turbomolecular pumps was developed by cobling the rotor with ceramic coating to achieve vacuum in the low  $10^{-12}$  Torr region. Sputter ion pumps and titanium sublimation pumps were also made from aluminum alloys. With the different aluminum components and pumps, an extremely high vacuum system of the order of  $10^{-13}$  Torr was developed using an aluminum alloy quadrupole mass filter. A very fast pump-down system was also developed employing special moisture traps to achieve vacuum of  $10^{-8}$  Torr region in less than 150 seconds.

Dr. Ishimaru is a Technical Consultant to Korea POSTECH 2 GeV synchrotron radiation source; DAØNE Collider Project for INFN Frascati, Italy; Taiwan 1.5 GeV Synchrotron; Spring-8, Japan; Space Shuttle's "WAKE" Project in collaboration with the Space Epitaxy Center in Houston University, and SSC Main Collider Beam Tube/HEB (now terminated). He was also instrumental in the design and development of a 40 m L-shaped aluminum alloy chamber and vacuum tank with laser beam reflecting mirror system for the National Astronomical Institute in Japan.

His work has been very extensively cited by others in the high vacuum field. He has authored and co-authored over 185 papers in vacuum journals and conference proceedings and four technical book publications. Dr. Ishimaru has 40 registered patents and over 100 patents pending. He is a Member of AVS, Japan Society of Vacuum, the Japan Society of Applied

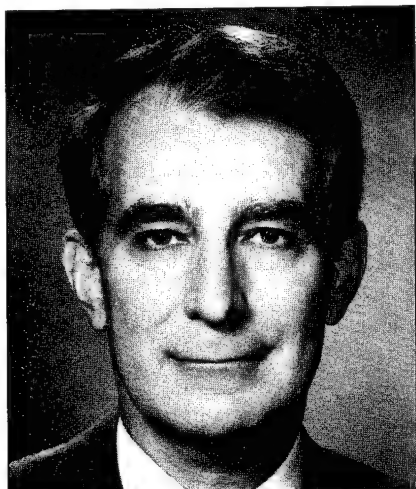
Physics, Japan Institute of Light Metals, and Member of the Editorial Advisory Board for "VACUUM," a British Vacuum Journal.

Dr. Ishimaru received numerous awards and honors for his work. In 1978, he received the Award of Excellence, Best Shop Note by the American Vacuum Society for the first bakeable metal-seal aluminum alloy flange system. Since it was the first award, he was not able to attend the award ceremony in New York due to budget constraints. In 1979, the Vacuum Society of Japan awarded Dr. Ishimaru for his contribution in the development of an 14 pin/BNC coaxial combination for cryogenic vacuum and microwave performance in the GHz region, and in 1982, for development of the first all aluminum alloy vacuum system. He received Japan's 42nd Remarkable Patent Award in 1983 for vacuum and cryogenic performance, high density, and quick connect and disconnect of the 14 pin/BNC coaxial combination feedthrough. In 1985, Japan's Remarkable Patent was awarded to Dr. Ishimaru for development of very thin and high performance thermal insulation with no particulates for vacuum systems. He received an award from the British Vacuum Society in 1985 for the first beryllium window mounted on aluminum by electron beam weld. In 1989, Physics News, from the American Institute of Physics, for the first practical  $10^{-13}$  Torr XHV aluminum system and in 1991 the TAKAGI AWARD from the Institute of Japan for the first Ball Screw and Ball Bearing in UHV with long life time. Dr. Ishimaru received Taiwan's highest honor for technical contribution to vacuum technology to the SRRC Project at a dedication ceremony on October 1993, Hsinchu, Taiwan.

Dr. Ishimaru was instrumental in the establishment of ALVALAB (Aluminum Vacuum Laboratory) in 1988, an international private research consortium to develop and promote aluminum ultrahigh technology. Today, 63 member firms worldwide offer aluminum vacuum components and system technology. Dr. Ishimaru is known as the "Father" of ALVALAB.

## JOHN A. THORNTON MEMORIAL AWARD AND LECTURE

To recognize outstanding research or technological innovation in the areas of interest to the American Vacuum Society, with emphasis on the fields of thin films, plasma processing, and related topics. The award is conferred annually or biannually as a suitable candidate may be identified. It consists of a cash prize, a commemorative plaque stating the nature of the award, and an honorary lectureship at a regular session of the National Symposium.



**DAVID W. HOFFMAN**

**Dr. David W. Hoffman**, Ford Motor Company, *"for basic contributions to the effects of magnetron sputtering on the stress and microstructure of thin films, gas dynamics and resputtering."*

David W. Hoffman studied physical metallurgy at The Ohio State University and the Massachusetts Institute of Technology, where he earned his doctorate in 1966. From 1966 until 1994 he was a member of the Scientific Research Laboratory at Ford Motor Company. Earlier this year he retired from Ford and is currently enjoying part time employment with Advanced Modular Power Systems in Ann Arbor, Michigan. Dr. Hoffman's research interests are rooted in physical metallurgy, where his early work at Ford dealt with discrete lattice Fourier representations of ordering and clustering in binary alloys. Using this formalism he deduced a simple, elegant expression for

the excess entropy of solution that greatly enhanced the accuracy of predictions of alloy ordering and clustering.

His interest in thin films was catalyzed by the automotive problem of coating plastic parts with vapor deposited decorative metals such as chromium as an alternative to electroplating without incurring failures caused by unexpectedly high residual stresses. A change meeting with John A. Thornton resulted in the discovery that chromium thin films deposited by then-new magnetron sputtering on plastic parts did not exhibit cracking from residual tensile stresses. This observation launched a decade-long collaboration that uncovered the remarkable stress transition to compressive intrinsic stress at low sputtering pressures accessible through magnetron sputtering, and established the phenomenon to be one of great generality. The stress transition was found to be associated with microstructural and physical property transitions in deposited films as controlled by sputtering pressure and many other process variables. This phenomenology was extensively mapped out and linked to the presence and control of inherent energetic neutral bombarding particles during sputter deposition through a variety of unique experiments. The main impact of the stress transition phenomenology developed by Hoffman and Thornton was to establish that the properties and growth structures of sputter-deposited materials are produced by the flux of energetic particles streaming from target to substrate, as controlled by the degree of gas-scatter dissipation and dis-alignment in transit and by the configuration of the target, substrates, and their relative deployment.

To simulate the observed sputter deposition phenomena, Dr. Hoffman pioneered the technique now widely known as ion peening or ion assisted deposition and published a seminal paper in this area. He also pioneered in the conceptualization and fabrication of a rotating magnets magnetron, specializing in a version with a helical rotating discharge. He was the first to observe and report gas dynamic effects caused by magnetron sputtering. He observed and named the phenomenon of intrinsic resputtering and deduced the theoretical explanation of its unusual universal curve. He quantified the flux of backscattered neutralized ions from sputtering targets and demonstrated the utility

of the analytic expressions by quantitative predictions of embedded inert gas in thin films. His work has appeared in over 50 publications and is extensively cited.

Dr. Hoffman was elected a Fellow of the American Vacuum Society with the first class of AVS Fellows in 1993. Professionally, Dr. Hoffman has been active in the American Vacuum Society, where he has served as Associate Editor of the *Journal of Vacuum Science and Technology A* and as Program Chairman of the Thin Films Division. He has lectured on applications of thin films in AVS Short Courses. In 1985 he was elected to the AVS National Board of Directors, where he initiated the AVS Investment Advisory Committee and was instrumental in establishing the John A. Thornton Memorial Award and Lecture. In 1988 he was elected President of the AVS for 1990. Since then he has served on the Investment Advisory Committee, the Long Range Planning Committee, and as AVS representative to the Governing Board of the American Institute of Physics, where he currently also serves on the Executive Committee of the Governing Board.

## PETER MARK MEMORIAL AWARD

The Peter Mark Memorial Award was established in 1979 in memory of Dr. Peter Mark who served as Editor of the *Journal of Vacuum Science and Technology* from 1975 to 1979. The award is presented to a young scientist or engineer (35 years of age or under) for outstanding theoretical or experimental work, at least some of which must have been published in JVST. The award consists of a cash prize and a certificate.

## MARJORIE OLMSTEAD

**Dr. Marjorie Olmstead**, University of Washington, *"For elucidating the nature of semiconductor surfaces and the heteroepitaxial growth of insulating materials on these surfaces."*

Marjorie Olmstead received her B.A. (Highest Honors) from Swarthmore College in Pennsylvania in 1979, majoring in physics with minors in applied mathematics and physical chemistry. She attended graduate school in physics at the University of California, Berkeley, where she received her M.A. in 1982 and her Ph.D in 1985. At Berkeley, she developed the technique of photothermal displacement spectroscopy to measure very small optical absorption signals, and used the technique to measure the optical adsorption of dangling bond states on cleaved Si and Ge. Her thesis work exploited these measurements to probe the symmetry, reconstructions, phase transitions and electron-phonon interaction on these surfaces.

Dr. Olmstead joined the Xerox Palo Alto Research Center as a Member of the Research Staff in 1985. She returned to Berkeley in 1986 as an Assistant Professor of Physics, and held a joint appointment as a Faculty Scientist at the Lawrence Berkeley Laboratory's Center for Advanced Materials from 1988 through 1993. She joined the faculty at the University of Washington, Seattle, in 1991, where she is currently an Associate Professor of Physics and Adjunct Associate Professor of Chemistry.

Beginning with her work at Xerox, Dr. Olmstead has pursued an interest in the chemical, structural and energetic constraints controlling the heteroepitaxy of strongly disparate materials. Using in-situ core-level and valence-band photoemission spectroscopy and X-ray standing wave fluorescence, Dr. Olmstead and her collaborators have shown how interface reactions, and the distinct surface energies and reaction tendencies of the resultant interface compounds, can control the structure and electronic properties of interfaces between strongly dissimilar materials, as well as the morphology of the resultant overlayer film.

Prof. Olmstead's current research centers on the kinetics of heteroepitaxy and on the structural and electronic properties of ultra-thin ionic materials. She and her students are among the first in the world to apply the technique of component-resolved X-ray photoelectron diffraction to study the kinetics of heteroepitaxial growth.

Their site-specific diffraction studies of calcium fluoride growth on silicon have yielded *in situ* kinetic information on the heteroepitaxy of strongly dissimilar systems, and have demonstrated the complex variety of growth modes accessible. Recently, her group has made both experimental and theoretical advances in understanding the role of thin film geometry on core-level energies in insulators.

Prof. Olmstead received a National Science Foundation Presidential Young Investigator Award and an IBM Faculty Development Award in 1986, and was the spokesperson for a multi-investigator project funded through the 1989 Department of Energy "2% Initiative" Competition. Prof. Olmstead enjoys teaching at both the graduate and undergraduate level. She is active in the American Vacuum Society, and is currently both a member of the Electronic Materials and Processing Division program committee and the Puget Sound Representative to the Pacific Northwest Chapter of the AVS.

### JVST SHOP NOTE AWARD

The JVST Shop Note Award was established in 1970 by the AVS Vacuum Technology Division. It is presented to encourage the publication of novel solutions to instrumental or experimental problems as JVST Shop Notes in the previous year. The award consists of a certificate and cash prize. U. Bischler and E. Bertel have been selected as the 1994 winners of the JVST Shop Note Award for their contribution to "Simple Source of Atomic Hydrogen for Ultrahigh Vacuum Applications," JVST A11, 458 (1993).

### NELLIE YEOH WHETTEN AWARD

The Nellie Yeoh Whetten Award was established in 1989, in the spirit of Nellie Yeoh Whetten, to recognize and encourage excellence by women in graduate studies in the sciences and technologies of interest to the American Vacuum Society. A fund to support the award was established by Timothy J. Whetten, friends and family of

Nellie Yeoh Whetten, and the AVS. The award consists of a \$1,000 cash prize, a certificate, and support of up to \$750 in reimbursed travel expenses to attend the National Symposium.

### 1994 NELLIE YEOH WHETTEN WINNER

Monica Katiyar, University of Illinois

### RUSSELL AND SIGURD VARIAN FELLOWSHIP

The Russell and Sigurd Varian Fellowship was established in 1982 to commemorate the pioneering work of Russell and Sigurd Varian in the Field of Vacuum Science and Technology. It is presented to recognize and encourage excellence in graduate studies in vacuum science. The Fellowship is supported by Varian Associates and consists of \$1,500, a miniature replica of the first Vac Ion pump, a certificate, and support of up to \$750 in reimbursed travel expenses to attend the National Symposium. The winner is selected from three finalists based on personal interviews with the Scholarships and Awards Committee at the National Symposium and will be announced at the Awards Assembly in October.

### 1994 VARIAN FINALISTS

Britt Turkot, University of Illinois  
Robert Turkot, Jr., University of Illinois  
Yajun Wang, University of Wisconsin

### AVS GRADUATE RESEARCH AWARDS

The AVS Graduate Research Award was established in 1984. They are awarded to recognize and encourage excellence in graduate studies in the sciences and technologies of interest to the American Vacuum Society. Each award consists of \$1,000, a certificate, and support of up to \$750 in reimbursed travel expenses to attend the AVS National Symposium.



## 1994 GRADUATE RESEARCH AWARD

Thomas R. Bramblett, University of Illinois  
Laurie Hackenberger, Pennsylvania State University  
Dong Li, Northwestern University  
Qian Liu, University of North Carolina  
David Patrick, University of Utah  
Britt Turkot, University of Illinois  
Robert Turkot, Jr., University of Illinois  
Yajun Wang, University of Wisconsin  
Huasheng Wu, Montana State University  
Frank Zimmerman, Cornell University

## AVS FELLOWS

The membership level designated "Fellow of the Society" was established in 1993 to recognize members who have made sustained and outstanding scientific and technical contributions in areas of interest to the AVS. These contributions can be in research, engineering, technical advancement, academic education, or managerial leadership. This is a prestigious membership level to which members are elected. The Fellow will receive a certificate.

## 1994 FELLOWS

Daniel Alpert, University of Illinois  
Ernst Bauer, Technical University, Clausthal  
Christopher R. Brundle, IBM Research  
Rointan F. Bunshah, University of California  
Robert J. Celotta, NIST  
John W. Coburn, Fraunhofer Inst fur Angewandte Festkorperphysik  
Jerome J. Cuomo, IBM Research Center  
Paolo della Porta, SAES Milano  
Francois M. d'Heurle, IBM Research Center  
Charles B. Duke, Xerox Webster Research Center  
Charles S. Fadley, Lawrence Berkeley Laboratory  
Randall M. Feenstra, IBM Research Center  
Maurice H. Francombe, Westinghouse R&D Center  
Barbara J. Garrison, Pennsylvania State University  
Richard A. Gottscho, AT&T Bell Labs.  
John T. Grant, University of Dayton  
Marsbed Hablanian, Varian Vacuum Products  
Robert J. Hamers, University of Wisconsin  
George H. Hass, Radiation Research Lab.  
Franz J. Himpsel, IBM Research Center  
Paul S. Ho, University of Texas  
Leslie Holland  
Jack E. Houston, Sandia National Laboratories  
Harald Ibach, Forschungszentrum Julich  
Hajime Ishimaru, Natl Lab for High-Energy Physics  
William J. Kaiser, Jet Propulsion Lab  
Harold Kaufman, Front Range Research  
Eric Kay, Stanford University  
Lawrence Kazmerski, Natl Renewable Energy Lab  
Max Lagally, University of Wisconsin  
Charles Magee, Evans East  
Dennis M. Manos, College of William and Mary  
John F. O'Hanlon, University of Arizona  
Marjorie Olmstead, University of Washington  
Daniel T. Pierce, NIST  
Cedric J. Powell, NIST  
Stephen M. Rossnagel, IBM Research Center  
John E. Rowe, AT&T Bell Labs  
Donald Santeler, Process Applications  
Martin Seah, National Physical Lab  
William Spicer, Stanford University  
Michel Van Hove, Lawrence Berkeley Lab  
John L. Vossen, John Vossen Associates  
Gottfried Wehner  
H.H. Wieder, University of California  
Jerry M. Woodall, Purdue University  
David P. Woodruff, Warwick University  
John T. Yates, Jr., University of Pittsburgh  
Russell Young, R.D. Young Consultants



# DIVISION AWARDS

## Morton M. Traum Surface Science Division Student Award

The AVS Surface Science Student Division Award was initiated in 1981. Morton M. Traum, then chair of the Surface Science Division, was the prime motivator in establishing the award. After Mort's untimely death on 1 December 1982, the Executive Committee of the Surface Science Division renamed the award in his memory. The Morton M. Traum Surface Science Division Student Award is presented annually for the best student paper based on work leading to a Ph.D thesis. The papers are judged on technical content and quality of presentation.

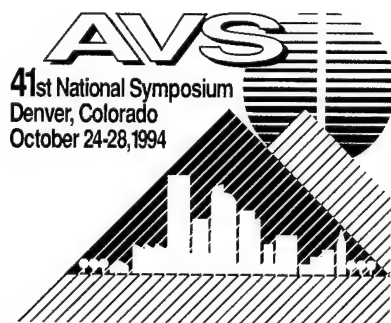
The winner of the award will be announced at the beginning of the Postdeadline Discovery Session held on Thursday evening, October 27.

### Past winners are:

1981	Eric Stuve
1982	Steven Gates
1983	Ann Smith
1984	Hans Gossman
1985	Duane Outka
1986	Greg Sitz
1987	Michael Henderson
1988	Jeff Hanson
1989	Yunong (Neal) Yang
1990	Benjamin Wiegand
1991	David Peale
1992	Chaochin Su
1993	Anna Swan

## John Coburn and Harold Winters Student Award in Plasma Science and Technology

The Plasma Science and Technology Division has established the John Coburn and Harold Winters Student Award. John Coburn and Harold Winters have made pioneering contributions to the field of plasma processing and plasma surface interactions. Their work has provided the inspiration for countless students to enter the field. Coburn and Winters have enhanced the graduate experiences of students by both example and by tutorship. In recognition of their work, the Coburn and Winters Student Award will be conferred on the student whose oral presentation of his/her paper at the Annual Symposium is judged most outstanding by a panel selected from the Executive Committee of the PSTD. The student winner will receive a prize of \$500.



## NEW PRODUCTS POSTER SESSION—SEE THE LATEST IN VACUUM TECHNOLOGY

At this year's exhibition, poster sessions will present the latest ideas in new technology. Don't miss the excellent opportunity (3–5 p.m. on Wednesday) to learn about new products being introduced to the market.

## SEE THE EXHIBITS—AND DON'T MISS A SINGLE EVENT

This year, you will have more time to tour the exhibit. There will be no plenary lunch-time lectures on exhibit days, and a full three-hour block of time has been opened on Wednesday when there will not be any technical sessions scheduled.

## REFRESHMENTS AND SPECIAL SNACKS

There are so many great technical sessions and interesting new technologies to see and so little time! So this year, there will be refreshments and snacks in the exhibition area. You can munch while you browse through the show.

# AVS TECHNOLOGY AND EQUIPMENT EXHIBITION

## WHY YOU SHOULD ATTEND

This will be an excellent opportunity to see products and services offered by over 150 participating companies. There is no fee to attend the exhibition, and it is open to members and nonmembers of the AVS. Everyone with an interest in keeping abreast of the current innovations in our industry is welcome and encouraged to attend. Many company scientists will be available to answer your questions.

Exhibits will be relevant to engineers, technicians, scientists, and purchasing professionals in the following fields:

- Thin-Film Deposition
- Fusion Technology
- Vacuum Metallurgy
- Nuclear and High-Energy Physics
- Surface Analysis
- Lasers and Optics
- Analytical Instruments
- Vacuum Technology
- Semiconductor Materials and Processing



# TECHNOLOGY AND EQUIPMENT EXHIBITORS

## NEW EXTENDED SHOW HOURS

A & N Corporation  
Academic Press  
Advanced Ceramics Corp.  
Advanced Energy Industries  
AJA International  
Alberta Microelectronic Centre  
Alcatel Vacuum Products  
Alta Group  
American Institute of Physics  
Ametek/Dycor  
Amplifier Research  
Angstrom Sciences  
APD Cryogenics  
Applied Science & Technology  
Applied Surface Technologies  
Arconium Specialty Alloys -  
PlasmArc Div.  
ATI Instruments N.A.  
Austin Scientific Co.  
Balzers  
Bertan High Voltage  
Bi-Braze  
Brooks Instruments  
Burleigh Instruments  
Cambridge Mill Products  
Cerac, Inc.  
Ceramaseal  
CHA Industries  
Commonwealth Scientific  
Cooke Vacuum Products  
CTI-Cryogenics  
CVC Products  
CVI Inc.  
Danielson Associates  
Denton Vacuum, Inc.  
Digital Instruments  
Duniway Stockroom  
DynaVac  
Edwards High Vacuum Int'l.  
Elnik Systems  
Evac International  
Charles Evans & Associates  
Extrel Mass Spectrometry  
FEI Co.  
Ferrofluidics  
Fil-Tech, Inc.  
Fison Instruments  
Fuji Seiki Inc.  
Geller Microanalytical  
GNB Corporation  
Granville-Phillips  
Helicoflex Co.  
Hiden Analytical Ltd.  
High Vacuum Apparatus Mfg.  
IBM Analytical Services

Inland Vacuum  
Innotec Group Inc.  
Integrated Vacuum Technology  
Ion Tech Inc.  
Jeol USA, Inc.  
John Crane Belfab  
KDF Electronic & Vacuum Svces.  
Key High Vacuum Products  
Kimball Physics  
Kratos Analytical  
L.D.S. Vacuum Products  
Larson Electronic Glass  
Kurt J. Lesker Co.  
Leybold Inficon Inc.  
Leybold Technologies  
Leybold Vacuum Products  
LK Technologies  
Luxtron Corporation  
Mass-Vac, Inc.  
Mat-Vac Technology  
Materials Science Inc.  
R.D. Mathis Co.  
Maxtek, Inc.  
McAllister Technical Services  
MDC Vacuum Products  
MeiVac, Inc.  
Metroline Industries  
MKS Instruments  
NIST/Standard Reference Data  
Nor-Cal Products  
Nordiko USA, Inc.  
Nuvac Innovations  
OCI Vacuum Microengineering  
Omicron Associates  
Osaka Vacuum Ltd.  
Oxford Instruments  
Park Scientific Instruments  
Perkin-Elmer  
Phelps Electronics  
Philips Semiconductors  
Plasma-Therm, Inc.  
PlasmaQuest, Inc.  
Plasmaterials, Inc.  
Polycold Systems  
Precision Flow Devices  
Precision Plus Vacuum Parts  
Princeton Research Instruments  
Princeton Scientific Corp.  
Process Systems Int'l.  
Pure Tech Inc.  
Quantar Technology  
Rees Instruments  
Research & PVD Materials  
RF Power Products  
RF Services Inc.

The hours are as follows:

<b>Tuesday</b>	<b>11 a.m.-6 p.m.</b>
<b>Wednesday</b>	<b>10 a.m.-5 p.m.</b>
<b>Thursday</b>	<b>10 a.m.-3 p.m.</b>

RHK Technology  
Rocky Mountain Laboratories  
Rushmore Technology Inc.  
SAES Getters U.S.A.  
Scienta Instrument AB  
Seiko Seiki Co., Ltd.  
Senior Flexonics, Inc.  
Service Physics  
Soleras Ltd.  
Specs GmbH  
Spectra Instruments  
Spectravac Inc.  
Staib Instrumente  
Stephens Analytical  
Stokes Vacuum Inc.  
Super Conductor Materials  
Surface/Interface  
Swagelok Co.  
Sycon Instruments  
T-M Vacuum Products Inc.  
Target Materials, Inc.  
Technotrade International  
Techware Systems  
Teledyne Brown Engineering  
Telemark  
Televac  
Tencor Instruments  
Terranova Scientific  
TFS Technologies  
Thermionics Lab.  
TopoMetrix  
Tylan General  
U-C Components, Inc.  
US Thin Film Products  
UTI Instruments  
Vacuum Engineering & MAT  
Vacuum Research Corp.  
Vacuum Technology  
Varian Associates  
VAT, Inc.  
Veeco Instruments  
VSI Vacuum Science Instruments  
GmbH  
John Wiley & Sons, Inc.  
Williams Advanced Materials  
Willson Scientific Glass  
J.A. Woollam Co.  
World Scientific Publ.  
Yeagle Technology

# THE 41ST NATIONAL SYMPOSIUM and TOPICAL CONFERENCES of the American Vacuum Society Denver, Colorado—October 24–28, 1994

The American Vacuum Society will hold its National Symposium and Topical Conferences at the Colorado Convention Center. This Symposium is the main gathering for scientists and technologists whose research interests or processing needs demand reduced pressure environments. Last year's meeting in Orlando attracted over 3000 registrants from academia, industry, and government.

## Technical Program

The meeting features a dynamic program comprised of 120 technical sessions including 18 poster sessions and 3 topical conferences — combined to offer a total of over 1000 papers. Distinguished invited speakers will keynote many of the technical sessions. A lunch-time plenary lecture on the world technological balance of power is scheduled to complement the technical program on the first day of the symposium.

## Exhibits

A very important part of each AVS National Symposium is the exhibit of vacuum and deposition equipment, vacuum system components, analysis systems, and vacuum-related services. As in previous years, an extensive commercial exhibit of current products will highlight progress in vacuum hardware and services. In Denver, the exhibits will be open Tuesday through Thursday (11 a.m.-6 p.m.; 10 a.m.-5 p.m.; 10 a.m.-3 p.m.). To encourage everyone to visit the exhibits, we have expanded the lunch hour on Wednesday, giving a full three hours for lunch and interaction with exhibitors.

## Morning Coffee/Tea and Announcements

We will be offering free coffee and tea in the foyer above the registration area on Monday through Friday before the first technical session (7:30-8:20). In addition, on Tuesday through Thursday free coffee and tea will be offered during the exhibit hours. Posters will be strategically located in the registration area of the Convention Center that will announce last minute changes in the sessions or other activities. Please check them.

## Short Courses

The Convention Center will also be the site for the short course program where courses on a variety of topics will be offered. These courses will run concurrently with the AVS Symposium. Full details are available in the preliminary program on pages 117.

## DIVISIONAL PROGRAM

The preliminary program is listed below for the 41st National Symposium of the American Vacuum Society. The program is organized by the Society's eight divisions. Various technical sessions will be keynoted by invited speakers of international reputation.

### Applied Surface Science Division

Session AS-MoM presents overviews of recent advances in Imaging and Small Area Analysis using ion, photon, and electron beams. Major topics include SIMS imaging techniques emphasizing organic surface characterization and advances in small area XPS and scanning AES instrumentation. Micro-Raman spectroscopy for strain imaging analysis will also be discussed.

The latest developments in data banks, data processing and reference materials for surface analysis will be presented in Session AS-MoA, Data Processing and Reference Methods. This is an area receiving a lot of attention worldwide. Information on a data model and data dictionary will be presented in a Tuesday poster session. Session AS-TuP illustrates the diversity of analytical techniques and applications. Areas of emphasis are: conductive polymers; organic surfaces and self-assembled monolayers; siloxane coatings; nanotopography and nanostructures, and metal oxide surfaces. Spectroscopic and imaging techniques include XPS, SIMS and AFM.

The location and identification of particulate contamination on surfaces are addressed in Session AS-TuM, Surface Chemistry and Contamination. This information has become critical in the area of manufacturing as the sizes of semiconductor devices have been reduced. The session on Electrochemistry and Liquid/Solid Interfaces, AS-TuA, will be joint with the Surface Science Division. The presentations will focus on: characterization of the liquid/solid interface, especially using scanning probe methods; passivation and corrosion of metal surfaces, adsorption from solution, and factors controlling surface reactivity.

Session AS-ThA, Polymer/Organic Surfaces, emphasizes ana-



lytical investigations of polymers such as: surface modification (ion beam, corona treatments), polymer interfaces (co-polymers), vibrational characterization (EELS), tacticity (SIMS), nanomechanical properties (AFM), and additives (silica in silicones, lubricants, plasticizers). XPS and/or TOF-SIMS are applied to various classes of polymers including halogenated species, polyethylenes, polystyrenes, polypropylenes and polymethacrylates.

The session on Adhesion and Adhesive Bonding, AS-FrM, will cover many aspects of adhesion including surface preparation and primers, characterization of polymer/metal interfaces and interfacial bond strengths. Applications range from structural bonding to microelectronics devices.

Code	Session
AS-MoM	Imaging and Small Area Analysis <i>H.-N. Migeon, Centre Univ. - Lux.</i>
AS-MoA	Data Processing and Reference Methods <i>R. W. Linton, Univ. North Carolina</i>
AS-TuM	Surface Chemistry and Contamination <i>T. Francis, Applied Materials</i>
ASSS-TuA	Electrochemistry and Liquid/Solid Interfaces <i>D. Baer, Pacific Northwest Lab.</i>
AS-WeM	Quantitative Analysis, Emphasizing Angle-Resolved XPS
AS-WeA	Depth Profiling <i>E. H. Cirlin, Hughes</i>
AS-ThM	Self-Assembled Monolayers <i>A. Ulman, Eastman Kodak</i>
AS-ThA	Polymer/Organic Surfaces
AS-FrM	Adhesion and Adhesive Bonding <i>J. Wightman, Va. Polytech. Inst</i>

## Electronic Materials and Processing Division

The Electronic Materials and Processing Division provides a forum for the discussion of research on electronic, optical, physical and chemical properties of semiconductors, metals and dielectrics and their interfaces, and on processing technologies for these materials. In this year's program, oral and poster sessions provide an exciting overview of the multiple connections between materials growth, structure and processing, and device fabrication and performance.

The EMPD program features sessions in all four of the Symposium's Focus Areas. Three sessions are devoted to Si based optoelectronics. The first is an all-invited session with overview talks describing the leading edge of optoelectronic device technologies. It is followed by two sessions on heterostructures for optoelectronics and wide band gap nitride materials which feature advances in II-VI and III-V blue/green emitters and lasers. In conjunction with other sessions focusing on sensors and diagnostics, EMPD will present a session on in-situ optical diagnostics for materials processing. It highlights a number of real-time techniques for characterization in situ, with a special focus on spectroscopic ellipsometry. A session on processing and characterization of materials for nanostructures is coordinated with a Surface Science session on nanoscale measurements on surfaces and a Nanometer-scale Science and Technology session

on the definition of nanoscale structures by lithography. Finally, a session on surface preparation and passivation will examine the current state of the art in surface cleaning and thin gate oxide formation. It is jointly sponsored by EMPD and the Manufacturing Science topical symposium, which will have a complementary session on tooling and manufacturing processes for wafer cleaning.

In conjunction with the topics covered in the focus areas, important progress in the growth, characterization and use of thin films in device structures is presented in two sessions covering materials for device integration, and thin film heterostructures. Areas highlighted include characterization and application of heterostructures, issues in interconnects and metallization, and new dielectric materials. Exciting progress in the science of electronic materials growth, characterization and processing is also presented in this year's program. Three sessions jointly sponsored by EMPD and the Surface Science Division will feature recent advances in fundamental understanding of microscopic mechanisms of surface modifications during materials processing, including important new insights made possible by use of the STM to characterize chemically modified surfaces. They are complemented by a session on interface characterization, presenting the state of the art in spectroscopic structural probes of heterogeneous interfaces. It will honor Marjorie Olmstead, 1994 Peter Mark Award winner.

In addition to the oral program, two exciting poster sessions will feature papers on core topics in this year's Electronic Materials and Processing Division program, as well as a wide range of other areas of interest to the division.

Code	Session
EM-MoM	Materials for Device Integration <i>B. Gnade, Texas Instr.</i>
EM-MoA	Thin Film Heterostructures <i>R. Ludeke, IBM; M. Asada, Tokyo Inst. of Tech.</i>
EMMS-TuM	Surface Preparation and Passivation <i>T. Ohmi, Tohoku Univ.</i>
EM-TuA	Silicon-based Optoelectronics <i>S. Yokoyama, Hiroshima Univ.; C. Henry, AT&amp;T; M. Koyonagi, Hiroshima Univ.; J. Michel, MIT; Y. Shiraki, Univ. Tokyo</i>
EM-WeM	Heterostructures for Optoelectronics <i>M. Ikeda, Sony; J. DePuydt, 3M; K. Bachmann, N. Carolina State Univ.</i>
EM-WeA	Wide-bandgap Nitrides <i>S. Nakamura, Nichia Chemical</i>
EM-ThM	Optical Diagnostics for Materials Processing <i>G. Maracas, Arizona State Univ.</i>
EMSS-ThM	Semiconductor Surface Reactions III <i>J. Weaver, Univ. Minnesota</i>
EM-ThA	Materials for Nanostructures <i>K. Martin, Georgia Inst. Tech.</i>
EM-FrM	Interface Characterization <i>R. Headrick, Cornell Univ.; M. Olmstead, Univ. Washington</i>

## The Nanometer-Scale Science and Technology NANO 3

This year, the Nanometer-scale Science and Technology Division (NSTD) will host the Third International Conference on Nanometer-scale Science and Technology (NANO 3). The NANO 3/NSTD program provides a multi-disciplinary forum focused on the science and technology of nanometer-scale phenomena in fields such as biology, chemistry, electronics, engineering, fabrication, materials science, medicine, metrology, optics, and physics.

NANO 3 follows the first conference held with STM '90 in Baltimore and NANO 2 held last year in Moscow. It was organized by a joint NSTD/international program committee. Members of the NSTD program committee include Rich Colton (Chair), Bob Hamers, Mark Reed, and Clayton Teague. The international committee members include Chair Christie Marrian (USA), Haroon Ahmed (UK), Chunli Bai (China), John Dagata (USA), Masa Hara (Japan), Young Kuk (Korea), Huguette Launois (France), Sharka Prokes (USA), Jurgen Rabe (Germany), Dan Rugar (USA), and Hiroshi Tokumoto (Japan). In addition to NSTD support, NANO 3 is being sponsored by the Office of Naval Research, the U.S. Army Research Office and the National Science Foundation.

The program begins Monday morning with an exceptional plenary session featuring three world-renowned keynote speakers: Prof. Wolfgang Göpel (Univ. Tübingen) on "Nanostructural Sensors for Molecular Recognition," Dr. Don Eigler (IBM Almaden Research Center) on "Quantum Corrals," and Dr. Yoshinobu Sugiyama (ETL) on "Recent Progress on Magnetic Sensors with Nanostructures and Applications." Briefly, Prof. Göpel is Director of the Institute of Physical Chemistry at the University of Tübingen. His work deals with the development of novel sensors based on the self-assembly of molecules at interfaces. Dr. Eigler is an IBM Fellow at the IBM Almaden Research Center. Using a cryogenic scanning tunneling microscope, he has shown that it is possible to individually move atoms to form structures that do not form naturally. Dr. Sugiyama is at the Electrotechnical Laboratory of the Ministry of International Trade and Industry in Japan. He has worked extensively on semiconductor magnetic sensors including the quantum Hall probe.

The invited and contributed program includes 16 oral and 4 poster sessions featuring 19 invited speakers and over 225 contributed papers. There will be poster sessions devoted to all aspects of nanometer-scale science and technology: Instrumentation and Metrology (Mo), Materials Characterization (Tu), Nanometer-scale Science and Technology (We), Nanoelectronics and Nanofabrication (Th).

The oral session are organized as follows. The Monday afternoon session focuses on advances in metrology at the nanometer-scale featuring an invited talk by Dr. J. Griffith (AT&T Bell Laboratories) on "Dimensional Metrology with Scanning Probe Microscopes." The session also includes talks on methods for fabricating and characterizing scanning probe tips and algorithms for overcoming some of the effects of finite tip geometry. The second session is the first of two sessions on the material properties of nanostructures including chemical, electrochemical, electronic, magnet, optoelectronic, and structural properties. This session focuses on electronic and structural properties of nanostructures exhibiting quantum size effects and is highlighted by an invited talk by Prof. H. Ahmed (Cambridge University).

On Tuesday morning, we begin a series of sessions devoted to the

materials science aspects of systems where structure and composition are controlled on the nanometer-scale. The session on nanostructured and nanocrystalline materials is headlined by an invited talk by Prof. H.-E. Schaefer (University Stuttgart) on "Nanostructured Solids as Interface-determined Systems." Nanoelectronics devices based on quantum effects such as resonant tunneling are close to 'real' applications. These recent advances are highlighted in a session on nanoelectronics with invited talks by Dr. J. Randall (Texas Instruments) on "Applications of Nanoelectronic Devices" and Dr. M. Peckerar (NRL) on "Manufacturing Considerations for Quantum-Effects Devices." The session concludes with a special presentation by Dr. V.N. Alfeev who will review recent developments in nanotechnology in Russia. On Tuesday afternoon, the sessions on material properties of nanostructures continue with a focus on chemical and electrochemical systems. The session features an invited talk by Dr. J. Frommer (IBM Almaden Research Center) on "Scanning Probe Microscopy on Organic Materials." We also feature part I of two sessions on nanomechanics and nanotribology with an invited talk by Prof. J.-M. Georges (University Lyon) on "Nanomechanics and Nanotribology of Lubricant Films."

Material manipulation has evolved to the point where structures can be assembled atom by atom and chemical functionality of surfaces and interfaces can be modified with molecular precision. On Wednesday morning, we begin a series of nanofabrication sessions with the topic of atomic manipulation. Invited speakers for this session are Prof. J. Lyding (University Illinois) speaking on "Nanometer-scale Patterning of Si Surfaces with an UHV STM" and J. McClelland (NIST) on "Nanofabrication with Laser Focused Atomic Deposition." We also explore various industrial applications of proximal probes in a session devoted to this topic. Invited speakers include Prof. H. Fuchs (University Munster) on "Industrial Application of Proximal Probes" and Dr. J. Mamin (IBM Almaden) on "Ultra-High Density Data Storage Based on Proximal Probes." This session also features a series of talks on using SPM-related techniques for 1-D and 2-D dopant profiling of semiconductor device structures. Since the discovery of photoluminescence from porous silicon, the role of surfaces and interfaces in determining the optical properties of silicon nanostructures has been recognized as a key issue. These effects are important in fabricated silicon nanostructures due to their large surface-to-volume ratio. A session on this topic will be held on Wednesday afternoon with an invited talk by Prof. H. Koch (Technical University Munich) on "Light from Silicon." The NANO 3 is also co-sponsoring three joint sessions with the Topical Conference on Biomaterial Interfaces. This afternoon we feature the first of two sessions on Biology at the Nanoscale with an invited talk by Dr. E. Betzig (AT&T Bell Labs) on "Scanning Near-Field Optical Microscopy."

On Thursday morning, the second session on biology at the nanoscale will feature an invited talk by Prof. L. Bottomley (Georgia Tech) on "SPM Visualization of Electrostatically Immobilized Intercalating Drug-Nucleic Acid Complexes." A second nanofabrication session devoted to proximal probe lithography will feature an invited talk by Prof. C. Van Haesendonck (Katholieke Univ-Leuven) on "Nanolithographic Patterning of Metal Films with the STM." This session will also feature several

talks on quantum conductance through thin wires. The afternoon session features part II of the session on nanomechanics and nanotribology. In addition, the biology joint sessions conclude with a session on micro-instrumentation and sensors which features an invited talk by Prof. G. Kovacs (Stanford University) on "Micromachined Neural Interface Technology."

On Friday we conclude our conference with two strong sessions devoted to innovations in proximal probe technology and novel nanofabrication techniques. Applications of proximal probes will be highlighted along with innovations such as instrumentation with high spatial and temporal resolution. Dr. G. McClelland (IBM Almaden) will deliver an invited talk on "Continuous Observation of the Motion of Single Adsorbed Atoms and Molecules with Picosecond and Sub-nanometer Resolution." The nanofabrication session will feature invited talks by J. Calvert (NRL) on "Chemistry and Applications of Self-assembled Films," and S. Fujima (NEC) on "Carbon Nanotubes."

Code	Session
NS1-MoM	NANO 3 Plenary Session <i>W. Göpel, Univ. Tübingen; Y. Sugiyama, Electrotech. Lab.; D. Eigler, IBM</i>
NS1-MoA	Nanostructure Properties: Structural and Electronic <i>H. Ahmed, Cambridge Univ.</i>
NS2-MoA	Nanometrology <i>J. Griffith, AT&amp;T</i>
NS1-TuM	Nanostructured Materials <i>H. Shaefer, Inst. Theor. u. Angew. Physik, Stuttgart</i>
NS2-TuM	Nanoelectronics <i>J. Randall, Texas Instr.; M. Peckerar, Naval Res. Lab</i>
NS1-TuA	Nanostructure Properties: Chemical and Electrochemical <i>J. Frommer, IBM</i>
NS2-TuA	Nanomechanics and Nanotribology: I <i>J. Georges, Ecole Centrale de Lyon</i>
NSMS-WeM	Industrial Applications of Scanned Probes <i>H. Fuchs, Univ. Muenster; J. Mamin, IBM</i>
NS2-WeM	Atomic Manipulation <i>J. Lyding, Univ. Illinois; J. McClelland, NIST</i>
NSBI-WeA	Biology at the Nanoscale: I <i>E. Betzig, AT&amp;T</i>
NS2-WeA	Optical Properties of Silicon Nanostructures <i>F. Koch, Tech. Univ. Munich</i>
NSBI-ThM	Biology at The Nanoscale: II <i>L. Bottomley, Georgia Inst. Tech.</i>
NS2-ThM	Proximal Probe Based Fabrication <i>C. Van Haesendonck, Katholieke Univ.</i>
NSBI-ThA	Micro-Instrumentation and Sensors <i>G. Kovacs, Stanford Univ.</i>
NS2-ThA	Nanomechanics and Nanotribology: II

NS1-FrM

Novel Materials and Methods for Nanofabrication

*J. Calvert, Naval Res. Lab.; S. Iijima, NEC*

NS2-FrM

Novel Probes

*G. McClelland, IBM*

## The Plasma Science and Technology Division

The Plasma Science and Technology Division will host eight oral sessions on the plasma processing of materials. The division will also sponsor one oral session on target fabrication for inertial confinement fusion. Two poster sessions will be offered. Eight students will compete for the John Coburn and Harold Winters Student Award in Plasma Science and Technology.

Rick Gottscho, the 1993 Division chairman, will lead off with an invited review of some of the key issues raised last year to help set the stage for this year. This talk will kick off the first two sessions on plasma etching and deposition, and one of the themes will be selective oxide etching. Yosuiro Horiike of Hiroshima University will present his work on highly selective oxide etching in an inductively coupled plasma. In the area of plasma deposition, Tom Mantei of the University of Cincinnati will provide an overview of diamond-like carbon film deposition, emphasizing plasma physics and chemistry aspects. The contributed papers in this session range over many of the issues involved with plasma generation, transport and surface interactions. Plasma deposition of metallic films for trench lining, trench filling, and contact via formation is addressed in a series of contributed papers.

Analysis and design of advanced plasma reactors continues to be an important topic in plasma materials processing. The contributed papers in this session examine problems and features in established designs such as ECR and ICP, along with some ideas for new reactor designs. The results of these studies are relevant to both deposition and etching.

Diagnostics are essential for understanding and controlling processing plasmas. Hideo Sugai of Nagoya University will present his work on diagnostic measurements of neutral and ionic radicals in an inductively coupled plasma reactor. The contributed papers include talks on gas phase and surface species detection. This session is one of the two focus areas in the 1994 Symposium in which PSTD is involved. Diagnostic sessions will be offered by seven other divisions.

Plasma-induced charging and contamination effects are among the most serious problems facing plasma technology. The session on these topics features an invited talk by Kouichi Hashimoto of Fujitsu, Ltd. on local differential charging of features, thought to be a new mechanism for gate oxide breakdown. Other papers in this session involve studies of profile distortion due to charging and charge-induced damage. Plasma-induced contamination, especially particle dynamics in plasma, is the focus of other contributed papers in this session. Surface contamination and control is the second of the two focus areas in which PSTD is included. Three other divisions will offer sessions related to this topic.

Charge free processing is an area attracting increasing attention, partly because of the charge damage and processing complications presented in the previous session. Chemical downstream etch and neutral beams are addressed in this session. Herb Sawin of MIT will present an overview of charge free processing applications,

including the current understanding of neutral-surface chemistry in charge free processing. Takachi Yunogami of Hitachi Ltd. will review recent work in the production of neutral beams, and their use for oxide etching. Among the key issues addressed in this talk are generation of high flux beams with large area uniformity.

Plasma-surface interactions are of course at the heart of plasma materials processing technologies. This year's session features an invited talk by Vince Donnelly of Bell Laboratories on measurements of spatially resolved surface adsorbate composition, termed 'chemical topography.' Contributed papers include experimental and theoretical studies of neutral and ionic species interacting with surfaces.

The session on target fabrication for inertial confinement fusion includes two invited talks. Michael Tobin of Lawrence Livermore National Laboratory will address target area design and system performance for the National Ignition Facility, Uichi Kubo of Kinki University will cover the historical development of microencapsulation for ICP capsules.

Code	Session
PS-MoM	Plasma Etching & Deposition <i>R. Gottscho, AT&amp;T; Y. Horiike, Hiroshima Univ.</i>
PS-MoA	Plasma Deposition <i>T. Mantei, Univ. Cincinnati</i>
PS-TuM	Plasma Process & Reactor Modeling <i>T. Bartel, Sandia Nat. Lab.; H. Feil, Philips</i>
PS-TuA	Advanced Plasma Reactor
PS-WeM	Plasma Diagnostics <i>H. Sugai, Nagoya Univ.</i>
PS-WeA	Plasma-Induced Charging and Contamination Effects <i>K. Hashimoto, Fujitsu</i>
PS-ThM	Charge Free Processing <i>H. Sawin, MIT; T. Yunogami, Hitachi</i>
PS1-ThA	Plasma Surface Interactions <i>V. Donnelly, AT&amp;T</i>
PS2-ThA	Target Fabrication For Inertial Confinement Fusion <i>M. Tobin, Lawrence Livermore Nat. Lab.; U. Kubo, Kinki Univ</i>

## Surface Science Division

The Surface Science Division is the largest division within the American Vacuum Society. One quarter of all the abstracts submitted for presentation at the symposium were submitted to the Division. Within the society, the Division has its main focus in the area of fundamental research. In this year's program, there will be presentations on all areas in surface chemistry and physics.

Two of the major awards given by the society this year are to individuals active in the Division. The Welch Award, given to recognize and encourage outstanding research in fields of interest to the society, will be awarded to Professor John T. Yates, Jr. from the University of Pittsburgh. Professor Yates will give an

invited talk on his recent research. The Gaede-Langmuir Award, given to recognize and encourage outstanding discoveries in the science and technologies of interest to the AVS, will be awarded jointly to Dr. Daniel Pierce and Dr. Robert Celotta, both from NIST. They are co-inventors of a new high resolution method of imaging magnetic domains, which will be discussed in their invited presentations.

A number of special sessions have been organized to focus attention on areas in which recent research has led to significant new understanding. Among these are sessions on the liquid/solid interface in which the development of atomic and molecular level structural probes now allow comparisons to be made with vacuum studies. This generates a close interaction between formerly disparate fields. Sessions on surface magnetism feature, among other topics, the discovery of a new type of magnetic material. It is a magnetic surface alloy which has potential applications to magnetic storage. Sessions on semiconductor surface reactions highlight recent experiments which give new insights into the role of atomic level steps in the oxidation and the etching of silicon surfaces by halogens.

Competition for the Morton M. Traum Award will focus on ten finalists who will be judged on their poster presentations on Monday and Tuesday afternoon.

In addition to these special sessions, the division has a very strong program in its traditional areas of surface structure, reactivity and characterization by spectroscopic means. These sessions are divided into groupings centered around materials and processes. They include sessions on surface reactions on metals, alloy and compound surface structure, surface electronic structure, semiconductor surface reactions, nucleation and growth of metals and semiconductors, heteroepitaxy, nanoscale measurements, and surface dynamics which include both thermal and non-thermal excitations.

On Thursday evening, a post deadline discovery session concerned with late breaking exciting or controversial recent developments in surface science will feature 15 minute presentations, accompanied by pretzels and beer. Abstracts for the post deadline session should be submitted on AVS forms to arrive by **Friday, September 2, 1994** to:

John C. Hemminger  
Department of Chemistry  
University of California, Irvine  
Irvine, CA 92717

Code	Session
SS1-MoM	Reactions on Metals: Hydrocarbons <i>J. Yates, Univ. Pittsburgh</i>
SS2-MoM	Alloy and Compound Surface Structure <i>H. Niehus, Humboldt Univ.</i>
SS1-MoA	Surface Mechanisms and Materials for Chemical Sensors <i>S. Semancik, NIST</i>
SS2-MoA	Nucleation and Growth: Semiconductors
SS1-TuM	Nucleation and Growth: Homoepitaxy
SS2-TuM	Non-Thermal Surface Dynamics <i>D. Jacobs, Univ. Notre Dame</i>

SS1-TuA	Dynamics and Kinetics of Surface Processes <i>M. Kordes, Ohio Univ.</i>
SS2-TuA	Nucleation and Growth: Metals
SS1-WeM	Surface Magnetism I
SS2-WeM	Reactions on Metals: Diatomics
SSEM-WeM	Semiconductor Surface Reactions I <i>J. Engstrom, Cornell Univ.;</i> <i>Y. Chabal, AT&amp;T</i>
SS1-WeA	Surface Magnetism II <i>H. Hopster, Univ. Calif. Irvine;</i> <i>S. Blugel, Forsch. Julich</i>
SS2-WeA	Solid Liquid Interfaces <i>D. Kolb, Univ. Ulm; B. Ocko,</i> <i>Brookhaven Nat. Lab.</i>
SSEM-WeA	Semiconductor Reactions II <i>K. Ragavachari, AT&amp;T</i>
SS1-ThM	Nanoscale Measurements <i>K. Kern, Ecole Polytech. Lausanne;</i> <i>R. Penner, Univ. Calif. Irvine</i>
SS2-ThM	Surface Interactions
SS1-ThA	Oxidation and Adsorption
SS2-ThA	Surface and Adsorbate Structure
SS1-FrM	Surface Electronic Structure
SS2-FrM	Group IV Semiconductor Surface Structure

Code	Session
TFVM-MoA	Diamond, Cubic Boron Nitride and Other Ultra-Hard Films I <i>P. Koidl, Fraunhofer Inst.;</i> <i>R. Collins, Penn. State Univ.</i>
TF-TuM	Thin Films for Sensors <i>Y. Taga, Toyota; A. Ricco, Sandia Nat. Lab.;</i> <i>J. Howard, IBM</i>
TFVM-TuA	Diamond, Cubic Boron Nitride and Other Ultra-Hard Films II <i>R. Davis, North Carolina State Univ.</i>
TF-WeM	Optical, Piezoelectric and Ferroelectric Films <i>A. MacLeod, Univ. Arizona; A. Kingon,</i> <i>North Carolina State Univ.</i>
TF-WeA	Deposition and Characterization Techniques of Nanostructures in Thin Films <i>J. Bilello, Univ. Michigan, R. Bradt,</i> <i>Univ. Nevada, Reno</i>
TFVM-ThM	Energetic Condensation: Processes, Properties and Products <i>J. Colligon, Univ. Salford; P. Martin,</i> <i>CSIRO; D. Hoffman, Ford</i>
TF-ThA	Thin Films for Energy Conversion and Efficiency / Active Films <i>J. Bates, Oak Ridge Nat. Lab.; R. Goldner,</i> <i>Tufts Univ.</i>
TF-FrM	In Situ Thin Film Characterization <i>M. Hammond, SI Diamond;</i> <i>S. Barnett, Northwestern Univ.</i>

## Thin Film Division

The Thin Film Division is sponsoring/co-sponsoring a number of sessions in the areas of innovative film deposition and characterization techniques and novel and practical applications.

Sessions with invited and contributed papers include:

- Thin Films for Energy Conversion and Efficiency/Active Films.
- Optical, Piezoelectric and Ferroelectric Films

In conjunction with the Vacuum Metallurgy Division, the Thin Film Division is sponsoring two sessions:

- Energetic Condensation: Process, Properties, and Products
- Diamond, Cubic Boron Nitride and other Ultra-Hard Films

Thin Film Division is also participating in the Sensors and Nanostructures. Focus Sessions with papers in the areas of:

- Thin Film Sensors
- In-situ Thin Film Characterization
- Deposition and Characterization Techniques of Nanostructures in Thin Films

The invited talks are focused on new and innovative applications for thin films as well as general review talks to help educate newcomers in the field. Finally, there will be an opportunity for extended interaction between presenters and audience in social sessions presented in the poster format and schedule for Wednesday and Thursday afternoons with focus in the areas of Post-deposition Film Characterization Techniques and Thin Film Applications.

## Vacuum Metallurgy Division

The Vacuum Metallurgy Division presents a session on mechanisms of thin film microstructure evolution covering effects of stress, surface thermodynamics as well as energetic bombardment on nucleation, texture, grain size, grain boundaries, etc. A special session is devoted to the novel area of pulsed laser and pulsed ion techniques for film deposition and surface modification. The session on surface engineering for wear and corrosion applications includes papers on protective coating techniques and treatments, particularly plasma-based process. The high level of interest in practical manufacturing technology for production of coatings and thin films prompted a special session in this area. Emphasized in the talks are processes for the deposition of large-area coatings or films. Also, an invited paper describes environmentally compliant coating processes to replace some electroplating processes that are no longer environmentally acceptable. VMD co-sponsors two sessions on ultra-hard coatings including diamond, cubic boron nitride, carbon nitride, and multilayer nitride films. Also of special interest is the session on energetic condensation which includes the John Thornton Award Lecture by D.W. Hoffman.

Code	Session
VM-WeA	Thin Film Microstructure Evolution <i>D. Srolovitz, Univ. Michigan;</i> <i>R. Camarata, Johns Hopkins Univ.</i>



VM-ThM	Pulsed Laser and Pulsed Ion Technology for Film Deposition and Surface Modification <i>L. Greer, Raytheon; D. McIntyre, Sandia Nat. Labs</i>	Code	Session
VM-ThA	Manufacturing Technology for Coatings <i>K. Legg, Northwestern Univ.; D. Glocker, Eastman Kodak; P. LeFebvre, OCLI</i>	VT-MoM	Total Pressure Gauging <i>S. Cho, Draper Labs</i>
VM-FrM	Surface Engineering for Wear and Corrosion Protection <i>A. Matthews, Univ. Hull</i>	VT-MoA	Gas Flow, Partial Pressure Analysis, and Leak Detection <i>M. Boeckmann, Vacuum Technology, Inc.; A. Fine, EPA</i>
		VT-TuM	Vacuum Systems for Accelerators and Fusion <i>P. LaMarche, Princeton Plasma Phys. Lab; R. Wavrick, Sandia Nat. Lab.</i>
		VT-TuA	Vacuum System Outgassing and Cleaning <i>S. Tison, NIST</i>

## Vacuum Technology Division

The 1994 Vacuum Technology Division program covers vacuum science and technology issues that are important to all users of vacuum equipment and processes. These topics include fundamentals of the production, measurement and control of the vacuum environment.

The program begins Monday morning with a session on total pressure measurement. Characterization of any system or process usually requires a reliable measurement of the pressure. This session presents pressure gauge calibration and reliability measurements and several promising new measurement methods. An invited paper and several contributed papers highlight silicon-based micro sensors. Partial pressure, gas flow, and leak detection methods are covered in Monday afternoon's session. Invited papers cover gas sampling techniques and the development of advanced vacuum insulation for use in energy conservation.

New to the Vacuum Technology Division program will be a technical poster session on Monday afternoon covering many aspects of vacuum science and technology. This session will provide excellent opportunity for questions and discussions with the presenters.

The large national and international facilities for particle physics and fusion research require complicated and high performance vacuum systems. Tuesday morning's session describes progress in the specialized materials, vacuum components, and vacuum vessel conditioning techniques developed for these large facilities that often find use in smaller systems for research and manufacturing. Invited talks will summarize the D-T experiments at Princeton which recently produced world's record fusion power with the TFTR tokamak, and the planned design of a new National Ignition Facility for inertial fusion research.

The understanding of the source of gas phase and surface contaminants is important for the design and operation of vacuum systems where impurity control is a critical parameter. The VTD's Focus Session on contamination control leads off with an invited talk by S. Tison from NIST who will summarize a recently held workshop sponsored by the Division on the measurement and control of water in vacuum systems. Related papers will discuss novel surface preparation methods and conditioning techniques which minimize thermal outgassing. The session concludes with a cluster of papers discussing new developments in vacuum materials for use in the next generation of storage rings for minimizing photodesorption gas loads.

## Topical Conferences

### Manufacturing Science and Technology

Building on last year's successful Topical Conference on manufacturing, and as a prelude to the recent establishment of a new Manufacturing Science and Technology Group within the AVS, this Second Topical Conference will comprise 3 1/2 days of technical sessions. The technical program of the Topical Conference has been jointly planned with the IEEE, which is a Technical Co-Sponsor.

The Topical Conference, focusing primarily on the microelectronics industry, is aimed at elucidating the scientific and technical issues which underpin effective manufacturing. An **Overview** session of primarily invited speakers will highlight the role of equipment, future manufacturing concepts, research opportunities, and environmental issues.

Two sessions are devoted to **Advanced Manufacturing Equipment** for both thermal and plasma processes, underscoring the importance of the equipment industry to microelectronics manufacturing. The equipment industry represents a critical component to microelectronics manufacturing competitiveness, and the AVS hopes to contribute significantly in this area, building on its scientific strengths and on the long-standing alliance between its university, government, and industrial members.

A session on **Diagnostics, Sensors, and Control** represents a crucial element for manufacturing and also draws on a traditional strength of the AVS; this session is part of a multi-session focus for the entire National Symposium. The session on **Micro-Contamination and Defects**, part of different multi-session focus in the meeting on surface contamination and control, will address particulate and molecular contamination, defects, and their relation to equipment and process. **The Process and Equipment Modeling** session will include an invited talk on the role of equipment modeling and process synthesis, as well as talks on both reactor-scale and microfeature-scale issues in chemical processes.

A joint session on **Vacuum Process Control** for manufacturing will emphasize aspects of vacuum technology with major manufacturing impact in microelectronics, particularly process and equipment control, ergonomics, and diagnostic sensors. Finally, the Topical Conference is co-sponsoring other sessions in the Symposium on Industrial Applications of Scanning Probe Microscopy and on Surface Preparation and Passivation.

Code	Session
MS-MoA	Process and Equipment Modeling <i>Z. Lemnios, ARPA</i>
MS-TuM	Manufacturing Overview and Environmental Issues <i>S. Harrell, Sematech; G. Pitts, MCT Corp., R. Kerby, EPA; D. Herr, Semicond. Res. Corp.</i>
MS-TuA	Advanced Manufacturing Equipment - A <i>R. Bachrach, Appl. Materials; E. van de Ven, Novellus; K. Okomura Toshiba</i>
MS-WeM	Advanced Manufacturing Equipment - B <i>R. Wright, Sematech; G. Selwyn, IBM</i>
MS-WeA	Diagnostics, Sensors, and Control <i>S. Butler, Texas Instr.; J. O'Neill, IBM; J. Wiczer, Sandia Nat. Lab.</i>
MS-ThM	Micro-Contamination and Defects <i>B. Hermsmeier, IBM; H. Walker, Texas A&amp;M Univ.</i>
MSVT-ThA	Vacuum Process Control for Manufacturing <i>D. Miller, Sandia Nat. Lab.; R. McMahon, Techware</i>

## Biomaterials Interfaces

The Second Biomaterials Interfaces Topical Conference has been organized to provide a special forum where biologists and interface scientists can share their unique perspectives to the R&D opportunities in biomaterials. This mixing of disciplines is important because many biological phenomena occur at the solid-liquid interface. Two sessions are devoted to the interactions of proteins and cells with solid-state interfaces. The perspectives of the speakers in these two sessions range from fundamental interactions to developed applications. A third session addresses the issues involved in sensors' interactions with biological systems, from design to applications. The fourth session, which is new to the Conference this year, described progress in the field of artificial cellular assemblies. The dominant theme in this session is the creation of artificial neuronal networks and their characterization. Most of the top groups in the world involved in this exciting frontier research are represented.

The conference also includes three joint sessions with the NANO 3 Conference. Two sessions deal with Biology at the Nanoscale, a collection of work that features applications of recent breakthroughs in Scanning Tunneling Microscopy/Spectroscopy, Force Microscopy, Near Field Optical Microscopy, and related technology. The investigation of DNA binding interactions is highlighted in one of these sessions. The final joint session lists developments in proximal probes, including medical and neuroual devices. The NANO 3 Conference also features related work in surface modification, nanomechanics, and nanotribology. In all, the combination of sessions give a good overview of the exciting area of biological-solid state interactions, with direct impact on human health issues and biotechnology.

Code	Session
BI-MoA	Cell-Solid Surface Interactions <i>J. Davies, Univ. Toronot; D. Okrongly, Appl. Immune Sci.</i>
BI-TuM	Protein-Solid Surface Interactions <i>P. Stayton, Univ. Washington; R. Marchant, Univ. Washington</i>
BI-TuA	The Biosensor-Biology Interface <i>M. Meyerhoff, Univ. Michigan; F. Ligler, Naval Res. Lab; D. Charych, Lawrence Berkeley Lab.</i>
BINS-WeM	Artificial Cellular Assemblies <i>T. Matsuda, Nat. Cardiovas. Res. Ctr. Japan</i>

## Focus Areas

"Focus Areas" are a new concept we are introducing at this meeting in order to highlight new technical areas that will likely be important topics at future symposia, and to highlight areas of common interest among a number of different divisions. We have scheduled sessions within each focus area to minimize conflicts, so that the attendee can obtain diverse perspectives from a number of AVS Divisions. The Focus Areas and sessions included in them are listed below. These sessions are also highlighted on the "Program at a Glance" in the rear of the program book.

## Si-based Optoelectronics

Sponsored primarily by the Electronic Materials and Processing Division, talks include materials, structures and devices for optoelectronics, based on silicon technology, including waveguides, light emitters, interconnects, and system applications.

Code	Session
EM-TuA	Silicon-based Optoelectronics
EM-WeM	Heterostructures for Optoelectronics
EM-WeA	Wide-bandgap Nitrides
NS2-WeA	Optical Properties of Silicon Nanostructures

## Sensors, *in-situ* Diagnostics and Process Control

This broadly defined area includes sessions on sensor materials and devices, use of sensors and other diagnostics in the process environment, and control of processes using *in-situ* diagnostic information.

Code	Session
SS1-MoA	Surface Mechanisms and Materials for Chemical Sensors
TF-TuM	Thin Films for Sensors
BI-TuA	The Biosensor-Biology Interface
PS-WeM	Plasma Diagnostics
MS-WeA	Diagnostics, Sensors, and Control

EM-ThM	Optical Diagnostics for Materials Processing
AS-ThM	Self-Assembled Monolayers
NSBI-ThA	Micro-Instrumentation and Sensors
TF-FrM	In Situ Thin Film Characterization

### **Nanostructure Fabrication and Atomic-scale Manipulation of Surfaces**

This area includes sessions on nanostructure fabrication processes and devices.

<b>Code</b>	<b>Session</b>
NS2-WeM	Atomic Manipulation
TF-WeA	Deposition and Characterization Techniques of Nanostructures in Thin Films
NS2-ThM	Proximal Probe Based Fabrication
SS1-ThM	Nanoscale Measurements
EM-ThA	Materials for Nanostructures
NS1-FrM	Novel Materials and Methods for Nano-fabrication

### **Surface Contamination and Control**

Here we focus on cleaning, passivation, particulate control, diagnostics, and contamination-free manufacturing.

<b>Code</b>	<b>Session</b>
EMMS-TuM	Surface Preparation and Passivation
VT-TuA	Vacuum System Outgassing and Cleaning
PS-WeA	Plasma-Induced Charging and Contamination Effects
MS-ThM	Micro-Contamination and Defects



# PLENARY LECTURE



*Dr. John A. Armstrong*

## **"The Role of Research in the Technological Balance of Power"**

No region of the modern developed world is able, or should seek, to dominate the world high-technology economy. What is desirable is that there be a stable technological balance of power among major economic regions. What contribution can research make to the achievement of such a balance? What can be done about the increasing difficulty of ensuring that the society which funds basic research will reap its share of the returns on new knowledge it has paid for?

John Armstrong, IBM Vice President, Science and Technology (retired) was born in Schenectady, NY, in 1934. He received an A.B. in Physics from Harvard College in 1956, and a Ph.D. from Harvard in 1961. He remained there as a Research Fellow working with Prof. N. Bloembergen in nonlinear optics until 1963, when he joined IBM as a Research Staff Member.

Between 1976 and 1980, as Director of Physical Sciences, he was responsible for a major part of the physics, chemistry, and materials science at IBM Research. In 1981 he moved to the IBM East Fishkill development lab as Manager of Materials and Technology Development, working on advanced bipolar semiconductor and packaging technology. In 1986 he was named IBM Director of Research, and in 1987 was elected an IBM Vice President. In 1989, he was elected a member of the Corporate

Management Board and named Vice President, Science and Technology. He retired from IBM in 1993.

Armstrong is the author or co-author of more than 50 papers on nuclear resonance, nonlinear optics, the photon statistics of lasers picosecond pulse measurements, the multiphoton spectroscopy of atoms, the management of research in industry, and issues of science and technology policy. He is a Fellow of numerous professional societies, was a member of the National Advisory Committee for Semiconductors, was a member of the National Science Board Special Commission on the Future of the NSF, and is a member of the NRC Board on Science, Technology and Economic Policy. He is Chair of the NRC study on The Future of Space Science.

He is a member of the National Academy of Engineering and of the Royal Swedish Academy of Engineering Sciences, and is a member of the Harvard University Board of Overseers. He received the 1989 George E. Pake Prize of the American Physical Society. In 1992, he was Regents' Lecturer of UCSB, and he was 1993-1994 Karl T. Compton Visiting Lecturer at MIT. He is currently Visiting Professor of Electrical Engineering and Computer Science at the University of Virginia.

# Association of Vacuum Equipment Manufacturers

Annual Seminar

held during the AVS 41st National Symposium  
at the

Radisson Hotel Denver

Tuesday, October 25, 1994 8:00 a.m. - 11:00 a.m.

**"Forecasting the Future Needs and Challenges for the Vacuum Industry"**

7:30 a.m. **Registration** (*refreshments served*)

8:00 a.m. **Welcome Address**

Joel McFadden, *President, Stokes Vacuum, Inc. and President, AVEM*

8:05 a.m. **Opening Remarks: Proactive Collaboration between AVS and the Vacuum Equipment Manufacturers**

John Noonan, *Argonne National Laboratory and President, AVS*

8:20 a.m. **A Forecast of the U.S. Economy with an Inside Look at the Vacuum Technology/Semiconductor Industry**

Kermit Baker, *Director of the Economics Dept. Cahners Publishing Company*  
**Sponsored by R&D Magazine**

Cahners Publishing Company publishes more than 80 magazines and directories covering virtually every sector of the U.S. economy, including R&D Magazine. Cahners Economics is the research and forecasting arm of Cahners Publishing and uses a wide range of microeconomic indicators for forecasting business trends. Dr. Baker will describe his forecast for the U.S. economy in general and will then focus on prospects for the field of vacuum technology and the semiconductor industry.

8:55 a.m. **The Changing Face of NIST**

David W. Norcross, *Acting Director, NIST*

The National Institute of Standards and Technology (NIST) began life in 1901 as the National Bureau of Standards. For 87 years, it was a respected measurement laboratory for the U.S. Government. In 1988 its name was changed and it was given an expanded mission - to work more directly with American industry. The Clinton Administration has made NIST the lead agency in helping industry modernize and solve tricky technical problems. In addition to its traditional laboratory programs, NIST now manages the Advanced Technology Program, the Manufacturing Extension Partnership, and the Malcolm Baldrige National Quality Award. NIST's budget is scheduled to grow from a modest \$250 million just a few years ago, to \$1.4 billion by 1997 - most of that new money will go for direct support to American industry.

9:30 a.m. - 9:50 a.m. Coffee break

9:50 a.m. **USDC - A Key Ingredient to FPD Success**

M. Robert Pinnel, *Chief Technical Officer, U.S. Display Consortium*

The U.S. flat panel display (FPD) Industry is entering a critical period which may represent the final opportunity for U.S. industry to be a significant player in this market. Among the factors which will determine success or failure for U.S. manufacturing capability in FPDs, will be the availability and supply of state-of-the-art equipment, materials, and process technology. The recognition of this issue led to the formation of the United States Display Consortium (USDC) and to the definition of its mission. Among the topics to be explored are the USDC's span of activities, its organizational structure, the approaches and key procedures established to fulfill its mission, the work projects undertaken, and an analysis of impact and benefits. A case will be made for the consortium approach as an effective solution to some of the significant barriers facing the U.S. FPD Industry.

10:25 a.m. **A Review of Capital Equipment Requirements from Component Products and Suppliers**

Alex Glew, *Core Technologist, Applied Materials*

In order for capital equipment suppliers to develop and introduce new equipment to the semiconductor industry, they must work closely with component suppliers. It is important to set expectations for component suppliers that will allow successful integration during equipment manufacture, a long robust component life during service, and overall product value. In order to achieve these goals in the ever shrinking development time cycles, the component supplier must develop products, plan capacity, distribution and service prior to or concurrently with the equipment developer. The component performance and reliability must be characterized by the component supplier in order for the equipment supplier to perform system level characterizations and cost of ownership models.

11:00 a.m. **Adjourn Seminar**

*AVS Equipment Show Opens*

11:30 a.m. **Luncheon and AVEM Annual Business Meeting**

(Non-members of AVEM are welcome. For the convenience of attendees, there are separate registration fees for the AVEM Seminar and the luncheon).

For registration information, contact the Association of Vacuum Equipment Manufacturers  
Telephone 505/856-6924; FAX 505/856-6716



# SPECIAL AND EVENING SESSIONS

## SUNDAY, OCTOBER 23, 1994

8:30 a.m.	Tutorial: Nanostructures Fabrication and Characterization .....	Terrace Room (H)
	<b>ASTM E-42 Subcommittee and Task Group Meetings</b>	
3:00 p.m.-4:00 p.m.	E42.03 AES Task Groups .....	Ballroom Section A (H)
3:15 p.m.-4:00 p.m.	E42.11 Standard Reference Data .....	Capitol Room (H)
4:00 p.m.-4:30 p.m.	E42.09 Standard Reference Materials .....	Capitol Room (H)
4:00 p.m.-5:00 p.m.	E42.03 AES .....	Ballroom Section A (H)
4:30 p.m.-5:30 p.m.	E42.08 Ion Beam Sputtering .....	Capitol Room (H)
5:00 p.m. - 5:30 p.m.	E42.02 Terminology .....	Capitol Room (H)
5:00 p.m.-6:00 p.m.	E42.06 SIMS .....	Ballroom Section A (H)
5:30 p.m.-6:00 p.m.	E42.01 Editorial .....	Capitol Room (H)
7:30 p.m.-8:30 p.m.	E42.04 XPS .....	Capitol Room (H)
7:00 p.m.-8:30 pm.	E42.14 STM/AFM .....	Ballroom Section A (H)
8:30 p.m.-9:15 p.m.	E42.00 Main Committee .....	Capitol Room (H)
9:15 p.m.-10:00 p.m.	E42 Executive Committee .....	Capitol Room (H)
1:00 p.m.	<b>Town Hall Meeting</b> .....	<b>Grand Ballroom (H)</b>
1:00 p.m.	<b>Tutorial: A Guideline for TQM: A Stepping Stone to ISO 9000</b> .....	<b>Columbine Room(H)</b>
1:00 p.m.	<b>Tutorial: Surface, Biology, and Biomaterials</b> .....	<b>Jr. Ballroom (H)</b>

## MONDAY, OCTOBER 24, 1994

9:00 a.m.	Science Educators Workshop .....	Denver Room (H)
12:00 Noon	Science Educators Lunch .....	Spruce Room (H)
12:45 p.m.	<b>Plenary Lecture "The Role of Research in the Technological</b> .....	<b>Ballroom 1 (CC)</b>
	<b>Balance of Power"</b>	
	<b>Dr. John Armstrong, Vice President, IBM (retired)</b>	
2:00 p.m.	Topical Conference on Biomaterials Interfaces .....	Room A106 (CC)
2:00 pm.	Topical Conference on Manufacturing Science and Technology .....	Room A110 (CC)
8:30 a.m.-5:00 p.m.	<b>Short Course Program</b> .....	<b>Various Rooms (CC)</b>

## TUESDAY, OCTOBER 25, 1994

8:20 a.m.	Topical Conference on Biomaterials Interfaces .....	Room A106 (CC)
8:20 a.m.	Topical Conference on Manufacturing Science and Technology .....	Room A110 (CC)
9:00 a.m.	Science Educators Workshop .....	Denver Room (H)
11:00 a.m.-6:00 p.m.	<b>Vacuum Equipment Exhibition</b> .....	<b>Exhibit Hall A</b>
12:00 Noon	Science Educators Luncheon .....	Spruce Room (H)
2:00 p.m.	Topical Conference on Biomaterials Interfaces .....	Room A106 (CC)
2:00 p.m.	Topical Conference on Manufacturing Science and Technology .....	Room A110 (CC)
6:30 p.m.	Placement Center Workshop .....	Columbine Room (H)
8:00 p.m.	ASTM E.42/ASSD Workshop .....	Jr. Ballrom (H)
8:30 a.m.- 5:00 p.m.	<b>Short Course Program</b> .....	<b>Various Rooms (CC)</b>

## WEDNESDAY, OCTOBER 26, 1994

8:20 a.m.	Topical Conference on Biomaterials Interfaces .....	Room A106 (CC)
8:20 a.m.	Topical Conference on Manufacturing Science and Technology .....	Room A110 (CC)
10:00 a.m.-5:00 p.m.	<b>Vacuum Equipment Exhibition</b> .....	<b>Exhibit Hall A</b>
3:00 p.m.-5:00 p.m.	New Vacuum Products Poster Session .....	Ballroom 4 (CC)
6:45 p.m.	<b>AVS Awards Assembly and Reception</b> .....	<b>Ballroom 1,2,3 (CC)</b>
8:30 a.m.-5:00 p.m.	<b>Short Course Program</b> .....	<b>Various Rooms (CC)</b>

## THURSDAY, OCTOBER 27, 1994

10:00 a.m.-3:00 p.m.	<b>Vacuum Equipment Exhibition</b> .....	<b>Exhibit Hall A</b>
8:00 p.m.	Surface Science "Post Deadline Discovery Session" .....	Grand Ballroom (H)
8:30 a.m. - 5:00 p.m.	<b>Short Course Program</b> .....	<b>Various Rooms (CC)</b>

## FRIDAY, OCTOBER 28, 1994

8:30 a.m.-5:00 p.m.	<b>Short Course Program</b> .....	<b>Various Rooms (CC)</b>
---------------------	-----------------------------------	---------------------------

H=Radisson Hotel  
CC=Colorado Convention Center

# BUSINESS AND COMMITTEE MEETINGS

## SATURDAY, OCTOBER 22, 1994

4:00 p.m. Education Committee Meeting and Dinner ..... Gold Room (H)

## SUNDAY, OCTOBER 23, 1994

8:00 a.m. Short Course Executive Committee Meeting..... Birch Room (H)  
 8:30 a.m. Tutorial: Nanostructures Fabrication and Characterization ..... Gold Room (H)  
 11:00 a.m. History Committee Meeting..... Colorado Room(H)  
 12:00 Noon History Committee Luncheon..... Aspen Room (H)  
 12:00 Noon Companions Program..... Silver Room (H)  
 1:00 p.m. Tutorial: A Guideline For TQM: A Stepping Stone to ISO 9000..... Spruce Room (H)  
 1:00 p.m. Tutorial: Surface, Biology, and Biomaterials ..... Century Ballroom (H)  
 1:00 p.m. Town Hall Meeting..... Grand Ballroom (H)

## MONDAY, OCTOBER 24, 1994

7:00 a.m. Companions Program (see insert)..... Silver Room (H)  
 8:00 a.m. Chapters & Divisions Newsletter Breakfast ..... Columbine Room (H)  
 8:30 a.m. Fundamentals of Surface Science Short Course ..... Capitol Room (H)  
 9:00 a.m. Science Educators Workshop..... Denver Room (H)  
 9:00 a.m. PPA Sampling..... Gold Room (H)  
 9:00 a.m. Cryo Pumps..... Aspen Room (H)  
 12:00 Noon Science Educators Workshop Luncheon..... Spruce Room (H)  
 12:00 Noon JVST Luncheon..... Century Room (H)  
 1:00 p.m. ICMC Abstract Selection Meeting..... Colorado Room (H)  
 1:00 p.m. Vacuum Symbols ..... Birch Room (H)  
 1:00 p.m. Leak Detection ..... Cedar Room (H)  
 5:00 p.m. 1995 Program Committee Meeting..... Columbine Room (H)  
 6:00 p.m. Chapters & Divisions Reception..... S. Convention Lobby (H)  
 6:30 p.m. Publications Committee Dinner ..... Century Room (H)  
 6:30 p.m. Applied Surface Science Executive Committee Meeting & Dinner..... Cedar Room (H)  
 6:30 p.m. Manufacturing Science and Technology Group Meeting and Dinner ..... Spruce Room (H)  
 6:30 p.m. Vacuum Technology Executive Committee Meeting & Dinner..... Gold Room (H)  
 6:30 p.m. Student Reception ..... A Upper Lobby (CC)  
 7:00 p.m. Chapters and Divisions Dinner ..... Jr. Ballroom (H)  
 7:00 p.m. NANO 3 Reception..... Majestic Ballroom (H)

## TUESDAY, OCTOBER 25, 1994

7:00 a.m. Companion's Program (see insert) ..... Silver Room (H)  
 8:00 a.m. AVEM Seminar..... Ballroom Section D (H)  
 9:00 a.m. Science Educators Workshop ..... Denver Room (H)  
 9:00 a.m. Ion Gauges ..... Birch Room (H)  
 12:00 Noon Science Educators Luncheon ..... Spruce Room (H)  
 12:00 Noon Topical Conferences Luncheon ..... Colorado Room (H)  
 12:00 Noon Recommended Practices Executive Committee Luncheon ..... Aspen Room (H)  
 12:00 Noon AVEM Luncheon..... Gr. Ballroom Section A (H)  
 5:20 p.m. Applied Surface Science Division Business Meeting..... Room A101 (CC)  
 5:20 p.m. Electronic Materials & Processing Division Business Meeting ..... Room A108 (CC)  
 5:20 p.m. Nanometer-Scale Science & Technology Division Business Meeting ..... Room A207 (CC)  
 5:20 p.m. Surface Science Division Business Meeting..... Room A205 (CC)  
 5:20 p.m. Thin Film Division Business Meeting ..... Room A105 (CC)  
 5:20 p.m. Vacuum Technology Division Business Meeting..... Room A102 (CC)  
 6:30 p.m. Vacuum Metallurgy Division Executive Committee Meeting ..... Birch Room (H)  
 6:30 p.m. EMPD Executive Committee Meeting & Dinner ..... Century Room (H)  
 6:30 p.m. Recommended Practices Committee Meeting & Dinner..... Gr. Ballroom Section B (H)  
 6:30 p.m. Surface Science Division Executive Committee Meeting & Dinner..... Gold Room (H)  
 6:30 p.m. Thin Film Division Executive Committee Meeting & Dinner ..... Aspen Room (H)  
 6:30 p.m. Nanometer Science and Technology Division Meeting & Dinner ..... Cedar Room (H)  
 6:30 p.m. Plasma Science & Technology Division Executive Committee Meeting & Dinner ..... Colorado Room (H)  
 6:30 p.m. Placement Center Workshop..... Columbine Room (H)  
 8:00 p.m. ASTM E42./ASSD Workshop ..... Jr. Ballroom (H)

**WEDNESDAY, OCTOBER 26, 1994**

7:00 a.m.	Companions Program (see insert).....	Silver Room (H)
8:00 a.m.	Newsletter/Publicity Breakfast .....	Colorado Room (H)
9:00 a.m.	Low Pressure Gauges Subcommittee.....	Spruce Room (H)
10:00 a.m.	Scholarship Meeting .....	Birch Room (H)
12:00 Noon	Scholarship Luncheon.....	Aspen Room (H)
5:20 p.m.	Plasma Science and Technology Division Business Meeting .....	Room A109 (CC)
5:20 p.m.	Vacuum Metallurgy Division Business Meeting .....	Room A106 (CC)

**THURSDAY, OCTOBER 27, 1994**

7:00 a.m.	Companions Program (see insert).....	Silver Room (H)
8:30 a.m.	Exhibitors Breakfast.....	Room C201 (CC)
12:00 Noon	1995 Program Committee Chairs.....	Aspen Room (H)
12:15 p.m.	AVS Business Meeting .....	Room A101 (CC)
6:00 p.m.	Surface Science Spectra Editorial Board Meeting & Dinner.....	Gold Room (H)
6:00 p.m.	1994-95 LAC/Program Committee Reception .....	Jr. Ballroom D (H)
7:00 p.m.	1994-95 LAC/Program Committee Dinner.....	Jr. Ballroom E (H)
8:00 p.m.	Surface Science Postdeadline Discovery Session .....	Grand Ballroom (H)

**FRIDAY, OCTOBER 28, 1994**

7:00 a.m.	Companions Program (see insert).....	Silver Room (H)
8:00 a.m.	Surface Science Database Committee Meeting .....	Denver Room (H)
12:00 Noon	Foreign Interactions .....	Gold Room (H)

H=Radisson Hotel  
CC=Colorado Convention Center

## TECHNICAL SESSIONS

### KEY TO SESSION/PAPER NUMBERS:

**AS**—Applied Surface Science Division

**EM**—Electronic Materials and Processing Division

**NS**—Nanometer Science and Technology Division and NANO 3

**PS**—Plasma Science and Technology Division

**SS**—Surface Science Division

**MS**—Topical Conference on Manufacturing Science and Technology

**BI**—Topical Conference on Biomaterials Interfaces

**TF**—Thin Film Division

**VM**—Vacuum Metallurgy Division

**VT**—Vacuum Technology Division

Sessions sponsored by two divisions are labeled with both acronyms (e.g. **SSEM**)

then: a number to indicate parallel sessions sponsored by the same Division (e.g. **SS1**, **SS2**)

then: **Monday**, **Tuesday**, **Wednesday**, **Thursday**, **Friday**

then: **Morning**, **Afternoon**, **Evening**, **Poster** then: a number to indicate the time slot scheduled for each paper

Example: **SS1-MOM9** (Surface Science, Monday morning, 11:00 a.m.)

# Monday Morning, October 24, 1994

## SURFACE SCIENCE

Room A205 - Session SS1-MoM pg. 114

### Reactions on Metals: Hydrocarbons

Moderator: D. Dwyer, University of Maine.

## SURFACE SCIENCE

Room A201 - Session SS2-MoM pg. 115

### Alloy and Compound Surface Structure

Moderator: B.E. Koel, University of Southern California.

8:20 am	<b>SS1-MoM1</b> Effects of Co-adsorbed Hydrogen on the Dehydrogenation of Cyclohexane on Pt(111). Identification of Cyclohexyl ( $C_6H_{11}$ ) Species. M.E. PANSOY-HJELVIK, P. SCHNABEL, J.C. HEMMINGER, University of California, Irvine.	<b>SS2-MoM1 INVITED</b> Surface Structure Investigation with Scanning Tunneling Microscopy (STM) and Low Energy Ion Backscattering. H. NIEHUS, Humboldt-Universität zu Berlin, Germany.
8:40 am	<b>SS1-MoM2</b> Oxygen Activated Combustion of Alkenes on Pd(100). X.-C. GUO, R.J. MADIX, Stanford University.	Invited talk continued.
9:00 am	<b>SS1-MoM3 INVITED</b> Surface Chemistry at Metallic Step Defect Sites. J.T. YATES, JR.,* University of Pittsburgh.	<b>SS2-MoM3</b> Anharmonicity on the NiAl(110) Bimetallic Alloy Surface. A.P. BADDORF, Oak Ridge National Laboratory. A.T. HANBICKI, University of Pennsylvania.
9:20 am	invited talk continued.	<b>SS2-MoM4</b> The Geometrical Structure of an Al(111)-(2x2)-Na Surface Alloy. M.M. NIELSEN, J. BURCHARDT, D.L. ADAMS, Aarhus University, Denmark. E. LUNDGREN, J.N. ANDERSEN, Lund University, Sweden. C. STAMPFL, M. SCHEFFLER, A. SCHMALZ, J. HAASE, Fritz Haber Institute, Germany.
9:40 am	<b>SS1-MoM5</b> Kinetics of Benzene Formation from Acetylene on Pd(111). I.M. ABDELREHIM, N.A. THORNBURG, C.M. GERTH, E. DELGADO, T.E. CALDWELL, J.T. SLOAN, D.P. LAND, University of California, Davis.	<b>SS2-MoM5</b> Structure of NiO(111) Films on a Ni(100) Substrate. O.L. WARREN, P.A. THIEL, Iowa State University.
10:00 am	<b>SS1-MoM6</b> Acetylene Di- and Trimerization Reactions at Pt(111) and the ( $\sqrt{3}\times\sqrt{3}$ )R30°-Sn/Pt(111). J. SZANYI, M.T. PAFFETT, Los Alamos National Laboratory.	<b>SS2-MoM6</b> Detailed Surface Structures of Ultrathin Films of Ice ( $H_2O$ ) and Rust ( $Fe_3O_4$ ) Grown on Pt(111), Determined by Automated Tensor LEED. M.A. VAN HOVE, A.B. BARBIERI, N. MATERER, U. STARKE, W. WEISS, M. RITTER, G.A. SOMORJAI, Lawrence Berkeley Laboratory.
10:20 am	<b>SS1-MoM7</b> The Surface Chemistry of 1,1-dimethylhydrazine on Pt and Ag-Modified Pt. A.L. SCHWANER, M. KOVAR, D.J. ALBERAS, J.M. WHITE, University of Texas, Austin.	<b>SS2-MoM7</b> Structural Studies of Quasicrystals. W.-B. CHIN, C.J. JENKS, S.-L. CHANG, C.-M. ZHANG, P.A. THIEL, Iowa State University.
10:40 am	<b>SS1-MoM8</b> Adsorption and Aggregation of HCN on Pt(111). D. JENTZ, H. CELIO, M. TRENARY, University of Illinois, Chicago.	<b>SS2-MoM8</b> A New Type of UHV - AFM: Studies on $KMnF_3$ Surfaces. Q. DAI, R. VOLLMER, R. CARPICK, D.F. OGLETREE, M. SALMERON, Lawrence Berkeley Laboratory.
11:00 am	<b>SS1-MoM9</b> The Chemistry of Phthalic Anhydride at a Clean and Oxygen Covered Copper Single Crystal Surface. S. HAO, R.C. BAINBRIDGE, N.V. RICHARDSON, University of Liverpool, United Kingdom.	<b>SS2-MoM9</b> Structure Determination of the InP(001) Surface. M.M. SUNG, H. BU, J.W. RABALAIS, University of Houston.
11:20 am	<b>SS1-MoM10</b> Cu(100) as a Model for the Methanol Catalyst. I. CHORKENDORFF, J. WAMBACH, M. KAZUTA, P.B. RASMUSSEN, Technical University of Denmark.	<b>SS2-MoM10</b> Surface Relaxation of PbTe(100). C.B. DUKE, A. LAZARIDES, A. PATON, Xerox Webster Research Center. A. KAHN, Princeton University.
11:40 am	<b>SS1-MoM11</b> Simulation and Sensitivity Analysis of the Heterogeneous Oxidation of Methane on a Platinum Foil. F. BEHRENDT, O. DEUTSCHMANN, J. WARNATZ, Universität Stuttgart, Germany.	<b>SS2-MoM11</b> Structure of the Ga-rich GaAs(001) 4x2 and 4x6 Phases. Q.K. XUE, T. HASHIZUME, J. ZHOU, T. SAKATA, T. SAKURAI, Tohoku University, Japan.

## 12:45 pm Plenary Lecture

### "The Role of Research in the Technological Balance of Power"

Dr. John A. Armstrong

Ballroom 1

**NANO 3/NANOMETER-SCALE SCIENCE AND TECHNOLOGY**  
Room BR1 - Session NS1-MoM pg. 117

**NANO 3 Plenary Session**

**Moderator:** C.R.K. Marrian, Naval Research Laboratory.

**APPLIED SURFACE SCIENCE**

Room A101 - Session AS-MoM pg. 118

**Imaging and Small Area Analysis**

**Moderator:** R.W. Linton, University of North Carolina, Chapel Hill.

8:20 am		<b>AS-MoM1 INVITED</b> Static and Dynamic SIMS with Sub-Micron Resolution: Sensitivity and Quantification Aspects. Y. GAO, F. SALDI, H.-N. MIGEON, CRP-CU, Luxembourg.
8:40 am	Introduction and Welcome: <b>C.R.K. MARRIAN</b> , Naval Research Laboratory.	Invited talk continued.
9:00 am	<b>NS1-MoM3 INVITED</b> Nanostructural Sensors for Molecular Recognition. <b>W. GÖPEL</b> , University of Tübingen, Germany.	<b>AS-MoM3</b> Surface Trimer Crystallization on Poly (Ethylene Terephthalate) Studied by Time-of-Flight Secondary Ion Mass Spectrometry (TOF-SIMS). <b>S. REICHLMAIER</b> , S.R. BRYAN, Perkin-Elmer Physical Electronics Division. D. BRIGGS, Wilton Research Centre, England.
9:20 am	Invited talk continued.	<b>AS-MoM4</b> TOF-SIMS Imaging of Organic Materials. <b>B. HAGENHOFF</b> , <b>D. RADING</b> , M. DEIMEL, A. BENNINGHOVEN, Universität Münster, Germany.
9:40 am	Invited talk continued.	<b>AS-MoM5</b> ToF SIMS Imaging of Self-Assembled Monolayers. <b>D.G. CASTNER</b> , University of Washington. P.J. MCKEOWN, Physical Electronics, Inc. D.W. GRAINGER, Colorado State University.
10:00 am	<b>NS1-MoM6 INVITED</b> Recent Progress on Magnetic Sensors with Nanostructures and Applications. <b>Y. SUGIYAMA</b> , Electrotechnical Laboratory, Japan.	<b>AS-MoM6</b> Scanning Photoelectron Microscope with Submicron Lateral Resolution Using Wolter-type X-ray Focusing Mirror. <b>K. NINOMIYA</b> , M. HASEGAWA, Hitachi, Ltd., Japan.
10:20 am	Invited talk continued.	<b>AS-MoM7</b> First Results from the Spectro-Microscopy Undulator Photoemission Beamline. <b>J. DENLINGER</b> , E. ROTENBERG, A. WARWICK, Advanced Light Source. S. KEVAN, University of Oregon. B.P. TONNER, University of Wisconsin, Milwaukee.
10:40 am	Invited talk continued.	<b>AS-MoM8</b> Identification and Quantification of Hidden Features using Imaging XPS. <b>J.E. FULGHUM</b> , L. PALEUDIS, T.A. ZUPP, Kent State University. D.J. SURMAN, Kratos Analytical, Inc.
11:00 am	<b>NS1-MoM9 INVITED</b> Quantum Corrales. <b>D.M. EIGLER</b> , IBM Almaden Research Center.	<b>AS-MoM9</b> Analysis of Insulating Materials using Field Emission Auger Electron Spectroscopy. <b>N.M. FORSYTH</b> , G. JONES, J. WOLSTENHOLME, Fisons Instruments Surface Systems.
11:20 am	Invited talk continued.	<b>AS-MoM10</b> SAM and XPS Studies of Roman Bronzes. <b>E. PAPAARAZZO</b> , L. MORETTO, ISM-CNR, Italy. P. NORTHOVER, University of Oxford, United Kingdom. C. D'AMATO, Museo della Civiltà Romana, Italy. E. SEVERINI, CSM SpA, Italy. A. PALMIERI, ITABC-CNR, Italy.
11:40 am	Invited talk continued.	<b>AS-MoM11</b> Strain Imaging Analysis using Raman Microscope. <b>J.P.H. SUKAMTO</b> , K. AJITO, K. HASHIMOTO, A. FUJISHIMA, University of Tokyo, Japan.



# Monday Morning, October 24, 1994

## PLASMA SCIENCE

Room A109 - Session PS-MoM pg. 120

### Plasma Etching & Deposition

Moderator: K.L. Seaward, Hewlett Packard Laboratories.

## VACUUM TECHNOLOGY

Room A102 - Session VT-MoM pg. 122

### Total Pressure Gauging

Moderator: N. T. Peacock, HPS Division of MKS Instruments Inc.

8:20 am	<b>PS-MoM1 INVITED</b> Recent Developments in Plasma Processing. <b>R.A. GOTTSCHO</b> , AT&T Bell Laboratories.	<b>VT-MoM1</b> Electron Path Length Calculation Using Finite Element Method for an Axial Emission Gauge. <b>A. AGARWAL</b> , <b>J. BASS</b> , <b>A.H. BASS</b> , National Research Council, Canada.
8:40 am	Invited talk continued.	<b>VT-MoM2</b> Observations of Electron Trapping Phenomenon Occurring in a Lafferty Gauge. <b>N. GOTOH</b> , The Graduate University for Advanced Studies, Japan. <b>R. PAITICH</b> , Terranova Scientific. <b>H. HISAMATSU</b> , <b>H. ISHIMARU*</b> , KEK National Laboratory for High Energy Physics, Japan.
9:00 am	<b>PS-MoM3</b> Self-Aligned-Contact (SAC) Dry Etch Process for 0.5 $\mu$ SRAM Technology. <b>J.E. NULTY</b> , <b>P.S. TRAMMEL</b> , Cypress Semiconductor.	<b>VT-MoM3</b> The Influence of Filament-Heating Waveform on the Sensitivity of Glass Envelope Bayard-Alpert Gages. <b>P.J. ABBOTT</b> , <b>J.P. LOONEY</b> , National Institute of Standards & Technology.
9:20 am	<b>PS-MoM4</b> The Correlation between Selective Oxide Etching and Thermodynamic Prediction. <b>S.C. MCNEVIN</b> , AT&T Bell Laboratories.	<b>VT-MoM4</b> Long-term Stability of Bayard-Alpert Gauge Performance: Results Obtained from Repeated Calibrations against the NIST Primary Vacuum Standard. <b>A.R. FILIPPELLI</b> , <b>P.J. ABBOTT</b> , <b>J.P. LOONEY</b> , <b>S. DITTMANN</b> , <b>C.R. TILFORD</b> , National Institute of Standards & Technology.
9:40 am	<b>PS-MoM5 INVITED</b> High Rate and Highly Selective SiO <sub>2</sub> Etching Employing Inductively Coupled Plasma. <b>Y. HORIIKE</b> , Tokyo University, Japan. <b>K. KUBOTA</b> , Hiroshima University, Japan. <b>T. FUKAZAWA</b> , TEL-Yamanashi, Japan.	<b>VT-MoM5 INVITED</b> Ultrasensitive Silicon Micromechanical Pressure Sensors. <b>S.T. CHO</b> , The Charles Stark Draper Laboratory.
10:00 am	Invited talk continued.	Invited talk continued.
10:20 am	<b>PS-MoM7</b> Tungsten Etching Using Electron Cyclotron Resonance Plasma. <b>T. MARUYAMA</b> , <b>K. SHIOZAWA</b> , <b>N. FUJIWARA</b> , <b>M. YONEDA</b> , Mitsubishi Electric Corporation, Japan.	<b>VT-MoM7</b> Vacuum Gauging with IC Technology Compatible Microsensors. <b>O. PAUL</b> , <b>O. BRAND</b> , <b>R. LENGGENHAGER</b> , <b>H. BALTES</b> , Physical Electronics Laboratory, ETH, Switzerland.
10:40 am	<b>PS-MoM8</b> Cu Metallization using Electron Cyclotron Resonance Plasmas. <b>S.M. GORBATKIN</b> , <b>R.L. RHOADES</b> , <b>L.A. BERRY</b> , Oak Ridge National Laboratory. <b>S.M. ROSSNAGEL</b> , IBM TJ Watson Research Center.	<b>VT-MoM8</b> A Miniaturized Silicon Based Thermal Vacuum Sensor. <b>W.J. ALVESTEFFER</b> , Hastings Instruments.
11:00 am	<b>PS-MoM9</b> Application of an Electron Cyclotron Resonance Plasma Source to Conductive Film Deposition. <b>M. SHIMADA</b> , <b>T. ONO</b> , <b>H. NISHIMURA</b> , <b>S. MATSUO</b> , NTT LSI Laboratories, Japan.	<b>VT-MoM9</b> Long-term Calibration Stability of Molecular Drag Gage Rotors. <b>R.W. HYLAND</b> , <b>J.P. LOONEY</b> , National Institute of Standards & Technology.
11:20 am	<b>PS-MoM10</b> Micro-Profile Simulations of Metal Ion and Neutral Deposition. <b>S. HAMAGUCHI</b> , <b>S.M. ROSSNAGEL</b> , IBM TJ Watson Research Center.	<b>VT-MoM10</b> An Optical Method for Low Pressure Measurements. <b>I. BELLO</b> , <b>S. BEDERKA</b> , University of Western Ontario, Canada. <b>L. HAWORTH</b> , University of Edinburgh, Scotland.
11:40 am	<b>PS-MoM11</b> High Density Metal Plasma Formation during DC Magnetron Sputtering in Self-Sustained Mode. <b>W.M. POSADOWSKI</b> , Technical University of Wroclaw, Poland. <b>Z.J. RADZIMSKI</b> , North Carolina State University.	<b>VT-MoM11</b> Validity of the Total Pressure of 5x10 <sup>-11</sup> Pa Estimated by Laser Ionization Method. <b>S. ICHIMURA</b> , <b>S. SEKINE</b> , <b>K. KOKUBUN</b> , Electrotechnical Laboratory, Japan.

**ELECTRONIC MATERIALS****Room A108 - Session EM-MoM pg. 123****Materials for Device Integration****Moderator:** L.L. Tedder, North Carolina State University.

8:20 am	<b>EM-MoM1 INVITED</b> Performance and Integration of Copper VLSI/ULSI Interconnects. D.C. EDELSTEIN, IBM TJ Watson Research Center.	
8:40 am	Invited talk continued.	
9:00 am	<b>EM-MoM3</b> Optimization of a Contact Metallization Scheme for 0.35 ASIC Technology. S. BOTHRA, T. TROWBRIDGE, VLSI Technology Inc.	
9:20 am	<b>EM-MoM4</b> The Effect of Oxygen Contamination on the Formation of $TiSi_2$ for Metallization Structures. M. LIN, J.F. BERNARD, A.R. RAHEEM, A. MCCOMAS, E.H. ADEM, T. LUKANC, S. FONG, D. MATSUMOTO, Advanced Micro Devices.	
9:40 am	<b>EM-MoM5</b> Al/Epitaxial-W Bilayer Model Diffusion Barrier Structures: Interfacial Reaction Pathways and Kinetics during Annealing. D.B. BERGSTROM, I. PETROV, L.H. ALLEN, J.E. GREENE, University of Illinois, Urbana.	
10:00 am	<b>EM-MoM6</b> Chemical Vapor Deposited TiCN - A New Barrier Metallization for Sub-micron Via and Contact Applications. M. EIZENBERG, K. LITTAU, S. GHANAHEIM, A. MAK, Y. MAEDA, M. CHANG, A.K. SINHA, Applied Materials.	
10:20 am	<b>EM-MoM7</b> Experiments and Simulations of High Pressure Chemical Vapor Deposition of TiN from Tetrakis-dimethylaminotitanium and Ammonia in Vias. H. LIAO, Arizona State University. R. GORDON, Harvard University. A. TOPRAC, SEMATECH. T.S. CALE, Arizona State University.	
10:40 am	<b>EM-MoM8</b> Using Poly(tetrafluoroethylene) as a Low Dielectric Constant Substrate for Microwave Circuit Fabrication. A.J. HOWARD, R.R. RYE, A.J. RICCO, D.J. RIEGER, M.L. LOVEJOY, L.R. SLOAN, M.A. MITCHELL, Sandia National Laboratories.	
11:00 am	<b>EM-MoM9 INVITED</b> Processing and Device Issues of High Permittivity Materials for DRAM Memories. B.E. GNADE, Texas Instruments.	
11:20 am	Invited talk continued.	
11:40 am	<b>EM-MoM11</b> PECVD $TiO_2$ in Microwave-RF Hybrid Plasma Reactor. Y.H. LEE, M.J. BRADY, K.K. CHAN, IBM TJ Watson Research Center.	

# MY SCHEDULE

## Monday Morning, October 24, 1994

TIME	SESSION	ROOM
8:20 am		
8:40 am		
9:00 am		
9:20 am		
9:40 am		
10:00 am		
10:20 am		
10:40 am		
11:00 am		
11:20 am		
11:40 am		
12:00 pm		
12:45 pm		
Lunch		
when		
with		where

### OTHER EVENTS MONDAY

7:00 a.m. Companions Program (see insert) (**Silver Room (H)**)  
 8:00 a.m. Chapters & Divisions Newsletter Breakfast (**Columbine Room (H)**)  
 9:00 a.m. Science Educators Workshop (**Denver Room (H)**)  
 9:00 a.m. PPA Sampling (**Gold Room (H)**)  
 9:00 a.m. Cryo Pumps (**Aspen Room (H)**)  
 12:00 Noon Science Educators Workshop Luncheon (**Spruce Room (H)**)  
 12:00 Noon JVST Luncheon (**Century Room (H)**)

H=Radisson Hotel  
 CC=Colorado Convention Hotel

### SHORT COURSES MONDAY

8:30 a.m. Fundamentals of Surface Science (**Vail Room (H)**)  
 8:30 a.m. Vacuum Technology (**Room C109 (CC)**)  
 8:30 a.m. A Comprehensive Course on Surface Analysis: AES,XPS,SIMS, Depth Profiling, & ISS/RBS (**Room C107 (CC)**)  
 8:30 a.m. Basics of Radio Frequency (RF) Technology (**Room C105 (CC)**)  
 8:30 a.m. Operation and Maintenance of Vacuum Pumping Systems (**Room C103 (CC)**)  
 8:30 a.m. Sputter Deposition (**Room C101 (CC)**)  
 8:30 a.m. Auger Electron Spectroscopy (**Room C107 (CC)**)  
 8:30 a.m. Controlling Contamination in Vacuum System (**Room C112 (CC)**)  
 8:30 a.m. CVD for Microelectronics (**Room C110 (CC)**)  
 8:30 a.m. An Introduction to Ion Sources: Principles and Techniques (**Room C108 (CC)**)  
 8:30 a.m. An Overview of Thin-Film Deposition and Etching Techniques (**Room C106 (CC)**)  
 8:30 a.m. Technological Aspects of Metal Semiconductor Contacts (**Room C104 (CC)**)  
 8:30 a.m. Understanding Thin-Film Optics (**Room C102 (CC)**)

### Special or Focus Area Sessions

NS1-MoM — Ballroom 1. NANO 3 Plenary Session

# MY SCHEDULE

## Monday Afternoon, October 24, 1994

TIME	SESSION	ROOM
2:00 pm		
2:20 pm		
2:40 pm		
3:00 pm		
3:20 pm		
3:40 pm		
4:00 pm		
4:20 pm		
4:40 pm		
5:00 pm		

### OTHER EVENTS MONDAY

- 1:00 p.m. ICMC Abstract Selection Meeting (**Colorado Room (H)**)
- 1:00 p.m. Vacuum Symbols (**Birch Room (H)**)
- 1:00 p.m. Leak Detection (**Cedar Room (H)**)
- 5:00 p.m. 1995 Program Committee Meeting (**Columbine Room (H)**)
- 6:00 p.m. Chapters & Divisions Reception (**S. Convention Lobby (H)**)
- 6:30 p.m. Publications Committee Dinner (**Century Room (H)**)
- 6:30 p.m. ASS Executive Committee Meeting & Dinner (**Cedar Room (H)**)
- 6:30 p.m. Manufacturing Science and Technology Group Meeting and Dinner (**Spruce Room (H)**)
- 6:30 p.m. Vacuum Technology Executive Committee Meeting & Dinner (**Gold Room (H)**)
- 6:30 p.m. Student Reception (**A Upper Lobby (CC)**)
- 7:00 p.m. Chapters and Divisions Dinner (**Jr. Ballroom (H)**)
- 7:00 p.m. NANO 3 Reception (**Majestic Ballroom (H)**)

H=Radisson Hotel  
CC=Colorado Convention Hotel

### SHORT COURSES MONDAY

- 8:30 a.m. Fundamentals of Surface Science **Vail Room (H)**
- 8:30 a.m. Vacuum Technology (**Room C109 (CC)**)
- 8:30 a.m. A Comprehensive Course on Surface Analysis: AES,XPS,SIMS, Depth Profiling, & ISS/RBS (**Room C107 (CC)**)
- 8:30 a.m. Basics of Radio Frequency (RF) Technology (**Room C105 (CC)**)
- 8:30 a.m. Operation and Maintenance of Vacuum Pumping Systems (**Room C103 (CC)**)
- 8:30 a.m. Sputter Deposition (**Room C101 (CC)**)
- 8:30 a.m. Auger Electron Spectroscopy (**Room C107 (CC)**)
- 8:30 a.m. Controlling Contamination in Vacuum System (**Room C112 (CC)**)
- 8:30 a.m. CVD for Microelectronics (**Room C110 (CC)**)
- 8:30 a.m. An Introduction to Ion Sources: Principles and Techniques (**Room C108 (CC)**)
- 8:30 a.m. An Overview of Thin-Film Deposition and Etching Techniques (**Room C106 (CC)**)
- 8:30 a.m. Technological Aspects of Metal Semiconductor Contacts (**Room C104 (CC)**)
- 8:30 a.m. Understanding Thin-Film Optics (**Room C102 (CC)**)

### Special or Focus Area Sessions

**Sensors, in-situ Diagnostics, Process Control**  
**SS1-MoA Surface Mechanisms and Materials for Chemical Sensors**

# Monday Afternoon, October 24, 1994

## SURFACE SCIENCE

Room A205 - Session SS1-MoA pg. 126

### Surface Mechanisms and Materials for Chemical Sensors

Moderator: R.M. Penner, University of California, Irvine.

## SURFACE SCIENCE

Room A201 - Session SS2-MoA pg. 127

### Nucleation and Growth: Semiconductors

Moderator: J.F. Wendelken, Oak Ridge National Laboratories.

2:00 pm	<b>SS1-MoA1</b> Surface Chemistry of Gold Doped $WO_3$ Hydrogen Sulfide Sensors. B. FRUHBERGER, D.J. DWYER, University of Maine.	<b>SS2-MoA1</b> Mixed-Morphology MTP Growth of Ag on Si(100)-2x1 Surface. G. JAYARAM, N. DORAISWAMY, L.D. MARKS, Northwestern University.
2:20 pm	<b>SS1-MoA2</b> Surface Chemistry of a Semiconducting Oxide Gas Sensor for Hydrogen Sulfide. G.S. HENSHAW, D.H. DAWSON, D.E. WILLIAMS, University of College London, England.	<b>SS2-MoA2</b> Modification of Overlayer Growth Kinetics by Surface Interlayers: The $Si(111)\sqrt{7}\times\sqrt{3}$ - Indium Surface. S. SURNEV, J. KRAFT, F.P. NETZER, Universität Graz, Austria.
2:40 pm	<b>SS1-MoA3</b> INVITED Surface, Interface and Thin Film Effects in Solid State Chemical Sensing. S. SEMANCIK, R.E. CAVICCHI, G.E. POIRIER, J.S. SUEHLE, M. GAITAN, National Institute of Standards & Technology.	<b>SS2-MoA3</b> K Islands on Si(111): Morphology Changes Induced by $O_2$ Exposure. B. LAMONTAGNE, F. SEMOND, D. ROY, Université Laval, Canada.
3:00 pm	Invited talk continued.	<b>SS2-MoA4</b> Kinetic Control in Epitaxial Growth: Chemisorption to Heteroepitaxy to Homoepitaxy in $CaF_2/Si(111)$ . U. HESSINGER, M. LESKOVAR, M.A. OLMSTEAD, University of Washington.
3:20 pm	<b>SS1-MoA5</b> Operation of Thin Film Gas Detectors in a Temperature Programmed Mode. R.M. MERCHANT, J.W. SCHWANK, J.L. GLAND, K.D. WISE, University of Michigan.	<b>SS2-MoA5</b> The Influence of Surface Topography on Epitaxial Growth. O.P. KARPENKO, D.P. ADAMS, S.M. YALISOVE, University of Michigan.
3:40 pm	<b>SS1-MoA6</b> Behavior and Kinetics of Palladium-Gated Hydrogen Sensors in UHV. R. BASTASZ, Sandia National Laboratories, Livermore. R.C. HUGHES, Sandia National Laboratories, Albuquerque. W.P. ELLIS, Los Alamos National Laboratory.	<b>SS2-MoA6</b> Structure of MBE-grown As-rich GaAs(001) Phases. T. HASHIZUME, Q.K. XUE, J. ZHOU, Tohoku University, Japan. A. ICHIMIYA, Nagoya University, Japan. T. SAKURAI, Tohoku University, Japan.
4:00 pm	<b>SS1-MoA7</b> Structure and Chemical Sensing Properties of Vanadium Oxide Sol-Gel Films. J.S. LEDFORD, P.A. ASKELAND, Michigan State University.	<b>SS2-MoA7</b> Simultaneous Measurement of Structure and Chemistry during Growth of GaAs by Chemical Vapor Deposition. P.H. FUOSS, AT&T Bell Laboratories. D.K. KISKER, G.B. STEPHENSON, IBM TJ Watson Research Center. I. KAMIYA, JRDC and Imperial College. S. BRENNAN, SSRL. L. MANTESE, D.E. ASPNES, North Carolina State University.
4:20 pm	<b>SS1-MoA8</b> High Resolution Photoemission and Auger Parameter Studies of Electronic Structure of Tin Oxides. L. KÖVÉR, Hungarian Academy of Sci., Inst. of Nuclear Res., Hungary. G. MORETTI, Università "La Sapienza", Italy. ZS. KOVÁCS, Hungarian Academy of Sci., Inst. of Nuclear Res., Hungary. R. SANJINÉS, Ecole Polytechnique Fédérale, Switzerland. E. CSERNY, Hungarian Academy of Sci., Inst. of Nuclear Res., Hungary. G. MARGARITONDO, Ecole Polytechnique Fédérale, Switzerland. J. PÁLINKÁS, Hungarian Academy of Sci., Inst. of Nuclear Res., Hungary. H. ADACHI, Kyoto University, Japan.	<b>SS2-MoA8</b> Heterostructures with Large Lattice Mismatch: Interaction of GaSe with GaAs(111). L.E. RUMANER, F.S. OHUCHI, University of Washington.
4:40 pm	<b>SS1-MoA9</b> Growth and Reactivity of Thin $TiO_x$ Films on W(110). G.S. HERMAN, C.H.F. PEDEN, Pacific Northwest Laboratory.	<b>SS2-MoA9</b> Morphology of GaAs(001) Grown by Solid- and Gas-Source Molecular Beam Epitaxy. J.E. VAN NOSTRAND, S.J. CHEY, D.G. CAHILL, A.E. BOTCHKAREV, H. MORKOC, University of Illinois, Urbana.
5:00 pm	<b>SS1-MoA10</b> Synthesis of Ordered Ultra-thin $Al_2O_3$ Films on Ru(0001) and Re(0001) Surfaces. Y. WU, E. GARFUNKEL, T.E. MADEY, Rutgers University.	<b>SS2-MoA10</b> Diffusion Barriers on GaAs:SN (100) Surfaces. S.M. SEUTTER, A.M. DABIRAN, X. SONG, B.E. ISHAUG, P.I. COHEN, University of Minnesota.

**NANO 3/NANOMETER-SCALE SCIENCE AND TECHNOLOGY**  
**Room A209 - Session NS1-MoA pg. 129**

**Nanostructure Properties: Structural and Electronic**  
**Moderator: J.N. Randall, Texas Instruments.**

**NANO 3/NANOMETER-SCALE SCIENCE AND TECHNOLOGY**  
**Room A207 - Session NS2-MoA pg. 131**

**Nanometrology**

**Moderator: E.C. Teague, National Institute for Standards and Technology.**

2:00 pm	<b>NS1-MoA1</b> Scanned-probe Measurements of CdSe Quantum Dot Structures. <b>B. ALPERSON, S.R. COHEN, G. HODES, I. RUBINSTEIN</b> , Weizmann Institute of Science, Israel.	<b>NS2-MoA1 INVITED</b> Dimensional Metrology with Scanning Probe Microscopes. <b>J.E. GRIFFITH</b> , AT&T Bell Laboratories.
2:20 pm	<b>NS1-MoA2</b> Low Temperature Scanning Tunneling Microscopy Studies of Granular Metal Films. <b>E. BAR-SADEH, D. PORATH, M. WOLOVELSKY, Y. GOLDSTEIN, O. MILLO</b> , The Hebrew University of Jerusalem, Israel. <b>Q. ZHANG, H. DENG, B. ABELES</b> , Exxon Research and Engineering.	Invited talk continued.
2:40 pm	<b>NS1-MoA3 INVITED</b> Properties of Nanostructures - Electronic. <b>H. AHMED</b> , University of Cambridge, UK.	<b>NS2-MoA3</b> Proximal Probe Characterization. <b>L.A. FILES, J.N. RANDALL</b> , Texas Instruments, Inc. <b>D. KELLER</b> , University of New Mexico.
3:00 pm	Invited talk continued.	<b>NS2-MoA4</b> Maximizing the Information Content of Scanning Probe Microscopy Data. <b>P.M. WILLIAMS, M.C. DAVIES, T.O. GLASBEY, D.E. JACKSON, C.J. ROBERTS, K.M. SHAKESHEFF, S.J.B. TENDLER</b> , University of Nottingham, United Kingdom.
3:20 pm	<b>NS1-MoA5</b> Voltage Oscillation Observed in Two Dimensional Nanostructures using Liquid Crystal Molecules at Room Temperature. <b>N. NEJOM, M. AONO, M. TSUKADA</b> , JRDC, RIKEN, and University of Tokyo, Japan.	<b>NS2-MoA5</b> Estimation of Proximal Probe Microscope Tip Geometry without Calibrated Reference Artifacts. <b>J.S. VILLARRUBIA</b> , National Institute of Standards & Technology.
3:40 pm	<b>NS1-MoA6</b> Charge Dissipation and Its Phase Transition of Densely Contact-Electrified Electrons on a Thin Silicon Oxide. <b>Y. SUGAWARA, Y. FUKANO, T. UCHIHASHI, T. OKUSAKO, T. TSUYUGUCHI, S. MORITA</b> , Hiroshima University, Japan. <b>Y. YAMANISHI, T. OASA</b> , Sumitomo Metal Industries, Ltd., Japan.	<b>NS2-MoA6</b> Stability and Engineering of Ultra-Sharp Tungsten Tips. <b>M.L. YU, B.W. HUSSEY, H.-S. KIM, T.H.P. CHANG</b> , IBM TJ Watson Research Center.
4:00 pm	<b>NS1-MoA7</b> Strain Relieving of Epitaxially Grown Ge Layers on Si Mesa Structure. <b>Y.-H. KHANG, Y. KUK</b> , Seoul National University, Korea.	<b>NS2-MoA7</b> Scanning Tunneling Microscope with Three-Dimensional Interferometer for Surface Roughness Measurement. <b>T. FUJII, M. YAMAGUCHI, M. SUZUKI</b> , Nikon Corporation, Japan.
4:20 pm	<b>NS1-MoA8</b> Atomic-Force Microscopy Measurements of Roughness Anisotropy on $\text{Si}_{1-x}\text{Ge}_x/\text{Si}$ Superlattice Film Surfaces. <b>C. TEICHERT, Y.H. PHANG</b> , University of Wisconsin, Madison. <b>L.J. PETICOLAS, J.C. BEAN</b> , AT&T Bell Laboratories. <b>E. KASPER</b> , Universität Stuttgart, Germany. <b>M.G. LAGALLY</b> , University of Wisconsin, Madison.	<b>NS2-MoA8</b> Automated Calibration of the Sample Image using Crystalline Lattice for Scale Reference in Scanning Probe Microscopy. <b>H. KAWAKATSU, T. HIGUCHI, H. KUGAMI, P. BLANALT</b> , University of Tokyo, Japan.
4:40 pm	<b>NS1-MoA9</b> Submicron Lithographically Patterned Magnetic Islands for Magnetic Recording. <b>R.M.H. NEW, R.F.W. PEASE, R.L. WHITE</b> , Stanford University.	<b>NS2-MoA9</b> Repeatability and Reproducibility Study of Si Wafer Micro-Roughness by Use of Atomic Force Microscopy. <b>A.R. RAHEEM, E.H. ADEM</b> , Advanced Micro Devices.
5:00 pm	<b>NS1-MoA10</b> Ferroelectric Domain Dynamics Investigated by Atomic Force Microscopy. <b>O. KOLOSOV</b> , Mechanical Engineering Lab and ATP and NAIR, Japan. <b>A. GRUVERMAN</b> , National Inst. for Research in Inorganic Materials, Japan. <b>J. HATANO</b> , Science University of Tokyo, Japan. <b>K. TAKAHASHI</b> , National Inst. for Research in Inorganic Materials, Japan. <b>H. TOKUMOTO</b> , ATP and NAIR, Japan.	<b>NS2-MoA10</b> An Optical Fiber Based Shear Force Microscope for Nanometer-Scale Dimensional Metrology on Large Samples. <b>H.M. MARCHMAN</b> , AT&T Bell Laboratories.



# Monday Afternoon, October 24, 1994

**APPLIED SURFACE SCIENCE**  
Room A101 - Session AS-MoA pg. 132

**Data Processing and Reference Methods**  
Moderator: G.C. Nelson, Sandia National Laboratories.

**PLASMA SCIENCE**  
Room A109 - Session PS-MoA pg. 134

**Plasma Deposition**  
Moderator: W. Holber, ASTeX, Inc.

2:00 pm	<b>AS-MoA1</b> Auger Electron Spectrometry Data Bank. <b>M.P. SEAH</b> , National Physical Laboratory, United Kingdom.	<b>PS-MoA1 INVITED</b> Plasma Assisted Deposition of Diamond Films. <b>T.D. MANTEI</b> , University of Cincinnati.
2:20 pm	<b>AS-MoA2</b> Multi-spectral Scanning Auger Microscopy of Rough, Chemically Inhomogeneous Samples. <b>I.R. BARKSHIRE</b> , M. PRUTTON, University of York, United Kingdom.	Invited talk continued.
2:40 pm	<b>AS-MoA3 INVITED</b> Surface Microanalysis and Imaging: Data Visualization and Pattern Recognition Applications. <b>R.W. LINTON</b> , University of North Carolina, Chapel Hill.	<b>PS-MoA3</b> An Investigation of SiO <sub>2</sub> PECVD using Attenuated Total Reflection Fourier Transform Infrared Spectroscopy. <b>S.C. DESHMUKH</b> , <b>E.S. AYDIL</b> , University of California, Santa Barbara.
3:00 pm	Invited talk continued.	<b>PS-MoA4</b> Step Coverage of Silicon Dioxide Films Deposited in Dual Frequency TEOS-Oxygen Plasma Systems. <b>F.R. MYERS</b> , M.W. PETERS, Motorola, Inc. <b>T.S. CALE</b> , Arizona State University.
3:20 pm	<b>AS-MoA5</b> Numerical Analysis of TOF-SIMS Data. <b>S.G. MACKAY</b> , 3M Corporation. <b>P.J. MCKEOWN</b> , Perkin-Elmer.	<b>PS-MoA5</b> Deposition of Silicon Oxide using Helicon Assisted Reactive Evaporation. <b>A. DURANDET</b> , R. BOSWELL, Australian National University.
3:40 pm	<b>AS-MoA6</b> SIMS vs. the TRIM Code for Depth Profiles of 100 to 350 keV Phosphorus in Silicon. <b>K. MIETHE</b> , W.H. GRIES, Deutsche Bundespost Telekom, Germany. <b>J.P. BIERACK</b> , Hahn-Meitner-Institut, Germany. <b>H. STRUSNY</b> , Ferdinand-Braun-Inst. für Höchstfrequenztechnik, Germany.	<b>PS-MoA6</b> ECR Oxygen Plasma-Assisted Deposition of Al <sub>2</sub> O <sub>3</sub> . <b>J.C. BARBOUR</b> , J.S. CUSTER, D.M. FOLLSTAEDT, M.B. SINCLAIR, B.G. PÖTTER, Sandia National Laboratories.
4:00 pm	<b>AS-MoA7</b> The Development of Standard Reference Material 2137 - A Boron Implant in Silicon Standard for Secondary Ion Mass Spectrometry. <b>D.S. SIMONS</b> , National Institute of Standards & Technology.	<b>PS-MoA7</b> Electron Cyclotron Resonance Plasma-Deposited Silicon Nitride from 25°C to 200°C. <b>K.L. SEAWARD</b> , F.F. MERTZ, K. NAUKA, Hewlett-Packard.
4:20 pm	<b>AS-MoA8</b> Elemental Binding Energies for X-ray Photoelectron Spectroscopy. <b>C.J. POWELL</b> , National Institute of Standards & Technology.	<b>PS-MoA8</b> Low Temperature Plasma Enhanced CVD of Main Group Nitrides using Organometallic Precursors. <b>D.J. ECONOMOU</b> , S.D. ATHAVALE, D.M. HOFFMAN, S.P. RANGARAJAN, J.-R. LIU, Z. ZHENG, W.-K. CHU, University of Houston.
4:40 pm	<b>AS-MoA9</b> On the Nature of the Use of Adventitious Carbon as a Binding Energy Standard. <b>T.L. BARR</b> , S. SEAL, University of Wisconsin, Milwaukee.	<b>PS-MoA9</b> Fast Deposition of a-Si:H for Solar Cell Application. <b>R.J. SEVERENS</b> , M.C.M. VAN DE SANDEN, G.J. MEEUSEN, <b>D.C. SCHRAM</b> , Eindhoven University of Technology, The Netherlands.
5:00 pm		<b>PS-MoA10</b> The Effects of the Process Parameters on the Low Temperature Si/SiGe Epitaxy by UHV-ECRCVD. <b>S.J. PARK</b> , K.H. HWANG, S.J. JOO, <b>E. YOON</b> , H.S. TAE, S.H. HWANG, Y.P. EO, K.W. WHANG, Seoul National University, Korea.

**VACUUM TECHNOLOGY****Room A102 - Session VT-MoA** pg. 135**Gas Flow, Partial Pressure Analysis, and Leak Detection****Moderator:** J.L. Provo, Martin Marietta Speciality Components Inc.**THIN FILM/VACUUM METALLURGY****Room A105 - Session TFVM-MoA** pg. 137**Diamond, Cubic Boron Nitride and Other Ultra-Hard Films I****Moderator:** R. Messier, Pennsylvania State University.

2:00 pm	<b>VT-MoA1</b> Transition Gas Flow in Drag Pumps and Capillary Leaks. <b>J.C. HELMER</b> , G. LEVI, Varian S.p.A. Italy.	<b>TFVM-MoA1 INVITED</b> Structural Control in the Vapour Growth of Oriented Diamond Films. <b>P. KOIDL</b> , C. WILD, R. LOCHER, Fraunhofer-Inst. für Angewandte Festkörperphysik, Germany.
2:20 pm	<b>VT-MoA2</b> Calculations of Orifice Flow in the Transition Regime. <b>J.P. LOONEY</b> , R.D. MOUNTAIN, National Institute of Standards & Technology.	Invited talk continued.
2:40 pm	<b>VT-MoA3 INVITED</b> High Precision, Gas Analysis System used to Analyze Grab Samples from the Space Shuttle Engine Compartment. <b>G.M. SOLOMON</b> , <b>M.D. BOECKMANN</b> , Vacuum Technology, Inc.	<b>TFVM-MoA3</b> Growth of High Quality Homoepitaxial Diamond with C/O/H Chemistry. <b>W.B. ALEXANDER</b> , P.H. HOLLOWAY, University of Florida, Gainesville. <b>P. DOERING</b> , R. LINARES, LMA Inc.
3:00 pm	Invited talk continued.	<b>TFVM-MoA4</b> Diamond Nucleation by Seeding from the Gas Phase. <b>Z. AJJI</b> , M. BUCK, Universität Heidelberg, Germany. <b>H. SCHWENK</b> , Wacker-Chemitronic, Germany. <b>CH. WÖLL</b> , Universität Heidelberg, Germany.
3:20 pm	<b>VT-MoA5</b> A Guide to Manual Tuning of Pressure Controllers. <b>L.D. HINKLE</b> , F. RUDOLPH, MKS Instruments, Inc.	<b>TFVM-MoA5</b> Low Temperature Plasma Synthesis of Diamond in a Pulsed Microwave ECR Discharge. <b>Z. RING</b> , S. TLALI, H.E. JACKSON, T.D. MANTEI, University of Cincinnati.
3:40 pm	<b>VT-MoA6</b> Fast Fine Leak Testing of Very Large Vessels. <b>L. BERGQUIST</b> , <b>Y.T. SASAKI</b> , Quantum Mechanics Corp.	<b>TFVM-MoA6</b> Effect of Substrate State on the Formation of the Diamond Film Using a Low Temperature Microwave Plasma System. <b>S.H. KIM</b> , Y.S. PARK, S.K. JUNG, J.-W. LEE, Samsung Advanced Institute of Technology, Korea.
4:00 pm	<b>VT-MoA7 INVITED</b> Vacuum Insulation: The Potential for Energy Conservation. <b>H.A. FINE</b> , U.S. Environmental Protection Agency.	<b>TFVM-MoA7 INVITED</b> Process-Property Relationships in Nanocrystalline Diamond Thin Film Preparation. <b>R.W. COLLINS</b> , B. HONG, W. DRAWL, R. MESSIER, Pennsylvania State University.
4:20 pm	Invited talk continued.	Invited talk continued.
4:40 pm	<b>VT-MoA9</b> Vacuum Process of Extremely Slow Leak from Fine Complicated Structures in Chamber Surfaces. <b>M. MIKI</b> , The Graduate University for Advanced Studies, Japan. <b>H. ISHIMARU</b> , National Laboratory for High Energy Physics, Japan.	<b>TFVM-MoA9</b> Diamond Deposition on Carbon Fibers. <b>S.I. SHAH</b> , M.M. WAITE, E.I. du Pont de Nemours and Company & University of Delaware.
5:00 pm	<b>VT-MoA10</b> Measurement of Metals Vapour Pressure as Function of Temperature. <b>V.I. RAKHOVSKY</b> , Research Center for Surface and Vacuum Investigation, Russia.	<b>TFVM-MoA10</b> Carbon Dimer, C <sub>2</sub> , as a Growth Species for Diamond Film Synthesis. <b>D.M. GRUEN</b> , <b>C.D. ZUIKER</b> , A.R. KRAUSS, Argonne National Laboratory.

# Monday Afternoon, October 24, 1994

## ELECTRONIC MATERIALS

Room A108 - Session EM-MoA pg. 139

### Thin Film Heterostructures

Moderator: L. J. Brillson, Xerox Webster Research Center.

## MANUFACTURING SCIENCE AND TECHNOLOGY

Room A110 - Session MS-MoA pg. 140

### Process and Equipment Modeling

Moderator: K. Uram, Lam Research Corporation.

2:00 pm	<b>EM-MoA1</b> Interface Quality in InP/InGaAs RTDs and 2 DEG in Delta-Doped HFET Channels as Observed by Scanning Tunneling Microscopy. <b>W. WU</b> , S.L. SKALA, J.R. TUCKER, K.-Y. CHENG, J.W. LYDING, University of Illinois, Urbana-Champaign. <b>A. SEABAUGH</b> , Texas Instruments Inc.	<b>MS-MoA1</b> Flux Distributions and Growth Rate Uniformities from Hexagonal Collimators. <b>Z. LIN</b> , T.S. CALE, Arizona State University.
2:20 pm	<b>EM-MoA2</b> Model for Metastable Defect Formation at Si-SiO <sub>2</sub> Interfaces. <b>G. LUCOVSKY</b> , Z. JING, J.L. WHITTEN, North Carolina State University.	<b>MS-MoA2</b> Modeling of Collimated Sputter-Deposition of Thin Films using Molecular Dynamics: A Study of Step Coverage and Film Properties. <b>C.C. FANG</b> , State University of New York, Stony Brook. <b>F. JONES</b> , J.J. HSIEH, R.V. JOSHI, IBM TJ Watson Research Center. <b>V. PRASAD</b> , State University of New York, Stony Brook.
2:40 pm	<b>EM-MoA3</b> High-Resolution Depth Profiling of Sequential Isotope Oxidation of Silicon. <b>H.C. LU</b> , T. GUSTAFSSON, E.P. GUSEV, E. GARFUNKEL, Rutgers University.	<b>MS-MoA3</b> <b>INVITED</b> Process and Equipment Modeling for Advanced Semiconductor Manufacturing. <b>Z.J. LEMNIOS</b> , Advanced Research Projects Agency.
3:00 pm	<b>EM-MoA4</b> FTIR Study of Rapid Thermal Annealing of Remote Plasma Chemical Vapor Deposited a-Si-Nitride Films. <b>Z. LU</b> , M.J. WILLIAMS, P.F. SANTOS, G. LUCOVSKY, North Carolina State University.	Invited talk continued.
3:20 pm	<b>EM-MoA5</b> <b>INVITED</b> Electrical Transport Properties of Hot Electrons at Metal, Insulator and Semiconductor Interfaces. <b>R. LUDEKE</b> , IBM TJ Watson Research Center. <b>A. BAUER</b> , Freie Universität Berlin, Germany.	<b>MS-MoA5</b> Comparison of the Sandia DSMC Molecular Flow Model to Experiment. <b>P.K. SHUFFLEBOTHAM</b> , Lam Research Corp. <b>T.J. BARTEL</b> , Sandia National Laboratories. <b>B. BERNEY</b> , Lam Research Corp.
3:40 pm	Invited talk continued.	<b>MS-MoA6</b> Modeling of Ion Flux Uniformity in Radio Frequency Discharges: Effect of Electrode Topography. <b>M. DALVIE</b> , M. SURENDRA, G.S. SELWYN, C.R. GUARNIERI, IBM TJ Watson Research Center.
4:00 pm	<b>EM-MoA7</b> Epitaxy in the Room Temperature Reaction of Ni on Si(111) Studied with Synchrotron X-ray Diffraction. <b>P. YANG</b> , M.Y. LEE, P.A. BENNETT, Arizona State University. <b>P.J. ENG</b> , AT&T Bell Laboratories. <b>I.K. ROBINSON</b> , University of Illinois, Urbana.	<b>MS-MoA7</b> Simulation of a Tungsten Filled Via Process Module for Process Integration. <b>D.S. BANG</b> , K. HSIAU, J.P. MCVITTIE, K.C. SARASWAT, Stanford University. <b>Z. KRIVOKAPIC</b> , Advanced Micro Devices.
4:20 pm	<b>EM-MoA8</b> Phonon Scattering of BEEM Electrons at Au/Si(100) Schottky Interfaces. <b>C.A. VENTRICE, JR.</b> , V. LABELLA, G. RAMASWAMY, L.J. SCHOWALTER, Rensselaer Polytechnic Institute.	<b>MS-MoA8</b> Reactor- and Feature-Scale Simulation of Tungsten Chemical Vapor Deposition. <b>A.H. LABUN</b> , Digital Equipment Corporation.
4:40 pm	<b>EM-MoA9</b> <b>INVITED</b> Metal (CoSi <sub>2</sub> )/Insulator (CaF <sub>2</sub> ) Resonant Tunneling Diodes. <b>M. ASADA</b> , M. WATANABE, T. SUEMASU, Y. KOHNO, Tokyo Institute of Technology, Japan.	<b>MS-MoA10</b> Deposition and Flow Planarization of Glasses. <b>H. LIAO</b> , T.S. CALE, Arizona State University.
5:00 pm	Invited talk continued.	

**BIOMATERIAL INTERFACES****Room A106 - Session BI-MoA** pg. 142**Cell-Solid Surface Interactions****Moderator:** J.J. Hickman, Science Applications International Corporation.

2:00 pm	<b>BI-MoA1 INVITED</b> The Bone Cell/Biomaterial Interface. <b>J.E. DAVIES</b> , University of Toronto, Canada.	
2:20 pm	Invited talk continued.	
2:40 pm	<b>BI-MoA3</b> Human Neutrophil Motility on Modified Surfaces. <b>L. HARVATH</b> , N.E. BROWNSON, CBER FDA. <b>K.E. FOSTER</b> , J.J. HICKMAN, Science Applications International Corporation.	
3:00 pm	<b>BI-MoA4</b> Nanofabricated Structures for the Measurement of Signals from Single Cells. <b>J.M. COOPER</b> , <b>A. GRIFFITHS</b> , <b>H. MORGAN</b> , University of Glasgow, United Kingdom.	
3:20 pm	<b>BI-MoA5 INVITED</b> Cell-Solid Surface Interactions. <b>D.A. OKRONGLY</b> , Xytronyx, Inc.	
3:40 pm	Invited talk continued.	
4:00 pm	<b>BI-MoA7</b> Nanofabricated Fibers for Studying the Phagocytosis of Inorganic Particulates by Macrophages. <b>J. GOLD</b> , <b>B. NILSSON</b> , <b>B. KASEMO</b> , Chalmers Univ. of Technology and Univ. of Göteborg, Sweden.	
4:20 pm	<b>BI-MoA8</b> Protein-Platelet and Platelet-Leukocyte Interaction at Materials in Contact with Human Blood. <b>H. NYGREN</b> , <b>M. BRAIDE</b> , <b>C. KARLSSON</b> , Department of Anatomy and Cell Biology, Sweden.	
4:40 pm	<b>BI-MoA9</b> Effect of Surface Mobility on Biointeractions. <b>C.D. RATNER</b> , <b>C.D. TIDWELL</b> , University of Washington.	
5:00 pm	<b>BI-MoA10</b> Secondary Ion Mass Spectrometry Studies of Covalently Bound Peptides to a Fluoropolymer: Imaging and Quantitation. <b>E.J. BEKOS</b> , <b>F.V. BRIGHT</b> , <b>J.A. GARDELLA, JR.</b> , State University of New York, Buffalo.	

# Monday Afternoon Poster Sessions

## SURFACE SCIENCE

Room BR4 - Session SS-MoP pg. 144

### Aspects of Surface Science

Moderator: J.C. Hemminger, University of California, Irvine.

Presenters present: 5:00-6:30 pm.

**SS-MoP1** In Situ, Real-Time Photoelectron Emission Microscopy & Scanning Auger & Low-Energy Electron Diffraction Studies of Oxygen Enhanced Diffusion of Sulfur on Mo(310) at 1000 K. **A. GARCIA**, M.E. KORDESCH, Ohio University.

**SS-MoP2** Multi-Bounce Direct Scattering of  $N_2$  from Cu(110). **J.L.W. SIDERS**, G.O. SITZ, University of Texas, Austin.

**SS-MoP3** Dynamics of  $D_2$  Recombinative Desorption from Ag(111). **R.N. CARTER**, F. HEALEY, A. HODGSON, University of Liverpool, United Kingdom.

**SS-MoP4** Epitaxial Domains of  $C_{60}$  on Ag(111). **J.E. ROWE**, R.A. MALIC, E.E. CHABAN, C.-M. CHIANG, AT&T Bell Laboratories.

**SS-MoP6** Deposition of Thin Layers of Inorganic Salts from Solution by Spin Coating. **R.M. VAN HARDEVELD**, M. GOEDBLOED, J.C. MUIJSERS, L.J. VAN IJZENDOORN, Eindhoven University of Technology, The Netherlands. **E.W. KUIPERS**, Shell Research, The Netherlands. **J.W. NIEMANTSVERDIET**, Eindhoven University of Technology, The Netherlands.

**SS-MoP7** Interaction of Fullerenes with the Cu(111) and Ag(111) Surfaces. **T. SAKURAI**, X.-D. WANG, T. HASHIZUME, J. KISHIMOTO, S. YAMAZAKI, V. YUROV, Tohoku University, Japan. **H. SHINOHARA**, Nagoya University, Japan. **H.W. PICKERING**, Pennsylvania State University.

**SS-MoP8** STM Study of the Clean and Cu Covered  $TiO_2(110)$  Surface. **D. NOVAK**, E. GARFUNKEL, T. GUSTAFSSON, Rutgers University.

**SS-MoP9** Low Energy Ion Beam Damage of Self-Assembled Monolayers. **E. ADA**, J.A. BURROUGHS, S.B. WAINHAUS, L. HANLEY, University of Illinois, Chicago.

**SS-MoP10** Vibrational Studies of Adsorbate Structure, Bonding and Reactivity: Alcohols, Thiols and Alkyl Iodides Adsorbed on Mo(110). **M.K. WELDON\***, P.U. UVDAL, C.M. FRIEND, Harvard University.

**SS-MoP11** Hydrogenation of Cyclohexene by Subsurface Hydrogen on Ni Surfaces. **G.-A. SON\***, M. MAVRIKAKIS, J.L. GLAND, University of Michigan.

**SS-MoP12** FT-IRAS of Adsorbed Alkoxides: Methoxide and Ethoxides on Cu(111). **S.C. STREET\***, University of Illinois, Urbana-Champaign. **A.J. GELLMAN**, Carnegie Mellon University.

**SS-MoP13** Dissociation Kinetics of NO on Rhodium (111). **H.J. BORG\***, R.A. VAN SANTEN, J.W. NIEMANTSVERDIET, Eindhoven University of Technology, The Netherlands.

**SS-MoP14** Two-Dimensional Surface Interactions and Dynamics of Benzene on Cu(111). **M.M. KAMNA\***, S.J. STRANICK, P.S. WEISS, The Pennsylvania State University.

**SS-MoP15** RAIRS of Rh Single Crystal Surfaces during NO Reduction at Moderate Pressures. **D.N. BELTON**, H. PERMANA, S.J. SCHMIEG, General Motors Research & Development Center. **K.Y. SIMON NG**, Wayne State University.

**SS-MoP16** Vibrational and Electron Spectroscopic Study of the Interaction of Nitric Oxide with the Ni(110) Surface. **D.H. HELLMOLDT**, C.M. AFFENTUSCHEGG, J.E. CROWELL, University of California, San Diego.

**SS-MoP17** The Role of C in O Removal from Ultra-Thin Layers of Oxidized La on Pd(100). **G.W. GRAHAM**, Ford Motor Company. **B.U.M. RAO**, M. AHMAD, Wayne State University.

**SS-MoP18** A Study of Oxygen Chemisorption Phases on Pt(111). **C. PUGLIA**, A. NILSSON, B. HERNNAS, K.O. KARIS, P. BENNICH, N. MÄRTENSSON, Uppsala University, Sweden.

**SS-MoP20** Selective Oxidation Reactions on Rh(111)-p(2x1)-O. **C.W.J. BOL**, C.M. FRIEND, Harvard University.

**SS-MoP21** The Early Stages of Ruthenium Oxidation. **J. HRBEK**, D. VAN CAMPEN, Brookhaven National Laboratory. **I. MALIK**, MEMC Electronic Materials.

**SS-MoP23** Activation Effects on the Surface Properties of Silica-Supported Cobalt Catalysts. **K. COULTER**, A.G. SAULT, Sandia National Laboratories.

**SS-MoP24** Disorder-Effects at the Al(110) Surface. **W. SCHOMMERS**, C. MAYER, H. GÖBEL, P. VON BLANCKENHAGEN, Institut für Materialforschung, Germany.

**SS-MoP25** Impact versus Dipole Scattering in HREELS of H/C(100). **B.D. THOMS**, J.E. BUTLER, Naval Research Laboratory.

**SS-MoP26** Scattering of  $^3He$  from the NiO (001) Surface. **J. BAKER**, G.G. BISHOP, E.S. GILLMAN, S.A. SAFRON, J.G. SKOFRONICK, Florida State University.

**SS-MoP27** The Chemisorption of  $F_2$  and  $O_2$  on Si(100) 2x1 and Si(111) 7x7. **H.C. FLAUM**, **E.R. BEHRINGER**, E.J. LANZENDORF, D. MASSON, D.J.D. SULLIVAN, A.C. KUMMEL, University of California, San Diego.

**SS-MoP28** Isothermal  $H_2$  Desorption Kinetics from Si(100) 2x1: Dependence on Disilane and Atomic Hydrogen Precursors. **L.A. OKADA**, M.L. WISE, S.M. GEORGE, University of Colorado, Boulder.

**SS-MoP29** Molecular Beam Reaction Studies of Trimethylgallium (TMGa) on Ga-rich GaAs(100). **B.A. BANSENAUER**, C.E. NELSON, University of Wisconsin, Eau Claire. **J.R. CREIGHTON**, Sandia National Laboratories.

**SS-MoP30** Inner-Shell Promotions in Low Energy  $Li^+$  - Al Collisions at Clean and Alkali - Covered Al(100). **K.A.H. GERMAN**, C.B. WEARE, J.A. YARMOFF, University of California, Riverside & Lawrence Berkeley Lab.

**SS-MoP31** Evolution of Surface Morphology of Si(100)-(2x1) during Oxygen Adsorption at Elevated Temperatures. **Y. HONG**, K. WURM, Y. WEI, I.S.T. TSONG, Arizona State University. **R. KLIESE**, B. RÖTTGER, H. NEDDERMEYER, Ruhr-Universität Bochum, Germany.

**SS-MoP32** Analysis of Chemisorption Sites:  $Cl_2$  on Si(111)-7x7. **C. YAN**, J.A. JENSEN, A.C. KUMMEL, University of California, San Diego.

**SS-MoP33** Resonantly Enhanced Multiphoton Ionization of SiO Desorbing from Si(111) in Reaction with  $O_2$ . **K.G. NAKAMURA**, M. KITAJIMA, National Research Institute for Metals, Japan.

**SS-MoP34** Charge Transfer Process of Low Energy Collisions of  $Li^+$  with Cs/Cu(111) Surfaces. **Q.B. LU**, Y.G. SHEN, D.J. O'CONNOR, B.V. KING, R.J. MACDONALD, University of Newcastle, Australia.

**SS-MoP35** The Site-Specific Neutralization Behavior of 2.0 keV  $^7Li^+$  Ions Scattered from Alkali/Al(100) Surfaces. **C.B. WEARE**, K.A.H. GERMAN, J.A. YARMOFF, University of California, Riverside & Lawrence Berkeley Lab.

**SS-MoP36** Isotope Effects in Electron-Stimulated Desorption from Physisorbed Monolayers of  $H_2$ , HD, and  $D_2$  on Graphite. **B. XIA**, S.C. FAIN, JR., University of Washington.

**SS-MoP37** Internal and Translational State Distributions and Alignment of a Photodesorbed Molecule: CO/Si(100) 2x1. **F.M. ZIMMERMAN**, P.L. HOUSTON, W. HO, Cornell University.

**SS-MoP38** Kinetic to Internal Energy Transfer during Polyatomic Ion-Surface Collisions. **J.A. BURROUGHS**, S.B. WAINHAUS, L. HANLEY, University of Illinois, Chicago.

**SS-MoP39** Application of Hyperthermal Beams to Achieve Adsorption and/or Abstraction of Adsorbates on Diamond Surfaces. **D. HAGGERTY**, C. BANDIS, **B.B. PATE**, Washington State University.

**SS-MoP40** The Effect of Preadsorbed Oxygen on the Dissociation Dynamics of Ethane on Ir(110). **W. HAGO**, D. KELLY, W.H. WEINBERG, University of California, Santa Barbara.

\*Finalist for the Morton M. Traum Award

**NANO 3/NANOMETER-SCALE SCIENCE AND TECHNOLOGY**  
**Room BR4 - Session NS-MoP pg. 150**

**Instrumentation and Metrology**

**Moderator:** E.C. Teague, National Institute of Standards and Technology.

Presenters present: 5:00-6:30 pm.

**NS-MoP1** Quantum Friction Observed with Two-Dimensional Frictional Force Microscope. **S. FUJISAWA**, E. KISHI, Y. SUGAWARA, S. MORITA, Hiroshima University, Japan.

**NS-MoP2** Microtribological Study of Lubricants using Friction Force Microscopy. **B. BHUSHAN**, **V.N. KOINKAR**, Ohio State University.

**NS-MoP3** Determining the Local Mechanical Properties of a Material using a Scanning Tunneling Microscope as a Surface Acoustic Wave Detector. **D.M. SCHAEFER**, R.J. COLTON, S.M. HUES, Naval Research Laboratory.

**NS-MoP4** Modeling of the Nanoindentation of Thin SiO<sub>2</sub> Layers on Si using Finite Element Analysis. **C.F. DRAPER**, Vanderbilt University. **D.M. SCHAEFER**, R.J. COLTON, S.M. HUES, Naval Research Laboratory.

**NS-MoP5** Measurement of Adhesive Force between poly-L-lysine Treated Mica and Colloidal Gold Particles. **J. CARNES**, J. VESENKA, R. MILLER, E. HENDERSON, Iowa State University.

**NS-MoP6** Ultrasound Influence on the Tribological Properties of CVD Diamond. **V. SNITKA**, Research Institute "Vibrotechnika", Lithuania. **V. BARANAUSKAS**, State University of Campinas, Brazil.

**NS-MoP7** Surface Roughness Characterization of Soft X-ray Multilayer Films on the Nanometer Scale. **J. YU**, Chubu University, Japan and SKLAO, P.R. China, J.L. CAO, SKLAO, P.R. China, Y. NAMBA, Chubu University, Japan. Y.Y. MA, SKLAO, P.R. China.

**NS-MoP8** Step Height Measurement using a Scanning Tunneling Microscope Equipped with a Crystalline Lattice Scale Reference and Interferometer. **T. FUJII**, M. SUZUKI, Nikon Corporation, Japan. **H. KUGAMI**, H. KAWAKATSU, T. HIGUCHI, University of Tokyo, Japan.

**NS-MoP9** Comparison of Magnetic Force Microscopy Techniques. **P. RICE**, J. MORELAND, National Institute of Standards & Technology.

**NS-MoP10** Scanning Thermal Microscopy with a Resistive Probe. **R.B. DINWIDDIE**, Oak Ridge National Laboratory. **R.J. PYLKKI**, P.E. WEST, TopoMetrix.

**NS-MoP11** An Integrated Lithography and Analysis Instrument. **G. ROSOLEN**, Leica Cambridge Ltd., England. **R. CLARK**, University of New South Wales, Australia.

**NS-MoP12** Low Noise Scanning Tunneling Microscope for Low Temperature Physics with an Electrically Isolated Circuit. **H. NAKAGAWA**, K. SAKUMOTO, E. KURAYA, S. ASAKURA, K. FUKUDA, Yokohama National University, Japan. **M. TANAKA**, Nippon Steel Co., Japan.

**NS-MoP13** Ar Atomic Emission Microscopy. **P.G. VAN PATTEN**, J.D. NOLL, M.L. MYRICK, University of South Carolina.

**NS-MoP14** Sub-Micron Lithography Employing Photoresist Channel-Constrained Electroless Metallization as an Etch Barrier. **C.S. DULCEY**, J.M. CALVERT, W.J. DRESSICK, M.S. CHEN, Naval Research Laboratory. **G.S. CALABRESE**, J.H. GERGER, JR., J.F. BOHLAND, Shipley Co.

**NS-MoP15** AFM Tip-Sample/Sample-Tip Deconvolution. **P.C. MARKIEWICZ**, M.C. GOH, University of Toronto, Canada.

**NS-MoP16** On the Recovery of Spectroscopic Image in Scanning Force Microscopy. **I.Y. SOKOLOV**, University of Toronto, Canada.

**NS-MoP17** Analysis of Resist Artifacts by AFM for use in SEM and In-house Line Width Standards. **D.A. CHERNOFF**, Advanced Surface Microscopy, Inc.

**NS-MoP18** PZT Thin Film Force Sensor for Atomic Force Microscope. **T. FUJII**, S. WATANABE, M. SUZUKI, T. FUJII, Nikon Corporation, Japan.

**NS-MoP19** The Design of an Atomic Force Microscope for Metrology. **J. SCHNEIR**, T. MCWALD, National Institute of Standards & Technology. **J. ALEXANDER**, B. WILFLEY, Park Scientific Instruments.

**NS-MoP20** UHV Setup with Original STM for Nanostructures Creating and Study. **K.N. ELTSOV**, A.N. KLIMOV, A.M. PROKHOROV, V.M. SHEVLYUGA, V.Y. YUROV, Russian Academy of Sciences.

**NS-MoP21** Scanning Potentiometry of YBCO Step-Edge Junctions. **J. MORELAND**, R.H. ONO, R.E. THOMSON, National Institute of Standards & Technology. **C. PRATER**, Digital Instruments.

**NS-MoP22** Development of Highly Conductive Cantilevers for Atomic Force Microscopy. **R.E. THOMSON**, J. MORELAND, National Institute of Standards & Technology.

**NS-MoP23** Effects of Potassium and Lithium Metal Deposition on the Emission Characteristics of Spindt-type Thin Film Field Emission Microcathode Arrays. **A.A. TALIN**, T.E. FELTER, Sandia National Laboratories. **D.J. DEVINE**, Coloray Display Corporation.

**NS-MoP24** A 25nm Resolution 1 keV SAFE Microcolumn. **E. KRATSCHMER**, H.S. KIM, M.G.R. THOMSON, K.Y. LEE, S.A. RISHTON, M.L. YU, T.H.P. CHANG, IBM T.J. Watson Research Center.



# Monday Afternoon Poster Sessions

## PLASMA SCIENCE

Room BR4 - Session PS-MoP pg. 153

### Plasma Etching and Deposition

Moderator: D.B. Graves, University of California, Berkeley.

Presenters present: 5:00-6:30 pm.

- PS-MoP1** Deposition of a-C:H Layers using an Expanding Ar/C<sub>2</sub>H<sub>2</sub>/CF<sub>4</sub> Plasma. J.W.A. GIELEN, M.C.M. VAN DE SANDEN, A.J.M. BUURON, D.C. SCHRAM, Eindhoven University of Technology, The Netherlands.
- PS-MoP2** Silicon Oxide Deposition in an ECR Plasma with Microwave Spectroscopy as a Diagnostic. K.H. CHEW, J. CHEN, R.C. WOODS, J.L. SHOHET, University of Wisconsin, Madison.
- PS-MoP3** Plasma Enhanced Chemical Vapor Deposition of Silicon Dioxide from Organosilanes. K.H.A. BOGART, E.R. FISHER, Colorado State University.
- PS-MoP4** Plasma Deposition of Diamond-like Carbon, Fluorocarbon Polymer, and Silicon Nitride Films. N. MACKIE, P.R. MCCURDY, E.R. FISHER, Colorado State University.
- PS-MoP5** The Ion Energy Distribution at the Substrate Surface in a RF Induction Plasma Source. J.B.O. CAUGHMAN, Oak Ridge National Laboratory.
- PS-MoP6** Analysis of the Oxygen Contamination Presented in SiN<sub>x</sub> Films Deposited by ECR. S. GARCIA, J.M. MARTIN, M. FERNANDEZ, I. MARTIL, G. GONZALEZ-DIAZ, Universidad Complutense, Spain.
- PS-MoP7** Comparison of Measured and Computed Magnetron Sputtering Tracks for Alloys of Differing Magnetic Susceptibility. D.R. JULIANO, D.N. RUZIC, University of Illinois, Urbana. B. MANRING, P. FRAUSTO, J. POOLE, Tosoh SMD.
- PS-MoP8** Synergistic Sputtering Effects during Ion Bombardment with Two Ion Species. S. BERG, I.V. KATARDJIEV, Uppsala University, Sweden.
- PS-MoP9** High Aspect Ratio Si Etching for Microsensor Fabrication. W.H. JUAN, S.W. PANG, University of Michigan.
- PS-MoP10** Plasma Etching of Pt and Ferroelectric Thin Films. R.L. RHOADES, D.B. POKER, Oak Ridge National Laboratory. B.S. MERCER, PlasmaQuest.
- PS-MoP11** Composition of the Oxygen Plasmas from Two Inductively Coupled Sources. M. TUSZEWSKI, J.T. SCHEUER, J.A. TOBIN, Los Alamos National Laboratory.
- PS-MoP12** Steady-State Helicon Plasma Experiments. J. GILLAND, R. BROWN, N. HERSHKOWITZ, R. BREUN, University of Wisconsin, Madison.

- PS-MoP13** Radio Frequency Hollow Cathode Discharge for Large Area Double Sided Foil Processing. D. KORZEC, M. SCHOTT, B. PFANNKUCHEN, K.-P. NINGEL, J. ENGEMANN, University of Wuppertal, Germany.
- PS-MoP14** Remote Source Characteristics of Helicon Discharges. I.D. SUDIT, F.F. CHEN, University of California, Los Angeles.
- PS-MoP15** High Density, Low Temperature Dry Etching in GaAs and InP Device Technology. S.J. PEARTON, C.R. ABERNATHY, University of Florida, Gainesville. F. REN, AT&T Bell Laboratories.
- PS-MoP16** Aspect Ratio Independent Etching of Silicon using a High Density Helicon Source. F.P. KLEMENS, C.W. JURGENSEN, D.E. IBOTSON, J.T.C. LEE, AT&T Bell Laboratories.
- PS-MoP17** Substrate Bias Effects in High-Aspect-Ratio SiO<sub>2</sub> Contact Etching using an ICP Reactor. A.C. WESTERHEIM, A.H. LABUN, J.H. DUBASH, Digital Equipment Corporation. J.C. ARNOLD, H.H. SAWIN, Massachusetts Institute of Technology. V. YU-WANG, Applied Materials.
- PS-MoP18** A Study of the Causes and Effects of Ion Angular Spread in High Density Plasma Sources. J. ZHENG, J.P. MCVITTIE, Stanford University.
- PS-MoP19** Modeling Simulation of Neutral Beam Processing using a Plasma Source. M.D. KILGORE, D.B. GRAVES, University of California, Berkeley.
- PS-MoP20** Influence of the Ponderomotive Force on Inductive-Source Plasma Profiles. G. DIPESO, T.D. ROGNLIEN, Lawrence Livermore National Laboratory. V. VAHEDI, Lawrence Livermore Nat'l Lab & Univ. of California, Berkeley. D.W. HEWETT, Lawrence Livermore National Laboratory.
- PS-MoP21** Modeling of Oxide Etching in a High Density ICP Tool. R.A. STEWART, J.D. BUKOWSKI, University of California, Berkeley. P. VITELLO, Lawrence Livermore National Laboratory. D.B. GRAVES, University of California, Berkeley.
- PS-MoP22** Spatially Averaged (Global) Model of Time Modulated High Density Electronegative Plasmas. S. ASHIDA, C. LEE, M.A. LIEBERMAN, University of California, Berkeley.
- PS-MoP23** 2D RF Sheath Structure due to Geometrical Discontinuities Outside the Wafer Edge. B. LANE, Plasma Dynamics.
- PS-MoP24** 2D Modeling of Time Modulated Inductive Discharges. V. VAHEDI, M.A. LIEBERMAN, University of California, Berkeley. G. DIPESO, D.W. HEWETT, Lawrence Livermore National Laboratory.

## VACUUM TECHNOLOGY

Room BR4 - Session VT-MoP pg. 157

### Vacuum Science and Technology

Moderator: L.D. Hinkle, MKS Instruments Inc.

Presenters present: 5:00-6:30 pm.

**VT-MoP2** Rotating Disc Gauge Using High Temperature Superconductor Suspension. **A. CHAMBERS**, A.D. CHEW, University of York, England. A.P. TROUP, Edwards High Vacuum International, United Kingdom.

**VT-MoP3** Measurement of Xe Pressure by Photoelectron Counting with the Imaging Counter. **S. SEKINE**, S. ICHIMURA, Electrotechnical Laboratory, Japan.

**VT-MoP4** Investigation of RGA's for High Sensitivity He Leak Detection. **J.A. SMITH**, MKS Instruments, Inc. M.G. RAO, Continuous Electron Beam Accelerator Facility.

**VT-MoP5** O<sub>3</sub> Treated Metal Surfaces with Less Carbon Detected on the Surface and in the Sputter-Profiled Layer by Auger Electron Spectroscopy (AES). **T. MOMOSE**, N. YAMADA, Miyagi National College of Technology, Japan. K. ASANO, H. ISHIMARU, National Laboratory for High Energy Physics, Japan.

**VT-MoP6** Outgassing Reduction of Type 304 Stainless Steel by Surface Oxidation in Air. **K. ODAKA**, S. UEDA, Hitachi Ltd., Japan.

**VT-MoP7** A Low Contamination Ultrahigh Vacuum System of the SRRC 1.3 GeV Electron Storage Ring. **G.Y. HSIUNG**, J.R. HUANG, D.J. WANG, J.G. SHYY, H.S. TZENG, S.N. HSU, S.Y. PERNG, K.M. HSIAO, W.D. WEY, Synchrotron Radiation Research Center, China. J.R. CHEN, Y.C. LIU, SRRC and National Tsing-Hua University, China.

**VT-MoP8** Selection of Beam Chamber Materials Cu, Cu/Al Hybrid, and Al for High Current Storage Ring. **H. ISHIMARU**, KEK National Laboratory for High Energy Physics, Japan. **A. KOMURA**, T. TAKAMA, A. KITAGAWA, Hitachi Zosen Corporation, Japan.

**VT-MoP9** Scaling Law of Outgassing with a Pumping Parameter. **K. AKAISHI**, Y. KUBOTA, Y. FUNATO, M. MUSHIAKI, O. MOTOJIMA, National Institute for Fusion Science, Japan.

**VT-MoP10** Enhancement of Hydrogen Evacuation by Injecting Flourine into the Exhaust System with Turbomolecular Pumps. **N. OGURE**, Ebara Research Co., Japan. A. SHIBATA, Ebara Solar, Inc. K. ONO, Ebara Corporation, Japan. N. HAYASAKA, H. OKANO, Toshiba Corporation, Japan. K. OKUMURA, Toshiba America Electronic Components, Inc.

**VT-MoP11** Pumping Behavior of Distributed Ion Pumps at High and Misaligned Magnetic Fields. **H.C. HSEUH**, W.S. JIANG, M. MAPES, Brookhaven National Laboratory.

**VT-MoP12** Modelling of a Multistage Claw Rotor Vacuum Pump. **I. IOFFE**, V. KOSS, The BOC Group, Inc. M. GRAY, R.G. LIVESEY, Edwards High Vacuum International, United Kingdom.

**VT-MoP13** H<sub>2</sub>O Pumping by Sputter Discharge with LaB<sub>6</sub> Cathode. **Y. FUNATO**, M. MIYOSHI, K. AKAISHI, Y. KUBOTA, M. MUSHIAKI, Suzuka College of Technology, Japan.

**VT-MoP14** Vacuum Characteristics of Titanium. **M. MINATO**, Y. ITOH, Vacuum Metallurgical Co., Ltd.

**VT-MoP15** Recombination Limited Outgassing of Stainless Steel. **B.C. MOORE**, Consultant.

## BIOMATERIAL INTERFACES

Room BR4 - Session BI-MoP pg. 160

### Biomaterial Interfaces

Moderator: M.J. Tarlov, National Institute of Standards and Technology.

Presenters present: 5:00-6:30 pm.

**BI-MoP1** Nanobiology: The Action of Picosecond Nanometer-Scale Pulse on DNA. **L.S. GONG**, J.H. WU, W.S. GONG, South China Normal University.

**BI-MoP2** STM Imaging of Oligonucleotides. **A. LIMANSKY**, O. LIMAN-SKAYA, Academy of Sciences of Ukraine. Y. KAMENSKY, Sci.-Res. Inst. of Radio Engineering Measurements, Ukraine.

**BI-MoP3** Fabrication of Patterned DNA Surfaces using Lithographic Modification of Self-Assembled Organic Monolayers. **L.A. CHRISSEY**, Naval Research Laboratory. **C.E. O'FERRALL**, P.M. ROBERTS, Naval Research Laboratory and Geo-Centers, Inc. W. DRESSICK, C.S. DULCEY, D.B. CHRISSEY, J.M. CALVERT, Naval Research Laboratory.

**BI-MoP4** Contact versus TappingMode™ AFM Imaging of Native Chromatin. **J. VESENKA**, L.D. MARTIN, R. MILLER, E. HENDERSON, D.D. LARSON, Iowa State University.

**BI-MoP5** Adsorption and Coadsorption of Water and Amino Acids on Pt(111). **P. LÖFGREN**, J. LAUSMAA, A. KROZER, B. KASEMO, Chalmers Univ. of Tech. & Univ. of Göteborg, Sweden.

**BI-MoP6** XPS and In Vitro Studies of TiNi Surfaces Modified Using Various Sterilization Procedures. **S.A. SHABALOVSKAYA**, J.W. ANDEREGG, J.E. CUNNICK, Iowa State University.

**BI-MoP7** Nano-Scale Mechanics and Morphology of Laser Ablated Tooth Enamel. **C.A. DIRUBIO**, P. TANGYUNYONG, J.E. HOUSTON, T.A. MICHALSKE, Sandia National Laboratories. O.L. WARREN, University of Western Ontario, Canada. P. WILDER-SMITH, University of California, Irvine.

**BI-MoP8** Surface Characterization of Titanium Implants. **G.N. RAIKAR**, J.C. GREGORY, University of Alabama, Huntsville. J.L. ONG, L.C. LUCAS, University of Alabama, Birmingham. D. KAWAHARA, M. NAKAMURA, Osaka Dental University, Japan.

**BI-MoP9** SIMS Characterization of Adsorbed Protein Films. **B. HAGENHOFF**, A. BENNINGHOVEN, Universität Münster, Germany. D.G. CASTNER, B.D. RATNER, University of Washington.

**BI-MoP10** Extraction of Quantitative Surface Information from Static SIMS using Partial Least Squares. **B.D. RATNER**, V.H. PÉREZ-LUNA, P. FAVIA, University of Washington.

**BI-MoP11** Sub-Angstrom Movements of Biological Specimens Detected by Microwaves. **P. GIZDULICH**, G. ASCHERO, Dpt Fisiopatologia Clinica, Italy. F. MANGO, Scuola Normale Superiore, Italy.

**BI-MoP12** Interactions of Cells and Proteins with Self-Assembled Monolayers (SAMs). **K.E. FOSTER**, J.J. HICKMAN, Science Applications International Corporation. D.A. STENGER, Naval Research Laboratory. A.E. SHAFFNER, J.L. BARKER, National Institutes of Health.

**BI-MoP13** Aminoacid Adsorption on Polyfunctional SAMs of Alkylthiols. **K.D. UVDAL**, University of Washington. S.V. ATRE, D. ALLARA, Pennsylvania State University. B.D. RATNER, University of Washington.

**BI-MoP14** One-step Immobilization of Biomolecules and Application in Biosensors. **A. HARTMANN**, D. BOCK, S. SEEGER, Universität Heidelberg, Germany.

**BI-MoP15** Polymeric Microcapsule Arrays - A Novel Method of Bioencapsulation. **R.V. PARTHASARATHY**, C.R. MARTIN, Colorado State University.

**BI-MoP16** Extreme Hydrophobicity Affecting the Adsorption of IgG on Methylated Surfaces. **B. WALIVAARA**, P. WARKENTIN, J. HEMMINGSSON, P. TENGVAL, Linköping University, Sweden.

# Tuesday Morning, October 25, 1994

## SURFACE SCIENCE

Room A205 - Session SS1-TuM pg. 163

### Nucleation and Growth: Homoepitaxy

Moderator: M.E. Kordesch, Ohio University.

## SURFACE SCIENCE

Room A201 - Session SS2-TuM pg. 164

### Non-Thermal Surface Dynamics

Moderator: J.P. Cowin, Pacific Northwest Laboratories.

8:20 am	<b>SS1-TuM1</b> Dynamics of the Si(100) Surface. C. PEARSON, R. CURTIS, X. SHI, E. GANZ, University of Minnesota.	<b>SS2-TuM1</b> Femtosecond Time-Resolved Desorption Dynamics: Vibrational Effects in the Electronically Driven Desorption of O <sub>2</sub> from Pd(111). J.A. MISEWICH, T.F. HEINZ, A. KALAMARIDES, P. WEIGAND, IBM TJ Watson Research Center.
8:40 am	<b>SS1-TuM2</b> STM Studies of Vacancy-Step Interaction Kinetics during Low-Energy Ion Bombardment of the Si(001) Surface. B.S. SWARTZENTRUBER, Sandia National Laboratories. C.M. MATZKE, University of New Mexico. J.E. HOUSTON, Sandia National Laboratories. D.L. KENDALL, University of New Mexico.	<b>SS2-TuM2</b> Dynamics of Surface Photochemistry: CO + O <sub>2</sub> on Pt(111). D.G. BUSCH, W. HO, Cornell University.
9:00 am	<b>SS1-TuM3</b> Stress-Induced Step Bunching on Vicinal Strained Layers. Z. ZHANG, University of Wisconsin, Madison. J.D. TERSOFF, IBM TJ Watson Research Center. Y.H. PHANG, M.G. LAGALLY, University of Wisconsin, Madison.	<b>SS2-TuM3</b> INVITED Reactions of Hyperthermal Energy (5-100 eV), Molecular Ions with Metal and Oxide Surfaces. D.C. JACOBS, University of Notre Dame.
9:20 am	<b>SS1-TuM4</b> Spatial Correlations in Surface Roughness during Low Temperature Epitaxial Growth of Ge(001). J.E. VAN NOSTRAND, S.J. CHEY, D.G. CAHILL, M.-A. HASAN, J.E. GREENE, University of Illinois, Urbana.	Invited talk continued.
9:40 am	<b>SS1-TuM5</b> Kinetic Smoothing of Vicinal Si(111). H.-C. KAN, R.J. PHANEUF, E.D. WILLIAMS, University of Maryland.	<b>SS2-TuM5</b> Low-Energy Electron-Stimulated Production of Molecular Hydrogen from Amorphous Water Ice. G.A. KIMMEL, R.G. TONKYN, T.M. ORLANDO, Pacific Northwest Laboratory.
10:00 am	<b>SS1-TuM6</b> Fractal Growth on Metal Surfaces. Z.G. ZHANG, X. CHEN, M.G. LAGALLY, University of Wisconsin, Madison.	<b>SS2-TuM6</b> Models for Positive Ion Emission by Photon Excitation at the (001) Surface of MgO. A. GIBSON, J.P. LAFEMINA, Pacific Northwest Laboratories. J.T. DICKINSON, Washington State University.
10:20 am	<b>SS1-TuM7</b> Computer Simulations of Diffusion and Island Growth. G. VIDALI, Syracuse University. O. BIHAM, Syracuse University and Hebrew University, Israel. M. KARIMI, Indiana University of Pennsylvania. R. KENNETT-FOX, H. ZENG, Syracuse University.	<b>SS2-TuM7</b> Non-Thermal Chemistry of Chemisorbed Ammonia: Dissociative Excitation and Dynamics. A.R. BURNS, E.B. STECHEL, D.R. JENNISON, Sandia National Laboratories.
10:40 am	<b>SS1-TuM8</b> On the Interlayer Atomic Diffusion Mechanism in Metal-on-Metal Epitaxy. Y. LI, A.E. DEPRISTO, Iowa State University.	<b>SS2-TuM8</b> Electron Stimulated Desorption of Hydrogen from Si(100):H Surfaces by STM. T.-C. SHEN, C. WANG, G. ABELN, J.W. LYDING, J.R. TUCKER, University of Illinois, Urbana-Champaign.
11:00 am	<b>SS1-TuM9</b> Surface Morphology Changes Upon Laser Heating of Pt(111). J. FROHN, J. REYNOLDS, T. ENGEL, University of Washington.	<b>SS2-TuM9</b> TOF and Internal State Distribution of Photodesorbed Species from N <sub>2</sub> O/Pt(111) by 193 nm Light. D.P. MASSON, E.J. LANZENDORF, A.C. KUMMEL, University of California, San Diego.
11:20 am	<b>SS1-TuM10</b> Configurational Stability and Surface Diffusion of Rhodium Clusters on Rh(100). G.L. KELLOGG, Sandia National Laboratories.	<b>SS2-TuM10</b> UV Irradiation of Physisorbed Overlayers: CD <sub>3</sub> I/MgO(100): Probing Photofragmentation Dynamics, Adsorbate Orientation and Overlayer Morphology. D.H. FAIRBROTHER, K.A. BRIGGMAN, P.C. STAIR, E. WEITZ, Northwestern University.
11:40 am	<b>SS1-TuM11</b> Scaling Properties of Fe Growth on Fe(001) Whiskers. J.A. STROSCIO, D.T. PIERCE, National Institute of Standards & Technology.	<b>SS2-TuM11</b> Molecular Desorption of Methyl Halides from GaAs(110). P.H. LU, P.J. LASKY, Q.Y. YANG, R.M. OSGOOD, JR., Columbia University.

**NANO 3/NANOMETER-SCALE SCIENCE AND TECHNOLOGY**  
**Room A209 - Session NS1-TuM pg. 166**

**Nanostructured Materials**

**Moderator:** D. Bonnell, University of Pennsylvania.

**NANO 3/NANOMETER-SCALE SCIENCE AND TECHNOLOGY**  
**Room A207 - Session NS2-TuM pg. 168**

**Nanoelectronics**

**Moderator:** T. Higman, University of Minnesota.

8:20 am	<b>NS1-TuM1</b> Nanocluster Surface Science by LDA Theory. <b>D.R. JEN-NISON</b> , Sandia National Laboratories. <b>Y.S. LI</b> , Biosym Technologies, Inc. <b>P.A. SCHULTZ</b> , M.P. SEARS, T. KLITSNER, P. FEIBELMAN, Sandia National Laboratories.	<b>NS2-TuM1</b> <b>INVITED</b> Application of Nanoelectronic Devices. <b>J.N. RANDALL</b> , Texas Instruments.
8:40 am	<b>NS1-TuM2</b> Kinetics and Thermodynamics of Organic Nanocluster Formation. <b>P.V. SHIBAEV</b> , Moscow State University, Russia. <b>K. SCHAUMBURG</b> , K. BRUNFELDT, CSMI, Denmark.	Invited talk continued.
9:00 am	<b>NS1-TuM3</b> <b>INVITED</b> Nanostructured Solids as Interface-determined Systems. <b>H.-E. SCHAEFER</b> , Stuttgart University, Germany.	<b>NS2-TuM3</b> Quantum Cellular Automata. <b>P.D. TOUGAW</b> , C.S. LENT, W. POROD, University of Notre Dame.
9:20 am	Invited talk continued.	<b>NS2-TuM4</b> Computational Behavior in Coulomb Blockade Arrays. <b>M.G. ANCONA</b> , <b>R.W. RENDELL</b> , Naval Research Laboratory.
9:40 am	<b>NS1-TuM5</b> Diffusion Controlled Growth of Metallic Nanoclusters at Selected Surface Sites. <b>G.M. FRANCIS</b> , R.E. PALMER, J.R.A. CLEAVER, Cavendish Laboratory, United Kingdom.	<b>NS2-TuM5</b> Photovoltaic Effect for Resonant Tunneling Structure of Quantum Dots. <b>M. SUMETSKII</b> , AT&T Bell Laboratories.
10:00 am	<b>NS1-TuM6</b> The Surface Composition of Semiconductor Nanocrystals. <b>J.E. BOWEN KATARI</b> , V.L. COLVIN, A.P. ALIVISATOS, University of California, Berkeley.	<b>NS2-TuM6</b> A Novel Method for Producing Nanostructures in Silicon Inversion Layers. <b>B. CAMPBELL</b> , G.H. BERNSTEIN, X. HUANG, University of Notre Dame.
10:20 am	<b>NS1-TuM7</b> Preparation and Characterization of Thiol Capped Silver Nanocrystals. <b>M.M. ALVAREZ</b> , <b>S. MURTHY</b> , R.L. WHETTEN, J.M. HAMPIKIAN, Georgia Institute of Technology.	<b>NS2-TuM7</b> Nanolithography: STM and 50 kV e-beam. <b>E.A. DOBISZ</b> , F.K. PERKINS, C.R.K. MARRIAN, S.L. BRANDOW, T.S. KOLOSKI, J.M. CALVERT, Naval Research Laboratory.
10:40 am	<b>NS1-TuM9</b> Polymer-Nanocrystal Composites - Integrated Materials for Electrooptical and Electronical Devices. <b>J.P. SPATZ</b> , A. ROESCHER, M. MÖLLER, Universität Ulm, Germany.	<b>NS2-TuM8</b> Patterning of Self-Assembled Monolayers by Electron Beams for High-Resolution Lithography. <b>J. LERCEL</b> , G.F. REDINBO, F.D. PARDO, M. ROOKS, R.C. TIBERIO, P. SIMPSON, <b>H.G. CRAIGHEAD</b> , Cornell University. C.W. SHEEN, A.N. PARIKH, D.L. ALLARA, Pennsylvania State University.
11:00 am	<b>NS1-TuM10</b> Characterization and Nanomanipulation of ZnS Nanoclusters via Atomic Force Microscopy. <b>J.E. COURY</b> , E.C. PITTS, L.A. BOTTOMLEY, R. SHORROSH, R.H. FELTON, Georgia Institute of Technology.	<b>NS2-TuM9</b> <b>INVITED</b> Manufacturing Considerations for Quantum-Effect Devices. <b>M. PECKERAR</b> , Naval Research Laboratory.
11:20 am	<b>NS1-TuM11</b> The Structure and Mechanical Properties of MoSi <sub>2</sub> -Based Nanolayer Composites. <b>H. KUNG</b> , T.R. JERVIS, N. YU, T.E. MITCHELL, M. NASTASI, Los Alamos National Laboratory.	Invited talk continued.
11:40 am		<b>NS2-TuM11</b> Results of NANO-II and Development of Nanotechnology in Russia. <b>V.N. ALFEEV</b> , Academy of Technological Sciences of the Russian Federation.

# Tuesday Morning, October 25, 1994

## APPLIED SURFACE SCIENCE

Room A101 - Session AS-TuM pg. 170

### Surface Chemistry and Contamination

Moderator: J.E. Fulghum, Kent State University.

## PLASMA SCIENCE

Room A109 - Session PS-TuM pg. 171

### Plasma Process & Reactor Modeling

Moderator: L.A. Berry, Oak Ridge National Laboratories.

8:20 am	<b>AS-TuM1 INVITED</b> Overview of Particle Detection on Silicon Wafers. <b>T. FRANCIS</b> , Applied Materials.	<b>PS-TuM1</b> Alternate Designs for High Plasma Density Inductively Coupled Etching Tools. <b>P.L.G. VENTZEK</b> , <b>M. GRAPPERHAUS</b> , <b>M.J. KUSHNER</b> , University of Illinois, Urbana.
8:40 am	Invited talk continued.	<b>PS-TuM2</b> Design of a Surface Reflection Neutral Beam Source for Semiconductor Processing. <b>C.A. NICHOLS</b> , <b>D.M. MANOS</b> , College of William & Mary.
9:00 am	<b>AS-TuM3</b> Limitations of Surface Analytical Techniques for Determining the Surface Composition of Bimetallic Particles. <b>A.G. SAULT</b> , Sandia National Laboratories.	<b>PS-TuM3</b> Modeling the Electromagnetic Field Excitation of Low-Pressure, High-Density Plasma Sources. <b>T.A. GROTHORN</b> , Michigan State University.
9:20 am	<b>AS-TuM4</b> Analysis and Imaging of Surfaces, Layers, and Particles by TOF - SIMS and Laser - SNMS. <b>B. HAGENHOFF</b> , <b>E. NIEHUIS</b> , <b>H.-G. CRAMER</b> , <b>R. MÖLLERS</b> , <b>H. RULLE</b> , <b>J. ZEHPFENNING</b> , <b>A. BENNINGHOVEN</b> , Universität Münster, Germany.	<b>PS-TuM4</b> The Effect of Time Varying Sheaths on Radially Dependent Ion Energy Distributions in Inductively Coupled Plasmas. <b>R.J. HOEKSTRA</b> , <b>M.J. KUSHNER</b> , University of Illinois, Urbana.
9:40 am	<b>AS-TuM5</b> Continuous Electron Stimulated Oxygen Atom Emission from Ag Permeation Membranes. <b>G.A. MINER</b> , <b>R.A. OUTLAW</b> , <b>M.R. DAVIDSON</b> , NASA Langley Research Center.	<b>PS-TuM5 INVITED</b> Modelling of Plasma Etching Discharges. <b>T.J. BARTEL</b> , Sandia National Laboratories. <b>D. ECONOMOU</b> , University of Houston.
10:00 am	<b>AS-TuM6</b> Oxidation of Gold by UV and Ozone at 25°C. <b>D.E. KING</b> , National Renewable Energy Laboratory.	Invited talk continued.
10:20 am	<b>AS-TuM7</b> Quantitative XPS Analysis of Complex Hydrated Inorganic Compounds. <b>C.R. ANDERSON</b> , Martin Marietta Laboratories.	<b>PS-TuM7</b> Modeling the Chemistry in Chlorine Plasmas using a Well Stirred Reactor Model with Comparison to Experimental Measurements. <b>E. MEEKS</b> , <b>J.W. SHON</b> , Sandia National Laboratories. <b>Y. RA</b> , <b>P. JONES</b> , Lam Research Corporation.
10:40 am	<b>AS-TuM8</b> The Influence of Hydrogen on LEIS Signals. <b>R.H. BERGMANS</b> , <b>M.J.H. VANHOMMERIG</b> , <b>A.W. DENIER VAN DER GON</b> , <b>H.H. BRONGERSMA</b> , Eindhoven University of Technology, The Netherlands.	<b>PS-TuM8</b> Role of Etch Products in Si Etching by Cl <sub>2</sub> in High Density Plasma Sources. <b>C. LEE<sup>†</sup></b> , <b>M.A. LIEBERMAN</b> , <b>D.B. GRAVES</b> , University of California, Berkeley.
11:00 am	<b>AS-TuM9</b> XPS and Infrared Spectroscopy of Cu-Implanted Silica and Borosilicate Glasses. <b>D.O. HENDERSON</b> , <b>M.A. GEORGE</b> , <b>A. BURGER</b> , <b>R. MU</b> , <b>S.H. MORGAN</b> , <b>W.E. COLLINS</b> , Fisk University. <b>R.H. MAGRUDER III</b> , Vanderbilt University. <b>C.W. WHITE</b> , <b>R.A. ZUHR</b> , Oak Ridge National Laboratory.	<b>PS-TuM9 INVITED</b> Molecular Dynamics Simulations of Si Etching. <b>H. FEIL</b> , Philips Research Laboratories, The Netherlands.
11:20 am	<b>AS-TuM10</b> Investigations of the Surface Chemistry of Pathogenic Silicates. <b>S. SEAL</b> , <b>S. HARDCASTLE</b> , <b>T.L. BARR</b> , University of Wisconsin, Milwaukee. <b>H. HE</b> , <b>J. KLINOWSKI</b> , <b>P. EVANS</b> , University of Cambridge, United Kingdom.	Invited talk continued.
11:40 am	<b>AS-TuM11</b> Characterization of Free Carbon in Silicon Carbide. <b>T.E. PAULSON</b> , <b>V.J. BOJAN</b> , <b>B.M. WICHTERMAN</b> , <b>C.G. PANTANO</b> , Pennsylvania State University.	<b>PS-TuM11</b> Ion-Neutral Synergism in Ar-Enhanced Fluorine Etching of Silicon: A Molecular Dynamics Simulation. <b>M.E. BARONE<sup>†</sup></b> , <b>D.B. GRAVES</b> , University of California, Berkeley.

**VACUUM TECHNOLOGY**

Room A102 - Session VT-TuM pg. 173

**Vacuum Systems for Accelerators and Fusion****Moderator:** M. A. Benapfl, Lawrence Livermore National Laboratory.**THIN FILM**

Room A105 - Session TF-TuM pg. 175

**Thin Films for Sensors****Moderator:** S. Semancik, National Institute of Standards and Technology.

8:20 am	<b>VT-TuM1</b> Theoretical Submonolayer Adsorption Isotherms for Hydrogen on a Heterogeneous Surface. <b>J.P. HOBSON</b> , National Vacuum Technologies, Inc.	<b>TF-TuM1 INVITED</b> Thin Film Sensors for Automobiles. <b>Y. TAGA</b> , Toyota Central Research & Development Laboratories, Japan.
8:40 am	<b>VT-TuM2</b> Cryosorption Pumping of H <sub>2</sub> and He in Cryogenic Accelerator Systems. <b>M.G. RAO</b> , H.F. DYLLA, Continuous Electron Beam Accelerator Facility. <b>W. TURNER</b> , Lawrence Berkeley Laboratory.	Invited talk continued.
9:00 am	<b>VT-TuM3 INVITED</b> D-T Experiments in TFTR. <b>P.H. LA MARCHE</b> , Princeton University.	<b>TF-TuM3 INVITED</b> Thin-Film-Based SAW Chemical Sensor Arrays. <b>A.J. RICCO</b> , Sandia National Laboratories. <b>C. XU</b> , R.M. CROOKS, Texas A&M University. <b>R.E. ALLRED</b> , Adherent Technologies, Inc.
9:20 am	Invited talk continued.	Invited talk continued.
9:40 am	<b>VT-TuM5</b> Pumping Characteristics of a Cryopump with Ar Sorbent in He and in D <sub>2</sub> /He Mixture. <b>M.M. MENON</b> , Oak Ridge National Laboratory. <b>G.J. LAUGHON</b> , General Atomics. <b>R. MAINGI</b> , M.R. WADE, D.L. HILLIS, Oak Ridge National Laboratory. <b>M.A. MAHDAVI</b> , General Atomics.	<b>TF-TuM5</b> Structure and Mass Sensing Properties of Zirconium Carboxylate Thin Films. <b>G.O. NOONAN</b> , K.G. SEVERIN, J.S. LEDFORD, Michigan State University.
10:00 am	<b>VT-TuM6</b> The Vacuum Integrity of the CEBAF Superconducting RF Cavity Assemblies. <b>H.F. DYLLA</b> , J. BENESCH, J. MAMMOSSER, M. WISEMAN, P. KNEISEL, M.G. RAO, W. SCHNEIDER, K. FINGER, Continuous Electron Beam Accelerator Facility.	<b>TF-TuM6</b> Effect of Deposition Parameters on Microstructure, Conductivity, and Sensitivity of WO <sub>3</sub> Thin Films for Gas Sensing Applications. <b>D.J. FRANKEL</b> , E.L. WITTMAN, K. SNOW, S.T. HESS, R.J. LAD, J.F. VETELINO, University of Maine.
10:20 am	<b>VT-TuM7</b> The Effect of Physisorbed Gases on the Quality Factor of Niobium Superconducting Radio Frequency Cavities. <b>P. KNEISEL</b> , M.G. RAO, Continuous Electron Beam Accelerator Facility.	<b>TF-TuM7</b> Increasing the Selectivity of Commercially Available Tin-Oxide Based Sensors for Process Environments. <b>R.M. HAWK</b> , A. NARAYANASWAMY, University of Arkansas, Little Rock.
10:40 am	<b>VT-TuM8</b> Ion Pump Speed Optimization for Low Pressure Operation. <b>M. DE SIMON</b> , M. SPAGNOL, Varian S.p.A., Italy.	<b>TF-TuM8</b> Fabrication of Thin Sensing Films by MicroCVD. <b>S. MAJOO</b> , J.W. SCHWANK, J.L. GLAND, K.D. WISE, University of Michigan.
11:00 am	<b>VT-TuM9 INVITED</b> NIF Vacuum Chamber. <b>R.W. WAVRIK</b> , Sandia National Laboratories. <b>D.A. MUIRHEAD</b> , Rockwell Power Systems. <b>V.P. KARPENKO</b> , Lawrence Livermore National Laboratory.	<b>TF-TuM9 INVITED</b> Magnetoresistive Sensors for Ultra-High Density Magnetic Recording. <b>J.K. HOWARD</b> , IBM Storage Systems Division.
11:20 am	Invited talk continued.	Invited talk continued.
11:40 am	<b>VT-TuM11</b> A Non-circular UHV Seal that Functions between $\pm 200^\circ\text{C}$ . <b>R.A. CHILDS</b> , <b>J.E. RICE</b> , Massachusetts Institute of Technology.	<b>TF-TuM11</b> Object Imaging with a Piezoelectric Tactile Integrated Circuit Sensor. <b>E.S. KOLESAR</b> , C.S. DYSON, Texas Christian University.



# Tuesday Morning, October 25, 1994

## ELECTRONIC MATERIALS/MANUFACTURING SCIENCE AND TECHNOLOGY

Room A108 - Session EMMS-TuM pg. 176

### Surface Preparation and Passivation

Moderator: S.M. George, University of Colorado, Boulder.

## MANUFACTURING SCIENCE AND TECHNOLOGY

Room A110 - Session MS-TuM pg. 178

### Manufacturing Overview and Environmental Issues

Moderator: G. W. Rubloff, North Carolina State University.

8:20 am	<b>EMMS-TuM1 INVITED</b> Very High Quality Thin Gate Oxide Film Formation Technology. T. OHMI, Tohoku University, Japan.	<b>MS-TuM1 INVITED</b> Environmental Consciousness: A Strategic Competitiveness Issue for the Microelectronics Industry. G.E. PITTS, Microelectronics & Computer Tech. Corp.
8:40 am	Invited talk continued.	Invited talk continued.
9:00 am	<b>EMMS-TuM3</b> STM/XPS Investigation on the Chemical Oxidation of Hydrogen Terminated Si(111) Surface. U. NEUWALD, U. MEMMERT, R.J. BEHM, Universität Ulm, Germany.	<b>MS-TuM3 INVITED</b> Integrating Regulatory Policy & Science -- Can It Be Done? B.C. JORDAN, U.S. Environmental Protection Agency.
9:20 am	<b>EMMS-TuM4</b> An MEIS Study of the Initial Stages of the Interaction of Oxygen with Si(111). E.P. GUSEV, E. GARFUNKEL, H.C. LU, T. GUSTAFSSON, Rutgers University.	Invited talk continued.
9:40 am	<b>EMMS-TuM5</b> Controlled Nitrogen-Atom Incorporation at Si-SiO <sub>2</sub> Interfaces by a Low-Temperature (300°C) Pre-Deposition Remote Plasma Oxidation Using N <sub>2</sub> O. D.R. LEE, G. LUCOVSKY, North Carolina State University.	<b>MS-TuM5 INVITED</b> Environment, Safety and Health Issues in Manufacturing. H.R. KERBY, SEMATECH.
10:00 am	<b>EMMS-TuM6</b> Silicon Oxide Etching using Gas Phase HF/Solvent Mixtures. A.J. MUSCAT, A.S. LAWING, H. XU, H.H. SAWIN, Massachusetts Institute of Technology.	Invited talk continued.
10:20 am	<b>EMMS-TuM7</b> Ion Beam Characterization of Si(100) Surfaces during Wet Chemical Cleaning. V. ATLURI, N. HERBOTS, P. YE, R.J. CULBERTSON, Arizona State University.	<b>MS-TuM7 INVITED</b> Factory of the Future: The "Whole Factory" View. S. HARRELL, SEMATECH.
10:40 am	<b>EMMS-TuM8</b> AFM Characterization of Pillar Structures on RCA Cleaned Silicon Surfaces. B.K. FURMAN, D.A. NEUGROSCHL, S.L. COHEN, R. TSAI, K. POPE, M. LIEHR, IBM TJ Watson Research Center. S. BASILIERE, S. ESTES, M.J. FLEMING, R. GAYLORD, C. GOW, W. SYVERSON, IBM Microelectronic Division.	Invited talk continued.
11:00 am	<b>EMMS-TuM9</b> Low Damage Surface Cleaning of CdTe by Hydrogen ECR Plasma. Y. LUO, P. LASKY, M. CHANG SHIH, R.M. OSGOOD, JR., Columbia University.	<b>MS-TuM9 INVITED</b> Research Opportunities in Semiconductor Manufacturing Science and Technology. D.J.C. HERR, The Semiconductor Research Corporation.
11:20 am	<b>EMMS-TuM10</b> The Thermal Stability and Effect of Atomic Deuterium Exposure on S-Passivated InP(100)-(1x1). G.W. ANDERSON, M.C. HANF, P.R. NORTON, University of Western Ontario, Canada. Z.H. LU, M.J. GRAHAM, National Research Council, Canada.	Invited talk continued.
11:40 am	<b>EMMS-TuM11</b> Thermal Effects on GaAs(001) Surface Prepared by Deoxygenated and Deionized Water Treatment. Y. HIROTA, T. OGINO, NTT Basic Research Labs, Japan. Y. WATANABE, M. OSHIMA, NTT Interdisciplinary Research Labs, Japan.	<b>MS-TuM11</b> Photocatalytic Oxidation for Point-of-Use VOC Abatement in Microelectronics Manufacturing. M. AMEEN, R. VARGHESE, J. NICO, G.B. RAUPP, Arizona State University.

**BIOMATERIAL INTERFACES****Room A106 - Session BI-TuM pg. 179****Protein-Solid Surface Interactions****Moderator:** B.D. Ratner, University of Washington.

8:20 am	<b>BI-TuM1 INVITED</b> Molecular Recognition at Protein-Biological Composite Interfaces. <b>P.S. STAYTON</b> , R. CLARK, C.L. LONG, L. KLUMB, A. CHILKOTI, A.A. CAMPBELL, G. DROBNY, University of Washington and Pacific Northwest Laboratories.	
8:40 am	Invited talk continued.	
9:00 am	<b>BI-TuM3</b> Surface Plasmon Imaging of Biotin-Streptavidin Binding on UV-Photopatterned Alkanethiol Monolayers Self-Assembled on Gold. <b>D. PISCEVIC</b> , Max-Planck Institute for Polymer Research, Germany. <b>M. TARLOV</b> , National Institute of Standards & Technology. <b>W. KNOLL</b> , Max-Planck Institute for Polymer Research, Germany.	
9:20 am	<b>BI-TuM4</b> Proteins at Surfaces Studied by Scanning Probe Microscopy. <b>C.J. ROBERTS</b> , M.C. DAVIES, D.E. JACKSON, K.M. SHAKESHEFF, S.J.B. TENDLER, P.M. WILLIAMS, University of Nottingham, United Kingdom.	
9:40 am	<b>BI-TuM5 INVITED</b> Plasma Protein Interactions with Solid Surfaces. <b>R.E. MARCHANT</b> , C. SIEDLECKI, S.J. EPELL, Case Western Reserve University.	
10:00 am	Invited talk continued.	
10:20 am	<b>BI-TuM7</b> The Effect of Oligo(ethyleneoxide) Chainlength on the Protein Resistance of Plasma Deposited Thin Films. <b>B.D. RATNER</b> , <b>E.E. JOHNSTON</b> , University of Washington.	
10:40 am	<b>BI-TuM8</b> Bioreactivity of Titanium Implant Alloys. <b>S.J. KERBER</b> , Material Interface, Inc.	
11:00 am	<b>BI-TuM9</b> Electrochemically and Glow Discharge Modified Titanium Surfaces used for Biological Evaluation. <b>B.-O. ARONSSON</b> , J. LAUSMAA, M. RODAHL, B. KASEMO, Chalmers University of Technology, Sweden.	
11:20 am	<b>BI-TuM10</b> Molecular Machining by Enzymatic Modification of a Chemisorbed Lipid Monolayer. <b>B.M. PEEK</b> , T.E. WERTZ, D.C. TURNER, D.D. ARCHIBALD, Naval Research Laboratory. <b>D. LEACH-SCAMPAVIA</b> , University of Washington. <b>B.P. GABER</b> , Naval Research Laboratory.	
11:40 am	<b>BI-TuM11</b> Static Secondary Ion Mass Spectrometry Study of Amino Acids on Acidic and Basic Polymer Surfaces. <b>S. KOVATCH</b> , Y. KIM, E. BEKOS, J.A. GARDELLA, JR., State University of New York, Buffalo.	

# MY SCHEDULE

## Tuesday Morning, October 25, 1994

TIME	SESSION	ROOM
8:20 am		
8:40 am		
9:00 am		
9:20 am		
9:40 am		
10:00 am		
10:20 am		
10:40 am		
11:00 am		
11:20 am		
11:40 am		
12:00 pm		
12:45 pm		
Lunch		
when		
with		where

### OTHER EVENTS TUESDAY

- 7:00 a.m. Companion's Program (see insert) (**Silver Room (H)**)
- 8:00 a.m. AVEM Seminar (**Ballroom Section D (H)**)
- 9:00 a.m. Science Educators Workshop (**Denver Room (H)**)
- 9:00 a.m. Ion Gauges (**Birch Room (H)**)
- 12:00 Noon Science Educators Luncheon (**Spruce Room (H)**)
- 12:00 Noon Topical Conferences Luncheon (**Colorado Room (H)**)
- 12:00 Noon Recommended Practices Executive Committee Luncheon (**Aspen Room (H)**)
- 12:00 Noon AVEM Luncheon (**Gr. Ballroom Section A (H)**)

H=Radisson Hotel  
CC=Colorado Convention Center

### SHORT COURSES TUESDAY

- 8:30 a.m. Vacuum Technology (**Room C109 (CC)**)
- 8:30 a.m. A Comprehensive Course on Surface Analysis: AES,XPS,SIMS, Depth Profiling, & ISS/RBS (**Room C107 (CC)**)
- 8:30 a.m. Basics of Radio Frequency (RF) Technology (**Room C105 (CC)**)
- 8:30 a.m. Operation and Maintenance of Vacuum Pumping Systems (**Room C103 (CC)**)
- 8:30 a.m. Sputter Deposition (**Room C101 (CC)**)
- 8:30 a.m. Fundamentals and Process Characterization of Ion Implantation (**Room C112 (CC)**)
- 8:30 a.m. Fundamentals of Semiconductor Characterization: Electrical and Optical Techniques (**Room C110 (CC)**)
- 8:30 a.m. Materials Microcharacterization (**Room C108 (CC)**)
- 8:30 a.m. Safety Concerns in the use of Vacuum Equipment
- 8:30 a.m. Vacuum System Design (**Room C104 (CC)**)
- 8:30 a.m. X-Ray Photoelectron Spectroscopy (XPS/ESCA) (**Room C107 (CC)**)

### Special or Focus Area Sessions

#### Sensors, In-situ Diagnostics, Process Control

TF-TuM Thin Films for Sensors

#### Surface Contamination and Control

EMMS-TuM Surface Preparation and Passivation

# MY SCHEDULE

## Tuesday Afternoon, October 25, 1994

TIME	SESSION	ROOM
2:00 pm		
2:20 pm		
2:40 pm		
3:00 pm		
3:20 pm		
3:40 pm		
4:00 pm		
4:20 pm		
4:40 pm		
5:00 pm		

### OTHER EVENTS TUESDAY

- 5:20 p.m. ASS Division Business Meeting (Room A101 (CC))
- 5:20 p.m. EMP Division Business Meeting (Room A108 (CC))
- 5:20 p.m. NST Division Business Meeting (Room A207 (CC))
- 5:20 p.m. SS Division Business Meeting (Room A205 (CC))
- 5:20 p.m. TF Division Business Meeting (Room A105 (CC))
- 5:20 p.m. VT Division Business Meeting (Room A102 (CC))
- 6:30 p.m. VM Division Executive Committee Meeting (Birch Room (H))
- 6:30 p.m. EMPD Executive Committee Meeting & Dinner (Century Room (H))
- 6:30 p.m. Recommended Practices Committee Meeting & Dinner (Gr. Ballroom Section B (H))
- 6:30 p.m. SS Division Executive Committee Meeting & Dinner (Gold Room (H))
- 6:30 p.m. TF Division Executive Committee Meeting & Dinner (Aspen Room (H))
- 6:30 p.m. NST Division Meeting & Dinner (Cedar Room (H))
- 6:30 p.m. PST Division Executive Committee Meeting & Dinner (Colorado Room (H))
- 6:30 p.m. Placement Center Workshop (Columbine Room (H))
- 8:00 p.m. ASTM E.42/ASSD Workshop (Jr. Ballroom (H))

H=Radisson Hotel  
CC=Colorado Convention Center

### SHORT COURSES TUESDAY

- 8:30 a.m. Vacuum Technology (Room C109 (CC))
- 8:30 a.m. A Comprehensive Course on Surface Analysis: AES,XPS,SIMS, Depth Profiling, & ISS/RBS (Room C107 (CC))
- 8:30 a.m. Basics of Radio Frequency (RF) Technology (Room C105 (CC))
- 8:30 a.m. Operation and Maintenance of Vacuum Pumping Systems (Room C103 (CC))
- 8:30 a.m. Sputter Deposition (Room C101 (CC))
- 8:30 a.m. Fundamentals and Process Characterization of Ion Implantation (Room C112 (CC))
- 8:30 a.m. Fundamentals of Semiconductor Characterization: Electrical and Optical Techniques (Room C110 (CC))
- 8:30 a.m. Materials Microcharacterization (Room C108 (CC))
- 8:30 a.m. Safety Concerns in the use of Vacuum Equipment
- 8:30 a.m. Vacuum System Design (Room C104 (CC))
- 8:30 a.m. X-Ray Photoelectron Spectroscopy (XPS/ESCA) (Room C107 (CC))

### Special or Focus Area Sessions

#### Silicon-based Optoelectronics

EM-TuA Silicon-based Optoelectronics

#### Sensors, In-situ Diagnostics, Process Control

BI-TuA The Biosensor-Biology Interface

#### Surface Contamination and Control

VT-TuA Vacuum System Outgassing and Cleaning

# Tuesday Afternoon, October 25, 1994

## SURFACE SCIENCE

Room A205 - Session SS1-TuA pg. 182

### Dynamics and Kinetics of Surface Processes

Moderator: D.C. Jacobs, University of Notre Dame.

## SURFACE SCIENCE

Room A201 - Session SS2-TuA pg. 183

### Nucleation and Growth: Metals

Moderator: D.M. Zehner, Oak Ridge National Laboratories.

2:00 pm	<b>SS1-TuA1</b> Dynamic of the Interaction of O Atoms with O <sub>2</sub> /Pt(111). C.T. RETTNER, J. LEE, D.J. AUERBACH, IBM Research Division.	<b>SS2-TuA1</b> STM Studies of Curvature Driven Mass Flow on the Au(111) Surface. J.G. MCLEAN, D.R. PEALE, B.H. COOPER, Cornell University.
2:20 pm	<b>SS1-TuA2</b> O <sub>2</sub> Adsorption on Silver Surfaces: F. BUATIER DE MONGEOT, M. ROCCA, U. VALBUSA, CFSBT-CNR and INFN, Italy.	<b>SS2-TuA2</b> Apparent Giant Applanation of Small 2D Ag Islands on Ag(100). P.J. BEDROSSIAN, Lawrence Livermore National Laboratory. B. POELSEMA, University of Twente, The Netherlands. G. ROSENFELD, IGV-Forschungszentrum Jülich, Germany. L. JORRITSMA, University of Twente, The Netherlands. N.N. LIPKIN, G. COMSA, IGV-Forschungszentrum Jülich, Germany.
2:40 pm	<b>SS1-TuA3</b> CO <sub>2</sub> Sticking on Pt(111); The Role of Kinetic Energy and Internal Degrees of Freedom. D. KULGINOV, M. PERSSON, C. ÅKERLUND, I. ZORIC, B. KASEMO, Chalmers University of Technology, Sweden.	<b>SS2-TuA3</b> A RHEED Specular Diffraction Spot Intensity Study of Ag(111) Homoepitaxy. K. ROOS, Bradley University. K. STANLEY, Iowa State University. C. PAPAGEORGIOPOULOS, University of Ioannine, Greece. M.C. TRINGIDES, Iowa State University.
3:00 pm	<b>SS1-TuA4</b> Investigations of the Adsorption and Desorption Dynamics of D <sub>2</sub> at Si Surfaces. K.W. KOLASINSKI, Fritz-Haber-Institut der Max-Planck-Gesellschaft, Germany.	<b>SS2-TuA4</b> Enhanced 2-Dimensional Growth of Cu on Cu(100) by Seeding. A.K. SWAN, J.F. WENDELKEN, Oak Ridge National Laboratory.
3:20 pm	<b>SS1-TuA5</b> INVITED Probing Reactive Deposition and Surface Dynamics using In Situ, Real-Time Emission Microscopy. M.E. KORDESCH, Ohio University.	<b>SS2-TuA5</b> Kinetic Roughening in a Multilayer Nucleation and Growth Model for M/M(100) Homoepitaxy. M.C. BARTELT, J.W. EVANS, Iowa State University.
3:40 pm	Invited talk continued.	<b>SS2-TuA6</b> First-Principles Calculations of Transition-Metal Surface Stress. P.J. FEIBELMAN, Sandia National Laboratories.
4:00 pm	<b>SS1-TuA7</b> Simulation of Complex Reaction/Desorption Kinetics using a Simple Stochastic Method. F.A. HOULE, W.D. HINSBERG, IBM Almaden Research Center.	<b>SS2-TuA7</b> Strain Induced Alloying of Immiscible Metals in Thin Film Systems. J.L. STEVENS, R.Q. HWANG, Sandia National Laboratories.
4:20 pm	<b>SS1-TuA8</b> Dynamics of Collisions between Inert Gases and the Surfaces of Liquid Metals. G.M. NATHANSON, W.R. RONK, D.V. KOWALSKI, University of Wisconsin, Madison.	<b>SS2-TuA8</b> Surface Alloying and Dealloying of Au on Ni(110) and Ni(111) Studied by STM and RBS. F. BESENBACHER, L. PLETH NIELSEN, I. STENSGAARD, E. LAEGSGAARD, Aarhus University, Denmark.
4:40 pm	<b>SS1-TuA9</b> Interactions between Coadsorbed Molecules. D.C. SKELTON, D.-H. WEI, S.D. KEVAN, University of Oregon.	<b>SS2-TuA9</b> Using STM to Understand Diffraction Oscillations: Fe Growth on Cu(100). D.D. CHAMBLISS, IBM Almaden Research Center. K.E. JOHNSON, Goucher College.
5:00 pm	<b>SS1-TuA10</b> A New Technique to Measure Surface Diffusion with the STM. M.L. LOZANO, M.C. TRINGIDES, Iowa State University.	<b>SS2-TuA10</b> Long Jumps in the Surface Diffusion of Adatoms: W, Ni, and Pd on W(211). D. COWELL SENFT, G. EHRLICH, University of Illinois, Urbana-Champaign.

**NANO 3/NANOMETER-SCALE SCIENCE AND TECHNOLOGY**

Room A209 - Session NS1-TuA pg. 185

**Nanostructure Properties: Chemical and Electrochemical****Moderators:** M. Hara, RIKEN, Japan. R.J. HAMERS, University of Wisconsin.**NANO 3/NANOMETER-SCALE SCIENCE AND TECHNOLOGY**

Room A207 - Session NS2-TuA pg. 186

**Nanomechanics and Nanotribology: I****Moderator:** S. Cohen, Weizman Institute of Science.

2:00 pm	<b>NS1-TuA1</b> Electron Tunneling through Water Clusters in Electrochemical STM. <b>S.M. LINDSAY</b> , T.W. JING, J. PAN, D. LAMPNER, A. VAUGHT, J.P. LEWIS, D.F. SANKEY, Arizona State University.	<b>NS2-TuA1</b> Atomistic Modelling of Friction and the Interaction between AFM Tips and Ionic Surfaces. <b>A.L. SHLUGER</b> , A.L. ROHL, D.H. GAY, The Royal Institution of Great Britain. R.M. WILSON, R.T. WILLIAMS, Wake Forest University.
2:20 pm	<b>NS1-TuA2</b> The Nature of Mixed Adlayers on Platinum Single Crystal Electrodes Probed by In Situ STM and Infrared Spectroscopy. <b>I. VILLEGAS</b> , M.J. WEAVER, Purdue University.	<b>NS2-TuA2</b> Molecular Dynamics Simulations of Metal-Oxide Surfaces and Interfaces. <b>F.H. STREITZ</b> , J.W. MINTMIRE, Naval Research Laboratory.
2:40 pm	<b>NS1-TuA3 INVITED</b> Scanning Probe Microscopy of Organic Materials. <b>J.E. FROMMER</b> , IBM Almaden Research Center.	<b>NS2-TuA3</b> Electron-Ion Dynamics: A New Technique for Simulating both Electronic Transitions and Atomic Motion in Molecules and Materials. <b>R.E. ALLEN</b> , Texas A&M University.
3:00 pm	Invited talk continued.	<b>NS2-TuA4</b> Scanning Near-Field Acoustic Microscopy: Nanoscale Material Properties. <b>N.A. BURNHAM</b> , A.J. KULIK, G. GREMAUD, Swiss Federal Institute of Technology, Switzerland.
3:20 pm	<b>NS1-TuA5</b> Molecular Scale Topographic Features and Electronic Structure in Thin Organic Films Observable by STM. <b>R.C. WHITE</b> , B. BIRCHFIELD, E.N. SCHULMAN, Columbia University.	<b>NS2-TuA5 INVITED</b> Tribology with the Atomic Force Microscope. <b>D.F. OGLETTREE</b> , J. HU, X.-D. XIAO, C. MORANT, M. SALMERON, Lawrence Berkeley Laboratory.
3:40 pm	<b>NS1-TuA6</b> Atomic Ordering within AlGaAs Alloys Studied using Cross-Sectional Scanning Tunneling Microscopy. <b>A.R. SMITH</b> , C.K. SHIH, Y.C. SHIH, B.G. STREETMAN, University of Texas, Austin.	Invited talk continued.
4:00 pm	<b>NS1-TuA7</b> Characterization of the Gallium Vacancy on GaAs(110). <b>G. LENGEL</b> , R. WILKINS, M. WEIMER, J. GRYKO, R.E. ALLEN, Texas A&M University.	<b>NS2-TuA7</b> Effect of Contact Area on Nanoindentation Curves Obtained using the Atomic Force Microscope. <b>C.F. DRAPER</b> , Vanderbilt University. D.M. SCHAEFER, R.J. COLTON, <b>S.M. HUES</b> , Naval Research Laboratory.
4:20 pm	<b>NS1-TuA8</b> Structure and Electronic States on Reduced SrTiO <sub>3</sub> (110) Surface Observed by Scanning Tunneling Microscopy and Spectroscopy. <b>H. BANDO</b> , Y. AIURA, Electrotechnical Laboratory, Japan. Y. HARUYAMA, University of Tsukuba, Japan. Y. NISHIHARA, Electrotechnical Laboratory, Japan.	<b>NS2-TuA8</b> The Nanomechanics of Single Crystal Au Surfaces. <b>J.E. HOUSTON</b> , P. TANGYUNYONG, Sandia National Laboratories. O.L. WARREN, University of Western Ontario, Canada. R.C. THOMAS, University of New Mexico. T.A. MICHALSKE, Sandia National Laboratories. R.M. CROOKS, Texas A&M University.
4:40 pm	<b>NS1-TuA9</b> An AFM Study of a Surface Bound Colloidal Pd Catalyst and Its Effect on Electroless Ni Particle Size. <b>S.L. BRANDOW</b> , W.J. DRESSICK, C.S. DULCEY, C.R.K. MARRIAN, G.M. CHOW, F.K. PERKINS, J.M. CALVERT, Naval Research Laboratory.	<b>NS2-TuA9</b> Surface Potential Control of Adhesion in an Atomic Force Microscope. <b>J. LARSEN</b> , T.W. JING, D. LAMPNER, S.M. LINDSAY, Arizona State University. Y.Q. LI, Texas A&M University. N.J. TAO, Florida International University.
5:00 pm	<b>NS1-TuA10</b> Direct Observations of Electric Field Gradients Near Field Emission Cathode Arrays. <b>Y. LIANG</b> , University of Pennsylvania. W. GOODHUE, Lincoln Laboratory. <b>D. BONNELL</b> , University of Pennsylvania.	<b>NS2-TuA10</b> Local Modification of Mechanical Properties of Polystyrene-Polyethyleneoxide Blend Surfaces. <b>H.-Y. NIE</b> , JRCAT-NAIR, Japan. M. MOTOMATSU, JRCAT-ATP, Japan. W. MIZUTANI, H. TOKUMOTO, JRCAT-NAIR, Japan.



# Tuesday Afternoon, October 25, 1994

## APPLIED SURFACE SCIENCE/SURFACE SCIENCE Room A101 - Session ASSS-TuA pg. 188

**Electrochemistry and Liquid/Solid Interfaces**  
**Moderator:** G.D. Davis, Martin Marietta Laboratories.

## PLASMA SCIENCE

Room A109 - Session PS-TuA pg. 190

## Advanced Plasma Reactors

**Moderator:** T.D. Mantei, University of Cincinnati.

2:00 pm	<b>ASSS-TuA1</b> Evidence of Specific and Non-Specific Adsorption of $\text{ClO}_4$ on $\text{Ag}(110)$ . <b>A. KRASNOPOLER</b> , E.M. STUVE, University of Washington.	<b>PS-TuA1</b> Helicon Plasma Source Excited by Flat Spiral Coil. <b>J.E. STEVENS</b> , Princeton Plasma Physics Laboratory. M.J. SOWA, Princeton University. J.L. CECCHI, University of New Mexico.
2:20 pm	<b>ASSS-TuA2</b> Surface Chemistry of Water and Hydrogen on Single Crystal $\text{Ni}_3(\text{Al,Ti})$ . <b>Y.-W. CHUNG</b> , <b>W.-J. CHIA</b> , Northwestern University.	<b>PS-TuA2</b> Comparison of High Density Plasma Sources for Silicon Etching: Helical Resonator, Helicon, and ECR. <b>K.V. GUINN</b> , I. TEPERMEISTER, N. BLAYO, F.P. KLEMENS, D.E. IBBOTSON, J.T.C. LEE, AT&T Bell Laboratories.
2:40 pm	<b>ASSS-TuA3</b> In Situ Study of 304 Stainless Steel's Passive Layer Exposed to HCl Acid using a Scanning Tunneling Microscope. <b>J.M. GALLIGAN</b> , <b>T.J. MCKRELL</b> , University of Connecticut.	<b>PS-TuA3</b> Ponderomotive Effects in Helicon Plasmas. <b>R. BROWN</b> , <b>J. GILLAND</b> , <b>N. HERSHKOWITZ</b> , R. BREUN, University of Wisconsin, Madison.
3:00 pm	<b>ASSS-TuA4</b> Tunnel Channels and Imaging Mechanisms in STM: W-, PtIr-, and Ag-Interfaces in Electrolytes. <b>G. REPPHUN</b> , IAC, UNI, 3000 BERN 9, Switzerland. <b>J. HALBRITTER</b> , K&K, IMF I, 76021 Karlsruhe, Germany.	<b>PS-TuA4</b> A High Etch Rate, Highly Selective, Sub-Half-Micron Contact Etch Process in a Low Pressure, High Density TCP Oxide Etcher. <b>P.K. GADGIL</b> , <b>A. ASTHANA</b> , I. MOREY, Lam Research Corporation.
3:20 pm	<b>ASSS-TuA5</b> In Situ Measurement of Thickness Changes with Electrolytic SPM. <b>R. NYFFENEGGER</b> , H. SIEGENTHALER, Universität Bern, Switzerland. <b>P. HÄRING</b> , R. KÖTZ, Paul Scherrer Institut, Switzerland.	<b>PS-TuA5</b> Construction and Characterization of a Multidipole-Confining RF Inductively-Coupled Plasma Etching Source. <b>C. LAI†</b> , B. BRUNMEIER, R.C. WOODS, University of Wisconsin, Madison.
3:40 pm	<b>ASSS-TuA6</b> Electrochemical Etching of $\text{Si}(111)$ Surfaces in Fluoride Solutions Studied by STM and AES. <b>R. HOUBERTZ</b> , Universität des Saarlandes, Germany. <b>U. MEMMERT</b> , Universität Ulm, Germany.	<b>PS-TuA6</b> Large Area Transformer Coupled Plasma for Microelectronics Processing. <b>Z. YU</b> , <b>D.M. SHAW</b> , G.J. COLLINS, Colorado State University.
4:00 pm	<b>ASSS-TuA7 INVITED</b> Effects of Structure and Chemistry on Surface Reactivity in Solution. <b>D.R. BAER</b> , A.S. LEA, Y. LIANG, L.-Q. WANG, M.H. ENGELHARD, Pacific Northwest Laboratory.	<b>PS-TuA7</b> Large Volume Electron Cyclotron Resonance Plasma Generation by Use of Slotted Antenna Microwave Applicator. <b>J. ENGEMANN</b> , M. SCHOTT, F. WERNER, D. KORZEC, University of Wuppertal, Germany.
4:20 pm	Invited talk continued.	<b>PS-TuA8</b> New ECR Plasma Source for UHV Epitaxy. <b>B.J. STANBERY</b> , T.J. ANDERSON, University of Florida, Gainesville.
4:40 pm	<b>ASSS-TuA9</b> AFM and STM Studies of Oxide Formation, Deposition, and Dissolution on Copper Single Crystal Surfaces. <b>A.A. GEWIRTH</b> , J.R. LAGRAFF, M. GE, University of Illinois, Urbana.	<b>PS-TuA9</b> Characteristics of the Non-Magnetic Type Microwave Plasma Etching Reactor with Slot Antenna. <b>H. TAMURA</b> , T. OTSUBO, I. SASAKI, K. OHARA, Y. YAMAGUCHI, S. KATO, Hitachi, Ltd., Japan.
5:00 pm	<b>ASSS-TuA10</b> In Situ Observation of Hg Amalgamation Formation and Stripping on Au using Atomic Force Microscopy. <b>L.A. NAGAHARA</b> , University of Tokyo, Japan. <b>X. YANG</b> , University of Tokyo, Japan & Southeast University, China. <b>K. TONAMI</b> , University of Tokyo, Japan. <b>Y. WEI</b> , Southeast University, China. <b>K. HASHIMOTO</b> , A. FUJISHIMA, University of Tokyo, Japan.	<b>PS-TuA10</b> Performance of a Permanent Magnet ECR Reactor. <b>A. SAPROD†</b> , D. DANE, T.D. MANTEI, University of Cincinnati.

**VACUUM TECHNOLOGY****Room A102 - Session VT-TuA pg. 191****Vacuum System Outgassing and Cleaning****Moderator:** H. F. Dylla, CEBAF.**THIN FILM/VACUUM METALLURGY****Room A105 - Session TFVM-TuA pg. 193****Diamond, Cubic Boron Nitride and Other Ultra-Hard Films II****Moderator:** W.D. Sproul, BIRL, Northwestern University.

2:00 pm	<b>VT-TuA1 INVITED</b> Water: Its Measurement and Control in Vacuum. <b>S.A. TISON</b> , J.P. LOONEY, National Institute of Standards & Technology.	<b>TFVM-TuA1 INVITED</b> Deposition and Characterization of Cubic Boron Nitride Thin Films. <b>R.F. DAVIS</b> , D.J. KESTER, K.S. AILEY, North Carolina State University.
2:20 pm	Invited talk continued.	Invited talk continued.
2:40 pm	<b>VT-TuA3</b> TiN Thin Film on Stainless Steel for Extremely High Vacuum Material. <b>K. SAITOH</b> , S. INAYOSHI, Y. IKEDA, Y. YANG, S. TSUKAHARA, ULVAC Japan, Ltd.	<b>TFVM-TuA3</b> An AES/XPS Study of Ti-B-N Thin Films. <b>M.A. BAKER</b> , A. STEINER, J. HAUPT, W. GISSLER, Institute for Advanced Materials, Italy.
3:00 pm	<b>VT-TuA4</b> SIMS Analysis for Aluminum Surfaces Treated by Glow Discharge Cleaning. <b>J.R. CHEN</b> , SRRC and National Tsing-Hua University, China. <b>G.Y. HSIUNG</b> , Synchrotron Radiation Research Center, China. <b>Y.C. LIU</b> , SRRC and National Tsing-Hua University, China. <b>W.H. LEE</b> , C.C. NEE, National Tsing-Hua University, China.	<b>TFVM-TuA4</b> Electron Cyclotron Resonance Plasma Assisted Growth of Thin Carbon Nitride Films on Si(100): Film Composition and Structure. <b>A. BOUSETTA</b> , A. BENSOUULA, M. LU, University of Houston.
3:20 pm	<b>VT-TuA5</b> Reduction of Water Outgassing from Metal Surfaces by Glow Discharge Cleaning. <b>M. LI</b> , College of William & Mary. <b>H.F. DYLLA</b> , Continuous Electron Beam Accelerator Facility.	<b>TFVM-TuA5</b> Sputtered Carbon Nitride Films. <b>K.G. KREIDER</b> , M.J. TARLOV, G. GILLEN, L.H. ROBINS, L.K. IVES, W.J. BOWERS, R. MARINENKO, National Institute of Standards & Technology.
3:40 pm	<b>VT-TuA6</b> XPS Analysis of Cleaning Procedures for Synchrotron X-ray Beamline Components at the Advanced Photon Source. <b>Y. LI</b> , R.A. ROSENBERG, D. RYDING, R. NIELSEN, C. LIU, D. SHU, T.M. KUZAY, Argonne National Laboratory.	<b>TFVM-TuA6</b> Thermal Behavior of Carbon Nitride and TiN/NbN Superlattice Coatings. <b>S. LOPEZ</b> , M.S. WONG, W.D. SPROUL, Northwestern University.
4:00 pm	<b>VT-TuA7</b> Thermal Outgassing Studies on Machinable Tungsten and TZM Molybdenum Alloy. <b>C. LIU</b> , R.W. NIELSEN, Y. LI, D. RYDING, T.M. KUZAY, Argonne National Laboratory.	<b>TFVM-TuA7</b> Deposition and Properties of Polycrystalline VN/NbN Superlattices. <b>X. CHU</b> , M.S. WONG, W.D. SPROUL, S.A. BARNETT, Northwestern University.
4:20 pm	<b>VT-TuA8</b> Photon Stimulated Desorption (PSD) Measurements of Extruded Copper and of Welded Copper Beam Chambers for the PEP II Asymmetric B-Factor. <b>C.L. FOERSTER</b> , C. LANNI, Brookhaven National Laboratory. <b>C. PERKINS</b> , Stanford Linear Accelerator Center. <b>M. CALDERON</b> , Lawrence Livermore National Laboratory.	<b>TFVM-TuA8</b> Growth Mechanism of Carbon and Related Diamondlike Films Deposited by High Energy C <sup>+</sup> Ions. <b>E. GROSSMAN</b> , G.D. LEMPERT, Soreq NRC, Israel. <b>J. KULIK</b> , J.W. RABALAIS, University of Houston. <b>Y. LIFSHTITZ</b> , Soreq NRC, Israel.
4:40 pm	<b>VT-TuA9</b> Photodesorption from Copper Chamber with Cutting Inner Surface by Broaching. <b>T. KOBARI</b> , M. MATUMOTO, N. HIRANO, MERL Hitachi Ltd., Japan. <b>M. KATANE</b> , M. MATSUZAKI, Hitachi Works, Japan. <b>Y. HORI</b> , M. KOBAYASHI, PF KEK, Japan. <b>M. NAGAI</b> , Hitachi Cable, Japan.	<b>TFVM-TuA9</b> Thickness-Distribution Control of Large-Area DLC Films Formed by CH <sub>4</sub> /H <sub>2</sub> Supremagnetron Plasma. <b>H. KINOSHITA</b> , S. NOMURA, M. HONDA, Shizuoka University, Japan.
5:00 pm	<b>VT-TuA10</b> Characteristics of Artificial Submerged Cavitation Water Jet. <b>S. HAMADA</b> , Ebara Research Co., Japan.	<b>TFVM-TuA10</b> Structural Analysis of Hydrogenated Carbon Films Obtained by Reactive dc Magnetron Sputtering. <b>S. FUJIMAKI</b> , M. KITOH, H. MATSUMOTO, Y. KOKAKU, Hitachi, Ltd., Japan.

# Tuesday Afternoon, October 25, 1994

## ELECTRONIC MATERIALS

Room A108 - Session EM-TuA pg. 194

### Silicon-based Optoelectronics

Moderator: K.J. Bachmann, North Carolina State University.

## MANUFACTURING SCIENCE AND TECHNOLOGY

Room A110 - Session MS-TuA pg. 195

### Advanced Manufacturing Equipment - A

Moderator: M. Liehr, IBM TJ Watson Research Center.

2:00 pm	<b>EM-TuA1 INVITED</b> Optical Waveguides on Silicon Chips. <b>S. YOKOYAMA</b> , Y. KURODA, T. MIYAMOTO, T. DOI, T. NAMBA, T. NAGATA, K. MIYAKE, S. MIYAZAKI, M. KOYANAGI, M. HIROSE, Hiroshima University, Japan.	<b>MS-TuA1 INVITED</b> The Semiconductor Equipment Industry: Applied Materials Role and Growth. <b>R.Z. BACHRACH</b> , Applied Materials.
2:20 pm	Invited talk continued.	Invited talk continued.
2:40 pm	<b>EM-TuA3 INVITED</b> Silicon Optical Bench Waveguide Technology. <b>C.H. HENRY</b> , AT&T Bell Laboratories.	<b>MS-TuA3 INVITED</b> Advances in Semiconductor Manufacturing Equipment. <b>E. VAN DE VEN</b> , T. BOWMAN, Novellus Systems, Inc.
3:00 pm	Invited talk continued.	Invited talk continued.
3:20 pm	<b>EM-TuA5 INVITED</b> Novel LSI Memories with Optical Interconnections. <b>M. KOYANAGI</b> , Tohoku University, Japan.	<b>MS-TuA5</b> MESC Cluster Tools for Advanced Metalization. <b>P.H. BALLENTINE</b> , T. OMSTEAD, M. MOSLEHI, CVC Products, Inc.
3:40 pm	Invited talk continued.	<b>MS-TuA6</b> Application of Motorola IRONMAN Methodology to Equipment Reliability Improvement. <b>R. DUFFIN</b> , K. MCCORMACK, Motorola SPS.
4:00 pm	<b>EM-TuA7 INVITED</b> Rare Earth Doped Silicon Emitters. <b>J. MICHEL</b> , L.C. KIMERLING, Massachusetts Institute of Technology.	<b>MS-TuA7 INVITED</b> The Development of the Fast Thermal Processor (FTP). <b>K. OKUMURA</b> , Toshiba.
4:20 pm	Invited talk continued.	Invited talk continued.
4:40 pm	<b>EM-TuA9 INVITED</b> SiGe/Si Quantum Well Light Emitters. <b>Y. SHIRAKI</b> , S. FUKATSU, University of Tokyo, Japan.	<b>MS-TuA9</b> Low Thermal Budget Gap Filling for Semiconductor Manufacturing. <b>K.J. URAM</b> , J.K. SHUGRUE, N.P. SANDLER, Lam Research Corporation.
5:00 pm	Invited talk continued.	<b>MS-TuA10</b> Sub-Atmospheric CVD (SACVD) Ozone/TEOS for SiO <sub>2</sub> Trench Filling. <b>I. SHAREEF</b> , IBM TJ Watson Research Center. G.W. RUBLOFF, North Carolina State University. M. ANDERLE, IBM TJ Watson Research Center. W. GILL, Rensselaer Polytechnic Institute. J. COTTE, IBM TJ Watson Research Center. D.-H. KIM, North Carolina State University.

**BIOMATERIAL INTERFACES****Room A106 - Session BI-TuA pg. 196****The Biosensor-Biology Interface****Moderator:** J.-J. Pireaux, Universitaires Notre-Dame, Belgium.

2:00 pm	<b>BI-TuA1 INVITED</b> In Vivo Electrochemical Sensors: The Challenge of Achieving Biocompatible Devices. <b>M.E. MEYERHOFF</b> , C. ESPADAS-TORRE, University of Michigan.	
2:20 pm	Invited talk continued.	
2:40 pm	<b>BI-TuA3</b> Neural Microsensors for Automated Toxicity and Pharmacology Assays. <b>D.A. STENGER</b> , V.C. KOWTHA, P.P. BEY, JR., Naval Research Laboratory. D. BORKHOLDER, G.T. KOVACS, Stanford University. K.E. FOSTER, J.J. HICKMAN, Science Applications International Corporation.	
3:00 pm	<b>BI-TuA4</b> Micrometre Resolution Molecular Patterning at Transducer Surfaces. <b>J.M. COOPER</b> , H. MORGAN, D.J. PRITCHARD, University of Glasgow, United Kingdom.	
3:20 pm	<b>BI-TuA5 INVITED</b> Activity of Antibodies Immobilized at the Solid-Liquid Interface in Biosensors. <b>D.W. CONRAD</b> , P.T. CHARLES, L.C. SHRIVER-LAKE, T.S. KOLOSKI, F.S. LIGLER, Naval Research Laboratory.	
3:40 pm	Invited talk continued.	
4:00 pm	<b>BI-TuA7 INVITED</b> Molecular Assemblies of Functionalized Polydiacetylenes. <b>D.H. CHARYCH</b> , A. REICHERT, Lawrence Berkeley Laboratory. R. STEVENS, G. KUZIEMKO, University of California, Berkeley. J. NAGY, Lawrence Berkeley Laboratory.	
4:20 pm	Invited talk continued.	
4:40 pm	<b>BI-TuA9</b> Preparation of an Immunosensing Surface by a Mixed Self-Assembled Monolayer. <b>P. HEIDUSCHKA</b> , J. RICKERT, W. BECK, G. JUNG, W. GÖPEL, University of Tübingen, Germany.	
5:00 pm	<b>BI-TuA10</b> Hydration and Dehydration of Adsorbed Protein Monolayers on Different Surfaces. <b>M. RODAHL</b> , F. HÖÖK, B. KASEMO, Chalmers Univ. of Technology and Univ. of Göteborg, Sweden.	

# Tuesday Afternoon Poster Sessions

## SURFACE SCIENCE

Room BR4 - Session SS-TuP pg. 198

### Aspects of Surface Science

Moderator: J.C. Hemminger, University of California, Irvine.

Presenters present: 5:00-6:30 pm.

- SS-TuP1** Simulation Studies of Electron Transfer at a Metal-Aqueous Electrolyte Interface. B.B. SMITH, J.W. HALLEY, University of Minnesota.
- SS-TuP2** Adsorption of Water on Oxidized Tungsten and Suppression of Electron Induced Oxygen Ion Emission by Molecular and Dissociated Water. M. AKBULUT, N.J. SACK, T.E. MADEY, Rutgers University.
- SS-TuP3** Adsorption, Desorption, Mixing, and Solvation Kinetics of Mixed Methanol and Water Multilayer Ices. R.S. SMITH, C. HUANG, E.K.L. WONG, B.D. KAY, Pacific Northwest Laboratory.
- SS-TuP4** The Interaction of HCl with Ultrathin Ice Films: Observation of Adsorbed and Absorbed States. J.D. GRAHAM, J.T. ROBERTS, University of Minnesota.
- SS-TuP5** Differences in the Surface Chemistry of Amorphous and Crystalline Ice Thin Films. J.E. SCHAFF, J.T. ROBERTS, University of Minnesota.
- SS-TuP6** SPA-RHEED - Spot Profile Analysis for In Situ Characterization. B. MÜLLER\*, M. HENZLER, Universität Hannover, Germany.
- SS-TuP7** Adsorption, Desorption and Diffusion of H<sub>2</sub>O on Single-Crystal Ice Surfaces. D.E. BROWN\*, J.T. NELSON, S.M. GEORGE, University of Colorado, Boulder.
- SS-TuP8** Microscopic Activation Energies Determined from the Time Structure of Step Jumps in Tunneling Images. M. GIESEN-SEIBERT\*, F. SCHMITZ, H. IBACH, Forschungszentrum Jülich, Germany.
- SS-TuP9** Atomically Resolved STM Study of the Interaction of Boron with Si(001). Y. WANG\*, R.J. HAMERS, University of Wisconsin, Madison.
- SS-TuP10** The Role of Energy Loss Mechanisms for the Trapping Dynamics of Alkanes on Platinum Surfaces. J.A. STINNETT\*, R.J. MADIX, Stanford University. J.C. TULLY, AT&T Bell Laboratories.
- SS-TuP11** Development of Surface Morphology and Microstructure during Si Homoepitaxial Growth. D.P. ADAMS, S.M. YALISOVE, University of Michigan. D.J. EAGLESHAM, AT&T Bell Laboratories.
- SS-TuP12** Nucleation Phenomena in the Chemical Vapor Deposition of Iron on Si(001). T.M. MAYER, D.P. ADAMS, L.L. TEDDER, B.S. SWARTZENTRUBER, Sandia National Laboratories.
- SS-TuP13** STM Observations of Hydrogen-Induced Ag Cluster Formation on the Si(111) $\sqrt{3}\times\sqrt{3}$ (R30°)-Ag Surface. I. KATAYAMA, Y. OHBA, Osaka Institute of Technology, Japan. H. OHNISHI, Y. YAMAMOTO, K. OURA, Osaka University, Japan.
- SS-TuP14** The Evolution of Growth Front in a Heteroepitaxial System: Pb on Cu(100). H. ZENG, G. VIDALI, Syracuse University.

- SS-TuP15** Island Growth and Energetics in Submonolayer Homoepitaxy on Cu(100). J.F. WENDELKEN, H. DÜRR, Oak Ridge National Laboratory. J.-K. ZUO, Oak Ridge National Lab & Southwest Missouri State Univ.
- SS-TuP16** An Atomic Scale View of Adsorbate Motion on Surfaces. P.S. WEISS, M.T. CYGAN, J.H. FERRIS, M.M. KAMNA, K.R. KROM, S.J. STRANICK, M.G. YOSHIKAWA YOUNGQUIST, The Pennsylvania State University.
- SS-TuP17** Local Morphology Effects on Mass Transport on Sputtered Au(111): An STM Study. T. CURCIC, J.G. MCLEAN, B.H. COOPER, Cornell University.
- SS-TuP18** Identification of Metastable bcc Ni Film Growth on Al(001) Surfaces using High-Energy Ion Scattering, X-ray Photoelectron Diffraction, and X-ray Photoelectron Spectroscopy. V. SHUTTHANANDAN, A.A. SALEH, R.J. SMITH, Montana State University.
- SS-TuP19** The Initial Growth of Ultrathin Pd Films on Cu(001). J. YAO, Y.G. SHEN, D.J. O'CONNOR, University of Newcastle, Australia.
- SS-TuP20** Structure and Stability of Steps on the GaAs(110) Surface. J.M. MCCOY, Montana State University. J.P. LAFEMINA, Pacific Northwest Laboratory.
- SS-TuP21** The Thermochemistry of CBr<sub>4</sub> on GaAs(100). M.T. MCELLISTREM, D. SLOAN, J.M. WHITE, University of Texas, Austin.
- SS-TuP22** Surface Chemistry of Dimethyl Hydrazine on GaAs(100). Y.-M. SUN, D. SLOAN, A. SCHWANER, J.M. WHITE, University of Texas, Austin.
- SS-TuP23** The Adsorption of Si on GaAs(001)-c(4x4); STM Evidence for Si Induced Disruption of As Layers. T.S. JONES, A.R. AVERY, D.M. HOLMES, M.R. FAHY, B.A. JOYCE, Imperial College, United Kingdom.
- SS-TuP24** Adsorption and Decomposition of Ammonia and Hydrazine on the GaAs(100)-c(8x2) Surface. E. APEN, J.L. GLAND, University of Michigan.
- SS-TuP25** Chemical Reactions of Triethylantimony on GaAs(100). J.M. HEITZINGER, J.G. EKERDT, University of Texas, Austin.
- SS-TuP26** The Interaction of Hydrogen Atoms with Ethyl Groups on Si(100). P.A. STEINER, J.M. HEITZINGER, M. MCELLISTREM, D.J. BONSER, J.M. WHITE, University of Texas, Austin.
- SS-TuP27** Infrared Evidence for an Electrically Conductive Diamond (110) Surface. B.L. MACKEY, Naval Research Lab and University of California, San Diego. J.N. RUSSELL, JR., Naval Research Laboratory. J.E. CROWELL, University of California, San Diego. J.E. BUTLER, Naval Research Laboratory.
- SS-TuP28** Surface Chemistry of Potential CVD Precursors, Diethylsilane and Diethylgermane on Ge(100). A. MAHAJAN, B.K. KELLERMAN, N. RUSSELL, S. BANERJEE, J.G. EKERDT, A. TASCH, J.M. WHITE, University of Texas, Austin.
- SS-TuP29** Surface Reactions of Ethylgermanes on Si(100). L. CHEN, L.A. KEELING, W. DU, C.M. GREENLIEF, University of Missouri, Columbia.
- SS-TuP30** An STM Study of Hydrogen Adsorption on Si(112). A.A. BASKI, L.J. WHITMAN, Naval Research Laboratory.

\*Finalist for the Morton M. Traum Award

**NANO 3/NANOMETER-SCALE SCIENCE AND TECHNOLOGY**  
**Room BR4 - Session NS-TuP pg. 203**

**Materials Characterization**

**Moderator:** R.J. Hamers, University of Wisconsin, Madison.

Presenters present: 5:00-6:30 pm.

**NS-TuP1** Selenium Nanoclustering in Vapor Grown ZnSe Crystals.

M.A. GEORGE, W.E. COLLINS, K.-T. CHEN, Z. HU, Y. ZHANG, A. BURGER, Fisk University. C.-H. SU, Y.-G. SHA, D.C. GILLES, S.L. LEHOCZKY, NASA/Marshall Space Flight Center.

**NS-TuP3** Chemistry in Nanoporous Materials: Semiconductor Particles Formed within a Solid Template. C.M. ZELENSKI, P.K. DORHOUT, Colorado State University.

**NS-TuP4** Scanning Tunneling Microscopy of Thin Films of TaS<sub>2</sub> Prepared by an Intercalation-Exfoliation Method. A. MANIVANNAN, C.R. CABRERA, University of Puerto Rico. A. FUJISHIMA, University of Tokyo, Japan.

**NS-TuP5** Oxidation Behavior of Aluminum Nanopowders. C.E. AUMANN, G.L. SKOFRONICK, J.A. MARTIN, Los Alamos National Laboratory.

**NS-TuP6** The Origin of Universality in the Top Layer Relaxation of Zincblende (110) and Wurtzite (10 $\bar{1}$ 0) Surfaces. G. BROWN, M. WEIMER, Texas A&M University.

**NS-TuP7** Nonlinear Optical Absorption in Asymmetric Quantum Wells. X. YANG, J.T. MCKINLEY, R.G. ALBRIDGE, A.V. BARNES, N.H. TOLK, Vanderbilt University. G. MARGARITONDO, Ecole Polytechnique Fédérale, Switzerland.

**NS-TuP8** Quantum Confinement Effects in Heteroepitaxial Si/ZnS Nanostructures Produced by MOCVD. E. BRETTSCHEIDER, A. DAVYDOV, J.E. YU, Z. HUANG, B. PATHANGEY, K.S. JONES, T.J. ANDERSON, University of Florida, Gainesville. H.P. MARUSKA, R. SUDHARSANAN, Spire Corporation.

**NS-TuP9** Luminescence of Nanostructures Induced by Carriers Injected from a Scanning Tunneling Microscope Emitter. L. MONTELIUS, J. LINDAHL, M.-E. PISTOL, L. SAMUELSON, Lund University, Sweden.

**NS-TuP10** Spectral and Structural Features of Porous Silicon Prepared by Chemical and Electrochemical Etching Processes. D.F. THOMAS, L.A. JONES, E. NAKAMICHI, L. ZAJCHOWSKI, University of Guelph, Canada.

**NS-TuP11** Mesostructure of Luminescent Porous Silicon. F. RUIZ, E. LÓPEZ-CRUZ, C. VÁZQUEZ-LÓPEZ, CINVESTAV-Salttillo, México. G. TORRES-DELGADO, CINVESTAV-DF, México. J. GONZÁLEZ-HERNÁNDEZ, CINVESTAV-Salttillo, México.

**NS-TuP12** The Size Effects Study on the Vibrational Properties of the Si Nanocrystalline Materials. H.F. ZHANG, T. JIN, Y.P. LI, C.S. WANG, S.D. XIA, University of Science and Technology of China.

**NS-TuP13** Atomic Force Microscopy and Scanning Tunneling Microscopy Study of Ge<sub>1-x</sub>Fe<sub>x</sub> Nanophase Materials. D.-M. ZHU, University of Missouri, Kansas City. J. SHI, University of Illinois, Urbana-Champaign.

**NS-TuP14** Growth, Structure and Diffusion of Small NaCl Clusters on the (001) Surface of MgO. A.L. SHLUGER, A.L. ROHL, The Royal Institution of Great Britain.

**NS-TuP15** Atomic Force Microscopy of Au Implanted in Sapphire. D.O. HENDERSON, M.A. GEORGE, A. BURGER, R. MU, S.H. MORGAN, Fisk University. R.H. MAGRUDER III, Vanderbilt University. C.W. WHITE, R.A. ZUHR, Oak Ridge National Laboratory.

**NS-TuP16** An STM Study of Molecular Intermediates in the Dissociative Adsorption of closo-1,2-dicarbododecaborane on Si(111). J.M. CARPINELLI, E.W. PLUMMER, Oak Ridge National Laboratory. D. BYUN, P.A. DOWBEN, University of Nebraska, Lincoln.

**NS-TuP17** Fabrication and Optical Characterization of Aluminum Nano-metal/Porous Aluminum Oxide Thin Film Composites. C.R. MARTIN, G.L. HORNYAK, B.P. BERGGREN, Colorado State University.

**NS-TuP18** Nanometer-scale Observations of the Corroded Surfaces of Metallic Glasses. Y. WATANABE, Y. NAKAMURA, S. HIRAYAMA, National Defense Academy, Japan.

**NS-TuP19** Dynamical Characteristics of Low Frequency Current Fluctuations from Local Areas of Semiconductor Field Emitter Surfaces. R.Z. BAKHTIZIN, S.S. GHOTS, Bashkir State University, Russia.

**NS-TuP20** Many-Particle Effects in Tunneling of Electrons from Metal and Semiconductor Surfaces. M.A. KOZHUSHNER, G.K. IVANOV, Russian Academy of Sciences.

**NS-TuP21** STM/STS Investigation of Ion Exchanged Polymer Multilayer LB Films: 2D Conductivity, Resonance Tunneling, Charge Superstructure. N. MASLOVA, Y.N. MOISEEV, V. NIKANOROV, V. PANOV, S. SAVINOV, R. YUSUPOV, Moscow State University, Russia.

**NS-TuP22** Determination of Large Heterogeneous Rate Constants using Nanoelectrode Ensembles. V.P. MENON, C.R. MARTIN, Colorado State University.



# Tuesday Afternoon Poster Sessions

## APPLIED SURFACE SCIENCE

Room BR4 - Session AS-TuP pg. 206

### Aspects of Applied Surface Science

**Moderator:** D.R. Baer, Battelle Pacific Northwest Laboratories.

Presenters present: 5:00-6:30 pm.

- AS-TuP1** A Study of Vapor-Deposited Polythiophene Thin Films. **T.R. DILLINGHAM**, D.M. CORNELISON, A.G. SYKES, M. VITTERA, S. TOWNSEND, Northern Arizona University.
- AS-TuP2** Highly Ordered Thin Films of Phthalocyanines Created by Self-Assembly and Langmuir Blodgett Deposition. **N.R. ARMSTRONG**, L.-K. CHAU, S.-Y. CHEN, E. OSBURN, D.F. O'BRIEN, University of Arizona. A. FERENCZ, G. WEGNER, Max Planck Institute für Polymerforschung, Germany.
- AS-TuP3** Metal Overlayers on Self-Assembled Monolayers: 5. ISS and XPS of the Ag/COOH Interface. **G.C. HERDT#**, A.W. CZANDERNA, National Renewable Energy Laboratory.
- AS-TuP4** Quantitative Analysis by Static SIMS of Mixed Self-Assembled Monolayer Films on Metal Substrates. **Y.-Z. DU**, R.W. JOHNSON, JR., J.A. GARDELLA, JR., State University of New York, Buffalo.
- AS-TuP5** Temperature Controlled TOF-SIMS Investigations of Polymer Materials. **M. DEIMEL**, B. HAGENHOFF, A. BENNINGHOVEN, Universität Münster, Germany.
- AS-TuP6** Radiation Damage on Some Organic Materials during S-SIMS and XPS Analysis. **M. KUDO**, T. NISHIHARA, Seikei University, Japan. T. HOSHI, ULVAC-PHI, Inc., Japan.
- AS-TuP7** XPS Characterization of Nylons. **S.N. RAMAN**, Monsanto.
- AS-TuP8** Surface Characterization of Silylated Substrates by TOF-SIMS. **B. HAGENHOFF**, M. DEIMEL, D. RADING, A. BENNINGHOVEN, J. GROBE, Universität Münster, Germany.
- AS-TuP9** Characterization of an Abrasion Resistant Coating on Polycarbonate. **R.M. FRIEDMAN**, Monsanto Corporate Research. R.W. LINTON, M.P. MAWN, University of North Carolina, Chapel Hill.
- AS-TuP10** Fundamental Characterization of Siloxane Adhesion Promoters on Metal and Metal Oxide Surfaces. **S. MISHRA#**, J.J. WEIMER, University of Alabama, Huntsville.
- AS-TuP11** Film Growth and Surface Structure of Methylene Blue on Mica. **G. HÄHNLER**, W.R. CASERI, N.D. SPENCER, ETH Zürich, Switzerland.
- AS-TuP12** Nanometer Resolution Imaging of the Growth of Water Monolayers on Mica from its Vapor. **J. HU#**, X. XIAO, D.F. OGLETREE, M. SALMERON, Lawrence Berkeley Laboratory.
- AS-TuP13** Surface Finish Characterization of Potassium Dihydrogen Phosphate (KDP) for Nonlinear Optical Applications. **E.C. HONEA**, R.L. MCEACHERN, Lawrence Livermore National Laboratory.
- AS-TuP14** Counterion and Dopant Induced Effects on the Structure of Electropolymerized Polyaniline Thin Films. **T.L. PORTER**, A.G. SYKES, Northern Arizona University.
- AS-TuP15** Contribution of Surface Roughness in the Nanometer Regime to the Depth Resolution in Sputter Profiling. **K.A. PISCHOW**, Lab. of Processing and Heat Treatment of Materials, Finland. S. HOFFMANN, Max-Planck-Institut für Metallforschung, Germany. A. ZALAR, Institute for Electronics and Vacuum Technique, Slovenia.

- AS-TuP16** Influence of Ion Species, Ion Energy and Substrate on Sputtering-Induced Ripple Topography. **J.J. VAJO**, R.E. DOTY, E.-H. CIRLIN, Hughes Research Laboratories.
- AS-TuP17** Use of Resonance Ionization Microprobe Analysis in Material Sciences. **H.F. ARLINGHAUS**, C.F. JOYNER, T.J. WHITAKER, Atom Sciences, Inc.
- AS-TuP18** Depth-Resolved Vibrational Characterization of Buried Interfaces. **N.H. FONTAINE**, T.E. FURTAK, Colorado School of Mines.
- AS-TuP19** Thickness Determination of Uniform Overlayers on Rough Substrates by Angle Dependent X-ray Photoelectron Spectroscopy. **P.L.J. GUNTER#**, J.W. NIEMANTSVERDIET, Eindhoven University of Technology, The Netherlands.
- AS-TuP20** Angle-resolved XPS Data Acquisition. **B.J. TIELSCH#**, J.E. FULGHUM, Kent State University.
- AS-TuP21** XPS Studies of Compositional Changes Induced by Ion Bombardment on  $\text{LaPO}_4$  Surface. **O.P. IVANOVA**, A.V. NAUMKIN, L.A. VASILYEV, V.I. RAKHOVSKY, Research Center for Surface and Vacuum Investigation, Russia.
- AS-TuP22** XPS Cerium(3d) Lineshape Analysis as a Measure of Oxygen Storage/Release in Automotive Catalysts. **S.J. SCHMIEG**, D.N. BELTON, D.R. MONROE, General Motors Research & Development Center.
- AS-TuP23** Quantitative Depth Profiling of Oxygen in Homoepitaxial  $\text{SrTiO}_3$  Films. **M. WATAMORI**, K. OURA, Osaka University, Japan. T. NAKAMURA, Sumitomo Electric Industries, Ltd., Japan.
- AS-TuP24** Negative Charge Production from Bombardment of a Cu Surface by Low Energy Oxygen Atoms and Ions. **T.M. STEPHEN**, **R.C. AMME**, B. VAN ZYL, University of Denver.
- AS-TuP25** The Effect of Copper Overlayers on the Thermal Stability of Chromium Carbide on HOPG. **J.J. BELLINA, JR.**, Saint Mary's College. K.A. BRIGGMAN, Northwestern University.
- AS-TuP26** Electric States of Segregated Metal Atom on Metal Surfaces and Potential Use for Field Emitter. **M. YOSHITAKE**, K. YOSHIHARA, National Research Institute for Metals, Japan.
- AS-TuP27** The Effect of Sample Bias on the Nitrogen Etching Products of Aluminum. **M.A. ROOKE**, **P.M.A. SHERWOOD**, Kansas State University.
- AS-TuP28** Local Density of State Analysis by AES. **H.J. ZHOU**, Y.C. WANG, W. HO, Tsinghua University, China.
- AS-TuP29** The Development of an Electron Spectroscopy Data Dictionary for the AVS Surface Science Spectral Database. **S.W. GAARENSTROOM**, General Motors R&D Center.
- AS-TuP30** A Generic Analytical Data Model: Ensuring that Surface Science Data Meet Analytical Chemistry Standards. **R.N. LEE**, Naval Surface Warfare Center.

#Candidate for the Applied Surface Science Division Award

## ELECTRONIC MATERIALS

Room BR4 - Session EM-TuP pg. 211

### Aspects of Electronic Materials and Processing I

Moderator: F. A. Houle, IBM Almaden Research Center.

Presenters present: 5:00-6:30 pm.

**EM-TuP1** Thermal Oxidation of Heteroepitaxial  $\text{Si}_{1-x-y}\text{Ge}_x\text{C}_y$  Alloy Thin Films. **J. XIANG**, N. HERBOTS, P. YE, S. HEARNE, Arizona State University.

**EM-TuP2** The Role of Temperature during Synthesis of Heteroepitaxial  $\text{Si}_{1-x-y}\text{Ge}_x\text{C}_y/\text{Si}$  (100) Synthesized by Combined Ion and Molecular Beam Deposition (CIMD). **N. HERBOTS**, P. YE, J. XIANG, S. HEARNE, Arizona State University.

**EM-TuP3** Growth of  $\text{Si}_{1-x}\text{Ge}_x$  Multiple Quantum Wells using Molecular Beam Epitaxy for Infrared Absorption. **T. KREIFELS**, Air Force Institute of Technology. **P.E. THOMPSON**, Naval Research Laboratory. **R. HENGHELD**, Y.K. YEO, Air Force Institute of Technology.

**EM-TuP4** Erbium Doped Si Films Prepared by Electron Cyclotron Resonance Plasma Enhanced Chemical Vapor Deposition. **J.L. ROGERS**, **W.J. VARHUE**, K. AHMED, F. LADIPPO, University of Vermont. **E. ADAMS**, M.A. LAVOIE, IBM Corporation.

**EM-TuP5** Silicon Nitride Encapsulation of Sulfide Passivated GaAs/AlGaAs Microdisk Lasers. **W.S. HOBSON**, F. REN, U. MOHIDEEN, R.E. SLUSHER, M. LAMONT SCHNOES, AT&T Bell Laboratories. **S.J. PEARTON**, University of Florida, Gainesville.

**EM-TuP6** Passivation of Compound Semiconductors: Improvement of the Dielectric/Sulfur/Semiconductor Interface. **C.I.H. ASHBY**, K.R. ZAVADIL, J.C. BARBOUR, R.J. SHUL, M.J. HAFICH, Sandia National Laboratories.

**EM-TuP7** Correlation of Surface Morphology with Chemical Structures of Sulfur-Passivated GaAs(100) Investigated by Scanning Tunneling Microscope and X-ray Photoelectron Spectroscopy. **J.S. HA**, S.-J. PARK, S.-B. KIM, E.-H. LEE, Electronics and Telecommunications Research Institute, Korea.

**EM-TuP8** Etching of Polysilicon with a Chlorine Trifluoride Beam. **H. XU**, A.J. MUSCAT, A.S. LAWING, H.H. SAWIN, Massachusetts Institute of Technology.

**EM-TuP9** Structural and Chemical Changes during Annealing of Gas-Phase Polysulfide Passivated InP. **R.W.M. KWOK**, G. JIN, The Chinese University of Hong Kong. **L. HUANG**, W.M. LAU, The University of Western Ontario, Canada. **C.C. HSU**, Institute of Semiconductors, PR China.

**EM-TuP10** Sputter-cleaning and Smoothing of GaAs(001) Surfaces using Glancing-Angle Ion Bombardment. **J.G.C. LABANDA**, Northwestern University. **L. HULTMAN**, Linköping University, Sweden. **S.A. BARNETT**, Northwestern University.

**EM-TuP11** Sputter Deposition of Yttria Stabilized Zirconia onto a Porous Au Substrate. **A.F. JANKOWSKI**, J.P. HAYES, Lawrence Livermore National Laboratory.

**EM-TuP12** Hydrogen Passivation of the Be Acceptor in p-InP (100). **M.D. WILLIAMS**, T.H. CHIU, F.G. STORZ, J.F. FERGUSON, AT&T Bell Laboratories.

**EM-TuP13** Studies of Strained Si-Ge Alloys Using Si-K and Ge-K X-ray Absorption Spectroscopy. **A.P. HITCHCOCK**, T. TYLISZCZAK, McMaster University, Canada. **T.E. JACKMAN**, McMaster University & National Research Council, Canada. **J.-M. BARIBEAU**, Z.H. LU, D.J. LOCKWOOD, National Research Council, Canada.

**EM-TuP14** Sb Ion Implantation and Annealing of SiGeC Heteroepitaxial Layers on Si(001). **R. GARCIA**, T. ALFORD, K. DALEY, S. SEGO, S.H. SHIU, R.J. CULBERTSON, D.B. POKER, Arizona State University.

**EM-TuP15** Strain Measurements of SiGeC Heteroepitaxial Layers on Si(001) using Ion Beam Analysis. **S. SEGO**, T. ALFORD, Z. ATZMON, A.E. BAIR, K. DALEY, P. YE, S.H. SHIU, R.J. CULBERTSON, N. HERBOTS, Arizona State University.

**EM-TuP16** Comparison of Trisdimethylaminoantimony and Sb as Sources for Growth of GaSb, AlSb and InSb by Metalorganic Molecular Beam Epitaxy. **C.R. ABERNATHY**, University of Florida, Gainesville. **D.A. BOHLING**, G.T. MUHR, Air Products and Chemicals Inc.

**EM-TuP17** Zincblende-CdSe on GaSb(110): Characterization of Epitaxial Growth and Electronic Structure. **G. NEUHOLD**, K. HORN, Fritz-Haber-Institut der MPG, Germany. **K.O. MAGNUSSON**, University of Karlstad, Sweden. **D.A. EVANS**, Athrofa Gogledd Ddwyrain Cymru (NEWI), Clwyd GB.

**EM-TuP18** Photoconductivity Decay Study of GaN Thin Films. **C.H. QIU**, Astralux Inc. and University of Colorado, Boulder. **C. HOGGATT**, Z.H. ZHANG, University of Colorado, Boulder. **M.W. LEKSONO**, Astralux Inc. **J.I. PANKOVE**, Astralux Inc. and University of Colorado, Boulder.

**EM-TuP19** Ohmic Electrical Contacts to p-ZnTe. **J.T. TREXLER**, J.J. FIJOL, P.H. HOLLOWAY, University of Florida, Gainesville.

**EM-TuP20** High Field Ni-SiC Schottky Barrier Diodes with Single-Metal Process. **J.N. SU**, A.J. STECKL, University of Cincinnati.

**EM-TuP21** Temperature-Dependent Optical Bandgap of Metastable Zincblende-Structure  $\beta$ -GaN. **A. LASTRAS-MARTÍNEZ**, H. NAVARRO-CONTRERAS, G. RAMÍREZ-FLORES, Universidad Autónoma de San Luis, México. **R.C. POWELL**, J.E. GREENE, University of Illinois, Urbana.

**EM-TuP22** Low Pressure Metalorganic Chemical Vapor Deposition of GaN on c-plane (0001) Sapphire Substrates. **C.-Y. HWANG**, W.E. MAYO, Y. LU, Rutgers University. **H. LIU**, Emcore Corporation.

**EM-TuP23** Growth of Crystalline 3C-SiC Films on 6H-SiC at 900°C by Chemical Vapor Deposition. **C. YUAN**, A.J. STECKL, University of Cincinnati. **J. CHAUDHURI**, R. THOKALA, Wichita State University. **M.J. LOBODA**, Dow Corning Corporation.

**EM-TuP24** Electron Emission from Wide-Bandgap Negative Electron Affinity Materials. **C. BANDIS**, D. HAGGERTY, B.B. PATE, Washington State University.

**EM-TuP25** Conformality of  $\text{SiO}_2$  Films from TEOS-sourced Remote Microwave Plasma-Enhanced Chemical Vapor Deposition. **D.A. LEVEDAKIS**, H. LIAO, T.S. CALE, G.B. RAUPP, Arizona State University.

## Tuesday Afternoon Poster Sessions

### MANUFACTURING SCIENCE AND TECHNOLOGY

Room BR4 - Session MS-TuP pg. 215

#### Manufacturing Science and Technology

Moderator: G.W. Rubloff, North Carolina State University.

Presenters present: 5:00-6:30 pm.

**MS-TuP1** Low-Cost Optical Reflectivity Temperature Measurement System. H.A. ATWATER, California Institute of Technology. D.S. GARDNER, Intel Corporation.

**MS-TuP2** Magnetron RIE System Using a Dipole-ring Magnet for Quarter Micron Etch Process. Y. TAHARA, Y. ISHIKAWA, M. OGASAWARA, K. INAZAWA, Tokyo Electron Ltd., Japan. Y. YOSHIDA, H. OKANO, Toshiba Corporation, Japan.

**MS-TuP3** Magnetron RIE without Charge-up Damage Using a Dipole-ring Magnet. I. SAKAI, S. IKEDA, M. SEKINE, K. HORIOKA, Y. YOSHIDA, H. OKANO, Toshiba Corporation, Japan. M. OGASAWARA, K. INAZAWA, Y. TAHARA, Tokyo Electron Ltd., Japan.

**MS-TuP4** Profile Modeling of High Density Plasma Oxide Etching. J.S. HAN, J.P. MCVITTIE, J. ZHENG, Stanford University.

**MS-TuP5** In Situ Monitoring and Control of MBE and MOCVD Growth using Multi-Wavelength Ellipsometry. J.A. WOOLLAM, S. PIT-TAL, B. JOHS, P. HE, J.A. Woollam Co., Inc. G.N. MARACAS, R. DROOPAD, C.H. KUO, S. ANAND, Arizona State University. S. DAKSHINA MURTHY, I. BHAT, Rensselaer Polytechnic Institute.

**MS-TuP6** Electrical Monitoring of Surface Conditions in a Plasma Reactor. M.A. SOBOLEWSKI, J.K. OLTHOFF, National Institute of Standards & Technology.

**MS-TuP7** Field Emission Tips for Micro-Column Lithography. W.K. LO, M. SKVARLA, M.S. ISAACSON, Cornell University.

**MS-TuP8** High Resolution Resists for Low Energy Electron Beam Lithography. C.W. LO, M.J. ROOKS, H.G. CRAIGHEAD, Cornell University.

**MS-TuP9** The Design and Testing of a Multi-Task, Multi-Instrument Sample Transfer System. S. THEVUTHASAN, D.R. BAER, Pacific Northwest Laboratory. J.N. WORTHINGTON, T.R. HOWARD, J.R. MUNN, Thermionics Northwest Instruments.

THE AMERICAN VACUUM SOCIETY

cordially invites you

to attend

the Awards Assembly

on

Wednesday, October 26, 1994

in

Ballroom 1

Colorado Convention Center

at 6:45 p.m.

followed by the

Awards Reception

# Wednesday Morning, October 26, 1994

## SURFACE SCIENCE

Room A205 - Session SS1-WeM pg. 218

### Surface Magnetism I

Moderator: H. Hopster, University of California, Irvine.

## SURFACE SCIENCE

Room A201 - Session SS2-WeM pg. 219

### Reactions on Metals: Diatomics

Moderator: G.B. Fisher, General Motors Research & Development Center.

8:00 am	<b>SS1-WeM0 INVITED</b> Spin-Polarized Electron Measurements: Foundations of Surface Magnetism Research. <b>R.J. CELOTTA*</b> , <b>D.T. PIERCE*</b> , National Institute of Standards & Technology.	<b>SS2-WeM0</b> Structure Sensitive Selectivity of the NO-CO Reaction over Rh(110) and Rh(111). <b>C.H.F. PEDEN</b> , Pacific Northwest Laboratory. <b>D.N. BELTON</b> , <b>S.J. SCHMIEG</b> , General Motors Research & Development Center.
8:20 am	Invited talk continued.	<b>SS2-WeM1</b> Dissociation Kinetics of NO on Rhodium (111). <b>H.J. BORG*</b> , <b>R.A. VAN SANTEN</b> , <b>J.W. NIEMANTSVERDIET</b> , Eindhoven University of Technology, The Netherlands.
8:40 am	<b>SS1-WeM2</b> Spin-Polarized Low Energy Electron Microscopy of Co/W(110). <b>T. DUDEN</b> , <b>K. GRZELAKOWSKI</b> , <b>E. BAUER</b> , <b>T.U. CLAUSTHAL</b> , Clausthal-Zellerfeld, Germany. <b>S. CHIANG</b> , <b>H. POPPA</b> , IBM Almaden Research Center.	<b>SS2-WeM2</b> Kinetics of the NO+CO+O <sub>2</sub> Reaction over Rh(111). <b>H. PERMANA</b> , <b>D.N. BELTON</b> , <b>S.J. SCHMIEG</b> , General Motors Research & Development Center. <b>K.Y. SIMON NG</b> , Wayne State University.
9:00 am	<b>SS1-WeM3</b> Scanning Ion Microscopy with Polarization Analysis (SIMPA) to Study Domain Structures of Metal Overlayers on Fe and Pd Single Crystal Surfaces. <b>N.L. NUNES</b> , Rice University. <b>H.P. OEPEN</b> , IGV-KFA Jülich, Germany. <b>G. STEIERL</b> , <b>C. RAU</b> , Rice University.	<b>SS2-WeM3</b> A Model for Chaos in Oscillatory Surface Reactions: Pt(100)/NO+CO. <b>G. VESER</b> , <b>R. IMBIHL</b> , <b>A. MIKHAILOV</b> , Fritz-Haber-Institut der Max-Planck-Gesellschaft, Germany.
9:20 am	<b>SS1-WeM4</b> Spin-Resolved X-ray Photoelectron Spectroscopy Study of the 2p <sub>3/2</sub> Level of Ferromagnetic Ni. <b>A.K. SEE</b> , <b>L.E. KLEBANOFF</b> , Lehigh University.	<b>SS2-WeM4</b> Particulate Cu on Ordered Al <sub>2</sub> O <sub>3</sub> : Reactions with Nitric Oxide and Carbon Monoxide. <b>M.-C. WU</b> , <b>D.W. GOODMAN</b> , Texas A&M University.
9:40 am	<b>SS1-WeM5</b> Electronic and Magnetic Properties of Pseudomorphic Ferromagnetic Alloy Films on Cu(100). <b>G.J. MANKEY</b> , <b>S.Z. WU</b> , <b>R.F. WILLIS</b> , Pennsylvania State University.	<b>SS2-WeM5</b> The Effect of Oxidizing and Reducing Environments on the Regeneration of a Sulfur Deactivated Pd Foil Catalyst. <b>c.L. DIMAGGIO</b> , <b>D.D. BECK</b> , General Motors NAO R&D Center.
10:00 am	<b>SS1-WeM6</b> Ferromagnetic Phases at the Fe/Si(111) Interface. <b>J.P. WOODS</b> , <b>Y.L. HE</b> , <b>D. WILIPITIYA</b> , University of Nebraska.	<b>SS2-WeM6</b> Structural Effects of Well-Defined Palladium Surfaces on CO+NO Coadsorption and Reaction. <b>S.M. VESECKY</b> , <b>X. XU</b> , <b>P. CHEN</b> , <b>D.W. GOODMAN</b> , Texas A&M University.
10:20 am	<b>SS1-WeM7</b> Circular Dichroism in Core-Level Photoemission. <b>H. XIAO</b> , Univ. of California, Davis & Lawrence Berkeley Laboratory. <b>A.P. KADUWELA</b> , <b>M.A. VAN HOVE</b> , Lawrence Berkeley Laboratory. <b>C.S. FADLEY</b> , Univ. of California, Davis & Lawrence Berkeley Laboratory.	<b>SS2-WeM7</b> On the Kinetics of Methanation of CO on Nickel. <b>I. ALSTRUP</b> , Haldor Topsøe Research Laboratories, Denmark.
10:40 am	<b>SS1-WeM8</b> Spin-Specific Photoelectron Diffraction Using Magnetic X-ray Circular Dichroism. <b>J.G. TOBIN</b> , <b>G.D. WADDILL</b> , Lawrence Livermore National Laboratory. <b>X. GUO</b> , <b>S.Y. TONG</b> , University of Wisconsin, Milwaukee.	<b>SS2-WeM8</b> Experimental and Numerical Study of OH Radical Distribution and Temperature above a Platinum Foil in H <sub>2</sub> /O <sub>2</sub> Mixtures. <b>F. BEHRENDT</b> , <b>F. GUDMUNDSON</b> , <b>B. KASEMO</b> , <b>A. ROSÉN</b> , Chalmers Univ. of Technology and Univ. of Göteborg, Sweden.
11:00 am		
11:20 am		
11:40 am		

**NANO 3/NANOMETER-SCALE SCIENCE AND TECHNOLOGY/  
MANUFACTURING SCIENCE AND TECHNOLOGY**

**Room A209 - Session NSMS-WeM pg. 221**

**Industrial Applications of Scanned Probes**

**Moderator:** J.E. Griffith, AT&T Bell Laboratories.

**NANO 3/NANOMETER-SCALE SCIENCE AND TECHNOLOGY**

**Room A207 - Session NS2-WeM pg. 222**

**Atomic Manipulation**

**Moderators:** H. Tokumoto, Joint Research Center for Atomic Technology, Japan. L.J. Whitman, Naval Research Laboratory.

8:00 am	<b>NSMS-WeM0</b> Industrial Applications of Friction Force Microscopy. <b>J. BURGER</b> , A. LEIJALA, M. BINGGELI, R. CHRISTOPH, CSEM, Switzerland.	<b>NS2-WeM0</b> Theory of Atom Extraction by the Scanning Tunneling Microscopy from the First-Principles Calculation. <b>K. HIROSE</b> , M. TSUKADA, University of Tokyo, Japan.
8:20 am	<b>NSMS-WeM1 INVITED</b> Industrial Applications of Proximal Probes. <b>H. FUCHS</b> , Universität Münster, Germany.	<b>NS2-WeM1</b> Investigation of the Mechanism for Removing Atoms from Si(001) Surfaces with the STM. <b>C.T. SALLING</b> , M.G. LAGALLY, University of Wisconsin, Madison.
8:40 am	Invited talk continued.	<b>NS2-WeM2</b> Atomic-scale Modification on Si(111)7x7 Surfaces. <b>N. LIU</b> , Q.J. GU, Z.L. MA, W.B. ZHAO, X. CHU, Z.Q. XUE, S. PANG, Academia Sinica, P.R. China.
9:00 am	<b>NSMS-WeM3</b> Lateral and Vertical Dopant Profiling in Semiconductors by Atomic Force Microscopy using Conducting Tips. <b>P. DE WOLF</b> , T. CLARYSSE, <b>W. VANDERVORST</b> , IMEC, Belgium. L. HELLEMANS, J. SNAUWAERT, University of Leuven, Belgium.	<b>NS2-WeM3 INVITED</b> Nanometer Scale Patterning of Silicon Surfaces with an Ultrahigh Vacuum Scanning Tunneling Microscope. <b>J.W. LYDING</b> , University of Illinois, Urbana-Champaign.
9:20 am	<b>NSMS-WeM4</b> Scanning Tunneling Microscopy/Spectroscopy Doping Determination of Si and GaAs Bulk Materials and Device Structures. <b>R.M. SILVER</b> , J.A. DAGATA, W. TSENG, National Institute of Standards & Technology.	Invited talk continued.
9:40 am	<b>NSMS-WeM5 INVITED</b> Ultra-High Density Data Storage Based on Proximal Probes. <b>H.J. MAMIN</b> , B. TERRIS, S. HOEN, L.S. FAN, D. RUGAR, IBM Almaden Research Center.	<b>NS2-WeM5</b> Nanolithography with the STM on Si. <b>N. KRAMER</b> , J. JORITSMA, H. BIRK, C. SCHÖNENBERGER, Philips Research, The Netherlands.
10:00 am	Invited talk continued.	<b>NS2-WeM6</b> Local Deposition of Si on Si(111)(7x7) with the STM. <b>H. RAUSCHER</b> , U. MEMMERT, R.J. BEHM, Universität Ulm, Germany.
10:20 am	<b>NSMS-WeM7</b> Quantitative Dopant Profile Measurements on Si by Scanning Capacitance Microscopy. <b>Y. HUANG</b> , C.C. WILLIAMS, University of Utah. J. SLINKMAN, IBM Microelectronics.	<b>NS2-WeM7 INVITED</b> Nanofabrication with Laser Focused Atomic Deposition. <b>J. MCCLELLAND</b> , R.E. SCHOLTEN, R. GUPTA, R.J. CELOTTA, National Institute of Standards & Technology.
10:40 am	<b>NSMS-WeM8</b> Two-Dimensional Delineation of Semiconductor Doping by Scanning Resistance Microscopy. <b>J.N. NXUMALO</b> , D. SHIMIZU, C. SHAFAL, D.J. THOMSON, University of Manitoba, Canada.	Invited talk continued.
11:00 am		
11:20 am		
11:40 am		

# Wednesday Morning, October 26, 1994

**APPLIED SURFACE SCIENCE**  
Room A101 - Session AS-WeM pg. 223

**Quantitative Analysis, Emphasizing Angle-Resolved XPS**  
Moderator: J.T. Grant, University of Dayton.

**PLASMA SCIENCE**  
Room A109 - Session PS-WeM pg. 225

**Plasma Diagnostics**  
Moderator: S. C. McNevin, AT&T Bell Laboratories.

8:00 am	<b>AS-WeM0</b> Depth-Profiling by Angle-Resolved XPS and AES; Elastic Scattering Corrections, and Intrinsic Limits on Depth-Resolution. <b>P.J. CUMPTON</b> , National Physical Laboratory, United Kingdom.	<b>PS-WeM0</b> Laser-Induced Thermal Desorption as an In Situ Surface Probe during Plasma Processing. <b>I.P. HERMAN</b> , AT&T Bell Laboratories and Columbia University. <b>C.C. CHENG</b> , K.V. GUINN, V.M. DONNELLY, AT&T Bell Laboratories.
8:20 am	<b>AS-WeM1</b> Assessment of Overlayer Thickness Determination Model by Controlled Monolayers. <b>B.C. BEARD</b> , Akzo Nobel. <b>R.A. BRIZ-ZOLARA</b> , Naval Surface Warfare Center.	<b>PS-WeM1</b> Transport of Ions through High Aspect Ratio Apertures: Simultaneous, High Resolution Measurement of Angular and Energy Distribution Functions. <b>B. QUINIOU</b> , Lawrence Livermore National Laboratory. <b>E.S. AYDIL</b> , University of California, Santa Barbara. <b>L. HARRIOTT</b> , J.A. GREGUS, R.A. GOTTSCHO, AT&T Bell Laboratories.
8:40 am	<b>AS-WeM2</b> Inelastic Mean Free Pathlengths of X-ray Photoelectrons for Quantitative Investigation of Technological Ultrathin Layers. <b>W.H. GRIES</b> , Deutsche Bundespost Telekom, Germany.	<b>PS-WeM2</b> Measurement of the Electron Energy Distribution Function with a Differentially Pumped Spherical Sector Energy Analyzer. <b>K.D. SCHATZ</b> , <b>D.N. RUZIC</b> , University of Illinois, Urbana.
9:00 am	<b>AS-WeM3</b> Corrections to the Angle-Resolved X-ray Photoelectron Spectroscopy with Consideration of the Solid Acceptance Angle. <b>K.W. WONG</b> , R.W.M. KWOK, The Chinese University of Hong Kong.	<b>PS-WeM3</b> Applications of Real Time Ellipsometry for Characterizing Etch Profiles in Sub-Micron Features. <b>N. BLAYD</b> , A. GREVOZ, J.T.C. LEE, D.E. IBBOTSON, AT&T Bell Laboratories.
9:20 am	<b>AS-WeM4</b> Variation of Effective Sampling Depths with Direction in Core Photoelectron Emission from Single Crystals. <b>R.X. YNZUNZA</b> , Univ. of California, Davis & Lawrence Berkeley Laboratory. <b>R.E. COUCH</b> , S.D. RUEBUSH, S.L. CHAMBERLAN, University of California, Davis. <b>S. THEVUTHASAN</b> , Pacific Northwest Laboratory. <b>A.P. KADUWELA</b> , M.A. VAN HOVE, Lawrence Berkeley Laboratory. <b>C.S. FADLEY</b> , Univ. of California, Davis & Lawrence Berkeley Laboratory.	<b>PS-WeM4</b> Spatial Distribution of Argon Metastables in RF Plasmas Measured by 2-D LIF Imaging. <b>B.K. MCMILLIN</b> , M.R. ZACHARIAH, National Institute of Standards & Technology.
9:40 am	<b>AS-WeM5</b> A Novel Algorithm for Quantitative Elemental Depth Profiling by Angle-Resolved XPS. <b>J.M. WILLIAMS</b> , T.P. BEEBE, JR., University of Utah.	<b>PS-WeM5 INVITED</b> Diagnostics and Control of Radicals in an Inductively-Coupled Etching Reactor. <b>H. SUGAI</b> , K. NAKAMURA, Nagoya University, Japan. Y. HIKOSAKA, M. NAKAMURA, Fujitsu Ltd., Japan.
10:00 am	<b>AS-WeM6</b> A Comparison of XPS Quantitation using Electrostatic and Magnetic Lens-Based Analyses. <b>D.J. SURMAN</b> , A.R. WALKER, Kratos Analytical Inc. <b>T.A. ZUPP</b> , J. LUCKAS, L. PALEUDIS, B.J. TIELSCH, J.E. FULGHUM, Kent State University.	Invited talk continued.
10:20 am	<b>AS-WeM7</b> Quantification in Molecular SIMS. <b>B. HAGENHOFF</b> , K. MEYER, M. DEIMEL, D. RADING, W. SICHTERMANN, A. BENNINGHOVEN, Universität Münster, Germany.	<b>PS-WeM7</b> The Third Peak in 'Bimodal' Ion Energy Distributions. <b>D. VENDER</b> , R.J.M.M. SNIJKERS, G.M.W. KROESEN, F.J. DE HOOG, Eindhoven University of Technology, The Netherlands.
10:40 am	<b>AS-WeM8</b> Simultaneous Dual-Element Analyses of Platinum-Group Elements in Natural Occurring Matrixes using Resonance Ionization of Sputtered Atoms. <b>W.F. CALAWAY</b> , Argonne National Laboratory. <b>R.C. WIENS</b> , D.S. BURNETT, California Institute of Technology. <b>D.M. GRUEN</b> , M.J. PELLIN, Argonne National Laboratory.	<b>PS-WeM8</b> Monitoring InP and GaAs Etched in Cl <sub>2</sub> /Ar Plasma Generated by Electron Cyclotron Resonance Source using Optical Emission Spectroscopy. <b>S. THOMAS III<sup>†</sup></b> , K.K. KO, S.W. PANG, University of Michigan.
11:00 am		
11:20 am		
11:40 am		



**SURFACE SCIENCE/ELECTRONIC MATERIALS**

Room A102 - Session SSEM-WeM pg. 226

**Semiconductor Surface Reactions I**

Moderator: K. Raghavachari, AT&amp;T Bell Laboratories.

**THIN FILM**

Room A105 - Session TF-WeM pg. 228

**Optical, Piezoelectric and Ferroelectric Films**

Moderator: D. K. Chatterjee, Eastman Kodak Company.

8:00 am	<b>SSEM-WeM0</b> Structure Sensitivity of Trimethylgallium Chemisorption on GaAs Surfaces. J.R. CREIGHTON, Sandia National Laboratories.	<b>TF-WeM0 INVITED</b> Thin Film Optical Coatings. H.A. MACLEOD, Thin Film Center Inc.
8:20 am	<b>SSEM-WeM1 INVITED</b> Molecular Beam Scattering as a Probe of Thin Film Deposition Processes. J.R. ENGSTROM, Cornell University.	Invited talk continued.
8:40 am	Invited talk continued.	<b>TF-WeM2</b> Composition and Morphology of Al Multilayer Thin Film Reflective Coatings. J. KIM, J.J. WEIMER, D. TORR, M. ZUKIC, University of Alabama, Huntsville.
9:00 am	<b>SSEM-WeM3</b> GaF <sub>3</sub> Thin Films Grown on GaAs via Exposure to XeF <sub>2</sub> . W.C. SIMPSON, P.R. VAREKAMP, J.A. YARMOFF, University of California, Riverside & Lawrence Berkeley Lab.	<b>TF-WeM3</b> Production and Characterisation of Multilayer KCl:LiF Thin Films on Glass. F. SOMMA, A. ERCOLI, Università di Roma, Italy. S. SANTUCCI, L. LOZZI, M. PASSACANTANDO, P. PICOZZI, Università dell'Aquila, Italy.
9:20 am	<b>SSEM-WeM4</b> Initial Stages of Phosphorous Desorption from InP(110) Surfaces. PH. EBERT, University of Wisconsin, Madison. M. HEINRICH, M. SIMON, K. URBAN, Institut für Festkörperforschung, Germany. M.G. LAGALLY, University of Wisconsin, Madison.	<b>TF-WeM4</b> Heat Transport in Sputtered Optical Coatings. S.-M. LEE, D.G. CAHILL, University of Illinois, Urbana. T.H. ALLEN, Optical Coatings Lab, Inc.
9:40 am	<b>SSEM-WeM5</b> Interaction of 50 eV Electrons with D <sub>2</sub> O on GaAs(100): Electron and Thermal Induced Oxidation. D.W. SLOAN, Y.-M. SUN, J.M. WHITE, University of Texas, Austin.	<b>TF-WeM5 INVITED</b> Review of Recent Developments in Ferroelectric, Piezoelectric and Electrooptic Thin Films. A.I. KINGON, H.N. AL-SHAREEF, A. CHOW, D.J. LICHTENWALNER, D. AUCIELLO, North Carolina State University.
10:00 am	<b>SSEM-WeM6 INVITED</b> Characterization of Silicon Surfaces and Interfaces by Vibrational Spectroscopy. Y.J. CHABAL, M.A. HINES, D. FEIJOO, AT&T Bell Laboratories.	Invited talk continued.
10:20 am	Invited talk continued.	<b>TF-WeM7</b> Smart Thin Film TiNi/Piezoelectric Heterostructures. A.P. JARDINE, P.G. MERCADO, State University of New York, Stony Brook.
10:40 am	<b>SSEM-WeM8</b> Surface IR Investigation of Arsine Adsorption on GaAs(001). H. QI, P.E. GEE, R.F. HICKS, University of California, Los Angeles.	<b>TF-WeM8</b> Microstructures of Sputtered Thin Films on PbTiO <sub>3</sub> Families. T. SATOH, K. TABATA, K. WASA, RITE, Japan.
11:00 am		
11:20 am		
11:40 am		

# Wednesday Morning, October 26, 1994

## ELECTRONIC MATERIALS

Room A108 - Session EM-WeM pg. 229

### Heterostructures for Optoelectronics

Moderator: C.W. Wilmsen, Colorado State University.

## MANUFACTURING SCIENCE AND TECHNOLOGY

Room A110 - Session MS-WeM pg. 230

### Advanced Manufacturing Equipment - B

Moderator: C.B. Whitman, CVC Products, Inc.

8:00 am	<b>EM-WeM0</b> MBE Growth of II-VI Blue/Green Laser Diodes. D.C. GRILLO, M.D. RINGLE, J. HAN, R.L. GUNSHOR, G.C. HUA, Purdue University. A. SALOKATVE, H. JEON, A.V. NURMIKKO, Brown University.	<b>MS-WeM0</b> Long-throw Low-pressure Sputtering Technology for ULSI Devices. Y. KADOKURA, Y. KASHIMOTO, T. KIYOTA, N. MOTEGI, I. NAKAYAMA, ULVAC Japan, Ltd.
8:20 am	<b>EM-WeM1 INVITED</b> MBE Growth of ZnMgSSe and its Application to Blue and Green Laser Diodes. M. IKEDA, A. ISHIBASHI, Sony Corporation Research Center.	<b>MS-WeM1</b> Polysilicon Gate Etch Linewidth and Profile Control in 0.25- $\mu\text{m}$ $L_{\text{eff}}$ Logic Technology: Effects and Length Scale of Pattern Loading. J.W. ADKISSON, S.J. HOLMES, C.C. SMOLINSKI, R.P. MALLETTE, M.C. CANTELL, T.A. KNOTTS, IBM Microelectronics.
8:40 am	Invited talk continued.	<b>MS-WeM2</b> Interlayer Dielectrics with Low Dielectric Constant for Multilevel Interconnection. R. AOKI, N. HAYASAKA, Y. NISHIYAMA, H. MIYAJIMA, Y. NAKASAKI, H. OKANO, Toshiba Corporation, Japan.
9:00 am	<b>EM-WeM3</b> Structural and Compositional Characterization of HgSe Contacts to p-ZnSe. J.J. FIJOL, P.H. HOLLOWAY, J. TREXLER, J. KIM, K. JONES, University of Florida, Gainesville.	<b>MS-WeM3 INVITED</b> Manufacturing Issues of Electrostatic Chucks. D.R. WRIGHT, L. CHEN, P. FEDERLIN, K. FORBES, SEMATECH.
9:20 am	<b>EM-WeM4</b> Deep Level Interface States Near ZnSe/GaAs(100) Heterointerfaces. A.D. RAISANEN, L.J. BRILLSON, Xerox Webster Research Center. G. BRATINA, L. SORBA, A. FRANCIOSI, University of Minnesota.	Invited talk continued.
9:40 am	<b>EM-WeM5 INVITED</b> Materials Issues in II-VI Semiconductor Lasers. J.M. DEPUYDT, S. GUHA, M.A. HAASE, J. QIU, G.E. HOFER, B.J. WU, G. MEIS-HAUGEN, H. CHENG, 3M Company.	<b>MS-WeM5 INVITED</b> Equipment Engineering Methods for Improvements in Particle and Uniformity Performance during Plasma Processing. G.S. SELWYN, M. DALVIE, C.R. GUARNIERI, M. SURENDRA, IBM TJ Watson Research Center.
10:00 am	Invited talk continued.	Invited talk continued.
10:20 am	<b>EM-WeM7 INVITED</b> Heteroepitaxy of Nearly Lattice Matched Compound Semiconductors on Silicon. K.J. BACHMANN, N. DIETZ, S. FLECHTER, J.T. KELLIHER, H. CASTLEBERRY, G. WOOD, North Carolina State University.	<b>MS-WeM7</b> Plasma Process Uniformity in a High Density System: Experiment and Modeling. C.R. GUARNIERI, M. SURENDRA, G.S. SELWYN, M. DALVIE, IBM TJ Watson Research Center.
10:40 am	Invited talk continued.	<b>MS-WeM8</b> The Complex Impedance of a Dusty Processing Plasma. W.C. ROTH, R.N. CARLILE, University of Arizona.
11:00 am		
11:20 am		
11:40 am		

**BIOMATERIAL INTERFACES NANO 3/NANOMETER-SCALE  
SCIENCE AND TECHNOLOGY**

**Room A106 - Session BINS-WeM pg. 231**

**Artificial Cellular Assemblies**

**Moderator:** D.A. Stenger, Naval Research Laboratory.

8:00 am	<b>BINS-WeM0</b> Electrical Characterization of Artificial Neuronal Networks. <b>J.J. HICKMAN</b> , K.E. FOSTER, R.C. OPRISON, Science Applications International Corporation. D.A. STENGER, Naval Research Laboratory. A.E. SHAFFNER, J.L. BARKER, National Institutes of Health.	
8:20 am	<b>BINS-WeM1</b> Neuronal Cells Cultured on Modified Microelectronic Device Surfaces. <b>A. OFFENHAUSER</b> , J. RUHE, Frontier Research Program, RIKEN, Japan. W. KNOLL, RIKEN, Japan & Max-Planck-Institute of Polymer Res., Germany.	
8:40 am	<b>BINS-WeM2</b> Using both Topographic Control and Micropatterned Protein Substrates in Controlling Neuron Extension and Connection in Culture. <b>A.S.G. CURTIS</b> , S. BRITLAND, C.D.W. WILKINSON, University of Glasgow, United Kingdom.	
9:00 am	<b>BINS-WeM3 INVITED</b> Photochemically-driven Surface Modifications and Cellular and Biomolecular Assemblies with Micron-order Precision. <b>T. MATSUDA</b> , National Cardiovascular Center Research Institute, Japan.	
9:20 am	Invited talk continued.	
9:40 am	<b>BINS-WeM5</b> Cell Patterns and Whole-Cell Biosensors using Photonic Tweezers Technology. <b>J. RENKEN</b> , <b>S. SEEGER</b> , Universität Heidelberg, Germany.	
10:00 am	<b>BINS-WeM6</b> Modification and Refunctionalization of Fluoropolymers for Controlling and Directing Neurons at Interfaces. <b>T.G. VARGO</b> , et al., State University of New York, Buffalo.	
10:20 am	<b>BINS-WeM7</b> Directed Growth of Uromyces Hyphae on Integrated Circuit Substrates. <b>M.N. KOZICKI</b> , R.W. ROBERSON, T.K. WHIDDEN, S.E. KERSEY, Arizona State University.	
10:40 am	<b>BINS-WeM8</b> Patterning of Microtubules Observed with Atomic Force Microscopy. <b>D.C. TURNER</b> , C. CHANG, S.L. BRANDOW, Naval Research Laboratory. D.B. MURPHY, Johns Hopkins University Medical School.	
11:00 am		
11:20 am		
11:40 am		

# MY SCHEDULE

## Wednesday Morning, October 26, 1994

TIME	SESSION	ROOM
8:20 am		
8:40 am		
9:00 am		
9:20 am		
9:40 am		
10:00 am		
10:20 am		
10:40 am		
11:00 am		
11:20 am		
11:40 am		
12:00 pm		
12:45 pm		
Lunch		
when		
with		where

### OTHER EVENTS WEDNESDAY

7:00 a.m.	Companions Program (see insert) ( <b>Silver Room (H)</b> )
8:00 a.m.	Newsletter/Publicity Breakfast ( <b>Colorado Room (H)</b> )
9:00 a.m.	Low Pressure Gauges Subcommittee ( <b>Spruce Room (H)</b> )
10:00 a.m.	Scholarship Meeting ( <b>Birch Room (H)</b> )
12:00 Noon	Scholarship Luncheon ( <b>Aspen Room (H)</b> )

H=Radisson Hotel  
CC=Colorado Convention Center

### SHORT COURSES WEDNESDAY

8:30 a.m.	Vacuum Technology ( <b>Room C109 (CC)</b> )
8:30 a.m.	A Comprehensive Course on Surface Analysis: AES,XPS,SIMS, Depth Profiling, & ISS/RBS ( <b>Room C107 (CC)</b> )
8:30 a.m.	Physics, Chemistry, and Mechanics of Adhesion (New) ( <b>Room C105 (CC)</b> )
8:30 a.m.	Cryopump Technology ( <b>Room C103 (CC)</b> )
8:30 a.m.	Partial Pressure Analyzers: Analysis and Applications ( <b>Room C101 (CC)</b> )
8:30 a.m.	Vacuum Sealing and Joining Techniques ( <b>Room C108 (CC)</b> )
8:30 a.m.	An Introduction to Ellipsometry ( <b>Room C106 (CC)</b> )
8:30 a.m.	Plasma Etching and RIE ( <b>Room C104 (CC)</b> )
8:30 a.m.	Secondary Ion and Neutral Mass Spectrometries (SIMS,SNMS,SALI) ( <b>Room C107 (CC)</b> )
8:30 a.m.	Surface Preparation for Thin-Film Deposition ( <b>Room C110 (CC)</b> )

### Special or Focus Area Sessions

#### Silicon-based Optoelectronics

**EM-WeM** Heterostructures for Optoelectronics

#### Sensors, In-situ Diagnostics, Process Control

**PS-WeM** Plasma Diagnostics

#### Nanostructure Fabrication and Atomic-scale Manipulation

**NS2-WeM** Atomic Manipulation

## MY SCHEDULE

### Wednesday Afternoon, October 26, 1994

TIME	SESSION	ROOM
2:00 pm		
2:20 pm		
2:40 pm		
3:00 pm		
3:20 pm		
3:40 pm		
4:00 pm		
4:20 pm		
4:40 pm		
5:00 pm		

#### OTHER EVENTS WEDNESDAY

- 5:20 p.m. PST Division Business Meeting (**Room A109 (CC)**)  
 5:20 p.m. Vacuum Metallurgy Division Business Meeting (**Room A106 (CC)**)

H=Radisson Hotel  
 CC=Colorado Convention Center

#### SHORT COURSES WEDNESDAY

- 8:30 a.m. Vacuum Technology (**Room C109 (CC)**)  
 8:30 a.m. A Comprehensive Course on Surface Analysis: AES,XPS,SIMS, Depth Profiling, & ISS/RBS (**Room C107 (CC)**)  
 8:30 a.m. Physics, Chemistry, and Mechanics of Adhesion (New) (**Room C105 (CC)**)  
 8:30 a.m. Cryopump Technology (**Room C103 (CC)**)  
 8:30 a.m. Partial Pressure Analyzers: Analysis and Applications (**Room C101 (CC)**)  
 8:30 a.m. Vacuum Sealing and Joining Techniques (**Room C108 (CC)**)  
 8:30 a.m. An Introduction to Ellipsometry (**Room C106 (CC)**)  
 8:30 a.m. Plasma Etching and RIE (**Room C104 (CC)**)  
 8:30 a.m. Secondary Ion and Neutral Mass Spectrometries (SIMS,SNMS,SALI) (**Room C107 (CC)**)  
 8:30 a.m. Surface Preparation for Thin-Film Deposition (**Room C110 (CC)**)

#### Special or Focus Area Sessions

##### Silicon-based Optoelectronics

- EM-WeA** Wide-bandgap Nitrides  
**NS2-WeA** Optical Properties of Silicon Nanostructures

##### Sensors, In-situ Diagnostics, Process Control

- MS-WeA** Diagnostics, Sensors, and Control

##### Surface Contamination and Control

- PS-WeA** Plasma-Induced Charging and Contamination Effects

##### Nanostructure Fabrication and Atomic-Scale Manipulation

- TF-WeA** Deposition and Characterization Techniques of Nanostructures in Thin Films

# Wednesday Afternoon, October 26, 1994

## SURFACE SCIENCE

Room A205 - Session SS1-WeA pg. 233

### Surface Magnetism II

Moderator: B.P. Tonner, University of Wisconsin, Milwaukee.

## SURFACE SCIENCE

Room A201 - Session SS2-WeA pg. 234

### Solid Liquid Interfaces

Moderator: E.M. Stuve, University of Washington.

2:00 pm	<b>SS1-WeA1 INVITED</b> Experimental Studies of Surface and Interface Magnetism. H. HOPSTER, University of California, Irvine.	<b>SS2-WeA1 INVITED</b> Surface Reconstruction at the Metal-Electrolyte Interface. D.M. KOLB, University of Ulm, Germany.
2:20 pm	Invited talk continued.	Invited talk continued.
2:40 pm	<b>SS1-WeA3</b> Strain Accommodation and Atomic Order in the Non-pseudomorphic Growth of Ultrathin Fe Films on Cu(001). D.E. FOWLER, J.V. BARTH, IBM Research Division.	<b>SS2-WeA3</b> Underpotential Deposition of Silver on the Au(111) Single Crystal Electrode in Sulfate Media. Ex Situ and In Situ Comparison. P. MROZEK, Y.-E. SUNG, A. WIECKOWSKI, C.-H. CHEN, A.A. GEWIRTH, University of Illinois, Urbana.
3:00 pm	<b>SS1-WeA4</b> Magnetic Structure of Ultra-thin Mn Films on Fe(100)/Pd(100). G. STEIERL, C. RAU, Rice University.	<b>SS2-WeA4</b> Characterization of Carbon and Sulfur Covered Pt(111) and Their Influence on CO Adsorption and Electrooxidation. D.E. SAUER, R.L. BORUP, E.M. STUVE, University of Washington.
3:20 pm	<b>SS1-WeA5</b> Mossbauer Spectroscopy Study of Tetragonal-Ir-Distorted fcc Fe(100). J.W. FREELAND, D.F. STORM, I.L. GRIGOROV, D.J. KEAVNEY, J.C. WALKER, Johns Hopkins University.	<b>SS2-WeA5 INVITED</b> Structure and Phase Behavior of Electrode Surfaces. B.M. OCKO, J. WANG, G.M. WATSON, O.M. MAGNUSSEN, R. ADZIC, Brookhaven National Laboratory.
3:40 pm	<b>SS1-WeA6</b> Magnetic Properties of Fe and Mn Overlayers on Ir(111) by Soft X-ray Circular Dichroism. W.L. O'BRIEN, B.P. TONNER, University of Wisconsin, Milwaukee.	Invited talk continued.
4:00 pm	<b>SS1-WeA7 INVITED</b> Impact of Magnetism on the Stability of Ultrathin Films: The Magnetically Driven Two Dimensional Surface Alloy. S. BLÜGEL, IFF, Forschungszentrum Jülich, Germany.	<b>SS2-WeA7</b> In Situ EXAFS of Cu on Pt under Electrochemical Control. L. WANG, T.E. FURTAK, Colorado School of Mines. L.B. LURIO, J. PANT, T.M. HAYES, Rensselaer Polytechnic Institute.
4:20 pm	Invited talk continued.	<b>SS2-WeA8</b> Model Electrochemical Interfaces in Ultrahigh Vacuum: Ionic and Surface Solvation Probed by Infrared Spectroscopy. M.J. WEAVER, N. KIZHKEVARIAM, I. VILLEGAS, Purdue University.
4:40 pm	<b>SS1-WeA9</b> Enhanced Exchange Splitting of Gd at the Monolayer Limit. D. LI, Argonne National Laboratory. J. ZHANG, P.A. DOWBEN, University of Nebraska, Lincoln. M. ONELLION, University of Wisconsin, Madison.	<b>SS2-WeA9</b> Thermal and Photon-stimulated Interactions of Oxygen and Water Coadsorbates with Potassium on Graphite. D. CHAKAROV, L. ÖSTERLUND, B. KASEMO, Chalmers Univ. of Technology and Univ. of Göteborg, Sweden.
5:00 pm	<b>SS1-WeA10</b> The Connection between Morphology and Magnetic Characteristics for Gd Thin Films Grown on W(110). E.D. TOBER, R.X. YNZUNZA, University of California, Davis & Lawrence Berkeley Lab. A.P. KADUWELA, Lawrence Berkeley Laboratory. C.S. FADLEY, University of California, Davis & Lawrence Berkeley Lab.	<b>SS2-WeA10</b> Adsorption, Desorption, and Phase Transformation Kinetics of Multilayer D <sub>2</sub> O and H <sub>2</sub> O on Au(111) and Ru(0001). C. HUANG, E.K.L. WONG, R.S. SMITH, B.D. KAY, Pacific Northwest Laboratory.

<b>NANO 3/NANOMETER-SCALE SCIENCE AND TECHNOLOGY/BIOMATERIAL INTERFACES</b> <b>Room A209 - Session NSBI-WeA pg. 236</b> <b>Biology at the Nanoscale: I</b> <b>Moderator: L. Bottomley, Georgia Institute of Technology.</b>		<b>NANO 3/NANOMETER-SCALE SCIENCE AND TECHNOLOGY</b> <b>Room A207 - Session NS2-WeA pg. 237</b> <b>Optical Properties of Silicon Nanostructures</b> <b>Moderator: O.J. Glembocki, Naval Research Laboratory.</b>	
2:00 pm	<b>NSBI-WeA1</b> Non-contact Scanning Force Microscopy of F-actin. <b>D. BRAUNSTEIN</b> , J.A. SPUDICH, Stanford University.	<b>NS2-WeA1 INVITED</b> Light from Silicon. <b>F. KOCH</b> , Technical University Munich, Germany.	
2:20 pm	<b>NSBI-WeA2</b> Atomic Force Microscopy of Collagen Monomers, Fibrils and Fibrillar Complexes. <b>E.A.G. CHERNOFF</b> , IUPUI. <b>D.A. CHERNOFF</b> , Advanced Surface Microscopy, Inc.	Invited talk continued.	
2:40 pm	<b>NSBI-WeA3</b> Imaging Biological Systems with Near-Field Scanning Optical Microscopy. <b>J. HWANG</b> , The Johns Hopkins University. <b>E. BETZIG</b> , AT&T Bell Laboratories. <b>M. EDIDIN</b> , The Johns Hopkins University.	<b>NS2-WeA3</b> Visible Luminescence from Plasma Deposited Nanocrystalline Silicon Thin Films. <b>R.E. HOLLINGSWORTH</b> , Materials Research Group, Inc. <b>M. ESTES</b> , University of Colorado, Boulder. <b>C. DEHART</b> , P.K. BHAT, Materials Research Group, Inc.	
3:00 pm	Invited talk continued.	<b>NS2-WeA4</b> The Mechanism of Room Temperature Red Light Emission in Porous Silicon and Fabricated Silicon Nanostructures. <b>S.M. PROKES</b> , W.E. CARLOS, O.J. GLEMBOCKI, Naval Research Laboratory.	
3:20 pm	<b>NSBI-WeA5</b> Imaging Individual Protein Molecules by Scanning Probe Microscopy. <b>S.L. TANG</b> , A.J. MCGHIE, DuPont Central Research and Development.	<b>NS2-WeA5</b> Properties of Ultrathin Films of Porous Silicon. <b>J. VON BEHREN</b> , Univ. of Rochester & Technical University of Munich, Germany. <b>Y. KOSTOULAS</b> , L. TSYBESKOV, University of Rochester. <b>J.V. VANDYSHEV</b> , University of Rochester and Moscow State University, Russia. <b>P.M. FAUCHET</b> , University of Rochester.	
3:40 pm	<b>NSBI-WeA6</b> Nanometer-Scale Modification of Biological Membranes by Field Emission Scanning Tunneling Microscopy. <b>J. TAMAYO</b> , <b>R. GARCEA</b> , Centro Nacional de Microelectrónica, Spain.	<b>NS2-WeA6</b> Luminescent Porous Silicon Layers Fabricated by Anodisation and Supercritical Drying. <b>L.T. CANHAM</b> , T.I. COX, Defence Research Agency, United Kingdom.	
4:00 pm	<b>NSBI-WeA7</b> SPM Studies of Supramolecular Architecture at Biological Interfaces. <b>M. HARA</b> , W. KNOLL, RIKEN, Japan.	<b>NS2-WeA7</b> Visible Electroluminescence from Ultrathin Stain-Etched Porous Films. <b>J. XU</b> , A.J. STECKL, University of Cincinnati.	
4:20 pm	<b>NSBI-WeA8</b> Control of the Adsorption of the Photoactive Biological Purple Membrane to Surfaces using Self-Assembled Monolayers. <b>R.A. BRIZZOLARA</b> , Naval Surface Warfare Center.	<b>NS2-WeA8</b> Properties of Partially Oxidized Porous Silicon. <b>L. TSYBESKOV</b> , <b>P.M. FAUCHET</b> , University of Rochester.	
4:40 pm	<b>NSBI-WeA9</b> Force Modulation Imaging of Protein Membranes. <b>H. YAMADA</b> , Joint Research Center for Atom Technology, Japan. <b>Y. HIRATA</b> , J. MIYAKE, National Institute for Bioscience & Human-technology, Japan.	<b>NS2-WeA9</b> Enhancement and Suppression of the Formation of Porous Silicon. <b>S.P. DUTTAGUPTA</b> , C. PENG, P.M. FAUCHET, University of Rochester. <b>S.K. KURINEC</b> , Rochester Institute of Technology. <b>T. BLANTON</b> , Eastman Kodak Company.	
5:00 pm	<b>NSBI-WeA10</b> LB Films of Disintegrated Purple Membranes: Photo-electrical Properties and STM Investigation. <b>E.A. FEDOROV</b> , V.V. KISLOV, V.V. PANOV, A.A. KONONENKO, E.P. LUKASHEV, D.S. CHERNAV-SKII, Russian Academy of Science.		



# Wednesday Afternoon, October 26, 1994

## APPLIED SURFACE SCIENCE

Room A101 - Session AS-WeA pg. 239

### Depth Profiling

Moderator: A.L. Testoni, Digital Equipment Corporation.

## PLASMA SCIENCE

Room A109 - Session PS-WeA pg. 240

### Plasma-Induced Charging and Contamination Effects

Moderator: M. G. Blain, Sandia National Laboratories.

2:00 pm	<b>AS-WeA1 INVITED</b> Fundamental Limits to Sputter Depth Profiling: Atomic Force Microscopy of Ion Beam-Induced Topography. <b>E.-H. CIRLIN</b> , Hughes Research Laboratories.	<b>PS-WeA1</b> Effect of Plasma Overetch of Polysilicon on Gate Oxide Damage. <b>J.P. MCVITTIE</b> , Stanford University. <b>C.T. GABRIEL</b> , VLSI Technology.
2:20 pm	Invited talk continued.	<b>PS-WeA2</b> Plasma-Induced Gate Oxide Charging Issues for sub-0.5 $\mu$ m CMOS Technologies. <b>A.K. STAMPER</b> , J.B. LASKY, J.W. ADKISSON, IBM Microelectronics.
2:40 pm	<b>AS-WeA3</b> Determination of the Electron Attenuation Length from High Resolution AES Depth Profiles. <b>S. HOFMANN</b> , Max-Planck-Institut für Metallforschung, Germany.	<b>PS-WeA3 INVITED</b> Gate Oxide Damage due to Local Charging Caused by Electron Shading. <b>K. HASHIMOTO</b> , Fujitsu Ltd., Japan.
3:00 pm	<b>AS-WeA4</b> Resolution in Sputter Depth Profiling Assessed by AlAs/GaAs Superlattices. <b>K. KAJIWARA</b> , Sony Corporation, Japan. <b>R. SHIMIZU</b> , Osaka University, Japan.	Invited talk continued.
3:20 pm	<b>AS-WeA5</b> The Effects of Misorientation of the GaAs(100) Surface on the Secondary Ion Yield during O <sub>2</sub> <sup>+</sup> or Cs <sup>+</sup> Ion Sputtering. <b>J.W. LEE</b> , S.H. KIM, W.J. CHOI, C.Y. KIM, S.T. KIM, GoldStar Central Research Laboratory, Korea.	<b>PS-WeA5</b> Plasma-Induced-Damage of GaAs during Etching of Refractory Metal Contacts. <b>R.J. SHUL</b> , M.L. LOVEJOY, A.G. BACA, J.C. ZOLPER, C.I.H. ASHBY, D.J. RIEGER, M.J. HAFICH, J.F. KLEM, Sandia National Laboratories.
3:40 pm	<b>AS-WeA6</b> Sputtering Effects in SIMS Depth Profiles of Multicomponent Glasses. <b>V.J. BOJAN</b> , T.E. PAULSON, C.G. PANTANO, Pennsylvania State University.	<b>PS-WeA6</b> 2-D Visualization of Powder Formation and Trapping Dynamics in Silane Plasmas. <b>J.-L. DORIER</b> , CH. HOLLENSTEIN, A.A. HOWLING, C. COURTEILLE, L. SANSONNENS, CRPP/EPFL, Switzerland.
4:00 pm	<b>AS-WeA7</b> The Effect of Tilt Angle on As Implants in Si. <b>J.M. ANTHONY</b> , J.A. KEENAN, Texas Instruments.	<b>PS-WeA7</b> The Role of Electrode Characteristics in Particulate Trapping in RF Discharges. <b>J.D. DAUGHERTY</b> , D.B. GRAVES, University of California, Berkeley.
4:20 pm	<b>AS-WeA8</b> Nondestructive and Quantitative Depth Profiling Analysis of Ion Bombarded Surfaces by Medium Energy Ion Scattering Spectroscopy. <b>J.C. LEE</b> , H.J. KANG, H.K. KIM, D.W. MOON, Korea Research Institute of Standards and Science.	<b>PS-WeA8</b> Strategies for Controlling Dust Particle Transport in Inductively Coupled Plasmas. <b>H.H. HWANG</b> , <sup>†</sup> M. GRAPPERHAUS, M.J. KUSHNER, University of Illinois, Urbana.
4:40 pm	<b>AS-WeA9</b> Nondestructive EPMA Depth Profiling of Buried Oxide Layers in Silicon. <b>A.P. ALEXEYEV</b> , Research Centre for Surface and Vacuum Investigation, Russia.	<b>PS-WeA9</b> The Dynamics of Particulates in the Afterglow of an RF Excited Plasma. <b>C.K. YEON</b> , J.H. KIM, <b>K.W. WHANG</b> , Seoul National University, Korea.
5:00 pm	<b>AS-WeA10</b> Real Time Monitoring of Depth Profiling. <b>L.A. VASILYEV</b> , A.V. NAUMKIN, V.I. RAKHOVSKY, Research Centre for Surface and Vacuum Investigation, Russia.	<b>PS-WeA10</b> Post-Plasma Particle Dynamics in a Gaseous Electronics Conference Standard Cell. <b>S.M. COLLINS</b> , J.F. O'HANLON, R.N. CARLILE, University of Arizona. <b>D.A. BROWN</b> , Sandia National Laboratories.

<b>SURFACE SCIENCE/ELECTRONIC MATERIALS</b> <b>Room A102 - Session SSEM-WeA pg. 242</b> <b>Semiconductor Reactions II</b> <b>Moderator: T.W. Engel, University of Washington.</b>		<b>THIN FILM</b> <b>Room A105 - Session TF-WeA pg. 244</b> <b>Deposition and Characterization Techniques of Nanostructures in Thin Films</b> <b>Moderator: R. Sargent, OCLI.</b>
2:00 pm	<b>SSEM-WeA1</b> Thermal Stability of Hydroxyl Species on the SiO <sub>2</sub> Surface. <b>D. SNEH</b> , S.M. GEORGE, University of Colorado, Boulder.	<b>TF-WeA1 INVITED</b> Deposition and Characterization Techniques for Nanostructures in Thin Films. <b>J.C. BILELLO</b> , S.M. YALISOVE, University of Michigan.
2:20 pm	<b>SSEM-WeA2</b> Correlation of Surface Core Levels and Structural Building Blocks through High Resolution Core Level Spectroscopy: Si(111)-(7x7). <b>J.J. PAGGEL</b> , W. THEIS, <b>K. HORN</b> , Fritz-Haber-Institut der MPG, Germany. <b>CH. JUNG</b> , C. HELLWIG, H. PETERSEN, BESSY GmbH, Germany.	Invited talk continued.
2:40 pm	<b>SSEM-WeA3</b> Abstraction of H from Group IV Surfaces by Atomic Hydrogen. <b>D.D. KOLESKE</b> , S.M. GATES, IBM TJ Watson Research Center. <b>B. JACKSON</b> , University of Massachusetts.	<b>TF-WeA3</b> Crystallographic Relations in Zirconia-Alumina Multilayer Nanolaminates. <b>M. GAJDARDZISKA-JOSIFOVSKA</b> , <b>C.R. AITA</b> , University of Wisconsin, Milwaukee.
3:00 pm	<b>SSEM-WeA4</b> Local Adsorbate Structures of F <sub>2</sub> Chemisorbed onto the Si(111)-7x7 Surface: A Molecular Beam/STM Study. <b>J.A. JENSEN</b> , C. YAN, A.C. KUMMEL, University of California, San Diego.	<b>TF-WeA4</b> A Novel Technique for Characterizing the Surface Coverage of CVD Films in Ultra-High-Aspect-Ratio Microstructures. <b>R.J. SOAVE</b> , G.W. TASKER, Galileo Electro-Optics Corporation. <b>J.W. MAYER</b> , Arizona State University. <b>Y. SHACHAM-DIAMAND</b> , Cornell University.
3:20 pm	<b>SSEM-WeA5 INVITED</b> First-Principles Study of Structures and Reactions on Si/SiO <sub>2</sub> Surfaces. <b>K. RAGHAVACHARI</b> , AT&T Bell Laboratories.	<b>TF-WeA5</b> Fabrication of Thin Films with Highly Porous Microstructures. <b>K. ROBBIE</b> , S.K. DEW, University of Alberta, Canada. <b>T. SMY</b> , Carleton University, Canada. <b>M.J. BRETT</b> , University of Alberta, Canada.
3:40 pm	Invited talk continued.	<b>TF-WeA6</b> Heteroepitaxial Growth of C <sub>70</sub> Films on MoS <sub>2</sub> and Their Characterization by LEED, XPS, and UPS. <b>B.Y. HAN</b> , <b>K. HEVESI</b> , L.M. YU, G. GENSTERBLUM, <b>J.-J. PIREAUX</b> , P.A. THIRY, R. CAUDANO, Facultés Universitaires Notre-Dame de la Paix, Belgium.
4:00 pm	<b>SSEM-WeA7</b> Translational-Energy-Induced Etching of n <sup>+</sup> Si(100) by Hyperthermal Cl <sub>2</sub> Molecular Beams. <b>Y. TERAOKA</b> , I. NISHIYAMA, NEC Corporation, Japan.	<b>TF-WeA7</b> Compositional and Microstructural Characterization of Fe-N Thin Films for Recording Sensor Applications. <b>Y.K. KIM</b> , P.B. NARAYAN, Rocky Mountain Magnetics, Inc.
4:20 pm	<b>SSEM-WeA8</b> Vacancy-Mediated and Ion-Enhanced Surface Diffusion on Semiconductors. <b>C.E. ALLEN</b> , <b>E.G. SEEBAUER</b> , University of Illinois, Urbana. <b>I.I. SUNI</b> , Clarkson University.	<b>TF-WeA8</b> Positron Annihilation Studies of Diamond-like Nanocomposite (DLN) Films. <b>P. ASOKA-KUMAR</b> , Brookhaven National Laboratory. <b>B.F. DORFMAN</b> , M.G. ABRAIZOV, Polytechnic University. <b>D. YAN</b> , F.H. POLLAK, Brooklyn College of CUNY.
4:40 pm	<b>SSEM-WeA9</b> Thermal and Photochemical Reactions of HN <sub>3</sub> on Ge(100): A Lower Temperature Route to Germanium Nitride. <b>C. TINDALL</b> , J.C. HEMMINGER, University of California, Irvine.	<b>TF-WeA9 INVITED</b> Microhardness Characterization of Substrates and Films. <b>R. BRADT</b> , University of Nevada, Reno.
5:00 pm	<b>SSEM-WeA10</b> Surface Phase Transformations in the Ni/Si(111) System: Real-Time Observations using LEEM and STM. <b>P.A. BENNETT</b> , M.Y. LEE, S.A. PARIKH, Arizona State University. <b>K. WORM</b> , University of Clausthal, Germany. <b>R.J. PHANEUF</b> , University of Maryland.	Invited talk continued.

# Wednesday Afternoon, October 26, 1994

## ELECTRONIC MATERIALS

Room A108 - Session EM-WeA pg. 245

### Wide-bandgap Nitrides

Moderator: P.D. Holloway, University of Florida, Gainesville.

## MANUFACTURING SCIENCE AND TECHNOLOGY

Room A110 - Session MS-WeA pg. 247

### Diagnostics, Sensors, and Control

Moderator: L.M. Cecchi, Sandia National Laboratories.

2:00 pm	<b>EM-WeA1</b> Low Carrier Concentration GaN Grown by MOCVD at Low Temperature (720°). J.C. CHEN, B. YANG, University of Maryland Baltimore County. F. SEMENDY, N. BAMBHA, Army Research Laboratory, Ft. Belvoir.	<b>MS-WeA1 INVITED</b> Process Control in Semiconductor Manufacturing. S.W. BUTLER, Texas Instruments.
2:20 pm	<b>EM-WeA2</b> Ohmic Contacts to Intrinsic n-Type GaN. S.J. MILLER, P.H. HOLLOWAY, University of Florida, Gainesville. J. PANKOVE, University of Colorado, Boulder.	Invited talk continued.
2:40 pm	<b>EM-WeA3 INVITED</b> InGaN/AlGaIn Blue-Light-Emitting Diodes. S. NAKAMURA, Nichia Chemical Industries Ltd., Japan.	<b>MS-WeA3</b> A Production Demonstration of Wafer-to-Wafer Plasma Gate Etch Control by Adaptive Real-Time Computation of the Over-Etch Time from In Situ Process Signals. E.A. RIETMAN, AT&T Bell Laboratories. S.H. PATEL, AT&T Microelectronics.
3:00 pm	Invited talk continued.	<b>MS-WeA4</b> Real-Time Process Control Method using Ellipsometry Applied to Gate Etching. J.T.C. LEE, N. BLAYO, A. GREVOZ, H.L. MAYNARD, D.E. IBBOTSON, AT&T Bell Laboratories.
3:20 pm	<b>EM-WeA5</b> Atomic Layer Deposition of Aluminum Nitride at Lower Temperatures Using Dimethylethylamine:alane and Ammonia. J.N. KIDDER, JR., J.W. ROGERS, JR., T.P. PEARSALE, J. KUO, H. LUI, A. LUDVIKSSON, University of Washington.	<b>MS-WeA5 INVITED</b> The Application of Real-Time Optical Monitors to Semiconductor Manufacturing. J. O'NEILL, IBM Microelectronics.
3:40 pm	<b>EM-WeA6</b> Growth of Epitaxial Aluminum Nitride Films on Hydrogen Terminated Si(111) Surfaces. F. AHMAD, T. LENANE, G. AUNER, R. NAIK, Wayne State University.	Invited talk continued.
4:00 pm	<b>EM-WeA7</b> Growth of $\text{In}_x\text{Al}_{1-x}\text{N}$ and $\text{In}_x\text{Ga}_{1-x}\text{N}$ by Metalorganic Molecular Beam Epitaxy. C.R. ABERNATHY, S.J. PEARTON, J.D. MACKENZIE, S. BHARATAN, K.S. JONES, University of Florida, Gainesville.	<b>MS-WeA7</b> Real-Time Process and Product Diagnostics in RTCVD using In Situ Mass Spectroscopic Sampling. L.L. TEDDER, G.W. RUBLOFF, North Carolina State University. I. SHAREEF, M. ANDERLE, D.-H. KIM, IBM TJ Watson Research Center. G.N. PARSONS, North Carolina State University.
4:20 pm	<b>EM-WeA8</b> Outdiffusion of Deuterium from GaN, AlN and InN. R.G. WILSON, Hughes Research Laboratories. S.J. PEARTON, C.R. ABERNATHY, University of Florida, Gainesville. J.M. ZAVADA, U.S. Army Research Office.	<b>MS-WeA8</b> Mass Spectrometric In Situ Process Monitoring Applied to Silicon Dioxide Electron Cyclotron Resonance Chemical Vapor Deposition. L.M. WILLIAMS, Lam Research Corp. L.C. FREES, T. VO, Leybold Inficon Inc.
4:40 pm		<b>MS-WeA9 INVITED</b> Microsensors for Process Control and Monitoring. R.C. HUGHES, J.J. WICZER, Sandia National Laboratories.
5:00 pm	<b>EM-WeA10</b> Dry Etching of GaN and AlGaIn. I. ADESIDA, A.T. PING, University of Illinois, Urbana-Champaign. M. ASIF KHAN, D.T. OLSON, J.N. KUZ-NIA, APA Optics, Inc.	Invited talk continued.

## VACUUM METALLURGY

Room A106 - Session VM-WeA pg. 248

### Thin Film Microstructure Evolution

Moderator: L. Hultman, Linköping University, Sweden.

2:00 pm	<b>VM-WeA1</b> Effects of High Flux Low Energy (~20 eV) Ion Irradiation during Growth on the Microstructure and Preferred Orientation in TiN Films Deposited by Magnetron Sputtering. <b>I. PETROV</b> , J.E. GREENE, University of Illinois, Urbana. <b>L. HULTMAN</b> , J.-E. SUNDGREN, Linköping University, Sweden.	
2:20 pm	<b>VM-WeA2</b> The Effect of 20-95 eV Ar Ion Bombardment on Molecular Beam Epitaxy of GaAs(100). <b>J. MIRECKI MILLUNCHICK</b> , S.A. BARNETT, Northwestern University. <b>L. HULTMAN</b> , Linköping University, Sweden.	
2:40 pm	<b>VM-WeA3 INVITED</b> Theoretical Considerations on Stress Effects on Thin Film Microstructure. <b>D.J. SROLOVITZ</b> , University of Michigan.	
3:00 pm	Invited talk continued.	
3:20 pm	<b>VM-WeA5 INVITED</b> Surface Thermodynamics Effects on Thin Film Microstructure. <b>R.C. CAMMARATA</b> , Johns Hopkins University.	
3:40 pm	Invited talk continued.	
4:00 pm	<b>VM-WeA7</b> A Molecular Dynamics Study of Transient Processes during Deposition on (001) FCC Metal Surfaces. <b>C.M. GILMORE</b> , The George Washington University & Naval Research Laboratory. <b>J.A. SPRAGUE</b> , Naval Research Laboratory.	
4:20 pm	<b>VM-WeA8</b> Synthesis of Epitaxial $\text{Sn}_x\text{Ge}_{1-x}$ Alloy Films by Ion Assisted Molecular Beam Epitaxy and Pulsed Laser Deposition. <b>G. HE</b> , M.E. TAYLOR, H.A. ATWATER, California Institute of Technology.	
4:40 pm	<b>VM-WeA9</b> Scanning Tunneling Microscopy Studies of the Effect of Annealing on Gold Films. <b>D. PORATH</b> , <b>E. BAR-SADEH</b> , <b>M. WOLOVELSKY</b> , <b>A. GRAYEVSKY</b> , <b>Y. GOLDSTEIN</b> , <b>O. MILLO</b> , The Hebrew University of Jerusalem, Israel.	
5:00 pm	<b>VM-WeA10</b> Structure-Property Relationships in Compositionally Modulated Titanium-Aluminum Thin Films. <b>R. AHUJA</b> , <b>H.L. FRASER</b> , The Ohio State University.	

# Wednesday Afternoon Poster Sessions

## SURFACE SCIENCE

Room BR4 - Session SS-WeP pg. 250

### Aspects of Surface Science

Moderator: J.C. Hemminger, University of California, Irvine.

Presenters present: 5:00-6:30 pm.

**SS-WeP1** Elevated Temperature Structures of the Ag on Si(111) System at Submonolayer Coverages. **G. NAVROTSKI**, J.M. BLAKELY, Cornell University.

**SS-WeP2** Surface Morphology Induced by Ga and Sn Overlayers on Si(100) and Si(311) Surfaces. **L. LI**, Y. WEI, I.S.T. TSONG, Arizona State University.

**SS-WeP3** STM Studies of Benzene Adsorption on both Clean and O-preadsorbed Ni(110). **L. RUAN**, I. STENSGAARD, F. BESENBACHER, E. LAEGSGAARD, Aarhus University, Denmark.

**SS-WeP4** Determination of the Reconstruction of Pt(100) Surface on Atomic Scale by Scanning Tunneling Microscope. **C.S. CHANG**, W.B. SU, T.T. TSONG, Academia Sinica, ROC.

**SS-WeP5** Multiple Tunneling Gap Resistance Imaging for Surface Structure Determination with the STM. **J.C. DUNPHY**, Lawrence Berkeley Laboratory. **P. SAUTET**, Inst. Recherche Catalyse & Lab. de Chimie Theorique, France. **D.F. OGLETREE**, M. SALMERON, Lawrence Berkeley Laboratory.

**SS-WeP6** Cu Deposition on Ru(0001) by Low Energy Li<sup>+</sup> Ion Scattering. **Y.G. SHEN**, D.J. O'CONNOR, J. YAO, R.J. MACDONALD, University of Newcastle, Australia. **H. VAN ZEE**, Eindhoven University of Technology, The Netherlands. **R.H. ROBERTS**, University of Newcastle, Australia. **K. WANDELT**, Universität Bonn, Germany.

**SS-WeP7** Morphological Effects of Ultrathin Metal Films on Mo(111). **J. GUAN**, **R.A. CAMPBELL**, T.E. MADEY, Rutgers University.

**SS-WeP8** Highly Angular Resolved Patterns of Photo- and Auger-Electron Diffraction from MgO(001). **Y. NIHEI**, H. ISHII, M. OWARI, Y. ICHINOHE, University of Tokyo, Japan.

**SS-WeP9** Structural Surface Phase Transitions during Segregation Competition. **M. MILITZER**, The University of British Columbia, Canada. **S. HOFMANN**, Max-Planck-Institut für Metallforschung, Germany.

**SS-WeP10** Direct Determination of Adsorbate Positions with Energy-Dependent and Angle-Resolved Photoelectron Diffraction. **H. WU**, G.J. LAPEYRE, Montana State University.

**SS-WeP11** Magneto-Optical Kerr Effect of Exchange Coupling in Co/Cr/Co Films on Pd(111) and Pd(100) Substrates. **J.D. MCKINLEY**, C. RAU, Rice University.

**SS-WeP12** Thickness- and Temperature-Dependent Spin Reorientation Transition of Epitaxial Ni Films on Single Crystal Cu Surfaces. **S.Z. WU**, G.J. MANKEY, R.F. WILLIS, Pennsylvania State University.

**SS-WeP13** Experimental Fermi Surface of Magnetic Multilayers. **C. CASADO**, J. AVILA, A. VJATKIN, Université Paris-Sud, France. **F. SORIA**, Instituto de Ciencia de Materiales de Madrid, Spain. **M.C. ASENSIO**, Université Paris-Sud, France.

**SS-WeP14** Combined XPD, STM, and LEED Study of Iron Oxide Films on Pt(111). **Y.J. KIM**, Lawrence Berkeley Laboratory & University of Hawaii. **C. WESTPHAL**, Lawrence Berkeley Laboratory and Univ.-GHS-Essen, Germany. **R.X. YNZUNZA**, H. XIAO, Z. WANG, Lawrence Berkeley Laboratory & Univ. of California, Davis. **H.C. GALLOWAY**, Lawrence Berkeley Laboratory & Univ. of California, Berkeley. **M. SALMERON**, M.A. VAN HOVE, Lawrence Berkeley Laboratory. **C.S. FADLEY**, Lawrence Berkeley Laboratory & Univ. of California, Davis.

**SS-WeP15** Surface-Specific Magnetic Order Transitions for Ising Ferromagnets and Antiferromagnets: Implications for Spin-Polarized Photoelectron Diffraction. **F. ZHANG**, Univ. of California, Davis & Lawrence Berkeley Laboratory. **S. THEVUTHASAN**, Pacific Northwest Laboratory. **R. SCALETTER**, R. SINGH, University of California, Davis. **C.S. FADLEY**, Univ. of California, Davis & Lawrence Berkeley Laboratory.

**SS-WeP16** Imaging Short-Range Magnetic Order by Spin-Polarized Photoelectron Holography. **Z. WANG**, Univ. of California, Davis & Lawrence Berkeley Laboratory. **A.P. KADUWELA**, Lawrence Berkeley Laboratory. **S. THEVUTHASAN**, Pacific Northwest Laboratory. **M.A. VAN HOVE**, Lawrence Berkeley Laboratory. **C.S. FADLEY**, Univ. of California, Davis & Lawrence Berkeley Laboratory.

**SS-WeP17** Magnetic Circular and Linear Dichroism in Angular Resolved Fe 3p Core Level Photoemission. **E. TAMURA**, G.D. WADDILL, J.G. TOBIN, P.A. STERNE, Lawrence Livermore National Laboratory.

**SS-WeP18** Investigation of the Curie Temperature of Iron Bilayer Components of Fe(110)/Ag(111) Multilayers Grown by Molecular Beam Epitaxy. **D.F. STORM**, D.J. KEAVNEY, J.W. FREELAND, I. GRIGOROV, J.C. WALKER, Johns Hopkins University.

**SS-WeP19** Reaction of HN<sub>3</sub> with Al(111): Growth of an AlN Film. **J.N. RUSSELL, JR.**, Naval Research Laboratory.

**SS-WeP20** Tailoring Sensing Film Selectivity and Sensitivity using Principles from the Hard/Soft Lewis Acid-Base (HSAB) Paradigm. **V. THOMAS**, J.W. SCHWANK, J.L. GLAND, University of Michigan.

**SS-WeP21** Differential-Conversion Temperature Programmed Desorption: A New Method for Obtaining Biomolecular Surface Rate Constants. **R.P. SOUTHWELL**, E.G. SEEBAUER, University of Illinois, Urbana.

**SS-WeP22** Effect of Fluorination on the Reaction Kinetics of the Phenyl Coupling Reaction on Cu(111). **J.M. MEYERS**, University of Illinois, Urbana. **A.J. GELLMAN**, Carnegie Mellon University.

**SS-WeP23** Thermal and Electron-Induced Chemistry of CF<sub>3</sub>I on Ni(100). **M.B. JENSEN**, P.A. THIEL, Iowa State University.

**SS-WeP24** Thermally Stimulated Desorption of Neutral CF<sub>3</sub> from CF<sub>3</sub>I on Ag(111). **K.H. JUNKER**, Z.-J. SUN, T.B. SCOGGINS, J.M. WHITE, University of Texas, Austin.

**SS-WeP25** Cyclopropyl on Cu(111): Area Selective Preparation and Vibrational Analysis Using a Dispersion-Compensation HREELS Spectrometer. **R. MARTEL**, A.P. ROCHEFORT, P.H. MCBREEN, Université Laval, Canada.

**SS-WeP26** Electron Induced Dissociation of Methanol Multilayers on Mo(110). **T.D. HARRIS**, D.H. LEE, M.Q. BLUMBERG, **C.R. ARU-MAINAYAGAM**, Wellesley College.

**SS-WeP27** Kinetics of Propene Desorption from Pd(111). **N.A. THORNBURG**, I.M. ABDELREHIM, C.M. GERTH, E.A. PICCIOTTO, D.P. LAND, University of California, Davis.

**SS-WeP28** Adsorption and Film Growth of BTA on the Clean and Oxygen Adsorbed Cu(110) Surfaces. **K. CHO**, J. KISHIMOTO, T. HASHIZUME, Tohoku University, Japan. **H.W. PICKERING**, Pennsylvania State University. **T. SAKURAI**, Tohoku University, Japan.

**SS-WeP29** Thermal Stability of Silver in Ion Exchanged Soda Lime Glasses. **P.W. WANG**, T. FAN, University of Texas, El Paso.

**SS-WeP30** First IR Spectroscopic Evidence of Strained Cyclic Reaction Sites on the Borosilicate Glass (BSG) Surface. **L.L. TEDDER**, J.E. CROWELL, University of California, San Diego. **K.J. URAM**, Lam Research Corporation.

**NANO 3/NANOMETER-SCALE SCIENCE AND TECHNOLOGY**  
**Room BR4 - Session NS-WeP pg. 254**

**Nanometer-Scale Science and Technology**

**Moderator:** R.J. Colton, Naval Research Laboratory.

Presenters present: 5:00-6:30 pm.

**NS-WeP1** The Nanometer-scale Structure of Isocyanide Functionalized Polyaniline Thin Films. T.L. PORTER, A.G. SYKES, Y. SHI, G. CAPLE, Northern Arizona University.

**NS-WeP2** Structural Characteristics of a Uniquely Nanostructured Organic Thin Film. M.K. DEBE, A.R. DRUBE, 3M Company.

**NS-WeP3** Nucleation and Growth Kinetics of Monolayer Organic Films Studied with Graphite Etch Pits and STM. V.J. CEE, D.L. PATRICK, T.P. BEEBE, JR., University of Utah.

**NS-WeP4** Scanning Force Microscopy of Quasi-single Crystalline Polyethylene and Nylon 6 Produced by Channel Dye Compression. C. WANG, R.-E. RIEMANN, M. DRECHSLER, H.-J. CANTOW, Albert-Ludwigs University, Germany.

**NS-WeP5** Nanoclusters of Polymethylene at Au(111) Surfaces. K. SESHADRI, S. ATRE, Pennsylvania State University. Y.T. TAO, Academia Sinica, ROC. D.L. ALLARA, Pennsylvania State University.

**NS-WeP6** Amorphous and Ordered Layers of Oligothiophenes: A Combined AFM-, UPS-, HREELS-, and Conductivity Study. O. BÖHME, D. OETER, C. ZIEGLER, W. GÖPEL, University of Tübingen, Germany.

**NS-WeP7** Substrate Effects on Two-Dimensional Ordering of Self-Assembled Layers on TMDs by STM. D.L. SAMPSON, B.A. PARKINSON, Colorado State University.

**NS-WeP8** Scanning Force Microscopy of Stearic Acid LB Film Deposited on Mica. J. LI, W. YAN, S. XI, E. WANG, Chinese Academy of Sciences.

**NS-WeP9** Atomic Force Microscopy Investigation of the Structure and Orientation Ordering in C<sub>70</sub> Single Crystal. L. JIANG, L.A. NAGAHARA, J. LI, N. KINO, T. IYODA, K. HASHIMOTO, K. KITAZAWA, A. FUJISHIMA, University of Tokyo, Japan.

**NS-WeP10** Force Microscopic Studies of Langmuir-Blodgett Film of Complex TTF<sub>3</sub>C<sub>60</sub>Br<sub>2</sub>. P.-C. ZHANG, C. BAI, D. ZHU, M. HAN, Y. XU, Y. LIU, Chinese Academy of Sciences.

**NS-WeP11** Structure and Electrical Property of C<sub>60</sub>/Ag Ultrafine Particle-Polymer Thin Films. H.J. GAO, Z.Q. XUE, Q.D. WU, Peking University, P.R. China. S. PANG, Academia Sinica, P.R. China.

**NS-WeP12** The AFM as a Tool for Metal Surface Modification. H. GÖBEL, P. VON BLANCKENHAGEN, W. SCHOMMERS, Kernforschungszentrum Karlsruhe, Germany.

**NS-WeP13** Nanometer Scale Modifications of Gold Surfaces by STM. A. OHI, JRCAT-ATP, Japan. W. MIZUTANI, H. TOKUMOTO, JRCAT-NAIR, Japan.

**NS-WeP14** Nano-scale Layer Removal of Metal Surfaces by SPM Scratching. T. SUMOMOGI, T. ENDO, K. KUWAHARA, Hiroshima-Denki Institute of Technology, Japan. R. KANEKO, NTT Interdisciplinary Research Laboratories, Japan.

**NS-WeP15** Nanofabrication of Gold Surface with Scanning Tunneling Microscope by Combination of Mechanical and Electrical Method. Y. ISHIKAWA, N. UMEDA, A. TAKAYANAGI, Tokyo University of Agriculture and Technology, Japan.

**NS-WeP16** Ordered Nanostructures Prepared by Oxidizing Treatment of Graphite Surface: STM and Angle-resolved XPS Study. M.O. BASHKIN, S.D. DUBROVENSKY, A.V. EMEL'YANOV, A.A. MALKOV, A.A. MAL'YGIN, S.M. PORTNOV, A.V. SCHUKAREV, A.V. ZIMIN, Zelenograd Research Institute of Physical Problems, Russia.

**NS-WeP17** Nanostructure of Cleaved Surface of Bi Crystal. A.M. TROIANOVSKII, V.S. EDELMAN, Academy of Science of Russia.

**NS-WeP18** Scanning Tunneling Microscopy of Transition-Metal Clusters. P.E. QUESENBERY, T.A. HANN, P.N. FIRST, Georgia Institute of Technology.

**NS-WeP19** Lateral Anisotropic Anodization Property of Silicon. I. YU, Kyungpook National Univ. & Kyungdong Junior College, Korea. K.-Y. PARK, J.-H. SIM, J.-K. SHIN, J.-H. LEE, J.-H. LEE, Kyungpook National University, Korea.

**NS-WeP20** Doping and Photoeffects in Layered Semiconductors Studied with Scanning Tunneling Microscopy. D.R. LOUDER, B.A. PARKINSON, Colorado State University.

**NS-WeP21** X-SFM, XPS, and SIMS Study of Cobalt Catalysts on Silica. K.A. PISCHOW, E.O. RISTOLAINEN, M.K. NIEMELÄ, K.O. KRAUSE, Helsinki University of Technology, Finland.

**NS-WeP22** Observation of Atomic Ordering in GaInP<sub>2</sub> by Scanning Probe Microscopy. Y. LENG, Y.J. HUANG, C.C. WILLIAMS, L.C. SU, G.B. STRINGFELLOW, University of Utah.

**NS-WeP23** Structural Analysis of Domain Boundaries on Si(111)7x7 Surfaces by STM. Q.J. GU, Z.L. MA, N. LIU, X. GE, W.B. ZHAO, X. CHU, Z.Q. XUE, S. PANG, Academia Sinica, P.R. China.

**NS-WeP24** Atomically Resolved Image of Cleaved Surface of Compound Semiconductors Observed with an Ultrahigh Vacuum Atomic Force Microscope. M. OHTA, Y. SUGAWARA, Hiroshima University, Japan. M. SUZUKI, NTT Interdisciplinary Labs, Japan. S. MISHIMA, T. OKADA, Olympus Optical Co., Ltd., Japan. S. MORITA, Hiroshima University, Japan.

**NS-WeP25** Studies of Etale Deposition of CdSe on the Low Index Planes of Gold. T.E. LISTER, R.D. HERRICK III, J.L. STICKNEY, University of Georgia.

**NS-WeP26** Effects of Current Stimulated Adsorption in STM Investigation of Si Surface in Ambient Air. A.A. BUKHARAEV, E.A. SAMARSKY, V.M. JANDUGANOV, N.V. BERDUNOV, P.G. ANTONOV, Kazan Physical Tech. Institute Russian Academy of Science.

# Wednesday Afternoon Poster Sessions

## PLASMA SCIENCE

Room BR4 - Session PS-WeP pg. 258

### Plasma Etching and Inertial Confinement Fusion Targets

Moderator: J.L. Cecchi, University of New Mexico.

Presenters present: 5:00-6:30 pm.

**PS-WeP1** Extraction of Oxygen for CO<sub>2</sub> using Glow-Discharge and Permeation Techniques. **D. WU**, R.A. OUTLAW, R.L. ASH, Old Dominion University.

**PS-WeP2** Temperature-dependent Reaction Kinetics for the Si/XeF<sub>2</sub> System. **M.J.M. VUGTS**, M.F.A. EURLINGS, G.L.J. VERSCHUEREN, L.J.F. HERMANS, **H.C.W. BEIJERINCK**, Eindhoven University of Technology, The Netherlands.

**PS-WeP3** Reactive Ion Etching-Induced Damages in GaAs/AlGaAs Quantum Well Structures and Recovery by Rapid Thermal Annealing and Hydrogen Passivation. **B.-S. YOO**, **S.-J. PARK**, K.-H. PARK, Electronics and Telecommunications Research Institute, Korea.

**PS-WeP4** Characterization of ECR Plasmas with a Quadrupole Mass Spectrometer and Cylindrical Mirror Energy Analyzer. **S. BEDERKA**, I. BELLO, H. IBRAHIM, W.M. LAU, University of Western Ontario, Canada.

**PS-WeP5** High Voltage Sheath Evolution in the Presence of Negative Ions. **J.T. SCHEUER**, T.B. MITCHELL, M. TUSZEWSKI, J.A. TOBIN, K.P. KREMEYER, A. WILLIAMS, Los Alamos National Laboratory.

**PS-WeP6** Power versus Time in Pulsed, Parallel Plate rf Discharges. **L.J. OVERZET**, University of Texas, Dallas.

**PS-WeP7** Electron Temperature Measurement in Magnetrons by Optical Emission Spectroscopy and Langmuir Probes. **K.F. LAI**, W. TSAI, Varian Associates.

**PS-WeP8** Ion and Neutral Ar Temperatures in MW ECR Plasmas by Doppler Broadened Emission Spectroscopy. **D.V. TSU**, R.T. YOUNG, S.R. OVSHINSKY, Energy Conversion Devices. **C.C. KLEPPER**, L.A. BERRY, Oak Ridge National Laboratory.

**PS-WeP9** Ion Chemistry Effects on SiO<sub>2</sub> to Si Selectivity in a High Density Fluorocarbon Plasma. **K.H.R. KIRMSE**, A.E. WENDT, R.A. BREUN, S.Y. PEREZ-MONTERO, J.A. MEYER, N. HERSHKOWITZ, University of Wisconsin, Madison.

**PS-WeP10** Determining the Neutral Radical Composition of Plasma Environments: Pulsed, Supersonic, Plasma Sampling Mass Spectrometry. **H. ZHU**, **R. BLUMENTHAL**, Auburn University.

**PS-WeP11** Fluid Simulations of Particle Contamination in Afterglow of Plasma Processes. **M.P. GARRITY**, T. PETERSON, L. GARRETT, J.F. O'HANLON, University of Arizona.

**PS-WeP12** Simulations of Damage Profiles due to Reactive Ion Etching and Ion-assisted Etching. **R.J. DAVIS**, P. JHA, Columbia University.

**PS-WeP13** Identification of Plasma Induced Failure Modes in the Development of a BiCMOS ASIC Process. **M.J. DION**, **J.J. HACKENBERG**, D.F. HEMMENWAY, L.G. PEARCE, J.W. WERNER, Harris Semiconductor.

**PS-WeP14** Modeling of Wafer Charging and Damage in High Plasma Density Etching Tools. **M. GRAPPERHAUS**, M.J. KUSHNER, University of Illinois, Urbana.

**PS-WeP15** Plasma Parameter Dependence of Thin-Oxide Damage from Wafer Charging during Electron-Cyclotron-Resonance Plasma Processing. **J.B. FRIEDMANN**, University of Wisconsin, Madison. **S.-M. MA**, J.P. MCVITTIE, Stanford University. **J.L. SHOHET**, University of Wisconsin, Madison.

**PS-WeP16** Impact of High-Z Limiters on Ion Fluxes in the Plasma Edge of the Textor Tokamak. **M. RUBEL**, B. EMMOTH, Royal Institute of Technology, Sweden. **L. KÖNEN**, V. PHILIPPS, A. POSPIESZCZYK, J. VON SEGGERN, Institute of Plasma Physics, KFA, Germany. **T. TANABE**, Y. UEDA, Osaka University, Japan. **P. WIENHOLD**, Institute of Plasma Physics, KFA, Germany.

**PS-WeP17** Mass Spectrometric Analysis of the Gas Phase Coating Environment in Plasma Polymerization. **S. LETTS**, R. BRUSASCO, Lawrence Livermore National Laboratory.

**PS-WeP18** Argon Permeation through Polyvinyl Alcohol (PVA) Coatings. **D.A. STEINMAN**, M.L. HOPPE, General Atomics.

**PS-WeP19** Preparation of Germanium Doped Plasma Polymerized Coatings as ICF Target Ablators. **R. BRUSASCO**, M. SACULLA, R. COOK, Lawrence Livermore National Laboratory.

**PS-WeP20** Liquid Hydrogen Layering Dynamics in Large Plastic Capsules. **T. BERNAT**, Lawrence Livermore National Laboratory. **D. BITTNER**, W.J. Schafer Associates. **G.W. COLLINS**, E.R. MAPOLES, J. SANCHEZ, Lawrence Livermore National Laboratory. **J. SATER**, W.J. Schafer Associates.

**PS-WeP21** Hollow Foam Microshells for Liquid-Layered Cryogenic ICF Targets. **G.E. OVERTURF, III**, R. COOK, B. REIBOLD, Lawrence Livermore National Laboratory. **D. SCHROEN-CAREY**, W.J. Schafer Associates.

**PS-WeP22** Determination of the Wall Thickness and Uniformity of Inertial-Fusion Capsules Using the Self-Interference Fringes Produced with Narrow-Bandwidth Illumination. **M.D. WITTMAN**, H.-G. KIM, A.S. CHOW, University of Rochester.



## THIN FILM

Room BR4 - Session TF-WeP pg. 262

### Aspects of Thin Films

Moderator: F. Sequeda, Conner Peripherals.

Presenters present: 5:00-6:30 pm.

#### TF-WeP1 A Novel Approach to the Calculation of ITO Films'

Figures of Merit. S.A. KNICKERBOCKER, A.K. KULKARNI, Michigan Technological University.

TF-WeP2 Protecting Silver Polymer Mirrors with Oxide Coatings for Solar Applications. C.E. KENNEDY, National Renewable Energy Laboratory.

TF-WeP3 UHV E-Beam Deposition of Pt and Ti on Single Crystal Si and SiO<sub>2</sub> Substrates for the Preparation of Pb(Zr,Ti)O<sub>3</sub> Thin Films by Laser Ablation. M. DUBEY, W. WILBER, L. CASAS, R. LAREAU, K.A. JONES, Army Research Lab, Fort Monmouth.

TF-WeP5 Microstructure and Characterization of Electron-trapping Stimulable Phosphor SrS:Eu,Sm Thin Film on Glass. T.J. HSIEH, R. REVAY, D. BROWER, Optex Communications Corporation. P.H. CHI, D.S. SIMONS, D.E. NEWBURY, S.W. ROBEY, National Institute of Standards & Technology.

TF-WeP6 The Structure and Magneto-Optical Properties of Ta/Fe and Ta/Co Bilayers. E.E. SHALIGINA, L.V. KOZLOVSKY, University of Daugavpils, Latvia.

TF-WeP7 Surface Compositions of Chemically Treated CdTe Thin Films for Photovoltaic Applications. D.W. NILES, X. LI, P. SHELDON, National Renewable Energy Laboratory.

TF-WeP8 Plasma-Deposition of Low Stress Electret Films for Electroacoustic and Solar Cell Applications. P. GÜNTHER, R. SCHELLIN, G. SESSLER, C. THIELEMANN, Technical University of Darmstadt, Germany. J.E. KLEMBERG-SAPIEHA, L. MARTINU, M.R. WERTHEIMER, Ecole Polytechnique, Canada.

TF-WeP9 Low Temperature Formation of Textured ZnO Transparent Electrodes by Magnetron Sputtering. T. MINAMI, H. SONOHARA, S. TAKATA, I. FUKUDA, Kanazawa Institute of Technology, Japan.

TF-WeP10 Vacuum Deposition Parameters for Thin Film Shape Memory Alloys. A.P. JARDINE, R. DANNENBERG, State University of New York, Stony Brook.

TF-WeP11 Low-Temperature Synthesis of High-Quality SiO<sub>2</sub> Thin Films from Low Energy Ion Beams. S.S. TODOROV, D. MARTON, K.J. BOYD, A.H. AL-BAYATI, J.W. RABALAIS, University of Houston.

TF-WeP12 A Compact Negative Metal Ion Beam Source for Low Energy Thin Film Deposition. S.I. KIM, Y.O. AHN, SKION Corporation.

TF-WeP13 Bias Sputter Deposition of Dense Yttria-Stabilized Zirconia Films on Porous Substrates. T. TSAI, S.A. BARNETT, Northwestern University.

TF-WeP14 Modeling and Experimental Studies of Multi-phase Formation in Reactive Sputtering. C. NENDER, T. NYBERG, S. BERG, Uppsala University, Sweden. K.O. LEGG, M. GRAHAM, P.J. RUDNIK, M.S. WONG, W.D. SPROUL, Northwestern University.

TF-WeP15 Ionized Magnetron Sputtering of Carbon Nitride Thin Films. D. LI, Y.W. CHUNG, S. LOPEZ, M.S. WONG, W.D. SPROUL, Northwestern University.

TF-WeP16 Developments in the Ionized Cluster Beam Deposition Technique. M.F. TABET, S. FENG, A.J. COX, F.K. URBAN, Florida International University.

TF-WeP17 Development of Vacuum Arc Metal Ion Sources and Techniques TAMEK for Material Surface Modification. A.M. TOLOPA, Ukraine Academy of Science and Pan TAMEK, Russia.

TF-WeP18 Synthesis and Properties of Polycrystalline CrN/TiN Superlattices. P. YASHAR, X. CHU, M.S. WONG, W. SPROUL, S.A. BARNETT, Northwestern University.

TF-WeP19 Neutralized Beam Assisted Evaporation of Cubic Boron Nitride on Si(100). M. LU, A. BOUSETTA, A. BENSADULA, University of Houston. K. WATERS, A. SCHULTZ, Ionwerks.

TF-WeP20 An X-ray Diffraction Study of Epitaxial Nitride Superlattices. A. MADAN, M. SHINN, S.A. BARNETT, Northwestern University.

TF-WeP21 Defect Structure of Low Energy Ion Modified Diamond(100) Surfaces. B.W. SUN, L.J. HUANG, I. BELLO, W.M. LAU, University of Western Ontario, Canada. S.-T. LEE, Eastman Kodak Company. P.A. STEVENS, B.D. DEVRIES, Exxon Research and Engineering Company.

TF-WeP22 The Effect of the Physical Vapor Deposition Techniques of Sputtering and Evaporation of Ti on the Formation and Transformation of C49 to C54 TiSi<sub>2</sub>. C. CABRAL, JR., R.A. ROY, L.A. CLEVINGER, K.L. SAENGER, IBM TJ Watson Research Center.

TF-WeP23 Residual Stress in Ion Implanted Titanium Nitride Films by Parallel Beam Glancing Incidence X-ray Diffraction. A.J. PERRY, J.R. TREGGIO, ISM Technologies Inc. D.E. GEIST, Martin Marietta.

## VACUUM TECHNOLOGY

Room BR4 - Session NP-WeP pg. 266

### New Products

Moderator: W. Weed, Sandia National Laboratories.

Presenters present: 5:00-6:30 pm.

NP-WeP2 Latest Developments on Valve Seat-Seal Assembly. R. DE VILLEPOIX, M. LEFRANCOIS, C. ROUAUD, Céfiliac-Etanchéité & Helicoflex.

NP-WeP3 Reliable In-Situ Gas Analysis for Aggressive Gas Processes. W. EISINGER, Leybold Inficon Inc.

NP-WeP4 Non-Reclosing Pressure Relief Device for Vacuum Systems. W.A. SWANSIGER, Sandia National Laboratories.

NP-WeP5 New Compact Total Pressure Gauges. A. SCHMID, R. STOCKER, Balzers Limited, Liechtenstein.

NP-WeP7 Combination Valve Enables In-Situ Zeroing and Calibration of Capacitance Manometers. J. SKUBA, HPS Division of MKS Instruments. J. DUNN, MKS Instruments.

# Thursday Morning, October 27, 1994

## SURFACE SCIENCE

Room A205 - Session SS1-ThM pg. 267

### Nanoscale Measurements

Moderator: J.E. Reutt-Robey, University of Maryland.

## SURFACE SCIENCE

Room A201 - Session SS2-ThM pg. 268

### Surface Interactions

Moderator: D.N. Belton, General Motors Research and Development Center.

8:20 am	<b>SS1-ThM1 INVITED</b> Nanostructuring of Surfaces by Diffusion Controlled Growth. <b>K. KERN</b> , Ecole Polytechnique de Lausanne.	<b>SS2-ThM1</b> Coadsorption of Alkalis and Hydrogen on W(100). <b>W. HAGO</b> , P.J. ESTRUP, Brown University.
8:40 am	Invited talk continued.	<b>SS2-ThM2</b> Comparative HREELS Study of H and CO on Pt(335). <b>H. WANG</b> , R.G. TOBIN, Michigan State University. <b>D.K. LAMBERT</b> , G.B. FISHER, C.L. DIMAGGIO, General Motors R&D Center.
9:00 am	<b>SS1-ThM3</b> Observation of Quantum Size Effects at Room Temperature on Metal Surfaces with STM. <b>PH. AVOURIS</b> , I.-W. LYU, Y. HASEGAWA, IBM TJ Watson Research Center.	<b>SS2-ThM3</b> The Adsorption of Hydrogen to the NiAl(110) Surface. <b>A.T. HANBICKI</b> , University of Pennsylvania. <b>E.W. PLUMMER</b> , University of Tennessee & Oak Ridge National Laboratory. <b>A.P. BADDORF</b> , Oak Ridge National Laboratory.
9:20 am	<b>SS1-ThM4</b> STM of Thin Film MgO Grown on Mo(001). <b>M.C. GALLAGHER</b> , M. FYFIELD, J.P. COWIN, S.A. JOYCE, Pacific Northwest Laboratories.	<b>SS2-ThM4</b> Thermal Desorption Studies of High-Coverage Hydrogen Overlayers Created with Gas-Phase Atomic Hydrogen on Ru(001). <b>T.A. JACHIMOWSKI</b> , B. MENG, D.F. JOHNSON, <b>W.H. WEINBERG</b> , University of California, Santa Barbara.
9:40 am	<b>SS1-ThM5</b> Nanosphere Lithography. <b>J.C. HULTEEN</b> , <b>R.P. VAN DUYN</b> , Northwestern University.	<b>SS2-ThM5</b> The Adsorption of Hydrogen on the $\text{Mo}_{0.75}\text{Re}_{0.25}$ (100), (110), and (111) Surfaces. <b>M. OKADA</b> , University of Tennessee. <b>D.B. POKER</b> , D.M. ZEHNER, Oak Ridge National Laboratory.
10:00 am	<b>SS1-ThM6</b> Nanofabrication on Electron Beam Resist using Scanning Tunneling Microscopy. <b>M.H. NAYFEH</b> , A. ARCHER, J.M. HETRICK, I. ADESIDA, University of Illinois, Urbana-Champaign.	<b>SS2-ThM6</b> Separating Ensemble and Electronic Effects on Bimetallic and Alloy Surfaces. <b>C. XU</b> , <b>B.E. KOEL</b> , University of Southern California.
10:20 am	<b>SS1-ThM7 INVITED</b> Nanometer-Scale STM Electrochemical Syntheses of Electronic Materials. <b>W. LI</b> , J. ZOVAL, J.A. VIRTANEN, <b>R.M. PENNER</b> , University of California, Irvine.	<b>SS2-ThM7</b> Adsorption of Sulfur on Bimetallic Surfaces. <b>M. KUHN</b> , J.A. RODRIGUEZ, Brookhaven National Laboratory.
10:40 am	Invited talk continued.	<b>SS2-ThM8</b> 'Nanocatalysis' by the Tip of a Scanning Tunneling Microscope Operating Inside a Reactor Cell. <b>B.J. MCINTYRE</b> , Lawrence Berkeley Laboratory. <b>U. SCHRÖDER</b> , Universität Bonn, Germany. <b>M. SALMERON</b> , G.A. SOMORJAI, Lawrence Berkeley Laboratory.
11:00 am	<b>SS1-ThM9</b> Self-Assembled Monolayers of Pendant Monomers: A Basis for Fabrication with the Scanning Tunneling Microscope. <b>R.J. WILLICUT</b> , <b>R.L. MCCARLEY</b> , Louisiana State University.	<b>SS2-ThM9</b> SPA-RHEED - Spot Profile Analysis for In Situ Characterization. <b>B. MÜLLER*</b> , M. HENZLER, Universität Hannover, Germany.
11:20 am	<b>SS1-ThM10</b> STM-Induced Etching of Ultra-thin Organic Resists: Structure, Mechanism, and Post-etching Elaboration. <b>J.K. SCHOER</b> , <b>R.M. CROOKS</b> , Texas A&M University. <b>T. CORBIT</b> , M.J. HAMPDEN-SMITH, University of New Mexico.	<b>SS2-ThM10</b> Experimental and Numerical Investigation of Ignition Conditions of $\text{H}_2/\text{O}_2$ Mixtures on Pt. <b>M. RINNEMO</b> , Chalmers University of Technology, Sweden. <b>O. DEUTSCHMANN</b> , Universität Stuttgart, Germany. <b>P. AHLSTRÖM</b> , Chalmers University of Technology, Sweden. <b>F. BEHRENDT</b> , Chalmers Univ. of Tech., Sweden & Univ. Stuttgart, Germany. <b>B. KASEMO</b> , Chalmers Univ. of Tech. & Univ. of Göteborg, Sweden.
11:40 am		<b>SS2-ThM11</b> The Synthesis of Ammonia on Ru(0001). <b>P.A. TAYLOR</b> , E. TÖRNQVIST, Haldor Topsoe Research Laboratories, Denmark.

<b>NANO 3/NANOMETER-SCALE SCIENCE AND TECHNOLOGY/BIOMATERIAL INTERFACES</b> <b>Room A209 - Session NSBI-ThM pg. 270</b> <b>Biology at the Nanoscale: II</b> <b>Moderator: S. Lindsay, Arizona State University.</b>		<b>NANO 3/NANOMETER-SCALE SCIENCE AND TECHNOLOGY</b> <b>Room A207 - Session NS2-ThM pg. 272</b> <b>Proximal Probe Based Fabrication</b> <b>Moderator: H.G. Craighead, Cornell University.</b>	
8:20 am	<b>NSBI-ThM1</b> Molecular Recognition between DNA Base Pairs by AFM. B.D. RATNER, T. BOLAND, University of Washington.	<b>NS2-ThM1</b> Electrical and Mechanical Properties of Metallic Nanowires: Conductance Quantization and Localization. J.I. PASCUAL, J. MÉNDEZ, J. GÓMEZ-HERRERO, A.M. BARÓ, N. GARCÍA, Universidad Autónoma de Madrid, Spain. U. LANDMAN, W.D. LUEDTKE, E.N. BOGACHEK, H.P. CHENG, Georgia Institute of Technology.	
8:40 am	<b>NSBI-ThM2</b> Direct Measurement of the Interaction Forces between Complementary Strands of DNA with the Atomic Force Microscope. G.U. LEE, L.A. CHRISSEY, R.J. COLTON, Naval Research Laboratory.	<b>NS2-ThM2</b> Quantized Conductance in an Atom-Sized Point Contact. F. BESENBACHER, L. OLESEN, E. LAEGSGAARD, I. STENSGAARD, Aarhus University, Denmark.	
9:00 am	<b>NSBI-ThM3 INVITED</b> Scanning Probe Microscopic Visualization of Electrostatically Immobilized Intercalating Drug-Nucleic Acid Complexes. L.A. BOT-TOMLEY, J.E. COURY, G. GARDNER, E.A. HANDLEY, L.D. WILLIAMS, Georgia Institute of Technology.	<b>NS2-ThM3</b> Nanoscale Mechanical and Chemical Processing of Surfaces: Molecular Dynamics Simulations. S.B. SINNOTT, R.J. COLTON, C.T. WHITE, D.W. BRENNER, Naval Research Laboratory.	
9:20 am	Invited talk continued.	<b>NS2-ThM4</b> Electrical Measurements on STM Patterned Silicon MOSFETS. T. FAYFIELD, T.K. HIGMAN, University of Minnesota.	
9:40 am	<b>NSBI-ThM5</b> Sequence Effects in the Images and Bonding of Single Stranded DNA on Au(111) Observed by Electrochemical STM. Y. LYUBCHENKO, D. REKESH, T.W. JING, S.M. LINDSAY, Arizona State University.	<b>NS2-ThM5 INVITED</b> Nanolithographic Patterning of Metal Films with the STM. C. VAN HAESSENDONCK, L. STOCKMAN, G. NEUTTIENS, C. STRUNK, Y. BRUYNSERAED, Katholieke Universiteit Leuven, Belgium.	
10:00 am	<b>NSBI-ThM6</b> Imaging Polytene Chromosomes with the Atomic Force Microscope. D.M. JONDLE, L. AMBROSIO, J. VESENKA, E. HENDERSON, Iowa State University.	Invited talk continued.	
10:20 am	<b>NSBI-ThM7</b> The Topology of Supercoiled DNA by SFM Imaging. B. SAMORI, C. NIGRO, I. MUZZALUPO, G. ZUCCHERI, C. QUAGLIARIELLO, University of Calabria, Italy.	<b>NS2-ThM7</b> Spectroscopic Investigation of PEDTA, an Ultrathin Resist for STM Lithography. F.K. PERKINS, E.A. DOBISZ, M.-S. CHEN, J.M. CALVERT, C.R.K. MARRIAN, Naval Research Laboratory.	
10:40 am	<b>NSBI-ThM8</b> Scanning Probe Microscopy Studies of Macromolecular Interactions. S.J.B. TENDLER, C.J. ROBERTS, P.M. WILLIAMS, M.C. DAVIES, D.E. JACKSON, University of Nottingham, United Kingdom.	<b>NS2-ThM8</b> Scanning Probe Lithography of Novel Langmuir-Schaeffer Films: Electrochemical Applications. U. DEMIR, K.K. BALASUBRAMANIAN, V. CAMMARATA, C. SHANNON, Auburn University.	
11:00 am	<b>NSBI-ThM9</b> DNA Surface Attachment Schemes for Scanning Probe Microscopy. L.A. WENZLER, T.P. BEEBE, JR., University of Utah.	<b>NS2-ThM9</b> Cyanide Etching of n-Alkanethiol-Modified Au (111) Surfaces Studied by Electrochemical Scanning Tunneling Microscopy. Y.Q. LI, O. CHAILAPAKUL, R.M. CROOKS, Texas A&M University.	
11:20 am	<b>NSBI-ThM10</b> Studying the Dynamics of Polymer Surface Degradation by Scanning Force Microscopy. K.M. SHAKESHEFF, M.C. DAVIES, University of Nottingham, United Kingdom. A. DOMB, Hebrew University of Jerusalem, Israel. C.J. ROBERTS, A. SHARD, S.J.B. TENDLER, P.M. WILLIAMS, University of Nottingham, United Kingdom.	<b>NS2-ThM10</b> Nanometer Structure Fabrication on Insulator and Magnetic Material using Scanning Probe Microscope. S. HOSAKA, H. HAJIME, A. KIKUKAWA, M. MIYAMOTO, T. SHINTANI, K. NAKAMURA, J. BRUGGER, R. IMURA, Hitachi, Ltd., Japan.	
11:40 am	<b>NSBI-ThM11</b> In Situ Observation of the Protonation of Cytosine on Au(111) by Electrochemical STM. D. LAMPNER, T.W. JING, J. PAN, S.M. LINDSAY, Arizona State University.	<b>NS2-ThM11</b> Field-induced Atom Transfer of Gold and Platinum Systems in the Scanning Tunneling Microscope Configuration. C.S. CHANG, H.N. LIN, W.B. SU, T.T. TSONG, Academia Sinica, ROC.	

# Thursday Morning, October 27, 1994

**APPLIED SURFACE SCIENCE**  
Room A101 - Session AS-ThM pg. 274

## Self-Assembled Monolayers

**Moderator:** A.W. Czanderna, National Renewable Energy Laboratory.

**PLASMA SCIENCE**  
Room A109 - Session PS-ThM pg. 276

## Charge Free Processing

**Moderator:** K.L. Maxwell, SEMATECH.

8:20 am	<b>AS-ThM1 INVITED</b> Surface Engineering using Mixed Alkanethiolate Monolayers on Gold. <b>A. ULMAN</b> , Polytechnic University.	<b>PS-ThM1 INVITED</b> An Overview of Charge-Free Processing - Mechanisms and Applications. <b>H.H. SAWIN</b> , Massachusetts Institute of Technology.
8:40 am	Invited talk continued.	Invited talk continued.
9:00 am	<b>AS-ThM3</b> Probing the Phase Transition in Alkyl Thiol Assemblies on Gold Surfaces. <b>F. BENSEBAA</b> , T. ELLIS, Univ. de Montréal, Canada. <b>A. BADIA</b> , B. LENNOX, Univ. de McGill, Canada.	<b>PS-ThM3</b> Charge Measurements and Damage Effects in the Reaction Chamber of a Remote Plasma Etcher. <b>D.J. BONSER</b> , P.K. AUM, T. TA, SEMATECH. <b>M.G. BLAIN</b> , T.L. MEISENHEIMER, Sandia National Laboratories. <b>W.M. HOLBER</b> , ASTeX, Inc.
9:20 am	<b>AS-ThM4</b> A NEXAFS-Investigation of the Adsorption of Pyromellitic Dianhydride (PMDA) on Pt(111). <b>C. THÜMMER</b> , T. STRUNSKUS, <b>A. SCHERTEL</b> , C.W. HUTCHINGS, H. WEGNER, CH. WÖLL, M. GRUNZE, Universität Heidelberg, Germany.	<b>PS-ThM4</b> In Situ Diagnostic Measurements of the Gas Phase Process Chemistry in the Reaction Chamber of a Remote Plasma Etcher. <b>M.G. BLAIN</b> , T.L. MEISENHEIMER, Sandia National Laboratories. <b>J.A. O'NEILL</b> , IBM Microelectronics. <b>D.J. BONSER</b> , P.K. AUM, T. TA, SEMATECH.
9:40 am	<b>AS-ThM5</b> Structure and Dynamics of Alkanethiol Self-Assembled Monolayers on Au(111) Characterized by Scanning Tunneling Microscopy. <b>G.E. POIRIER</b> , M.J. TARLOV, H.E. RUSHMEIER, National Institute of Standards & Technology.	<b>PS-ThM5</b> Effects of Reactor Wall on Downstream Stripping. <b>M. NAKAMURA</b> , K. NISHIKAWA, K. SHINAGAWA, Fujitsu Ltd., Japan.
10:00 am	<b>AS-ThM6</b> Metal Overlayers on Self-Assembled Monolayers: 6. XPS of Cr/COOH on Mercaptohexadecanoic Acid. <b>D.R. JUNG</b> , A.W. CZANDERNA, National Renewable Energy Laboratory.	<b>PS-ThM6</b> UV-Stimulated Dry Stripping of Silicon Nitride Films. <b>D.C. GRAY</b> , J.W. BUTTERBAUGH, C.F. HIATT, FSI International.
10:20 am	<b>AS-ThM7</b> An Unexpected Packing of Fluorinated n-Alkane Thiols on Au(111): An Atomic Force Microscopy Study. <b>G. LIU</b> , University of California, Berkeley. <b>C.E.D. CHIDSEY</b> , Stanford University. <b>D.F. OGLETREE</b> , <b>M.B. SALMERON</b> , Lawrence Berkeley Laboratory.	<b>PS-ThM7 INVITED</b> Neutral-Beam-Assisted Etching. <b>T. YUNOGAMI</b> , K. YOKOGAWA, T. MIZUTANI, Hitachi Ltd., Japan.
10:40 am	<b>AS-ThM8</b> The Surface Chemistry of Self-Assembled and Vapor Deposited Perfluorinated n-Alkanoic Acid Monolayers on Native Aluminum-oxide. <b>R.M. WALLACE</b> , S.A. HENCK, P. CHEN, D.A. WEBB, Texas Instruments Inc.	Invited talk continued.
11:00 am	<b>AS-ThM9</b> Quantitative Analysis of Monolayer Molecular Films using "Molecule Corrals" and STM. <b>D.L. PATRICK</b> , V.J. CEE, T.P. BEEBE, JR., University of Utah.	<b>PS-ThM9</b> Hyperthermal Neutral Beam Etching. <b>K.P. GIAPIS</b> , T.A. MOORE, T.K. MINTON, California Institute of Technology.
11:20 am	<b>AS-ThM10</b> In Situ AFM/STM Study of Nucleation, Growth and Electron Transfer Reactions of Purines at the Graphite-Water Interface. <b>N.J. TAO</b> , Z. SHI, Florida International University.	<b>PS-ThM10</b> A Thermalized Neutral Radical Source for Charge-Free Processing. <b>L. CHEN</b> , Q. YANG, D.R. WRIGHT, K.L. MAXWELL, SEMATECH.
11:40 am	<b>AS-ThM11</b> Multi-Step Assembly of Polymeric Monolayers. <b>D.W. GRAINGER</b> , G. MAO, F. SUN, Colorado State University. <b>D.G. CASTNER</b> , University of Washington.	<b>PS-ThM11</b> Hyperthermal Neutral Beam Anisotropic Etching for Submicron Patterning of Electronic Materials. <b>J.B. CROSS</b> , M.A. HOFFBAUER, Los Alamos National Laboratory.

**ELECTRONIC MATERIALS/SURFACE SCIENCE**

Room A102 - Session EMSS-ThM pg. 277

**Semiconductor Surface Reactions III**

Moderator: J.R. Engstrom, Cornell University.

**THIN FILM/VACUUM METALLURGY**

Room A105 - Session TFVM-ThM pg. 279

**Energetic Condensation: Processes, Properties and Products**

Moderator: D.A. Glocker, Eastman Kodak Research Laboratories.

8:20 am	<b>EMSS-ThM1</b> Sputtering of GaAs(110) Studied with Scanning Tunneling Microscopy. <b>R.J. PECHMAN</b> , X.-S. WANG, J.H. WEAVER, University of Minnesota.	<b>TFVM-ThM1 INVITED</b> Energetic Condensation: Processes, Properties and Products. <b>J.S. COLLIGON</b> , University of Salford, England.
8:40 am	<b>EMSS-ThM2</b> Atomically-resolved Decomposition of Phosphine and Formation of P-terminated Layers on Si(001). <b>R.J. HAMERS</b> , Y. WANG, University of Wisconsin, Madison.	Invited talk continued.
9:00 am	<b>EMSS-ThM3 INVITED</b> Semiconductor Etching with Halogens: Scanning Tunneling Microscopy Investigations. <b>J.H. WEAVER</b> , University of Minnesota.	<b>TFVM-ThM3</b> Primary-ion Deposition of Al on a-C and Ge on Si(001): Role of Low-energy Ion/Surface Interactions. <b>Y.-W. KIM</b> , I. PETROV, H. ITO, J.E. GREENE, University of Illinois, Urbana.
9:20 am	Invited talk continued.	<b>TFVM-ThM4</b> Topography and Structure of Homoepitaxial Si Films Grown by Mass Selected Ion Beam Deposition. <b>A.H. AL-BAYATI</b> , S.S. TODOROV, D. MARTON, K.J. BOYD, J.W. RABALAIS, University of Houston. Y. LIFSHITZ, Nuclear Research Center, Soreq, Israel.
9:40 am	<b>EMSS-ThM5</b> Analysis of Nanometer-Scale Surface Roughness with Reflection Inelastic Electron Scattering from Silicon Surfaces. <b>H.N. FRASE</b> , <b>H.A. ATWATER</b> , S.S. WONG, C.C. AHN, California Institute of Technology.	<b>TFVM-ThM5</b> Formation of Thin C-N Films by Ion Beam Deposition. <b>K.J. BOYD</b> , D. MARTON, S.S. TODOROV, A.H. AL-BAYATI, J. KULIK, J.W. RABALAIS, University of Houston.
10:00 am	<b>EMSS-ThM6</b> Sub-surface Diffusion of Ni on Si(100) and (111). <b>M.Y. LEE</b> , P.A. BENNETT, Arizona State University.	<b>TFVM-ThM6 INVITED</b> Energetic Condensation Using Filtered Arc Evaporation. <b>P.J. MARTIN</b> , A. BENDAVID, T.J. KINDER, X. WANG, CSIRO Division of Applied Physics, Australia.
10:20 am	<b>EMSS-ThM7</b> Chemical Vapor Deposition of $\text{TiSi}_2$ using $\text{SiH}_4$ and $\text{TiCl}_4$ . <b>M.A. MENDICINO</b> , R.P. SOUTHWELL, E.G. SEEBAUER, University of Illinois, Urbana.	Invited talk continued.
10:40 am	<b>EMSS-ThM8</b> FTIR Study of Intrinsic TEOS Surface Reaction Kinetics on $\text{SiO}_2$ at CVD Process Temperatures and Pressures. <b>M.E. BARTRAM</b> , H.K. MOFFAT, Sandia National Laboratories.	<b>TFVM-ThM8 INVITED</b> The Deposition of AlCu and TiN Films for Microelectronic Applications using Ionized Magnetron Sputter Deposition. <b>S.M. ROSSNAGEL</b> , IBM TJ Watson Research Center.
11:00 am	<b>EMSS-ThM9</b> Investigation of the Chemical Mechanisms of Ta/Ta-oxide Halogen Etch Selectivity. <b>L.A. DELOUISE</b> , Xerox Webster Research Center.	Invited talk continued.
11:20 am	<b>EMSS-ThM10</b> Scanning Tunneling Microscopy and Spectroscopy of the Reaction of $\text{NH}_3$ with GaAs(110). <b>G. BROWN</b> , M. WEIMER, Texas A&M University.	<b>TFVM-ThM10 INVITED</b> Further Perspectives on Stresses in Sputter-Deposited Thin Films. <b>D.W. HOFFMAN*</b> , Advanced Modular Power Systems.
11:40 am	<b>EMSS-ThM11</b> MBE Growth of $\text{SnS}_2$ and $\text{SnSe}_2$ on Cleaved Mica, Single Crystal $\text{SnS}_2$ , $\text{WSe}_2$ and Other Layered Semiconductors - RHEED, LEED, Photoemission and STM Characterization. <b>R. SCHLAF</b> , D. LOUDER, O. LANG, C. PETTENKOFER, W. JAEGERMANN, Colorado State University. <b>K. NEBESNY</b> , P. LEE, B.A. PARKINSON, <b>N.R. ARMSTRONG</b> , University of Arizona.	Invited talk continued.

# Thursday Morning, October 27, 1994

## ELECTRONIC MATERIALS

Room A108 - Session EM-ThM pg. 280

### Optical Diagnostics for Materials Processing

Moderator: P. Herman, Columbia University.

## MANUFACTURING SCIENCE AND TECHNOLOGY

Room A110 - Session MS-ThM pg. 282

### Micro-Contamination and Defects

Moderator: A.C. Diebold, SEMATECH.

8:20 am	<b>EM-ThM1 INVITED</b> Ellipsometry for III-V Epitaxial Growth Diagnostics. <b>G.N. MARACAS</b> , C.H. KUO, S. ANAND, R. DROOPAD, Arizona State University. G.R.L. SOHIE, General Electric Corporate Research Lab.	<b>MS-ThM1 INVITED</b> The Effect of Contamination on the Reliability of Magnetic Materials and Storage Disks. <b>B. HERMSMEIER</b> , IBM Advanced Magnetic Recording Lab.
8:40 am	Invited talk continued.	Invited talk continued.
9:00 am	<b>EM-ThM3</b> Real-Time Monitoring of Resonant Tunneling Diode Growth using Spectroscopic Ellipsometry. <b>F.G. CELII</b> , Y.-C. KAO, W.M. DUNCAN, T.S. MOISE, A.J. KATZ, Texas Instruments.	<b>MS-ThM3</b> An In Situ XPS Study of Metal Surface Recontamination and Hollow Cathode Plasma Cleaning. <b>H. LI</b> , A. BELKAND, <b>Z. ORBAN</b> , BOC Group Technical Center. F. JANSEN, Airco Coating Technology.
9:20 am	<b>EM-ThM4</b> Real-time Spectroscopic Ellipsometry (RTSE) Monitoring of Si <sub>1-x</sub> Ge <sub>x</sub> /Si Epitaxial Growth. <b>C. PICKERING</b> , D.A.O. HOPE, R.T. CARLINE, D.J. ROBBINS, Defence Research Agency, United Kingdom.	<b>MS-ThM4</b> Generation of Standard Test Wafers for Cleaning Evaluations in Semiconductor Manufacturing. <b>M. LIEHR</b> , S.L. COHEN, R. TSAI, K. POPE, B. FURMAN, R. PURTELL, IBM TJ Watson Research Center. K. ALBAUGH, S. BASILIERE, S. ESTES, M.J. FLEMING, R. GAYLORD, C. GOW, W. SYVERSON, IBM Microelectronic Division.
9:40 am	<b>EM-ThM5</b> Real Time Investigation of Nucleation and Growth of Si on SiO <sub>2</sub> Using Silane and Disilane in a Rapid Thermal Processing System. <b>Y.Z. HU</b> , D. DIEHL, C.Y. ZHAO, Q. LIU, E.A. IRENE, University of North Carolina, Chapel Hill. K.N. CHRISTENSEN, D.M. MAHER, North Carolina State University.	<b>MS-ThM5 INVITED</b> Rapid Yield Learning. <b>D.M.H. WALKER</b> , Texas A&M University.
10:00 am	<b>EM-ThM6</b> Real Time Monitoring of the Electron Cyclotron Resonance Etching of Semiconductors by In Situ Spectroscopic Ellipsometry. <b>N.J. IANNO</b> , P.G. SNYDER, S. AHMER, University of Nebraska, Lincoln. S. PITTAL, B. JOHS, J.A. WOOLLAM, J.A. Woollam Co.	Invited talk continued.
10:20 am	<b>EM-ThM7</b> Bulk Ordering and Optical Anisotropy of In <sub>x</sub> Ga <sub>1-x</sub> As/InP. <b>D.E. ASPNES</b> , North Carolina State University. K. HINGEL, J. KAMIYA, L.T. FLOREZ, Bellcore. B. PHILLIPS, S. MAHAJAN, Carnegie Mellon University. J.P. HARBISON, Bellcore.	<b>MS-ThM7</b> New Ashing Technology with Multi-Plasma-Mode Reactor. <b>R.L. BERSIN</b> , M. KIKUCHI, I. NAKAYAMA, ULVAC Technologies, Inc.
10:40 am	<b>EM-ThM8</b> Monitoring of Deposition and Dry Etching of Si/SiGe Multiple Stacks. <b>B. TILLACK</b> , G. RITTER, H.H. RICHTER, A. WOLFF, G. MORGENSTERN, Institut für Halbleiterphysik, Germany. C. EGGS, Universität Greifswald, Germany.	<b>MS-ThM8</b> Vapor Phase SiO <sub>2</sub> Etching and Pre-gate Oxide Cleaning in an Integrated Cluster System. <b>Y. MA</b> , M.L. GREEN, AT&T Bell Laboratories. D. MARCH, Submicron System, Inc. K. HANSON, J. SAPJETA, D. BRASEN, AT&T Bell Laboratories.
11:00 am	<b>EM-ThM9</b> Observation of Etching Reaction using Second Harmonic Generation. <b>S. HARAICHI</b> , F. SASAKI, S. KOBAYASHI, M. KOMURO, T. TANI, Electrotechnical Laboratory, Japan.	<b>MS-ThM9</b> Detection and Analysis of Ultra-Small Particles on 8" Unpatterned Si Wafers. <b>C.R. BRUNDLE</b> , C.R. Brundle and Associates. Y. URITSKY, Applied Materials.
11:20 am	<b>EM-ThM10</b> Hydrogen Annealing Effect on SHG from SiO <sub>2</sub> /Si(111) Interfaces. <b>H. HIRAYAMA</b> , F. ITO, K. WATANABE, NEC Corporation, Japan.	<b>MS-ThM10</b> The Nature of Copper Precipitation from Dilute HF Solutions onto Si Surfaces. <b>T.S. SRIRAM</b> , R. SAMPSON, J. SHYU, W.C. HARRIS, D. LIU, S. BILL, Digital Equipment Corporation.
11:40 am	<b>EM-ThM11</b> Single Photon Ionization Time-of-Flight Mass Spectrometric Probing of III-V Semiconductor Growth. <b>S.M. CASEY</b> , National Institute of Standards & Technology. A.L. ALSTRIN, A.K. KUNZ, University of Colorado, Boulder. S.R. LEONE, National Institute of Standards & Technology.	

**VACUUM METALLURGY****Room A106 - Session VM-ThM pg. 284****Pulsed Laser and Pulsed Ion Technology for Film Deposition and Surface Modification****Moderator:** B. Sartwell, Naval Research Laboratory.

8:20 am	<b>VM-ThM1</b> Dual Laser Ablation of Particulate Free Optical Films. <b>S. WITANACHCHI</b> , K. AHMED, P. SAKTHIVEL, P. MUKHERJEE, University of South Florida.	
8:40 am	<b>VM-ThM2</b> Nanostructured Films and Particles Produced by Femtosecond Pulsed-Laser Ablation. <b>S.L. ROHDE</b> , A. LATEEF, B. ROBERTSON, T. VOILES, D. DOERR, D.R. ALEXANDER, University of Nebraska.	
9:00 am	<b>VM-ThM3 INVITED</b> Large-Area Pulsed Laser Deposition: Techniques and Applications. <b>J.A. GREER</b> , M.D. TABAT, Ratheon Company - Research Division.	
9:20 am	Invited talk continued.	
9:40 am	<b>VM-ThM5</b> Laser Induced Fluorescence Studies of Atomic and Molecular Species in Laser Generated Plumes. <b>T.L. THIEM</b> , P.J. WOLF, USAF Academy.	
10:00 am	<b>VM-ThM6</b> GeO <sub>2</sub> Films Prepared by Pulsed Laser Deposition. <b>B.M. PATTERSON</b> , P.J. WOLF, M. SCOTT, USAF Academy. T. CHRISTENSEN, University of Colorado, Colorado Springs.	
10:20 am	<b>VM-ThM7 INVITED</b> High Energy, High Flux, Pulsed Ion Beams for Rapid Thermal Surface Treatment. <b>D.C. MCINTYRE</b> , R.W. STINNETT, R.G. BUCHHEIT, Sandia National Laboratories. D.J. REJ, R. MUENCHHAUSEN, Los Alamos National Laboratory. J. GREENLY, M. THOMPSON, Cornell University. G. JOHNSTON, University of New Mexico.	
10:40 am	Invited talk continued.	
11:00 am	<b>VM-ThM9</b> Carbon and Nitrogen Implantation in a Large-Scale PSII Experiment. <b>B.P. WOOD</b> , J.T. SCHEUER, D.J. REJ, I. HENINS, W.A. REASS, R.J. FAEHL, K.C. WALTER, M.A. NASTASI, Los Alamos National Laboratory.	
11:20 am	<b>VM-ThM10</b> Film Deposition and Surface Modification using Intense Pulsed Ion Beams. C.A. MELI, <b>K.S. GRABOWSKI</b> , D.D. HINSELWOOD, S.J. STEPHANAKIS, Naval Research Laboratory. D.J. REJ, W.J. WAGANAAR, Los Alamos National Laboratory. M.O. THOMPSON, Cornell University.	
11:40 am	<b>VM-ThM11</b> Reactive DC Magnetron Sputtering of Oxide Coatings. <b>W.D. SPROUL</b> , M.E. GRAHAM, M.S. WONG, Northwestern University. R.A. SCHOLL, Advanced Energy Industries, Inc.	



# MY SCHEDULE

## Thursday Morning, October 27, 1994

TIME	SESSION	ROOM
8:20 am		
8:40 am		
9:00 am		
9:20 am		
9:40 am		
10:00 am		
10:20 am		
10:40 am		
11:00 am		
11:20 am		
11:40 am		
12:00 pm		
12:45 pm		
Lunch		
when		
with		where

### OTHER EVENTS THURSDAY

- 7:00 a.m. Companions Program (see insert) (**Silver Room (H)**)  
 8:30 a.m. Exhibitors Breakfast (**Room C201 (CC)**)  
 12:00 Noon 1995 Program Committee Chairs (**Aspen Room (H)**)

H=Radisson Hotel  
 CC=Colorado Convention Center

### SHORT COURSES THURSDAY

- 8:30 a.m. Vacuum Technology (**Room C109 (CC)**)  
 8:30 a.m. A Comprehensive Course on Surface Analysis: AES,XPS,SIMS, Depth Profiling, & ISS/RBS (**Room C107 (CC)**)  
 8:30 a.m. Physics, Chemistry, and Mechanics of Adhesion (New) (**Room C105 (CC)**)  
 8:30 a.m. Hard Coatings by PVD Methods (**Room C103 (CC)**)  
 8:30 a.m. Depth Profiling (**Room C107 (CC)**)  
 8:30 a.m. Mass Flow Controllers: Fundamentals, Techniques, and Applications (**Room C101 (CC)**)  
 8:30 a.m. Plasma-Enhanced CVD: Fundamentals, Techniques, and Applications (**Room C108 (CC)**)  
 8:30 a.m. Total Pressure Gauging Techniques (**Room C106 (CC)**)  
 8:30 a.m. Transparent Conducting Oxides: Their Science, Fabrication, Properties, and Applications (**Room C104 (CC)**)  
 8:30 a.m. Vacuum Evaporation/Deposition Technology (**Room C110 (CC)**)  
 8:30 a.m. Vacuum Leak Detection (**Room C112 (CC)**)

### Special or Focus Area Sessions

#### Sensors, In-situ Diagnostics, Process Control

- EM-ThM** Optical Diagnostics for Materials Processing  
**AS-ThM** Self-Assembled Monolayers

#### Surface Contamination and Control

- MS-ThM** Micro-Contamination and Defects

#### Nanostructure Fabrication and Atomic-Scale Manipulation

- NS2-ThM** Proximal Probe Based Fabrication  
**SS1-ThM** Nanoscale Measurements

# MY SCHEDULE

## Thursday Afternoon, October 27, 1994

TIME	SESSION	ROOM
2:00 pm		
2:20 pm		
2:40 pm		
3:00 pm		
3:20 pm		
3:40 pm		
4:00 pm		
4:20 pm		
4:40 pm		
5:00 pm		

### OTHER EVENTS THURSDAY

- 12:15 p.m. AVS Business Meeting (**Room A101 (CC)**)
- 6:00 p.m. Surface Science Spectra Editorial Board Meeting & Dinner (**Gold Room (H)**)
- 6:00 p.m. 1994-95 LAC/Program Committee Reception (**Jr. Ballroom D (H)**)
- 7:00 p.m. 1994-95 LAC/Program Committee Dinner (**Jr. Ballroom E (H)**)
- 8:00 p.m. Surface Science Postdeadline Discovery Session (**Grand Ballroom (H)**)

H=Radisson Hotel  
CC=Colorado Convention Center

### SHORT COURSES THURSDAY

- 8:30 a.m. Vacuum Technology (**Room C109 (CC)**)
- 8:30 a.m. A Comprehensive Course on Surface Analysis: AES,XPS,SIMS, Depth Profiling, & ISS/RBS (**Room C107 (CC)**)
- 8:30 a.m. Physics, Chemistry, and Mechanics of Adhesion (New) (**Room C105 (CC)**)
- 8:30 a.m. Hard Coatings by PVD Methods (**Room C103 (CC)**)
- 8:30 a.m. Depth Profiling (**Room C107 (CC)**)
- 8:30 a.m. Mass Flow Controllers: Fundamentals, Techniques, and Applications (**Room C101 (CC)**)
- 8:30 a.m. Plasma-Enhanced CVD: Fundamentals, Techniques, and Applications (**Room C108 (CC)**)
- 8:30 a.m. Total Pressure Gauging Techniques (**Room C106 (CC)**)
- 8:30 a.m. Transparent Conducting Oxides: Their Science, Fabrication, Properties, and Applications (**Room C104 (CC)**)
- 8:30 a.m. Vacuum Evaporation/Deposition Technology (**Room C110 (CC)**)
- 8:30 a.m. Vacuum Leak Detection (**Room C112 (CC)**)

### Special or Focus Area Sessions

- Sensors, In-situ Diagnostics, Process Control**
- NSBI-ThA Micro-Instrumentation and Sensors
- Nanostructure Fabrication and Atomic-Scale Manipulation**
- EM-ThA Materials for Nanostructures

# Thursday Afternoon, October 27, 1994

## SURFACE SCIENCE

Room A205 - Session SS1-ThA pg. 286

### Oxidation and Adsorption

Moderator: J.W. Rogers, University of Washington.

## SURFACE SCIENCE

Room A201 - Session SS2-ThA pg. 288

### Surface and Adsorbate Structure

Moderator: P. Avouris, IBM T.J. Watson Research Center.

2:00 pm	<b>SS1-ThA1</b> Molecular Beam Homoepitaxial Growth and Surface Characterization of MgO(001). T.T. TRAN, T.A. HILEMAN, S.A. CHAMBERS, Pacific Northwest Laboratory.	<b>SS2-ThA1</b> Br/Si(211)2x1 Structure Investigated by X-ray Standing Waves. V. ETELÄNIEMI, E.G. MICHEL, G. MATERLIK, HASYLAB at DESY, Germany.
2:20 pm	<b>SS1-ThA2</b> Step Fluctuation Kinetics and the Formation of (nx1)-O/Ag(110). W.W. PAI, M.R. PENG, N.C. BARTELT, J.E. REUTT-ROBEY, University of Maryland.	<b>SS2-ThA2</b> The Structural Characterization of Ga on Si(112). J.E. YATER, A. SHIH, Y. IDZERDA, Naval Research Laboratory.
2:40 pm	<b>SS1-ThA3</b> Oxidation Behavior of the (100) and (110) FeAl Surfaces. H. GRAUPNER, L. HAMMER, K. MÜLLER, University of Erlangen, Germany. D.M. ZEHNER, Oak Ridge National Laboratory.	<b>SS2-ThA3</b> Transition Metal Induced Ring-Cluster Structures on Si(111) Studied by STM. S.A. PARIKH, M.Y. LEE, P.A. BENNETT, Arizona State University.
3:00 pm	<b>SS1-ThA4</b> Electron Stimulated Oxidation of Metals at Low Temperature: Ni(111) at 120K. W. LI, M.J. STIRNIMAN, S.J. SIBENER, University of Chicago.	<b>SS2-ThA4</b> Surface Geometry of S-Passivated InP(100)-(1x1). D.L. WARREN, G.W. ANDERSON, M.C. HANF, P.R. NORTON, University of Western Ontario, Canada.
3:20 pm	<b>SS1-ThA5</b> Cesium/Oxide Interactions for Ultrathin Films on an $\alpha$ -Al <sub>2</sub> O <sub>3</sub> (0001) Surface. K.R. ZAVADIL, Sandia National Laboratories. J.L. ING, AEA Technology.	<b>SS2-ThA5</b> Structural Determination of Methyl Halides on GaAs(110): Analysis of NEXAFS and TOF Measurements of Photodissociation. P.J. LASKY, P.H. LU, Q.Y. YANG, R.M. OSGOOD, JR., Columbia University.
3:40 pm	<b>SS1-ThA6</b> Infrared Spectroscopy of Oxygen and Formate on Cu(100): Broadband Reflectance and Low-Frequency Vibrations. K.C. LIN, R.G. TOBIN, Michigan State University. P. DUMAS, LURE, France.	<b>SS2-ThA6</b> Structure of Sulfided Ultra-thin Ni Films on W(001). S.H. OVERBURY, Oak Ridge National Laboratory.
4:00 pm	<b>SS1-ThA7</b> Atomically Resolved STM Study of the Interaction of Boron with Si (001). Y. WANG*, R.J. HAMERS, University of Wisconsin, Madison.	<b>SS2-ThA7</b> Morphology and Mobility of Steps on a Metallic Surface Cu(1 1 1). Influence of Sulphur Adsorption. L. MASSON, L. BARBIER, J. COUSTY, B. SALANON, C.E.A. SRSIM, France.
4:20 pm	<b>SS1-ThA8</b> The Structure and Stability of Methyl Thiolate on Ni(111). D.R. HUNTLEY, D.R. MULLINS, S.H. OVERBURY, Oak Ridge National Laboratory. H. YANG, North Carolina State University.	<b>SS2-ThA8</b> Second Harmonic Generation from Alkali Metal Overlayers on Al(111) Surface. J. WANG, Z.C. YING, University of Pennsylvania. E.W. PLUMMER, University of Tennessee.
4:40 pm	<b>SS1-ThA9</b> A Comparative Study of P(CH <sub>3</sub> ) <sub>3</sub> and PH <sub>3</sub> Decomposition on Ru(0001). H.-S. TAO, T.E. MADEY, Rutgers University. U. DIEBOLD, Tulane University. N.D. SHINN, Sandia National Laboratories.	<b>SS2-ThA9</b> Depolarization and Phase Behavior in a Model for Alkali Adsorption on Simple Metals. L.D. ROELOFS, D. FROMOWITZ, Haverford College.
5:00 pm	<b>SS1-ThA10</b> Long Range Periodicity and Local Order in Complex Molecule Chemisorption. B.G. FREDERICK, F.M. LEIBSLE, S. DHESI, M.B. LEE, K. KITCHING, N.V. RICHARDSON, University of Liverpool, United Kingdom.	<b>SS2-ThA10</b> The Structures of CO and O on the Rh(110) Surface as Determined by Tensor LEED. J.D. BATTEAS, A. BARBIERI, E.K. STARKEY, M.A. VAN HOVE, G.A. SOMORJAI, University of California, Berkeley.

**NANO 3/NANOMETER-SCALE SCIENCE AND TECHNOLOGY/BIOMATERIAL INTERFACES**  
Room A209 - Session NSBI-ThA pg. 290

**Micro-Instrumentation and Sensors**

**Moderator:** M.H. Hecht, Jet Propulsion Laboratory.

**NANO 3/NANOMETER-SCALE SCIENCE AND TECHNOLOGY**  
Room A207 - Session NS2-ThA pg. 291

**Nanomechanics and Nanotribology: II**

**Moderator:** N.A. Burnham, École Polytechnique Fédérale de Lausanne.

2:00 pm	<b>NSBI-ThA1 INVITED</b> Micromachined Neural Interface Technology. <b>G.T.A. KOVACS</b> , Stanford University.	<b>NS2-ThA1</b> Observation of Superlubricity by Using Scanning Tunneling Microscope Method. <b>M. HIRANO</b> , NTT Interdisciplinary Research Labs, Japan. <b>K. SHINJO</b> , ATR Optical & Radio Communications Research Labs, Japan. <b>R. KANEKO</b> , NTT Interdisciplinary Research Labs, Japan. <b>Y. MURATA</b> , The University of Tokyo, Japan.
2:20 pm	Invited talk continued.	<b>NS2-ThA3</b> Influence of Water Vapor on Nanotribology Studied by Friction Force Microscopy. <b>M. BINGGELI</b> , Ctr. Suisse d'Electronique et de Microtechnique, Switzerland. <b>C.M. MATE</b> , IBM Almaden Research Center.
2:40 pm	<b>NSBI-ThA3</b> Fabrication and Characterization of a Nanosensor for Admittance Spectroscopy of Biomolecules. <b>L. MONTELIUS</b> , J.T. TEGENFELDT, T. LING, Lund University, Sweden.	<b>NS2-ThA4</b> AFM Studies of Corrosive Tribological Wear: Single Crystal $\text{NaNO}_3$ Exposed to Moist Air. <b>S. NAKAHARA</b> , J.T. DICKINSON, S.C. LANGFORD, Washington State University.
3:00 pm	<b>NSBI-ThA4</b> Interfacial Aspects of Acoustic Plate Mode (APM) Biosensor Response. <b>J. RENKEN</b> , R. DAHINT, Universität Heidelberg, Germany. <b>F. JOSSE</b> , Marquette University. <b>M. GRUNZE</b> , Universität Heidelberg, Germany.	<b>NS2-ThA5</b> Nanotribology in Electrochemically Controlled Environment. <b>M. BINGGELI</b> , J. BURGER, R. CHRISTOPH, Ctr. Suisse d'Electronique et de Microtechnique, Switzerland.
3:20 pm	<b>NSBI-ThA5</b> Fast Temperature Modulation for Selective Gas Sensor Operation. <b>R.E. CAVICCHI</b> , J.S. SUEHLE, National Institute of Standards & Technology. <b>P. CHAPARALA</b> , University of Maryland. <b>K.G. KREIDER</b> , M. GAITAN, National Institute of Standards & Technology.	<b>NS2-ThA6</b> Friction and Adhesion Properties of Hard Carbon Surfaces Measured by Atomic Force Microscopy. <b>S.S. PERRY</b> , G.A. SOMORJAI, University of California, Berkeley. <b>C.M. MATE</b> , IBM Almaden Research Center.
3:40 pm	<b>NSBI-ThA6</b> New Techniques of Thermal Imaging using the Atomic Force Microscope. <b>M. CHANDRACHOOD</b> , O. NAKABEPPU, Y. WU, J. LAI, A. MAJUMDAR, University of California, Santa Barbara.	<b>NS2-ThA7</b> Orientational Ordering of Polymers with A.F.M. in Contact Mode: An Application to Conjugated Polymers. <b>Z. ELKAAKOUR</b> , J.P. AIMÉ, T. BOUHACINA, C. ODIN, Université Bordeaux I, France. <b>T. MASUDA</b> , Kyoto University, Japan.
4:00 pm	<b>NSBI-ThA7</b> Initial Tests of a Micromachined SEM. <b>D.A. CREWE</b> , A.D. FEINERMAN, University of Illinois, Chicago.	<b>NS2-ThA8</b> Nanotribological Investigations of Epitaxial $\text{C}_{60}$ Films on $\text{GeS(001)}$ by Lateral Force Microscopy and Force Spectroscopy. <b>W. ALLERS</b> , U.D. SCHWARZ, University of Hamburg, Germany. <b>G. GENSTERBLUM</b> , Universitaires Notre-Dame de la Paix, Belgium. <b>R. WIESENDANGER</b> , University of Hamburg, Germany.
4:20 pm	<b>NSBI-ThA8</b> Localized Photodiode for Near-Field Photodetection Optical Microscopy. <b>R.C. DAVIS</b> , C.C. WILLIAMS, University of Utah.	<b>NS2-ThA9</b> UHV Boundary Lubrication of the $\text{Cu(111)/Cu(111)}$ Interface by Submonolayer Coverages of Trifluoroethanol. <b>C.F. MCFADDEN</b> , University of Illinois, Urbana-Champaign. <b>A.J. GELLMAN</b> , Carnegie Mellon University.
4:40 pm	<b>NSBI-ThA9</b> Production and Characterization of High Aspect Ratio Probes for Resonance-Mode Atomic Force Microscopy. <b>K.F. JARAUSCH</b> , K.M. EDENFELD, C.B. MOONEY, D.P. GRIFFIS, G.M. SHEDD, P.E. RUSSELL, North Carolina State University.	<b>NS2-ThA10</b> Interfacial Friction of Physisorbed Rare-Gas Films on Metal Surfaces. <b>C. DALY</b> , J. KRIM, Northeastern University.
5:00 pm	<b>NSBI-ThA10</b> Tunnel Sensors for High Spatial Resolution and Sensitivity Force Sensors. <b>R.C. WHITE</b> , <b>J.C. JIANG</b> , Columbia University.	

# Thursday Afternoon, October 27, 1994

**APPLIED SURFACE SCIENCE**  
Room A101 - Session AS-ThA pg. 293

**Polymer/Organic Surfaces**

**Moderator:** A.B. Ulman, Eastman Kodak Company.

**PLASMA SCIENCE**

Room A109 - Session PS1-ThA pg. 294

**Plasma Surface Interactions**

**Moderator:** M. Nakamura, Fujitsu Ltd., Japan.

2:00 pm	<b>AS-ThA1</b> Polymer Surface Damage by X-ray Photoelectron Spectroscopy. <b>W.F. STICKLE</b> , P.E. SOBOL, H. IWA, Physical Electronics Laboratories.	<b>PS1-ThA1 INVITED</b> Chemical Topography of Masked Poly-Si Films Etched in Cl <sub>2</sub> and HBr-Containing, High Density Plasmas. <b>V.M. DONNELLY</b> , C.C. CHENG, K.V. GUINN, AT&T Bell Laboratories. I.P. HERMAN, AT&T Bell Laboratories & Columbia University.
2:20 pm	<b>AS-ThA2</b> Surface Vibrational Characterization of Thick Polymer Films using High Resolution Electron Energy Loss Spectroscopy. <b>G.R. APAI</b> , W.P. MCKENNA, L. GERENSER, C.A. FLEISCHER, Eastman Kodak Company.	Invited talk continued.
2:40 pm	<b>AS-ThA3</b> Surface Studies of Filled Silicone Elastomers. <b>B.D. RATNER</b> , D. LEACH-SCAMPAVIA, W. CIRIDON, C.D. TIDWELL, T. BOLAND, University of Washington. P. YANG, Mentor, Inc.	<b>PS1-ThA3</b> Reactivity of Plasma Radicals with the Surface of Depositing Films. <b>N.F. DALLESKA</b> , <b>E.R. FISHER</b> , Colorado State University.
3:00 pm	<b>AS-ThA4</b> High Resolution XPS and ToFSIMS Studies of Polyamidoamines. <b>A.G. SHARD</b> , M.C. DAVIES, S.J.B. TENDLER, University of Nottingham, United Kingdom. G. BEAMSON, SERC, Daresbury Laboratory. A.J. PAUL, CSMA Ltd. L. SARTORE, P. FERRUTI, Università di Brescia.	<b>PS1-ThA4</b> Molecular Dynamics Simulation of Atomic Layer Etching of Si(100). <b>S.D. ATHAVALA</b> , <sup>‡</sup> D.J. ECONOMOU, University of Houston.
3:20 pm	<b>AS-ThA5</b> Mass Spectra of Low-Molecular-Weight Materials on Corona-Treated Polypropylene. O. KORNIENKO, J.A. BURROUGHS, L. HANLEY, University of Illinois, Chicago.	<b>PS1-ThA5</b> Generation of Ionic Radicals by a Fragmentation Process on Surface. <b>Y. MITSUOKA</b> , Nagoya University & Nippondenso Co., Ltd., Japan. S. TAKAHASHI, H. TOYODA, Nagoya University, Japan. S. MUKAINAKANO, T. HATORI, Nippondenso Co., Ltd., Japan. H. SUGAI, Nagoya University, Japan.
3:40 pm	<b>AS-ThA6</b> Addition of a Single Chemical Functional Group to a Polymer Surface with a Mass-Separated Low Energy Ion Beam. <b>P. NOWAK</b> , N.S. MCINTYRE, Surface Science Western and Univ. of Western Ontario, Canada. I. BELLO, W.M. LAU, University of Western Ontario, Canada.	<b>PS1-ThA6</b> Aspect Ratio Dependent Etching of Polysilicon. <b>T.J. DALTON</b> , H.H. SAWIN, Massachusetts Institute of Technology.
4:00 pm	<b>AS-ThA7</b> Polyfluoroether Lubricant Analysis by TOF-SIMS. <b>P. KASAI</b> , <b>A.M. SPOOL</b> , IBM Storage Systems Division.	<b>PS1-ThA7</b> Real-Time Investigation of DC Bias Effects on Ultra Thin Silicon Oxide Growth in an Oxygen Plasma. <b>M. KITAJIMA</b> , I. KAMIOKA, K.G. NAKAMURA, National Research Institute for Metals, Japan.
4:20 pm	<b>AS-ThA8</b> Time of Flight-Secondary Ion Mass Spectrometry Analysis of Langmuir-Blodgett Films of Isotactic, Syndiotactic, and Atactic Poly(Methyl Methacrylate). <b>R.W. NOWAK</b> , J.A. GARDELLA, JR., P.A. ZIMMERMAN, D.A. HERCULES, State University of New York, Buffalo.	<b>PS1-ThA8</b> Defect Production and Recombination during Low-Energy Ion Processing. <b>B.K. KELLERMAN</b> , <sup>‡</sup> J.A. FLORO, E. CHASON, D.K. BRICE, S.T. PICHAUX, Sandia National Laboratories. J.M. WHITE, University of Texas, Austin.
4:40 pm	<b>AS-ThA9</b> Probing the Interfacial Properties of Poly(vinyl acetate-ethylene) Copolymers and Poly(vinyl chloride) Laminations by Time-of-Flight Secondary Ion Mass Spectrometry. <b>P.A. CORNELIO CLARK</b> , S.A. GARDNER, D. HORWAT, Air Products and Chemicals, Inc.	<b>PS1-ThA9</b> Characterization of Ion Directionality in Plasma Enhanced Chemical Vapor Deposition of Silicon Dioxide. <b>J. LI</b> , C. CHANG, J.P. MCVITTIE, K.C. SARASWAT, Stanford University.
5:00 pm	<b>AS-ThA10</b> Morphological and Nanomechanics Investigations of Surface Modified Poly(tetrafluoroethylene). <b>A.J. HOWARD</b> , R.R. RYE, P. TANGYUNYONG, J.E. HOUSTON, Sandia National Laboratories.	<b>PS1-ThA10</b> An Auger and XPS Study of Ar <sup>+</sup> Sputtering Yield and Angular Distribution of Al. <b>P.C. SMITH</b> , R.B. TURKOT, J.P. KELLY, D.N. RUZIC, University of Illinois, Urbana.

**PLASMA SCIENCE****Room A102 - Session PS2-ThA pg. 296****Target Fabrication For Inertial Confinement Fusion****Moderator:** H. G. Kim, University of Rochester.**THIN FILM****Room A105 - Session TF-ThA pg. 298****Thin Films for Energy Conversion and Efficiency / Active Films****Moderator:** B.P. Hichwa, Optical Coating Laboratory Inc.

2:00 pm	<b>PS2-ThA1 INVITED</b> Target Area Design Basis and System Performance for the National Ignition Facility. <b>M.T. TOBIN</b> , V. KARPENKO, K. HAGANS, A. ANDERSON, Lawrence Livermore National Laboratory. <b>R. WAVRIK</b> , R. GARCIA, Sandia National Laboratories.	<b>TF-ThA1 INVITED</b> Thin-Film Rechargeable Lithium Batteries. <b>J.B. BATES</b> , Oak Ridge National Laboratory.
2:20 pm	Invited talk continued.	Invited talk continued.
2:40 pm	<b>PS2-ThA3</b> Precision Shell Characterization using Radial Averaging of X-ray Images. <b>R.B. STEPHENS</b> , General Atomics.	<b>TF-ThA3</b> Sputter Deposition of Cermet Fuel Electrodes for Solid Oxide Fuel Cells. <b>T. TSAI</b> , S.A. BARNETT, Northwestern University.
3:00 pm	<b>PS2-ThA4</b> High Yield Fabrication of Uniform, Large Diameter Foam Shells for Laser Fusion Targets using Polymerization by Photo Initiation with UV Light. <b>M. TAKAGI</b> , Y. KOBAYASHI, T. NORIMATSU, Y. IZAWA, S. NAKAI, Osaka University, Japan.	<b>TF-ThA4</b> Morphology of Precursors and $\text{CuIn}_{1-x}\text{Ga}_x\text{Se}_2$ Thin Films Prepared by Two-Stage Selenization Process. <b>N.G. DHERE</b> , S. KUTATH, Florida Solar Energy Center. <b>H.R. MOUTINHO</b> , National Renewable Energy Laboratory.
3:20 pm	<b>PS2-ThA5 INVITED</b> The Historical Development of the Microencapsulation Technique used to Fabricate ICF Capsules. <b>U. KUBO</b> , H. NAKANO, H. TSUBAKIHARA, Kinki University, Japan.	<b>TF-ThA5</b> Structure, Morphology, and Properties of $\text{CuIn}_x\text{Ga}_{1-x}\text{Se}_2$ Epitaxial Layers on GaAs. <b>G.A. BERRY</b> , D. SCHROEDER, L.-C. YANG, H.Z. XIAO, <b>A. ROCKETT</b> , University of Illinois, Urbana.
3:40 pm	Invited talk continued.	<b>TF-ThA6</b> Growth of Chalcopyrite $\text{Cu}(\text{Ga},\text{In})\text{Se}_2/\text{CuIn}_3\text{Se}_5$ Absorbers by r.f. Sputtering. <b>J.L. HERNÁNDEZ-ROJAS</b> , I. MÁRTIL, G. GONZÁLEZ-DÍAZ, J. SANTAMARIA, F. SÁNCHEZ-QUESADA, Universidad Complutense, Spain.
4:00 pm	<b>PS2-ThA7</b> Vapor Deposited Solid Hydrogen Crystals: Size, Structure, and Roughening. <b>G.W. COLLINS</b> , E. MAPOLES, W. UNITES, T. BERNAT, Lawrence Livermore National Laboratory.	<b>TF-ThA7 INVITED</b> Attaining a Solar Energy Economy with Active Thin Film Structures. <b>R.B. GOLDNER</b> , Tufts University.
4:20 pm	<b>PS2-ThA8</b> The Design, Performance, and Application of an Atomic-Force Microscope-based Profilometer. <b>R.L. MCEACHERN</b> , C.E. MOORE, R.J. WALLACE, Lawrence Livermore National Laboratory.	Invited talk continued.
4:40 pm	<b>PS2-ThA9</b> Cryogenically Resealable Vacuum Seals. <b>N.B. ALEXANDER</b> , General Atomics.	<b>TF-ThA9</b> Low Temperature, High Rate Deposition of Electrochromic Materials/Devices with MetaMode. <b>N.A. O'BRIEN</b> , J.G.H. MATHEW, B.P. HICHWA, Optical Coating Laboratory, Inc.
5:00 pm	<b>PS2-ThA10</b> Estimation for Heating Uniformity on a Solid Fuel Layer by a Glow Discharge Plasma in Plasma Layering Technique to Make a Uniform Cryogenic Fuel Layer Inside an ICF Target. <b>T. NORIMATSU</b> , M. ISHIHARA, M. TAKAGI, Y. IZAWA, S. NAKAI, Osaka University, Japan.	<b>TF-ThA10</b> Properties of Transparent Conducting Zinc-Stannate Films Prepared by RF Magnetron Sputtering. <b>T. MINAMI</b> , <b>S. TAKATA</b> , H. SATO, H. SONOHARA, Kanazawa Institute of Technology.

# Thursday Afternoon, October 27, 1994

## ELECTRONIC MATERIALS

Room A108 - Session EM-ThA pg. 299

### Materials for Nanostructures

Moderator: H.P. Gillis, Georgia Institute of Technology.

## MANUFACTURING SCIENCE AND TECHNOLOGY/VACUUM TECHNOLOGY

Room A110 - Session MSVT-ThA pg. 301

### Vacuum Process Control for Manufacturing

Moderator: W. Weed, Sandia National Laboratories.

2:00 pm	<b>EM-ThA1 INVITED</b> Magnetotransport in Semiconductor Nanostructures. <b>K.P. MARTIN</b> , Georgia Institute of Technology.	<b>MSVT-ThA1 INVITED</b> Top Ten List of User-Hostile Interface Design. <b>D.P. MILLER</b> , Sandia National Laboratories.
2:20 pm	Invited talk continued.	Invited talk continued.
2:40 pm	<b>EM-ThA3</b> Nanoscale Structures in III-V Semiconductors Using Sidewall Masking and High Ion Density Dry Etching. <b>F. REN</b> , AT&T Bell Laboratories. <b>S.J. PEARTON</b> , <b>C.R. ABERNATHY</b> , University of Florida, Gainesville. <b>J.R. LOTHIAN</b> , AT&T Bell Laboratories.	<b>MSVT-ThA3 INVITED</b> Advanced Control Methodologies into the Future. <b>R.W. MCMAHON</b> , Techware Systems Corporation, Canada.
3:00 pm	<b>EM-ThA4</b> Optical Evaluation and Surface Passivation of Quantum Structures Fabricated by Neutral Atom Etching at Cryogenic Temperatures. <b>M.B. FREILER</b> , <b>M.C. SHIH</b> , <b>S. KIM</b> , <b>M. LEVY</b> , <b>R. SCARMOZZINO</b> , <b>I.P. HERMAN</b> , <b>R.M. OSGOOD, JR.</b> , Columbia University.	Invited talk continued.
3:20 pm	<b>EM-ThA5</b> Room Temperature Photoluminescence and Electroluminescence from Ge Nanocrystals in SiO <sub>2</sub> formed by Ion Implantation and Precipitation. <b>C.M. YANG</b> , <b>K.V. SHCHEGLOV</b> , <b>S.S. WONG</b> , <b>H.A. ATWATER</b> , California Institute of Technology.	<b>MSVT-ThA5</b> Adaptive Extensions to a Multi-Branch Run-to-Run Controller for Plasma Etching. <b>J.R. MOYNE</b> , <b>N. CHAUDHRY</b> , <b>R. TELFEYAN</b> , University of Michigan.
3:40 pm	<b>EM-ThA6</b> Direct Characterization of a 2 Dimensional Electron Gas in Heterostructure FETs with Scanning Tunneling Microscope. <b>S.L. SKALA</b> , <b>W. WU</b> , <b>J.R. TUCKER</b> , <b>K.-Y. CHENG</b> , <b>J.W. LYDING</b> , University of Illinois, Urbana-Champaign.	<b>MSVT-ThA6</b> Real-Time Feedback for Sidewall Profile Control. <b>B. RASHAP</b> , <b>J. FREUDENBERG</b> , <b>M. ELTA</b> , University of Michigan.
4:00 pm	<b>EM-ThA7</b> Temporal Evolution of Nanoscale Interfacial Phases between GaAs and Metal Films. <b>T.-J. KIM</b> , <b>P.H. HOLLOWAY</b> , University of Florida, Gainesville.	<b>MSVT-ThA7</b> Process Monitoring with Residual Gas Analyzers. <b>C.R. TILFORD</b> , National Institute of Standards & Technology.
4:20 pm	<b>EM-ThA8</b> Selective Chemical Vapor Deposition of Copper on Pd-Activated Self-Assembled Films. <b>S.J. POTOCHNIK</b> , <b>D.S.Y. HSU</b> , <b>J.M. CALVERT</b> , <b>P.E. PEHRSSON</b> , Naval Research Laboratory.	<b>MSVT-ThA8</b> An Improved Method of Non-Intrusive Deposition Rate Monitoring by Atomic Absorption Spectroscopy. <b>C. LU</b> , <b>Y. GUAN</b> , Intelligent Sensor Technology, Inc.
4:40 pm	<b>EM-ThA9</b> Surface Chemistry of Al <sub>2</sub> O <sub>3</sub> Deposition using Al(CH <sub>3</sub> ) <sub>3</sub> and H <sub>2</sub> O in a Binary Reaction Sequence. <b>A.W. OTT</b> , <b>A.C. DILLON</b> , <b>S.M. GEORGE</b> , University of Colorado, Boulder. <b>J.D. WAY</b> , Colorado School of Mines.	<b>MSVT-ThA9</b> A Model Based Technique for Estimation of Fluorine in a CF <sub>4</sub> /Ar Plasma. <b>P.D. HANISH</b> , <b>J.W. GRIZZLE</b> , <b>M.D. GILES</b> , University of Michigan.
5:00 pm	<b>EM-ThA10</b> Study of Polycrystalline CdTe Thin Films by Atomic Force Microscopy. <b>H.R. MOUTINHO</b> , <b>F.A. HASOON</b> , <b>F. ABULFOTUH</b> , <b>L.L. KAZMERSKI</b> , National Renewable Energy Laboratory.	<b>MSVT-ThA10</b> Role of Inert Carrier Gases in Modeling, Design and Operation of a Single Wafer APCVD Reactor for Manufacturing. <b>P.N. GADGIL</b> , Queen's University, Canada.



**VACUUM METALLURGY****Room A106 - Session VM-ThA** pg. 302**Manufacturing Technology for Coatings****Moderator:** D.C. Carmichael, Vacuum Technology Inc.

2:00 pm	<b>VM-ThA1 INVITED</b> Environmentally Compatible Coating Technology. K.O. LEGG, A. ADAM-SKI, C. WEST, P. RUDNICK, Northwestern University. F. RASTAGAR, Cummins Piston Ring Division. J. SCHELL, GE Aircraft Engines. A. GONZALES, Corpus Christi Army Depot. B. SARTWELL, Naval Research Laboratory.	
2:20 pm	Invited talk continued.	
2:40 pm	<b>VM-ThA3 INVITED</b> Development of a Manufacturing Process to Sputter AlN Barrier Layers on MO Recording Disks. D.A. GLOCKER, Eastman Kodak Company.	
3:00 pm	Invited talk continued.	
3:20 pm	<b>VM-ThA5</b> Simultaneous Deposition and Lamination Process in Vacuum. A.W. FREELAND, J.R. GERMUNDSON, R.L. SWISHER, K. BARNES, C.T. WAN, Sheldahl Inc.	
3:40 pm	<b>VM-ThA6</b> Anode Effects in Magnetron Sputtering. A. BELKIND, F. JANSEN, Z. ORBAN, J. VOSSEN, The BOC Group Technical Center.	
4:00 pm	<b>VM-ThA7 INVITED</b> Recent Technology Advancements in Optical Thin Film Manufacturing. P.M. LEFEBVRE, B.P. HICHA, R.W. ADAIR, Optical Coating Laboratory Inc.	
4:20 pm	Invited talk continued.	
4:40 pm	<b>VM-ThA9</b> Sputter Deposition of Indium Tin Oxide (ITO) from a Cylindrical Ceramic Target. K.P. GIBBONS, T. VAN SKE, C.K. CARNIGLIA, Airco Coating Technology.	
5:00 pm		

# Thursday Afternoon Poster Sessions

## NANO 3/NANOMETER-SCALE SCIENCE AND TECHNOLOGY Room BR4 - Session NS-ThP pg. 304

### Nanoelectronics and Nanofabrication

**Moderator:** J.D. Dagata, National Institute of Standards and Technology.

Presenters present: 5:00-6:30 pm.

**NS-ThP1** Voltage Controlled Nanometer Scale Oxidation of Si(100) Surface by STM. **E. PÉREZ-MURANO**, G. ABADAL, N. BARNIOL, X. AYMERICH, Universitat Autònoma Barcelona, Spain.

**NS-ThP2** Local Electrical Switching Effects in CuTCNQ Films Studied by Surface Modification with STM. **L. WANG**, C.W. YUAN, J.W. LIANG, H. CHEN, Y. WEI, Southeast University, PR China.

**NS-ThP3** Deep-Etch Silicon MM-Waveguide Structure for the Relativistic Acceleration of Electrons. **T.L. WILLKE**, A.D. FEINERMAN, University of Illinois, Chicago.

**NS-ThP4** Measurement of the Piezoelectricity of Thin Films with STM. **R. WINTERS**, M. REINERMANN, C. ENSS, G. WEISS, Universität Heidelberg, Germany.

**NS-ThP5** Chemically Assisted Micromachining of Diamond with a Focused Ion Beam. **G.M. SHEDD**, T.J. STARK, D.P. GRIFFIS, P.E. RUSSELL, North Carolina State University.

**NS-ThP6** Nanometer-Scale Definition of Conductors on Insulators using the AFM. **M. FALVO**, D. GLICK, **R. SUPERFINE**, University of North Carolina, Chapel Hill.

**NS-ThP7** Electrochemical Nanoscale Patterning of Surfaces with Electrically Conductive Polymers. **X.Y. ZHENG**, Y. DING, C. TONG, L.A. BOTTOMLEY, J. KOWALIK, L.M. TOLBERT, Georgia Institute of Technology.

**NS-ThP8** Local Fusion of Metallic Surfaces and Dots Formation using STM. **L. LIBIOLLE**, J.-M. GILLES, Facultés Notre-Dame de la Paix, Belgium.

**NS-ThP9** Nanometer-Size Features Produced by Highly Charged Ions. **D.C. PARKS**, M.P. STÖCKLI, Kansas State University. **R.W. SCHMIEDER**, R.J. BASTASZ, Sandia National Laboratories.

**NS-ThP10** The Self-Assembled Ordered Structures for Nano-electronics: Stability and Local Modification. **A.V. EMEL'YANOV**, V.V. PROTASENKO, **V.N. RYABAKON**, Zelenograd Research Institute of Physical Problems, Russia.

**NS-ThP11** Mechanical Nanofabrication based on Scanning Force Methods. **S. LUKAS**, M. LÖHNDORF, C. HAHN, U.D. SCHWARZ, **R. WIESEN-DANGER**, University of Hamburg, Germany.

**NS-ThP12** New Design for STM-CVD Nanofabrication. **S. RUBEL**, X.-D. WANG, **A.L. DE LOZANNE**, University of Texas, Austin.

**NS-ThP13** Submicron Pattern Transfers in HgCdTe and GaAs by Reactive-Ion Etching through Nanochannel Glass Lithographic Masks. **C.R. EDDY, JR.**, R.J. TONUCCI, Naval Research Laboratory.

**NS-ThP14** The Technological Aspects of Cluster Film Application in Nanoelectronics with Use of STM. **P.N. LUSKINOVICH**, E.E. GUTMAN, I.A. RYZHIKOV, "Delta" R&D Institute, Russia.

**NS-ThP15** Nanoscale STM Patterning of Silicon Dioxide Thin Films by Catalyzed HF Vapor Etching. **J. ALLGAIR**, M.N. KOZICKI, H.J. SONG, **T.K. WHIDDEN**, Arizona State University.

**NS-ThP16** Ambient Dependence of Nanometer Scale Writing on Silicon (100) Surfaces by an Atomic Force Microscope. **L. TSAU**, D. WANG, K.L. WANG, University of California, Los Angeles.

**NS-ThP17** The Formation of Nanometer-Scale Molecular Memory by STM. **K. MATSUSHIGE**, Kyoto University, Japan. **S. TAKI**, Kyushu University, Japan.

**NS-ThP18** Using Scanning Tunneling Microscopy for Control and Revision of Strongly Ruffled Surfaces of Plane Carbon Field Emitters Modified by Ion Beams. **A.L. SUVOROV**, V.V. PROTASENKO, V.G. STOLYAROVA, E.P. SHESHIN, Institute of Theoretical & Experimental Physics, Russia.

**NS-ThP19** Negative-Differential Conductivity Observed on a Germanium Layer on Si(001). **H.-J. MÜSSIG**, D. KRÜGER, S. HINRICH, Institut für Halbleiterphysik, Germany. **P.O. HANSSON**, Max-Planck-Institut für Festkörperforschung, Germany.

**NS-ThP21** Manipulation of Nanometer-Scale Structures in Langmuir-Blodgett Films using Atomic Force Microscopy. **J. GARNAES**, Danish Institute for Fundamental Metrology, Denmark. **N.B. LARSEN**, University of Copenhagen, Denmark. **T. BJØRNHOLM**, Danish Institute of Fundamental Metrology, Denmark.

**NS-ThP22** Experimental Design for Determining the Duration of Quantum Tunneling with Laser-Illuminated Field Emission. **M.J. HAGMANN**, Florida International University.

**NS-ThP23** Cross-sectional Characterization of Thin Film Transistors with Transmission Electron Microscopy. **S. TSUJI**, M. TANAKA, H. IWAMA, N. TSUTSUI, K. KURODA, H. SAKA, IBM Japan, Ltd.

**NS-ThP24** Single Crystal Epitaxial Ge Based Ohmic Contacts to III-V Nanoelectronic and Mesoscopic Devices. **M. DUBEY**, K.A. JONES, L.M. CASAS, Army Research Laboratory.

**NS-ThP25** Nanoscale Lithography and Pattern Transfer on Si(100) with a UHV Scanning Tunneling Microscope. **G.C. ABELN**, T.-C. SHEN, C. WANG, J.R. TUCKER, J.W. LYDING, University of Illinois, Urbana-Champaign.

## ELECTRONIC MATERIALS

Room BR4 - Session EM-ThP pg. 308

### Aspects of Electronic Materials and Processing II

Moderator: A. Rockett, University of Illinois, Urbana.

Presenters present: 5:00-6:30 pm.

**EM-ThP1** Study of Damage Caused by W Etchback and Effect on Subsequent AlCu Deposition. **L.R. ALLEN**, J.M. GRANT, Sharp Microelectronics Technology, Inc.

**EM-ThP2** Low-Resistivity Ohmic Contacts to Moderately Doped n-GaAs with Low Temperature Processing. **M.L. LOVEJOY**, A.J. HOWARD, Sandia National Laboratories. **P.A. BARNES**, Auburn University. **D.J. RIEGER**, K.R. ZAVADIL, R.J. SHUL, J.C. ZOLPER, Sandia National Laboratories.

**EM-ThP3** Excimer Laser Induced Deposition of Tungsten on GaAs from  $WF_6$  and  $SiH_4$ . **M. TABBAL**, M. MEUNIER, R. IZQUIERDO, A. YELON, Ecole Polytechnique de Montréal, Canada.

**EM-ThP4** The Effect of Chemical Etchants on Back Contact Formation to CdTe-Based Solar Cells. **X. LI**, D. NILES, F. HASOON, P. SHELTON, National Renewable Energy Laboratory.

**EM-ThP5** STM Observations of Sub-Surface Donor and Acceptors in GaAs. **J.-F. ZHENG**, D.F. OGLETTREE, E. WEBER, M. SALMERON, Lawrence Berkeley Lab & University of California, Berkeley.

**EM-ThP6** Microscopic-Scale Lateral Inhomogeneities of Heterostructure Energy Barriers. **F. GOZZO**, H. BERGER, I.R. COLLINS, G. MARGARITONDO, Ecole Polytechnique Fédérale de Lausanne, Switzerland. **W. NG**, A.K. RAY-CHAUDHURI, S. SINGH, F. CERRINA, University of Wisconsin, Madison.

**EM-ThP7** Interface Electronic Structure in the Ceramic-ZnO/Bi System: Evidence for the Varistor Effect. **K.O. MAGNUSSON**, University of Karlstad, Sweden. **S. WIKLUND**, University of Lund, Sweden.

**EM-ThP8** Internal Photoemission of Adjustable Band-offset Heterojunctions. **G. MENSING**, R. ALBRIDGE, A. BARNES, J. MCKINLEY, N. TOLK, J. DAVIDSON, T. STULTZ, Vanderbilt University. **B. MCCOMBE**, A. PETROU, State University of New York, Buffalo.

**EM-ThP9** Interface Exciton Luminescence: Indication of Interface Inhomogeneities in Single GaAs/GaAlAs Heterostructures. **V.N. BESSOLOV**, **V.V. EVSTROPOV**, M.V. LEBEDEV, V.V. ROSSIN, A.F. Ioffe Physico-Technical Institute, Russia.

**EM-ThP10** The Nature of Ambient (100) GaAs Surfaces. **O.J. GLEM-BOCKI**, J.A. TUCHMAN, Naval Research Laboratory. **K.K. KO**, S.W. PANG, University of Michigan. **J.A. DAGATA**, National Institute of Standards & Technology. **R. KAPLAN**, Naval Research Laboratory. **C.E. STUTZ**, Wright Patterson Laboratories.

**EM-ThP11** Surface Studies of MBE Grown GaAs(111)A by HREELS, XPS, UPS and LEED. **J. WU**, G.J. LAPEYRE, Montana State University.

**EM-ThP12** Geometric and Electronic Structure of Ni Silicide on Si(100). **Y. KHANG**, Seoul National University, Korea. **D. JEON**, Myong-ji University, Korea. **Y. KUK**, Seoul National University, Korea.

**EM-ThP13** Electronic Band Structure of Epitaxial  $\gamma$ -FeSi<sub>2</sub>(111)2x2. **J. ALVAREZ**, C. LIMONES, E.G. MICHEL, R. MIRANDA, M.E. DAVILA, J. MARTIN-GAGO, Universidad Autonoma de Madrid, Spain.

**EM-ThP14** Sensor for Measuring the Atomic Fraction in Highly Dissociated Hydrogen. **W.L. GARDNER**, Oak Ridge National Laboratory.

**EM-ThP15** Spectroscopic Ellipsometry Studies of a-Si<sub>1-x</sub>C<sub>x</sub>:H Film Growth by Reactive Magnetron Sputtering. **Y.H. YANG**, M. KATYAR, **J.R. ABELSON**, University of Illinois, Urbana.

**EM-ThP16** Numerical Ellipsometry; Applications of a New Algorithm for Real Time, In Situ Film Growth Monitoring. **J.C. COMFORT**, **F.K. URBAN III**, Florida International University.

**EM-ThP17** ARXPS-Studies of Oxidation of 6H SiC Single Crystal (001) Si- and (001) C-Surfaces. **B. HORNETZ**, UNI, 76131 Karlsruhe, Germany. **H.-J. MICHEL**, J. HALBRITTER, K&K, IMF I, 76021 Karlsruhe, Germany.

**EM-ThP18** Adsorption and Co-adsorption of Boron and Oxygen on Ordered  $\alpha$ -SiC Surfaces. **V.M. BERMUDEZ**, Naval Research Laboratory.

**EM-ThP19** Oxide Layer Growth on Gallium Arsenide using High Kinetic Energy Neutral Atomic Oxygen. **M.A. HOFFBAUER**, J.B. CROSS, Los Alamos National Laboratory. **J.C. GREGORY**, University of Alabama.

**EM-ThP20** Oxidation-Induced Roughening and Oxide Nucleation on Si(001)-2x1 Surfaces: An STM Study. **J.P. PELZ**, **J.V. SEIPLE**, Ohio State University.

**EM-ThP21** Growth of Layered Semiconductors by Molecular Beam Epitaxy: Formation and Characterization of GaSe, and MoSe<sub>2</sub> Layers on Sulfur Passivated GaP(111) and GaAs(111). **C. HAMMOND**, University of Arizona. **M. LAWRENCE**, Concordia University, Canada. **K. NEBESNY**, P. LEE, University of Arizona. **R. SCHLAF**, Hahn Meitner Institute, Germany. **N.R. ARMSTRONG**, University of Arizona.

**EM-ThP22** An Atomically-resolved STM Study of the Interaction of Trimethyl Gallium with Si(001). **M.J. BRONIKOWSKI**, R.J. HAMERS, University of Wisconsin, Madison.

**EM-ThP23** Reactions of Tetraethoxysilane (TEOS) Vapor on Titanium Dioxide Surfaces. **T.A. JURGENS**, University of Washington and Pacific Northwest Laboratory. **G.S. HERMAN**, University of Washington. **T.T. TRAN**, S.A. CHAMBERS, C.H.F. PEDEN, Pacific Northwest Laboratory. **J.W. ROGERS, JR.**, University of Washington.

**EM-ThP24** Synchrotron Radiation Induced Decomposition of closo-1,2-dicabado-decaborane. **D. BYUN**, S.-D. HWANG, University of Nebraska, Lincoln and Syracuse University. **J. ZHANG**, University of Nebraska, Lincoln. **H. ZENG**, Syracuse University. **F.K. PERKINS**, Naval Research Laboratory. **G. VIDALI**, Syracuse University. **P.A. DOWBEN**, University of Nebraska, Lincoln.

**EM-ThP25** Interaction of Tungsten Hexafluoride with W(100). **W. CHEN**, J.T. ROBERTS, University of Minnesota.

**EM-ThP26** Chemisorption and Thermally Activated Etching of Iodine on Si(100)-2x1. **D. RIOUX**, F. STEPNIAK, R.J. PECHMAN, J.H. WEAVER, University of Minnesota.

# Thursday Afternoon Poster Sessions

## THIN FILM

Room BR4 - Session TF-ThP pg. 312

### Thin Film Characterization and Sensors Applications

Moderator: A.C. Wall, IBM Corporation.

Presenters present: 5:00-6:30 pm.

**TF-ThP1** Auger Electron Spectroscopy as a Real-Time Probe of Film Composition during MBE Growth. **S.A. CHAMBERS**, T.T. TRAN, Pacific Northwest Laboratory.

**TF-ThP2** B-Doped Si(001) Grown by Gas-Source Molecular-Beam Epitaxy from  $\text{Si}_2\text{H}_6$  and  $\text{B}_2\text{H}_6$ : B Incorporation and Electrical Properties. **Q. LU**, T.R. BRAMBLETT, N.-E. LEE, M.-A. HASAN, T. KARASAWA, J.E. GREENE, University of Illinois, Urbana.

**TF-ThP3** Mass Spectroscopy of Recoiled Ions (MSRI) as a Tool both for Surface Analysis of Boron Nitride Thin Films during Deposition and Ex Situ. **L. WOOLVERTON**, J.A. SCHULTZ, K. EIPERS-SMITH, K. WATERS, IONWERKS.

**TF-ThP4** Deposition of Polysilicon by ECRCVD and RTCVD. **P. MÜLLER**, E. CONRAD, Hahn-Meitner-Institut, Germany. T.R. OMSTEAD, CVC Products, Inc.

**TF-ThP5** Oxygen Content of Indium Tin Oxide Films Fabricated by Reactive Sputtering. **S. HONDA**, A. TSUJIMOTO, M. WATAMORI, K. OURA, Osaka University, Japan. F. SHOJI, Kyushu Kyoritsu University, Japan.

**TF-ThP6** Thin-Film and Buried Interface Characterization using High Brightness Synchrotron Radiation. **J.J. JIA**, T.A. CALLCOTT, University of Tennessee. F.J. HIMPSEL, H. AKATSU, IBM TJ Watson Research Center. M.G. SAMANT, J. STOHR, IBM Almaden Research Center. D.L. EDERER, Tulane University. J.A. CARLISLE, E.A. HUDSON, L.J. TERMINELLO, Lawrence Livermore National Laboratory. R.C.C. PERERA, D.K. SHUH, Lawrence Berkeley Laboratory.

**TF-ThP7** Structure and Composition of Hydrogenated  $\text{Ti}_x\text{C}_y$  Thin Films Prepared by Reactive Sputtering. **M.P. DELPLANCHE**, V. VASSILERIS, R. WINAND, Université Libre de Bruxelles, Belgium.

**TF-ThP8** Ion Beam-Induced SiC Crystallization of Carbon Implanted Layers in Si(100) Studied by Electron Spectroscopy. **H.J. STEFFEN**, V. HEERA, R. KOEGLER, W. SKORUPA, Research Center Rossendorf Inc., Germany.

**TF-ThP9** Interfacial Properties of FCC-Iron Grown on Diamond. **R. SWINEFORD**, F. YUE, D.P. PAPPAS, Virginia Commonwealth University.

**TF-ThP10** Study of Adsorption and Desorption of 1,5-Cyclooctadiene on Cu(111) Surface. **Q. CHENG**, K. GRIFFITHS, S. SERGHINI, Z. YAN, P.R. NORTON, R.J. PUDDEPHATT, University of Western Ontario, Canada.

**TF-ThP11** Spatial Grating Formation in Amorphous Chalcogenide Thin Films. **E. LÓPEZ-CRUZ**, J. GONZÁLEZ-HERNÁNDEZ, F. RUIZ, C. VÁZQUEZ-LÓPEZ, CINVESTAV-Saltito, México. E. HARO-PONIATOWSKI, Universidad Autónoma Metropolitana-Iztapalapa, México.

**TF-ThP12** Synchrotron Radiation Photoelectron Emission Microscopy of Natural and Chemical Vapor Deposited Diamond Surfaces. **J.D. SHOVLIN**, M.E. KORDESCH, Ohio University. D. DUNHAM, B.P. TONNER, University of Wisconsin, Milwaukee. W. ENGEL, Fritz Haber Institute, Germany.

**TF-ThP13** Surface Spectroscopic Studies of the Deposition of TiN Thin Films from Tetrakis-(dimethylamido)-Titanium and Ammonia. **P.J. CHEN**, C.M. TRUONG, J.S. CORNEILLE, W.S. OH, D.W. GOODMAN, Texas A&M University.

**TF-ThP14** Phase Stability and Al Solubility in Epitaxial  $\text{Nb}_{1-x}\text{Al}_x\text{N}$  Films Grown on MgO(001) by Reactive Sputtering. **T.I. SELINDER**, D.J. MILLER, K.E. GRAY, Argonne National Laboratory. L. HULTMAN, M.R. SARDELA, JR., Linköping University, Sweden.

**TF-ThP15** Growth and Structure of Silicon Oxide Thin Films on Polymers by AFM and XPS. **H. LI**, S. KROMMENHOEK, E. EZELL, BOC Group Technical Center. F. JANSEN, Airco Coating Technology.

**TF-ThP16** Characterization of Aluminum based Oxide Layers formed by Microwave Plasma. **Z. KATZ**, Ben-Gurion-University, Israel. A. RAVEH, NRC-Negev, Israel.

**TF-ThP17** Investigation of Pyroelectric Characteristics of Lead Titanate Thin Films for Microsensor Applications. **K.K. DEB**, Army Research Laboratory, Fort Belvoir. K.W. BENNETT, P.S. BRODY, Army Research Laboratory, Adelphi.

**TF-ThP18**  $\text{ReSi}_2$  Thin Film Infrared Detectors. **J.P. BECKER**, J.E. MAHAN, Colorado State University. R.G. LONG, Hewlett-Packard Co.

**TF-ThP19** Detection of Chlorinated Hydrocarbon Vapors using 1,3, bis-(1-pyrene)propane in a Poly (vinyl alcohol) Film. **S.L. ROSE-PEHRSSON**, J. KRECH, Naval Research Laboratory.

**TF-ThP20** Electrochemical and Surface Properties of a Unique Electro-Ceramic Sensor for Selective Detection of Chlorinated Organics. **J. VETRONE**, J.R. STETTER, W.R. PENROSE, W.R. BUTTNER, Transducer Research, Inc.

**TF-ThP21** Surface Characterization of Ultra-thin Metallic Sensing Films. **H. LIU**, J.L. GLAND, J.W. SCHWANK, K. WISE, University of Michigan.

**TF-ThP22** Electron Spectroscopy (XPS, UPS, HREELS) Study of the  $\text{Cu/SrTiO}_3$  (100) Interface. **T. CONARD**, A.-C. ROUSSEAU, R.L. SPORKEN, J. GHIJSEN, R. CAUDANO, Facultés Universitaires Notre Dame de la Paix, Belgium.

**TF-ThP23** AlN Thin Film Structure Development and Quality during Magnetron Sputter Deposition on Si(100) and Si(111), Studied by XRD, AES, and FE SEM. **B. LADNA**, M. CHASON, S. VOIGHT, Motorola.

**TF-ThP24** Microstructural Characterization of Pd/InP and Ag/InGaAs Films Grown at Room Temperature and 77K. **M.E. HAWLEY**, Q.X. JIA, Los Alamos National Laboratory. J. PALMER, H.J. LEE, W. ANDERSON, State University of New York, Buffalo. D. HOELZER, Alfred University.

## NOTES

# Friday Morning, October 28, 1994

## SURFACE SCIENCE

Room A205 - Session SS1-FrM pg. 317

### Surface Electronic Structure

Moderator: R. Hwang, Sandia National Laboratories.

## SURFACE SCIENCE

Room A201 - Session SS2-FrM pg. 319

### Group IV Semiconductor Surface Structure

Moderator: R. Hamers, University of Wisconsin.

8:20 am	<b>SS1-FrM1</b> Theory of Clean and H-covered Be(0001). <b>R. STUMPF</b> , P.J. FEIBELMAN, Sandia National Laboratories.	<b>SS2-FrM1</b> New Method for Empirically Determining Surface Electronic Species from Multiple-bias STM Images: A Multivariate Classification Approach. <b>A.M. BOUCHARD</b> , G.C. OSBOURN, B.S. SWARTZEN-TRUBER, Sandia National Laboratories.
8:40 am	<b>SS1-FrM2</b> Core-Level Spectroscopy of Metal Monolayers and Interfaces. <b>N.D. SHINN</b> , Sandia National Laboratories. <b>B. KIM</b> , Pohang University of Science & Technology, Korea. <b>K.J. KIM</b> , Kon-Kuk University, Korea. <b>T.-H. KANG</b> , Pohang University of Science & Technology, Korea. <b>J.L. ERSKINE</b> , University of Texas, Austin.	<b>SS2-FrM2</b> High Resolution TEM Determination of the (5x2) Au/Si(111) Structure. <b>R. PLASS</b> , L.D. MARKS, Northwestern University.
9:00 am	<b>SS1-FrM3</b> Core Level Shifts in Trimetallic Systems. <b>D.R. RAINER</b> , J.S. CORNEILLE, D.W. GOODMAN, Texas A&M University.	<b>SS2-FrM3</b> FT-IRAS of Adsorbed Alkoxides: Methoxide and Ethoxides on Cu(111). <b>S.C. STREET*</b> , University of Illinois, Urbana-Champaign. <b>A.J. GELLMAN</b> , Carnegie Mellon University.
9:20 am	<b>SS1-FrM4</b> Substrate Core-level Response to Nucleation and Growth of Ultra-thin Ni Films on W(001). <b>S.H. OVERBURY</b> , <b>D.R. MULLINS</b> , P.F. LYMAN, Oak Ridge National Laboratory. <b>N.D. SHINN</b> , Sandia National Laboratories.	<b>SS2-FrM4</b> Boron Induced Structures on the Si(111) Surface. <b>C. WANG</b> , T.C. SHEN, J.W. LYDING, J.R. TUCKER, University of Illinois, Urbana-Champaign.
9:40 am	<b>SS1-FrM5</b> Nature of the 4s-derived States of Adsorbed K Studied by X-ray Absorption Spectroscopy and the Core Hole Clock Method. <b>A. SANDELL</b> , <b>A. NILSSON</b> , P.A. BRÜHWILER, N. MARTENSSON, Uppsala University, Sweden.	<b>SS2-FrM5</b> Surface-Induced Optical Anisotropies of Single-Domain (2x1)-Reconstructed (001) Si and Ge Surfaces. <b>L. MANTESE</b> , T. YASUDA, D.E. ASPNES, North Carolina State University.
10:00 am	<b>SS1-FrM6</b> Photoemission Study of Alkali Metal Adsorption on the Passivated Si(111)1x1-As Surface. <b>M.C. HÅKANSSON</b> , M. JOHANSSON, L.S.O. JOHANSSON, University of Lund, Sweden.	<b>SS2-FrM6</b> High-Temperature Structural Phases of the Si(111) Surface Studied with High-Resolution, Energy-Resolved Helium Atom Scattering. <b>C.A. MELI</b> , Naval Research Laboratory. <b>G. LANGE</b> , J.P. TOENNIES, Max-Planck-Institut für Strömungsforschung, Germany.
10:20 am	<b>SS1-FrM7</b> Spectroscopic Characterization of Unique Electronic and Catalytic Properties of Vanadium Carbide Films on V(110). <b>J.G. CHEN</b> , B. FRÜHBERGER, B.D. DEVRIES, Exxon Research and Engineering Co.	<b>SS2-FrM7</b> Two-Dimensional Surface Interactions and Dynamics of Benzene on Cu(111). <b>M.M. KAMNA*</b> , S.J. STRANICK, P.S. WEISS, The Pennsylvania State University.
10:40 am	<b>SS1-FrM8</b> Electronic Transitions and Excitations in Solid C <sub>70</sub> Studied by HREELS and XPS C1s Shakeup Structures. <b>B.Y. HAN</b> , L.M. YU, K. HEVESI, G. GENSTERBLUM, P. RUDOLF, J.-J. PIREAUX, P.A. THIRY, R. CAUDANO, Facultés Universitaires Notre-Dame de la Paix, Belgium.	<b>SS2-FrM8</b> Strain-induced Surface Morphology on Si(111)-(7x7). <b>Y. WEI</b> , L. LI, I.S.T. TSONG, Arizona State University.
11:00 am	<b>SS1-FrM9</b> Inverse Photoemission Study of CO Chemisorption on Metallic Quantum Wells. <b>F.G. CURTI</b> , R.A. BARTYNSKI, Rutgers University.	<b>SS2-FrM9</b> A Novel Facet Reconstruction of Si(112) Revealed by STM. <b>A.A. BASKI</b> , L.J. WHITMAN, Naval Research Laboratory.
11:20 am	<b>SS1-FrM10</b> A Core Level Spectroscopy Study of Different Adsorption States of Ethylene on Pt(111). <b>B. HERNNÄS</b> , A. NILSSON, O. KARIS, C. PUGLIA, A. SANDELL, N. MARTENSSON, Uppsala University, Sweden.	<b>SS2-FrM10</b> Structural Determination of the Dimerized Si(100) Surface. <b>Y. QIAN</b> , M.J. BEDZYK, G.E. FRANKLIN, S. TANG, A.J. FREEMAN, Argonne National Laboratory & Northwestern University.
11:40 am	<b>SS1-FrM11</b> The Auger Relaxation of <sup>37</sup> Cl Following Electron Capture Decay of <sup>37</sup> Ar. <b>L. ZHU</b> , R. AVCI, G.J. LAPEYRE, Montana State University. <b>M.M. HINDI</b> , R.L. KOZUB, S.J. ROBINSON, Tennessee Technological University.	<b>SS2-FrM11</b> Fluctuations of Monatomic Steps on Si(001). <b>H.J.W. ZANDVLIET</b> , B. POELSEMA, University of Twente, The Netherlands. <b>H.B. ELSWIJK</b> , Philips Research Laboratories, The Netherlands.

**NANO 3/NANOMETER-SCALE SCIENCE AND TECHNOLOGY**  
Room A209 - Session NS1-FrM pg. 320

**Novel Materials and Methods for Nanofabrication**

**Moderator:** Y. Kuk, Seoul National University, Korea.

**NANO 3/NANOMETER-SCALE SCIENCE AND TECHNOLOGY**  
Room A207 - Session NS2-FrM pg. 322

**Novel Probes**

**Moderator:** D. Rugar, IBM Almaden Research Center.

8:20 am	<b>NS1-FrM1 INVITED</b> Chemistry and Applications of Self-Assembled Films. <b>J.M. CALVERT</b> , Naval Research Laboratory.	<b>NS2-FrM1</b> Applications of an AFM Probe with Ultrafast Time Resolution. <b>B.A. NECHAY</b> , F. HO, A.S. HOU, D.M. BLOOM, Stanford University.
8:40 am	Invited talk continued.	<b>NS2-FrM2</b> Measurement of Ultra Fast Optoelectronic Phenomena in Organic Molecular Assembly by Scanning Maxwell Stress Microscopy. <b>T. INOUE</b> , H. YOKOYAMA, Electrotechnical Laboratory, Japan.
9:00 am	<b>NS1-FrM3</b> Preparation and Characterization of Highly Organized Self-Assembled Monolayers as Substrates for Nanoelectronics. <b>C.W. SHEEN</b> , A.N. PARIKH, <b>D.L. ALLARA</b> , Pennsylvania State University. <b>M.J. LERCEL</b> , H.G. CRAIGHEAD, Cornell University.	<b>NS2-FrM3</b> High Frequency Pattern Extraction in Digital Integrated Circuits using Scanning Electrostatic Force Microscopy. <b>G.E. BRIDGES</b> , R.A. SAID, M. MITTAL, D.J. THOMSON, University of Manitoba, Canada.
9:20 am	<b>NS1-FrM4</b> Nanometer Resolution Near-field Optical Lithography. <b>M. RUDMAN</b> , A. SHCHEMELININ, K. LIEBERMAN, A. LEWIS, Hebrew University of Jerusalem, Israel.	<b>NS2-FrM4</b> Room Temperature Quantum Mechanical Capacitance Measured with the Ultrafast Scanning Probe Microscope. <b>D. BOTKIN</b> , S. WEISS, D.F. OGLETREE, M. SALMERON, D.S. CHEMLA, University of California, Berkeley.
9:40 am	<b>NS1-FrM5</b> Fabrication of 10nm Holes on a 20nm Hexagonal Lattice in Si(100). <b>T.A. WINNINGHAM</b> , S.D. WILLIAMS, K. DOUGLAS, University of Colorado, Boulder. <b>D. CHOUTOV</b> , J.D. PIPER, K.P. MARTIN, H.P. GILLIS, Georgia Institute of Technology.	<b>NS2-FrM5 INVITED</b> Continuous Observation of the Motion of Single Adsorbed Atoms and Molecules with Picosecond and Sub-nanometer Resolution. <b>G.M. MCCLELLAND</b> , F. WATANABE, H. HEINZELMANN, IBM Almaden Research Center.
10:00 am	<b>NS1-FrM6</b> New Compound Quantum Dot Materials Produced by Electron-Beam Induced Deposition. <b>M. WEBER</b> , Technische Hochschule Darmstadt, Germany. <b>H.W.P. KOOPS</b> , Deutsche Bundespost Telekom, Germany. <b>M. RUDOLPH</b> , J. KRETZ, Technische Hochschule Darmstadt, Germany. <b>G. SCHMIDT</b> , Universität Hamburg, Germany.	Invited talk continued.
10:20 am	<b>NS1-FrM7</b> Synthesis of Polymers at Highly Ordered Pyrolytic Graphite Templates via Flow Injection Scanning Tunneling Microscopy. <b>M.L. MYRICK</b> , P.G. VAN PATTEN, <b>J.D. NOLL</b> , University of South Carolina.	<b>NS2-FrM7</b> Magnetic Resonance Detection and Imaging using Force Microscope Techniques. <b>O. ZUEGER</b> , S. HOEN, C.S. YANNONI, D. RUGAR, IBM Almaden Research Center.
10:40 am	<b>NS1-FrM8</b> Nanoarchitectures of Poly(di-n-alkylsilylene)s. <b>S. SHEIKO</b> , H. FREY, M. MÖLLER, Universität Ulm, Germany.	<b>NS2-FrM8</b> Parallel Imaging with an Atomic Force Microscope. <b>S.C. MINNE</b> , PH. FLUECKIGER, H. SÖH, C.F. QUATE, Stanford University.
11:00 am	<b>NS1-FrM9 INVITED</b> Carbon Nanotubes. <b>S. IIJIMA</b> , NEC R&D Group, Japan.	<b>NS2-FrM9</b> Detection of Sub-Femtonewton Forces. <b>S. HOEN</b> , O. ZÜGER, C.S. YANNONI, H.J. MAMIN, K. WAGO, D. RUGAR, IBM Almaden Research Center.
11:20 am	Invited talk continued.	<b>NS2-FrM10</b> Atomic Force Microscope Tip Modification with Self-Assembled Monolayer Molecules. <b>T. HAN</b> , J. WILLIAMS, T.P. BEEBE, JR., University of Utah.
11:40 am	<b>NS1-FrM11</b> C <sub>60</sub> on Silicon: Self-Organization, Film Growth, and SiC Formation. <b>D. SARID</b> , D. CHEN, University of Arizona, Tucson.	<b>NS2-FrM11</b> Photon Channeling: A New Approach to Photoelectron Microscopy. <b>J.E. ROWE</b> , R.A. MALIC, E.E. CHABAN, N.V. SMITH, AT&T Bell Laboratories.



# Friday Morning, October 28, 1994

**APPLIED SURFACE SCIENCE**  
Room A101 - Session AS-FrM pg. 324

**Adhesion and Adhesive Bonding**  
Moderator: C.R. Anderson, Martin Marietta Laboratories.

**THIN FILM**  
Room A105 - Session TF-FrM pg. 326

**In Situ Thin Film Characterization**  
Moderator: C.R. Aita, University of Wisconsin, Milwaukee.

8:20 am	<b>AS-FrM1</b> Plasma Polymerized Primers for Adhesive Bonding of Aluminum. I. SEGALL, C.E. TAYLOR, F.J. BOERIO, W.J. VAN OOIJ, University of Cincinnati. R.A. DICKIE, D.J. ONDRUS, Ford Motor Company.	<b>TF-FrM1</b> In Situ Ellipsometric Monitoring and Post-Deposition Characterization of Dielectric Optical Multilayers. P. HE, S. PITTAL, B. JOHS, J.A. WOOLLAM, J.A. Woollam Co., Inc. J.H. KIM, CVI Laser Corp.
8:40 am	<b>AS-FrM2</b> Plasma Sprayed Coatings as Surface Treatments of Aluminum Adherends. G.D. DAVIS, D.K. SHAFFER, P.L. WHISNANT, G.B. GROFF, Martin Marietta Laboratories. J.D. VENABLES, Venable and Associates.	<b>TF-FrM2</b> Real Time Monitoring of the Deposition and Growth of Thin Organic Films by In Situ Ellipsometry. J.F. WALL, E. CLAUBERG, R.W. MURRAY, E.A. IRENE, University of North Carolina, Chapel Hill.
9:00 am	<b>AS-FrM3 INVITED</b> Characterization of the Interphase Formed on Adhesion of Polymers to Metal Oxides. J.P. WIGHTMAN, Virginia Tech.	<b>TF-FrM3 INVITED</b> Surface Analysis at Low to Ultra-High Vacuum by Ion Beam Recoil Spectroscopy. M.S. HAMMOND, SI Diamond Technology Inc. J.A. SCHULTZ, Ionwerks Inc.
9:20 am	Invited talk continued.	Invited talk continued.
9:40 am	<b>AS-FrM5</b> Practical Multi-Technique Analysis of Metal Surfaces for Adhesive Bonding Applications. A.P. DIWANJI, A.R. MADURA, R. MARTIN, LORD Corporation.	<b>TF-FrM5 INVITED</b> Deposition and Characterization of Transition-Metal Nitride Superlattices. S.A. BARNETT, Northwestern University.
10:00 am	<b>AS-FrM6</b> Strained Siloxane Rings in the Surface of Silica: Their Reaction with Organosiloxanes. A. GRABBE, T.A. MICHALSKE, W.L. SMITH, Sandia National Laboratories.	Invited talk continued.
10:20 am	<b>AS-FrM7</b> A New Probe of Plastic Deformation Accompanying Metal-Ceramic Interfacial Failure. J.T. DICKINSON, S. NAKAHARA, S.C. LANGFORD, L.C. JENSEN, Washington State University.	<b>TF-FrM7</b> Spectroscopic Ellipsometry of Thin Films on Transparent Substrates: A Formalism for Data Interpretation. Y.H. YANG, J.R. ABELSON, University of Illinois, Urbana.
10:40 am	<b>AS-FrM8</b> Improved Adhesion at the Copper/Polyimide Interface using an Organometallic Additive. D. COULMAN, The DuPont Company.	<b>TF-FrM8</b> Optical Emission Spectroscopy of Plasmas for Diamond Growth. R. MANUDONDA, R. DILLON, University of Nebraska.
11:00 am	<b>AS-FrM9</b> Observing Bond Orientation and Chemistry at the Buried Metal/Benzocyclobutene (BCB) Polymer Interface with Near Edge X-ray Absorption Fine Structure (NEXAFS). B.M. DEKOVEN, Dow Chemical Company. D.A. FISCHER, National Institute of Standards & Technology. S.J. BABINEC, J.J. CURPHY, Dow Chemical Company. J.L. GLAND, University of Michigan. G.E. MITCHELL, D.H. PARKER, C.A. WEDELSTAEDT, Dow Chemical Co.	<b>TF-FrM9</b> Optical Second Harmonic Generation (SHG) as an In Situ Technique to Monitor the Growth and to Analyse the Structure of Thin Films. M. BUCK, CH. DRESSLER, M. GRUNZE, Universität Heidelberg, Germany. F. TRÄGER, Universität Kassel, Germany.
11:20 am	<b>AS-FrM10</b> Adhesive Bonding between Self-Assembling Monolayer Films Measured by Interfacial Microscopy. R.C. THOMAS, University of New Mexico. R.M. CROOKS, University of New Mexico and Texas A&M University. T. KIM, Texas A&M University. J.E. HOUSTON, T.A. MICHALSKE, Sandia National Laboratories.	<b>TF-FrM10</b> Real Time Infrared Spectroscopy of Chemical Bonding during Thin Film Growth and Surface Modification: A Review of Techniques. M. KATIYAR, Y.H. YANG, J.R. ABELSON, University of Illinois, Urbana.
11:40 am	<b>AS-FrM11</b> Micromachining Induced Adhesion Enhancement between High Performance Polymer and Silicon Dioxide Substrate. H.-S. JEONG, Institute of Advanced Engineering, Korea. J. JIANG, Thomas Electronics, Inc.	<b>TF-FrM11</b> In Situ Analysis of Thin Film Deposition Processes using Time-of-Flight (TOF) Ion Beam Analysis Methods. Y. LIN, Argonne National Laboratory & Northwestern University. A.R. KRAUSS, Argonne National Laboratory. O. AUCIELLO, Microelectronics Center of North Carolina. D.M. GRUEN, Argonne National Laboratory. R.P.H. CHANG, Northwestern University.

**ELECTRONIC MATERIALS**

Room A108 - Session EM-FrM pg. 327

**Interface Characterization**

Moderator: S. A. Chambers, Pacific Northwest Laboratory.

**VACUUM METALLURGY**

Room A106 - Session VM-FrM pg. 329

**Surface Engineering for Wear and Corrosion Protection**

Moderator: C.R. Parent, The Gillette Company.

8:20 am	<b>EM-FrM1 INVITED</b> High Resolution X-ray Reflectivity Characterization of Interface Roughness and Correlation. <b>R.L. HEADRICK</b> , Cornell University.	<b>VM-FrM1</b> Friction and Wear of Gas Lubricated SiC/Mo Couples in Sliding Contact. <b>I.L. SINGER</b> , Naval Research Laboratory. <b>TH. LE MOGNE</b> , CH. DONNET, J.M. MARTIN, Ecole Centrale de Lyon, France.
8:40 am	Invited talk continued.	<b>VM-FrM2</b> Microstructural Effects on Tribological Properties of Electron Enhanced Magnetron Sputtered Coatings. <b>J.M. SCHNEIDER</b> , A.A. VOEVODIN, C. REBHOLZ, A. MATTHEWS, University of Hull, United Kingdom. D.B. LEWIS, Sheffield Hallam University, United Kingdom.
9:00 am	<b>EM-FrM3</b> Buffer Layer- Superlattice Interactions in the AlAs/GaAs Superlattice System. <b>J.G. PELLEGRINO</b> , National Institute of Standards & Technology. S.B. QADRI, Naval Research Laboratory. B. ROUGHANI, GMI Engineering and Management Institute. C.A. RICHTER, NRC Research Associate. D. CHANDLER-HOROWITZ, N.V. NGUYEN, P.M. AMIRTHARAJ, National Institute of Standards & Technology.	<b>VM-FrM3</b> Coatings Defects on Corrosion Behavior of Hard Nitride Coatings on Steel. Y.B. WANG, <b>M.S. WONG</b> , R. KRUEGER, W.D. SPROUL, T.J. BARLO, Northwestern University.
9:20 am	<b>EM-FrM4</b> Interfacial Properties of Metal-Insulator Semiconductor Capacitors on GaAs(110). <b>L.J. HUANG</b> , R. KRISHNAMURTHY, W.M. LAU, University of Western Ontario, Canada. S. INGLEY, Bell Northern Research, Canada. D. LANDHEER, J.-P. NOËL, National Research Council, Canada.	<b>VM-FrM4</b> Thermo-Mechanical and Chemical Properties of SiC-C Functionally Gradient Coatings on C/C Composites. <b>M.R. RICHARDS</b> , A.C. RICHARDS, M. TAYA, F.S. OHUCHI, University of Washington.
9:40 am	<b>EM-FrM5 INVITED</b> Growth Kinetics and Interface Chemistry: Site-specific Diffraction and Spectroscopy of Ultra-thin Insulators. <b>M.A. OLMSTEAD*</b> , U. HESSINGER, M. LESKOVAR, J. DENLINGER, E. ROTENBERG, University of Washington.	<b>VM-FrM5 INVITED</b> Plasma-based Surface Engineering Processes for Wear and Corrosion Protection. <b>A. MATTHEWS</b> , A. LEYLAND, B. DORN, P.R. STEVENSON, M. BIN-SUDIN, C. REBHOLZ, A. VOEVODIN, J. SCHNEIDER, University of Hull, United Kingdom.
10:00 am	Invited talk continued.	Invited talk continued.
10:20 am	<b>EM-FrM7</b> Modified Surface Charge Spectroscopy for the Characterization of Insulator-Semiconductor Structures. <b>W.M. LAU</b> , L.J. HUANG, University of Western Ontario, Canada. R.W.M. KWOK, G. JIN, Chinese University of Hong Kong.	<b>VM-FrM7</b> Vacuum Technology for Coating TiCN-Based Cermets. <b>I.Y. KONYASHIN</b> , Hardmetal Technologies, Russia.
10:40 am	<b>EM-FrM8</b> Buried Contaminant Structure Determination with Component-Resolved X-ray Photoelectron Diffraction in $\text{CaF}_2/\text{O}/\text{Si}(111)$ Heterostructures. <b>M. LESKOVAR</b> , U. HESSINGER, M.A. OLMSTEAD, University of Washington.	<b>VM-FrM8</b> Fluoroplastic Coating of Cold Drying - "TETRON". <b>V.J. DEMIN</b> , V.I. RAKHOVSKY, Research Center for Surface and Vacuum Investigation, Russia.
11:00 am	<b>EM-FrM9</b> A Study of Thermal Oxidation of Rough Silicon Surfaces. <b>Q. LIU</b> , L. SPANOS, E.A. IRENE, University of North Carolina, Chapel Hill.	
11:20 am	<b>EM-FrM10</b> Interfacial and Microstructural Study of Epitaxial Aluminum Nitride Films using Atomic Force Microscopy and Transmission Electron Microscopy. <b>T.D. LENANE</b> , F. AHMAD, G.W. AUNER, R. NAIK, Wayne State University.	
11:40 am		

# MY SCHEDULE

## Friday Morning, October 28, 1994

TIME	SESSION	ROOM
8:20 am		
8:40 am		
9:00 am		
9:20 am		
9:40 am		
10:00 am		
10:20 am		
10:40 am		
11:00 am		
11:20 am		
11:40 am		
12:00 pm		
12:45 pm		
Lunch		
when		
with		where

### OTHER EVENTS FRIDAY

- 7:00 a.m. Companions Program (see insert) (**Silver Room (H)**)  
 8:00 a.m. Surface Science Database Committee Meeting (**Denver Room (H)**)  
 12:00 Noon Foreign Interactions (**Gold Room (H)**)

H=Radisson Hotel  
 CC=Colorado Convention Center

### SHORT COURSES FRIDAY

- 8:30 a.m. Vacuum Technology (**Room C109 (CC)**)  
 8:30 a.m. A Comprehensive Course on Surface Analysis: AES,XPS,SIMS,  
 Depth Profiling, & ISS/RBS (**Room C107 (CC)**)  
 8:30 a.m. Hard Coatings by PVD Methods (**Room C103 (CC)**)  
 8:30 a.m. Gas Flow in Vacuum Systems (**Room C112 (CC)**)  
 8:30 a.m. Ion Scattering and Rutherford Backscattering Spectroscopies  
 (**Room C107 (CC)**)  
 8:30 a.m. Nucleation, Growth, and Microstructure Evolution (**Room C110 (CC)**)  
 8:30 a.m. Optical Diagnostic Techniques for Plasma Processing (**Room C104 (CC)**)  
 8:30 a.m. Pumping Hazardous Gases (**Room C105 (CC)**)  
 8:30 a.m. Rapid Thermal Processing: Equipment, Technology, and Process  
 (**Room C106 (CC)**)  
 8:30 a.m. Scanning Tunneling and Atomic Force Microscopy (**Room C108 (CC)**)  
 8:30 a.m. Throughput Pump Technology: Mechanical,Turbomolecular,  
 and Diffusion Pumps (New) (**Room C102 (CC)**)  
 8:30 a.m. UHV Design and Practices (**Room C101 (CC)**)

### Special or Focus Area Sessions

- Sensors, In-situ Diagnostics, Process Control**  
 TF-FrM In-situ Thin Film Characterization  
**Nanostructure Fabrication and Atomic-Scale Manipulation**  
 NS1-FrM Novel Materials and Methods for Nanofabrication

# AVS SHORT COURSE GENERAL INFORMATION

## Location

Colorado Convention Center  
700 14th Street  
Denver, CO 80202  
303/640-8000

The short courses, symposium technical sessions, and equipment exhibit will take place at the Colorado Convention Center.

## Schedule

All courses will begin at 8:30 a.m. and finish at 5:00 p.m. with a hour break for lunch. Lunch is not included.

## Certificates

Certificates of completion will be given to all students attending the full course.

## Textbook and Course Notes

The fee for most courses includes a set of class notes. With

many of the short courses offered, the fee for the course includes the cost of a published, hardcover textbook. Plain notebooks are not provided.

## Registration Locations and Hours

All short courses will take place at the Colorado Convention Center. All pre-registered students must check in at the Short Course Registration desk located in ??? to collect their course materials and badges.

Registration hours are as follows:

Sun, October 23	4:00 p.m. to 7:00 p.m.
Mon, October 24	7:00 a.m. to 5:00 p.m.
Tues, October 25–Thurs, October 27	7:30 a.m. to 5:00 p.m.
Fri, October 28	7:30 a.m. to 12:00 noon

## Further Information

For further information contact:  
Margaret Stringer, AVS, 120 Wall Street, 32nd Floor, New York, NY 10005; 212/248-0326.

## SURFACE SCIENCE

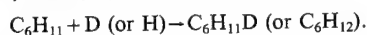
Room A205 - Session SS1-MoM

### Reactions on Metals: Hydrocarbons

Moderator: D. Dwyer, University of Maine.

8:20 am SS1-MoM1 Effects of Co-adsorbed Hydrogen on the Dehydrogenation of Cyclohexane on Pt(111). Identification of a Cyclohexyl ( $C_6H_{11}$ ) Species, M. E. Pansoy-Hjelvik, P. Schnabel and John C. Hemminger, Department of Chemistry and Institute for Surface and Interface Science, University of California, Irvine, CA 92717.

Effects of co-adsorbed hydrogen on the dehydrogenation of cyclohexane on Pt(111) have been studied using Thermal Desorption Spectroscopy (TDS), Laser Induced Thermal Desorption-Fourier Transform Mass Spectrometry (LITD-FTMS), and Auger Electron Spectroscopy (AES). The co-adsorption experiments have been performed by first adsorbing 0.25 ML cyclohexane and then saturating the Pt surface at 150 K with hydrogen. Without co-adsorption of hydrogen the onset for desorption and dehydrogenation occurs at about 195 K. With hydrogen coadsorbed the onset for desorption and dehydrogenation occurs also simultaneously, but is shifted to 165 K. The branching ratio between dehydrogenation and desorption is 4:1 without co-adsorbed hydrogen and 2:1 when hydrogen is co-adsorbed. Evidently, the co-adsorption of hydrogen decreases the temperature at which the dehydrogenation and desorption of cyclohexane commences and it enhances desorption. The TD spectra of cyclohexane with co-adsorbed hydrogen show two desorption maxima one at 195 K and another at 240 K. Deuterium co-adsorption experiments reveal that the high temperature desorption signal is a result of the rehydrogenation of a cyclohexyl ( $C_6H_{11}$ ) surface species:



Since the high temperature desorption maximum occurs at 255 K when deuterium is co-adsorbed it is obvious that this recombination reaction exhibits an isotope effect.

8:40 am SS1-MoM2 Oxygen Activated Combustion of Alkenes on Pd(100), X.-C. Guo and R. J. Madix, Department of Chemical Engineering, Stanford University, Stanford, CA 94305-5025.

Palladium has recently gained much attention in automotive catalysis as a possible substitute for Rh and Pt because of its lower cost. However, little fundamental work has been done towards understanding the process of hydrogen combustion on Pd surfaces. In this work, we investigate alkene combustion on Pd(100) under UHV conditions using temperature programmed reaction spectroscopy, combined with isotopic labeling and isotope coadsorption methods. The alkenes studied are ethylene, propene, 1-butene, and 1,3-butadiene. Alkene adsorption and reaction have been studied on both clean Pd(100) and atomic oxygen covered Pd(100)-p(2×2)-O surfaces. On the clean surface, all alkenes dehydrogenate through a series of intermediates in a temperature range from 200 to 900 K. No self-hydrogenation occurs for monoenes although multiple H-D exchange is facile. Butadiene can self-hydrogenate to butene. On Pd(100)-p(2×2)-O, while atomic oxygen inhibits ethylene dehydrogenation, the hydrogenation of higher alkenes is activated, yielding  $H_2O$  and  $CO_2$  below the dehydrogenation temperature on clean Pd(100). The total dehydrogenation yields for higher alkenes are similar (~0.10 alkene/Pd) to that on the clean surface. At low alkene coverages, the whole molecule is dehydrogenated below 450 K forming  $H_2O$ ;  $CO_2$  evolves in two states at 350 and 530 K. At high alkene coverages,  $CO$  evolution occurs at 450 and 600 K. The high temperature  $CO$  and  $CO_2$  evolutions are from  $C(a) + O(a)$  reactions. The low temperature  $CO_2$  production below 400 K resembles that from  $CO(a) + O(a)$ . Together with desorption-limited  $CO$  evolution at 450 K, this indicates that the C—O bond is formed before dehydrogenation is completed. A direct O(a)-alkene(a) reaction mechanism is thus identified, distinct from indirect scavenging reactions: dehydrogenation on clean sites and subsequent oxidation of H(a) and C(a).

9:00 am SS1-MoM3 Surface Chemistry at Metallic Step Defect Sites\*, John T. Yates, Jr., Surface Science Center, Department of Chemistry, University of Pittsburgh, Pittsburgh, PA 15260.

The role of defect sites on metals in catalysis and surface chemistry has been of interest since the historical postulate of the active site by

H. S. Taylor in 1925. Modern surface spectroscopic and structural methods have addressed this problem in more recent times. In this talk, a model chemical reaction, the formation of  $CO_2$  from  $CO$  and oxygen on stepped Pt single crystal surfaces, will be described, identifying the most active site on two related Pt single crystal surfaces. In addition, step defect sites have been used for trapping mobile molecules to observe and characterize a new surface phenomenon, electron stimulated migration, ESM.

INVITED

\*Work supported by The Office of Basic Energy Sciences (DOE), and The Air Force Office of Scientific Research (AFOSR).

9:40 am SS1-MoM5 Kinetics Of Benzene Formation From Acetylene On Pd(111), I. M. Abdelrehim, N. A. Thornburg, C. M. Gerth, E. Delgado, T. E. Caldwell, J. T. Sloan, and D. P. Land, Department of Chemistry, UC Davis, Davis, CA 95616.

Laser-induced thermal desorption with post-ionization and FT mass spectrometry (LITD/FTMS) is utilized to study the cyclotrimerization of acetylene to benzene on Pd(111). A Nd:YAG laser (1064 nm, 5 ns,  $\sim 10^7$ – $10^8$  W/cm<sup>2</sup>) is used to desorb neutrals without substrate ablation. A 70 eV electron beam post-ionizes the neutrals and FTMS is used for detection of the ionized species. LITD/FTMS yields the desorption of intact products and intermediates.

Heating acetylene on Pd(111) causes cyclotrimerization to benzene even at 1L exposures. In addition, 6L exposures of acetylene with submonolayer coverages of sulfur (.06 ML) produce low temperature (200 K) formation of thiophene, as well as benzene.<sup>1</sup> These desorbates form in similar quantities on the surface, but thiophene preferentially decomposes during slow heating and very little is observed in TDS.

Kinetic studies of benzene formation from acetylene (2.5 L) on clean Pd(111) were initiated resulting from our preliminary TDS and laser desorption surveys. Isothermal rate investigations were conducted at temperatures ranging from 170 K–205 K. The results indicate that benzene formation has an activation energy of  $10 \pm 1$  kcal/mol and a preexponential factor of  $7 \times 10^9$  s<sup>-1</sup>. The effects of sulfur on the rates and selectivity of benzene and thiophene formation will also be reported.

<sup>1</sup>I. M. Abdelrehim, N. A. Thornburg, J. T. Sloan, and D. P. Land, *Surf. Sci. Lett.*, **298**, L169 (1993).

10:00 am SS1-MoM6 Acetylene Di- and Trimerization Reactions at Pt(111) and the ( $\sqrt{3} \times \sqrt{3}$ )R30°-Sn/Pt(111) Surface Alloy, Janos Szanyi and M. T. Paffett, CST-1, Los Alamos National Laboratory, Los Alamos, NM 87545.

The di- and trimerization reactions of acetylene were studied over Pt(111) and ( $\sqrt{3} \times \sqrt{3}$ )R30°-Sn/Pt(111) model catalysts at moderate pressures (20–100 Torr). The overall catalytic activity of ( $\sqrt{3} \times \sqrt{3}$ )R30°-Sn/Pt(111) surface alloy was ~4–5 times higher than that of Pt(111). Both surfaces produced  $C_4$  and chain and cyclic  $C_6$  hydrocarbons as di- and trimerization products with  $C_4$  production rates being about an order of magnitude higher than that for  $C_6$  hydrocarbons. For both the  $C_4$  and  $C_6$  product groups the degree of unsaturation of the hydrocarbon molecules depended upon the experimental conditions applied ( $P_{H_2}/P_{C_2H_2}$ ; T). The formation of carbonaceous surface residues were seen under all experimental conditions but did not eliminate the di- and trimerization of acetylene even at high coverages. The very good correlation found between the formation rates of butadiene and cyclic  $C_6$  hydrocarbons suggests that the formation of ring  $C_6$  products proceeds through a metallocyclopentadiene intermediate. These observations will be further discussed in the context of additional UHV characterization studies (C. Xu, J. Peck, and B. E. Koel, *J. Am. Chem. Soc.*, **1993**, 115, 751).

10:20 am SS1-MoM7 The Surface Chemistry of 1,1-dimethylhydrazine on Pt and Ag-Modified Pt, A. L. Schwane, M. Kovar, Diann J. Almeras, and J. M. White, Department of Chemistry and Biochemistry, University of Texas at Austin, Austin, TX 78712.

Alkylhydrazines are potential precursors for surface nitridation, and are more stable than hydrazine. In addition, C–N surface bonds, which are used in catalysis to improve selectivity in hydrogenation reactions, can be formed. To further our understanding of alkylhydrazine surface chemistry, the thermal decomposition of 1,1-dimethylhydrazine (DMH),  $(CH_3)_2N-NH_2$ , at 100 K on Pt and Ag-modified Pt surfaces

has been studied by temperature programmed desorption, temperature programmed static secondary ion mass spectrometry, high resolution electron energy loss spectroscopy, X-ray and ultraviolet photoelectron spectroscopy. Our interests centered on the thermal decomposition pathway and dehydrogenation of DMH, and how the dehydrogenation properties of Pt are influenced by increasing Ag coverage (0.5–14 ML). On clean Pt, DMH adsorbs molecularly at coverages >1 ML, and dissociatively at <1 ML. Thermal N-N bond cleavage occurs at 300 K creating two surface fragments,  $\text{-NH}_2$  and  $(\text{CH}_3)_2\text{N-}$ . Each fragment has its own independent decomposition pathway. Interestingly, hydrogen (320 K), ammonia (340 K) and nitrogen (855 K) desorb via thermal decomposition of  $\text{-NH}_2$ , while decomposition of  $(\text{CH}_3)_2\text{N-}$  yields hydrogen (430 K), cyanide (610 K), cyanogen (780 K) desorption products and surface carbon (>1000 K). On thickly Ag-covered Pt surfaces (~14 ML), only parent desorption was observed. At Ag coverages <1 ML, similar products to those observed desorbing from Pt were detected. However, the desorption temperatures were higher on Ag/Pt than clean Pt; thus, we believe that Ag lowers the reactivity of Pt. The chemistry associated with the decomposition of DMH on Pt and Ag-modified Pt will be described, and our results compared with thermal decomposition of other alkylated amines and hydrazines. Supported by the U.S. Department of Energy, Office of Basic Sciences.

10:40 am **SS1-MoM8 Adsorption and Aggregation of HCN on Pt(111)**, *D. Jentz, H. Celio, and M. Trenary*, Department of Chemistry, M/C (111), University of Illinois at Chicago, 845 W. Taylor St., Room 4500, Chicago, IL 60607-7061.

We have investigated the adsorption of HCN on Pt(111) at 85 K, 200 K and 300 K from low to high exposures by Fourier transform infrared reflection absorption spectroscopy (FT-IRAS) and thermal desorption spectroscopy (TDS). Based on the IR spectra we conclude that at 85 K HCN weakly adsorbs onto the surface at low exposures since the spectra resemble that reported for HCN in an Argon matrix isolation study [1]. At higher exposures (>1 L) aggregation occurs which is determined by the formation of hydrogen bonded species on the surface which leads to a shifting of  $\nu_{\text{CH}}$  to lower frequencies and a broadening of this band. These multimers continue to form until at 20 L the IR spectrum resembles that for solid HCN which is composed of long chains of hydrogen bonded linear HCN. Upon annealing to 300 K, HCN irreversibly rehybridizes and forms a bent di- $\sigma$  bonded species with the C=N bond parallel to the surface. This is determined by the appearance of an intense band at  $\sim 1570 \text{ cm}^{-1}$  characteristic of a C=N double bond. At high exposures at 300 K, hydrogen isocyanide monomer and HCN multimers form and exist on the surface simultaneously with the HCN monomer. At all temperatures, strong adsorbate-adsorbate interactions occur which lead to aggregation; however, above 200 K the metal surface mediates these interactions by strongly interacting with the adsorbate leading to irreversible rehybridization of the HCN monomer.

I. J. Pecansky and G. V. Calder, *J. Mol. Structure* **14** (1972) 363.

11:00 am **SS1-MoM9 The Chemistry of Phthalic Anhydride at a Clean and Oxygen Covered Copper Single Crystal Surface**, *S. Haq, R. C. Bainbridge and N. V. Richardson*, Surface Science Research Centre, University of Liverpool, Liverpool L69 3BX, UK.

As part of a programme of research aimed at controlled, oligimide, thin film growth at metal surfaces, initiated by chemisorption of an appropriate dianhydride, we have studied the chemisorption behaviour of the model aromatic anhydride, phthalic anhydride over a range of temperatures (100–600 K), as a function of coverage on both clean Cu{110} and  $\text{p}(2 \times 1)\text{-O/Cu}\{110\}$  surfaces. Experiments have been carried out in UHV with background dosing of the phthalic anhydride; a volatile solid. Thermal desorption mass spectroscopy allied to Fourier Transform reflection absorption Infra-red (FT-IR) spectroscopy has been used to characterise the evolution of the surface chemistry. FT-IR reveals a number of distinct species with well-defined surface orientations. On the clean surface at low temperature, bands characteristic of the parent molecule are observed. With increasing temperature, the anhydride ring opens to permit a carboxylate link to the copper surface, indicated by a band at  $\sim 1400 \text{ cm}^{-1}$ . Major re-orientation of the aromatic ring is a consequence. The lower temperature dominance of the in-phase, out-of-plane C-H bending mode ( $720 \text{ cm}^{-1}$ ) is lost. At 270 K, CO is lost from the molecule into the gas-phase and a species ( $\text{C}_6\text{H}_4\text{CO}_2$ ) closely related to benzoate is the result. Thermal decomposition of this species occurs at 550 K. In contrast, adsorption on the  $\text{p}(2 \times 1)\text{-O/Cu}\{110\}$  surface inhibits the loss of CO and oxidative

conversion to a di-carboxylate species occurs instead. This species is stable to 550 K when explosive decomposition and desorption takes place.

11:20 am **SS1-MoM10 Cu(100) as a Model for the Methanol Catalyst**, *J. Chorkendorff, J. Wambach, Mayumi Kazuta and Peter B. Rasmussen*, Physics Department, Technical University of Denmark, DK-2800 Lyngby, Denmark.

Industrially methanol is synthesized from a mixture of CO, CO<sub>2</sub>, and H<sub>2</sub> over a catalyst containing Cu/ZnO/Al<sub>2</sub>O<sub>3</sub>. The active phase and the structure of the catalyst has been a subject of controversy and so is the reaction mechanism. In order to address some of these questions we have investigated the synthesis rate of methanol on a Cu(100) single crystal from a mixture of CO<sub>2</sub> and H<sub>2</sub>. All experiments were performed in a high pressure cell build into an UHV apparatus equipped with surface sensitive methods so that the crystal could be characterized prior to, and after the experiments. It was found that methanol could indeed be synthesized from this gas mixture (CO<sub>2</sub>:H<sub>2</sub>=1:1) at a total pressure of 2 bar and the turnover frequency was found to be  $2.7 \times 10^{-4} (\text{site} \cdot \text{sec})^{-1}$  at 543 K with an activation energy of 69 kJ/mol. Furthermore was the synthesis rate investigated both as a function of total pressure and as a function of gas composition. The influence of CO has also been investigated. A micro kinetic model based on the above results was constructed and good agreement with measurements on a real methanol catalyst was obtained.

11:40 am **SS1-MoM11 Simulation and Sensitivity Analysis of the Heterogeneous Oxidation of Methane on a Platinum Foil**, *F. Behrendt, O. Deutschmann, and J. Warnatz*, Universität Stuttgart, Institut für Technische Verbrennung, Pfaffenwaldring 12, D-70569 Stuttgart, Germany.

Catalytic combustion of methane has potentially practical applications like improved flame stability, generation of low-temperature process heat, and reduced pollutant emissions. Quantitative simulations will play an important role in accelerating the development in this field. Methane is the major constituent of natural gas, and reactions of the methyl radical are among the rate limiting steps in the gas phase combustion of larger hydrocarbons. Thus, understanding of heterogeneous ignition and extinction of methane and the role of intermediate radicals at the surface is crucial to use heterogeneous combustion processes efficiently and safely.

Earlier treatments of the catalytic methane oxidation often used simplified global surface chemistry. However, heterogeneous combustion processes are determined by interaction of diffusion processes from and to the gas phase, of adsorption and desorption, and of surface reactions. Depending on the conditions, each of these processes can be rate-limiting thus leading to a completely different behaviour of the global surface reaction.

Here, the heterogeneous oxidation of methane-air mixtures in a stagnation point flow onto a platinum foil is investigated numerically and results are compared with experiments. The analysis includes detailed reaction mechanisms for the gas phase as well as the surface. Gas phase transport and its coupling to the surface is described using detailed multi-component models. The heterogeneous ignition, extinction, and autothermal behaviour are interpreted in terms of elementary steps at the gas-surface interface.

A sensitivity analysis of the surface reactions is performed to identify crucial steps in the mechanism, thus pointing to those reactions for which better kinetic and thermodynamic data are needed urgently.

## SURFACE SCIENCE

### Room A201 – Session SS2-MoM

#### Alloy and Compound Surface Structure

**Moderator:** B. E. Koel, University of Southern California

8:20 am **SS2-MoM1 Surface Structure Investigation with Scanning Tunneling Microscopy (STM) and Low Energy Ion Backscattering**, *Horst Niehus*, Humboldt-Universität zu Berlin, Institut für Physik, Oberflächenphysik und Atomstoßprozesse, Invalidenstr. 110, D10115 Berlin, Germany.

Ultra high resolution microscopy STM in combination with a highly surface structure sensitive probe as 180° low energy ion scattering and detection of neutrals (NICISS) gives a powerful probe for surface



structure investigations. The determination of structure parameters of metal, metal alloy and semiconductor surfaces can be made element specific and well resolved for the first few surface layers with NICISS. The obtained lateral averaged surface data have been used for a proposal of a structure model, which in turn can be verified and complemented by atomically resolved microscopy for measuring unit cell parameters, and additionally with no need of atomic resolution to show morphological features as growth mechanisms, step or other defect distributions. The usefulness of the combination of methods will be demonstrated at metal and metal alloy surfaces, i.e. at  $\text{Cu}_3\text{Au}$ . After prolonged annealing of  $\text{Cu}_3\text{Au}(110)$ , a LEED ( $4 \times 1$ ) superstructure appears at room temperature. The ( $4 \times 1$ ) also shows up in the STM images. From the NICISS investigation the gold rich termination has been found. Upon oxygen exposure at 330K and subsequent annealing at 800K a segregation of Cu atoms to the surface occurs. In case of nitrogen at  $\text{Cu}_3\text{Au}(110)$ , the STM images indicate the same chain like structure elements as at  $\text{Cu}(110)-(2 \times 3)\text{-N}$  surfaces. Structure models based on NICISS and STM measurements will be discussed.

INVITED

9:00 am **SS2-MoM3 Anharmonicity on the NiAl(110) Bimetallic Alloy Surface**, *Arthur P. Baddorf*, Oak Ridge National Laboratory,<sup>†</sup> Oak Ridge, TN 37831-6024, and *Aubrey T. Hanbicki*, Univ. of Pennsylvania, Philadelphia, PA.

Anharmonicity of an alloy surface has been directly measured for the first time by examining the temperature dependence of the energy and lifetime of a surface phonon on NiAl(110). This surface consists of an ordered array of Ni and Al atoms, is rippled with the Ni contracted and the Al expanded, and exhibits an optical phonon at the zone center whose energy lies in the bulk band gap. High-resolution electron energy loss spectroscopy was employed to determine the energy and linewidth (lifetime) of the optical phonon between 40 and 960 K. Over this range, the phonon energy decreases from 27.6 to 25.1 meV, following a functional form which is a signature for anharmonicity: little change at low T, and linear dependence at high T. The rate of decrease observed is 2/3 that found at the zone center on Cu(110). Since the two materials have a similar bulk thermal expansion, the enhancement of anharmonicity by the surface appears to be smaller on NiAl(110). Based on this comparison, the NiAl(110) surface appears to be about 50% more anharmonic than bulk NiAl.

<sup>†</sup>Operated by Martin Marietta Energy Systems, Inc., under US DOE contract No. DE-AC05-84OR21400.

9:20 am **SS2-MoM4 The Geometrical Structure of an Al(111)-(2 × 2)-Na Surface Alloy**, *M. M. Nielsen, J. Burchhardt, D. L. Adams, E. Lundgren\*, J. N. Andersen\*, C. Stampfl\*\*, M. Scheffler\*\*, A. Schmalz\*\*, and J. Haase\*\**, Institute of Physics, Aarhus University, DK-8000 Aarhus C, Denmark, \*Institute of Physics, Lund University, S-22362 Lund, Sweden, and \*\*Fritz Haber Institute, D-14195 Berlin, Germany.

Recent experimental and theoretical studies of the  $(\sqrt{3} \times \sqrt{3})\text{R}30^\circ$  structures formed by adsorption of Na, K, and Rb on Al(111) at room temperature have surprisingly revealed that for each system the alkali atoms adsorb in substitutional sites formed by disrupting the outermost substrate layer<sup>1</sup>. No such consistent picture has yet emerged for the even more complicated structures which form at coverages other than 1/3 monolayer. We report here on a LEED determination of the geometry of the  $(2 \times 2)$  structure formed by adsorption of 1/2 monolayer Na. The LEED results are shown to be in very good agreement with the results of ab initio calculations, with SEXAFS results, and with previous core level photoemission measurements<sup>2</sup>. The structure, which can best be described as a surface alloy, contains two  $(2 \times 2)$  Na layers interspersed by a  $(2 \times 2)$  Al layer. Na atoms in the lower Na layer are adsorbed in substitutional sites on the first, reconstructed layer of the substrate.

<sup>1</sup>M. M. Nielsen *et al.*, Phys. Rev. Lett., **72**, (1994), and references therein.

<sup>2</sup>J. N. Andersen *et al.*, Phys. Rev. Lett., **68**, 94 (1992).

9:40 am **SS2-MoM5 Structure of NiO(111) Films on a Ni(100) Substrate**, *O. L. Warren and P. A. Thiel*, Department of Chemistry and Ames Laboratory, Iowa State University, Ames, IA 50011 USA.

NiO can be grown in the (111) epitaxy on metallic Ni substrates. We have performed a full dynamical LEED structure analysis of such a film on Ni(100). The film is sufficiently thick and contiguous that metallic Ni is not probed by the electron beam. The oxide is oxygen-

terminated with oxygen in fcc sites, and with a 15% contraction in the first interlayer spacing (relative to the bulk spacing). Deeper layers retain cubic symmetry while compressing to align uniaxially with the metallic substrate. Comparison with other work suggests that oxygen termination, strong contraction in the first interlayer spacing, and retention of cubic symmetry in deeper layers may be general features of metal oxide, rocksalt films with unreconstructed, (111) surface orientations.

10:00 am **SS2-MoM6 Detailed Surface Structures of Ultrathin Films of Ice ( $\text{H}_2\text{O}$ ) and Rust ( $\text{Fe}_3\text{O}_4$ ) Grown on Pt(111), Determined by Automated Tensor LEED**, *M. A. Van Hove, A. B. Barbieri, N. Materer, U. Starke, W. Weiss, M. Ritter and G. A. Somorjai*, Lawrence Berkeley Laboratory, University of California, Berkeley, CA 94720, USA.

Ice was grown at 90 K by deposition of water vapor on Pt(111), until the Pt(111) LEED pattern could no longer be seen. Annealing to 140 K produced a moderately sharp LEED pattern, corresponding to a  $(1 \times 1)$  termination of the oriented hexagonal (1h) or cubic (1c) bulk phases of ice. Fitting of LEED IV curves with automated tensor LEED favors the (0001) face of the hexagonal form (most common in nature) with minimal relaxations from the bulk structure and undetectable hydrogen atoms. The data are most satisfactorily explained by a full-bilayer termination in which the outermost half-bilayer of  $\text{H}_2\text{O}$  molecules vibrates so strongly at 90 K as to become invisible to LEED.

Iron oxide was grown on Pt(111) by successive cycles of monolayer iron deposition and oxidation, until the Pt(111) LEED pattern could no longer be seen. The resulting moderately sharp LEED pattern corresponds to an unreconstructed (111) termination of bulk  $\text{Fe}_3\text{O}_4$ . With automated tensor LEED, 6 possible bulk terminations and many other models were tested. The favored structure has a bulk termination with an exposed "1/4" monolayer of Fe atoms on a dense monolayer of O atoms. Strong relaxations of atomic positions perpendicular to the surface are found, up to about 0.5 Å from bulk positions: these are likely related to strong local elastostatic fields.

10:20 am **SS2-MoM7 Structural Studies of Quasicrystals**, *W.-B. Chin, C. J. Jenks, S.-L. Chang, C.-M. Zhang, and P. A. Thiel*, Department of Chemistry and Ames Laboratory, Iowa State University, Ames, IA 50011.

Quasicrystals are materials with long range aperiodic order and crystallographically forbidden rotational symmetries. Quasicrystals show great promise for use as protective coatings because of their hardness, low coefficient of friction, resistance to oxidation, and more environmentally friendly manner with which they can coat metals compared to standard chromium coatings. Although many studies have been conducted on the bulk properties of quasicrystals, little has been done to determine the surface properties of quasicrystals. We have investigated the surface properties of the five-fold surface of a "single crystal" of  $\text{Al}_{70}\text{Pd}_{21.5}\text{Mn}_{8.5}$  in the presence of adsorbates using low energy electron diffraction and thermal desorption spectroscopy. Our results show that oxygen affects the quasicrystal's surface structure while hydrogen does not. Implications for the resistance of quasicrystals to oxidation will be discussed.

10:40 am **SS2-MoM8 A New Type of UHV-AFM: Studies on  $\text{KMnF}_3$  Surfaces**, *Q. Dai, R. Vollmer, R. Carpick, D. F. Ogtree, M. Salmeron*, Material Science Division, Lawrence Berkeley Laboratory.

For the first time, an Ultra High Vacuum Atomic Force Microscope (AFM) which operates at variable temperatures (100K–500K) has been developed. The instrument has been used in the study of  $\text{KMnF}_3$  surfaces cleaved under UHV condition. It has been found that after cleavage, two different types of terminations, KF and  $\text{MnF}_2$ , coexist on the surface. One type of termination forms large domains ( $\geq 1000\text{Å}$ ), while the other appears as small islands, about 200 Å across. AFM images with atomic resolution taken on both of these two terminations show no lattice constant nor lattice orientation changes. It is hence proposed that on KF surface, because the ionic radius of  $\text{K}^+$  and  $\text{F}^-$  are very close, they are both imaged by the AFM tip, while on  $\text{MnF}_2$  surface, since  $\text{Mn}^{2+}$  is much smaller than  $\text{F}^-$ , only  $\text{F}^-$  is imaged. Friction images taken on both of these terminations indicate that friction force is different for the two surfaces with different chemical compositions.

11:00 am **SS2-MoM9 Structure Determination of the  $\text{InP}(001)$  Surface**, *M. M. Sung, H. Bu, and J. W. Rabalais*, Department of Chemistry, University of Houston, Houston, TX 77204-5641.



InP is an important substrate for growing lattice matched epitaxial films of alloy semiconductors, such as GaInAsP, for electronic and photonic devices. The polar {001} face is the important surface for device fabrication, yet no atomic structure model has been determined for this crystal. A qualitative missing row dimer structure, based on that proposed for GaAs{001}, has been discussed previously for this  $(4 \times 2)$  surface. As part of a project to study metal/InP {001} interfaces using time-of-flight scattering and recoiling spectrometry (TOF-SARS), we have investigated the various reconstructions of InP{001}, such as  $(1 \times 1)$ ,  $(4 \times 1)$ ,  $(4 \times 2)$ , and  $c(8 \times 2)$ . Analysis of the results leads to the surprising conclusion that the structure of the {001}— $(4 \times 2)$  reconstructed surface is different from the previously proposed model. The  $(1 \times 1)$  surface could not be considered an intrinsic structure of clean InP as the TOF spectra contained H, C, and O impurity peaks. No peaks such impurities were observed on the sharp  $(4 \times 2)$  surface, confirming the surface cleanliness. The proposed structure for this surface is an autocompensated **In missing-row-trimer P dimer model (MRTD)** in which every fourth In row is missing and the first-layer In atoms form trimers along the [011] azimuth with intratrimer spacing of  $3.65 \pm 0.1 \text{ \AA}$ . The exposed 2nd-layer P atoms are dimerized along [011] with an intradimer spacing of  $2.95 \pm 0.1 \text{ \AA}$ . The  $(8 \times 2)$  structure observed at higher temperature can be formed by phase shifted domains between such  $(4 \times 2)$  units. This model is quite different from that discussed earlier based on the GaAs structure.

11:20 am **SS2-MoM10 Surface Relaxation of PbTe(100)**, C. B. Duke, A. Lazarides, A. Paton, Xerox Webster Research Center, Webster, NY 14580; A. Kahn, Princeton University, Princeton, NJ.

An analysis of surface core level shifts [G. Allen, Phys. Rev. B 43 (1990), 9594] from rock salt structure PbTe(100) suggests large contractions of the top layer of this material, in contradiction to expectations from other binary cubic semiconductors like MgO. To test this hypothesis we have performed a structure analysis on PbTe(100) using eight beams of diffracted low energy electrons ( $50 \text{ eV} < E < 250 \text{ eV}$ ) from PbTe(100) at 100K. An intensity analysis, based on relativistic potentials shown to be accurate for other fifth row elements in addition to Pb, leads to the conclusion that the Pb sublattice in the top layer is contracted by  $0.24 \text{ \AA}$  (7%), whereas the Te species in the top layer is unrelaxed. A search for second layer relaxations did not improve the description of the measured intensities. An error analysis, performed using a new procedure yielding statistically significant errors, suggests a 95% confidence in this structure to within  $\pm 0.08 \text{ \AA}$  for both layers. Thus, our analysis gives results analogous to those found for the (100) surfaces of other cubic materials rather than the large uniform top-layer contraction suggested by the analysis of the core-level shifts.

11:40 am **SS2-MoM11 Structure of the Ga-rich GaAs(001)  $4 \times 2$  and  $4 \times 6$  Phases**, Q. K. Xue, T. Hashizume, J. Zhou, T. Sakata\* and T. Sakurai, Institute for Materials Research (IMR), Tohoku University, Sendai 980-77, Japan.

Among a wide variety of reconstructions being realized using molecular-beam epitaxy (MBE), the Ga-rich GaAs(001) surfaces has not been systematically studied, while the As-rich  $2 \times 4$  reconstruction is extensively studied. By taking advantage of the migration enhanced epitaxy (MEE) technique, we have investigated the  $4 \times 2$  and  $4 \times 6$  phases using a high-performance MBE-STM instrument, which is a combination of a MBE and the FI-STM (field-ion scanning tunneling microscope).

We have found that the  $4 \times 2$  structure is so-called "a bilayer model" with the unit structure of two Ga dimers and another Ga dimer in the third layer. In the high resolution STM images of the filled states, the Ga dimers in the first layer are observed as the bifurcated dim protrusions, while the dangling bond-derived filled states of the second layer As appears bright, much brighter than the first layer Ga dimers. By changing the As<sub>4</sub>/Ga flux ratio in MEE growth or post annealing temperature, we have shown that the  $4 \times 6$  phase is more Ga-rich than the  $4 \times 2$  phase, which has been reported otherwise in some of the previous publications. In the case of the  $4 \times 6$  filled states images, we observe the Ga dimers brighter than the As dangling bond-derived feature, which is explained by a charge transfer from the extra Ga atoms to the empty band localized at the dangling bond of the Ga dimers.

\*Permanent address: Faculty of General Science, Osaka Prefecture University, Sakai 591, Japan.

## NANO 3/NANOMETER-SCALE SCIENCE AND TECHNOLOGY

Room BR1 – Session NS1-MoM

### NANO 3 Plenary Session

Moderator: C. R. K. Marrian, Naval Research Laboratory

9:00 am **NS1-MoM3 Molecular Recognition of Volatile Compounds (VOC's) with Self-Assembled Monolayers of Supramolecular Compounds**, Wolfgang Göpel<sup>1</sup>, Klaus Dieter Schierbaum<sup>1</sup>, Tilo Weiss<sup>1</sup>, and David N. Reinhoudt<sup>2</sup>, <sup>1</sup>Institute of Physical and Theoretical Chemistry, University of Tübingen, Auf der Morgenstelle 8, D-72076 Tübingen (FRG), <sup>2</sup>Department of Organic Chemistry, MESA Research Institute, PO Box 217, 7500 AE Enschede (Netherlands).

Monolayers of resorcin[4]arenes on clean Au surfaces have been prepared by self-assembly through thiol bonds in ethanol/chloroform solutions. Angle-resolved photoelectron spectra give evidence that the monolayers are well-ordered and that resorcin[4]arene macrocycles determine the outermost surface. Their interaction with organic molecules like C<sub>2</sub>Cl<sub>4</sub> was studied with quartz microbalance oscillators. It leads to a fast and reversible mass increase. The latter results from an incorporation of C<sub>2</sub>Cl<sub>4</sub> within the molecular "cavities" formed by the resorcin[4]arenes. Comparative thermal desorption spectra indicate binding sites with high interaction energies of C<sub>2</sub>Cl<sub>4</sub> molecules. These monolayers serve as a model supramolecular compound for SXM studies which provide well-defined surface recognition structures for organic molecules.

10:00 am **NS1-MoM6 Recent Progress on Magnetic Sensors with Nanostructures and Applications**, Yoshinobu Sugiyama, Electrotechnical Laboratory, 1-1-4, Umezono, Tsukuba 305, Japan.

A billion-per-year of semiconductor Hall devices and magnetoresistors are used for a displacement sensor of brushless motor in a video tape recorder and a disk driver, a banknote detector of vending machine and a contactless switch. The conventional magnetic sensor has a few hundredmicrons of active area and a micron thickness. Recently, a low dimensional Hall device made of InAlAs/InGaAs pseudomorphic heterostructure semiconductors with high electron mobility of  $16,000 \text{ cm}^2/\text{Vs}$  at 300 K and  $160,000 \text{ cm}^2/\text{Vs}$  at 10 K has been developed. The new device has a very thin active layer of two-dimensional electron gas (2DEG), and the high device performance with a large dynamic sensitivity from nano tesla to a few tesla and a wide temperature range from cryogenic temperature to some hundred centigrade. A nanoscale of 2DEG Hall sensor with a very thin active layer of about 10 nm can be designed. The  $1/f$  current noise decreases with decreasing the device dimension, that is the decrease of Hooge's parameter. The high signal-to-noise ratio given by the ratio of the large magnetic sensitivity to the small current noise is promising on the low dimensional microsensor. A magnetic image sensor made of a one- or two-dimensional array integration of three-terminal Hall elements are very useful for an inspection of magnetic microdomain. The operating principle is based on the differential detection with one reference element integrated monolithically. The linear magnetic property is shown in this device, but a half sensitivity.

Another new type of magnetic sensor is based on galvanomagnetic effects in vacuum. The vacuum magnetic sensor (VMS) is made of three metal electrodes on the quartz substrate, that is a comb-shaped microstructure emitter, a high-field gate and a pair of splitted collectors. An electron emitted in vacuum by high electric field is deflected by an external magnetic field. The device has higher magnetic sensitivity of  $1,000 \text{ \%}/\text{T}$  compared with semiconductor sensors.

INVITED

11:00 am **NS1-MoM9 Quantum Corrals**, D. M. Eigler, IBM Research Division, Almaden Research Center, 650 Harry Rd., San Jose, CA 95120.

Electrons occupying surface states on the closepacked faces of noble metals form a two-dimensional (2-d) nearly-free electron gas. Because this system is accessible to the scanning tunneling microscope (STM), it provides a unique opportunity to study the local properties of electrons in reduced dimensions. We have observed standing wave patterns in the surface local density of states due to the interference of 2-d surface state electrons scattering off of step edges and adsorbate atoms. Analysis of the energy dependence of the periodicity of the standing waves gives an independent measure of the surface state dispersion. We have found that Fe adatoms strongly scatter the surface state

electrons. Using the atomic manipulation capabilities of the STM, we have assembled Fe adatoms into barriers which reflect the surface state electrons. By closing these barriers on themselves we create a new kind of electron confinement structure: a "Quantum Corral." The energies of the eigenstates of the corral may be directly measured by tunneling spectroscopy. The spatial distribution of the electron density of energy-selected eigenstates of the corral may be directly imaged with the STM. The main features of the electron density in the corrals are consistent with the solutions of the classic quantum mechanics problem of a particle in a box. Our experience is that BEING a quantum mechanic, that is, engineering and constructing a quantum state, can provide seemingly endless hours of enjoyment. **INVITED**

## APPLIED SURFACE SCIENCE Room A101 - Session AS-MoM

### Imaging and Small Area Analysis

**Moderator:** R. W. Linton, University of North Carolina, Chapel Hill.

8:20 am **AS-MoM1 Static and Dynamic SIMS with Sub-Micron Resolution: Sensitivity and Quantification Aspects**, Y. Gao, F. Saldi, H.-N. Migeon, Laboratoire d'Analyse des Matériaux, CRP-CU 162a, avenue de la Faïencerie, L-1511 Luxembourg.

The latest developments in SIMS instrumentation have made possible the analysis with lateral resolutions in the 100 to 200 nm range. Together with this resolution obtained by means of finely focused ion beams (Gallium, Cesium, Oxygen) the use of secondary optical systems allowing high transmission and high mass resolution makes useful SIMS analysis with good lateral resolution.

In this paper, we intend to review the capabilities for both static and dynamic SIMS applications in terms of ionisation efficiencies under different bombarding conditions, ionisation efficiencies of different elements and their influence on detection limits in microvolumes, image acquisition time. The figures of merit of double focusing magnetic sector and Time of Flight spectrometers will be outlined for static, dynamic and intermediate regimes.

If those performances can be predicted when dealing with SIMS measurements either in the static or in the dynamic regimes, the major limitation for the use of SIMS on laterally heterogeneous samples is related to the matrix effect. Some examples of such artefacts will be pointed out under different bombarding conditions. In order to minimise the matrix effect in dynamic SIMS we will concentrate on two alternatives, cationisation (MCs<sup>+</sup>) and SNMS, as well as laser positionisation for the static SIMS measurements. **INVITED**

9:00 am **AS-MoM3 Surface Trimer Crystallization on Poly-(Ethylene Terephthalate) Studied by Time-of-Flight Secondary Ion Mass Spectrometry (TOF-SIMS)**, S. Reichlmaier<sup>1</sup>, S. R. Bryan<sup>1</sup> and D. Briggs<sup>2</sup>, 1) Perkin-Elmer Physical Electronics Division, Eden Prairie, MN 55344, 2) ICI plc., Wilton Research Centre, Middlesbrough, Cleveland TS90 8JE.

Film poly (ethylene terephthalate) (PET) is used as substrate material in a great variety of applications, because of its excellent physical properties. Film strength is an important requirement for magnetic recording tapes as used in every VCR. Surface properties like adhesion and friction are also extremely crucial in this application. Under certain thermal treatments or exposure to some solvents PET is known to crystallize oligomeric material on the surface. This oligomeric material is dominated by the cyclic trimer. We investigated the generation and spatial distribution of the cyclic trimer on PET film samples. The film samples were heat treated in an air oven at 170°C for different periods of time (1-48h). Quite dense distributions of trimer crystals were observed for both materials even after only 1h of treatment. Domains with different characteristic were observed under an optical microscope and crystal size varied from 1µm to 50µm. The surfaces were then chemically characterized using TOF-SIMS. High mass resolution allows unambiguous assignments of the observed surface species and was used to verify previous observations using a quadrupole SIMS instrument<sup>1</sup>. The high sensitivity and transmission of the TOF analyzer also allowed chemical imaging of these surfaces. Retrospective image analysis was used to determine mass spectral differences between the

PET substrate surface and the crystallite surface. Relative peak intensities from these areas were used to investigate the presence of non crystallized trimer in the areas between the crystals.

1) D. Briggs, SIA, Vol. 8, pp. 133-136 (1986).

9:20 am **AS-MoM4 TOF-SIMS Imaging of Organic Materials**, B. Hagenhoff, D. Rading, M. Deimel, A. Benninghoven, Physikalisches Institut der Universität, Wilhelm-Klemm-Str. 10, D-48149 Münster, Germany.

Surface properties like adhesion, wetting behaviour, friction and corrosion play a key role in many fields of technology. As these properties are determined by the molecular composition and structure in the uppermost monolayer an analytical technique is required which allows to localize, identify and quantify the molecules present in this area.

We applied imaging TOF-SIMS to the characterization of structured SA monolayers (domain structure, monitoring of patterning processes), coated fibers (surface coverage, molecular distribution in two component systems) and defects in car paint (failure analysis). Although TOF-SIMS instruments equipped with liquid metal ion guns meanwhile allow lateral resolutions of ≤100 nm we found that the useful lateral resolution for organic imaging in most cases is limited to 1 µm. This is mainly due to the static conditions required for organic SIMS (only the uppermost monolayer can be consumed if intact molecules have to be detected) and the generally low transformation probabilities of molecular species ( $P(M \rightarrow X) = 10^{-2}-10^{-8}$ ). The results presented will, however, show that imaging TOF-SIMS nevertheless can offer most valuable information which is not accessible with other analytical techniques.

9:40 am **AS-MoM5 ToF SIMS Imaging of Self-Assembled Monolayers**, D. G. Castner, Univ. of Washington, Seattle, WA and P. J. McKeown, Perkin-Elmer PHI, Eden Prairie, MN, and D. W. Grainger, Colorado State University.

Self-assembly of organic monolayers (SAMs) via silane or sulfur anchor groups provides a versatile method of preparing bound thin films with well-defined surface chemistries. Variation of monolayer structure in the vertical direction can be obtained by assembly of multifunctional polymers onto surfaces. This study examines methods of preparing well-defined lateral patterns of surface chemistries. A series of 20 µm long lines varying in width from 0.2 to 2 µm were etched into SAMs of octadecane thiol and perfluoro siloxane polymers on Au with a 20 keV Ga<sup>+</sup> focused ion beam. The octadecane thiol SAM was then exposed to perfluorothione to fill the etched regions. The etched perfluoro siloxane was imaged without further treatment. The ToF SIMS images were obtained in the static mode (ion dose ≤ 10<sup>12</sup>) using a 25 keV Ga<sup>+</sup> source. All lines were readily resolved on both samples. The perfluoro siloxane polymer was also self-assembled onto a SiO<sub>2</sub> substrate with 2 µm wide Au lines. ToF SIMS images showed the SAM was only present on the Au lines. Full mass spectral analysis in the different regions of the patterned SAMs confirmed the surface structure of each region. This selected area analysis also provided information about contamination and oxidation processes occurring on these samples. These SIMS results show patterned SAMs can be prepared with submicron resolution. Additional characterization of the SAMs has been done with XPS, ellipsometry, contact angle, and FTIR.

10:00 am **AS-MoM6 Scanning Photoelectron Microscope with Submicron Lateral Resolution Using Wolter-type X-ray Focusing Mirror**, Ken Ninomiya, and Masaki Hasegawa, Central Research Laboratory, Hitachi, Ltd., Kokubunji, Tokyo 185, Japan.

Photoelectron microscopy is a powerful tool providing detailed chemical and electronic state information at high spatial resolution. We have recently improved lateral resolution of a scanning photoelectron microscope (SPEM) in the soft X-ray beamline of the 2.4 GeV electron storage ring at the Photon Factory. The microscope is characterized by the use of a Wolter-type grazing incidence X-ray mirror for generating a focused soft X-ray microbeam.<sup>1</sup> The mirror, fabricated by epoxy resin method<sup>2</sup> in combination with vacuum replication, has a demagnification of 1/29.8 and an X-ray reflectivity of 77% for 150 eV soft X-rays. When the microbeam (sagittal beam size: 1.8 µm) one-dimensionally scans aluminum stripe patterns formed on a SiO<sub>2</sub> wafer, the 4 to 0.6 µm stripes are clearly detected using the total yield of photoelectrons with modulations between 0.33 and 0.08. In addition, the 16%-84% width of the photoelectron count rate change at the pattern edge gives a still higher resolution of 0.5 µm.

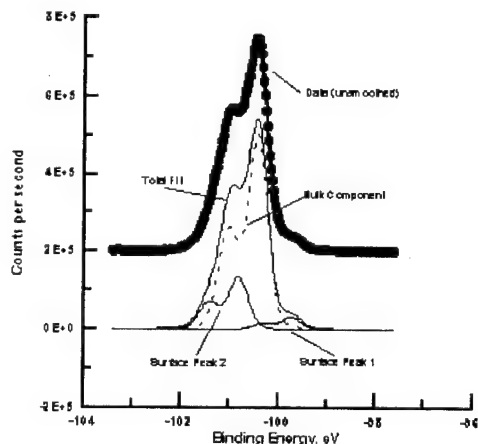
These results indicate that our SPEM has a lateral resolution better than 0.6  $\mu\text{m}$ . The present study demonstrates photoelectron imaging at the highest lateral resolution that has ever been achieved using grazing incidence mirrors in the soft X-ray region. A submicron focused beam is also presented that will soon be used for higher-resolution photoelectron imaging. This work has been performed under the approval of the PAC of the Photon Factory (Proposal No. 93-Y003).

<sup>1</sup>K. Ninomiya and Masaki Hasegawa, *Jpn. J. Appl. Phys.* **33**, L550 (1994).

<sup>2</sup>M. Hasegawa, H. Taira, T. Harada, S. Aoki, and K. Ninomiya, *Rev. Sci. Instrum.* (to be published).

10:20 am **AS-MoM7 First Results from the Spectro-Microscopy Undulator Photoemission Beamline**, *J. Denlinger<sup>1</sup>, E. Rotenberg<sup>1</sup>, A. Warwick<sup>1</sup>, S. Kevan<sup>2</sup>, and B. P. Tonner<sup>3</sup>*, <sup>1</sup>Advanced Light Source, Berkeley, CA 94720, <sup>2</sup>Univ. of Oregon, Eugene, OR, <sup>3</sup>Univ. of Wisconsin-Milwaukee, Milwaukee, WI.

The term "ultraESCA" is used to refer to a high performance photoemission spectroscopy system, which optimizes small analysis area, spectral resolution, atomic species detection sensitivity, and count rate. The implementation at the Advanced Light Source is based on a 5 cm period undulator and spherical grating monochromator with adaptive focussing optics, coupled with a high efficiency electron energy analyzer. The first results show simultaneous achievement of analysis areas below 50 micron, energy resolution below 0.2 eV, and count rates above 1 MHz. The tunable photon energy permits optimization of surface or near-surface sensitivity, and cross-section enhancement of dilute species by orders of magnitude in comparison to typical fixed-wavelength laboratory instruments. A spectrum showing surface core level shifts from Si(111)-7  $\times$  7 is shown here, with a total collection time of 20 seconds. This corresponds to an enhancement of a factor of 800 over Al  $K\alpha$  sources. Many applications will be discussed.



10:40 am **AS-MoM8 Identification and Quantification of Hidden Features using Imaging XPS**, *J. E. Fulghum, L. Paleudis and T. A. Zupp*, Chemistry Department, Kent State University, Kent, OH 44242 and *D. J. Surman*, Kratos Analytical, 535 East Crescent Ave., Ramsey, NJ 07446.

XPS images are predominantly used to display changes in surface composition or to locate features for small area analysis. However, a more three-dimensional picture of the sample can be developed in some cases. Vertical and horizontal changes in composition contained within the XPS sampling depth can be quantitatively evaluated using XPS images from different sample components. Step heights, layer thicknesses, and feature sizes can be determined if changes in composition occur within the first  $\approx$  10 nm in depth or within the image field of view (up to 10 mm<sup>2</sup>). Information which can be obtained will be demonstrated using both organic and inorganic samples containing buried layers and patterns. Quantitative information will be compared to line scans and small area analyses.

This work is partially supported by the W. M. Keck Foundation and the NSF Science and Technology Center for Advanced Liquid Crystalline Optical Materials (ALCOM) under DMR89-20147.

11:00 am **AS-MoM9 Analysis of Insulating Materials Using Field Emission Auger Electron Spectroscopy**, *N. M. Forsyth, G. Jones and J. Wolstenholme*, Fisons Instruments Surface Systems, The Birches Industrial Estate, Imberhorne Lane, East Grinstead, West Sussex, RH19 1UB, UK.

Traditionally the major uses of Auger electron spectroscopy (AES) have been in the analysis of conducting samples requiring high spatial resolution. The electron beam primary source with its relatively large dissipation of energy into the sample can lead to serious charging problems on insulating samples. The analysis of insulating samples requires the ability to use either very high (25 keV) or very low (3 keV) primary beam energies and the geometry of the instrument must allow a range of sample tilt angles to satisfy each individual sample requirement. The MICROLAB 310-F is the Fisons Instruments dedicated Auger microprobe with a Schottky field emission electron source which is capable of giving high spatial resolution even at low beam energies. It also has a co-planar geometry which allows a wide range of sample tilt angles to be used in orienting the sample to combat charging effects without compromising the sensitivity of the instrument.

Examples will be shown of the spectroscopy and mapping capabilities of this instrument on ceramics and insulating composite materials showing the analysis of sub-micron sized grains and describing the contribution this capability can make to solving surface related problems on insulating samples with small features.

11:20 am **AS-MoM10 SAM and XPS Studies of Roman Bronzes**, *E. Paparazzo, L. Moretto*, ISM-CNR, Via E. Fermi 38, Frascati, Italy, *P. Northover*, Dept. of Materials, University of Oxford, UK, *C. D'Amato*, Museo della Civiltà Romana, Roma, Italy, *E. Severini*, CSM SpA, Roma, Italy, *A. Palmieri*, ITABC-CNR, Monterotondo, Italy.

A series of Roman bronzes of the 3d century B.C. is studied with scanning Auger microscopy (SAM) and x-ray photoemission spectroscopy (XPS). The object is to characterize the chemical species present at the surface and to highlight their lateral distribution. Cu oxides, SnO<sub>2</sub>, PbO, PbCl<sub>2</sub> and carbonates are the main corrosion products, and the surface composition is related to bulk quantitative analysis obtained with the electron microprobe and atomic emission spectrometry. A huge lateral dishomogeneity is found when Ar sputter-profiles obtained with XPS in large area (1 cm<sup>2</sup>) analysis are compared with those given by Auger point spectra recorded over an area 1  $\mu\text{m}^2$  large. The microchemistry of the materials is further explored using Auger imaging, which highlights Sn, Cu and O segregations with a spatial resolution of 0.5  $\mu\text{m}$ . We show that SAM and XPS techniques feature unique advantages in the study of the surface microchemistry of archaeological objects, markedly as regards the direct identification of chemical species and the quantitation of light elements.

11:40 am **AS-MoM11 Strain Imaging Analysis Using Raman Microscope**, *J. P. H. Sukanto<sup>†</sup>, K. Ajito, T. Minabe, L. Jiang, L. A. Nagahara, K. Hashimoto, and A. Fujishima*, Department of Applied Chemistry, Faculty of Engineering, The University of Tokyo, Hongo, Bunkyo-ku, Tokyo 113, Japan.

Micro-Raman spectroscopy has been used to study the local mechanical stress in micro fabricated structures on a silicon substrate. Large stress can give rise to defects in the silicon substrate and even to structural defects such as breaking of an oxide pad, which makes further processing of these structures impossible. Furthermore, mechanical stress has a strong influence on the electrical characteristics and the degradation behavior of metal-oxide-semiconductor (MOS) integrated circuits. In order to investigate the local stress, we used a Raman mapping system which combined a commercial high light throughput spectrometer with a cold CCD detector and a XYZ stepper stage.

We present the ability to image stress fields (2-D) using Raman microprobe. Images of the stress field of a Si wafer will be presented. The local stress field was obtained from the shift of 520 cm<sup>-1</sup> Si peak as calculated using a curve fitting program. A shift in the Raman peak, corresponding to a compressive strain, was found in regions where SiO<sub>2</sub> was thermally grown on the Si wafer. Discussion of the strain resolution in relation to the standard deviation of the peak position as calculated by a Monte Carlo method will be presented. The resolution of our system is about 0.1 cm<sup>-1</sup>. The total exposure time to generate a strain in 500 by 500  $\mu\text{m}$  image consisting of 2500 data points (50 by 50) was 625 seconds.

<sup>†</sup>The present address is Corrosion Research Center, Department of Chemical Engineering and Materials Science, University of Minnesota, Minneapolis, MN 55455, U.S.A.

# PLASMA SCIENCE

## Room A109 - Session PS-MoM

### Plasma Etching & Deposition

**Moderator:** K. L. Seaward, Hewlett Packard Laboratories

8:20 am **PS-MoM1 Recent Developments in Plasma Processing,** Richard A. Gottscho, AT&T Bell Laboratories, Murray Hill, NJ 07974.

The purpose of this talk is to highlight advances presented at last year's national symposium of the American Vacuum Society and those that will be presented during this week's symposium. I will also venture slightly beyond this mandate to outline future directions for the plasma science and technology community to consider.

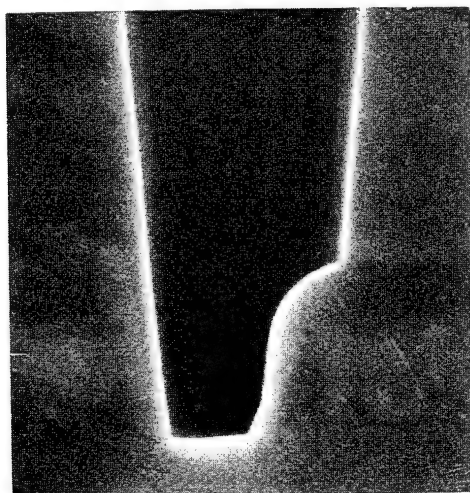
Last year's meeting featured some healthy controversy and discussion on the relationships between ion and neutral transport, etching mechanisms, and that troublesome problem referred to as microloading, RIE lag, aspect ratio dependent etching, . . . In my mind, seemingly contradictory results were reconciled by considering the competition between etching and deposition and their different dependencies on the ion to neutral flux ratio. I will review last year's talks along these lines and shed new light on the subject.

In going forth, we are witnessing the advent of large area, high performance plasma processing. While Si wafer sizes are increasing to 300 and 400 mm diameters, flat panel displays are already made on  $360 \times 485$  mm glass plates. These sizes place unprecedented demands on etching uniformity and throughput while linewidth control and selectivity demands also grow more stringent. As a result, the plasma processing and reactor design communities are being challenged as never before. I will highlight some of the approaches being taken in dealing with etching and deposition processes and where significant challenges remain.

INVITED

9:00 am **PS-MoM3 Self-Aligned-Contact (SAC) Dry Etch Process for  $0.5\mu$  SRAM Technology,** J. E. Nulty, P. S. Trammel, Cypress Semiconductor, San Jose, CA 95134.

Self-Aligned-Contact (SAC) technology is a preferred method to reduce cell size in CMOS SRAM technology while maintaining low manufacturing costs. Key to this technology is the SAC etch, which requires a blanket etch-stop layer to protect underlying topography from oxide etch plasma during contact hole formation. We report a SAC etch technology utilizing BPTEOS as an oxide dielectric and CVD Nitride as a blanket etch stop. CVD Nitride is used extensively in existing technologies, demonstrates good step coverage in high aspect ratios, and is a good insulator for semiconductor devices. In the course of our development, we addressed the following key issues: ARDE effects, flat substrate nitride loss, and alignment-sensitive topography-corner nitride loss. Solutions to each issue will be discussed. We will present both SEM and electrical test structure verification results for our work as applied to  $0.5\mu$  SRAM.



0.3 $\mu$

9:20 am **PS-MoM4 The Correlation between Selective Oxide Etching and Thermodynamic Prediction,** S. C. McNevin, AT&T Bell Laboratories, 600 Mountain Ave., Murray Hill, NJ 07974.

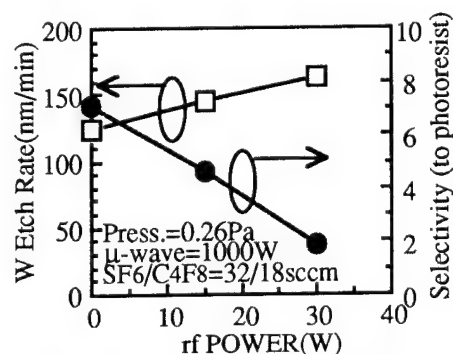
This talk will report the connection between the chemical predictions based on thermodynamics and the experimentally observed selective oxide etching in a hot wall commercial HDP system. The relation between the protective carbon-based deposit on non-oxide surfaces (Si, TiN etc.) and the theoretically predicted selective deposition of carbon will be explored. While carbon is deposited on both Si and  $\text{SiO}_2$ , the oxygen in the  $\text{SiO}_2$  leads to the selective removal of the carbon so that plasma etching of the oxide can continue. It will be shown that CO and the chamber/wafer temperature play a major role in this carbon deposition. The chemical role of H in increasing this deposit will also be examined. The model predicts that the CO responsible for the carbon deposition can have many collisions with the  $\text{SiO}_2$  sidewalls but will only deposit on the non-oxide at the bottom of an opened contact. This is consistent with the experimental observation that increasing chamber temperature increases the protective deposition, but does not change the sidewall angle.

9:40 am **PS-MoM5 High Rate and Highly Selective  $\text{SiO}_2$  Etching Employing Inductively Coupled Plasma,** Y. Horike, K. Kubota\*, and T. Fukazawa\*\*, Toyo Univ., Kujirai, Kawagoe, \*Hiroshima Univ., Saijo, Higashi-Hiroshima, \*\*TEL-Yamanashi, Nirasaki, Yamanashi, Japan.

The kinetics of high selectivity of  $\text{SiO}_2$  etching achieved by inductively coupled plasma (ICP) employing  $\text{C}_4\text{F}_8 + \text{H}_2$  mixture will be discussed. Selectivity depended strongly on the gap distance, d between a quartz plate on which a single turn antenna coupled with 13.56 MHz power was set, and a wafer stage biased by 100 KHz power. This resulted from a sheet-like structure of ICP. Higher electron density in narrower gap of d < 50 mm dissociated HF products to produce F atoms which were responsible for the Si etching, while HF products were exhausted readily at the downstream diffusive region in wider gap of d > 75 mm, thus increasing the selectivity. The effect was confirmed by the result that selectivity increased with increasing flow rate. Scavenging of F atoms also resulted in deposition of carbon-rich polymer films on the Si surface which protected the Si surface from ion bombardment. Selective deposition of the films in contact holes with feature size less than  $0.8\mu\text{m}$  which led to infinite selectivity was observed. The SEM cross sectional pictures demonstrated that films covered uniformly whole wall surfaces of holes for 30%  $\text{H}_2$  addition to  $\text{C}_4\text{F}_8$ , while films deposition was limited to opening areas of holes for  $\text{C}_4\text{F}_8$  alone. Since film thickness on hole bottom increased with increasing self bias voltage, resputtered side wall films was considered to accumulate on the bottom of holes. Appearance voltage mass analysis of radicals in the  $\text{C}_4\text{F}_8/\text{H}_2$  plasma showed that CF and  $\text{CF}_2$  radicals were dominant in spite of with and without  $\text{H}_2$  addition to  $\text{C}_4\text{F}_8$ . Above drastic change of step coverage of films on wall surfaces in the presence of 30%  $\text{H}_2$  may be ascribable to a reaction between introduction of CF radicals into hole and H atoms adsorbed on inner wall surfaces.

INVITED

10:20 am **PS-MoM7 Tungsten Etching Using Electron Cyclotron Resonance Plasma,** T. Maruyama, K. Shiozawa, N. Fujiwara, M. Yoneda, ULSI Lab., Mitsubishi Elec. Corp., 4-1 Mizuhara, Itami, Hyogo 664, Japan.



The dependance of selectivity on rf power

Tungsten (W) is widely used as wire materials instead of aluminum alloys or poly-Si due to its low resistivity, good step coverage and electromigration resistance. However, in W etching, it was difficult



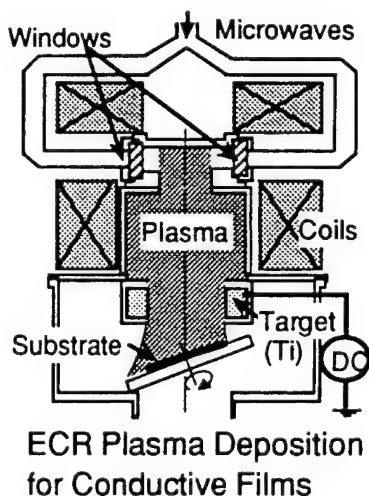
to realize high selectivity to photoresist and anisotropic etching simultaneously. The electron cyclotron resonance (ECR) plasma is one of the suitable methods to realize highly selective etching. In this paper, we study W etching by the ECR plasma using  $\text{SF}_6/\text{C}_4\text{F}_8$  gas mixture. Samples used in this experiment were chemical vapor deposition (CVD) W films on TiN films masked with photoresist pattern. Stage temperature and gas pressure was set at  $30^\circ\text{C}$  and at  $0.26\text{Pa}$ , respectively. The selectivity to photoresist increases with decreasing of rf power. The highest value of selectivity is 7.9, which is obtained with applying no rf-bias. Furthermore, the selectivity increases with increasing magnetic field where the sample was located. The reason for this result is supposed that sheath potential decreases as magnetic field increases. Concerning etch profiles, in the case of etching using pure  $\text{SF}_6$  gas, the side etching is observed in sidewall of W. This side etching is reduced by  $\text{C}_4\text{F}_8$  gas addition, and an anisotropic etching is achieved with addition of 36%  $\text{C}_4\text{F}_8$ . Moreover, it is clear that the addition of  $\text{C}_4\text{F}_8$  reduce reactive ion etching (RIE) lag in W etching. The reason for the decrease of RIE lag is that the flux of deposition precursors, which is generated by  $\text{C}_4\text{F}_8$  decomposition, decreases due to low conductance in high aspect ratio patterns.

10:40 am **PS-MoM8 Cu Metallization Using Electron Cyclotron Resonance Plasmas**, S. M. Gorbalkin, R. L. Rhoades, and L. A. Berry, Oak Ridge National Laboratory, Oak Ridge, TN 37831-6057 and S. M. Rossnagel, IBM Research, P.O. 218, Yorktown Heights, NY 10598.

A permanent magnet electron cyclotron resonance (ECR) plasma source has been redesigned to accommodate powers up to 5 kW and used with a solid metal sputter target for Cu deposition over 200-mm diameters. Sputter target current densities of  $\sim 40\text{ mA/cm}^2$  have been measured at 1400 W, and the results of operation at higher powers, along with thin-film deposition rates, uniformities, and resistivities, will be reported. Measurements of the ion energy required for no net deposition have been used to deduce the ratio of Ar ions to all Cu species. At pressures  $\sim 4\text{ mTorr}$  and microwave powers  $\sim 1000\text{ W}$ , the ratio is  $\sim 1.5\text{--}3$ . The ratio of the Cu ion to neutral flux has been estimated using observations on the filling characteristics of submicron, 1:1 to 3:1 aspect ratio features combined with modeling.

Research is managed by the Division of Materials Sciences, U.S. Department of Energy, under contract DE-AC05-84OR21400 with Martin Marietta Energy Systems, Inc.

11:00 am **PS-MoM9 Application of an Electron Cyclotron Resonance Plasma Source to Conductive Film Deposition**, M. Shimada, T. Ono, H. Nishimura, and S. Matsuo, NTT LSI Laboratories, Atsugi, Kanagawa 243-01, Japan.



A new electron cyclotron resonance (ECR) plasma source for conductive film deposition has been developed<sup>(1)</sup>. In this source, 2.45 GHz microwaves are divided into two directions and transported into the composer through quartz windows. The windows are arranged in the blind space from the ECR plasma and in a region where the magnetic field is higher than that of the ECR condition (875 Gauss). Two coils with different inner diameters are set for the generation of highly uniform plasma<sup>(2)</sup>. High ion current densities above  $10\text{ mA/cm}^2$  and

good uniformity of  $\pm 5\%$  over a 6-inch diameter area have been obtained. TiN films were deposited by ECR plasma deposition using a sputtering material supply. The ratio of Ti to N was about 0.9 at a  $\text{N}_2$  partial pressure of  $0.01\text{ Pa}$ , and a resistivity of only  $25\text{ }\mu\Omega\cdot\text{cm}$  was obtained with  $\text{Ar/N}_2$  plasma at  $300^\circ\text{C}$ . Advantageous features, good step coverage and filling to the bottom, were obtained by using a rotative inclined substrate holder. The target current was very stable for deposition over 100 hours. In applying this source to CVD, SiC films were deposited with high reliability using  $\text{C}_2\text{H}_4/\text{SiH}_4$  plasma.

- (1) T. Ono, *et al.*, Proceeding of 40th AVS, 171 (1993).
- (2) H. Nishimura, *et al.*, Jpn. J. Appl. Phys. 32, 332 (1993).

11:20 am **PS-MoM10 Micro-Profile Simulations of Metal Ion and Neutral Deposition**, S. Hamaguchi and S. M. Rossnagel, IBM, Thomas J. Watson Research Center, P.O. Box 218, Yorktown Heights, N.Y. 10598.

Numerical simulations in parallel with experimental depositions have been performed to model the deposition of metal neutrals AND ions into trench structures. This type of topographical feature is commonly used for interconnect metallization techniques on semiconductors. The work is intended to describe the deposition and etching dynamics occurring deposition from metal plasmas, such as in the case of metal ECR plasmas or Ionized Magnetron Sputter Deposition systems. The numerical model is based on the shock-tracking algorithms for a moving boundary and the etch/deposition rate is calculated from the fluxes of metal ions, metal neutrals and inert gas ions incident on the sample surface. The model is versatile enough to simulate semi-isotropic deposition of neutral metal atoms (conventional sputter deposition), deposition of angle-limited neutral metal atoms (collimated sputtering) and the deposition and etching dynamics of depositing metal ions (ionized magnetron sputter deposition or metal ECR plasma deposition), which may also cause local sputtering and redistribution at the sample surface. Combinations of these effects are also describable. Comparison with experimental depositions in each of these three areas shows good agreement. The model is used to optimize trench/via filling as a function of feature size and aspect ratio for the case of neutral and metal ion deposition at various flux ratios and energies.

11:40 am **PS-MoM11 High Density Metal Plasma Formation During DC Magnetron Sputtering In Self-Sustained Mode**, W. M. Posadowski<sup>(1)</sup> and Z. J. Radzinski<sup>(2)</sup>, <sup>(1)</sup>Institute of Electron Technology, Technical University of Wroclaw, Wroclaw, Poland; <sup>(2)</sup>Analytical Instrumentation Facility, North Carolina State University, Raleigh, NC 27609.

During a conventional DC magnetron sputtering with an inert gas, a target material is sputtered in form of neutrals and ions. Majority of sputtered species are neutrals which traveling through the plasma region above the magnetron source may be ionized. If high ionization is guaranteed then one may expect that a high ratio of target ions to neutrals can be achieved. With an electric potential across the dark space field in the order of few hundreds eV, the target ions will have enough energy to sputter target material. If a self-sputtering yield is high enough the process can transition without an inert gas into the self-sustained mode. A high ionization efficiency of target secondary species which has been achieved in the ETERNA<sup>TM</sup> 2.5, 4 and 8" diameter sources enables one to perform sputtering in self-sustained mode for a variety of materials at the chamber background pressure of  $8 \times 10^{-6}\text{ Torr}$ . During such sputtering, the target species are the primary component of plasma. It will be shown that, the plasma impedance, calculated as a ratio of target voltage to target current can be a good indicator of these threshold conditions for self-sustained sputtering, i.e. the formation of high density metal plasma. An interesting tendency can be observed when the plasma impedance is plotted vs. working pressure with target current as the parameter. The plasma impedance is almost independent of working pressure in a wide range from  $10^{-2}$  to  $10^{-6}\text{ Torr}$  for materials with high sputtering yield. The results will be presented for various materials (e.g. stainless steel, Cu, Ag, Ta, W) using the ETERNA<sup>TM</sup> sources.



## VACUUM TECHNOLOGY

### Room A102 - Session VT-MoM

#### Total Pressure Gauging

**Moderator:** N. T. Peacock, HPS Division of MKS Instruments Inc.

8:20 am **VT-MoM1 Electron Path Length Calculation Using Finite Element Method for An Axial Emission Gauge**, *A. Agarwal, J. Bass, A. H. Bass*, INMS, National Research Council, Ottawa, Ontario, Canada K1A 0R6.

The axial emission gauge (AEG) is an ionization gauge which is used to measure pressure in the ultra high vacuum (UHV) region. The gauge is similar in construction to a Bayard Alpert gauge (BAG), except that the filament and ion collector are located at the two ends, on the symmetry axis of the accelerating grid. As with a BAG, the sensitivity of an AEG is also proportional to the path length of ionizing electrons, which is determined by the potential field present within the gauge. To be able to improve the gauge sensitivity, we have developed a computer model of the AEG to study the trajectories and calculate the total path length of the electrons. Using axial symmetry finite element topography, the potential field used to accelerate the electrons has been calculated by solving the Laplace equation using appropriate boundary conditions. The same topography is then used to compute the electron trajectories and path lengths for both a predetermined direction of electrons and random electron emissions whose speeds have been determined using Monte Carlo techniques assuming a Maxwell velocity distribution. The mathematical model indicates that it is possible to find maximum path length by varying gauge parameters.

8:40 am **VT-MoM2 Observations of Electron Trapping Phenomenon Occurring in a Lafferty Gauge**, *N. Gotoh*, The Graduate University for Advanced Studies, 1-1 Oho, Tsukuba 305 Japan, *R. Paitich*, Terranova Scientific, 5481 Bell Road, Auburn, CA 95602 U.S.A., *H. Hisamatsu*, and *H. Ishimaru*, KEK National Laboratory for High Energy Physics, 1-1 Oho, Tsukuba 305 Japan.

We have been studying a Lafferty gauge for extreme high vacuum pressure measurement. The Lafferty gauge has high sensitivity due to electron trapping by applied magnetic field. We found experimentally an electron trapping phenomenon. Ion current of the Lafferty gauge came to zero several minutes after filament power was OFF. The several minutes "life time" of ion current means that electron trapping phenomenon was occurred by magnetic field within the Lafferty gauge. The life time of ion current depended on a magnitude of magnetic field and a filament-to-anode voltage. We observed that the most longest life time obtained was five minutes on the condition that the filament-to-anode voltage: 800 volts, and magnetic field: 400 gauss, and emission: 1 nA. Pressure, when the life time measurement was performed, was on the order of  $10^{-10}$  Pa. The life time of ion current has close relationship with the electron storage mechanism within the anode and the electron scattering mechanism to the anode. Therefore experimental results of the life time measurement and theoretical sensitivity analysis by calculating electron's motion within the gauge including electron-electron scattering, electron-molecule scattering will enable us to realize the sensitivity of the Lafferty gauge.

N. Gotoh, T. Momose, H. Ishimaru, R. Paitich: Residual Current of a Modified Lafferty Gauge, 40th AVS, Orlando (1993).

9:00 am **VT-MoM3 The Influence of Filament-Heating Waveform on the Sensitivity of Glass Envelope Bayard-Alpert Gages**, *P. J. Abbott and J. P. Looney*, Thermophysics Division, NIST, Gaithersburg, MD 20899.

Non-linearities of about ten to fifteen percent in the sensitivity of glass enveloped Bayard-Alpert (BA) gages have been observed in the pressure range  $10^{-7}$  to  $10^{-2}$  Pa which are due to a time-dependent potential on the inner glass surface of the gage tube which arises as a result of the use of chopped AC filament-heating waveforms. These non-linearities were studied using modified BA gage tubes with platinum coatings on their inner glass surfaces and measuring the equilibrium potential of the platinum coating as a function of pressure and waveform characteristics. The sensitivities of the gage systems (gage tube plus controller) were found to depend on the inner surface potential, and this potential was found to depend on the pressure and on the details of the filament heating waveform. It was found that the nonlinearities could be minimized by holding the inner surface

potential to a fixed DC potential, by modifying the AC filament-heating waveform, or by using a controller that provides a noise free DC filament-heating current.

9:20 am **VT-MoM4 Long-term Stability of Bayard-Alpert Gauge Performance: Results Obtained from Repeated Calibrations Against the NIST Primary Vacuum Standard**, *Albert R. Filippelli, Patrick J. Abbott, John P. Looney, Sharrill Dittmann, and Charles R. Tilford*, National Institute of Standards and Technology, Gaithersburg, MD 20899.

Over the past 10 years, the Vacuum Standards Laboratory at NIST has performed more than 165 Bayard-Alpert ionization gauge calibrations for a wide variety of industrial and government laboratories. For 16 gauge "tube"/controller combinations the calibration has been carried out more than once, with time intervals typically 1 or 2 years between the repeat calibrations.  $\text{ThO}_2/\text{Ir}$ -filament and tungsten-filament gauges of both the nude and glass-tubulated type are included in this group. These calibration results will be presented and discussed. In most cases, we find that the repeat calibration results for a given gauge "tube"/controller combination differ by 5% or less from the previous results. In a few cases, this difference is as large as 10%.

9:40 am **VT-MoM5 Ultrasensitive Silicon Micromechanical Pressure Sensors**, *Steve T. Cho*, The Charles Stark Draper Laboratory, Cambridge, MA 02139.

In many low pressure industrial applications, there is a need for small, low cost pressure sensors. Micromechanical pressure sensors offer several advantages over conventional sensing devices, including high sensitivity, wide dynamic range, auto calibration, and self-test. Differential capacitive pressure sensors fabricated from thin silicon membranes can resolve pressures on the order of 1 mTorr, while covering a dynamic range of 6 orders of magnitude. These devices are inherently rugged and can withstand overpressures greater than 1 ATM. Furthermore, unique readout schemes have been developed for this transducer to implement advanced features such as auto-calibration and self-test. Electrostatic signals that simulate pressure impulses are generated in the electronics; these calibrated signals are used as self-test or auto-calibration signals. These devices are fabricated using a novel silicon-on-glass technology.

For vacuum applications in the uTorr and sub-uTorr operating regions, silicon resonant devices are being used as absolute pressure sensors. The operation of these devices are dependent on the damping of the ambient and are very sensitive to small pressure changes. They are currently being employed as leak detectors for measuring rates much less than standard instrumentation ( $10^{-14}$  SCCM).

10:20 am **VT-MoM7 Vacuum Gauging with IC Technology Compatible Microsensors**, *O. Paul, O. Brand, R. Lenggenhager, H. Baltes*, Physical Electronics Laboratory, ETH, CH-8093 Zurich, Switzerland.

Micromachined silicon devices used for the measurement of vacuum pressures have a number of advantages such as small size and low cost, and the possibility of batch fabrication and cointegration with on-chip signal-conditioning circuitry. Such a perspective however requires the compatibility of the devices with commercial IC processes.

We have realized thermal vacuum sensors fabricated with the commercial 1.2  $\mu\text{m}$  CMOS process of AMS (Austria Mikro Systeme, Unterpörschach, A) and post-processed at our laboratory in two ways. A first category of structures was obtained by silicon bulk micromachining with EDP solution, leaving silicon dioxide cantilevers of typical dimensions  $200 \times 200 \mu\text{m}^2$ . The power dissipated by an integrated polysilicon heater leads to a pressure dependent temperature increase of the device which in turn is measured by integrated thermopiles located on the heater beam itself or on a second beam opposite to it. The range of maximum sensitivity is between 10 and  $10^4$  Pa. A second category of structures was obtained by local and selective removal of the lower metallization layer of the CMOS process, creating a 0.6  $\mu\text{m}$  thin air gap between a heated membrane and the silicon substrate. Due to the small size of the gap, the sensitivity of these structures is maximum between  $10^2$  and  $10^6$  Pa.

A third type of devices uses the pressure dependence of the resonant behavior of thermally driven microstructures. The resonators were realized by the anisotropic etching of silicon. Their resonance frequency decreases linearly between  $10^4$  and  $10^5$  Pa, whereas their quality factor shows a strong decrease between 1 and  $10^3$  Pa.

By combining the above principles, seven decades in pressure can in principle be covered by a single silicon chip of a few  $\text{mm}^2$ .

10:40 am **VT-MoM8 A Miniaturized Silicon Based Thermal Vacuum Sensor**, *D. C. Jacobs and W. J. Alvesteffer*, Teledyne Brown Engineering—Hastings Instruments, Hampton, VA 23661.

A new miniaturized silicon based, Pirani type thermal vacuum sensor that detects pressure from 760 Torr to  $1 \times 10^{-5}$  Torr has been developed. The compact instrument is attitude insensitive, rugged and has rapid response to pressure variations. The very small passageways prevent the flow from entering into the viscous flow regime thus resulting in predominately conductive heat transfer over the entire pressure range. This removes the complexities introduced into the pressure versus output curve by convective heat transfer. The output is linear from  $1 \times 10^{-4}$  up to 0.1 Torr and monotonically increases to 760 Torr.

A unique feature of this instrument is the use of a microprocessor to compute power from the analog voltage and current. In the molecular flow regime the absolute pressure is directly proportional to the power dissipated by the surrounding gas. By measuring the power the sensor rejects most of the errors introduced by ambient temperature variations. The analog to digital converters for both the current and the voltage signals use the  $\Sigma\Delta$  conversion method to reject electrical noise by an averaging technique. This results in stable signal detection of pressure down to  $1 \times 10^{-5}$  Torr.

The instrument is thermally stable over an ambient temperature range of 0–50°C when the pressure is between  $10^{-4}$  and 760 Torr.

11:00 am **VT-MoM9 Long-Term Calibration Stability of Molecular Drag Gage Rotors**, *R. W. Hyland, and J. P. Looney*, Thermophysics Division, NIST, Gaithersburg, MD 20899.

The NIST has been keeping historical records of calibrations of molecular drag gage (MDG) rotors for about 10 years. Over 250 individual calibrations involving over 105 customer rotors, as well as numerous calibrations of NIST-owned rotors, have been performed. These records will be reviewed to determine patterns of long-term stability and ranges of parameters which can be expected with use and handling of the rotors.

11:20 am **VT-MoM10 An Optical Method for Low Pressure Measurements**, *I. Bello and S. Bederka\**, Department of Materials Engineering, University of Western Ontario, London, Canada N6A 5B9, and *L. Haworth*, Department of Electrical Engineering, University of Edinburgh, Edinburgh, EH9 3JL Scotland.

Pressure measurements from  $10^{-3}$  to  $10^3$  Pa were performed by an optical method. In this method, a radiofrequency electrodeless discharge is initiated in a small glass chamber and discharge radiation is sensed by a photosensitive element. The radiation intensity was found to increase initially with an increasing pressure but decrease above a certain pressure threshold. Thus two pressure values are often associated with each radiation intensity reading. However, it was also found that the dc current passing through the radiofrequency oscillator, which is related to the loss in the electric discharge, could be used to identify if the radiation data are taken below or above the "deflection point" pressure in the calibration curve of radiation vs. pressure. Hence, simultaneous measurements of the radiation intensity and dc oscillator current always give a unique pressure. This optical contactless method is particularly useful for the determination of pressure in chemically aggressive environments, and for automatic pressure stabilization in a radiofrequency plasma system.

\*Permanent address: Microelectronics Department, Slovak Technical University Bratislava, Ilkovicova 3, Bratislava, Slovakia.

11:40 am **VT-MoM11 Validity of the Total Pressure of  $5 \times 10^{-11}$  Pa Estimated by Laser Ionization Method**, *S. Ichimura, S. Sekine, and K. Kokubun*, Electrotechnical Laboratory, 1-1-4, Umezono, Tsukuba 305, Japan.

Laser ionization method is one of the promising technique for total pressure measurement in extreme high vacuum (XHV) ranges. Using second harmonics of a pico-second YAG laser, we estimated an ultimate pressure in an XHV chamber. Above  $7 \times 10^{-10}$  Pa ( $H_2$  equivalent), which was a detection limit of an ionization (extractor) gage used in this experiment, the number of detected ions changed linearly with pressure. Only ion detection rate decreased further to a minimum level of one count during 500 laser shots. Pressure corresponds to the count rate was estimated by extrapolation to be  $5 \times 10^{-11}$  Pa.

To verify the validity of the estimated pressure, the size of the ionization region was measured under same experimental condition of incident laser energy (30 mJ/pulse) and focussing with a spherical lens (focal length; 250 mm). An ion imaging detector<sup>1)</sup> was used for

the measurement. The size of the ionization region having a spindle shape was about  $60 \mu\text{m}$  (maximum diameter)  $\times$  2.5 mm (length) at a pressure of  $2 \times 10^{-7}$  Pa. It was shown that the volume of the ionization region was constant when the product of pressure in the XHV chamber and the number of video images used for the estimation was kept constant. The volume is roughly  $2 \times 10^{-3} \text{ mm}^3$ . This small volume supports the fact that we could count only one ion during 500 laser shots, since molecular density at  $5 \times 10^{-11}$  Pa is about 5 molecules/ $\text{mm}^3$ .

1) S. Ichimura *et al.*, Jpn. J. Appl. Phys. 33, L135 (1994).

## ELECTRONIC MATERIALS

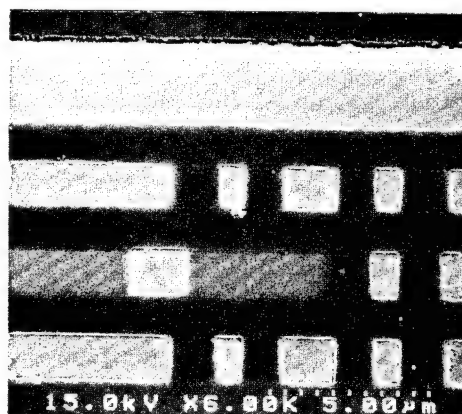
### Room A108 – Session EM-MoM

#### Materials for Device Integration

**Moderator:** L. L. Tedder, North Carolina State University.

8:20 am **EM-MoM1 Performance and Integration of Copper VLSI/ULSI Interconnects**, *D. C. Edelstein*, IBM T. J. Watson Research Center, Yorktown Heights, NY 10598.

It has long been proposed that on-chip interconnection systems should eventually migrate to copper/low dielectric constant insulators for improved performance. However, advances in CMOS circuit integration density, microprocessor architecture, and custom layout currently afford geometrical performance improvements as compared with more incremental cycle time enhancements predicted from the change in materials. On the other hand, evidence will be presented that migration to copper dual-damascene (combined line/stud metal fill and chem-mech polish) interconnects may offer incremental improvements not only in performance but also cost, yield, chip power consumption, and reliability-related impacts. Furthermore, the currently-practiced copper interconnect process may be more extendable to deep-submicron ULSI groundrules and high aspect ratios than aluminum-based technologies. This talk will present data to support the above statements from detailed electrical modeling, high-speed and other electrical measurements, and process integration and materials issues associated with the first successful demonstration of fully-integrated multilevel copper submicron interconnects. **INVITED**



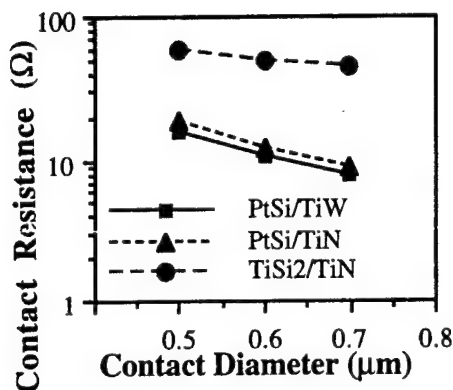
Cross-section of 4-level copper polyimide VLSI interconnects.

9:00 am **EM-MoM3 Optimization of a Contact Metallization Scheme for 0.35 ASIC Technology**, *Subhas Bothra and Teresa Trowbridge*, VLSI Technology Inc., San Jose, CA 95131.

The performance of a contact metallization scheme developed for a 0.35  $\mu\text{m}$  ASIC technology will be presented. The main features of the contact structure are a reactive sputtered TiN glue layer and CVD W plug for contact fill. A DOE approach was used to optimize the contacting layer and process for a low contact resistance with an adequate thermal stability. Since TiN does not form a low contact resistance to  $p^+$  and  $n^+$  silicon, two silicide contact layers, namely,



PtSi and TiSi<sub>2</sub> were investigated. The PtSi contacting layer results in a low contact resistance to both n<sup>+</sup> and p<sup>+</sup> silicon, while TiSi<sub>2</sub> shows a higher contact resistance to p<sup>+</sup> silicon. The contact resistances to p<sup>+</sup> Si vs contact diameter are shown below. The barrier properties of the PtSi/TiN and TiSi<sub>2</sub>/TiN were compared by annealing the wafers after subsequent deposition of AlCu alloy metal and patterning. The TiSi<sub>2</sub>/TiN barrier layer was found to be superior and necessary to achieve an adequate barrier over the worst case contact aspect ratio. Further, use of a W plug improved the barrier stability, along with a small lowering in contact resistance. DOE results on the effects of contact sputter etch, RTP TiSi<sub>2</sub> formation, TiN barrier thickness, tungsten deposition conditions and stack combinations will be presented.



9:20 am **EM-MoM4 The Effect Of Oxygen Contamination on the Formation of TiSi<sub>2</sub> for Metallization Structures**, M. Lin, J. F. Bernard, A. R. Raheem, A. McComas, E. H. Adem, T. Lukanc, S. Fong, D. Matsumoto, Advanced Micro Devices, Sunnyvale, CA 94088.

Titanium disilicide as a refractory metal silicide is ideal for use as a metallization material in VLSI technology, primarily due to its low resistivity, high temperature stability and its compatibility with standard processing techniques. However the presence of oxygen in the starting films can adversely effect the formation of a uniform and homogeneous silicide. In this paper we describe the results of an extensive experimental study where Ti (300–500 Å) and Si (700–1200 Å) films have been sputter deposited on Si and SiO<sub>2</sub> substrates by physical vapor deposition (PVD). Titanium disilicide was formed by use of furnace anneal (FA), rapid thermal anneal (RTA) and in situ ultra-high vacuum (UHV) anneal at various temperatures ranging from 400°C to 700°C. The formation of silicide, surface and interface reactions were monitored by use of AES, XPS and RBS. Oxygen and other contaminants in the sputter deposited Si/Ti films were measured by SIMS. Sheet resistance measurements were made by the four-point probe method. The results from FA and RTA thermal treatments indicate that for the amorphous-Si (a-Si) films with O levels above 10<sup>19</sup> atoms/cm<sup>3</sup> the Si/Ti reaction did not go to completion due to formation of an SiO<sub>2</sub> interface layer between unreacted a-Si and newly formed TiSi<sub>x</sub> films. These films gave high sheet resistance and had a blue discoloration. Same films when annealed in UHV successfully formed TiSi<sub>2</sub> with evolution of O and SiO into UHV ambient. The paper will further discuss the formation of surface and interface reaction products as TiSi<sub>2</sub> is formed on Si and SiO<sub>2</sub> substrates.

9:40 am **EM-MoM5 Al/Epitaxial-W Bilayer Model Diffusion Barrier Structures: Interfacial Reaction Pathways and Kinetics During Annealing**, D. B. Bergstrom, I. Petrov, L. H. Allen, and J. E. Greene, Dept. Materials Science, University of Illinois, 1101 W. Springfield Ave., Urbana, IL 61801.

Single crystal bcc W layers, 140 nm thick, were grown on Mg(001) substrates by ultra-high-vacuum (UHV) magnetron sputtering at T<sub>s</sub> = 600°C. 190-nm-thick Al films, with weak (001) preferred orientation and an average grain size of 350 nm, were then deposited at T<sub>s</sub> = 100°C without breaking vacuum. Changes in bilayer resistivity ρ during UHV annealing were monitored continuously as a function of temperature T during temperature-ramping and as a function of time t during isothermal annealing. In addition, Rutherford backscattering spectroscopy, x-ray diffraction, transmission electron microscopy (TEM), and scanning TEM in which cross-sectional specimens were analyzed by energy-dispersive x-ray analysis with a 1 nm resolution were used to follow area-averaged and local interfacial reaction paths as well as microstructural changes as a function of annealing condi-

tions. The initial reaction products were discontinuous regions of monoclinic-structure WAl<sub>4</sub> with the WAl<sub>4</sub> (240) planes frequently oriented perpendicular to the W interface with a very close lattice match, within 0.5%, to the underlying W (110) planes, bcc WAl<sub>12</sub> forms at a later stage and grows conformally to cover both W and WAl<sub>4</sub>. The WAl<sub>4</sub> and the WAl<sub>12</sub> phases continue to grow until the Al layer is completely consumed. Information from microchemistry and microstructural analyses was used to model the ρ(T, t) results, based upon a novel multi-element equivalent circuit approach which accounts for the observed non-planar nature of the reaction front, and determine reaction kinetics and activation energies. The results show that the growth of WAl<sub>4</sub> is diffusion limited with an activation energy E<sub>a</sub> of 3.1 eV while the formation of WAl<sub>12</sub> is reaction limited with E<sub>a</sub> = 3.3 eV.

10:00 am **EM-MoM6 Chemical Vapor Deposited TiCN—A New Barrier Metallization for Sub-micron Via and Contact Applications**, M. Eizenberg<sup>a</sup>, K. Littau, S. Ghanaheim, A. Mak, Y. Maeda, M. Chang, and A. K. Sinha, Applied Materials, Santa Clara, CA 95054.

High quality chemical vapor deposited (CVD) TiCN films were produced in a single wafer reactor using a metallorganic (TDMAT) precursor. The films have excellent step coverage (>75%) over high aspect-ratio contacts as well as very low particle content. These properties are obtained because the films were deposited under surface-reaction controlled conditions; the measured activation energy is 0.9 eV. The stress levels of the films are relatively low, below 5 × 10<sup>9</sup> dyne/cm<sup>2</sup>. The films show also excellent barrier properties against Al and WF<sub>6</sub> attack, which are attributed to their amorphous component, to the high C content of the films, and to the high step coverage. The electrical properties of the CVD TiCN films were evaluated at the via level, and the resistance was shown to be comparable to that of sputtered TiN. These properties make this material a superb barrier material for contact and via applications in ULSI devices.

<sup>a</sup>Permanent address: Dept. Materials Eng., Technion, Haifa, 32000, Israel.

10:20 am **EM-MoM7 Experiments and Simulations of High Pressure Chemical Vapor Deposition of TiN from Tetrakisdimethylaminotitanium and Ammonia in Vias**, Hung Liao\*, Roy Gordon\*\*, Anthony Toprac\*\*\* and Timothy S. Cale\*, \*Center for Solid State Electronics Research, Arizona State University, Tempe, AZ 85287-6006, \*\*Chemistry Department, Harvard University, \*\*\*SEMA-TECH.

We present EVOLVE-HIP, which consists of EVOLVE [1] and a high pressure chemical vapor deposition process simulator based on the continuum transport and reaction model (CTRM) [2]. EVOLVE-HIP is used to simulate high pressure deposition of TiN films from tetrakisdimethylaminotitanium (TDMAT) and ammonia. The total deposition process is divided into several small time intervals. Within each simulation time step, EVOLVE-HIP solves the steady-state version of the multicomponent continuum diffusion-reaction equations to get the local partial pressures. The local species partial pressures at the wafer surface are then used to get local film growth rates. We use the conservation law based moving algorithms in EVOLVE to update the film profile for each time step. This procedure is repeated until a desired film thickness or deposition time is reached. We use experimental TiN film profiles in vias, in addition to growth rate data on flat substrates, to estimate the kinetic parameters for a proposed rate expression for TDMAT and ammonia. The kinetic parameters are estimated by comparing predicted film profiles with experimental results (SEMs).

1. EVOLVE is a low pressure deposition process simulator developed by T. S. Cale at ASU and Motorola, Inc. with funding from the SRC and NSF.

2. H. Liao and T. S. Cale, *J. Vac. Sci. Tech.*, in press.

10:40 am **EM-MoM8 Using Poly(tetrafluoroethylene) as a Low Dielectric Constant Substrate for Microwave Circuit Fabrication**, A. J. Howard, R. R. Rye, A. J. Ricco, D. J. Rieger, M. L. Lovejoy, L. R. Sloan, and M. A. Mitchell, Sandia National Laboratories, Albuquerque, NM 87185.

By combining the low (~2.0) dielectric constant material poly(tetrafluoroethylene) (PTFE or Teflon®) with conventional integrated-circuit processing techniques, we have developed processes for the fabrication of fine circuit features directly on PTFE substrates.

Metal features are defined using a liftoff technology, electroless plating, or a combination of electroless and electroplating. The most versatile technique has achieved 4  $\mu\text{m}$ -thick metal features with high lateral resolution ( $<20 \mu\text{m}$ , a factor of five smaller than existing printed wiring board-based technology). These processes result in a less expensive process to pattern adherent, conducting metal lines on an etched PTFE substrate. Adhesion of the metal features depends upon successful substrate preparation by etching the PTFE in a sodium naphthalenide solution. Using the processes discussed above, coupled-line quadrature (Lange) couplers that demonstrate equal power splitting between 5 and 14 GHz have been fabricated directly on a PTFE substrate. Lange couplers have extensive applications as passive hybrid device components in microwave and radio-frequency (RF) systems. Details of the developed process sequences and preliminary test results for our Lange couplers on PTFE will be presented. This work demonstrates the utility of PTFE in challenging high frequency device applications where low dielectric constant substrates are essential. This work was performed at Sandia National Laboratories and supported by the U.S. Dept. of Energy under contract DE-AC04-94AL85000.

**11:00 am EM-MoM9 Processing and Device Issues of High Permittivity Materials for Dram Memories, B. E. Gnade, Materials Science Laboratory, Texas Instruments, Dallas, TX 75265.**

The development of high permittivity materials for capacitor dielectrics will significantly reduce the cell topography and complexity anticipated for  $\geq 256$  Mbit DRAMs using current dielectric technology. While cell architectures could be simplified with the introduction of high permittivity materials, there are many materials, processing and device issues which need to be resolved before high permittivity materials will be realized in a ULSI DRAM. This presentation will discuss

manufacturing and device requirements which need to be met in order for high permittivity materials to replace  $\text{SiO}_2$  and  $\text{Ta}_2\text{O}_5$  in high density DRAMs.

**11:40 am EM-MoM10 PECVD  $\text{TiO}_2$  In Microwave-RF Hybrid Plasma Reactor, Young H. Lee, Michael J. Brady and Kevin K. Chan, IBM T. J. Watson Research Center, Yorktown Heights, NY 10598.**

Plasma-enhanced chemical vapor deposition (PECVD) tool and process have been developed for  $\text{TiO}_2$  thin films of a high dielectric constant for DRAM storage capacitors. Microwave (2.45 GHz) generates a highly dense plasma ( $\sim 10^{12}$  electrons/ $\text{cm}^3$ ) through electron cyclotron resonance (ECR) and a RF hollow cathode made of a high-purity titanium sheet for electron confinement in the ECR chamber. Additional RF (13.56 MHz) was applied to the substrate electrode to extract low energy ions ( $<100$  eV) toward a Si substrate during film deposition. Our deposition process includes (1) removal of the Si native oxide in He plasma, (2) regrowth of an ultra thin ( $<1$  nm)  $\text{SiO}_2$  buffer layer in  $\text{O}_2$ /He plasma, and (3) deposition of a 30 nm thick rutile  $\text{TiO}_2$  in  $\text{TiCl}_4/\text{O}_2$ /He plasmas. All three process steps were performed near 1 mTorr and monitored by the emission spectroscopy (OES), residual gas mass/energy analyzer (RGA) and 'in situ' ellipsometer. The  $\text{SiO}_2$  buffer layer is essential to prevent diffusion of Ti into Si and consequently improves the leakage current below  $10^{-10}$  A/ $\text{cm}^2$  at the bias of  $\pm 2$  V with a 'good' thermal stability at  $1000^\circ\text{C}$ . X-ray diffraction shows the anatase phase at a low deposition temperature below  $200^\circ\text{C}$  but dominantly the rutile phase at higher temperatures. The  $\text{TiO}_2$  films deposited at  $400^\circ\text{C}$  show the dielectric constant of  $60(\pm 5)$  at 1 MHz, independent of a film thickness (20~200 nm). Low energy ion bombardment has improved the quality and thickness uniformity of  $\text{TiO}_2$  films over 125 mm Si wafers.

## SURFACE SCIENCE

Room A205 - Session SS1-MoA

### Surface Mechanisms and Materials for Chemical Sensors

**Moderator:** R. M. Penner, University of California, Irvine.

2:00 pm **SS1-MoA1 Surface Chemistry of Gold Doped WO<sub>3</sub> Hydrogen Sulfide Sensors**, *Bernd Fruhberger and Daniel J. Dwyer*, Laboratory for Surface Science and Technology, University of Maine, Orono, ME 04469-5764.

Gas sensors that detect H<sub>2</sub>S in the ppm range have been developed based on the fact that thin WO<sub>3</sub> films doped with gold exhibit resistivity changes upon exposure to H<sub>2</sub>S. In an attempt to understand the chemical mechanism by which these sensors operate, we have explored the interaction of H<sub>2</sub>S with a variety of relevant surfaces. These surfaces include: clean Au single crystal surfaces, Au polycrystals, WO<sub>3</sub> thin films and Au doped WO<sub>3</sub> thin films. These studies used a variety of ultra-high vacuum surface science techniques including X-ray Photoelectron Spectroscopy (XPS), Low Energy Electron Diffraction (LEED), Temperature Programmed Desorption (TPD) and High Resolution Electron Energy Loss Spectroscopy (HREELS). Data obtained from these surface chemistry studies has lead us to suggest a chemical mechanism for the sensor. This mechanism involves dissociative adsorption of H<sub>2</sub>S on the surface of the Au dopant followed by the chemical reduction of the WO<sub>3</sub> substrate by a spillover mechanism. Oxygen vacancies produced during the chemical reduction of the WO<sub>3</sub> films induce an n-type conductivity increases in the films. It is this conductivity increase that triggers the sensor response. The conductivity increase in the sensors is a dynamic process in which the vacancies produced by the reaction with H<sub>2</sub>S are re-oxidized by atmospheric oxygen. It is the balance between creation and re-oxidation of the vacancies which defines the dynamic range of the sensors.

2:20 pm **SS1-MoA2 Surface Chemistry of a Semiconducting Oxide Gas Sensor for Hydrogen Sulfide**, *G. S. Henshaw, D. H. Dawson and D. E. Williams*, Department of Chemistry, University College London, London WC1H 0AJ, England.

Titanium-substituted chromium oxides, in the single phase region at low titanium content (compositions around Cr<sub>1.8</sub>Ti<sub>0.2</sub>O<sub>(3+x)</sub>), act as gas sensitive resistors at elevated temperature with high sensitivity towards H<sub>2</sub>S. Upon first exposure to ppm levels of H<sub>2</sub>S in air the materials exhibit an increased baseline resistance. This pretreatment appeared permanent below about 720 K. The surface modification of the material following exposure to H<sub>2</sub>S was studied by x-ray photoelectron spectroscopy (XPS) and temperature programmed desorption (TPD). The S 2p region indicated a change in the speciation of surface sulfur during pre-treatment from, initially, sulfide and elemental sulfur, to sulfate at the completion of the pretreatment, as judged by the effects on the baseline resistance. Vacuum TPD studies of Cr<sub>1.8</sub>Ti<sub>0.2</sub>O<sub>(3+x)</sub> following H<sub>2</sub>S exposure at room temperature showed H<sub>2</sub>S and SO<sub>2</sub> desorption peaks at 720 K. This corresponded to the temperature at which the effect of pre-treatment was lost. Subsequent exposures to H<sub>2</sub>S did not reproduce the 720 K SO<sub>2</sub> desorption peak unless O<sub>2</sub> was co-adsorbed. It was concluded H<sub>2</sub>S reacted with chemisorbed oxygen during pre-treatment to form sulfate species which resulted in a reduction of electron acceptor states and a decrease in conductivity for this p-type material. The mechanism of response of Cr<sub>1.8</sub>Ti<sub>0.2</sub>O<sub>(3+x)</sub> was explained in terms of specific surface sites identified by XPS and adsorption studies.

2:40 pm **SS1-MoA3 Surface, Interface and Thin Film Effects in Solid State Chemical Sensing**, *S. Semancik, R. E. Cavicchi, G. E. Poirier, J. S. Suehle and M. Gaitan*, National Institute of Standards and Technology, Gaithersburg, MD 20899.

The increasing need for sensors that can perform reliable compositional analyses for environmental monitoring, industrial process control, personal safety and a variety of other applications has elevated the level of interest in chemical sensing considerably in recent years. Improvements in the performance characteristics of future generations of chemical sensors can be expected to relate closely to research efforts aimed at understanding transduction mechanisms, exploring new detection schemes and developing and incorporating improved planar

materials. After providing a general overview on sensing concepts, we illustrate the importance of surface chemical, structural and electronic characterization in the development of advanced, conductometric microsensor arrays for analyses of gas mixtures. Among the specific topics to be discussed are electron transport properties in crystalline and polycrystalline semiconducting oxides (including ultrathin films), metal/oxide interface formation, approaches used to impart selectivity and microstructure/performance issues. We describe both the challenges encountered and major opportunities realized when active sensing films are combined with micromachined Si array configurations with on-chip circuitry, and also indicate the roles of controlled thermal manipulation of chemisorption phenomena (static and dynamic—at ~10 msec) and neural networks in attaining optimized performance. Finally, the reciprocal nature of research benefits that can occur between surface science and the evolving field of sensor science are discussed.

INVITED

3:20 pm **SS1-MoA5 Operation of Thin Film Gas Detectors in a Temperature Programmed Mode**, *R. M. Merchant, J. W. Schwank, J. L. Gland, K. D. Wise\**, Chemical Engineering Department, Electrical Engineering and Computer Science Department\*, University of Michigan, Ann Arbor, MI 48109-2136.

The response of a thin film conductivity based gas detector to aromatic hydrocarbons is monitored by using the detector in both a temperature-programmed desorption and a temperature-programmed reaction mode. The detector structure consists of a Pt/TiO<sub>x</sub> sensing film supported by a 1 mm<sup>2</sup> micromachined dielectric window. A boron-diffused silicon heater beneath the window allows the window temperature to be varied between ambient and 1000°C. The thin film resistance is measured using Pt/Ti electrodes arranged in a four point probe configuration.

Experimental data of resistance changes induced by adsorption and temperature programmed desorption of aromatic hydrocarbons such as benzene and toluene in UHV will be presented. Use of the detector in a temperature programmed reaction mode will also be discussed. In this mode, the adsorbed species will show a characteristic reaction temperature with a typical "cleaning gas" such as oxygen, giving additional information about the nature of adsorbed species.

Results from characterization of the active sensing film using prototypical 1 cm<sup>2</sup> samples of the active film supported on a silica substrate will also be discussed. The prototypical sensing films are used for ex-situ XPS and correlation of temperature programmed desorption to the gas phase with changes in thin film resistance during desorption.

3:40 pm **SS1-MoA6 Behavior and Kinetics of Palladium-Gated Hydrogen Sensors in UHV**, *R. Bastasz*, Sandia National Laboratories, Livermore, CA 94551, *R. C. Hughes*, Sandia National Laboratories, Albuquerque, NM 87185, and *W. P. Ellis*, Los Alamos National Laboratory, Los Alamos, NM 87545.

Catalytic-metal-gated field effect devices, such as Pd-MOS capacitors and transistors, can detect small partial pressures of hydrogen in UHV. Their sensitivity and time response are strongly affected by surface impurities and substrate temperature. To help understand how these parameters affect the kinetics of sensor response, we have studied the behavior of Pd-MOS hydrogen sensors in UHV to short pulses (1–200 msec) of H<sub>2</sub> gas at pressures in the range of 10–300 μPa as a function of surface condition and temperature. Sputter cleaning of sensor surfaces improves response and recovery times, evidently by removing impurities that impede H<sub>2</sub> dissociation and recombination. At 300 K, hydrogen accumulates at the sensing junction giving a saturable response initially related to the total gas fluence. At 450 K the hydrogen concentration at the internal interface is more representative of the external partial pressure of hydrogen. These results are interpreted using a model in which hydrogen equilibrates among the internal interface, the metal film, and the internal sensing junction.

This work was supported by the US Department of Energy under contract DE-AC04-94AL85000.

4:00 pm **SS1-MoA7 Structure and Chemical Sensing Properties of Vanadium Oxide Sol-Gel Films**, *J. S. Ledford, P. A. Askeland*, Department of Chemistry and the Center for Fundamental Materials Research, Michigan State University, East Lansing, MI 48823.

The structure of vanadium oxide films prepared by hydrolysis of vanadium isopropoxide oxide has been examined using Fourier trans-

form infrared spectroscopy (FTIR) and X-ray photoelectron spectroscopy (XPS). Vanadium centers in the bulk of the film are partially reduced and retain some of their isopropoxide ligands. XPS analysis shows that the surface of the polymer film is hydroxylated, but contains no alkoxide ligands. Mass sensor results for a series of normal alcohols indicate that the vanadium oxide film has molecular sieving properties which lead to the exclusion of alcohols larger than *n*-propanol from the pores of the film. Film/analyte interactions monitored by FTIR-attenuated total reflectance spectroscopy (FTIR-ATR) revealed the formation of water at the vanadium oxide film upon exposure to alcohols ( $C_2$  and higher). The conductimetric sensor response to alcohols ( $C_2$  and higher) in air and nitrogen has been explained in terms of changes in the proton conductivity of the film that arise from water generated by alcohol dehydration reactions. For methanol, the conductimetric response is attributed to reduction of the vanadium oxide lattice. The extent of reduction of the vanadium oxide film in air and nitrogen atmospheres leads to differences in the magnitude of methanol response.

4:20 pm **SS1-MoA8 High Resolution Photoemission and Auger Parameter Studies of Electronic Structure of Tin Oxides**, *L. Kövér, G. Moretti<sup>1</sup>, Zs. Kovács, R. Sanjinés<sup>2</sup>, I. Csérny, G. Margaritondo<sup>3</sup>, J. Pálkás and H. Adachi<sup>3</sup>*, Institute of Nuclear Research of the Hungarian Academy of Sciences, H-4001 Debrecen, P.O.B. 51, Hungary, <sup>1</sup>Centro di Studio del CNR "SACSO", Dipartimento di Chimica, Università "La Sapienza", Piazzale A. Moro 5, 00185 Rome, Italy, <sup>2</sup>Institut de Physique Appliquée, Ecole Polytechnique Fédérale, CH-1015 Lausanne, Switzerland, <sup>3</sup>Dept. of Materials Science and Engineering, Kyoto University, Yoshida-honmachi, Kyoto 606, Japan.

Surface electronic structure of tin oxides (Sn and SnO<sub>2</sub>) is an important subject of study from point of view of better understanding of their mechanisms in gas sensing and catalytic actions. In order to obtain information on local electronic and geometric structure, around the core-ionized atoms, high resolution core and valence band photoemission as well as photoinduced Auger measurements of Sn metal, SnO and SnO<sub>2</sub> samples were performed. SnO surfaces were obtained without the use of ion sputtering by using a special preparation procedure based on in situ surface scraping. Comparing the valence band spectra to the theoretical spectra calculated by a cluster MO DVX<sub>α</sub> model, unambiguous information was gained on the local geometries. From the Sn core photoemission and Auger measurements it was found, in agreement with the estimation using a simple model, that the initial state effects are the same for SnO and SnO<sub>2</sub>. This was supported by the chemical state plot as well, indicating the magnitude of the initial state parameters. The oxygen K-Auger parameter shifts show that SnO<sub>2</sub> belongs to the class of oxides, hydroxides and metallic anions and indicate larger polarisability, similar to that of NiO. In summary, the use of the Auger parameter approach for obtaining information on initial state effects, polarisability and final state hole-hole repulsion energies has been demonstrated for the case of tin oxides.

4:40 pm **SS1-MoA9 Growth and Reactivity of Thin TiO<sub>x</sub> Films on W(110)**, *G. S. Herman and C. H. F. Peden*, Pacific Northwest Laboratory\*, Richland, WA 99352.

The growth and reactivity of thin TiO<sub>x</sub> films on W(110) have been studied using x-ray photoelectron spectroscopy (XPS), Auger electron spectroscopy (AES), ion scattering spectroscopy (ISS), low energy electron diffraction (LEED), and temperature programmed desorption (TPD). Growths at different oxygen partial pressures in the  $1 \times 10^{-9}$  torr to  $1 \times 10^{-7}$  torr range and at different substrate temperatures in the 300 K to 1200 K range resulted in films with varying stoichiometries and order. Final film stoichiometry was determined by AES and cross-calibrated against Ti 2p/O 1s photoemission intensity ratios. These two techniques also provide Ti oxidation state information. Initial oxidation of the Ti films at 700 K and oxygen partial pressure of  $2.5 \times 10^{-7}$  torr resulted in stable TiO. Films grown at room temperature, followed by an annealing cycle at 900–1500 K possess long range crystallographic order, as observed by LEED. However, at annealing temperatures above 1500 K tungsten AES and ISS signals can be detected, indicative of the formation of islands. In addition, TPD data indicate that the TiO<sub>x</sub> films desorb at approximately 1800 K. Finally, the reactivity of these films were investigated using several different probe molecules including D<sub>2</sub>O and CH<sub>3</sub>OH.

\*Pacific Northwest Laboratory is operated for the U.S. Department of Energy by Battelle Memorial Institute under contract DE-AC06-76RLO1830.

5:00 pm **SS1-MoA10 Synthesis of Ordered Ultra-thin Al<sub>2</sub>O<sub>3</sub> Films on Ru(0001) and Re(0001) Surfaces**, *Yutong Wu, Eric Garfunkel and Theodore E. Madey*, Departments of Chemistry and Physics, and Laboratory for Surface Modification, Rutgers, the State University of New Jersey, P.O. Box 849, Piscataway, NJ 08855-0849.

Ultra-thin Al<sub>2</sub>O<sub>3</sub> films (about 15–20 Å thick) are synthesized by two different methods on Ru(0001) and Re(0001) surfaces and monitored by XPS, LEIS and LEED. This work is part of an effort to synthesize ultra-thin crystalline films of insulating oxides on conducting substrates. On Ru(0001) post-oxidation of deposited Al films generates Al<sub>2</sub>O<sub>3</sub> films that do not have ordered LEED patterns. When Al is deposited in  $\sim 1 \times 10^{-5}$  torr oxygen at elevated substrate temperatures ( $\sim 900^\circ\text{C}$ ) the resultant films have hexagonal LEED patterns characteristic of  $\alpha$ - or  $\gamma$ -Al<sub>2</sub>O<sub>3</sub>. On the Re(0001) substrate hexagonal LEED patterns are observed from the films synthesized by both methods. Generally, the films synthesized by evaporation of Al in oxygen show better LEED patterns than those oxidized following deposition, and Re(0001) surfaces yield better LEED structure than Ru(0001). XPS results show that the films are nearly stoichiometric, and LEIS results show that the substrates are well covered. The differences between Ru and Re substrates are discussed in terms of lattice constants and alloying properties between Al and the substrates.

## SURFACE SCIENCE

### Room A201 – Session SS2-MoA

#### Nucleation and Growth: Semiconductors

**Moderator:** J. F. Wendelken, Oak Ridge National Laboratories.

2:00 pm **SS2-MoA1 Mixed-Morphology MTP Growth of Ag on Si(100)-2 × 1 Surface**, *G. Jayaram, N. Doraiswamy and L. D. Marks*, Northwestern University, Dept. of Mat. Sci. and Eng., Evanston, IL 60208.

Although the Ag/Si(100) system has received relatively less attention than Ag/Si(111), more than thirty papers have investigated the growth mode both at the initial stages and for thicker films. STM, LEED and AES studies suggest that the nucleation and growth mode is layer plus island, with a mixture of  $\langle 100 \rangle$ ,  $\langle 110 \rangle$  and  $\langle 111 \rangle$  epitaxy normal to the surface. All studies have reported, more correctly assumed, a simple structure for these islands. However, little is really known about their structure. We present the first such study of Ag islands grown on Si(100)-2 × 1 surfaces using ultrahigh vacuum high resolution transmission electron microscopy (UHV-HREM) imaging and diffraction (TED) techniques.

Several monolayers of Ag were deposited onto clean Si(100)-2 × 1 surfaces at room temperature inside the UHV-HREM facility. TED revealed a complicated pattern which could be interpreted in terms of a mixed epitaxy. HREM images showed that this was due to a mixture of multiply twinned particles (MTP's) and single crystals of Ag which grow with different epitaxies on the Si(100)-2 × 1 surface.

This data demonstrates that one of the most fundamental questions about the growth mode of silver on clean Si(100), i.e. the particle structure, has escaped more than a decade of study. Rather than being a simple Stranski-Krastanov growth system, this is a classic mixed morphology MTP growth system [1].

1. S. Ino, J. Phys. Soc. Japan 21 (1966) 346.

2:20 pm **SS2-MoA2 Modification of Overlayer Growth Kinetics by Surface Interlayers: The Si(111)  $\sqrt{7} \times \sqrt{3}$ -Indium Surface**, *S. Surnev, J. Kraft and F. P. Netzer*, Institut für Experimentalphysik, Universität Graz, A-8010 Graz, Austria.

Indium-on-Silicon is a prototypical metal-semiconductor system which exhibits unusual growth properties in the transition region from 2-D layer to 3-D island growth. Of particular interest in this context is the  $(\sqrt{7} \times \sqrt{3})$  structure of In on Si(111), which develops at elevated temperature for around one monolayer coverage ( $\theta_{1m} = 6/5$ ). The atomic structure of the  $(\sqrt{7} \times \sqrt{3})$  surface has been investigated by STM and LEED: it consists of a densely packed In overlayer with a local arrangement similar to a (001) face of face-centered tetragonal bulk In. AES and thermal desorption measurements indicate that the further In uptake on the  $(\sqrt{7} \times \sqrt{3})$  surface is reduced as compared to In on Si (111) without this ordered interlayer. The mobility of In



on the ( $\sqrt{7} \times \sqrt{3}$ ) surface is very high as evidenced by STM, where only few but very large In islands are observed, leaving a major portion of the surface uncovered even for nominal depositions as high as 500 Å. Epitaxially grown In islands are detected at elevated substrate temperature which displays a hexagonal array of In atoms on their surfaces.

**2:40 pm SS2-MoA3 K Islands on Si(111): Morphology Changes Induced by O<sub>2</sub> Exposure, Boris Lamontagne, Fabrice Sémont, Denis Roy, Laboratoire de Physique Atomique et Moléculaire, Département de Physique, Université Laval, Québec, Canada G1K 7P4.**

The morphology of the K overlayer is a controversial issue associated with the research field of Si oxidation promoted by alkali metals. Using SAES getter sources, K overlayers have been deposited in-situ on ( $7 \times 7$ ) Si(111) kept at 150 K. Various techniques (XPS, AES, SEM and SIMS) attached to the same UHV system allowed us to characterize precisely the K overlayers. For high K coverages, islands with average dimension of 1–2 µm have been found to coalesce and form long parallel islands (~10 µm in length) on the top of a continuous K layer of ~3 ML coverage. During a temperature annealing up to 300 K the islands desorb and leave a uniform K monolayer. Surprising and interesting results have been obtained upon the exposure of K islands to O<sub>2</sub>. K islands are partially levelled under the low pressure O<sub>2</sub> exposure (~10<sup>-8</sup> mbar) as they freeze under high pressure (~10<sup>-6</sup> mbar). The O<sub>2</sub> exposure induces a modification of the surface energy via an O-K interaction. After the high pressure O<sub>2</sub> exposure of the K islands, a subsequent annealing to desorb K yields SiO<sub>2</sub> islands characterized by SEM, AES and AFM. K islands levelling favors the consecutive K desorption as observed with SIMS. While several studies have suggested the formation of K islands, this work is the first of its kind to report the direct observation of K islands as well as the pronounced effect of a subsequent O<sub>2</sub> exposure on their morphology.

**3:00 pm SS2-MoA4 Kinetic Control in Epitaxial Growth: Chemisorption to Heteroepitaxy to Homoepitaxy in CaF<sub>2</sub>/Si(111)<sup>1</sup>, Uwe Hessinger, M. Leskovar and Marjorie A. Olmstead, Department of Physics, FM-15, Univ. of Washington, Seattle, WA 98195.**

Crystal growth by molecular beam epitaxy is inherently a kinetic process, and the growth mode and morphology depend on the chosen kinetic parameters—flux and substrate temperature—in relation to the materials parameters—diffusion barriers, adsorption energies, and island or terrace sizes. For heteroepitaxial growth of dissimilar materials, these materials parameters will be different for each of the first few layers. We have applied kinetic models to explain the complex system of growth modes we observe with transmission electron microscopy and X-ray photoelectron diffraction for such a heteroepitaxial system, CaF<sub>2</sub> on Si(111).

The extent of dissociation of CaF<sub>2</sub> to CaF in the first layer can be controlled with temperature. The high temperature (≥600°C) CaF interface layer exhibits lower adsorption energies and diffusion barriers for second-layer CaF<sub>2</sub> molecules than either the undissociated CaF<sub>2</sub> interface (T < 600°C) or subsequent CaF<sub>2</sub> layers. This leads to bilayer growth of the second and third layers at high temperatures, nucleating at surface steps and/or on terraces, depending on the kinetics. The event of nucleating the fourth and subsequent layers with respect to the event of bilayer coalescence determines the extent of a layer-by-layer versus island growth mode. We extend the model to propose a kinetic range for a layer-by-layer growth mode without bilayer formation.

<sup>1</sup>Work supported by the U.S. Dept. of Energy.

**3:20 pm SS2-MoA5 The Influence of Surface Topography on Epitaxial Growth, O. P. Karpenko, D. P. Adams and S. M. Yalisove, Department of Materials Science and Engineering, University of Michigan, Ann Arbor, MI 48109-2136.**

Growth onto non-planar Si substrates was used to study the relationship between starting surface topography and thin film microstructure for heteroepitaxial growth of CoSi<sub>2</sub>. In this study, substrates were prepared by lithographically etching trenches (λ ~ 4 µm, depth ~ 3000 Å) into Si(001) wafers. Following high temperature (T ~ 625°C) Si buffer layer growth and annealing (T ~ 950°C) a number of well defined, high index surfaces including Si(117), (115) and (113) were observed at the sidewalls. Subsequently, these substrates were equilibrated to lower temperatures in order to study the growth of CoSi<sub>2</sub> (using the "template" technique) on each of these surfaces. Heteroepitaxy of CoSi<sub>2</sub> onto each Si(hkl) surface resulted in the nucleation of epitaxial films with different epitaxial orientations. The structure of these films as it relates to the morphology of the starting

surface (different Si(hkl) surfaces and the distribution of facets) will be presented. Based on these results, possible mechanisms for the nucleation of misoriented CoSi<sub>2</sub>(110) grains during heteroepitaxial growth of CoSi<sub>2</sub>(001) onto planar Si(001) substrates will be suggested. These results will be discussed in the context of other materials systems where the initial surface topography has been shown to influence the structure of the resulting film (i.e. Si homoepitaxy).

**3:40 pm SS2-MoA6 Structure of MBE-grown As-rich GaAs(001) Phases, T. Hashizume, Q. K. Xue, J. Zhou, A. Ichimiya<sup>a</sup> and T. Sakurai, Institute for Materials Research (IMR), Tohoku University, Sendai 980-77, Japan, <sup>a</sup>Department of Applied Physics, Nagoya University, Nagoya 464, Japan.**

Understanding the structure of the GaAs(001) surfaces grown by molecular-beam epitaxy (MBE) is one of the most important issues of the recent semiconductor industry. In order to thoroughly study this system, we have applied a MBE-STM instrument, which is a combination of a commercial MBE and the FI-STM (field-ion scanning tunneling microscope) equipped with AES, RHEED.

Three phases of the As-rich (2 × 4); α, β and γ phases, classified by Farrell and Palmstrom<sup>1</sup>, and c(4 × 4) phase are analyzed in detail based on the high resolution STM images, simultaneous RHEED observations and dynamical RHEED calculations. We have found that the unit cell of the (2 × 4)-α, β and γ phases *all has the same structure of two As dimers and two dimer vacancies* in the topmost layer, in contrast to the general belief that a unit of the three As-dimers and one dimer vacancy is energetically favored. Our systematic study shows that the α and β phases have different second and third layer structures which are exposed by the As dimer vacancy rows and that the γ phase is the locally ordered β phase with large open areas exposing the As double layer structures which is the locally ordered c(4 × 4) phase. The two As-dimer structure we propose agrees with the recent theoretical calculation by Northrup and Froyen.<sup>2</sup>

<sup>1</sup>H. H. Farrell and C. J. Palmstrom, J. Vac. Sci. Technol. **B8**, 903 (1990).

<sup>2</sup>J. E. Northrup and S. Froyen, Bull. Amer. Phys. Soc. **39**, No. 1 (1994) p. 215.

**4:00 pm SS2-MoA7 Simultaneous Measurement of Structure and Chemistry During Growth of GaAs by Chemical Vapor Deposition, P. H. Fuoss<sup>a</sup>, D. W. Kisker<sup>b</sup>, G. B. Stephenson<sup>b</sup>, I. Kamiya<sup>c</sup>, S. Brennan<sup>d</sup>, L. Mantese<sup>c\*</sup>, and D. E. Aspnes<sup>c\*</sup>, <sup>a</sup>AT&T Bell Laboratories, <sup>b</sup>IBM T. J. Watson Research Laboratory, <sup>c</sup>JRDC and Imperial College, <sup>d</sup>SSRL, and <sup>e</sup>NCSU.**

Chemical vapor deposition (CVD) represents a complex interplay between chemistry and surface structure, making detailed understanding difficult to achieve. As a step toward this goal we report the first simultaneous measurement of surface chemistry and atomic order using reflectance-difference spectroscopy (RDS) and grazing-incidence X-ray scattering (GIXS), respectively, specifically on (001) GaAs. We use GIXS to determine both short- and long-range order, i.e., surface reconstructions and island sizes, and RDS to determine surface-induced optical anisotropy, which is sensitive to local surface reconstructions and chemical effects. During layer-by-layer growth both GIXS and RDS signals exhibit oscillations whose periods are identical, thereby unambiguously connecting the RDS oscillations to layer-to-layer growth. Using these complementary probes, we have performed a systematic investigation of CVD as a function of temperature, growth rate, V-III ratio, and precursor species. Here, we focus on dynamic measurements during growth. Key results are that the crossover between layer-by-layer and step-flow growth modes depends on the V-III ratio, and that the amplitudes of GIXS and RDS oscillations depend differently on process parameters, in particular on the partial pressure of tertiarybutylarsine. Additional results that take advantage of this unique combination of data to develop a more complete picture of CVD will also be discussed.

\*Supported by ONR Contract N-00014-93-1-0255.

**4:20 pm SS2-MoA8 Heterostructures with Large Lattice Mismatch: Interaction of GaSe with GaAs(111), L. E. Rumaner and F. S. Ohuchi, Department of Materials Science and Engineering, University of Washington, FB-10, Seattle, WA 98195.**

Van der Waals Epitaxy (VDWE) allows for the growth of heterostructures, where the films are chosen based on the property of interest rather than lattice matching constraints. Films of GaSe have been grown on the surface of GaAs(111) by VDWE, overcoming a lattice

mismatch of 6%. In this study, GaSe was sublimated from a single solid GaSe source. Detailed RHEED and XPS studies of the nucleation of GaSe on the GaAs(111) surface indicates Se termination of the GaAs surface dangling bond occurs prior to GaSe formation. Randomly oriented GaSe islands nucleate at submonolayer coverages and are observed in RHEED by relatively broad, randomly oriented streaks corresponding to the GaSe lattice spacing. While the interaction of the substrate with the film is not strong enough to form an epitaxial structure, it is strong enough to dictate a favorable orientation relationship. As the nucleated grains grow larger, the broad streaks in the RHEED pattern become narrower and a six-fold rotational symmetry is observed. This corresponds to one favorable orientation of GaSe on the GaAs(111) surface, with the GaSe symmetrically oriented parallel to the underlying GaAs.

**4:40 pm SS2-MoA9 Morphology of GaAs(001) Grown by Solid- and Gas-Source Molecular Beam Epitaxy, Joseph E. Van Nostrand, S. Jay Chey, David G. Cahill, A. E. Botchkarev and H. Morkoc,** Materials Research Lab, Coordinated Science Lab, and the Department of Materials Science, University of Illinois, Urbana, IL.

We use a scanning tunneling microscope operating in UHV to compare the growth morphology of GaAs(001) prepared using solid-source ( $\text{As}_2$ ) and gas-source ( $\text{AsH}_3$ ) MBE. We evaluate the effect of temperature and the presence of hydrogen on surface morphology. Films were deposited on the (001) surface miscut  $0.25^\circ$  towards [110] at both  $585^\circ\text{C}$  and  $650^\circ\text{C}$  with a deposition rate of  $1 \mu\text{m/hr}$ . Samples were cooled from the growth temperature to  $400^\circ\text{C}$  in approximately 300 seconds. They were then transferred in UHV from the growth chamber to the STM analysis chamber. Surfaces grown at  $585^\circ\text{C}$  using solid-source As and an As cracker display an ordered multilevel system of elongated terraces  $5000 \times 700 \text{ \AA}$ , where the larger dimension is along the [110] direction. The surface morphology of GaAs(001) prepared using  $\text{AsH}_3$  is isotropic with irregular shaped steps. Domains of the surface reconstruction on the gas-source grown buffer layer are approximately  $600 \text{ \AA}$  in diameter. At  $650^\circ\text{C}$ , island sizes for both the solid-source and gas-source grown surfaces become considerably smaller than the terrace width.

Supported by the US Department of Energy grant no. DEFG02-91-ER45439 through the University of Illinois Materials Research Laboratory.

**5:00 pm SS2-MoA10 Diffusion Barriers on GaAs:Sn (100) Surfaces\*, S. M. Seutter, A. M. Dabiran, X. Song, B. E. Ishaug, and P. J. Cohen,** University of Minnesota, Minneapolis, MN 55455.

Ultra-high vacuum, scanning tunneling microscopy (UHV-STM) and atomic force microscopy (AFM) in air have been used in conjunction with reflection high-energy electron diffraction (RHEED) to study the molecular beam epitaxial growth of GaAs on a delta-doped layer of Sn. Fractional monolayers (ML) of Sn were adsorbed onto singular GaAs(100) surfaces in an  $\text{As}_4$  flux and at a substrate temperature of  $600^\circ\text{C}$ . For growth at these temperatures, Sn is known to segregate to the surface; and dramatic changes in the growth kinetics have been observed by RHEED. The latter includes an enhancement of the layer by layer growth, an increase in Ga and Al surface diffusion, and strong beats in the RHEED intensity oscillations. Sn covered surfaces, with and without GaAs overgrowth, were characterized by AFM and STM. For surfaces without GaAs overgrowth, the surface morphology was relatively unchanged from that without a Sn layer. With 20 nm of GaAs growth, the step density increased and monolayer deep holes formed. UHV-STM images showed the surface to be covered with small islands oriented in skewed rows parallel to the step edges. On the upper side of step edges a denuded zone formed while the small islands bunched together on the lower side of step edges and inside the holes. There was no directional anisotropy to the denuded zone. The results are interpreted in terms of diffusion barriers at step edges.

\*Partially supported by the National Science Foundation (DMR93-07852).



## NANO 3/NANOMETER-SCALE SCIENCE AND TECHNOLOGY

Room A209 – Session NS1-MoA

### Nanostructure Properties: Structural and Electronic

Moderator: J. N. Randall, Texas Instruments.

**2:00 pm NS1-MoA1 Scanned-Probe Measurements of CdSe Quantum Dot Structures, B. Alpers, S. Cohen, G. Hodes, and I. Rubinstein,** Weizmann Institute of Science, Rehovot, ISRAEL 76100.

Size-controlled quantum dots provide a means for tailoring band gaps in semiconductor material. We have electrochemically deposited the semiconductor CdSe on gold with densities ranging from isolated clusters with dimensions of several nm, up to coherent coatings of nominal thickness exceeding 30 nm. The electrical characteristics and morphology of these films have been examined using a combined SFM/STM. A standard STM may be problematic in these measurements due to the enormous conductivity differential between the gold substrate and semiconductor, leading to difficulty in selecting bias conditions. STM images also cannot yield accurate height information under such conditions. However, by using the force between tip and surface for feedback control, surface topography could be obtained, together with conductivity and I/V behavior. Measurements were performed under ambient conditions. Tunneling resistances measured on the gold indicated that point contact between metallized (Pt) tip and the surface was frequently not observed, but mediated by a contaminant layer. By varying operating conditions and comparing the results from different sized particles, it was possible to deduce information regarding the size-dependent electrical characteristics.

**2:20 pm NS1-MoA2 Low Temperature Scanning Tunneling Microscopy Studies of Granular Metal Films, E. Bar-Sadeh, D. Porath, M. Wolovelsky, Y. Goldstein and O. Millo,** Racah Institute of Physics, The Hebrew University of Jerusalem, ISRAEL, and Q. Zhang, H. Deng and B. Abeles, Exxon Research and Engineering, Annandale, NJ.

We are using a cryogenic scanning tunneling microscope to study the electrical-transport and structural properties of very thin granular  $\text{Au/Al}_2\text{O}_3$  films, having metal volume fractions close to and below the percolation threshold. The granular films typically are  $\sim 15 \text{ nm}$  thick and sputter-deposited on top of gold films. We have measured simultaneously topographic images and local tunneling current-voltage (I-V) characteristics perpendicular to the films at cryogenic temperatures. The I-V curves were found to vary qualitatively from one tip position to another over distances of the order of a few nanometers, indicating rapid spatial variations of the local transport properties. Some I-V traces show metallic behavior, whereas others exhibit pronounced structure due to single-electron charging effects of the small metal grains. Among these latter traces we observed Coulomb blockade and the Coulomb-staircase, similar to those observed for double-barrier tunnel junction systems. Many of our I-V characteristics exhibit, however, novel Coulomb-staircase structures having unusual variations in step heights and widths due to complex electron tunneling paths. These characteristics cannot be explained assuming a double-barrier tunnel junction geometry. We have developed a triple-barrier tunnel junction model, based on the "orthodox" theory for single electron tunneling, where electrons tunnel through two small metallic grains along their path. This model accounts very well for the experimental results.

**2:40 pm NS1-MoA3 Properties of Nanostructures—Electronic, Haroon Ahmed,** Cavendish Laboratory, University of Cambridge, UK.

Nanometre scale structures in semiconductors offer possibilities of making electronic devices in the future that overcome some of the limitations that arise when conventional devices are scaled down to smaller and smaller sizes. The transport of electrons in lateral and vertical nanostructures in systems such as 2DEGS can be reduced to 1D or 0D conditions. Novel quantum effects can be observed in such structures such as electron interference and ballistic transport. Another example of such devices exploit the well known Coulomb blockade effect. This effect is observed when current flow is interrupted by the presence of a single electron on an isolated nanoscale island. The requirement is that  $e^2/2C$  where  $C$  is the island capacitance is much greater than  $kT$ . The effect is observed in many systems at low temperature but for room temperature observation the islands must be reduced to nanometre scales so that  $C \leq 10^{-18} \text{ F}$ . Another interesting

example of nanotechnology in electronics arises from the need to make artificial silicon structures that mimic the properties of porous silicon. In this case the pores are  $\sim 2$  nm or less in diameter and therefore nanostructures of this size must be created in arrays as artefacts in silicon. There are several fabrication techniques that are contenders for making sub 10 nm structures in semiconductors, electron beam lithography, STM and single atom lithography. With these methods quantum effect devices and single electron devices may be realised.

**3:20 pm NS1-MoA5 Voltage Oscillation Observed in Two Dimensional Nanostructures Using Liquid Crystal Molecules at Room Temperature, H. Nejoh, M. Aono and M. Tsukada,** Aono Atomcraft Projects, JRDC, 5-9-9 Tohkohdai, Tsukuba 300-26 Japan, RIKEN and University of Tokyo.

When liquid crystal (LC) molecules are used as the central electrodes of an array of two-dimensional tunnel junction (TDTJ) which consists of LC molecules and metal islands, the capacitance between molecules and islands is restricted by the size of the LC molecule ( $0.5 \text{ nm} \times 1.5 \text{ nm}$ ). Conventionally, tunnel junction arrays have been fabricated using lithography so that the characteristic size was of the order of 100 nm. Single electron charging has been observed in such systems only at cryogenic temperatures. Since the size of the TDTJ using LC molecules is of the order of nm, the corresponding Coulomb energy becomes larger than room temperature. We have observed voltage oscillation across the current biased TDTJ where the STM tip was held above an LC molecule and acted as a gate by ramping the tip voltage at room temperature. This structure has the disadvantage that the TDTJ is not properly isolated from the external circuit. We propose to overcome this problem by using a metal-coated AFM cantilever, where this cantilever will act as gate and a double tunnel junction will be fabricated by scratching a lead wire with the AFM cantilever and placing LC molecules in the groove.

**3:40 pm NS1-MoA6 Charge Dissipation and its Phase Transition of Densely Contact-Electrified Electrons on a Thin Silicon Oxide, Y. Sugawara, Y. Fukano, T. Uchihashi, T. Okusako, T. Tsuyuguchi, S. Morita, Y. Yamanishi\* and T. Oasa\*,** Department of Physics, Faculty of Science, Hiroshima University, Higashi-Hiroshima, Hiroshima 724, Japan, \*Advanced Technology Research Laboratories, Sumitomo Metal Industries, Ltd., Amagasaki, Hyogo 660, Japan.

Recently, Saurenbach and Terris [1] and we [2], independently, succeeded in performing reproducible and controllable contact electrification of a thin insulator using an atomic force microscope (AFM) with a conductive cantilever.

In the present experiment, we investigated the charge dissipations of the densely contact electrified electrons on a thin silicon oxide surface quantitatively, using the newly developed contact-electrification method. As a result, by increasing the density of the deposited electrons, we observed an appearance of a stable state of the densely deposited electrons and its disappearance due to the charge dissipation, i.e., a kind of stable-unstable phase transition. We also observed a saturation of the density of the deposited electrons with the spatial spread of deposited electrons. We further observed the electrostatic force related to positively charged trap site in a silicon oxide layer in addition to that induced by the deposited electrons on the silicon oxide surface. By comparing the charge dissipation in vacuum with that in air, finally, we discussed the dissipation processes of the contact electrified electrons.

[1] F. Saurenbach and B. D. Terris: IEEE Trans. on Industry Applications, 28 (1992) 256.

[2] S. Morita et al.: Jpn. J. Appl. Phys. 32 (1993) 2983.

**4:00 pm NS1-MoA7 Strain Relieving of Epitaxially Grown Ge Layers on Si Mesa Structure, Y.-H. Khang and Young Kuk,** Department of Physics, Seoul National University, Seoul 151-742, Korea.

Though the critical thickness and other elastic properties have been well understood in the  $\text{Ge}_x\text{Si}_{1-x}/\text{Si}$  system, the misfit dislocation and/or misfit strain have been one of the biggest stumbling blocks for the better performance of the devices.

In a small island, the epitaxial film with rather large misfit strain (larger than Frank-van der Merwe limit) can be grown. In order to understand the electronic structural dependence on the misfit strain, we have grown Ge epitaxial layer on Si mesa structures: with varying sizes ranging  $0.6 \mu\text{m} \sim 30 \mu\text{m}$  patterned by electron lithography. The strain dependence was studied by scanning tunneling microscope/spectroscopy, UPS and Raman spectroscopy. The strain relieving via step arrangement was observed in STM/STS and the shift of phonon peak

was observed in Raman spectroscopy. We'll compare these observed electronic structural changes with the calculation by perturbation theory. In addition, we'll suggest the possible configuration of the direct bandgap in the strain relieved Ge/Si system. The mechanism and possible application will be discussed.

**4:20 pm NS1-MoA8 Atomic-force Microscopy Measurements of Roughness Anisotropy on  $\text{Si}_{1-x}\text{Ge}_x/\text{Si}$  Superlattice Film Surfaces\*, C. Teichert, Y. H. Phang, L. J. Peticolas<sup>1</sup>, J. C. Bean<sup>1</sup>, E. Kasper<sup>2</sup>, M. G. Lagally,** University of Wisconsin-Madison, WI 53706, <sup>1</sup>AT&T Bell Laboratories, Murray Hill, NJ 07974, <sup>2</sup>Universität Stuttgart, Germany.

The surface roughness of  $\text{Si}_{1-x}\text{Ge}_x/\text{Si}$  superlattices grown by molecular-beam epitaxy on vicinal Si(001) has been characterized by *ex situ* atomic-force microscopy. At high Ge concentration in the alloy layers the surface exhibits a one-dimensional waviness with an average ripple spacing of about 450 nm to 1  $\mu\text{m}$  and an amplitude of  $\leq 1$  nm. The ripple orientation is always parallel to the substrate steps. The characteristics of this waviness, including cross section of the ripples, domain size of areas with undisturbed waviness, and lateral correlation length of the underlying isotropic roughness are determined as a function of the substrate miscut, the individual-layer thickness, and the number of bilayers. On the basis of these morphological data, together with corresponding x-ray diffraction results on the buried interfaces [1], a model, based on stress accommodation, for the origin of this roughness anisotropy and its spatial evolution is developed.

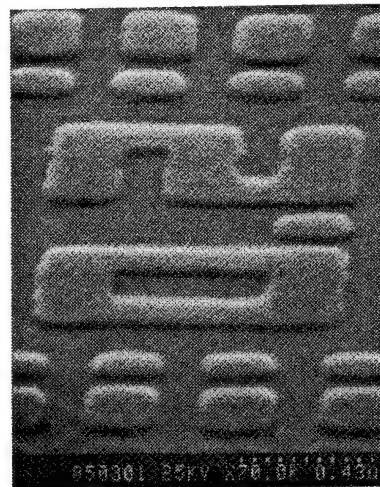
\*Research supported by NSF Grant No. DMR 92-01856. One of us (C. T.) acknowledges support by the German Academic Exchange Service.

[1] Y. H. Phang, C. Teichert, L. J. Peticolas, J. C. Bean, E. Kasper, M. G. Lagally, submitted to Phys. Rev. B.

**4:40 pm NS1-MoA9 Submicron Lithographically Patterned Magnetic Islands for Magnetic Recording, R. M. H. New, R. F. W. Pease, R. L. White,** Stanford University, Stanford, CA 94305.

In conventional hard-disk magnetic recording systems, the signal to noise ratio is limited by "transition" noise which occurs due to the irregular zig-zag domain walls between adjacent recorded bits. In order to address this problem, we have been studying recording media composed of submicron lithographically defined islands of magnetic material. We have developed a procedure using direct write electron-beam lithography for high resolution patterning of magnetic thin films, and we have used this procedure to define large arrays of small magnetic particles. We are studying the characteristics of these particles with both bulk measurement techniques and with high resolution magnetic imaging methods to determine if they will be suitable for high density recording systems. Theory suggests that sufficiently small magnetic islands will behave like single-domain particles with only two stable magnetisation states. Such particles would be ideal for storing a single bit of information.

The scanning electron micrograph to the right shows a patterned thin film of cobalt. The film is 200 Å thick, and the smallest feature size is 0.2  $\mu\text{m}$ . The picture is taken from an angle of 15°, measured from the surface of the film. This work was performed under NSF contract number ECS 8920652.



5:00 pm **NS1-MoA10 Ferroelectric Domain Dynamics Investigated By Atomic Force Microscopy**, O. Kolosov<sup>1,2</sup>, A. Gruverman<sup>3</sup>, J. Hatano<sup>4</sup>, K. Takahashi<sup>3</sup> and H. Tokumoto<sup>2</sup>, <sup>1</sup>Mechanical Engineering Laboratory, Tsukuba, Ibaraki 305, JAPAN, <sup>2</sup>Joint Research Center for Atom Technology, ATP and NAIR, Tsukuba, Ibaraki 305, JAPAN, <sup>3</sup>National Institute for Research in Inorganic Materials, Tsukuba, Ibaraki 305, JAPAN, <sup>4</sup>Science University of Tokyo, Faculty of Industrial Science and Technology, Noda, Chiba 278, JAPAN.

The domain structure in ferroelectric crystal guanidinium aluminum sulfate hexahydrate (GASH) and its evolution under the action of electric field were studied by atomic force microscopy (AFM) with nanoscale resolution. The ferroelectric domains were directly observed on the cleavage surface of crystal using AFM operating in both contact and noncontact modes. To distinguish the contrast associated with topography from that related to electrostatic interaction between tip and polarization charges, two types of cantilevers were used, namely, standard nonconductive Si<sub>3</sub>N<sub>4</sub> tip and gold coated conductive one. To investigate the domain dynamics a constant potential was applied to the bottom electrode, while conductive tip was held at zero potential.

The domain structure in the form of rows of cylinder domains along with configuration consisting of domains of one sign embedded into the larger domain of opposite sign was observed in topography image. The origin of domain contrast was discussed. The AFM images were compared with domain patterns revealed by powder deposition technique.

The domain dynamics in applied electric field was studied for the first time with nanoscale resolution. It was directly observed that sidewise growth of domains proceeds through nucleation on the domain wall. The estimations of nucleus size as well as of electric field, required for domain growth, showed a good agreement with experimental results. The ability of effective control of the domain structure with AFM was directly demonstrated.

## NANO 3/NANOMETER-SCALE SCIENCE AND TECHNOLOGY

Room A207 - Session NS2-MoA

### Nanometrology

**Moderator:** E. C. Teague, National Institute for Standards and Technology.

2:00 pm **NS2-MoA1 Dimensional Metrology with Scanning Probe Microscopes**, J. E. Griffith, AT&T Bell Laboratories, Murray Hill, NJ 07974-0636.

By the end of the decade, semiconductor manufacturers will need measurements of surface topography with lateral uncertainties of a few nanometers and vertical uncertainties of less than a nanometer. Scanning probe microscopes have the potential to meet these needs, but only if the microscopes' behavior is tightly controlled. The dominant source of measurement error arises from the probe tip, which interacts with the measured surface in an intrinsically nonlinear manner. A fundamental requirement is that the probe shape be stable and well characterized. In our instrument we use conical Ir probes formed with focused ion beams and cylindrical glass probes chemically etched from optical fibers. Our force microscope is able to employ a wide range of probe types because of the force sensor, which does not depend on microlithographically patterned cantilevers. We use instead a force-balance scheme that drives a rather large, and rugged, balance beam. The pivots for the beam are small ball bearings constrained by a magnet, which allows easy tip exchange. Balancing of the beam is effected through two capacitors, which also provide force sensing. A set of three capacitors are also used to monitor the position of the scan head. Though capacitors can be extremely precise position sensors, significant position measurement uncertainties can arise from Abbe offsets between the probe and the monitor. The extent to which this affects measurements will be discussed. Our probe microscope has been used to nondestructively measure high-aspect-ratio features on lithographically patterned photomasks and wafers. **INVITED**

2:40 pm **NS2-MoA3 Proximal Probe Characterization**, Leigh Ann Files, John N. Randall, Texas Instruments, Inc., and David Keller, University of New Mexico.

One of the primary problems with the transition of Scanning Probe Microscopes (SPMs) from the "picture" to the metrology stage is the difficulty in extracting the true profile of a sample from the apparent

profile obtained as a result of convolution of the tip shape with the sample. High aspect ratio tips have been fabricated to help alleviate this problem, but it is difficult to fabricate such tips reproducibly, and they are rather fragile. This can present difficulties when using an SPM to monitor feature sizes in a wafer fabrication area. If the tip breaks while scanning a small feature, much larger dimensions may be measured, and it may erroneously be presumed that the lithography of the sample being scanned is the problem. Thus a method to characterize the tip is needed. It has been proposed that one could scan a standard feature of known dimension and combine two halves of the scan line to obtain an inverted image or replica of the probe tip<sup>1</sup>. Such a standard could be used to qualify or "grade" tips as they are fabricated to determine the maximum sidewall and minimum dimensions they are suitable for measuring. It could also be used to monitor the tip quality at appropriate intervals during scanning. We have used electron beam lithography to pattern such a standard. Arrays of features up to 0.5  $\mu\text{m}$  in height and ranging from 0.1 to 5  $\mu\text{m}$  in diameter with a 20 nm thick ledge are formed by anisotropic dry etching followed by isotropic selective etching of a multilayer stack. Envelope image analysis<sup>2</sup> has been used in conjunction with this standard to extract probe shapes from profiles to determine the structure of a number of commercially available probes.

<sup>1</sup>Griffith, et al., "Technology of Proximal Probe Lithography," Vol. IS10 SPIE (1993).

<sup>2</sup>D. Keller and F. Franke, "Surface Science" Vol. 409 (1993).

3:00 pm **NS2-MoA4 Maximizing the Information Content of Scanning Probe Microscopy Data**, P. M. Williams, M. C. Davies, T. O. Glasbey, D. E. Jackson, C. J. Roberts, K. M. Shakesheff and S. J. B. Tendler, Laboratory of Biophysics and Surface Analysis, Department of Pharmaceutical Sciences, The University of Nottingham, Nottingham, NG7 2RD, UK.

Scanning probe microscopy has revolutionized the field of surface science. Recently, however, much emphasis has been placed on the mechanisms of image formation and the degradations imposed on image data. The effect of probe geometry has been studied by several workers and mechanisms have been proposed and adopted for image refinement. Here we detail a method for the derivation of probe geometry from any probe microscopy image. The method eliminates all assumptions concerning probe profile and permits the reconstruction of image surfaces without any prior knowledge of the tip.

An algorithm will be described that extracts a possible probe geometry from an image and is demonstrated on scanning force microscopy studies of semiconductor and polymer samples. The derived probe profiles are then validated by their comparison with electron microscopy images. Furthermore, details will be given of an image reconstruction technique which permits the assignment of true sample features allowing the quantification of image degradation. Such assignments are critical to the rigorous validation of image data by comparison with those from complementary imaging techniques. Finally, recent progress in developing a novel technique for extracting surface friction and compliance data, as an extension to the algorithms described, will be presented.

3:20 pm **NS2-MoA5 Estimation of Proximal Probe Microscope Tip Geometry without Calibrated Reference Artifacts**, J. S. Villarrubia, National Institute of Standards and Technology, Gaithersburg, MD 20899.

Proximal probe techniques such as scanning tunneling microscopy (STM) or atomic force microscopy (AFM) routinely achieve image resolutions of 1 nm or better, making them good candidates for dimensional measurement tools in the otherwise difficult sub- $\mu\text{m}$  regime. However, the tip shape is "convolved" (strictly, dilated) with the surface, resulting in imaging errors which can be significant at the size scales of interest. Parts of the actual surface which were touched by the tip may be reconstructed if the geometry of the tip is known. For this reason, much attention has recently focused on reconstructing tip shapes by imaging known reference artifacts. Mathematically this procedure is well-defined, but calibrating and maintaining stable reference artifacts to nanometer accuracies is not trivial. Fortunately, for many purposes it may not be necessary. Using a mathematical model of the imaging process, I will show that for each point on an image there is a corresponding surface which is an upper bound on the tip. The actual tip must be smaller than or equal to the largest tip which satisfies all of the bounds. Images of surfaces with high relief and narrow, steep features provide tight bounds on the tip geometry. Model calculations indicate good reconstruction of tips for easily manufacturable reference artifacts, *the geometry of which need not be known in detail*.



3:40 pm **NS2-MoA6 Stability and Engineering of Ultra-Sharp Tungsten Tips**, *Ming L. Yu, Brian W. Hussey, Ho-Seob Kim, and T. H. Philip Chang*, IBM Research Division, T. J. Watson Research Center, Yorktown Heights, NY 10598.

Engineering of ultra-sharp tips has made significant progress recently. Procedures encompass oxygen treatment, ion bombardment, and thermal-field build-up. These tips with atomic sharpness are particularly attractive for scanning probe microscopies and as high brightness field emission electron sources such as in our STM aligned electron-beam microcolumns. Emission stability of these tips is frequently a major concern. We have made a systematic study of the stability issue using field emission and correlated the results with the structures of the tips as determined by field ion microscopy. We found that ultra-sharp tips are particularly vulnerable to instabilities caused by the surface migration of tungsten atoms near the apex. There are two driving forces for the motion of the atoms. The first one is from surface tension which moves the atoms in a direction to minimize the gradients of the principal radii of curvature. The second is from electrostatic stress which drives the atoms to locations with maximum local electric field. The mobility of the atoms, on the other hand, depends both on the activation energy for surface diffusion and the operation temperature. We shall report our results on  $W\langle 100 \rangle$ ,  $W\langle 111 \rangle$  and  $W\langle 310 \rangle$  single crystal tips to illustrate the importance of low mobility on the facet at the apex, and demonstrate how to engineer the geometry of the tip to modify the field distribution for better stability.

Research partially supported by ARPA Contract F49620-93-C-0068.

4:00 pm **NS2-MoA7 Scanning Tunneling Microscope with Three-Dimensional Interferometer for Surface Roughness Measurement**, *Toru Fujii, Masataka Yamaguchi and Masatoshi Suzuki*, Nikon Corporation, 1-10-1, Asamizodai, Sagamihara, Kanagawa 228, JAPAN.

Scanning tunneling microscope (STM) has been well known for its high lateral resolution and non-destructive surface profiling capability but its potential as a profiler for roughness and step height measurement has been rarely exploited to its maximum extent because of its unreliable vertical accuracy. We have for the first time developed an STM which is capable of 300  $\mu\text{m}$  line scanning secured by a parallel spring mechanism in X direction with interferometric monitoring STM tip feed-back controlled motion in Z direction along with X and Y raster scanning motion. Step height and pitch measurement on a surface topography standard agrees well with the certified value of the standard. In this study we were successful in combining the superior lateral resolution of the STM with the better vertical accuracy of interferometric measurement. The result of high accuracy roughness measurement with our STM supports the common observation that STM measurement gives larger roughness than interferometric measurement.

Part of this work was conducted in the program: 'Advanced Material-Processing and Machining System,' consigned to AMMTRA from NEDO, which is carried out under the Industrial Science and Technology Frontier Program enforced by the Agency of Industrial Science and Technology.

4:20 pm **NS2-MoA8 Automated Calibration of the Sample Image Using Crystalline Lattice for Scale Reference in Scanning Probe Microscopy**, *Hideki Kawakatsu, \*Toshiro Higuchi, Hiroshi Kougami, and Pierre Blanalt*, Institute of Industrial Science, \*Faculty of Engineering, University of Tokyo.

In the first part of the paper, automated calibration of the sample image using a dual tunneling-unit scanning tunneling microscope and a scale reference graphite crystal is discussed. Measurements in the hundred nanometer range showed accuracy of around 99.99%. In the latter part of the paper, the use of scanning force microscopy and a crystal to linear scale measurement is introduced. In this technique, the periodic meandering motion of the end point of the tip observed in scanning force microscopy was used. The technique proved to be more robust compared to the method using scanning tunneling microscopy since atomic periodicity is less likely to be lost due to outer disturbances.

4:40 pm **NS2-MoA9 Repeatability and Reproducibility Study of Si Wafer Micro-Roughness by Use of Atomic Force Microscopy**, *A. R. Raheem, E. H. Adem*, Advanced Micro Devices, Sunnyvale, CA 94088.

In the semiconductor industry the Atomic Force Microscope (AFM) has become an invaluable tool for the measurement of surface micro-roughness and topography with sub- $\text{\AA}$  height resolution. Tunnel and gate oxide integrity are a strong function of micro-roughness which depends on the physical and chemical processing of the starting Si

wafers and oxides. The semiconductor industry is demanding improvements in precision, accuracy, repeatability and reproducibility, so that AFMs' can be put on a more metrological footing for routine in-line process control. In this paper the results of an AMD sponsored AFM round robin from 9 laboratories are presented and discussed. Starting Si wafers were etched in a solution of 40:1  $\text{NH}_4\text{F}:\text{HF}$  to create various grades of micro-roughness from 0.5  $\text{\AA}$  to 5  $\text{\AA}$  RMS. In the repeatability study 30 continuous  $2\mu \times 2\mu$  area scans were made using the same probe tip without re-positioning. In the reproducibility study each wafer was sequentially scanned twice using a single tip and re-scanned with a new tip. The results indicate that all the participants were able to resolve each grade of roughness. The minimum reported micro-roughness for polished starting wafers was 0.2  $\text{\AA}$  and maximum was 1.5  $\text{\AA}$  RMS. For the roughest wafer the reported RMS differed by only  $2\times$ . This paper will discuss microroughness variation from tip to tip and pass to pass, seek correlation between contact and non-contact mode of AFM operation and derive a relationship between RMS and PV.

5:00 pm **NS2-MoA10 An Optical Fiber Based Shear Force Microscope For Nanometer-Scale Dimensional Metrology On Large Samples**, *H. M. Marchman*, AT&T Bell Laboratories, Murray Hill, NJ 07974 USA.

The ability to measure topography of micro-fabricated structures in all three dimensions with nanometer-scale accuracy and precision is crucial for the development of sub micrometer (and below) device fabrication techniques as well as a product qualification yardstick for existing ones. A shear force microscope has been constructed for performing dimensional measurements of nanometer-scale features on large samples, such as five inch wafers or lithographic masks. Tip-to-sample regulation is accomplished by optically monitoring the change in vibration amplitude of a light-emitting optical fiber probe, oscillating near its mechanical resonance, as it encounters forces from the sample surface. Attractive mode sensing in the lateral scan direction (for sidewalls) is also possible with this system. The frequency and quality factor (Q) of the mechanical resonance of the light-emitting tip can also be tuned by tailoring the probe shape during fabrication. The cylindrical and undercut etched fiber probes used in this system are also ideal for making accurate dimensional measurements on high aspect ratio structures. In addition, the Abbe offset error that normally occurs during tip position monitoring is significantly reduced by detecting the position of the light that is emitted near the apex of the tip, or proximal point.

## APPLIED SURFACE SCIENCE Room A101 - Session AS-MoA

### Data Processing and Reference Methods

**Moderator:** G. C. Nelson, Sandia National Laboratories.

2:00 pm **AS-MoA1 Auger Electron Spectrometry Data Bank**, *M. P. Seah*, Division of Materials Metrology, National Physical Laboratory, Teddington, Middlesex, TW11 0LW, UK.

An Auger electron spectral data bank has been acquired for most elements in the direct spectral mode at high energy resolution (0.25 eV) with both 5 and 10 keV electron beams. The energy dependence of the spectrometer transmission and its absolute value are calibrated. By removal of (i) the reflected primary electrons, (ii) the secondary electron cascade and (iii) the inelastically scattered Auger electrons, the true Auger electron peak areas may be determined. These true peak area intensities are compared with theoretical predictions using the best available general sources for the cross sections, backscattering, inelastic mean free paths etc at the absolute level with no adjustable parameters. Agreement is excellent. Divergencies do occur, however, in well-defined regions of kinetic energy and atomic number. The reasons for these divergencies will be discussed with recommendations for more convergent approaches. This analysis gives great confidence in the general use of AES for quantitative analysis since all parameters now have traceability to a basic system of accepted theory or the SI measurement system. Recommendations are given for the best way to use the data bank for quantitative analysis.

2:20 pm **AS-MoA2 Multi-spectral Scanning Auger Microscopy of Rough, Chemically Inhomogeneous Samples**, *I. R. Barkshire and M. Prutton*, Department of Physics, University of York, Heslington, York, YO1 5DD, UK.

Auger microscopy is widely used for surface characterisation. However, the presence of surface topography or sub-surface composition variations can often result in the technique being unable to provide even qualitative information. MULSAM has been developed to allow quantitative microanalysis of rough, chemically inhomogeneous systems. MULSAM is a strategy for the acquisition and analysis of multi-spectral image sets, and involves the simultaneous acquisition of secondary electron, sample absorption current, characteristic X-rays, Auger and backscattered electron signals. The exploitation of correlations between the various signals combined with models enables the removal of artefacts due to both topography and sub-surface composition variations. These techniques will be demonstrated with two different types of sample. The first example demonstrates the characterisation of the chemical and topographical variations across wear scars generated using a Plint foil test with model oil formations. The image manipulations prove sufficiently robust to allow meaningful analysis of samples with gross topography. The second example investigates the depth distribution of  $\text{Al}_2\text{Cu}$  precipitates formed in  $1\text{ }\mu\text{m}$  wide  $\text{AlCu}$  interconnects which have undergone electromigration stressing. Ion beam bevelling is employed to expose laterally the depth distribution of elements along the length of the track. The combination of characteristic X-ray, backscattered electron and Auger images allow the determination of the location of surface and sub-surface precipitates.

2:40 pm **AS-MoA3 Surface Microanalysis and Imaging: Data Visualization and Pattern Recognition Applications**, *R. W. Linton*, Department of Chemistry, University of North Carolina, Chapel Hill, NC 27599-3290.

A critical issue in the evolution of surface imaging applications is the effective correlation of multi-dimensional data, both for classification and visualization. One illustration involves the use of imaging secondary ion mass spectrometry, for the 3-D dynamic depth profiling of solid surfaces or the 2-D static mode imaging of molecular microstructures. Even if artifact contrast contributions such as chemical, topographic, and chromatic effects can be evaluated, a problem remains to view 3-D multielemental concentration images with high dynamic range. Possibilities include stereo pairs, holographic display, surface rendering, and true volume rendering using ray tracing. The latter approach is used in combination with shadowing, thresholding and control of voxel opacities to reveal internal structures within a 3-D volume. Pseudocolor is employed to indicate depth scale, multielement correlations, or intensity (concentration) gradients for a given element. Another critical step in the process of reducing SIMS images to chemical or compositional information is segmentation: dividing the images into regions that correspond to structural units. The data intensive nature of SIMS imaging, such as the possibility for acquisition of full mass spectra at each pixel, is a driving force toward the application of multivariate techniques for image classification. This is especially true considering the high dynamic range available in SIMS: the presence or absence of a mass peak often is less informative than the pattern of intensities for various masses. The application of pattern recognition for data classification involves the use of statistical techniques (e.g. principal component analysis, cluster analysis) or artificial neural networks (e.g. Kohonen self-organizing feature maps) to associate each image element (pixel or voxel) with a major group or class. Both approaches are of value in correlating mass selected images to localize molecular species on heterogeneous surfaces. **INVITED**

3:20 pm **AS-MoA5 Numerical Analysis of TOF-SIMS Data**, <sup>1</sup>*Susan G. MacKay*, <sup>2</sup>*Patrick J. McKeown*, <sup>3</sup>*3M Corporation*, 3M Center, 201-25-16, St. Paul, MN 55144, <sup>2</sup>*Perkin-Elmer*, Physical Electronics Division, 6509 Flying Cloud Drive, Eden Prairie, MN 55344.

Interpretation of TOF-SIMS data often involves the recognition of a characteristic fragmentation pattern for a particular species. In the cases of heterogeneous samples or complex mixtures, identification of unknown species becomes increasingly difficult due to chemical interferences. Currently there is a growing interest in applying numerical analysis techniques to help resolve multicomponent spectra, and to aid in searching of spectral databases. In order for statistical techniques to be successfully applied to TOF-SIMS data analysis, some fundamental data processing issues need to be addressed. Preliminary work has been performed which explores instrumental effects on spectral reproducibility. Data was acquired from a model system (acrylate

copolymers) using two different geometry TOF-SIMS instruments. A data matrix was then compiled which combined data acquired on both instruments from identical samples, and from samples prepared from the same copolymer mixtures. The data was then processed and analyzed using partial least squares (PLS) analysis. Various data processing and normalization procedures will be discussed pertaining to both qualitative and quantitative applications.

3:40 pm **AS-MoA6 SIMS vs. the TRIM Code for Depth Profiles of 100 to 350 keV Phosphorus in Silicon**, *K. Miethe, W. H. Gries, J. P. Biersack\*, H. Strusny\*\**, Research and Technology Center, Deutsche Bundespost Telekom, P.O. Box 10 00 03, 64276 Darmstadt, \*Hahn-Meitner-Institut, 14109 Berlin, \*\*Ferdinand-Braun-Institut für Höchstfrequenztechnik, 12489 Berlin, Germany.

Computer simulation of ion-implanted depths profiles and of the broadening function resulting from ion-bombardment during measurement of these profiles by secondary ion mass spectrometry (SIMS) is of cardinal importance for certification of these profiles in ion-implanted reference materials (e.g. W. H. Gries, J. Vac. Sci. Technol. A7, 1639, 1989, and Proc. 9th Int. Conf. on SIMS, Yokohama, 1993). A feasibility study is being undertaken on the system phosphorus in silicon at a dose density level of  $10^{18}\text{ cm}^{-2}$ . Phosphorus has been ion-implanted in pre-amorphized silicon wafers in an energy-calibrated research implanter at six energies between 100 and 350 keV. SIMS measurements (in a scanning-beam quadrupole instrument) are accompanied by computer simulations of the broadening function by a dynamic TRIM code, while the as-implanted profiles are simulated by use of another TRIM code. A status report is being presented.

4:00 pm **AS-MoA7 The Development of Standard Reference Material 2137—A Boron Implant in Silicon Standard for Secondary Ion Mass Spectrometry**, *D. S. Simons*, Chemical Science and Technology Laboratory, National Institute of Standards and Technology, Gaithersburg, MD 20899.

Ion implants are recognized as valuable reference materials for secondary ion mass spectroscopy (SIMS), because the integral of the concentration as a function of depth is equal to the retained ion dose or fluence. We chose to develop a Standard Reference Material for SIMS based on ion implantation of boron in silicon. Boron is the most common dopant in silicon semiconductor technology, and the dose of the isotope  $^{10}\text{B}$  can be measured by a nuclear reaction method known as Neutron Depth Profiling. The starting material for the standards was a batch of 24 commercial n-type silicon (100) single crystal wafers of 76-mm diameter, polished on one side. The polished side of the wafer was implanted with  $^{28}\text{Si}$  ions to render the surface sufficiently disordered that it would appear to be amorphous to the  $^{10}\text{B}$  ion beam. The purpose was to eliminate ion channeling of the boron that would otherwise produce a more complicated profile shape, which could vary across the surface of a wafer. The  $^{28}\text{Si}$  ions were implanted at three different energies to create lattice disorder over the entire range of the boron implant. The  $^{10}\text{B}$  was implanted at a nominal energy of 50 keV and a nominal dose of  $1 \times 10^{15}\text{ atoms/cm}^2$ . The wafers were then cut into  $1 \times 1\text{ cm}$  squares with a wafer saw. Twenty-one squares, each at least 7 mm from the outer edge, were obtained from each wafer. Extensive NDP measurements were made on three wafers to determine the certified boron ion dose. Thirty-one dose measurements were made on 21 individual samples, with 10 replicates. The final certified dose of  $^{10}\text{B}$  is  $1.018 \pm 0.035 \times 10^{15}\text{ atoms/cm}^2$ , the stated uncertainty being a 95% coverage, 95% confidence tolerance interval that takes into account the spatial variation of the implantation process.

4:20 pm **AS-MoA8 Elemental Binding Energies for X-Ray Photoelectron Spectroscopy**, *C. J. Powell*, National Institute of Standards and Technology, Gaithersburg, MD 20899.

The binding energies (BEs) of core electrons in elemental solids have been measured and reported by many scientists but there are, unfortunately, significant discrepancies among the published data. I will report on an analysis of BE data from four sources [1-4]. For each set of data, a single instrument has been used to measure BEs for many elements. In order to compare BEs from these sources, it was necessary to recalibrate the instrumental BE scales of three instruments using NPL reference data [5] and a draft ASTM E-42 standard. Mean BEs were then computed for elements and core levels for which there were two or more measurements. Finally, individual differences from the mean values were calculated; this analysis disclosed several discrepancies in data due either to differences in specimens or to possible

mistakes. Plots of differences in BE values from mean values versus BE indicated systematic trends in the BE measurements from each source.

1. S. Svensson *et al.* J. Elect. Spectr. **9**, 51 (1976); A. Berndtsson *et al.* Phys. Stat. Sol. (b) **93**, K103 (1979); N. Martensson *et al.*, J. Electron Spectr. **19**, 299 (1980); R. Nyholm and N. Martensson, J. Phys. C **13**, L279 (1980); R. Nyholm *et al.*, *ibid.* **13**, L1091 (1980); A. Lebugle *et al.* Phys. Scripta **23**, 825 (1981).
2. N. Ikeo *et al.*, *Handbook of X-Ray Photoelectron Spectroscopy* (JEOL, 1991).
3. J. F. Moulder *et al.*, *Handbook of X-Ray Photoelectron Spectroscopy* (Perkin-Elmer, 1992).
4. B. V. Crist (private communication).
5. M. P. Seah, Surf. Interface Anal. **14**, 488 (1989).

4:40 pm **AS-MoA9 On the Nature of the Use of Adventitious Carbon as a Binding Energy Standard**, Tery L. Barr, Sudipta Seal, University of Wisconsin-Milwaukee 53201.

It has become common practice to employ as a binding energy reference for XPS studies of nonconductive materials the C(1s) spectra of the ubiquitous (adventitious) carbon that seems to exhibit an instantaneous presence on all air exposed materials. Despite this commonality, surface scientists, including many practitioners, have substantial concerns about the validity of this approach. A detailed discussion is presented of the method including a consideration of the types of materials and the electronic energy states involved, e.g., Fermi edges, vacuum levels, etc., and the couplings that must exist between these states. Also described is the physical status that the material being examined and the adventitious carbon must be in for the referencing method to be correctly applied. A number of other surface environments are presented for which the carbon referencing method may be fallacious. This leads to a consideration of the ESCA results for the different types of adventitious species and how the presence of some of these may confuse the use of the method. In this regard, we will also discuss the use of other methods to establish binding energy scales, such as Fermi edge coupling and select doping (e.g., the Au dot approach). Finally, we will consider the use of the carbon referencing method and the status of adventitious carbon during studies of polymers and other carbonaceous materials.

## PLASMA SCIENCE

### Room A109 - Session PS-MoA

#### Plasma Deposition

Moderator: W. Holber, ASTeX, Inc.

2:00 pm **PS-MoA1 Plasma Assisted Deposition of Diamond Films**, T. D. Mantei, Department of Electrical and Computer Engineering, University of Cincinnati, Cincinnati, Ohio 45221.

The synthesis of diamond by chemical vapor deposition (CVD) methods has opened a new regime of diamond film applications at moderate temperatures and pressures. Synthetic diamond can be grown from carbon-containing gases on a variety of substrates at temperatures below 1000°C and at subatmospheric pressures, with gas activation furnished by a heated filament, laser irradiation, or electron impact in a radio frequency or microwave plasma. The emphasis in this paper will be on plasma assisted CVD of diamond from methane or other gaseous hydrocarbon precursors in a hydrogen plasma environment. Although diamond is metastable with respect to graphite and the kinetics of graphite growth are faster than for diamond, the barrier to diamond growth can be overcome by providing an adequate supply of atomic hydrogen; a principal role of the plasma deposition reactor is thus to generate sufficient atomic hydrogen while controlling the accompanying ion flux. Current diamond deposition reactors will be compared, including microwave applicators and ECR sources. The effects of additives, including oxygen and halogens, will be considered, and recent results on low temperature and low pressure diamond growth in pulsed magnetoactive microwave discharges will be discussed.

INVITED

2:40 pm **PS-MoA3 An Investigation of SiO<sub>2</sub> PECVD Using Attenuated Total Reflection Fourier Transform Infrared Spectroscopy**, S. C. Deshmukh and E. S. Aydil, Department of Chemical and Nuclear Engineering, University of California Santa Barbara, CA 93106.

*In situ* attenuated total reflection Fourier transform infrared (ATR-FTIR) spectroscopy was used to study surface processes during plasma enhanced chemical vapor deposition (PECVD) of silicon dioxide through tetraethylorthosilicate (TEOS) and oxygen. ATR-FTIR studies were conducted on thin (50–100 Å) silicon dioxide films deposited on GaAs. This approach allowed us to obtain the infrared spectrum of SiO<sub>2</sub> surfaces in the spectral region 4000 cm<sup>-1</sup>–770 cm<sup>-1</sup> and to determine the surface species and their relative surface concentrations as a function of deposition conditions in a helical resonator plasma reactor. Studies were conducted where SiO<sub>2</sub> surface was exposed to TEOS and O<sub>2</sub>-plasma sequentially and/or simultaneously. Surface processes were studied as a function of TEOS exposure and substrate temperature. *In situ* ATR-FTIR studies of adsorption of TEOS on SiO<sub>2</sub> surface show that TEOS adsorbs physically onto the SiO<sub>2</sub> surface below ≈ 100°C. Hence, during PECVD of SiO<sub>2</sub> below this temperature, physically adsorbed TEOS can be trapped in the growing oxide giving rise to increased ethoxy and O-H species which in turn adversely affect the film integrity and quality. At higher temperatures (> 100°C), TEOS adsorbs irreversibly and chemically onto SiO<sub>2</sub>. SiO<sub>2</sub> growth was found to occur even without an oxygen plasma at temperatures as low as 200°C, albeit very slowly. Exposure of adsorbed TEOS to O atoms (oxygen plasma) removed the ethoxy ligands of the surface ethoxy-siloxanes, produced surface OH species and resulted in deposition of SiO<sub>2</sub>. The insight gained from the ATR-FTIR studies allowed us to deposit, from an O<sub>2</sub>/TEOS plasma, high quality SiO<sub>2</sub> films even at room temperature.

3:00 pm **PS-MoA4 Step Coverage of Silicon Dioxide Films Deposited In Dual Frequency TEOS-Oxygen Plasma Systems**, F. R. Myers, M. W. Peters, Motorola, Inc., Chandler, Arizona 85224, T. S. Cale, Arizona State University, Tempe, Arizona 85287-6206.

The deposition of SiO<sub>2</sub> films from TEOS is a commonly used process in the manufacturing of semiconductor devices. Control over film properties such as film stress, composition, density, and the step coverage over features is critical in maintaining device yield and reliability. Dual frequency radio frequency power is being utilized in plasma enhanced chemical vapor deposition (PECVD) manufacturing equipment for the deposition of silicon nitride, oxynitride, and silicon dioxide. The use of both high (13.56 MHz) and low (300–400 KHz) frequency rf power has been shown to provide additional control over film properties such as stress, density, and composition. The use of dual frequency power has also been shown to improve step coverage of SiO<sub>2</sub> films deposited using TEOS.

A dual frequency plasma sheath model is utilized to supply the necessary input parameters to a Monte Carlo simulator to predict the ion energy and angular distributions [1]. A plasma model is utilized to predict the concentrations of the relevant species at the feature mouth. The ion energy and angular distributions and the concentrations of the reactive species are used as inputs to EVOLVE [2], a physically based feature scale simulator, to predict the step coverage in the TEOS-oxygen system. Using this modular approach, experimentally observed trends in step coverage and deposition rate with plasma operating conditions are reproduced. Trends in step coverage observed with the amount of low frequency power applied to the system are also reproduced.

[1] F. R. Myers, M. Ramaswami, and T. S. Cale, J. Electrochem. Soc. **141**, 1313 (1994).

[2] EVOLVE is a deposition process simulator developed by T. S. Cale at ASU and Motorola, with funding from the SRC and NSF.

3:20 pm **PS-MoA5 Deposition of Silicon Oxide Using Helicon Assisted Reactive Evaporation**, Antoine Durandet and Rod Boswell, Plasma Research Laboratory, R. S. Phys. S. E., Australian National University, ACT0200 AUSTRALIA.

The Helicon Assisted Reactive Evaporation (HARE) is a new plasma assisted reactive evaporation device that combines an evaporation source (Electron Beam) and a high density plasma source (Helicon plasma source), in a configuration where the evaporant material is transported through the plasma source. This technique allows deposition of a large variety of materials without requiring the handling of hazardous chemical precursors.

In this paper, we present results of silicon oxide deposition; deposition rates in the range of 100 nm/min are obtained. Films growth is monitored by in-situ ellipsometry, and films are characterised using FTIR. Evidence of the ionisation of the evaporated silicon passing through the high density plasma source is given using optical emission measurements and energy selective mass spectrometry.

3:40 pm **PS-MoA6 ECR Oxygen Plasma-Assisted Deposition of  $\text{Al}_2\text{O}_3$** , J. C. Barbour, J. S. Custer, D. M. Follstaedt, M. B. Sinclair, and B. G. Potter, Sandia National Laboratories, Albuquerque, NM 87185-1056.

The deposition of  $\text{Al}_2\text{O}_3$  films was investigated using an electron cyclotron resonance (ECR)  $\text{O}_2$  plasma in conjunction with electron-beam evaporation of Al. This work is a first step in obtaining dielectric waveguides on GaAs photonic devices which require a low temperature process for deposition of high refractive index material ( $\text{Al}_2\text{O}_3$ ,  $n = 1.6-1.7$ ) on a low index cladding layer ( $\text{SiO}_2$ ,  $n = 1.45$ ). A magnetic shield was designed and used to permit electron-beam evaporation in the vicinity of the high magnetic fields from the broad-area ECR source. Diverse Al-O alloys were formed by varying the plasma parameters to change the film composition from  $\text{Al}_2\text{O}_3$  to  $\text{AlO}_{0.1}$ . For a low flow rate (1 sccm) and constant Al deposition rate, the oxygen content of the film was predominantly affected by the microwave power used to generate the ECR plasma. Increasing the microwave power from 50 to 150 Watts increased the electron density, ion density, and the number of reactive species. Stoichiometric  $\text{Al}_2\text{O}_3$  films deposited at  $130^\circ\text{C}$  were amorphous with  $n = 1.62$  at 633 nm. These films crystallized into  $\gamma\text{-Al}_2\text{O}_3$  during annealing at  $800^\circ\text{C}$ . This anneal also increased  $n$  to 1.65 and reduced the waveguide loss by an order of magnitude. The effect of sample temperature and bias during deposition were also investigated and correlated to the structural and optical properties. Erbium was incorporated into the  $\text{Al}_2\text{O}_3$  as an optically active species and the photoluminescence (PL) intensity and lifetime ( $\tau$ ) were measured as a function of temperature and plasma conditions. Vacuum annealing or an ECR-hydrogenation of Er-implanted  $\text{Al}_2\text{O}_3$  increased  $\tau$  but decreased the PL intensity.

This work was supported by the US DOE contract DE-AC04-94AL85000.

4:00 pm **PS-MoA7 Electron Cyclotron Resonance Plasma-Deposited Silicon Nitride from  $25^\circ\text{C}$  to  $200^\circ\text{C}$** , K. L. Seaward, F. F. Mertz, and K. Nauka, Hewlett-Packard, Palo Alto, CA 94303.

Electron cyclotron resonance (ECR) plasma has been used to explore the low-temperature limit of high-quality silicon nitride deposition. There is interest in this technology for use on temperature-sensitive materials such as compound semiconductors, polymers, and plastics. The literature contains reports of high quality silicon nitride deposited by ECR plasma at low temperatures, on the order of  $100^\circ\text{C}$ . Temperature generally has not been well-controlled and substrates are usually heated simply by exposure to the plasma. In addition, in order to maintain high quality, deposition rates are usually low, 100–200  $\text{\AA}/\text{min}$ .

We have investigated the properties of silicon nitride films deposited on substrates with temperature controlled at 25, 60, 100, 150 and  $200^\circ\text{C}$  using helium-backside cooling combined with plasma heating. Films deposited at  $100^\circ\text{C}$  and below were found to have similar values of stress, wet etch rate, and N-H and Si-H content from FTIR. In comparison, films deposited at  $150\text{--}200^\circ\text{C}$  had about half the hydrogen content, the compressive stress was reduced by a factor of 3, and the wet etch rate was reduced by a factor of 8. This is consistent with publications on rf PECVD silicon nitride that report a large decrease in hydrogen content for silicon nitride films deposited above  $150^\circ\text{C}$ . We have also investigated increasing the deposition rate up to 1000  $\text{\AA}/\text{min}$  by using higher pressure. In order to maintain film quality, it is necessary to increase the ion flux. Data demonstrating the competing constraints of deposition rate, ion flux, and temperature on the deposition of high quality ECR silicon nitride below  $200^\circ\text{C}$  will be shown.

4:20 pm **PS-MoA8 Low Temperature Plasma Enhanced CVD of Main Group Nitrides Using Organometallic Precursors**, D. J. Economou, S. D. Athavale, D. M. Hoffman, S. P. Rangarajan, J.-R. Liu, Z. Zheng, and W.-K. Chu, University of Houston, Houston, TX 77204.

Main group nitride thin films are important in microelectronic device fabrication and as protective coatings. Currently, there is considerable interest in developing methods for the low temperature deposition of these films. It is well known that plasma enhanced chemical vapor deposition (PECVD) allows lower substrate temperature ( $150\text{--}400^\circ\text{C}$ ) as compared to thermal CVD.

In this work, we have studied the use of homoleptic amido precursors of the general formula  $\text{M}(\text{NR}_2)_4$  [ $\text{M} = \text{Si}, \text{Ge}, \text{Sn}, \text{R} = \text{CH}_3$ ] and ammonia, to deposit nitride thin films by plasma CVD. Depositions were carried out in a low pressure (0.1–1 torr) discharge excited by a coil at 13.56 MHz. Ammonia was passed through the plasma, and the organometallic precursor was injected downstream of the plasma, just before the substrate.

We have deposited nearly stoichiometric films, at temperatures below  $400^\circ\text{C}$ , with growth rates of 120, 300, and 1800  $\text{\AA}/\text{min}$  for Si-, Ge- and Sn-nitride respectively. The film growth rate was increased by lowering pressure and/or increasing plasma power. The film composition (measured by RBS, Auger and ERS) depended mainly on the ammonia to precursor flow ratio and the substrate temperature. Further characterizations of the films included IR, UV-VIS spectrophotometry and ellipsometry. At optimum deposition conditions, the films were carbon and oxygen free.

4:40 pm **PS-MoA9 Fast Deposition of a-Si:H for Solar Cell Application**, R. J. Severens, M. C. M. van de Sanden and G. J. Meeusen and D. C. Schram, Department of Physics, Eindhoven University of Technology, P.O. Box 513, 5600 MB Eindhoven, The Netherlands.

Amorphous hydrogenated silicon is used as the intrinsic layer in amorphous silicon solar cells. As the growth rate of a-Si:H using conventional techniques as PECVD is low (typically 0.1 nm/s), a successful commercial introduction of solar energy is hampered. Considerable higher growth rates are therefore desirable. In this paper a newly developed deposition technique, based on an expanding thermal arc in an argon hydrogen mixture seeded with  $\text{SiH}_4$  will be discussed. As the opto-electronic properties are essential, the aim was to increase the deposition rate while maintaining the quality of the deposited layers. Properties such as bandgap, refractive index, bonding type ( $\text{SiH}/\text{SiH}_2$  ratio) and light to dark conductivity, oxygen and nitrogen impurity content were monitored as function of the deposition parameters. Layers showing good opto-electronic properties (light to dark conductivity  $> 10^5$ ,  $n > 3.8$ ,  $E_{\text{gap}} = 1.6 - 1.8 \text{ eV}$ ) were produced at high growth rates (typically  $> 10 \text{ nm/s}$ ) as measured with in situ HeNe ellipsometry. The good layers also show low oxygen and nitrogen content. As the ion energy is low (typically  $< 2 \text{ eV}$ ) it is demonstrated that the beneficial effect of DC bias in RF deposition is not essential. Also the refractive index seems to be independent of the substrate temperature. The particular role of ions, radicals and the possible presence of clusters is addressed.

5:00 pm **PS-MoA10 The Effects of the Process Parameters on the Low Temperature Si/SiGe Epitaxy by UHV-ECRCVD**, S. J. Park, K. H. Hwang, S. J. Joo, E. Yoon, Department of Inorganic Materials Engineering, H. S. Tae, S. H. Hwang, Y. P. Eo, K. W. Whang, Department of Electrical Engineering, Seoul National University, Seoul 151-742, Korea.

The low temperature Si/SiGe epitaxy is investigated using Ultrahigh Vacuum Electron Cyclotron Resonance Chemical Vapor Deposition (UHV-ECRCVD). The effects of process parameters on the hydrogen plasma cleaning and on the Si/SiGe epitaxy are examined by RHEED, TEM, and dilute Shimmel etching. It is observed that the defect formation on the Si substrates during *in situ* ECR hydrogen plasma cleaning is strongly dependent on the process parameters such as the microwave power, the remoteness of ECR layer from the substrate, and the substrate DC bias, and the plasma exposure time. The hydrogen ion dose plays a significant role in the low temperature *in situ* plasma cleaning, and consequently the precise control of both process parameters and the plasma exposure time is very important in preparing the damageless clean Si surfaces prior to epitaxial growth. The defect production in the Si/SiGe epilayers during plasma deposition is mainly caused by the energetic ions impinging on the substrate and can be effectively suppressed by the proper control of the ion energy influx. It has been found that the control of the DC substrate bias can be used for this purpose and a high quality, dislocation-free Si/SiGe epilayers are obtained in the UHV-ECRCVD system under optimum conditions. The effect of process parameters on the Si/SiGe epitaxy will be also reported.

## VACUUM TECHNOLOGY

### Room A102 – Session VT-MoA

#### Gas Flow, Partial Pressure Analysis, and Leak Detection

**Moderator:** J. L. Provo, Martin Marietta Specialty Components Inc.

2:00 pm **VT-MoA1 Transition Gas Flow in Drag Pumps and Capillary Leaks**, J. C. Helmer, Menlo Park, CA, G. Levi, Varian SpA, Via F.lli Varian 54, 10040 Leini (Torino) Italy.



Modern turbopumps include a drag state that operates in the pressure range of .01–10 torr or higher. Flow conditions range from molecular flow at the drag inlet, to viscous flow at the outlet. This is called “transition” flow. In general, transition flow models of pumps have not been developed. Models of transition conductance in tubes have been considered by Knudsen and others, for capillary leaks to atmosphere. These models add the two conductances of the tube at low and high pressure, multiplied by weighting functions of the average pressure.

If the tube surface moves with a velocity in the axial direction, it becomes a Gaede pump [1]. We have developed a model of the Gaede pump that proceeds from transition flow in a differential element, integrated over the length of the pump. The predictions of this model are modified by a new, “pumping leak” theory of the gas stripper, which separates inlet from outlet. The result is compared with experimental measurements.

If the surface velocity is zero, the model predictions agree with Knudsen’s data for capillary leaks, while giving a better account of the controversial, “conductance minimum”.

[1] G. Levi, M. De Simon, J. Helmer, “Use of the Clausing Equation to Evaluate the Pumping Effect of Molecular Pumps,” 4th European Vacuum Conference, Uppsala (June, 1994).

2:20 pm **VT-MoA2 Calculations of Orifice Flow in the Transition Regime, J. P. Looney, and R. D. Mountain**, Thermophysics Division, NIST, Gaithersburg, MD 20899.

The flow of gas through an ideal orifice has been investigated theoretically and experimentally for large Knudsen numbers ( $Kn$  = mean free path to orifice diameter ratio) by several investigators<sup>1–5</sup> since the pioneering work of Knudsen. To date, calculations of the gas flow or orifice conductance for nearly free molecular flow conditions at large  $Kn$  either do not exhibit good agreement with experiment<sup>2,4</sup>, are only valid<sup>2,3</sup> for first-order deviations from ideal molecular flow (i.e.  $Kn \gg 1$ ), or so mathematically complex<sup>3,5</sup> the physics is obscured. In this talk I will discuss a model that we have developed which is based upon mean free path kinetic theory and the numerical solution of this problem through the use of Monte Carlo methods. The physical interpretation of this model is straightforward, and the results of these calculations are in excellent agreement with experimental data that has been reported in the literature<sup>1,2</sup> and obtained in our laboratory for  $Kn$  as small as 0.3. We also find good agreement with the theoretical results from numerical solution of the Boltzmann Equation<sup>3</sup> for  $Kn > 1$ .

<sup>1</sup>K. Poulter, Vacuum **28** (1977) 135 and references therein.

<sup>2</sup>Lieppmann, H. W., J. Fluid Mech., **10** (1961) 65 and references therein.

<sup>3</sup>Rotenburg, A. and Weitzner, H., Phys. of Fluids, **12** (1969) 1573.

<sup>4</sup>Hibey, J. W. and Paul, M. Phys. Rev. **88** (1952) 414 and Z. Naturforsch **11a** (1956) 533.

<sup>5</sup>D. R. Willis, J. Fluid Mech. **21** (1965) 21.

2:40 pm **VT-MoA3 High Precision, Gas Analysis System Used to Analyze Grab Samples from the Space Shuttle Engine Compartment, G. M. Solomon and M. D. Boeckmann**, Vacuum Technology, Inc., 1003 Alvin Weinberg Drive, Oak Ridge, TN 37830.

A system was built to analyze grab samples taken from the space shuttle engine compartment. The gas samples varied from 3 torr to 200 torr in a 210 cc sample cylinder which uses explosive charges on a valve to “grab” the gas samples. The analysis system uses three expansion volumes to reduce the sample pressure to between 0.5 to 1 torr in a 650 cc inlet volume. During the pump out of the sample volume, the mass peak ions signals were extrapolated to zero time. Pure gases were used to measure the system time constant, verify the molecular flow assumption and determine cracking pattern ratios for the gases of interest. The gases of interest were hydrogen, helium, carbon monoxide, methane, nitrogen, oxygen, argon and carbon dioxide. It was found that the active gases changed the partial pressure sensitivities of all gases by more than 10%, initially. An ion source conditioning step was performed using an oxygen mixture to stabilize the gas sensitivity factors with time, before the analysis was performed. Mixed gas standards of varying percentages were intercompared to test the system. Batch inlet system design criteria, calibration standards and analysis software will be reviewed.

3:20 pm **VT-MoA5 A Guide to Manual Tuning of Pressure Controllers, L. D. Hinkle and F. Rudolph**, MKS Instruments, Inc., Andover, MA 01810.

Most vacuum processes require pressure control which is stable, quick to achieve set point, and responsive to perturbations. In common practice, a pressure control system using a proportional-integral-derivative (PID) algorithm drives a downstream throttle valve or an upstream bleed valve. As with any PID controller, the tuning of the parameters which govern the system behavior is critical to its performance. To complicate matters, vacuum systems are inherently non-linear as a function of pressure and gas throughput and so a fixed tuning may not span the entire operating range effectively. A controller which stores multiple tuning recipes may be employed but it still requires manual tuning of each recipe for its application.

Two approaches to manually tuning a PID controller are (1) a close loop method and (2) an open loop method. Since the tuning parameters for the desired response in a given PID application are closely constrained, either method should yield similar results; however the relative ease and efficiency of the tuning processes may vary from case to case. A test where various vacuum systems are tuned using each method is used to form comparisons and recommendations.

3:40 pm **VT-MoA6 Fast Fine Leak Testing of Very Large Vessels, Lyle Bergquist, Y. Tito Sasaki**, Quantum Mechanics Corp., PO Box 1885, Sonoma, CA 95476.

Conventional helium leak detectors cannot detect fine leaks in vessels measuring tens of cubic meters. Because of the large amount of desorbed gases such as  $H_2$  and  $H_2O$  relative to the amount of the tracer gas, concentration of helium becomes extremely low. If we want the helium partial pressure to be high enough for the mass spectrometer to detect it, then the background pressure becomes too high for the spectrometer’s proper functioning. Conversely, if we lower the total pressure, the partial pressure of helium becomes too low to be detectable. An added problem is the long response time that will make it uneconomical to locate the leak and fix it. A simple solution to all these problems has been developed by combining the principles of helium compression and selective accumulation. A system we designed will detect leaks in the order of  $10^{-12}$  sccHe/s in a 40 m<sup>3</sup> vessel under 5 seconds. An additional minute will establish the exact leak rate. This design uses a turbomolecular pump of a high pumping speed and high helium compression ratio. It compresses the residual gas in the vessel—both the leaked-in helium and the desorbed gases—into the mass spectrometer region. Then a chemical getter and a cryocondensation pump remove all but helium. In this manner the leaked-in helium is immediately concentrated in the detector region while the background pressure therein is kept low. The paper discusses this and other possible designs and applications.

4:00 pm **VT-MoA7 Vacuum Insulation: The Potential for Energy Conservation, H. Alan Fine**, Global Change Division, U.S. Environmental Protection Agency, Washington, DC.

A number of advanced insulation systems are currently under development. These systems generally consist of a filler material maintained under vacuum within a gas-tight barrier/container. With the exception of gas-filled panels, the improved thermal performance of these systems results from the vacuum.

Filler materials incorporated into advanced insulation systems include ceramic spacers, precipitated silica or other powders, fiberglass, aerogel tiles and open-cell foam. Barrier have generally been fabricated from laminated polymeric structures, glass or stainless steel. Vacuum requirements range from soft vacuums of approximately 50 Torr for aerogel tiles to hard vacuums of less than a micron for ceramic spacers.

The state-of-the-art of advanced insulations is reviewed. Emphasis is placed on the achieved and potential thermal performance of the insulation systems, and their potential for energy conservation when they are used to improve the energy efficiency of appliances and buildings. The barriers which must be overcome before wide spread implementation of this technology will occur are outlined. The advantages of advanced insulations, as compared to more traditional forms of insulation, and the cost effectiveness of advanced insulations are also discussed.

INVITED

4:40 pm **VT-MoA9 Vacuum Process of Extremely Slow Leak from Fine Complicated Structures in Chamber Surfaces, M. Miki**, The Graduate University for Advanced Studies, 1-1 Oho, Tsukuba, Ibaraki 305, Japan, **H. Ishimaru**, National Laboratory for High Energy Physics, 1-1 Oho, Tsukuba, Ibaraki 305, Japan.

Elementary processes in vacuum pump-down were studied in an aluminum ultrahigh vacuum system, using super-dry nitrogen and argon. The system is constituted of a roughing pump line, a main pump line with a residual gas analyzer, a venting gas line and a main chamber with vacuum gauges. The venting gas line can reduce other



suggests that surface reactions on the diamond seed produce volatile species which diffuse to the substrate to form nucleation centers.

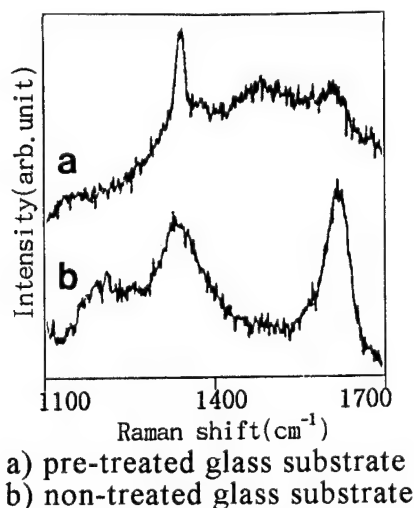
[1] Z. Ajji, M. Buck and Ch. Wöll, *Diamond and Related Materials*, 2 (1993) 1525.

3:20 pm **TFVM-MoA5 Low Temperature Plasma Synthesis of Diamond in a Pulsed Microwave ECR Discharge**, Z. Ring, S. Tiali, H. E. Jackson, and T. D. Mantei, University of Cincinnati, Cincinnati, Ohio 45221.

High quality diamond films have been synthesized in  $\text{CH}_4\text{-H}_2\text{-O}_2$  mixtures at substrate temperatures down to  $350^\circ\text{C}$ , using a pulse-modulated electron cyclotron resonance (ECR) microwave discharge. The minimum temperature for diamond deposition was lowered by decreasing the gas pressure. High quality diamond films were grown at gas pressures of 0.3 to 3 Torr and substrate temperatures of 350 to  $550^\circ\text{C}$  by combining magnetic field discharge activation and plasma modulation. A static applied axial magnetic field established by a permanent magnet structure provided ECR enhancement, increasing gas dissociation and ionization by approximately an order of magnitude. Pulse modulation of the input microwave power provided high atomic hydrogen fluxes to the substrate without accompanying ion or electron bombardment fluxes over most of the discharge cycle. The low temperature diamond films exhibit sharp characteristic  $1333\text{ cm}^{-1}$  Raman phonon peaks with a small nondiamond carbon response; the linewidth is  $4\text{ cm}^{-1}$  at  $350^\circ\text{C}$ . Vertical growth rates range from 400 nm/min at  $550^\circ\text{C}$  to 100 nm/min at  $350^\circ\text{C}$ .

3:40 pm **TFVM-MoA6 Effect of Substrate State on the Formation of the Diamond Film Using a Low Temperature Microwave Plasma System**, S. H. Kim, Y. S. Park, S. K. Jung, J.-W. Lee, New Materials Laboratories, Samsung Advanced Institute of Technology, P.O. Box 111, Suwon, 440-600, Korea.

Diamond thin films were deposited on the various substrates (pre-treated glass, non-treated glass, pre-treated silicon, and pre-treated quartz) using a low temperature MPECVD (microwave plasma enhanced chemical vapor deposition) system. The substrate temperature can be lowered below  $500^\circ\text{C}$  by removing the substrate from the plasma. Among the various substrates, the diamond films form only on the pre-treated glass and the pre-treated quartz substrate. For the non-treated glass and the pre-treated silicon, the formation of graphite is an occurrence. Therefore we can confirm that the pre-treated glass and the pre-treated quartz substrate are promising substrates for the diamond formation at low temperature. In addition, we deposited the films on the pre-treated glass substrate by varying  $\text{CH}_4$  concentration. The growth rate of the film decreases with increasing the  $\text{CH}_4$  concentration. The best quality of the diamond film can be acquired at 4%  $\text{CH}_4$ . Microstructure of the films was also investigated by TEM. From these results, we will discuss the preferred formation of the diamond films on the pre-treated glass and the pre-treated quartz substrates.



4:00 pm **TFVM-MoA7 Process-Property Relationships in Nanocrystalline Diamond Thin Film Preparation**, R. W. Collins, Byungyou Hong, W. Drawl, and R. Messier, Materials Research Laboratory, Penn State University, University Park, PA 16802, USA.

Insights into the process-property relationships for diamond thin film preparation have been obtained from real time spectroscopic ellipsometry (SE) studies. SE has been performed during nanocrystalline diamond film growth by microwave plasma-enhanced chemical vapor deposition onto c-Si substrates, seeded to obtain high nucleation densities ( $\sim 4 \times 10^{10}\text{ cm}^{-3}$ ). Thus, the grain size is much smaller than the probe wavelengths ( $> 3000\text{ Å}$ ), and SE data analysis yields the time evolution of bulk and surface roughness layer thicknesses and the non-diamond carbon ( $\text{sp}^2\text{C}$ ) and void volume fractions in the bulk layer. We have studied these characteristics versus substrate temperature and process gas composition over the C-H-O phase diagram. For conditions under which diamond crystallites form, the SE data reveal a reproducible nucleation and coalescence sequence. In the nucleation stage, when the diamond consists of a layer of isolated particles (thickness,  $d < 300\text{ Å}$ ), a relatively low  $\text{sp}^2\text{C}$  volume fraction ( $< 0.05$ ) is observed and represents defects within grains. As nuclei coalesce, a large intergranular contribution to the  $\text{sp}^2\text{C}$  volume fraction (0.2–0.3) develops in the first 500 Å of bulk film growth. The subsequent evolution of the average  $\text{sp}^2\text{C}$  content with bulk layer thickness is found to be very sensitive to process gas composition. Under C-rich conditions, the high level of intergranular  $\text{sp}^2\text{C}$  stabilizes as the film increases in thickness. With increasing O additions to the gas phase, however, the average  $\text{sp}^2\text{C}$  content shows increasingly rapid decays with thickness. This latter result suggests that O species are effective at penetrating intergranular voids and preventing defects from forming on shadowed nuclei surfaces. Diamond films prepared using C-H-O mixtures at the growth/etching boundary exhibit a minimum of intergranular  $\text{sp}^2\text{C}$  trapped at the substrate interface. Further insights into diamond growth mechanisms are obtained from studies of the surface roughness evolution and the growth rate versus temperature, measured at different points in the C-H-O phase diagram.

INVITED

4:40 pm **TFVM-MoA9 Diamond Deposition on Carbon Fibers**, S. Ismat Shah and M. M. Waite, E. I. du Pont de Nemours and Company, Central Research and Development, Experimental Station, P.O. Box 80356, Wilmington, DE 19880-0356 and Department of Physics and Astronomy, University of Delaware, Newark, DE 19716.

Due to the inherent nature of the CVD diamond deposition process which involves preferential etching of non-diamond carbon phases, diamond deposition on carbon substrates is non-trivial. Thick graphite substrates can be used for deposition in which the initial etching of the substrate can be tolerated and as the diamond film forms, further etching of the substrate halts. Diamond deposition on low dimensional objects is difficult because the substrate gets etched away before the formation of a continuous protective diamond film. We have successfully deposited diamond films on carbon fibers using a pretreatment process which ensures fiber protection until a continuous layer of diamond has been formed on the fibers. Diamond films were deposited on these pretreated fibers by plasma assisted CVD. In this paper we will describe the pretreatment process and present the results of the characterization of the diamond coated carbon fibers. We will also discuss the optimum process parameters for the film deposition.

5:00 pm **TFVM-MoA10 Carbon Dimer,  $\text{C}_2$ , as a Growth Species for Diamond Film Synthesis\***, D. M. Gruen, C. D. Zuiker, and A. R. Krauss, Materials Science and Chemistry Divisions, Argonne National Laboratory, Argonne, IL 60439.

It was shown recently that nanocrystalline diamond films can be grown using fullerenes as precursors in an argon microwave plasma without hydrogen or oxygen additions [Appl. Phys. Lett. 64, 1502 (1994)]. Extensive fragmentation of  $\text{C}_{60}$  in the microwave discharge leads to copious production of the carbon dimer molecule,  $\text{C}_2$ , as evidenced by intense Swan-band emission. We propose a mechanism for diamond film growth on the (100) surface using  $\text{C}_2$  as the growth species. This surface is known to reconstruct to the (100)-(2 × 1): H form, and at 1573K in vacuum to the (100)-(2 × 1) form, by loss of surface hydrogen. The latter reconstruction is the one most likely to obtain, under the high temperature ( $\sim 850^\circ\text{C}$ ), argon atmosphere (100 Torr) deposition conditions characteristic of our plasma experiments. In the event, each surface carbon atom is bonded twice to carbons in the bulk and twice to a surface carbon ( $\pi$ -bonding) making a "dimer" and forming a five-member ring. With  $\text{C}_2$  as the growth species, no hydrogen abstraction reactions are required. Because of its very high energy of adsorption (815 KJ/mol C), the  $\text{C}_2$  molecule can insert directly into the dimer bonds, and a second  $\text{C}_2$  can add across the adjoining trough. The added carbons would then dimerize with their neighbors, forming a new (2 × 1) surface on a new layer, with dimer rows orthogonal to the original rows. Because the requirement for

multiple hydrogen abstraction reactions is lifted with  $C_2$  as the growth species, the kinetics of carbon incorporation into the diamond lattice would be expected to be vastly increased, and therefore growth rates can be much higher.

\*Work supported by the U.S. Department of Energy, BES-Materials Sciences Division of Advanced Energy Projects, under Contract W-31-109-ENG-38.

## ELECTRONIC MATERIALS Room A108 - Session EM-MoA

### Thin Film Heterostructures

**Moderator:** L. J. Brillson, Xerox Webster Research Center.

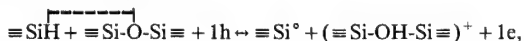
2:00 pm **EM-MoA1 Interface Quality in InP/InGaAs RTDs and 2 DEG in Delta-Doped HFET Channels as Observed by Scanning Tunneling Microscopy<sup>†</sup>**, W. Wu, S. L. Skala, J. R. Tucker, K.-Y. Cheng, and J. W. Lyding, Department of Electrical and Computer Engineering, Beckman Institute and Microelectronics Laboratory, University of Illinois at Urbana-Champaign, Urbana, IL 61801, A. Seabaugh, Texas Instruments Incorporated, Central Research Laboratories, M/S 147, Dallas, TX 75265.

Cross-sectional Scanning Tunneling Microscopy (XSTM) observations of the cleaved (110) surface of InP/InGaAs RTDs show marked differences between the normal and inverted interfaces. The inverted interface exhibits "microroughness" on a length scale of 10–30 Å along the interface, while the normal interface, in contrast, is very smooth with only occasional monolayer steps occurring on a length scale of over 100 Å. Preliminary results also indicate the ability to observe the decay of conduction band electron wavefunctions within the InP barrier. XSTM images of a delta-doped InGaAs channel HFET directly show the spatial extent of a 2 DEG. The electron wavefunction of the first subband is observed in both the occupied and unoccupied state STM images. Measurements clearly show the peak of the electron wavefunction to be ~60 Å from the barrier-channel interface on a sample with a Si delta-doping level of  $5 \times 10^{12} \text{ cm}^{-2}$ .

<sup>†</sup>This work was supported by JSEP under contract N00014-90-J-1270 and NSF under contract NSF ECD 89-43166.

2:20 pm **EM-MoA2 Model for Metastable Defect Formation at Si-SiO<sub>2</sub> Interfaces**, G. Lucovsky, Z. Jing and J. L. Whitten, Departments of Physics and Chemistry, North Carolina State University, Raleigh, NC 27695-8202.

A key issue in semiconductor device processing is reliability; i.e., under operating conditions, what are the factors that contribute to the rate at which current/voltage stress creates electronically-active defect states that can render device operation below acceptable limits? We focus on *initially-passive* local bonding arrangements at Si-SiO<sub>2</sub> interfaces which can serve as precursor sites for stress-induced defect formation. The model is based on identification of a similar metastable defect generation mechanism that has been applied to the photo-induced defect generation process in amorphous silicon (a-Si) alloys; i.e., the Staebler-Wronski Effect [1]. The relevant local bonding configurations in a-Si alloys are associated with electronegative impurity atoms or groups, such as O and NH (the NH group has similar chemical properties as O), and the proximity of near-neighbor silicon monohydride (SiH) bonds, creating *bridging H-bonds* between the H-atom of the SiH, and the electronegative species. The same types of SiH and =Si-O-Si= local bonding arrangements are present at Si-SiO<sub>2</sub> interfaces, whereas bonding arrangements involving NH groups can be introduced in forming nitrated oxides, or composite oxide-nitride-oxide dielectrics from HN<sub>3</sub> sources. The defect generation (→) neutralization(←) reaction is



where |----| represents the H-bond. Defect states: a Si dangling ( $\equiv \text{Si}^{\bullet}$ ) bond, and the ( $\equiv \text{Si}-\text{OH}-\text{Si} \equiv$ )<sup>+</sup> charged center are created by hole trapping (→), and relaxed by electron trapping (←). Ab-initio calculations have shown that the positively charged center is stable, and that trapping an electron returns the local bonding to its original state.

We have shown that incorporation of NH groups increases both interfacial traps, ( $D_{it}$ ) and fixed charge. In contrast, the controlled incorporation of N-atoms, which cannot participate in H-bond formation, generally decreases  $D_{it}$ , and does not contribute to fixed charge in the dielectric near the Si-SiO<sub>2</sub> interface.

[1] G. Lucovsky, *et al.*, MRS Symp., Spring 1994, paper A9.12.

2:40 pm **EM-MoA3 High-Resolution Depth Profiling of Sequential Isotope Oxidation of Silicon<sup>\*</sup>**, H. C. Lu, T. Gustafsson, E. P. Gusev, and E. Garfunkel, Depts. of Physics and Chemistry, and Laboratory for Surface Modification, Rutgers University, Piscataway, NJ 08855.

The mechanism of ultra-thin (1–5 nm) silicon oxide growth is still under intensive discussion. In this paper, we present results obtained with a novel method that shed important new light on the complex initial oxidation of Si(100) at 750–900°C. To help elucidate the mechanism of oxide growth, we have used medium energy ion scattering (MEIS) with <sup>18</sup>O<sub>2</sub> followed by <sup>16</sup>O<sub>2</sub> isotope oxidation. MEIS distinguishes <sup>18</sup>O from <sup>16</sup>O and gives the depth distribution for both in the thin oxide films with an accuracy of ~0.4 nm. The isotope distribution calculated from deconvolution of an MEIS energy spectrum is found to be non-uniform, with isotropic mixing for very thin (1–4 nm) films, inconsistent with any existing model of silicon oxidation. For thicker films, sequential isotope oxidation results in an isotropic mixture near the surface, and Si<sup>16</sup>O<sub>2</sub> near the interface. We have also observed oxygen loss during oxidation.

\*Supported in part by NSF DMR 90-19868 and 93-06899.

3:00 pm **EM-MoA4 FTIR Study of Rapid Thermal Annealing of Remote Plasma Chemical Vapor Deposited a-Si-nitride Films**, Z. Lu, M. J. Williams, P. F. Santos-Filho and G. Lucovsky, Departments of Physics, Electrical and Computer Engineering, and Electrical and Computer Engineering, North Carolina State University, Raleigh, NC 27695-8202.

Si-nitride films are widely used in the microelectronics industry. PECVD deposited silicon nitrides are known to have bonded hydrogen in the form of Si-H and SiN-H. There is ample evidence that electrical performance of the Si-nitride films can be improved through high temperature rapid thermal annealing (RTA). This study uses FTIR to study behavior of bonded-H in Si-nitride films after RTA from room temperature to 1200°C, to establish correlations between electrical performance of Si-nitride and the amount of bonded hydrogen. The silicon nitride films were deposited using NH<sub>3</sub> and SiH<sub>4</sub> as source gases in a remote PECVD reactor. Different Si-nitride films were prepared ranging from Si-rich, to quasi-stoichiometric, and finally to heavily hydrogenated. The temperature dependencies for Si-H and SiN-H reductions are different depending upon the initial bonding stoichiometry of the nitride film. A bonding model is proposed to account these results which associates the H-release with generation of molecular H<sub>2</sub>. Additional data will be presented for silicon nitride films made using ND<sub>3</sub> as N-source gas, where insights into the film and evolution chemistry and can be gained. For near-stoichiometric nitrides, the SiN-H bonding feature progressively decreases as the RTA temperature increases from room temperature to ~900°C. At the same time, Si-N peak increases, indicating rebonding of nitrogen to silicon after bonded hydrogen (Si-H and SiN-H) has been thermally released. This phenomena is supported in a Si-rich nitrides, where the initial Si-H and SiN-H concentrations are comparable. These observations are consistent with electrical performance improvement of Si-nitride film. They indicate that the SiN-H group, which is abundant in near-stoichiometric nitride films produced by low temperature PECVD is mainly responsible for the poor electrical performance. Reduction of SiN-H by RTA significantly improves the quality of the PECVD nitride films grown from NH<sub>3</sub> source gases.

3:20 pm **Em-MoA5 Electrical Transport Properties of Hot Electrons at Metal, Insulator and Semi-Conductor Interfaces**, R. Ludeke, IBM T. J. Watson Research Center, P.O. Box 218, Yorktown Heights, NY 10598, and A. Bauer, Institut für Experimentalphysik, Freie Universität Berlin, D-14195 Berlin, Germany.

Hot electron transport across interfaces is dominated by a variety of scattering processes that have been difficult to study by conventional techniques. The advent of a variant of the STM, Ballistic Electron Emission Microscopy, or BEEM allows the investigation of scattering phenomena and related issues in heterostructures over a broad electron energy range and at near-atomic resolution. A number of applications of BEEM spectroscopy over an energy range up to 10 eV will be



discussed. The technique has recently been used to show that transverse momentum is largely conserved for electron transport across the commensurate  $\text{NiSi}_2/\text{Si}(111)$  interface, whereas it is not conserved for incommensurate metal-semiconductor systems. The energy dependence of elastic and inelastic mean free paths of hot electrons in Pd layers deposited on  $\text{Si}(100)$  and  $(111)$  substrates has been obtained as well. BEEM can be used to measure directly the quantum yield of electron-hole pair generation by impact ionization of injected hot electrons, which will be discussed for Si. Of current interest is the characterization of transport properties of thin insulating layers (2–6 nm) placed between the metal and the semiconductor. Transport takes place mainly through electron injection into the conduction band of the insulator. The application of a bias across the insulator provides an additional variable to study the de-excitation processes of hot carriers in the conduction band of the insulator. Recent results for  $\text{SiO}_2$  interlayers will be presented. **INVITED**

4:00 pm **EM-MoA7 Epitaxy in the Room Temperature Reaction of Ni on Si(111) Studied with Synchrotron X-ray Diffraction**, P. Yang, M. Y. Lee and P. A. Bennett, Physics Dept., ASU, Tempe, AZ 85287-1504, P. J. Eng, AT&T Bell Labs, Murray Hill, NJ 07974 and I. K. Robinson, Physics Dept., UI, Urbana, IL 61810.

We find that deposition of Ni on  $\text{Si}(111)-7 \times 7$  at room temperature produces a commensurate, epitaxial silicide at the buried metal/silicon interface. Intensity oscillations occur signifying a layerwise etching of the substrate, similar to the Pd/Si case.[1] Model calculations of the intensity profile along several crystal truncation rods allows a clear structure assignment as  $\text{Ni}_2\text{Si}$ -theta. For the first several Å, the integrated intensities in the  $\text{Ni}_2\text{Si}$  reflections account for all the deposited metal, ie: no other phase forms. The structure factors show a Debye-Waller like variation against Q with an extremely large atomic displacement  $u_{\text{rms}} \sim 0.4$  Å. Diffuse intensity appears throughout the Brillouin zone, suggesting a high density of point defects. The nature of disorder in the silicide film explains why epitaxy has not been seen at room temperature using other techniques such as MEIS, LEED, etc. Implications for low temperature epitaxial growth are discussed.

[1] P. A. Bennett, B. Devries, I. K. Robinson and P. J. Eng, Phys. Rev. Lett. **69**, 2539 (1992).

4:20 pm **EM-MoA8 Phonon Scattering of BEEM Electrons at Au/Si(100) Schottky Interfaces**, C. A. Ventrice, Jr., V. LaBella, G. Ramaswamy, and L. J. Schowalter, Rensselaer Polytechnic Institute, Troy, NY 12180 U.S.A.

The relative importance of temperature dependent scattering mechanisms (i.e., acoustic phonon scattering within the metal overlayer and optical phonon scattering within the semiconductor) on ballistic electron emission microscopy (BEEM) electron transport across Au/Si(100) Schottky interfaces is not well understood. To better quantify the effects of phonon scattering, BEEM measurements on Au/Si(100) interfaces have been performed at both room temperature (RT) and 77 K for several Au overlayer thicknesses on n-type Si ( $\rho = 2-4$  ohm-cm). The onset of the BEEM collector current, which determines the Schottky barrier height, was measured to be 0.82 eV at 77 K and 0.78 eV at RT. The observed shift in the onset of the collector current results from both a narrowing of the band gap of Si at elevated temperatures and thermal broadening of the tip's Fermi function at RT. Measurements of the average BEEM electron transmittance for energies up to  $\sim 0.4$  eV above the 0.8 eV Schottky threshold have revealed a reduction in BEEM electron transmittance at RT for each Au film thickness. The measured relative transmittance at RT to that at 77 K ranged from 0.55 to 0.68 for Au overlayer thicknesses of 67 Å to 140 Å. Calculations of the temperature dependent attenuation length within the Au overlayer have indicated that multiple reflections of the BEEM electrons within the Au overlayer must be taken into account to explain the observed functional dependence of the BEEM electron transmittance. (This research was supported in part by the U.S. Air Force and the Office of Naval Research).

4:40 pm **EM-MoA9 Metal ( $\text{CoSi}_2$ )/Insulator ( $\text{CaF}_2$ ) Resonant Tunneling Diodes and Transistors**, M. Asada, M. Watanabe, T. Suemasu, and Y. Kohno, Tokyo Institute of Technology, Meguro-Ku, Tokyo 152, Japan.

Metal/insulator heterostructures can be considered attractive material for high-speed quantum electron devices, because high carrier density of metal and low dielectric constant of insulator are suitable for the size reduction and high-speed operation. Also, in certain material combination, strong quantum interference is expected due to

very large band discontinuity at the heterointerface ( $\sim 10$  eV), which can be utilized for multifunctional and high-transconductance devices.

In this paper, we report epitaxial growth of metal/insulator heterostructure and its application to quantum electron devices.  $\text{CoSi}_2$  and  $\text{CaF}_2$  were chosen for metal and insulator because of their small lattice mismatch to Si ( $-1.2$  and  $+0.6\%$ , respectively).  $\text{CaF}_2$  was grown at low temperature ( $\sim 450^\circ\text{C}$ ) by the partially ionized beam epitaxy to suppress the thermal damage of  $\text{CoSi}_2$  underlayers.  $\text{CoSi}_2$  was grown by the two-step growth of Si and Co to avoid island formation. By these technique, a few nanometer-thick  $\text{CoSi}_2/\text{CaF}_2$  multilayer was obtained on  $\text{Si}(111)$ . Resonant tunneling diodes with two metal quantum wells showed negative differential resistance (NDR) at 77 K and room temperature. The change of the applied voltage at NDR with quantum well thickness agreed with theoretical calculation. Resonant tunneling transistors were fabricated by connecting the base electrode to one of the quantum wells of the resonant tunneling diode with high-selective wet chemical etching process. Transistor action with NDR was observed at 77 K. Depending on the choice of the two wells as the base, two different characteristics were obtained. Transfer efficiency close to unity was obtained for electrons from emitter to collector through the resonant levels in these transistors. **INVITED**

## MANUFACTURING SCIENCE AND TECHNOLOGY

### Room A110 - Session MS-MoA

#### Process and Equipment Modeling

**Moderator:** K. Uram, Lam Research Corporation.

2:00 pm **MS-MoA1 Flux Distributions and Growth Rate Uniformities from Hexagonal Collimators**, Z. Lin and T. S. Cale, Center for Solid State Electronics Research, Arizona State University, Tempe, AZ 85287-6006.

We use the Monte Carlo method to simulate collisionless transport through collimator cells and collisional transport from the collimator to the substrate [1]. Three dimensional flux distributions are obtained for species exiting a single hexagonal collimator cell as functions of collimator aspect ratio, the sticking factor of the sputtered material in the collimator, and the flux distribution of moieties entering the collimator. We consider specular as well as diffuse re-emission, for species which have subunity sticking factors in the collimator. The larger the sticking factor and the higher aspect ratio, the higher the 'beaming' effect of the collimator and the smaller the fraction of moieties which make it through the collimator. Diffuse re-emission produces a more collimated beam than specular re-emission, but the fraction of the moieties which make it through the collimator is lower for diffuse re-emission.

After establishing the film growth rate profile on a flat wafer due to one collimator cell, local growth rates due to all of the cells are obtained by summing the fluxes from all contributing collimator cells. For a given collimator design, the variation in deposited film thickness is a function of collimator to wafer distance and sputter gas pressure. The longer the distance from the collimator to the wafer and the shorter the mean free path of the sputtered gas, the more collisions between molecules and the smoother the deposition profile. For hexagonal cells, the positions of the maxima in the deposition profile are under the corners of the cells, and the minima are under their middles.

1. D. Liu, S. K. Dew, M. J. Brett, *Thin Solid Films* **236**, 267 (1993).

2:20 pm **MS-MoA2 Modeling of Collimated Sputter-Deposition of Thin Films Using Molecular Dynamics: A Study of Step Coverage and Film Properties**, C. C. Fang, State University of New York at Stony Brook, Department of Mechanical Engineering, NY 11794-2300, F. Jones, J. J. Hsieh, R. V. Joshi, IBM Watson Research Center, P.O. Box 218, Yorktown Heights, NY 10598, and V. Prasad, State University of New York at Stony Brook, Department of Mechanical Engineering, NY 11794-2300.

In the manufacture of sub- $0.5 \mu\text{m}$  generation devices, the coverage of the liner on the bottom and the sidewall of the contact/via imposes severe limitations on the deposition process. Collimated sputtering is generally used to improve the coverage in high aspect ratio contacts and resolve several of the step coverage problems. Although this technique is widely used in electronics industry, the basic phenomena

associated with this process are poorly understood. This paper reports simulations of collimated sputter-deposition of thin films in micro-sale trench using a two-dimensional molecular dynamics model (MD) and examines the effects of process parameters on film properties and step coverage. The microstructure, intrinsic stresses and step coverage are calculated as a function of working pressure, power input, and aspect ratio of the collimator. The numerical results demonstrate that the non-unity stick coefficient strongly depends on the energetic neutral argon ejected from the target. The MD simulation technique is found to be helpful in optimization of the collimated sputter processes with high demands on uniformity and edge coverage. The simulation results for depositions in deep trenches are presented for a wide range of collimator aspect ratio, to explain the physics of the process.

**2:40 pm MS-MoA3 Process and Equipment Modeling for Advanced Semiconductor Manufacturing, Zachary J. Lemnios, Program Manager, Advanced Research Projects Agency (ARPA).**

Enormous development costs and excessive cycle times to transition new ideas into the manufacturing environment have limited semiconductor technology innovation. Through sequential and iterative process development, new process technologies require approximately 5-years to mature while process derivatives require 2-3 years to mature.

This paper addresses use of advanced process and equipment models to synthesize leading edge manufacturing tools. It also presents the use of these models in an integrated environment to synthesize of new manufacturing processes. This approach, will combine a new set of programmable factory tools with a set of embedded manufacturing models and computer aided design tools. The resulting architecture will provide the capability to concurrently design a circuit along with its associated process, significantly improving the yield learning curve for new products and technologies. The ability to make appropriate tradeoffs in performance, reliability, manufacturability, life cycle cost and cycle time will be possible with the availability of a process synthesis framework. **INVITED**

**3:20 pm MS-MoA5 Comparison of the Sandia DSMC Molecular Flow Model to Experiment<sup>1</sup>, Paul K. Shuffelebotham, Lam Research Corp., 4650 Cushing Pkwy., Fremont, CA 94538, Timothy J. Bartel, Sandia National Laboratories, Albuquerque, NM 87185-5800, Butch Berney, Lam Research Corp.**

The Sandia DSMC rarefied gas dynamics model is used for the simulation of axisymmetric transition and molecular gas flow. This code has potential as a CAD tool for use in the vacuum design of low pressure plasma processing equipment, which typically operates in the transition flow regime. This assumes that the model is accurate and predictive. We have constructed an axisymmetric, transition flow, vacuum test cell (VTC) to test the model through direct comparison with experiment. The VTC was equipped with numerous capacitance manometers, a mass flow controller and a 2000 l/s compound magnetically levitated turbopump. Spatially-resolved pressure measurements were made at dry N<sub>2</sub> flows from 50 to 500 sccm. The inputs to the model were the VTC geometry and surface temperatures, input mass flow rates and output pumping speeds. Tens of thousands of computational particles were tracked for hundreds of thousands of time steps. After a brief discussion of the known model and experimental uncertainties, the capability of the DSMC code to predict the absolute values, flow rate dependencies and spatial variations of the pressures measured in the VTC will be described in detail. The utility of the model as a vacuum system CAD tool will also be briefly discussed.

<sup>1</sup>Work supported by Lam Research, Sematech and DOE.

**3:40 pm MS-MoA6 Modeling of Ion Flux Uniformity in Radio Frequency Discharges: Effect of Electrode Topography, M. Dalvie, M. Surendra, G. S. Selwyn, C. R. Guarnieri, IBM T. J. Watson Research Center, POB 218, Yorktown Heights, NY 10598.**

Plasma process non-uniformity is a major cause of yield loss during integrated circuit fabrication. Correlation of yield with chip placement on the wafer shows that yield falls off near the edge of the wafer, leading to an "edge exclusion" zone on the wafer. One possible cause of this is a non-uniformity in the ion flux. This is studied here by means of a 2-d self-consistent fluid model of a radio frequency discharge. Time-dependent electron and ion continuity, ion momentum balance, and electron energy balance equations are solved along with Poisson's equation. A semi-implicit time integration scheme and Galerkin Finite elements are used to solve the equations.

The simulation domain includes electrode topography that simulates

clamprings and wafer edges. Results indicate that electrical property variation (e.g., conducting wafer to non-conducting clampring) causes the ion flux to fall off near the wafer edge. This may be partially responsible for the commonly observed edge exclusion on plasma processed wafers. Effect of the topography is related to plasma parameters, e.g., pressure, through the sheath thickness. Under high pressure (low sheath thickness) conditions, the ion flux is more sensitive to the topographical perturbation due to ionization rate enhancement in the corner. At low pressure, electrical property variation is more important. We also compare uniformity predictions obtained from the complete ion momentum balance to those from the drift-diffusion approximation (no ion inertia).

**4:00 pm MS-MoA7 Simulation of a Tungsten Filled Via Process Module for Process Integration, D. S. Bang, K. Hsiao, J. P. McVittie, and K. C. Saraswat, Integrated Circuits Lab, Stanford University, CA 94305, Zoran Krivokapic, Advanced Micro Devices, P.O. Box 3453, Sunnyvale, CA 94088.**

Tungsten is widely used for sub-micron VLSI via plugs because of the gap fill advantages of W-CVD over Al-PVD. A typical W-plug process contains multiple etching and deposition steps whose interactions become increasingly important in determining via characteristics as dimensions shrink. The use of computer simulation to examine equipment and process trade offs for an integrated Tungsten filled via process is demonstrated. Previous work in deposition and etching modeling has centered on developing topography models for specific process steps and equipment. This paper presents the development of modeling multistep fabrication processes for VLSI metallization. The interactions between different process steps during the fabrication of sub-micron Tungsten vias are examined. Process integration issues considered are the influence of oxide etch and glue layer deposition profiles on void formation during W-CVD, tradeoffs in collimated and non-collimated Ti/TiN PVD systems, and the effects of stop on oxide and stop on TiN W-etchback profiles on subsequent metallization. Simulations are tested with experimental results.

**4:20 pm MS-MoA8 Reactor- and Feature-Scale Simulation of Tungsten Chemical Vapor Deposition, A. H. Labun, Digital Equipment Corp., Hudson, MA 01749.**

Models of tungsten chemical vapor deposition (WCVD) by the hydrogen reduction of tungsten hexafluoride (WF<sub>6</sub>) are presented which span both the reactor and device scales, providing the capability of predicting tungsten step coverage in features from reactor settings. Comparisons of model predictions with experiments are made at both scales. A chemical kinetic scheme consisting of 16 elementary gas-surface reactions has been adopted from the work of Arora and Pollard [1] simulating low pressure WCVD and extended to 40 Torr using SURFACE CHEMKIN software [2]. A one-dimensional, stagnation-flow model of a single wafer reactor predicts deposition rate over a wide variety of process conditions, including deviations from the desired zero-order dependence of deposition rate on WF<sub>6</sub> partial pressure. The 'starvation' of the final elementary deposition reaction step for intermediate adsorbed WF<sub>x</sub> surface species, observed in the simulations, is evidently responsible for the resulting highly nonconformal deposition under these conditions. A simple model of an entire sub-micron feature as a single perfectly stirred reactor shows that as feature aspect ratio changes, so too does the internal chemical balance and hence the WF<sub>6</sub> partial pressure at which deviations from the zero-order deposition rate begin. A submicron feature in the zero-order deposition rate regime may also be modeled as a pair of communicating perfectly-stirred reactors, the first extending approximately one mean free path from the feature opening and the second comprising the remainder of the feature, with the gas concentrations at the feature opening determined by the reactor-scale simulation. The variation in starvation conditions between the two reactors which model the feature correlates with observed step coverage, from which a sticking coefficient may be deduced. The resulting sticking coefficient-based deposition model for WCVD has been integrated with a model for collimated TiN sputter deposition, permitting the submicron plug-filling process to be handled by a standard topography simulator.

[1] R. Arora and R. Pollard, J. Electrochem. Soc. **138** 1523 (1991).

[2] M. Coltrin, R. Kee, F. Rupley, Sandia Report SAND90-8003B (1991).

**4:40 pm MS-MoA10 Deposition and Flow Planarization of Glasses, H. Liao and T. S. Cale\*, Center for Solid State Electronics Research, Arizona State University, Tempe, AZ 85287-6006.**

We present our physically based simulation package (EVOLVE-

FLOW), which consists of EVOLVE [1] and a thin film thermal flow process simulation program. EVOLVE's algorithms for simulating profile evolution during low and high pressure deposition have been discussed [2]. The thermal flow process is modeled as two-dimensional, incompressible, free-boundary flow, and has been discussed by Bornside *et al.* [3]. The flow simulator generates a mesh in the deposited film, and solves the Navier-Stokes equations using the penalty function finite element method. The deposition/flow process is divided into a number of time steps, and the location of the free boundary is determined as a function of time. Within each simulation time step, the local film deposition rates are determined by EVOLVE, then the thermal flow simulation program predicts the flow induced film velocity. These velocities are combined and the free surface profile is updated using the movement algorithms in EVOLVE.

As an example application of EVOLVE-FLOW, we present simulated film profiles during the simultaneous deposition and fusion flow planarization of borophosphosilicate glasses in high aspect ratio trenches. The process is based on tetraethoxysilane-oxygen chemistry with triethylborate and phosphine as dopant sources, and is conducted in a LPCVD reactor. We compare the planarization performance of the single step process to that of a two step process (deposition then reflow) in order to explain its reported superior trench filling capability.

1. EVOLVE is a deposition process simulator developed by T. S. Cale at ASU and Motorola, Inc. with funding from the SRC and NSF.
2. T. S. Cale and G. B. Raupp, *JVST*, B8(6), 1242 (1990).
3. D. E. Bornside, R. A. Brown, S. Mittal and F. T. Geyling, *Appl. Phys. Lett.*, 58(11), 1181 (1991).

## BIOMATERIAL INTERFACES

Room A106 - Session BI-MoA

### Cell-Solid Surface Interactions

**Moderator:** J. J. Hickman, Science Applications International Corporation.

2:00 pm **BI-MoA1 The Bone Cell/Biomaterial Interface**, J. E. Davies, Centre for Biomaterials, University of Toronto, Ontario, M5S 1A1, Canada.

The future for Biomaterials lies in creating a marriage between materials science and biotechnology. Fundamental understanding of interfacial reactions between biological systems and artificial substrates will simultaneously lead to considerable advance in: (1) design of new materials for implantation in the body (Biomaterials), (2) creation of substrates for engineering of biological reactions in vitro (Biotechnology), and (3) creating substrates for diagnostic tests of biological processes in health and disease (Health Care). It has long been accepted that mechanistic explanations of reactions at solid liquid interfaces, within the biological milieu, will only emerge as a result of the deconvolution of molecular events at surfaces. However, there is currently a wide gap between our understanding of the physicochemistry of surfaces and the application of this knowledge to interpretations of cell behaviour. This gap is slowly closing as a result of the considerable efforts of surface scientists who have applied themselves to biological interfacial problems, and the emergence of analytical techniques which provide information on the intact solid/liquid interface. Specific examples of the need for a surface analytical approach to understand the behaviour of both major bone cell types, osteoblast and osteoclasts, at surfaces will be provided. These examples will include studies of corrosion behaviour, as a function of passivation treatment, of metal alloys in biological systems; bone cell adhesion and cell spreading as functions of the charged, or polar, nature of a polymer substrate; changes in bone protein adsorption as a function of polymer surface modifications and the means by which bone growth can be dictated by materials surfaces.

2:40 pm **BI-MoA3 Human Neutrophil Motility on Modified Surfaces**, L. Harvath, N. E. Brownson, K. E. Foster<sup>1</sup>, J. J. Hickman<sup>1</sup>, CBER FDA, Bethesda, MD 20892, <sup>1</sup>SAIC, McLean, VA 22102.

Human neutrophil migration in the absence of a stimulus (random motility) and in the presence of various concentrations of a chemotactic stimulus (chemotaxis) was evaluated on modified and unmodified polycarbonate membranes. Neutrophils are the first blood cells found at an inflammatory site. The assay is routinely used to evaluate neu-

trophil migration through 5  $\mu$ m pores in the polycarbonate membranes in response to medium alone or the chemoattractant, N-formylmethionyl-leucyl-phenylalanine (FMLP). Neutrophils that have migrated from the upper surface through the pores to the lower polycarbonate membrane surface are quantified by image analysis (Harvath *et al.*, 1980, *J. Immunol. Methods*, 37: 39-45). To investigate the role of the surface in neutrophil responses to a chemotactic agent, we modified the polycarbonate membranes with various self-assembled monolayers (SAMs). The silane monolayers used in this study contained various functionalities, including amines, thiols, and hydrophobic groups. The surfaces were analyzed by X-ray photoelectron spectroscopy and contact angle measurements. These modifications increased neutrophil random migration, in some cases, 3 to 4-fold over control responses. The surface modifications did not inhibit neutrophil chemotactic responses to FMLP, however, amine-containing modifications substantially increased (>6-fold) the chemotactic response to suboptimal concentrations of FMLP. The significance of enhanced neutrophil migration to suboptimal concentrations of chemoattractant may be directly relevant to *in vivo* responses to implanted materials.

3:00 pm **BI-MoA4 Nanofabricated Structures for the Measurement of Signals from Single Cells**, J. M. Cooper, A. Griffiths, and H. Morgan, Bioelectronics Group, Department of Electronics, University of Glasgow, Glasgow, G12 8LT, UK.

Dielectrophoresis is a technique which enables non-uniform electric fields generated at micro-electrodes to be used in order to guide or to position cells on the basis of their dielectric properties. By fabricating suitable geometries of such electrodes, it has proved possible to position individual cells within a two dimensional array of nano-scale amperometric biosensors. The sensors, which are based upon the immobilisation of cytochrome c on self-assembled thiol monolayers on gold, have a potential application in the detection of superoxide for cell signalling. To this end, measurements have been made on stimulated single neutrophils.

3:20 pm **BI-MoA5 Cell-Solid Surface Interactions**, D. A. Okrongly, Xytronix, Inc., San Diego, CA 92121.

Methods to effect specific cell adhesion to biomaterials is an area of intense investigation. In addition, recombinant protein technology has created a number of new biological drugs for diagnosing and treating disease. Combination of the products of biotechnology with biomaterials research has created an exciting new field of hybrid medical devices. A hybrid medical device can be defined as any medical device that uses a biological material, usually a recombinant protein, to effect its intended medical application. The current investigation will be a case study of a medical device used in human clinical trials to separate immune stem cells and CD8+ lymphocytes. The discussion of the methodology employed in the development of these highly specific cell adhesion devices will highlight a new type of biomaterial, surface analysis techniques such as ESCA and Attenuated Total Reflectance FT-IR and the use of monoclonal antibodies directed to cell surface antigens. Preliminary results of human clinical trials will be presented.

**INVITED**

4:00 pm **BI-MoA7 Nanofabricated Fibers for Studying the Phagocytosis of Inorganic Particulates by Macrophages**, J. Gold, B. Nilsson, and B. Kasemo, Chalmers University of Technology and University of Göteborg, 412 96 Göteborg, Sweden.

Inorganic particulates occur in the body due to e.g. wear debris generated by articulating surfaces in orthopaedic implant devices, or by inhalation of mineral dusts and fibers. Empirical observations have indicated that these particulates can lead to failure of the implant and lung diseases, respectively. Macrophages attempt to remove particulates from the body via phagocytosis into the cell, and send out signals indicating the presence of either an inert or a toxic foreign object. Several physical and chemical characteristics of the particulates appear to play a role in determining this phagocytic response of macrophages.

Typically, particulates used in these types of studies are produced by e.g. grinding raw/bulk materials, spin casting, or atomization. However, these techniques generate inherent distributions in the size, shape and chemical composition of particulates even within a given production lot. In the present work we have produced fibers having controlled shapes, dimensions, sized distributions, and compositions for studying the role of these factors in the cellular response. By using nanofabrication techniques, fibers can be made in a large number of materials and in a wide range of dimensions (nm's to mm's). Significant quantities for cell culture studies can be made with tight control over the fiber size distribution.

Ti, SiO<sub>2</sub>, and Au fibers of dimensions 0.1, 1 and 10  $\mu$ m, have been

produced and are currently being used in cell culture studies of the phagocytic response of alveolar macrophages. The preparation and characterization of these fibers will be presented. Reference will be made to the ongoing cell culture studies at the Dept. of Environmental Medicine, Univ. of Gothenburg, Sweden.

**4:20 pm BI-MoA8 Protein-Platelet and Platelet-Leukocyte Interaction at Materials in Contact with Human Blood, Håkan Nygren, Magnus Braide and Christin Karlsson, Department of Anatomy and Cell Biology, Medicinaregatan 5, S-413 90 Göteborg, Sweden.**

The adhesion and activation of platelets and leukocytes at blood-material interfaces was studied by fluorescence microscopy, and photometry using specific anti-CD antibodies, anti-plasma protein antibodies and the calcium ion probe Fura-2. Gold or titanium were evaporated onto glass slides and capillary blood was placed as droplets on the surfaces in a humidified chamber. The adsorption of plasma protein was monitored with FITC-labelled antibodies and the adhesion of platelets was shown by anti-CD 61 antibodies, specific for this cell type.

Adhering platelets were found after 15 seconds incubation time on both surfaces, and the number of cells increased slowly. The cells spread over the surface, aggregated and developed stress fibers in contact with the surface. The distribution of fibrinogen was heterogeneous with higher surface concentration in connection with adhering cells. Platelet-derived microvesicles were found after 8 minutes of incubation. These microvesicles showed intense staining with anti-C3c antibodies.

In other experiments, granulocytes were isolated and incubated with Fura-2. The supernatant of hirudin-treated blood, incubated with material surfaces was added to the cells and the fluorescence was recorded after emission at 340 and 380 nm. A rapid peak was shown indicating influx of  $\text{Ca}^{++}$  into the cytoplasm. The results suggest a functional relationship between adsorbed plasma proteins, platelets and leukocytes, which may be important in the non-self recognition of foreign materials.

**4:40 pm BI-MoA9 Effect of Surface Mobility on Biointeractions, B. D. Ratner, C. D. Tidwell, Univ. of Washington, Seattle, WA 98195.**

Correlations between biomaterial surface properties and biological responses involves consideration of many factors including surface chemistry, charge, and morphology. One parameter affecting biointeractions which has received limited attention is surface mobility, due in part, to difficulties in making well-defined, mobile surfaces. Molecular self-assembly provides an effective means of fabricating organic surfaces with well-defined structure and chemistry for elucidating relationships between surface structure and bioresponses. "Mixed" self-assembled monolayers (SAMs), prepared by the coadsorption of alkanethiols of differing alkyl chain length onto gold, form monolayers

comprised of a highly ordered inner region and a disordered, liquid-like outer region. Using a series of mixed SAMs with varying interfacial disorder, biointeractions can be investigated.

A series of mixed SAMs were formed by competitive adsorption of 1 mM ethanolic solutions of mixtures of octadecyl mercaptan and dodecanethiol onto evaporated gold substrates. SAM surface composition, compositional depth profile, and thickness were determined by X-ray photoelectron spectroscopy (XPS). Monolayer wetting characteristics were assessed by contact angle goniometry. Biointeraction characteristics of the mixed SAMs are being investigated by albumin and fibronectin adsorption and elutability studies followed by a determination of endothelial cell growth on the SAMs.

Thicknesses of the hydrocarbon portion of the monolayers, as determined by XPS, were approximately 13–19 Å. Cosines of the advancing contact angles for water and the natural logarithm of the ratio of C(1s) and Au(4f) XPS intensities varied in a sigmoidal fashion with the log of the ratio of components in solution. A solution concentration ratio of 5:1 (Dodecanethiol/octadecyl mercaptan) was required to obtain a SAM composed of an equimolar mixture of the two components.

**5:00 pm BI-MoA10 Secondary Ion Mass Spectrometry Studies of Covalently Bound Peptides to a Fluoropolymers: Imaging and Quantitation, Evan J. Bekos, Frank V. Bright, and Joseph A. Gardella, Jr., SUNY Buffalo, Chemistry Department, Buffalo, New York 14214.**

We have recently reported the covalent binding of peptides, by both the N- and C-termini, to a modified fluoropolymer.<sup>1</sup> The binding of a pentapeptide, YIGSR (Tyr-Ile-Gly-Ser-Arg), has been analyzed and quantified using a variety of surface sensitive techniques: secondary ion mass spectrometry (SIMS), electron spectroscopy for chemical analysis (ESCA), and attenuated total reflectance-Fourier transform infrared spectroscopy (ATR-FTIR). In the current study, we are using SIMS to analyze and quantify a broad range of peptide sequences bound to a fluoropolymer substrata. The higher mass fragments unique to each peptide will be used to analyze mixtures of peptides. In the case of lithographically patterned surfaces, images of peptides restricted to defined domains will be presented. Also, an established quantitative method will be used for these peptide mixtures.<sup>2</sup> The use of these peptide-modified materials in neural cell tissue regeneration is currently being explored.

(1): T. G. Vargo, E. J. Bekos, Y. S. Kim, J. P. Ranieri, R. Belamkonda, P. Aebischer, D. E. Margevich, P. M. Thompson, F. V. Bright, and J. A. Gardella, Jr., *J. Biomed. Mater. Res.*, submitted April 1994.

(2): P. A. Cornelio and J. A. Gardella, Jr., *J. Vac. Sci. Technol. A*, **8**(3), 2283–2286 (1990).



## SURFACE SCIENCE

### Room BR4 - Session SS-MoP

#### Aspects of Surface Science

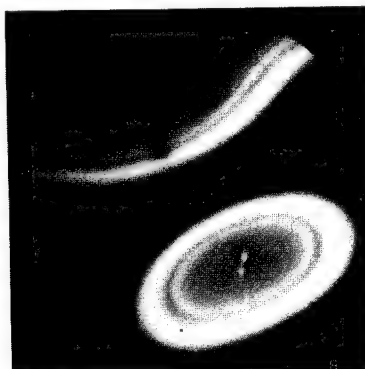
**Moderator:** J. C. Hemminger, University of California, Irvine.

**SS-MoP1 In Situ, Real-Time Photoelectron Emission Microscopy and Scanning Auger and Low-Energy Electron Diffraction Studies of Oxygen Enhanced Diffusion of Sulfur on Mo(310) at 1000 K,** A. Garcia, M. E. Kordesch, Ohio University, Athens, OH 45701.

In situ, real-time observations of sulfur diffusion from bulk Mo(310) to the oxygen covered Mo surface with the photoelectron emission microscope shows two major routes for sulfur transport on the O/Mo(310) surface. One type is characterized by annular structures centered on impurity particles. The second type is in the form of a two-dimensional front of macroscopic dimensions (several millimeters) extending over the crystal surface. Both annular and front-like features exhibit well developed, structured leading edges (see micrograph<sup>†</sup>). Post-reaction Auger analysis confirms the removal of oxygen from the substrate and reveals sulfur wherever oxygen was removed. Low-energy electron diffraction shows an ordered sulfur overlayer. We present data suggesting that the oxygen surface concentration regulates sulfur transport to and over the surface.

<sup>†</sup>Field of view is 260  $\mu\text{m}$ .

Supported by ONR/BMDO Grant No. N0014-J-91-1596.



**SS-MoP2 Multi-Bounce Direct Scattering of N<sub>2</sub> from Cu(110),** J. L. W. Siders and G. O. Sitz, Department of Physics, University of Texas, Austin, Texas 78712.

Resonantly enhanced multiphoton ionization and time resolved molecular beam techniques were used to study the rotational state and velocity distributions of N<sub>2</sub> scattered from Cu(110). The final rotational temperature of the scattered molecules was found to depend linearly on incident energy,  $E_i$ , indicating a direct scattering process. Unlike the previous results of N<sub>2</sub> scattering on silver (Sitz, J. Chem. Phys. **89**, 2558), tungsten and platinum (Hanisco, J. Chem. Phys. **99**, 7076), the surface temperature dependence is found to be strong on copper. An anticorrelation between the final translational energy and final rotational state,  $J$ , was present for an incident energy of 0.79 eV, but was washed out at 0.09 eV. For  $E_i = 0.09$  eV the N<sub>2</sub> molecules scattered into the highest  $J$  states have more final rotational energy than incident energy available, which suggests that surface energy is being converted into rotational energy. The final total energy remains less than the incident energy for  $E_i = 0.79$  eV, therefore energy is being transferred to the surface. Rotational rainbows were observed at high incident energies ( $>0.25$  eV), but were washed out at low energies and low surface temperatures (300 K). As the surface temperature is raised the rotational rainbow becomes more pronounced. The strong surface temperature dependence and absence of rotational rainbows at low  $E_i$  and  $T_s$  is attributed to multiple bounces which appear to play a large role in the dynamics and energy transfer of the N<sub>2</sub>/Cu system. Work supported by the Robert A. Welch Foundation, grant F-1198.

**SS-MoP3 Dynamics of D<sub>2</sub> Recombinative Desorption from Ag(111),** R. N. Carter, F. Healey, and A. Hodgson, Surface Science Research Centre, University of Liverpool, Liverpool L69 3BX, U.K.

The interaction of deuterium atoms with Ag(111) has been investigated with temperature-programmed desorption (TPD) and low energy electron diffraction (LEED). Atomic deuterium is found to adsorb on this surface at a temperature near 110 K, resulting in a TPD feature near 185 K at lowest coverages. With increasing exposure, this feature shifts up in temperature to an ultimate value of 220 K and is joined by two lower temperature peaks near 200 and 180 K. The lowest temperature feature does not saturate but grows linearly with exposure and is attributed to deuterium atoms absorbed into the subsurface. LEED shows a  $(2 \times 2)$  pattern at 110 K for low coverages where only the highest temperature peak is observed in TPD. At coverages above this, a superposition of  $(2 \times 2)$  and  $(3 \times 3)$  patterns is observed at 110 K, which reorders to  $(4 \times 4)$  after annealing at 150 K. The angular distribution of the low coverage desorption peak is sharply peaked with respect to the surface normal, with a  $P(\theta) = \cos^2\theta$  distribution. The implications of these results for the D<sub>2</sub>-Ag(111) potential energy surface as well as the kinetic analysis of the TPD will also be discussed.

**SS-MoP4 Epitaxial Domains of C<sub>60</sub> on Ag(111),** J. E. Rowe, R. A. Malic, E. E. Chaban, and C.-M. Chiang, AT&T Bell Laboratories, Murray Hill, New Jersey 07974.

Epitaxial C<sub>60</sub> films have been grown on Ag(111) substrates for thickness up to  $\sim 100$  monolayers (ML). For ultrathin layers (0-2 ML) we observe growth of (111) layers of C<sub>60</sub> which have a  $(2\sqrt{3} \times 2\sqrt{3})R30^\circ$  superstructure with respect to the fundamental Ag(111) 2-D lattice. Low energy electron diffraction (LEED) with a computer controlled CCD camera allowed accurate images and angular profiles to be measured. Two domains are observed at low electron energies,  $E \lesssim 40$  eV as well as multiple scattering between domains due to an anti-phase boundary structure. These thin layers do not exhibit the low temperature phase transition associated with orientation ordering in the bulk. This is likely due to the strong C<sub>60</sub>-Ag(111) interaction previously reported by Altman and Colton [1]. As growth continues above 2 ML a gradual transition occurs to a twinned (111) layer structure which interacts less strongly with the substrate. These thicker layers display the low temperature phase transition associated with orientation ordering in the bulk. However, the surface of these films show anti-phase domain effects as well as the twinning with respect to the Ag(111) substrate. Domain sizes of the twinned commensurate structure are in the range 40-50 Å which is more than a factor of two smaller than the best epitaxial films grown on Cu(111) substrates. Soft X-ray photoemission of the C-1s core level shows an asymmetric shape similar to that of C<sub>60</sub> on Cu(100) which we interpret as evidence of local orientation ordering as reported for epitaxial films grown on Cu(111). The shift with respect to the bulk C-1s position can be interpreted as a charge transfer of  $\sim 1$  electron per C<sub>60</sub>. This local ordering may be the cause of the anti-phase domains observed with LEED.

[1] E. I. Altman and R. J. Colton, Surface Science, **295**, 13-33 (1993).

**SS-MoP6 Deposition of Thin Layers of Inorganic Salts from Solution by Spin Coating,** R. M. van Hardeveld, M. Goedbloed, J. C. Muijsers, L. J. van IJendoorn, E. W. Kuipers<sup>a</sup> and J. W. Niemantsverdriet, Eindhoven University of Technology, Eindhoven, and <sup>a</sup>Shell Research, Amsterdam, The Netherlands.

Spin coating is a well known technique for the preparation of thin polymeric photo resist layers on silicon wafers. Recently, the method has attracted attention as a highly useful procedure for the deposition of thin layers (between less than one and several monolayers) of inorganic salts on flat supports, of interest as models for catalysts. Here we show that a slightly modified theoretical description of the spin coating process predicts the amount of deposited material within 15% accuracy, on the basis of the following parameters: evaporation time, density, viscosity and concentration of the solution, and rotor speed. The method has been applied to deposit submonolayers of molybdenum and chromium on flat oxides of silicon and aluminum. Ruthenium Backscattering Spectrometry (RBS) and X-ray photoelectron spectroscopy (XPS) have been used to determine the amount of deposited material.

**SS-MoP7 Interaction of Fullerenes with the Cu(111) and Ag(111) Surfaces**, T. Sakurai, X.-D. Wang, T. Hashizume, J. Kishimoto, S. Yamazaki, V. Yurov, H. Shinohara\*, and H. W. Pickering#, Institute for Materials Research (IMR), Tohoku University, Sendai 980-77, Japan, \*Faculty of Science, Nagoya University, Nagoya 464-01, Japan, #Department of Materials Science and Engineering, The Pennsylvania State University, University Park, PA 16802, USA.

Adsorption and the monolayer film formation of fullerenes ( $C_{60}$ ,  $C_{70}$ ,  $C_{60(x)}C_{70(1-x)}$ ,  $Sc_2@C_{84}$ , etc.) on the Cu(111)  $1 \times 1$  and Ag(111)  $1 \times 1$  surfaces have been studied by the field ion-scanning tunneling microscope (FI-STM). The fullerene molecules are mobile on the terrace at room temperature, segregate to the steps and form two-dimensional islands with a close-packed configuration. Monolayers of the  $C_{60}$  and  $C_{60(x)}C_{70(1-x)}$  ( $x > 30\%$ ) molecules on the Cu(111) surface form a highly ordered  $4 \times 4$  commensurate phases and the intramolecular structures are observed. This indicates a strong interaction between fullerenes and the Cu substrate to suppress fullerene's internal rotation. The intramolecular structures are interpreted in terms of the local density of the states of the  $C_{60}$  and  $C_{70}$  molecules.

For the case of the  $Sc_2C_{84}$  monolayer film on the Ag(111) surface, we observe eight different phases having a similar nearest neighbour distance but distinctly different rotation angles with respect to the substrate, similar to the case of the  $C_{60}$  adsorption on the Ag(111) surface. These indicate that the interaction between fullerene and the Ag(111) surface is weak comparing with that among fullerene molecules. The rotation angle is dictated by the adsorption configurations which produce higher number coincidence lattice sites.

**SS-MoP8 STM Study of the Clean and Cu Covered  $TiO_2(110)$  Surface\***, D. Novak, E. Garfunkel, and T. Gustafsson, Departments of Physics and Chemistry, and Laboratory for Surface Modification, Rutgers, The State University of New Jersey, Piscataway, NJ 08855.

We have used a UHV Scanning Tunneling Microscope (STM) to study the atomic scale structure of  $TiO_2(110)$  ( $1 \times 1$ ) and the nature of defects on this surface. Samples have been prepared which are atomically flat over large areas, and on which the ( $1 \times 1$ ) structure is resolved with STM. On some samples, we also find a highly elongated defect structure in addition to the ( $1 \times 1$ ) structure. These rowlike structures ( $\sim 2 \text{ \AA}$  in height and  $\sim 12 \text{ \AA}$  FWHM) are oriented along the [001] direction in registry with the ( $1 \times 1$ ) structure and can extend for up to  $1000 \text{ \AA}$  when not intersecting a step edge. We have also studied the morphology of Cu overlayers on this surface. For deposition at 300 K, Cu is found to form three dimensional islands in the low coverage regime. Upon annealing, a coarsening process is observed in which the size of an average cluster increases. The clusters are found to be weakly bound to the substrate and are easily moved with the STM tip.

\*Supported by NSF DMR 90-19868 and 93-06899.

**SS-MoP9 Low Energy Ion Beam Damage of Self-Assembled Monolayers**, E. Ada, J. A. Burroughs, S. B. Wainhaus, and L. Hanley, University of Illinois at Chicago, Chicago, IL 60607-7061.

These experiments examine the effect of low energy atomic and molecular ion beam exposure upon self-assembled monolayers of alkanethiols. Methane and hexanethiolate adsorbates on Ag(111) are exposed to low energy ( $< 100 \text{ eV}$ ) molecular ions of pyridine, furan, and thiophene. The degree of ion beam damage of the adsorbate is then measured by infrared reflection absorption spectroscopy. Ion beam damage of the adsorbate ranges up to 50% for exposures of  $\sim 10^{14}$  ions/cm<sup>2</sup>. More recent experiments utilize x-ray photoelectron spectroscopy to probe the effect of low energy  $Ar^+$ ,  $O_2^+$ , and  $N_2^+$  ions on alkanethiolates adsorbed on polycrystalline gold surfaces. These results indicate that low energy ion beams can be utilized in lithographic applications via modification of self-assembled monolayers for selective electroless metal deposition.

**SS-MoP10 Vibrational Studies of Adsorbate Structure, Bonding and Reactivity: Alcohols, Thiols and Alkyl Iodides Adsorbed on Mo(110)**, M. K. Weldon, P. U. Uvdal and C. M. Friend, Department of Chemistry, Harvard University, Cambridge, MA 02138.

The bonding and reactivity of methanol and methyl iodide adsorbed on Mo(110) as well as benzenethiol adsorbed on sulfided Mo(110) were investigated using temperature programmed reaction, Fourier transform infrared reflection adsorption and electron energy loss spectroscopies in combination with isotropic labelling studies. At low coverages, methoxy adsorbs in a pseudo- $C_{3v}$  geometry, based on the observation of a single C-H stretch at  $2930 \text{ cm}^{-1}$  in the infrared

spectrum of  $CHD_2O$ . At high coverage two methoxy species are apparent, both with  $C_6$  symmetry, based on the appearance of two distinct symmetric C-H stretching modes as well as two asymmetric C-H stretching modes in the surface infrared spectra. The average tilt angle of these species is estimated to be  $\sim 30 \pm 10^\circ$ , from the relative intensity of the symmetric and asymmetric deformation modes. The C-O bond is found to be extremely anharmonic, based on the observation of the overtone of the C-O stretch with an anharmonicity of  $\sim 50 \text{ cm}^{-1}$ . We estimate a C-O bond energy of  $\sim 20 \text{ kcal/mol}$ , by assuming a Morse potential. Surface methyl exhibits considerable C-H bond softening on adsorption on Mo(110). The molecular symmetry is lower than  $C_{3v}$  over the entire coverage range, based on the dipole character of both the symmetric and asymmetric C-H stretching modes in the electron energy loss spectrum. Facile conversion to surface methylene occurs below 250 K. We propose that the methylene groups bridge along the [001] directions, by consideration of the selection rules operative in electron energy loss spectroscopy. Phenyl disulfide is formed via S-H bond scission and S-S bond formation in benzenethiol on 0.35 ML S Mo(110) at 100 K. The S-S linkage is oriented perpendicular and the phenyl ring parallel to the surface, based on electron energy loss spectroscopy. The disulfide subsequently forms an upright phenyl thiolate species, prior to the onset of gaseous benzene and phenyl formation.

**SS-MoP11 Hydrogenation of Cyclohexene by Subsurface Hydrogen on Ni Surfaces**, Gyeong-A Son, Manos Mavrikakis, John L. Gland, Department of Chemistry, University of Michigan, Ann Arbor, MI 48109.

Subsurface hydrogen can be formed at low pressure by absorption of pre dissociated hydrogen in Ni(100) and Ni(111) samples. Subsurface hydrogen selectively hydrogenates cyclohexene to cyclohexane on both surfaces at about 176K. In contrast, no hydrogenation by surface hydrogen is observed. Desorption of molecular cyclohexene dominates on both Ni(100) and Ni(111) surfaces in the presence of surface hydrogen. Dehydrogenation of cyclohexene to benzene is a dominant thermal path way on both surfaces in the absence of hydrogen. Reaction mechanism of cyclohexene hydrogenation were suggested by TPD, EELS and isotopic experiments. We have demonstrated that absorbed hydrogen is quite reactive even at low temperature. Temperature programmed desorption and high resolution electron energy loss spectra were combined to probe the dynamics of surface and bulk phenomena involved.

**SS-MoP12 FT-IRAS of Adsorbed Alkoxides: Methoxide and Ethoxides on Cu(111)**, Shane C. Street, University of Illinois Urbana-Champaign 61801, and Andrew J. Gellman, Carnegie Mellon University, Pittsburgh, PA 15213.

The surface chemistry and structure of methoxide and ethoxide adsorbed on Cu(111) has been studied by FT-IRAS and TPD. The structure of methoxy on Cu(111) has been a matter of debate. Previous IRAS results were interpreted to show that the  $C_{3v}$  axis of methoxy at saturation coverage lies perpendicular to the surface. Subsequent X-ray diffraction and backscattering photoelectron diffraction experiments support this orientation. However recent work with methoxy cluster compounds has led to the proposal that at low coverages methoxy is tilted, and that steric crowding reorients the molecular axis towards the surface normal at saturation. We present high resolution spectra for methoxy at a range of coverages. For the more complex ethoxy adsorbate we present the FT-IRAS spectra for a set of seven deuterated and isotopically ( $^{13}C$ ) labelled ethoxides. This is by far the most detailed labelling study to assign vibrational modes of an adsorbate. The  $C_{3v}$  axis of the methyl group of ethoxy is found to lie roughly parallel with the surface.

**SS-MoP13 Dissociation Kinetics of NO on Rhodium(111)**, H. J. Borg, R. A. van Santen and J. W. Niemantsverdriet, Schuit Institute of Catalysis, TU Eindhoven, P.O. Box 513, 5600 MB Eindhoven, The Netherlands.

Temperature programmed static secondary ion mass spectrometry (TPSSIMS) and temperature programmed desorption (TPD) have been used to study the kinetics of adsorption, dissociation, and desorption of NO on Rh(111). At 100 K, NO adsorbs molecularly via mobile precursor state kinetics. SSIMS suggests threefold adsorption at low coverage, with increasing amounts of bridged NO at higher coverages. Three characteristic coverage regimes appear with respect to NO dissociation. At coverages below 0.25 ML, NO dissociates completely at temperatures between 275 and 340 K, with an activation energy of  $39 \pm 6 \text{ kJ/mol}$  and a preexponential factor of  $10^{6 \pm 1} \text{ s}^{-1}$ . Nitrogen atoms desorb as  $N_2$ , with kinetics that is strongly influenced by the presence



of coadsorbed oxygen. In the medium coverage range,  $0.25 < \theta_{\text{NO}} < 0.50$  ML, part of the NO desorbs molecularly, with a desorption barrier of  $116 \pm 10$  kJ/mol and a preexponential of  $10^{16.5 \pm 1.0} \text{ s}^{-1}$ , suggestive of a mobile transition state. Dissociation of NO becomes progressively inhibited, the onset shifting from 275 K at 0.25 ML to 400 K, the NO desorption temperature, at a coverage of 0.50 ML. On these highly covered surfaces nitrogen atoms become destabilized, resulting in an additional low temperature  $\text{N}_2$  desorption state. For initial NO coverages higher than 0.50 ML, NO dissociation is completely self-inhibited, indicating that all sites required for dissociation are blocked. The desorption of the more weakly bound bridged NO does not generate the sites required for dissociation; these become only available after the desorption of triply coordinated NO.

**SS-MoP14 Two-Dimensional Surface Interactions and Dynamics of Benzene on Cu{111}, M. M. Kamna, S. J. Stranick, and P. S. Weiss,** Department of Chemistry, The Pennsylvania State University, University Park, PA 16802.

We seek to understand the interactions that determine the chemistry, structure, and dynamics of surface adsorbates. We have used ultrahigh vacuum scanning tunneling microscopy to study the low temperature behavior of benzene adsorbed on Cu{111}. Electron standing waves are apparent in STM images of Cu{111} at low temperature due to scattering of surface states from step edges, defects, and benzene molecules. The resulting charge density modulations influence the binding of the benzene molecules. We find that at low coverage, adsorbed benzene binds along Cu step edges and at other high charge density sites. The molecules form a tightly bound 2-D solid at the step edges while benzene molecules on terraces move across the surface as a 2-D molecular gas. At the interface between the solid and gas we observe 2-D adsorption and desorption in real time. We discuss the relative strengths of the interactions at various step and terrace sites due to these nanometer scale variations in the surface electronic structure.

This work was supported by BRDC, NSF, and ONR.

**SS-MoP15 RAIRS of Rh Single Crystal Surfaces During NO Reduction at Moderate Pressures, D. N. Belton, H. Permana, S. J. Schmieg, General Motors R&D, Warren, MI 48090-9055, and K. Y. Simon Ng, Wayne State University, Detroit, MI 48202.**

Although CO and HC emissions from passenger cars are primarily determined by the amount of time required to heat up the catalyst, NO emissions tend to occur primarily under conditions where the catalyst is fully warmed-up. This simple observation means that NO reduction kinetics play an important role in determining the amount of NO that will escape from the catalytic converter of a vehicle. Our research has focused on obtaining a detailed kinetic mechanism that can quantitatively describe NO reduction kinetics. To achieve this goal we have measured reaction kinetics at pressures realistic for automotive exhaust and modeled those kinetics with a mechanism consisting of elementary steps and UHV-measured rate constants. Currently we reproduce the observed reaction rates using reasonable rate constants that can be justified on the basis of UHV measurements; however, we have not been able to measure the rates of every elementary step at all applicable coverages. In order to constrain the permissible surface coverages in our model, we have recently used reflection-absorption infrared spectroscopy to measure CO and NO coverages during the  $\text{NO} + \text{CO}$  and  $\text{NO} + \text{CO} + \text{O}_2$  reactions over Rh single crystals. Our results show that there is both NO and CO on the surface under most reaction conditions. Further, as the reaction temperature or the CO pressure is raised, there is a strong tendency for CO to displace NO from the surface. These measurements will be put in context of the reaction mechanism and the effect of these experimental measurements on our modeling efforts will be discussed.

**SS-MoP16 Vibrational and Electron Spectroscopic Study of the Interaction of Nitric Oxide with the Ni(110) Surface, D. H. Hellmoldt, C. M. Affentauschegg and J. E. Crowell, Department of Chemistry, University of California at San Diego, La Jolla, CA 92093-0314.**

The understanding of  $\text{NO}_x$  reactions with metal surfaces is of fundamental importance to the development of efficient catalysts for automobile exhaust pollution control. In an effort to understand these processes we have studied the reaction of NO with clean, as well as oxygen and hydrogen-precovered, Ni(110) surfaces. At saturation NO coverage, reflection-absorption Fourier transform infrared spectroscopy (FT-RAIRS) shows two distinct NO stretching vibrations: A sharp, intense peak at  $1867 \text{ cm}^{-1}$ , assigned to atop site adsorption,

and a broad medium strength peak at  $1678 \text{ cm}^{-1}$ , which we have assigned to bridge site adsorption. Additionally, a weak, broad band at  $1740 \text{ cm}^{-1}$  is observed; this feature may be a result of NO adsorption at defect sites. The coadsorption of hydrogen suppresses the higher frequency ( $1867 \text{ cm}^{-1}$ ) peak, thus stabilizing the bridge site, while  $\text{O}_2$  preadsorption favors NO adsorption at atop sites. X-ray photoelectron spectroscopy (XPS) analysis of the above surfaces suggests that at least two types of adsorption occur. This data, together with the RAIRS data, indicates that NO decomposition predominates upon initial NO exposure at 125 K, with molecular adsorption possible with increasing exposure after a critical coverage of N and O atoms at the surface is reached. Also, it is found that NO decomposes at the surface with heating, leading to little or no NO molecular species at the surface above 400 K. With further heating, the O atoms remain on the surface, while the N atoms combine to desorb as  $\text{N}_2$  by  $\sim 850$  K. The implications of the above findings will be discussed.

**SS-MoP17 The Role of C in O Removal from Ultra-Thin Layers of Oxidized La on Pd(100), G. W. Graham<sup>a</sup>, B. U. M. Rao<sup>b</sup>, and M. Ahmad<sup>b</sup>, <sup>a</sup>Ford Motor Company, MD 3179, Bldg. SRL, P.O. Box 2053, Dearborn, MI 48121, <sup>b</sup>Wayne State University, Department of Physics and Astronomy, Detroit, MI 48202.**

The complete removal of O from ultra-thin layers of oxidized La on Pd(100), effected by heating to temperatures as low as 625 K in UHV (1, 2), was found to be influenced by C present at levels not detected by Auger electron spectroscopy due to interference with Pd. Measurements in which Pd was replaced by Rh, where correspondingly small levels of C could be detected, show that C from the Rh is able to reduce oxidized La under such conditions. The elimination of C from the Pd(100) surface by means of heat treatments in  $\text{O}_2$  (tested by temperature programmed desorption of CO) led to only a modest increase (100 K) in thermal stability of the oxidized La, however, and the thermal stability of ultra-thin layers of oxidized Al was essentially unchanged. A difference in sensitivity to C of the thermal stability of oxidized La versus Al layers on Pd could be indicative of a difference in the interfacial structure which might also account for other known differences in chemisorption and sintering behavior.

(1) M. Ahmad, Md. M. Rahman, B. U. M. Rao, and G. W. Graham, J. Vac. Sci. Technol. (in press).  
(2) A. D. Logan and G. W. Graham, Surf. Sci. 277, L47 (1992).

**SS-MoP18 A Study of Oxygen Chemisorption Phases on Pt(111), C. Puglia, A. Nilsson, B. Hernnäs, K. O. Karis, P. Bennich and N. Mårtensson, Department of Physics, Uppsala University, Box 530, S-751 21 Uppsala, Sweden.**

$\text{O}_2/\text{Pt}(111)$  is a system that has been object of a great number of studies during a long period of time. We now present new results concerning the identification and characterization of three different chemisorption states studied by means of different spectroscopic techniques such as XPS, XAS and DES. From our data we can conclude that oxygen chemisorbes on Pt(111) in two different molecular phases which are precursors for the thermal activated dissociation process. A first molecular state is obtained at a temperature of about 90 K. It is weakly chemisorbed and we have identified it as a superoxo-like configuration of the oxygen molecule ( $\text{O}_2^-$ ). At around 135 K a second molecular phase, more strongly involved in the hybridization with the substrate, has been characterized as a peroxo-like configuration ( $\text{O}_2^{2-}$ ). The atomic phase, with the characteristic ( $2 \times 2$ ) LEED patterns, occurs at a substrate temperature higher than 150 K. For this phase we will discuss the results according to a model which describes the density of states induced by the hybridization of the oxygen 2p orbitals with the 6sp-states and 5d-band of the metal.

**SS-MoP20 Selective Oxidation Reactions on Rh(111)-p(2 × 1)-O: C. W. J. Bol and C. M. Friend, Department of Chemistry, Harvard University, Cambridge, MA 02138.**

Oxygen addition reactions on Rh(111)-p(2 × 1)-O were investigated using temperature programmed reaction and high resolution electron energy loss spectroscopy. Ketones are formed in the oxidation of secondary thiols and halides. Olefin elimination and decomposition are competing pathways. The selectivities strongly depend on the initial oxygen coverage. At low oxygen coverage no ketone production is observed and olefin elimination and decomposition are the major pathways. Small amounts of the corresponding alkane are also formed.

Vibrational studies show that the, at low temperature formed, thiolates and the alkyl halides stay intact up till the reaction temperature. Carbon-sulfur (carbon-halide) bond cleavage is proposed to be the

rate determining step in the formation of both ketones and olefins. The reaction temperature correlates well with the C-X bond strength in different secondary thiols and alkylhalides. Further studies will address the nature of the C-X bond cleavage; homolytic, resulting in a radical, or heterolytic, forming a carbocation.

The proposed mechanism is different than those observed in the oxidation of secondary alkoxides on Rh(111)-p(2 × 1)-O. Here  $\beta$ -hydrogen abstraction at low temperature leads to the formation of ketones and reaction with surface oxygen at higher temperature gives rise to a surface carboxylate, which subsequently reacts to form a ketone. These mechanisms are not feasible in the oxidation of secondary thiolates and halides because of geometric reasons.

**SS-MoP21 The Early Stages of Ruthenium Oxidation,\* J. Hrbek, D. van Campen and I. Malik\*,** Chemistry Department 555, Brookhaven National Laboratory, Upton, NY 11973-5000; \*MEMC Electronic Materials, P.O. Box 8, St. Peters, MO 63376.

Although Ru is known to be an excellent catalyst for several processes, it is not used by the industry because it forms volatile oxides. In order to understand the initial stages of the process, we studied the interaction of atomic oxygen with a Ru(001) surface by X-ray photoelectron spectroscopy, thermal desorption and electron diffraction. Atomic oxygen reacts with ruthenium in three distinct stages: chemisorption is followed by subsurface diffusion and oxidation. Large concentration of oxygen can be dissolved in the subsurface region without a noticeable change of the Ru core levels. We observe the onset of reaction of dissolved oxygen with the Ru host only for concentrations corresponding to equivalent coverages of more than ~50 ML. A new Ru 3d core level, shifted by 0.50 eV toward higher binding energy, grows with increasing oxygen exposure. An additional weak feature 2.60 eV above the metallic Ru 3d binding energy appears for higher oxygen coverages. The asymmetric O 1s peak shows a shoulder 2.0 eV higher than the main oxygen level. At the highest coverage studied (~870 ML) almost all the Ru metal within the probing depth of the photoelectrons is oxidized; the binding energy of the main component agrees well with previous measurements on RuO<sub>2</sub>. Completely diffused LEED patterns show that the surface is disordered for coverages higher than 3 ML. The oxidized Ru surface is thermally stable up to 900 K with the majority of oxygen desorbing between 950 and 1150 K. Heating the Ru crystal to 1560 K removes all detectable oxygen and restores the perfect structural order of Ru(001).

\*This research was carried out at Brookhaven National Laboratory under contract DE-AC02-76CH-00016 with the U.S. Department of Energy and supported by its Division of Chemical Sciences, Office of Basic Energy Sciences.

**SS-MoP23 Activation Effects on the Surface Properties of Silica-Supported Cobalt Catalysts, Kent Coulter and Allen G. Sault,** Sandia National Laboratories, Albuquerque, NM 87185-0710.

XPS shows that the surface properties of Co/SiO<sub>2</sub> catalysts exhibit a strong dependence on catalyst pretreatment conditions with the formation of cobalt oxide, cobalt silicate, cobalt silicide, and metallic Co determined by the activation environment. Heating a Co(NO<sub>3</sub>)<sub>2</sub>·6H<sub>2</sub>O precursor on a silica support at 400°C in air, after drying at 100°C in either air or vacuum, produces Co<sub>3</sub>O<sub>4</sub> that is easily reduced in H<sub>2</sub>. In contrast, samples dried at 100°C and then annealed in UHV to 400°C exhibit drastically different characteristics. Initially, the cobalt phase on the dried samples is a surface silicate. Annealing air dried samples in UHV converts the surface silicate to an irreducible bulk cobalt silicate. Remarkably, UHV annealing of vacuum dried samples promotes the formation of a cobalt silicide. The nature of the Co species formed depends upon the concentration of nitrate, H<sub>2</sub>O, and O<sub>2</sub> species at the surface during the decomposition of the precursor. For example, conversion of the intermediate surface silicate to silicide in UHV entails reduction by NO generated from nitrate decomposition. The implications of these results for the CO hydrogenation activity of Co/SiO<sub>2</sub> catalysts will be discussed.

This work was performed at Sandia National Laboratories for the U.S. Department of Energy under Contract DE-AC04-76DP000789.

**SS-MoP24 Disorder-Effects at the Al(110) Surface, W. Schommers, C. Mayer, H. Göbel and P. von Blanckenhagen,** Kernforschungszentrum Karlsruhe, Institut für Materialforschung I, P.O. Box 3640, 76012 Karlsruhe, Germany.

We have investigated the temperature dependence of the structure

and dynamics of the Al(110) surface by molecular dynamics. The following model has been used: The Al particles were arranged as a slab-shaped fcc crystal with two (110) planes as free surfaces. The slab consisted of 11 layers, and its total number of particles in the calculations was  $N = 528$ . For the interaction between the particles we have used a realistic pseudopotential (in the long range part of the potential interactions of van der Waals-type were considered).

The behaviour of the following quantities have been studied: Pair correlation function, generalized phonon density of states, and the mean-square displacement as a function of time. Significant effects concerning disorder and diffusivity were found for temperatures  $T > 600$  K (melting temperature: 933 K). These results will be compared with experimental structure factors measured by low energy electron diffraction for momentum transfers between 0.2 and 2.2 Å<sup>-1</sup> and at temperatures between 800 and 900 K.

**SS-MoP25 Impact versus Dipole Scattering in HREELS of H/C(100), B. D. Thomas and J. E. Butler,** Code 6174, Naval Research Laboratory, Washington, DC 20375.

Several researchers, including the authors, have recently used high resolution electron energy loss spectroscopy (HREELS) to study structure and bonding on diamond surfaces. However, the selection rules which apply must be known to be able to correctly interpret these spectra. The selection rules in effect are determined by the mechanism for vibrational excitation. For this reason, we have investigated the mechanism for vibrational excitation during the scattering of low energy electrons from hydrogen terminated C(100):2 × 1. We find that the scattering mechanism is dependent on surface smoothness which we characterize using low energy electron diffraction (LEED). For surfaces prepared with standard procedures, we observe that impact scattering dominates the vibrational loss spectra. In addition, we have developed a method to create extremely smooth hydrogen terminated C(100) as demonstrated by the observation of half order LEED spots at an incident electron energies as low as 13 eV. Only for these extremely smooth surfaces is dipole scattering seen to contribute significantly in the excitation of C-H vibrations. We will discuss reasons for the dominance of impact scattering and implications for the interpretation of HREEL spectra from nonmetals.

**SS-MoP26 Scattering of <sup>3</sup>He from the NiO (001) Surface, Jeff Baker, G. G. Bishop, E. S. Gillman, S. A. Safran, J. G. Skofronick,** Florida State University, Tallahassee, FL 32306.

An experiment scattering <sup>3</sup>He from the NiO (001) surface has been performed in an attempt to measure the magnetic structure of the NiO surface. A nozzle beam of 5% <sup>3</sup>He in a carrier gas of <sup>4</sup>He was used to produce a narrow velocity spread of the incident <sup>3</sup>He atoms,  $\Delta v/v \approx 5.6\%$ . This beam was scattered from the surface and the <sup>3</sup>He in the beam was detected using a quadrupole mass spectrometer. Measurements of the scattered intensity versus incident angle produced narrow Bragg peaks, indicating that a high quality surface had been produced by cleaving *in situ*. The diffraction pattern obtained with <sup>3</sup>He is slightly different from that obtained with <sup>4</sup>He. A careful study of the region in which the magnetic Bragg peaks were expected set the maximum intensity of the magnetic peak at  $4 \times 10^{-5}$  times smaller than the intensity of the specular peak. These results are discussed in terms of a comparison of the standard helium-surface interaction potential with the interaction between the nuclear magnetic dipole of the <sup>3</sup>He and the electronic spins of the Ni<sup>2+</sup> ions. The narrow velocity distribution obtained for <sup>3</sup>He by this technique shows that high resolution experiments measuring the dynamics of crystal surfaces can be performed with both <sup>3</sup>He and <sup>4</sup>He, which should prove useful for other surfaces, both magnetic and non-magnetic.

**SS-MoP27 The Chemisorption of F<sub>2</sub> and O<sub>2</sub> on Si(100)-(2 × 1) and Si(111)-(7 × 7): An Inverse Temperature Effect, H. C. Flaum, E. R. Behringer, D. J. D. Sullivan, and A. C. Kummel,** Chemistry Department, University of California at San Diego, La Jolla, CA 92093 U.S.A.

We have measured the initial sticking probability ( $S_0$ ) of O<sub>2</sub> and F<sub>2</sub> as a function of incident translational energy ( $0.03\text{ eV} < E_i < 1.4\text{ eV}$ ) and surface temperature ( $300\text{ K} < T_s < 900\text{ K}$ ) on both Si(111)-(7 × 7) and Si(100)-(2 × 1). For all four systems, at high incident translational energy ( $E_i \sim 0.3\text{ eV}$ ), the sticking probability increases with surface temperature ("inverse temperature effect"), but at the highest incident translational energies ( $E_i > 1.0\text{ eV}$ ) the sticking probability is ( $S_0 \approx 1.0$  for  $300\text{ K} < T_s < 900\text{ K}$ ) independent of the surface temperature ("normal temperature effect"). The inverse temperature effect for O<sub>2</sub>/Si(100)-(2 × 1) was first observed by D'Evelyn, Nelson, and Engel. The appearance and disappearance of the inverse temper-

ature effect as a function of incident translational energy for both  $F_2$  and  $O_2$  suggests that thermal carriers are important in the activated chemisorption process.

**SS-MoP28 Isothermal  $H_2$  Desorption Kinetics from Si(100)  $2 \times 1$ : Dependence on Disilane and Atomic Hydrogen Precursors,** *Lynne A. Okada, Michael L. Wise, and Steven M. George*, Dept. of Chemistry and Biochemistry, Univ. of Colorado, Boulder, CO 80309-0215, USA.

The isothermal  $H_2$  desorption kinetics from the Si(100)  $2 \times 1$  surface were studied using laser induced thermal desorption (LITD) techniques. Disilane ( $Si_2H_6$ ) and atomic hydrogen were used as the hydrogen precursors. Atomic hydrogen deposits only hydrogen adatoms and  $H_2$  subsequently desorbs from an atomically-flat Si(100)  $2 \times 1$  surface. Disilane deposits both hydrogen and silicon adatoms which may produce an atomically-rough Si(100) surface. This surface roughening with silicon adatoms simulates silicon chemical vapor deposition (CVD) and may affect the  $H_2$  desorption kinetics. The isothermal LITD studies revealed first-order  $H_2$  desorption kinetics for both precursors. An activation barrier of  $E_d = 57.2 \pm 2.6$  kcal/mol and a pre-exponential factor of  $\nu_d = 2.21 \times 10^{15 \pm 1} s^{-1}$  were measured for the atomic hydrogen precursor. An activation barrier of  $E_d = 54.3 \pm 2.3$  kcal/mol and a pre-exponential factor of  $\nu_d = 2.32 \times 10^{14 \pm 1} s^{-1}$  were determined for the disilane precursor. Within the experimental error, the isothermal  $H_2$  desorption kinetics were not significantly affected by the hydrogen source. The similar desorption kinetics are attributed to the surface mobility of the silicon adatoms deposited with disilane.  $H_2$  presumably does not desorb from an atomically-rough surface because the silicon adatoms can diffuse to step edges or form Si(100)  $2 \times 1$  islands on the underlying Si(100)  $2 \times 1$  surface. The first-order  $H_2$  desorption kinetics are explained by the concerted desorption of  $H_2$  from two hydrogen atoms paired on the same silicon dimer on the Si(100)  $2 \times 1$  surface.

**SS-MoP29 Molecular Beam Reaction Studies of Trimethylgallium (TMGa) on Ga-rich GaAs(100),** *Barbara A. Bansenauer and Christine E. Nelson*, University of Wisconsin-Eau Claire, Eau Claire, WI 54702-4004, and *J. Randy Creighton*, Sandia National Laboratories, Albuquerque, NM 87185.

We have used molecular beam experiments to probe the reactivity of TMGa (an important organometallic precursor used in GaAs ALE and MOMB) on the GaAs surface. We have measured saturation coverages and sticking coefficients of TMGa on the Ga-rich surface of GaAs(100) at low temperatures, where adsorption and desorption are the major reaction processes, and at high temperatures, where TMGa decomposition is the dominant surface process. We have found that the TMGa saturation coverage ranges from  $1.7 \times 10^{14}$  to  $6.0 \times 10^{13}$  molecules/cm<sup>2</sup> at 173 and 613 K, respectively. Also, the shape of the sticking coefficient vs. coverage plot suggests that precursor-mediated adsorption kinetics are operative. Kinetic modeling of the molecular beam data confirms that precursor mediated adsorption kinetics are active and uses a Kisliuk expression for the sticking coefficient. Using arrhenius parameters from thermal desorption and SIMS work, we have modeled the sticking coefficient vs. coverage curves using a multi-step mechanism that includes adsorption, desorption, and TMGa decomposition into DMGa and MMGa.

**SS-MoP30 Inner-Shell Promotions in Low Energy  $Li^+$ -Al Collisions at Clean and Alkali-Covered Al(100),** *K. A. H. German<sup>1</sup>, C. B. Weare and J. A. Yarmoff*, Department of Physics, University of California, Riverside, CA 92521 and Materials Sciences Division, Lawrence Berkeley Laboratory, Berkeley, CA 94720.

The success of low energy ion scattering (LEIS) in determining surface geometries hinges on the use of accurate models for the energy loss and neutralization experienced by scattered ions. The present study reveals that the inelastic loss and charge exchange that occur during low energy, i.e., 0.4 to 5.0 keV,  $Li^+$  scattering from clean and alkali-covered Al(100) are greatly affected by inner-shell excitations, a mechanism that is not usually considered in the interpretation of LEIS data. Spectra of backscattered  $Li^+$  ions exhibit discrete loss features associated with single scattering from Al target atoms. The loss features are resistant to the usual increase in neutralization produced by the deposition of alkali atoms on the surface. Spectra of ion-induced electron emissions show that Li 1s promotions initiate the formation of autoionizing  $Li^+(1s\ 2s^2)$ . It is the production of ions away from the surface via autoionization that is responsible for the lack of response of the loss features to alkali-adsorption. The results also show that, while Li 1s electrons are promoted during hard Li-Al collisions, they are not promoted during Li-K or Li-Na collisions. Because Li 1s electron promotion is dependent on the target atom species, the inelastic

loss and neutralization processes for  $Li^+$  ions scattered from alkali-covered Al are also site-dependent.

<sup>†</sup>Present address: *Pacific Northwest Laboratories, Richland, WA 99352.*

**SS-MoP31 Evolution of Surface Morphology of Si(100)-(2  $\times$  1) During Oxygen Adsorption at Elevated Temperatures,** *Y. Hong, K. Wurm, Y. Wei and I. S. T. Tsong*, Arizona State University, Tempe, AZ 85287, *R. Kliese, B. Röttger and H. Neddermeyer*, Ruhr-Universität Bochum, 44780 Bochum, Germany.

We used scanning tunneling microscopy (STM) and low-energy electron microscopy (LEEM) to study the etching of the Si(100)-(2  $\times$  1) surface by oxygen at low pressures and elevated temperatures. At  $5 \times 10^{-8}$  torr partial pressure of oxygen, the transition from random etching of terraces to step-etching occurs at  $\sim 580^\circ C$ , while at a higher partial pressure of  $5 \times 10^{-7}$  torr, the transition temperature is  $\sim 625^\circ C$ . The diffusing species is a dimer vacancy, formed by the deposition of two SiO molecules. Anisotropic diffusion of the vacancies is observed, with a preferred direction along the dimer rows. The reaction probability, defined as the number of desorbed SiO molecules to the number of incident  $O_2$  molecules, is estimated to be  $0.010 \pm 0.005$ , almost exactly twice that of the sticking probability of  $O_2$  on Si(100) reported previously. This suggests that virtually all adsorbed  $O_2$  molecules were converted to volatile SiO giving rise to etching at the pressure and temperature ranges studied.

**SS-MoP32 Analysis of Chemisorption Sites:  $Cl_2$  on Si(111)-7  $\times$  7,** *C. Yan, J. A. Jensen, A. C. Kummel*, U.C. San Diego Chemistry, La Jolla, CA 92093.

Using scanning tunneling microscopy, we have analyzed the different types of dimer/pair adatom chemisorption sites which result from the chemisorption of molecular chlorine as function of their incident translational energy,  $E_{trans}$ . On the Si(111)-7  $\times$  7 reconstructed surface, there are five different types of adjacent adatom pairs (ignoring the stacking fault of one half of the unit cell): corner-corner adatoms, corner-center adatoms within one half of a unit cell, corner-center adatoms from to adjacent half unit cells, etc. We observe that at high  $E_{trans}$  (0.44 eV) where dimer/pair adatom adsorption is dominant, one type of adatom pair accounts for a majority (60%) of all double adatom adsorption: two center adatoms from adjacent half unit cells. It should be noted that this pair has the lowest degeneracy of all possible nearest-neighbor pairs (3 sets in one unit cell vs. 6 or 12). A possible explanation of this preference is that this is the closest set of center adatoms; another is the fact that these two adatoms are electronically decoupled across the stacking fault. At low  $E_{trans}$  (0.11 eV), single site adatom adsorption is most common other than large islands formed by precursor mediated chemisorption. In addition, at low  $E_{trans}$  there is no double adsorbate sites preference. This lack of adatom pair selectivity and the appearance of many single adatom sites suggests that either adatom-rest atom dissociative chemisorption, or as suggested by Bolland, et al., abstraction of one Cl atom onto an adatom, is the dominant non-precursor mediated chemisorption mechanism at low  $E_{trans}$ .

**SS-MoP33 Resonantly Enhanced Multiphoton Ionization of SiO Desorbing from Si(111) in Reaction with  $O_2$ ,** *K. G. Nakamura and M. Kitajima*, National Research Institute for Metals, Tsukuba, Ibaraki 305, Japan.

Internal state distribution of SiO desorbing from Si(111) surface in reaction with  $O_2$  molecular beam have been studied using resonantly enhanced multiphoton ionization mass spectroscopy (REMPI). The  $F^1\Sigma^+ - X^2\Sigma^+$  transition is used for (2 + 1) REMPI with a wavelength of 290–295 nm. The experiments were performed in an ultrahigh vacuum chamber (base pressure  $< 10^{-7}$  Pa). Si(111) surface is exposed to pulse  $O_2$  molecular beam ( $\sim 1$  ms of FWHM) at substrate temperature of  $\sim 1250$  K. The SiO molecule produced by the Si surface oxidation reaction  $Si(s) + O_2(g) \rightarrow SiO(g)$  is observed and its waveform is almost same as that of the incident  $O_2$  beam. Well separated vibrational bands [FX(0, 0), FX(1, 1), and FX(2, 2)] have been observed in the (2 + 1) REMPI spectrum. Intensity ratios of vibrational bands are comparable to the vibrational distribution of SiO with a Boltzmann distribution at the surface temperature. The rotational distribution of SiO will be also discussed.

**SS-MoP34 Charge Transfer Process of Low Energy Collisions of  $Li^+$  with Cs/Cu(111) Surfaces,** *Q. B. Lu, Y. G. Shen, D. J. O'Connor, B. V. King and R. J. MacDonald*, Department of Physics, University of Newcastle, New South Wales 2308, Australia.



Charge transfer process from Cs-covered Cu(111) surfaces has been studied using low energy  $\text{Li}^+$  ion scattering. Energy distributions and polar angle dependences of the scattered both  $\text{Li}^+$  and  $\text{Li}^-$  ion intensities are collected as a function of Cs coverage. The results indicate that the  $\text{Li}^+$  single scattering intensity from Cs is almost completely neutralized, while the  $\text{Li}^-$  intensity behaves totally differently, showing maximum at certain Cs coverage near the work function minimum ( $\Delta\Phi = -3.5$  eV). Quantitative agreement is achieved with the observed work function dependence. The experimental results can be well interpreted by a resonant charge transfer theory which includes electron excitation, negative ion formation and level crossings. The effects of oxygen adsorption on various pre-coverages of Cs by observing the variations of the  $\text{Li}^+$ -Cs and  $\text{Li}^-$ -Cs single scattering intensities are also investigated. These results are discussed in connection with the electron structure of alkalis on metal surfaces.

**SS-MoP35 The Site-Specific Neutralization Behavior of 2.0 keV  $^7\text{Li}^+$  Ions Scattered from Alkali/Al(100) Surfaces,** C. B. Weare, K. A. H. German and J. A. Yarmoff, Department of Physics, University of California, Riverside, CA 92521 and Materials Sciences Division, Lawrence Berkeley Laboratory, Berkeley, CA 94720.

The effects of alkali adsorption on metal surfaces is of fundamental importance in many processes. Numerous experiments have investigated these effects by studying the neutralization behavior of alkali ions scattered from alkali-covered metallic surfaces. However, previous experiments were unable to separate the neutralization probabilities, or neutral fractions, of alkali atoms scattered from substrate and adsorbate sites. Site-specific sensitivity of the neutral fraction is made possible in the present study by combining a large scattering angle ( $168^\circ$ ) with time-of-flight (TOF) detection of Li scattered near the surface normal. This yields spectra in which the single scattering signals from substrate and adsorbate sites are well separated, thus allowing independent measurements of the neutral fractions. For low K coverages,  $\text{Li}^+$  ions scattering from K sites experience essentially complete neutralization, while the neutral fraction for  $\text{Li}^+$  scattering from Al sites is on the order of 50%. For K coverages approaching 0.4 ML, however, the measured neutral fractions for Li scattering from K and Al become nearly equal (at about 80%). The data support a picture in which, at low K coverages, K adsorbates behave as independent dipoles, creating an inhomogeneous surface electrostatic potential. At higher K coverages, on the other hand, K forms a uniform dipole layer. Data for Na and Cs adsorbates are also presented.

**SS-MoP36 Isotope Effects in Electron-Stimulated Desorption from Physisorbed Monolayers of  $\text{H}_2$ , HD, and  $\text{D}_2$  on Graphite,** Bin Xia and S. C. Fain, Jr., Department of Physics, FM-15, Univ. of Washington, Seattle, WA 98195.

Time-of-flight and retarding field energy measurements using positive ions desorbed by 62 eV electrons from physisorbed  $\text{H}_2$ , HD, and  $\text{D}_2$  monolayers on graphite have been used to estimate cross sections  $\sigma$  and most probable energies  $E$ . The monatomic ion cross sections are  $10^{-2}$  to  $10^{-3}$  of the gas phase value; the diatomic ion cross sections are  $10^{-5}$  to  $10^{-6}$  of the gas phase value. The reduction of the ion cross sections relative to the gas phase is qualitatively consistent with greater quenching by the surface electrons for ions with lower kinetic energy and higher mass. In gas phase measurements, conservation of linear momentum in electron-induced dissociation causes the ratio of H+ energy to D+ energy from HD to be 2.0. The larger energy ratio observed here may be due to the quenching by the surface affecting dissociation via the antibonding HD+ state differently than dissociation via autoionizing states. By lowering the electron energy to 32 eV, dissociation via the antibonding HD+ state is strongly suppressed. Newly analyzed time-of-flight data indicate a decrease from 3 to 2 for the ratio of the number of H+ ions to the number of D+ ions as the incident electron energy is lowered from 62 eV to 32 eV. Ion energy distributions from the HD time-of-flight data as a function of incident electron energy will be presented.

Supported by NSF grant DMR-91-19701.

**SS-MoP37 Internal and Translational State Distributions and Alignment of a Photodesorbed Molecule: CO/Si(100)  $2 \times 1$ ,** Frank M. Zimmermann, Paul L. Houston, and W. Ho, Materials Science Center, Cornell University, Ithaca, NY 14853.

We have studied photochemical (308 nm) desorption of CO from Si(100)  $2 \times 1$  at 82 K, using state resolved detection by laser induced fluorescence. The process has two remarkably large cross sections ( $\sim 1 \times 10^{-16}$  and  $7 \times 10^{-18}$  cm<sup>2</sup>), which correlate with two thermal desorption peaks. Internal and translational energy distributions provide

insight into the dynamics of the photodesorption process. Most notable is a very high degree of vibrational excitation, which, together with the large cross sections, may indicate relatively weak electronic quenching. The rotational as well as the translational energy distributions are bimodal, with the hotter component of the translational distribution correlating with the colder part of the rotational distribution. Both of these components individually exhibit positive rotational-translational correlations, however, in qualitative agreement with a simple dynamical model. We report the first angular momentum alignment measurements of a photodesorbed molecule. The results indicate that the colder component of the rotational distribution is not strongly aligned, whereas the J-vectors of the rotationally hotter component show preferential alignment parallel to the surface (cartwheeling motion).

**SS-MoP38 Kinetic to Internal Energy Transfer during Polyatomic Ion-Surface Collisions,** J. A. Burroughs, S. B. Wainhaus, and L. Hanley, University of Illinois at Chicago, Chicago, IL 60607-7061.

Low energy polyatomic ion-surface collisions occur in a wide variety of mass spectrometric, plasma, and ion beam etching processes. The transfer of kinetic to internal energy can lead to the surface-induced dissociation of the primary ions, an effect which has begun to be utilized in mass spectrometry to obtain ionic structural information. 20 to 120 eV  $\text{Cr}(\text{CO})_6^+$  ions are collided with monolayers of hexanethiol and heptafluorobutyric acid adsorbed on Ag(111) and the fragment ions formed in the surface collision are monitored by a mass spectrometer.  $\text{Cr}(\text{CO})_6^+$  fragmentation patterns from surface-induced dissociation are fit to an impulsive collision model originally used to describe gas phase collision-induced dissociation. This simple model can at least partially describe the variation in kinetic to internal energy transfer between the hydrogenated and fluorinated surfaces. Additional data on the secondary ion kinetic energy distributions of the  $\text{Cr}(\text{CO})_6^+$  fragments is used to obtain a more detailed description of the ion-surface collision.

**SS-MoP39 Application of Hyperthermal Beams to Achieve Adsorption and/or Abstraction of Adsorbates on Diamond Surfaces,** D. Haggerty, C. Bandis, B. B. Pate, Department of Physics, Washington State University, Pullman, WA 99164-2814.

Hydrogen stabilization of the diamond surface against reconstruction is thought to be a key element enabling low pressure diamond growth. However, if every surface atom was terminated by hydrogen, carbon deposition (diamond growth) would be hindered due to a lack of chemically active sites. In a typical diamond CVD apparatus, the steady state fraction of active (hydrogen-free) sites is thought to be directly related to growth rate. The production of active sites during growth is attributed to the abstraction of surface-bound hydrogen by gas-phase atomic hydrogen (activation energy ca. 7 kcal/mole). Due to activation barriers and relaxation phenomena, adsorption and abstraction phenomena is likely to be dependent upon the excitation state (eg. kinetic energy, ionization, etc.) of the gas phase species (such as hydrogen).

In this experimental study, we employ a mass-selected low kinetic energy (10-50 eV) hydrogen source to interact species at controlled impact kinetic energy with the diamond surface. Our objective is to better understand the role of hydrogen kinetic energy in the hydrogen adsorption/abstraction mechanisms which are key to understanding low pressure diamond growth. We report the effects of hyperthermal hydrogen exposure upon both hydrogen coverage and surface structure of clean and hydrogenated diamond surfaces.

Work supported by NSF and Washington State University.

**SS-MoP40 The Effect of Preadsorbed Oxygen on the Dissociation Dynamics of Ethane on Ir(110)\*,** W. Hago, D. Kelly, and W. H. Weinberg, Department of Chemical Engineering, University of California, Santa Barbara, California 93106.

As part of an ongoing effort to understand the basic mechanisms of alkane activation, and to find new methods of oxidizing hydrocarbons, we have examined the effect of chemisorbed oxygen on the dissociation dynamics of ethane on Ir(110). In particular, we have examined, using a supersonic molecular beam, the effect of preadsorbed oxygen on the initial probability of ethane activation on this surface at various coverages. We preadsorbed oxygen up to a saturated monolayer, and found that oxygen, while not affecting the initial trapping probability, significantly affects the initial probability of dissociation chemisorption for both trapping-mediated and direct dissociation. For trapping-mediated adsorption, 0.5 monolayer of oxygen is sufficient to significantly inhibit any ethane activation. Furthermore, by following changes in surface carbon and oxygen with Auger spec-

troscopy, we have monitored the reaction of the dissociation products of the ethane (for direct dissociation) with the preadsorbed oxygen as a function of surface temperature.

\*Supported by the Department of Energy (grant DE-FG03-89ER14048).

## NANO 3/NANOMETER-SCALE SCIENCE AND TECHNOLOGY

### Room BR4 - Session NS-MoP

#### Instrumentation and Metrology

**Moderator:** E. C. Teague, National Institute of Standards and Technology.

**NS-MoP1 Quantum Friction Observed with Two-Dimensional Frictional Force Microscope, S. Fujisawa, E. Kishi, Y. Sugawara and S. Morita,** Department of Physics, Faculty of Science, Hiroshima University, 1-3-1 Kagamiyama, Higashi-Hiroshima 724 Japan.

We investigated nature of the atomic scale friction between a single asperity of  $\text{Si}_3\text{N}_4$  and an atomically flat surface of  $\text{MoS}_2$ , where the frictional force becomes two-dimensional vector. Using the two-dimensional frictional force microscope (2D-FFM) which detects both the components separately and simultaneously [1, 2], we found that the single asperity shows the two-dimensional quantized jump with the lattice periodicity of the  $\text{MoS}_2$ , namely "two-dimensional stick-slip" phenomenon [1]. We also found that this quantized behavior shows fluctuation [2]. This phenomenon shows that on an atomic scale the frictional force is quantized two-dimensionally and acts not only along the scan direction but also across the scan direction, although there is contradiction to the principle of the classical friction. Further, we will discuss the nature of the quantized friction, using the simple two-dimensional stick-slip model with effective adhesive radius.

[1] S. Fujisawa et al: *Nanotechnology* 4 (1993) 138-142.

[2] S. Fujisawa et al: *Jpn. J. Appl. Phys.* 33 (1994) in press.

**NS-MoP2 Microtribological Study of Lubricants Using Friction Force Microscopy, Bharat Bhushan and Vilas N. Koinkar,** Computer Microtribology and Contamination Laboratory, Department of Mechanical Engineering, The Ohio State University, Columbus, Ohio 43210-1107.

Atomic force microscopy (AFM)/Friction force microscopy (FFM) is used for microtribological studies on the unlubricated and lubricated single-crystal silicon. The single-crystal silicon is coated with few nanometer thick polar and non polar lubricants. Friction dependence upon the normal load, shear velocity and different environments are studied in detail. The friction of lubricated and unlubricated samples sliding against silicon, silicon nitride and diamond tip is also investigated. It is observed that lubricant depletion/degradation on a microscale can easily be detected with FFM. Normal load and shear velocity significantly affect the lubricant performance. Some friction studies on unlubricated and lubricated thin-film magnetic rigid disks have been performed and are discussed briefly. FFM appears to be an useful tool to study boundary lubrication properties on a nanoscale.

**NS-MoP3 Determining the Local Mechanical Properties of a Material using a Scanning Tunneling Microscope as a Surface Acoustic Wave Detector, David M. Schaefer, Richard J. Colton, and Steven M. Hues,** Code 6170, Naval Research Laboratory, Washington, D.C. 20375-5342 USA.

A scanning tunneling microscope (STM) has been modified to detect surface acoustic waves (SAW) across the surface of bulk materials and thin films with a lateral resolution on the nanometer length scale. The surface acoustic waves are excited using interdigital transducers configured to produce a SAW with a frequency of 79 MHz. An rf signal of comparable frequency is also applied to the STM tip. With this configuration, the tip acts as a mixer, and the difference term in the frequency components of the tunnel current is detected with conventional STM electronics. The amplitude and phase of the SAW are directly observed on an oscilloscope, and are related to the local mechanical properties of the substrate. By imaging the surface with the STM, surface acoustic wave measurements can be performed at se-

lected positions on the surface. The effects of surface morphology and defects on the local mechanical properties of the material will be discussed.

**NS-MoP4 Modelling of the Nanoindentation of Thin  $\text{SiO}_2$  Layers on Si Using Finite Element Analysis, Charles F. Draper<sup>1</sup>, David M. Schaefer<sup>2</sup>, Richard J. Colton<sup>2</sup>, and Steven M. Hues<sup>2</sup>,** <sup>1</sup>Department of Mechanical Engineering, Vanderbilt University, Nashville, TN, 37205 USA, <sup>2</sup>Code 6170, Naval Research Laboratory, Washington, D.C., 20375-5342 USA.

A main forte of the atomic force microscope (AFM) as a nanoin-denter is its ability to measure mechanical properties of thin films. The properties measured, however, are composite properties that reflect not only the intrinsic properties of the film, but also the underlying substrate. Upon tip/surface contact, a stress field is generated which penetrates into the sample. The magnitude of the composite modulus is determined by the relative distribution of the stress and strain fields between the layer and substrate. We have studied this effect experimentally using thermally-grown oxide layers (2-30 nm) on  $\langle 100 \rangle$  Si wafers. Finite element analysis (FEA) is used to model the stress and strain fields within the overlayer/substrate system and quantitatively describe the nanoindentation behavior of the film/substrate system as a function of oxide thickness. Details of the FEA modeling and comparison with experimental results will be presented and discussed.

**NS-MoP5 Measurement of Adhesive Force between poly-L-lysine Treated Mica and Colloidal Gold Particles, J. Carnes, J. Vesenka, R. Miller\*, and E. Henderson,** Department of Zoology and Genetics and Department of Mathematics\*, Iowa State University, Ames, Iowa 50011.

The adhesion force between 5, 15 and 30 nm colloidal particles and poly-L-lysine treated mica (pllm) was measured using atomic force microscopy. Through incremental increases in the normal force, the lateral force needed to break the presumed weak electrostatic bond between the gold particles and pllm was determined. Key to accurate measurements of these forces is accurate knowledge of the tip geometry<sup>1,2</sup>, cantilever spring constant<sup>3</sup>, and monitoring of the piezo-translator drift. The results were compared with a model of a charged sphere in close proximity to countercharged infinite plane. Measurements of both macroscopic properties (coefficient of friction) and microscopic properties (force between opposite paired charges) are discussed.

<sup>1</sup>R. Miller, J. Vesenka, & E. Henderson, "Three Dimensional Reconstruction of Scanning Probe Apex from Colloidal Gold Specimens," Submitted.

<sup>2</sup>J. Vesenka, R. Miller, & E. Henderson, "Three Dimensional Probe Reconstruction for the Atomic Force Microscope," *Rev. Sci. Instr.*, in press (July 1994).

<sup>3</sup>J. Cleveland, S. Manne, D. Bocek, & P. K. Hansma, "A Nondestructive Method for Determining the Spring Constant of Cantilevers for Scanning Force Microscopy," *Rev. Sci. Instr.*, 64: 403-405 (1993).

**NS-MoP6 Ultrasound Influence on the Tribological Properties of CVD Diamond, V. Snitka,** Research Institute "Vibrotechnika", Kaunas, 3000 LITHUANIA, V. Baranauskas, State University of Campinas, 13081-970 Campinas SP BRASIL.

The friction and wear behavior CVD diamond film sliding against alumina, iron, steel and itself has been investigated under strong ultrasound conditions at the friction interface. Experiments were performed on an alternating "pin-on-plate" tribometer constructed as an ultrasonic motor. The bimodal mechanical vibrations were in the frequency range (25-80) kHz. The diamond samples were deposited on the molybdenum by the Hot-filament assisted CVD from  $\text{CF}_4/\text{CH}_4$  gas mixture with typical 5-10  $\mu\text{m}$  lateral grain size and film thickness up to 100  $\mu\text{m}$ . AFM and SEM were used for the characterization of the surface morphology. The experimental results have shown that ultrasound makes strong influence on the alumina and diamond wearing, friction and surface deformation. XPS analysis of the worn diamond crystallites indicated the occurrence of tribochemical reactions between ceramics, iron and diamond. Fast friction coefficient decrease in time was observed in the case of sliding CVD diamond against CVD diamond films. Presence of ultrasound during the sliding decrease the friction coefficient to zero. The diamond wearing in the lower hardness materials friction pair case can be explained by high share stresses and high oxidation rate of diamond in presence of ultrasound. Raman scattering have shown low level of induced defects during ultrasonic assisted friction. The diamond films were mechanically polished from

initial surface roughness 3  $\mu\text{m}$  to 20 nm, as measured by the AFM height surface histograms. The high quality and speed of ultrasonic polishing of CVD diamond suggests that this technique is interesting for a high number of diamond applications where almost atomic flat surface is needed.

**NS-MoP7 Surface Roughness Characterization of Soft X-Ray Multilayer Films on the Nanometer Scale,** *J. Yu\**<sup>#</sup>, *J. L. Cao*<sup>#</sup>, *Y. Namba*<sup>\*</sup>, *Y. Y. Ma*<sup>#</sup>, \*Dept. of Mech. Engg., Chubu University, 1200 Matsumotocho, Kasugai, Aichi 487, Japan, <sup>#</sup>SKLAO, Changchun Institute of Optics and Fine Mechanics, Changchun 130022, P. R. China.

The more common availability of monochromatic, well-collimated beams of X rays, from sources such as electron storage rings, has motivated a study of the optical elements used at these short wavelengths. One of the important parameters governing the performance of x-ray optics is the surface roughness. Surface roughness measurements have been achieved by the stylus method and many kinds of optical interferometric methods. However, it is difficult to measure the lateral period of the surface roughness of less than about 1000 Å by these methods. We use the STM to investigate the surface roughness statistics characterization of some kinds of soft x-ray multilayer films, such as Mo/Si, Mo/C, and W/Si films, on the nanometer scale. The experiment results show that the surface roughness will be larger after sputtering films, for Mo/Si (61 layers): 0.50 nm rms  $\rightarrow$  1.37 nm rms, for Mo/C (45 layers): 0.50 nm rms  $\rightarrow$  1.41 nm rms, which is depended on the kind of film system, layer numbers and thickness of every layer. In addition, we will give the correlated-roughness analysis.

**NS-MoP8 Step Height Measurement Using a Scanning Tunneling Microscope Equipped with a Crystalline Lattice Scale Reference and Interferometer,** *Toru Fujii and Masatoshi Suzuki*, Nikon Corporation, 1-10-1, Asamizodai, Sagami-hara, Kanagawa 228 JAPAN, *Hiroshi Kougami and Hideki Kawakatsu*, Institute of Industrial Science, University of Tokyo, 7-22-1, Minato-Ku, Tokyo 106 JAPAN, *Toshiro Higuchi*, Faculty of Engineering, University of Tokyo, 7-3-1, Hongo, Bunkyo-Ku, Tokyo 113 JAPAN.

Scanning tunneling microscope (STM) has been well known for its high resolution and non-destructive surface profiling capability but its potential as a profiler for step height measurement has been rarely exploited to its maximum extent because of its unreliable vertical accuracy. Recently, an STM equipped with three-dimensional interferometer was developed and step height and pitch measurement with nanometer accuracy was achieved. However, all the features of the interferometer are not always required in step height measurement. An STM equipped with scale reference crystal for X and Y directions was simple and compact compared to the STM with interferometer, and offers subnanometer resolution using lattice image which consumes large memory area so that high resolution short range measurement is effective. We have successfully combined reference crystal technique and high accuracy mechanisms, and developed new method which can measure both scanning direction and feedback direction simultaneously. Interferometry was also applied to verify measured step height using reference crystal.

**NS-MoP9 Comparison of Magnetic Force Microscopy Techniques,** *Paul Rice and John Moreland*, National Institute of Standards and Technology, Boulder, CO 80303 USA.

We compare magnetic force microscopy (MFM) images of a computer hard disk obtained with four MFM techniques. MFM is becoming a widely used tool for studying the data written on magnetic storage disks. Interpreting the information obtained from various MFM techniques is paramount to understanding the magnetization of the disk. The four MFM techniques include two types of ac MFM, that detect either changes in amplitude or changes in frequency of a vibrating cantilever. The third is a dc MFM technique that detects the deflection of a non-vibrating cantilever. Finally we compare tunneling stabilized magnetic force microscopy (TSMFM) which detects the deflection of a non-vibrating cantilever using a tunneling current to stabilize the tip-sample contact. The sample imaged in this comparison has bit densities and magnetic properties typical of most currently available hard disks. The ac MFM techniques measure the force derivative between the tip and sample. In contrast, dc MFM and TSMFM techniques measure the force between the tip and sample. We have tried, from this comparison, to emphasize the differences of these various techniques in a current industrial application. We hope to provide more quantitative MFM measurements so that magnetic fields can be extrapolated from the images.

**NS-MoP10 Scanning Thermal Microscopy with a Resistive Probe,** *R. B. Dinwiddie*, High Temperature Materials Laboratory, Oak Ridge National Laboratory, Oak Ridge, TN, 37831; *R. J. Pylkki and P. E. West*, TopoMetrix, Santa Clara, CA 95054.

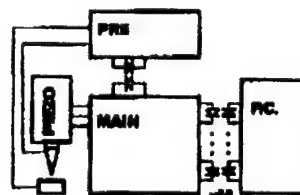
A unique thermal probe has been developed utilizing a resistive element integrated with an atomic force microscope cantilever. Two operating modes of the thermal probe will be described. In one mode, surface temperatures are mapped by monitoring the resistance of the thermal probe. In the second operating mode, the heat flow from the self-heating thermal probe to the sample is monitored. Variations in the thermal properties of the sample (heat capacity, thermal diffusivity, thermal conductivity, etc.), as well as temperature, affect this flow of heat, changing the power necessary to keep the probe at a constant temperature. Integration of the thermal probe with a scanning probe microscope allows simultaneous acquisition of topography with the thermal data. Applications include the investigation of heat generating component or defect structures in electronic devices. The self-heating probe could be used to study the thermal properties of microscopic structures such as particles, fibers and intergranular phases. Examples of both operating modes will be shown.

**NS-MoP11 An Integrated Lithography and Analysis Instrument,** *Grahame Rosolen\** and *Robert Clark*<sup>†</sup>, \*Leica Cambridge Ltd., Clifton Road, Cambridge, CB1 3QH, England, <sup>†</sup>University of New South Wales, P.O. Box 1, Kensington 2033, Australia.

We have developed a PC based integrated electron beam lithography and microscopy instrument for device research and development. This instrument has been used to expose and examine structures ranging from curved optical devices down to nanostructures used as precursors for tunnelling devices. To minimise scattering in the resist material the electron optics is designed to provide a finely focused beam of energy up to 100 kV suitable for fabricating nanostructures. The pattern data may be prepared using either PC CAD packages or a text based input, which is subsequently processed for writing utilising a Digital Signal Processor (DSP) interfaced to the PC. The combines the flexibility of software control in programming the DSP, with the considerable processing capability of the DSP. The pattern data is further processed by dedicated low noise analogue lithography hardware to enhance the stability and resolution of the electron optics. In addition the instrument may be operated as a high resolution electron microscope for examining the results of the lithography. This is particularly important for examining structures in the nanometre scale. The design methodology enables the instrument to be used as an integrated tool for pattern design, conversion, exposure and subsequent investigation.

**NS-MoP12 Low Noise Scanning Tunneling Microscope For Low Temperature Physics With An Electrically Isolated Circuit,** *H. Nakagawa, K. Sakumoto, E. Kuraya, S. Asakura, K. Fukuda*, Fac. of Eng., Yokohama National Univ., Yokohama, Japan, *M. Tanaka*, R&D Labs., Nippon Steel Co., Kawasaki, Japan.

A cryogenic scanning tunneling microscope (STM) was constructed. It was designed to characterize superconducting materials under cryogenic (4.2 K) and magnetic (8 T) conditions. An attention was paid to reduce electrical noises, especially digital switching noise and ground loop noise. The preamplifier is battery-operated and is electrically isolated from the main control circuit by analog optical couplers. The digital portion of the main control circuit is static and no system clock is generated. The main control circuit is interfaced with a personal computer via 52 optical couplers. Dual electrical isolation eases the ground loop problem and shows good atomic resolution.



**NS-MoP13 Arc Atomic Emission Microscopy,** *P. G. Van Patten, J. D. Noll, and M. L. Myrick*, Department of Chemistry and Biochemistry, University of South Carolina.

The scanning tunneling microscope is extremely useful in determining the topology of conductive surfaces. However, little if any other information is available to complement the topographic image obtained. Such information could eliminate doubt concerning the con-



stitution of an imaged surface and could lend great insight into the observation of various surface phenomena.

This work has resulted in the development of hardware and software additions for the STM which allow the instrument to provide chemical information about the substrate via nano-scale arc atomic emission spectroscopy which takes advantage of the convenient geometry of the STM experiment. This experiment is performed by arcing across the tunneling gap with short-lived, large-amplitude (up to 150 V) pulses of the bias voltage. Previous results have shown that this arc reaches temperatures in excess of 6500 K and emits intense light. Collection of this light into fiber optics and direction of the light into a spectrometer should allow elemental analysis of the surface directly under the tip.

**NS-MoP14 Sub-Micron Lithography Employing Photoresist Channel-Constrained Electroless Metallization as an Etch Barrier, C. S. Dulcey, J. M. Calvert, W. J. Dressick, M. S. Chen, G. S. Calabrese\*, J. H. Georger, Jr.\* and J. F. Bohland\*,** Center for Bio/Molecular Science and Engineering Naval Research Laboratory, Washington, DC 20375, \*Shipley Co., Marlborough, MA 01752.

We demonstrate a new technique for selective metallization combining photoresist technology with self-assembled monolayers (SAMs) and electroless (EL) metallization. A substrate coated with a ligand functional SAM is coated with photoresist and then exposed according to standard photoresist protocols. Upon development, the resist is removed, exposing the underlying SAM. A Pd catalyst is attached to the exposed SAM regions, followed by EL Ni metallization to produce channel constrained metal patterns at high resolution. The high etch resistance of even extremely thin Ni films towards RIE means that the patterned Ni may be employed as a highly selective etch barrier for pattern transfer into the underlying substrate. The application of this technique for sub-half micron patterning at DUV wavelengths and ~0.1 micron patterning by e-beam will be demonstrated.

**NS-MoP15 AFM Tip-Sample/Sample-Tip Deconvolution, Peter C. Markiewicz, M. Cynthia Goh,** Department of Chemistry, University of Toronto, Toronto, Ontario, Canada, M5S 1A1.

A simple algorithm has been implemented to directly extract information on the probe tip geometry used in the Atomic Force Microscope. The program uses known sample geometries in the deconvolution. These can be man-made arrays or calibration standards which can be co-deposited with samples. Being able to resolve the tip geometry in such a manner provides an effective means of inspecting the tips for manufacturing defects or the adhesion of debris. The tip information can then be used to deconvolute the subsequent AFM images to improve their quality. Examples of the deconvolution and their uses in various applications will be presented.

**NS-MoP16 On the Recovery of Spectroscopic Image in Scanning Force Microscopy, Igor Yu. Sokolov,** Dept. of Physics, University of Toronto, ON M5S 1A7, Canada.

A principal opportunity of detection of the sort of materials a surface consists of (spectroscopic image of the surface) is discussed for the scanning force microscopy method. It is shown that the problem can be reduced to the Fredholm integral equation of the first kind with the kernel of Hilbert-Schmidt type. Such a problem is demonstrated has a unique solution here provided we consider the case of exact measurements. Moreover, we suggest that the surface topology is known in advance. The possibility of spectroscopic image recovery for the case of the measurements with errors is discussed.

As an example, we demonstrate the obtaining of the Hamaker constant for unknown longitude plan impregnation from SFM scanning.

**NS-MoP17 Analysis of Resist Artifacts by AFM for Use in SEM as In-house Line Width Standards, D. A. Chernoff,** Advanced Surface Microscopy, Inc., 6009 Knyghton Rd., Indianapolis, IN 46220.

Photoresist line widths are presently controlled by inspecting wafers in plan view with a 'metrology SEM'. Proprietary algorithms convert signal intensity to a pseudo-topographic profile and place markers at the inferred foot of the photoresist. No standard reference materials exist for checking this measurement. This report shows the feasibility of creating an in-house standard for this purpose. Three specimens of 0.5- $\mu$ m wide photoresist line test patterns with a range of defocus conditions, in order to produce both aberrated and good line shapes. The specimens were examined in cross-section using the AFM and in plan view using the SEM. The AFM images had crisp edges defining the line profile. Pitch, line width, and slope angles were measured from the AFM images and compared with the pitches and line widths reported by the SEM. Differences are noted and discussed. The basis

for edge contrast in the AFM is explored and a method is proposed for mathematical analysis. This work has shown that the AFM can directly examine resist line profiles and provide images of useful precision, without adding a conductive coating as is commonly done in high resolution SEM. (A conductive coating would modify both the physical width of the structure and its electron scattering characteristics.)

The author thanks Dennis Schrope, for the initial concept of this research and for supplying the specimens and SEM images, and AT&T Bell Laboratories for financial support.

**NS-MoP18 PZT Thin Film Force Sensor for Atomic Force Microscope, Toru Fujii, Shunji Watanabe, Masatoshi Suzuki and Takamitsu Fujiu,** Nikon Corporation, 1-10-1, Asamizodai, Sagamihara, Kanagawa 228 JAPAN.

Atomic force microscope (AFM) is a powerful tool for observing not only conducting surfaces but also nonconducting surfaces with nanometer resolution. AC mode operation AFM which has the potential to profile surfaces with non-contact mode becomes important for non-destructive surface measurements, especially for measuring semiconductor surfaces covered with soft resist. The configuration of AFM is severely restricted by the detector used for measuring the deflection of the cantilever probe. This configuration which requires sample scanning and feedback sample positioning is inconvenient especially for large sample measurement such as semiconductor devices and optics. A piezoresistive cantilever capable of lever scanning and positioning was developed, however, it did not have the potential to oscillate itself for AC operation. ZnO film has been widely used in electronic appliances such as saw devices. This thin film forming technique was applied in fabricating cantilevers with sputtered zinc oxide film which was used as thin film actuator in STM as well as thin film sensor in AFM. PZT is one of the promising piezoelectric materials for both sensing distortion and oscillating the cantilever because it has high piezoelectric constant compared to other piezoelectric materials. We have successfully achieved combining the process for fabricating Si cantilever and forming thin PZT films without deteriorating their characteristics. Preliminary images were taken using this cantilever to which electrochemically etched tungsten stylus was manually glued. Details around the pits of a surface of compact disk and textures of sputtered platinum were clearly observed.

**NS-MoP19 The Design of An Atomic Force Microscope for Metrology, J. Schneir<sup>1</sup>, Thomas McWaid<sup>1</sup>, J. Alexander<sup>2</sup>, and B. Wilfley<sup>2</sup>,** <sup>1</sup>National Institute of Science and Technology, Precision Engineering Division, Gaithersburg, MD 20899, <sup>2</sup>Park Scientific Instruments, 1171 Borregas Ave., Sunnyvale, CA 94089.

We have initiated a project to develop and calibrate artifacts which can be imaged on a commercial AFM. These images can then be used to calibrate the commercial AFM so that subsequent AFM measurements will be accurate and traceable back to the wavelength of light. To avoid systematic errors between different types of metrology tools we plan to calibrate our artifacts using a specially design AFM system which we call the Calibrated AFM. This system has been constructed as much as possible out of commercially available components. We use a flexure stage driven by piezoelectrics for scanning; a heterodyne interferometer system to measure the X-Y position of the sample; a capacitance sensor to measure the Z position of the sample; an integrated piezoresistive force sensor; and a commercially available AFM control system. The control system has two feedback loops which read from the X and Y interferometers and adjust the piezoelectric voltages to keep the X-Y scan position accurate. This feedback loop can hold the X and Y interferometer readings constant to within 1.2 nm rms.

The critical electromechanical and metrology issues involved in the construction and operation of such a system will be discussed in detail.

**NS-MoP20 UHV Setup with Original STM for Nanostructures Creating and Study, K. N. Eltsov, A. N. Klimov, A. M. Prokhorov, V. M. Shevlyuga, V. Yu. Yurov,** General Physics Inst., Russian Academy of Sciences, Moscow.

Perfect nanostructures obviously should be created in controlled conditions of ultra high vacuum. Here we would like to represent a UHV setup in which STM is combined with analytical module equipped with AES, TDS, SIMS, LEED and controlled chlorination of sample. There are also abilities of sample surface preparation: ion etching, annealing up to 1300 K, and cooling to 100 K, etc.

The major tool of this UHV combine is original STM with following features: a) no mechanical drives from outside for coarse tip movement, b) topography, spectroscopy & lithography modes, c) construction is extremely opened that allows to adsorb gases and treat the

sample surface by radiation or particle beams in situ during scanning, d) tips & samples transfer system easily allows to use the STM in combination with other surface science techniques.

For correct measurements of interatomic distances on atomic structures we used original algorithm of STM calibration and reconstruction of real STM image in presence of noticeable drift of the STM tip. Using this algorithm we measured piezoceramics sensitivities along all three axes and also followed their changes after annealing of UHV chamber.

Preliminary study of chlorine adsorption on copper surface confirms ability to create nanostructures (copper clusters inside copper chloride islands) with very interesting properties for nanoelectronics by STM tip.

**NS-MoP21 Scanning Potentiometry of YBCO Step-Edge Junctions,** John Moreland, R. H. Ono, R. E. Thomson, National Institute of Standards and Technology, Boulder, CO 80303 and Craig Prater, Digital Instruments, Santa Barbara, CA 93103.

One of the first variations of scanning tunneling microscopy (STM) was scanning tunneling potentiometry (STP). STP has nanoscopic spatial resolution and submicrovolt voltage resolution. It works well on conductive samples where a reasonable tunneling contact can be maintained during scanning. The atomic force microscope (AFM) has also been adapted for scanning potentiometry. The advantage of AFM is that the sample being scanned can be partially insulating. The likely superiority of a AFM potentiometry over STP becomes evident when one considers imaging of submicrometer structures. In such cases it will be difficult to land a STM tip on small conducting areas on the sample without crashing into insulating regions. We are presently optimizing AFM potentiometry for simultaneous topographic and surface potential measurements of patterned YBCO step-edge junctions and junction arrays. In addition, we are developing STP for low temperature measurements of an unpatterned step edge.

**NS-MoP22 Development of Highly Conductive Cantilevers for Atomic Force Microscopy,** R. E. Thomson and J. Moreland, National Institute of Standards and Technology, Boulder, CO 80383 USA.

We are investigating several techniques for improving the electrical conductivity of standard silicon cantilevers for atomic force microscopy. One easy technique we have tried is to evaporate thin layers of gold, platinum or indium onto the lower surface of the cantilever to create a conducting metal layer. Such coated cantilevers suffer from the problem that the metal covering the apex of the tip may be worn away during the process of scanning the tip. A more promising method is to dope silicon cantilevers with boron or phosphorus. This is done by baking the cantilevers at temperatures above 900°C in proximity to industry standard planar diffusion sources in an atmosphere of flowing nitrogen. This is followed by a short etch in dilute hydrofluoric acid. These cantilevers have a sheet resistance of less than 100  $\Omega$ /square. Because of the formation of an oxide layer, the contact resistance to the cantilevers slowly increases over a period of several days. We are investigating using these cantilevers for a variety of applications including scanning potentiometry, simultaneous STM and AFM, and making electrical contact to submicrometer thin-film multilayer dots for vertical giant magnetoresistance measurements.

**NS-MoP23 Effects of Potassium and Lithium Metal Deposition on the Emission Characteristics of Spindt-type Thin Film Field Emission Microcathode Arrays,** A. A. Talin,<sup>1</sup> T. E. Felter,<sup>1</sup> and D. J. Devine,<sup>2</sup> Sandia National Laboratories, Livermore, CA 94551, <sup>2</sup>Coloray Display Corporation, Fremont, CA 94539.

In this paper we discuss the effects K and Li deposition on the emission characteristics of Spindt-type thin film field emission microcathode arrays (TFEMC) with Mo tips. We report the amount by which each alkali metal lowered the effective work function of a TFEMC, and compare this data to results of similar measurements performed with single-crystal (100)Mo surfaces. We discuss both short- and long-term fluctuations in the emission current and how these fluctuations are affected by the alkali metal adsorbates. In addition, we show that the emission current produced at a given gate voltage during alkali metal deposition is significantly larger than the emission current collected when the deposition source is turned off. We discuss the emission current fluctuations and the increase in emission during deposition using a model based on adsorbate diffusion.

**NS-MoP24 A 25 nm Resolution 1 keV SAFE Microcolumn,** E. Kratschmer, H. S. Kim, M. G. R. Thomson, K. Y. Lee, S. A. Rishton, M. L. Yu, and T. H. P. Chang, IBM Research Division,

T. J. Watson Research Center, Yorktown Heights, New York 10598, USA.

The microcolumn is a complete electron optical column consisting of a field emission source, electrostatic lenses and deflector with a total column length of only 3.5 mm for operation at 1 keV electron energy in ultra high vacuum. The electron source is a scanning tunneling microscope (STM) aligned field emission (SAFE) source, which uses a  $\langle 111 \rangle$  W field emitter with a tip radius of about 50 nm for a low extraction voltage. A selectively scaled dual electrode accelerating lens forms a source lens with low aberrations. The beam is imaged onto a sample at 1 mm working distance by a symmetrical einzel lens. All lenses are assembled from silicon membrane chips and insulating pyrex spacers held together by anodic bonding. With the present microcolumn we have measured a beam diameter of 20–25 nm. This paper will discuss the microcolumn design and give a comparison of the electron optical modelling and experimental results obtained, such as the scanning transmission imaging of grid samples.

A portion of this work has been sponsored by ARPA under an AFOSR contract.

## PLASMA SCIENCE

### Room BR4 – Session PS-MoP

#### Plasma Etching and Deposition

**Moderator:** D. B. Graves, University of California, Berkeley.

**PS-MoP1 Deposition of a-C:H Layers Using an Expanding Ar/C<sub>2</sub>H<sub>2</sub>/CF<sub>4</sub> Plasma,** J. W. A. Gielen, M. C. M. van de Sanden, A. J. M. Buuron and D. C. Schram, Department of Physics, Eindhoven University of Technology, P.O. Box 513, 5600 MB Eindhoven, The Netherlands.

Amorphous hydrogenated carbon layers are used as optical, corrosion and wear resistant layers. These properties depend critically on, for e.g.,  $sp^3/sp^2$  ratio, density and bandgap. In this study an expanding thermal arc in argon is used ( $I_{arc} = 20-90$  A,  $Q_{Ar} = 10-100$  scc/s,  $P_{arc} = 100-500$  mbar) in which the monomer ( $Q_{C_2H_2} = 1-3$  scc/s) is added downstream ( $p_{reactor} = 0.2$  mbar). To influence the layer properties, an etching agent CF<sub>4</sub> ( $Q_{CF_4} = 0-3$  scc/s) is injected. As in this method ion bombardment is absent, the use of the etching agent is to manipulate bandgap,  $sp^3/sp^2$ , refractive index and microstructure of the deposited layers. First results indicate an increase of the  $sp^3/sp^2$  ratio with increasing CF<sub>4</sub> flow, as determined using FTIR. No CF<sub>2</sub> and CF<sub>3</sub>-bonds are identified in the deposited layers whereas CF is dominantly present. From in situ ellipsometry it is shown that the growth rate depends linearly on the C<sub>2</sub>H<sub>2</sub> flow and is unaffected by the etching gas CF<sub>4</sub>. The growth rates are typically 10 nm/s but larger rates can be obtained by increasing the arc power and monomer flow. The microstructure is investigated using an atomic force microscope. The dimensions of the structures observed seem to decrease with increasing CF<sub>4</sub>-flow, indicating the influence of etching during deposition. In this paper the role of the etching agent will be addressed with respect to the influence on plasma radicalisation and deposition mechanism. Relation with other work on a-C:H:F deposition will be discussed.

**PS-MoP2 Silicon Oxide Deposition in an ECR Plasma with Microwave Spectroscopy as a Diagnostic\*,** Kok Heng Chew, Jian Chen, R. Claude Woods, and J. Leon Shohet, Engineering Research Center for Plasma-Aided Manufacturing, University of Wisconsin-Madison, 1410 Johnson Dr. Room 101, Madison, WI 53706.

A 2.45 GHz electron cyclotron resonance (ECR) reactor was used to deposit silicon oxide films using both tetraethoxysilane (TEOS) + O<sub>2</sub> and silane (SiH<sub>4</sub>) + O<sub>2</sub>. This reactor is also equipped with an *in situ* microwave spectrometer in the frequency range of 75–110 GHz, which is used to monitor the gas phase chemical species in this environment. The  $J = 1 \rightarrow 2$  rotational transition of the vibrational ground state of silicon monoxide (SiO) was detected and monitored in ECR plasmas of TEOS + O<sub>2</sub> and SiH<sub>4</sub> + O<sub>2</sub>. The integrated intensity of this microwave transition was used to obtain absolute line-integrated densities of SiO in both of these plasma chemistries. The deposition is done on a silicon wafer clamped onto a water-cooled wafer stage located 20–40 cm away from the ECR zone. Silicon oxide films were

deposited at a pressure of a few mTorr and at low wafer temperature. The chemical composition of the deposited films was obtained using infrared absorption and electron spectroscopy for chemical analysis (ESCA). The refractive indices of the films are estimated to be 1.45 by a single color ellipsometry. Dry and wet etch rates for plasma deposited silicon oxide films were compared to those for thermal oxide films and deposition rates were determined as a function of TEOS/oxygen or silane/oxygen flow rate.

\*This work is supported by the National Science Foundation under Grant No. ECD-8721545. Most of the equipment for constructing the microwave spectrometer was donated by Hewlett-Packard Co. and the absolute temperature controller and TEOS were donated by Schumacher Co.

**PS-MoP3 Plasma Enhanced Chemical Vapor Deposition of Silicon Dioxide from Organosilanes, K. H. A. Bogart and Ellen R. Fisher,** Department of Chemistry, Colorado State University, Fort Collins, CO 80523.

Plasma enhanced chemical vapor deposition (PECVD) of thin films is used extensively in the semiconductor industry. Understanding the process by which deposition of silicon dioxide,  $\text{SiO}_2$ , occurs from organosilanes is important for the development of superior dielectric materials for microelectronics. Several studies of the deposition of  $\text{SiO}_2$  from tetraethoxysilane (TEOS) by PECVD have been published, although investigations of novel organosilane precursors have been few. Using an inductively coupled rf PECVD reactor, we have investigated the deposition conditions and the resulting films from a 100% TEOS plasma. FTIR analysis of  $\text{SiO}_2$  films from our reactor indicate hydrocarbon incorporation in the film. Results from FTIR, SEM, and ellipsometry analyses will be presented for TEOS as well as for triethoxysilane, tetramethoxysilane, trimethoxysilane, and triethoxychlorosilane plasmas. Addition of oxidants, such as  $\text{O}_2$ , to the feed gases will also be investigated. Trends in film compositions produced by varying plasma conditions such as rf input power, starting materials, and substrate temperature will also be presented. Optimization of deposition conditions for  $\text{SiO}_2$  films will allow further elucidation of deposition mechanisms using the Imaging of Radicals Interacting with Surfaces (IRIS) technique.

**PS-MoP4 Plasma Deposition of Diamond-like Carbon, Fluorocarbon Polymer, and Silicon Nitride Films, N. Mackie, P. R. McCurdy, and Ellen R. Fisher,** Department of Chemistry, Colorado State University, Fort Collins, CO 80523.

Plasma enhanced chemical vapor deposition (PECVD) of thin films has found extensive use in the semiconductor industry. Additionally, plasma deposited polymers can be used for membranes, sensors and protective coatings. The chemical mechanisms for plasma depositions, however, are not well understood. We are fundamentally interested in elucidating these mechanisms. We have recently investigated the deposition of thin films from inductively coupled rf plasmas. Plasma environments are characterized by optical emission spectroscopy and deposited films are characterized using ellipsometry, FTIR spectroscopy, and scanning electron microscopy (SEM). Results from deposition of "diamond-like" carbon and teflon-like fluorocarbon polymer films from fluorocarbon feeds ( $\text{C}_2\text{F}_6/\text{H}_2$ ,  $\text{C}_2\text{F}_4/\text{H}_2$  and  $\text{CF}_4/\text{H}_2$ ) will be presented. We will also present results from plasma deposition of silicon nitride films from various silicon ( $\text{SiH}_4$ ,  $\text{SiCl}_4$ ,  $\text{SiBr}_4$ ) and nitrogen ( $\text{NH}_3$ ,  $\text{N}_2$ ) sources. Further, films with distinctive compositions deposited from organosilane/ $\text{NH}_3$  plasmas have also been produced. Trends in film compositions produced from varying plasma conditions such as input power, plasma pressure, starting materials, and substrate temperature are presented. Optimization of deposition conditions in these systems will allow further elucidation of deposition mechanisms using the imaging of radicals interacting with surfaces (IRIS) technique.

**PS-MoP5 The Ion Energy Distribution at the Substrate Surface in a RF Induction Plasma Source, J. B. O. Caughman,** Oak Ridge National Laboratory\*.

The energy of the ions bombarding the substrate can have an effect on the etching or deposition processes occurring on the surface, such as etch selectivities, etching/deposition rates, and thin film quality. The distribution of ion energies incident on the surface of the substrate in a high density radio-frequency induction source has been measured. The plasma source consists of a planar spiral induction coil and a multipole magnet bucket, with an i.d. of 20 cm. A gridded energy analyzer is embedded in a grounded substrate and can be located 10–

25 cm from the coil. Plasmas of argon, helium, and hydrogen have been studied, with rf powers up to 2 kW and operating pressures of 0.5–10 mTorr. Measurements indicate that the ion energy distribution is initially broad ( $>50$  eV) at low rf powers and narrows ( $<10$  eV) as the discharge transforms from a low-density capacitive mode to a high-density inductive mode. The rf power range where the transition occurs can change dramatically with different gases and operating pressures. For example, at a pressure of 2 mTorr, the transition occurs at a power of  $\sim 100$  W for argon and at a power of  $\sim 1000$  W for hydrogen. In general, more rf power is needed to stay in the inductive mode as the pressure is reduced. The relationship between the ion energy distribution, the rf potential of the plasma, and the rf potential of the induction coil will be presented, along with processing implications.

\*Research managed by the U.S. Department of Energy, under contract DE-AC05-84OR21400 with Martin Marietta Energy Systems, Inc.

**PS-MoP6 Analysis of the Oxygen Contamination Presented in  $\text{SiN}_x$  Films Deposited by ECR, S. Garcia, J. M. Martin, M. Fernandez, I. Martil and G. Gonzalez-Diaz,** Departamento de Electricidad y Electronica, Facultad Fisicas, Universidad Complutense, Madrid 28040, Spain.

One of the problems found in the  $\text{SiN}_x$  ECR deposition is the oxygen contamination of the films in some of the deposition conditions, but the origin of the oxygen has not been clarified. In this paper, the oxygen source and the deposition conditions for the oxygen incorporation to the  $\text{SiN}_x$  films, deposited at different microwave powers, P, (50–250 W) and  $\text{N}_2/\text{SiH}_4$  gases flow ratios, R, (1.6–9) are determined. Refractive index, infrared absorption spectra and film composition measured by AES are used to investigate the presence of oxygen. Oxygen content (7%) is detected in the films deposited at  $R \geq 5$  and  $P \geq 150$  W. At  $R \geq 5$ , the oxygen content is lower (3%) for the films deposited at 200 W and no oxygen is found in the films deposited at others powers. According to the presence of oxygen, the Si-N vibration mode is located at high wavenumbers ( $880\text{ cm}^{-1}$ ) for the films deposited at  $R \geq 5$  and  $P \geq 150$  W. Films with lower oxygen content or without it show the Si-N mode at  $830\text{--}850\text{ cm}^{-1}$ , depending on the Si/N ratio. Refractive index between 1.72–1.77 are obtained for the films deposited at  $R \geq 5$  and  $P \geq 150$  W and between 1.82–2.71 for the rest of the films. The analysis clearly shows a threshold in the deposition conditions ( $R = 5$  and  $P = 150$  W) for the oxygen incorporation into the films. Beyond this threshold value, the oxygen content remains constant. These results, and the fact that the oxygen only appears in the films deposited at high deposition rates, indicate that the source can not be the oxygen background pressure, but the sputtering of the quartz liner located into the ECR source, more effective at high microwave powers and  $\text{N}_2/\text{SiH}_4$  gases flow ratios.

**PS-MoP7 Comparison of Measured and Computed Magnetron Sputtering Tracks for Alloys of Differing Magnetic Susceptibility, Daniel R. Julian, David N. Ruzic,** University of Illinois, 103 S. Goodwin, Urbana, IL 61801, Bill Manning, Phil Frausto, John Poole, Tosoh SMD, Grove City, OH 43123.

An electron tracking code was developed in order to predict ionizations inside a magnetron. The sputtering track is then predicted from the ionization profile. The code was modeled after T. E. Sheridan *et al.*<sup>1</sup> The code requires as inputs the cathode composition and voltage, the geometry of the device, the magnetic field configuration inside the device, the gas composition, pressure, and density, and data on sputtering yields. The magnetic field configuration was calculated with a finite element analysis code.<sup>2</sup> The sputtering yields depend on the energy and weight of the impacting ion (and hence the gas type) and are calculated using VFTRIM.<sup>3</sup> Two types of cathodes were studied—a non-magnetic Chromium and a magnetic Cobalt alloy. Differences in alloy magnetic susceptibility cause significant perturbations in the sputtering track pattern and target utilization. Sputtering tracks calculated with the code compared favorably with those measured in the magnetron. The code also compiles data for collision processes (elastic, excitation, and ionization) and outputs calculated spatial distribution of radiation for comparison to optical diagnostics in addition to predicting the sputtering track.

<sup>1</sup>T. E. Sheridan *et al.*, J. Vac. Sci. Technol. A 8, 30 (1990).

<sup>2</sup>ANSYS 5.0A, Swanson Analysis Systems.

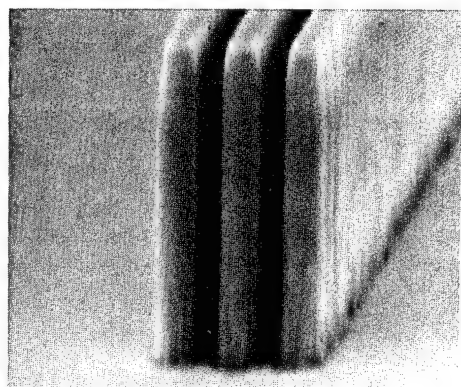
<sup>3</sup>D. Ruzic, Nucl. Instrum. Methods B 47, 118 (1990).

**PS-MoP8 Synergistic Sputtering Effects During Ion Bombardment With Two Ion Species, S. Berg and I. V. Katardjiev, Inst. Technology, Uppsala University, Box 534, S-75121 Sweden.**

The modification of the sputtering yield during ion bombardment with two ion species of different masses is studied with the dynamic Monte Carlo code T-DYN. Specifically, the sputtering yield of low mass targets with low to medium mass primary ions is substantially enhanced when a second ion species of higher mass is introduced. This enhancement is due to the incorporation of the heavier ion species into the target material thus changing significantly the collision cascade behaviour of the primary ions. As a result, the energy deposited at the surface is increased and hence the sputtering yield is also increased. This sputter yield enhancement is found to be a function of the ion energy, angle of incidence, masses and atomic densities of the two ion species, steady state concentration of the secondary ion species at the surface (primary to secondary ion ratio), etc. The effect is found to be most pronounced at low energies where the sputter yield enhancement is predicted to increase by a factor of two or more. The mechanisms of the sputter yield enhancement as well as the modification of the energy deposition function are discussed in detail. These computer simulations have been verified experimentally in a number of situations.

**PS-MoP9 High Aspect Ratio Si Etching for Microsensor Fabrication, W. H. Juan and S. W. Pang, Solid State Electronics Laboratory, Department of Electrical Engineering and Computer Science, The University of Michigan, Ann Arbor, MI 48109-2122.**

To improve the sensitivity of micro-electromechanical devices, high aspect ratio Si etching for bulk micromachining is developed. Si is etched in a  $\text{Cl}_2$  plasma generated by an electron cyclotron resonance (ECR) source. The ECR source provides fast etch rate with high selectivity since the reactive species density and ion energy can be controlled independently. Si etch rate increases with microwave and rf power but decreases with Ar and  $\text{CF}_4$  percentage in  $\text{Cl}_2$ . Among different etch masks used for Si etching, Ni provides the highest selectivity ( $\sim 50$ ) compared to thermal  $\text{SiO}_2$  ( $\sim 7$ ) and polyimide/novolac resist ( $\sim 1-2$ ). Etch profile becomes more isotropic with increasing microwave power and temperature, but shows no significant dependence on pressure for the conditions used. Figure 1 shows Si structures etched with 10:1 aspect ratio. With 700 nm electroplated Ni as a mask, 1  $\mu\text{m}$  wide features in Si were etched down to 10  $\mu\text{m}$  deep with vertical profile. This high aspect ratio Si etching was carried out with 100 W microwave power, 100 W rf power, and 20 sccm  $\text{Cl}_2$  at 3 mTorr. The influence of etch mask on etch profile and surface morphology will be presented. Resonant based microsensors with high aspect ratio sensing elements will be fabricated.



H  
1  $\mu\text{m}$

**PS-MoP10 Plasma Etching of Pt and Ferroelectric Thin Films, R. L. Rhoades and D. B. Poker, Oak Ridge National Laboratory\*, Oak Ridge, TN; and B. S. Mercer, PlasmaQuest, Richardson, TX.**

Ferroelectric materials such as PZT (lead zirconate titanate) and BST (barium strontium titanate) are of growing interest for ULSI memories, optical shutters, piezoelectric microtransducers, and a wide variety of sensors and detectors. Much progress has been made on depositing these materials as thin films; however, patterning and etching remains as a major obstacle to their use in devices and circuits. Etch rates of PZT, BST, and Pt with  $\text{Ar}/\text{Cl}_2$  plasmas have been studied using an electron cyclotron resonance plasma etching system. Plasma

parameters were varied over a broad range to determine near optimal values for microwave power, RF sample bias,  $\text{Ar}/\text{Cl}_2$  ratio, substrate carrier temperature, and total pressure. Etch rates for these films were measured in the following ranges: PZT (275–1075  $\text{\AA}/\text{min}$ ), BST (105–473  $\text{\AA}/\text{min}$ ), and Pt (205–800  $\text{\AA}/\text{min}$ ). Etch rate data was then used to determine a preliminary process for patterning of Pt/PZT/Pt layers typical of integrated circuit requirements. Selectivity of PZT:Pt was controllable in the range of 1:1 to 5:1.



SEM cross section of Pt/PZT/Pt layers etched by  $\text{Ar}/\text{Cl}_2$  plasma. (Sloped wall due to transfer of pattern from original photoresist.)

\*Research sponsored in part by the Division of Materials Sciences, U.S. Department of Energy, under contract DE-AC05-84OR21400 with Martin Marietta Energy Systems, Inc.

**PS-MoP11 Composition of the Oxygen Plasmas from Two Inductively Coupled Sources, M. Tuszewski, J. T. Scheuer, and J. A. Tobin, Los Alamos National Laboratory, Los Alamos, NM 87545.**

Two r.f. inductively coupled plasma sources are studied: a cylindrical source with a 12-turn coil of 0.3 m diameter powered by a 0.5 kW, 0.46 MHz generator, and a planar source with a 3-turn spiral coil of 0.25 m outer diameter powered by a 1 kW, 13.56 MHz generator. These sources generate pure oxygen plasmas in a 0.4 m diameter, 1.2 m length, vacuum vessel with gas fills of 1–10 mTorr. The unknown ionic ( $\text{O}^+$ ,  $\text{O}_2^+$ , and  $\text{O}^-$ ) plasma composition is of particular interest to our oxide growth studies which take place 0.18 m inside the vacuum vessel. Hence, plasma composition at that location is investigated with several measurements: (1) a combination of Langmuir probe radial scans and line-integrated microwave interferometry measurements, (2) optical emission spectroscopy, including Argon actinometry of selected oxygen lines, and (3) mass spectrometry with a compact instrument built for these studies. The results of these measurements will be presented for the two inductive sources and compared to the plasma compositions predicted by a global source model.

**PS-MoP12 Steady-State Helicon Plasma Experiments, J. Gilland, R. Brown, N. Hershkovitz, R. Breun, University of Wisconsin, Department of Nuclear Engineering and Engineering Physics, 1500 Johnson Drive, Madison, WI 53706-1687.**

Helicon waves are studied in steady-state argon and helium helicon plasma created in a solenoidal magnetic field. Maximum plasma densities are the order of  $10^{13} \text{ cm}^{-3}$ . Three types of antenna structures (Nagoya Type III, Dual-Half-Turn and Spiral) are investigated. Helicon waves at 13.56 MHz are excited and identified by the wavelengths of standing waves detected by B-dot probes mounted external to and inside the plasma. Plasma parameters are measured with Langmuir probes. Both radial temperature and density profiles are measured. A microwave interferometer provides a non-intrusive measurement of plasma density. A power balance between ambipolar diffusion losses and rf power deposition is found to agree with the experimental scaling with power, B field and neutral gas. Studies of the power balance are being extended to establish the self-consistent nature of the plasma column radius.

Supported by NSF Grant No. ECS-9120326.

**PS-MoP13 Radio Frequency Hollow Cathode Discharge for Large Area Double Sided Foil Processing, D. Korzec, M. Schott, B. Pfannkuchen, K.-P. Ningel, and J. Engemann.**

A large area surface modification of membranes for medical applications is an important field of plasma processing [1]. A rf hollow cathode discharge is known as an efficient method to generate large area plasmas [2]. A slotted hollow cathode discharge (SHCD) plasma source [3] has been developed for large area treatment of fast moving membranes with a width of 35 cm. A membrane is moved between two symmetrical, capacitively coupled active rf electrodes (cathodes)



with slots perpendicular to the direction of membrane motion. The slots are open at both ends to establish an electrical contact between the plasma and the rf grounded electrodes (anodes). The dependence between the plasma density and the geometrical dimensions of the hollow cathode slots were examined. For measurements of the ion density and its distribution along the slots a double Langmuir probe system has been used. A dense plasma with ion densities up to  $1 \times 10^{12} \text{ cm}^{-3}$  is produced with up to 1000 W power of 13.56 MHz excitation for a pressure range from  $5 \times 10^{-2}$  to 10 mbar with argon, oxygen and nitrogen as working gases. A rapid surface modification of the membrane allows for a membrane processing speed of 20 m/min. An important advantage of the SHCD concept is its up scale ability. A plasma module for membranes with a width of 1200 cm is currently under development and will be described elsewhere.

[1] Man, N. K. *et al.*, *Artif. Organs*, **14**, pp. 44-50 (1990).

[2] Horwitz, C. M. *et al.*, *J. Vac. Sci. Technol.* **A6**, pp. 1837-1844 (1988).

[3] J. Engemann and D. Korzec, *Verfahren und Vorrichtung zur Plasmabehandlung bahnförmiger Materialien*, german patent pending (1992).

**PS-MoP14 Remote Source Characteristics of Helicon Discharges**, Isaac D. Sudit and Francis F. Chen, EE Department, University of California, Los Angeles, 90024-1594.

Etching of silicon in helicon sources has been shown to decrease with increasing magnetic field, even though the plasma density rises<sup>1</sup>. Presumably this is because at high fields the active neutral species is depleted by the extremely high ionization rate. To increase the etch rate, one has to decrease the electron temperature while maintaining high plasma density. We have made measurements of the downstream behavior of a helicon discharge several decimeters away from the antenna. The density is observed to rise and the temperature to fall, just as desired. Using the helicon discharge as a truly "remote" source not only makes the ion flux more uniform, but also increases the ion flux and the population of the etchant species. This feature distinguishes helicon sources from inductively coupled RFI sources, where the density is highest in the near field of the antenna.

<sup>1</sup>R. W. Boswell and R. K. Porteous, *J. Appl. Phys.* **62**, 3123 (1987).

**PS-MoP15 High Density, Low Temperature Dry Etching in GaAs and InP Device Technology**, S. J. Pearton<sup>1</sup>, C. R. Abernathy<sup>1</sup> and F. Ren<sup>2</sup>, <sup>1</sup>Department of Materials Science and Engineering, University of Florida, Gainesville, FL 32611, <sup>2</sup>AT&T Bell Laboratories, Murray Hill, NJ 07974.

ECR etching of GaAs, AlGaAs and GaSb in  $\text{Cl}_2/\text{Ar}$  or  $\text{BCl}_3/\text{Ar}$  and of InP in  $\text{CH}_4/\text{H}_2/\text{Ar}$  discharges is performed down to  $-30^\circ\text{C}$  substrate temperature and characterized in terms of rate, anisotropy, damage introduction and near-surface stoichiometry. Below  $-10^\circ\text{C}$  the vertical etch rates of all these semiconductors decrease due to reduced volatility of the products, and there is suppression of lateral etching with chlorine-based mixtures, but no change in anisotropy of  $\text{CH}_4/\text{H}_2/\text{Ar}$ -etched features. Etching of typical dielectrics ( $\text{SiN}_x$ ,  $\text{SiO}_2$ ) and metals (W,  $\text{WSi}_x$ ) used in bipolar or FET devices in  $\text{SF}_6/\text{Ar}$  discharges was also characterized, and for substrate temperatures below  $-20^\circ\text{C}$  increased concentration of fluorine-containing residues are found on the exposed semiconductor surfaces after removal of the dielectric or metal. These can be removed by a 500 W microwave ECR  $\text{H}_2$  plasma with low additional ( $\sim 25\text{V}$ ) dc bias on the sample. The effect of additional lower collimating magnets on the etch anisotropy was also examined, and found to have a significant improvement at low ion energies. Condensation of the etch gas occurs at  $-30^\circ\text{C}$  for  $\text{BCl}_3$ , but is absent with  $\text{Cl}_2$  or  $\text{CH}_4/\text{H}_2$ . The question of sample heating during high density etching or deposition will also be addressed. The uniformity of etching was measured both with and without the lower collimating magnet operational and no significant change was found.

**PS-MoP16 Aspect Ratio Independent Etching of Silicon using a High Density Helicon Source**, F. P. Klemens, C. W. Jurgensen, D. E. Ibbotson, and J. T. C. Lee, AT&T Bell Laboratories, Murray Hill, NJ 07974.

The fabrication of ultra-large-scale integrated (ULSI) circuits requires increasingly tighter control of wall profiles in order to achieve high circuit densities. Low pressure, high plasma density sources are becoming the accepted technology in many development laboratories and will be installed in significant numbers in production lines in the near future. The advantages of these sources include more anisotropic

etching, high etching rate uniformity, high etching rates, and independent control of the ion energy through wafer biasing.

In order to evaluate the etching performance of these new source technologies, high aspect ratio etching needs to be studied since ULSI devices impose even greater demands with respect to aspect ratio. In this paper, we report results for the etching of silicon trenches with HBr and  $\text{Cl}_2$  chemistry using a low pressure, high density helicon plasma source. We explore the effect of trench depths from 0.50 to  $1.5 \mu\text{m}$ , oxide mask thicknesses of 0.5, 1.0, and  $2.0 \mu\text{m}$ , and rf-bias's of 150 W and 300 W on the resulting profiles of  $0.35 \mu\text{m}$  and  $0.60 \mu\text{m}$  wide trenches and a sidewall next to an open field. The presence of microtrenching, mask undercutting, mask faceting, and wall angle are quantified. For wafers with the  $0.5 \mu\text{m}$  thick masks, we do not observe any aspect ratio dependent etching; however, the etching rate does decrease with etching time.

**PS-MoP17 Substrate Bias Effects in High-Aspect-Ratio  $\text{SiO}_2$  Contact Etching Using an ICP Reactor**, A. C. Westerheim, A. H. Labun, J. H. Dubash, Digital Equipment Corporation, 77 Reed Road, Hudson, MA 01749, J. C. Arnold, H. H. Sawin, Dept. of Chemical Engineering, MIT, Cambridge, MA 02139, V. Yu-Wang, Applied Materials, Santa Clara, CA 95054.

We etched high-aspect-ratio sub-half-micro contacts in  $\text{SiO}_2$  using a high-density  $\text{C}_2\text{F}_6$  plasma generated by an inductively coupled, low-pressure reactor. As expected, oxide and resist etch rates increased with increasing bias. We also observed increasingly vertical sidewall angles and increasing microtrenching depth for higher rf bias conditions on contacts, trenches, and steps. Topography modeling shows that the microtrench profiles are consistent with specular ion reflection from sidewalls and the increase in their depths with rf bias is consistent with the energy-dependent etching yields in high density, fluorocarbon plasma etch chemistries reported by Oehrlein, *et al.*<sup>1,2</sup>

<sup>1</sup>G. S. Oehrlein, Z. Zhang, D. Vender, and M. Haverlag, *J. Vac. Sci. Technol. A* **12**, 323 (1994).

<sup>2</sup>G. S. Oehrlein, Z. Zhang, D. Vender, and O. Joubert, *J. Vac. Sci. Technol. A* **12**, 333 (1994).

**PS-MoP18 A Study of the Causes and Effects of Ion Angular Spread in High Density Plasma Sources**, J. Zheng, J. P. McVittie, CIS, Stanford University, Stanford, CA 94305.

In plasma etching processes, the demand for the directionality of energetic ions on the wafer surface increases as feature sizes shrink. It was believed that sheath collisions were the main cause of the ion angular spread at the wafer surface. Therefore, by moving from conventional plasma sources to high density plasma sources, where the sheaths are basically collisionless, we would expect highly directional (beam-like) ions at the wafer surface. However, with the use of our overhang test structures, we have found a significant amount of ion angular spread in these systems, especially in those with low bias powers.

The possible causes for this ion angular spread are (1) the ion temperature in the bulk plasma, which can be much higher than what was believed ( $k_B T_i > 0.2 \text{ eV}$ ); (2) the higher ion plasma frequency due to its higher density, and the shorter transit time in the sheath due to the smaller sheath thickness, which can make the ions responding to an AC field instead of a DC field in the sheath; and (3) distortion of the electric field in the vicinity of the feature owing to its topography and state of surface charging. All these factors can broaden the ion angular distribution but in different ways. The ion angular spread caused by charging is feature geometry dependent, and that caused by AC sheath field is always accompanied by a much wider ion energy distribution.

We have used silicon wafers with overhang test structures to obtain experimental data. The most important feature of these structures is to let all ions including those very off-normal angled ones to arrive on a flat surface through apertures of different sizes. With the assistance of our etching and deposition profile simulator, SPEEDIE, which also includes a Monte Carlo sheath simulator, we are able to identify the causes and effects of the ion angular spread in various etching processes.

**PS-MoP19 Modelling and Simulation of Neutral Beam Processing Using a Plasma Source**, M. D. Kilgore and D. B. Graves, Dept. of Chemical Engineering, Univ. of California, Berkeley, CA 94720-1462.

Charge-free processing has been proposed as a means of avoiding damage to substrates that may occur as a result of plasma processing. We use simulation to investigate a system in which a high density inductively coupled plasma is used as a source of energetic, directed

neutrals for surface processing. The beaming neutrals are produced by charge exchange collisions as well as by surface neutralization on a grid which separates a plasma source chamber from a wafer processing chamber. We apply a coupled plasma and neutral transport simulation to study the properties of the energetic neutrals at the wafer surface as a function of operating conditions. The inductively coupled plasma simulation includes fluid treatments of ion and electron transport coupled with Poisson's equation for the self-consistent potential as well as a solution of Maxwell's equations for the power input from the external coil. The neutral simulation is a kinetic treatment using the direct simulation Monte Carlo method. Our simulation results show the effects of varying plasma power, operating pressures and geometries of the two chambers, as well as gas flowrate and pumping speed. We model the interchamber grid to investigate how its design influences the beaming neutrals' angular and energy distributions. We show results which illustrate trade-offs which must be considered for the downstream chamber operating pressure. Low pressure is desirable for beam directionality while high pressure is desirable for process rate and uniformity.

**PS-MoP20 Influence of the Ponderomotive Force on Inductive-Source Plasma Profiles, G. DiPeso\*, T. D. Rognlien\*, V. Vahedi<sup>†</sup>, and D. W. Hewett\*,** \*Lawrence Livermore National Laboratory, Livermore, CA 94550; <sup>†</sup>EECS Department, UC Berkeley, CA 94720.

We present results of the influence of the ponderomotive force on the density and electrostatic potential profiles in inductive discharges. The ponderomotive force can be written as a gradient of a potential, and the resulting electron force scales with the discharge power and inversely with the discharge pressure. The effect of the force on density profiles is demonstrated using a one dimensional analytic theory and a two dimensional fluid simulation. For a cylindrical discharge with an inductive coil on one axial face, this force results in a reduced particle outflow toward the coil, and increases the density peak in the discharge center. The smaller flow toward the coil can reduce erosion on a dielectric window between the coil and the plasma. The higher overall density increases the density at the opposite axial face by a multiplicative factor which gives a higher etch rate but minimal change in radial uniformity for the top-coil configuration. For the side-coil configuration, the ion density at the wafer increases, the ion flux to the side-wall (and assumed dielectric window) is reduced, and the radial uniformity at the wafer improves.

**PS-MoP21 Modeling Of Oxide Etching In A High Density ICP Tool, R. A. Stewart, J. D. Bukowski, P. Vitello\*, and D. B. Graves,** Department of Chemical Engineering, University of California, Berkeley, CA 94720.

We present results from a two dimensional (r, z) model of an inductively coupled plasma tool used for etching of SiO<sub>2</sub>. Both inductive and capacitive coupling from the coils are included in the model. Capacitive coupling from the rf biased substrate is also included. The discharge physics model is based on fluid equations for electrons, positive and negative ions. Neutral species transport and chemistry are coupled to the equations for charged species, including the creation and deposition of film precursors. We use a variety of fluorocarbon mixtures, similar to those used industrially. Results are compared to experiment where possible.

\*Lawrence Livermore National Laboratory, Livermore, CA 94551.

**PS-MoP22 Spatially Averaged (Global) Model of Time Modulated High Density Electronegative Plasmas, S. Ashida\*, C. Lee, and M. A. Lieberman,** Univ. of California, Berkeley, Berkeley, California 94720.

The operation of plasma sources utilizing time modulated input power has attracted much attention recently because the technique yields another discharge parameter. In this study, a spatially averaged (global) model of time modulated plasmas has been developed and used to investigate argon and Cl<sub>2</sub> gas discharges. The advantage of this model is that it requires much smaller computational resources than such models as Fluid or PIC simulations. It has been found that higher plasma densities can be obtained by selecting an appropriate pulse period, for the same average power as in the case of continuous wave operation. Other parameters, such as the duty ratio and the shape of the modulation waveform also affect the plasma density. In addition, we discuss the dependence of the radical density and the

electronegativity of the Cl<sub>2</sub> plasma as a function of the duty ratio and the pulse period.

This work is performed with support in part from NSF Grant ECS-9217500, DOE Grant DE-FG03-87ER13727, and LLNL Contract W-7405-ENG-48.

\*On leave from R&D Center, Toshiba Corp., Japan.

**PS-MoP23 2D RF Sheath Structure due to Geometrical Discontinuities Outside the Wafer Edge, B. Lane,** Plasma Dynamics.

2D simulation results of the time dependent RF sheath in the vicinity of the wafer edge are presented. Geometrical obstacles such as steps in the underlying electrode, dielectric focus rings and grooves affect the shape of the RF sheath and hence the flux and directionality of ions impinging on the wafer edge. The simulation follows fluid ions under the assumption that the directed velocity is much greater than the random thermal velocity; electrons are assumed to have a Maxwell-Boltzmann distribution and thus have an exponential dependence on the potential. The electrostatic potential is obtained by direct solution of the Poisson equation. All material surfaces are taken to be covered by insulators and the surface charge density is self-consistently integrated. The simulation volume focuses on the wafer edge and the effects of the core plasma enter through boundary conditions. This provides a detailed look at this critical region in a computationally feasible fashion at the expense of simplifying global processes which sustain the plasma. It is found that the sheath curvature near the wafer edge can be either concave towards or away from the wafer with consequent focussing or defocussing of the ion flux to the wafer edge; the curvature depends on the details of the geometry outside the wafer edge.

Work supported by SEMATECH.

**PS-MoP24 2D Modeling of Time Modulated Inductive Discharges, V. Vahedi<sup>†</sup>, M. A. Lieberman<sup>†</sup>, G. DiPeso\*, and D. W. Hewett\*,** \*Lawrence Livermore National Laboratory, Livermore, CA 94550; <sup>†</sup>EECS Department, UC Berkeley, CA 94720.

Recent measurements and reports of plasma behavior in time modulated discharges have increased the general interest in these types of discharges. The current belief is that a very short time (< 1 μsec) after the power is turned off, the fast electrons in the system, on the tail of the electron energy distribution, are depleted. As a result, ionization, and most other electron impact dissociative mechanisms with high energy thresholds, will be greatly reduced after this short time, and the time-average concentration of certain free radicals can be significantly modified.

We will present results from 2D fluid simulations of time modulated inductive discharges showing the dependence of the time-averaged electron temperature and plasma density on the duty-cycle and duration of the RF power signal. We will also show modifications to the plasma density profile due to the modulation.

## VACUUM TECHNOLOGY

### Room BR4 - Session VT-MoP

#### Vacuum Science and Technology

**Moderator:** L. D. Hinkle, MKS Instruments Inc.

**VT-MoP2 Rotating Disc Gauge Using High Temperature Superconductor Suspension, A. Chambers and A. D. Chew,** University of York, England, and A. P. Troup, Edwards High Vacuum International, Crawley, UK.

The rotating disc gauge measures high and potentially ultra-high vacuum by sensing the torque transferred by molecular drag between a disc rotating at high speed ~ 1000 Hz and a close coaxial disc which intercepts molecules leaving the rotor. In an early version of the device (J Vac Sci Technol A 10(4) 2655) in which the torque on the sensing disc was measured by a classical torsion balance method we showed that it is capable of absolute measurements at  $2 \times 10^{-7}$  mbar with accuracy of order  $\pm 3\%$ . The achievement of better sensitivities—closer to the expected theoretical limit ~ few  $10^{-10}$  mbar—was limited by vibrational problems.

In a new version of the RDG the sensor disc is freely supported by



a high temperature superconductor/magnet suspension and a dynamic technique used to measure its acceleration from rest. A principal aim of the work is to achieve a torque-free suspension system so that all the induced motion can be attributed to molecular drag, thus eliminating the term which corresponds to 'residual drag' in the spinning rotor gauge, and which limits the sensitivity of that device.

Progress towards this aim will be reported with particular emphasis placed on the development of a novel UHV compatible HTS-magnet suspension.

**VT-MoP3 Measurement of Xe Pressure by Photoelectron Counting with the Imaging Counter, Shigeyuki Sekine and Shingo Ichimura,** Electrotechnical Laboratory, 1-1-4 Umezono, Tsukuba, Ibaraki 305, JAPAN, e-mail: sekine@etl.go.jp, FAX: +81-298-58-5733.

Measurement of xenon (Xe) pressure was carried out by the photoelectron-counting method adopting a laser ionization technique. Second harmonics of a picosecond pulsed Nd:YAG laser was used for the non-resonant multiphoton ionization of Xe atoms. Produced photoelectrons were extracted by an electrostatic lens and were detected by a combination of a microchannel plate and a fluorescence screen. Each bright spot on the screen corresponded to a photoelectron. The spot image was photographed by a CCD camera with a repetition rate of the laser, and the number of spots on the screen was counted by an image processor for each laser shot.

The number was measured as a function of Xe pressure in the ultrahigh vacuum (UHV) region, and a simple proportion was successfully observed. The number of photoions was also counted with the same apparatus by changing a polarity of the extraction voltage. The overall detection efficiency for both results was evaluated.

**VT-MoP4 Investigation of RGA's for High Sensitivity He Leak Detection\*, J. A. Smith,** MKS Instruments Inc., Walpole, MA 02081 and **M. G. Rao,** Continuous Electron Beam Accelerator Facility, Newport News, VA 23606.

Continuous Electron Beam Accelerator Facility (CEBAF) and MKS Instruments have recently signed a Cooperative Research and Development Agreement (CRADA) for developing an ultrahigh sensitivity He leak detector. This new leak detector is based on the technique of dynamic adsorption and desorption of He, which was developed at CEBAF for the production of ultra leak tight Superconducting Radio Frequency Cavity pairs operating at 2 K<sup>1</sup>. A closed cycle He refrigerator operating at ~8 K and a low mass range quadrupole electron multiplier RGA are required for this leak detector development program. A low He detection limit (~10<sup>-14</sup> torr) in the presence of a large hydrogen (~10<sup>-8</sup> torr) background is an essential requisite for the RGA with an electron multiplier detector. In this paper we present the results of our investigation of high frequency operation of RGA's for achieving the above goals. The long term stability of the RGA's will also be presented in this paper.

1. M. G. Rao, J. Vac. Sci. and Technol. A 11, 1598 (1993).

\*This work supported by U.S. DOE Contract No. DE-AC05-84ER40150.

**VT-MoP5 O<sub>2</sub> Treated Metal Surfaces with Less Carbon Detected on the Surface and in the Sputter-Profiled Layer by Auger Electron Spectroscopy (AES), T. Momose\*, N. Yamada\*, K. Asano, and H. Ishimaru,** \*Miyagi National College of Technology, Natori, 981-12, National Laboratory for High Energy Physics (KEK), 1-1 Oho, Tsukuba, 305 Japan.

The authors have been engaged in efforts to reduce gas desorption of UHV materials, especially on aluminum alloys. The special extrusion technique succeeded in making thermal gas desorption three orders lower. An oxygen plasma treatment improved dynamic gas desorption about one order. In both treatments however, carbon remains on the surface and in sputter-profiled layer. Carbon deteriorates dynamic gas desorption coefficient. To eliminate carbon, ozone treatment was applied on metal surfaces. The surfaces of aluminum, copper, and stainless steel without any treatments were exposed to ozone using air including ozone of 250 ppm with flowing rate of 1 l/min for 24 hours. The samples were shown to become less carbon, especially on Cu and Al surfaces, by AES with a turbomolecular and a dry backing pump. In addition, no carbon was detected in the sputter-profiled layer. The detectability of AES is on the order of 10<sup>-3</sup> and number of carbon atoms could be 3 × 10<sup>13</sup> cm<sup>-2</sup>. The thickness of the oxidized layer was 6.3, 8.1 and 3.0 times of the native oxide layer for Cu (120 Å), Al (170 Å) and stainless steel (60 Å), respectively. X-ray photoelectron spectroscopy shows: 1) The ratio (O/Al) is 1.5 for the treated and 1.3

for the non treated. 2) Cu<sup>+</sup> is included in the treated but Cu<sup>2+</sup> is dominant for the non treated. The surfaces are further expected with low carbon adsorption characteristics because no carbon detected by AES on the surfaces stored in a covered glass dish more than four days. The photo-desorption yield of similarly treated aluminum surface was 1.7 × 10<sup>-4</sup> molecules per photon at a dose of 1.4 × 10<sup>19</sup> photons-cm<sup>-2</sup> using TRISTAN accumulation ring synchrotron radiation facility. This is two times of the yield of copper, obtained with the same system at a same dose. The layer, in conjunction with the simple ozone treatment, makes an ideal construction material for storage rings and other XHV systems and components.

**VT-MoP6 Outgassing Reduction of Type 304 Stainless Steel by Surface Oxidation in Air, K. Odaka, S. Ueda,** Mechanical Engineering Research Laboratory, Hitachi Ltd., 502 Kandatsu, Tsuchiura-shi, Ibaraki 300, Japan.

The effect of surface oxidation in air on the outgassing reduction from stainless steel were investigated. The outgassing measurement system of throughput method was fabricated from type 304 commercial-grade stainless steel and was buff- and electro-polished before the prebaking at 450°C for 30 h. The test chamber had surface area of 1.5 m<sup>2</sup> and was evacuated with a TMP. The orifice was 5.6 mm in diameter. The two extractor gauges were calibrated using a spinning rotor gauge. An evacuation cycle including 18 h-baking at 200°C was repeated four times. An outgassing rate of 6 × 10<sup>-11</sup> Pam<sup>3</sup>s<sup>-1</sup>m<sup>-2</sup> was obtained after 200°C baking. Then, the system at room temperature was exposed to air and was heated and kept at 200°C for 3 h to oxidize the surface. Oxidation in air resulted in remarkable reduction of the outgassing rate after baking. During the first evacuation after oxidation in air, 2 × 10<sup>-11</sup> Pam<sup>3</sup>s<sup>-1</sup>m<sup>-2</sup> was obtained. In the following 3 evacuation cycles, outgassing rate reached 3 × 10<sup>-11</sup> Pam<sup>3</sup>s<sup>-1</sup>m<sup>-2</sup> repeatedly. Residual gas analysis showed a significant reduction in the amount of hydrogen after oxidation in air. On the other hand, oxidation in air did not affect the outgassing characteristics before baking. This may be due to an oxide layer on the stainless steel surface preventing hydrogen from diffusing out of the metal and escaping into the vacuum.

**VT-MoP7 A Low Contamination Ultrahigh Vacuum System of the SRRC 1.3 GeV Electron Storage Ring, G. Y. Hsiung, J. R. Huang, D. J. Wang, J. G. Shyy, H. S. Tzeng, S. N. Hsu, S. Y. Perng, K. M. Hsiao, W. D. Wey, J. R. Chen<sup>a)</sup> and Y. C. Liu<sup>b)</sup>,** Synchrotron Radiation Research Center, No. 1 R&D Road VI, Hsinchu Science-Based Industrial Park, Hsinchu, Taiwan 300, R.O.C.

The vacuum system of the SRRC 1.3 GeV electron storage ring is designed as a low contamination ultrahigh vacuum system. In addition to the standard treatments for the UHV components, several contamination reduction methods were adopted in the manufacturing processes such as oil-free machining processes, completely oil-free pumping system and dust controlled installation processes. The profits of the low contaminated treatments were proved from the results of fast beam cleanup, low dust trapping effect and low carbonaceous residual gases in the vacuum system.

- a) also at Institute of Nuclear Science, National Tsing-Hua University.
- b) also at Department of Physics, National Tsing-Hua University.

**VT-MoP8 Selection of Beam Chamber Materials Cu, Cu/Al Hybrid, and Al for High Current Storage Ring, H. Ishimaru,** National Laboratory for High Energy Physics, KEK, 1-1 Oho Tsukuba 305 Japan, **A. Komura, T. Takama, and A. Kitagawa,** Hitachi Zosen, 1-3-40 Sakurajima, Konohana Osaka 554 Japan.

Electron storage rings tends to be operated for high beam current, especially for a beam pipe in B-Factor which is constructed by KEK-Japan and SLAC-US. Copper has been currently used the beam pipe materials under high current, however it costs higher than an aluminum alloy which is inferior under heat load for photons. Actually it is necessary to consider both cost and heat load limits. We have considered three models. 1) Cu, 2) Cu/Al hybrid, and 3) Al. We have analyzed three dimensionally by super-computer on temperature distribution, heat deformation, and heat stress in the heat load 5 kW/m, 7.5 kW/m and 10 kW/m. Particularly in model 2) Cu/Al hybrid method, we proposed a new configuration mentioned below. a) Material of an photon absorber is used copper bar/water cooled aluminum alloy clad. The beam chamber is an extruded aluminum alloy. b) Cu/Al clad is an explosion bonding method. c) Structure of weld parts is simplified to enable automatic TIG. d) Many slits of the absorber can reduce heat stress and heat strain. e) The particle free can be kept for

the cycle heat strain between the absorber and the beam pipe. Highest temperature of the absorber is 190°C for 10 kW/m of heat load in aluminum alloy, 160°C in Cu/Al hybrid systems, and 145°C in copper. In the analysis of heat stress, the hybrid system can be used in wide range heat load with slits of the absorber.

H. Ishimaru, T. Momose, Y. Suetsugu, and H. Hirayama: Hybrid Cu-Al Beam Pipe for KEK-B Factory, *J. Vac. Sci. Technol.*, A11, No. 6, Nov/Dec (1993) 3121.

**VT-MoP9 Scaling Law of Outgassing with a Pumping Parameter, K. Akaishi, Y. Kubota, Y. Funato, M. Mushiaki and O. Motojima,** National Institute for Fusion Science, Nagoya 464-01, Japan.

In order to investigate the dependence of outgassing rate on pumping speed in a vacuum chamber which is pumped at room temperature, a small test chamber made of 304 stainless steel which has a volume of 20 l and a surface area of 7200 cm<sup>2</sup> has been constructed. The chamber has been pumped after air exposure for 3 days with six kinds of pumping speeds in a range from 200 l/s to 0.36 l/s through orifices and the outgassing rate of the chamber has been determined from the measured final pressure at the pumping time of 72 h. As a result of the experiment, it is shown that the observed outgassing rates  $q$  are expressed with two sets of power functions of  $q = q_0(S/A)^{-n_1}$  and  $q = q_0'(S/A)^{-n_2}$  where  $S/A$  is a pumping parameter defined as the ratio of pumping speed  $S$  to surface area  $A$ , exponents of  $n_1$  and  $n_2$  are  $n_1 = 0.8282$  for  $S/A \geq 10^{-3}$  l/scm<sup>2</sup> and  $n_2 = 0.4655$  for  $S/A \leq 10^{-3}$  l/scm<sup>2</sup>, respectively.

**VT-MoP10 Enhancement of Hydrogen Evacuation by Injecting Fluorine into the Exhaust System with Turbomolecular Pumps, N. Ogure,** Ebara Research Co., A. Shibata, Ebara Solar, Inc., K. Ono, Ebara Corp., N. Hayasaka, H. Okano, Toshiba Corp., and K. Okumura, Toshiba America Electronic Components, Inc.

We propose a novel evacuation system with fluorine being injected into the discharge port of a turbomolecular pump (TMP) to improve effective hydrogen compression ratio. The mechanism of this improvement is to convert hydrogen into heavy weight molecule, such as HF, which has high compression ratio, by the reaction between fluorine and hydrogen in the discharge port.

It was confirmed that the effective compression ratio increases to  $10^4$ – $10^6$  from  $10^3$  in the range where the hydrogen partial pressure in the evacuated chamber was more than  $10^{-8}$  torr by the TMP system.

**VT-MoP11 Pumping Behavior of Distributed Ion Pumps at High and Misaligned Magnetic Fields,\* H. C. Hseuh, W. S. Jiang, and M. Mapes,** AGS Department, Brookhaven National Laboratory, Upton, New York 11973-5000.

In order to optimize the design of the distributed ion pumps (DIPs) to be used for a muon storage ring currently under construction at Brookhaven, the pumping speeds of several DIPs were studied in various magnetic fields. The DIPs were subjected to magnetic field  $B$ , ranging from several hundred Gauss up to 15 Kilogauss, and misalignment angles (angles between the direction of  $B$  and the anode axis) from 0 to 13 degrees. The pumping speeds of the DIPs with cell radii of 9 and 12 mm peaked at the transition magnetic field,<sup>1</sup> then dropped off rapidly with an increasing magnetic field. The pumping speeds of these DIPs were not as sensitive to misalignment with respect to  $B$  as the DIPs with smaller radii. The pumping speeds of DIPs with cell radii of 5 and 6 mm remained relatively constant with an increasing magnetic field, but decreased rapidly when subjected to misalignment. The results of this study are in reasonable agreement when compared to the calculated pumping speeds using Suetsugu's empirical formula.<sup>2</sup>

\*Work performed under the auspices of the U.S. Department of Energy.

<sup>1</sup>Hartwig and J. S. Kouptsidis, *J. Vac. Sci. Technol.*, 11, 1154 (1974).

<sup>2</sup>Y. Suetsugu and M. Nakagawa, *Vacuum* 42, 761 (1991).

**VT-MoP12 Modelling of a Multistage Claw Rotor Vacuum Pump, I. Ioffe, V. Koss,** The BOC Group, Inc. Technical Center, USA, M. Gray, R. G. Livesey, Edwards High Vacuum International, UK.

Claw rotor compressors are used in a wide variety of vacuum pumping applications. However, the published literature on these machines offers little guidance on the physical processes which occur during pump operation, their effect on pump performance or the influence of design and operating parameters. Equations describing a multistage pump mechanism are derived. The equations are based on the laws of conservation of mass and energy and uses a lumped parameters

approximation. The equations describe pressure and temperature changes due to volume variation, gas flux between stages, leakage within and between stages, gas mixing, and heat exchange. Expressions for the pumping speed and power consumption are also provided. Predictions based on the model are compared with experimental data.

**VT-MoP13 H<sub>2</sub>O Pumping by Sputter Discharge with LaB<sub>6</sub> Cathode, Y. Funato, M. Miyoshi, K. Akaishi\*, Y. Kubota\* and M. Mushiaki\*\*,** Dept. of Electronic and Information Engineering, Suzuka College of Technology, Suzuka 510-02, JAPAN.

Characteristics of H<sub>2</sub>O water pumping by glow discharge with LaB<sub>6</sub> cold cathode are studied. For the purpose of the development of a new type of sputter ion pumps, Lanthanum Hexaboride (LaB<sub>6</sub>) is applied for the cathode material on the basis of the preliminary study. Use of LaB<sub>6</sub> for the cathode of a sputter ion pump was proposed to develop a low outgassing wall for vacuum chamber. The study showed that the vacuum chamber with the LaB<sub>6</sub> sputter coating reached a low ultimate pressure than that without coating. The QMS analysis showed that the pressure of residual water vapor was remarkably reduced before coating. The experiment shows that LaB<sub>6</sub> coating by glow discharge on stainless steel wall is effective to reduce the H<sub>2</sub>O outgassing rate of a vacuum wall. And the pumping speed of H<sub>2</sub>O is also estimated.

**VT-MoP14 Vacuum Characteristics of Titanium, M. Minato and Y. Itoh,** Vacuum Metallurgical Co., Ltd., 516 Yokota, Sambu, Chiba, 289-12 Japan.

It is true that little attention has been paid to the metals other than stainless steels and aluminum alloys for the materials of vacuum chambers in UHV (Ultra High Vacuum). Titanium is another candidate new material for UHV and XHV (Extreme High Vacuum). It has such advantages as light weight, high corrosion resistivity, and small thermal deformation.

To obtain basic data for the application of titanium to UHV and XHV, various samples made of stainless steel and titanium with specific fabrications and surface treatments were prepared. The outgassing rates of those samples in the bake out process at 200°C have been measured. It was found that titanium has low outgassing rate and can be used for the material in UHV. Coating with TiN is also found to lower the outgassing rate. The gases outgassed from those samples were analyzed by quadrupole mass analyzer. Interesting results were obtained in the change of outgassing rates of hydrogen of those samples.

Taking those results into consideration, a vacuum chamber made of electro-polished stainless steel and a vacuum chamber made of titanium coated with TiN were prepared and pumped down into XHV region. The pump down curves were compared and discussed.

**VT-MoP15 Recombination Limited Outgassing of Stainless Steel, Boude C. Moore,** Consultant.

It is common practice to bake stainless steel vacuum chambers and equipment in order to reduce hydrogen outgassing. The removal of atomic hydrogen from the bulk metal follows classic diffusion theory, at least at the start of bake. When low levels of outgassing are sought, experiment diverges radically from these expectations. Observed hydrogen outgassing of vacuum baked 304 stainless steel can be as much as a factor of  $10^{30}$  larger than predicted by diffusion theory. This theory assumes that all of the atomic hydrogen diffusing to the surface recombines into molecular hydrogen and escapes into the vacuum; none returns into the bulk metal. However as the surface coverage of atomic hydrogen is reduced, the recombination rate falls as the square of the coverage. It has been suggested that a recombination limit could be the cause of the high outgassing rates. It is the objective of this paper to test this suggestion. Recombination rates for atomic deuterium have been reported. These are used as a rough approximation to hydrogen rates. A numeric analysis is used to estimate the outgassing rates and the internal concentration profiles for specific bake procedures. The results are much closer to experiment than the simple diffusion theory. Adding the recombination limit is a useful step towards the reliable prediction of postbake outgassing rates.



## BIOMATERIAL INTERFACES

### Room BR4 - Session BI-MoP

#### Biomaterial Interfaces

**Moderator:** M. J. Tarlov, National Institute of Standards and Technology.

**BI-MoP1 Nanobiology: The Action of Picosecond Nanometer-Scale Pulse on DNA, Gong Lisan, Wu Junhan and Gong Weisui** (South China Normal University, Guangzhou, GD 510631, China).

**EXPERIMENT SAMPLE DNA** (Biological Informational Source) was treated with YAG (Ultrafast Source).

**PURPOSES:** 1. to study the action of ultrafast nanometer-scale pulse on DNA; 2. to explore the possibility of cleavage of DNA.

**MATERIALS:** 1. Sample DNA ( $\lambda$ -DNA,  $\lambda$ -DNA-HindIII); 2. YAG 265 nm.

**METHODS:** Sample DNA was irradiated by YAG (265 nm, 30 ps, 50 uJ) and then examined by spectrophotography and electrophoresis.

**RESULTS:** 1. the spectra of the tested was DNA's typical spectra; 2. the forms of the DNA spectra did not change after the treatment of ultrafast pulses, and their peaks were still at 260 nm, but their peak values increased, showing hyperchromic effect. 3. the result of agarose gel electrophoresis revealed tailing of the DNA treated by pulse.

**DISCUSSION:** 1. the hyperchromic effect and the tailing indicated that the structural bonds of DNA were cleaved by ultrafast pulses; 2. DNA was broken into structural units at different levels; 3. DNA photolytic products (photodimer, photohydrate, photosensitizer and transient species, etc.) were created. Obviously, ultrafast pulses can change DNA molecular structure and cleave DNA. Unfortunately, under the condition of this experiment, we did not observe the cleavage on the predesignatory site of DNA by YAG. As to the prospect for the future, it is possible that the combination of molecular biotechnology and transient ultrafast optical technique may eventually achieve cleavage on predesignatory site and splicing of DNA in order to create new species.

**BI-MoP2 STM Imaging of Oligonucleotides, A. Limansky, O. Limanskaya, Yu Kamensky\***, Institute for Low Temperature Physics and Engineering, Academy of Sciences of Ukraine, 47 Lenin Ave., Kharkov 310164; \*Scientific-Research Institute of Radio Engineering Measurements, 271 Acad. Pavlov Str., Kharkov 310054, Ukraine.

Double-stranded DNA is a weak conducting structure. Besides, even when using pAO3 DNA of the known length (50 nm), we were not always able to distinguish unambiguously the sticklike structure on HOPG surface and DNA real molecules. Therefore to simplify STM image interpretation, we used single-stranded oligonucleotides of 20 nucleotide length. At low ionic strength corresponding to the melted state of DNA, its contour length is from 17 to 18 nm. At high ionic strength of the solution ( $I = 0.1$ ), double-stranded oligonucleotide with the length of 20 nucleotide pairs are in the helical state in solution at room temperature. The oligonucleotide length measured at  $I = 0.1$  was 14–15 nm. Our value for DNA length (17–18 nm) obtained at low ionic strength indicates the more flexible bonds of DNA sugar-phosphate bone.

**BI-MoP3 Fabrication of Patterned DNA Surfaces Using Lithographic Modification of Self-Assembled Organic Monolayers, Linda A. Chrisey<sup>1</sup>, C. Elizabeth O'Ferrall<sup>1,2</sup>, Paul M. Roberts<sup>1,2</sup>, Walter Dressick<sup>1</sup>, Charles S. Dulcey<sup>1</sup>, Douglas B. Chrisey<sup>1</sup> and Jeffrey M. Calvert<sup>1</sup>**, <sup>1</sup>Naval Research Laboratory, Center for Bio/Molecular Science and Engineering (Code 6900), Washington, DC 20375-5348, and <sup>2</sup>Geo-Centers, Inc., Fort Washington, MD 20744.

Self-assembled monolayer (SAM) films of various organosilanes have been characterized as surfaces for the spatially-controlled, selective attachment of single-stranded synthetic DNA. Patterns of DNA on silica substrates have been created by photochemical modification of the SAMs through lithographic masks to produce regions which promote or resist DNA attachment. The attachment of DNA to SAM-modified surfaces was followed using UV spectroscopy, radioassay, ellipsometry, and enzyme-linked immunoassay. We have also demonstrated that the immobilized DNA is capable of selective hybridization to a complementary oligomer, thus this attachment format has potential for the development of multiplexed DNA-based biosensors.

**BI-MoP4 Contact versus Tapping Mode<sup>TM</sup> AFM Imaging of Native Chromatin, J. Vesenska, L. D. Martin, R. Miller\*, E. Henderson, and D. D. Larson**, Dept. of Zoology and Genetics and Dept. of Mathematics\*, Iowa State University, Ames, IA 50011.

Associated and dissociated chromatin structures<sup>1</sup> are examined in both contact and TappingMode<sup>TM,2</sup> atomic force microscopy (AFM). Probe apices are characterized using colloidal gold standards<sup>3,4</sup>. AFM probes of nominally same radius of curvature obtain significantly different lateral structural details of the chromatin, though similar vertical height, in these two imaging modes. These comparisons provide more evidence for lateral broadening of specimens due to shear forces<sup>5</sup>. The consequence of this broadening mechanism on image reconstruction, the process of removing the image distortion due to finite tip radius, is discussed.

<sup>1</sup>L. D. Martin, J. Vesenska, E. Henderson, and D. D. Larson, "Observation of Individual Histones in Dissociated Nucleosome Cores Derived from Native Chromatin," Submitted.

<sup>2</sup>TappingMode<sup>TM</sup> is a registered trademark of Digital Instruments Inc., Santa Barbara, CA.

<sup>3</sup>R. Miller, J. Vesenska, and E. Henderson, "Three Dimensional Reconstruction of Scanning Probe Apex from Colloidal Gold Specimens," Submitted.

<sup>4</sup>J. Vesenska, R. Miller, and E. Henderson, "Three Dimensional Probe Reconstruction for the Atomic Force Microscope," *Rev. Sci. Instr.*, in press (July 1994).

<sup>5</sup>K. A. Barbee, P. F. Davies, and R. Lal, "Shear Stress-Induced Reorganization of the Surface Topography of Living Endothelial Cells Imaged by Atomic Force Microscopy," *Circ. Res.* **74**(1): 163–171, 1994.

**BI-MoP5 Adsorption and Coadsorption of Water and Amino Acids on Pt(111), P. Löfgren, J. Lausmaa, A. Krozer, and B. Kasemo**, Chalmers University of Technology and University of Göteborg, 412 96 Göteborg, Sweden.

Adsorption of water, (hydrated) ions and biomolecules constitute important early events at the interface between materials and tissue, such as in medical implants. Model experiments, using surface science methods (UHV techniques, single crystals, ...), are potentially useful for obtaining information about the molecular interactions taking place at such interfaces. In this work we are studying the adsorption and coadsorption of water and different amino acids on a Pt(111) surface, using TDS and XPS as the main analytical techniques.

High resolution TDS of water adsorption shows that water starts to form multilayers and clusters after 80% saturation of the first monolayer. The sticking coefficient is slightly higher on clusters/multilayers than on the clean Pt surface. Under certain conditions bilayer formation can be observed, as evidenced by an additional peak that appears before clusters and multilayers start to form.

Depending on their side-chains and physical properties, different amino acids offer wide spectrum of possible adsorbate-surface and adsorbate-adsorbate interactions, for example different binding energies, adsorbate orientations, proton exchange reactions, and surface solvation. Platinum is a particularly interesting substrate in this respect, in view of its catalytic activity for many reactions involving H<sub>2</sub>, O<sub>2</sub>, H<sub>2</sub>O, CO, ... Results from experiments exploring the effects mentioned above will be reported.

**BI-MoP6 XPS and In vitro Studies of TiNi Surfaces Modified Using Various Sterilization Procedures, S. A. Shabalovskaya, J. W. Anderson, J. E. Cunnick**, Ames Laboratory—D.O.E., and Department of Microbiology, Immunology, and Preventive Medicine, Iowa State University, Ames, IA 50011.

TiNi has emerged as shape memory implant material with unexpectedly good biocompatibility. Despite widespread applications of these alloys in Russia, China, and Germany, nothing is known about their surface Chemistry. Since nickel is a well-known antagonist of living tissues, there is a question regarding the role the alloy components play in the surface formation. The results of the first XPS surface studies of nearly equiatomic TiNi alloys chemically etched, autoclaved in steam and in water, exposed to hydrogen peroxide solution are presented. The type of oxide layer, its thickness as well as depth distribution of elements critically depend on the layer formation conditions. In general, TiNi alloys revealed a tendency to be covered by TiO<sub>2</sub> based oxides with Ni atoms incorporated in the oxide lattice. Chemical etching selectively removes nickel from the surface. Hydrogen peroxide produces oxide with the highest nickel concentration (~20–30 at. %). The increase of the duration of autoclaving affects the surface nickel concentration in opposite ways depending on whether

environment is water or steam. The appropriate choice of treatment allows us to reduce the Ni concentration down to 5 at. % in surface layers as deep as 5–15 nm. Surface treatment procedures allowing to completely eliminate nickel from the surface have been developed. Variation of the alloy composition in the range 49–51 at. % Ni accompanied by structural change does not affect the surface state.

XPS investigation was followed by *in vitro* studies of rat spleen cells behavior. Exposure of cells to autoclaved TiNi samples induced a slight increase in plating efficiency compared with cells exposed to the control Ti samples and "cells alone". Samples exposed to hydrogen peroxide reveal a severe toxic effect comparable with that of pure nickel. Different biological response to TiNi surfaces requires further studies.

**BI-MoP7 Nano-Scale Mechanics and Morphology of Laser Ablated Tooth Enamel.** C. A. DiRubio\*, P. Tangyungyong\*, J. E. Houston\*, T. A. Michalske\*, O. L. Warren<sup>†</sup>, and P. Wilder-Smith\*\* (\*): Surface and Interface Science Department, Sandia National Laboratories, Albuquerque, NM; (†) Department of Chemistry, University of Western Ontario, London, Ontario, Canada; (\*\*) Beckman Laser Institute & Medical Clinic, University of California, Irvine, CA.

It has been observed that human tooth enamel which has been surface treated with an excimer laser ( $\lambda = 308$  nm) prior to fluoridation is more decay resistant than enamel which has been fluoridated alone<sup>1</sup>. We have studied the surface of tooth enamel which has undergone this pre-treatment using interfacial force microscopy (IFM) to probe the mechanical properties of the surface, and both IFM and atomic force microscopy (AFM) to probe the surface morphology. The enamel consists of apatite crystallites imbedded in a protein rich organic matrix that makes up less than 1% of the enamel mass. Preliminary results indicate that the laser preferentially ablates the organic material between the crystallites, resulting in a rougher enamel surface. In addition, the irradiated enamel can be permanently deformed in IFM loading experiments, whereas the non-irradiated enamel exhibits an anelastic response to loading (i.e., there is a large hysteresis in the force vs. displacement curve, but no permanent deformation). We will discuss possible models for the enhanced decay resistance of the laser pre-treated enamel in light of these results.

<sup>1</sup>P. Wilder-Smith, A. Arrastia, J. Neev, L. H. Liaw, and N. W. Burns, J. Dental Res. 72, Abstr. 1949 (1993). This work performed at Sandia National Laboratories is supported by the U.S. Department of Energy under contract DE-AC04-94AL85000.

**BI-MoP8 Surface Characterization of Titanium Implants.** G. N. Raikar and J. C. Gregory, Surface Science Labs, University of Alabama, Huntsville, AL 35899; J. L. Ong and L. C. Lucas, Dept. of Biomedical Engineering, University of Alabama, Birmingham, AL 35294; D. Kawahara and M. Nakamura, Dept. of Biomaterials, Osaka Dental University, Osaka 540, Japan.

The initial biocompatibility of titanium (Ti) implants is associated with surface and not bulk properties; hence surface characterization of these implants is critical for their clinical success. A goal of this study was to characterize the surface composition of Ti oxides after different surface treatments. In this paper, we present the results of XPS, AES, FTIR, and Raman spectroscopy performed on surface modified Ti (ASTM F76) samples which were immersed in  $\alpha$ -MEM solution. Initial surface studies revealed an amorphous oxide layer on all the samples similar in composition to TiO<sub>2</sub>. After exposure to  $\alpha$ -MEM medium, deposition of elements such as Ca and P increased, and exhibit a chemistry similar to brushite. The Ca/P ratio increased gradually, approaching 1.2 after 12 days of immersion in solution. FTIR analyses indicated an amorphous/finely crystalline Ca-P layer after immersion in  $\alpha$ -MEM solution. In summary, an amorphous/finely crystalline Ca-P layer, having a chemistry similar to brushite was observed on all immersed samples.

**BI-MoP9 SIMS Characterization of Adsorbed Protein Films.** B. Hagenhoff, A. Benninghoven, Univ. Munster, Munster, FRG and D. G. Castner, B. D. Ratner, Univ. of Washington, Seattle, WA.

One of the first events that occurs when a material is placed in the biological environment is the adsorption of proteins. The structure of the adsorbed protein film can have a significant effect on further biological events (e.g., cell attachment) and the biocompatibility of the material. This study uses ToF SIMS and XPS to investigate the structure of albumin and fibrinogen films adsorbed from buffer onto PTFE and Ti substrates. Protein concentrations from 0.0005 to 0.5 mg/ml were exposed to the substrates for 2 hrs, then the samples were rinsed and dried. Characteristic secondary ion fragments from the

constituent amino acids (glycine, alanine, serine, proline, valine, cysteine, leucine, tyrosine, etc.) of the proteins were detected by SIMS. On the PTFE samples, both protein and PTFE fragments were detected at all protein concentrations studied. Since the thickness of the protein molecules is larger than the SIMS sampling depth of  $\sim 20$  Å, this indicates that PTFE surface is not fully covered by protein, in agreement with previous XPS studies. The intensities of the amino acid fragments correlated directly with the amount of N detected by XPS, and therefore the amount of protein present. The intensity of these ions did vary as a function of the protein, substrate, and protein concentration. These differences indicate that SIMS intensities of the constituent amino acid fragments can be used to identify both the type and conformation of adsorbed proteins. This will require correlating SIMS intensities to biochemical measurements of protein conformation.

**BI-MoP10 Extraction of Quantitative Surface Information from Static SIMS Using Partial Least Squares.** B. D. Ratner, V. H. Pérez-Luna and P. Favia, Department of Chemical Engineering, University of Washington, Seattle, WA 98195.

Plasma deposited films (PDFs) of fluorinated precursors exhibit low thrombogenicity which correlates with the high retention of the proteins adsorbed on them. This high retention has been ascribed to the presence of CF<sub>3</sub> groups at their surface, which promotes strong hydrophobic interactions between substrate and adsorbed proteins. Because of the complex surface chemistry of PDFs, other groups may also be implicated in the high protein retention observed. To ascertain the role of other functional groups in protein adsorption and retention, a set of fluorinated substrates were prepared by plasma deposition of C<sub>2</sub>F<sub>6</sub>/H<sub>2</sub> and C<sub>2</sub>F<sub>6</sub>/CH<sub>4</sub> mixtures. Surface characterization of these substrates was performed by ESCA (elemental composition and C<sub>1s</sub> spectra), static SIMS (positive and negative ions in the range of  $m/z = 0-300$ ) and wettability measurements. <sup>125</sup>I-Fibrinogen (Fb) was adsorbed from a 1% baboon plasma solution and the adsorbed Fb was eluted with a 1% sodium dodecyl sulfate solution. The percentage of the initially adsorbed Fb remaining on the surface after the elution step is referred to as the retention. Fb adsorption and surface properties were correlated by using partial least squares (PLS) regression. Preliminary results show that wettability ( $\cos \theta$ ), CF and C-CF<sub>n</sub> groups correlate positively with the amounts of Fb adsorbed. F/C ratio, CF<sub>3</sub>, CF<sub>2</sub> and CH<sub>x</sub> groups correlated negatively with the amounts of Fb adsorbed. F/C ratio, CF and CF<sub>3</sub> groups correlated positively with retention. C-CF<sub>n</sub> and CH<sub>x</sub> groups correlated negatively with retention. In addition, several SIMS peaks were also identified that correlated with the retention or the amounts of adsorbed Fb, specifically, certain sulfur contaminants were found to have a significant effect in protein adsorption even at trace levels. This work illustrates the application of multivariate calibration methods to build quantitative models and the extraction of qualitative information from them.

**BI-MoP11 Sub-Angstrom Movements of Biological Specimens Detected by Microwaves.** P. Gizdulich, G. Aschero, F. Mango<sup>†</sup>, Fisica Medica, Dpt. Fisiopatologia Clinica, I-50134 Firenze <sup>†</sup>Laboratorio di Fisica, Scuola Normale Superiore, I-56126 Pisa.

Bones are considered piezoelectric, but inverse effect has not been properly checked yet, because of the predicted elongation,  $\ll 1$  Å when 100V are applied to the sample.

We used two resonant microwave cavities. One acts as a reference. The length of the other is controlled by the deformation of a bone sample, when a square-wave voltage is applied. A klystron provides a periodic sweep in frequency. The resonance peaks from the two cavities are electronically compared. This results in a measure of displacements, after averaging over 300 ÷ 400 cycles.

Such a device measures displacements down to 0.05 Å. When no averaging procedure is used, the system is still capable to detect 50 Å displacements. Reproducibility is 10% and improvements are shown to be achievable. The output is a linear function of displacements. Measurements up to 1 ÷ 10  $\mu$ m are possible in a single run. We could therefore measure at the same time both the "piezoelectric" tensor's coefficients and the thermal capacity of the bone sample.

In conclusion, our device is suitable to measure displacements on a sub-Angstrom scale. The detection is linear over a wide range, while other methods are known to be strongly nonlinear. No similar microwave device is at present commercially available.

Our numerical results support doubts on the true piezoelectric nature of the electromechanical effect in bones, and on some procedures currently used in estimating bones' piezoelectricity. This will be of help in the search of a satisfactory model for bone growth and remodelling.



**BI-MoP12 Interactions of Cells and Proteins with Self-Assembled Monolayers (SAMs),** K. E. Foster, J. J. Hickman, K. E. Foster, D. A. Stenger<sup>1</sup>, A. E. Shaffner<sup>2</sup>, and J. L. Barker<sup>2</sup>; Science Applications International Corporation, McLean, VA 22102; <sup>1</sup>Center for Bio/Molecular Science and Engineering, Naval Research Laboratory, Washington, DC 20375; <sup>2</sup>Laboratory for Neurophysiology, BNP, DIR, NINDA, National Institutes of Health, Bethesda, MD 20892.

We have been using silane SAMs to modify surfaces and then studying how neurons interact with these modified surfaces. We have surveyed over 20 SAMs with two different cell types, rat spinal cord neurons and hippocampal neurons, and with different growth media. The growth media and cell preparation has also been varied in certain experiments. We find that the protein adsorption during cell culture is variable on different types of surfaces and has profound effects on neuronal survivability and viability. We have characterized the surfaces before culture by X-ray photoelectron spectroscopy (XPS) and contact angle and after culture by XPS, contact angle and ellipsometry. We will report on some interesting correlations of cellular responses to initial surface characteristics.

**BI-MoP13 Aminoacid Adsorption on Polyfunctional SAMs of Alkylthiols,** K. Uvdal, S. V. Atrre\*, D. Allara\* and B. D. Ratner, University of Washington, Seattle, WA 98195, Penn State University\*, University Park, PA 16802.

Amino acid adsorption on alkylthiol monolayers is investigated by high resolution X-ray photoelectron spectroscopy (XPS). Alkylthiol, (HS(CH<sub>2</sub>)<sub>15</sub>X), monolayers with four different terminating groups are studied. The terminating groups are -CH<sub>3</sub>, -OH, -COOH and -COOCH<sub>3</sub>.

The properties of the alkyl monolayer modified gold surface is strongly correlated to the functionality of the terminating groups of the thiol monolayer. Glycine adsorption on to these alkylthiol monolayers is studied and the pH for the amino acid adsorption solution is varied as well as the adsorption time. Alkylthiol monolayers prior to adsorption are used as references to the alkylthiol monolayers immersed into glycine solution.

High resolution XPS spectra for alkylthiol monolayers immersed into glycine solution are presented. The amino acid adsorption on to the alkylthiol monolayers is detected in both the C1s and the N1s core level spectra. The peak position of the N1s peak indicates the type of surface interaction. The affinity for glycine on these alkylthiols is strongly dependent of the choice of the terminating groups.

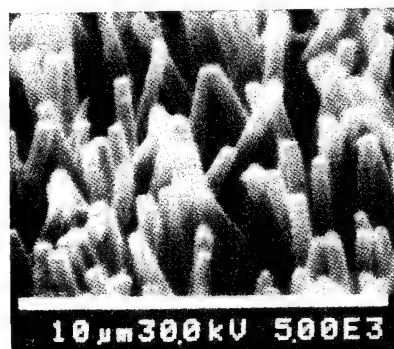
**BI-MoP14 One-Step Immobilization of Biomolecules and Application in Biosensors,** A. Hartmann, D. Bock, and S. Seeger.

Immobilization of biomolecules has advanced to become a major topic in biosensor research. So far, classical immobilization techniques have the disadvantage of the high number of preparative steps in combination with long incubation times. The Langmuir-Blodgett (LB-) technique allows a one-step transfer of biofilms from the air-water interface to the substrate. Therefore stable transferable monolayers of e.g. antibodies—incorporated in a photopolymerizable matrix—are prepared. Film stabilization can be achieved by irradiation of mixed monolayers of phthalocyaninato-polysiloxane-derivatives and the biomolecules. Photochemical crosslinking is monitored by the film area decrease with irradiation time and significantly enhanced density and stability of active immobilized antibodies. Using an evanescent wave biosensor, laser diode induced fluorescence emission of dye-linked antigens is observed so that antigens can be detected. The

presented method allows the preparation of films of high stability in only a few minutes. Furthermore, this new procedure can be highly parallelized and automatized.

**BI-MoP15 Polymeric Microcapsule Arrays—A Novel Method of Bioencapsulation,** Ranjani V. Parthasarathy, Charles R. Martin, Department of Chemistry, Colorado State University, Fort Collins, CO 80523.

We describe a novel method for encapsulating enzymes in conductive polymer microcapsules. Microporous polycarbonate filtration membranes were used as “templates” to prepare microcapsules of polypyrrole. The microcapsule arrays are prepared via a combination of electrochemical and chemical polymerizations. These polymeric microcapsules are hollow and typically have uniform diameters of 400 nm and lengths of 10  $\mu$ m. They are arranged in a high density array in which the individual capsules protrude from a surface like the bristles of a brush. Five enzymes—catalase, glucose oxidase, subtilisin, trypsin and alcohol dehydrogenase have been encapsulated using this method. Standard array methods were used to show that the encapsulated enzymes are catalytically active. The enzyme-loaded microcapsule arrays can function as enzymatic bioreactors in both aqueous solution and organic solvents. A scanning electron microscopic image (See attached figure) revealed the unique brush-like arrangement of these capsules. This general route to enzyme immobilization should find applications in both bioreactors and biosensors.



**BI-MoP16 Extreme Hydrophobicity Affecting the Adsorption of IgG on Methylated Surfaces,** Bengt Walivaara, Peter Warkentin, Jan Hemmingsson, and Pentti Tengvall, Linköping University, IFM, Laboratory of Applied Physics, S-58183 Linköping, Sweden.

Adsorption of IgG onto methylated surfaces in static protein solutions was studied using tapping mode AFM in air.

Incubation of DDS (dichloro dimethyl silane)-treated silicon surfaces in IgG (1–15  $\mu$ g/ml) was found to induce dendrite-like structures of IgG on the surfaces. These aggregates were highly dependent on the degree of methylation (surface energy) and on the concentration of IgG in solution. Surfaces were required to have water contact angles above 91° in order to induce dendrite formation. Similar patterns were also observed on SH(CH<sub>2</sub>)<sub>15</sub>CH<sub>3</sub> modified gold surfaces (water contact angle = 100°) after incubation in IgG suggesting the outermost chemical properties were responsible for the behaviour.

## SURFACE SCIENCE

Room A205 - Session SS1-TuM

### Nucleation and Growth: Homoepitaxy

Moderator: M. E. Kordes, Ohio University.

8:20 am **SS1-TuM1 Dynamics of the Si(100) Surface**, *Chris Pearson, Rob Curtis, Xin Shi and Eric Ganz*, Department of Physics, University of Minnesota, Minneapolis, MN 55455.

We have used a hot STM to create movies of the Si (100)-2 × 1 reconstructed surface at sample temperatures between 200°C and 300°C with a 30 second frame rate. By measuring the attachment and detachment rates of groups of Si atoms we determine the activation and binding energies for the predominant processes on this time scale for various step and kink configurations. In addition to attachment or detachment of pairs of dimers<sup>1</sup>, we also observe blocks of multiple pairs of dimers moving in concert.

<sup>1</sup>N. Kitamura, B. S. Swartzentruber, M. G. Lagally, and M. B. Webb, *Phys. Rev. B* **48**, 5704 (1993).

Supported by NSF grant #DMR-9222493.

8:40 am **SS1-TuM2 STM Studies of Vacancy-Step Interaction Kinetics During Low-Energy Ion Bombardment of the Si(001) Surface\***, *B. S. Swartzentruber<sup>1</sup>, C. M. Matzke<sup>2</sup>, J. E. Houston<sup>1</sup>, and D. L. Kendal<sup>2</sup>*, <sup>1</sup>Sandia National Laboratories, and <sup>2</sup>University of New Mexico, Albuquerque, NM.

Low-energy ion bombardment has been suggested as a nonthermal means for tailoring surface morphology during thin-film growth. In this work, we explore a specific aspect of such a scheme by studying the kinetics of Si(001) surfaces sputtered by low-energy Xe ions (~300 eV) at substrate temperatures between 350 and 525°C. Just as adatoms preferentially stick to the ends of substrate dimer rows on Si(001), vacancies are found to preferentially annihilate at the ends of dimer rows. Because the surface is comprised of two types of steps, those running parallel (SA) or perpendicular (SB) to the upper terrace dimer rows, ion bombardment tends to retract the SB step from its equilibrium position midway between neighboring SA steps, leading to a domain asymmetry. The resulting step morphology is determined by the competition between vacancy annihilation events which retract the SB steps and the intrinsic rate at which the SB steps return to their equilibrium position. At temperatures where the vacancy diffusion is large enough so that no vacancy islands are formed on the terraces (step flow), the surface reaches a steady state asymmetry as the competing kinetic contributions balance. At lower temperatures vacancy islands form on the terraces leading to a layer-by-layer removal. We analyze the overall recovery kinetics of the surface with LEED and investigate the detailed surface morphologies as a function of ion dose and substrate temperature with STM. The recovery of the two-domain surface upon annealing is hindered by the presence of anti-phase domain boundaries which form during ion bombardment as vacancy islands coarsen. We discuss these results in terms of their possible implications on evolving morphologies during surface preparation by growth and ion bombardment.

\*This work performed at Sandia National Laboratories is supported by the U.S. Department of Energy under contract DE-AC04-94AL85000.

9:00 am **SS1-TuM3 Stress-Induced Step Bunching on Vicinal Strained Layers\***, *Zhenyu Zhang<sup>(1)</sup>, Jerry D. Tersoff<sup>(2)</sup>, Yew H. Phang<sup>(1)</sup>, and Max G. Lagally<sup>(1)</sup>*, <sup>(1)</sup>University of Wisconsin-Madison, Madison, WI 53706, <sup>(2)</sup>IBM T. J. Watson Research Center, Yorktown Heights, NY 10598.

Recently there has been great interest in stress-induced "roughening" of strained epitaxial films. However, theoretical treatments to date have focused on continuum models. Including discrete steps in the analysis leads to a qualitatively different picture of the morphological instability. We show that, for a vicinal surface, elastic relaxation around each step leads to a long-ranged attractive interaction between steps. Stress-induced roughening then initiates as step bunching. As in the continuum case, there is a true instability, but now only in the direction of the vicinality. Also, the length scale and kinetics of rough-

ening are controlled by completely different factors than in the continuum model. We perform numerical simulations of the step bunching, within an elastic model, and compare the results with the anisotropic roughening observed in Ge layers grown on vicinal Si(001) and Ge/Si multilayer films.

\*Supported by NSF, Materials Research Group Grant (#DMR91-21074), and by NSF, Electronic Materials Program Grant (#DMR92-01856).

9:20 am **SS1-TuM4 Spatial Correlations in Surface Roughness During Low Temperature Epitaxial Growth of Ge(001)**, *Joseph E. Van Nostrand, S. Jay Chey, David G. Cahill, M.-A. Hasan, J. E. Greene*, University of Illinois, Urbana, IL.

For many materials, molecular beam epitaxy (MBE) can be used to grow single crystal layers at temperatures below any other technique. To better understand the limits to the capabilities of MBE growth, we measure the surface morphology of Ge(001) grown at low temperatures. After growing a Ge buffer layer on a Ge(001) substrate, we deposit epitaxial layers over a wide range of thicknesses, 5 to 1000 Å, and temperatures, 60 to 275°C; the samples are transferred to a scanning tunneling microscope without leaving the ultrahigh vacuum environment. The surface morphology shows spatial correlations of the surface roughness in the plane of the film. The length scale of the correlations increases from less than 100 Å at 60°C to approximately 1000 Å at 275°C. The surface roughness becomes more pronounced as the film thickness approaches the critical thickness for the transition from crystalline to amorphous growth.

9:40 am **SS1-TuM5 Kinetic Smoothing of Vicinal Si(111)\***, *H.-C. Kan, R. J. Phaneuf and E. D. Williams*, Department of Physics, University of Maryland, College Park, MD 20742-4111 U.S.A.

Processes such as growth can push surface structure far from equilibrium. One example of this is the formation of kinetically stabilized step structures, which can often remain after growth as metastable structures with long lifetimes for decay to equilibrium. We report on an unusual example of such a process, the formation of a metastable uniformly stepped surface from an equilibrium faceted surface during homo-epitaxy. The initial equilibrium structure is the faceted [1] vicinal Si(111) surface misoriented by 6° toward [211]. We have used low energy electron diffraction (LEED) to study the evolution of the step structure *in situ* as a function of Si flux and sample temperature. We find that growth reverses the thermodynamically induced faceting at sufficiently high flux. This smoothing can be interpreted as due to an anisotropic step velocity function such as the Schwoebel effect [2, 3]. The transition to a uniform step train requires growth of hundreds of layers, suggesting the anisotropy is weak. We compare the time dependent diffraction profiles with the results of models of growth on a faceted surface, including the Schwoebel effect, and generalized models [4].

\*Work supported by DOD.

1. R. J. Phaneuf, E. D. Williams and N. C. Bartelt, *Phys. Rev. B* **38**, 1984 (1988).

2. R. L. Schwoebel and E. J. Shipsey, *J. Appl. Phys.* **37**, 3682 (1966).

3. J. Villain, *J. de Phys.* **II**, 19 (1991).

4. D. Kandel and J. D. Weeks, *Phys. Rev. B*, in press (1994).

10:00 am **SS1-TuM6 Fractal Growth on Metal Surfaces\***, *Zhenyu Zhang, Xun Chen, and Max G. Lagally*, University of Wisconsin-Madison, Madison, WI 53706.

In recent scanning tunneling microscopy (STM) studies of metal-on-metal growth at submonolayer coverages, fractal-like islands have frequently been observed on substrates of triangular or hexagonal geometry, but to date only compact islands have been observed on substrates with square geometry. To understand this striking phenomenon, we have investigated theoretically the formation mechanisms of fractal islands by taking specific atomic-bonding geometry into proper consideration [1]. We found that three growth regimes can be defined as the surface temperature is increased: the standard diffusion limited aggregation regime; the *extended* fractal regime; and the compact regime. The extended fractal regime is characterized by significant local relaxation by edge diffusion. The temperature range defining this regime is relatively wide for triangular lattices, but vanishingly



small for square lattices, explaining why fractal growth has been observed only on triangular lattices. By comparing experimental and theoretical results, we also give estimates of the activation barriers against edge diffusion for several systems.

[1] Z. Y. Zhang, X. Chen, and M. G. Lagally, Phys. Rev. Lett. (submitted).

\*Supported by NSF, Materials Research Group Grant (#DMR91-21074), and by NSF, Solid State Chemistry Grant (#DMR93-04912).

10:20 am **SS1-TuM7 Computer Simulations of Diffusion and Island Growth**, *G. Vidali<sup>a</sup>, O. Biham<sup>a,b</sup>, M. Karim<sup>c</sup>, R. Kennett-Fox<sup>a</sup>, and H. Zeng<sup>a</sup>*, a. Physics Department, Syracuse University; b. Hebrew University; c. Indiana University of Pennsylvania.

Motivated by recent experiments of epitaxial growth<sup>1</sup>, we have performed computer simulations of submonolayer island growth of Cu on Cu(001) using realistic deposition rates and energy barriers. The key and novel aspect of our work is that in calculating the hopping rate of an adatom we take into account the environment in which it moves. We have calculated the energy barriers using the Embedded Atom Method<sup>2</sup>. We find that island density during deposition quickly saturates over a broad range of coverage for realistic deposition rates. Islands are rather compact. These results are in agreement with recent island growth experiments of Pb on Cu(001)<sup>1a</sup> and Ni on Ni(001)<sup>1b</sup>. We then introduce a model that with only four parameters which realistically describes island growth on (001) surface of metallic substrates. We will show that such model differs in a very important aspect from the "bond-counting model" and that it gives a qualitatively correct description of island growth on metal surfaces.

<sup>1</sup>Wei Li, G. Vidali, and O. Biham, Phys. Rev. B48, 8336 (1993); E. Kopatzki, J. Schroder, C. Gunther and R. J. Behm, Surf. Sci. 284, 154 (1993). <sup>2</sup>G. T. Barkema, O. Biham, M. Breeman, D. O. Boerma and G. Vidali, Surf. Sci. Lett. 306, L569 (1994). \*Supported by NSF grant DMR 9119735.

10:40 am **SS1-TuM8 On the Interlayer Atomic Diffusion Mechanism in Metal-on-Metal Epitaxy**, *Yinggang Li and Andrew E. DePristo*, Chemistry Department and Ames Laboratory, USDOE, Iowa State University, Ames, IA 50011.

From an atomistic point of view, low temperature metal-on-metal growth (on both fcc(111) and (100) surfaces) is not well understood. To help elucidate the elementary processes in growth, we have determined the potential energy barriers (PEB) for interlayer mass transport by performing minimum-energy-path calculations. The systems studied were transition metals with filled or nearly filled d-bands while the interactions were described by the Corrected Effective Medium theory. The dependence of the PEB on the size and shape of the 2D islands on the surfaces was investigated. As a function of the size, the PEB showed non-monotonic behaviors that differed considerably from metal to metal. We will explain the implications of these results for experimental observations (e.g., reentrant and surfactant-induced layer-by-layer growth) and predict that the reentrant growth could be observed for the Pd/Pd(111) system. Incorporation of small clusters (dimers and trimers) into the islands at the island edges will also be discussed.

\*Work supported by NSF grant CHE-9224884.

11:00 am **SS1-TuM9 Surface Morphology Changes Upon Laser Heating of Pt(111)**, *Josef Frohn, Jane Reynolds and Thomas Engel*, Department of Chemistry, BG-10, University of Washington, Seattle, WA 98195.

The surface morphology of Pt(111) has been studied as a function of irradiation energy produced by a pulsed laser at 1064 nm. Substantial changes from the ideal crystal structure are observed at temperatures greater than approximately half the melting point. These changes are due to the nucleation of dislocations associated with the large temperature gradient normal to the surface. Using scanning tunneling microscopy, we observe dislocations with near atomic resolution. Stress caused by the normal temperature gradient is relieved by slip parallel to the (111) planes inclined to the surface. Increasing the stress by increasing the maximum temperature to which the surface is heated increases the density of dislocations rather than the average slip along a dislocation. For maximum surface temperatures below 1000 K, atomic diffusion along steps does not occur during the 5 nanosecond time in which the surface is heated. For  $T_{\max}$  above 1100 K, this diffusion

becomes rapid. For  $T_{\max}$  above values leading to surface damage in the form of slip bands which are visible by light microscopy, the surface is highly disordered.

11:20 am **SS1-TuM10 Configurational Stability and Surface Diffusion of Rhodium Clusters on Rh(100)**, *G. L. Kellogg*, Sandia National Labs., Albuquerque, NM 87185-0344.

The properties of small clusters adsorbed on single-crystal terraces play a key role in defining the nature of epitaxial growth processes. I have used field ion microscopy to examine the stability and mobility of Rh clusters containing two to twelve atoms adsorbed on the Rh(100) plane. In contrast to Pt on Rh(100), where stable chain configurations are observed for clusters up to pentamers, all Rh clusters larger than trimers are stable as two-dimensional islands. The activation energy of surface diffusion exhibits an interesting, oscillatory behavior as a function of cluster size. Compact geometric structures (squares and rectangles) have a consistently higher activation energy than structures with extra atoms at the periphery. For example, a 9-atom cluster (square configuration) is immobile up to 440 K, whereas a 10-atom cluster becomes mobile at 380 K. Apparently, the periphery atoms destabilize the cluster leading to a lower diffusion barrier. Possible mechanisms for the diffusion process and the relationship of surface diffusion to cluster stabilities are discussed.

\*Work supported by the U.S. Department of Energy under contract DE-AC04-94AL85000.

11:40 am **SS1-TuM11 Scaling Properties of Fe Growth on Fe(001) Whiskers**, *Joseph A. Stroscio and D. T. Pierce*, National Institute of Standards and Technology, Gaithersburg, MD 20899.

Central to recent growth theories describing molecular beam epitaxy has been the scaling of various distributions describing the evolution of film growth. Our work on the homoepitaxial growth of Fe on Fe(001) whiskers elucidates many of scaling properties of island distributions predicted in the early stages of growth, but shows characteristic length scales in subsequent thin film growth not found in conventional statistical growth theories. In this presentation, we describe the evolution of Fe film growth from the submonolayer regime through thin films using scanning tunneling microscopy (STM) and reflection-high-energy-electron-diffraction (RHEED) measurements. Scaling of island size and separation distributions as a function of the ratio of surface diffusion to deposition rate is observed. The measured scaling functions for the island size distributions indicate a critical nucleus size of 1 atom for growth at 300°K, and show evidence of an increase in critical size to ~3 atoms for growth above 550°K. In the case of thin film growth, we observe a characteristic length,  $\xi$ , in real space images and height correlation functions obtained from STM measurements and also in the splitting of RHEED diffraction features. For growth at room temperature, this length scale is initially ~5 nm, set by the average island separation at submonolayer coverage, and is observed to increase slowly with increasing film thickness, for example,  $\xi \sim 10$  nm for a 600 layer thick film.

\*This work is supported in part by the Office of Naval Research.

## SURFACE SCIENCE

### Room A201 - Session SS2-TuM

#### Non-Thermal Surface Dynamics

**Moderator:** J. P. Cowin, Pacific Northwest Laboratories.

8:20 am **SS2-TuM1 Femtosecond Time-Resolved Desorption Dynamics: Vibrational Effects in the Electronically Driven Desorption of O<sub>2</sub> from Pd(111)**, *J. A. Misewich, T. F. Heinz, A. Kalamarides, and P. Weigand*, IBM Research Division, T. J. Watson Research Center, Yorktown Heights, NY 10598-0218.

Recently, several investigators have applied femtosecond laser techniques to examine the dynamics of desorption at a metal surface in the time domain<sup>1,2</sup>. In these papers it has been demonstrated that femtosecond laser light can result in highly efficient desorption. This effect has been associated with a novel mechanism for activation occurring at the high substrate electronic temperatures induced by the

ultrashort laser pulses. In this talk we present time-resolved correlation results for  $O_2/Pd(111)$  in which the desorption yield is monitored as a function of delay time between a pair of strong femtosecond pulses<sup>3</sup>. This technique provides information on the lifetime of the excitation responsible for desorption. The correlation results are dominated by a subpicosecond feature, consistent with a mechanism of strong coupling of the adsorbate to the substrate electronic excitation. However, a weaker feature lasting  $\geq 10$  ps is also observed. The presence of such a long-time feature is interpreted as an enhancement of the electronic mechanism through vibrational excitation of the adsorbate resulting from the first laser pulse. A detailed analysis of the data in terms of models for the vibrational excitation and the effect of such excitation on electronic desorption mechanisms will be presented.

<sup>1</sup>F. Budde, T. F. Heinz, M. M. T. Loy, J. A. Misewich, F. de Rougemont, and H. Zacharias, *Phys. Rev. Lett.* **66**, 3044 (1991).

<sup>2</sup>J. A. Prybyla, H. W. K. Tom, and G. D. Aumiller, *Phys. Rev. Lett.* **68**, 503 (1992).

<sup>3</sup>J. A. Misewich, A. Kalamarides, T. F. Heinz, U. Höfer, and M. M. T. Loy, *J. Chem. Phys.* **100** 736 (1994).

8:40 am **SS2-TuM2 Dynamics of Surface Photochemistry: CO + O<sub>2</sub> on Pt(111)**, *Darryl G. Busch and W. Ho*, Department of Physics, Cornell University, Ithaca, NY 14853.

Photo-induced desorption of CO<sub>2</sub> and O<sub>2</sub> from CO and O<sub>2</sub> coadsorbed on Pt(111), and O<sub>2</sub> from O<sub>2</sub> on Pt(111) at 80 K, has been studied using nanosecond and femtosecond laser pulses, and time-of-flight detection with a quadrupole mass spectrometer. The CO<sub>2</sub> TOF distribution obtained with 10 ns, 355 nm pulses can be fit to a modified Maxwell-Boltzmann with mean kinetic energy 2800 K and reduced width 0.89. The O<sub>2</sub> TOF distributions are bimodal Maxwell-Boltzmanns with temperatures of 600 K and 85 K for O<sub>2</sub> alone, and 950 K and 90 K for the coadsorbed system. The low energy O<sub>2</sub> peaks vary with fluence and may be attributed to conversion to physisorbed O<sub>2</sub> followed by thermal desorption. Desorption of O<sub>2</sub> from O<sub>2</sub>/Pt(111) using femtosecond pulses produces a nearly Maxwell-Boltzmann TOF distribution with temperature 1400 K, which corresponds to the calculated peak electronic temperature for the fluence used. This gives evidence, along with the nonlinear dependence of yield on fluence and two pulse correlation results, that desorption by femtosecond pulses is mediated through coupling to the hot, nonequilibrium electronic distribution which results from an intense, ultra-short laser pulse.

9:00 am **SS2-TuM3 Reactions of Hyperthermal Energy (5-100 eV), Molecular Ions with Metal and Oxide Surfaces**, *D. C. Jacobs*, Department of Chemistry and Biochemistry, University of Notre Dame, Notre Dame, IN 46556.

Often, reactions performed under thermal conditions only access a restricted range of product channels. However, hyperthermal energy collisions activate a variety of chemical processes which are important to ion etching applications, low-earth orbit spacecraft environments, and mass-spectrometric instrumentation. Studying the dynamics of hyperthermal molecular reactions on metal and oxide surfaces provides detailed mechanistic information for this important class of systems.

Our lab has conducted experiments which probe novel reaction mechanisms involving hyperthermal energy molecules with Ag, O/Ag, and SiO<sub>x</sub> surfaces. Multiphoton laser ionization is employed to prepare molecular ions in a particular quantum state, i.e., with a controlled amount of electronic, vibrational, and rotational energies, as well as a restricted distribution of reagent orientations. These ions are accelerated to a collision energy ranging from 5-100 eV and strike a well-characterized surface under UHV conditions. Dissociation, electron transfer, and abstraction reactions are studied with attention to the specific roles that energetic and steric effects play in determining the outcome of a reactive collision.

INVITED

9:40 am **SS2-TuM5 Low-Energy Electron-Stimulated Production of Molecular Hydrogen from Amorphous Water Ice**, *Greg A. Kimmel, Russell G. Tonkyn and Thomas M. Orlando*, Molecular Science Research Center, Pacific Northwest Laboratory\*, Richland, WA USA 99352.

Low-energy electron-stimulated processes on or within molecular multilayers are important in many conventional areas of physics, chemistry, and radiation biology. We have investigated the stimulated production of D<sub>2</sub> during low energy (5-150 eV) electron-beam irradiation of D<sub>2</sub>O amorphous ice using quadrupole mass spectrometry and resonance-enhanced multiphoton ionization spectroscopy. The D<sub>2</sub> production threshold is 6.3 eV  $\pm$  0.5 eV, well below the first excited state

of condensed water at 7.3 eV. We assign the 6.3 eV threshold to D<sup>-</sup> + D<sub>2</sub>O  $\rightarrow$  D<sub>2</sub> + OD<sup>-</sup> condensed phase (primarily surface) reactions that are initiated by dissociative attachment. The D<sub>2</sub> yield increases gradually until another threshold is reached at  $\sim 17$  eV and continues to increase at higher energies. We associate the yield above  $\sim 11$  eV mainly to the recombination of D<sub>2</sub>O<sup>+</sup>, or D<sub>3</sub>O<sup>+</sup>, with quasifree or trapped electrons. Exciton dissociation and ion-electron recombination processes can produce reactive energetic D atom fragments or D<sub>2</sub> directly via molecular elimination. The importance of D<sup>+</sup> interactions increases at  $\sim 17$  eV (dipolar threshold) and at energies  $\geq 21$  eV where multi-hole and multi-electron final states are energetically accessible. The state distribution of the D<sub>2</sub> desorbates produced by 100 eV electrons is highly non-thermal. Although the D<sub>2</sub> desorbates have very little translational energy ( $\sim 20$  meV), they are vibrationally ( $v = 0, 1, 2$ ) and rotationally ( $j = 0-10$ ) excited. The internal state distributions are consistent with non-thermal reactive scattering and/or dissociative recombination events. This study of the neutral reaction products suggest that several types of electronic excitations are important in understanding non-thermal reactions in molecular ices.

\*PNL is operated for the U.S. Department of Energy by Battelle Memorial Institute under contract DE-AC06-76RLO 1830.

10:00 am **SS2-TuM6 Models for Positive Ion Emission by Photon Excitation at the (001) Surface of MgO**, *A. Gibson, J. P. LaFemina*, Molecular Science Research Center, Pacific Northwest Laboratories, Richland, WA, and *J. T. Dickinson*, Department of Physics, Washington State University, Pullman, WA.

Desorption of positive ions, principally Mg<sup>+</sup>, from MgO surfaces during sub-bandgap 248 nm irradiation has been shown to be accompanied by photoelectron emission. The ion emission is highly collimated along the surface normal, and exhibits a complicated energy dependence. Anion vacancy defects (F centers) in the surface region are necessary for this emission. To understand the desorption process, the relative energetics of Mg emission from different defect sites at the (001) surface have been computed using density functional theory, and in the local density approximation. In particular, a comparison is made between two models which describe cation emission from the (001) surface. The first model, which has also been used to explain Na ion emission from NaCl (001), involves the emission of a cation from a site adjacent to a surface F center, thereby forming a surface P center. The second model involves the emission of the cation from its initial configuration adsorbed atop the surface F center. In both cases the initial and final products are considered as a function of their charge state, and compared to the experimentally observed ion kinetic energy and angular distributions.

Pacific Northwest Laboratories are operated for the U.S. Department of Energy by Battelle Memorial Institute under contract DE-AC06-76RLO 1830. J. T. D. acknowledges partial support from the D.O.E., B.E.S. under contract DE-SG06-92ER14252.

10:20 am **SS2-TuM7 Non-Thermal Chemistry of Chemisorbed Ammonia: Dissociative Excitation and Dynamics\***, *A. R. Burns, E. B. Stechel, and D. R. Jennison*, Sandia National Laboratories, MS 0344, Albuquerque, New Mexico 87185-0344.

Non-thermal or "stimulated" surface chemistry has been of great interest over the years, both in fundamental surface science and in its potential for selective area processing. Recent activity includes the stimulated chemistry of adsorbed ammonia, which have applications in substrate nitridation. We have studied experimentally and theoretically the electronic excitations and the subsequent dynamics for both *desorption* and *dissociation* of chemisorbed NH<sub>3</sub> and ND<sub>3</sub> on Pt(111). We have shown that the two processes are due to *distinct* adsorbate electronic excitations that have identifiable thresholds and naturally produce very different dynamics.

In this presentation we discuss the ammonia dissociation channel, where gas-phase H and D products are detected by 2 + 1 resonance-enhanced multiphoton ionization. Whereas desorption correlates with the 8 eV excitation of the lone-pair 3a<sub>1</sub> electrons, dissociation correlates with the deeper 14 eV excitation of the 1e N-H bonding electrons. The H/D yield ratio *varies with translational energy* in the range (0.01-0.5 eV). It increases from near unity at energies  $< 0.05$  eV to approximately 3 at 0.5 eV. This effect can be qualitatively understood in terms of simple one-dimensional potentials, where the lighter H atoms acquire more kinetic energy during the excited state lifetime and thus leave the surface with greater probability. This is supported by calculations. The relatively low H/D ratio implies that the lifetime

of the dissociative excitation is relatively long, consistent with the high dissociation yields noted in previous studies.

\*This work performed at Sandia National Laboratories is supported by the U.S. Department of Energy under contract DE-AC04-94AL8500.

10:40 am **SS2-TuM8 Electron Stimulated Desorption of Hydrogen from Si(100):H Surfaces by STM**, T.-C. Shen, C. Wang, G. Abeln, J. W. Lyding and J. R. Tucker, University of Illinois at Urbana-Champaign, Urbana, IL 61801.

The hydrogen desorption mechanism from Si(100) surface has been under intensive investigation recently. Most of the previous studies were performed by thermal desorption. We will present the results of hydrogen desorption induced by the electron beam from a STM probe. The STM probe can deliver a very high current density (about  $10^5$  A/cm<sup>2</sup>) locally. Combining this with the atomic scale resolution provides a unique tool to study the electron stimulated desorption (ESD) process. Hydrogen passivated Si(100)-2 × 1 and 3 × 1 surfaces were prepared in an UHV chamber. Atomic scale desorption was achieved by bombarding the surface with electrons at STM probe biases as small as negative 4 V relative to the sample. Our observation agrees with previous reports about the recombinative nature of the hydrogen desorption, however, we find in some cases that the newly formed clean Si atoms can re-dimerize themselves with a shift relative to the original dimer rows. The existence of these shifted dimers suggests a possible scenario in which the  $\sigma$  bonds between Si atoms are broken during desorption. We have also obtained electron-hydrogen conversion efficiency as a function of electron kinetic energy. The relation of desorption area to electron dosage, and threshold voltage will be discussed. These ESD results could be complementary to those obtained from thermal desorption and shed some light on the much disputed hydrogen recombinative desorption mechanism from this surface.

Supported by the Office of Naval Research URI:N00014-92-J-1519.

11:00 am **SS2-TuM9 TOF and Internal State Distribution of Photo-desorbed Species from N<sub>2</sub>O/Pt(111) by 193 nm Light**, D. P. Masson, E. J. Lanzendorf and A. C. Kummel, Department of Chemistry, University of California at San Diego, La Jolla, CA 92093.

Polarized ultraviolet light from an excimer laser (193 nm) was used to photodesorb and photodissociate N<sub>2</sub>O adsorbed on a cold Pt(111) surface. The desorbed species and their time-of-flight (TOF) were monitored by resonantly enhanced Multi Photon Ionization (MPI) spectroscopy. We have identified three major channels. The photo-desorption of molecular N<sub>2</sub> was observed only in the slowest channel where N<sub>2</sub> produced by fragmenting the N<sub>2</sub>O is thermalized on the surface before desorbing. Evidence for this behavior includes both a low (~90 K) rotational and translational temperature of the N<sub>2</sub> fragments as well as a lack of correlation between rotational and translational energy. In the next fastest channel, only ground electronic state N<sub>2</sub>O (exit kinetic energy;  $0.4 \pm 0.1$  eV) was seen to photodesorb. The analysis of the N<sub>2</sub>O photofragments O(<sup>1</sup>D) and N<sub>2</sub>(J) produced by the probe laser suggests a substantial degree of rotational and vibrational excitation exists upon leaving the surface. The angular distribution of this N<sub>2</sub>O channel is also more peaked toward the surface normal than the angular distribution of the thermal N<sub>2</sub>. The desorption yield of the above two channels decreases when the polarization of the desorption laser is changed from p-polarized to s-polarized in agreement with hot carrier mediated chemistry. In the fastest channel, we have detected O(<sup>3</sup>P) which, we believe, originates predominantly from the probe laser dissociation of electronically excited N<sub>2</sub>O(<sup>3</sup>Π or <sup>3</sup>Σ) with an exit kinetic energy of  $0.90 \pm 0.15$  eV. This may be the first experimental evidence that electronically excited species photodesorb from a metal surface.

11:20 am **SS2-TuM10 UV Irradiation of Physisorbed Overlayers: CD<sub>3</sub>I/MgO(100): Probing Photofragmentation Dynamics, Adsorbate Orientation and Overlayer Morphology**, D. Howard Fairbrother, K. A. Briggman, P. C. Stair and Eric Weitz, Department of Chemistry, Northwestern University, Evanston, Illinois 60208.

The 257 nm photodissociation dynamics of CD<sub>3</sub>I multilayers adsorbed on an MgO(100) substrate have been studied using resonantly enhanced multiphoton ionization time-of-flight mass spectrometry (REMPI-TOFMS) to detect both CD<sub>3</sub> and I photofragments. The photofragments result from direct adsorbate photolysis of methyl iodide chromophores present in the near surface region, leading to the production of both neutral methyl and iodine fragments. Data on the morphology of the evolving film was obtained by monitoring the

variation in photofragment intensity with adsorbate coverage. Methyl produced with velocities as fast as those found in gas-phase dissociation were observed with a narrow angular distribution ( $\approx \cos^{20}\theta$ ) consistent with a preferential orientation of the C-I bond along the surface normal. Collisionally slowed fragments, characterized by a temperature close to that of the overlayer, were also observed with a much broader dependence upon the angle of ejection ( $\approx \cos^{3.5}\theta$ ). Iodine fragments with velocities in excess of the gas-phase limit result from energy transfer with faster moving methyl fragments. A fraction of the iodine photofragments are trapped within the adlayers and give rise to photoinduced chemistry.

11:40 am **SS2-TuM11 Molecular Desorption of Methyl Halides from GaAs (110)**, P. H. Lu, P. J. Lasky, Q. Y. Yang, and R. M. Osgood, Jr., Columbia Radiation Laboratory, Columbia University, NY, NY 10027.

Temperature Programmed Desorption (TPD) has been used to study the molecular desorption of methyl halides from the GaAs (110) surface. The TPD spectra are strongly coverage dependent. For example, the peak position shifts from 155K to 125K for CH<sub>3</sub>Cl when the coverage is changed from 0.1 to 1 monolayer. A dipole-dipole interaction model has been used successfully to explain and analyze the TPD spectra. The fitting results for CH<sub>3</sub>Cl show that the effective dipole moment is 1.3D, the effective polarizability is  $3.0\text{\AA}^3$ , and the zero-coverage desorption energy is 40.0 KJ/mol. The gas phase dipole moment of CH<sub>3</sub>Cl is 1.86D. The decrease may be due to the fact that the molecules are inclined towards the surface, such that their dipole axes form an angle of 43° with the surface normal. The orientation of the molecules on the surface has been confirmed by NEXAFS and angular-resolved measurements of photodissociated methyl radicals. The angular distribution of thermally desorbed CH<sub>3</sub>Cl molecules, about  $(\cos\theta)^2$  for 0.5 monolayer coverage, has also been determined. The results show that even though the molecules are oriented at an angle on the surface, the thermally desorbed molecules are collected along the surface normal. Similar results are also obtained for both CH<sub>3</sub>Br and CH<sub>3</sub>I. We discuss the implications of these findings for the understanding of desorption, and likewise adsorption, dynamics of physisorbed molecules, particularly on strongly covalently bonded semiconductor surfaces. This work is supported by DOE.

## NANO 3/NANOMETER-SCALE SCIENCE AND TECHNOLOGY

Room A209 - Session NS1-TuM

### Nanostructured Materials

Moderator: D. Bonnell, University of Pennsylvania.

8:20 am **NS1-TuM1 Nanocluster Surface Science by LDA Theory**, D. R. Jennison<sup>a</sup>, Y. S. Li<sup>b</sup>, P. A. Schultz<sup>a</sup>, M. P. Sears<sup>a</sup>, T. Klitsner<sup>a</sup>, and P. Feibelman<sup>a</sup>, <sup>a</sup>Sandia National Laboratories\*, Albuquerque, NM 87185-0344; <sup>b</sup>Biosym Technologies Inc., San Diego, CA 92121-3752.

Using the local density approximation (LDA) and massively-parallel computing, we examine from first principles some structural and adsorbate properties of Cu, Ru, Pd, and Ag clusters with up to ~55 atoms, with a goal of uncovering basic principles. Our results include the following:

a) **Structure:** Preferred structures vary considerably. For example, we find that Ag<sub>13</sub> prefers the optet structure proposed by McAdon and Goddard for lithium (*J. Phys. Chem.* 91 (1987) 2607). Pd<sub>13</sub>, however, prefers the icosahedral structure over either fcc or the optet. This result supports the polyicosahedral structures proposed by Parks *et al.* (*JCP* 96 (1992) 8267) for clusters between icosahedral shell closings of 13 and 55 atoms. These trends are understood based on the locality of metal bonding.

b) **"Electrostatically" Bound Adsorbates:** Binding to a cluster may be quite different than to extended surfaces. For example, ammonia prefers an atop site on Pd<sub>13</sub>, a site shown experimentally *not* to be favored on extended Pd(111) (Burns, *et al.*, *PRL*, in press); in addition, NH<sub>3</sub> is bound almost 50% more strongly than on the extended surface. Furthermore, we observe very slow convergence to the preferred extended-surface site with increasing cluster size. The binding energy of ammonia is well-given by standard LDA theory, i.e., without a gradient correction.

c) *Covalently Bound Adsorbates*: Adsorbates with strong covalence, such as  $\text{CH}_3$ , bind at similar sites on finite clusters and extended surfaces. They are also well-described by standard LDA. However, adsorbates with weak covalence, such as NO, have a large error in adsorption energy without the gradient correction to LDA, while site preference, geometry, and vibrational frequencies are well-given without the gradient correction. For example, NO is found to prefer the hollow site on a 19-atom Pd cluster which mimics Pd(111), in agreement with recent experimental results (Materer, *et al.*, *Surf. Sci.* 303 (1994) 319).

\*Work supported by US DOE under Contract No. DE-AC04-94AL8500.

8:40 am **NS1-TuM2 Kinetics and Thermodynamics of Organic Nanocluster Formation**, P. V. Shibaev\*, K. Schaumburg\*\*, K. Brunfeldt\*\*\*; \*119899, Moscow State University, Physical Electronics Dept., Russia; \*\*CISM1, Fruebjergvej 3, 2100 Copenhagen, Denmark.

The theory of oriented growth of organic clusters and films during vacuum deposition is presented. Theory is based on the consideration of thermodynamic of the system and generalization of the kinetic rate equations to the spatially anisotropic rigid molecules. Molecules and clusters are considered to have two possible orientations of long molecular axis parallel (P) and normal (N) with respect to the surface substrate. Concentrations of clusters with definite structure are determined for the equilibrium conditions. Transformations of cluster structure are investigated in terms of transition state theory (TST). Applicability of this theory is discussed. Basing on the data obtained the set of kinetic equations for the P- and N-oriented clusters is derived. To estimate adsorption energies and diffusion coefficients the atom-atom potential calculations of interaction energies between some covalent substrates and linear molecules were performed.

The developed theory predicts concentrations of N- and P-clusters appeared on the substrate in different deposition conditions. It was found that for the fixed substrate temperature and molecular length there is a critical flux of molecules onto the substrate for which the rate of P-cluster formation becomes higher than for N-clusters. The higher the temperature the less is the critical flux of molecules. These results are in a good agreement with recently obtained experimental ones which are also intensively discussed.

9:00 am **NS1-TuM3 Nanostructured Solids as Interface-Determined Systems**, H.-E. Schaefer, Stuttgart University, Institut für Theoretische und Angewandte Physik, 70550 Stuttgart, Germany.

Nanostructured solids are characterized by ultrafine crystallites with a typical diameter of ca. 10 nm and therefore contain a high number density of structurally disordered interfaces which comprise a substantial fraction of the atoms. Due to the high number of these interfaces the properties of a nanostructured solid are profoundly modified compared to the chemically identical solid with a long-range periodic crystalline order. The structure of the interfaces depends on the technique of preparation as well as on the thermal relaxation and a wide variety of preparation routes as gas-phase condensation of crystallites and compaction, chemical synthesis, severe plastic deformation, crystallization from amorphous precursors etc. are available. In order to study the structure of the interfaces on a local atomistic level nuclear probes as, e.g., positrons were used. By means of positron lifetime spectroscopy a distribution of atomic free volumes from the size of vacancies (1V) in the interfaces to nanovoids of about 10 missing atoms (10V) in triple junctions can be detected. These free volumes exhibit a high compressibility in the comparatively "soft" interfaces and tend to agglomerate upon annealing. The high diffusivities of substitutional atoms in nanocrystalline metals and the high desorption rates of gases will be correlated to these free volumes. The magnetic properties as the Curie temperature,  $T_C$ , the magnetic moment per atom,  $\mu$ , and the coercive field,  $H_C$ , are taken as examples to demonstrate the modification of the macroscopic properties in nanocrystalline solids.

INVITED

9:40 am **NS1-TuM5 Diffusion Controlled Growth of Metallic Nanoclusters at Selected Surface Sites**, G. M. Francis, R. E. Palmer and J. R. A. Cleaver, Cavendish Laboratory, Madingley Road, Cambridge CB3 0HE, UK.

The nucleation and growth of atomic clusters at artificially created defects on a substrate is an attractive route to producing low-dimensional quantum structures [1]. We have therefore investigated the phenomenon of three dimensional particle growth at an atomic step due to the diffusion of silver adatoms across the surface of Highly

Oriented Pyrolytic Graphite (HOPG) in a high vacuum ( $10^{-6}$  mbar). By controlling the growth conditions (temperature, deposition rate), cluster growth has been confined to steps on the surface avoiding terrace nucleation. This leads to the approximately 10 nm diameter as determined with a scanning electron microscope (SEM). The results suggest the viability of an important new route to the creation of controlled nanoscale quantum structures.

In order to explore in more detail the kinetics of the nanocluster growth process, we have also performed a quantitative analysis of the spatial distribution of the clusters on the surface steps. Using a recently published theory [2] we have been able to calculate atomic diffusion parameters along the steps and determine that the graphite surface has several types of straight surface steps, with different diffusion barriers varying over a range of 0.17 eV. At substrate temperatures above 50°C we find that the adatoms are able to diffuse to the steps, across defect-free terraces up to 140 nm wide without terrace nucleation and in this regime the steps act as perfect adatom sinks. By contrast, at room temperature we find that terrace nucleation competes with step nucleation down to the lowest deposition rates available.

1. R. W. Siegel, *Physics Today* 46 No. 10 (1993) 64.

2. A. D. Gates and J. L. Robins, *Surface Sci.* 191 (1987) 449.

10:00 am **NS1-TuM6 The Surface Composition of Semiconductor Nanocrystals**, J. E. Bowen Katari, V. L. Colvin and A. P. Alivisatos, Department of Chemistry, University of California, Berkeley, CA 94720.

The surface of a semiconductor nanocrystal plays an important role in determining its electronic structure because of the large ratio of surface atoms to interior atoms. However, because of low symmetry and absence of long range order on the crystal surface, many traditional probes of surface structure are not applicable, and thus little is known about the surface of nanocrystals.

We have studied the surface composition of chemically synthesized CdSe nanocrystals using x-ray photoelectron spectroscopy (XPS). The samples as prepared are not suitable for XPS, as they will charge nonuniformly, causing shifts and broadening of peaks. Thus, the crystals were covalently bound to gold, resulting in submonolayer coverage of nanocrystals placed  $\sim 10$  Å above the conducting surface.

Using the position and relative areas of the relevant core level peaks, we have determined that the nanocrystal surface initially contains as many capping molecules as are sterically allowed. As the radius of the nanocrystal increases from 9 Å to 30 Å, the surface gets flatter, allowing less capping molecules to fit on the surface and decreasing the surface coverage. We have also demonstrated that it is possible to displace the original surface ligand, creating a bare surface.

This method for determining surface composition, combining a unique sample preparation with XPS, is easily extendible to a variety of surface ligands and to other chemically synthesized nanocrystal systems. In combination with other techniques, such as valence band photoemission, this work will allow us to quantify the effect of the nanocrystal surface on its electronic properties.

10:20 am **NS1-TuM7 Preparation and Characterization of Thiol Capped Silver Nanocrystals**, M. M. Alvarez,<sup>1</sup> Srihari Murthy,<sup>1</sup> R. L. Whetten<sup>1,2</sup> and J. M. Hampikian<sup>3</sup>, <sup>1</sup>School of Physics, Georgia Institute of Technology, Atlanta, GA 30332-0430, <sup>2</sup>School of Chemistry and Biochemistry, Georgia Institute of Technology, Atlanta, GA 30332-0400, <sup>3</sup>School of Materials Science and Engineering, Georgia Institute of Technology, Atlanta, GA 30332-0245.

Silver nanocrystals (8–40 nm) are prepared in a flowing aerosol device and solubilized by bubbling through appropriate thiol solutions. They remain in solution for days and they can be dried, handled in air and resolubilized without noticeable change in observable properties. By contrast, when silver nanocrystals are prepared in the flowing aerosol device and bubbled through neat liquids, they settle out of solution. Transmission electron microscopic studies and energy-dispersive X-ray analysis of nanocrystals prepared by these methods will be used to discuss the effectiveness of thiols in acting as capping and solubilizing agents for silver nanocrystals. Atomic force microscopic studies of arrays of nanocrystals prepared on mica substrates will be presented and the applicability of atomic force microscopy as a routine technique for the determination of the sizes and shapes of nanocrystals will be discussed.

10:40 am **NS1-TuM9 Polymer-Nanocrystal Composites—Integrated Materials for Electrooptical and Electronical Devices**, J. P. Spatz, A. Roescher, M. Möller, Organische Chemie III, Universität Ulm, D-89069 Ulm.



We report a new method of producing nanostructured metal and semiconductor clusters which can be used to improve the properties of nanoscaled devices and therefore to investigate effects which are hidden behind the limit of conventional methods. The chemical structure and properties of the used polymer in which the crystallite is embedded can be tailored for optimisation of physical properties and applications.

Functional block copolymers with ionic endgroups are employed to bind different metal ions or coordination complexes in ordered nanostructures and in defined concentration within a polymer matrix. Subsequently, the transition metal ions are converted to small crystallites (active component) by reduction. The size of the micro domains in which the transition metal ions or complexes are concentrated (crystallite substrate) can be rigorously controlled between a few and up to 1000 nanometers. Also the distance between the micro domains can be controlled within the same range. The maximal size of the crystallites can be controlled by the absolute amount of the transition metal per domain. Crystallite dimensions can be reduced behind the 1 nm scale. Molecular mobility and thus crystal growth can be controlled by making use of the glass transition. These new samples are characterised by X-RAY scattering, TEM, UV-VIS absorption and photoluminescence measurements, which determine the size, size distributions and electron confinement effects. Applications (devices and quantum lasers) which could be improved or new developed will be discussed.

11:00 am **NS1-TuM10 Characterization and Nanomanipulation of ZnS Nanoclusters via Atomic Force Microscopy**, *J. E. Coury, E. C. Pitts, L. A. Bottomley, R. Shorosh and R. H. Felton*, School of Chemistry & Biochemistry, Georgia Institute of Technology, Atlanta, GA 30332-0400 USA.

Semiconductor clusters, also known as nanoclusters or quantum dots, have recently been the object of intensive study because of their potential use in high-speed electronics applications. We have prepared and characterized ZnS nanoclusters utilizing x-ray absorption fine structure techniques, x-ray diffraction (XRD), structure simulations, and chemical analysis. The nanoclusters were "capped" with alkanethiols possessing chemically-polarizable end-groups enabling their electrostatic immobilization to similarly-modified gold, bare mica, and Mg-modified mica for atomic force microscopic (AFM) analysis. Size distributions were easily obtained; mean particle diameters correlated well with values obtained by XRD. Compressibility studies were performed and showed that the nanoclusters were relatively incompressible under typical imaging forces. The transport of these nanoclusters via the probing tip between different substrates and their subsequent electrostatic deposition into well-defined arrays has been achieved. The "striking behavior" of these clusters upon repeated AFM scanning will be noted. This report describes the reliable and reproducible AFM imaging of semiconductor nanoclusters as well as their controlled nanomanipulation.

11:20 am **NS1-TuM11 The Structure and Mechanical Properties of MoSi<sub>2</sub>-Based Nanolayer Composites**, *H. Kung, T. R. Jervis, N. Yu, T. E. Mitchell and M. Nastasi*, Los Alamos National Laboratory, Los Alamos, NM.

Enhancement of the mechanical properties of nanoscale materials has been observed in a number of multilayer structures. Specifically, metal-metal systems have shown increased yield and fracture strength. One potential application of the nanolayers is for high temperature coating. The layer stability and its effect on the mechanical properties are of main concern. In this study, the layer structure evolution and its influence on the mechanical properties as a function of temperature is investigated in two MoSi<sub>2</sub>-based composites, namely, MoSi<sub>2</sub>-SiC

and MoSi<sub>2</sub>-MoSi<sub>2</sub>N<sub>3</sub>. Nanoindentation is employed to measure the hardness and modulus of the nanolayers. Cross-sectional transmission electron microscopy (XTEM) is used to examine the microstructure and the layer structure evolution when exposing to different temperatures. An amorphous structure is observed in the as-sputtered nanolayers in both types of composites. For MoSi<sub>2</sub>-SiC, crystallization of MoSi<sub>2</sub> and SiC occurs at 500°C and 700°C respectively. Figure 1 shows a XTEM image of a 500°C-1h annealed multilayer. Significant increase in both hardness and modulus is observed accompanying the crystallization process. A 900°C-2h anneal causes the complete layer breakdown to form a nanocrystalline equiaxed microstructure. For MoSi<sub>2</sub>-MoSi<sub>2</sub>N<sub>3</sub>, MoSi<sub>2</sub> crystallize at 500°C while MoSi<sub>2</sub>N<sub>3</sub> layers remain amorphous up to ~900°C; the layered structure is preserved after annealing at 900°C for 1h. The difference in the layer stability at temperatures between the two composites will be discussed. The results on the influence of micro-structure and reinforcing geometry on the mechanical properties of the nano-layer composites will be presented.

## NANO 3/NANOMETER-SCALE SCIENCE AND TECHNOLOGY

Room A207 - Session NS2-TuM

### Nanoelectronics

**Moderator:** T. Higman, University of Minnesota.

8:20 am **NS2-TuM1 Application of Nanoelectronic Devices**, *John N. Randall*, Texas Instruments, PO Box 65936, MS 134, Dallas, TX 75265.

Resonant tunneling devices are finding applications in small scale integrated circuits with specialized applications. These devices are scaled to nanometer dimensions only in their epitaxial structure. A vision for the future of ultra-scaled integrated circuits described by Bate [1] includes resonant tunneling through heterostructure confined quantum dots in a limited interconnect massively parallel architecture. A universal quantum dot cell that could be used in a functionally complete edge-fed cellular cascade will be described. There is a current effort to produce lateral heterostructure resonant tunneling devices that will be the basis for the universal quantum dot cell. The critical fabrication processes that will be used to fabricate the lateral resonant tunneling devices will be presented: Lateral patterning techniques using e-beam lithography and sidewall processing will be utilized to produce 15 nm features. Ion beam assisted etching that uses separate ion and molecular halogen beams, will etch InP and related compounds. Epitaxial regrowth of InP by Chemical Beam Epitaxy or MOCVD will be employed to create lateral tunnel barriers.

**INVITED**

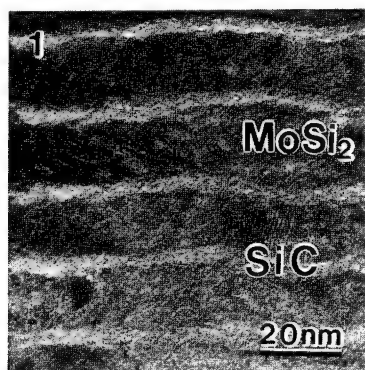
[1] R. T. Bate, Nanotechnology Vol. 1, page 1, 1990.

9:00 am **NS2-TuM3 Quantum Cellular Automata**, *\*P. Douglas Tougaw, Craig S. Lent, and Wolfgang Porod*, Department of Electrical Engineering, University of Notre Dame, Notre Dame, IN 46556.

We discuss a new paradigm for computing based on connecting quantum dot devices in a cellular automata architecture—quantum cellular automata (QCA). The architecture is designed so that the ground state of the array, subject to the boundary conditions determined by the inputs, yields a useful computational result.

One realization of these ideas uses two-electron cells composed of quantum dots and is within the reach of current fabrication technology. The charge density is highly aligned along one of two cell axes, making this cell ideal for a two-state CA. The polarization of one cell induces a polarization in a neighboring cell in a very nonlinear way, and this interaction is used to make QCA wires which can transmit the binary information encoded in the quantum state of the cells.

We analyze the behavior of these arrays by solving the time-independent Schrödinger equation to find the many-particle ground state, and show how useful computing structures may be built from a set of logical primitives. These primitives include wires, coplanar wire crossings, inverters, and a flexible three-input structure<sup>1</sup>. The three-input device can be configured as an AND gate, an OR gate, or a majority logic device. Devices as complicated as a full adder have been



simulated<sup>2</sup>. We will also discuss recent work on time-dependent calculations of the switching of this class of devices.

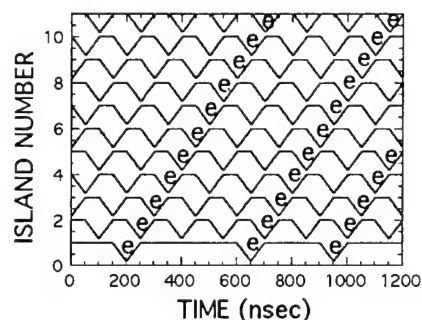
\*Work supported by ARPA/ONR.

1. C. S. Lent, P. D. Tougaw, W. Porod, and G. H. Bernstein, *Nanotechnology* **4**, 49 (1993).
2. P. D. Tougaw and C. S. Lent, *J. Appl. Phys.* **75** 1818 (1994).

9:20 am **NS2-TuM4 Computational Behavior in Coulomb Blockade Arrays**, M. G. Ancona and R. W. Rendell, Code 6813, Naval Research Laboratory, Washington, DC 20375 USA.

The limitations on device scaling due to interconnects has led to an interest in locally-interconnected architectures composed of quantum devices. To better understand the potential of such architectures in a "realistic" context, we have studied models of locally-interconnected one-dimensional tunneling arrays operating in the Coulomb blockade regime from a computational point-of-view. Bits of information are represented by single electrons on the islands between junctions and we find that computational behaviors can be obtained if the size of an electron plus its polarization cloud is sufficiently small. We show that linear tunneling arrays can be made to act as "charge-coupled devices" for single electrons. Arbitrary patterns of electrons can be transferred by applying a regular 3+ phase biasing cycle to a set of phase gates in a way similar to that in a single electron pump [1]. This behavior, which could be used for array input/output, is depicted in the figure. We further demonstrate that other regular gate biasings can produce "useful" computations, e.g., simulation of diffusion. These preliminary results suggest that such arrays may be more broadly useful in a technology that should be scalable to molecular dimensions. We discuss these prospects, the fabrication issues, and various error sources such as cotunneling and polarization charge which can impact performance.

[1] H. Pothier et al., *Physica B* **169**, 573 (1991).



9:40 am **NS2-TuM5 Photovoltaic Effect for Resonant Tunneling Structure of Quantum Dots**, M. Sumetskii, AT&T Bell Laboratories, Murray Hill, NJ 07974-0636.

This report is devoted to the study of influence of the external radiation on the transport properties of nanometer device. This problem is specially important for the future nanoelectronics when one aims to create a structure that could serve as an effective detector of the information carried by the incident electromagnetic field. The task for theory is, evidently, to find how this information will be transformed by the structure i.e. the problem of current response to the applied alternating field should be solved.

The structure studied in the present paper consists of two leads and few quantum dots between them each having resonant level close to the energy of incident electrons. We model the dots by the small-radius potential wells [1] when the Green function of the stationary problem can be found in analytical form. The photovoltaic effect caused by the arbitrary time- and coordinate-dependent applied field is studied using the quantum perturbation theory. The influence of harmonic field is found without perturbation theory. Different simplest situations are analyzed (single barrier, single and double quantum dot structures, two coupled parallel linear chains of quantum dots). In particular cases, the answers for the photocurrent coincide with the ones found previously by more cumbersome methods [2].

1. M. Sumetskii, *J. Phys.: Condens. Matter*, **3**, 2651 (1991); *Phys. Rev. B* **48**, 4586 and 14288 (1993); *Appl. Phys. Lett.* **63**, 3185 (1993).
2. M. Sumetskii and M. L. Felshtyn, *Sov. Phys. JETP* **67**, 1610 (1988); *JETP Lett.* **53**, 24 (1991).

10:00 am **NS2-TuM6 A Novel Method for Producing Nanostructures in Silicon Inversion Layers**, B. Campbell, G. H. Bernstein, X. Huang, Department of Electrical Engineering, University of Notre Dame, Notre Dame, IN 46556.

A novel method for fabricating nanostructures based on the interactions of the MOS material system with an e-beam has been investigated. A positive charge located at the SiO<sub>2</sub>-Si interface which is both positionally and temporally stable<sup>1</sup> results from the interaction of the beam with the sample. The trapped charge at the SiO<sub>2</sub>-Si interface modulates the surface potential creating a Q-1D channel. There then exists a voltage that when applied to the gate inverts the region underneath the induced oxide charge while leaving the remaining area in depletion. The transport properties of the exposed devices were measured at 1.8 K. The width of the induced channel and the carrier concentration are modulated by varying the gate voltage. Electrical transport characteristics of the post-irradiated silicon MOSFET structures reveal quantized conductance with a step size less than  $e^2/h$ . A point contact in series with a large resistance would account for the non-integer quantization value. The transport characteristics of the exposed transistors are comparable to work published by Tang<sup>2</sup> et al. who used a long and narrow wire gate defined by EBL and RIE to study reduced dimensional transport. We believe that this novel technique could be applied to create a wide range of quantum structures with relatively simple processing requirements.

<sup>1</sup>G. H. Bernstein, S. W. Polchlopek, and W. Porod, *Scanning* **14**, 345 (1992).

<sup>2</sup>Y. S. Tang, G. Jin, J. H. Davies, J. G. Williamson, and C. D. Wilkinson, *Phys. Rev. B* **45**, 13799 (1992).

10:20 am **NS2-TuM7 Nanolithography: STM and 50 kV e-beam**, E. A. Dobisz, F. K. Perkins, C. R. K. Marrian, S. L. Brandow, T. S. Koloski, J. M. Calvert, Naval Research Laboratory, Washington, DC 20375 USA.

To be viable, nanolithography must be performed in a manner which permits transfer of the lithographically defined pattern to the desired device of nanostructured material. In this context, low voltage e-beam lithography with the STM and high voltage e-beam lithography with commercial and experimental resists are compared. The key issues are resolution, process latitude, sample preparation, and transfer of a pattern from resist to substrate. With commercial resists, we have achieved 12 nm lines in a 60 nm period grating in a 60 nm thick layer of PMMA, with a 50 kV e-beam. In contrast, in 50 nm of SAL-601 (Shipley, Corp.), the best 50 kV results were 50 nm lines on a 100 nm line-to-line spacing; whereas with STM lithography 20 nm lines were achieved with a 45 nm line-to-line spacing. Sample preparation is critical for STM lithography. It can only operate with certain resists, of limited resist thicknesses, and on clean passivated substrate surfaces. To achieve the finest resolution ( $\leq 10$  nm), crystallographically smooth surfaces are required. The advantages of STM lithography arise from the smaller scattering lengths of low voltage electrons. The resulting localized high contrast exposure allows for very high resolution, no proximity effects, and a large resist process latitude. To move beyond a research technique, STM lithography requires the development of ultra thin resist films, which accentuates the problems of pattern transfer. The alternatives such as atomic manipulation or surface modification cannot be applied to a wide range of materials. Our results with self assembling imaging layers indicate that a viable STM lithographic technique can be developed which can be extended to a production nanolithography once the limited throughput is overcome.

10:40 am **NS2-TuM8 Patterning of Self-Assembled Monolayers by Electron Beams for High-Resolution Lithography**, M. J. Lercel, G. F. Redinbo, F. D. Pardo, M. Rooks, R. C. Tiberio, P. Simpson, and H. G. Craighead, Cornell University, Ithaca, NY 14853, C. W. Sheen, A. N. Parikh, and D. L. Allara, Pennsylvania State University, University Park, PA 16802.

We have demonstrated the use of self-assembled monolayers as high-resolution resists by modifying them on a small scale by the use of electron beams and transferring patterns with standard chemical etches.

Focused electron beams of energies 1-50 keV have been used to pattern monolayers of octadecylsiloxanes on SiO<sub>2</sub> and TiO<sub>2</sub> and octadecylthiols on GaAs. Line widths down to 25 nm have been formed. Currently, resolution of this patterning is still limited by the size of the exposing beam, but we are exploring the ultimate resolution of these materials. The critical doses for modification have been determined—both by direct observation of the material after patterning (using an atomic force microscope) and after wet chemical etching. Also, lithography based on scanned probe microscopy with energies



of  $\sim 10$  eV has been used to modify the chemical properties of these monolayers down to 15 nm feature sizes.

Patterns have been etched into silicon to a depth of  $> 120$  nm using octadecylsiloxane as a resist. The etch resistance to many common etchants has been measured and we are exploring other etches that may take advantage of the chemical properties of the monolayer.

The exact mechanism of the electron beam damaged is being explored using infrared and x-ray spectroscopy. An understanding of the damage mechanism should allow for better preparation of the monolayers and methods to improve their use in pattern transfer.

This work is supported by the Advanced Research Projects Agency ULTRA project.

**11:00 am NS2-TuM9 Manufacturing Considerations for Quantum-Effect Devices, Martin Peckerar, US Naval Research Laboratory, Surface and Interface Sciences Branch, Washington, D.C. 20375.**

As a result of evolutionary trends in microelectronic device development, we are currently at the threshold of large-scale deployment of quantum effect devices. These are devices making use of quantum interference and/or tunneling in their basic functioning. Heterostructure bipolar are in use in the microwave industry. Texas Instruments has announced a logic device, operating at room temperature, which makes use of a resonant tunneling transistor. The increased number of output states of this device allows reduced part-count on chip. Reduced dimensionality transport and single electron transport structures may see utilization by the end of the decade. Each of these novel structures presents a particular fabrication challenge, either due to the resolution requirements of the lithography employed or the requirements for minimally damaging etch processes. Laboratory demonstrations prove concept feasibility. But the barriers to scale-up to manufacturing are formidable. This talk reviews progress in movement toward a manufacturing base for quantum devices. **INVITED**

**11:40 am NS2-TuM11 Results of NANO-II and Development of Nanotechnology in Russia, V. Alfeev, Academy of Technological Sciences of the Russian Federation, Moscow, Russia.**

The overview presents the main achievements on nanotechnology, obtained by leading Russian scientific bodies, participated at the Second International Conference on Nanotechnology NANO-II and Exhibition in Moscow, in 1993. Success of NANO-II, in which took part well-known scientists from the USA, UK, Switzerland, Germany, Italy, France, Japan, China, etc. promoted the further development of nanotechnology in many countries especially in Russia. The attained results served the base for forming of Nanotechnology Program, including parts devoted to nanomechanical processing, atom assembling, multifunctional nanocomplexes and basic elements of nanocomputer. The Program is authorized by the Russian Government. The more success were attained on subprograms such as: "Diamond nanotechnology", "Superhigh terabit memory" and "Nanotron". The first results of nanodiamond biotesting have attracted attention due especially to the behaviour of diamond particles, which have sizes proper to protein molecules. The study of thin structure of modified nanoparticles concerning their electronic properties allows new approaches to clean carbon nanoelectronics to be defined. Within the framework of the Program a device for storage of information volume up to 1 Tbit on the base of STM was created. Range of data cell is near 10 nm. Density of data recording exceeds laser disk one. The one-year realization of the Program also allowed to construct new samples of nanotechnological equipment for studying of surface and biological objects and for atom assembling of nanoelectronics elements. The Program is opened for participation of all interested international bodies and now we have already contacted Chinese and Ukrainian scientists as attendees of this Program. There is the Nanometer Science and Technology Division under the Russian Academy of Technological Sciences in Russia, which co-ordinates this Program.

## **APPLIED SURFACE SCIENCE** **Room A101 - Session AS-TuM**

### **Surface Chemistry and Contamination**

**Moderator: J. E. Fulghum, Kent State University.**

**8:20 am AS-TuM1 Overview of Particle Detection on Silicon Wafers, Terry Francis.**

Contamination Reduction is the battleground of the ninety's on

Silicon Wafers. Detection of the particle on the wafers is a key issue but is not sufficient to meet the criteria for contamination reduction. To meet this criteria it is necessary to identify the location of the contamination in a precise manner and then to identify the specific contaminate back to its initial root cause. This overview will cover application of Contamination/Particle Analysis by SEM, EDAX, Auger, ESCA, ICPMS, GCMS, FTIR and Surface Photoacoustic Measurement and their correlation to root cause. **INVITED**

**9:00 am AS-TuM3 Limitations of Surface Analytical Techniques for Determining the Surface Composition of Bimetallic Particles, Allen G. Sault, Fuel Science Department, Sandia National Laboratories, MS 0710, Albuquerque, NM 87185-5800.**

Calculations of expected X-ray photoelectron spectroscopy intensity ratios for both homogeneous and segregated bimetallic particles demonstrate that a minimum particle size exists, below which reliable differentiation between homogeneous alloy particles and particles in which one component has segregated to the surface cannot be made. This minimum particle size varies between 3 and 8 nm, depending on the specific metal combination in question. In cases of partial segregation of one component, the minimum particle size is even larger. The implications of these results for the study of surface segregation in supported bimetallic catalyst particles is discussed.

This work was performed at Sandia National Laboratories for the U.S. Department of Energy under contract DE-AC04-94AL85000.

**9:20 am AS-TuM4 Analysis and Imaging of Surfaces, Layers, and Particles by TOF-SIMS and Laser-SNMS, B. Hagenhoff, E. Niehuis, H.-G. Cramer, R. Möllers, H. Rulle, J. Zehnpfennig, and A. Benninghoven, Universität Münster, D-48149 Münster, Germany.**

New concepts and instrumental developments have increased considerably the performance of time-of-flight mass spectrometry. Most important developments concern ion sources, sample stage, instrument control, and data handling and evaluation. These developments allow considerable improvements, e.g. in quantitative surface and micro area analysis, micro area depth profiling, particle identification, direct analysis of very large samples, thermal characterization of molecular surface contaminants, the analysis of volatile materials, etc.

We will report on these new developments and their application in particular for the analysis of microelectronic devices and molecular surfaces and overlayers.

**9:40 am AS-TuM5 Continuous Electron Stimulated Oxygen Atom Emission From Ag Permeation Membranes, G. A. Miner, R. A. Outlaw, M. R. Davidson, NASA Langley Research Center, Mail Stop 493, Hampton, VA 23681-0001.**

The emission characteristics of atomic oxygen generated by electron stimulated desorption (ESD) from the downstream surface of polycrystalline Ag membrane have been studied. The oxygen is supplied by permeation through the membrane where it emerges into an atomically bound state at the down stream ultrahigh vacuum surface and then desorbed by ESD. The flux levels of atomic oxygen were linear with electron bombardment current and measured up to approximately  $1 \times 10^{14} \text{ cm}^{-2} \text{ s}^{-1}$  (electron bombardment flux of 5 mA  $\text{cm}^{-2}$  at 2.8 kV). The emission pattern appeared to be highly directed approaching a  $\cos^4 \alpha$  angular dependence. The oxygen atom to ion ratio emitted was determined to be in excess  $1 \times 10^5$ , but the specific ESD mechanism in operation is still under study. The kinetic energy of the oxygen ions was measured by TOF methods and found to have a mean energy of approximately 5 eV with a FWHM of 4 eV for large grain polycrystalline Ag. The addition of a small amount of Zr (0-.5 wt. %) substantially broadened the distribution to a FWHM of 6 eV, presumably because of the increase in the adatom bond energy distribution on the alloy surface. Neutral atom energy measurements indicate that the energies are in excess of 2 eV, but the distribution has not yet been determined.

**10:00 am AS-TuM6 Oxidation of Gold by UV and Ozone at 25 °C, David E. King, NREL, 1617 Cole Blvd., Golden, CO 80401.**

Gold surfaces have been found to be hydrophilic only after exhaustive preparation and with the ultimate care in sample preparation and treatment. The use of a combination of UV and ozone has been described as a viable method of producing a clean, hydrophilic, gold surface. We have found that gold surfaces stored in the laboratory after vacuum deposition and purchased high purity standards, are oxidized by a combination of UV light and ozone generated from a mercury lamp. The samples were characterized with XPS and ISS prior to and after exposure to UV/ozone in a stainless steel box in laboratory air. After the cleaning process gold surfaces were found by XPS to

contain less carbon, to be enriched in oxygen, and often contain detectable residual nitrogen. The O1s on the cleaned surface, which was not present on the untreated surface, consisted of two peaks that are attributed to gold oxide and water, presumably adsorbed onto the oxide. The oxide layer was found to be  $17 \pm 4$  Å thick by variable angle XPS depth profiling with an initial stoichiometry of  $\text{Au}_2\text{O}_3$ . The oxide was found to be stable to extended exposure to UHV and water rinse. ISS compositional depth profiles confirmed the oxide layer thickness and that the hydrated surface layer is removed in the initial sputtering of the oxidized gold. Implications of these results about the mechanism of self-assembly of thiols on Au will be discussed.

\*Performed under DOE contract DE-AC02-83CH10093.

10:20 am **AS-TuM7 Quantitative XPS Analysis of Complex Hydrated Inorganic Compounds**, *Charles R. Anderson*, Martin Marietta Laboratories Baltimore, Baltimore, MD 21227-3898.

Many hydrated inorganic compounds are technologically important, yet little investigated due to their complex, often multiphase, structures and their sensitivity to many processing parameters. An example is aluminum hydroxide, often called aluminum trihydrate, which is used as a fire retardant filler in polymer matrices. Adhesive bonding properties of such composite materials are strongly affected by differences in aluminum hydroxide feedstock materials. These differences could not be detected by XRD, IR, or low energy resolution XPS. High energy resolution XPS had to contend with differential surface potentials, which paradoxically proved effective in separating the multiple hydration states of the aluminum hydroxide materials. Two materials each had two charging potentials associated with two phases of quantifiable  $\text{H}_2\text{O}$  and  $\text{CO}_2$  content for a total of four unique phases. Despite these differences, the average oxygen to aluminum ratios of each material were identical and the photoelectron binding energies were virtually identical after corrections for the respective surface potentials. The aluminum hydroxide phases exhibited stepped multiple hydration and carbonation levels. Examples of this quantification technique with magnesium oxides and ferric oxides will also be presented.

10:40 am **AS-TuM8 The Influence of Hydrogen on LEIS Signals**, *R. H. Bergmans, M. J. H. Vanhommerig, A. W. Denier van der Gon and H. H. Brongersma*, Eindhoven University of Technology, Faculty of Physics, P.O. Box 513, 5600 MB Eindhoven, The Netherlands.

Hydrogen is often used as a pretreatment of samples to remove oxygen, when sputtering is not allowed. This leaves a hydrogen covered surface which may affect the surface composition or the determination thereof. In Low Energy Ion Scattering (LEIS) the composition of the topmost atomic layer of a sample is deduced from the energy distribution of the scattered ions. Because of its low mass, hydrogen can not be detected in most LEIS-geometries nor with many other surface sensitive techniques. It is known that hydrogen can obscure other elements in LEIS [1], but most of this knowledge is limited to  $\text{He}^+$  scattering from single elements. In this work the influence of hydrogen on LEIS signals is studied using 4 keV  $\text{Ne}^+$ . The samples investigated consisted of Pt, Pd and Ge or combinations hereof. It was found that the presence of hydrogen can cause a decrease in the intensity of LEIS signals of nearly 100%, due to neutralization. The hydrogen did not affect the surface composition of the samples investigated, nor did it obscure one element in the alloys more effectively than another. The removal of hydrogen by sputtering was fitted to a model. From the results of the fitting sputter yields for hydrogen were determined.

[1] E. Taglaier, U. Beitz, W. Heiland, Nucl. Instr. and Meth. B 149, 605, (1978).

11:00 am **AS-TuM9 XPS and Infrared Spectroscopy of Cu-Implanted Silica and Borosilicate Glasses**, *D. O. Henderson, M. A. George, A. Burger, R. Mu, S. H. Morgan, W. E. Collins*, Fisk University, Physics Dept., Nashville, TN 37208, *R. H. Magruder III*, Dept. of Applied and Engineering Sciences, Vanderbilt University, Nashville, TN 37235, *C. W. White and R. A. Zuhr*, Oak Ridge National Laboratory, P.O. Box 2008, Oak Ridge, TN 37831-6057.

Copper implanted in silica exhibits a large nonlinear index of refraction, i.e. a large third order optical nonlinearity. The nonlinear response is thought to arise from the formation of metal colloids. Other highly polarizable metal ions, e.g. Pb implanted in silica also gives rise to a third order optical nonlinearity, however lead incorporates into the glass as a  $\text{PbO}$  phase. Nonlinearities may also occur from ion induced damage in the host substrate. The formation of metallic colloids or a product resulting from a reaction of the glass

with the implanted ion depends on the chemistry between the host glass and the implanted ion. In order to characterize these effects we have measured the infrared and XPS spectra of Cu implanted in optical grade silica and a borosilicate glass. These results are discussed in terms of ion induced damage and the chemistry of the Cu ion in these glass hosts.

The research at ORNL was sponsored by the Division of Materials Sciences, under contract DE-ACD5-84OR21400 with Martin Marietta Systems Inc.

11:20 am **AS-TuM10 Investigations of the Surface Chemistry of Pathogenic Silicates**, *Sudipta Seal, Stephen Hardcastle, Tery L. Barr*, University of Wisconsin-Milwaukee, Milwaukee, WI 53201; and *Heyong He, Jacek Klinowski and Peter Evans*, University of Cambridge, Cambridge, U.K.

The following is a continuation of our extensive investigations of the chemistry of complex silicate systems employing a combination of MAS-NMR and ESCA. In this case, we have extended the study to include the pathogenic asbestoses, including the amphibole, riebeckite, and the serpentine, chrysotile. The materials have been investigated both before and following alterations of their physical conditions (e.g., crushing) and also before and after contact with select in-vitro tissue samples. In our studies to date, we have been able to track the "in-lattice" chemistry of the constituents of these, and related, silicates, differentiating such features as the aluminum in the tetrahedral and octahedral sites and the iron in M-4, as opposed to M-3 or M-1 octahedral positions (of the amphiboles). We are comparing our results for the present fibrous silicates with those achieved with related non-fibrous forms. In this manner, we are trying to confirm (or deny) the views of the biomedical community regarding the structural and chemical features of the fibrous silicates that are suspected to be primarily responsible for their pathogenic behavior.

11:40 am **AS-TuM11 Characterization of Free Carbon in Silicon Carbide**, *T. E. Paulson, V. J. Bojan, B. M. Wichterhan, C. G. Pantano*, The Pennsylvania State University, Materials Characterization Lab, University Park, PA 16802.

SiC materials are of great interest as advanced structural ceramics, protective coatings, and as reinforcements in composites for high temperature applications. The presence of excess carbon in the microstructure has a pronounced effect on the observed thermomechanical properties; i.e. grain growth, creep resistance and oxidation behavior. The ability to quantitatively measure excess carbon in SiC materials could provide valuable insight into predicting and/or explaining the thermomechanical behavior of SiC. Secondary Ion Mass Spectrometry ( $\text{Cs}^+$  primary beam, negative SIMS mode) of single crystal SiC and highly oriented pyrolytic graphite (HOPG) has revealed "fingerprints" for graphitic carbon in the higher mass carbon clusters. Specifically, the useful yield of the  $\text{C}_6^-$  cluster ion signal was a factor of 2 higher in the HOPG. However, the signal intensity ratio  $\text{C}_6^-/\text{C}^-$  was strongly dependent on instrument conditions, such as contrast aperture size and field aperture position. Depth profiles of SiC coatings deposited by CVD on SCS-6 fibers best illustrated the usefulness of the  $\text{C}_6^-$  molecule in identifying the presence of free carbon. The  $\text{C}_6^-$  signal intensity levels matched perfectly in the SiC coating and SiC core fiber. Within the outer coatings of the SCS-6 fiber, which are comprised of carbon reinforced with SiC particles, the  $\text{C}_6^-$  signal intensity increased dramatically. In addition, the  $\text{C}_6^-$  signal increased sharply within the 100 nm turbostatic carbon layer between the carbon-rich coatings. This work has confirmed the ability to use the  $\text{C}_6^-$  cluster ion to identify and quantify free carbon in the presence of SiC.

## PLASMA SCIENCE

### Room A109 - Session PS-TuM

#### Plasma Process & Reactor Modeling

**Moderator:** L. A. Berry, Oak Ridge National Laboratories.

8:20 am **PS-TuM1 Alternate Designs for High Plasma Density Inductively Coupled Etching Tools**,<sup>1</sup> *Peter L. G. Ventzek*,<sup>2</sup> *Michael Grapperhaus and Mark J. Kushner*, University of Illinois, Dept. Electrical and Computer Engineering, Urbana, IL 61801.

Inductively coupled plasma (ICP) reactors are being developed for high plasma density, low gas pressure etching of semiconductors and metals. As a result of experimental development and computer modeling, design rules to optimize the uniformity of ion and neutral etching precursors in these reactors have recently been proposed. For example, modeling and experiments have shown that at pressures <10–15 mTorr ion sources located at intermediate or large radii produce a more uniform ion flux to the wafer. We have developed a 2-dimensional hybrid model for ICP reactors (<10–15 mTorr,  $>10^{11}$  cm<sup>-3</sup> plasma density) with which we are investigating these design issues. Our goals are to optimize the uniformity of etching precursors to the wafer in metal and p-Si etching gas mixtures. The validation of the model will be discussed using electron densities measured using microwave interferometry.<sup>3</sup> We will discuss results for radially dependent ion and radical fluxes in chlorine gas mixtures (rare gas/Cl<sub>2</sub>, rare gas/BCl<sub>3</sub>) for reactor designs using alternate coil configurations and “triode” structures. The effect of substrate topography (sacrificial surfaces, focus rings, discontinuities in material properties) on the directionality of the ion flux and uniformity of the radical flux will be demonstrated.

<sup>1</sup>Work supported by Sandia/Sematech, SRC, NSF and Univ. of Wisconsin ERC for Plasma Aided Manufacturing.

<sup>2</sup>Present Address: Department of Electrical Engineering, Hokkaido University, Sapporo 060, Japan.

<sup>3</sup>K. Greenberg, Sandia National Labs, 1994.

**8:40 am PS-TuM2 Design of a Surface Reflection Neutral Beam Source for Semiconductor Processing, C. A. Nichols and D. M. Manos, College of William & Mary, Applied Science Program, Williamsburg, VA 23187.**

We have developed a computational model to optimize the design of a surface reflection neutralization source of hyperthermal neutrals for charge-free processing. For the deployment of this technique to large scale ( $\geq 8$ " wafers) processing, a system design study has been completed. The model calculates particle transport of ions from a single RFI source or multiple sources through the neutral background to a reflector plate. The resulting hyperthermal neutral density uniformity at the wafer is calculated for various plasma source density profiles. Angular dependence of etch rate and surface reflection distribution are modeled using observations from previous experiments. The model assumes specular or diffuse (or both) reflection from the neutralizer, followed by an off-line Monte Carlo simulation of elastic and inelastic collisions with the plasma stream. Charge exchange between the plasma ions and hyperthermal neutrals is considered and compared to the effect of Frank-Condon and charge exchange neutrals from the plasma on the above profiles. Fine line (<0.5  $\mu$ ) feature evolution under this hyperthermal neutral bombardment is calculated and presented as a function of the source density profile.

This work supported in part by SEMATECH contract #731234120P, Project J85.4415.

**9:00 am PS-TuM3 Modeling the Electromagnetic Field Excitation of Low-Pressure, High-Density Plasma Sources, T. A. Grotjohn, Dept. of Electrical Engineering, Michigan State University, East Lansing, MI 48824.**

Low-pressure/high-density plasma sources are finding increased use in a variety of materials processing applications. Several design variations have been developed using microwave and RF excitation of the plasma discharges. The modeling of these sources requires the solution of the electromagnetic fields, plasma discharge physics and chemistry, and plasma-surface interactions. This paper focuses on the self-consistent solution of the electromagnetic fields and plasma discharge physics in microwave and RF plasma sources. Previous work has concentrated on solving the electromagnetic fields in unmagnetized microwave plasma sources [1], whereas, the plasma sources studied for this paper include multipolar ECR plasma sources, divergent field (electromagnet) ECR plasma sources, and RF inductively coupled plasma sources. The electromagnetic fields are solved by a finite-difference time-domain solution of Maxwell's equations in two or three dimensions. The plasma discharge behavior is modeled using particle and fluid descriptions. The techniques for coupling the electromagnetic field solutions and plasma discharge behavior solution together self-consistently will be examined. Additionally, example power absorption profiles, electric field strengths, and plasma uniformities will be presented. The sensitivity of the spatial power absorption profile across an input power and pressure parameter space will be presented and its implications for uniformity will be discussed. Lastly, the electro-

magnetic field/plasma discharge simulations of the various sources will be examined with respect to identifying dominant plasma heating mechanisms.

[1] W. Tan and T. A. Grotjohn, "Modeling the Electromagnetic Excitation of a Microwave Cavity Plasma Reactor," to appear, J. of Vacuum Sci. and Technol., 1994.

**9:20 am PS-TuM4 The Effect of Time Varying Sheaths on Radially Dependent Ion Energy Distributions in Inductively Coupled Plasmas<sup>1</sup>, Robert J. Hoekstra, and Mark J. Kushner, University of Illinois, Dept. Electrical and Computer Engineering, Urbana, IL 61801.**

In moderate pressure (10s–100s mTorr), low plasma density ( $10^9$ – $10^{10}$  cm<sup>-3</sup>) reactive ion etching (RIE) tools, the ion transit time is often long enough that ions “see” an average sheath potential. Ion transit across the sheath may also be collisional. High plasma density ( $10^{11}$ – $10^{12}$  cm<sup>-3</sup>), low pressure (<10 mTorr) etching tools, such as inductively coupled plasmas (ICPs), use rf biasing of the substrate. The thinner rf sheath allows ions to transit the sheath more rapidly. The ions may then “see” the instantaneous sheath potential resulting in the ion energy distribution (IED) being broadened. We have developed a 2-dimensional Plasma Chemistry Monte Carlo Simulation (PCMCS) with which we are investigating spatially dependent IEDs in high plasma density ICP etching tools. The PCMCS uses 2-d time dependent electric fields and source functions as input. These quantities are produced by a comparison hybrid equipment model of ICPs. The PCMCS tracks the trajectories of ions and radicals while accounting for ion-neutral and ion-radical collisions. IEDs as a function of position on the wafer will be discussed for multicomponent chlorine gas mixtures for p-Si and metal etching (Ar/Cl<sub>2</sub>); and fluorocarbon gas mixtures for oxide etching (CF<sub>4</sub>/H<sub>2</sub>). The effect of electrode topography on ion angular distributions will also be discussed.

<sup>1</sup>Work supported by SRC, NSF, Sandia/Sematech and Univ. of Wisconsin ERC for Plasma Aided Manufacturing.

**9:40 am PS-TuM5 Modelling of Plasma Etching Discharges, Timothy J. Bartel, Sandia National Labs, Albuquerque, NM 85185-0826, and Demetre Economou, University of Houston, Houston, TX 77204.**

Low-pressure high-density plasma reactors are currently under development to meet the demands of gigascale integrated circuit fabrication. These sources operate at pressures less than 50 mTorr. Traditional numerical simulation tools employ a fluid approximation for the transport of the neutral and ion species; this assumption will begin to breakdown at these low pressures where the mean-free-path is the order of the wafer dimensions.

We will present 2- and 3-D results using the Direct Simulation Monte Carlo (DSMC) particle simulation method for the neutral and ion transport in plasma reactors; a fluid model was used for the electron transport. The DSMC technique has been shown to be valid from free molecular to very high pressures (2 atm.). The only limitation of the method, computational resources, has been minimized by using massively parallel computers. A 1024 node nCUBE-2 and a 1872 node Intel Paragon were used in the simulations; the Paragon is several hundred times faster than a single Cray Y/MP processor.

The etching of polysilicon in a chlorine discharge was selected as an example material system. The feed gas (Cl<sub>2</sub>), etchant (Cl radicals), product (SiCl<sub>4</sub>), and ion (Cl<sup>+</sup>, Cl<sub>2</sub><sup>+</sup>) transport were modelled with millions of computational particles with species dependent weights. Their energy and angular distribution on the wafer is a natural output from a particle-based simulation. Results of comparing 2-D and 3-D simulations for injector and vacuum pump placement will also be discussed.

**INVITED**

**10:20 am PS-TuM7 Modeling the Chemistry in Chlorine Plasmas Using a Well Stirred Reactor Model with Comparison to Experimental Measurements, E. Meeks and J. W. Shon, Sandia National Laboratories, Livermore, California, Y. Ra and P. Jones, Lam Research Corporation, Fremont, California.**

We present results from a plasma chemistry model that incorporates well-stirred reactor approximations to provide predictions of spatially and temporally averaged plasma properties. The solution of species, mass, and electron-energy balance equations determines steady-state electron energy and species compositions for ions, electrons, and neutral species. The electron energy equation includes a detailed power balance with losses to ions and electrons through the sheath, as well as inelastic and elastic collision losses in the plasma bulk. Model

predictions compare and test reaction-rate coefficients that are generated from solution of the Boltzmann equation and from a Maxwellian electron energy distribution function (EEDF). The model is then applied to chlorine-etch process conditions typical of high plasma density inductively coupled plasma (ICP) reactors. Model results show the dependence of species concentrations on the atomic chlorine recombination rate at both wafer and reactor-wall surfaces, as well as the effects of assumptions in the EEDF. The effect of inelastic collisions on the 'tail' of the EEDF is to reduce the ionization and excitation rates in the plasma. The dominance of surface reaction rates in determining plasma properties is expected to be equally important in higher-dimensional ICP models, due to the highly diffuse nature of these low-pressure reactors. Finally, we compare model predictions to the concentrations of ions, electrons and radicals measured by a Langmuir probe and optical spectroscopic methods in the transformer coupled plasma (TCP) source.

10:40 pm **PS-TuM8 Role of Etch Products in Si Etching by  $\text{Cl}_2$  in High Density Plasma Sources**, C. Lee, M. A. Lieberman\*\*, D. B. Graves, Dept. of Chem. Eng., Univ. of California, Berkeley, CA 94720 (\*\*Dept. of Elect. Eng.).

For low pressure, high density plasma systems, etch products can play a significant role in affecting the plasma parameters such as the density of etchant species and electron temperature, and therefore overall processing parameters. We used a spatially-averaged global model to include both gas phase and surface chemistry in the study of silicon etching by chlorine. In this process, the etch products leaving the wafer surface are assumed to be composed of  $\text{SiCl}_x$  species ( $x = 1-4$ ). These species, upon colliding with energetic electrons in the plasma, will undergo fragmentation and ionization. In addition, the formation of  $\text{Cl}^-$  from  $\text{SiCl}_x$  is also possible, which affects the electronegativity of the discharge when etch products are important neutral components.

The relatively high degree of dissociation in high density plasmas leads to the formation of elemental Si, which can deposit on the chamber walls and wafer surface. We have included surface models for both the wall and the wafer in an attempt to better understand the role of etch products as a function of flowrate, pressure, input power, and species residence time. The phenomenological model for surface chemistry in the plasma was developed based on the available experimental data.

11:00 am **PS-TuM9 Molecular Dynamics Simulations of Si Etching**, H. Feil, Philips Research Laboratories, Eindhoven, The Netherlands.

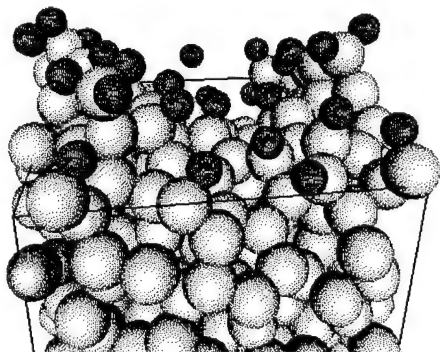
Chemical sputtering of Si in a chlorine environment has been examined with molecular dynamics simulations. Two important processes are identified.

Ion bombardment causes a rough surface and the chlorine passivation of the Si surface prevents the flattening of the surface due to the high activation barrier for surface diffusion. The rough surface contains reactive intermediates which can be desorbed onto the gas phase when, after an ion impact, the region has a large energy content.

Secondly, the desorption of  $\text{SiCl}_x$  molecules is facilitated by the strong decrease of the free energy of activation with increasing temperature.

**INVITED**

Rough Cl-covered Si surface with volatile  $\text{SiCl}_x$  molecules.



11:40 am **PS-TuM11 Ion-Neutral Synergism in Ar-Enhanced Fluorine Etching of Silicon: a Molecular Dynamics Simulation**, M. E. Barone and D. B. Graves, University of California, Berkeley, CA 94720.

We explore the role of low energy Ar ion bombardment (100, 50 and 20 eV) in enhancing fluorine etching of silicon, using molecular dynamics simulations. The key results from the simulations can be compared to various experimental measurements to help put together a more complete picture of the ion-neutral synergism, and the role it plays in etching. The simulations suggest that the source of the ion-neutral synergism is the creation of weakly bound species (wbs) during the short but intense collision cascade. These wbs are created throughout the  $\text{Si-F}_x$  layer and build up to an appreciable concentration during steady state etching. The formation of wbs occurs on short timescales, but the rate-limiting steps in etching often proceed on much longer timescales. Analysis of long timescale phenomena such as direct thermal desorption of wbs from the surface, and chemical reactions between surface wbs and thermal F impacting the surface, suggests that most of the experimental observations can be accounted for with this model. The overall yield is found to follow a square root dependence on ion energy. Kinetic energy distributions of etched species, yield as well as product distributions obtained from the simulation are compared with experiment.

Video illustrations of events occurring during ion-assisted etching will be presented.

## VACUUM TECHNOLOGY

### Room A102 - Session VT-TuM

#### Vacuum Systems for Accelerators and Fusion

**Moderator:** M. A. Benapfl, Lawrence Livermore National Laboratory.

8:20 am **VT-TuM1 Theoretical Submonolayer Adsorption Isotherms for Hydrogen on a Heterogeneous Surface**, J. P. Hobson, National Vacuum Technologies Inc., Box 4160, Postal Station E, Ottawa, Canada K1S 5B2.

Theoretical submonolayer adsorption isotherms for Argon, Nitrogen, and Helium on a heterogeneous surface, over wide ranges of pressure and temperature, were calculated by the author many years ago (1). These calculations showed good agreement with available experimental data. Since then the widespread development of large accelerators with cryogenically cooled tubes (cold bore) has made the analogous calculation of hydrogen isotherms of relevance. This paper presents such a calculation over the pressure range  $10 \exp - 16 < P < 10 \exp 3$  (torr), and at temperatures of 3.0, 4.2, 6.0, 10, 15, 20, 25, 30, 40 K. The values of relative coverage,  $\Theta$ , span the range  $10 \exp - 11$  up to 1. The form of the isotherm used was  $\ln \Theta = -B(RT \ln P/P_0)^2$  with  $B = 528$  Cal/Mole,  $R = 1.9865$  Cal/Mole Degree, and  $P_0$  = Vapor pressure of hydrogen at the chosen temperature. In regions where this isotherm is not quantitatively applicable the results have been rounded off to give the correct limiting values, i.e.  $P = P_0$  for  $\Theta \gg 1$ , and  $\Theta = kP$  (i.e. Henry's Law with  $k$  constant) for Temperatures of 30 and 40 K. The results should be useful for comparison with the experimental data being assembled by Rao et al. (2). In particular the calculations which predict only relative coverage provide a useful way of evaluating the surface "roughness factor" of an experimental substrate.

(1) J. P. Hobson, Jour. Vac. Sci. Tech., 3, 281, 1966.

(2) M. G. Rao, et al., "Collider Cryosorber Development Studies," presented at the 40th National Symposium of the American Vacuum Society, Orlando, Florida, November 1993.

8:40 am **VT-TuM2 Cryosorption Pumping of  $\text{H}_2$  and He in Cryogenic Accelerator Systems\***, M. G. Rao, H. F. Dylla, Continuous Electron Beam Accelerator Facility, Newport News, VA 23606 and W. Turner, Lawrence Berkeley Laboratory, Berkeley, CA 94720.

Residual background pressures of helium and hydrogen are the main contributing factors to the total pressure in beam line tubes of many cryogenically cooled particle accelerators and colliders. In the absence of He leaks and high  $\text{H}_2$  outgassing from room temperature components, the required base pressure of less than  $10^{-10}$  torr is easily maintained in these systems by cryosorption pumping of all residual gas species. In reality, additional pumping needs to be provided for keeping the system pressure at the required low levels. Cryosorption pumping of He by molecular sieves and charcoals have been investigated for



this purpose at 4.2 K. These studies indicate that high adsorption capacities could not be reached under dynamic conditions either due to the plugging of the pores and/or by the reduced mobility of hydrogen at this low operating temperature. Further, the low pressure adsorption isotherm data does not follow the Polanyi's potential theory. Large surface area clean metal oxides are likely to provide the enhanced pumping speeds at low pressures with high adsorption capacities because of their open micropore structure. We have been investigating metal oxides for dynamic adsorption and desorption of hydrogen and helium. In this paper we present the theoretical analysis of the adsorption isotherm data of the molecular sieves, charcoals and metal oxides with respect to their suitability for cryogenic accelerator systems. We also discuss Polanyi's potential theory with reference to low pressure adsorption isotherm data on metal oxides.

\*This work supported by U.S. DOE Contract No. DE-AC05-84ER40150.

9:00 am **VT-TuM3 D-T Experiments in TFTR**, *P. H. La Marche and the TFTR Team*, Princeton University, Princeton, NJ 08543.

The first weeks of December 1993 witnessed the realization of the first deuterium-tritium (D-T) fueled plasma discharges in the Tokamak Fusion Test Reactor (TFTR). This exciting time saw world records in fusion power output broken on an hourly basis, with output exceeding 6 megawatts. In the intervening time, although D-T high power plasma discharges are not yet commonplace, multi-megawatt discharge operation is reproducible to the point of on-demand-performance and the operation of TFTR with tritium has become routine. These accomplishments represent the steady improvement in power output over the years by a number of fusion research devices from the microwatt range of the sixties to the megawatt range of today, with a doubling time of less than one year. This steady progress is matched with a coupled improvement in several disciplines, particularly in vacuum pumping and vessel wall conditioning techniques. One technological objective for these experiments is to develop experience and expertise with safe handling and processing of tritium and tritium contaminated waste. Another objective is to understand and manage the changes in operation of the facility due to the increased levels of regulatory and safety controls brought by the use of tritium. We shall review results of D-T operation in TFTR along with tritium processing, vacuum pumping and vessel conditioning in support of this operation.

INVITED

This work supported by USDOE Contract DE-AC02-76-CHO-3073.

9:40 am **VT-TuM5 Pumping Characteristics of a Cryopump with Ar Sorbent in He and in D<sub>2</sub>/He Mixture\***, *M. M. Menon, G. J. Laughon, R. Maingi, M. R. Wade, D. L. Hillis, and M. A. Mahdavi*, Oak Ridge National Laboratory, Oak Ridge, TN 37831. <sup>1</sup>General Atomics, San Diego, CA 92186.

The He ash that will result from DT burn in a fusion reactor must be exhausted from the plasma to avoid serious fuel dilution effects. In view of this, transport and exhaust studies of He in fusion plasmas are getting increasing attention in recent years. To date, most of the He pumping investigations were conducted with pure He. In fusion plasmas, though, the exhaust gas will be a mixture of D<sub>2</sub> and He, with He forming only a small fraction. D<sub>2</sub> condensation on the pumping surface is shown to have an adverse effect on He cryosorption, although systematic data on this topic could not be found. We have investigated the pumping of pure He and a mixture of D<sub>2</sub> and He (90% D<sub>2</sub>) using layers of Ar gas condensed at 4.35 K as the sorbent. The experiment revealed that: 1) cryosorption pumping speed of pure He drops precipitously if the Ar/He ratio falls below about 20, 2) the pumping speed for He in a D<sub>2</sub>/He mixture decreases in an exponential manner with the amount of D<sub>2</sub> pumped, 3) increasing the thickness of Ar in the range of 1–20  $\mu\text{m}$  showed no clear trend in the pumping speed for He in a D<sub>2</sub>/He mixture, and 4) with the pumping surface coated with a 2  $\mu\text{m}$  layer of Ar, surrounded by a radiation shield having a transparency of about 17%, a He pumping speed of about 12,000  $\text{l s}^{-1}$  could be obtained with 100 millibar of D<sub>2</sub> condensed on 1  $\text{m}^2$  of the pumping surface.

\*Work supported by the U.S. Department of Energy, under Contract No. DEAC05-84OR21400 with Martin Marietta Energy Systems, Inc., and DEAC03-89ER51114 with General Atomics.

10:00 am **VT-TuM6 The Vacuum Integrity of the CEBAF Superconducting RF Cavity Assemblies\***, *H. F. Dylla, J. Benesch, J. Mammoser, M. Wiseman, P. Kneisel, M. G. Rao, W. Schneider, K. Finger*, Continuous Electron Beam Accelerator Facility, Newport News, VA 23606.

The 4 GeV recirculated linac at CEBAF uses 338 superconducting rf cavities to accelerate a cw electron beam for basic nuclear physics research. Pairs of superconducting rf cavities, fabricated from high purity niobium, are carefully chemically cleaned, rinsed, and assembled into hermetic units, prior to final assembly within cryostats for low temperature operation at 2K. Each cavity pair assembly contains 22 flanged joints and several meters of electron beam welds which must maintain leak tightness to UHV standards while submerged in a super fluid helium environment. Particular attention was given to the design, surface preparation, and assembly techniques for the indium wire-sealed niobium and stainless steel flanges employed in the cavity assemblies. Finite element models of the flange geometry, and flange test assemblies that were temperature cycled to ensure vacuum integrity of the critical seals before the production cavities were assembled. After assembly of each production cavity pair, total integrated leak rates were measured in a 2K environment using an ultra sensitive ( $<10^{-15}$  atm cc/s) leak detection method.

\*This work supported by U.S. DOE Contract No. DE-AC05-84ER40150.

10:20 am **VT-TuM7 The Effect of Physisorbed Gases on the Quality Factor of Niobium Superconducting Radio Frequency Cavities\***, *P. Kneisel, and M. G. Rao*, Continuous Electron Beam Accelerator Facility, Newport News, VA 23606.

The quality factor  $Q_0$  of Superconducting Radio Frequency (SRF) cavities is inversely proportional to the surface resistance of the Nb cavity walls. The residual resistance is a combination of many contributions including that of the physisorbed hydrocarbons, residual gases and physisorbed and/or chemically bound hydrogen. In this paper we will present the results of our controlled studies on the effect of the quantity of the physisorbed moist air and hydrogen on the  $Q_0$  of a single cell Nb cavity. In these studies an extractor gauge is used at 2 K to monitor the pressure and quantity of the residual gases adsorbed. A monolayer of hydrogen is introduced onto the cavity at 4.3 K. The cavity is warmed to 100 K and held there for few hours, to form a hydride and the cavity is cooled back to 2 K. The quality factor of the cavity is measured as a function of the accelerating gradient. These studies are conducted with different physical and chemical treatments of the Nb cavity wall surface. The results of these investigations will be presented in this paper.

\*This work supported by U.S. DOE Contract No. DE-AC05-84ER40150.

10:40 am **VT-TuM8 Ion Pump Speed Optimization for Low Pressure Operation**, *M. De Simon, M. Spagnol*, Varian S.p.A., 10040 Leini (TORINO) Italy.

Ion pumps are widely utilized and recognized as the best pumps for UHV conditions. Despite their actual use, for historical reasons, the pumping speed in the UHV range is far from the maximum value. To analyze the pumping behaviour in UHV conditions a new pumping model is proposed, based on the direct evaluation of the sputtering rate of the getter material from the cathode. Different from former models, the present one uses a restricted set of empirical parameters; these have been evaluated fitting the theoretical results to the actual pumping speed and ion current measured on different ion pump configurations. The model allows to estimate the pumping speed as a function of the geometrical, physical and electrical parameters that define an ion pump. Introducing the correlations between all these parameters (e.g. the magnetic field depends on the element height), the pumping performance has been optimized in the low pressure range. In particular, the ratio between pumping speed and total volume (element plus magnets) has been maximized as function of cell radius, element height and anode to cathode gap. This model shows a maximum of pumping efficiency for a flat element configuration operated at high magnetic field values.

11:00 am **VT-TuM9 NIF Vacuum Chamber**, by *R. W. Wavrik*, Sandia National Laboratories, *Dennis A. Muirhead*, Rockwell Power Systems, Albuquerque, NM, and *V. P. Karpenko*, Lawrence Livermore Laboratory, Livermore, CA.

The National Ignition Facility (NIF) will be a facility capable of

generating about 20 MJ of fusion yield. Laser beams, 240 in number, will be directed at a fusion target located at the center of a 10 m spherical aluminum vacuum chamber. The required pump down time of  $5 \times 10^{-5}$  Torr in 2 hours of the 18,800 cf chamber, coupled with tritium contaminated debris, outgassing of diagnostics, neutronic activation of the materials used in the chambers construction, as well as the dimensional stability of the chamber result in a unique design for both the chamber, decontamination systems, and vacuum pumping systems. The additional requirements of oil free and full sized stand-by equipment poses additional design constraints for the vacuum system. One 36" cryopump is capable of meeting the requirements if .2 Torr can be reached in 75 minutes however, a 48" pump is less expensive and offers more safety factor in design. Three pumps will be required as a minimum, one running, one on stand by, and one in regeneration. Steam ejectors, which are used in most other large volume high altitude chambers, are not permitted due to the tritium's affinity for water. The tritium constraint also eliminates liquid ring pumps. The large Roots style blowers being used for second stage pumping don't like to be started at atmospheric pressure. The oil-free requirement may eliminate the use of straight vane type mechanical fore pumps, although when used with inert gas back-streaming or LN2 cold traps the fore pumps are usually of small capacity by design, therefore gas back-streaming is not recommended. These constraints and the conceptual design for meeting them will be discussed in the presentation.

INVITED

11:40 am **VT-TuM11 A Non-circular UHV Seal That Functions Between  $\pm 200^\circ\text{C}$** , R. A. Childs, J. E. Rice, Massachusetts Institute of Technology, Plasma Fusion Center, Cambridge, MA 02139.

The Alcator C-MOD tokamak fusion experiment has over 40 large and small smoothed faced flanged ports that require reliable all metal seals to interface with the various diagnostic experiments and pumps that make up it's 4000 liter volume. In at least 10 of these ports the environment is such that the flanges and seals can experience temperature excursions between  $\pm 200^\circ\text{C}$ . These particular flanges are large racetrack shaped flanges that have an I.D. of 8" wide by 24.75" tall. They are located inside the massive confinement vessel which is cooled to LN2 temperatures. Because of their location in the tokamak they can inadvertently have LN2 applied to parts of the flanges while the rest of the flange has heat being applied to maintain the vacuum vessel near room temperature or occasionally at bakeout temperatures. This can create local differentials of over  $100^\circ$  from one end to the other on a single flange. We will report on the development of the seal under extensive testing and after more than a year of actual use.

## THIN FILM

### Room A105 - Session TF-TuM

#### Thin Films for Sensors

**Moderator:** S. Semancik, National Institute of Standards and Technology.

8:20 am **TF-TuM1 Thin Film Sensors for Automobile**, Y. Taga, Toyota Central Research and Development Laboratories, Nagakute, Aichi 480-11, JAPAN.

A great amount of effort has been devoted to the constant improvement of such basic automobile performance as drivability, safety and environmental protection. As a result, the total combination of various technologies has made it possible to produce safer and more comfortable automobiles. Among these technologies, surface and thin film techniques are mainly concerned with sensors, optics and electronics and surface modifications.

This review paper first describes a new concept of thin film process in materials synthesis on the basis particle-surface interaction during deposition. Some examples of practical applications of thin films for sensors are then given. These include (1) a poly(vinylidene fluoride) thin films for integrated pyroelectric infrared sensors, (2) a new piezoelectric thin films of Cr-O-X system for pressure sensors and (3) a niobium pentoxide films for oxygen sensors.

Based on the recent progress of thin film technology, it has now become possible to control thin film nanostructure and to guarantee the durability for automobile applications.

Finally, future challenges of thin film sensors for automobile are discussed.

9:00 am **TF-TuM3 Thin-Film-Based SAW Chemical Sensor Arrays**, A. J. Ricco, Microsensor R&D, Sandia National Laboratories, Albuquerque, NM 87185-0351; C. Xu, R. M. Crooks, Dept. of Chemistry, Texas A&M University, College Station, TX 77843-3255; R. E. Allred, Adherent Technologies, Inc., Albuquerque, NM 87123.

Chemical sensor arrays offer the promise of selective chemical detection without perfectly selective thin films, but the chosen films must have a degree of *chemical orthogonality* (preferential response to different classes of chemicals by each film). Using a six-device array of 97-MHz, ST-quartz surface-acoustic wave (SAW) delay lines, we have studied the chemical sensor response of two classes of thin film; self-assembling monolayers (SAMs) and plasma-grafted polymer films (PGFs). The sensitivity of the SAW to very small surface mass changes ( $< 100 \text{ pg/cm}^2$ ) and a range of other perturbations is necessary for characterization of analyte/film interactions for SAMs and PGFs that range in thickness from a single molecular layer to 100 nm. SAMs were terminated by methyl, cyano, amino, and carboxylic acid functionalities, and by carboxylate-coordinated  $\text{Cu}^{2+}$ ,  $\text{Ni}^{2+}$ ,  $\text{Fe}^{2+}$ , and  $\text{Zr}^{2+}$ . PGFs were derived from acrylic acid, vinylphosphonic acid, and eugenol (a phenol derivative). Arrays of SAW devices were exposed to 14 analytes representing saturated, aromatic and chlorinated hydrocarbons; alcohols; ketones; organophosphonates; and water. Adsorption/desorption isotherms were obtained for each analyte over the zero to 50%-of-saturation vapor pressure range. Analysis of array data using multidimensional cluster analysis techniques under development in Sandia's Vision Science Dept. results in very accurate identification of individual analytes. This work supported by the U.S. DOE under contract DE-AC04-94AL-85000.

INVITED

9:40 am **TF-TuM5 Structure and Mass Sensing Properties of Zirconium Carboxylate Thin Films**, G. O. Noonan<sup>1</sup>, K. G. Severin<sup>1</sup>, and J. S. Ledford<sup>1</sup>. <sup>1</sup>Department of Chemistry and The Center for Fundamental Materials Research, Michigan State University, East Lansing, Michigan 48824-1322.

Zirconium carboxylate polymer oxide glass thin films have been prepared by hydrolysis of zirconium(IV) *n*-propoxide in excess valeric or acetic acid. Fourier transform infrared spectroscopy (FTIR) and X-ray photoelectron spectroscopy (XPS) have been used to determine the structure of these films. Results of spectroscopic analysis show that the polymer film consists of a Zr-O backbone coordinated with bridging and chelating bidentate carboxylate ligands. The mass sensing properties of the films for simple alcohols and alkanes have been determined using a quartz crystal microbalance (QCM). Our results show that altering surface structure by changing carboxylate ligands affects the mass sensing properties of the films. The zirconium acetate film selectively responds to alcohols and rejects alkanes. The selective alcohol response has been attributed to hydrogen bonding interactions between the alcohol hydroxyl group and O atoms (Zr-O backbone and acetate ligands) in the zirconium acetate film. The zirconium valerate film exhibits a higher response for alkanes, but shows only limited sensitivity for the alcohols. Recent efforts to control the chemical affinity of zirconium carboxylate films using various carboxylic acids will be presented.

10:00 am **TF-TuM6 Effect of Deposition Parameters on Microstructure, Conductivity, and Sensitivity of  $\text{WO}_3$  Thin Films for Gas Sensing Applications**, D. J. Frankel, E. L. Wittman, K. Snow, S. T. Hess, R. J. Lad, J. F. Vetelino, Laboratory for Surface Science & Technology, 5764 Sawyer Research Center, University of Maine, Orono, ME 04469-5764.

Surface acoustic wave (SAW) gas microsensors utilizing a gas sensitive doped metal oxide semiconducting thin film deposited between the input and output transducers of a SAW delay line oscillator provide higher sensitivity than chemi-resistive sensors. The SAW sensor response to a target gas is maximized when the electrical conductivity of the film is within a critical range which depends on the piezoelectric substrate properties. The sensor selectivity, sensitivity, long term stability and reliability are directly related to the film microstructure. Reactively RF sputtered  $\text{WO}_3$  and Au-doped  $\text{WO}_3$  films which show high sensitivity and selectively to  $\text{H}_2\text{S}$  have been deposited on quartz and  $\text{LiNO}_3$  substrates and characterized using two point probe conductivity measurements and atomic force microscopy (AFM). Film stability is improved by annealing the initially amorphous films to form polycrystalline  $\text{WO}_3$ . Conductivity is increased by decreasing the RF power or total sputter pressure during deposition. The changes in conductivity are correlated with changes in microstructure observed with the AFM. The results show that manipulation of the film mi-



crostructure by variation of the deposition conditions can be used to optimize the performance of SAW gas microsensors.

\*Supported by NSF grants ECS-8806875 & ECS-9112282.

\*NSF-REU student supported by NSF grant EEC-9300004.

10:20 am **TF-TuM7 Increasing the Selectivity of Commercially Available Tin-Oxide Based Sensors for Process Environments**, Roger M. Hawk and Arvind Narayanaswamy, University of Arkansas at Little Rock, Department of Electronics and Instrumentation, 2801 S. University, Little Rock, AR 72204.

The use of semiconductors to detect changes in gas composition was discovered in the early 1950's. The dominant device available now is the Taguchi sensor, which uses a sintered form of the n-type semiconductor, tin-oxide. This sensor is sensitive to alcohols and combustible gases and is used widely as a detector to monitor gas leakage. However, there are limits in many applications due to the lack of selectivity. Presently, a sensor must be tuned when several gases are to be detected. This paper presents data on the enhanced specificity of commercially available gas sensors using a combination of temperature cycling and multi-dimensional signal processing techniques. Sensor parameters include: 1) surface current and voltage, and 2) complex impedance. Our investigations generated a data bank with I-V/temperature and complex impedance/temperature surfaces for known mixtures of reducing gases. The application of neural networks as a pattern recognition technique allowed trace detection of the different gases chemisorbed on the surface of the semiconductor gas sensor. This approach allows the use of a single sensor instead of multi-sensor arrays for the detection of different reducing gaseous agents, eliminates problem calibration, and results in enhancement of sensor selectivity. Concomitantly, the cost of sensor operation in industrial multi-gas environments will be reduced.

10:40 am **TF-TuM8 Fabrication of Thin Sensing Films by MicroCVD**, Sanjeev Majoo, Johannes W. Schwank, John L. Gland\* and Kensall D. Wise†, Departments of Chemical Engineering,\* Chemistry, †Electrical Engineering and Computer Science, University of Michigan.

A novel CVD method for localized thin film growth on a microscale with an immediate application in chemical sensing is reported. Previously, films used in monolithic microelectronic gas sensors were fabricated by vacuum deposition. A drawback of this method is that many promising sensing film materials are incompatible with the final etch used in micromachining of the device. The new method overcomes this limitation by depositing films on completely fabricated devices lacking only the transducing film. Thermally-activated CVD is achieved on the heated, stress-relieved, micromachined dielectric window. The window has an area of  $350 \mu\text{m} \times 350 \mu\text{m}$ , and is  $1.3 \mu\text{m}$  thick. It is composed of layers of  $\text{SiO}_2$  (3000 Å),  $\text{Si}_3\text{N}_4$  (2000 Å) and  $\text{SiO}_2$  (7000 Å). A  $5 \mu\text{m}$  thick meandering boron-diffused heater under the window permits the window temperature to be varied between ambient and over  $1000^\circ\text{C}$ . This structure represents a micro-hotplate with excellent temperature uniformity and rapid thermal response. The device has four-point probe electrodes to measure resistance changes. These electrodes are already in place and operational prior to thin film deposition. Film growth occurs only on the heated region of the window and is monitored *in situ* using resistance measurements. End-point recognition is obtained by removing the heater current once a desired film resistance is reached. We illustrate microCVD of platinum (Pt) from tetrakisfluorophosphine platinum,  $\text{Pt}(\text{PF}_3)_4$ , and titanium dioxide ( $\text{TiO}_2$ ) from titanium isopropoxide,  $\text{Ti}[\text{OCH}(\text{CH}_3)_2]_4$ . The deposited films are extensively characterized *ex situ* using optical microscopy, spectrophotometry, ESEM/SEM and XPS.

11:00 am **TF-TuM9 Magnetoresistive Sensors for Ultra-High Density Magnetic Recording**, J. Kent Howard, IBM Storage Systems Division, San Jose, CA 95193.

Magnetic recording technology has been the dominant technology for information storage since the invention of the computer. Computer disk drives have doubled in areal density every 2.5 years for the past 40 years. The areal density in the state of the art disk drives approaches  $1 \text{ gigabit/in}^2$  ( $1 \text{ billion bits/in}^2$ ) since the introduction of the magnetoresistive read head sensor by IBM in 1991. This presentation will review the concept of magnetic recording, magnetoresistive head materials issues and the challenges to extend the magnetoresistive head to even higher areal densities. Recently, the discovery of a giant magnetoresistance effect in magnetic multilayer structures was announced. It is expected that the giant magnetoresistive effect can extend the read

head sensor technology to areal densities of  $10 \text{ gigabits/in}^2$  ( $10 \text{ billion bits/in}^2$ ). We will discuss the giant magnetoresistive effect and the different options for fabrication as well as the challenges for implementation.

INVITED

11:40 am **TF-TuM11 Object Imaging with a Piezoelectric Tactile Integrated Circuit Sensor**, Edward S. Kolesar and Craig S. Dyson, Texas Christian University, Department of Engineering, Electrical Engineering Laboratory, Fort Worth, TX 76129.

A two-dimensional, electrically-multiplexed tactile sensor has been realized by coupling a piezoelectric polyvinylidene fluoride (PVDF) polymer film to a monolithic silicon integrated circuit (IC). The IC incorporates 64 sensor electrodes arranged in a symmetrical  $8 \times 8$  matrix. A corresponding set of *in situ* high-input impedance metal-oxide-semiconductor field-effect transistor amplifiers are used to capture each taxel's pseudo steady-state response. With an electrical multiplexing circuit, the sensor's unprocessed data can currently be measured in approximately 100 microseconds. Off-line computational assets are used to generate a tactile object image. Each electrode occupies a  $400 \times 400 \mu\text{m}$  square area, and they are separated from each other by  $300 \mu\text{m}$ ; this taxel density is consistent with the tactile nerve density of a human adult. A  $40\text{-}\mu\text{m}$  thick piezoelectric PVDF polymer film was attached to the electrode array with an electrically non-conductive urethane adhesive. The response of the tactile sensor is linear for loads spanning 0.8 to 135 grams-of-force (gmf). The response bandwidth is 25 Hz, the hysteresis level is minimal, and, for operation in the sensor's linear range, taxel crosstalk is negligible. The historically persistent stability and response reproducibility limitation associated with piezoelectric-based tactile sensors has been resolved by implementing a novel pre-charge voltage bias technique to establish consistent pre- and post-load sensor responses. The pre- and post-load stabilization bias responses are used in concert with the sensor's response to a load, to generate a three-dimensional tactile object image. A rudimentary tactile object image measurement procedure for applied loads has been devised to recognize the silhouette of a sharp edge, square, trapezoid, isosceles triangle, circle, toroid, slotted screw, and cross-slotted screw.

## ELECTRONIC MATERIALS/MANUFACTURING SCIENCE AND TECHNOLOGY Room A108 - Session EMMS-TuM

### Surface Preparation and Passivation

Moderator: S. M. George, University of Colorado, Boulder.

8:20 am **EMMS-TuM1 Very High Quality Thin Gate Oxide Film Formation Technology**, Tadahiro OHMI, Tohoku University, Sendai, 980 JAPAN.

To realize highly reliable ULSI fabrication, the wafer surface should be free from: 1) Particle, 2) Organic contamination, 3) Metallic contamination, 4) Native oxide and 5) Surface micro-roughness. Qualities of ultrapure DI water, liquid chemicals and wafer cleaning technology have been drastically improved for last several years under the leadership of Tohoku University. Recently we found that once wafers are exposed to clean room air, organic materials adsorb on the wafer surface. This organic contamination degrades thin gate oxide integrity. However, organic contaminants on the wafer surface can be partly eliminated during a temperature ramp-up process by desorption or reaction with a little  $\text{O}_2$  in inert gas, which is commonly used to avoid pitting of wafer surface. However, oxide growth during a ramp-up process can not be neglected for deep submicron processes which requires ultra-thin gate oxide. Also a slower ramp-up rate is required for larger size wafers to reduce thermal stress that causes slip formation may enhance this problem. Therefore, the approach using a little  $\text{O}_2$  during ramp-up to protect wafer surface may not be applicable to deep submicron devices. In order to solve these problems, we propose the following approach. First, wafers are cleaned with ozonated ultra pure water and dried using a newly developed spin cleaner in an  $\text{N}_2$  ambient. This process provides a high quality pre-oxide without organic contamination. Then, the wafers are transported into an oxidation furnace in an  $\text{N}_2$  ambient. Finally, the wafers are ramp-up to an oxidation temperature in inert gases and oxidation is carried out

in a reductive ambient with H radicals. This approach can completely eliminate organic contamination and uncontrolled oxide growth and provide very high quality thin gate oxide. **INVITED**

**9:00 am EMMS-TuM3 STM/XPS Investigation on the Chemical Oxidation of Hydrogen Terminated Si(111) Surfaces, U. Neuwald, U. Memmert and R. J. Behm, Abt. Oberflächenchemie u. Katalyse, Universität Ulm, D-89069 Ulm, Germany.**

We used STM and XPS to investigate the chemical oxidation of hydrogen-passivated Si(111) surfaces in a variety of oxidizing media (air, 30% H<sub>2</sub>O<sub>2</sub>, conc. HNO<sub>3</sub>). Prior to oxidation, we prepared smooth and well ordered Si(111) (1 × 1)-H surfaces by etching in 40% NH<sub>4</sub>F solution. These samples were exposed to the different oxidizing media at room temperature for durations of up to one year. The thicknesses of the resulting thin oxide layers were determined by XPS. The geometrical interface structure was imaged by STM after selectively removing the newly grown oxide by a short dip in conc. HF.

Initially, oxide growth proceeds for all oxidizing media used in this study exclusively within the topmost Si(111) bilayer, via nucleation of homogeneously distributed 10–20 Å wide oxide patches. We found the oxidation of the first bilayer to be completed after 20 s in conc. HNO<sub>3</sub>, after 20 min in 30% H<sub>2</sub>O<sub>2</sub> and after 1 month in the case of humid air. In dry air the first layer was only partly oxidized even after 1/2 year.

The second Si(111) bilayer reacts much slower than the first layer. Interestingly, we found that for the second layer the oxidation rates are independent of the nature of the oxidant.

The oxide thickness vs. time curves, determined from both the XPS and the STM data, can be fitted assuming simple Langmuir adsorption kinetics for the first layer and field assisted oxidation according to the Mott-Cabrera mechanism for the subsequent growth of the second oxide layer.

**9:20 am EMMS-TuM4 An MEIS Study of the Initial Stages of the Interaction of Oxygen with Si(111)\*, E. P. Gusev, E. Garfunkel, H. C. Lu, and T. Gustafsson, Depts. of Chemistry and Physics, and Laboratory for Surface Modification, Rutgers University, Piscataway, NJ 08855.**

The question of whether the initial oxidation of silicon proceeds in a layer-by-layer fashion or through 3D islands is a matter of intensive debate. For example, recent STM experiments<sup>1</sup> were interpreted as supporting in-depth island oxidation at 600°C, starting at submonolayer coverages. We have used high resolution medium energy ion scattering (MEIS) with approximately monolayer depth resolution to investigate the growth mode. The width of the oxygen energy spectra during oxidation at 600–700°C is found to be nearly constant up to an oxygen coverage of ~3 ML (3 atoms per Si(100) unit cell). This fact suggests that the surface oxide does not grow deeper until the entire surface is covered by this surface oxide. This conclusion is also supported by results on Si atom displacements, as deduced from Si angular spectra. Above 3 ML, the oxygen energy peak gets broader, indicating oxidation in deeper layers. From our ion scattering experiments, we believe that the difference between submonolayer oxidation at 250°C and 600°C, observed previously by STM, is more likely due to differences in local stoichiometry rather than simply the oxygen depth distribution.

<sup>1</sup>Y. Ono, M. Tabe, and H. Kageshima, Phys. Rev. B 48, 14291 (1993).

\*Supported in part by NSF DMR 90-19868 and 93-06899.

**9:40 am EMMS-TuM5 Controlled Nitrogen-Atom Incorporation at Si-SiO<sub>2</sub> Interfaces by a Low-Temperature (300°C) Pre-Deposition Remote Plasma Oxidation Using N<sub>2</sub>O, D. R. Lee, and G. Lucovsky, Departments of Materials Science and Engineering, Electrical and Computer Engineering, and Physics, North Carolina State University, Raleigh, NC 27695-8202.**

Device-quality Si-SiO<sub>2</sub> structures can be formed by a two-step low-temperature (300°C) process that includes (i) formation of the Si-SiO<sub>2</sub> interface on a H-terminated Si surface by remote plasma-assisted oxidation, and (ii) deposition of an SiO<sub>2</sub> layer by remote PECVD [1]. The source gas for the oxidation step is O<sub>2</sub>; for the PECVD, they are N<sub>2</sub>O and SiH<sub>4</sub>. The oxidation step (i) removes residual C-atom contamination to a level of ~10<sup>12</sup> cm<sup>-2</sup> (SIMS), (ii) promotes formation of a low defect density Si-SiO<sub>2</sub> interface (D<sub>it</sub> ~ 1–3 × 10<sup>10</sup> cm<sup>-2</sup>·eV<sup>-1</sup>) that can withstand processing temperatures to ~900°C, (iii) forms ~0.5 to 0.6 nm of SiO<sub>2</sub> which serves as a platform for the oxide depositions, and (iv) prevents uncontrolled incorporation of N-atoms at the Si-SiO<sub>2</sub> interface during oxide deposition from N<sub>2</sub>O, thereby

preventing increases in D<sub>it</sub>. A similar process has been used with other remote PECVD dielectrics: silicon oxynitride alloys and SiO<sub>2</sub>/Si<sub>3</sub>N<sub>4</sub> composites. In this paper we describe a new process that replaces O<sub>2</sub> with N<sub>2</sub>O for the pre-deposition oxidation. The use of N<sub>2</sub>O does not degrade the effectiveness of this process in reducing C-atom contamination, but increases the interfacial N-content in a controllable way from ~1.5 × 10<sup>14</sup> cm<sup>-2</sup> to ~8.6 × 10<sup>14</sup> cm<sup>-2</sup>. C-V measurements on MOS capacitors using the O<sub>2</sub> and N<sub>2</sub>O processes showed that D<sub>it</sub>, and fixed charge (Q<sub>f</sub>) near the Si-SiO<sub>2</sub> interface were not degraded by the > five-fold increase of N-atoms, in fact D<sub>it</sub> levels decreased from ~1.5 × 10<sup>10</sup> cm<sup>-2</sup>·eV<sup>-1</sup> to ~1.0 × 10<sup>10</sup> cm<sup>-2</sup>·eV<sup>-1</sup>. Performance and stress data will be presented for MOS devices with 100 Å thick SiO<sub>2</sub> dielectrics fabricated on Si-SiO<sub>2</sub> interfaces formed by changing the O<sub>2</sub> to N<sub>2</sub>O ratio in the oxidation step, and thereby controlling the level of N-concentration at the Si-SiO<sub>2</sub> interface. Values of D<sub>it</sub> and Q<sub>f</sub>, and their stress dependences will be reported as functions of the N-atom concentrations (by SIMS) at the Si-SiO<sub>2</sub> interface.

[1] T. Yasuda, et al., Appl. Phys. Lett. 60, 434 (1992).

**10:00 am EMMS-TuM6 Silicon Oxide Etching using Gas Phase HF/solvent Mixtures, Anthony J. Muscat, A. Scott Lawing, Han Xu, and Herbert H. Sawin, Department of Chemical Engineering, Bldg. 66-225, Massachusetts Institute of Technology, Cambridge, MA 02139.**

Gas phase mixtures of anhydrous HF and solvent have the potential to replace liquid phase solutions for silicon oxide removal in wafer cleaning applications. Both water and alcohols have been shown to be effective solvents in the gas phase but their role in the etching reaction is incompletely understood. We have constructed an ultra-high vacuum compatible apparatus with a base pressure of 10<sup>-8</sup> Torr to study the contribution of various solvents in the etching of silicon oxide with anhydrous HF under well-defined conditions. Solvents were vaporized and introduced into the apparatus along with anhydrous HF in regulated amounts. The etching rate monitored *in situ* by ellipsometry was studied as a function of total pressure from 100 to 400 Torr and process temperature from 25 to 100 °C. A water or alcohol partial pressure of approximately five percent of its vapor pressure at the process temperature was found to be necessary to obtain good etch uniformity and control at etch rates in the range of 300 Å/min. Results will be presented showing the importance of the solvent in the etching of silicon oxide using anhydrous HF.

**10:20 am EMMS-TuM7 Ion Beam Characterization of Si(100) Surfaces During Wet Chemical Cleaning, V. Atluri, N. Herbots, P. Ye, and R. J. Culbertson, Dept. of Physics and Astronomy, Arizona State University, Tempe, AZ.**

This study is motivated by the development of low-temperature surface cleaning methods for Si. Epitaxial growth requires an initial surface that is ordered and as free as possible of contaminants such as C, O, or metallic impurities. Wet etching of Si by a solution of HF in alcohol after a modified RCA clean, has been shown to produce (1 × 1) H-terminated hydrophobic Si surfaces that are ordered at room temperature<sup>1,2</sup>. Our purpose is to measure in a quantitative fashion the removal of C and O, the H-coverage as well as residual disorder at the surface. Hydrogen is detected by the elastic recoil at 2.8 MeV, whereas, O and C are detected by nuclear resonance analysis (NRA) at 3.05 MeV and 4.265 MeV respectively. NRA is combined with ion channeling along the Si<111> direction to increase sensitivity to C and O as well as measure the surface peak to correlate it to surface disorder. Our results demonstrate that NRA for C and O combined with ion channeling can measure in a quantitative fashion, the change in C and O and H-coverage at the different steps of wet cleaning. For instance, the total amount of C on Si(100) sample decreases by a factor of 1.5 after the first step in the surface cleaning, by immersing in a solution of H<sub>2</sub>O:H<sub>2</sub>O<sub>2</sub>:NH<sub>4</sub>OH (4:1:1) at 80°C for 10 minutes, that is intended to remove hydrocarbon from the surface. The total amount of native oxide is found to increase by a factor of 2, while the H content of the oxide does not change.

1. P. J. Grunthaner, et al., Thin Solid Films, 183 (1989), 197–212.

2. Y. J. Chabal, et al., J. Vac. Sci. Technol. A 7 (3), May/June 1989, 2104–2109.

**10:40 am EMMS-TuM8 AFM Characterization of Pillar Structures on RCA Cleaned Silicon Surfaces, B. K. Furman, D. A. Neugroschl, S. L. Cohen, R. Tsai, K. Pope, M. Liehr, IBM T. J. Watson Research Center, P.O. Box 218, Yorktown Heights, NY 10598, S. Basiliere,**

S. Estes, M. J. Fleming, R. Gaylord, C. Gow, W. Syverson, IBM Microelectronic Division, Essex Junction, VT.

The combination of an HF etch and RCA clean is widely recognized as an effective cleaning process to remove metallic and particulate contamination from silicon wafers. Recently it has been observed that these cleaning processes may also cause nanoscale roughening of silicon surfaces and generate silicon pillars (spikes) and light point defects (LPDs), both potential yield detractors.

Atomic Force Microscopy (AFM) was used to measure these silicon features as a function of etching variables. This paper will discuss the role of process chemistry (temperature, pH, megasonics, time) and metallic contamination on pillar formation. Interestingly, in contrast to previous literature, pillar formation has been observed on both hydrophilic and hydrophobic wafers. Comparison of AFM features with conventional light scattering data will also be shown.

In addition to conventional post clean analysis data, we will also show in-situ AFM results which allow one to directing observe changes in surface morphology during a simulated cleaning process.

11:00 am **EMMS-TuM9 Low Damage Surface Cleaning of CdTe by Hydrogen ECR Plasma**, Yi Luo, Peter Lasky, Ming Chang Shih, and R. M. Osgood, Jr., Microelectronics Sciences Laboratories, Columbia University, New York, NY 10027.

We present a low damage, in-situ process for surface cleaning of CdTe semiconductor by hydrogen Electron Cyclotron Resonance (ECR) plasma. The hydrogen ECR plasma is generated by a 2.5 GHz microwave source operated at 25–30 W. The pressure in the ECR processing chamber is about  $5 \times 10^{-4}$  Torr. Surface cleaning of CdTe by Ar-ion sputtering has been reported, however it is known that the ion bombardment can cause surface damage. By using reactive hydrogen atoms generated in an ECR plasma with low kinetic energy to remove surface oxides, surface damage can be avoided. CdTe (110) single crystal surfaces were used in our experiments. X-ray photoelectron spectroscopy (XPS) and Auger spectroscopy are used to trace the change of the surface composition due to hydrogen ECR plasma processing. Low energy electron diffraction (LEED) is used to monitor the surface structure after cleaning. The Te(3d), Cd(MNN) and O(1s) XPS spectra show that at room temperature, a hydrogen ECR plasma can remove CdTe surface oxides effectively. We also present the results of the oxide reduction rate at various substrate temperatures. In addition, hydrogen ECR surface cleaning for both a native oxide and an oxide grown by oxygen ECR is discussed. The results of surface cleaning by hydrogen ECR are compared with those of Ar-ion sputtering and thermal desorption methods. Our results show that CdTe surface oxide can be grown and removed effectively by using ECR plasmas. This work is supported by National Science Foundation.

11:20 am **EMMS-TuM10 The Thermal Stability and Effect of Atomic Deuterium Exposure on S-Passivated InP(100)-(1 × 1)**, G. W. Anderson, M. C. Hanf and P. R. Norton, University of Western Ontario, London, Ontario, Canada and Z. H. Lu and M. J. Graham, National Research Council, Ottawa, Ontario, Canada.

Surface cleaning/passivation is a key step in semiconductor manufacturing processes, such as epitaxial overgrowth. For InP(100), the conventional approach has been to remove the native oxide by annealing at 820K. This technique cannot be utilized in some situations (ie. growth on a patterned surface) where the thermal budget is very low, as such high temperatures would destroy the initial structure. In this investigation we have examined the potential of S passivation in an aqueous (NH<sub>4</sub>)<sub>2</sub>S solution as a low temperature technique to produce InP(100) substrates suitable for further processing.

We have investigated the thermal stability and effect of atomic deuterium exposure on S-passivated InP(100) – (1 × 1). The S passivated surfaces are found to be thermally stable to ~700K where the samples begin to evaporate, giving rise to roughened surfaces displaying macroscopic In islands. Atomic deuterium exposure was observed to result in the removal of S from the surface. At elevated temperatures (>500K) a clean InP(100) – (4 × 2) reconstructed surface is formed, which shows a regular distribution of In islands. For samples held at 300 or 400K a D-terminated InP(100) – (1 × 1) surface is obtained, which shows the same morphology as the initial sample.

These results illustrate several potential methods for producing InP(100) substrates suitable for use in semiconductor manufacturing. Depending on the substrate requirements, S-passivation can be utilized to produce a S-terminated (1 × 1), D-terminated (1 × 1) or clean (4 × 2) InP(100) surface at low temperature.

11:40 am **EMMS-TuM11 Thermal Effects on GaAs(001) Surface Prepared by Deoxygenated and Deionized Water Treatment**, Y. Hirota, T. Ogino, \*Y. Watanabe, and \*M. Oshima, NTT Basic Research Labs, 3-1, Morinosato Wakamiya, Atsugi-shi, Kanagawa 243-01, Japan. \*NTT Interdisciplinary Research Labs, 3-9-11 Midori-cho, Musashino-shi, Tokyo 180, Japan.

Surface defects of GaAs degrade optical and electrical device characteristics such as efficiency of luminescence intensity and electron mobility. To prevent surface defects during cleaning process, we have recently proposed a new method based on electrochemical reaction. Deoxygenated and deionized water (DODIW) treatment, in extremely low concentration of dissolved oxygen (1 ppb), completely removes surface oxides and produces a passivation layer of elemental As and/or hydrogenated As on the surface due to the liberation of Ga atoms after removal of oxides.<sup>1</sup> After heating the DODIW treated-GaAs (001) and (111)B surfaces in high vacuum, RHEED observation shows spotty  $2 \times 4$  and  $3 \times 6$  surface reconstruction patterns,<sup>2</sup> and STM observation shows  $2 \times 2$  and  $\sqrt{19} \times \sqrt{19}$  structures, respectively.<sup>3</sup>

In the present study, we investigate the temperature dependence of surface Fermi level ( $E_F$ ) by using synchrotron-radiation photoelectron spectroscopy (SRPES) in ultra-high vacuum. SRPES reveals that the  $E_F$  for the DODIW treated n-type ( $8 \times 10^{16}/\text{cm}^3$ ) GaAs (001) surface lies at  $E_{\text{VBM}} + 0.9$  eV at room temperature, moves toward  $E_{\text{VBM}} + 0.6$  eV on heating to 500°C, and returns to near-flat-band position ( $E_{\text{VBM}} + 1.0$  eV) after cooling to room temperature. These results suggest that the changes in  $E_F$  is due to the reduction in density of surface state, which is achieved with the DODIW treatment. This is because the DODIW treatment is essentially a low energy process and the DODIW treated surface is initially passivated with excess elemental As and/or hydrogenated As layer.

<sup>1</sup>Y. Hirota, J. Appl. Phys., 75 (1994) 1798.

<sup>2</sup>Y. Hirota, Y. Homma, and K. Sugii, Sur. Sci. 60/61 (1992) 619.

<sup>3</sup>T. Fukuda, and Y. Hirota, J. Vac. Sci. Technol. B11 (1993) 1982.

## MANUFACTURING SCIENCE AND TECHNOLOGY

### Room A110 – Session MS-TuM

#### Manufacturing Overview and Environmental Issues

**Moderator:** G. W. Rubloff, North Carolina State University.

8:20 am **MS-TuM1 Environmental Consciousness: A Strategic Competitiveness Issue for the Microelectronics Industry**, Gregory E. Pitts, Director, Environmental Programs, Microelectronics and Computer Technology Corp. (MCC), 3500 W. Balcones Center Dr., Austin, TX 78759-5398, (512) 338-3790, (512) 338-3814, pitts@mcc.com.

The electronics industry has become increasingly aware of the need to develop a strategic approach to identify cost-effective, long-term solutions for environmental issues. Many organizations have invested resources to address environmental issues and business opportunities. As these efforts have evolved, it has become apparent that a strategic, coordinated approach for addressing environmental issues and business opportunities will help the electronics industries maintain a competitive edge in the international market and keep up with competitors who have long-range planning partnerships in the industry and government for addressing environmental issues. This paper will discuss several activities to develop a broad environmental strategy and solutions for priority environmental issues.

**INVITED**

9:00 am **MS-TuM3 Integrating Regulatory Policy & Science—Can It Be Done?** Bruce C. Jordon, Director, Emission Standards Division, MD-13, U.S. EPA, Research Triangle Park, NC 27711.

Regulatory activity within the United States is placing a heavy burden on industry. The economic consequences of government regulations have increased many fold in the last few years. Too often, industry has left in the hands of lawyers, and non-scientific oriented employees, or professional lobbyist its role in regulatory activity. Yet, within most industries lies the knowledge and capability to achieve the most cost-effective approach to meeting environmental objectives.

This presentation will review how industry and the academic community can take a more active role in regulation development. A review of the regulatory process for the Clean Air Act will be presented.

Examples where industry can and have become actively involved in regulation development will be discussed and results reviewed. Finally, the future of the relationship between the industry and regulator is outlined and options illustrated.

**9:40 am MS-TuM5 Environment, Safety and Health Issues in Manufacturing.**

One of the roadmaps in the National Technology Roadmap for semiconductor technology is the 15 year strategy for Environment, Safety and Health improvements in semiconductor chips and package manufacturing. Materials and process changes are a significant part of this strategy which will be discussed in this paper.

SEMATECH, a consortium of leading United States semiconductor manufacturers and ARPA, is a major implementor/facilitator of the national roadmap. The SEMATECH ESH program trends in semiconductor manufacturing and their relation to the national roadmap will be presented. **INVITED**

**10:20 am MS-TuM7 Factory of the Future: The "Whole Factory" View, Dr. Sam Harrell, Chief Strategy Officer, SEMATECH.**

The primary task of a semiconductor factory is to produce integrated circuits of outstanding performance at a steeply declining cost per electronic function delivered. The semiconductor industry over the next decade will need to continue to drive costs down in order to maximize manufacturing productivity in the climate of rising product complexity, equipment cost, and risk. Historically we have concentrated on aggressive yield improvement and declining wafer fab cost per  $\text{cm}^2$  as the dominant factors for increasing productivity. To continue to be competitive, SEMATECH is extending its focus beyond cost per  $\text{cm}^2$  to the more total view of cost per function. We are working toward a combination of solutions to meet our manufacturing challenges recognizing that no single solution will provide enough benefit to achieve the productivity gains end users expect. The "Whole Factory" View is a useful strategic planning tool for defining the future of manufacturing in the semiconductor industry. **INVITED**

**11:00 am MS-TuM9 Research Opportunities in Semiconductor Manufacturing Science and Technology, Daniel J. C. Herr, The Semiconductor Research Corporation, 79 Alexander Drive, Research Triangle Park, North Carolina 27709.**

This talk describes several opportunities for long-range research at the academic-industrial interface that could significantly impact future generations of semiconductor manufacturing technology. A vision for success is emerging within the semiconductor industry that calls for increased cooperation and collaboration in tackling critical precompetitive issues. This vision is driven by the need for leading-edge, high-performance, semiconductor-based electronics. It comprehends the importance of balancing the escalating cost, complexity, and sophistication of the research and development processes required to bring new science and technology to an environmentally conscious market place. The pressure to continuously shorten product and process research and development cycle times is engendering effective and innovative working partnerships between independent companies, government, and university R&D programs. These pioneering efforts have led to industry consensus on identifying several critical gaps and potential showstoppers on the path to future technologies. These recognized critical issues provide opportunities for long-term research that will increase fundamental understanding of chemical and physical processes, enable high-performance and robust technologies, and strengthen the supporting infrastructure of trained scientists and engineers. **INVITED**

**11:40 am MS-TuM11 Photocatalytic Oxidation for Point-of-Use VOC Abatement in Microelectronics Manufacturing, Mahbub Ameen, Ronnie Varghese, Jill Nico, and Gregory B. Raupp, Department of Chemical, Bio & Materials Engineering, Arizona State University, Tempe, AZ 85287-6006.**

In response to the Montreal Protocol of 1989, many microelectronics manufacturing firms are replacing chlorofluorohydrocarbons (CFCs) used in cleaning processes with volatile organic compounds (VOCs) such as acetone, isopropanol and glycol ethers. Although these solvents provide acceptable cleaning capabilities, these, as well as other VOCs, are on the 1990 Clean Air Act Amendments list of hazardous compounds. As a result, a threshold has been established for VOC emissions, forcing the industry to consider VOC abatement equipment to limit their emissions. We have recently initiated a research and development program aimed at establishing the commercial viability of gas-solid heterogeneous photocatalytic oxidation (PCO) for point-of-use abatement of VOCs in air streams. In PCO, VOCs present in

process or air vents can be rapidly and completely oxidized to innocuous byproducts over near-UV illuminated titanium dioxide thin film catalyst at room temperature. Photocatalytic oxidation appears to be well-suited to the special requirements of the semiconductor processing industry. In this paper we review these requirements in the context of the recently-published SIA roadmap. The specific requirements for VOC abatement from (i) a typical photolithography track, and (2) solvent cleaning stations are presented, as are bench scale PCO kinetics for target VOCs.

## **BIOMATERIAL INTERFACES**

**Room A106 - Session BI-TuM**

### **Protein-Solid Surface Interactions**

**Moderator:** B. D. Ratner, University of Washington.

**8:20 am BI-TuM1 Molecular Recognition at Protein-Biological Composite Interfaces, P. S. Stayton, R. Clark, C. L. Long, L. Klumb, A. Chilkoti, A. A. Campbell, G. Drobny, University of Washington, Seattle, WA 98195 and Battelle Pacific Northwest Laboratories, Richland, WA 99352.**

The Materials Science community has focused much recent attention on the way in which biological composites and ceramics are synthesized and processed. Biology provides many examples of exquisitely constructed hard materials, ranging from bone to seashell nacre, and "lessons from nature" may prove valuable in attempts to improve ceramic/composite processing strategies. In most known examples, proteins provide the molecular control necessary to control the hierarchical microstructure of composites with unparalleled specificity and structural resolution. Despite their well established importance, however, there is little known of the direct molecular recognition mechanisms used by protein surfaces to control the nucleation and growth of biological composites such as calcium oxalate and hydroxyapatite. We have utilized a combination of site-directed mutagenesis, functional characterization of protein-crystal interactions, and high-resolution structural analysis to elucidate molecular recognition processes at the protein-biological composite interface. These studies are providing a detailed molecular picture of the mechanisms utilized by proteins to control composite structure. The principles and rules defining biological composite engineering should be generally useful to materials scientists interested in improving ceramic engineering technologies. **INVITED**

**9:00 am BI-TuM3 Surface Plasmon Imaging of Biotin-Streptavidin Binding on UV-Photopatterned Alkanethiol Monolayers Self-Assembled on Gold, D. Piscevic, M. Tarlov\*, and W. Knoll, Max-Planck Institute for Polymer Research, Ackermannweg 10, D-6500 Mainz, Germany and \*National Institute of Standards and Technology, Gaithersburg, MD 20899.**

We report the surface plasmon imaging of UV-photopatterned alkanethiol self-assembled monolayers (SAMs) on gold and subsequent biomolecular recognition reactions on these surfaces. To photopattern the monolayers, a SAM of desired surface functionality is formed, irradiated with UV light through a mask, and then immersed in a solution containing a second alkanethiol molecule of different terminal functionality. Using this procedure, patterned monolayers are formed containing two regions of different surface properties with micron-scale features. Surface plasmon resonance was used to ascertain the effectiveness of the UV-photopatterning process by measuring changes in SAM thickness following UV exposure and immersion in a second alkanethiol solution. The binding of the protein streptavidin to biotin-terminated alkanethiols was used as the model biomolecular recognition system. The specific binding of streptavidin to the surface was maximized by using a mixed monolayer consisting of the biotinylated thiol diluted into a hydroxy-terminated SAM. A pure hydroxy-terminated monolayer was used to retard the non-specific binding of streptavidin to selected regions of the surface. In this talk the use of surface plasmon microscopy to detect and image in real time the binding of streptavidin to the patterned biotinylated SAM surfaces will be demonstrated. In addition, the potential use of surface plasmon microscopy for parallel addressing of biosensing and diagnostic arrays will be discussed.



9:20 am **BI-TuM4 Proteins at Surfaces Studied by Scanning Probe Microscopy**, C. J. Roberts, M. C. Davies, D. E. Jackson, K. M. Shakesheff, S. J. B. Tendler and P. M. Williams, The Laboratory of Biophysics and Surface Analysis, Department of Pharmaceutical Sciences, The University of Nottingham, Nottingham, NG7 2RD, UK.

The routine application of scanning probe microscopy (SPM) to the analysis of biomolecular structure and function is a goal sought by a number of laboratories. We have developed a number of widely applicable immobilization techniques to allow reproducible SPM imaging of proteins on a variety of substrates, including gold, mica and polystyrene. Here we will present molecular resolution data of biotinylated antibody-antigen complexes bound to polystyrene via a streptavidin linkage. Specifically the SPM data will compare a passively adsorbed antiferritin antibody to a biotinylated antiferritin antibody, both for surface coverage and functionality to the antigen, ferritin. To validate SPM data and to aid in its interpretation we commonly employ complementary biophysical techniques, and in this case we have used surface plasmon resonance to supply data on antibody and antigen adsorption rates to a polystyrene surface.

The biophysical and biomolecular information which may be retrieved from such data will be demonstrated by the observation of an approximate ten-fold increase in functionality of the biotinylated antibody bound *via* streptavidin to polystyrene as opposed to the antibody passively adsorbed to the polystyrene surface.

9:40 am **BI-TuM5 Plasma Protein Interactions with Solid Surfaces**, R. E. Marchant, C. Siedlecki and S. J. Eppell, Department of Biomedical Engineering, Case Western Reserve University, Cleveland, Ohio, 44106.

This presentation will review our recent studies directed towards understanding the nature of protein interactions with synthetic surfaces. We describe a molecular-level study by atomic force microscopy (AFM) of von Willebrand Factor (vWF) on hydrophilic and hydrophobic solid surfaces. vWF is large multimeric plasma glycoprotein, which is an important biopolymer involved in thrombus formation, particularly in areas of the vascular circulation where high shear stresses are prevalent. vWF is composed of extended linear chains, with a distribution of molecular weights ranging up to  $20 \times 10^6$ , making it the largest globular protein in plasma. In our early experiments on hydrated vWF deposited on mica and imaged by AFM, the protein molecules were easily swept across the surface by the lateral force applied by the probe tip. Removal of interfacial water by drying increased protein-surface adhesion and permitted molecular level imaging in air, in which the distinctive globular domains of vWF were resolved and analyzed. When vWF was studied by AFM on a hydrophobic surface of octadecyltrichlorosilane (OTS) self-assembled monolayer under phosphate buffered saline, strong protein-surface adhesion was observed. The self-assembled monolayer deposited on glass was sufficiently smooth to permit identification of adsorbed vWF. The frictional force between the adsorbed protein and the surface was sufficient to withstand an estimated applied lateral force of 19 nN, showing that vWF experiences strong interaction with a hydrophobic surface in aqueous media. This allowed repeated scanning by the AFM probe, and images of vWF on a submolecular scale were obtained. Statistical analysis of adsorbed vWF shows that the protein is composed of large globular domains with elliptical cross sections of average dimensions 56 nm (major axis) 26 nm (minor axis) and 2.8 nm (height). On the basis of our analysis of the globular domains, a model describing the three-dimensional structure of vWF dimer adsorbed on a hydrophobic surface in a physiological solution will be presented.

INVITED

10:20 am **BI-TuM7 The Effect of Oligo(ethyleneoxide) Chain-length on the Protein Resistance of Plasma Deposited Thin Films**, B. D. Ratner, E. E. Johnston, U. of Washington, Seattle, WA 98195.

There is an established need in industry for surface coatings which resist fouling by organic macromolecules and bacteria. Poly(ethylene oxide) (PEO) films have been recognized in the biomaterials literature as having desirable protein- and cell-resistant properties. Radio frequency plasma deposition of oligo(ethylene oxide) monomers create molecularly smooth PEO-like thin films on a variety of substrates from the gas phase. IA project was undertaken to learn whether plasma-deposited longer oligo(ethyleneoxide) chains improve the protein resistance of the films. Films were prepared on glass substrates by RF-plasma deposition of monomers containing from 2 to 12 ethyleneoxide units in a tubular, capacitively-coupled reactor. Depositions were performed under controlled pressure and flow, graduating the deposition power to enhance film adhesion. Film thickness, roughness, composition and surface energy were subsequently characterized by AFM,

XPS, SSIMS, and contact angle goniometry. The protein-resistance of the film was determined by I-125 radiolabeled fibrinogen adsorption. Partial least squares modelling was performed to determine whether protein resistance could be correlated to oligo(ethylene oxide) fragment length in the mass spectra of the films.

10:40 am **BI-TuM8 Bioreactivity of Titanium Implant Alloys**, Susan J. Kerber, Material Interface Inc., Sussex, WI 53089-2244.

A study was conducted regarding the adsorption of peptides on cp-Ti and Ti-6Al-4V. The peptides used were arginine-glycine-aspartic acid-alanine (RGDA), arginine-glycine-aspartic acid-serine (RGDS), and arginine-phenylalanine-aspartic acid-serine (RFDS). The tripeptide RGD is known to be important for biologically specific adhesion reactions. This research was conducted to investigate the reason for a tendency toward thrombus formation with Ti-6Al-4V that is not observed with cp-Ti. After argon plasma cleaning, coupons of the titanium alloys were inserted into solutions with variable concentrations (0.0625 mg/ml to 2 mg/ml) of an individual peptide group under constant temperature and time conditions. The samples were rinsed, dried, and analyzed with x-ray photoelectron spectroscopy (XPS). Adsorption isotherms were obtained by plotting the relative amount of peptide adhesion as a function of solution concentration. It was determined with XPS that the major adhesion mechanism for the peptides to the titanium alloys was hydrogen bonding. CP titanium and Ti-6Al-4V were hypothesized to react differently as implants because Ti-6Al-4V has a more electropositive surface which allows fewer hydrogen bonds to form. Hydrophilic reactions were of secondary importance during bioadhesion, influencing the structure of the second layer adsorbed. There was no correlation found between the net charge of the peptide groups and their adhesion to the alloys.

11:00 am **BI-TuM9 Electrochemically and Glow Discharge Modified Titanium Surfaces Used for Biological Evaluation**, B.-O. Aronsson, J. Lausmaa, M. Rodahl, and B. Kasemo, Chalmers University of Technology and University of Göteborg, 412 96 Göteborg, Sweden.

Titanium is a suitable model material for studying how different surface properties influence biological response since; (i) it is a commonly and successfully used biomaterial, and (ii) its surface properties can be varied over a wide range. In this work we have used differently prepared titanium surfaces for studying how protein adsorption in vitro and bone response in vivo is influenced by different structural and chemical properties.

Electrochemical methods and glow discharge plasma methods were used for preparing Ti surfaces with varied surface structures, oxide thicknesses, and/or surface compositions. Characterisation of the prepared samples was done by AES, XPS, AFM, SEM, and FT Raman spectroscopy. Enzymelinked immunosorbent assay (ELISA) was used to measure the amount of proteins (fibrinogen and albumin) adsorbed onto the surfaces. Screw shaped Ti samples were implanted in rabbit bone and, after different time periods, retrieved and sectioned for bone histomorphometry analysis.

Electrochemical preparation results in a titanium dioxide (TiO<sub>2</sub>) surface layer of different thickness (4–200 nm). Glow discharge treatment results in either a TiO<sub>2</sub> (thickness 2–300 nm) or a nitride (TiN<sub>x</sub>, thickness 2–7 nm) surface layer depending on the gas (O<sub>2</sub> or N<sub>2</sub>) and other discharge parameters. On top of the surface there were always a contamination layer, in most cases consisting of mainly hydrocarbons.

The results of the protein adsorption and bone response studies will also be summarized and discussed.

11:20 am **BI-TuM10 Molecular Machining by Enzymatic Modification of a Chemisorbed Lipid Monolayer**, Brian M. Peek, Thomas E. Wertz, David C. Turner, Douglas D. Archibald, Deborah Leach-Scampavia<sup>2</sup>, and Bruce Paul Gaber, Center for Bio/Molecular Science and Engineering, Code 6900, Naval Research Laboratory, Washington, DC 20375 and <sup>2</sup>National ESCA and Surface Analysis Center for Biomedical Problems, University of Washington, Seattle, WA 98185.

We wish to combine the nanometer-scale control of the atomic force microscope (AFM) with the specificity of enzyme chemistry. An enzyme on the tip of an AFM cantilever could be used to write a pattern on a surface modified with the enzyme's substrate. Ideally, this could allow the creation of patterns with molecular resolution. Thus, we have modified silicon wafers with an amino-terminal silane (EDA), and attached a carboxylic acid derivative of dimyristoylphosphatidylcholine (DMPC) to create an immobilized lipid monolayer. The resulting lipid layer, characterized by AFM, electron spectroscopy for chemical analysis (ESCA), and ellipsometry, was also treated with phospholipase C (PLC), the enzyme which catalyzes the cleavage of

the glycerol-phosphate ester bond of the lipid headgroup. Analysis of the resulting surface, by the above methods, shows that the enzyme modified the immobilized lipid layer. We are currently examining different methods to immobilize PLC on a surface in an oriented fashion while retaining full enzymatic activity.

11:40 am **BI-TuM11 Static Secondary Ion Mass Spectrometry Study of Amino Acids on Acidic and Basic Polymer Surfaces**, *S. Kovatch, Y. Kim, E. Bekos, J. A. Gardella Jr.*, State University of New York at Buffalo, Buffalo, NY 14214.

Characterization of adsorbed proteins on polymer surfaces is an important step in the development of new biomaterials. Static SIMS is one tool used to gain information on the adsorbed chemical species,

and has successfully been employed for analysis of polymers on metal substrates. In order to apply SSIMS to protein analysis on polymer surfaces, an understanding of the secondary ion emission of proteins is essential. In developing a protocol to study these systems, we have chosen to investigate a more fundamental system: the adsorption of amino acids on polymer surfaces. Adsorption on chemically modified polystyrene sulfonic acid and poly aminostyrene is used to investigate the effect of surface acidity or basicity on the secondary ion yields of phenylalanine and tyrosine. These results are compared to previous work on polycrystalline metals.<sup>1</sup>

<sup>1</sup>L. M. Jirikowsky and A. Benninghoven, *Surf. Sci.* 136 (1984) 419.  
A. Benninghoven, D. Jaspers and W. Sichtermann, *Appl. Phys.* 11 (1976) 35.



## SURFACE SCIENCE

Room A205 - Session SS1-TuA

### Dynamics and Kinetics of Surface Processes

**Moderator:** D. C. Jacobs, University of Notre Dame.

2:00 pm **SS1-TuA1 Dynamic of the Interaction of O Atoms with O<sub>2</sub>/Pt(111), C. T. Rettner, J. Lee, and D. J. Auerbach**, IBM Res. Division, 650 Harry Road, K33/801, San Jose, CA 95120.

Exposing an <sup>18</sup>O<sub>2</sub>-covered Pt(111) surface to a beam of <sup>16</sup>O atoms at a surface temperature,  $T_s$ , of 80 K yields a prompt <sup>16</sup>O<sup>18</sup>O product. In addition, <sup>18</sup>O<sub>2</sub> molecules are displaced from the surface. In both cases, the nascent O<sub>2</sub> leaves the surface with a bimodal velocity distribution that is clearly different from that obtained for laser-induced thermal desorption. We find no evidence for O<sub>3</sub> leaving the surface. The <sup>16</sup>O<sup>18</sup>O product is attributed to a simple chemical reaction. The <sup>18</sup>O<sub>2</sub> product appears to result from a new desorption mechanism in which the adsorbate is directly displaced by the incident species. In this latter case, the desorbed molecule must carry away part of the adsorption energy of the incident O atom. Photodesorption at 213 nm gives a velocity distribution that is identical to that for the displacement reaction, indicating that the desorbed molecules are actually displaced by photofragments at this wavelength, rather than being directly photoejected. Our findings also provide insight into the mechanism of the thermal desorption and dissociation of O<sub>2</sub> on Pt(111), which occur simultaneously at  $T_s \sim 150$  K. The fact that the velocity distribution for thermal desorption is different from that for displacement by O atoms indicates that desorption must precede dissociation in this system.

2:20 pm **SS1-TuA2 O<sub>2</sub> Adsorption on Silver Surfaces, F. Buatier de Mongeot, M. Rocca and U. Valbusa**, CFSBT-CNR and INFN, Dip. di Fisica, via Dodecaneso 33, 16146 Genova, Italy.

We have studied the interaction of O<sub>2</sub> with Ag(100) and Ag(111) with a supersonic molecular beam to investigate the dependence on crystal face and temperature of the sticking probability  $S$ , which was measured both by using the method of King and Wells, and by evaluating the derivative of surface coverage versus exposure via EELS measurement [1].

For Ag(111) at  $T_s = 100$  K the initial sticking coefficient  $S_0$  is lower than our experimental sensitivity of  $2 \cdot 10^{-6}$ . For longer exposures we find that the coadsorption of H<sub>2</sub>O originating from the background of the vacuum chamber (base pressure  $\approx 10^{-11}$  mbar) induces the formation of OH. We find no evidence for the presence of adsorbed superoxydic oxygen, in contrast with literature [3], neither for the clean surface, nor in presence of H<sub>2</sub>O contamination as the observed losses can be assigned to H<sub>2</sub>O.

The reactivity of Ag(100) towards oxygen is comparable with the one of Ag(110), recorded in our laboratory [3]. For molecular adsorption we find  $S_0 = 0.5$  at  $T_s = 100$  K,  $E_i = 0.65$  eV and normal incidence.  $S_0$  depends strongly on surface temperature, showing an abrupt decrease above the dissociation temperature of 200°K. Preliminary data indicate that low temperature molecular adsorption follows normal energy scaling, while dissociative adsorption follows nearly total energy scaling. Such a behaviour is observed for the first time to our knowledge.

[1] M. Rocca, U. Valbusa, A. Gussoni, G. Maloberti and L. Racca, Rev. Sci. Instrum. **62**, 2172 (1991).

[2] A. F. Carley et al., Surf. Sci. Lett. **238** (1990) L467.

[3] L. Vattuone, C. Boragno, M. Pupo, P. Restelli, M. Rocca and U. Valbusa, Phys. Rev. Lett. **72**, 510 (1994).

2:40 pm **SS1-TuA3 CO<sub>2</sub> Sticking on Pt(111): The Role of Kinetic Energy and Internal Degrees of Freedom, Dmitri Kulginov\*, Mats Persson, Claes Åkerlund, Igor Zoric and Bengt Kasemo**, Department of Applied Physics, Chalmers University of Technology, 412 96 Gothenburg, Sweden.

The characteristic features of CO<sub>2</sub> adsorbed on Pt(111) include low energy intramolecular vibration (80 meV) and a probable free rotation of the adsorbed molecule. This system is suitable for studies of the role of internal degrees of freedom on the sticking process. We have

carried out measurements of nondissociative sticking coefficient,  $S_0$ , of CO<sub>2</sub> on the Pt(111) surface as a function of incident kinetic energy,  $E_k$ , ( $60 \text{ meV} < E_k < 1.2 \text{ eV}$ ) at different incident angles. The observed features include a high initial sticking coefficient of 0.6 at 60 meV which declines sharply with increasing incident energy to  $S_0 \approx 0.2$  at 0.4 eV followed by a slow decline towards a value of  $S_0 \approx 0.1$  at highest measured energy independent of the incident angle. Such a behavior, unexpected for a physisorption system (the binding energy of CO<sub>2</sub> on Pt(111) is  $\approx 0.2 \text{ eV}$ ) suggests an important role of the intramolecular degrees of freedom in the sticking process. Simple modeling based on a soft cube model shows that the main features of the observed behavior may be rationalized in terms of rotationally mediated sticking, while the effect of the intramolecular vibrations is negligible. In addition, a more realistic modeling of the energy transfer to phonons via rotations will be presented based on classical trajectory studies of a rotating rigid molecule scattered from a slab of substrate atoms.

\*Permanent address: Institute of Interphase Interactions, POB 1146, St. Petersburg 194291, Russia.

3:00 pm **SS1-TuA4 Investigations of the Adsorption and Desorption Dynamics of D<sub>2</sub> at Si Surfaces, Kurt W. Kolasinski**, Fritz-Haber-Institut der Max-Planck-Gesellschaft, Faradayweg 4-6, D-14195 Berlin, Germany.

Adsorption and desorption in the hydrogen/Si system have been investigated by means of supersonic molecular beam and laser techniques. The dependence of the molecular D<sub>2</sub> sticking coefficient,  $S$ , on surface temperature,  $T_s$ , and nozzle temperature,  $T_n$ , has been measured. The sticking coefficient increases with both increasing  $T_s$  and increasing  $T_n$ . This directly demonstrates for the first time that hydrogen adsorption on Si is activated. The increase in the effective sticking coefficient with  $T_s$  shows that surface excitations play an important role in the reaction dynamics. An attempt is made to formulate a unified description of the reaction dynamics. The role of surface configurations in the dynamics and their interpretation within a Marcus-like theory will be discussed.

3:20 pm **SS1-TuA5 Probing Reactive Deposition and Surface Dynamics Using In Situ, Real-Time Emission Microscopy, Martin E. Kordes**, Ohio University, Athens, OH 45701.

Emission microscopy is one of the oldest forms of electron microscopy. The images obtained are direct maps of the surface electron yield under illumination by various sources, including light from UV to soft x-rays, low energy electrons, ions, energetic neutral atoms, and thermionic and field emission. The image composition is a complex combination of sample topography, surface electron yield, and microscope design. Ultraviolet and soft x-ray Photoelectron Emission Microscopy (PEEM) images of surface processes during chemical vapor deposition and atomic layer epitaxy of diamond show a number of reaction phenomena that illustrate the problems suitable for observation with the emission microscope: nucleation of adsorbed layers, adsorbate controlled diffusion from the bulk, pattern formation, melting and the evolution of topographical features during "reverse growth". Neutral impact images of layers deposited using a seeded molecular beam will be presented, as well as examples of surface dynamics on Mo and Diamond surfaces.

INVITED

Work supported by NATO and the ONR-BMDO.

4:00 pm **SS1-TuA7 Simulation of Complex Reaction/Desorption Kinetics Using a Simple Stochastic Method, F. A. Houle and W. D. Hinsberg**, IBM Research Division, Almaden Research Center, San Jose, CA 95120.

We describe a computational approach which allows realistic, quantitative models of temperature programmed desorption kinetics to be devised from experimental data. It is based on the exact stochastic solution to the master equation described by Bunker and Gillespie, modified to simulate reactions under the influence of arbitrary time-temperature profiles. It is well-suited to modelling many types of adsorbate systems, including those with attractive and repulsive inter-adsorbate interactions, and those which undergo phase transitions and chemical reactions in competition with desorption. By combining stochastic simulations with experiment, it is possible to access the wealth of information on surface kinetics and instantaneous coverages con-

tained in temperature programmed reaction and desorption data for even quite complicated systems. Examples of simulations of CO reaction and desorption on several transition metals will be described. The characteristics of models built using this method will be discussed, including their extension to include adsorption kinetics. The main features will be compared to those obtained using analytic functions and Monte Carlo simulations of adsorbate systems.

4:20 pm **SS1-TuA8 Dynamics of Collisions Between Inert Gases and the Surfaces of Liquid Metals**, *Gilbert M. Nathanson, Warren R. Ronk, D. V. Kowalski*, Department of Chemistry, University of Wisconsin, Madison, 53706-1322.

We are bouncing gases off the surfaces of liquid metals and alloys in order to probe the microscopic stiffness and roughness of the surfaces of atomic liquids. In these experiments, a nearly monoenergetic beam of gas atoms is directed at a liquid metal, and the energy of the scattered gas is monitored by mass spectrometry using time-of-flight velocity analysis. The gases chosen for these experiments are the inert atoms He, Ne, Ar, and Xe. Metals included in the study are liquid gallium, indium, and the In/Ga eutectic. Due to large differences in the surface tensions of Ga and In, the top layer of In/Ga is enriched in indium, while the subsurface layers are enriched in gallium. By comparing the In/Ga alloy with pure In and Ga, we can begin to understand the roles of surface and subsurface atoms in controlling energy transfer between atomic gases and atomic liquids.

4:40 pm **SS1-TuA9 Interactions Between Coadsorbed Molecules**, *D. C. Skelton, D.-H. Wei, S. D. Kevan*, Department of Physics, University of Oregon, Eugene, OR 97403.

The energetic interactions between adsorbed atoms and molecules govern a diverse array of finite coverage surface phenomena ranging from formation of ordered overlayers to growth of thin films to determination of reaction pathways. Several groups have combined adsorption and desorption isotherm measurements with a quasiequilibrium analysis to probe the interaction potential between identical adsorbed molecules. We will report experiments which extend these efforts to coadsorption of CO with NO or NH<sub>3</sub> on Pt(111) and Ni(111). Using time-resolved EELS coupled to pulsed molecular beam dosing, we have measured the low coverage desorption rate constant of, e.g., NO, as a function of CO coverage. We thus can isolate the CO-NO lateral interaction energetics from the simultaneous complexity of NO-NO interactions. We find that some systems exhibit kinetic compensation characterized by compensation temperatures as high as ~350K, while other systems do not exhibit significant compensation. Prior results from single-adsorbate systems implies a substantially attractive lateral potential energy well in the former but not the latter type of system. We employ the lattice gas approximation and extend the currently-popular transfer matrix approach to quantify this conclusion. While the interactions are statistically coupled, we find a direct and nearly linear relationship between the magnitude of the attractive lateral well and the compensation temperature. We discuss these attractions in terms of residual gas phase potential energy surfaces and through-surface interactions which arise from screening of the adsorbed molecules.

5:00 pm **SS1-TuA10 A New Technique to Measure Surface Diffusion with the STM**, *M. L. Lozano, M. C. Tringides*, Department of Physics and Astronomy, Iowa State University—USDOE, Ames Laboratory, Ames, IA 50011.

We present preliminary results on a new technique using the STM to characterize surface diffusion. The time dependence of the tunneling current is analyzed through its spectral density. The spectra of clean, stepped Si(111) shows no temperature dependence. If  $\Theta \sim 0.3$  ML of oxygen is dosed onto the surface, broadening of the spectra with temperature is observed, indicating adatom mobility. The data agree with theoretical work<sup>1</sup> which indicates that the power spectrum of the tunneling current when adsorbates move on the surface takes the form  $W(f) \sim \ln(f)/D$ ,  $f \rightarrow 0$ . It is also shown with Monte Carlo simulations that this form is characteristic of single-diffusion processes. When simultaneous diffusion on the surface and on the tip is simulated a different power spectrum dependence is observed, so most likely only diffusion on the Si(111) surface is probed. These measurements demonstrate that the STM can be used in "real-time" to measure diffusion coefficients on surfaces.

<sup>1</sup>Sumetskii and Kornyshev, in press.

\*Ames Laboratory is operated for U.S. Department of Energy by Iowa State University under Contract No. W-7405-ENG-82.

## SURFACE SCIENCE

### Room A201 - Session SS2-TuA

#### Nucleation and Growth: Metals

**Moderator:** D. M. Zehner, Oak Ridge National Laboratories.

2:00 pm **SS2-TuA1 STM Studies of Curvature Driven Mass Flow on the Au(111) Surface**, *J. G. McLean, D. R. Peale, and B. H. Cooper*, Dept. of Physics, Cornell University, Ithaca, NY 14853.

We have observed mass flow on the Au(111) surface at room temperature using time-lapse sequences of STM images. In these sequences, layered nanoscale nonequilibrium structures decay in size and highly curved monatomic step edges become less curved [1]. This behavior suggests mass flow driven by curvature and mediated by adatom movement both across the terrace and along step edges. Further, this behavior is strongly dependent on conditions at the surface; for instance, the mass flow can be greatly enhanced by the presence of adsorbates.

Based on earlier works [2], we have developed a macroscopic, thermodynamic theory of mass flow driven by step edge curvature which is consistent with the temporal behavior of the observed decay. This theory suggests that adatom attachment and detachment at step edges is the controlling step in the mass flow. Ongoing Monte Carlo solid-on-solid simulations have successfully reproduced consequences of step edge curvature as predicted by the macroscopic theory. These simulations are being used to probe the connection between the thermodynamic and atomistic explanations for the experimentally observed behavior.

[1] D. R. Peale and B. H. Cooper, *J. Vac. Sci. Tech.*, **A 10**, 2210 (1992).

[2] e.g. C. V. Thompson, *Acta metall.*, **36**, 11, p. 2929 (1988).

This work supported by F49620-93-1-0504 and the Cornell Materials Science Center (NSF-DMR-9121654).

2:20 pm **SS2-TuA2 Apparent Giant Appliance of Small 2D Ag Islands on Ag(100)**, *P. Bedrossian<sup>1</sup>, B. Poelsema<sup>2</sup>, G. Rosenfeld, L. Jorritsma<sup>2</sup>, N. N. Lipkin, and G. Comsa*, IGV-Forschungszentrum Jülich, Germany. Permanent Addresses: <sup>1</sup>Lawrence Livermore National Laboratory, Livermore, CA; <sup>2</sup>University of Twente, Enschede, The Netherlands.

Rocking curves acquired with Thermal Energy He-Atom Scattering (TEAS) indicate a giant contraction of small, homoepitaxial, 2D Ag islands on Ag(100) normal to the surface, reaching 25% at 180K but vanishing at room temperature, for 1/2 ML coverage. In contrast, high resolution SPA-LEED measurements reveal no corresponding normal relaxation of atoms within the islands. The apparent discrepancy between the LEED and TEAS data can be reconciled by attributing the anomaly observed in TEAS to a smoothening of the electronic corrugation (Smoluchowski effect), which is probed by the He atoms, for small, densely-spaced islands. The dependence of the magnitude of the effect on growth temperature indicates that it is related to the size and separation of the Ag islands and is most pronounced for a high density of small islands, as would occur with 1/2 ML coverage at low temperatures. At 180K, SPA-LEED data indicate that these islands typically consist of 20-40 atoms.

P.B. and NNL were supported by the Alexander von Humboldt Foundation. PB was also supported by Lawrence Livermore National Laboratory, under the auspices of the US Dept. of Energy, under Contract W-7405-Eng-48.

2:40 pm **SS2-TuA3 A RHEED Specular Diffraction Spot Intensity Study of Ag(111) Homoepitaxy**, *K. Roos<sup>1</sup>, K. Stanley<sup>2</sup>, C. Papageorgopoulos<sup>3</sup>, M. C. Tringides<sup>2</sup>*, <sup>1</sup>Bradley U.; <sup>2</sup>Iowa State U.; <sup>3</sup>U. of Ioannine, Greece.

The homoepitaxial growth of Ag on Ag(111) was studied as a function of substrate temperature and the flux rate using RHEED. The decay in the intensity of the specularly diffracted beam was observed. This allows probing the film morphology at low coverages ( $\theta < 0.2$ ), necessary to test the scaling theory of nucleation. Surprisingly, the intensity as a function of coverage,  $I(\theta)$ , did not noticeably depend on the flux rate, but varied significantly with temperature. Flux rates between 1/30 and 1/3000 monolayers/sec and temperatures from 150 to 310K were used.

Our results are not consistent with the temperature and flux independent  $I(\theta)$  predicted by the kinematic approximation which is based

solely on the interference of the reflections from different levels. If instead, the step density is assumed to be dominantly responsible for the intensity decay, an activation energy and growth exponents  $x$ ,  $y$  for the island density,  $N \approx (F/D)^{x+y}$ , can be extracted. The results do not agree with simple nucleation theory which for irreversible growth predicts the island density to have the same dependence on temperature as it does on the flux rate. Results from Monte Carlo simulations will also be presented supporting the scaling of the step density vs. flux and temperature in model systems.

\*S. Clarke & D. D. Vvedensky, J. Appl. Phys. **63** (1988) 2272.

3:00 pm **SS2-TuA4 Enhanced 2-Dimensional Growth of Cu on Cu(100) by Seeding**, Anna K. Swan and John F. Wendelken, Oak Ridge National Laboratory, \* Oak Ridge, TN 37831-6057.

Typical growth experiments are performed at temperatures and flux rates far from equilibrium, where kinetic effects determine the growth behavior. Therefore, the diffusion rate and deposition rate determine the island density distribution in the submonolayer regime. For layer-by-layer growth to occur, atoms landing on top of islands have to be transported to the lower terrace before nucleation takes place on the top layer. This interlayer mass transport depends on both the "step down" activation barrier and the island density.<sup>1</sup> In this work, the role of the island density and the step down barrier are examined independently with high-angular resolution low-energy electron diffraction. At a given temperature, the surface is seeded at a high flux,  $F_1$ , producing a high-island density with an average island separation,  $S_1$ . Growth is then continued at a lower rate  $F_2$ , which on the unseeded surface would produce a larger average island separation  $S_2$ . The degree of 2-dimensional growth of the first layer is determined by monitoring the specular intensity in out-of-phase condition as a function of coverage. An increase of the ratio of the intrinsic length scales,  $R = S_2/S_1$  enhances the 2-dimensional growth. Using the same length scales at different temperatures, the effect of the step down barrier is examined. The work is performed in a temperature region where the critical nucleation size is a dimer<sup>2</sup> and where the islands retain a compact square shape.

1. G. Rosenfeld et al., Phys. Rev. Lett. **71**, 895 (1993).

2. H. Dürr et al., submitted.

\*Research sponsored in part by the Division of Materials Sciences, U.S. Department of Energy, under contract DE-AC05-84OR21400 with Martin Marietta Energy Systems, Inc.

3:20 pm **SS2-TuA5 Kinetic Roughening in a Multilayer Nucleation and Growth Model for M/M(100) Homoepitaxy**, M. C. Bartelt and J. W. Evans, Iowa State University, Ames, IA 50011.

We analyze kinetic roughening in a realistic model for metal/metal(100) homoepitaxial thin film growth, where nucleation and growth of near square islands occurs with critical size  $i = 1$  in each layer, and where a key additional parameter is the Schwoebel barrier for downward interlayer diffusive transport. This model applies to, e.g., Fe/Fe(100) homoepitaxy, where it has been shown to reproduce full size and separation distributions observed for submonolayer growth between 290 and 500K<sup>1</sup>. We obtain and elucidate the experimentally observed crossover from a split diffraction profile for ultra-thin films to the non-split scaled form of Yang et al.<sup>2</sup> for thicker films. We also examine the effective exponent,  $\beta$ , describing roughening of the film. At least for lower temperatures, we argue that modeling and interpretation of roughness and  $\beta$ -values requires realistic treatment of nonuniversal features of the growth process such as crystal geometry, deposition dynamics, and island separation and structure, and illustrate this point with the example of Cu/Cu(100). Control of interface roughness through modulation of deposition flux or substrate temperature is also explored.

<sup>1</sup>Strosio and Pierce, Phys. Rev. B **49**, 8522 (1994); Bartelt and Evans, Surface Sci. **298**, 421 (1993).

<sup>2</sup>Yang, Lu and Wang, Phys. Rev. Lett. **68** 2612 (1992).

This work was supported by NSF Grant CHE-9317660.

3:40 pm **SS2-TuA6 First-Principles Calculations of Transition-Metal Surface Stress**, Peter J. Feibelman, Sandia National Laboratories, Albuquerque, NM 87185-0344.

Despite their fundamental role in crystal growth morphology, absolute surface stress are not yet measured directly. Values are extracted from surface phonon spectra, via use of empirical elastic models.<sup>1</sup> To

provide a reliable foundation for intuition and to help improve surface-phonon analyses, I have developed a novel first-principles method to compute surface stress, and applied it to several Group VIII metal crystal faces. For the anisotropic Pd(110) surface, I obtain (001) and (110) tensile stresses of 0.10 and 0.16 eV/Å<sup>2</sup>. The (001) stress is expected to be smaller because surface relaxation reduces the tension in the first to second layer bonds. This, however, disagrees with the ordering of the results for Ni(110)<sup>1</sup> based on a central-force model.<sup>2</sup> In that case, analysis of surface phonon data yields the counter-intuitive result that the stress in the (001) direction is larger by a factor of two than in the (110) direction. \*Work supported by the U.S. Department of Energy under Contract DE-AC04-94AL85000.

<sup>1</sup>See, e.g., S. Lehwald, et al., Surf. Sci. **192**, 131 (1987).

<sup>2</sup>This model works surprisingly well for Ni(110), but not perfectly. See M. Balden, et al. Phys. Rev. **B46**, 4172 (1992).

4:00 pm **SS2-TuA7 Strain Induced Alloying of Immiscible Metals in Thin Film Systems**, J. L. Stevens and R. O. Hwang, Sandia National Laboratories, Livermore, CA 94550.

The influence of stress induced by lattice mismatch in thin film superlattice systems is known to influence the interface structure greatly. In multi-component overlayer systems, the different stresses acting on the film constituents alter their mutual interactions and can lead to drastic departures from their bulk phase diagrams. We have investigated these effects in the growth and structure of the thin film systems of Ag/Cu [1] and Ag/Co on Ru(0001) using scanning tunneling microscopy. Due to the opposite signs of the lattice mismatch of the substrate with the respective film components, mixing of the overlayer metals is found despite their bulk immiscibilities. New two dimensional alloys of specific stoichiometry are stabilized. By studying the details of the morphology and composition of the resulting films, the driving mechanism for this behavior can be attributed to strain relief. Furthermore, domain formation of the various phases is observed which can also be understood in terms of strain relief. Such effects are expected to play a central role in the formation of interfaces in superlattice systems and could also lead to the formation of novel materials. Supported by DOE Contract No. DE-AC04-94AL85000.

1. M. Schick, J. Schäfer, K. Kalki, G. Ceballos, P. Reinhardt, H. Hoffschulz, and K. Wandelt, Surf. Sci. **287/288** (1993) 960.

4:20 pm **SS2-TuA8 Surface Alloying and Dealloying of Au on Ni(110) and Ni(111) Studied by STM and RBS**, F. Besenbacher, L. Pleth Nielsen, I. Stensgaard, and E. Lægsgaard, Center for Atomic-scale Materials Physics and Institute of Physics and Astronomy, Aarhus University, DK 8000 Aarhus C, Denmark.

The growth of Au on Ni(110) and Ni(111) have been studied at room temperature by in-situ Scanning Tunneling Microscopy (STM) and Rutherford Backscattering-Spectroscopy (RBS).

On Ni(110) we observe that incoming Au atoms are replacing surface Ni atoms up to Au coverage of 0.4 ML, i.e. forming a surface Au-Ni alloy, and that the hereby squeezed out Ni atoms agglomerate into Ni islands on the surface. Increasing the Au coverage above 0.4 ML causes an abrupt phase transition from two to three-dimensional growth through the formation of [001] directed Au chains. From a detail analysis of the amount of Au incorporated in the Au chains it can be concluded that the phase transition involves a dealloying mechanism where Au atoms are 'popping' out of the alloyed surface and nucleated into Au chains leaving behind Ni vacancies. Correlated with this concentration induced dealloying we observe a reversed Ni-mass transport from the Ni islands back into the leftover vacancies.

STM results of the growth of Au on Ni(111) reveals that even this clocked packed surface shows the formation of an Au/Ni surface alloy. However the substitution of Au for Ni is only observed at elevated temperatures indicating that this is an activated process.

The formation of an Au/Ni surface alloys on both Ni(110) and Ni(111) and the concentration induced dealloying on Ni(110) will be discussed and supported by total energy calculations within the effective medium theory.

4:40 pm **SS2-TuA9 Using STM to Understand Diffraction Oscillations: Fe Growth on Cu(100)**, David D. Chambliss, (IBM Research Division, Almaden Research Center, 650 Harry Road, San Jose, CA 95120 USA) and Kevin E. Johnson (Department of Chemistry, Goucher College, Baltimore, MD 21204 USA).

Intensity oscillations in surface-sensitive electron diffraction (RHEED and MEED) are widely used to analyze epitaxial growth, so

an understanding of the origin of intensity variations is needed. Direct comparisons of RHEED with scanning tunneling microscopy (STM) results have verified the qualitative correspondence between surface roughness and decreased intensity.<sup>1,2</sup> We examine *quantitatively* the relationship between experimental diffraction intensity variations for room-temperature growth of Fe on Cu(100)<sup>3</sup> and topography measured with the scanning tunneling microscope (STM). Variations in spot profiles and integrated intensity are predicted from STM data using Fourier transform methods to implement kinematical formulas. When the detector size is explicitly included, the agreement is good with the experimental MEED results of Thomassen et al.<sup>3</sup> The agreement demonstrates the similarity of samples prepared in the different laboratories and the applicability of kinematical analysis to MEED oscillations. A significant conclusion is that the detector defines a characteristic length of the measurement that must be included in a quantitative interpretation of MEED data.

<sup>1</sup>J. A. Strosio, D. T. Pierce and R. A. Dragoset, Phys. Rev. Lett. **70**, 3615 (1993).

<sup>2</sup>J. Sudijono et al., Phys. Rev. Lett. **69**, 2811 (1992).

<sup>3</sup>J. Thomassen, B. Feldmann, and M. Wuttig, Surf. Sci. **264**, 406 (1992).

5:00 pm **SS2-TuA10 Long Jumps in the Surface Diffusion of Adatoms: W, Ni, and Pd on W(211),\* D. Cowell Senft and Gert Ehrlich,** University of Illinois at Urbana-Champaign.

Molecular dynamics simulations indicate that atomic jumps longer than a nearest-neighbor spacing may become important at high temperatures, but there has been little experimental evidence that this is a significant effect in the actual diffusion of isolated metal adatoms. Field ion microscopic observations have now been made for W, Pd, and Ni adatoms on W(211), for which migration is one-dimensional. The measurements reveal that for these atoms, diffusion obeys a simple Arrhenius relation, with entirely normal prefactors. Analyses of the displacement distribution function, to determine contributions from different types of jumps, show that W moves entirely by single jumps. Ni atoms make occasional double jumps, even at the lowest temperature examined, but the number of long jumps is not much affected by temperature. For Pd, the number of long jumps increases rapidly with temperature, and double as well as triple jumps contribute significantly—the first experimental indication of long jumps in one-dimensional diffusion.

\*Supported by the National Science Foundation under Grant DMR 91-01429.

## NANO 3/NANOMETER-SCALE SCIENCE AND TECHNOLOGY

Room A209 – Session NS1-TuA

### Nanostructure Properties: Chemical and Electrochemical

**Moderator:** M. Hara, RIKEN, Japan, R. J. Hamers, University of Wisconsin.

2:00 pm **NS1-TuA1 Electron Tunneling through Water Clusters in Electrochemical STM, S. M. Lindsay, T. W. Jing, J. Pan, D. Lampner, A. Vaught, J. P. Lewis and O. F. Sankey,** Department of Physics and Astronomy, Arizona State University, Tempe, AZ 85287.

When measured in electrochemically clean conditions, tunnel current versus distance curves in aqueous electrolytes yield decay constants bigger than  $1 \text{ \AA}^{-1}$ . Interpreted in terms of a simple barrier, this corresponds to several eV. In non-binding electrolytes, however, the decay constant depends strongly upon the voltage applied between the tip and the substrate, the barrier showing a sharp dip near zero volts. The effect is independent of the conductance at which the measurement is initiated and also independent of the electrochemical potential of the substrate. We will show that, operated at  $G\Omega$  resistance, the gap probably contains at least 4 water molecules and the current is dominated by the through-bond tunneling of a chain of hydrogen bonded molecules. When the electric field in the tunnel gap is high enough to 'freeze' the cluster, the strain imposed by movement of the tip results in stretching of hydrogen bonds with a consequent rapid decay of

current. If, on the other hand, rotational transitions are permitted (i.e., at low fields) the strain may be taken up by rotations of molecules about the hydrogen bonds, resulting in a slow decay of current with tip movement.

These results are consistent with a simple 1-electron calculation of the gap resistance and suggest that the ability of the STM to image wide band-gap materials stems from (a) the fact that the decay of the wavefunction at energies well into the gap is not as rapid in a small cluster as it is in the bulk and (b) electronic interactions, even in a weakly bonded material like wafer, lead to significant residual conductance even far from the band edges.

This work was supported by grants 1R21 HG00818-01A1 from the National Institutes of Health and N00014-90-J-1455 from the Office of Naval Research.

2:20 pm **NS1-TuA2 The Nature of Mixed Adlayers on Platinum Single Crystal Electrodes Probed by In-Situ STM and Infrared Spectroscopy, I. Villegas and M. J. Weaver,** Department of Chemistry, Purdue University, West Lafayette, Indiana 47907-1393, USA.

The coadsorption of carbon monoxide with metal adatoms, e.g. bismuth or lead, is of particular interest in studies on the catalytic activity of platinum electrode surfaces towards the electrooxidation of numerous organic molecules. The unprecedented real-space structural information obtained from scanning tunneling microscopy (STM) images of electro-chemical adlayers when combined with infrared reflection-absorption spectroscopy can provide further insight on coadsorbate interactions for in-situ electrode surfaces. CO containing adlayers are excellent model systems for these studies due to the sensitivity of the  $\nu_{\text{CO}}$  IR absorption frequency to the binding site on platinum-group transition metals. Consequently, CO binding site as well as coverage changes induced by the metallic coadsorbates can readily be deduced from IR spectra. STM images obtained from Pt(111) electrode surfaces predosed with irreversibly adsorbed Bi and immersed in CO saturated acid solutions indicate that most of the surface ( $\approx 70\%$ ) is covered by an atomically intermixed adlayer of Bi and CO. This finding is consistent with the corresponding in-situ IR data. The rest of the surface, however, displays structures previously observed for pure CO adlayers on Pt(111). An interesting observation is that, although no complete segregation of Bi and CO domains occurs, regions free of Bi atoms are clearly distinguishable. The catalytic implication of such findings on this and other Pt single-crystal surfaces will also be noted.

2:40 pm **NS1-TuA3 Scanning Probe Microscopy of Organic Materials, J. E. Frommer,** IBM Almaden Research Center, 650 Harry Road, San Jose, CA 95120.

The requirements for successfully imaging organic materials in SPM experiments are at once the same and different from other classes of materials. This is because overall, the class of organic materials is characterized by diversity. Bonding within organics involves covalent, van der Waals, ionic, electrostatic, and hydrogen bonds, in many combinations. Therefore, the strongest point to bring to the imaging of organics is an awareness of the multiple modes of behavior that they can take on. This awareness is necessary in sample preparation, setting scanning parameters, and in interpreting results.

This overview will cover a broad range of organic materials, from molecular crystals to weakly anchored liquids. Intermolecular interactions will be discussed, and how the scanning instruments probe these forces. The organic samples will be discussed in the context of the broad range of environments in which they are found, e.g., friction, adhesion, membranes, manipulation.

**INVITED**

3:20 pm **NS1-TuA5 Molecular Scale Topographic Features and Electronic Structure in Thin Organic Films Observable by STM, R. C. White, B. Birchfield, and E. N. Schulman,** Columbia University, New York, NY 10027 USA.

We have characterized the structural and electronic properties of a polymer thin film on the molecular scale using a scanning tunneling microscope (STM). The polymer studied was a polyimide (PMDA-ODA) commonly employed as an insulating layer in microelectronics. Results of this work lead to an understanding of the mechanism by which poorly conducting organic materials can be imaged by STM. Prolonged exposure to ultra-high vacuum (UHV) was employed to eliminate extraneous current sources such as mobile ions, and allow the small electronic conductivity present in such materials to dominate the tunneling current. This resulted in an increased topographic resolution, and we have obtained the first STM images of an un-modified



polyimide surface, verified by measurement of contact between tip and film. In addition, we have distinguished nanometer scale, spatially localized regions of the polymer film which exhibit strong, voltage dependent switching between discrete conductance levels, similar to a localized two state switching previously observed in thin SiO<sub>2</sub> films. This process in SiO<sub>2</sub> is due to simple electron trapping and de-trapping, while that observed in the organic film displays more complex kinematics similar to multilevel fluctuators in metal micro bridges. Thus the conductance mechanism in the organic film is related to trapping and de-trapping, in localized "defect states" which result from intermolecular interactions. This mechanism of electron current supply through the film dominates and thus no intramolecular electronic states are accessible by STM.

3:40 pm **NS1-TuA6 Atomic Ordering Within AlGaAs Alloys Studied Using Cross-Sectional Scanning Tunneling Microscopy**, *A. R. Smith and C. K. Shih*, University of Texas at Austin, Austin, TX 78712, *Y. C. Shih and B. G. Streetman*, Microelectronics Research Center and Department of Computer and Electrical Engineering, University of Texas, Austin, TX 78712.

We have investigated the composition fluctuations of AlGaAs alloys with atomic resolution using X-STM. Clean cross-sectional (110) surfaces are prepared in UHV by cleaving samples in-situ. Experiments are performed on *p*-type samples with an aluminum content of 30%. Within the AlGaAs regions, we have observed localized alloy fluctuations similar to those seen by Johnson et al. in which Al-rich regions were observed which align preferentially along the [112] and [112] directions.<sup>1</sup> The alloy concentration modulation wavelength in this case is on the order of 40–50 Å. In addition to this long wavelength modulation in the alloy composition, we have also observed alternating rows of AlAs/GaAs within the AlGaAs alloy region which lie along the [112] and [112] directions. This observation indicates that there are locally ordered regions consisting of alternating AlAs/GaAs (111) planes in the bulk. The influence of the growth conditions on the observed alloy ordering will be discussed. Further investigations are currently underway to identify the atomistic mechanisms behind these ordered features.

<sup>1</sup>M. B. Johnson, U. Maier, H.-P. Meier, and H. W. M. Salemink, *Appl. Phys. Lett.* **63**, 1273 (1993).

4:00 pm **NS1-TuA7 Characterization of the Gallium Vacancy on GaAs (110)**, *G. Lengel, R. Wilkins, M. Weimer, J. Gryko, and R. E. Allen*, Texas A&M University, College Station, TX 77843.

Using scanning tunneling microscopy and spectroscopy, together with tight-binding molecular dynamics simulations, we previously characterized the geometry and electronic structure of the As vacancy at the (110) surface of GaAs [1]. Here we apply the same techniques to the Ga vacancy. There is an interesting symmetry between the two defects: In both cases, the neighboring atoms (Ga neighbors for the As vacancy, As neighbors for the Ga vacancy) are observed to relax upward relative to their positions on the pristine surface. Also, there are three defect levels (per spin) associated with the three new dangling bonds around the vacancy site. For an As vacancy, these can be viewed as pulled down from the Ga-derived conduction band; and for a Ga vacancy, as pushed up from the As-derived valence band. The energetics of the calculated levels indicates that the As vacancy is preferred on *p*-type GaAs, and the Ga vacancy on *n*-type, in agreement with the observations. The levels also indicate that the As vacancy (on *p*-GaAs) should be positively charged, and the Ga vacancy (on *n*-type) negatively charged; these results are again consistent with the experiments. There is just one principal difference between the As and Ga surface vacancies: The Ga neighbors around an As vacancy are found to spontaneously relax upward in the molecular dynamics simulations. The As neighbors around a Ga vacancy, however, relax upward only in the presence of a modest electric field. We therefore attribute the latter relaxation to an interaction between the surface atoms and STM tip. The As neighbors can be pulled up rather easily because they have only two remaining bonds: According to both the simulations and the measurements, these atoms do not shift laterally to rebond.

[1] G. Lengel et al., *Phys. Rev. Lett.* **72**, 836 (1994). This work was supported by the U.S. Office of Naval Research and the Robert A. Welch Foundation.

4:20 pm **NS1-TuA8 Structure and Electronic States on Reduced SrTiO<sub>3</sub> (110) Surface Observed by Scanning Tunneling Microscopy and Spectroscopy**, *H. Bando, Y. Aiura, Y. Haruyama\*, and Y. Ni-*

*shihara*, Electrotechnical Laboratory, Tsukuba, Ibaraki 305, Japan. \*Institute of Physics, University of Tsukuba, Tsukuba, Ibaraki 305, Japan.

SrTiO<sub>3</sub> (110) surface has been used as a substrate of off-c-axis oriented high-T<sub>c</sub> superconductor thin films, and it is important to observe microscopically the behavior of the surface under heat treatment in vacuum. Recently two types of mid-gap electronic states were observed on reduced SrTiO<sub>3</sub> (110) surface by photoemission spectroscopy: a metallic state with a sharp Fermi cut-off appeared after annealing at 800°C, whereas a broad state centered at ~1.1 eV below E<sub>F</sub> was seen after annealing at 1000°C. The latter state was similar to one observed on reduced SrTiO<sub>3</sub> (100) surface. We observe the same (110) surface by scanning tunneling microscopy and spectroscopy. The surface after annealing at 800°C is dominated by flat regions where tunneling spectra are of metallic character. After annealing above 1000°C, step edges along [110] and row-like structures along [001] with the spacing ~3 nm are observed together with an electronic state around 1 eV below E<sub>F</sub>, which are consistent with formation of micro-facets.

4:40 pm **NS1-TuA9 An AFM Study of a Surface Bound Colloidal Pd Catalyst and Its Effect on Electroless Ni Particle Size**, *S. L. Bradow, W. J. Dressick, C. S. Dulcey, \*C. R. K. Marrian, G. M. Chow, \*F. K. Perkins, and J. M. Calvert*, Center for Biomolecular Science and Engineering (Code 6900), \*Electronics Science and Technology Division (Code 6864), Naval Research Laboratory, Washington, D.C. 20375 USA.

We have previously reported a new approach for selective electroless metal deposition utilizing chemisorbed ligating organosilane films in conjunction with a tin-free, aqueous based Pd(II) catalyst. This process provides several advantages over traditional methods including patternability, a well defined interaction between catalyst and surface through ligation, and elimination of the acceleration step during processing. From recent STM experiments it appears that formation of the latent image in the monolayer is not the limiting factor in the resolution of this process. Rather the particle size of the electroless metal is large enough to degrade the patterning resolution. Using a combination of AFM, SEM, and TEM we have examined how variations in the metal bath and catalyst effect the particle size of the electroless metal. It was found that the size and distribution of catalyst particle sizes depends on the age of the catalyst solution, the deposition time, the formulation, and the nature of the ligating surface. Shifting the size distribution of bound catalyst particles to smaller sizes results in a dramatic reduction in the metal particle size. Results are discussed in terms of current electroless metallization theory. Selective metallization with the new catalyst was used to produce features with linewidths to approximately 100 nm by high voltage e-beam lithography and features ranging from 35–100 nm using STM exposure. In both cases pattern transfer was accomplished using reactive ion etching to depths of 200–500 nm in Si.

5:00 pm **NS1-TuA10 Direct Observations of Electric Field Gradients Near Field Emission Cathode Arrays**, *Y. Liang, D. Bonnell*, The University of Pennsylvania, Philadelphia, PA 19104, *W. Goodhue, D. Rathman, C. Bozler*, Lincoln Lab, Boston, MA.

The variation of electric field gradients above arrays of field emission cathodes is characterized with atomic force microscopy (AFM) using both imaging techniques and force-displacement measurements. Cathodes have submicron diameters at the base, decreasing to nanometer scale tips. Effects of AFM tip convolution will be considered explicitly. The dependence of the spatial distribution of field gradient on applied bias and height above the arrays is compared to theoretical predictions. Results confirm a parabolic relationship between sample bias and field gradient and power law dependence on height.

## NANO 3/NANOMETER-SCALE SCIENCE AND TECHNOLOGY

### Room A207 – Session NS2–TuA

#### Nanomechanics and Nanotribology: I

**Moderator:** S. Cohen, Weizman Institute of Science.

2:00 pm **NS2-TuA1 Atomistic Modelling of Friction and the Interaction Between AFM Tips and Ionic Surfaces**, *A. L. Shluger, A. L. Rohl and D. H. Gay*, The Royal Institution of Great Britain,

21 Albemarle St., London W1X 4BS, U.K., *R. M. Wilson and R. T. Williams*, Department of Physics, Wake Forest University, Winston-Salem, NC 27109, USA.

Interaction of nano-asperities with ionic surfaces is relevant to the micro-mechanisms of friction, nanolithography, modification of surfaces, and AFM imaging of their structure. Periodic surface structures of several alkali halides, alkali-earth fluorides and oxides have been recently obtained by Scanning Force and Friction Microscopy. Several images of steps, corners and point defects have also been obtained in our and other groups. Correct interpretation of these experiments requires theoretical studies of the basic mechanisms of the interaction of realistic nano-structures, such as surface roughness and AFM tips, with ionic surfaces. In this study we focus on the chemical nature and the interaction of different nano-asperities with ionic surfaces at long and short distances, including surface penetration and scanning. In particular, we consider the interaction of three different types of asperities, composed of protonated  $\text{SiO}_2$  and  $\text{MgO}$  and consisting of up to 66 atoms, with the perfect, stepped and kinked (001) surfaces of  $\text{LiF}$ ,  $\text{NaCl}$  and  $\text{CaO}$  by quantum-chemical and atomistic simulation techniques. The associated surface distortions caused by this interaction were investigated. Friction and AFM images of steps, kinks and point defects at different tip-surface separations and forces were analysed both experimentally and theoretically. From the AFM perspective, it is demonstrated that the optimal tip-surface distance for 'atomic resolution' is about 3–5 Å.

2:20 pm **NS2-TuA2 Molecular Dynamics Simulations of Metal-Oxide Surfaces and Interfaces**, *F. H. Streitz and J. W. Mintmire*, Naval Research Laboratory, Washington, DC 20375, USA.

The metal-oxide/metal-oxide and metal-oxide/metal interfaces are ubiquitous in the adhesion of ceramics and metals. A range of technologically important materials applications are critically dependent on the properties of these interfaces: ceramic-metal composite materials, conductive metals on metal-oxide substrates in electronic devices, and anticorrosive surface oxide layers on structural metals are just a few representative examples. Atomic-scale simulations of metal-oxide materials can be important in understanding and predicting the effect of the interface region on materials properties. One primary objective we have in our current research effort is to simulate the atomic-scale dynamics and energetics of technologically important metal/metal-oxide interfaces. We need an empirical method that allows the local cation valence to vary according to the local environment and which includes the Coulombic electrostatic interaction among the anions and cations. We have investigated the use of an electronegativity-based model for direct calculation of charge transfer in metal-oxide systems and incorporated the resulting electrostatic potential into an overall model potential. We present a brief outline of our approach for modeling the electrostatic component of the potential energy of ionic systems, and how standard empirical potential techniques can be effectively merged with this approach. We then discuss our results for  $\alpha$ -alumina, looking at both surface relaxation of low-index faces of alumina, and strain effects on an alumina/aluminum interface. Our results indicate that this approach will be able to provide physically realistic empirical potentials for future simulations on mixed metal/metal-oxide systems.

2:40 pm **NS2-TuA3 Electron-Ion Dynamics: A New Technique for Simulating Both Electronic Transitions and Atomic Motion in Molecules and Materials**, *Roland E. Allen*, Texas A&M University, College Station, TX 77843.

In 1964, Aneesur Rahman introduced the technique of *molecular dynamics*, in which the motion of atoms and molecules is computed from classical potentials. Twenty years later, we introduced *quantum molecular dynamics*, in which the forces on atoms are computed from the electronic structure, via the Hellmann-Feynman theorem. We have now developed a much more general technique, *electron-ion dynamics*, which permits electronic transitions and atomic motion to be treated simultaneously. The key features of this technique are the following: (1) Use of the *interaction picture* in solving the time-dependent Schrödinger equation  $i\hbar\partial\psi/\partial t = H\psi$ . (2) A *generalized Hellmann-Feynman theorem* which is valid for excited states, and even during the course of electronic transitions. (3) An Einstein detailed-balance argument for treating spontaneous emission of radiation. (Absorption and stimulated emission are treated directly, through a classical description of the radiation field.) (4) A time-dependent self-consistent-field approach, which is equivalent to the random phase approximation. This technique is not limited to one-photon and one-phonon processes; it can be applied to arbitrarily strong radiation fields and arbitrarily violent ionic motion. It is suitable for both *ab initio* and semiempirical calculations, but our first illustrative calculations are for excited state chemistry in tight-binding models.

This work was supported by the Office of Naval Research and the Robert A. Welch Foundation.

3:00 pm **NS2-TuA4 Scanning Near-Field Acoustic Microscopy: Nanoscale Material Properties**, *N. A. Burnham, A. J. Kulik and G. Gremaud*, Department of Physics, Swiss Federal Institute of Technology, 1015 Lausanne, Switzerland.

A Scanning Near-field Acoustic Microscope (SNAM) is an atomic-force microscope that detects transmitted high-frequency acoustic waves. By exciting the cantilever above its resonant frequency, its effective stiffness increases. Hence, normal-force images at low loads and SNAM images may be simultaneously acquired, eliminating the limiting compromise between force resolution and cantilever rigidity. Greater detail is evident in the SNAM images than in the normal-force images. The SNAM contrast is related to the local surface forces, adhesion and elastic properties.

The principles of this new technique will be explained, and a few example SNAM images of graphite and a test structure with varying elastic properties will be shown and compared to the usual low-frequency force modulation images. Data interpretation will be emphasized, and in particular the relative roles of adhesion and elastic modulus will be examined.

3:20 pm **NS2-TuA5 Tribology with the Atomic Force Microscope**, *D. Frank Ogletree, Jun Hu, Xu-dong Xiao, C. Morant, and M. Salmeron*, Materials Sciences Division, Lawrence Berkeley Laboratory, Berkeley, California 94720.

The atomic force microscope is a powerful tool to study adhesion and friction in single asperity contacts under well defined conditions. Using the AFM, we have obtained atomic lattice resolution images in both topographic and lateral force modes on a variety of ordered surfaces, including mica,  $\text{NaCl}(001)$ ,  $\text{LiF}(001)$ ,  $\text{KMnF}_3(001)$ ,  $\text{Au}(111)$  films and self-assembled organic molecular layers on  $\text{Au}(111)$ . Friction has been measured as a function of load on these surfaces in ambient laboratory conditions. Additional friction vs. load measurements on some of these surfaces have been carried out under controlled humidity, in liquids and in ultra-high vacuum. Absolute calibration of normal and lateral forces in the AFM is difficult, so comparative measurements have been made with the same tip on different surfaces. We have also carried out a systematic study of friction on mica to see if this surface is a suitable "AFM friction standard". Results of friction measurements for different mica samples, for different scan directions, for different levers, as a function of humidity and in different environments will be presented. Issues involved in quantitative tribological measurements with the AFM will be discussed. **INVITED**

4:00 pm **NS2-TuA7 Effect of Contact Area on Nanoindentation Curves Obtained Using the Atomic Force Microscope**, *Charles F. Draper<sup>1</sup>, David M. Schaefer<sup>2</sup>, Richard J. Colton<sup>2</sup>, and Steven M. Hues<sup>2</sup>*, <sup>1</sup>Department of Mechanical Engineering, Vanderbilt University, Nashville, TN 37205 USA, <sup>2</sup>Code 6170, Naval Research Laboratory, Washington, D.C., 20375-5342 USA.

Nanoscale mechanical properties may be quantitatively measured by nanoindentation using the atomic force microscope (AFM). However, a lack of understanding of the exact size and nature of the contact area between the tip and surface severely hampers the extraction of absolute material property values from raw nanoindentation data. Commonly used AFM tips (diamond, W,  $\text{Si}_3\text{N}_4$ ) have ill-defined nanoscale tip apex geometries and consequently greatly complicated absolute mechanical property measurements. The contact of spherical indentors, however, are well-described by Hertzian contact mechanics. In order to study the effect of contact area in greater detail, we have indented a variety of materials with spheres of decreasing diameter (micron to nanometer range) and have studied the effect of the contact area changes on the nanoindentation curves and derived mechanical properties.

4:20 pm **NS2-TuA8 The Nanomechanics of Single Crystal Au Surfaces\***, *J. E. Houston<sup>1</sup>, P. Tangyonyong<sup>1</sup>, O. L. Warren<sup>2</sup>, R. C. Thomas<sup>3</sup>, T. A. Michalske<sup>1</sup> and R. M. Crooks<sup>4</sup>*, <sup>1</sup>Sandia National Labs., Albuquerque, NM, <sup>2</sup>University of Western Ontario, London, Ontario, Canada, <sup>3</sup>University of New Mexico, Albuquerque, NM, <sup>4</sup>Texas A&M University, College Station, TX.

We have used Interfacial Force Microscopy (IFM) to quantitatively measure the mechanical properties of various surfaces of single-crystal Au in order to study the effect of crystal-face and probe-tip radius when the tip size is nanoscale, i.e., 50–500 nm. The etched W probes are analyzed by SEM profiling and the Au surfaces are passivated with self-assembling monolayers of alkanethiol molecules. The IFM tech-



nique is used because it is quantitative, mechanically stable, has a zero-compliance sensor and can readily accept characterizable probes. Contact mechanics permit a determination of the elastic modulus and the shear-stress threshold for plastic deformation. Measured values for the elastic constants follow the expected trend for the various faces. However, unexpected deviations in the measured elastic constants, the shear-stress thresholds and the plastic-strain thresholds are observed for truly nanoscale deformations. We discuss these findings in terms of a non-continuum model which takes account of the tip size relative to the substrate lattice constant.

\*Work performed at Sandia National Laboratory supported by the US Department of Energy under Contract DE-AC04-94AL85000.

4:40 pm **NS2-TuA9 Surface Potential Control of Adhesion in an Atomic Force Microscope**, J. Larsen, T. W. Jing, D. Lampner, and S. M. Lindsay, Dept. Physics and Astronomy, Arizona State University, Tempe, AZ 85287, Y. Q. Li, Dept. of Chemistry, Texas A&M University, College Station, TX 77843, N. J. Tao, Dept. of Physics, Florida International University, University Park Campus, Miami, FL 33199.

Control of adhesion is possible by varying the potential of the conducting surfaces of both a probe and a substrate in an electrochemical cell for an atomic force microscope. We have studied adhesion between a gold-coated force sensing probe and a gold (111)  $23 \times \sqrt{3}$  surface under potential control in perchlorate electrolytes. The maximum adhesion, at the potential for zero charge (PZC), is in reasonable agreement with predictions based on the known surface energy of gold. The adhesion is reduced to zero by relatively small excursions of the surface potential each side of the PZC.

This work was supported by grants 1R21 HG00818-01A1 from the National Institutes of Health and N00014-90-J-1455 from the Office of Naval Research.

5:00 pm **NS2-TuA10 Local Modification of Mechanical Properties of Polystyrene-Polyethyleneoxide Blend Surfaces**, H.-Y. Nie, M. Motomatsu\*, W. Mizutani, and H. Tokumoto, JRCAT-NAIR and JRCAT-ATP\*, Higashi 1-1-4, Tsukuba, Ibaraki 305, Japan.

We report the modification of local mechanical properties of polystyrene (PS)-polyethyleneoxide (PEO) blend surfaces with atomic force microscopy (AFM) and force modulation microscopy (FMM). In the course of the experiments, the slopes of force curves are quite informative to examine mechanical properties.

We used PS-PEO blend films annealed at 90°C for 1 day, exhibiting phase separations. In this particular case, it is possible to distinguish PS and PEO from topography because only PEO crystallizes.<sup>1)</sup> Force curves on PS and PEO measured before and after FMM scanning changed remarkably. Before scanning, the slope of force curve on PEO was smaller than that on PS, indicating PEO is softer than PS. After scanning, however, the slope of force curve on PEO became close to or larger than that on PS, depending on stiffness of cantilevers and scanning rates. This can be explained as follows: during FMM scanning, applied forces resulted in plastic deformation of PEO, causing PEO stiffer than PS. We point out possibilities of controlling elastic properties and of recognizing molecules of polymers with this technique.

<sup>1)</sup>M. Motomatsu *et al.*, Proceedings of "Forces in Scanning Probe Microscopies," NATO-ASI series (Kluwer Academic Publishers).

## APPLIED SURFACE SCIENCE/SURFACE SCIENCE

Room A101 – Session ASSS-TuA

### Electrochemistry and Liquid/Solid Interfaces

Moderator: G. D. Davis, Martin Marietta Laboratories.

2:00 pm **ASSS-TuA1 Evidence of Specific and Non-Specific Adsorption of ClO<sub>4</sub> on Ag(110)**, A. Krasnopolov and E. M. Stuve, Dept. of Chem. Eng., BF-10, University of Washington, Seattle, WA 98195.

The coadsorption of ClO<sub>4</sub> and of HClO<sub>4</sub> with H<sub>2</sub>O on Ag(110) has been studied with HREELS as a model of anion adsorption at the solid-liquid interface. The vibrational spectrum of adsorbed ClO<sub>4</sub> shows losses at 470, 615, 905, 1020 and 1230 cm<sup>-1</sup>, indicating a lowering of symmetry due to adsorption. A model for the adsorption is proposed. When coadsorbed with H<sub>2</sub>O, the vibrational spectrum resembles that of the fully solvated ClO<sub>4</sub><sup>-</sup>, suggesting the formation of a nonspecifically adsorbed anion in UHV. The vibrational structure of the water shows signs of the "structure breaking" effect of ClO<sub>4</sub> in aqueous solution.

Coadsorption of HClO<sub>4</sub> and H<sub>2</sub>O produces adsorbed perchlorate and hydronium, as indicated by the  $\nu(\text{Cl-O})$  at 1260 cm<sup>-1</sup> and  $\delta_s$  of H<sub>3</sub>O<sup>+</sup> at 1080 cm<sup>-1</sup>. Additional H<sub>2</sub>O partially ionizes the perchlorate, although not as completely as for coadsorption of H<sub>2</sub>O and ClO<sub>4</sub>, due to preferential hydration of H<sub>3</sub>O<sup>+</sup>. The symmetric bend of H<sub>3</sub>O<sup>+</sup> shifts to 1130 cm<sup>-1</sup>, suggesting a more aqueous environment. The combination of adsorbed and hydrated ClO<sub>4</sub> with hydrated H<sub>3</sub>O<sup>+</sup> represents a model of specific and non-specific adsorption. Reversing the dosing order results in formation of aqueous H<sub>3</sub>O<sup>+</sup> at the acid/water interface. However, some molecular acid remains undissociated in the top layer, making this an inadequate model of non-specific adsorption.

2:20 pm **ASSS-TuA2 Surface Chemistry of Water and Hydrogen on Single Crystal Ni<sub>3</sub>(Al, Ti)**, Yip-Wah Chung and Wen-Jui Chia, Northwestern University, Dept. of Materials Sci. & Eng., Evanston, IL 60208.

Intermetallic compounds such as Ni<sub>3</sub>Al have low tensile ductility when tested in normal room temperature air ambients. This is believed to be due to hydrogen embrittlement, hydrogen being produced by the interaction of water vapor in air and fresh metal surfaces exposed during tensile testing. In this talk, we present results of the interaction of water and hydrogen using TPD, Auger and X-ray photoelectron spectroscopy. The interaction depends strongly on surface orientation. On the (111) surface, water adsorbs molecularly. On the (533) stepped surface and the (100) surface, water dissociates to produce hydrogen. Water desorption was not observed up to 700K. AES/XPS showed that adsorbed oxygen or hydroxyl remains on the surface. The absence of water evolution during desorption suggests complete dissociation of water into hydrogen and oxygen atoms on the (533) and (100) surface. The mechanism of environmental embrittlement of intermetallic compounds by water dissociation to produce hydrogen atoms is demonstrated.

2:40 pm **ASSS-TuA3 In Situ Study of 304 Stainless Steel's Passive Layer Exposed To HCl Acid Using A Scanning Tunneling Microscope**, J. M. Galligan, T. J. McKrell, University of Connecticut, Storrs, CT, 06268.

The nature of 304 stainless steel's passive layer and how it is altered as a function of exposure time in HCl acid has been studied using a Scanning Tunneling Microscope (STM). This device offers the distinct advantage of in situ studies, on a microscopic scale, of the electrical character of the surface in the presence of a corrosive environment. In the present paper we present evidence which shows how the surface structure of 304 stainless steel is altered by hydrochloric acid (HCl) while the surface is probed with an STM. In particular, the in situ current (I) and bias voltage (V) curves were measured as a function of etchant exposure time. The important region, concerning passivation, is the extent and the slope of the curve near where the current is zero. This region corresponds to corrosion resistance and shows a low or zero slope near where the current is equal to zero. The research method establishes a quantitative measure of the extent of protection and the kinetics of the removal of the passive layer. The findings of this research are correlated with nanoscale STM images of the 304 stainless steel's surface.

3:00 pm **ASSS-TuA4 Tunnel Channels and Imaging Mechanisms in STM: W-, PtIr-, and Ag-Interfaces in Electrolytes**, G. Repphun, Inst. of Physical Chemistry, University, CH-3000 Bern 9, Switzerland; J. Halbritter, KfK, IMF I, Postfach 3640; 76021 Karlsruhe, Germany.

In scanning tunneling microscopy (STM) operation in fluids, air and, usually also in UHV, tips and substrates are covered by adsorbates, hydroxides or oxides. These coatings are difficult to identify and to control. In an electrolytic environment receipts exists for cleaning tip and substrate. In addition, the potential electrolyte-tip or electrolyte-substrate changes the interface in a well defined way.

STM charge transfer is far from being simple, like direct tunneling in vacuum given by  $\exp(-2d\sqrt{2m\phi}/\hbar)$  with the gap width  $d$  and  $\phi$  as tunnel barrier height. For example, the observed tunnel currents

often decay very slowly with  $d_{\text{eff}} = d/(n + 1)$  by  $n$  intermediate states simulating a low tunnel barrier  $\Phi_{\text{eff}} = \phi_0/(n + 1)^2$ . Thus, reported  $\phi_{\text{eff}}$ -values are often not a barrier height but resemble intermediate state tunneling bridging the gap and reducing so the effective tunnel distance to  $d_{\text{eff}} \leq d/2$ . We identify the imaging processes and tunnel channels via  $n$  intermediate states by voltage and distance spectroscopy and separated up to 7 intermediate tunneling states in the: oxide-, hydroxide- and solid part of the double-layer. We relate the intermediate states in this electrolyte interface to dipole resonances of the ordered, solid-like HOH-OH<sup>-</sup> dipole layer changing with interface potential. The thickness and dipole moment of the interface layer are obtained from distance and potential dependencies of  $\phi_{\text{eff}}$ . The importance of the dipole layer interfaces on deposition and growth is discussed.

**3:20 pm ASSS-TuA5 In-situ Measurement of Thickness Changes with Electrolytic SPM, R. Nyffenegger, H. Siegenthaler, P. Häring\* and R. Kötz\*,** Institut für Anorganische, Analytische und Physikalische Chemie, Universität Bern, 3012 Bern, Switzerland; \*Paul Scherrer Institut, 5232 Villigen, Switzerland.

Scanning Probe Methods (SPM) not only allow a mapping of surface topography in real space but also enable the measurement of time dependent thickness changes of the sample. Assuming a constant distance between tip and sample during the entire experiment, the tip will follow the thickness change of the sample and the corresponding driving signal of the piezo can be recorded and assigned to this thickness change.

This method has been used to measure in-situ thickness changes of electrochemically formed surface films in electrolytic environment, that can be charged or discharged (e.g. conducting or redox polymer). This change of the oxidation state often leads to a surface modification, e.g. formation of hydroxide or oxide layers or swelling/shrinking of polymers phases induced by ion exchange. Typical examples include nickel hydroxide films and polyaniline layers. Both are investigated in view of their practical application in novel types of batteries.

The obtained results can be assigned to the corresponding thickness changes. Experimental and principal considerations suggest a lower detection limit of ca. 1 nm. Below this limit, alterations of relevant imaging parameters (e.g. inverse depth length for STM, stiffness of the sample in the case of AFM) may affect the thickness measurements and falsify the experiment.

**3:40 pm ASSS-TuA6 Electrochemical Etching of Si(111) Surfaces in Fluoride Solutions Studied by STM and AES, R. Houbertz\* and U. Memmert,** Abt. Oberflächenchemie, Universität Ulm, D-89069 Ulm, Germany, \*Fr 10.2, (Experimentalphysik), Universität des Saarlandes, D-66041 Saarbrücken, Germany.

The electrochemical etching of Si(111) surfaces in conc. NH<sub>4</sub>F solution in dependence of etch potential and etch time was investigated by I-V curves, AES and STM. The samples were etched under full potentiostatic control in an ex-situ electrochemical cell and transferred afterwards into a UHV system for the AES and STM measurements. Within the potential regime considered in this study we were able to characterize five distinct potential regions in the I-V curves: A cathodic range, the open circuit potential (OCP) and three anodic ranges, separated each other by two current maxima. During etching at cathodic potentials and the OCP no oxides are formed on the surfaces. STM imaging shows that an anisotropic etch mechanism leads to very smooth and regular surfaces. Etching at anodic potentials yields much rougher surfaces

to the formation of large, several Si(111) bilayers deep holes. The AES measurements display still no oxide below the first current peak, while in the second anodic region between the two peaks app. one bilayer is oxidized. The oxide thickness increases drastically for potentials above the second current peak. The anisotropic etching for cathode potentials and the OCP is explained by the local binding situation for different surface sites, while for anodic potentials long-range effects have to be considered. Anodically in NH<sub>4</sub>F etched samples show quite different topographies than samples which were treated in HF/ethanol solution. While in NH<sub>4</sub>F solution the holes on the surface stay rather shallow, for the HF/ethanol solution the formation of very narrow and deep pores was found. This difference is explained by the different ability of these solutions to attack clean Si even without an external anodic current applied.

**4:00 pm ASSS-TuA7 Effects of Structure and Chemistry on Surface Reactivity in Solution, D. R. Baer, A. S. Lea, Y. Liang, Li-Qiong Wang, and M. H. Engelhard,** Pacific Northwest Laboratory, Richland, WA 99352.

The solid-solution interface is the location where many environmentally important reactions take place. Results from two different approaches for examining the effects of surface structure and chemistry on surface reactivity in solution will be described. Crystals which readily dissolve and grow in ground water have significant potential for storing or releasing contamination. Atomic Force Microscopy (AFM) has been used to observe and measure the dissolution of the cleavage face of CaCO<sub>3</sub> in aqueous solutions. Dissolution occurs at steps and the step velocities differ by a factor of three (or more) depending upon the step structure. Impurities, such as Mn, can alter the rate of dissolution and change the structure of a dissolving pit. Current efforts are to relate a model of relative surface reactivities for different sites to the observed dissolution patterns and rates. Although defects are known to strongly influence the reactivity of oxide surfaces, the defects observed or created in vacuum, may not be those present in solution. The reaction of water with "undamaged" and defected surfaces of TiO<sub>2</sub> (110) has also been examined by transferring a specimen prepared in vacuum to solution and then returning the specimen to the spectrometer. These results are compared to the effects of low-pressure ( $p < 10^{-6}$  Torr) and higher pressure ( $10^{-6} < p < 10^{-3}$  Torr) exposure to water vapor.

INVITED

**4:40 pm ASSS-TuA9 AFM and STM Studies of Oxide Formation, Deposition, and Dissolution on Copper Single Crystal Surfaces, Andrew A. Gewirth, John R. LaGraff, and Mauhui Ge,** Department of Chemistry, University of Illinois, 505 S. Mathews Avenue, Urbana, IL 61801 USA.

We used the AFM to image the initial stages of oxidation on Cu(110), Cu(100), and Cu(111) electrode surfaces in dilute acid solutions. On Cu(110) images obtained in H<sub>2</sub>SO<sub>4</sub> and HClO<sub>4</sub> solutions with a pH near 2.5 revealed oxide monolayers consisting of (1T0) and (001) chains. These chains represent the initial oxide layer growing on the Cu surface. After completion of this monolayer, the images revealed formation of  $n \times 1$  structures where  $n = 1, 2, 3, 4$ , which were attributed to precursor structures which develop prior to bulk oxide development. In solutions where Cl<sup>-</sup> was deliberately added, a different overlayer exhibiting a  $c(2 \times 2)$  lattice structure was observed. On the Cu(100) face we observed that a  $(\sqrt{2} \times \sqrt{2})$  R45° adlattice is formed on this material at potentials negative of the rest potential. The oxide monolayer is amorphous on Cu(111), but becomes ordered at neutral pH values.

The oxide monolayer controls the initial nucleation of Cu deposits onto Cu surfaces. We found in addition that deposition could be preferentially enhanced on Cu by scanning the AFM tip over areas on the surface. The tip removes the oxide layer and forms nucleation sites on the Cu substrate.

**5:00 pm ASSS-TuA10 In-situ Observation of Hg Amalgamation Formation and Stripping on Au using Atomic Force Microscopy, L. A. Nagahara<sup>†</sup>, X. Yang<sup>†,\*</sup>, K. Tonami<sup>†</sup>, Y. Wei<sup>\*</sup>, K. Hashimoto<sup>†</sup>, and A. Fujishima<sup>†</sup>,** <sup>†</sup>Department of Applied Chemistry, Faculty of Engineering, University of Tokyo, Hongo, Bunkyo-ku, Tokyo 113, Japan; <sup>\*</sup>National Laboratory of Molecular & Biomolecular Electronics, Southeast University, Nanjing 210018, China.

We have used atomic force microscopy (AFM) to investigate in-situ the initial stages of Hg amalgamation on Au films as well as Hg stripping from the amalgamated film. The Au(111) on a glass substrate used in this study were prepared via vacuum-deposition at elevated substrate temperatures. In the case of Hg deposition, amalgamation occurred in the form of small islands. Further deposition resulted in the growth of these islands as well as the formation of new islands. Adjacent to these islands, a portion of the Au film is observed to be preferentially removed at pinhole sites and resulted in larger and deeper pits. Highly ordered regions also showed dissolution as evident by the increase in mono-atomic stepped terraces. When the Hg was removed from the amalgamated film, the entire surface became noticeably rougher indicating that the amalgamation process has occurred even in well-ordered regions. The AFM results and the mechanism for amalgam formation and stripping will be presented.



Advanced Plasma Reactors

Moderator: T. D. Mantei, University of Cincinnati.

2:00 pm **PS-TuA1 Helicon Plasma Source Excited by Flat Spiral Coil,\*** J. E. Stevens, Princeton Plasma Physics Laboratory, M. J. Sowa, Princeton University, Department of Chemical Engineering, and J. L. Cecchi, University of New Mexico, Department of Chemical and Nuclear Engineering.

We have operated and characterized a new helicon plasma source with an end-launch antenna configuration. Power at 13.56 MHz is coupled via a four-turn flat spiral coil into an  $m = 0$  helicon mode with the application of a weak ( $B > 5G$ ) axial magnetic field. Plasma parameters were measured with Langmuir probes and the structure and absorption of the helicon wave fields were determined with magnetic induction probes. Plasma densities of  $10^{11}$ – $10^{12}$   $\text{cm}^{-3}$  are produced in Ar for pressures in the 1–50 mTorr range with a 5–60 G magnetic field. RF power absorption occurs primarily via collisionless Landau and ECR damping for pressure below  $\approx 10$  mTorr. Above this pressure, collisional damping dominates. Absorption is strongest for magnetic fields less than  $\approx 20$  G. This source requires no separate source chamber, and thus combines the compactness of flat coil inductively coupled sources, with the advantages of remote plasma generation found in wave-supported sources. Additionally, by not constraining the helicon parallel wavelength, the source can be easily optimized for a variety of operating conditions.

\*Work supported by the Semiconductor Research Corporation.

2:20 pm **PS-TuA2 Comparison of High Density Plasma Sources for Silicon Etching: Helical Resonator, Helicon, and ECR,** K. V. Guinn, I. Tepermeister, N. Blay, F. P. Klemens, D. E. Ibbotson, and J. T. C. Lee, AT&T Bell Laboratories, Murray Hill, NJ 07974.

As part of research efforts to develop sub 0.35  $\mu\text{m}$  design rule devices, we are etching in a dual reaction chamber cluster tool made by Lucas Labs of Sunnyvale, California. The reaction chambers are geometrically, electrically, and mechanically the same; thus, allowing direct side-by-side comparisons of different plasma sources while excluding platform dependent effects. In this study, we present the results from the continuation of our effort to compare commercially available, low pressure, high density sources. The first two sources were a multipole ECR manufactured by Wavemat of Plymouth, Michigan and an rf-inductively coupled helicon manufactured by Lucas Labs. The third source is a 12" diameter helical resonator manufactured by Prototech Research of Tempe, Arizona.

We first perform a statistical evaluation of blanket polysilicon etching rate and etching rate uniformity as a function of source power, reactor pressure (2–5m Torr) and rf-bias (25–75 W). Based on these results, operating conditions for optimum uniformity for each source are determined. The effect of process parameters on polysilicon profiles is then evaluated and compared. The etching process in each source is optimized to give vertical profiles and the optimized recipes are compared. Finally, we also present the radial Langmuir probe measurements of the plasma properties above the wafer corresponding to the etching conditions explored above.

2:40 pm **PS-TuA3 Ponderomotive Effects in Helicon Plasmas,** R. Brown, J. Gilland, N. Hershkowitz, R. Breun, University of Wisconsin, Department of Nuclear Engineering and Engineering Physics, 1500 Johnson Drive, Madison, WI 53706-1687.

Computer modeling of Nagoya Type III, Dual-Half-Turn and Spiral antennas, used to excite helicon waves, has been carried out with the code ANTENA. The code considers a cylindrical plasma with an arbitrary radial density and temperature profile and realistic antenna structures, in a uniform magnetic field. With the exception of end conditions, it provides a good model of the experimental configuration in our laboratory helicon plasma in which the helicon wavelength  $\lambda \ll L$ , the plasma length. We report investigations of the role of rf radial ponderomotive force in providing or reducing MHD stability of the helicon plasma with emphasis on the roles of the  $m = +1$  and  $m = -1$  azimuthal modes. Comparisons are presented to experimental data.

Supported by NSF Grant No. ECS-9120326.

3:00 pm **PS-TuA4 A High Etch Rate, Highly Selective, Sub-half-micron Contact Etch Process in a Low Pressure, High Density TCP Oxide Etcher,** P. K. Gadgil, A. Asthana, and I. Morey, Lam Research Corporation, Fremont, California 94538.

A low pressure, high density transformer coupled plasma (TCP) source with independent RF bias control has been characterized for etching sub-half-micron contact holes in silicon dioxide on 200 mm substrates. The dependence of etch selectivities of silicon dioxide to photoresist, to silicon nitride, and to silicon on different process parameters has been investigated. This paper discusses the effects of feed gas chemistry, the ratio of inductive-to-capacitive nature of plasma generation, and TCP power on the etch selectivities and the tradeoffs therein. The etch selectivity of oxide-to-nitride increases with more inductive plasma generation, and with more polymerizing chemistries. A high aspect ratio (6:1) contact etch process with high oxide etch rate ( $> 8000$  A/min), high oxide-to-resist selectivity ( $> 5$ ), high oxide-to-nitride selectivity ( $> 20$ ); and low RIE lag in 0.35  $\mu\text{m}$  contacts has been achieved by optimizing the process parameters. The results indicate that the TCP technology is a promising candidate for future sub-half-micron contact and via etch applications.

3:20 pm **PS-TuA5 Construction and Characterization of a Multi-dipole-Confined RF Inductively-Coupled Plasma Etching Source\*,** C. Lai, B. Brunmeier, and R. Claude Woods, The Engineering Research Center for Plasma-Aided Manufacturing, University of Wisconsin, Madison, WI 53706.

A planar rf inductively-coupled plasma etching system has been constructed. The plasma is confined by an external multidipole magnetic bucket made of strong Nd-Fe-B magnets. The system is equipped with a helium-backside-cooled electrostatic wafer chuck and a loadlock chamber. A single-sided Langmuir probe was used to measure electron velocity distribution functions (EVDFs) radially and axially for both Ar and  $\text{N}_2$  plasmas with rf powers up to 1 kW at lower pressures ( $\leq 10$  mTorr). By rotating the single-sided probe we found that the EVDFs are noticeably anisotropic. The values of the plasma potential, which were highly uniform radially, were independent of the probe orientation, but those of the floating potential depended strongly on it. The radial uniformity of the plasma potentials was confirmed by measurements using an emissive probe. The Langmuir probe measurements also showed non-Maxwellian EVDFs for both Ar and  $\text{N}_2$  plasmas. Because of the multidipole confinement, the plasma densities are quite uniform axially and the radial uniformity improves as the axial distance from the quartz window increases. The system was further characterized using a capacitive probe and an electromagnetic (B-dot) probe.

\*This work was supported by the National Science Foundation under Grant ECD-8721545.

3:40 pm **PS-TuA6 Large Area Transformer Coupled Plasma For Microelectronics Processing,** Z. Yu, D. M. Shaw, and G. J. Collins, Colorado State University, Fort Collins, CO 80523.

Radio-frequency (rf) transformer coupled plasma (TCP) provides for a better way to generate spatially confined high density gas discharge plasmas for microelectronics processing. Commercial processing equipment using this technique is currently available; however, it is limited in size to 8-inch diameter by problems with plasma uniformity and window erosion. We have developed a new TCP design that allows for larger dimensions with good uniformity. The current equipment requires an expensive thick quartz plate vacuum window that separates the rf inductor and the plasma. The thick quartz plate reduces coupling efficiency and causes uniformity problems. Our device incorporates the rf inductor and dielectric window inside of the vacuum chamber, allowing for a thin layer of quartz or other dielectric material, as required by the process, to be placed between the coil and the excited plasma. This thin dielectric layer, as well as a newly designed rf tuning network, allow the plasma to be scaled to larger dimensions while maintaining good uniformity. Plasma ashing results for an 8-inch device show 2% uniformity across 6-inch wafers. Characterization of the plasma generated by a larger scale device, as well as ashing results for the device, will be presented.

This work supported by NSF grants DDM-9108531 and DDM-9311697.

4:00 pm **PS-TuA7 Large Volume Electron Cyclotron Resonance Plasma Generation by Use of Slotted Antenna Microwave Applicator,** J. Engemann, M. Schott, F. Werner, and D. Korzec.

The generation of large area, low pressure (below  $10^{-3}$  mbar) mi-

crowave plasmas is of high technological interest for etching, deposition, plasma modification and production of nanomaterials [1]. A slotted antenna concept described in detail elsewhere [2] allows generation of high volume 2.45 GHz discharge. The microwave applicator used in this work for ECR plasma generation consists of ten horn antennas positioned around a fused silica cylindrical plasma chamber with a diameter of 16 cm. The horn antennas are supplied with microwave power from a wave guide ring resonator through transversal slots. SmCo magnets are placed between the horn antennas directly at the plasma chamber wall. Three types of magnetic field architecture are regarded: toroidal, multicusp and hybrid. All these geometries allow to generate argon plasma at pressure down to  $2 \times 10^{-4}$  mbar. An effective air cooling allows for long term stable operation of the source at microwave powers up to 2 kW. The plasma was characterized by use of a double Langmuir probe in the weak magnetic field area in a distance of two cm from the plasma chamber wall. The toroidal permanent magnets configuration allows the highest plasma density and the best azimuthal plasma homogeneity. The ion concentration of  $5 \times 10^{12} \text{ cm}^{-3}$  for this configuration can be achieved. An important advantage of the presented plasma source architecture is its up scale ability. The 64 cm diameter version of the slotted antenna source will be described elsewhere.

[1] Asmussen, J., *J. Vac. Sci. Technol. A.*, 7, pp. 883-893 (1989).

[2] Werner, F. et al., *Plasma Sources Science and Technol.* to be published (1994).

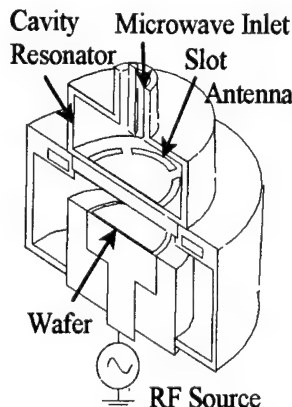
4:20 pm **PS-TuA8 New ECR Plasma Source for UHV Epitaxy**, B. J. Stanbery, T. J. Anderson, Department of Chemical Engineering, University of Florida, Gainesville, FL 32611-2022.

Conventional and commercially available ECR plasma sources for UHV epitaxy are based on plasma excitation of a gas source, such as methane or arsine. This approach suffers two principal limitations for application to reactive deposition. First, independent control of the supply of hydrogen, hydrides, and elemental species to the growth surface is unavailable. Thus the competitive etching reactions which have been reported in the case of, for example, GaAs, are not separably controllable. Second, the hydride gas sources are hypertoxic relative to their elemental constituents (*eg*: arsine *vs.* arsenic), resulting in additional cost and risk when they are used.

We have developed an ECR plasma "cracker" to address these problems. It couples to a conventional MBE effusion cell for the volatile species, in our case selenium. The source includes a gas injector which enables generation of the plasma in mixtures of the effusion cell's vapors and other gases. We use helium and hydrogen as a buffer and for control of hydride generation, respectively.

The first iteration of design used permanent magnets and a flux shunt to generate the magnetic field required for ECR resonance. Inhomogeneity of the resulting field limited the discharge to a small fraction of the intended reaction zone, resulting in a minimum operating pressure of  $\sim 10^{-4}$  torr. We are substituting solenoidal electromagnetic field coils to increase the resonance zone's pathlength and reduce the operating pressure. The design approach, operating characteristics and flux energy distribution will be reported.

4:40 pm **PS-TuA9 Characteristics of the Non-Magnetic Type Microwave Plasma Etching Reactor with Slot Antenna**, H. Tamura, T. Otsubo, I. Sasaki, K. Ohara, Y. Yamaguchi, S. Kato\*, Production Engineering Research Laboratory, Hitachi, Ltd., Yokohama, Japan, \*Device Development Center, Hitachi, Ltd., Ome Japan.



The etching process in ULSI fabrication demands high plasma uniformity. For high precision and uniform processing, ions must strike the wafer uniformly at a  $90^\circ$  angle. Achieving this requires a highly-controllable plasma generation region, low-temperature ion generation and readily diffusible electrons. It is therefore important to generate plasma at low pressure and without a magnetic field. Using a cavity resonator and slot antenna, we recently developed a compact microwave plasma reactor with virtually no magnetic field adjacent to the wafer. We have termed it the Microwave Slot Antenna (MSA) reactor.

Microwaves are introduced to the cavity resonator in order to enhance the electric field. The microwaves are radiated through the slot antenna to the processing chamber. The plasma generation region can be controlled by adjusting the slot antenna. Uniform control of the plasma and RF bias distribution is readily achievable because the electrons near the wafer can easily diffuse.

We numerically simulated the distribution of the electron temperature and density and the microwave EM field. We applied the MSA reactor to the Si etching process. After achieving uniformity of  $< 5\%$  and an undercut of  $< 20$  nm, we confirmed that the MSA reactor is efficient for the ULSI process.

5:00 pm **PS-TuA10 Performance of a Permanent Magnet ECR Reactor**, A. Saproo, D. Dane, and T. D. Mantei, University of Cincinnati, Cincinnati, Ohio 45221.

A permanent magnet electron cyclotron resonance high density reactor has been developed and characterized for plasma assisted etching applications. The axial magnetic field required for ECR operation is established by a Nd-Fe-B permanent magnet structure which provides a resonance plane ( $\sim 0.0875$  Tesla) approximately 10 cm below the magnet face, with no electrical input or cooling power required. The process plasma is radially confined by a multipolar magnetic field layer. High plasma densities ( $\sim 10^{11} \text{ cm}^{-3}$ ) and high ion current densities ( $\sim 10 \text{ mA-cm}^{-2}$ ) are generated in  $100\% \text{ Cl}_2$  at a pressure of 2 mTorr, measured at the wafer position 30 cm below the ECR plane. The radial plasma parameter uniformity is better than 1% across a 200 mm diameter, in agreement with the predictions of a two dimensional plasma diffusion model. Polysilicon etch results obtained on 150 mm patterned Si wafers in  $\text{Cl}_2$  will also be presented.

## VACUUM TECHNOLOGY

### Room A102 - Session VT-TuA

#### Vacuum System Outgassing and Cleaning

Moderator: H. F. Dylla, CEBAF.

2:00 pm **VT-TuA1 Water: Its Measurement and Control in Vacuum**, S. A. Tison and J. P. Looney, National Institute of Standards and Technology, Gaithersburg, MD 20899.

The presence of water vapor in vacuum systems has many deleterious effects which can influence the yield of vacuum manufacturing processes, the ultimate pressure of vacuum systems, and the stability of vacuum instrumentation. Water vapor can enter the vacuum system from the process gas, can desorb from interior surfaces or diffuse through polymer seals. Although the presence of water vapor is well known, the ability to measure its abundance with conventional gaging is not well understood. Additionally although many models exist for predicting water adsorption and desorption from surfaces, their reliability or applicability is not well established. Some recent advances in water measurement, such as using optical techniques to measure water vapor abundance, have promise to advance the understanding of water dynamics in vacuum systems. A workshop dedicated to examining the current state of water vapor measurement and control in vacuum was held at the National Institute of Standards and Technology in May of 1994. This paper will summarize the contents of the workshop and review recent progress in water measurement and control.

INVITED

2:40 pm **VT-TuA3 TiN Thin Film on Stainless Steel for Extremely High Vacuum Material**, K. Saitoh, S. Inayoshi, Y. Ikeda, Y. Yang, and S. Tsukahara, Tsukuba Institute for Super Materials, ULVAC JAPAN, Ltd. Tsukuba, JAPAN 300-26.

We noticed TiN films on stainless steel (TiN/SS) as one of the most promising candidate materials for extremely high vacuum (XHV) use. All the TiN films were vapor deposited at the optimum conditions



determined previously and vacuum properties of the TiN/SS samples have been compared with those of the electrolytically polished SS samples.

The outgassing of the short samples of  $20 \text{ mm}^2 \times 0.5 \text{ mm}$  was measured by thermal desorption spectroscopy heating up to  $450^\circ\text{C}$  in ultrahigh vacuum. The total outgassing of TiN/SS was always lower than that of SS when they were measured in the same conditions.

Hydrogen permeation of membrane samples were measured varying the temperature and the thickness of TiN films. The TiN film works as the barrier to hydrogen desorption from stainless steel surface. The TiN/SS membranes showed about two orders less permeation rate than those of SS at  $350^\circ\text{C}$  and the difference of them is the higher at the lower temperature.

As the final experiments the chamber samples of  $254 \text{ mm } \phi \times 380 \text{ mm}$  were examined. The temperature depending outgassing rates of the chambers after the bake-out at  $150^\circ\text{C}$  for 2 days were measured by the throughput method with special consideration to completely exclude the outgassing of the gauges and spectrometer tubes under measurements. At the ultimate upstream pressures of about  $1 \times 10^{-9} \text{ Pa}$  and the downstream pressure at XHV range the residual gas component was only hydrogen and the specific outgassing rate of the TiN/SS and the SS chambers were  $6 \times 10^{-12}$  ( $6 \times 10^{-11}$  for hydrogen) and  $9.7 \times 10^{-10} \text{ Pa} \cdot \text{ms}^{-1}$  for nitrogen at  $21.4^\circ\text{C}$ , respectively. The result proves that the TiN films on stainless steel are applicable to wall material for XHV apparatus.

3:00 pm **VT-TuA4 SIMS Analysis for Aluminum Surfaces Treated by Glow Discharge Cleaning**, J. R. Chen<sup>a)</sup>, G. Y. Hsiung, Y. C. Liu<sup>b)</sup>, Synchrotron Radiation Research Center, No. 1 R&D Road VI, Hsinchu Science-Based Industrial Park, Hsinchu, Taiwan 300, R.O.C., W. H. Lee and C. C. Nee, Institute of Nuclear Science, National Tsing-Hua University, Hsinchu, Taiwan 300, R.O.C.

The glow discharge cleaning treatments on aluminum surfaces were studied by the SIMS method. The cleaning effects of DC and RF glow discharge with different gases were compared. The elements or compounds of the contamination or reaction products were identified from the analyses of mass and energy distribution of the secondary ions. The secondary ion energy distribution was similar for the elements with the same group. The results and discussions are to be described in this paper.

a) also at Institute of Nuclear Science, National Tsing-Hua University.  
b) also at Department of Physics, National Tsing-Hua University.

3:20 pm **VT-TuA5 Reduction of Water Outgassing from Metal Surfaces by Glow Discharge Cleaning\***, Minxu Li, College of William & Mary, Williamsburg, VA 23185, and H. F. Dylla, Continuous Electron Beam Accelerator Facility, Newport News, VA 23606.

The effectiveness of glow discharge cleaning (GDC) as a means of decreasing the pump-down time of vacuum systems was studied. We measured the outgassing rate of an electropolished stainless steel surface after it was exposed to glow discharges fueled by various gases ( $\text{He}$ ,  $\text{He}/1\sim 3\%\text{H}_2$ ,  $\text{He}/1\sim 3\%\text{CH}_4$ ,  $\text{H}_2$ ) following a standard one hour of venting to ambient air. It is shown that  $\text{He}$  GDC is most effective in reduction of outgassing rate: a  $\text{He}$  GDC trial with a dose of  $0.8 \text{ coulomb}/\text{cm}^2$  reduces the outgassing rate and subsequently the pump-down time by a factor of 13. For given glow discharge currents, the outgassing reduction factor is linearly proportional to the glow discharge duration. The reduction of post-GDC outgassing is a result of enhanced desorption of  $\text{H}_2$ ,  $\text{CO}$ , and  $\text{CO}_2$  by  $\text{He}$  GDC as observed by residual gas analysis during the discharge. The GDC results are consistent with our previously proposed diffusion models for water outgassing from metal surfaces.

\*This work supported by U.S. DOE Contract No. DE-AC05-84ER40150.

3:40 pm **VT-TuA6 XPS Analysis of Cleaning Procedures for Synchrotron X-Ray Beamline Components at the Advanced Photon Sources**, \*Y. Li, R. A. Rosenberg, D. Ryding, R. Nielsen, C. Liu, D. Shu, and T. M. Kuzay, Advanced Photon Source, Argonne National Laboratory, Argonne, IL 60439.

The Advanced Photon Source (APS), currently under construction at Argonne National Laboratory, will be one of the most powerful synchrotron x-ray photon sources in the world. The beamline sections where the x-ray will be transported will contain high thermal load ultrahigh vacuum (UHV) compatible components, such as photon shutters, fixed masks, slits, and bellows. These components are made

of OFHC copper (for photon shutters), GlidCop<sup>®</sup>  $\text{Al}_2\text{O}_3$  dispersion strengthened copper (for fixed masks and photon shutter face-plates), TZM high temperature molybdenum alloy (for slits), machinable tungsten (for safety shutters) and 304 or 316 stainless steels (for UHV component joints and bellows). Before any of these components can be assembled, they must be cleaned to remove surface contaminants so that the ultrahigh vacuum necessary for successful operation can be achieved. Fabrication of the components will also involve joining processes, such as explosion bonding, brazing and soldering, et al. Removal of surface oxides of joining materials is crucial to obtain secure bonding. Although the vacuum and mechanical properties of the cleaned surface are of prime importance, environmental and safety factors are also of great concern. Both conventional and environmentally safe, commercially available cleaning detergents were investigated, and the surface cleanliness was evaluated using x-ray photoelectron spectroscopy (XPS). Several important results have been learned in this study. Some of the commercial cleaning detergents were as effective as conventional etching solutions for the materials. The effect of the material microstructure on the surface cleanliness and XPS analysis results will also be discussed in detail.

\*Work supported by U.S. Department of Energy, BES-Materials Sciences, contract No. W-31-109-ENG-38.

4:00 pm **VT-TuA7 Thermal Outgassing Studies on Machinable Tungsten and TZM Molybdenum Alloy\***, C. Liu, R. W. Nielsen, Y. Li, D. Ryding, and T. M. Kuzay, Advanced Photon Source, Argonne National Lab, Argonne, IL 60439.

Machinable tungsten and molybdenum alloys are extensively used as safety shutters and optical slits at the Advanced Photon Source (APS) front ends. These materials may present a vacuum problem because of their porosity. Also, environmentally acceptable cleaning procedures have to be used for these materials. We have chosen specially heat-treated machinable tungsten with a density of  $18 \text{ g}/\text{cm}^3$  for safety shutters and TZM (a molybdenum alloy containing 0.5% titanium and ~0.1% zirconium) for optical slits. Thermal outgassing tests have been performed for a machinable tungsten set with a total surface area of  $4500 \text{ cm}^2$  and a  $2.8 \times 4.6 \times 32.6 \text{ cm}^3$  piece of TZM. A cleaning procedure using alkaline detergent ultrasonic washes and vacuum furnace baking was used prior to the outgassing measurements. Outgassing rates 10 h after initial pump down at room temperature are  $1.6 \times 10^{-10} \text{ Torr l/s cm}^2$  for machinable tungsten and  $8.0 \times 10^{-10} \text{ Torr l/s cm}^2$  for TZM. The outgassing rates 24 h after an *in situ* bake at  $160^\circ\text{C}$  for two days decreased to  $2.2 \times 10^{-12} \text{ Torr l/s cm}^2$  for machinable tungsten and  $1.2 \times 10^{-11} \text{ Torr l/s cm}^2$  for TZM, respectively. Optical studies confirmed that the TZM sample is more porous than the machinable tungsten sample. Further studies of a denser TZM sample have been planned to study the effect of porosity on the outgassing rate.

\*Work supported by the U.S. Department of Energy BES Materials Science under contract W-31-109-ENG-38.

4:20 pm **VT-TuA8 Photon Stimulated Desorption (PSD) Measurements of Extruded Copper and of Welded Copper Beam Chambers for the PEP II Asymmetric B-Factory**, C. L. Foerster, C. Lanni, Brookhaven National Laboratory, Upton, NY 11973, and C. Perkins, Stanford Linear Accelerator Center, Stanford, CA 94305 and M. Calderon, Lawrence Livermore National Laboratory, Livermore, CA 94551.

PEP II is being built as a higher luminosity electron-positron collider, with asymmetric beams of 9 GeV and 3.1 GeV, having maximum currents of 3.0 A. Based on our previous work on the NSLS VUV beamline U10B, a copper was selected for construction of UHV beam chambers and absorbers to minimize the pressure rise from synchrotron radiation during operation. An extruded beam chamber and a welded beam chamber were fabricated from the selected copper for PSD measurements on NSLS X-ray beamline X28A. The chambers were exposed to white light with a critical energy of 5 Kev, both direct and through a 0.010 inch thick Beryllium filter. Each chamber was exposed to a dose of approximately  $10^{23}$  photons per meter at an incidence angle of 30 mrad, after argon glow conditioning and a  $150^\circ\text{C}$  vacuum bake. Desorption yields for  $\text{H}_2$ ,  $\text{CO}$ ,  $\text{CO}_2$ , and  $\text{CH}_4$  are reported as a function of accumulated photon flux, critical energy, and chamber preparation. The results are compared with the previous work on beamline U10B and with those of other published work for copper.

\*Work performed under the auspices of the U.S. Department of Energy, under contract DE-AC02-76CH00016.

4:40 pm **VT-TuA9 Photodesorption From Copper Chamber With Cutting Inner Surface By Broaching**, *T. Kobari, M. Matumoto and N. Hirano*, MERL Hitachi Ltd., Tsuchiura 300 Japan, *M. Katane and M. Matsuzaki*, Hitachi works, Hitachi 317, *Y. Hori and M. Kobayashi*, PF KEK, Tsukuba 305, *M. Nagai*, Hitachi Cable, Tsuchiura 300.

We had reported that the photodesorption yields due to synchrotron radiation of OFC chamber with machined surface was especially lower than those of stainless steel or aluminum alloy. It is also reported that a new OFC chamber with machined inner surface installed in the PF ring and the photodesorption yield of the chamber showed quick decreasing. The chamber was manufactured by machining the inner surface of extruded half shell of a chamber, then a beam chamber was formed by electron beam welding.<sup>1)</sup> But, the manufacturing method requires high cost.

A new surface treatment has been developed for cutting the inner surface of a beam chamber and to get lower photodesorption easily. A OFC test chamber was extruded, then the inner surface was cut by broaching. Photodesorption yield of the chamber has been measured in BL21 of PF beamline. The comparison with other treatments and surface analysis will be presented.

<sup>1)</sup> Y. Hori, M. Kobayashi, Y. Takiyama, JVST A12(4), Jul./Aug., 1994 (in printing).

5:00 pm **VT-TuA10 Characteristics of Artificial Submerged Cavitation Water Jet**, *S. Hamada*.

Water jet is one of general methods of cleaning wafers, liquid crystals, and some materials. Increase of cleaning effect can be expected by water jet with cavitations more than conventional water jet. Although cavitation water jet requires some form of artificial submergence for in-air cleaning operations, good performance of cavitation water jets has mainly been documented under submerged conditions for a given set of operating conditions.

The purpose of this study is establish the usefulness and limitations of cavitation water jets for wide spread practical applications. Sample results of flow visualization, impinging pressure distribution are presented in an attempt to elucidate the influence of geometrical and operating parameters on the performance of the cavitation water jets. Possible advantages of artificial submergence through surrounding nozzle are also explored.

## THIN FILM/VACUUM METALLURGY

Room A105 - Session TFVM-TuA

### Diamond, Cubic Boron Nitride and Other Ultra-Hard Films II

**Moderator:** W. D. Sproul, BIRL, Northwestern University.

2:00 pm **TFVM-TuA1 Deposition and Characterization of Cubic Boron Nitride Thin Films**, *Robert F. Davis, Daniel J. Kester, and K. Shawn Ailey*, Department of Materials Science and Engineering, North Carolina State University, Raleigh, North Carolina 27695.

Boron nitride (BN) thin films have been grown on Si(100) and diamond (100) substrates by ion beam assisted deposition (IBAD) using electron beam evaporation of B together with simultaneous bombardment by N and Ar ions. Characterization by FTIR and TEM showed that the films consisted of initial amorphous and hexagonal BN layers, followed by the growth of cubic BN. This growth sequence is attributed primarily to increasing compressive intrinsic stress in the films. The effect of deposition conditions, specifically substrate temperature and bombardment intensity, on the film growth was studied. It was found that increasing the substrate temperature above 400°C led to the onset of the cubic phase at a greater film thickness, while increased bombardment led to earlier c-BN growth. These results are explained by the relaxation of intrinsic stress in the films at higher temperatures due to increased adatom mobility and to increased intrinsic stress in the films resulting from increased bombardment. Lower temperatures led to mixed phase growth. There also seems to be a minimum substrate temperature (200–300°C) required for single phase cubic boron nitride growth. BN was also grown on single crystal Cu and Ni substrates.

INVITED

2:40 pm **TFVM-TuA3 An AES/XPS Study of Ti-B-N Thin Films**, *M. A. Baker, A. Steiner, J. Haupt, W. Gissler*, Commission of the European Communities, Joint Research Centre, Institute for Advanced Materials, 21020 Ispra, Italy.

Boron nitride based transition metal coatings are presently being considered as potential materials for coating applications requiring high hardness, high temperature and corrosion resistance. Ti-B-N layers have been produced by sputter deposition from a BN target onto which small Ti platelets have been positioned. By changing the number of platelets, the Ti-B-N composition has been varied and the films studied by AES and XPS. Quantification of the film composition by AES is discussed, considering the Ti  $L_{23}M_{23}M_{23}$  and N  $KL_{23}L_{23}$  peak overlap. Changes in the Ti  $L_{23}M_{23}M_{23}$  and B  $KL_{23}L_{23}$  peak regions with composition are examined and correlated with DOS calculations. Using XPS, shifts in the B1s and N1s peaks have been used to compare the phase composition with that predicted by the thermodynamic phase diagram. Correlations of the compositional and mechanical testing data show that films of highest hardness are obtained when a composition of approximately  $TiBN_{0.5}$  is obtained, the phase composition being a combination of  $TiB_2$  and TiN.

3:00 pm **TFVM-TuA4 Electron Cyclotron Resonance Plasma Assisted Growth of Thin Carbon Nitride Films on Si(100): Film Composition and Structure**, *A. Bousetta, A. Bensaoula, and M. Lu*, Space Vacuum Epitaxy Center, University of Houston, Houston, Texas 77204-5505.

We report compositional and structural properties of thin carbon nitride films on Si(100) substrates at temperatures in the range of 100–650°C using e-beam evaporation of graphite assisted with ECR plasma generated nitrogen beam. The effects of a SiN buffer layer, a varying nitrogen gas flow into the ECR source, and the substrate temperature, on the C/N composition ratio, and  $C_xN_y$  crystal structure were investigated using Fourier transform infrared spectroscopy (FTIR), X-ray photoelectron spectroscopy (XPS), Rutherford backscattering spectroscopy (RBS), and Raman spectroscopy. From both RBS and XPS, the nitrogen concentration in the film was calculated in the range of 20 to 38% and varied directly with the nitrogen partial pressure in the ECR source. FTIR spectra from films with low nitrogen content exhibited a high visible- to infrared-transmittance and were dominated by amine groups ( $NH_2$ ) with the presence of C-N stretching modes. Raman spectra however show no evidence of CN bonding and were characteristic of a graphitic carbon. In contrast, in high nitrogen content thin films, both the transmittance and  $NH_2$  absorption band decreased whereas the C-N absorption band increased. Raman spectra of these films show a well resolved peak at  $1275\text{ cm}^{-1}$  suggesting the formation of a  $C_xN_y$  phase with predominately  $sp^3$  bonding.

3:20 pm **TFVM-TuA5 Sputtered Carbon Nitride Films**, *K. G. Kreider, M. J. Tarlov, G. Gillen, L. H. Robins, L. K. Ives, W. J. Bowers, and R. Marinenko*, NIST, Gaithersburg, MD 20899.

The recent announcement of the synthesis of  $C_3N_4$  by plasma enhanced laser ablated deposition has increased interest in this unique material. Carbon nitride may have several useful properties for wear and corrosion resistant coatings, electrical insulators, and optical coatings. We have produced carbon nitride coatings containing up to 40% nitrogen using ion assisted planar magnetron RF sputtering in a nitrogen atmosphere. Up to 2  $\mu\text{m}$  thick coatings are produced on alumina, silicon,  $SiO_2$ , and glass substrates using a graphite target. Films with greater than 95% transparency in the visible wavelengths and harder than alumina have been produced. The electrical properties of these films are correlated with composition, fabrication conditions, and subsequent heat treatments. Typical compositional measurements from energy dispersive X-ray measurements indicate 36–40% by weight nitrogen in an amorphous phase. XPS studies appear to confirm the stability of a carbon nitride phase up to 600°C. Compositional variations and oxygen presence were monitored with SIMS depth profiling and the Raman spectra are compared with those of other carbon and carbon nitride films.

3:40 pm **TFVM-TuA6 Thermal Behavior of Carbon Nitride and TiN/NbN Superlattice Coatings**, *S. Lopez, M. S. Wong and W. D. Sproul*, BIRL Industrial Research Laboratory, Northwestern University, 1801 Maple Avenue, Evanston, Illinois 60201-3135, USA.

Hard coatings are commonly used today to enhance the life of numerous tools (drills, cutters) and wear parts (bearings). Carbon nitride ( $CN_x$ ) and TiN/NbN superlattice films are being evaluated for such tribological applications, and it was necessary to test their behavior under thermal treatment. The coatings were reactively sputtered on various substrates. Thermal annealings of both coatings were per-



formed at temperatures up to 1000°C either under high vacuum ( $10^{-7}$  Torr) or in air. Several properties of the coatings before and after annealing were evaluated including hardness (nano-indentation), adhesion/cohesion (critical load), structure (XRD), and composition (AES). In vacuum, the carbon nitride coatings lost part of their nitrogen as the annealing temperature was increased and a critical temperature for stability was found to be around 600°C. No change in composition and slight changes in layer structure were observed for the TiN/NbN superlattice films annealed at temperatures up to 800°C under vacuum for 2 hours.

4:00 pm **TFVM-TuA7 Deposition and Properties of Polycrystalline VN/NbN Superlattices**, X. Chu\*, M. S. Wong\*\*, W. D. Sproul\*\* and S. A. Barnett\*, \*Department of Materials Science and Engineering; \*\*BIRL, Northwestern University, Evanston, Illinois 60201.

A larger difference in shear modulus between neighboring layers was attributed to the hardening effects observed in TiN/NbN and TiN/VN superlattices studied previously. A new transition metal nitride superlattice VN/NbN with little difference in shear modulus was investigated in order to verify the superlattice hardening theory. The NbN/VN superlattices were deposited on steel substrates by an opposed dual-cathode unbalanced magnetron sputtering system. Despite a large lattice mismatch of 5.7% between NbN and VN, XRD results show that the superlattice structure exists in all the films studied, when the superlattice period ranged from 2.4 nm to 50 nm. The structures and properties of superlattices were investigated under different deposition and superlattice modulation parameters including nitrogen partial pressure, superlattice period, and relative layer ratio. Microhardnesses measured by both a Vickers microhardness and nanoindentation tester showed no appreciable hardness enhancement as a function of superlattice period or relative layer ratio. The results were compared with TiN/NbN and TiN/VN superlattices, in which hardness enhancements of over 2 times either nitride layer was shown. This study supports the theory that the difference in layer shear modulus is a major factor affecting the superlattice hardness.

4:20 pm **TFVM-TuA8 Growth Mechanism of Carbon and Related Diamondlike Films Deposited by High Energy  $C^+$  Ions**, E. Grossman<sup>a</sup>, G. D. Lempert<sup>b</sup>, J. Kulik<sup>b</sup>, J. W. Rabalais<sup>b</sup> and Y. Lifshitz<sup>a</sup>, a. Soreq NRC, Yavne 81800 Israel, b. Univ. of Houston, Houston 77204-5641 TX, USA.

Carbon films were deposited on Si substrates using mass selected  $C^+$  ions at deposition energies of 2 to 45 KeV and substrate temperatures from 25°C to 250°C. A recent publication<sup>1</sup> described the growth mechanism of similar films deposited at lower ions energy (<2KeV) and the dependence of their structure and properties on the deposition parameters. The present study investigates the growth mechanisms and properties at higher energies.

The main characterized features were: (i) morphology at the nanometer scale, by Atomic Force Microscopy (AFM) (ii) density, by Rutherford Backscattering Spectroscopy (RBS) in conjunction with profilometry (iii) chemical composition and depth profile by Auger Electron Spectroscopy (AES) and (iv) bonding configuration ( $sp^3/sp^2$ ) by Electron Energy Loss Spectroscopy (EELS).

In the low deposition energy regime a smooth surface was an indication of internal subsurface growth with a higher  $sp^3$  component, while rougher surfaces were consistent with a higher  $sp^2$  component. At higher  $C^+$  energies, films with relatively smooth surfaces evolved. The mechanisms (different from those at the low energy regime) affecting the films growth, surface morphology and bulk properties are discussed.

1. Y. Lifshitz, G. D. Lempert and E. Grossman, Phys. Rev. Lett. 72 (1994) 2753.

4:40 pm **TFVM-TuA9 Thickness-Distribution Control of Large-Area DLC Films Formed by  $CH_4/H_2$  Supermagnetron Plasma**, H. Kinoshita, S. Nomura, and M. Honda, Research Institute of Electronics, Shizuoka University, 3-5-1 Johoku, Hamamatsu 432, Japan.

Supermagnetron plasma<sup>1)</sup> was first applied to CVD with adjusting both rf phase difference (RFPD) and rf power ratio (13.56 MHz) whose powers were supplied to two parallel cathodes. In most experiments, stationary magnetic field of 45G was applied parallel to a lower cathode, on which a 5-in. Si wafer was set. Thickness uniformities of diamondlike carbon (DLC) films were evaluated as a function of rf phase difference. When RFPD was 0°, its uniformity became poor ( $\pm 9\%$ ), and at about 180° it became excellent ( $\pm 3\%$ ). Based on this result, we measured the upper cathode rf power (UPRF) de-

pendence of its thickness distribution at the fixed conditions of RFPD of 180°, electrode spacing of 45mm, lower cathode rf power (LORF) of 400W, and gas pressure of 6 mTorr. When UPRF was set to OW, linearly graded thickness-distribution was observed along perpendicular direction to magnetic field lines, which shows a typical magnetron mode<sup>2)</sup>. At UPRF of 100W, almost uniform distribution of  $\pm 2.9\%$  was obtained, and at 200W inverse distribution to that of OW was observed, i.e. inverse magnetron mode. Extremely high uniformity of  $\pm 1.4\%$  was observed at RFPD of 180° by rotating the magnetic field. Rather high hardness of about 1400 kg/mm<sup>2</sup> was obtained in this condition. From this experiment it was confirmed that, at RFPD of about 0° secondary electrons emitted from the upper cathode drift along it and generate plasma over the upper cathode. At about 180°, on the contrary, that emitted from the upper cathode drift toward the lower cathode and generate plasma over the lower cathode.<sup>1)</sup>

<sup>1)</sup>H. Kinoshita and K. Nomoto, J. Vac. Sci. Technol. A10, 1092 (1992).

<sup>2)</sup>H. Kinoshita et al., J. Appl. Phys. 62, 4269 (1987).

5:00 pm **TFVM-TuA10 Structural Analysis of Hydrogenated Carbon Films Obtained by Reactive dc Magnetron Sputtering**, S. Fujimaki, M. Kitoh, Production Engineering Research Laboratory, Hitachi, Ltd., Totsuka-ku, Yokohama 244, Japan; H. Matsumoto, Y. Kokaku, Data Storage & Retrieval Systems Division, Hitachi, Ltd., Kozu, Odawara 256, Japan.

Amorphous hydrogenated carbon films were prepared by reactive dc magnetron sputtering in argon plasma containing methane as the reactant gas. The films were characterized using various spectroscopic measurements such as Raman scattering, optical absorption spectroscopy in the ultraviolet (UV)—visible (VIS) region and infrared (IR) absorption spectroscopy.

The spectral analyses indicated that changes in Raman spectral intensity occurring with increasing methane gas content were determined to be caused by changes in optically resonant components in the films.

Furthermore, significant correlation was seen between the relative intensity of IR peaks and wear durability. It can be concluded that the increase of  $CH_3$  bonds at  $sp^3$ -carbon sites is assumed to restrict the network of C-C connections and thus reduce the film's wear durability. Also, the chain-like structure of olefinic compounds, as compared with the ring structure of aromatic compounds, was assumed to increase the wear durability at  $sp^2$ -carbon sites. From this, the films formed at a methane gas content of about 20% were found to have the highest wear resistance.

## ELECTRONIC MATERIALS Room A108 – Session EM-TuA

### Silicon-based Optoelectronics

Moderator: K. J. Bachmann, North Carolina State University.

2:00 pm **EM-TuA1 Optical Waveguides on Silicon Chips**, S. Yokoyama, Y. Kuroda, T. Miyamoto, T. Doi, T. Namba, T. Nagata, K. Miyake, S. Miyazaki, M. Koyanagi and M. Hirose, Research Center for Integrated Systems, Hiroshima University, 1-4-2 Kagamiyama, Higashi-Hiroshima 724, Japan.

The signal propagation delay for metal interconnections is increasing with down-scaling of device sizes. In order to overcome this problem, optical interconnections are attracting great interest due to their high functional performance and high speed. In this study we have developed technologies to fabricate optical waveguides consisting of  $SiO_xNy$  core and  $SiO_2$  cladding layers at low temperatures (300°C). The propagation loss for curved waveguides has also been simulated and compared with experimental results.

Remote plasma enhanced CVD was employed for the deposition of  $SiO_xNy$  and  $SiO_2$  films to reduce plasma-induced damage. The source gases were  $SiH_4$ ,  $N_2O$  and  $NH_3$ . The refractive index of the  $SiO_xNy$  core layer can be precisely controlled from 1.5 to 1.95 by changing the gas flow ratio. The propagation loss of the slab waveguides with  $SiO_xNy$  core (470 nm) and  $SiO_2$  cladding layers (800 nm) ranges from 0.93 to 1.54 dB/cm depending on the core index used.

Simulation of the loss for curved waveguides is necessary for design of optical interconnection networks. We have developed a simulator for the propagation loss in the optical waveguides by means of the

beam propagation method. The loss for curved waveguides increases drastically for radii of curvature shorter than 400  $\mu\text{m}$ , which is in good agreement with experiment results from a simple test chip with integrated LEDs, Si-mirrors, curved waveguides and LED-based detectors.

In summary, the fundamental technologies to realize the optoelectronic integrated circuits have been developed. **INVITED**

**2:40 pm EM-TuA3 Silicon Optical Bench Waveguide Technology, Charles H. Henry, AT&T Bell Laboratories, Murray Hill, N.J. 07974.**

This technology makes optical waveguides similar to those in optical fibers by depositing thick films of doped silica on silicon substrates, primarily by low pressure chemical vapor deposition. The films are patterned by photolithography and etching into complex optical integrated circuits. Components include taps, splitters, star couplers, broad and narrow band multiplexers and low speed switches. Commercial application of optical integrated circuits require nearly perfect optical waveguides with very low loss, polarization independence, control of the absolute refractive index and control over the optical phase difference between different paths. The SiOB waveguide technology has the potential to meet all of these needs. The waveguide fabrication, properties, components of current interest and opportunities for systems applications areas will be reviewed. **INVITED**

**3:20 pm EM-TuA5 Novel LSI Memories with Optical Interconnections, M. Koyanagi, Tohoku University, Sendai, Japan.**

The performance of the microprocessor has been significantly improved owing to the progress of LSI technology. However, even if the microprocessor performance is rapidly improved, the overall performance of the computer system is not always so rapidly improved because it is eventually limited by the data transfer speed or the data bandwidth of the buses. In particular, this bottleneck in the bus becomes more serious in the parallel processing computer system. We have been interested in employing optical interconnection as an intrachip or interchip interconnection to increase the data transfer speed among processors and memories in the parallel processing computer system. In this paper, we describe new LSI memories with optical interconnection such as Optical RAMbus (ORAMbus) memory. Optical RAM (ORAM)-link and Optically Coupled Common (OCC) memory which have been proposed to increase the data transfer speed and the data bandwidth by transferring data among many memories through optical interconnection. These memories have three-dimensional (3D) structure which consist of several 2D memory layers with LEDs and photoconductors or photodiodes. The memory layers are connected each other through many free-space optical interconnections in the vertical direction. The basic functions and performances of these new memories are evaluated using an optical-electrical circuit simulator. In addition, the test chips are fabricated to confirm their basic functions. **INVITED**

**4:00 pm EM-TuA7 Rare Earth Doped Silicon Emitters, J. Michel and L. C. Kimerling, Department of Materials Science and Engineering, Massachusetts Institute of Technology, Cambridge, MA 02139.**

Recent results on the improvement and understanding of light emission from the Si:Er system are reviewed. Erbium emits light at 1.54  $\mu\text{m}$ , a wavelength ideal for optical communication. While most recent studies focused on co-doping with oxygen to optically activate erbium, fluorine co-doped samples show two orders of magnitude efficiency improvement at low temperatures. Room temperature performance of Si:Er based edge emitting LED's, capable of direct waveguide coupling, will be shown and discussed in the context of system requirements for integrated optical interconnection. **INVITED**

**4:40 pm EM-TuA9 SiGe/Si Quantum Well Light Emitters, Yasuhiro Shiraki and Susumu Fukatsu, Research Center for Advanced Science and Technology, The University of Tokyo, Komaba, Meguro-ku, Tokyo 153, Japan.**

Highly luminescent SiGe/Si heterostructures are now fabricated by various growth techniques such as molecular beam epitaxy (MBE), UHV/CVD, rapid thermal CVD and so on. Especially, gas source MBE where hydrogenated gases,  $\text{Si}_2\text{H}_6$  and  $\text{GeH}_4$ , are used as molecular beam sources can provide extremely promising results for light emitting device application. Quantum wells (QWs) grown by this method show a clear quantum confinement effect as the well width is changed and their luminescence properties are well understood in terms of effective mass approximation. The temperature dependence reflects the band alignment at the heterostructures and carrier dynamics in multi-QWs provide strategies to realize light emitting devices. These results indicate that device properties of this system are predictable

from the quantum mechanical consideration, suggesting high potentials in band engineering and device designing. Some examples of LEDs including room temperature operation are demonstrated and new concepts of optical devices exploiting the nature of this material system are proposed. **INVITED**

## **MANUFACTURING SCIENCE AND TECHNOLOGY**

**Room A110 - Session MS-TuA**

### **Advanced Manufacturing Equipment - A**

**Moderator: M. Liehr, IBM TJ Watson Research Center.**

**2:00 pm MS-TuA1 The Semiconductor Equipment Industry: Applied Materials Role and Growth, Robert Z. Bachrach, Applied Materials, 3050 Bowers Ave., MS 1250, Santa Clara, CA 95054.**

Applied Materials celebrated its 25th anniversary in 1993 and in 1994 became the first Semiconductor Equipment Manufacturer to achieve revenue of one billion dollars per year. An overview will be presented of some of the factors and circumstances that have allowed Applied Materials to differentiate itself in the industry both technically and in business performance. Applied Materials now provides its customers with advanced manufacturing equipment for Etch, CVD, PVD, Implant, and HTF (High Temperature Films) for 6"/8" wafer processing. Applied Materials has focused on single wafer processing with common architecture multi-chamber mainframes: Precision 5000®, Endura®, and Centura™. A major thrust is to extend these capabilities to the next wafer size of 12" and 14" silicon which is expected to be manufacturing starting in 1998. **INVITED**

**2:40 pm MS-TuA3 Advances in Semiconductor Manufacturing Equipment, Evert van de Ven, Tom Bowman, Novellus Systems, San Jose, California.**

The Semiconductor Industry is maturing rapidly and with its requirements for manufacturing equipment have been changing from process capable hardware to turnkey production systems with guaranteed performance.

This paper will review the main issues critical to high volume manufacturing and how changes, historically and in the future, are affecting the equipment requirements and design approach. With these changes, the main focus on equipment is shifting to productivity cost/performance and production reproducibility. To determine performance to these requirements, new metrics, such as equipment productivity index, value added time, and sigma six processing are being added to defect density and cost of ownership. Using these and other criteria, the advantages and limitations of various equipment concepts will be compared and examples of successful implementation presented. Finally, an overview will be given of the challenges for next generation equipment. **INVITED**

**3:20 pm MS-TuA5 MESC Cluster Tools for Advanced Metalization, P. H. Ballentine, T. Omstead, M. Moseleh, CVC Products, Inc., Rochester, NY 14603.**

Cluster tools are playing an increasingly important role in semiconductor manufacturing. Individual process steps may be integrated into a single vacuum environment to reduce surface contamination and minimize operator handling. By using a modular approach to system design, individual process modules may be taken off line for service and burn in while the rest of the tool remains in production, thus reducing qualification time. From an equipment development point of view, process modules may be developed and characterized independent of the wafer transport platform and cluster control architecture. This provides a significant reduction in time-to-market for new process equipment. The adoption of the SEMI MESC (Modular Equipment Standards Committee) standards has provided additional benefits by allowing two or more equipment suppliers to integrate "best of breed" process modules into a single cluster tool. We have used our CVC Connexion platform to rapidly develop thin film deposition tools for both the data storage and semiconductor industries. Process modules for PVD, RTP, MOCVD, and soft etch have been developed in parallel and combined for use in production of thin film recording heads and development of advanced multilevel metalization schemes. Portions of the process modules have been based on tech-

nology licensed from the MMST program at Texas Instruments. We will present examples of individual process results as well as calculations of cost of ownership for specific integrated applications.

**3:40 pm MS-TuA6 Application of Motorola IRONMAN Methodology to Equipment Reliability Improvement, Robert Duffin, Kathleen McCormack, Motorola SPS.**

The cost to build and equip a modern IC manufacturing area is increasing rapidly. At the same time the useful life of the area is being shortened by the decreasing time required to develop new IC products. Some trend watchers have even questioned the economic viability of the IC industry past the 64 megabit DRAM.

These trends will be countered with faster fab startups, a better ROI early on, and fab life extensions. Improvements such as these will require manufacturing equipment to achieve a high degree of reliability immediately after installation and have the potential to be upgraded in the field for next generation products. These upgrades must be fully qualified at the equipment supplier site before commercial introduction.

There is a clear need for equipment suppliers and IC manufacturers to work together in a systematic way to achieve these goals. This will require an equipment development and improvement methodology that gets accurate information to the equipment manufacturer quickly to accelerate cycles of learning. Reliance on field data will slow this down and may even be misleading. If equipment manufacturers can develop and evaluate new equipment and processes in their factories, accuracy and speed will increase and the time required to improve reliability will be greatly reduced.

Motorola has developed, and successfully used, a methodology called IRONMAN for working with equipment suppliers to achieve mutual reliability and speed-of-introduction goals. This paper gives specific examples of how IRONMAN works and proposes an industry wide application of the principles involved.

**4:00 pm MS-TuA7 The Development of the Fast Thermal Processor (FTP), Katsuya Okumura, Toshiba.**

Furnace operations (oxidations, anneals and LPCVD) account for a large percentage of integrated circuit fabrication cycle time and short cycle time is necessary to minimize product development time and manufacturing capital investment. Therefore, further innovation is needed in the areas of furnace tooling and processing in order to improve ULSI fab productivity.

Today, hot processes are carried out in either conventional furnaces or newer rapid thermal processors (RTPs). Furnaces have relatively slow ramp rates (3–10°C/minute) compared to RTPs (500–1000°C/minute), but furnaces can typically process 100–150 wafers at once while RTPs are usually single-slice (single-wafer) processors. Also, there exists a large body knowledge related to conventional furnaces and processes which has yet to be duplicated in RTPs. But because of the large difference in operating regimes, it is difficult to transfer learning between the two types of equipment. Moreover, there are many unresolved problems that are unique to RTP.

In order to combine the best features of furnaces and RTPs, Toshiba and TEL collaborated to develop the Fast Thermal Processor (FTP). The FTP utilizes a standard vertical furnace configuration with a small batch size (50 wafers) and enhanced heating and cooling capability to achieve ramp rates of 50–100°C/minute. In addition, thermal and CVD processes can be done sequentially in the same chamber to achieve cost-effective process development and manufacturing. **INVITED**

**4:40 pm MS-TuA9 Low Thermal Budget Gap Filling for Semiconductor Manufacturing, Kevin J. Uram, John K. Shugrue, and Nathan P. Sandler, Lam Research Corp., 49026 Milmont Dr., Fremont, CA 94538.**

Advanced device designs and new material compatibility are placing greater demands on the gap filling capability of interlayer dielectric films. In this paper we present results of recent studies of the deposition of borophosphosilicate glass (BPSG) from the reaction of tetraethylorthosilicate (TEOS), triethylborate (TEB), phosphine (PH<sub>3</sub>), and oxygen in the temperature range of 750–800°C for high aspect ratio gap filling and interlayer isolation applications. Our studies have shown that at least three different mechanisms contribute to gap filling by BPSG in this temperature range. Viscous flow of the deposited glass is the predominant mechanism for gap fill at temperatures in excess of the glass transition temperature. A simple physical attraction between approaching side-walls has been observed to contribute to gap fill. Finally, some degree of chemical selectivity can be achieved from the deposition of BPSG from the above mentioned reactants. This chemical selectivity contributes to preferential gap fill from the corner

of structures. All of these mechanisms contribute to gap filling capability of BPSG on high aspect ratio structures (>2.5:1) with small openings <0.17 µm at temperatures as low as 750°C.

**5:00 pm MS-TuA10 Sub-Atmospheric CVD (SACVD) Ozone/TEOS for SiO<sub>2</sub> Trench Filling, I. Shareef<sup>1</sup>, G. W. Rubloff<sup>2</sup>, M. Anderle<sup>1</sup>, W. Gil<sup>3</sup>, J. Cotte<sup>1</sup>, and D.-H. Kim<sup>2</sup>; <sup>1</sup>IBM Research, Yorktown Heights, NY 10598, <sup>2</sup>North Carolina State Univ., Raleigh, NC 27695, <sup>3</sup>Rensselaer Polytechnic Institute, Troy, NY.**

Equipment for sub-atmospheric CVD (SACVD) is already in commercial use for ozone/TEOS processes to achieve low temperature (400°C), conformal, planar SiO<sub>2</sub> films for interlevel dielectric and possibly trench isolation applications, despite experimental complexities and poor understanding of its multicomponent gas and surface reactions. We report the first systematic study kinetics, conformality, and material properties over a broad pressure range (30–300 Torr), using an ultraclean MOCVD reactor with showerhead, O<sub>3</sub> generator, liquid TEOS delivery system, and O<sub>3</sub> quantification by chemical reaction/titration. SACVD rates exceed those for atmospheric pressure CVD; rates increase and then saturate with either O<sub>3</sub> or TEOS overabundance, providing an intermediate process window for optimizing rates, conformality, and film quality. Increasing O<sub>3</sub>/TEOS ratio decreases rates but enhances SiO<sub>2</sub> quality (O<sub>3</sub>/TEOS > 3 is required for low BHF etch rates, indicative of good SiO<sub>2</sub> quality). Conformality and trench filling properties at 30, 200, and 280 Torr are enhanced for higher O<sub>3</sub>/TEOS ratio and higher total pressure, as seen for shallow and deep trenches (aspect ratios ~1.5 and 10, respectively), with excellent conformality observed for shallow trenches. Gas phase deposition precursors and O<sub>3</sub> supply appear crucial in assuring complete oxidation of film constituents and volatilization of organic products.

## **BIOMATERIAL INTERFACES** **Room A106 – Session BI-TuA**

### **The Biosensor–Biology Interface**

**Moderator:** J.-J. Pireaux, Universitaires Notre-Dame, Belgium.

**2:00 pm BI-TuA1 In Vivo Electrochemical Sensors: The Challenge of Achieving Biocompatible Devices, M. E. Meyerhoff and C. Espadas-Torre, Department of Chemistry, The University of Michigan, Ann Arbor, MI 48109.**

The effective management of critically ill patients usually requires the frequent measurement of blood gases (pH, PCO<sub>2</sub>, and PO<sub>2</sub>) and electrolytes (Na<sup>+</sup>, K<sup>+</sup>, Ca<sup>++</sup>, and Cl<sup>-</sup>) in whole blood. In recent years, there has been an increase in efforts to provide such test results at the patient's bedside on a continuous basis via the use of intra-arterial chemical sensors. Such *in vivo* sensors can be based on either electrochemical or optical measurements. The electrochemical type catheters are essentially miniaturized versions of the polymer membrane-based sensors already in use within commercial *in vitro* blood gas-electrolyte instruments. The reliability of values obtained by these small devices within the *in vivo* environment depends on chemical and instrument stability (drift), as well as sensor biocompatibility (thrombus formation). Indeed, adhesion of cells to the surface of implanted sensors will cause significant errors in blood gas/pH measurements owing to local changes in these values due to the cellular metabolic activity present at the sensor/blood interface. Reducing thrombus formation represents an especially difficult challenge with respect to the polymer materials used for fabrication/coating of the sensors, since chemical derivatization of the materials used (e.g., immobilization of heparin, etc.) can dramatically alter the analytical response properties (including selectivity) of the catheters. Approaches aimed at overcoming this biocompatibility issue with respect to developing implantable potentiometric ion-selective sensors will be the main focus of this paper. Specifically, the modification of polymer membrane ion-selective electrode materials (various polyurethanes) via cross-linked polyethylene oxide hydrogels, etc., will be shown to reduce platelet adhesion while maintaining electroanalytical performance of the electrochemical devices. **INVITED**

**2:40 pm BI-TuA3 Neural Microsensors for Automated Toxicity and Pharmacology Assays, D. A. Stenger\*, V. C. Kowtha, P. P. Bey, Jr., D. Borkholder<sup>1</sup>, G. T. Kovacs<sup>1</sup>, K. E. Foster<sup>2</sup>, and J. J. Hickman<sup>2</sup>,**

Center for Bio/Molecular Science and Engineering, Naval Research Laboratory, Washington, DC 20375; 1: Dept. of Electrical Engineering, Stanford University, Stanford, CA 94305; 2: Science Applications International Corporation, McLean, VA 22102.

We are developing a simple neural-based biosensor that detects the presence of wide ranges of toxic threats capable of interfering with many types of cellular and electrical functions. This approach uses neural cells as device components that must be integrated into a hybrid device consisting of electronic microcircuits and hardware dedicated to environmental control and sample processing. Silicon nitride-passivated iridium microelectrode arrays are surface-modified using self-assembled monolayers and used for detection of repetitive action potentials. Repetitive APs of the NG108-15 cells can be used to monitor both direct channel activation/block and modulation by receptor/second messenger interaction. A key aspect of this integration involves the interfacing of cells to the surface, the nature of the electrical signals produced by the cells, and the electronics used to translate these signals into useful measurements. We will discuss our progress in modulating the physical, chemical, and electrical characteristics of this interface.

**3:00 pm BI-TuA4 Micrometre Resolution Molecular Patterning at Transducer Surfaces, J. M. Cooper, H. Morgan and D. J. Pritchard,** Bioelectronics Group, Department of Electronics, University of Glasgow, Glasgow, G12 8LT, UK.

Techniques for controlling the architecture of immobilized biomolecular films onto transducer surfaces have a wide range of potential applications in bioelectronics, particularly in biosensing and in the control of cell guidance. In this paper, a novel method for the site-specific attachment of biological molecules onto glass, gold and silicon is described. The technique, which is based upon the modification of the sensor surface and the activation of a bound photosensitive ligand, provides a method for two dimensional patterning of proteins onto precise areas whilst preventing non-specific binding to non-designated sites. Different molecules, including enzymes and antibodies, have been immobilized with a micrometre scale resolution whilst retaining their biochemical activity. Initial results are presented on the application of this system to multianalyte immunosensors.

**3:20 pm BI-TuA5 Activity of Antibodies Immobilized at the Solid-Liquid Interface in Biosensors, D. W. Conrad<sup>1</sup>, P. T. Charles<sup>2</sup>, L. C. Shriver-Lake<sup>3</sup>, T. S. Koloski<sup>2</sup>, and F. S. Ligler<sup>3</sup>,** <sup>1</sup>NRC Postdoctoral Fellow, <sup>2</sup>ONT Postdoctoral Fellow, <sup>3</sup>Center for Bio/Molecular Science and Engineering, Code 6900, Naval Research Laboratory, Washington, DC 20375.

The incorporation of biomolecules into optoelectronic devices to serve as molecular recognition elements is becoming an accepted methodology for the fabrication of ultrasensitive detection devices. The choice of biomolecule, its method of incorporation, and the chemical and physical environment in which it functions, are all critical parameters in determining specificity, sensitivity, and long-term use of the biosensor. While much is known about the interaction of biomolecules under solution conditions, the biochemical and physical interactions at the solvent-substrate interface in heterogeneous systems are yet to be fully defined.

Our own research effort has relied on the use of antibodies to serve as the detection component in several different biosensors systems. These devices employ a variety of substrates for antibody immobilization and operate under diverse chemical environments. In order for such sensors to function reproducibly with long-term stability, specialized immobilization methods and chemically-tailored substrates must be employed. These are required to maintain antibody activity and prevent the deleterious effects of non-specific adsorption or denaturation at the interface.

**INVITED**

**4:00 am BI-TuA7 Molecular Assemblies of Functionalized Polydiacetylenes, Deborah H. Charych<sup>1</sup>, Anke Reichert<sup>1</sup>, Raymond Stevens<sup>2</sup>, Geoff Kuziemko<sup>2</sup>, Jon Nagy<sup>1</sup>,** <sup>1</sup>Center for Advanced Materials, Lawrence Berkeley Laboratory, Berkeley, CA 94720, <sup>2</sup>Department of Chemistry, University of California, Berkeley, CA 94720.

Self organized membrane-like structures such as Langmuir-Blodgett films and liposomes provide new materials with well defined surface chemical functionality. If the lipid molecules which comprise these structures are endowed with biologically-active functional groups and with polymerizable groups, new multifunctional materials can be created. The applications of these materials will be discussed, particularly with respect to colorimetric sensor devices and pharmaceutical drug discovery.

**INVITED**

**4:40 pm BI-TuA9 Preparation of an Immunosensing Surface by a Mixed Self-Assembled Monolayer, P. Heiduschka<sup>1</sup>, J. Rickert<sup>1</sup>, W. Beck<sup>2</sup>, G. Jung<sup>2</sup> and W. Göpel<sup>1</sup>,** University of Tübingen, <sup>1</sup>Institute of Physical and Theoretical Chemistry, <sup>2</sup>Institute of Organic Chemistry, Auf der Morgenstelle, D-72076 Tübingen.

Thiols adsorb very strongly onto gold surfaces. When long-chained alkanethiols are used, so-called self-assembled monolayers of crystalline order may be formed which are stable over months in different media. In order to utilise these monolayers for analytical purposes in a biochemical sensor, they have to be modified chemically by incorporating molecules with appropriate recognition properties. We choose epitope peptides. Epitopes represent the sequence of amino acids of an antigen (e.g., a virus) which is recognised by the specific antibody. In our studies, the epitope of the virus of the foot-and-mouth disease was synthesised chemically and served as the antigen. The peptide was modified by coupling with hydroxyundecanethiol (HUT). The resulting derivative adsorbs onto gold and yields dense layers. The adsorbed layer was stabilised and optimised with respect to its surface density by coadsorption of the unmodified HUT with the HUT-peptide. The binding conditions of the specific antibody were characterised by electrochemical impedance measurement. After the molecular recognition step, the complex of the antibody with the epitope could be destroyed in 6 M urea solution. The recognition properties of the peptide layer remained after the removal of the antibodies. Therefore, reproducible detection of antibodies was possible with the same monolayer coating.

**5:00 pm BI-TuA10 Hydration and Dehydration of Adsorbed Protein Monolayers on Different Surfaces, M. Rodahl, F. Höök, and B. Kasemo,** Chalmers University of Technology and University of Göteborg, 412 96 Göteborg, Sweden.

An apparatus for sensitive hydration/dehydration studies based on the quartz-crystal microbalance (QCM) is described. The system is intended for studies of water equilibrium uptakes and uptake/release kinetics, respectively, at different humidities, at approximately 1 atm total pressure. The sensitivity is in the *submonolayer* regime, i.e. better than 3 ng/cm<sup>2</sup>. The mass sensitive crystal is AT-cut and operating at 10 MHz fundamental resonant frequency.

In the present work we have applied this method to study hydration and dehydration of adsorbed monolayers of the proteins ferritin and myoglobin on (i) UV/ozone cleaned (hydrophilic) gold surfaces and (ii) gold modified by self-assembled monolayers of thiols (rendering the surface hydrophobic). For comparison, results are presented for the same surfaces without adsorbed proteins.

Information about the adsorbed layers and their water uptake is obtained by the observed frequency shift of the QCM and the simultaneously measured Q-factor of the oscillator. This provides information both about mass changes (due to hydration/dehydration) and about the viscoelastic properties of the adsorbed layers.



## SURFACE SCIENCE

### Room BR4 - Session SS-TuP

#### Aspects of Surface Science

**Moderator:** J. C. Hemminger, University of California, Irvine.

**SS-TuP1 Simulation Studies of Electron Transfer at a Metal-Aqueous Electrolyte Interfaces, B. B. Smith, J. W. Halley,** School of Physics and Astronomy, University of Minnesota, Minneapolis, MN 55455.

We report new simulation studies of the rate of ferrous-ferric and cuprous-cupric electron transfer at a metal electrolyte interface. In contrast with earlier work, new features in our study include a detailed account of the effects of the field associated with the charging of the electrode, inclusion of entropic effects in the calculated free energy barriers, and a study of the dependence of the relevant free energy surfaces on the distance of the ion from the electrode. The qualitative picture of the reaction mechanism which emerges is significantly more detailed than that in earlier work. The dominant factors in determining the rate and mechanisms of electron transfer are the distance dependence of the following: the work function of the metal, the concentration profile, and the electronic matrix element. Calculated free energy barriers for the ferrous-ferric reaction are consistent with experimentally measured ones. We also estimate the equilibrium potential for this reaction from the model and find a value which is within 0.1 V of the measured one. For the cuprous-cupric reaction we find a more pronounced effect of the electric field arising from the charge on the electrode. In the cuprous-cupric case, we present the limits within which a single step mechanism is relevant to the more complicated real world reaction.

INVITED

**SS-TuP2 Adsorption of Water on Oxidized Tungsten and Suppression of Electron Induced Oxygen Ion Emission by Molecular and Dissociated Water, M. Akbulut\*, N. J. Sack and T. E. Madey,** Rutgers University, Department of Physics and Astronomy, and Laboratory for Surface Modification, Piscataway, NJ 08855.

We have studied the adsorption and decomposition of water on an oxidized W(100) surface, and have measured the transmission of low energy ( $< 10$  eV)  $^{16}\text{O}^+$  ions through ultrathin films of water,  $\text{H}_2^{18}\text{O}$ , condensed at 20 K. Our goal is to address the fundamental scattering and charge transfer processes that influence ion transport through molecular layers.  $^{16}\text{O}^+$  ions with a peak energy of 7 eV and a narrow angular distribution (FWHM  $\sim 15^\circ$ ) are generated by means of electron stimulated desorption (ESD) from the  $^{16}\text{O}$  oxidized W(100) surface and their yield, energy and angular distributions are measured as a function of  $\text{H}_2^{18}\text{O}$  coverage with a digital ESDIAD (ESD ion angular distribution) detector. Thermal desorption spectroscopy (TDS) demonstrates that the majority of water adsorbed in the first monolayer remains molecular and desorbs with a peak temperature of 155 K. However, both TDS and ESD measurements indicate that a small percentage of  $\text{H}_2^{18}\text{O}$  dissociates upon adsorption. We find complete suppression of the  $^{16}\text{O}^+$  ESD emission upon adsorption of only a fraction of a monolayer of  $\text{H}_2^{18}\text{O}$ . We suggest that charge transfer between  $^{16}\text{O}^+$  and  $\text{H}_2^{18}\text{O}$  is the main reason for the attenuation of  $^{16}\text{O}^+$ .

\*Permanent address: Stevens Institute of Technology, Physics Department, Hoboken, NJ 07030.

**SS-TuP3 Adsorption, Desorption, Mixing, and Solvation Kinetics of Mixed Methanol and Water Multilayer Ices, R. Scott Smith, C. Huang, E. K. L. Wong, and Bruce D. Kay,** Molecular Science Research Center, Pacific Northwest Laboratory\*, Richland, WA 99352.

In an effort to understand the surface chemistry of ice and its applicability to processes occurring in liquid solutions we have studied binary mixtures of water and methanol ices grown using molecular beam deposition. It is well-known that liquid mixtures of methanol and water exhibit non-ideal solution behavior due to hydrogen bonding and hydrophobic solvation. Molecular beam scattering and programmed desorption (both TPD and isothermal) are used to study the adsorption, desorption, mixing, and solvation kinetics of mixed multilayer (5-100 ML) ices of water and methanol. Compositionally tailored multilayers of methanol and water are grown on Ru(0001) using

both sequential and simultaneous beam dosing techniques. The desorption spectra exhibit complex features that depend strongly on both the mole fraction and the thickness of the multilayer. Analysis of the desorption spectra reveal both the extent of mixing and the details of the solvation kinetics. These kinetics depend strongly on the initial phase of the ice (amorphous or crystalline). The experimental results are analyzed using a kinetic model that describes liquid solution evaporation. From this analysis we can extract a binary phase diagram. The mixed water and methanol ices exhibit non-ideal behavior reminiscent of the liquid solution results. Details of the experimental techniques, results, and implications regarding ice solutions at low temperatures will be presented.

\*Pacific Northwest Laboratory is operated for the U.S. Department of Energy by Battelle Memorial Institute under contract DE-AC06-76RLO 1830.

**SS-TuP4 The Interaction of HCl With Ultrathin Ice Films: Observation of Adsorbed and Adsorbed States, J. D. Graham and J. T. Roberts,** Department of Chemistry, University of Minnesota, Minneapolis, MN 55455.

To gain understanding of heterogeneous chemistry that occurs in the polar stratosphere, the temperature programmed desorption and Fourier transform infrared reflection absorption spectra of hydrogen chloride interacting with amorphous and crystalline ultrathin (4-20 monolayers) ice films were studied. The desorption spectra reveal two distinct HCl states, at 140 and 180 K, labeled  $\alpha$ - and  $\beta$ -HCl respectively. The  $\beta$  state, which is formed exclusively at low HCl exposures, evolves concurrently with water sublimation. This state is assigned to the sublimation of a stoichiometric HCl water phase. Infrared spectra suggest this phase is  $\text{HCl}\cdot 6\text{H}_2\text{O}$ . The  $\alpha$  state is associated with HCl adsorbed on the hexahydrate surface. Experiments conducted on ice- $d_2$  show a much smaller amount of H-D exchange between HCl and  $\text{D}_2\text{O}$  than would be expected from dissociative adsorption. Thus it is believed that HCl adsorbs molecularly. The activation energy of  $\alpha$ -HCl desorption is  $33 \pm 5$  kJ mol $^{-1}$ , which strongly suggests hydrogen bond formation. This is supported by the infrared spectra with the disappearance of the surface O-H stretching mode upon adsorption of HCl. A comparison of crystalline and amorphous films shows that the rate of  $\text{HCl}\cdot 6\text{H}_2\text{O}$  formation is much slower in crystalline films. This is due to a lower sticking coefficient of HCl on the crystalline films.

**SS-TuP5 Differences in the Surface Chemistry of Amorphous and Crystalline Ice Thin Films, Jason E. Schaff, Jeffrey T. Roberts,** University of Minnesota, Dept. of Chemistry, 207 Pleasant St. SE, Minneapolis, MN 55455.

The interactions of several small molecules with thin ( $\sim 80$  ML) films of both amorphous and crystalline ice have been studied using temperature programmed desorption spectroscopy (TPD) and infrared reflection absorption spectroscopy (IRAS). Amorphous and crystalline films can be clearly distinguished using IRAS. Those adsorbate molecules which are good hydrogen bond acceptors show one more desorption state from amorphous ice than they do from crystalline ice, and also show differences in their IR spectra when adsorbed on the two different types of ice films. This is interpreted as indicating either a reduction in the number of free-OH bonds on the surface of crystalline ice, or as a reduction in the accessibility of such dangling bonds to adsorbate molecules. This conclusion is supported by the significant reduction in intensity of the free-OD stretching peak which is observed upon crystallization of deuterated ice films in IRAS experiments. Molecules which do not readily form hydrogen bonds show no significant differences in behavior when adsorbed on the two types of ice films. To the best of our knowledge, this represents the first conclusive evidence for a difference in the chemical behavior of crystalline and amorphous ice surfaces.

**SS-TuP6 SPA-RHEED-Spot Profile Analysis for *in situ* Characterization, B. Müller and M. Henzler,** University of Hannover, Appelstr. 2, D-30167 Hannover, Germany.

The morphology of the surface dominates the quality of the epitaxial growth. In order to tailor low dimensional artificial structures the surface must be characterized during growth. One of the most powerful methods for *in situ* studies is RHEED. The quantitative analysis on island sizes and step distributions, however, is mainly performed by



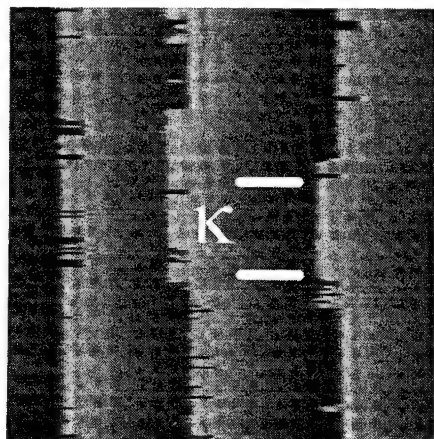
LEED because of the more complicated geometry of RHEED and the influence of inelastic scattering. To overcome these difficulties, a novel RHEED instrument with extremely high angular resolution (0.1 mrad) and energy resolution of about 2 eV is developed. For the first time the SPA-RHEED instrument points out the important contribution of inelastic processes to the intensity distribution of the spot profiles. Electronic losses due to plasmons and band transitions are clearly detected and quantitatively described by the dipole scattering theory. A meaningful evaluation of the profiles with respect to defects is only possible with a good energy resolution. For well prepared Si(111) with various island sizes in different azimuths the elastic and inelastic scattering is investigated throughout several Brillouin zones. Mean terrace sizes between 50 and 5000 Å are detected. Characteristic structures are correlated with the scattering vectors and are separated into surface and bulk related phenomena because of the refraction effect. The extremely high angular resolution of SPA-RHEED enables determination of island size up into the micrometer range and lattice constants with an accuracy <0.1 %. Surface damage is reduced due to the extremely low current. Therefore the features of the SPA-RHEED instrument offer new applications for RHEED.

**SS-TuP7 Adsorption, Desorption and Diffusion of H<sub>2</sub>O on Single-Crystal Ice Surfaces, D. E. Brown, J. T. Nelson and S. M. George, University of Colorado, Department of Chemistry, Boulder, CO 80309.**

Ice surfaces are important in ozone depletion involving heterogeneous chemistry on polar stratospheric clouds. The adsorption, desorption and diffusion of H<sub>2</sub>O on single-crystal ice grown epitaxially on Ru(001) were measured using optical interference and laser-induced thermal desorption (LITD) techniques. Low energy electron diffraction (LEED) studies confirmed that the ice films were crystalline to thicknesses of at least 140 Bilayers (1 Bilayer defined according to Thiel et al., JCP 75 (1981) 5556). Condensation and evaporation coefficients were measured using optical interference. The condensation coefficient,  $\alpha$ , was measured at temperatures between 95 and 170 K and decreased versus temperature from  $\alpha = 1.00 \pm 0.08$  at 95 K to  $\alpha = 0.68 \pm 0.11$  at 170 K. The evaporation coefficient,  $\gamma$ , was obtained using isothermal desorption measurements and remains constant at  $\gamma = 0.62 \pm 0.08$  from 160 K to 193 K. An Arrhenius analysis of the desorption rates revealed zero-order desorption with an activation barrier of  $E_{des} = 12.8 \pm 0.5$  kcal/mol and a preexponential of  $\nu_0 = 4.5 \times 10^{31 \pm 0.3}$  molecules/(cm<sup>2</sup>s). Isotope experiments were performed to investigate the desorption of a single bilayer of H<sub>2</sub>O<sup>18</sup> from a multilayer of H<sub>2</sub>O<sup>16</sup> ice on Ru(001). The isothermal desorption of H<sub>2</sub>O<sup>18</sup> measured with LITD followed first-order desorption kinetics. These measured kinetics allowed the residence time for H<sub>2</sub>O on ice to be determined at different temperatures. LITD studies also examined the surface diffusion of H<sub>2</sub>O on ice. A step coverage profile of H<sub>2</sub>O<sup>18</sup> on a multilayer of H<sub>2</sub>O<sup>16</sup> ice was created using a masking technique. By following the decay of the H<sub>2</sub>O<sup>18</sup> coverage profile with LITD, an upper limit of  $D = 6 \times 10^{-9 \pm 0.4}$  cm<sup>2</sup>/s was placed on the diffusion coefficient of H<sub>2</sub>O on ice at 140 K.

**SS-TuP8 Microscopic Activation Energies Determined from the Time Structure of Step Jumps in Tunneling Images, Margret Giesen-Seibert, Frank Schmitz, Harald Ibach, Forschungszentrum Jülich, IGV, D-52425 Jülich, Germany.**

Steps on copper surfaces are mobile for temperatures larger than 300K. Due to the finite scan speed the tunneling tip finds the step in different positions in consecutive scan lines. Therefore, steps in STM images display sudden jumps in the step position. For Cu(1 1 19) we



have measured the probability distribution  $P(\kappa, \tau)$  to find time intervals of  $\kappa$  scan lines, each requiring a time  $\tau$  (see figure). A different dependence of  $P(\kappa, \tau)$  is found for short and long intervals between two consecutive step jumps. Short intervals obey a  $\kappa^{-3/2}$ -law which is caused by the emission of adatoms from kink sites and their subsequent return. For long intervals an exponential tail is found in  $P(\kappa, \tau)$  which is due to uncorrelated kink motion. We have developed analytical models for  $P(\kappa, \tau)$  in the two regimes in terms of the microscopic events of adatom generation and migration along the steps. The models were tested employing Monte-Carlo simulations. With the help of these models we have determined the activation energies for adatom generation and migration from the experimental data.

**SS-TuP9 Atomically Resolved STM Study of the Interaction of Boron with Si(001), Yajun Wang, and Robert J. Hamers, Department of Chemistry, University of Wisconsin, Madison, WI 53706, USA.**

The interaction of boron with Si(001) is very important for semiconductor processing. STM, tunneling spectroscopy and surface photovoltage measurement have been used to study the geometric and electronic structures of boron-induced reconstructions produced by thermal decomposition of diborane on Si(001). At  $T > 675$  K, boron atoms organize into ordered structures on the surface. STM images reveal a number of boron-induced reconstructions which arise from the arrangements of three structural subunits. Boron atoms bond at substitutional sites and form a delta-doped layer. These boron-induced structures are chemically inactive, but electrically active. Over 1075K, most boron atoms diffuse into bulk and it also produces surface faceting. This is the first atomic-scale study of boron-induced reconstructions on Si(001) and it will provide a deeper understanding of semiconductor doping. The formation process of new structures and their effects on further silicon film growth will be discussed. This work is supported by the U.S. Office of Naval Research.

**SS-TuP10 The Role of Energy Loss Mechanisms for the Trapping Dynamics of Alkanes on Platinum Surfaces, J. A. Stinnett, R. J. Madix, Stanford University, Stanford, CA 94305, and J. C. Tully, AT&T Bell Labs, Murray Hill, NJ 07974.**

The molecular adsorption of methane, ethane, and propane on several platinum surfaces were studied by simulation to examine the relative importance of the energy loss mechanisms available to assist trapping. Methane was simulated as a spherical species. Ethane and propane were considered to be pseudo diatomic and triatomic molecules, respectively, interacting with a vibrating periodic solid slab. Three dimensional stochastic trajectory calculations with a Morse pairwise methyl-platinum potential were used to represent the gas-solid interaction. The potential parameters were determined by fitting to experimental initial trapping probabilities and scattered angular distributions of ethane interacting with Pt(111). Examination of the flow of energy during the trapping process of ethane shows that cartwheel rotational energy serves as an important energy storage mechanism which, if dissipated, can assist trapping. These potential parameters were then employed for methane, ethane, and propane interacting with other platinum surfaces. For example, the application of these potential parameters to the Pt(110)-(1 × 2) surface predicts the azimuthal dependence and the enhancement in the trapping probability for ethane seen experimentally. These calculations suggest that ethane trapping on Pt(110)-(1 × 2) is enhanced relative to Pt(111) due to increased conversion of normal momentum to parallel momentum. Methane and propane simulations were also successful at representing the incident angle and energy dependence on trapping. The wide range success of all these calculations provides confidence for the prediction of adsorption probabilities and dynamics from a very limited data set.

**SS-TuP11 Development of Surface Morphology and Microstructure During Si Homoepitaxial Growth, D. P. Adams and S. M. Yalisove, Department of Materials Science and Engineering, University of Michigan, Ann Arbor, MI 48109-2136, D. J. Eaglesham, AT&T Bell Laboratories, Murray Hill, N.J. 07974.**

The development of surface morphology and microstructure has been studied for homoepitaxial growth onto both patterned, nonpolar Si substrates and flat Si(100) surfaces. Growth onto nonplanar substrates was useful for studying changes in morphology over a range of temperatures. First, growth at higher temperatures has been characterized in terms of a number of well developed high index surfaces (including Si(117), (115) and (113)) which form at a sidewall. Subsequent low temperature growth onto each of these surfaces has also been studied. Each Si(hkl) surface was found to exhibit a crystalline to amorphous transition at low temperatures; however, the epitaxial thicknesses,  $h_{epi}$ , are different for each {hkl} surface (in general,

$h_{\text{epi}}(001) > h_{\text{epi}}(117) > h_{\text{epi}}(115) > h_{\text{epi}}(113)$ ). Furthermore,  $h_{\text{epi}}(\text{hkl})$  was found to follow an Arrhenius relation with substrate temperature. The "activation energies", characteristic of this breakdown in epitaxy, were then determined for each surface by measuring the epitaxial thickness over a range of temperatures below  $\sim 300^\circ\text{C}$ .  $E_{\text{act}}(\text{hkl})$  was determined to be 0.35 eV, 0.33 eV, 0.30 eV and 0.27 eV for (001), (117), (115) and (113) surfaces, respectively.

The origin of this breakdown in epitaxy has also been identified. Work using flat Si(100) starting surfaces showed that surface roughening leads to the formation of amorphous material (a phenomenon intrinsic to low temperature growth). In this investigation, the role of H on changing the epitaxial thickness was also elucidated. Increased amounts of atomic D, introduced to the growth surface were found to lower  $h_{\text{epi}}$ , but also increase the roughening rate within the epitaxial portion of the film and permit a larger roughness amplitude before nucleation of the amorphous phase. Interestingly, the surface roughening rates, measured here by TEM (using thin Ge marker layers to mark the profile) and RHEED, indicate that growth of Si at low temperatures is characterized by a large roughening exponent, i.e.  $\beta > 1$ .

**SS-TuP12 Nucleation Phenomena in the Chemical Vapor Deposition of Iron on Si(001), T. M. Mayer, L. L. Tedder, B. S. Swartzentruber, Sandia National Laboratories, Albuquerque, NM 87185.**

We report studies of the initial stages of growth of Fe films on single crystal Si (001) surfaces by chemical vapor deposition (CVD). *In-situ* high temperature scanning tunneling microscopy (STM) is used to image surface reactive sites, island morphology and size distributions as a function of coverage. At temperatures of 100–150°C we observe selective decomposition of the  $\text{Fe}(\text{CO})_5$  precursor at Si dimer sites, with no reaction observed at step or defect sites. Isolated atom-sized features are initially observed, followed by linear chains of atoms aligned along Si dimer rows at increasing coverage. At coverage in excess of one monolayer, larger islands characteristic of three dimensional growth appear. We observe no residual C or O in complementary x-ray photoelectron spectroscopy (XPS) experiments, nor do we see evidence for C or O contamination in the STM. The shape and size distribution of nuclei are consistent with an autocatalytic growth process, in which selective decomposition of the precursor occurs at existing metallic nuclei. The small sticking coefficient and short residence time of  $\text{Fe}(\text{CO})_5$ , and apparent low mobility of Fe atoms on Si at 100–150°C suggest that site-selective adsorption and reaction of the precursor gas molecule is responsible for the morphology of the Fe nuclei. Kinetic Monte-Carlo simulations are presented to examine the dynamic processes of nucleation. Low energy electrons from the STM tip are also effective at enhancing local area nucleation of Fe through electron induced decomposition of  $\text{Fe}(\text{CO})_5$ .

This work is supported by the U.S. Department of Energy under contract DE-AC04-94AL85000.

**SS-TuP13 STM Observations of Hydrogen-Induced Ag Cluster Formation on the Si(111)  $\sqrt{3} \times \sqrt{3}(\text{R}30^\circ)$ -Ag Surface, Itsuo Katayama and Yasuyuki Ohba, Department of Applied Physics, Faculty of General Education, Osaka Institute of Technology, Asahi-ku, Osaka 535 Japan, Hideaki Ohnishi, Yasuji Yamamoto and Kenjiro Oura, Department of Electronic Engineering, Faculty of Engineering, Osaka University, Suita, Osaka 565 Japan.**

Scanning tunneling microscope (STM) has been used to study structural transformation of the Si(111)  $\sqrt{3} \times \sqrt{3}(\text{R}30^\circ)$ -Ag surface caused by atomic hydrogen adsorption. When atomic hydrogen adsorbed on the  $\sqrt{3}$ -Ag surface, the surface structures dramatically change. The atomic hydrogen attack the  $\sqrt{3}$ -Ag surface at the domain boundaries or step edges, and the clusters are found to be formed on the  $\sqrt{3}$ -Ag domain. This suggest that H atoms break the Ag-Si bond followed by the formation of both the bonding of H atoms to the Si dangling bonds thus formed and the clusters formed by Ag free atoms released from the  $\sqrt{3}$  lattice. The hexagonal shape observed and its orientation suggest the formation of Ag(111) clusters, and the size of the clusters has been confirmed to be less than 15 nm. These STM results are in agreement with our previous ion scattering results. Spatial distributions of the clusters, observed as a function of the exposure to atomic hydrogen, reveal that surface diffusion of Ag atoms over the hydrogen-covered regions is largely suppressed compared with that on the  $\sqrt{3}$ -Ag surface. It has been disclosed that hydrogen adsorption has two critical roles: the first is that hydrogen atoms break Ag-Si bonds and release free Ag atoms on the  $\sqrt{3}$ -Ag surface. The second role of hydrogen is to suppress surface migration of the Ag atoms over the hydrogen adsorption region on the specimen surface.

**SS-TuP14 The Evolution of Growth Front in a Heteroepitaxial System: Pb on Cu(100)\*, Hong Zeng and G. Vidali, Department of Physics and the Solid State Science and Technology Program, Syracuse University, Syracuse, NY 13244.**

We have measured in real time the evolution of the growth front in the kinetically driven low temperature (150 K) growth of Pb on Cu(100). Films from above 1 layer up to 450 layers were studied using helium beam scattering apparatus, LEED and Auger electron spectroscopy. The large lattice mismatch, the difference in bonding strengths and symmetry between substrate and film produces a rather complex growth pattern. The first Pb layer is ordered with a square supercell ( $5 \times 5$ ) rotated by  $37^\circ$ . The second layer grows by islands with a double step of about  $4.87 \text{ \AA}$ . Overall the second and third layer grow in a disordered fashion. The next layers grow in a quasi-layer-by-layer mode. The LEED pattern shows the presence of (111)Pb exposed surfaces with domains rotated by  $90^\circ$ . From about 16 equivalent monolayers (ML) until 450 ML the average terrace width changes little. The interface width grows as  $t^\beta$  with  $\beta \approx 0.3$  until about 40 ML. The lateral correlation length grows with deposition time as  $t^{\beta\alpha}$  with  $\alpha \approx 1$ . After that the growth saturates and a groove instability develops; the  $\alpha$  value is slightly smaller than 1 due to a logarithmic correction. Manipulation of the growth of the film have also been achieved by preparing a first layer with different structures or by annealing.

\*Supported by NSF grant DMR 9119735.

**SS-TuP15 Island Growth and Energetics in Submonolayer Homoepitaxy on Cu(100)\*, J. F. Wendelken,<sup>a</sup> H. Dürr,<sup>a</sup> and J.-K. Zuo,<sup>a,b</sup> <sup>a</sup>Oak Ridge National Laboratory, Oak Ridge, TN 37831-6030 and <sup>b</sup>Southwest Missouri State University, Springfield, MO 65804-0094.**

Submonolayer epitaxial growth may be described in terms of a scaling relationship  $L \sim (D/F)^{p/2}$  where  $L$ ,  $D$ , and  $F$  are the average island separation, adatom diffusion constant, and deposition flux, respectively. The scaling exponent  $p$  reflects the critical nucleus size required to begin the growth of an island. High angular resolution LEED was used to observe the island morphologies and separations as a function of flux and deposition temperature  $T$  in the steady state regime. Two dimensional diffraction profiles at temperatures of 220 to 305 K and STM topographic images at  $\sim 300 \text{ K}$  reveal square islands with close-packed [110] step edges indicating a low energy barrier for diffusion along this step direction. From measurements of the island separation as a function of flux, the critical island size is found to change from a dimer at 223 K to a tetramer at 263 K and above. An Arrhenius plot of the island separation vs  $1/T$  for a fixed flux can be best fit with two line segments with a turning point at 225 K indicating the onset of dimer dissociation. The slope of this plot in the low temperature (dimer) regime indicates a diffusion energy barrier of  $\sim 0.36 \text{ eV}$ . From the change in slope, the average binding energy of dimers and trimers is estimated to be 0.14 eV.

\*Research sponsored by the Division of Materials Science, U.S. Department of Energy, under contract DE-AC05-84OR21400 with Martin Marietta Energy Systems, Inc.

**SS-TuP16 An Atomic Scale View of Adsorbate Motion on Surfaces, P. S. Weiss, M. T. Cygan, J. H. Ferris, M. M. Kamna, K. R. Krom, S. J. Stranick, and M. G. Yoshikawa Youngquist, Department of Chemistry, The Pennsylvania State University, University Park, PA 16802.**

Adsorbate mobility is critical to the growth, stability, and structure of surface films and structures. We use the scanning tunneling microscope to obtain an atomic scale view of the motion of adsorbates on surfaces. For sufficiently slow diffusion, we follow this motion in real time. Reducing the rate of motion can be accomplished by chemically modifying the adsorbate under study to increase the strength of lateral interactions or by reducing the temperature at which the measurements are performed. We have used both these strategies to enable the study of adsorbate diffusion. For faster adsorbate motion we are able to observe the partial occupancy of surface sites on the time scale of our measurements. For lateral motion induced by surface processes such as adsorption or chemical reaction, we are able to analyze the positions of the adsorbates or reaction products in order to measure the distances covered and to elucidate the means by which energy is accommodated to the surface. For sufficient adsorbate mobility, we observe molecules nucleating, clustering and forming ordered structures at steps and other surface defects.

This work has been supported by BRDC, NSF, and ONR.

**SS-TuP17 Local Morphology Effects on Mass Transport on Sputtered Au(111): an STM Study\***, T. Curcic, J. G. McLean, B. H. Cooper, LASSP, Cornell University, Ithaca, NY 14853.

We have performed a UHV study of nanoscale clusters of vacancies on a clean Au(111) surface at room temperature. The vacancy clusters were formed by sputtering the surface with a low energy (500 eV) Ar ion beam. Time-lapse sequences of STM images reveal the following: (1) while vacancy clusters persist as highly stable features on Au(111) at room temperature, changes in local morphology do occur, and (2) dramatic changes in mass transport coincide with certain changes in local morphology. We discuss two microscopic mechanisms which may be responsible for the changes in mass transport: (1) onset of vacancy diffusion (intralayer mass transport) and (2) enhanced interlayer mass transport due to the increased adatom pressure near curved step edges.

\*Supported by the Cornell Materials Science Center (DMR-9121654); additional support from F49620-93-1-0504.

**SS-TuP18 Identification of metastable bcc Ni Film Growth on Al(001) Surfaces Using High-Energy Ion Scattering, X-Ray Photoelectron Diffraction, and X-Ray Photoelectron Spectroscopy**, V. Shutthanandan, Adli A. Saleh, R. J. Smith, Physics Department, Montana State University, Bozeman, MT 59717\*.

High-energy ion scattering spectroscopy (HEIS), x-ray photoelectron diffraction (XPD), and x-ray photoelectron spectroscopy (XPS) were used to determine the interface structure of ultrathin Ni films deposited on Al(001) surfaces at room temperature. The HEIS/channeling experiments were performed in the normal direction, and the surface peak areas of Al and Ni were monitored as a function of Ni coverage. Following each HEIS measurement the XPS spectra of the Al 2p and Ni 2p core levels were collected. In the XPD experiments polar-angle scans for both the Al 2p and Ni 3p emission were collected for three different coverages of Ni, namely at 1, 5 and 11 monolayers (ML), and for emission along the [010] and [110] azimuths of the substrate surface. The forward scattering peaks obtained in these experiments suggest that up to 5 ML of Ni coverage, a Ni film grows as a metastable bcc(001) structure in a Stranski-Krastanov (SK) like growth mode. That is, first a flat overlayer forms, approximately 2 layer thick, and not necessarily commensurate with the substrate lattice. This is followed by Ni island formation. After 5 ML of coverage, the bcc islands coalesce to cover the surface. These results are significantly different from the Ni/Al(110) results in which a strong Ni-Al interface reaction was observed.

\*Supported by Montana Space Grant Consortium, NASA grant #NGT40041.

**SS-TuP19 The Initial Growth of Ultrathin Pd Films on Cu(001)**, J. Yao, Y. G. Shen and D. J. O'Connor, Department of Physics, University of Newcastle, New South Wales 2308, Australia.

The deposition of Pd on Cu(001) at 300 K was studied by low energy alkali ion scattering and low energy electron diffraction (LEED). The results of the azimuthal scans at grazing incidence showed evidence for surface alloying by the substitution of Cu with Pd atoms in the first layer even at very low coverages. However, the penetration of Pd atoms into the second layer was not observed at coverages below 0.3 ML. A clear maximum in the best  $c(2 \times 2)$  LEED pattern intensity corresponded to an ordered 50% Pd-50% Cu in the first layer, while there was 30% Pd-70% Cu in the second layer. Further growth of the Pd beyond the surface  $c(2 \times 2)$  mixed layer was found to promote more Pd atoms in the top two layers, destroying the ordered arrangement of the surface  $c(2 \times 2)$  structure. The disordered Pd clustering effect at higher coverages was evidenced by measuring the Pd-Pd pair double scattering peak using 2 keV  $K^+$  ion scattering. The structure of the Cu(001)- $c(2 \times 2)$  Pd surface phase was also probed by measuring the intensity of  $Li^+$  ion scattering as a function of the incident angle along the main azimuthal directions. The results showed that the Pd and Cu atoms were located at the same plane within the experimental uncertainty of 0.05 Å.

**SS-TuP20 Structure and Stability of Steps on the GaAs(110) Surface**, J. M. McCoy\*, Department of Physics, Montana State University, Bozeman, MT 59717, and John P. LaFemina, Pacific Northwest Laboratory\*\*, Richland, WA 99352.

An improved understanding of the behavior and structure of steps at semiconductor surfaces is important for device fabrication, as well as being of fundamental interest. Using a tight-binding total energy calculation procedure [1], we have calculated the atomic geometries

and energies of monolayer and bilayer steps running in the  $[1\bar{1}0]$  and  $[1\bar{1}2]$  directions on the GaAs(110) surface. These computations provide important insight into the dependence of the relative step stability upon the direction of the step and upon the step-edge atomic configuration. We find steps in the  $[1\bar{1}2]$  direction to be much more stable than steps in the  $[1\bar{1}0]$  direction, in agreement with STM results which suggest such a stability difference on the basis of extreme differences in step structure [2].

[1] C. Mailhot, C. B. Duke, and D. J. Chadi, Phys. Rev. B **31**, 2213 (1985).

[2] Y.-N. Yang, B. M. Trefas, R. L. Siefert, and J. H. Weaver, Phys. Rev. B. **44**, 3218 (1991).

\*Present address: Pacific Northwest Laboratory\*\*, Richland, WA 99352.

\*\*Operated for the U.S. Department of Energy by Battelle Memorial Institute under contract DE-AC06-76RLO 1830.

**SS-TuP21 The Thermochemistry of CBr<sub>4</sub> on GaAs(100)**, M. McEllistrem, D. Sloan and J. M. White, NSF Science and Technology Center, University of Texas, Austin, TX 78712.

Recent GaAs film growth studies have shown carbon tetrabromide (CBr<sub>4</sub>) to be a promising precursor for carbon doping. We have investigated the thermochemistry of CBr<sub>4</sub> on GaAs(100) using temperature programmed desorption (TPD), X-ray photoelectron spectroscopy (XPS) and static secondary ion mass spectrometry (SSIMS). Our TPD results, following low temperature (~100 K) adsorption of CBr<sub>4</sub>, show a physisorbed state for doses greater than 1 monolayer, from which the molecule desorbs intact at 195 K. For submonolayer coverages, desorption of molecular CBr<sub>4</sub> is not seen; instead, bromine desorbs as GaBr<sub>x</sub> ( $x = 1-3$ ) at 650 K, leaving carbon behind on the surface. XPS studies confirm the submonolayer decomposition of CBr<sub>4</sub>, and indicate that the C-Br bond has broken and bromine migrated onto the GaAs surface at temperatures as low as 400 K. The kinetics of the CBr<sub>4</sub> decomposition have been investigated by SSIMS. The results will be related to film growth studies.

**SS-TuP22 Surface Chemistry of Dimethyl Hydrazine on GaAs(100)**, Y.-M. Sun, D. Sloan, A. Schwaner and J. M. White, Department of Chemistry and Biochemistry, The University of Texas at Austin, Austin, Texas 78712.

The thermal chemistry of dimethyl hydrazine (DMH) on GaAs(100) has been studied by X-ray photoelectron spectroscopy and temperature programmed desorption. DMH molecularly adsorbs on GaAs(100) at 150 K, and forms three dimensional islands as indicated by TPD spectra. Molecular desorption occurs at 180 K with a high temperature shoulder extending to 400 K. No evidence for dissociation during the temperature ramp was found. Dissociation did occur during dosing at 400 K. N(1s) XP spectra show that N-N bond breaking occurs. Two decomposition products, dimethyl amine and ammonia, desorbed at 490 and 580 K, respectively. GaN formation was observed when DMH was dosed at surface temperature above 600 K, and carbon contamination was below the detection limit of XPS. There was no evidence for C-N bond breaking at reaction temperatures below 500 K.

This work was supported by the NSF Science and Technology Center, Grant CHE 8920120.

**SS-TuP23 The Adsorption of Si on GaAs(001)- $c(4 \times 4)$ ; STM Evidence for Si Induced Disruption of As Layers**, T. S. Jones<sup>1,2</sup>, A. R. Avery<sup>1,2</sup>, D. M. Holmes<sup>1,2</sup>, M. R. Fahy<sup>2</sup>, B. A. Joyce<sup>2</sup>, <sup>1</sup>Department of Chemistry and <sup>2</sup>IRC for Semiconductor Materials, Imperial College, London, UK.

Atomic resolution scanning tunnelling microscopy (STM) has been used to study the adsorption of Si onto GaAs(001) surfaces, grown *in situ* by molecular beam epitaxy (MBE), with a view to understanding the incorporation of Si in  $\delta$ -doped GaAs structures. For surfaces prepared at 400°C, the clean GaAs surface is characterised by a well-defined  $c(4 \times 4)$  RHEED pattern, a structure terminated with two layers of As. Filled states STM images of this surface indicate that the basic structural unit, when complete, consists of rectangular blocks of six As atoms, with the As-As bond in the surface layer aligned along the  $[110]$  direction. Deposition of Si onto this surface at 400°C and relatively low coverages ( $<0.5$  ML), causes disruption of the  $c(4 \times 4)$  layer and formation of dimer rows on the surface. The Si resides in what was the topmost As layer, while displaced As forms dimer rows on top of this Si. In contrast, deposition of Si at 400°C on the GaAs(001)-(2  $\times$  4) surface, shows no evidence for such a disruption.



The importance of the underlying GaAs surface reconstruction in determining the incorporation of Si into the growing structure will be discussed, in particular relating this to the electrical behaviour in Si  $\delta$ -doped GaAs.

**SS-TuP24 Adsorption and Decomposition of Ammonia and Hydrazine on the GaAs(100)-c(8  $\times$  2) Surface, Elizabeth Apen and John L. Gland,** Department of Chemistry, University of Michigan, Ann Arbor, MI 48109-1055.

Temperature programmed desorption (TPD), x-ray photoelectron spectroscopy (XPS), and high resolution electron energy loss spectroscopy (HREELS) have been used to study the adsorption and decomposition of ammonia and hydrazine on the GaAs(100)-c(8  $\times$  2) surface. Ammonia was found to decompose at moderate (250K) temperatures as evidenced by a  $\text{NH}_2$  deformation mode in the HREELS spectrum. Hydrazine was found to adsorb in a "side-on" (vs. "end-on") fashion by XPS. At low coverages, hydrazine dissociation is complete with ammonia the major gas phase product. At higher coverages,  $\text{N}_2$  is the major decomposition product. The absence of a high temperature TPD recombination peak indicates the formation of  $\text{N}_2$  occurs via an intramolecular mechanism. Both  $\text{N}_2\text{H}_y$  and  $\text{NH}_x$  are identified as reaction intermediates for hydrazine decomposition on the GaAs(100)-c(8  $\times$  2) surface. Above 350 K, only  $\text{NH}_x$  species are present on the surface.

**SS-TuP25 Chemical Reactions of Triethylantimony on GaAs(100), John M. Heitzinger and J. G. Ekerdt,** NSF Science and Technology Center, University of Texas, Austin, TX 78712.

Antimony based materials are potentially important for a number of device applications where a small band gap is desirable. Materials such as GaSb and InSb have been successfully grown from organometallic sources using a number of techniques. However, several problems including relatively high growth temperatures and carbon incorporation persist. In an effort to understand the underlying reasons for these problems and evaluate the effect of various ligands on film growth, we have initiated a surface science study of antimony precursors. Our result for triethylantimony indicate that both molecular and dissociative adsorption occur for a substrate temperature of 55°C. A small amount of triethylantimony desorbs from the surface between 55 and 100°C. Upon heating the surface to 300°C, the ethyl ligands undergo a  $\beta$ -hydride elimination reaction to form ethylene. No evidence for ethyl radical desorption is observed indicating homolysis is not an important pathway for ligand removal. This behavior is different than that observed for triethylgallium where both homolysis and  $\beta$ -hydride elimination reactions occur. Most of the triethylantimony initially chemisorbed on the surface is converted to atomic Sb by 380°C. This indicates that once triethylantimony is chemisorbed, its reaction probability is high. We have also performed exposures of triethylantimony at 400°C. For equivalent exposures, more Sb is deposited at 400°C relative to substrate temperatures of 55°C. This is the expected result of site blocking by ethyl groups which remain adsorbed on the surface at the lower adsorption temperature. These, and other results will be related to film growth results.

**SS-TuP26 The Interaction of Hydrogen Atoms with Ethyl Groups on Si(100), P. A. Steiner, J. M. Heitzinger, M. McEllistrem, D. J. Bonser and J. M. White,** NSF Science and Technology Center, University of Texas, Austin, TX 78712.

We have investigated the interaction of hydrogen atoms with ethyl groups adsorbed on Si(100) with Auger electron spectroscopy and temperature programmed desorption (TPD). Ethyl bromide was exposed to the Si(100) surface at 350 K and produced adsorbed ethyl groups and Br atoms. TPD results show ethylene desorption occurs at 590 K via a  $\beta$ -hydride elimination reaction. When H atoms are exposed to an ethyl + Br saturated surface at 350 K, the Br is removed efficiently by hydrogen atoms. However, only a small fraction of the ethyl groups are removed at this temperature. Removal of the Br atoms causes the ethylene desorption temperature to increase by 100 K. This indicates that adsorbed Br decreases the activation energy for the  $\beta$ -hydride elimination reaction. The removal rate of ethyl groups by H atoms increases with increasing substrate temperature; the ethyl and Br removal rate become comparable at 450 K. Arrhenius plots indicate an activation energy for ethyl group removal of 4 kcal/mol. These results, along with the hydrogen flux dependence and kinetic order will be discussed. The data are consistent with a "hot" precursor mechanism in which the majority of the activation energy required

for the reaction to remove ethyl groups is acquired from the precursor, i.e., the H atom, and not the substrate.

This work was supported by the National Science Foundation, Grant #CHE8920120.

**SS-TuP27 Infrared Evidence for an Electrically Conductive Diamond (110) Surface, Bob L. Mackey<sup>1,2,\*</sup>, John N. Russell Jr.<sup>1</sup>, John E. Crowell<sup>2</sup>, James E. Butler<sup>1</sup>,** 1) Naval Research Laboratory, Washington, DC 20375; 2) University of California, San Diego, La Jolla, CA 92123.

The internal reflectivity of the diamond (110) surface was observed by multiple internal reflection infrared spectroscopy (MIRIRS). Surprisingly large variations in the broadband infrared reflectance were seen with annealing or hydrogen dosing. The broadband internal reflectance of the H-terminated surface is found to decrease substantially on thermal desorption of the hydrogen. The reflectivity of the surface was restored by exposure to atomic hydrogen. The change in reflectivity increased with frequency, and is greater for S-polarization.

A simple Drude electron gas model and Fresnel reflectance calculation is used to predict the reflectance of a diamond surface modified by a thin conductive layer for a range of frequencies. The model shows that the observed optical effects are consistent with electrical conductance changes in a thin surface layer. Broadband reflectivity changes may provide a sensitive and generally applicable method of measuring surface electrical conductivity *in situ*.

\*Fannie and John Hertz Foundation Fellow, additional support provided by ONR and ARPA.

**SS-TuP28 Surface Chemistry of Potential CVD Precursors, Diethylsilane and Diethylgermane, on Ge(100), A. Mahajan, B. K. Kellerman, N. Russell, S. Banerjee, J. G. Ekerdt, A. Tasch, J. M. White,** National Science Foundation Science and Technology Center, University of Texas at Austin, Austin, TX 78712.

The adsorption and desorption kinetics of diethylsilane (DES) and diethylgermane (DEG) on a Ge(100) (2  $\times$  1) surface have been studied using temperature programmed desorption (TPD), Auger electron spectroscopy (AES) and high resolution electron energy loss spectroscopy. DES and DEG adsorb at room temperature in a self-limiting fashion. Data indicate that both precursors dissociatively chemisorb, producing a hydrogen- and ethyl-terminated surface. TPD of DES-saturated and DEG-saturated surfaces revealed only two species, ethylene and hydrogen, desorbing from the surface. The ethylene signal evolved from the decomposition of the ethyl groups via  $\beta$ -hydride elimination, with the desorption peak temperature of 620 K for both precursors. The hydrogen TPD spectra were also similar for both precursors and consisted of two peaks: a low temperature peak corresponding to hydrogen desorption from the monohydride state and a high temperature peak corresponding to desorption of hydrogen rate-limited by  $\beta$ -hydride elimination of the ethyl groups. The area under the hydrogen peak in the TPD spectra was calibrated against the areas for known hydrogen coverages. Using this area, the Si/Ge atom coverage following DES/DEG saturation exposure was found to be approximately 0.3 ML, assuming complete  $\beta$ -hydride elimination of the ethyl groups. No carbon contamination was detected on the surface by AES following exposure and TPD cycles of either DES or DEG.

This work was supported by Science and Technology Center under NSF Grant CHE-8920120 and ONR Contract No. N00014-91-J1213.

**SS-TuP29 Surface Reactions of Ethylgermanes on Si(100), Li Chen, Lori A. Keeling, Wei Du, and C. Michael Greenlief,** Department of Chemistry, University of Missouri-Columbia, Columbia, MO 65211.

The adsorption and decomposition of mono-, di-, and tri-ethylgermane on the Si(100)-(2  $\times$  1) surface was investigated with the intent of elucidating the surface processes leading to the deposition of epitaxial Ge films from gaseous Ge-containing sources. The low temperature adsorption of each molecule was investigated, as well as, their thermal decomposition. Similarities in the thermal decomposition of these molecules was observed.  $\text{H}_2$  and  $\text{C}_2\text{H}_4$  are observed in temperature programmed desorption experiments. The ethylene is produced through a  $\beta$ -hydride elimination reaction within the adsorbed ethyl group. The kinetics of ethyl group decomposition are also determined. The amount of Ge that can be deposited in a reaction cycle is correlated with the number of sites occupied by the ethyl groups upon dissociation

of a given ethylgermane. The interactions of ethylgermanes with Si(100) will be discussed in detail and the implications for Ge atomic layer epitaxy will also be explored.

**SS-TuP30 An STM Study of Hydrogen Adsorption on Si(112),** A. A. Baski and L. J. Whitman, Naval Research Laboratory, Washington, DC 20375.

An ideally terminated Si(112) surface would consist of short (111) terraces separated by monoatomic-height steps running along the [110] direction. [It can be considered a (111) surface "miscut" by 19.5°.] Assuming such an ordered array of steps exists, this surface has been used as a potential substrate for quantum wire growth and heteroepitaxy. However, our recent STM studies revealed that this surface undergoes a major reconstruction. The novel facet-reconstruction consists of 50–100 Å wide (337) terraces separated by a variety of short downward-sloping regions [necessary to maintain the (112) plane]. In order to further elucidate the nature of this reconstruction, and investigate possible effects of processing, we have studied the affect of H adsorption on this surface.

Following room temperature adsorption of atomic hydrogen (produced by a hot W filament ~3 cm from the sample and H<sub>2</sub> pressures ~1 × 10<sup>-7</sup> Torr), the facet-reconstruction to (337) terraces is still observed, but the atomic-scale structure is disordered. We attribute the disordered features to the presence of SiH, SiH<sub>2</sub>, and SiH<sub>3</sub> groups on the surface, similar to those observed on Si(001). The (337) terraces persist even if the surface is exposed to H at ~400°C under conditions which normally produce a monohydride-covered Si(001) surface. However, at this higher temperature the atomic-scale structure within the reconstruction is modified by the adsorbed H, producing new ordered structures. These structures and their evolution with increasing H coverage reveal new details about the atomic-scale structure of the clean surface reconstruction. Models of the H-covered surface and the implications of our observations for processing of this substrate will be discussed.

## NANO 3/NANOMETER-SCALE SCIENCE AND TECHNOLOGY

Room BR4 – Session NS-TuP

### Materials Characterization

**Moderator:** R. J. Hamers, University of Wisconsin, Madison.

**NS-TuP1 Selenium Nanoclustering in Vapor Grown ZnSe Crystals,** M. A. George, W. E. Collins, K.-T. Chen, Zhiyu Hu, Y. Zhang, and A. Burger, Center for Photonic Materials and Devices, Department of Physics, Fisk University, Nashville, TN 37208, and C.-H. Su, Y.-G. Sha, D. C. Gilles and S. L. Lehoczky, Space Science Laboratory, NASA/Marshall Space Flight Center, Huntsville, AL 35812.

This study reports on the chemical identification, distribution and morphology of Se nanoclusters formed during the crystal growth process of ZnSe single crystals. The ZnSe crystals were grown by the Physical Vapor Transport method from prepurified starting materials. The surfaces were examined using Scanning Auger electron spectroscopy (SAES) and X-ray photoelectron spectroscopy (XPS) and Atomic Force Microscopy (AFM). The formation of nanoclusters and its relation to the crystal growth procedure was investigated. The occurrence of the nanoclusters was linked to the purity and stoichiometry of the starting materials as well as the surface morphology of the crystal growth facets. Acknowledgement: This work was performed through funding provided by the NASA through the Fisk Center for Photonic Materials and Devices, Grant #NAGW-2925, and partial support from NASA Lewis Research Center, Grant #NAG3-1430.

**NS-TuP3 Chemistry in Nanoporous Materials: Semiconductor Particles Formed Within a Solid Template,** Catherine M. Zelenski and Peter K. Dohout, Colorado State University, Fort Collins, CO 80523.

Metal sulfide semiconductors have been synthesized within the nanometer-sized pores of an aluminum oxide template. Several solution methods for the formation of nanoparticles of semiconductors within this template have been studied. A method of dipping the film into precursor solutions produced fine particles of the semiconductors trapped within the pores near the surface of the film. A second method utilizing a U-tube apparatus produced a thin coat of metal sulfide

particles along all inner surfaces of the aluminum oxide template. Primary methods of characterization include UV-vis spectroscopy, TEM, SEM, energy dispersive X-ray microanalysis, and electron and X-ray powder diffraction. Thus far, particles have not grown to entirely fill the 50–70 nm diameter pores of the template; however, several other methods for these syntheses are being studied.

**NS-TuP4 Scanning Tunneling Microscopy of Thin Films of TaS<sub>2</sub> Prepared by an Intercalation-Exfoliation Method,** A. Manivannan, C. R. Cabrera and A. Fujishima\*, Dept. of Chem. and Materials Research Center, Univ. of Puerto Rico, P.O. Box 23346, San Juan, PR 00931 USA, \*Dept. of Synthetic Chem., Faculty of Engineering, The Univ. of Tokyo, Hongo, Bunkyo-Ku, Tokyo-113, Japan.

Two dimensional atomic and electronic systems are of specific interest with respect to their phase transitions due to the formation of charge density waves (CDWs). Layered transition metal dichalcogenides (LTMDs) are the suitable candidates for two dimensional studies when they are prepared as single molecular layer form. In this work, single layer suspensions of metallic layered compounds TaS<sub>2</sub> were prepared by a lithium intercalation-exfoliation procedure. These suspended layers were directly deposited on a titanium substrate and heat treated at 250°C in vacuum for 2 hrs. Scanning electron microscopy (SEM) measurements revealed a lamellar microstructure with the basal plane of TaS<sub>2</sub> crystallites oriented parallel to the substrate. Scanning tunneling microscopy (STM) investigations indicated the existence of CDWs having peak spacings of ~12 Å similar to that of single crystals. The surface atomic structure has also been imaged by STM which showed lattice distortions and deviations. The existence of CDWs in these restacked single layer(s) of TaS<sub>2</sub> allows us to study the intralayer interactions and also supports the theoretical work of a two dimensional model of CDWs in one layer. Moreover, the presence of CDWs in these films contradicts the failure to observe a CDW diffraction pattern in the previous electron microscopy study. Thus, STM seems to be a powerful and unique technique to study the existence and dynamics of CDWs in these single layer(s) of TaS<sub>2</sub> films.

**NS-TuP5 Oxidation Behavior of Aluminum Nanopowders,** C. E. Aumann, G. L. Skofronick, and J. A. Martin, Physical Chemistry and Process Technology Group, CST-2, Chemical Science and Technology Division, Los Alamos National Laboratory, Mail Stop J565, Los Alamos, NM 87545.

Interest in nanostructures is fueled by the potential for finding novel properties in material structures that have small physical dimensions. Indeed, composite materials assembled from nanosized components exhibit properties very different than bulk depending on the size and characteristics of their individual constituents. A dramatic example is found in the reaction rate of mixtures of Al and MoO<sub>3</sub> nanopowders. Powder mixtures with average diameters of 2–500 Å achieve reactive powers 1000 times that of conventional thermite powders. Also, reactive power is tunable by mixing together powders with other average particle sizes. Nanostructures can be manipulated to yield changes in the behavior of the composite, e.g., partial oxidation of Al nanoparticles reduces total energy released in reactions of Al and MoO<sub>3</sub> powders. Often, properties of nanosized components can be inferred from macroscopic changes that occur in a bulk quantity of material. We have used thermogravimetric analysis (TGA) to measure changes in mass of Al powder samples annealed at a particular temperature during exposure to oxygen. Samples are characterized using transmission electron microscopy (TEM) and Rutherford backscattering spectrometry (RBS). As-prepared Al particles consist of a core of crystalline Al protected by a ~30 Å thick shell of amorphous alumina. Activation energy for oxidation is determined from a series of isothermal TGA measurements taken at different temperatures for powder samples with different average particle sizes. Activation energy is found to depend on the average size of the Al particles and to be much smaller than for flat Al samples.

**NS-TuP6 The Origin of Universality in the Top Layer Relaxation of Zincblende (110) and Wurtzite (1010) Surfaces,** G. Brown and M. Weimer, Department of Physics, Texas A&M University, College Station, TX 77843-4242.

Extensive experimental and theoretical studies have confirmed the "universal" nature of the relaxation that occurs at zincblende (110) and wurtzite (1010) cleavage surfaces. This relaxation can be parameterized in terms of a nearly rigid bond rotation of the top layer atoms, with a "universal" tilt angle for each structure that is independent of chemical composition. No precise origin for this chemical independence, or transparent model of what happens to the orientation and character of the dangling bonds as relaxation proceeds, has yet



been proposed. In addition to enriching our understanding of the perfectly periodic surface, such a picture might well provide a semi-quantitative basis for describing more complex phenomena such as defect formation and chemisorption.

To address such questions, we have examined these relaxations within the context of a simple analytical model, considering those bond length conserving reorientations that preserve the symmetries consistent with experiments and more detailed theoretical calculations. We derive a general mathematical relationship between the top layer atom hybrid orbital energies and the constraining local geometry. Our results show a relaxation that is constrained by orthogonality limits on the amount of anion orbital rehybridization, so that the minimum energy configuration is determined explicitly and obviously by the bonding geometry, and not by atomic term values. This leads to a universal tilt angle for each structure that is in good agreement with the accepted values.

A particularly noteworthy feature of the model, in addition to its simplicity, is that it allows both zincblende and wurtzite surfaces to be treated equivalently within a single framework, where the same driving forces and limiting factors govern the relaxation. The model furthermore provides an explicit representation for the hybrid character and orientation of the dangling orbitals during all stages of the relaxation.

**NS-TuP7 Nonlinear Optical Absorption in Asymmetric Quantum Wells, Xinxing Yang, J. T. McKinley, R. G. Albridge, A. V. Barnes, N. H. Tolk, Vanderbilt University; Nashville, TN 37235, and G. Margaritondo, Ecole Polytechnique Fédérale, CH-1015 Lausanne, Suisse.**

We have probed the nonlinear optical properties of asymmetric GaAs/AlAs multiple quantum wells in the mid-infrared spectral range using the z-scan technique and the Vanderbilt Free-Electron Laser (FEL). The z-scan method gives an accurate and absolute measurement of the nonlinear index of refraction and the nonlinear absorption coefficient while not requiring sophisticated instrumentation. The FEL is a source of high intensity (15 MW) radiation with tunable wavelength (1–8  $\mu\text{m}$ ) and tunable pulse width (0.7–1.5 ps). In a z-scan measurement, a thin semiconductor sample is scanned along the optical axis (z-axis) of a focusing element causing strong nonlinear effects to occur as the sample moves through the beam waist. The nonlinear coefficients are obtained by fitting the normalized transmission spectrum to well-known analytic expressions. In the bulk semiconductors, the studies focused on the near optical band gap nonlinear refractive index and the two-photon absorption coefficient. In the quantum well materials, the intensity dependence of the intersubband separation was measured. Saturation effects and free-carrier absorption are also discussed. These are the first successful z-scan measurements performed at the Vanderbilt FEL.

**NS-TuP8 Quantum Confinement Effects in Heteroepitaxial Si/ZnS Nanostructures Produced by MOCVD,\* E. Brettschneider, A. Davydov, J. E. Yu, Z. Huang, B. Pathangey, K. S. Jones, T. J. Anderson, University of Florida, Gainesville, FL 32611, H. P. Maruska, R. Sudharsanan, Spire Corp., Bedford, MA 01730.**

Silicon multi-quantum wells with closely lattice matched ZnS barriers were grown on silicon substrates by metalorganic chemical vapor deposition (MOCVD) in a horizontal-flow reactor. Photoluminescence studies revealed emissions peaks which were blue-shifted with respect to the photon-assisted emission from bulk silicon substrates. The observation of an emission shift to shorter wavelengths is consistent with our calculations of quantum confinement effects in silicon nanostructures. A high temperature (900°C) silicon buffer layer was first grown from disilane on both (100) and (111) oriented Si substrates, followed by the epitaxial ZnS cladding layer. Silicon films with thickness ranging from 3 to 15 nm were then deposited on the ZnS at low temperatures (350–500°C) using disilane. A ZnS capping layer completed the structures. Multiquantum well structures featuring as many as six wells were grown, and emission peaks at wavelengths as short as 830 nm were observed. The Si thicknesses were determined by transmission electron microscopy. The presence of the Si quantum wells were further substantiated by SIMS depth profiling and from emission shifts detected by micro-Raman spectroscopy.

\*Work supported by the US Department of Energy.

**NS-TuP9 Luminescence of Nanostructures Induced by Carriers Injected from a Scanning Tunneling Microscope Emitter, Lars Montelius, Joakim Lindahl, Mats-Erik Pistol and Lars Samuelson, Lund University, Department of Solid State Physics and The Nanometer Structure Consortium, PO Box 118, S-221 00 LUND, SWEDEN.**

In recent years the interest for devices based upon the properties of

low-dimensional structures has increased substantially. In order to reveal the electrical and optical properties of such structures scanning probe microscopy techniques have proven to be particularly useful. The main advantage with these techniques is the possibility to locally characterize the material. One such technique is the combination of local injection of carriers using a scanning tunneling microscope (STM) and simultaneous luminescence detection of the tip sample region. The modes of operation are either a mechanism that is similar to high-energy cathodoluminescence (CL) spectroscopy, where the injected carriers generate electron hole pairs which in turn recombine radiatively, or direct radiative recombination of the injected carriers with holes (or electrons). In this paper CL excitation and STM excitation will be compared. The sample studied is an AlGaAs/GaAs quantum well and quantum wire sample making it possible to inject carriers directly into a single quantum wire using STM injection.

**NS-TuP10 Spectral and Structural Features of Porous Silicon Prepared by Chemical and Electrochemical Etching Processes, D. F. Thomas, L. A. Jones, E. Nakamichi, L. Zajchowski, Department of Chemistry and Biochemistry, University of Guelph, Guelph, Ontario, Canada. N1G 2W1.**

It is known that fluorescent porous silicon can be formed by both electrochemical and chemical etching procedures. The continuing effort to understand the formation mechanisms involved and the nature of the resulting photo- and electroluminescence is complicated by the wide variety of resulting structural features with relevant dimensions that span several orders of magnitude. Porous silicon was formed from both n- and p-doped Si(111) and Si(100) using both an HF-electrochemical process and a HF/HNO<sub>3</sub> chemical etchant. Both fluorescence and excitation spectra were acquired to analyze the spectral properties of the samples. The electrochemically prepared samples generally produced fluorescence peaked around 650 nm while the chemically prepared samples peaked around 610 nm. Excitation spectra show a monotonic increase in fluorescent intensity when the excitation wavelength is scanned from 500 nm down to 275 nm (the instrumental limit). One notable exception to these trends was a chemically prepared sample which showed blue fluorescence at 440 nm in addition to the orange fluorescence. The structural properties of these samples were studied by scanning electron microscopy (SEM) and scanning force microscopy (SFM). On the scale of microns, the surface features varied widely between sample preparation techniques. Three types of surface porosity are identified with remarkably different surface roughness characteristics. The correlation between sample preparation procedures, the resulting surface roughness, and the subsequent photoluminescence will be presented.

**NS-TuP11 Mesostructure of Luminescent Porous Silicon\*, F. Ruiz\*\*, E. López-Cruz, C. Vázquez-López, G. Torres-Delgado\*\*\*, and J. González-Hernández, Programa Multidisciplinario de Materiales Avanzados, CINVESTAV-Saltillo, Saltillo, Coah., México, \*\*On leave from Universidad Autónoma de San Luis Potosí, \*\*\*CINVESTAV-DF.**

Scanning Electron Microscopy, Scanning Force Microscopy (SFM), Raman Spectroscopy, and Photoluminescence were used to characterize samples of highly optical efficient porous silicon. Preparation conditions of the samples were as follows: p-Si(100) substrates with electrical resistivity in the 1–2 ohm-cm range were electrochemically etched by means of an HF:H<sub>2</sub>O:ethanol solution, at the proportion: 1:1:2. Anodization time was 15 minutes and the current density employed were 1, 5, 25, and 40 mA/cm<sup>2</sup>. The Raman and photoluminescence measurements were correlated to the microstructure as determined by SFM. By using images both from the surface as well as from the side it was possible to construct a three dimensional model of the mesostructure of porous silicon. It is concluded that the presence of photoluminescence in this type of samples do not necessarily have its origin in the fibrous-type structures as reported by several authors.

\*This work was partially sponsored by CONACyT-México.

**NS-TuP12 The Size Effects Study on the Vibrational Properties of the Si Nanocrystalline Materials, H. F. Zhang, T. Jin, Y. P. Li, C. S. Wang, S. D. Xia, Department of Physics, University of Science and Technology of China, Hefei 230026, P.R. China.**

With the growing study on the nanometer materials and the porous silicon, it is obvious that the predominant reason for these materials having special properties is the size effect of the crystallites. As we know, not only the electronic structure and optical properties study are important aspects for us to explain the experimental results, but also the Raman scattering and infrared absorption study are also

important techniques, and the latter ones are correlated to the vibrational properties. In this paper, The Extension Hukel Tight-binding method (EHT), the Recursion Method as well as the Dean method were used to study the vibrational densities of states on the real Si structure with the size from 4.70 Å to 50.7 Å were systematically studied. The results that when the crystallite sizes are different, the densities of states are varied (the peaks become sharp and shift to higher energies, as the size growing) are presented and discussed, which are in good agreement with experiment. On the other hand, when the number of the atoms in one crystallite is up to 3109, that means the diameter of the crystallite is 21.7 Å, the densities of states are the same more or less, and all close to that of the crystalline Si, these results agree well with the electronic structure study on the hydrogenated Si clusters.

**NS-TuP13 Atomic Force Microscopy and Scanning Tunneling Microscopy Study of  $\text{Ge}_{1-x}\text{Fe}_x$  Nanophase Materials,** *Da-Ming Zhu*, Department of Physics, University of Missouri-Kansas City, Kansas City, MO 64110, USA; *Jin Shi*, Department of Physics, University of Illinois at Urbana-Champaign, Urbana, IL, USA.

We have conducted a study of nanophase  $\text{Ge}_{1-x}\text{Fe}_x$  materials using atomic force and scanning tunneling microscopies. Our goals are to characterize the size and shape distributions of nanoparticles in the materials and to detect possible interfacial diffusion of atoms between particles. The materials were synthesized via gas-condensation in an ultrahigh vacuum system. The condensed particles were compressed *in situ* to form thin disks before exposure to air. We have prepared a series of samples with Fe concentration varying from 6% to 86%. The sample with 6% concentration of Fe is almost insulating. We have obtained images with an atomic force microscope which clearly identify each individual nanoparticles. The sizes of the Ge and Fe particles are very uniform, being about 50 nm. For the samples with high concentration of Fe, we have used scanning tunneling microscope to examine the boundaries between different particles, in an attempt to study the atomic diffusions between particles. We will compare our results with the those of transport measurements conducted on the same samples.

**NS-TuP14 Growth, Structure and Diffusion of Small NaCl Clusters on the (001) Surface of MgO,** *A. L. Shluger and A. L. Rohl*, The Royal Institution of Great Britain, 21 Albemarle St., London W1X 4BS, U.K.

Study of the stability, atomic and electronic structure and mobility of clusters adsorbed at insulating surfaces can provide deeper insights into the micro-mechanisms of growth of materials by molecular beam epitaxy and vapour deposition, and the formation of nanostructures. Comparison of the structural and optical properties of adsorbed clusters with analogous properties of the bulk materials and free clusters is important for further understanding of the properties of materials as a function of their dimensions. In this study we have investigated atomic and electronic structure, stability and mobility of  $\text{Na}_x\text{Cl}_x$  ( $x = 1, 3, 6$ ) clusters adsorbed on the (100) surface of MgO using atomistic simulation and quantum-chemical MO LCAO calculation techniques. Crystal and cluster optical absorption spectra were calculated using the configuration interaction technique. We considered attachment of new NaCl molecules to existing surface structures, modelling their growth. It was demonstrated that starting from  $\text{Na}_4\text{Cl}_4$  clusters they begin to form two-layered rectangular structures which are isotropic and grow by filling the kink sites. The stability of the clusters increases slowly with their size. Due to a large mismatch of the MgO lattice constant and interionic separation within the clusters, at large cluster sizes ( $x > 24$ ) only average cluster-surface interactions play a role. The mobility of large clusters is anisotropic and much higher than that of small ones. The optical excitation energies and other electronic structure parameters are calculated as a function of cluster size and structure.

**NS-TuP15 Atomic Force Microscopy of Au Implanted in Sapphire,** *D. O. Henderson, M. A. George, A. Burger, R. Mu, S. H. Morgan*, Fisk University, Physics Dept., Nashville, TN 37208, *R. H. Magruder III*, Dept. of Applied and Engineering Sciences, Vanderbilt University, Nashville, TN 37235, *C. W. White and R. A. Zuhr*, Oak Ridge National Laboratory, P.O. Box 2008, Oak Ridge, TN 37831-6057.

Ion implantation is an attractive technique for modifying the near surface properties of a wide variety of materials. The implantation of Au into  $\text{Al}_2\text{O}_3$  leads to the disruption of the long range order in the crystal producing an amorphous layer. Annealing the implanted crystal at 1373 K restores the crystallinity of the sample. The annealing also imparts a purple color to the Au implanted sample which is attributed to the surface plasmon resonance of gold colloids. The width of the

surface plasmon resonance depends on the colloid size, whereas the resonance frequency depends on the colloid shape. In order characterize the size and shape of Au colloids formed by ion implantation, we have performed AFM measurements on Au implanted sapphire. Infrared spectra for the Au implanted sapphire are also reported and are discussed in terms of ion induced damage.

The research at ORNL was sponsored by the Division of Materials Sciences, under contract DE-ACD5-84OR21400 with Martin Marietta Systems.

**NS-TuP16 An STM Study of Molecular Intermediates in the Dissociative Adsorption of closo-1,2-dicarbadoecaborane on Si(111),** *J. M. Carpinelli and E. W. Plummer*, Oak Ridge National Labs, Oak Ridge, TN 37831-6057; *D. Byun and P. A. Dowben*, University of Nebraska, Lincoln, NE 68588-0111.

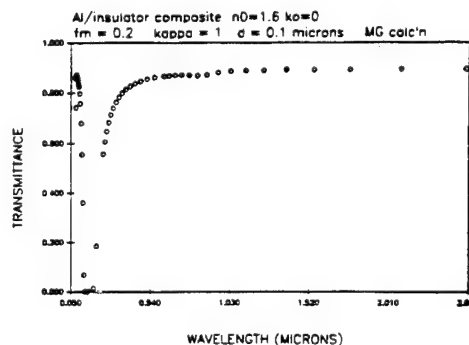
Closo-1,2-dicarbadoecaborane ( $\text{C}_2\text{B}_{10}\text{H}_{12}$ ) is a source compound for the deposition of a high resistivity form of boron-carbide ( $\text{B}_3\text{C}$ ) and has been used to make  $\text{B}_3\text{C}/\text{Si}(111)$  heterojunction diodes [1]. The goal in employing this source compound is "direct writing" or selective area deposition of boron-carbide using very short wavelength (high resolution) radiation. For success in the direct writing technique, the source molecule must exhibit a molecular precursor state on Si(111). Using an STM, we have imaged such molecular icosahedra after exposure to closo-1,2-dicarbadoecaborane. Prolonged exposure to our source leads to a reconstruction of the Si(111)-(7 × 7) surface. Based upon Auger electron spectroscopy data, we postulate that following dissociation of the surface intermediate species, some boron atoms substitutionally occupy selvedge sites. This selvedge layer of boron is believed to cause the surface reconstruction.

[1] Dongjin Byun, S.-d. Hwang, P. A. Dowben, F. K. Perkins, F. Filipps, and N. J. Ianno, Appl. Phys. Lett. (1994) in press.

**NS-TuP17 Fabrication and Optical Characterization of Aluminum Nanometal/Porous Aluminum Oxide Thin Film Composites,** *C. R. Martin, G. L. Hornyak, B. P. Berggren*, Department of Chemistry, Colorado State University, Fort Collins, CO 80523.

An aluminum nanometal inclusion/porous aluminum oxide host composite thin film is predicted to be transparent in the visible range of the spectrum so long as the dimensions of the particles are very small (circa 10 nm) according to our computer simulations. The theoretical plasmon resonance absorption maximum derived from those simulations is near 190 nm wavelength (please consult the figure given below). We present an experimental strategy for fabrication of these transparent composite thin films by means of electroplating in a toluene/aluminum bromide/potassium bromide/trimethylchlorosilane solution under an inert atmosphere blanket.

For aluminum oxide composites which contain nanometals of greater dimensions, where scattering phenomena cannot be neglected, we employ our dynamical Maxwell-Garnett effective medium theory model to explain spectral characteristics. In addition to the apparent transparency as described above, these composite films can be made to possess electrical conductivity with respect to the transverse direction of the film. Film structures are characterized by transmission and scanning electron microscopy.



**NS-TuP18 Nanometer-Scale Observations of the Corroded Surfaces of Metallic Glasses,** *Y. Watanabe, Y. Nakamura and S. Hirayama*, National Defense Academy, Yokosuka, Kanagawa 239, Japan.

In order to study the influence of crystallization on corrosion re-

sistance of metallic glasses, surfaces of as-cast and annealed metallic glasses,  $\text{Fe}_{40}\text{Ni}_{38}\text{Mo}_4\text{B}_{18}$ , are observed with atomic force microscope and the change in the surface morphology before and after corrosion by nital is examined on the nanometer-scale. On the surface of the as-cast specimen before corrosion, several protrusions with a height of less than 50 nm are observed on the smooth matrix, while on the surface of the as-cast specimen after corrosion the matrix becomes rough and the protrusions are found to grow although the corrosion has occurred at room temperature. This may be explained by the assumptions that (1) protrusions are metal boride crystallites and they are not corroded by nital, (2) the matrix is corroded by nital because of its iron-rich composition and (3) crystallites buried under the matrix has appeared by corrosion of the matrix. On the surface of the 873 K-annealed specimen before corrosion, the surface is covered with protrusions of 100 to 200 nm height and the smooth matrix is also observed, but the surface of the annealed specimen after corrosion is almost covered over with protrusions of less than 100 nm and the smooth matrix has disappeared. These observations suggest that during corrosion larger crystallites have been peeled from the surface because the corrosion of the matrix progressed. This peeling of crystallites seems to result in deterioration of corrosion resistance of metallic glasses after annealing.

**NS-TuP19 Dynamical Characteristics of Low Frequency Current Fluctuations from Local Areas of Semiconductor Field Emitter Surfaces**, *R. Z. Bakhtizin and S. S. Ghots*, Department of Physical Electronics Bashkir State University, Ufa 450074, RUSSIA.

Semiconductor field emitter surfaces are by no means static and surface structure changes of nanometer scale can occur spontaneously near or slightly above room temperatures especially if high electric field is applied. Such changes can not be studied simultaneously both in terms of space and time using conventional Scanning Probe Methods (STM, AFM), whereas they give rise to current fluctuations.

In this paper we describe the dynamical characteristics of elementary low-frequency current fluctuations which originate from local surface areas of the p-type Si field emitter. We also present the results of noise measurement providing the possibility of single atom movement observation within the local areas of 10 nm. All types of linear elementary fluctuations, i.e., oscillating, relaxing and aperiodic processes as well as non-linear oscillating (i.e. telegraph form) process are considered.

**NS-TuP20 Many-Particle Effects in Tunneling Electrons from Metal and Semiconductor Surfaces**, *M. A. Koshushner, G. K. Ivanov*, Institute of Chemical Physics, Moscow 117997, RUSSIA and *I. I. Olinik*, Volgograd State University, Volgograd 400087, RUSSIA.

We develop theory of tunneling processes in many-particle systems on the grounds of Lippman-Schwinger integral equation that gives us possibility to calculate the asymptotics of many-electron wave functions with accuracy provided by standard quantum-chemical methods in the main region of electron localization (MREL) [1]. In this approach, interaction between electrons and inter-electron correlations are naturally included into consideration.

Application of the theory to calculate parameters for tunneling from metal surfaces displays two main effects of interaction between electrons. First, the effective tunneling potential depends on topology of Fermi surface, quantum numbers of the tunneling electron and does not coincide with widely used image potential. Second, tunneling transition is accompanied by inter-electron exchange of energy, that results in effective change of tunneling probability energy dependence.

We obtained general expression for tunneling current in STM, that gives the possibility of solution of reverse STM problem—extraction of wave functions data for surface and tip atoms from tunneling current measurements. The specific examples of STM imaging in case of graphite, Cu and Au surfaces illustrate the general scheme of direct and reverse STM problems' solution.

[1] Ivanov, G. K., and Koshushner, M. A., Asymptotics of Many-Electron Wave Functions and Calculation of Tunnel Transitions, Chemical Physics, 1993, 170, 303.

**NS-TuP21 STM/STS Investigation of Ionexchanged Polymer Multilayer LB Films: 2D Conductivity, Resonance Tunneling, Charge Superstructure**, *N. Maslova, Yu. Moiseev, V. Nikanorov, V. Panov, S. Savinov, R. Yusupov*, Moscow State University, Physical Department, 119899, Moscow, Russia.

The Langmuir-Blodgett (LB) films of ionexchanged polymers have been investigated by scanning tunneling microscopy (STM) and scanning tunneling spectroscopy (STS) methods.

For the ionexchanged polymer films with odd layers number some peculiarities have been discovered. In this case the  $dI/dV(V)$  dependencies have a peak (local maximum) with the width about 250 mV near the zero bias. Surface reconstruction corresponding to charge density wave and the oscillating character of  $I(V)$  dependencies have been observed. The STM feedback loop generation was observed when the setpoint of STM is in the negative slope area of  $I(V)$  curve.

This effects are explained by theoretical model taking into account that the overall electronic density of states is determined by the superposition of effects connected with the two-dimensional conductivity character and charge density wave.

**NS-TuP22 Determination of Large Heterogenous Rate Constants Using Nanoelectrode Ensembles**, *Vinod P. Menon and Charles R. Martin*, Department of Chemistry, Colorado State University, Fort Collins, CO 80523.

An electroless deposition method has been developed for the fabrication of nanoelectrode ensembles using commercially available polycarbonate membrane filters as templates. Ensembles with individual electrode radii as small as 50 Å have been fabricated. These ensembles act as partially blocked electrodes and have a very low fractional electrode area. Due to the apparent slowing down of rate constants at partially blocked electrodes, these ensembles can be used to determine heterogenous rate constants for extremely fast redox couples. Rate constants as high as 70 cm/s have been obtained for a derivatized ferrocene redox couple. Furthermore these ensembles show detection limits three orders of magnitude lower than conventional macrosized electrodes. Some of these kinetic and detection limit data will be presented.

## APPLIED SURFACE SCIENCE Room BR4 – Session AS-TuP

### Aspects of Applied Surface Science

**Moderator:** D. R. Baer, Battelle Pacific Northwest Laboratories.

**AS-TuP1 A Study of Vapor-Deposited Polythiophene Thin Films**, *T. R. Dillingham, D. M. Cornelson, A. G. Sykes, M. Vittera and S. Townsend*, Department of Physics and Astronomy, Northern Arizona University, Flagstaff, Arizona 86011.

Thin polythiophene films, prepared using a vacuum evaporation process, have been studied using x-ray photoelectron spectroscopy (XPS). Emphasis is placed on the chemical structure of the deposited films and the results are compared to films synthesized using more conventional chemical or electrochemical methods. The films were deposited, with a starting material of polythiophene powder, using a resistively heated quartz crucible under high vacuum conditions. The as-deposited films have a mirror-like quality and the XPS analysis of the film, which is compared to that of the initial powder, indicates that no chemical change occurs during the deposition process. Results are also presented concerning the oxidation of these films in an iodine environment and this analysis is related to conductivity measurements of the vapor-deposited films.

\*Supported by the National Science Foundation under grant No. DMR-9217526 and the NAU Organized Research Program.

**AS-TuP2 Highly Ordered Thin Films of Phthalocyanines, Created by Self-Assembly and Langmuir Blodgett Deposition**, *N. R. Armstrong\*, L.-K. Chau\*, S.-Y. Chen\*, E. Osburn\*, D. F. O'Brien\*, A. Ferencz†, G. Wegner†* (\*) = Department of Chemistry, University of Arizona, Tucson, Arizona 85721; † = Max Planck Institut für Polymerforschung, Mainz, Germany.

Densely packed and highly ordered thin films of various phthalocyanines are obtainable by deposition from solution, provided that side chain modification of the Pc's has been carried out to improve processability. Silicon phthalocyanines can be polymerized along the central axis, to form an O-Si-O-Si ... linkage, which provides for close packing of the cofacial Pc rings—processability as LB thin films is produced through various alkane side chains (4 per ring system). Divalent metal Pc's (CuPc and ZnPc), with the appropriate side chains, will self-organize during simple solution casting, and/or through the formation of LB thin films. Both types of thin films show a high

degree of organization, which impacts on both the electrochemical and optical properties of these assemblies. The degree to which electrochemical oxidation of the Pc rings is possible is difficult to determine—however, since these films are vacuum compatible, surface analysis techniques such as angle resolved XPS can be used to determine oxidation stoichiometry (i.e. the degree of counter ion incorporation into the near surface region of these thin films).

**AS-TuP3 Metal Overlayers on Self-Assembled Monolayers: 5. ISS and XPS of the Ag/COOH Interface, G. C. Herdt, and A. W. Czanderna, NREL, Golden, CO 80401\*.**

The purpose of our research is to study the interactions or processes between vacuum deposited metals and self-assembled monolayers (SAMs) under controlled conditions. In this work, XPS and ISS were used to characterize mercaptoundecanoic acid (MUA,  $\text{HS}(\text{CH}_2)_{10}\text{COOH}$ ) and mercaptohexadecanoic acid (MHA,  $\text{HS}(\text{CH}_2)_{15}\text{COOH}$ ) SAMs before and after depositing up to 1.0 nm Ag at ca.  $10^{-7}$  torr. The SAMs were prepared by self-assembly onto gold films on <100> silicon substrates in an ethanolic thiol solution. XPS spectra indicate that no strong interaction occurs between the deposited Ag and the COOH organic functional group (OFG). ISS compositional depth profiles (CDPs) for Ag on MHA and MUA (this work) and octadecanethiol (ODT,  $\text{HS}(\text{CH}_2)_{17}\text{CH}_3$ )<sup>1</sup> are compared over a temperature range of 113 to 293 K. The ISS results indicate that Ag remains on the surface of MUA and MHA for up to 1 h after deposition, whereas Ag penetrates ODT in less than 5 min at 295 K. The time dependence of the slower Ag penetration through MUA and MHA will be compared with that for ODT at temperatures below 295 K. Although Ag/OFGs are expected to have relatively weak interactions, the Ag/COOH system was anticipated to be more interactive than was found, so rapid penetration of Ag through the COOH SAM is an unexpected result.

<sup>1</sup>GCH & AWC, JVST A, 12 (1994) July/August.

\*Performed under DOE contract DE-AC02-83CH10039.

**AS-TuP4 Quantitative Analysis by Static SIMS of Mixed Self-Assembled Monolayer Films on Metal Substrates, Yue-Zhong Du, Robert W. Johnson, Jr., Joseph A. Gardella, Jr., Department of Chemistry, State University of New York at Buffalo, Buffalo, New York 14214.**

Self-Assembled monolayer films (SAMs) allow the construction of thin organic films with highly specific properties. The effect of hydrocarbon chain length on the orientation of these films has been extensively characterized using contact angle, ellipsometry, external-reflection infrared spectroscopy, and electron spectroscopy for chemical analysis. However, the effect of hydrocarbon chain length on the composition of films formed from solutions of mixed adsorbates has been studied less extensively. In the current study, static secondary ion mass spectrometry (SSIMS) is used to address this question. Specifically, quantitative techniques that have been developed for the analysis of monolayer films will be utilized. These techniques, which involve the quantification of molecular secondary ions as a function of ion dose, have been used to determine the composition of mixed monolayer Langmuir-Blodgett films. Results from mixed monolayer Langmuir-Blodgett films are used to quantify Self-Assembled monolayer films. Surface excess of long chain acids in mixed Self-Assembled monolayer films are quantified.

**AS-TuP5 Temperature Controlled TOF-SIMS Investigations of Polymer Materials, M. Deimel, B. Hagenhoff, A. Benninghoven, Physikalisches Institut der Universität, Wilhelm-Klemm-Str. 10, D-48149 Münster, Germany.**

The temperature dependence of secondary ion (SI) yields can give a deeper insight into the ion formation process in SIMS. Up to now, however, such investigations were limited to relatively small molecules adsorbed on clean metal surfaces due to the use of quadrupole instruments. We added a device for temperature control to a time-of-flight (TOF) mass spectrometer such making use of the higher accessible mass range and sensitivity of TOF analyzers.

We investigated the temperature dependence of SI yields for several polymers including Polystyrene (PS), Polydimethylsiloxane (PDMS), Polymethylmethacrylate (PMMA), a perfluorinated polyether (Krytox) and Polyethyleneglycol (PEG) prepared as monolayers on different metal substrates. The results show that the temperature behaviour in principle is independent of the respective substrate material. Intact polymer molecules disappear from the surface at well defined temperatures when the target is heated. For PEG a common disappearance temperature  $T_D = 500$  K is observed independent of the polymer chain

length caused by a thermal fragmentation process. For all other polymers the observed desorption temperatures increase with the number of repeat units. From these observations we determined the activation energy for the desorption as a function of the polymer chain length according to the Polanyi-Wigner model.

**AS-TuP6 Radiation Damage on Some Organic Materials During S-SIMS and XPS Analysis, M. Kudo\*, T. Nishihara\* and T. Hoshi\*\*, \*Seikei Univ., Musashino, Tokyo 180, Japan, \*\*ULVAC-PHI Incorporated, Chigasaki, Kanagawa 253, Japan.**

It is generally recognized both Static-SIMS and XPS are non-destructive analytical techniques. However, in S-SIMS, the obtainable mass spectra change a great deal according to the primary ion dosage. In XPS, both monochromatic and non-monochromatic x-ray sources also cause sample damages, the latter, generally, more serious due to the higher energy Bremsstrahlung x-rays irradiation. Although some systematic analysis data have been presented for some typical materials, the detailed interpretations and standard criteria for practical analysis have not been established yet.

In this study, we investigated systematically the damages on some radiation sensitive materials such as Poly Tetrafluoroethylene (Teflon), Poly Caprolactam (Nylon 6), Poly Carbonate (PC), Poly Ethylene Terephthalate (PET) and some others. The S-SIMS mass spectra were recorded at an appropriate dosage intervals, each followed with XPS analysis. The x-ray irradiation damage was also evaluated using both XPS spectra and S-SIMS mass spectra analysis. The results are discussed in terms of the dependence of damages on the chemical bonding of the materials investigated and on the energy and beam densities of the primary probes, as well as differences in nature between the ion and photon induced damages.

**AS-TuP7 XPS Characterization of Nylons, Sankar N. Raman, Physical and Analytical Science Center, Monsanto, 730 Worcester Street, Springfield, MA 01151.**

Nylon is a material of very high commercial importance, in the aviation industry, as fabrics, numerous molded parts and carpets. In this paper XPS spectra for a variety of Nylons is presented. Spectra for Carbon, Oxygen and Nitrogen and the entire energy range, is presented along with curve fit results for C 1s, O 1s and N 1s peaks. The concentrations and curve fit results are consistent with theoretical predictions. These results are extremely useful reference data in the characterization of commercially manufactured nylons. The nylons studied here are pure materials with no additives. In the real world commercial case there may be additives and other materials incorporated in nylon to improve performance, which will tend to change the chemical bonding thereby leading to slightly different peak shapes and different atomic concentrations.

**AS-TuP8 Surface Characterization of Silylated Substrates by TOF-SIMS, B. Hagenhoff, M. Deimel, D. Rading, A. Benninghoven, J. Grobe, Universität Münster, D-48149 Münster, Germany.**

The treatment of hydroxylated surfaces with functionalized silanes is a commonly used modification technique in technological areas reaching from biosensing to the environmental protection of building materials. Silylated substrates are normally analyzed by IR and NMR techniques providing information on surface near layers and the bulk material. The knowledge about the molecular structure and composition of the uppermost monolayer which governs important surface properties like wetting, adhesion, and long-term stability, however, is still sparse.

We applied time-of-flight secondary ion mass spectrometry (TOF-SIMS) which offers molecular information about the uppermost monolayer with high sensitivity to the characterization of hydroxylated surfaces modified by organosilicon compounds  $\text{RSiX}_3$  ( $\text{R} = \text{CH}_3$ , Phe,  $\text{X} = \text{OCH}_3$ ,  $\text{OC}_2\text{H}_5$ , Cl). In order to be comparable with standard application process of protective agents the silanes were allowed to react with the substrate for three weeks in ambient air without additional amounts of water. The spectra reveal that in all cases the uppermost monolayer consists of totally hydrolyzed polymeric siloxanes which do not contain the reactive group X (silsequioxanes of the structure  $(\text{CH}_3\text{SiO}_{1.5})_n$ ). A comparison with additionally performed IR and NMR experiments shows that the surprising occurrence of silsequioxanes under the reaction conditions used is definitely restricted to the uppermost monolayers.

**AS-TuP9 Characterization of an Abrasion Resistant Coating of Polycarbonate, R. M. Friedman<sup>1</sup>, R. W. Linton<sup>2</sup> and M. P. Mawn<sup>2\*</sup>, <sup>1</sup>Analytical Sciences Center, Monsanto Corporate Research, St. Louis,**



MO 63167-0001 and <sup>2</sup>Department of Chemistry, University of North Carolina, Chapel Hill, NC 27599-3290.

Plastics and polymers are being used increasingly in place of traditional materials of construction because of their light weight, impact resistance, and low cost. Unfortunately, plastics are generally soft and subject to abrasion, fracture, or other forms of mechanical failure. To offset these limitations, surface coatings are being used to protect against degradation. Two key properties of the coatings are hardness and clarity reflecting the chemical composition and microstructure of the material. For example, GE offers a line of structural plastics, such as sheet polycarbonate, marketed under the trademarked name LEXAN®MR5 with an abrasion resistant surface, MARGARD®. The material is described in an extensive array of patents, but there is little discussion in the literature concerning its molecular or microstructural characterization. A commercial sample of the material was analyzed by TOF-SIMS, angle-resolved XPS and ATR-FTIR. TOF-SIMS yielded identification of the surface siloxyl building blocks through analysis of characteristic fragment ions. ATR-FTIR helped to differentiate between molecular species with the same empirical formula, e.g.,  $\text{SiO}_2(\text{H})(\text{OCH}_3)$  and  $\text{SiO}_2(\text{OH})(\text{CH}_3)$ , as well as to indicate a gradient in composition within the surface coating as confirmed by angular resolved photoemission. Coupling the TOF-SIMS results with the quantitative elemental composition determined by XPS yielded detailed insight into the nature of the siloxane surface coating. The correlation of analytical techniques with different sampling depths (TOF-SIMS < XPS < FTIR) and information about long range molecular structure (XPS < FTIR < TOF-SIMS) provides a broadly applicable approach to characterizing abrasion resistance coatings.

\*Present address: DuPont Co., Wilmington, DE.

**AS-TuP10 Fundamental Characterization of Siloxane Adhesion Promoters on Metal and Metal Oxide Surfaces**, *Sourabh Mishra and Jeffrey J. Weimer*, Joint Materials Science Ph.D. Program, University of Alabama in Huntsville, Huntsville, AL 35899.

Silane adhesion promoters have the form  $\text{X}_n\text{-Si-R}_{4-n}$  where R is an organic functionality and X is a group that hydrolyzes to form a siloxane. They are used extensively to enhance bonding of polymers to metals, however the fundamental bonding mechanisms are not well characterized. Silination of Cu and oxidized Cu surfaces using trimethyl-chloro- and trimethyl-methoxy-silane has been investigated to determine the mechanisms involved in bonding. Compositions and oxidation states of elements on the substrates were determined using x-ray photoelectron spectroscopy (XPS). Glancing incidence Fourier transform infrared spectroscopy (FTIR) was used to characterize vibrational frequencies at the immediate promoter-metal interface. Silane deposition was carried out using wet chemistry techniques, and the layers were cured under vacuum at high temperature. Chlorosilane reduced oxides on the surfaces during silination, and curing led to removal of residual chlorine and unbound chlorosilane. Surface oxides were not reduced by the methoxysilane until curing. The results signify the relative importance of physisorption and hydrogen bonding of silane prior to formation of a covalently bonded siloxane. This work is being continued with chloro-, methoxy-, and other monofunctional silanes used in bonding polymers and proteins to biocompatible and metal surfaces.

**AS-TuP11 Film Growth and Surface Structure of Methylene Blue on Mica**, *G. Hähner, W. R. Caseri, and N. D. Spencer*, Materials Dept., ETH Zürich, CH-8092 Zürich, Switzerland.

Methylene blue (MB) is often used to determine specific surface areas of high-surface-area materials. The molecule is generally considered to be a rectangular parallelepiped and to adsorb in a flat orientation. We have investigated the adsorption of MB on a mica substrate with AFM/LFM, XPS, ToF-SIMS, and NEXAFS in order to monitor film growth, film thickness, coverage, homogeneity, and the orientation of the molecules. It was found that the growth depends critically upon the preparation conditions. Under our experimental conditions a flat orientation was not detected. These results may also have some impact on our understanding of the surface properties of layered silicates, which are of ever increasing interest in colloid science.

**AS-TuP12 Nanometer Resolution Imaging of the Growth of Water Monolayers on Mica from its Vapor**, *Jun Hu, Xudong Xiao, D. F. Ogletree and M. Salmeron*, Material Science Division, Lawrence Berkeley Laboratory.

For the first time we have been able to image with nanometer resolution the layer by layer condensation and evaporation of water films on mica as a function of humidity. This has been done using a non-

contact AFM imaging method based on the polarizability of materials under applied electric fields. Using a biased AFM tip and an insulating mica surface, the polarization forces can be detected from a few hundred Å's away from the surface. We found that wetting proceeds by formation and growth of 2D islands. The islands often adopt polygonal shapes with edges that are aligned with the mica crystallographic directions. This suggests ordering of the molecules beyond the first layer, as in ice. Studies of the time dependence of the polarization force due to the motions of charges and molecular dipoles will be presented as well.

**AS-TuP13 Surface Finish Characterization of Potassium Dihydrogen Phosphate (KDP) for Nonlinear Optical Applications**, *E. C. Honnea, R. L. McEachern*, Lawrence Livermore National Laboratory, Livermore, CA 94551.

Atomic Force Microscopy (AFM) was used to characterize the influence of various cleaning and surface finishing processes on potassium dihydrogen phosphate (KDP) crystals used for nonlinear optical applications. Diamond turning off the surface results in a visible periodic structure, with 0.2–0.3 micron sized features distributed along the path of the diamond cutting tool. Various surface cleaning methods, including oxygen plasma cleaning, were investigated. Surface morphology and degradation (fogging) were related to process history and environmental factors.

Work performed under the auspices of the U.S. Department of Energy by Lawrence Livermore National Laboratory under Contract W-7405-ENG-48.

**AS-TuP14 Counterion and Dopant Induced Effects on the Structure of Electropolymerized Polyaniline Thin Films**, *T. L. Porter, A. G. Sykes*, Northern Arizona University, Flagstaff, AZ 86011.

The transport of charge in polyaniline and polyaniline based materials is highly dependent upon a number of chemical and structural factors. Polyaniline in an amorphous state may display the conductive characteristics of a Fermi glass. Polyaniline in a semicrystalline state exhibits metallic properties on a local scale and characteristics of a granular conductor on the macroscopic scale. The structural state of polyaniline in turn is determined largely by the chemical preparation parameters. We have used the technique of scanning probe microscopy in the non-contact mode to study the dependence of electropolymerized film nanostructure on several of these parameters, including choice of counterion, dopant concentration and film thickness. We have obtained the first direct, real space evidence of a nanometer-scale island structure in HCl doped unsubstituted electropolymerized polyaniline. The effects of chemical preparation on the film structure and the resulting conductivity will be discussed in terms of models based on a granular conductor. Earlier studies on polyaniline and substituted polyanilines using SPM in the contact mode will also be compared to the noncontact results presented here.

**AS-TuP15 Contribution of Surface Roughness in the Nanometer Regime to the Depth Resolution in Sputter Profiling**, *K. A. Pischow, S. Hoffmann and A. Zalar*, Laboratory of Processing and Heat Treatment of Materials, Vuorimiehentie 2 A, FIN-02150 Espoo, FINLAND <sup>a</sup>Max-Planck-Institut für Metallforschung, D-70174 Stuttgart, Germany, <sup>b</sup>Institut für Electronics and Vacuum Technique, P.O.B. 59, 61111 Ljubljana, Slovenia.

Ion bombardment induced surface roughness is one of the most important effects degrading the depth resolution in sputter profiling of thin films. Because usual depth resolution measurements at abrupt bilayer interfaces always involve many other possible contributions, particularly ion induced atomic mixing, it is important to separate these effects from catch other. Scanning force microscopy (SFM) is ideally suited to obtain a precise measurement of the surface roughness within the analyzed area, typically  $10 \times 10 \mu\text{m}^2$ , in AES depth profiling. Comparison of Ni/Cr multilayer sample roughness after sputtering with and without sample rotation showed a considerable variation of the surface roughness between 2 nm and 20 nm. The nanomorphology of the Ni and Cr layers is different and can be correlated with the difference in the physico-chemical properties of Ni and Cr. Surface roughness distributions will be given and SFM tip effects on the achieved surface roughness values will be considered.

**AS-TuP16 Influence of Ion Species, Ion Energy and Substrate on Sputtering-Induced Ripple Topography**, *John J. Vajo, Robert E. Doty and Eunhee Cirlin*, Hughes Research Laboratory, Malibu, CA 90265.

The influence of ion species ( $\text{O}_2^+$ ,  $\text{N}_2^+$ , and  $\text{Ar}^+$ ), ion energy (1 to



10 keV) and substrate (Si, Ge, and  $\text{Al}_x\text{Ga}_{1-x}\text{As}$  with  $x = 0$  to 0.8) on the sputtering-induced formation of surface ripples has been studied using changes in secondary ion yields, scanning electron microscopy and atomic force microscopy. Attention is focused on the initial stages of ripple formation, which we characterized primarily by the ripple wavelength as a function of ion-substrate combination and ion sputtering conditions. Depth profiling using 0.5 keV  $\text{Ar}^+$  together with Auger electron spectroscopy was used to determine the amount of retention and the distribution of  $\text{O}_2^+$  and  $\text{N}_2^+$  primary ions. For  $\text{O}_2^+$  sputtering of Si at an angle of incidence of  $40^\circ$  from the normal the ripple wavelength increases linearly from 1.5 to 9 keV. Sputtering of Si with  $\text{N}_2^+$  also produces ripples but with a shorter wavelength. This difference between  $\text{O}_2^+$  and  $\text{N}_2^+$  is interesting because the ballistic aspects of both species are similar. The ripple wavelength is also found to decrease with increasing Al content in  $\text{Al}_x\text{Ga}_{1-x}\text{As}$  alloys. Ripples do not form when sputtering any of the substrates with  $\text{Ar}^+$ , or on Ge with any of the sputtering conditions used. These results are discussed in terms of several mechanisms they may initiate ripple formation such as surface diffusion, surface stress, retention of primary ions, and variations in sputtering yields.

**AS-TuP17 Use of Resonance Ionization Microprobe Analysis in Material Sciences,** *Heinrich F. Arlinghaus, Charles F. Joyner and Tom J. Whitaker*, Atom Sciences, Inc., Oak Ridge, TN 37830.

We have built a new analytical time-of-flight instrument capable of sputter-initiated resonance ionization microprobe (SIRIMP) measurements. This instrument has the ability to obtain quantitative element concentration images with high spatial resolution and virtually no matrix effects. The SIRIMP technique is especially valuable for ultratrace element analysis in samples where the complexity of the matrix is frequently a serious source of interferences. The instrument utilizes three different ion guns for sputtering, a liquid metal gallium ion gun, a mass-filtered microbeam ion gun and a mass-filtered low energy sputtering ion gun which can be used either independently or simultaneously.

In our presentation we will describe the implementation of the new SIRIMP system to solve a number of analysis problems and illustrate its salient characteristic with data from a wide range of applications. Results presented will include a) depth profiles of dopants implanted in various matrices, b) studies of surface and bulk contaminations in semiconductor samples and c) high-resolution lateral distributions of trace elements in semiconductors. The practical capabilities of SIRIMP to determine trace elements as a function of depth and lateral position in semiconductors will be discussed.

This work was partly supported by the Advanced Research Projects Agency.

**AS-TuP18 Depth-Resolved Vibrational Characterization of Buried Interfaces,\*** *N. H. Fontaine and T. E. Furtak*, Colorado School of Mines, Golden, CO 80401.

Adhesion between polymers, or between a polymer and a more rigid solid, is difficult to study without destroying the bonded interface. Post-failure analysis of rupture surfaces is only indirectly related to the nature of the system prior to failure. We have developed a non-destructive method of extracting the vibrational signature of polymers as a function of depth in a laminated construct. Our approach is based upon Raman scattering. It employs high precision control of the evanescent field beyond a dielectric under internal reflection conditions. Through detailed angle-dependent measurements, and the use of Laplace transforms, we are able to reconstruct the spatial distribution of molecular structure. Demonstration experiments on model systems related to polymer adhesion are presented.

\*This research was supported by the Office of Naval Research, contract No. N00014-93-1-0101.

**AS-TuP19 Thickness Determination of Uniform Overlayers on Rough Substrates by Angle Dependent X-ray Photoelectron Spectroscopy,** *P. L. J. Gunter and J. W. Niemantsverdriet*, Schuit Institute of Catalysis, Eindhoven University of Technology, PO Box 513, 5600 MB Eindhoven, the Netherlands.

It is well known that ADXPS can be used for determining the thickness of thin overlayers. In the straight-line approximation to photoelectron transport a simple expression relates the intensity ratio of overlayer and substrate signals to the thickness of a uniform overlayer on a flat substrate. This expression is a very popular one and

has been used often to evaluate the thickness of all kinds of overlayers on flat as well as rather rough substrates.

We have analysed the errors involved in applying the simple expression mentioned for thickness determination of overlayers on rough substrates. We have used an algorithm for simulation of fractional Brownian motion to model substrate roughness in a realistic way on the computer and then calculated signal intensities by a Monte Carlo method for electron trajectory simulation. Our calculations indicate that the local steepness of the surface determines the deviation in XPS signal intensities as compared to those of a flat surface. We have applied Atomic Force Microscopy and ADXPS on aluminum foils and roughened silicon wafers, and confirmed the calculated link between local steepness and signal intensity.

The errors made in thickness evaluation based on the simple flat substrate model can be as large as 50%. An important result of our work, however, is that the error is only a few percent for an off-axis angle (between analyser and surface normal) of  $35^\circ$ , independent of roughness, overlayer thickness, and type of material.

**AS-TuP20 Angle-Resolved XPS Data Acquisition,** *B. J. Tielsch and J. E. Fulghum*, Chemistry Department, Kent State University, Kent, OH 44242.

In order to develop standard methods for angle-resolved XPS (ARXPS), it is important to evaluate not only data analysis methods, but also the effect of data acquisition conditions. Comparisons of algorithms have shown that a careful choice of algorithm parameters is required to obtain reasonable and reproducible results. However, practical variations in data acquisition parameters have remained largely unexamined. The effect of the range and number of angles for which data is acquired, the signal-to-noise ratio of the data set, and variation in analyzer acceptance angle will be discussed for a variety of sample types and algorithms. We will demonstrate that for some sample types, it is possible to obtain useful information from noisy data acquired at only two or three angles. Practical guidelines for ARXPS data acquisition will be outlined.

This work is partially supported by the W. M. Keck Foundation and the NSF Science and Technology Center for Advanced Liquid Crystalline Optical Materials (ALCOM) under DMR89-20147.

**AS-TuP21 XPS Studies of Compositional Changes Induced by Ion Bombardment on  $\text{LaPO}_4$  Surface,** *O. P. Ivanova, A. V. Naumkin, L. A. Vasilyev, V. I. Rakhovsky*, Research Center for Surface and Vacuum Investigations, 6 bld.1, Kazarmenny per., 109028 Moscow, Russia.

It was previously shown that ion-induced chemical processes play an important role in formation of altered layer. We have investigated compositional and chemical changes in  $\text{LaPO}_4$  induced by 6 keV  $\text{Ar}^+$  ion bombardment in terms of possible chemical reactions between decomposed species during relaxation process. It is clear that ion energy is large enough to disrupt numerous chemical bonds and to form decomposed components in the near surface region. The relaxation process depends on the preferential sputtering, chemical activity of decomposed species, the formation of thermodynamically stable phases and on the structure of the undamaged layers. The chemical composition of altered layer was determined by the  $\text{O}1s$  and  $\text{P}2p$  lines curve fitting procedures. The intensity ratios separation and binding energies were obtained from the initial surface spectra measurements of  $\text{LaPO}_4$  and  $\text{La}_2\text{O}_3$ . It was found that chemical composition may be presented as  $\text{LaPO}_4$ ,  $\text{LaPO}_3$ ,  $\text{P}_2\text{O}_5$  and  $\text{La}_2\text{O}_3$  with relative intensities of 0.3, 0.22, 0.09 and 0.38 respectively. The chemical aspects of preferential sputtering are discussed.

**AS-TuP22 XPS Cerium(3d) Lineshape Analysis as a Measure of Oxygen Storage/Release in Automotive Catalysts,** *S. J. Schmieg, D. N. Belton, and D. R. Monroe*, General Motors R&D Center, Physical Chemistry Department, Warren, MI 48090.

Ceria is an important component in current catalyst formulations for the removal of CO, hydrocarbons, and nitrogen oxides during the oscillatory behavior present in automotive exhaust. The amount of oxygen storage in the converter correlates with the ceria content in the catalyst. We have studied the effect of thermal aging on the oxygen storage/release and activity in a Pt/Rh/Ce and several highly-loaded Pd/Ce catalysts. X-ray photoelectron spectroscopy (XPS) was used to measure changes in the oxidation state of the catalyst after various oxidation and reduction treatments and rate measurements of the CO oxidation reaction were used to determine the reaction kinetics and activity. These measurements were then compared to the oxygen storage/release characteristics measured in a pulse reactor system. The catalysts were tested fresh and after cycled aging at  $1000^\circ\text{C}$ . To de-

termine which Ce species were present on the surface, we fit the XPS Ce(3d) data with combinations of spectra from standard materials ( $\text{CeO}_2$  and  $\text{Ce}_2\text{O}_3$ ). Aging the Pt/Rh catalyst causes a loss of oxygen storage capacity by forming compounds which do not allow the Ce to cycle between oxidation states. For the fresh catalyst, the observed kinetics for the CO oxidation reaction show all of the signatures attributable to a catalyst with a high degree of ceria/noble metal interaction. Changes in the kinetics upon aging are consistent with a loss of ceria/noble metal contact area. The degradation of the oxygen storage in the Pd/Ce catalysts was found to be similar to the Pt/Rh/Ce catalyst. The XPS results correlate well with the oxygen storage measurements from the pulse reactor system.

**AS-TuP23 Quantitative Depth Profiling of Oxygen in Homoepitaxial  $\text{SrTiO}_3$  Films,** *M. Watanori and K. Oura*, Dept. of Electronic Eng., Fac. of Eng. Osaka Univ., 2-1 Yamadaoka, Suita, Osaka 565, Japan, *T. Nakamura*, Sumitomo Electric Industries LTD., 1-1-3 Shimaya, Konohaku, Osaka City, Osaka 554, Japan.

We have investigated the quantitative depth profiling of oxygen content in  $\text{SrTiO}_3$  substrates and  $\text{SrTiO}_3$  films on  $\text{SrTiO}_3$  substrates using  $^{16}\text{O}(\alpha, \alpha)^{16}\text{O}$  3.045 MeV resonant backscattering spectrometry.  $\text{SrTiO}_3$  films were evaporated onto  $\text{SrTiO}_3$  substrates by MBE methods with an introduction of reactive  $\text{O}_3$  gas.  $^{16}\text{O}(\alpha, \alpha)^{16}\text{O}$  resonant backscattering was corrected and an absolute volume of oxygen concentration could be accurately estimated with other metallic elements. For  $\text{SrTiO}_3$  substrates, one  $\text{SrTiO}_3$  substrate fabricated at A company had a different composition from a chemical stoichiometry (namely, that is  $\text{Sr}:\text{Ti}:\text{O} = 1:1:3$ ) and indicated the remarkable deficiency of Sr and oxygen component, while one  $\text{SrTiO}_3$  substrate fabricated at another company had a chemical stoichiometric composition.  $\text{SrTiO}_3$  film compositions were strongly affected by the compositions of  $\text{SrTiO}_3$  substrates, and nearly constant depth profilings were obtained from film surfaces to substrate surfaces in spite of  $\text{O}_3$  flux densities. These results are consistent with depth profiling results of  $\mu$ -AES performed as cross checking. Continuity of oxygen volume at the interface will be demonstrated for  $\text{SrTiO}_3$  films on  $\text{SrTiO}_3$  substrates and other superconducting films on  $\text{SrTiO}_3$  substrates.

**AS-TuP24 Negative Charge Production from Bombardment of a Cu Surface by Low Energy Oxygen Atoms and Ions,\*** *Thomas M. Stephen, R. C. Amme and Bert Van Zyl*, Department of Physics, University of Denver, Denver, Colorado 80208.

At atomic beam apparatus capable of producing oxygen atoms and ions has been used to investigate negative charge production from copper, as well as stainless steel, surfaces over a range of energy of 15 eV to 500 eV. The yield in all cases rapidly approaches zero as the beam energy diminishes towards approximately 20 eV; a ten percent yield is observed for all species at beam energies in the vicinity of 150 eV. The neutral oxygen atoms are generated by electron photodetachment of  $\text{O}^-$  in an extended laser cavity producing visible radiation (ca. 450 to 530 nm wavelength). A 25W Spectra Physics argon ion laser was employed for this purpose; the cavity radiation was chopped at 40 Hz and the resulting ion currents measured to permit absolute neutral beam intensity determinations. The neutrals are 100% ground state  $\text{O}^3\text{P}$ , since no excited states are accessible for the ions and radiation employed. A model will be discussed which provides fair agreement for the negative charge production observed.

\*Work supported by Air Force OSR Grant 90-0119.

**AS-TuP25 The Effect of Copper Overlayers on the Thermal Stability of Chromium Carbide on HOPG,** *J. J. Bellina, Jr.*, Saint Mary's College, Notre Dame, IN 46556 and *K. A. Briggman*, Northwestern University, Evanston, IL 60208.

Recent reports indicate that the wetting of graphite by copper improves with the addition of small amounts of carbide-forming metals, such as chromium. Since there are applications for these copper-graphite materials at high temperatures, the formation and thermal stability of chromium carbide films on graphite with and without copper overlayers have been studied. Our results from reactions of chromium films with highly-oriented pyrolytic-graphite (HOPG) indicate that chromium carbide is metastable. It only forms on an ion-damaged surface, and decomposes above 500°C. Thus, there remains a question of whether the improved wetting of graphite by chromium-doped copper is in fact due to chromium carbide formation at the interface.

Experiments were performed in-situ in UHV by thermally evaporating chromium and/or copper onto the basal plane of a HOPG substrate, and observing the Auger electron spectra as a function of

annealing temperature. Changes in the peak shapes and intensities of the carbon KVV and the chromium and copper LMM and MVV Auger transitions are interpreted in terms of metal film structure, and carbide formation and decomposition. The results are used to evaluate the role of carbide formation in the wetting of graphite by chromium-doped copper films.

**AS-TuP26 Electric States of Segregated Metal Atom on Metal Surfaces and Potential Use for Field Emitter,** *M. Yoshitake and K. Yoshihara*, National Research Institute for Metals, Ibaraki, JAPAN.

The segregation phenomena of substrate copper atoms onto the deposited titanium film were observed using Auger electron spectroscopy (AES) and X-ray photoelectron spectroscopy (XPS). The Ti film of 1  $\mu\text{m}$  thickness was deposited by r.f. magnetron sputtering on polycrystal Cu surface. The specimens were heated in XPS apparatus. After a certain time, Cu atom diffused onto the surface of Ti film from the substrate with the 60% of the activation energy of bulk diffusion. The surface concentration of Cu saturated at about 5%. When the segregated surface was destroyed, Cu-saturated surface structure was easily reformed. The binding energy of Cu 2p<sub>3/2</sub> of the segregated Cu was 0.24 eV higher than that of pure metal. It suggests that the electron belongs to Cu is attracted to Ti and the segregated Cu slightly charges positively. This direction of charge transfer was also observed when Ti was deposited on Cu substrate. The binding energy of Cu 2p<sub>3/2</sub> of Cu, on which surface was covered with Ti was almost same as segregated Cu. It is well known that when adsorbed atom causes charge transfer and forms electric dipole, the work function changes.

In the case of Cu segregation on Ti film, the charge transfer from Cu to Ti is estimated to be 0.11e from the above binding energy. It is concluded that when this value is used for the calculation of the dipole moment, about 0.62 eV decrease in work function is expected and this material has great potential for a field emitter.

**AS-TuP27 The Effect of Sample Bias on the Nitrogen Etching Products of Aluminum,** *M. A. Rooke, P. M. A. Sherwood*, Department of Chemistry, Willard Hall, Kansas State University, Manhattan, KS 66506-301.

The paper will report the effect that biasing of a sample has on the products of a reactive etching process. When aluminum metal is etched using a saddle-field argon ion etcher with nitrogen as the etching gas the aluminum metal is first converted into an oxy-nitride. The oxy-nitride is formed because of residual oxygen in the etching gas. If etching is continued past an initial two minute etch, then the surface continues with approximately the same composition. Surface composition is determined by core and valence band X-ray photoelectron spectroscopy, with the valence band data interpreted by spectra generated by multiple scattered wave  $X\alpha$  calculations.

If the aluminum sample is subjected to a 15 volt d.c. negative bias, then oxy-nitride is formed after the initial two minute etch, but continued etching leads to the formation of a surface that is almost entirely aluminum oxide. In addition in the case of the biased sample a number of N1s XPS features are seen, including nitride, adsorbed  $\text{N}_2$ , and a peak at high binding energy due to implanted  $\text{N}_2$ . This latter peak is only seen when the sample is negatively biased. The paper will suggest reasons for the chemical changes that occur when the sample is biased.

This material is based upon work supported by the Air Force Office of Scientific Research under Grant No. F496620-92-J-0144.

**AS-TuP28 Local Density of State Analysis,** by *Aes. H. J. Zhou, Y. C. Wang, W. Ho*, Department of Electronic Engineering, Tsinghua University, Beijing 100084, China.

In order to measure the local density of state on each depth profile of the GaAs/Si interface by AES, the Auger lineshape is carefully processed and the Auger lineshape analysis is performed with the help of objective factor analysis. Fast Fourier transform is applied for AES spectral background subtraction and a series of corrections to remove the distortion of the peak shape are carried. The contributive weighting factor of the electrons of different atomic orbitals for the AES spectrum are determined from the measured peaks in comparison with theoretical results.

**AS-TuP29 The Development of an Electron Spectroscopy Data Dictionary for the AVS Surface Science Spectral Database,** *Stephen W. Gaarenstroom*, General Motors R&D Center, Analytical Chemistry Dept., 30500 Mound Road, Warren, MI 48090-9055.

For a spectral database to be useful to an analyst, each data record

must include data elements which fully describe all aspects of the record, such as the specimen, the instrument, the experiment, the calibration, the spectral data, the data analysis methods, and the results. The list of data elements making up the database and their definitions is called the data dictionary. The data dictionary for electron spectroscopy used by the American Vacuum Society's Surface Science Spectral Database contains 188 data elements grouped into 8 information classes. In developing the data elements to use in the database, consideration was given to existing surface analysis standards, existing standards and databases in other spectroscopies, and input from the user community. Several areas of complications required substantial dialogue with users and instrument manufacturers to achieve a satisfactory solution. For example, the variety of instrument designs and measurement strategies makes it difficult to define a universal set of data elements that can be applied to describe the commonly used electron spectrometers. Also, since data records are contributed from the entire user community and peer-reviewed by the same wide community, explicit guidance must be given to describe the various quality level and completeness requirements.

**AS-TuP30 A Generic Analytical Data Model: Ensuring that Surface Science Data Meets Analytical Chemistry Standards, R. N. Lee, NSWC, Carderock Div., Silver Spring, MD 20903.**

Development of the Auger, XPS and SIMS data dictionaries for the AVS Surface Science Database was carried out in close coordination with parallel efforts in the broader analytical chemistry community. This collaboration between the surface science and analytical chemistry communities has been directed toward the specification of a unified data model that would permit merging and cross-referencing of data from different analytical techniques. Attempts to find a common data model for such diverse analytical techniques as XPS, IR, NMR and chromatography have been frustrated by the inherent limitations of available information management technology. We have been able to extend conventional data modeling concepts to provide a natural environment for describing analytical measurements in general. The generic data model that has emerged employs a matrix array to describe the measurement process as well as the instruments and specimens that are involved. This new data model is being proposed as a standard for both surface science and analytical chemistry information systems.

## ELECTRONIC MATERIALS

### Room BR4 - Session EM-TuP

**Aspects of Electronic Materials and Processing I**  
**Moderator: F. A. Houle, IBM Almaden Research Center.**

**EM-TuP1 Thermal Oxidation of Heteroepitaxial  $\text{Si}_{1-x-y}\text{Ge}_x\text{C}_y$  Alloy Thin Films<sup>†</sup>, Jiong Xiang, Nicole Herbots, Peihua Ye\*, Sean Hearne, Department of Physics and Astronomy, \*Department of Chemical and Bio and Materials Engineering, Arizona State University, Tempe, AZ 85287-1504.**

Heteroepitaxial  $\text{Si}_{1-x}\text{Ge}_x$  alloys have found wide applications in Si-based technology. However, good quality dielectric on  $\text{Si}_{1-x}\text{Ge}_x$  are not obtained by thermal oxidation. Our motivation is to explore the effect of carbon in thermal oxidation of  $\text{Si}_{1-x}\text{Ge}_x$  alloys as well as its role on strain compensation in  $\text{Si}_{1-x}\text{Ge}_x$  alloys. Pre-cleaned Si(100) wafer, MBE-grown Ge,  $\text{Si}_{1-x}\text{Ge}_x$  and  $\text{Si}_{1-x-y}\text{Ge}_x\text{C}_y$  alloys on Si(100) were oxidized at 1000°C in dry oxygen atmosphere for two hours. The thickness and the composition of all samples before and after oxidation were measured by Rutherford Backscattering Spectrometry (RBS) combined with ion channeling at 2 MeV and carbon nuclear resonance measurements at 4.3 MeV using  $^4\text{He}^{+}$ . The structures were also characterized by Secondary Ion Mass Spectrometry (SIMS), High Resolution TEM (HRTEM), FTIR and Raman Spectroscopy. As expected, 2.0 MeV RBS analysis shows that a uniform layer of 1040 Å  $\text{SiO}_2$  is grown on pure Si(100) sample during thermal oxidation. For all other samples, a layer of  $\text{SiO}_2$  is also formed, while Ge segregates towards the top surface and at the  $\text{SiO}_2/\text{Si}_{1-x}\text{Ge}_x$  and  $\text{SiO}_2/\text{Si}_{1-x-y}\text{Ge}_x\text{C}_y$  interfaces. However, RBS analysis also shows that carbon in  $\text{Si}_{1-x}\text{Ge}_x$  reduces the amount of Ge segregated during thermal

oxidation. This observation will be discussed in conjunction with SIMS, HRTEM, FTIR and Raman data.

<sup>†</sup>Research supported by AFSOR/ARPA contract F49620-93-C-0018.

**EM-TuP2 The Role of Temperature During Synthesis of Heteroepitaxial  $\text{Si}_{1-x-y}\text{Ge}_x\text{C}_y/\text{Si}(100)$  Synthesized by Combined Ion and Molecular Beam Deposition (CIMD)<sup>†</sup>, Nicole Herbots\*, Peihua Ye, Jiong Xiang\*, Sean Hearne\*, Dept. of Chemical and Bio and Materials Engineering, \*Dept. of Physics & Astronomy, Arizona State University, Tempe, AZ 85287-1504.**

The motivation for this study is to investigate a new ternary group IV semiconductor,  $\text{Si}_{1-x-y}\text{Ge}_x\text{C}_y$  for strain and bandgap engineering. Heteroepitaxial  $\text{Si}_{1-x-y}\text{Ge}_x\text{C}_y/\text{Si}(100)$  is synthesized by Combined Ion and Molecular beam Deposition (CIMD). Characterization involves Nuclear Resonance Rutherford Backscattering Spectrometry (NRA) combined with ion channeling. Secondary Ion Mass Spectroscopy (SIMS), High Resolution Transmission Electron Microscopy (HRTEM), Fourier Transformation Infrared Spectroscopy (FTIR), and Raman Spectroscopy. NRA shows that up to 2% C can be incorporated in heteroepitaxial  $\text{Si}_{1-x-y}\text{Ge}_x\text{C}_y$  films, which is about three orders of magnitude above the C solid solubility in Si. TEM shows that  $\text{Si}_{1-x-y}\text{Ge}_x\text{C}_y$  films are epitaxial with a well defined interface between films and substrate. Cross section TEM also shows that films deposited at 600°C exhibit a crystalline secondary phase coherent with the matrix and localized in small regions (2 nm in diameter), while the film deposited at 500°C exhibits uniform phase contrast. FTIR spectra for films deposited at 500°C show a distinct absorption mode at 604  $\text{cm}^{-1}$ , which is characteristic of substitutional carbon in Si. However, FTIR spectra for films deposited at 600°C neither exhibit silicon carbide precipitates (wave number 800  $\text{cm}^{-1}$ ) nor substitutional C (wave number 604  $\text{cm}^{-1}$ ). Raman and FTIR spectra will be discussed in light of microstructural findings by HRTEM.

<sup>†</sup>Research supported by AFSOR/ARPA contract F49620-93-C-0018.

**EM-TuP3 Growth of  $\text{Si}_{1-x}\text{Ge}_x$  Multiple Quantum Wells Using Molecular Beam Epitaxy for Infrared Absorption, T. Kreifels\*, P. E. Thompson\*\*, R. Hengehold\*, and Y. K. Yeo\*, \*Air Force Institute of Technology, Wright Patterson AFB, OH 45433-7765, \*\*Naval Research Laboratory, Washington, DC 20375-5347.**

Multiple SiGe quantum wells were grown by MBE on Si (100), (110), and (111) substrates in order to determine the optimum growth conditions for these structures to be used as infrared (IR) detectors. The nominal structure was: five to fifteen 4 nm  $\text{Si}_{0.8}\text{Ge}_{0.2}$  quantum wells separated by 30 nm Si, with the center 3 nm of each quantum well doped with B at concentrations ranging from 1 to  $5 \times 10^{19} \text{ cm}^{-3}$ . The photoluminescence (PL) measurements at 4.2K showed that bandedge, phonon-resolved PL was most intense for the quantum wells grown at 710°C on the Si(100) substrates and grown at 800°C on the Si(110) and Si(111) substrates. However the quantum well IR absorption was strongest for the samples grown at 550°C. Using a single pass, normal incident light technique, the strong absorption observed in doped structures between 4.0 and 5.0  $\mu\text{m}$  on each of the substrate orientations has been tentatively associated with bound-to-continuum quantum well transitions. Using a waveguide structure, polarization-dependent quantum well intersubband IR absorption was observed at 8.4  $\mu\text{m}$  and 10.5  $\mu\text{m}$ , corresponding to  $\text{HH}_1 \rightarrow \text{SO}_1$  and  $\text{HH}_1 \rightarrow \text{HH}_2$  transitions, respectively, for the samples grown on Si(100). Both SIMS and TEM analysis of the structures, as a function of growth temperature, will be reported.

**EM-TuP4 Erbium Doped Si Films Prepared by Electron Cyclotron Resonance Plasma Enhanced Chemical Vapor Deposition, Jim L. Rogers and Walter J. Varhue, Dept. of Electrical Engineering, University of Vermont, Burlington, VT 05405, Kazi Ahmed and Folami Ladipo, Dept. of Chemistry, University of Vermont, Burlington, VT 05405, Edward Adams, and Mark A. Lavoie, IBM Corp., Essex Junction, VT 05452.**

Epitaxial Si films doped with Er have been grown at low substrate temperatures by plasma enhanced chemical vapor deposition. The Er gas sources used were sublimed organo-metallic compounds fed into the process chamber. The goal of this investigation was to reduce the inadvertent incorporation of carbon into the film while depositing an optically active Er centers. Optically active Er centers are believed to be Er surrounded by strong electro-negative atoms such as oxygen and fluorine. One of the organometallic precursors used, [tris(triphenylsiloxy) Erbium (III)], was design specifically to perform this task.

The deposition process in general relies on the beneficial effects of low energy ion bombardment to reduce the growth temperature. This bombardment may also lead to the enhanced incorporation of carbon into the deposited film. Processing conditions were varied to gain an understanding of the impurity incorporation mechanism. Film quality and impurity concentration were determined by Rutherford backscattering spectrometry and secondary ion mass spectrometry.

**EM-TuP5 Silicon Nitride Encapsulation of Sulfide Passivated GaAs/AlGaAs Microdisk Lasers, W. S. Hobson, F. Ren, U. Mohideen, R. E. Slusher, and M. Lamont Schnoes, AT&T Bell Laboratories, Murray Hill, NJ 07974; S. J. Pearton, Dept. of Materials Science, University of Florida, Gainesville, FL 32611.**

Surface recombination of carriers is an important process during the operation of semiconductor devices such as heterojunction bipolar transistors and lasers. This is especially true as device dimensions decrease. In particular, GaAs-based materials have very high surface recombination velocities and much effort has been devoted to reducing surface recombination through surface passivation. Sulfide passivation is an effective method, but the improvement is only temporary if the surface is exposed to oxygen. We have examined silicon nitride encapsulation of sulfide passivated surfaces as a technique to improve the stability of the passivating effect. This passivation scheme was applied to GaAs/AlGaAs microdisk lasers. There is interest in both the fundamental physics and potential applications of these lasers. From our perspective, these microlasers serve as a sensitive probe of the surface processes since the optical mode volume follows the surface at the edge of the disk. These lasers have diameters ranging from 2 to 10  $\mu\text{m}$ . The microdisks did not lase without the sulfide treatment when optically pumped at 77K using 632 nm up to 10 kW/cm<sup>2</sup>. With sulfide treatment cw laser was achieved but the lifetime was only a few seconds. Silicon nitride encapsulation of the sulfide passivated microdisks resulted in a dramatic increase in the laser lifetime. Furthermore, the laser output could be increased by nearly an order of magnitude by annealing at 400°C for 300 s or by cw operation over a period of several hours. Results on test structures using photoluminescence and secondary ion mass spectrometry will also be discussed.

**EM-TuP6 Passivation of Compound Semiconductors: Improvement of the Dielectric/Sulfur/Semiconductor Interface, C. I. H. Ashby, K. R. Zavadil, J. C. Barbour, R. J. Shul, and M. J. Hafich, Sandia National Laboratories, Albuquerque, NM 87185.**

Sulfidation of III-V semiconductor surfaces markedly improves their electronic properties, but exposure to atmosphere results in loss of passivation. Dielectric encapsulation halts atmosphere-induced decay, but passivation can be reduced through loss of sulfur and other damage during dielectric deposition. For retention of maximum passivation, improved methods of dielectric deposition must be developed. To that end, we are studying the electronic and chemical properties of the SiN<sub>x</sub>/S/GaAs interface using optical (photoluminescence (PL) and Raman) and surface analysis (XPS and x-ray-excited Auger) techniques. Thin (~40 Å) SiN<sub>x</sub> films are deposited on photosulfided GaAs using an electron cyclotron resonance (ECR) plasma deposition system that permits variation of ion incidence angle, ion energy, surface illumination, temperature, and gas composition. Film thicknesses are selected to permit Auger and photoelectron escape from the buried SiN<sub>x</sub>/S/GaAs interface for chemical characterization. For commonly employed ECR deposition conditions, approximately 50% of the S is lost during deposition, and a second (SKLL) peak joins the single peak observed on uncapped S/GaAs. Both Raman and PL measurements reveal shallower depletion regions and improved electronic properties over the native oxide surface, but at levels reduced from the original S/GaAs surface. The effects of altered deposition conditions on surface composition and electronic properties and alternatives for improved passivation will be discussed.

This work was performed at Sandia National Laboratories and supported by the U.S. Department of Energy under Contract No. DE-AC04-94AL85000.

**Em-TuP7 Correlation of Surface Morphology with Chemical Structures of Sulfur-Passivated GaAs(100) Investigated by Scanning Tunneling Microscope and X-ray Photoelectron Spectroscopy, Jeong Sook Ha, Seong-Ju Park, Sung-Bock Kim, and El-Hang Lee, Research Department, Electronics and Telecommunications Research Institute, P.O. Box 106, Taeduk Science Town, Taejeon 305-606, Korea.**

Nanometer-scale characterization of semiconductor surfaces and preparation of atomically flat and chemically stable surfaces are of particular interest for precise control of ultrafine device structures. In

this paper, the surface morphology and the chemical structures of the n-GaAs(100) samples after etching with sulfuric acid and sulfur passivation with (NH<sub>4</sub>)<sub>2</sub>S<sub>x</sub> solution were systematically investigated by scanning tunneling microscope (STM) and X-ray photoelectron spectroscopy (XPS). STM measurements were performed in a constant current mode under ambient condition. The surface morphology was observed to be quite different depending on the surface treatments. In particular, the effect of water rinse between etching and sulfur passivation on the surface morphology was examined. The sulfur passivated surface with post-etch water rinse showed a roughness similar to that of the as-etched sample with a surface undulation of 20 Å. However, sulfur passivation without post-etch water rinse dramatically improved the surface flatness giving a surface undulation of 5 Å. It was also shown that the surface roughness induced by etching with sulfuric acid was improved after HCl treatment for 10 minutes. Such effects could be explained by the preferential removal of gallium oxide and arsenic oxide by HCl and water, respectively. XPS measurements were found to support this reaction mechanism. In this work, we will discuss the correlation of the surface morphology with the chemical reaction on the surface revealed by STM and XPS investigation.

**EM-TuP8 Etching of Polysilicon with a Chlorine Trifluoride Beam, Han Xu, Anthony J. Muscat, A. Scott Lawing and Herbert H. Sawin, Department of Chemical Engineering, Bldg. 66-225, Massachusetts Institute of Technology, Cambridge, MA 02139.**

Thermally excited molecular beams (Cl<sub>2</sub>, SF<sub>6</sub>, ClF<sub>3</sub>, etc) have the potential to replace wet cleans for removing metal contaminants and repairing damage on wafer surface *in situ*. These "dry" beams etch silicon surface rapidly without damaging the underlying silicon lattice as ion-assisted processes do.

We have studied the etching of *n*-doped polysilicon with a room temperature ClF<sub>3</sub> beam under high vacuum conditions. Etching rates were measured at silicon temperatures between 13 and 250°C. An Arrhenius plot of the data gave an apparent activation energy of 0.4 kcal/mol. The etched surface was terminated by F atoms as shown by the intense SIMS SiF<sup>+</sup> peak after etching. Samples on which a submonolayer of copper atoms were deposited before etching showed that the etching rates at room temperature were similar to those without Cu. When the sample temperature was raised to 250°C, the etching rates after Cu deposition were an order of magnitudes higher. The apparent activation energy was 3.0 kcal/mol in the latter case, and the etched surface was terminated by Cl as well as F atoms. These results suggest that the copper atoms catalyzes the halogenation of the silicon surfaces. The correlation between the etching rate and the surface roughness will be discussed as well.

**Em-TuP9 Structural and Chemical Changes During Annealing of Gas-Phase Polysulfide Passivated InP, R. W. M. Kwok, G. Jin, Department of Chemistry, The Chinese University of Hong Kong, Hong Kong; L. Huang, W. M. Lau, Department of Materials Engineering, The University of Western Ontario, London, Ontario, B6A 5B7 Canada; C. C. Hsu, Institute of Semiconductors, CAS, Beijing, PR China.**

The structural and chemical changes induced by annealing in InP exposed to gas-phase polysulfide, a heat treatment which is known to activate the passivation for surface state reduction (J. Vac. Sci. Technol. A11, 990 (1993)), were investigated using *in situ* low energy electron diffraction (LEED), thermal desorption spectrometry, and X-ray photoelectron spectroscopy (XPS). A blurred InP (1 × 1) LEED pattern was observed on InP exposed to UV/O<sub>3</sub> and then etched by a 1:30 HF solution, which became sharper with an additional exposure to gas-phase polysulfide. Vacuum annealing of the polysulfide treated InP gave a more ordered sulfide passivated InP surface as suggested by a further sharpness improvement of the LEED pattern. The sharpest pattern obtained was after annealing at 400°C. Accompanying to these structural changes were the desorption of species containing H and S at 300°C, and those containing P and S at 400°C. Further, XPS showed that the P-S bonding species and weakly chemisorbed In-S species, which were present in the polysulfide passivated surface, disappeared with the annealing at 400°C. Further annealing at 450°C resulted in the destruction of the surface sulfide passivation as indicated by the reduction of the surface sulfur, desorption of sulfur as well as phosphorus, and an increase of surface state densities by capacitance-voltage measurements. The resultant surface showed a blurred (2 × 1) LEED pattern.

**EM-TuP10 Sputter-Cleaning and Smoothing of GaAs(001) Surfaces Using Glancing-Angle Ion Bombardment, J. G. C. Labanda, Dept. of Physics and Astronomy, Northwestern Univ., Evanston, IL 60208, L. Hultman, IFM, Linköping University, Linköping, Sweden,**



S. A. Barnett, Dept. of Materials Sci. and Eng., Northwestern Univ., Evanston, IL 60208.

Glancing-angle argon ion bombardment has the advantages over normally incident ions of reducing ion damage and ion implantation projected ranges, reducing channeling, and preferentially removing surface asperities leading to flat surfaces. The effect of different bombardment conditions on the surface morphology and perfection of GaAs(001) substrates was studied. Initially rough surfaces become smoother with irradiation as evidenced by spotty reflection high energy electron diffraction (RHEED) patterns becoming streaky and by atomic force microscope (AFM) images. Optimal surfaces with AFM roughness  $< 0.4$  nm and showing short bulk and reconstruction RHEED streaks arrayed in an arc were obtained at  $510^\circ\text{C}$  as an  $\text{As}_4$  overpressure after a dose of  $2 \times 10^{16}$  Ar ions/cm<sup>2</sup> with energy  $E = 1000$  eV incident at an angle  $\theta = 15^\circ$  from the surface plane. Lower  $E$ ,  $\theta$ , and dose values were not as effective in smoothing and removing contamination, while larger values yielded rougher surfaces. Cross-sectional transmission electron microscope (XTEM) images of bombarded GaAs surfaces showed that ion damage increased with increasing dose,  $E$ , and  $\theta$ . Damage was resolved for the optimal smoothing and cleaning conditions noted above. However, defects were eliminated by using  $\theta = 6^\circ$ . Defect-free GaAs and InGaAs layers were grown on the sputtered surfaces by molecular beam epitaxy even when sub-surface ion damage was present. X-ray diffraction results for these films will also be reported.

**EM-TuP11 Sputter Deposition of Yttria Stabilized Zirconia onto a Porous Au Substrate**, A. F. Jankowski and J. P. Hayes, University of California, Lawrence Livermore National Laboratory, Livermore, CA 94551-9900.

Thin film synthesis of solid-oxide fuel cells is motivated by the objective to increase power densities for applications as in the light transportation industry. Process issues key to manufacturing a fuel cell stack from single cells include the ability to transport gas through porous conducting electrodes, deposit a defect-free electrolyte on the porous electrodes, and provide sufficient structural integrity for stack assembly as well as temperature cycling. This study addresses the issue of electrolyte layer deposition on a substrate under conditions appropriate for stack assembly. Our initial approach is to use a porous metal substrate to permit measurement of the electrolyte performance as well as provide a pore size similar to conventionally used electrode materials, e.g. sintered compacts. The sputter deposition of Au, under proper process parameters, serves as the porous substrate for the electrolyte layer. An optimum choice for the electrolyte material is yttria stabilized zirconia (YSZ). The focus of the study is to evaluate the process parameters of rf sputtering a YSZ target to densely coat a porous substrate and provide a defect-free, 2–5  $\mu\text{m}$  thick electrolyte suitable for operation at temperatures of  $750^\circ\text{C}$  or less. With consideration to the scattering effects of sputtered neutrals, an elevated working gas pressure of Argon facilitates filling surface voids of the porous substrate leading to the formation of a defect-free layer of cubic YSZ as examined with electron microscopy techniques. Whereas many deposition processes call for an elevated substrate temperature to produce the cubic phase, we use a room temperature substrate. This is advantageous with respect to our objective of utilizing a coefficient of thermal expansion—matched porous substrate for the planar electrodes. Electrolyte coated, anode and cathode pairs will be sintered together to form a fuel cell stack. Therefore, the electrolyte and electrodes will be subject to the same thermal history during processing and future temperature cycling.

**EM-TuP12 Hydrogen Passivation of the Be Acceptor in p-InP (100)**, M. D. Williams, T. H. Chiu, F. G. Storz, J. F. Ferguson, AT&T Bell Laboratories, Holmdel, NJ 07733-3030.

Gas-source molecular and chemical beam epitaxial techniques are being increasingly utilized in the production of III-V optoelectronic devices. It has been demonstrated that all of the donor and acceptor impurities in GaAs can be passivated with atomic hydrogen by the formation of complexes. The "hydrogenation" of the charge carriers provides a simple means of patterning and isolating discrete components in integrated device structures such as tunable externally modulated lasers and is a viable alternative to ion implantation. Atomic hydrogen sources can easily be incorporated in growth systems for *in situ* processing. The passivation mechanism for the shallow-level cation-site acceptors is presumed to be similar in the phosphide based III-V's. The exception to this, to date, is the column IIA acceptor, Mg, in GaP which exhibits little or no passivation. This suggests that Be (also column IIA), the preferred acceptor dopant in beam epitaxial systems, may also be difficult to passivate in InP. We show that the carrier concentration of Be-doped InP (100) can be compensated by

more than four orders of magnitude by diffusion of atomic hydrogen generated by an electron cyclotron resonance plasma source. Chemical beam epitaxy allows doping to  $3 \times 10^{19} \text{ cm}^{-3}$  with an effective carrier density of  $4 \times 10^{18} \text{ cm}^{-3}$ . C-V depth profiling shows effective compensation of the carriers within the first 0.4  $\mu\text{m}$  from the surface. Be has a larger electronegativity than that of Mg and its compensation may be explained by its higher affinity for  $\text{H}^+$  [J. Weber and M. Singh, Mater. Res. Soc. **104**, 325 (1988)].

**EM-TuP13 Studies of Strained Si-Ge Alloys Using Si-K and Ge-K X-Ray Absorption Spectroscopy**, A. P. Hitchcock<sup>1</sup>, T. Tylliszczak<sup>1</sup>, T. E. Jackman<sup>1,2</sup>, J.-M. Baribeau<sup>2</sup>, Z. H. Lu<sup>2</sup> and D. J. Lockwood<sup>2</sup>, <sup>1</sup>Inst. Materials Research, McMaster University, Hamilton, Canada L8S 4M1; <sup>2</sup>Inst. Microstructural Sciences, National Research Council, Ottawa, Ont. CANADA.

The structures of a series of strained and relaxed single crystal  $\text{Si}_x\text{Ge}_{100-x}$  alloy thin films grown by MBE on Si(100) and Ge(100) substrates have been studied by Ge-K and Si-K X-ray absorption spectroscopy. A constrained multi-file analysis of the extended fine structure signal<sup>[1]</sup> has been used to evaluate the Si-Si, Si-Ge and Ge-Ge bond lengths in order to investigate a controversy concerning the extent to which these bond lengths vary with composition. The results are discussed in terms of a recent "topological rigidity" model<sup>[2]</sup>. Polarisation dependent Si-K near edge spectra of the strained alloys<sup>[3]</sup> are related to band structure calculations<sup>[4]</sup> in order to demonstrate the sensitivity of the Si-K spectral features to the influence of strain on the conduction band electronic structure.

Research supported by NSERC and the Ontario Centre for Materials Research. Experiments at CHESS and SRC, supported by NSF.

[1] P. Aebi et al. Phys. Rev. B **45** (1992) 13579.

[2] N. Mousseau and M. F. Thorpe, Phys. Rev. B **46** (1992) 15887, *ibid* **48** (1993) 5172.

[3] A. P. Hitchcock et al. Surf. Sci. **301** (1994) 260; J. Vac. Sci. Tech. A (1994) in press.

[4] Q. M. Ma et al. Phys. Rev. B **47** (1993) 1936.

**EM-TuP14 Sb Ion Implantation and Annealing of SiGeC Heteroepitaxial Layers on Si(001)**<sup>†</sup>, R. Garcia\*, T. Alford\*\*, K. Daley\*\*, S. Segó\*\*, S. H. Shiu\*, R. J. Culbertson\*\*, D. B. Poker\*\*\*, \*Chemical, Bio and Materials Engineering, Arizona State University, Tempe, AZ, \*\*Dept. of Physics and Astronomy, Arizona State University, Tempe, AZ, \*\*\*Solid State Division, Oak Ridge National Laboratory, Oak Ridge, TN.

Si-capped SiGeC samples grown by CVD were implanted with several doses of 200 keV Sb ions. In order to completely amorphize the layer, one sample was implanted with  $1 \times 10^{16}$  ions/cm<sup>2</sup> of 200 keV Si ions at LN<sub>2</sub> temperature. Rapid thermal annealing was performed for 200 seconds at both  $600^\circ\text{C}$  and  $960^\circ\text{C}$ . Since samples annealed at  $600^\circ\text{C}$  exhibited little epitaxial regrowth, they were subsequently annealed at  $800^\circ\text{C}$  for 200 seconds. Samples were studied using Rutherford backscattering spectrometry (RBS) and ion channeling. Carbon was quantified using the  $^{12}\text{C}(\alpha, \alpha)^{12}\text{C}$  ion beam resonance at 4.265 MeV. It was found that the regrowth kinetics were significantly different from those of SiGe alloys. A greater thermal budget is required for regrowth. Furthermore, at the higher temperatures the carbon diffuses greatly out of the layer leaving a carbon depleted region. This has a possible negative impact on the doping of this material.

<sup>†</sup>Research conducted at Arizona State University was supported by AFOSR (Darpa), contract F49620-93-0081. Research at Oak Ridge National Laboratory is partially supported by the Division of Materials Science, U.S. Department of Energy, contract DE-AC05-84OR21400 with Martin-Marietta Energy Systems, Inc.

**EM-TuP15 Strain Measurements of SiGeC Heteroepitaxial Layers On Si(001) Using Ion Beam Analysis**<sup>†</sup>, S. Segó\*, T. Alford\*\*, Z. Atzmon\*\*, A. E. Bair\*\*, K. Daley\*, P. Ye\*\*, S. H. Shiu\*\*, R. J. Culbertson\*, N. Herbots\*, \*Dept. of Physics and Astronomy, Arizona State University, Tempe, AZ, \*\*Chemical Bio and Materials Engineering, Arizona State University, Tempe, AZ.

The strain in commensurate SiGeC heteroepitaxial films grown on Si(100) substrates has been quantified using ion channeling. The films were grown by molecular beam epitaxy (MBE) and chemical vapor deposition (CVD). Rutherford backscattering spectrometry (RBS) was used to quantify the Ge concentration as well as the film thickness. Nuclear resonance elastic ion scattering was used to quantify the carbon. Channeling was done using 2MeV  $\text{He}^{++}$  ions which yielded



angular scans in theta. The layers were etched using a 4 molar solution of HF and HNO<sub>3</sub> in order to obtain a reliable scan in the substrate. The shift in minima in the angular scans gave the tetragonal strain which ranged from 0 to 1.8%. This indicates that carbon is compensating for at least part of the strain caused by the high Ge content above the critical thickness of these layers.

†Research conducted at Arizona State University was supported by AFOSR (Darpa), contract F49620-93-C-0081.

**EM-TuP16 Comparison of Trisdimethylaminoantimony and Sb as Sources for Growth of GaSb, AlSb and InSb by Metalorganic Molecular Beam Epitaxy.** C. R. Abernathy, D. A. Bohling\* and G. T. Muhr\*, Department of Materials Science and Engineering, University of Florida, Gainesville, FL 32611, \*Air Products and Chemicals Inc., 7201 Hamilton Blvd., Allentown, PA 18195.

Gaseous alternatives to Sb and alkyl-Sb sources are actively being sought. Trisdimethylaminoantimony (DMASb) appears to be a promising precursor for use in Metalorganic Molecular Beam Epitaxy (MOMBE), though at present little is known regarding the use of this source in ultrahigh vacuum (UHV) growth environments. This paper will present a comparison of Sb and DMASb as Sb sources for growth of InSb and AlSb from trimethylindium (TMI) and trimethylamine alane (TMAA) respectively. The feasibility of GaSb growth from triethylgallium (TEG) and elemental Ga will also be discussed for each of the two Sb sources. In addition to their impact on growth rate and morphology, the role of the Sb precursor on carbon incorporation will be examined as a function of V/III ratio and growth temperature. Finally, the feasibility of carbon doping from CBr<sub>4</sub> will be discussed, paying particular attention to the incorporation of other impurities such as Br and hydrogen.

**EM-TuP17 Zincblende-CdSe on GaSb(110): Characterization of Epitaxial Growth and Electronic Structure.** G. Neuhold, K. Horn, Fritz-Haber-Institut der MPG, 14195 Berlin, Germany, K. O. Magnusson, Department of Natural Sciences, University of Karlstad, S-650 09 Karlstad, Sweden, and D. A. Evans, Athrofa Gogledd Ddwyrain Cymru (NEWI), Clwyd GB.

Substrate-stabilized pseudomorphic growth offers the chance to study the electronic structure of a particular semiconductor in different crystal structures, and to investigate the influence of structural differences on bulk and surface states. We have grown layers of CdSe, which in the bulk crystallizes in the stable wurtzite structure, in the zincblende modification on cleaved GaSb(110) surfaces by molecular beam epitaxy in an ultrahigh vacuum photoelectron spectrometer. The growth mode and structure of the overlayer were studied by means of LEED and core as well as valence level photoemission, using synchrotron radiation. The attenuation of substrate core level intensities with CdSe deposition indicate layer wise growth. An interface reaction, the amount of which depends on growth temperature, leads to the liberation of Sb, which floats on the growth front, and the formation of a Ga-Se compound, as signaled by changes in substrate and overlayer core level line shape. The valence band offset for this lattice-matched heterojunction interface system was determined, and found to be of the staggered type. This is in agreement with predictions based on the dielectric midgap energy model. Angle-resolved valence band spectra were interpreted in terms of direct transitions, and yielded good agreement with band structure calculations for the cubic phase.

**EM-TuP18 Photoconductivity Decay Study of GaN Thin Films.** C. H. Qiu<sup>(a,b)</sup>, C. Hoggatt<sup>(b)</sup>, Z. H. Zhang<sup>(b)</sup>, M. W. Leksono<sup>(a)</sup>, and J. I. Pankove<sup>(a,b)</sup>; a) Astralux Inc., 2386 Vassar Drive, Boulder, CO 80303; b) University of Colorado, Dept. of Electrical and Computer Engineering, Boulder, CO 80309-0425.

GaN is a potential candidate material for high temperature electronics and for blue-UV lasers. Though there are many reports on the Hall mobility measurement, few studies of the carrier lifetime have been reported. Since the minority carrier lifetime is an important parameter in device design and operation, we performed a photoconductivity (PC) decay study on GaN films grown by low pressure MOCVD. The PC measured with coplanar geometry was excited by a KrF excimer laser and was recorded with a storage oscilloscope. The films examined included undoped n-type GaN and a Mg-doped insulating p-type GaN. Negative PC is observed from films with high electron concentrations, while positive PC is observed from the slightly n-type samples and the p-type sample. For all the films, the PC decay obeys a power law of  $t^{-\alpha}$ , with an  $\alpha$  value in the range of 0.2 to 0.5.  $\alpha$  depends very slightly on the laser excitation power. The implications of the results and device design considerations will be discussed.

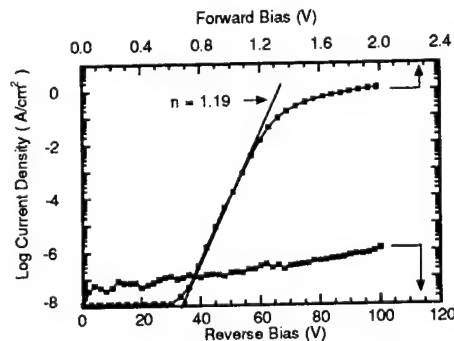
**EM-TuP19 OHMIC Electrical Contacts to p-ZnTe\***, Jeffrey T. Trexler, J. J. Fijol, and P. H. Holloway, Dept. of Materials Science and Engineering, University of Florida, Gainesville, FL 32611.

Formation of electrical contacts to MBE grown p-type (nitrogen doped to  $\sim 3 \times 10^{18} \text{ cm}^{-3}$ ) ZnTe using sputter deposited Au films (1500 Å) has been studied using Current-Voltage (I-V) data, Auger electron spectroscopy (AES), secondary ion mass spectroscopy (SIMS), and optical and scanning electron microscopy. I-V measurements were performed on the samples as deposited as well as after annealing at  $T > 150^\circ\text{C}$  in forming gas for times  $< 90$  minutes in order to determine the optimum annealing temperature and time. Lower resistances were measured for  $150^\circ\text{C}$  and  $200^\circ\text{C}$  for 15 minutes, while the resistance increased slightly with longer anneals. At  $250^\circ\text{C}$  the I-V data were still linear, but higher resistances were measured for all annealing times. For an optimum anneal of  $200^\circ\text{C}$  for 15 minutes, a current density of  $2.0 \times 10^3 \text{ mA/cm}^2$  was obtained at 5V. Reactions at the interface have been studied by AES and doping profiles have been determined by SIMS. Microscopy shows a planar surface with minor perturbations of morphology of the Au contacts. These results will be compared with previous studies of the reaction of Au and Ag with p-ZnSe with respect to current density, compound formation and surface morphology.

\*This work supported by ONR/ARPA Grant N00014-92-J-1895.

**EM-TuP20 High Field Ni-SiC Schottky Barrier Diodes with Single-Metal Process.** J. N. Su and A. J. Steckl, Department of Electrical and Computer Engineering, University of Cincinnati, Cincinnati, Ohio 45221-0030.

Wide-bandgap silicon carbide is receiving increased attention for high power and high temperature applications. Metal-SiC Schottky junction is a promising approach for the development of high power SiC MESFETs. We report the use of Ni as both Schottky and ohmic contact metal to fabricate a high breakdown field ( $\sim 1\text{E}6 \text{ V/cm}$ ) Schottky barrier diode (SBD) on a thin ( $1.6 \mu\text{m}$ ) 6H-SiC epi-layer ( $n = 2\text{E}16 \text{ cm}^{-3}$ ) grown on p<sup>+</sup> SiC substrate. Ni metallizations are carried out by sputtering deposition at room temperature followed by different thermal processes to distinguish the ohmic and Schottky contact regions. I-V characteristics show the Ni/SiC SBD has a high breakdown voltage of 150V, an extremely low leakage current density and excellent thermal stability. The ideality factor of less than 1.2 is an indication of a well-behaved thermionic emission mechanism. To compare with a commonly used SiC Schottky structure, Pt/6H-SiC diodes have also been fabricated using the same process and SiC material. Although the Pt/SiC diodes have a leakage current density as low as the best results reported, the Ni/SiC exhibited electrical characteristics and thermal stability superior to those of the Pt/SiC structure. For example, Ni-SiC diodes have a leakage current density of  $\sim 1\text{E}-6 \text{ A/cm}^2$  at blocking voltage of 100V,  $100\times$  less than that of a Pt-SiC structure. Subjected to thermal exposure, Pt-SiC structures show thermal degradation for temperatures beyond  $400^\circ\text{C}$ , while the Ni/6H-SiC Schottky junction exhibits a stable performance to a temperature stress as high as  $600^\circ\text{C}$ . Furthermore, using Ni as both Schottky and ohmic contact metal greatly simplifies the fabrication process.



J-V characteristics of a Ni/6H-SiC diode

**EM-TuP21 Temperature-Dependent Optical Bandgap of Metastable Zincblende-Structure  $\beta$ -GaN.** A. Lastras-Martinez, H. Navarro-Contreras, and G. Ramirez-Flores, Instituto de Investigación en Comunicación Óptica, Universidad Autónoma de San Luis Potosí, 78000, San Luis Potosí, SLP, México; R. C. Powell\* and J. E. Greene, Materials Science Dept., Coordinated Science Laboratory, and Ma-

terials Research Laboratory, University of Illinois, 1101 West Springfield Avenue, Urbana, IL 61801.

Epitaxial metastable zincblende-structure  $\beta$ -GaN(001)  $4 \times 1$  has been grown on MgO(1  $\times$  1) by reactive-ion molecular beam epitaxy in which the primary source of nitrogen is a low-energy (35 eV)  $N_2^+$  ion beam extracted from an ultra-high vacuum hot-cathode single-grid source with magnetic confinement. The incident  $N_2^+$  to thermal Ga ratio at the substrate was 2.0 with a film growth temperature of 650°C. Film thickness range from 1 to 1.5  $\mu$ m. The temperature-dependent (10–300 K) optical bandgap  $E_0(T)$  of epitaxial metastable zincblende-structure  $\beta$ -GaN(001)  $4 \times 1$  has been determined by modulated photoreflectance and used to interpret low-temperature photoluminescence spectra.  $E_0$  in  $\beta$ -GaN varied from  $3.302 \pm 0.004$  eV at 10 K to  $3.231 \pm 0.008$  eV at 300 K with the temperature dependence given by  $E_0(T) = 3.3022 - 6.697 \times 10^{-4} T^2 / (T + 600)$  eV. The spin-orbit splitting  $\Delta_0$  in the valence band was determined to be  $17 \pm 1$  meV. The oscillations in the photoreflectance spectra were very sharp with a broadening parameter  $\Gamma$  of only 10 meV at 10 K.  $\Gamma$  is comparable to modulated electroreflectance data from GaAs obtained at 4.2 K and, hence, an indication of the relatively high quality of the epitaxial  $\beta$ -GaN layers. The dominant transition observed in temperature-dependent luminescence was attributed to radiative recombination between a shallow donor, at  $\approx 11$  meV below the conduction band edge, and the valence band.

\*Present address: Sollar Cells Inc., 1702 N. Westwood Ave., Toledo, Ohio 43607.

**EM-TuP22 Low Pressure Metalorganic Chemical Vapor Deposition of GaN on c-plane (0001) Sapphire Substrates, C.-Y. Hwang, W. E. Mayo,** Department of Mechanics and Materials Science, Y. Lu, Department of Electrical and Computer Engineering, Rutgers University, Piscataway, NJ 08855, and H. Liu, Encore Corp., Somerset, NJ 08873.

GaN films were grown on c-plane sapphire substrates by low pressure metalorganic chemical vapor deposition (LPMOCVD) using a GaN buffer layer grown at lower temperatures. The quality and surface morphology of the GaN films were strongly affected by the growth conditions of the buffer layer as well as those of the GaN film. We have achieved a carrier concentration in the range of  $2 \times 10^{16} - 5 \times 10^{17}$  and mobility in the range of 100–300  $\text{cm}^2/\text{V}\cdot\text{S}$ . A systematic study of the influence of the buffer layer to the GaN film properties will be reported including the effects of the buffer layer thickness, growth temperature and the annealing of the buffer layer. The GaN films were evaluated by photoluminescence, Hall measurement, X-ray rocking curve, transmission and scanning electron microscopy.

**EM-TuP23 Growth of Crystalline 3C-SiC Films on 6H-SiC at 900°C by Chemical Vapor Deposition from Silacyclobutane, C. Yuan and A. J. Steckl,** Nanoelectronics Laboratory, Department of Electrical and Computer Engineering, University of Cincinnati, Cincinnati, OH 45221-0030; J. Chaudhuri and R. Thokala, Department of Mechanical Engineering, Wichita State University, Wichita, KS 67260-0035; M. J. Loboda, Dow Corning Corporation, Midland, MI 48686-0994.

Reduction of the growth temperature has been an important goal in the fabrication of SiC devices. We have previously reported the successful growth of crystalline 3C-SiC films on Si (100) and (111) at the reduced temperatures of 800–900°C from the single-source organosilane precursor silacyclobutane ( $\text{C}_3\text{H}_6\text{SiH}_2$ , SCB). In this paper, we report on the chemical vapor deposition of 3C- on 6H-SiC substrates using SCB. SiC growth by SCB has been investigated over the temperature range of 800–1100°C. The growth was carried out at low pressure (5 torr) with 1 sccm of SCB and 1.9 lpm of  $\text{H}_2$ . UV and visible spectrophotometry was used to determine an optical absorption edge for the films of  $\sim 2.27$  eV, corresponding approximately to the energy band-gap of 3C-SiC. The structure, strain and dislocation density in the 3C-SiC thin films grown on 6H-SiC are determined using X-ray double crystal diffractometry and compared with values obtained for 3C-SiC grown on Si(111). The SiC films grown by SCB on Si at 900–1000°C were found to be 3C-type crystalline and with an excellent surface morphology. The films grown at 1100°C were found to be a mixture of cubic and hexagonal polytypes of SiC. Although the dislocation density of SiC on Si(111) was in the low to mid- $10^{10}/\text{cm}^2$ , which is a considerable improvement over the values present in 3C-SiC films grown on Si(100), an even more significant reduction in the dislocation density has been achieved for 3C-SiC grown on 6H-SiC (0001). These films exhibit a dislocation density in the low to mid- $10^7/\text{cm}^2$ , which is within range of the substrate dislocation density.

The results obtained indicate that use of SCB as precursor for growth of 3C- on 6H-SiC is very promising for low temperature deposition of crystalline films.

**EM-TuP24 Electron Emission from Wide-Bandgap Negative Electron Affinity Materials, C. Bandis, D. Haggerty, and B. B. Pate,** Department of Physics, Washington State University, Pullman, WA 99164.

The diamond (111)  $1 \times 1$  surface was found to exhibit negative electron affinity (NEA) over a decade ago [1]. Our recent work [2] on electron emission properties of the NEA diamond (111) surfaces find that the creation of free excitons play an important role in the high quantum yield which has been obtained with near threshold photoexcitation. We found that bound electron-hole pairs transport to the surface and breakup in the electric field of the surface dipole. In this report, we present evidence for the existence of such an emission mechanism in other wide bandgap materials. These results suggest that the exciton-derived emission mechanism is common, and is likely to apply to a wide variety of wide-bandgap materials.

[1] F. J. Himpsel et al. Phys. Rev. B20, 624 (1979).

[2] C. Bandis and B. B. Pate, in preparation.

Work supported by the National Science Foundation.

**EM-TuP25 Conformality of  $\text{SiO}_2$  Films from TEOS-Sourced Remote Microwave Plasma-Enhanced Chemical Vapor Deposition, D. A. Levedakis, H. Liao, T. S. Cale and G. B. Raupp,** Department of Chemical, Bio & Materials Engineering, Arizona State University, Tempe, AZ 85287.

The dependence of silicon dioxide step coverage in micron scale trenches on substrate temperature, absorbed microwave power, total pressure and  $\text{O}_2/\text{TEOS}$  flow ratio were systematically investigated in a remote plasma configuration in which oxygen is excited upstream of the deposition chamber in a microwave discharge. This configuration allows us to investigate the plasma-induced deposition of  $\text{SiO}_2$  from TEOS in the absence of charged species (ions and electrons). Of the independent parameters investigated, temperature has the strongest effect on film conformality. For example, step coverage in a long rectangular trench of aspect ratio two is greater than 90% at 250°C., but less than 40% at 400°C at otherwise fixed conditions. Experimental film profiles in trenches are compared to simulations using EVOLVE, a ballistic transport and reaction simulator. In our simulations we assume that deposition proceeds through oxidative attack of TEOS or TEOS fragments adsorbed on the growing film surface by oxygen atoms. A thermally activated, heterogeneous oxygen atom recombination reaction consumes oxygen atoms without leading to deposition. A plasma chemistry model of the excitation and afterglow regions of the plasma source is used to provide an estimate of the flux of oxygen atoms to the feature mouth. We demonstrate how physically-based modeling can be used to extract kinetic rate parameters from experimental data, and how to use physically-based simulation to predict operating windows for high step coverage and good film quality.

## MANUFACTURING SCIENCE AND TECHNOLOGY

### Room BR4 – Session MS-TuP

#### Manufacturing Science and Technology

**Moderator:** G. W. Rubloff, North Carolina State University.

**MS-TuP1 Low-Cost Optical Reflectivity Temperature Measurement System, H. A. Atwater<sup>(a)</sup> and D. S. Gardner<sup>(b)</sup>,** (a) California Institute of Technology, Pasadena, CA 91125 and (b) Intel Corporation, Santa Clara, CA 95052.

We describe the results of a project to assess the use of a low-cost ( $\leq \$700.00$ ) optical reflectivity system as a practical surface temperature diagnostic for on-wafer measurements during sputter deposition. The physical processes which lead to temperature-dependent optical reflectivities are material-dependent, but are large enough for many integrated circuit materials (e.g., Al, Si, Cu) to be useful for thermometry. Correlation of thermocouple temperature measurements made in an isothermal environment with optical reflectivity allows

system calibration via an empirical fit to the nonlinear dependence of reflectivity with temperature. Dividing the reflectivity data for a given material by the fitting function allows relative temperature measurement with precision of  $\pm 4^\circ\text{C}$  at temperatures above  $170^\circ\text{C}$ , for Al and Si. *In situ* optical reflectivity measurements during sputter deposition of Cu indicated a large temperature rise during film deposition. Limits to optical reflectivity thermometry, as well as extensions to rapid thermal annealing and chemical vapor deposition will be discussed.

**MS-TuP2 Magnetron RIE System Using a Dipole-Ring Magnet for Quarter Micron Etch Process.** *Y. Tahara, Y. Ishikawa, M. Ogasawara, K. Inazawa,* Etch System Dept. SPE Div., Tokyo Electron Limited, Sumiyoshi-cho, Fuchu 183 Japan, *K. Horioka, H. Hayashi, \*Y. Yoshida, H. Okano,* Research and Development Center, \*Semiconductor Div., Toshiba Corporation, Saiwai-ku, Kawasaki 210 Japan.

A Dipole-ring Magnet (DRM) has a capability of producing high fields up to 600G with excellent uniformity. Its low stray magnetic field outside of the ring eliminates interference between chambers, and makes it suitable for compact new mainframe systems. We have developed new processes for quarter micron oxide and Si trench etching employing magnetron RIE system using the DRM.

Si etch rate was found to increase with magnetic field strength due to higher plasma density in high fields. The 600G DRM enables  $\phi 0.25\mu\text{m}$  deep trench etch with a rate of more than  $1.2\mu\text{m}/\text{min}$ , which is twice that of the current magnetron RIE. For the  $\text{SiO}_2$  process, a magnetic field around 120~200G was adopted according to the optimization of Vdc, ion flux and F radical concentration variations to field strength, to obtain the best etching performance. Finally, contact hole etch process with high selectivity over poly-Si(50),  $\text{Si}_3\text{N}_4$ (20), and Al(40) was accomplished with the 120G DRM using fluorocarbon gas and CO chemistry.

The process technologies with DRM are concentrated in a next generation "UNITY" mainframe supported by an advanced control system.

**MS-TuP3 Magnetron RIE Without Charge-up Damage Using a Dipole-Ring Magnet.** *J. Sakai, S. Ikeda, M. Sekine, K. Horioka, \*Y. Yoshida, H. Okano,* Research and Development Center, \*Semiconductor Div., Toshiba Corporation, Toshiba-cho, Saiwai-ku, Kawasaki 210 Japan, *M. Ogasawara, K. Inazawa, Y. Tahara,* Etch System Dept. SPE Div., Tokyo Electron Limited, Sumiyoshi-cho, Fuchu 183.

We have introduced a new plasma etching system using a Dipole-ring Magnet (DRM) as a promising etch tool for quarter micron devices. DRM provides a parallel magnetic field up to 600 Gauss with excellent uniformity, and has achieved excellent performances such as high etch rate in Si deep trench and high selectivity of more than ten in  $\text{SiO}_2$  etching over  $\text{Si}_3\text{N}_4$  as well as low charge-up damage (1).

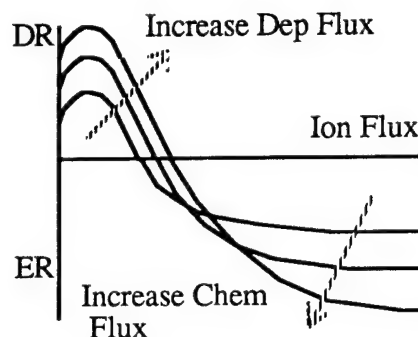
For further improvement of the gate oxide reliability in  $\text{SiO}_2$  etching, we have succeeded in compensation of the plasma non-uniformity due to  $\mathbf{E} \times \mathbf{B}$  electron drift, realized by use of an optimized magnetic field distribution. This enabled the use of higher rf power for higher etch rates, and a compact magnet design, still with no degradation of the gate oxide in a TDDb test. Finally, the DRM's low level of stray magnetic field eliminates interference between chambers, which makes it suitable for compact mainframe systems.

(1) M. Sekine et al. Proc. 13th Symp. Dry Process, (Tokyo, 1993) p. 17. (The Inst. of Electrical Engineer of Japan).

**MS-TuP4 Profile Modeling of High Density Plasma Oxide Etching.** *J. S. Han, J. P. McVittie, J. Zheng,* Stanford University, Center for Integrated Systems, Stanford, CA 94305.

Plasma dry etching is increasingly becoming a central part of IC manufacturing. As device dimensions continually decrease, the contact vias and lines begin to push the sub  $0.35\mu\text{m}$  regime. In addition, aspect ratios approaching 5:1 for contacts and more than 20:1 for trenches are now commonplace. Such geometry can only be processed using dry etching techniques. To understand and predict etch profiles becomes essential to reduce costs in process optimization. In this paper, several profile issues that result from an industry accepted inductively couple high density plasma oxide etch system are investigated using oxide overhang test structures and vias. The key features observed from the test structures include ion enhanced polymer deposition, etch rate saturation effect, redeposition, direct polymer deposition (CVD polymer), and etch lag. In addition, vias show trends of reverse lag and microtrenching. A new model is presented and implemented in SPEEDIE, a topography simulator developed at Stanford design to use phenomenological models to predict profile evolution. The model

separates the neutral flux into a deposition flux and a chemical flux, where the deposition species contribute to the growth of polymer and the chemical species contribute to the etching of the substrate, in this case,  $\text{SiO}_2$ . Deposition or etching takes place at a rate dependent on the ratio of the deposition flux to the ion (energy) flux or chemical flux to the ion (energy) flux. In addition, microtrenching is modeled by an ion induced chemical desorption component. Comparison with SEM results show that the new model can be used to accurately simulate profile evolution.



**MS-TuP5 Insitu Monitoring and Control of MBE and MOCVD Growth Using Multi-Wavelength Ellipsometry.** *John A. Woollam, S. Pittal, B. Johs, and P. He,* J. A. Woollam Co., Inc., 650 'J' St. #39, Lincoln, NE 68508, *G. N. Maracas, R. Droopad, C. H. Kuo, and S. Anand,* Arizona State University, Tempe, AZ 85287, *S. Dakshina Murthy and I. Bhat,* Rensselaer Polytechnic Institute, Troy, NJ 12180.

In this paper we describe real-time growth control of MBE grown GaAs/AlGaAs multiple quantum well, and MOCVD grown HgCdTe using a novel and low cost insitu multi-wavelength ellipsometer. This ellipsometer acquires insitu ellipsometric data in real-time at 44 wavelengths in the spectral range of 415~750 nm with maximum acquisition rate of 25 measurements/second (typical 1 measurement/second).

A GaAs/AlGaAs multiple quantum well with varying well thicknesses was MBE grown on a GaAs substrate. In this experiment layer thicknesses of the multiple quantum well were controlled by the ellipsometer. The substrate was rotated at all times during the MBE growth. The insitu ellipsometer was also used in the composition control of MOCVD grown HgCdTe. Alloy compositions of 0.25 and 0.3 were stabilized by regulating the  $\text{H}_2$  flow through a DMCD source. And, when an intentional temperature disturbance was introduced during the control experiment, the ellipsometer re-adjusted the  $\text{H}_2$  flow to maintain the as-grown composition. Results from SIMS will also be described.

**MS-TuP6 Electrical Monitoring of Surface Conditions in a Plasma Reactor.** *Mark A. Sobolewski and James K. Olthoff,* National Institute of Standards and Technology, Gaithersburg, MD 20899.

Measurements of the voltage and current of radio-frequency discharges can be used to detect plasma etching endpoints and monitor the conditioning of plasma reactor surfaces. However, the mechanisms that relate plasma electrical characteristics to surface properties are not well understood. We have therefore undertaken a detailed investigation of these mechanisms. In this work, voltage and current waveforms were measured at both electrodes of a parallel-plate reactor as gas composition and surface conditions were varied. To further characterize the electrical properties of the plasma, the rf voltage in the glow region of the plasma was measured, using a capacitive probe. Absolute concentrations of gas-phase species were measured simultaneously using a calibrated mass spectrometer.

Plasma electrical properties can depend indirectly on surface chemistry, through changes in the gas-phase concentration of species arising from the surfaces. We have also observed, for aluminum surfaces exposed to oxidizing plasmas, electrical changes that depend directly on surface conditions. At fixed gas-phase oxygen concentration, slow changes were observed in plasma impedance and dc self bias, due to absorption of oxygen species by the aluminum. The electrical changes arise because the adsorbed oxygen increases secondary electron emission from the aluminum surface, producing greater electron density in the plasma. The electrical changes can be reversed by exposing the surface to an argon plasma, which removes the adsorbed oxygen by sputtering.

We have developed a model of the electrical behavior of rf discharges

that can be used to interpret the data and to distinguish changes in surface conditions from competing effects. The model suggest that electrical sensors of surface conditions would succeed in a wide variety of plasmas. The model also allows values of other relevant plasma properties (such as the plasma potential and incident ion energies) to be obtained from the electrical data.

**MS-TuP7 Field Emission Tips for Micro-Column Lithography,** *W. K. Lo<sup>\*</sup>, M. Skvarla<sup>1</sup>, M. S. Isaacson<sup>\*</sup>*, <sup>\*</sup>Applied and Engineering Physics, Cornell University, Ithaca, NY 14853, <sup>1</sup>National Nanofabrication Facility, Cornell University, Ithaca, NY 14853.

We have tailor made field-emission tips with differing geometrical shapes using controlled electrochemical etching in combination with nanofabrication techniques including focused ion beam milling and reactive ion etching. Current investigations include studying the effects that a microfabricated Schottky electrode, formed integrally with the tip, has on the tip's emission angle, extraction voltage, and energy distribution.

These emission properties are all relevant to micro-column based electron lithography<sup>1</sup> which requires electron sources exhibiting: 1) low extraction voltages ( $\sim 1$  kV) to accommodate low-voltage microcolumn operation, 2) narrow energy distributions to reduce the effect of chromatic aberration on spot size, 3) narrow emission angles to reduce the effect of spherical aberration on spot size, 4) high current densities to allow faster scanning for a given electron dose, and 5) stable emission to minimize unintended dose variation.

Field-emission sources, best known for their narrow energy distributions and high current densities, have the potential to satisfy all these requirements simultaneously. Conventional sources of this type are, however, notoriously sensitive to contamination and sputter damage by ionized residual gases and usually operate under ultra-high vacuum conditions ( $\sim 5 \times 10^{-11}$  Torr) for stability. They also have relatively high extraction voltages (few kV) and emission angles ( $\sim 10^\circ$ ). These properties are affected by the geometry of the tip and the tip material which can be controlled.

Recent results from our study will be presented here.

1. T. H. P. Chang, D. P. Kern and L. P. Muray, *J. Vac. Sci. Technol. B* 10 (1992) 2743.

**MS-TuP8 High Resolution Resists for Low Energy Electron Beam Lithography,** *C. W. Lo<sup>1</sup>, M. J. Rooks<sup>2</sup>, H. G. Craighead<sup>1</sup>*, <sup>1</sup>Applied and Engineering Physics, Cornell University, Ithaca, NY 14853, <sup>2</sup>National Nanofabrication Facility, Cornell University, Ithaca, NY 14853.

Low energy electron beam lithography has been suggested for use in high resolution patterning because of low proximity effects and high resist-sensitivity at low energy. However, resists and electron-beam columns optimized for use in low energy lithography are not yet well developed. Micro-column lithography is one approach which

addresses the difficulties of obtaining a finely focused, low energy electron beam. Using a miniature, micro-fabricated electron column (a few mm in length), scanning electron beams with diameters of tens of nm at 1 keV have been achieved<sup>1</sup>. The response of resists to electrons of different energies must be considered for the development of low energy resists. For instance since electrons at low energy have very shallow penetration depths, the resists has to be very thin. (tens of nm for 1 keV electrons). Some resists are capable of high resolution pattern-transferring, but because of their low electron sensitivities at high energies, they are impractical to employ for conventional lithography. These resists are, however, attractive for use in low energy lithography because cross sections for 1 keV electrons are approximately two orders of magnitude higher than those for 30 keV electrons.

We are currently investigating several promising processes for use in low energy, high resolution pattern transferring. The resists are exposed using a low energy, field emission SEM, which has been modified to include a pattern generator. It has been used successfully to expose patterns with 1 keV electrons on PMMA and self-assemble monolayers. In addition, a Monte-Carlo program has also been developed for simulating the non-classical, low energy electron-matter interactions. We will discuss our most recent experimental results which include comparisons to the predictions of Monte-Carlo simulations.

<sup>1</sup>Chang et al., *J. Vac. Sci. Technol. B* 10, 2749 (1992).

**MS-TuP9 The Design and Testing of a Multi-Task, Multi-Instrument Sample Transfer System,** *S. Thevuthasan and D. R. Baer*, Pacific Northwest Laboratory, Richland, WA and *J. N. Worthington, T. R. Howard, and J. R. Munn*, Thermionics Northwest Instruments, Port Townsend, WA.

A prototype multi-instrument, multi-task UHV sample transfer system has been developed for integration with a wide range of synthesis and analysis instruments. This capability will be utilized in the Environmental Molecular Sciences Laboratory (EMSL), a new U.S. Department of Energy user facility under construction at Pacific Northwest Laboratory (PNL). The EMSL will have several state-of-the-art systems that can be used by scientists from around the world. A primary focus of EMSL is understanding the molecular level interactions that influence waste processing and contaminant transport in the environment. Because interfaces play a large role in these environmental issues, there is a significant element of interface science in EMSL. The specimen transfer capability allows a sample to be synthesized, processed, and characterized by several surface science techniques without exposing the sample to air. The temperature range of the specimen can be as high as 2000 K during heating and as low as 50 K during cooling. Components of the system are designed to allow pumped or ambient transfer of specimens from different locations. Several tests have been performed to verify the functional limitations and capabilities of the system. We will discuss the design and the capabilities of the transfer system along with test results.



## SURFACE SCIENCE

Room A205 - Session SS1-WeM

### Surface Magnetism I

**Moderator:** H. Hopster, University of California, Irvine.

8:00 am **SS1-WeM0 Spin-Polarized Electron Measurements: Foundations of Surface Magnetism Research**, Robert J. Celotta and Daniel T. Pierce, Electron Physics Group, National Institute of Standards and Technology, Gaithersburg, MD 20899.

Electron spectroscopies have long been used in investigations of atoms and solid surfaces. Although the number of electrons at a given energy or momentum resulting from a particular emission or scattering process is typically measured, new insights are obtained in many investigations if another parameter is considered, namely, the electron spin polarization. Such measurements have been facilitated in the last two decades by the development of improved electron polarization techniques, i.e., the GaAs polarized electron source and a variety of spin polarization analyzers. Surface magnetic properties such as the spontaneous magnetization, Curie temperature, temperature dependence of the magnetic order, anisotropy, spin-dependent electronic structure, magnetization curves, elementary excitation, and magnetic microstructure have been determined with spin-dependent techniques. Examples will be drawn from the work of the Electron Physics Group at NIST and from other laboratories. The outgrowth of this early work is evident in the current exciting investigations involving electron spin polarization. **INVITED**

Supported in part by the Office of Naval Research.

8:40 am **SS1-WeM2 Spin-Polarized Low Energy Electron Microscopy of Co/W(110)**, T. Duden, K. Grzelakowski, E. Bauer, T. U. Clausthal, Clausthal-Zellerfeld, Germany, and S. Chiang, H. Poppa, IBM Almaden Research Center, San Jose, CA 95120-6099.

We have used a new spin-polarized low energy electron microscope (SPLEEM) to measure the topography and magnetic domain structure of thin layers of Co on W(110). In contrast to the first SPLEEM instrument,<sup>1</sup> the design of this new instrument<sup>2</sup> is characterized by three main features: a) compactness of construction, b) multi-directional spin electron gun, and c) integration with a versatile sample preparation and exchange system. The new GaAs based and laser excited spin gun uses a combination of electrical and magnetic beam deflection elements to allow positioning of the electron beam polarization vector in any direction with respect to the sample surface.<sup>3</sup> Lateral resolution obtained to date with this microscope is of the order of 20 nm. The observed variations in the magnetic contrast for different angles of the electron beam polarization, both in and out of the plane of Co/W(110) sample, will be discussed. SPLEEM images have been measured both as a function of  $\theta$  at constant  $\varphi$  and as a function of  $\varphi$  at constant  $\theta$ . These images show that the magnetization of the domains is fully in-plane for 3-6 ML Co, in contrast to the considerable out-of-plane magnetization previously measured for Co/Au(111) by secondary electron microscopy with polarization analysis (SEMPA).<sup>4</sup> Correlations between the magnetic and topographic structure of the Co/W(110) sample will also be shown.

1. M. S. Altman, H. Pinkvos, J. Hurst, H. Poppa, G. Marx, and E. Bauer, *Mat. Res. Symp. Proc.*, Vol. 232, 125 (1991).
2. K. Grzelakowski and E. Bauer, to be published.
3. T. Duden and E. Bauer, to be published.
4. R. Allenspach, M. Stampanoni, A. Bischof, *Phys. Rev. Lett.*, 66, 3344 (1990).

9:00 am **SS1-WeM3 Scanning Ion Microscopy with Polarization Analysis (SIMPA) to Study Domain Structures of Metal Overlayers on Fe and Pd Single Crystal Surfaces**, N. L. Nunes, H. P. Oepen\*, G. Steierl and C. Rau, Department of Physics & Rice Quantum Institute, Rice University, Houston, TX 77251-1892, USA.

Scanning ion microscopy with spin analysis (SIMPA) is a novel high-resolution magnetic imaging technique. In SIMPA, a highly focussed Ga ion beam from a liquid metal ion source (minimum spot size: 40 nm) induces the emission of spin-polarized electrons during

scanning at ferromagnetic surfaces. At low beam intensities, the topographical and magnetic domain structures are obtained by collecting the emitted electrons and analyzing the electron spin polarization (ESP). The ESP is used as a measure of the surface magnetization. At high beam intensities, the scanning ion beam is used to etch out desired geometric nanostructures of various magnetic and nonmagnetic overlayers deposited on nonmagnetic or magnetic substrates. We report on first SIMPA studies of micromagnetic domain structures obtained from various metal substrate combinations. The microscopic structure of the metal overlayers is further studied using UHV scanning tunneling microscopy.

\*Supported by the National Science Foundation, the Welch Foundation and the Texas Higher Education Coordinating Board.  
\*IGV-KFA Jülich, Germany.

9:20 am **SS1-WeM4 Spin-Resolved X-ray Photoelectron Spectroscopy Study of the  $2p_{3/2}$  Level of Ferromagnetic Ni**, A. K. See, L. E. Klebanoff, Department of Chemistry, Lehigh University.

We have studied the spin polarization of the  $2p_{3/2}$  main line and "6-eV" satellite photoemission features from Ni(110) by using Spin-Resolved X-ray Photoelectron Spectroscopy (SRXPS). The main line of the  $2p_{3/2}$  spectrum displays a significant minority-spin polarization while the satellite displays a strong spin polarization and sizable exchange splitting of  $\sim 0.5$  eV. The observation of the polarization in the  $2p_{3/2}$  main peak indicates that the final state valence configuration upon core hole creation is not  $3d^{10}$  for the main peak, in contrast with previous assignments, but is more likely  $3d^9$ . The SRXPS data directly reveal that the  $3d$  electron count in the satellite is smaller than in the main line, and is most likely  $3d^8$ .

9:40 am **SS1-WeM5 Electronic and Magnetic Properties of Pseudomorphic Ferromagnetic Alloy Films on Cu(100)**, G. J. Mankey, S. Z. Wu and R. F. Willis, Department of Physics, The Pennsylvania State University, University Park, Pennsylvania 16802.

Ultrathin films of Fe, Co and Ni on Cu(100) exhibit a variety of magnetic phases which depend on film growth conditions, film thickness and temperature. We have measured the energy band dispersions<sup>1</sup> and magnetic properties<sup>2</sup> of these films. Fe films exhibit a perpendicular magnetization below 6 ML which switches to in-plane for thicker films.<sup>3</sup> Co films exhibit an in-plane magnetization for both ultrathin and thick films. Ni films exhibit an in-plane magnetization below 7 monolayers which switches to perpendicular for thicker films. By simultaneously depositing Fe or Co and Ni on Cu(100) we can produce alloy films with a controlled stoichiometry. The electronic properties of the films are measured with angle resolved ultraviolet photoemission spectroscopy and the ferromagnetic properties are measured with the surface magneto-optic Kerr effect. We show that by varying the alloy stoichiometry the average spin moment of the ferromagnet can be tuned and demonstrate the effect of tuning the spin moment on the magnetic anisotropy behavior.

1. G. J. Mankey, R. F. Willis and F. B. Himpsel, *Phys. Rev. B* 48, 10284 (1993).
2. F. Huang, M. T. Kief, G. J. Mankey and R. F. Willis, *Phys. Rev. B* 49, 3962 (1994).
3. Dongqi Li, M. Freitag, J. Pearson, Z. Q. Qiu and S. D. Bader, *Phys. Rev. Lett.* 72, 3112 (1994).

10:00 am **SS1-WeM6 Ferromagnetic Phases at the Fe/Si(111) Interface**, J. P. Woods, Y. L. He and D. Welipitiya, Department of Physics and Center for Materials Research and Analysis, University of Nebraska, 116 Brace Laboratory, Lincoln, NE 68588-0111.

Fe/Si layered structures have exhibited unique magnetic properties and the ferromagnetic Fe silicides at the Fe/Si interface are investigated. Fe is evaporated on the Si(111) surface at room temperature; the Fe concentration is measured with Auger and core-level electron spectroscopy and the surface order is monitored with low energy electron diffraction. The magnetic phases of atomically thin layers of Fe/Si(111) are identified with magneto-optic Kerr effect and photoemission experiments. Ferromagnetic ordering is first observed with Fe/Si Auger intensity ratio of 1.2 and an additional ferromagnetic phase ( $\alpha$  Fe) is evident in hysteresis loops with additional Fe evapo-



ration. The photoemission spectra are dominated by the Fe 3d electrons even at Si rich non-ferromagnetic phases, and the spin-resolved valence-band electronic structure is measured. The diffusion of Fe into the Si substrate with various annealing steps and the diminishing ferromagnetic order is investigated.

Supported by ACS-PRF and NSF-EPSCoR.

10:20 am **SS1-WeM7 Circular Dichroism in Core-Level Photoemission**, *H. Xiao<sup>a,b</sup>, A. P. Kaduwela<sup>b</sup>, M. A. Van Hove<sup>b</sup>, and C. S. Fadley<sup>a,b</sup>*, <sup>a</sup>Department of Physics, University of California, Davis, CA 95616, <sup>b</sup>MSD, Lawrence Berkeley Laboratory, Berkeley, CA 94720.

We have calculated the circular dichroism associated with core-level photoemission from both non-magnetic and magnetic systems using a multiple-scattering photoelectron diffraction theory. Our simulations for the non-magnetic cases of C 1s emission from CO on Pd(111) and Si 2p emission from Si(100) well predict the dichroism found in experimental results due to Schönhense et al. [1] and Daimon et al. [2], respectively. Magnetic circular dichroism has also been treated for the case of Fe 2p emission from Fe(110), including a generalization of the theory to allow for spin-orbit coupling in the initial state and spin-dependent scattering in the final state. Both total intensities and spin-resolved intensities resulting from circularly-polarized excitations will be discussed. A strong interplay between normal (non-magnetic) dichroism and magnetic dichroism is found. Photoelectron diffraction theory thus provides a general framework for modeling dichroism in core-level photoemission from both non-magnetic and magnetic systems.

[1] G. Schönhense, *Phys. Scripta T* **31**, 255 (1990).

[2] H. Daimon, T. Nakatani, S. Imada, S. Suga, Y. Kagoshima, and T. Miyahara, *Jpn. J. Appl. Phys.* **32**, L1480 (1993).

10:40 am **SS1-WeM8 Spin-Specific Photoelectron Diffraction Using Magnetic X-Ray Circular Dichroism**, *J. G. Tobin, and G. D. Waddill*, Lawrence Livermore National Laboratory, *X. Guo and S. Y. Tong*, University of Wisconsin-Milwaukee.

The first observation of spin-dependent photoelectron diffraction using circularly-polarized x-rays is reported for monolayer ferromagnetic fcc Fe films on Cu(001). Circularly-polarized x-rays are used to produce spin-polarized photoelectrons from the Fe 2p spin-orbit split doublet, and intensity asymmetries in the 2p<sub>3/2</sub> level of  $\approx 3\%$  are observed. The asymmetry is dependent on the relative orientation of the x-ray polarization vector and the Fe magnetic moment, and is sensitive to the electron kinetic energy. Our results are compared to multiple scattering calculations which reproduce the experimental observations. A strong angular dependence is predicted by theory and is observed in the experiment. This spin-dependent technique promises the direct, element-specific determination not only of local atomic structure, but magnetic structure as well.

Work performed under the auspices of the US Department of Energy by the Lawrence Livermore National Laboratory under contract number W-7405-END-48. Work at Wisconsin was supported by the US Department of Energy.

## SURFACE SCIENCE

### Room A201 – Session SS2-WeM

#### Reactions on Metals: Diatomics

**Moderator:** G. B. Fisher, General Motors Research & Development Center.

8:00 am **SS2-WeM0 Structure Sensitive Selectivity of the NO-CO Reaction over Rh(110) and Rh(111)**, *C. H. F. Peden*, Pacific Northwest Laboratory\*, Richland, WA 99352, *D. N. Belton and S. J. Schmieg*, General Motors Research and Development Center, Warren, MI 48090.

We have studied the effects of temperature, NO conversion, and NO-CO ratio on the activity and selectivity of the NO-CO reaction at high (1 torr < P < 100 torr) pressures over the Rh(110) and Rh(111) surfaces. Under the conditions used in this study, the NO-CO activity is between 1.3 and 6.3 times faster over Rh(110) than over Rh(111).

The (110) surface exhibits a lower apparent activation energy ( $E_a$ ), 27.2 vs. 34.8 kcal/mol, than does the (111) surface. Although the turnover numbers for NO reduction can be quite similar on the two different surfaces, we find large differences between Rh(110) and Rh(111) with regard to their selectivities for the two competitive nitrogen-containing products, N<sub>2</sub>O vs. N<sub>2</sub>. The more open Rh(110) surface tends to make significantly less N<sub>2</sub>O than Rh(111) under virtually all conditions that we probed with these experiments. These results can be understood in terms of the relative surface coverages of adsorbed NO and N-atoms on the two surfaces. Notably, more facile NO dissociation on Rh(110) appears to lead to greater steady-state concentrations of adsorbed N-atoms than is present on the (111) surface. Higher N coverages on the (110) surface favor N-atom recombination (N<sub>2</sub> formation) more than the NO + N reaction (N<sub>2</sub>O formation) on Rh(110) relative to Rh(111). Indeed, Rh(110) surfaces were found to be largely composed of adsorbed N and lesser quantities of NO in post-reaction XPS measurements. In contrast, Rh(111) surfaces only showed XPS features due to adsorbed NO.

\*Pacific Northwest Laboratory is operated for the U.S. Dept. of Energy by Battelle Memorial Institute under contract DE-AC06-76RLO 1830.

8:20 am **SS2-WeM1 Dissociation Kinetics of NO on Rhodium(111)**, *H. J. Borg, R. A. van Santen and J. W. Niemantsverdriet*, Schuit Institute of Catalysis, TU Eindhoven, P.O. Box 513, 5600 MG Eindhoven, The Netherlands.

Temperature programmed static secondary ion mass spectrometry (TPSSIMS) and temperature programmed desorption (TPD) have been used to study the kinetics of adsorption, dissociation, and desorption of NO on Rh(111). At 100 K, NO adsorbs molecularly *via* mobile precursor state kinetics. SSIMS suggests threefold adsorption at low coverage, with increasing amounts of bridged NO at higher coverages. Three characteristic coverage regimes appear with respect to NO dissociation. At coverages below 0.25 ML, NO dissociates completely at temperatures between 275 and 340 K, with an activation energy of  $39 \pm 6$  kJ/mol and a preexponential factor of  $10^{6 \pm 1} \text{ s}^{-1}$ . Nitrogen atoms desorb as N<sub>2</sub>, with kinetics that is strongly influenced by the presence of coadsorbed oxygen. In the medium coverage range,  $0.25 < \theta_{\text{NO}} < 0.50$  ML, part of the NO desorbs molecularly, with a desorption barrier of  $116 \pm 10$  kJ/mol and a preexponential of  $10^{16.5 \pm 1.0} \text{ s}^{-1}$ , suggestive of a mobile transition state. Dissociation of NO becomes progressively inhibited, the onset shifting from 275 K at 0.25 ML to 400 K, the NO desorption temperature, at a coverage of 0.50 ML. On these highly covered surfaces nitrogen atoms become destabilized, resulting in an additional low temperature N<sub>2</sub> desorption state. For initial NO coverages higher than 0.50 ML, NO dissociation is completely self-inhibited, indicating that all sites required for dissociation are blocked. The desorption of the more weakly bound bridged NO does not generate the sites required for dissociation; these become only available after the desorption of triply coordinated NO.

8:40 am **SS2-WeM2 Kinetics of the NO + CO + O<sub>2</sub> Reaction over Rh(111)**, *H. Permana, D. N. Belton, S. J. Schmieg*, General Motors R&D, Warren, MI 48090-9055, and *K. Y. Simon Ng*, Wayne State University, Detroit, MI 48202.

The competition between NO and O<sub>2</sub> to be the oxidant for CO is one of the primary determinants of the amount of NO emitted from the catalytic converter of a passenger car. Because Rh is the most active NO reduction catalyst, we have an ongoing program to understand the NO reduction over Rh single crystal catalysts with a combination of moderate pressure reaction kinetics and UHV measurements of elementary steps. Previously we focused on the NO + CO reaction over Rh(111) and Rh(110) and demonstrated that reaction can be understood in some detail when we have reliable measurements of the rates of elementary steps. In this talk we present new kinetic measurements for the NO + CO + O<sub>2</sub> reaction over Rh(111) and show that the understanding we gained in the simpler NO + CO system extends quite readily to the more complex ternary mixture. Under our reaction conditions, addition of O<sub>2</sub> to the NO + CO mixture has no effect on the NO reduction rate, the N<sub>2</sub> and N<sub>2</sub>O formation rates, nor the NO and CO pressure dependencies. In addition, we find that O<sub>2</sub> is consumed with kinetics that are remarkably similar to those observed for the CO + O<sub>2</sub> reaction. We understand these kinetics to mean that the dissociative adsorption of oxygen is proceeding on the surface vacant sites that are left-over by the NO + CO reaction. Surface NO and N coverages are not affected by gas phase oxygen because the CO + O – CO<sub>2</sub> elementary step is so fast that surface O coverages remain quite low during the NO + CO + O<sub>2</sub> reaction. Qualitatively, our

results suggest that for the  $\text{NO} + \text{CO} + \text{O}_2$  system, both the  $\text{NO} + \text{CO}$  and  $\text{CO} + \text{O}_2$  reactions are occurring on the same surface with very little recognition that the other reaction is simultaneously occurring.

9:00 am **SS2-WeM3 A Model for Chaos in Oscillatory Surface Reactions: Pt(100)/NO + CO**, *G. Vesper\*, R. Imbuhl and A. Mikhailov*, Fritz-Haber-Institut der Max-Planck-Gesellschaft, Faradayweg 4-6, D-14195 Berlin (Dahlem), Germany.

The NO reducing reactions with CO or  $\text{H}_2$  on Pt(100) exhibit a number of similarities with respect to their dynamical behavior. Both reactions show sustained rate oscillations in the  $10^{-6}$  mbar range which take place on a largely hex-reconstructed surface, and both oscillatory systems display a period-doubling cascade into deterministic chaos. Rate oscillations in the NO + CO reaction take place on a macroscopically uniform surface, i.e. the different local oscillators are completely synchronised via the gas phase. We propose a model for the occurrence of deterministic chaos in both reactions which is based upon the breakdown of synchronization as the system becomes chaotic. The key feature of the model is the synchronization via a critical dependence of the  $1 \times 1 \rightleftharpoons \text{hex}$  phase transition on  $p_{\text{CO}}$  and  $p_{\text{NO}}$  leading to nonlinear growth kinetics of  $1 \times 1$ -islands. The resulting 3-variable model exhibits complex dynamical behavior due to the time delay between generation and dissolution of  $1 \times 1$ -islands. Since the equations have been constructed on the basis of experimental data, we consider them to be the first realistic model for the occurrence of deterministic chaos in oscillatory surface reactions.

(\*present address: Department of Chemical Engineering and Materials Science, University of Minnesota, Minneapolis, MN 55455)

9:20 am **SS2-WeM4 Particulate Cu on Ordered  $\text{Al}_2\text{O}_3$ : Reactions with Nitric Oxide and Carbon Monoxide**, *Ming-Cheng Wu, and D. Wayne Goodman*, Department of Chemistry, Texas A&M University, College Station, TX 77843-3255.

The growth of small Cu particles, prepared by vacuum vapor deposition, on  $\text{Al}_2\text{O}_3$  films on Mo(100) has been studied in the 80–800K temperature range with Auger electron spectroscopy (AES) and temperature programmed desorption (TPD). A model based on Auger measurements has been utilized to examine the number density and the average size of the Cu particles on  $\text{Al}_2\text{O}_3$ . Nitric oxide decomposition on the Cu particles has been further investigated using TPD and high resolution electron energy loss spectroscopy (HREELS). TPD and HREELS data clearly show that a fraction of NO molecules reacts with the Cu particles to produce gaseous  $\text{N}_2$  and  $\text{N}_2\text{O}$  in the 90–250K temperature range. The formation of  $\text{N}_2$  at 770K is also evident and is due to the recombination of adsorbed N atoms from NO dissociation. The effects of retained oxygen, adsorption temperature and particle size on the production of high-temperature  $\text{N}_2$  have been examined. The reaction between nitric oxide and carbon monoxide has also been studied. The results show that besides the  $\text{N}_2$  and  $\text{N}_2\text{O}$  products arising from NO decomposition, a small quantity of  $\text{CO}_2$  is produced by the reaction between adsorbed CO and adsorbed oxygen.

9:40 am **SS2-WeM5 The Effect of Oxidizing and Reducing Environments on the Regeneration of a Sulfur Deactivated Pd Foil Catalyst**, *Craig L. DiMaggio and Donald D. Beck*, General Motors NAO R&D Center, Warren, MI 48090-9055.

A Pd foil has been treated in a reactor cell/UHV chamber with  $\text{O}_2$ ,  $\text{H}_2$ , and  $\text{SO}_2$  in an attempt to understand the mechanism by which sulfur poisons the Pd metal in a catalyst and test the effects of oxidizing and reducing environments on regenerating the catalytic activity of the Pd. Results indicate the chemical state of the adsorbed surface sulfur to be zero valent and independent of treatment scheme. Auger measurements of the surface strongly suggest that the sulfur penetrates the surface at temperatures in excess of 300°C and then rediffuses out at temperatures above 500°C.

Although sulfur severely reduces the ability of the Pd catalyst to oxidize CO by blocking CO adsorption sites, the degree to which catalyst activity could be regained was dependent on the gas mix used during or after the  $\text{SO}_2$  exposure. Auger measurements show that lean environments during  $\text{SO}_2$  exposure maintain 50% to 75% of the CO adsorption activity while post exposure of a sulfur deactivated catalyst to  $\text{O}_2$  removes greater than 90% of the sulfur present at relatively low temperatures. Conversely, rich environments ( $\text{H}_2$ ) during  $\text{SO}_2$  exposure or post exposures to  $\text{H}_2$  were ineffective in removing more than 20% of the sulfur from the catalyst even though significantly higher temperature treatments were employed. This evidence supports the ob-

servation that a sulfur deactivated Pd foil under reducing conditions will not regain CO oxidation activity while oxidizing environments effectively remove sulfur and restore activity.

10:00 am **SS2-WeM6 Structural Effects of Well-Defined Palladium Surfaces on CO + NO Coadsorption and Reaction**, *Scott M. Vesecky, Xueping Xu, Peijun Chen and D. Wayne Goodman*, Department of Chemistry, Texas A&M University, College Station, TX 77843-3255.

The coadsorption of CO and NO has been studied on well-defined Pd particles supported on silica and alumina and compared with coadsorption data on low index single crystals. At low pressures ( $<10^{-6}$  Torr), temperature programmed reaction spectroscopy (TPRS) was used to study the desorption temperatures of the reactants (CO and NO) and the products ( $\text{CO}_2$ ,  $\text{N}_2\text{O}$  and  $\text{N}_2$ ). Under these conditions,  $\text{N}_2\text{O}$  production is strongly correlated to a high temperature (600 K) desorption feature. The concentration of this high temperature NO state and the rate of  $\text{N}_2\text{O}$  production increases with increasing Pd particle size (from 100–500 Å). At higher pressures (2–20 Torr), infrared reflection absorption spectroscopy (IRAS) was used to monitor the surface intermediate and gas phase product concentrations at thermal equilibrium. On the close-packed surfaces (Pd(111) and large ( $>100$  Å) Pd particles), a high temperature (600 K) NO surface state was again observed, which strongly correlates to the gas phase production of  $\text{N}_2\text{O}$ . On the lower coordination sites of Pd(100), Pd(110) and smaller Pd particles ( $<100$  Å), NO was found to be considerably less stable, with desorption occurring at 500 K under both high and low pressure conditions. The fact that  $\text{N}_2\text{O}$  production was practically negligible in comparison to  $\text{N}_2$  production on these low coordination sites has important implications for the design of Pd-only exhaust gas catalysts. The strong correlation between the low and high pressure data validates the comparison of UHV measurements with higher, more "realistic" adsorption and reaction conditions in these experiments.

10:20 am **SS2-WeM7 On the Kinetics of Methanation of CO on Nickel**, *I. Alstrup*, Haldor Topsøe Research Laboratories, Nymøllevej 55, DK-2800 Lyngby, Denmark.

A large number of macrokinetic models have in the past been suggested to account for experimental rates of CO methanation on nickel catalysts. However, it turns out that none of them can account for the published results obtained for nickel single crystal surfaces or foils. A set of microkinetic models with formation of carbon as an intermediate followed by stepwise hydrogenation of the carbon to methane is presented. Most of the parameters are determined from surface science experiments or from theoretical calculations. Agreement is obtained with the single crystal and foil results for a model with the hydrogenation of the  $\text{CH}^*$  surface intermediate as the rate controlling step. Analysis of this model shows that the surface is almost saturated by CO in the temperature range where the overall activation energy  $E_a$  of the reaction is approximately constant.  $E_a$  is mainly determined by the chemisorption energy of CO in this temperature region. The decrease of  $E_a$  at higher temperatures is mainly due to changes in the equilibrium constants of the hydrogen chemisorption and of the methyl formation step.

10:40 am **SS2-WeM8 Experimental and Numerical Study of OH Radical Distribution and Temperature above a Platinum Foil in  $\text{H}_2/\text{O}_2$  Mixtures**, *F. Behrendt<sup>1,2</sup>, F. Gudmundson<sup>1</sup>, B. Kasemo<sup>2</sup>, A. Rosén<sup>1</sup>*, <sup>1</sup>Department of Physics and <sup>2</sup>Department of Applied Physics, Chalmers University of Technology and University of Göteborg, S-412 96 Göteborg, Sweden.

During the last years the formation of water in catalytic reactions of  $\text{H}_2$  and  $\text{O}_2$  on a platinum foil in a flow reactor at pressures from 10 to 200 mTorr have been studied. The formation of water proceeds through dissociative adsorption of molecular hydrogen and oxygen giving hydrogen and oxygen atoms on the surface, which then recombine to OH radicals. The vast majority of OH radicals are consumed in the formation of water, but if the catalytic foil is kept at high temperature a minor fraction of them leave the surface where they can be detected using laser-induced fluorescence (LIF). The studies have given detailed information about surface reaction steps.

In this work a flow of hydrogen and oxygen of various compositions at a total pressures of 0.2–10 Torr is directed towards the foil, which is resistively heated to 1000–1400 K. Under steady-state conditions two-dimensional LIF (2D-LIF) is used to determine the distribution of OH radicals outside the heated platinum foil. The fluorescence light from OH radicals excited by an excimer pump dye-laser system is imaged with a two-dimensional intensified CCD camera, and is used

to determine relative concentration profiles and the temperature outside the foil.

A code to simulate laminar reactive stagnation point flows above catalytically active surfaces is applied to model the experiment. A detailed mechanism with elementary reactions is used to describe the gas phase reactions as well as a detailed mechanism for the surface reactions. The gas phase transport is described by a multicomponent transport model. The experimentally found spatial distribution of OH radicals and temperatures as function of the distance from the platinum foil are compared with numerical results. The results are found to be well predicted by the detailed model calculations.

## **NANO 3/NANOMETER-SCALE SCIENCE AND TECHNOLOGY/MANUFACTURING SCIENCE AND TECHNOLOGY**

**Room A209 - Session NSMS-WeM**

### **Industrial Applications of Scanned Probes**

**Moderator:** J. E. Griffith, AT&T Bell Laboratories.

8:00 am **NSMS-WeM0 Industrial Applications of Friction Force Microscopy**, J. Burger, A. Leijala, M. Binggeli and R. Christoph, Centre Suisse d'Electronique et de Microtechnique S.A. (CSEM), 2007 Neuchâtel, Switzerland.

Scanning probe microscopy has become a well established tool to enhance knowledge about nanometer scale properties of materials and has found applications in many fields of scientific interest. A new instrument developed at CSEM, the Atomic Scale Tribometer, is a very compact standalone force and friction microscope is being presented and its application to industrial problems, like surface characterization in general and questions of quality insurance in particular will be discussed. Due to the particular standalone design, our SFM/FFM is especially well suited to investigate samples under working conditions, i.e. realistic industrial environments as oils or other liquids (e.g. corrosive), or to investigate large samples as there is no need to scan the sample itself. A recently developed software module enables for the distinction of chemical heterogeneities on the sample surface by generating a friction histogram from the simultaneously acquired normal and lateral force data, thus providing further local analytical information on cleanliness and process yield. The characterization of surface roughness on bonding capillaries for microelectronics as well as nanotribological studies on SiC-Coatings and quantitative 3-dimensional measurements on prototype optical structures will be presented.

8:20 am **NSMS-WeM1 Industrial Applications of Proximal Probes**, H. Fuchs, Universität Münster, Physikalisches Institut, D-48149 Münster.

Proximal probe microscopies have displayed great versatility in analysing materials from a wide range of fields and with varied properties. The scanning force microscope not depending on electrically conducting surfaces is currently of special interest of many industrial applications such as surface roughness measurements, local friction and stiffness investigations. Its derivatives such as magnetic force microscopy will likely be developed as additional appropriate methods for industrial applications [1].

As compared to conventional surface analytical methods, AFM does not require any specific surface preparation techniques or vacuum conditions.

Examples for the industrial applications of proximal probes are given. The potential of novel techniques such as the scanning near field acoustical microscope (SNAM) and the scanning near field optical microscope (SNOM) for industrial applications are discussed.

**INVITED**

[1] SCANNING (topical issue) Vol. 15, 1993.

9:00 am **NSMS-WeM3 Lateral and Vertical Dopant Profiling in Semiconductors by Atomic Force Microscopy Using Conducting Tips**, P. De Wolf, T. Clarysse and W. Vandervorst, IMEC, Kapeldreef 75, B-3001 Leuven, Belgium, L. Hellemans and J. Snauwaert, Department of Chemistry, University of Leuven, Celestijnenlaan 200 D, B-3001 Leuven, Belgium.

The determination of the spatial distribution of charge carriers in semiconducting structures with an atomic force microscope (AFM) is presented. This new technique is based on the measurement of the spreading resistance of a conducting AFM tip on a sample as the tip is scanned over the surface. The advantage of this method is that it can be applied on the cross section of a device providing 1D (vertical) and 2D (lateral) profile information.

First, a detailed study was made regarding the properties of the tip (tip material and preparation, lifetime) and the evolution of I-V characteristics with pressure on uniformly doped silicon. From this work a model of the electric properties of the microcontact is emerging. It includes an Ohmic contribution to the overall resistance which is related to the plastically deformed area, and contributions from a Schottky barrier as well as from tunneling. Second, a calibration curve has been established by measuring on homogeneously doped substrates with varying resistivities. Finally, this method has been applied for junction delineation with 50 nm resolution and with sufficient sensitivity to encompass a dynamic range of concentrations between  $10^{14}$  and  $10^{19}$  at/cm<sup>3</sup>. These measurements were found to be in good agreement with those performed by the classical spreading resistance profiling technique.

9:20 am **NSMS-WeM4 Scanning Tunneling Microscopy/Spectroscopy Doping Determination of Si and GaAs Bulk Materials and Device Structures**, R. M. Silver, J. A. Dagata and W. Tseng, National Institute of Standards and Technology, Gaithersburg, MD 20899.

Scanning tunneling microscopy/spectroscopy (STM/S) of n- and p-doped bulk GaAs and Si was performed in *air and UHV* using recently developed passivation techniques to better understand the electronic nature of the passivated surfaces and air ambient STM [1]. The spectroscopic data, obtained over a range of doping densities for both Si and GaAs, is interpreted in a previously proposed model which includes thermionic emission, space-charge tunneling, and vacuum tunneling [2]. Here, we extend this work to an investigation of the electronic properties of GaAs pn-junction heterostructures and Si device structures using STM imaging and position-dependent current-voltage spectroscopy. These results can be well understood by including electronic tip-induced effects on the bulk pn-junction depletion characteristics and surface states. This complete treatment of bandbending correctly predicts the apparent pn-junction locations observed in the STM imaging mode and the current-voltage characteristics across the junction.

<sup>1</sup>J. A. Dagata, W. Tseng, J. Bennett, J. Schneir, and H. H. Harary, Appl. Phys. Lett. **59**, 3288 (1991).

<sup>2</sup>R. M. Silver, J. A. Dagata, and W. Tseng, J. Appl. Phys. Submitted.

9:40 am **NSMS-WeM5 Ultra-High Density Data Storage Based on Proximal Probes**, H. J. Mamin, B. Terris, S. Hoen, L. S. Fan and D. Rugar, IBM Research Division, Almaden Research Center, 650 Harry Road, San Jose, CA 95120.

Scanning probe microscopes have been used in a variety of ways to "write" on surfaces, on scales ranging from sub-micron down to the atomic. This technology thus forms an attractive approach to high density data storage, provided that some of the fundamental problems can be overcome. A number of formidable technical challenges must be met in order to produce a device with realistic data rate, error rate, and overall reliability. We will review a number of the modification techniques which have been demonstrated, and discuss their suitability for data storage. In particular, we will describe some techniques based on the atomic force microscope which appear to be among the most promising. We will also look at an alternative approach based on near-field optical recording with a high index solid immersion lens.

**INVITED**

10:20 am **NSMS-WeM7 Quantitative Dopant Profile Measurements on Si by Scanning Capacitance Microscopy**, Y. Huang and C. C. Williams, Physics Department, University of Utah, Salt Lake City, UT 84112 USA, J. Slinkman, IBM Microelectronics, Essex Jct., VT 05452 USA.

The direct measurement of local dopant profiles on a nanometer scale will benefit sub-micron semiconductor device design and simulation. Presently, a nanometer scale capacitance-voltage (C-V) method for the quantitative measurement of the dopant density distribution near a semiconductor surface is being established. An atomic force microscope is used to position a nanometer scale tip at a semiconductor surface, and local capacitance measurements are performed by a high-sensitivity capacitance sensor. The C-V measurements have been performed with tips of sub-50nm radius on test wafers in which the dopant

density varies laterally by more than four orders of magnitude in a region of 300 nm. The experimental SCM data was inverted to provide quantitative dopant density profiles. The inverted dopant profiles were compared with profiles obtained by process simulation. First order agreement was found between the SCM profiles and the simulation profiles.

10:40 am **NSMS-WeM8 Two-Dimensional Delineation of Semiconductor Doping by Scanning Resistance Microscopy**, *J. N. Nxumalo, D. Shimizu, C. Shafai, D. J. Thomson*, Department of Electrical and Computer Engineering, University of Manitoba, Winnipeg, Manitoba, R3T 5V6.

In order to meet the challenge of miniaturization of microelectronic devices on integrated circuits there is an increased demand for nanometer scale diagnostic tools for mapping out semiconductor doping profiles. We recently developed the scanning resistance microscope (SRM) as a nanometer scale technique for two dimensional delineation of P-N junctions [1]. The SRM utilizes a conducting probe to perform localized resistance measurements while scanning over a surface. Experimental results show that this technique can localize a P-N junction with a lateral spatial resolution of less than 35 nm. We will present images of surface polysilicon that demonstrate an artifact of the SRM technique where topographic features are coupled into resistance images. We will also be presenting results of SRM imaging of implant cross sections and silicon on insulator cross sections. In addition we will be presenting results from a new imaging technique that uses voltage modulation to maintain a constant current. This technique should overcome some of the limitations of the SRM and enhance the accuracy and dynamic range of the SRM technique.

1. C. Shafai and D. J. Thomson, *J. Vac. Sci. Technol. B* 12(1), Jan/Feb 1994.

## NANO 3/NANOMETER-SCALE SCIENCE AND TECHNOLOGY

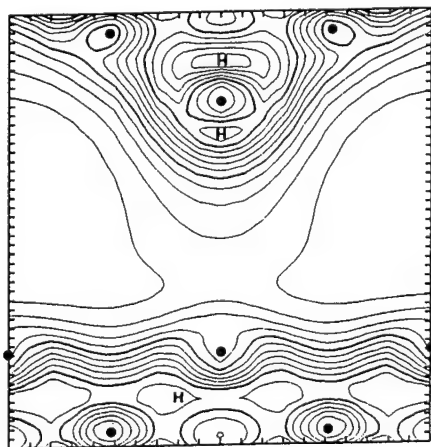
Room A207 – Session NS2-WeM

### Atomic Manipulation

**Moderator:** H. Tokumoto, Joint Research Center for Atom Technology, Japan, and L. J. Whitman, Naval Research Laboratory.

8:00 am **NS2-WeM0 Theory of Atom Extraction by the Scanning Tunneling Microscopy from the First-Principles Calculation**, *Kenji Hirose and Masaru Tsukada*, Department of Physics, University of Tokyo, Tokyo 113, Japan.

We present a method of the first-principles calculation of the electronic states under strong fields and currents. This method is effective for the bielectrode systems with atomic structure. A microscopic distribution of the fields and currents is calculated self-consistently with the electron density in the surface region. Here the method is applied to the problem of atom extraction by the tip.



The picture shows the electron density for the surface bias of +8V. It is found, when a bridge structure of the electron density is formed between the tip and the surface, a strong extracting force is acted on the top surface atom. This explains the extreme specificity of the extraction site found in the experiments.

8:20 am **NS2-WeM1 Investigation of the Mechanism for Removing Atoms from Si(001) Surfaces with the STM\***, *C. T. Salling and M. G. Lagally*, Univ. of Wisconsin-Madison, Madison, WI 53706.

We have used the scanning tunneling microscope (STM) to define regular crystalline structures as small as two atoms wide and one atom thick [1] by removing atoms from the Si(001) surface at small values of tip-sample separation (1–3 Å). Three types of features can result from an attempt to remove atoms [2]: a hillock, a hillock surrounded by a moat, or a pit. We have investigated the nature of the atom removal process by 1) measuring the probability of forming the three types of features as a function of voltage and tip-sample separation, 2) measuring the threshold voltage for forming a pit as a function of tip-sample separation, and 3) monitoring the piezo drive voltage and current during a removal attempt. At a tip-sample separation of 1.5 Å, we find that the most probable outcome is a hillock for low voltages, a hillock surrounded by a moat for higher voltages, and a pit for voltages at or above the threshold value. The threshold voltage is observed to increase with increasing tip-sample separation. The current during a removal attempt has been used to determine whether the atoms are transferred during or after the voltage pulse. We will use our results to evaluate possible mechanisms for atom removal, including chemically-assisted field evaporation [2] and simple thermal evaporation, and examine the hypothesis [2] that a bridge of atoms forms between the tip and sample as an intermediate state.

\*Research supported by the NSF and AFOSR.

[1] C. T. Salling and M. G. Lagally, submitted to *Science*.

[2] In-Wan Lyo and Ph. Avouris, *Science* 253, 173 (1991).

8:40 am **NS2-WeM2 Atomic-scale Modification on Si(111) 7×7 Surfaces**, *N. Liu, Q. J. Gu, Z. L. Ma, W. B. Zhao, X. Chu, Z. Q. Xue, S. Pang*, Beijing Laboratory of Vacuum Physics, Academia Sinica, Beijing 100080, P. R. China.

As silicon is a very important material, so nanometer-scale structure modification on silicon surfaces is essential in developing new quantum devices. To do so, reliable modification and manipulation techniques must be found. We present a method to manipulate atom clusters and single atoms on silicon surfaces using the scanning tunnelling microscope. With this method, we can remove a single atom at a predetermined site as well as deposit a single atom on a selected position. With this method, we can reproducibly scoop out nanometer-scale hollow lines (grooves), specially when it is along one of the three lattice elementary-vector-directions, the grooves appear a very regular structure, the linewidth can be easily controlled to be less than 1.5 nm. With this method we can routinely and alternatively create hollow lines (grooves) and protruding lines (ridges) on the Si(111) 7×7 reconstructed surface. We also give a detailed discussion about the mechanical principle of the process.

9:00 am **NS2-WeM3 Nanometer Scale Patterning of Silicon Surfaces with an Ultrahigh Vacuum Scanning Tunneling Microscope†**, *J. W. Lyding*, Department of Electrical and Computer Engineering and Beckman Institute, University of Illinois at Urbana Champaign.

Hydrogen passivation on silicon represents the simplest possible resist system for nanolithography experiments. We have achieved one nanometer resolution on the Si(100)-2×1:H monohydride surface by selectively desorbing hydrogen with an ultrahigh vacuum (UHV) scanning tunneling microscope (STM). The monohydride surface is prepared by exposing a heated sample (650K) to atomic hydrogen. This surface is structurally and chemically uniform and ideal for subsequent UHV-STM patterning. By operating the STM in field emission, the hydrogen passivation is selectively desorbed leaving behind atomically clean silicon. Depassivation occurs when the classical kinetic energy of the STM electrons exceeds the Si-H bond strength, and approximately 2×10<sup>6</sup> electrons are required to depassivate each silicon atom. The atomic hydrogen recombines to evolve as H<sub>2</sub>, preventing repassivation of previously patterned areas of the surface. Depassivation of individual atomic dimer rows is possible by this technique. Results will be shown that demonstrate the variations in patterning as functions of the electron energy and dose. The recovery of clean silicon after STM patterning is suggestive of many interesting possibilities for selective surface chemistry. We have demonstrated selective oxidation



of the patterned areas without degradation of the pattern resolution. Progress in applying these techniques to the nanofabrication schemes will also be presented.

INVITED

<sup>†</sup>Supported by the ONR URI under contract N00014-92-J-1519.

9:40 am **NS2-WeM5 Nanolithography with the STM on Si**, *N. Kramer, J. Jorritsma, H. Birk and C. Schönenberger*, Philips Research, Eindhoven, The Netherlands.

The STM has been used to locally oxidize hydrogen passivated silicon and hydrogenated amorphous silicon (a-Si:H). Oxide lines as narrow as 5 nm have been made on H-passivated Si. The oxide pattern acts as an etch mask. A proper choice of etch liquid enabled us to transfer 50 nm wide oxide lines 500 nm deep into the substrate; yielding trenches with a width below 50 nm and an aspect ratio > 10.

Oxide patterns can also be made in thin films of a-Si:H. a-Si:H clearly has the advantage that it can be deposited in very thin films (<20 nm) on almost any surface, this makes a-Si:H a resist suitable for many applications.

In addition to the STM patterning we studied the chemistry of electron induced oxidation. An UHV system was built that allowed us to expose a Si surface to electrons in an oxygen environment. Auger analysis revealed information about the oxide thickness as a function of electron energy and dose and the oxygen pressure.

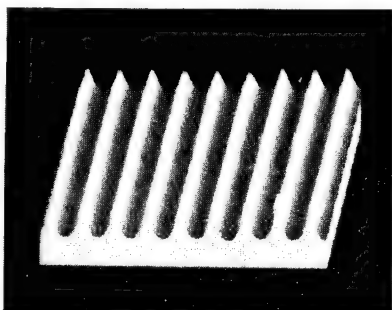
The direct patterning of oxide on Si is not only interesting for the fabrication of etch masks, many other applications are possible. The oxide patterns can form a mask for selective growth of metals with CVD or for the selective chemisorption of molecules.

10:00 am **NS2-WeM6 Local Deposition of Si on Si(111)(7×7) with the STM**, *H. Rauscher, U. Memmert, R. J. Behm*, Abteilung für Oberflächenchemie und Katalyse, Universität Ulm, D-89069 Ulm, Germany.

In search for a method to produce small artificial surface structures, the STM is used for direct local deposition of Si from a SiH<sub>4</sub> precursor on Si(111)(7×7). For material deposition, the tip is brought into the field emission regime and the emitted electron beam is utilized for direct proximal probe lithography at room temperature. The SiH<sub>4</sub> precursor gas is activated by electron bombardment from the STM tip with energies from 40 to 100 eV and emission currents of up to 100 nA. This produces local accumulation of the dissociation products on the surface just below the tip. Direct writing of nanostructures with lateral dimensions of down to 40 nm is accomplished. Structures with a height from ~3 Å (1 ML) up to ~50 Å have been produced. Deposition and imaging of the cracking products is carried out with the same tip. Possible deposition/activation mechanisms and the chemical nature of the deposited species will be discussed.

10:20 am **NS2-WeM7 Nanofabrication with Laser Focused Atomic Deposition**, *J. J. McClelland, R. E. Scholten, R. Gupta, and R. J. Celotta*, Electron Physics Group, National Institute of Standards and Technology, Gaithersburg, MD 20899 USA.

When an atomic beam passes through a laser beam, the optical field can act as a lens, focusing the atomic beam to a spot which can reach the nanometer scale. Such a laser-atomic lens can be used to focus atoms as they deposit onto a substrate, creating nanostructures. When the laser field is generated in an interference pattern, such as a standing wave, a large array of micro-lenses is created, each with dimension of the order of an optical wavelength. This arrangement allows massively parallel fabrication of nanostructures with potential dimensions of 10 nm or less. We have demonstrated this technique by focusing chromium atoms as they deposit onto a silicon substrate. A one-dimensional



AFM image of laser focused Cr lines

standing wave was used, and the resulting pattern is a series of lines with width 65 nm, spaced at 212.78 nm, covering an area of approximately 0.5 mm<sup>2</sup> (see figure). Future applications and extensions of this technique include two dimensional patterns, use of the chromium as an etch mask, and generalization to other atomic species and arbitrary patterns.

INVITED

\*Work supported in part by NSF grant PHY-9312572.

## APPLIED SURFACE SCIENCE Room A101 - Session AS-WeM

### Quantitative Analysis, Emphasizing Angle-Resolved XPS

**Moderator:** J. T. Grant, University of Dayton.

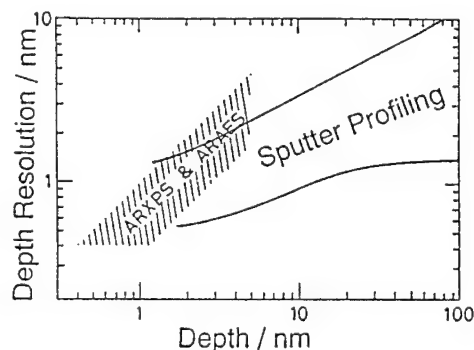
8:00 am **AS-WeM0 Depth-Profiling by Angle-Resolved XPS and AES; Elastic Scattering Corrections, and Intrinsic Limits on Depth-Resolution**, *P. J. Cumpson*, National Physical Laboratory, Teddington, UK.

Angle-resolved data has often been used to obtain information on variations of concentration with depth, down to about 5 nm below the specimen surface. For a decade this has been a successful method of measuring the thicknesses of overlayers, but a number of algorithms for the reconstruction of complete depth profiles have also been proposed. The usefulness of these methods is limited by the low information content of angle-resolved data; this is quantified, and used to show that the fractional depth-resolution in ARXPS or ARAES is limited to;

$$(\Delta z/z) \approx 0.8 \exp[\epsilon/8.9(n-1)^{1/2}]$$

where  $\epsilon$  is the %-precision of the peak intensities measured at  $n$  emission angles. It is shown how this limit can be improved by a factor of about 2 using *a priori* information which is justified for some specimens.

Elastic scattering leads to deviations from commonly used quantitation equations. Results of efficient Monte-Carlo calculations are used to define precisely the angular range for which these equations are reliable.



8:20 am **AS-WeM1 Assessment of Overlayer Thickness Determination Model by Controlled Monolayers**, *Bruce C. Beard<sup>a</sup>, and Robert A. Brizzolara<sup>b</sup>*, a) Akzo Novel, 1 Livingstone Ave., Dobbs Ferry, NY, 10522, b) Naval Surface Warfare Center, 10901 New Hampshire Ave., Silver Spring, MD 20903.

Thickness determination of carbonaceous overlayers on solid surfaces is of great importance for the quantitative analysis of x-ray photoelectron spectroscopy data. Several approaches can be taken for the determination of such overlayer thicknesses. In this discussion the C(1s)/C(KW) peak area ratio method will be evaluated. This approach depends on the difference in energy dependent inelastic mean free path of the two electron emission transitions to act as a measure of the overlayer thickness. A theoretical formalism was previously presented employing a ratio of the classic overlayer intensity equation:

$$I_x = I_0 N_x T(E_x) \lambda(E_x) \sigma_x L_x [1 - \exp\{-d/\sin \theta \lambda(E_x)\}]$$

Earlier investigators have found this formalism to poorly represent



experimental data. In this study self assembled overlayers of alkane thiols have been employed to more closely evaluate the potential sources for error in the theoretical expression. Thickness of the overlayers was determined by angle dependant XPS and confirmed with published ellipsometry values. These results also do not fall on the theoretically predicted curve. Evaluation of the theoretical formalism will be discussed in light of these results to provide an indication of the source of error and means for correction.

**8:40 am AS-WeM2 Inelastic Mean Free Pathlengths of X-Ray Photoelectrons for Quantitative Investigation of Technological Ultrathin Layers, Werner H. Gries,** Research and Technology Center, Deutsche Bundespost Telekom, P.O. Box 10 00 03, 64276 Darmstadt, Germany.

Angle-Resolved Self-Ratio X-ray Photoelectron Spectroscopy is being developed for the quantitative investigation of (disordered) technological ultrathin layers (this author, at previous AVS symposia and elsewhere). The thicknesses and stoichiometries of a succession of surface layers within a total depth of 10 nm can be derived from angle-dependent intensity measurements, provided (1) the layers are sufficiently dissimilar for each to give rise to at least one unique spectral line and (2) the inelastic mean free pathlengths (IMFP) of the characteristic x-ray photoelectrons are known for each material involved. The rather work-intensive procedure of evaluation has now been simplified to the extent that routine application to technological surfaces is possible. The major obstacle to quantitative interpretation, i.e. the lack of IMFP data for the great variety of technological materials, has been overcome by the introduction of a new universal predictive formula which allows IMFP to be predicted for all elements, atomic mixtures and compounds of varying stoichiometry found on technological surfaces. The formula has been derived on the basis of a recently published selection of IMFP data (Tanuma, Powell and Penn) as well as a large collection of stopping power data of charged particles from various sources.

**9:00 am AS-WeM3 Corrections to the Angle-resolved X-ray Photoelectron Spectroscopy with Consideration of the Solid Acceptance Angle, Wong Ka Wai and R. W. M. Kwok,** Department of Chemistry, The Chinese University of Hong Kong.

Angle-resolved X-ray photoelectron spectroscopy (ARXPS) is a non-destructive depth profile technique in which "lines" or "columns" of photoelectrons are assumed to be ejected from the sample. However, it is well known that "cones" of photoelectrons are actually collected and the cone is characterised by the so-called solid acceptance angle. As most scientists neglect this factor even in quantitative XPS analysis, the author found that there was an uncertainty of over 20% for the deduced thickness of SiO<sub>2</sub> overlayer in an ARXPS analysis on a SiO<sub>2</sub>/Si sample at three polar angles: 0°, 15° and 30°, and three solid acceptance angles (controlled by iris). Therefore the author derives a set of basic equations that describe the signal intensity detected from these "cones" in terms of acceptance angle, polar angle and the thickness of layers in multilayer structure. The aim is to improve the accuracy of the current ARXPS technique.

**9:20 am AS-WeM4 Variation of Effective Sampling Depths with Direction in Core Photoelectron Emission from Single Crystals, R. X. Yin<sup>a,b</sup>, R. E. Couch<sup>a</sup>, S. D. Ruebush<sup>a</sup>, S. L. Chamberlan<sup>a</sup>, S. Thevuthasan<sup>c</sup>, A. P. Kaduwela<sup>b</sup>, M. A. Van Hove<sup>b</sup>, C. S. Fadley<sup>a,b</sup>,** <sup>a</sup>Physics Department, U.C. Davis, Davis, CA 95616, <sup>b</sup>MSD, Lawrence Berkeley Laboratory, Berkeley, CA 94720, <sup>c</sup>MSRC, Pacific Northwest Laboratories, Richland, WA 99352.

We have studied theoretically the variation of effective sampling depths with direction for core photoelectron emission from single crystals, including the effects of isotropic inelastic scattering and single and multiple elastic scattering with real and complex phase shifts. Our calculations were carried out for emission in the 1 keV energy range on both simple chains of atoms embedded in an isotropic inelastic medium, and on larger atomic clusters that should more realistically simulate emission from a semi-infinite single-crystal substrate or epitaxial overlayer. The mean emitter depth is found to vary by as much as ±30% with direction, being lowest just adjacent to low-index chains of atoms because of destructive interferences in photoelectron diffraction, and highest along low-index directions due to forward scattering, in spite of well-known reductions in intensity along such directions due to multiple-scattering defocussing effects. These variations of effective sampling depths due to photoelectron diffraction effects (as well as analogous Auger diffraction effects) thus should be taken into account in the quantity analysis of surfaces and surface concentration profiles using photoelectrons and Auger electrons.

**9:40 am AS-WeM5 A Novel Algorithm for Quantitative Elemental Depth Profiling by Angle-Resolved XPS, John M. Williams and Thomas P. Beebe, Jr.,** Dept. of Chemistry, University of Utah, Salt Lake City, Utah, 84112.

We have developed an algorithm for analysis of angle-resolved x-ray photoelectron spectra (ARXPS) that allows quantitative depth profiling of the surface elemental composition with *atomic resolution*. This method has non-destructively yielded valuable new information about adsorbate bonding and conformation for several of the chemical systems listed below, permitting adsorbate modeling at the atomic level. The computation implements a profile-smoothing search, gives error limits on the profiles, and requires only minutes on a 33-MHz processor. The method is capable of computing at least six simultaneous elemental profiles, is robust to as much as 10% experimental error, and performs well even under unfavorable conditions such as patchy overlayers, complex organic adsorbates (such as DNA), and trace elemental quantities (<10%). The depth profiles obtained for Cu on Ru(0001), and for sulfur-modified DNA, Cl(CH<sub>2</sub>)<sub>3</sub>SH, and cystamine adsorbed onto Au(111) show close correspondence to scale molecular models and to expected elemental percentages for the surface structure. The algorithm also has verified depth profiles from other researchers on other chemical systems.

**10:00 am AS-WeM6 A Comparison of XPS Quantitation using Electrostatic and Magnetic Lens-Based Analyses, D. J. Surman and A. R. Walker,** Kratos Analytical Inc., 535 E. Crescent Ave., Ramsey, NJ 07446, and T. A. Zupp, J. Lucacs, L. Paleudis, B. J. Tielsch, and J. E. Fulghum, Chemistry Department, Kent State University, Kent, OH 44242.

Magnetic immersion lenses have not, until recently, been incorporated into X-ray photoelectron spectrometers. These lenses do, however, overcome the limitations of electrostatic lens-based systems for small area analysis and imaging. The spherical aberrations that provide a practical limit of low magnifications and collection angles in electrostatic lenses are minimized by magnetic immersion lenses, which provide large magnifications and collection angles. This results in a dramatic improvement in sensitivity from small analysis areas.

An important aspect of X-ray Photoelectron Spectroscopy, (XPS), is the ability to obtain quantitative information. Previous work evaluating spectrometer transmission functions in order to improve quantification has focussed on spectrometers incorporating only electrostatic lenses. This paper will compare XPS data acquired using both electrostatic and magnetic lenses on the same instrument. The results demonstrate that operation of the spectrometer with either the electrostatic or magnetic lens results in a similar transmission function, and that qualitative results are easily obtainable from small analysis areas using a magnetic immersion lens. The discussion will also illustrate quantitative imaging XPS.

**10:20 am AS-WeM7 Quantification in Molecular SIMS, B. Hagenhoff, K. Meyer, M. Deimel, D. Rading, W. Sichtermann, and A. Benninghoven,** Physikalisches Institut der Universität, Wilhelm-Klemm-Str. 10, D-48149 Münster, Germany.

In the last years TOF-SIMS has been proven to be a suitable tool for the qualitative characterization of molecular species with high surface sensitivity. However, quantification in molecular SIMS is difficult because of the dependence of secondary ion yields (transformation probabilities) on the chemical composition of the sample surface. This matrix effect is determined by the nature of the surface species considered and by its chemical environment (matrix, substrate). Nevertheless, quantification can be realized by three different procedures. The application of 1. additional quantitative surface analytical techniques (e.g. XPS, Laser-SNMS), 2. external standards, and 3. internal standards.

We applied these calibration techniques to a variety of organic molecules (e.g. cyclosporin and steroids), several functional groups on polymers (e.g. OH), self assembling layers (e.g. binary mixtures of different thiols on Au), etc.

Our investigation reveal that the application of internal standards—a well established technique in general mass spectrometry—is most valuable for molecular SIMS. Not only isotopically labelled molecules but also chemically similar molecules could be applied successfully as internal standards.

Examples for molecular quantification, in particular for organic molecules, will be presented in detail.

**10:40 am AS-WeM8 Simultaneous Dual-Element Analyses of Platinum-Group Elements in Natural Occurring Matrixes using Resonance Ionization of Sputtered Atoms,\* W. F. Calaway,<sup>1</sup> R. C. Wiens,<sup>2</sup>**

D. S. Burnett,<sup>2</sup> D. M. Gruen,<sup>1</sup> and M. J. Pellin,<sup>1</sup> <sup>1</sup>Argonne National Laboratory, Argonne, IL 60439, <sup>2</sup>California Institute of Technology, Pasadena, CA 91125.

The combination of secondary neutral mass spectrometry (SNMS) and resonance ionization spectroscopy (RIS) has been shown to be a powerful tool for the detection of low levels of elemental impurities in solids. Drawbacks of the technique have been the laser-repetition-rate-limited low duty cycle of the analysis and the fact that RIS schemes are limited to determinations of a single element. These problems have been addressed as part of an on going program to explore the usefulness of RIS/SNMS instruments for the analysis of naturally occurring samples. Efficient two-color/two-photon resonance ionization schemes were identified for five platinum-group elements (Mo, Ru, Os, Ir, and Re). Careful selection of the ionization schemes allowed Mo or Ru to be measured simultaneously with Re, Os, or Ir using two tunable dye lasers and a XeCl excimer laser. Resonance frequencies could be switched easily under computer control, so that all five elements were analyzed while removing less material than the depth resolution of ion sputtering methods (~1 nm). Quantitative measurements of these elements in metal grains of five meteorites at sub-ppm levels were determined. Detection limits were calculated from the sensitivity of each element and the background signal. From the analyses, estimates of the accuracy and precision our RIS/SNMS instrument were determined.

\*Work supported by the U.S. Department of Energy, BES-Materials Sciences, under Contract W-31-109-ENG-38 (ANL).

## PLASMA SCIENCE

### Room A109 - Session PS-WeM

#### Plasma Diagnostics

**Moderator:** S. C. McNevin, AT&T Bell Laboratories.

**8:00 am PS-WeM0 Laser-Induced Thermal Desorption as an *in situ* Surface Probe During Plasma Processing of Si, I. P. Herman,<sup>(a)</sup> C. C. Cheng, K. V. Guinn, and V. M. Donnelly,** AT&T Bell Laboratories, Murray Hill, NJ 07974.

Laser-induced thermal desorption (LITD) is used to detect adsorbates in real time during plasma processing. The steady-state surface layer formed during etching of Si(100) in a helical resonator is examined with Cl<sub>2</sub>, HBr, Cl<sub>2</sub>/O<sub>2</sub>, and Cl<sub>2</sub>/HBr gases. During Si etching by Cl<sub>2</sub>, pulsed XeCl excimer laser irradiation of the surface produces transient heating and thermal desorption of SiCl. The desorbing products can be detected by either laser-induced fluorescence (LIF) excited by the same pulse or by plasma induced emission resulting from electron impact excitation. LIF analysis provides time-resolved measurements on a scale that is less than the time required to etch one monolayer, and has been used to show that the surface layer formed during plasma etching of Si by Cl<sub>2</sub> remains essentially unchanged after processing, so post-processing XPS analysis probes a layer that is representative of the real-time processing conditions. Supportive XPS measurements are also presented. Using this LITD technique, the steady-state surface layer during chlorination is observed to contain twice as much chlorine and to be more weakly bound when the plasma is on *vis-a-vis* when the plasma is turned off. Near typical operating conditions, the Cl coverage depends weakly on discharge power, substrate bias voltage, and pressure, which suggests that ion flux, and not neutral etchant flux (i.e., Cl and Cl<sub>2</sub>) apparently still limits the etch rate, even in a high-density, low pressure plasma. Competitive chlorination/bromination of the surface layer during etching by Cl<sub>2</sub>/HBr mixtures is also probed, by comparing LIF by desorbed SiCl and SiBr.

<sup>(a)</sup>Also with the Department of Applied Physics, Columbia University, New York, NY; IPH was supported in part by the Petroleum Research Fund administered by the ACS.

**8:20 am PS-WeM1 Transport of Ions through High Aspect Ratio Apertures: Simultaneous, High Resolution Measurement of Angular and Energy Distribution Functions, Bertrand Quiniou,** Lawrence Livermore National Laboratory, Livermore, CA, **Eray S. Aydil,** University of California, Santa Barbara, CA, **Lloyd Harriott, Jeffrey A.**

**Gregus, and Richard A. Gottscho,** AT&T Bell Laboratories, Murray Hill, NJ 07974.

The transport of ions through high aspect ratio features is an important element in controlling rate and linewidth in sub-micron etching for ULSI applications. Not only the incident ion angular and energy distributions, but also the modification of these distributions by sidewall scattering are important considerations.

We report the study of ion transport through micron-size apertures as a function of aspect ratio. Argon ions are produced in a 13.56 MHz excited helicon plasma. After passing through a gridded analyzer that provides energy resolution of 1 eV, ions impact a microchannel plate which creates a spatially resolved electron avalanche. The electrons are then accelerated to a phosphor screen and the resultant phosphorescent pattern is imaged onto a CCD camera to provide simultaneous angular resolution of 0.2°. Ion energy and angular distribution functions are measured as a function of rf power, Ar pressure, axial magnetic field strength, and aperture aspect ratio. The ion energy distributions in the absence of applied rf bias exhibit either a sharp single peak or a bimodal structure. The origin of the bimodal structure is discussed along with the dependence of the distribution functions on aspect ratio.

**8:40 am PS-WeM2 Measurement of the Electron Energy Distribution Function with a Differentially Pumped Spherical Sector Electrostatic Energy Analyzer, Ken D. Schatz, David N. Ruzic,** University of Illinois, Urbana, IL 61801.

The fundamental information about a plasma is contained within its electron energy distribution function (EEDF). Typically the EEDF is derived from Langmuir probe measurements by taking the first or second derivative of the probe electron current versus voltage data. Several difficulties are inherent with this scheme, including, smoothing and fitting of data prior to differentiating, subtraction of ion current, and accounting for a drifting EEDF. A diagnostic which avoids these difficulties is the spherical sector energy analyzer. This type of energy analyzer is energy discriminating rather than energy integrating as is the Langmuir probe.

The diagnostic apparatus samples the plasma through a 100. micron diameter pinhole into a differentially pumped diagnostic chamber. The energy analyzer, located within the low pressure, ~10E-5 Torr, diagnostic chamber, records electron collection rates with an energy resolution of ~1. eV around the detection energy. Also the potential of the 6. mm diameter pinhole disk is adjustable, and disk voltage and current are recorded. This feature allows the pinhole to be biased at plasma potential and so remove the effects of the sheath as much as possible from in front of the pinhole.

Results are presented for the EEDF of an electron-beam sustained discharge in 100. to 400. mTorr of Helium. The discharge, powered by the combination of an electron beam and DC electric field, is measured to produce plasmas with electron temperatures between 0.2 eV and 5. eV and interesting, non-maxwellian, beam effects are observed. Also, deviation of the EEDF from a simple inverse exponential at energies corresponding to excitation and ionization thresholds is observed. A comparison is made with Langmuir probe data for the same discharge conditions.

**9:00 am PS-WeM3 Applications of Real Time Ellipsometry for Characterizing Etch Profiles in Sub-Micron Features, Nadine Blayo, A. Grevoz, J. T. C. Lee, and D. E. Ibbotson,** AT&T Bell Laboratories, Murray Hill, NJ 07974.

Microelectronics processing of ULSI devices, which incorporate thin films and sub-micron design rules, requires sensitive diagnostic techniques to achieve tightly controlled processes. Wafer film thickness and etch profiles are commonly characterized by post-process or destructive techniques such as cross-sectional scanning electron microscopy. *In situ* spectroscopic ellipsometry is a preferable diagnostic because of its sensitivity and compatibility with plasma processing environments, but until recently was thought to require a sacrificial section of unpatterned wafer, which could provide film thickness, but not etch profile information. We show, that with careful analysis, ellipsometry can be used to distinguish between undercut, tapered and vertical sidewall profiles, and thus provide real time information about multilayer stack etching and film thicknesses without the use of the sacrificial pad. To assist in distinguishing etch profiles, *in-situ* UV-visible spectroscopy is collected in addition to the real time ellipsometry. We discuss the sensitivity of the technique to detect changes in linewidth and wall angle and present different models to understand how the ellipsometric traces relate to the etch profiles and line features.

9:20 am **PS-WeM4 Spatial Distribution of Argon Metastables in RF Plasmas Measured by 2-D LIF Imaging**, *B. K. McMillin and M. R. Zachariah*, National Institute of Standards and Technology, Gaithersburg, MD 20899.

The time-averaged spatial concentration distribution of the argon ( $1s_5$ ) metastable in pure argon and argon/ $CF_4/O_2$  rf plasmas, generated in a parallel-plate, asymmetric discharge, have been studied using planar laser-induced fluorescence imaging. This metastable state was examined with reactor gas pressures ranging from 100–1000 mT and applied rf voltages from 75–300 V. The measurements were obtained using pulsed, laser-sheet excitation of the  $1s_5-3p_2$  transition at 394.9 nm and right angle detection of the fluorescence (at 418 and 433 nm) with an intensified, cooled CCD camera. The fluorescence signals were corrected for the excited state quenching, based on the observed fluorescence lifetime at each condition. The imaged region covered one-half of the discharge, extending from the centerline to ~1 cm beyond the edge of the electrodes.

In general, the measurements indicate that the metastable density increases with pressure and, to a lesser extent, with applied voltage. At a given pressure, significant radial variations in the metastable concentration are observed, with the peak occurring near the outer edge of the plasma. While radial variation in the metastable density is observed at all conditions examined, it is most pronounced at the lower applied voltages where the variations are as high as 50%. Significant axial variations in the metastable density are observed as well. For example, as the pressure is increased from 100–1000 mT, the distribution changes from a parabolic type profile, with a peak at the discharge center, to one in which the metastables peak sharply near the glow/sheath interface of the powered electrode. By providing two-dimensional spatial distributions and the relative concentrations of the argon ( $1s_5$ ) metastable state over a range of discharge conditions, these results provide insight into the uniformity of these plasmas and valuable data for the validation of 2-D plasma processing models.

9:40 am **PS-WeM5 Diagnostics and Control of Radicals in an Inductively-Coupled Etching Reactor**, *H. Sugai,<sup>a</sup> K. Nakamura,<sup>a</sup> Y. Hikosaka,<sup>b</sup> M. Nakamura,<sup>b</sup>* <sup>a</sup> Nagoya University, Nagoya 464-01, Japan; <sup>b</sup> Process Development Division, Fujitsu Ltd., Kawasaki 211, Japan.

Advanced high-density etching reactors such as ECR, helicon and ICP (inductively coupled plasma) have common problems of irreproducibility and a low etch selectivity of  $SiO_2$  to Si. Lack of information on radical behaviors have hindered from understanding and controlling the high-density plasma etching. In this paper, we report comprehensive measurements of ionic and neutral radicals in a fluorocarbon ICP, together with an innovative radical control based on a reactor temperature and/or pulse modulation. Neutral radical  $CF_m$  ( $m = 1-3$ ) is detected by appearance mass spectrometry and F atom by an actinometry technique. The measured densities and surface loss probabilities are presented in comparison with a low-density high-pressure CCP (capacitively coupled plasma). The most abundant ionic species is  $CF^+$  in the ICP and  $CF_3^+$  in the CCP. The density of F atom is an order of magnitude higher in the ICP than in the CCP while the densities of  $CF_m$  radicals are lower in the ICP than in the CCP. The high etching rates and low selectivity of  $SiO_2$  to Si observed in the ICP are tentatively attributed to numbers of F atoms with less  $CF_m$  radicals. In order to control the radical composition of ICP, the reactor vessel was heated up to 100–200°C. The measurement revealed a drastic increase in the  $CF_m$  densities with the F atom density almost unchanged. As a result, a high etch selectivity of  $SiO_2/Si$  was obtained in the hot ICP reactor. Another possibility of radical control by a pulse modulation will be presented. **INVITED**

10:20 am **PS-WeM7 The Third Peak in 'Bimodal' Ion Energy Distributions**, *D. Vender, R. J. M. M. Snijkers, G. M. W. Kroesen and F. J. de Hoog*, Eindhoven University of Technology, PO Box 513, 5600 MB Eindhoven, The Netherlands.

The energy distribution of ions exiting a plasma through an rf modulated sheath is important in many surface processing applications, and also as a plasma diagnostic. As is well known, when the rf excitation frequency lies between the ion and electron plasma frequencies, the collisionless energy distribution is made up of two peaks (the so-called 'bimodal' distribution) at energies related to the amplitude of the rf modulation and the ion transit time across the sheath. We have measured almost collisionless, mass-resolved ion energy distributions in a 13.56 MHz rf plasma at very low pressures (5 to 20 mTorr) and compared the results to numerical simulations of ion loss in both model and self-consistently obtained electric fields. Contrary to expectation, the distributions of light minority species (such as He<sup>+</sup>

in a mixture of Ar + 8% He) clearly show the presence of a third peak. The simulations are used to study the genesis of this third peak and its dependence on the plasma and sheath parameters. The results support the conclusion that the third peak is a direct indication of the Bohm velocity of the ions entering the sheath. The measurement of its position can thus be a valuable diagnostic of the plasma sheath and presheath. Results from both electropositive and electronegative plasmas (obtained by mixing a few percent  $CF_4$  with Ar) are discussed and a previously unexplained feature of collisionless ion energy spectra is clarified.

10:40 am **PS-WeM8 Monitoring InP and GaAs Etched in  $Cl_2/Ar$  Plasma Generated by Electron Cyclotron Resonance Source Using Optical Emission Spectroscopy**, *S. Thomas III, K. K. Ko, and S. W. Pang*, Department of Electrical Engineering and Computer Science, The University of Michigan, Ann Arbor, Michigan 48109-2122.

Optical emission spectroscopy (OES) has been shown to be a valuable tool for monitoring the etching of III-V materials. This non-invasive in-situ diagnostic can be related to the etch rate, surface morphology, and end point. A  $Cl_2/Ar$  plasma generated by an electron cyclotron resonance (ECR) source is used for the etching of InP and GaAs since it can provide low surface damage. Additionally, there is no polymer deposition when  $Cl_2/Ar$  is used compared to  $CH_4/H_2$ , and the process is more controllable and reproducible.

110  $\mu m$  deep, 30  $\mu m$  wide via holes in InP have been etched with  $Cl_2/Ar$  discharges. The etch rate is ~3  $\mu m/min$  and a vertical profile with smooth morphology is obtained. Etching should be stopped at a 40 nm thick Ti layer to prevent sputtering of the underlying Au which can cause device failure and contamination. Therefore, end point detection using OES is essential. It is found that the optical emission signals for In at 410.2 and 451.1 nm can be used to monitor the end point.

For GaAs etching, the optical emission signal for Ga at 417.1 nm shows close correlations with changes in the etch rate for varying microwave power, rf power,  $Cl_2$  percentage in Ar, and pressure. For example, the Ga signal increases 9x for 5%  $Cl_2$  addition to Ar which results in 8x increase in etch rate. The response time for the increase in Ga signal is found to be <5 sec. Monitoring the Ga signal as a function of time, the etching of surface oxide can be detected and the removal rate is found to increase with ion energy. The sensitivity of OES will be investigated for controlling via hole etching in InP and emitter etching for heterojunction bipolar transistors and the results will be compared to mass spectrometry.

## **SURFACE SCIENCE/ELECTRONIC MATERIALS Room A102 – Session SSEM-WeM**

### **Semiconductor Surface Reactions I**

**Moderator:** K. Raghavachai, AT&T Bell Laboratories.

8:00 am **SSEM-WeM0 Structure Sensitivity of Trimethylgallium Chemisorption on GaAs Surfaces**, *J. Randall Creighton*, Org. 1126, MS 0601, Sandia National Laboratories, Albuquerque, NM 87185-0601.

Compound semiconductor deposition by metal organic chemical vapor deposition (MOCVD) and atomic layer epitaxy (ALE) often exhibits a marked structural sensitivity, i.e. a large variation in growth rate for different surface crystallographic orientations. We have investigated the chemisorption and reactivity of trimethylgallium (TMGa) on non-polar (i.e. [110]) and polar (i.e. [100] and [111]) surfaces of GaAs and found significant differences in behavior. Surface infrared spectroscopy and static-SIMS were used to examine the surface intermediates formed during TMGa dissociation, while TPD was used to monitor the overall reaction pathway. Results indicate that the dominant factor in determining reactivity is the presence or absence of atom vacancies at the surface. The polar (111) and (100) surfaces generally reconstruct into structures with intrinsic vacancies or ad-atoms, whereas the (110) surface is stoichiometric. During TPD a significant fraction (10–30%) of a monolayer of TMGa chemisorbs irreversibly on the gallium-rich (100) and (111)A surfaces, evolving methyl radicals at 705 and 730 K, respectively. In contrast, there is a complete lack of methyl radical desorption from the (110) surface. Although TMGa chemisorbs strongly on the (110) surface, the process is reversible and virtually all of the TMGa desorbs at 400 K during

TPD. Apparently the gallium atom vacancies intrinsic to the (100) and (111)A reconstructions offer a convenient site for the gallium atom to occupy during TMGa dissociation, while the stoichiometric (110) surface has no atom vacancies and cannot accommodate the extra gallium atoms into a stable surface structure.

8:20 am **SSEM-WeM1 Molecular Beam Scattering as a Probe of Thin Film Deposition Processes**, *J. R. Engstrom*, School of Chemical Engineering, Cornell University, Ithaca, NY 14853.

Supersonic molecular beam scattering techniques have been employed to examine the prerequisite reaction to the deposition and growth of thin films: dissociative chemisorption. Concerning the reactions of  $\text{Si}_2\text{H}_6$  and  $\text{SiH}_4$  on clean Si surfaces we have found that incident translational energy ( $E_{tr}$ ) and incident angle ( $\theta_i$ ) are the dominant variables controlling the probability of dissociative chemisorption,  $S_R$ . In addition, these variables couple so as to produce a single universal relationship between  $S_R$  and a scaled kinetic energy given by the quantity  $E_{tr}\theta_i(\theta_i/\alpha)$ , where the dimensionless quantity  $\alpha$  can be associated with surface microcorrugation. In the case of  $\text{Si}_2\text{H}_6$ , the dissociation pathway is also sensitive to the surface structure. For example, a surface-induced pyrolysis reaction,  $\text{Si}_2\text{H}_6(g) \rightarrow \text{Si}(a) + \text{H}_2(g) + \text{SiH}_4(g)$  is observed on  $\text{Si}(111)-(7 \times 7)$ , whereas it is completely absent on the  $\text{Si}(100)$  and  $\text{Si}(111)-(1 \times 1)$  surfaces. Our most recent work concerns similar studies of organosilanes (e.g.,  $\text{SiH}_3\text{CH}_3$ ) on Si and SiC substrates, and work examining a dopant precursor,  $\text{PH}_3$ . Concerning the reaction of  $\text{PH}_3$  on clean Si we find for  $E_{tr}$  as large as 0.8 eV that a precursor-mediated dissociation mechanism is operative. The effect of  $\text{PH}_3$  on the reactions of  $\text{SiH}_4$  and  $\text{Si}_2\text{H}_6$  has also been examined. We find that for all incident translational energies examined adsorbed P acts to inhibit chemisorption of both silanes in a sub-linear fashion, i.e.,  $S_R = S_{R,0}(1 - \theta_P)^n$ , where  $n < 1$ , and  $\theta_P$  is the fractional coverage of P(a). Adsorbed P(a) is also observed to influence the dissociation pathway for  $\text{Si}_2\text{H}_6$  on  $\text{Si}(100)$ , where at finite values of  $\theta_P$ , a  $\text{SiH}_4(g)$  production channel is operative.

#### INVITED

9:00 am **SSEM-WeM3 GaF<sub>3</sub> Thin Films Grown on GaAs via Exposure to XeF<sub>2</sub>**, *W. C. Simpson, P. R. Varekamp and J. A. Yarmoff*, Department of Physics, University of California, Riverside, CA 92521, and Materials Sciences Division, Lawrence Berkeley Laboratory, Berkeley, CA 94720.

A study of the interaction of atomic F (via  $\text{XeF}_2$ ) with GaAs(110) and (100) has been carried out, employing soft x-ray photoelectron spectroscopy (SXPS), photon and electron stimulated desorption (PSD and ESD) and electron energy loss spectroscopy (EELS). It is found that the fluorination of GaAs results in the formation of a thin film of  $\text{GaF}_3$ , which is a  $\sim 10$  eV band gap insulator. This is a simple chemical process for growing an insulator on GaAs, (similar to how  $\text{SiO}_2$  is grown on Si via exposure to  $\text{O}_2$ ) and thus has potential technological importance, motivating further study of  $\text{GaF}_3$  films grown in this manner.

From the results of this work, a model of the film growth mechanism is proposed and the nature of the film/substrate interface is discussed. In addition, the electronic structure of  $\text{GaF}_3$  films are investigated. It is found that, once the films reach a thickness of  $\sim 10$  Å, they acquire the electronic characteristics of bulk  $\text{GaF}_3$ . From SXPS and EELS measurements, the band-gap of the films and the band line-up of the films with the substrate are determined. From the PSD data, absorption spectra of the  $\text{GaF}_3$  films are obtained, which provide information on the unoccupied density of states.

9:20 am **SSEM-WeM4 Initial Stages of Phosphorous Desorption from InP(110) Surfaces**, *Ph. Ebert<sup>a</sup>, M. Heinrich<sup>b</sup>, M. Simon<sup>b</sup>, K. Urban<sup>b</sup>, M. G. Lagally<sup>a</sup>*, <sup>a</sup>University of Wisconsin, Madison, WI 53706; <sup>b</sup>Institut für Festkörperforschung, Forschungszentrum Jülich GmbH, D-52425 Jülich, Germany.

The initial stages of phosphorous desorption from InP(110) surfaces were investigated quantitatively on the atomic scale as a function of the duration of thermal treatment in a temperature range between room temperature and 200°C. The measurements were performed using a scanning tunneling microscope to investigate in particular the phosphorous monovacancies created during the thermal treatments. The formation rate of the P vacancies increases up to 160°C. Above 160°C the formation rate decreases. This non-Arrhenius behavior is explained by the interaction of two thermal processes, a vacancy-adatom pair formation, creating vacancies, and a P segregation from the bulk toward the surface, annihilating vacancies. The evaporation of P itself occurs through diffusion of P adatoms along the surface

and formation of  $\text{P}_2$  molecules, which immediately desorb. A saturation of the vacancy density is observed and explained by a charge-induced repulsion between vacancies.

\*P. E. thanks the Humboldt Foundation for a Lynen Research Fellowship. Permanent address: Institut für Festkörperforschung, Forschungszentrum Jülich GmbH, D-52425 Jülich, Germany.

9:40 am **SSEM-WeM5 Interaction of 50 eV Electrons with D<sub>2</sub>O on GaAs(100): Electron and Thermal Induced Oxidation**, *Derrell W. Sloan, Yang-Ming Sun, and J. M. White*, Department of Chemistry and Biochemistry, University of Texas at Austin, Austin, TX 78712.

The interaction of 50 eV electrons with  $\text{D}_2\text{O}$  on GaAs(100) has been investigated using temperature programmed desorption (TPD), x-ray photoelectron spectroscopy (XPS), and high resolution electron energy loss spectroscopy (HREELS). The interest in this study was to determine if an oxide layer could be produced on a semiconductor surface by a nonthermally activated pathway.  $\text{D}_2\text{O}$  adsorbs molecularly on GaAs(100) at  $\sim 100$  K as indicated by XP spectra that show an O(1s) binding energy of 534 eV. Substantial hydrogen bonding at submonolayer coverages is seen in both TPD and HREELS results. Electron irradiation induces both desorption and dissociation of  $\text{D}_2\text{O}$  forming OD, O, and D. XP spectra taken after electron irradiation show that the O(1s) binding energy shifts to 532 eV and broadens. HREEL spectra show that hydrogen bonding as well as  $\text{D}_2\text{O}$  bending decreases after electron irradiation. These results are consistent with molecular desorption and dissociation leaving OD, O, and D. Flashing to 600 K following electron irradiation removes OD and D leaving an oxide surface as indicated by an O(1s) binding energy of 530 eV and the loss of all  $\text{D}_2\text{O}$  and OD features in the HREELS spectrum. The results indicate that electron irradiation can produce an oxide but not a clean oxide layer. D and OD that remain on the surface after electron irradiation must be removed thermally.

10:00 am **SSEM-WeM6 Characterization of Silicon Surfaces and Interfaces by Vibrational Spectroscopy**, *Y. J. Chabal, M. A. Hines and D. Feijoo*, AT&T Bell Laboratories, Murray Hill, NJ 07974.

The understanding of chemical reactions at silicon surfaces and interfaces required spectroscopic characterization of the chemical species (reactants, reaction products and intermediate species). We consider here the various techniques available (Infrared Absorption, Raman and Sum-frequency spectroscopies as well as Electron Energy Loss Spectroscopy) for the study of etching and bonding of silicon wafers.

Etching plays a key role in wet chemical processing, including chemo-mechanical polishing. The use of aqueous fluorine etch lead to a termination of silicon surfaces often involving hydrogen with contamination species such as OH,  $\text{CH}_x$ , F. The combination of electron and photon spectroscopies have made it possible to characterize both flat and stepped surfaces. The data have been used to suggest specific chemical reactions responsible for the preferential etching observed in buffered HF solutions.

Silicon bonding occurs upon mechanical contact of oxidized (hydrophilic) wafers. It is an important technique to produce Silicon-on-insulator substrates, to substitute for epitaxial growth and to manufacture micro-mechanical systems. We have used multiple internal reflection (MIR) infrared absorption spectroscopy to characterize the concentrations of water, hydrogen, hydroxyl and hydrocarbon species at the interface of both hydrophobic and hydrophilic Si(100) wafers as a function of bonding temperatures. This sandwich geometry provides a large ( $\approx 40$ ) enhancement (of the component of vibrations perpendicular to the interface plane) over the standard MIR geometry, traditionally used to study semiconductor external surfaces. The magnitude and polarization dependence of this enhancement factor make it possible to perform accurate measurements in air without interference from impurities adsorbed on the outer surfaces, and to detect as few as 1% monolayers of various species in these chemically complex interfaces. The data are used to critically evaluate the various proposed bonding mechanisms.

#### INVITED

10:40 am **SSEM-WeM8 Surface IR Investigation of Arsine Adsorption on GaAs(001)**, *Haihua Qi, Paul E. Gee and Robert F. Hicks*, Chemical Engineering Department, University of California, Los Angeles, Los Angeles, CA 90024-1592.

We report the first observation of surface infrared spectra of adsorbed arsine on the  $c(2 \times 8)$  and  $(1 \times 6)$  reconstructions of GaAs(001). Arsine dissociatively adsorbs on the  $c(2 \times 8)$  reconstruction forming  $\text{AsH}_2$  and  $\text{AsH}$  species with vibrational frequencies of 2080 and 2140



$\text{cm}^{-1}$ . Polarized infrared spectroscopy reveals these arsine species bond to the second-layer gallium atoms exposed at As-dimer vacancies. Infrared peaks for arsine adsorption on  $(1 \times 6)$  reconstruction appear at 2135 and 2100  $\text{cm}^{-1}$ . Increasing the arsine adsorption temperature causes additional peaks to appear at 2045 and 2020  $\text{cm}^{-1}$ . This indicates that arsine adsorbs on gallium dimer sites and decomposes to form arsenic dimers. These results are used to present a mechanism for arsine adsorption and decomposition on GaAs(001) surface.

## THIN FILM

Room A105 - Session TF-WeM

### Optical, Piezoelectric and Ferroelectric Films

**Moderator:** D. K. Chatterjee, Eastman Kodak Company.

8:00 am **TF-WeM0 Thin Film Optical Coatings, H. A. Macleod**, Thin Film Center Inc., 2745 E Via Rotonda, Tucson, AZ 85716-5227.

Optical materials are quite limited in their range of intrinsic optical properties. Thin-film optical coatings open up an almost limitless range of possible performance by combining optical materials into regular layered structures. The resulting behavior may be far from that of the component materials and this includes properties such as mechanical, thermal, electronic and acoustic. The distinguishing feature of an optical coating is that its primary purpose is optical but all the other properties may be, and often are, involved. The optical properties are normally achieved by controlled interference and this implies a high degree of uniformity and precision of layer thickness. The structures may range from just a few to several thousand layers. Their optical purpose may be to reflect strongly, to select or reject spectral regions, to control polarization, to suppress reflection, to combine or split beams. The list is almost limitless. Optical considerations have traditionally been dominant and optimum, with mechanical, thermal and other considerations of secondary importance. As requirements change this situation is also changing and much effort is now directed at improved understanding of these other factors and especially at the influence of the various processes that may be used for optical film deposition.

INVITED

8:40 am **TF-WeM2 Composition and Morphology of Al Multilayer Thin Film Reflective Coatings, J. Kim\*, J. J. Weimer\*\*, D. Torr\*, and M. Zukic\***, \*Department of Physics, \*\*Department of Chemistry and Department of Chemical & Materials Engineering, University of Alabama in Huntsville, Huntsville, AL 35899.

Successful design of Al multilayer optical devices depends critically on accurate knowledge of optical constants for the device. Obtaining detailed information about thicknesses, compositions, and morphologies of layers in such devices is therefore vital. Multilayer Al thin films with interleaving and protective  $\text{MgF}_2$  dielectric layers for use as far and extreme UV reflectors have been characterized using x-ray photoelectron spectroscopy (XPS) and atomic force microscopy (AFM) with this goal in mind. The devices were prepared in a conventional high vacuum system, and sputter depth profiles were obtained using XPS in a separate UHV system. Thin, oxidized regions were found at the top- and bottom-most interfaces of the Al layers. These oxide regions may be thicker than previously reported from optical measurements. Interdiffusion of elements was apparent at boundaries between the Al and  $\text{MgF}_2$  layers. The AFM images showed columnar-like growth of the Al and  $\text{MgF}_2$  layers, and roughnesses were determined across these surfaces at the microscopic scale. Since oxidation of Al is probably the main cause of discrepancies between design and actual performance, a relationship was derived to predict the extent of oxidation in Al layers from parameters measured *in situ* during film deposition. A model for determining optical parameters of multilayer devices is presented that incorporates Al oxide layers as a first step toward improving agreement with design values.

9:00 am **TF-WeM3 Production and Characterisation of Multilayer KCl:LiF Thin Films on Glass, F. Somma, A. Ercoli**, Dipartimento di Fisica, III Università di Roma, 00146 Roma, Italy, **S. Santucci, L. Lozzi, M. Passacantando, P. Picozzi**, Dipartimento di Fisica, Università dell'Aquila, 67010 Coppito (AQ), Italy.

Alkali halide films with colour centres have important applications in information storage, lithography, radiation dosimetry and solid state lasers. KCl:LiF multilayers have been grown by thermal evap-

oration on glass substrates at  $p < 10^{-6}$  mbar under continuous monitoring of the substrate temperature ( $T = 30\text{--}300^\circ\text{C}$ ) and deposition rate ( $V = 0.4\text{--}0.6$  nm/s). The colour centres have been produced by low energy (3 keV) electrons. The complete characterisation of the samples has been performed using depth profile XPS, for the profile composition, X-ray diffraction and SEM, for the structural analysis and optical absorption, for the optical properties. When the substrate temperature is low ( $30^\circ\text{C}$ ) the LiF layer deposited onto KCl (h00) film grows as (111) and a low diffusion between KCl and LiF layers are observed. Instead when the substrate temperature is high ( $250\text{--}300^\circ\text{C}$ ) a (100) growth of LiF onto KCl (h00) and a strong diffusion are shown.

9:20 am **TF-WeM4 Heat Transport in Sputtered Optical Coatings, S.-M. Lee, David G. Cahill**, University of Illinois, Urbana, IL; and **Thomas H. Allen**, Optical Coatings Lab Inc., Santa Clara, CA.

The thermal conductivity of dielectric optical coatings is thought to be a major factor in determining the laser damage threshold. Micron thick films of  $\text{TiO}_2$ ,  $\text{SiO}_2$ ,  $\text{Al}_2\text{O}_3$ , and stabilized zirconia are deposited on single crystal Si and MgO substrates using radio-frequency and ion-beam sputtering. We measure the thermal conductivity of the films in the temperature range 80 to 400 K using a new extension of the 3 $\omega$  method. The accuracy of this technique is demonstrated by the fact that the thermal conductivity of a-SiO<sub>2</sub> grown thermally on Si(001) is identical to bulk a-SiO<sub>2</sub>. The temperature dependence of the data for sputtered oxide films is comparable to bulk a-SiO<sub>2</sub> and the magnitude of the conductivity at high temperatures is in good agreement with the predicted minimum thermal conductivity for these materials.

9:40 am **TF-WeM5 Review of Recent Developments in Ferroelectric, Piezoelectric and Electrooptic Thin Films, A. I. Kingon, H. N. Al-Shareef, A. Chow, D. J. Lichtenwalner, and O. Auciello**, Department of Materials Science and Engineering, North Carolina State University, Raleigh, NC 27695-7919.

We review recent developments in ferroelectric, piezoelectric and electrooptic films, with special emphasis on research at NCSU.

Ferroelectric films are of current interest for non-volatile memories (NVMs) and DRAMs. Lead zirconate titanate (PZT) solid solutions are a leading choice for NVMs. Successful utilization requires careful control of stoichiometry and microstructure, *via* the chosen process method. We show the importance of the early stages of film growth on the resultant microstructure. The control of key properties such as polarization fatigue and film leakage is discussed.

Electrooptic films have potential application for optical switches and frequency doubling (for blue light sources). In this case, high quality epitaxial films are required. Improvement of optical losses is the major technical obstacle to exploitation. The situation is discussed with reference to niobate films ( $\text{KNbO}_3$  and  $\text{LiNbO}_3$ ).

The final portion of the presentation deals with the status of piezoelectric films. Applications include microelectromechanical (MEMs) and surface acoustic wave (SAW) devices. The review covers simple oxides such as ZnO as well as perovskite solid solutions.

INVITED

10:20 am **TF-WeM7 Smart Thin Film TiNi/Piezoelectric Heterostructures, A. Peter Jardine and Peter G. Mercado**, Dept. of Materials Science and Engineering, SUNY at Stony Brook, Stony Brook, NY 11794-2275.

The development of smart materials relies on developing heterostructures with both sensing and actuation capabilities which are coupled by an intrinsic control mechanism. It has been previously demonstrated that heterostructures of Shape Memory Effect TiNi and piezoelectric (53/47)  $\text{Pb}(\text{Zr,Ti})\text{O}_3$  (PZT) coupled by a  $\text{TiO}_2$  interface are capable of being considered as "smart". As TiNi naturally passivates with a titania surface, the use of piezoelectric titanates was a natural system for exploring these heterostructures. In this paper, we outline the development processing of TiNi using UHV deposition techniques and the development of the ceramic layers using sol-gel techniques.

The current post-deposition state of the heterostructures was initially amorphous. Of particular concern to smart materials development is that the post-deposition processing to crystallize the correct phase of one component of the smart heterostructure can adversely affect the microstructure and active properties of the second phase of the material. We have found that there is a narrow range of processing temperatures between  $550^\circ\text{C}$  and  $600^\circ\text{C}$  where the PZT thin film is in its perovskite phase, the TiNi is in superelastic austenitic state and the  $\text{TiO}_2$  interface between the TiNi and PZT is rutile. Detailed characterization of the physical properties was performed using SEM, XRD and optical microscopy and the piezoelectric properties of these het-



erostructures was performed using an RT-11 Ferroelectric Test station. These results will be presented and implications for possible devices discussed.

10:40 am **TF-WeM8 Microstructures of Sputtered Thin Films of PbTiO<sub>3</sub> Families**, *Toshifumi Satoh, Kenji Tabata and Kiyotaka Wasa*, Research Institute of Innovative Technology for the Earth (RITE), 9-2 Kizugawadai, Kizu-cho, Kyoto 619-02 Japan.

Surface and/or microstructures of thin films of the perovskites, which will affect their physical and chemical properties, have been not fully understood yet, although the extensive works have been done on a deposition of the perovskites including sputtering, reactive evaporation, laser ablation, and chemical vapor deposition. This study describes the surface and the microstructures of perovskites lead titanate (PT) thin films of PbTiO<sub>3</sub> families grown on (100) MgO and (0001) sapphire. Their surface and microstructures have been studied by a scanning electron microscopy (SEM) and a transmission electron microscopy (TEM). Rf magnetron sputtering was used for the deposition of the perovskite thin films. It was found that the (001) lead titanate thin films were epitaxially grown on the (100) MgO single crystal at stoichiometric composition. The composition of the resultant thin films and the thin film thickness have strongly influenced their surface and microstructures.

This research was supported in part by the NEDO Environmental Catalyst Research Programme.

## ELECTRONIC MATERIALS

### Room A108 - Session EM-WeM

#### Heterostructures for Optoelectronics

**Moderator:** C. W. Wilmsen, Colorado State University.

8:00 am **EM-WeM0 MBE Growth of II-VI Blue/Green Laser Diodes**, *D. C. Grillo, M. D. Ringle, J. Han, R. L. Gunshor, G. C. Hua*, Purdue University, West Lafayette, IN 47907, *A. Salokatve, H. Jeon, A. V. Nurmikko*, Brown University, Providence, RI 02912.

The high-injection lasing conditions mandated for semiconductor laser diodes present stringent challenges to both material and device scientists. Issues such as defects, dopings, contacts, and processing have to all be properly addressed in order to achieve prolonged operation at room temperature under continuous wave (CW) excitation. In this paper we describe the MBE growth and characterizations of widegap II-VI (Zn,Mg)(S,Se)/Zn(S,Se)/(Zn,Cd)Se separate-confinement heterostructure (SCH) quantum well lasers. By employing an elevated temperature during growth of the active regions (confinement region and quantum wells), we were able to reduce, as evident from photoluminescence, device degradation, and TEM characterizations, the density of non-radiative point defects. Devices operated at room temperature have CW lifetime exceeding 30 seconds with threshold current densities at low as 250 A/cm<sup>2</sup> and lasing voltage below 6 volts. To eliminate the residual strain built-in to the (Zn,Mg)(S,Se) cladding layers due to compositional drifting, as manifested by the presence of multiple diffraction peaks in the x-ray rocking curves, the substrate temperature was carefully monitored by an infrared pyrometer taking into account the thin-film interference effect arising from the II-VI/III-V heteroepitaxy; rocking curves with single diffraction peak of 24 arcsec were obtained from a 2  $\mu$ m quaternary epilayer.

This work was supported by ARPA/ONR University Research Initiative grant number 286-25043, AFOSR grant number F49620-92-J-0440, NSF/MRG grant number 9221390-DMR, and NSF grant number 9202957-DMR.

8:20 am **EM-WeM1 MBE Growth of ZnMgSSe and Its Application to Blue and Green Laser Diodes**, *M. Ikeda and A. Ishibashi*, Sony Corporation Research Center, 174 Fujitsuka-cho, Hodogaya-ku, Yokohama 240, Japan.

The ZnMgSSe alloy, which was originally developed by Sony researchers in 1991 (1), is a suitable material as cladding layers of wide band gap II-VI laser diodes because it offers a wide range of band gap energy from 2.7 to ~4 eV at room temperature maintaining the

zinc-blende structure lattice-matched to GaAs or ZnSe. The electrical and optical properties as well as doping behaviors of ZnMgSSe layers epitaxially grown by MBE on GaAs have been studied extensively, and those results will be reviewed briefly.

When the ZnMgSSe cladding layers are employed instead of conventional ZnSSe cladding layers in II-VI laser diodes, the carrier and optical confinement within the active region will be enhanced significantly, which results in the improved laser performance. Indeed, we have achieved room-temperature continuous-wave operation of II-VI laser diodes for the first time using ZnCdSe/Zn(S)Se/ZnMgSSe strained quantum-well separate-confinement heterostructures (2, 3). The device characteristics of the state-of-the-art II-VI laser diodes in the blue and green spectral region will be presented.

Important subjects for future improvements in ohmic contacts and longer device lifetimes will be finally discussed. **INVITED**

1. H. Okuyama, K. Nakano, T. Miyajima, and K. Akimoto, *Jpn. J. Appl. Phys.* 30, L1620 (1991).

2. N. Nakayama, S. Itoh, T. Ohata, K. Nakano, H. Okuyama, M. Ozawa, A. Ishibashi, M. Ikeda, and Y. Mori, *Electron. Lett.* 29, 1488 (1993).

3. N. Nakayama, S. Itoh, H. Okuyama, M. Ozawa, T. Ohata, K. Nakano, M. Ikeda, A. Ishibashi, and Y. Mori, *Electron. Lett.* 29, 2194 (1993).

9:00 am **EM-WeM3 Structural and Compositional Characterization of HgSe Contacts to p-ZnSe**, *J. Fijol, P. H. Holloway, J. Trexler, J. Kim, and K. Jones*, Department of Materials Science and Engineering, University of Florida, P.O. Box 116400, Gainesville, FL 32611\*.

HgSe contacts to MBE grown p-ZnSe (nitrogen doped to  $3 \times 10^{17}$  cm<sup>-3</sup>) have been formed by the reaction of an amorphous Se capping layer with Hg vapor, yielding pseudo ohmic behavior. This process was performed using atmospheric processing which involves heating the Se capped samples to 150°C in Hg vapor. Current densities of 2.5 A/cm<sup>2</sup> at 10 volts were observed for these contacts and temperature dependant I-V measurements have been used to identify thermionic field emission as the mechanism of current transport across the HgSe/ZnSe interface. The properties of the amorphous Se capping layer such as glass transition temperature (T<sub>g</sub>) and peak recrystallization temperature (T<sub>c</sub>) have been identified as critical factors in the formation of HgSe. To improve contact performance, the reaction of Hg with Se and the structural and compositional properties of the resulting HgSe contacts have been studied. Auger electron spectroscopy (AES) and X-ray diffraction (XRD) have been used to determine contact composition and structure at stages throughout the reaction. TEM analysis indicates that under specific processing conditions, regions of HgSe are formed which are epitaxed to the p-ZnSe. The implications of these reactions to the contact properties will be discussed.

\*This work supported by ONR grant N00014-92-J-1895.

9:20 am **EM-WeM4 Deep Level Interface States Near ZnSe/GaAs(100) Heterointerfaces**, *A. D. Raisanen and L. J. Brillson*, Xerox Webster Research Center, Webster, NY 14580, *L. Vanzetti, L. Sorba, and A. Franciosi*, Dept. of Chemical Engineering and Materials Science, Univ. of Minn., Minneapolis, MN 55455.

We have used low energy cathodoluminescence spectroscopy (CLS) and laser photoluminescence spectroscopy (PL) to characterize the energies, and depth distribution of deep levels near the buried, MBE-grown ZnSe/GaAs(100) heterointerface. Previous studies have described a variation in heterojunction band offset with Zn/Se beam pressure ratio (BPR) during epilayer growth.<sup>1</sup> Using a combination of electron excitation energies and laser wavelengths to obtain CLS/PL "depth profiles" through the interface regions of 50, 1500, and 5000 Å ZnSe/GaAs structures, we find that deep electronic states are formed near the heterojunction and within the epilayer whose relative emission intensities vary dramatically with BPR. For Zn (Se)-rich interfaces, features at 0.9 and 1.0 eV (1.3 and 1.9 eV) photon energies are dominant. In general, intensities of the 0.9 and 1.0 eV features decrease away from the free epilayer surface, whereas the 1.3 and 1.9 eV features appear most intense for excitation depths corresponding to the buried interface regions. The CLS/PL spectra reveal characteristic features of intermixing at elevated temperatures consistent with known atomic diffusion behavior.<sup>2</sup> These spectral features demonstrate substantial differences in the localized interface states formed under variant epi-

layer growth conditions. In addition, they provide effective in-situ monitors of heterointerface quality and stability.

1. R. Nicolini et al., Phys. Rev. Lett. 72, 294 (1994).
2. J. Gutowski, N. Presser, and G. Kudlek, Phys. Stat. Sol.(a) 120, 11 (1990).

9:40 am **EM-WeM5 Materials Issues in II-VI Semiconductor Lasers**, J. M. DePuydt, S. Guha, M. A. Haase, J. Qiu, G. E. Hofler, B. J. Wu, G. Meis-Haugen and H. Cheng, 3M Company, St. Paul, MN 55144-1000.

Since the first report of II-VI blue-green laser diodes in 1991 rapid progress has been made in advancing both the II-VI materials and devices. Although continuous operation of laser diodes at room temperature has been demonstrated, the lifetimes of the best devices are limited to a few minutes. TEM, cathodoluminescence and electroluminescence studies have shown that laser degradation proceeds by the evolution of dark defects that are formed in the vicinity of pre-existing defects such as V-shaped stacking faults. The stacking faults responsible for the degradation appear to be formed during the nucleation of the II-VI layers on the GaAs substrate. Possible causes of the stacking faults and efforts to eliminate them will be discussed.

**INVITED**

10:20 am **EM-WeM7 Heteroepitaxy of Nearly Lattice Matched Compound Semiconductors on Silicon**, K. J. Bachmann, N. Dietz, S. Fiechter, J. T. Kelliher, H. Castleberry, and G. Wood, Department of Materials Science and Engineering, North Carolina State University, Raleigh, NC 27695.

The control of the properties of heteroepitaxial films of compound semiconductors on silicon is impeded by surface structure/chemistry and strain effects that result in the generation of defects. In this paper, the low temperature growth of nearly lattice-matched heterostructures of compound semiconductors on silicon is reviewed, separating the study of surface structure and chemistry effects from the problem of strain-induced defect formation. Using GaP on silicon as an example, the growth of heteroepitaxial structures under the conditions of interrupted cycle chemical beam epitaxy is discussed. Excellent selectivity of GaP heteroepitaxy on Si as compared to SiO<sub>2</sub> and SiC covered surface areas is observed. Although selectivity is a desirable aspect in the context of device processing, the impediment of epitaxial overgrowth by residual oxygen and carbon on the silicon surface points to the fundamental importance of surface cleaning and the maintenance of a clean silicon surface during the initial stages of nucleation and GaP growth. The kinetics of heteroepitaxial GaP growth is evaluated on the basis of RBS, AFM, HREM, RHEED and mass spectrometric studies that focus on the evolution of chemical and structural changes during the heating of the initially hydrogen terminated silicon surface in the presence of a phosphorus precursor beam and the subsequent nucleation and sealing stage that establishes a contiguous GaP epilayer on the silicon surface. Also, the heteroepitaxial growth of related nearly lattice-matched II-IV-V<sub>2</sub> compounds and alloys is considered, using the ZnSi<sub>x</sub>Ge<sub>1-x</sub>P<sub>2</sub> system as an example. **INVITED**

## MANUFACTURING SCIENCE AND TECHNOLOGY

**Room A110 - Session MS-WeM**

### Advanced Manufacturing Equipment-B

**Moderator:** C. B. Whitman, CVC Products, Inc.

8:00 am **MS-WeM0 Long-throw Low-pressure Sputtering Technology for ULSI Devices**, Yoshiyuki Kadokura, Yuzou Kashimoto, Tetsuji Kiyota, Nobuhiro Motegi, I. Nakayama, ULVAC Japan, Ltd., Shizuoka, Japan.

The process of metallizing contact/via holes plays a very important role in semiconductor device fabrication. As LSI becomes increasingly high integrated, the size of the contact/via holes shrinks, producing higher aspect ratios. As a result, sufficient bottom coverage cannot be obtained by the conventional sputtering techniques. To solve this problem, a collimated sputtering technique has been investigated recently. Though it has been shown that the bottom coverage is highly improved by using a collimator, the technique has still disadvantage for production, such as generation of particles, degassing from the

collimator, and clogging of the collimator itself. We have developed a new technology, called long-throw low-pressure sputtering technology, for sputtering high-aspect-ratio ULSI devices without employing collimators in the system. The basic feature of our design is to make the distance between target and substrate much longer than that of the conventional sputtering method so that sputtered atoms are incident perpendicular to the wafer, while lowering the discharge pressure by one order of magnitude in deposition (10<sup>-2</sup> Pa range) so that sputtered atoms are not scattered by gas molecules between the target and the substrate. Our results indicate that this technique has very good potential for applications in high-aspect-ratio ULSI sputtering processes. In this paper, we will describe the basic principle of our design, the unique properties of metal thin films, such as TiN/Ti and Al-alloy formed by our method, and the various advantage of the method as an advanced manufacturing technology for next generation ULSI devices.

8:20 am **MS-WeM1 Polysilicon Gate Etch Linewidth and Profile Control in a 0.25- $\mu$ m L<sub>eff</sub> Logic Technology: Effects and Length Scale of Pattern Loading**, J. W. Adkisson, S. J. Holmes, C. C. Smolinski, R. P. Mallette, M. C. Cantell, T. A. Knotts, IBM Microelectronics, Essex Junction, VT 05452.

Faster circuit performance requires tight control of gate linewidth and profile to avoid short-channel reliability failures or speed degradation; to provide this control, the gate etch process must be insensitive to variations in loading. Problematic loading densities include very local (<1 $\mu$ m), intermediate (1-20mm) and global (100mm) interactions. Our efforts to quantify and reduce these effects are discussed in this paper.

For this study, we used an integrated three-step gate-etch process in a single wafer RIE tool which included a F-based breakthrough etch, followed by a two-step HBr/Cl<sub>2</sub>/O<sub>2</sub> polysilicon etch. Cross-sectional and plan-view SEM and electrical linewidth measurements were used to characterize the etch results.

The optimized process showed similar profiles and negligible offset between nested and isolated lines. For very local effects, the offset between isolated and dense features was increased by the passivation produced in the breakthrough step, the degree of sputtering in the first polysilicon etch step, and the oxygen flow ratio in the final gate-oxide selective step. The local loading effects were further perturbed by the intermediate- and global-scale loadings. The length scale of the intermediate loading effects for the gate etch process was determined by using a variable loading structure positioned next to an array of measurement structures. For the most severe loading changes, significant variations in the isolated features extended over 20mm, while nested lines were almost unaffected. Higher global resist loading was observed to decrease etch bias and increase the isolated-dense offset.

8:40 am **MS-WeM2 Interlayer Dielectrics with Low Dielectric Constant for Multilevel Interconnection**, R. Aoki, N. Hayasaka\*, Y. Nishiyama, H. Miyajima\*, Y. Nakasaki\* and H. Okano\*, Integrated Circuit Advanced Process Eng. Department, Toshiba Corp., \*ULSI Research Center, Toshiba Corp.

The high quality insulator with low dielectric constant for interlayer dielectrics is the key technology for future high speed ULSI devices. We realized F doped SiO<sub>2</sub> with low dielectric constant (less than 3.5) and high water absorption resistance. F was incorporated into SiO<sub>2</sub> by adding fluorine contained gases into TEOS/O<sub>3</sub> dual frequency excited plasma.

We studied the CVD mechanism by investigating the plasma chemistry and physics, and we have clarified the role of F on film formation properties (film quality and step coverage). And also the mechanism of reducing dielectric constant due to F addition into SiO<sub>2</sub>, which was clarified by using molecular orbital calculation, will be presented.

9:00 am **MS-WeM3 Manufacturing Issues of Electrostatic Chucks**, D. R. Wright, L. Chen, P. Federlin, K. Forbes, SEMATECH, Austin, TX 78741.

In the past few years, Electrostatic Chucks (ESCs) have become much more widespread in semiconductor manufacturing equipment. In addition to the elimination of moving parts, ESCs hold the promise to decrease the wafer edge exclusion, that is, to allow more good chips to be made on each wafer. A number of technical, material, and business challenges remain in making ESCs workable and reliable in all tools across the semiconductor factor, or fab.

We will discuss issues of clamping force, clamping and declamping time, and wafer temperature control, describing how they affect design and choice of materials. The effect of these choices on adapting ESCs

to various tools over various temperature ranges will also be discussed. The role of models and test results in accelerating development will be addressed.

Finally, we will list some of the business challenges to implementing ESCs. Despite technical successes, many high-volume fab lines are always reluctant to risk installing new technology, despite promises of improvement. SEMATECH has addressed these issues with Working Groups, which help address standard specifications, study early testing results, and share manufacturing performance data.

#### INVITED

9:40 am **MS-WeM5 Equipment Engineering Methods for Improvements in Particle and Uniformity Performance during Plasma Processing**, G. S. Selwyn, M. Dalvie, C. R. Guarnieri and M. Surendra, IBM Research Division, Yorktown Heights, NY 10598.

Particle contamination and process uniformity are key yield detractors in plasma processing. Often, these issues are viewed as separate problems with separate corrective actions. However, recent results demonstrate that uniformity and contamination problems can be *inter-linked* by the formation of locally-disturbed plasma regions called "traps". Traps are induced by changes in the electrode including the electrode topography and the emission of secondary electrons. Traps are characterized by a localized increase in the plasma potential. Wafers, clamp rings, focus rings and wafer patterning induce trap formation. In addition to these causes, we demonstrate for the first time that *changes in materials under the electrode surface also induce traps*, by altering the coupling of rf power into the sheath. Traps influence contamination problems by helping to confine particles. Similarly, traps can influence process uniformity by altering the flux and trajectory of ions to the wafer. The latter effect has strong influence on the wafer edge exclusion, the highly nonuniform region close to edge of the wafer. Typically, product yield is lowest in this region.

We correct this problem through the use of specially-designed buried layers of metal and dielectric to compensate edge effects and topography changes. The results are verified by optical emission studies, uniformity mapping and improvement in particle contamination performance.

#### INVITED

10:20 am **MS-WeM7 Plasma Process Uniformity in a High Density System: Experiment and Modeling**, C. R. Guarnieri, M. Surendra, G. S. Selwyn, and M. Dalvie, IBM T. J. Watson Research Center, Box 218, Yorktown Heights, NY 10598.

In plasma processing of large area substrates, nonuniformities in etching or deposition result in lower yields or a wide distribution of device characteristics. Process uniformity is affected by variations in ion flux, energy, and direction.

Experiments have been carried out in a high density, rf inductively coupled system with a rf capacitively coupled substrate. Results indicate that by spatially varying the rf coupling to the substrate alone, we are able to vary the etch rate uniformity of SiO<sub>2</sub> on blanket wafers from a profile that is higher in the center by ~20% to one which is lower in the center by ~10%. The rf coupling impedance is varied by both controlling the shape of the metal electrode and the use of dielectrics. The effect of spatially varying substrate rf coupling is dependent on substrate resistivity and applied frequency. Situations where substrate rf coupling is unintentionally nonuniform, e.g. wafer bowing due to backside cooling gas pressure, are also examined.

Process rate uniformity has been modeled with two dimensional analytic models of the plasma source and rf sheaths, coupled to an equivalent circuit element discretization of the electrode assembly, substrate, plasma source and sheath. Results from the model are in reasonable agreement with experimental measurements, and serve as a useful design tool for electrode assembly design.

10:40 am **MS-WeM8 The Complex Impedance of a Dusty Processing Plasma**, Weston C. Roth and Robert N. Carlile, Dept. of Electrical and Computer Engineering, University of Arizona, Tucson AZ 85721.

It is now understood that all plasmas used for processing silicon wafers contain large numbers of particles (dusty plasma) which have the potential to contaminate the wafer being processed. It is the purpose of this paper to examine the complex impedance of a dusty plasma. Specifically, we measured the complex impedance (magnitude and angle) at the fundamental frequency of 13.56 MHz and also at the first, second, and third harmonics as a function of time at the RF input to a modified Tegal MCR-1 etch chamber. The plasmas were derived from argon and also SF<sub>6</sub>. For SF<sub>6</sub>, using a Si wafer on an aluminum electrode, there were rapid variations of all angles at early times, probably indicating initial particle nucleation and growth within

the plasma volume and transport to particle traps at the plasma-sheath interface. Subsequent to this period, the angles changed slowly. For argon, with a silicon wafer on a graphite electrode, there was no initial rapid variation, but only a slow change with time, probably suggesting that particle formation is a surface phenomenon. It may be possible to correlate the slow changes in the impedance angles at long times with particle deposition on the wafer, thus eliminating the need for the common and expensive use of witness wafers.

## BIOMATERIAL INTERFACES NANO 3/ NANOMETER-SCALE SCIENCE AND TECHNOLOGY

Room A106 - Session BINS-WeM

### Artificial Cellular Assemblies

Moderator: D. A. Stenger, Naval Research Laboratory.

8:00 am **BINS-WeM0 Electrical Characterization of Artificial Neuronal Networks**, J. J. Hickman, K. E. Foster, R. C. Oprison, D. A. Stenger<sup>1</sup>, A. E. Shaffner<sup>2</sup>, and J. L. Barker<sup>2</sup>, Science Applications International Corporation, McLean, VA 22102; <sup>1</sup>Center for Bio/Molecular Science and Engineering, Naval Research Laboratory, Washington, DC 20375; <sup>2</sup>Laboratory for Neurophysiology, BNP, DIR, NINDA, National Institutes of Health, Bethesda, MD 20892.

We are creating *in vitro* circuits of mammalian neurons by controlling their adhesion and neurite outgrowth on artificial surfaces. We are using self-assembled monolayers (SAMs) to control the intrinsic and geometric properties of the culture growth surfaces. The ability to control the surface composition as well as other variables, such as growth media and cell preparation, all play important roles in neuron pattern viability. We have recorded the electro-physiological signals produced by neurons on the artificial surfaces in response to stimuli. The surfaces have been characterized by XPS and contact angle measurements and we are relating the intrinsic properties of the surfaces to the cellular development. We are using what we learn for a more fundamental understanding of neuronal circuit development as well as to develop new algorithms for training neural networks.

8:20 am **BINS-WeM1 Neuronal Cells Cultured on Modified Microelectronic Device Surfaces**, A. Offenhausser<sup>1</sup>, J. Ruhe<sup>1</sup>, W. Knoll<sup>1,2</sup>, <sup>1</sup>Frontier Research Program, RIKEN, 351-01 Wako-shi, Japan and <sup>2</sup>Max-Planck-Institute of Polymer Research, 55128 Mainz, Germany.

The recording of the electrical activity of a large number of neurons in tissue culture over a period of weeks or even months should be very helpful in the understanding of the development and function of biological neuronal networks. Ideally, a method for the detection of the changes in intercellular voltage in such a system should have both high spatial and temporal resolution. One approach could be to record with a fixed electrode array built into the floor of the tissue culture chamber.

We have chosen to detect the electrical signal of the neuron by direct coupling with a field effect transistor. Such a coupling is the first step towards multisite recording in neuronal nets and the development of neuronal network on a microelectronic device surface it is necessary, to control adhesion and outgrowth of neurons on a microscopic scale. To achieve biocompatibility the chemical composition of the surfaces of such devices have to be modified.

Our approach to control the chemical architecture at the interface is to attach ultra thin polymer films to the device surface by using a novel "grafting from" procedure. It could be shown, that the chemical composition of the interface could be tuned in such a way that Purkinje neurons show good adhesion to such a surface and survive and grow on it for weeks.

8:40 am **BINS-WeM2 Using Both Topographic Control and Micropatterned Protein Substrates in Controlling Neuron Extension and Connection in Culture**, Professor A. S. G. Curtis, Department of Cell Biology, University of Glasgow G12 8QQ, Dr. Stephen Britland and Professor C. D. W. Wilkinson, Department of Electronics and Electrical Engineering, University of Glasgow G12 8LT.

We describe techniques of combining topographical guidance and patterning of protein molecules on the surface and other adhesive, non-adhesive and activating and inactivating molecules on surfaces,

to control and to aid the formation of functional neuronal networks *in vitro*. These techniques have been used with rat CNS neurons in culture to obtain good guidance and electrical activity in culture. The activity of the cells is either spontaneous or can be stimulated with extracellular electrodes. The same electrodes also fabricated in the substrate can be used for long-term multisite recording. Problems associated with patterning proteins over electrodes will be reported.

9:00 am **BINS-WeM3 Photochemically-driven Surface Modifications and Cellular and Biomolecular Assemblies with Micron-order Precision**, *T. Matsuda*, National Cardiovascular Center Research Institute, 5-7-1 Fujishirodai, Suita, Osaka 565, Japan.

If we can manipulate precisely surface microprocessing, three dimensional (3-D) functionalized surfaces can be created to provide advanced artificial organs, microbiosensors and micromachines in which surface properties play a decisive role in functioning. To this end, precise control of the surface chemical composition at XY-plane and microstructure at Z-axis is essentially needed. Since photochemical process proceeds only at irradiated portions, such a surface modification can be dimensionally controlled with micron-order precision in principle.

In this talk, our recent several years-efforts focusing on the development of surface photochemical modification methods will be summarized. At first, XY-manipulation was attained by photoreactivities of p-azidophenyl group, dithiocarbamate group and benzophenone group, all of which can form a covalent bond with a neighboring chemical group upon ultraviolet (UV) irradiation. Photoreactive group-derivatized synthetic and biological polymers were prepared and cast on a substrate. Subsequently UV light was irradiated. Chemical fixation was noticed. When UV was irradiated through a photomask, a patterned surface was created, which was clearly observed under atomic force microscopy. Photoreactive proteins such as albumin and gelatin were also chemically fixed at UV-irradiated portions. Z-axis manipulation was attained by an excimer laser ablation technique combined with surface photochemical process, resulting in the formation of microtextured surface.

When 2-D surfaces with cell-adhesion promoting regions such as hydrophobic or gelatin-fixed parts and cell-adhesion-free regions such as nonionic, hydrophilic or albuminated parts were created, cells adhered, spread, migrated and proliferated only on cell-adhesion promoting regions, resulting in the formation of a 2-D tissue. 2-D and 3-D neural circuits were also demonstrated. **INVITED**

9:40 am **BINS-WeM5 Cell Patterns and Whole-cell Biosensors Using Photonic Tweezers Technology**, *J. Renken and S. Seeger*, Universität Heidelberg, Physikalisch-Chemisches Institut, Im Neuenheimer Feld 253, 69120 Heidelberg, Germany.

Photonic tweezers technology exploits the light pressure in order to trap and transport microscopic particles such as mammalian cells. In our photonic tweezers system, a Nd:YAG laser (1064 nm) is directed into an inverted microscope, which is equipped with a computer-controlled XY-stage and an image processor. This set-up was used for the transport of cells from chambers showing weak cellular adhesivity to chambers coated with Cell-Tak<sup>®</sup>, a strong cell adhesive allowing the rapid immobilization of cells within cell diameter accuracy. Patterns of different cell lines were fabricated on a single chip. Thus the direct observation of the interaction between different cell classes is possible. By staining the cells with different ion-sensitive fluorescent dyes, concentrations of various ions can be monitored simultaneously and related to the metabolic responses of various cells to drugs. This way, a new tool for *in vitro*-toxicology is established.

10:00 am **BINS-WeM6 Modification and Refunctionalization of Fluoropolymers for Controlling and Directing Neurons at Interfaces**, *T. G. Vargo et al.*, State University of New York at Buffalo, Buffalo, NY 14214.

Recent modifications to fluoropolymer substrata have been shown which allows their surfaces to be refunctionalized either homogeneously or in patterns with a variety of materials including conducting metals, proteins or bioactive molecules. Covalent attachment of peptides with bioactive receptor sites for neurons is one of the most recent results. Through lithographic techniques, fluoropolymer surfaces can be patterned with peptides which can act to influence or direct specific attachment of neurons via their active receptors. In this discussion results will be shown illustrating the specificity of NG 108-15 neuro-

blastoma and PC12 cells to well characterized FEP (fluorinated ethylene propylene) surfaces refunctionalized with laminin derived oligopeptides. Receptor mediated cell attachment is determined using competitive binding assays. Detailed analysis of the refunctionalized FEP surfaces is obtained using ESCA, ToF-SIMS, ATR-FTIR, and fluorescent spectroscopy. FEP films having covalently immobilized 19 mer IKVAV sequences are used to demonstrate the high percentage of receptor mediated cell attachment sites on the IKVAV sequence. Results are shown where a 6 fold decrease in PC12 cell attachment is observed as determined through a competitive binding assay medium containing the IKVAV oligopeptide.

10:20 am **BINS-WeM7 Directed Growth of Uromyces Hyphae on Integrated Circuit Substrates**, *M. N. Kozicki, R. W. Roberson\*, T. K. Whidden, S. E. Kersey*, Center for Solid State Electronics Research, Arizona State University, Tempe, AZ 85287 (\*Department of Botany, Arizona State University).

We report on the initial findings of a program to investigate the directed growth of fungal hyphae on custom-designed integrated test circuits. The motivation behind such a combination is to allow the study of hyphal growth/steering mechanisms at the microscale and to determine the electrical characteristics of the resulting bio-hybrid integrated system. The primary biological element in this work is *Uromyces appendiculatus*, an organism which has been shown to exhibit precise and unique topographical signal recognition. The integrated circuit substrate is fabricated using standard semiconductor processing techniques. Guiding or "vectoring" elements, a series of 1 micron wide and 0.1 micron high ridges, are etched into the final layer of metallization (aluminum). A self-assembling hydrophobic monolayer is then applied to the circuit to create a suitable bio-compatible layer for cell attachment and growth. The *Uromyces* spore is placed on a contact pad in the center of the circuit, where it takes in water to allow it to begin the germination process. Germination results in the formation of a germ tube from the spore which grows out to touch the surface. This narrow, cytoplasm-filled structure is then guided by the vectoring elements toward another contact. Since the vectoring structures are part of the metallization pattern, they may be biased to control ion movement in the tube. The integrated test structures have been used to determine the influence of topography and surface coatings on hyphal growth. The vectoring structures were shown to be capable of steering the hyphae to intended connection/termination points through a wide range of angles. In addition, self-assembled monolayers of n-octyltrichlorosilane on the circuit materials resulted in superior germination characteristics compared to untreated surfaces.

10:40 am **BINS-WeM8 Patterning of Microtubules Observed with Atomic Force Microscopy**, *D. C. Turner, C. Chang, S. L. Brandow, and D. B. Murphy<sup>1</sup>*, Center for Biomolecular Science and Engineering, Code 6900, Naval Research Laboratory, Washington, D.C. 20375-5348, and <sup>1</sup>Department of Cell Biology, Johns Hopkins University Medical School, Baltimore, MD 21205.

Microtubules are cylindrical microstructures of diameter 25 nm that self-assemble from monomeric tubulin protein in the presence of the nucleotide GTP. In the cell microtubules act structurally, as part of the cytoskeleton, and as substrates for active transport of organelles. This transport is mediated by molecular motor proteins, such as kinesin and dynein, which "walk" along microtubules in the presence of ATP, carrying cargo along with them. We have been studying the adhesion characteristics of microtubules on silane modified surfaces with the goal of producing biologically active, patterned microtubules for the examination of two-dimensionally constrained molecular motor traffic *in vitro*. Silanes which promote adhesion and surfaces which reduce adhesion will be discussed, as well as a silane which causes depolymerization of the microtubules. Characterization of the silane films was carried out using AFM, ellipsometry and wettability. Biological activity of microtubules immobilized on the silane surfaces was assayed by observing ATP induced binding and movement of kinesin coated beads on the microtubules. Silanes which promoted adhesion were patterned using the method of Calvert and coworkers (Calvert, J. (1993) *J. Vac. Soc. B* 11, 2155) to produce substrates for selective adhesion of microtubules. Patterns of isotropic and aligned microtubules which were imaged with AFM will be discussed.

Supported by the Office of Naval Research.



## SURFACE SCIENCE

Room A205 - Session SS1-WeA

### Surface Magnetism II

**Moderator:** B. P. Tonner, University of Wisconsin, Milwaukee.

#### 2:00 pm SS1-WeA1 Experimental Studies of Surface and Interface Magnetism, H. Hopster, University of California, Irvine, CA 92717.

The magnetic coupling between ferromagnetic films through spacer layers is of great current interest due to the associated giant magnetoresistance (GMR) effects. The exchange coupling at various transition metal interfaces between ferromagnetic and non-ferromagnetic materials has been studied by spin polarized electron spectroscopies (secondary electrons, core level photoemission, Auger electrons, and energy loss spectroscopy) by several groups [1-6]. Although surface magnetic moments are difficult to extract directly from the data there is evidence that the surface moment at Fe(100) is enhanced with respect to the bulk value. Monolayers of Cr, Mn and V have been shown to couple antiferromagnetically to Fe(100). While Cr and Mn(100) layers order in a layer-by-layer antiferromagnetic structure on Fe(100) no intrinsic magnetic structure has been found in thicker V layers on Fe(100). A largely enhanced surface moment is found on the Cr(100) overlayers.

INVITED

1. F. U. Hillebrecht et al., Europhys. Lett. 19, 711 (1992).
2. T. G. Walker et al., Phys. Rev. Lett. 69, 1121 (1992).
3. J. Unguris et al., Phys. Rev. Lett. 69, 1125 (1992).
4. T. G. Walker, H. Hopster, Phys. Rev. B 48, 3563 (1993).
5. T. G. Walker, H. Hopster, Phys. Rev. B 49, 7687 (1994).
6. P. Fuchs, K. Totland, M. Landolt, to be published.

#### 2:40 pm SS1-WeA3 Strain Accommodation and Atomic Order in the Nonpseudomorphic Growth of Ultrathin Fe Films on Cu(001), D. E. Fowler and J. V. Barth, IBM Research Division, 650 Harry Rd., San Jose, CA 95120.

The detailed role of atomic order and of strain in a magnetic film and its interfaces in determining the magnetic anisotropy of the film is not well understood. To probe connections between these properties, we have made a structural study of Fe on Cu(001). Fe films from 0.5 ML to 6 ML were grown at 310 K and at 100 K, then annealed to 300 K. Medium Energy Ion Scattering (MEIS) measurements clearly show that there are deviations from pseudomorphic growth for even low Fe coverages. Structural changes continue to occur as the Fe coverage increases suggesting that the Fe film is attempting to take up a non-Cu fcc-like lattice introducing strain at the interface. By 6 ML (310 K growth) the Fe almost completely achieves this new lattice and, also, shows a surface reconstruction. Our MEIS data are consistent with a recently proposed nonpseudomorphic model (1). For 100 K growth and to a lesser extent for 310 K, the interfacial strain is apparently taken up by disruption of the near-interface Cu layers as shown by increased ion scattering from Cu. On increasing from 3 to 4 ML of Fe there is a particularly large increase in Cu scattering from the 2nd and 3rd layers below the interface. At 6 ML (100 K growth) of Fe nearly 5 full Cu layers are exposed to the ion beam. We compare these structural changes with the changes in the perpendicular, magnetic anisotropy constants of these Fe films as determined by an insitu Magneto-Optic Kerr Effect (MOKE).

(1.) P. Bayer et al., Phys. Rev. B, 48, 17611 (1993).

#### 3:00 pm SS1-WeA4 Magnetic Structure of Ultra-Thin Mn Films on Fe(100)/Pd(100)\*, G. Steierl and C. Rau, Department of Physics and Rice Quantum Institute, Rice University, Houston, TX 77251-1892.

The electronic and magnetic structure of Mn films epitaxially grown on Fe(100)/Pd(100) is studied using spin-polarized electron emission spectroscopy (SPEES). In SPEES surface reflected protons with an energy of typically 150 keV are used to induce the emission of Auger and secondary electrons. Spin analysis of the emitted electrons allows us to determine the spin polarization in the topmost Mn layer. We report on the thickness dependence of the Mn surface magnetization

within a thickness range of 1 to 20 monolayers. The relevance of our results towards the exchange coupling mechanism found between ferromagnetic layers separated by a spacer material is discussed.

\*Supported by the National Science Foundation, the Welch Foundation and the Texas Higher Education Coordinating Board.

#### 3:20 pm SS1-WeA5 Mössbauer Spectroscopy Study of Tetragonally-Distorted fcc Fe(100), J. W. Freeland, D. F. Storm, I. L. Grigorov, D. J. Keavney, and J. C. Walker, Johns Hopkins University, Baltimore, MD 21218.

Ultrathin films of fcc Fe(100) have been grown by MBE on Cu(100) and Cu<sub>1-x</sub>Au<sub>x</sub>(100) substrates, and their magnetic properties studied by Mössbauer spectroscopy and SQUID magnetometry in an effort to determine the effect of substrate lattice parameter on the magnetic moment of fcc Fe. The alloy substrates were grown *in-situ* by co-deposition, and their composition was varied between pure Cu and x=19.7% Au. This composition range corresponds to a lattice parameter range of 3.61 Å to 3.702 Å. RHEED and Mössbauer structural information suggested that the Fe is pseudomorphic with the substrate, with a tetragonal contraction to compensate for the in-plane expansion.

Mössbauer spectroscopy detected two different magnetic phases coexistent in the film: an antiferromagnetic (AF) phase with low spin, and a higher spin ferromagnetic (FM) phase. Interestingly, the moments of these phases appear to be independent of the substrate lattice parameter. Rather, the relative amounts of the film that exist in each phase changes dramatically with the alloy substrate composition. Over the lattice parameter range studied, the FM phase increases in intensity from about 20% to more than 60% of the film, at the expense of the AF phase. Therefore, it appears that there are two metastable states, and increasing the lattice parameter drives the Fe structure closer to one of those states. SQUID magnetometry observed this as an increase in average moment per Fe atom, in agreement with other total moment studies done on fcc Fe(100).

#### 3:40 pm SS1-WeA6 Magnetic Properties of Fe and Mn Overlayers on Ir(111) by Soft X-ray Circular Dichroism, W. L. O'Brien and B. P. Tonner, Synchrotron Radiation Center, Univ. of Wisconsin-Madison, Stoughton 53589.

A comparison has been made between the structure and magnetic properties of Mn and Fe ultrathin films grown on an fcc(111) substrate. Initially, Mn/Ir(111) gives split (1 × 1) LEED spots, which evolve into a simple (1 × 1) pattern between 2 and 4 monolayer thicknesses. Above 4 ML, a new structure with a (√3 × √3) LEED pattern forms. In the Fe/Ir(111) case, however, the films grow in the more common Kurdjumov-Sachs bcc(110)-fcc(111) structure. A combination of X-ray absorption, photoemission, and X-ray magnetic circular dichroism (XMCD) spectroscopies was used to correlate the changes in film structure with local magnetic moment and long-range ferromagnetic (FM) order. Only the Fe films show FM ordering at room temperature (as detected by XMCD). The XMCD data does not support a model of magnetic "dead layers" at the Ir interface, as proposed to explain earlier Fe/Ir superlattice experiments. The Mn/Ir(111) films show an enhancement of the Mn local atomic magnetic moment for atoms at the surface, but this is not associated with the structural changes that occur for different film thicknesses. A small change in the Mn 3s core-level photoemission exchange splitting is found to accompany the increased local moment. These results will be compared to other studies of Mn magnetic films, including c(2 × 2) MnCu and c(2 × 2) MnNi alloys.

#### 4:00 pm SS1-WeA7 Impact of Magnetism on the Stability of Ultrathin Films: The Magnetically Driven Two Dimensional Surface Alloy, S. Blügel, IFF, Forschungszentrum Jülich, D-52425 Jülich, FRG.

The magnetism of 3d, 4d, and 5d transition metal monolayers on various noble metal (100) substrates is shortly reviewed. The existence of two magnetic phases (p(1 × 1) ferromagnetic and c(2 × 2) antiferromagnetic) will be discussed. The main emphasis of this talk will be on the importance of magnetism for the structure and stability of ultrathin magnetic films. Exemplary for 3d transition metal monolayers on noble metal substrates detailed calculations for 3d monolayers on Cu(100) have been performed, which show a clear trend: i) Magnetism acts against interdiffusion. At low coverage, where the



magnetism of Cr and Mn is very large, interdiffusion is suppressed. ii) Magnetism reduces clustering and promotes alloy formation. For Mn we find a strong tendency for alloy formation. From i) + ii) we expect for the case of the Cu substrate a thermodynamically stable, two dimensional surface alloy: Cu(100)c(2×2)Mn. Although in detail, the results depend on the Cu substrate, the trends presented above have an universal character. Therefore, Cu(100)c(2×2)Mn is only an example of a much wider class of magnetic surface alloys. Ab-initio calculations have been performed using the FLAPW-method (Full-Potential Linearized Augmented Plane-Wave) and are based on the density functional theory in the local spin density approximation.

INVITED

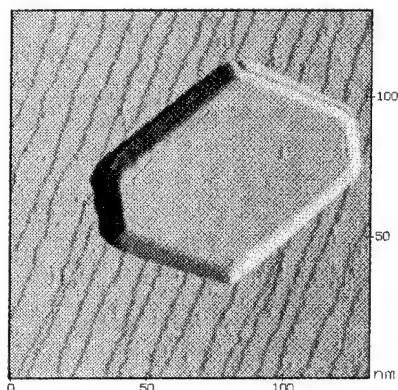
4:40 pm **SS1-WeA9 Enhanced Exchange Splitting of Gd at the Monolayer Limit**, Dongqi Li\*, Materials Science Division, Argonne National Lab, Argonne, IL 60439, Jiandi Zhang, P. A. Dowben, Dept. of Physics, Univ. of Nebraska, Lincoln, NE 68588, M. O'Neill, Dept. of Physics, Univ. of Wisconsin, Madison, WI 53706.

Ultrathin Gd films on W(110) have been studied with constant-initial-state spectroscopy (CIS) for photoemission utilizing linearly polarized light of synchrotron radiation. The photoemission cross-section of a 5d surface state near  $E_F$  shows strong photon energy dependence, i.e., sharp peaks in CIS spectra near the Gd 5p<sub>3/2</sub> adsorption edge. These peaks originate from resonant photoemission processes involving the occupied 5p and unoccupied 5d levels. In particular, mainly the 5d surface states/resonances were utilized in this resonant process. The symmetry of the unoccupied states were determined experimentally by changing the polarization of light, where p-polarized light excites only to the unoccupied  $d_{z^2}$  or  $d_{xz,yz}$  states and s-polarized light to all the d states including  $d_{x^2-y^2}$  and  $d_{xy}$  states. The lower bound of the exchange splitting of the Gd 5d<sub>z<sup>2</sup></sub> surface state can therefore be abstracted. This minimum exchange splitting increases when the thickness of Gd film decreases. The effect is particularly apparent at the monolayer limit, where the minimum exchange splitting increases by about 1 eV compared to that of bulk. Our results are qualitatively consistent with the theoretical predictions that the systems with lower coordination numbers have larger magnetic moments, and therefore larger exchange splitting.

\*Work at Argonne was supported by the US DOE BES-Materials Sciences under contract #W-31-109-ENG-38.

5:00 pm **SS1-WeA10 The Connection Between Morphology and Magnetic Characteristics for Gd Thin Films Grown on W(110)**, \*E. D. Tober, \*R. X. Ynzunza, \*A. P. Kaduwela, and \*C. S. Fadley, \*Physics Dept., U.C. Davis, Davis, CA 95616, \*Materials Sciences Division, Lawrence Berkeley Laboratory, Berkeley, CA 94720.

Post-deposition annealing of Gd thin films grown epitaxially on W(110) substrates has been observed in prior studies to drastically alter the magnetic properties of these films. We have used Scanning Tunneling Microscopy to examine the morphology of such films for two different post-deposition annealing temperatures (530 and 710 K). For coverages between 7 and 20 ML, annealing to 530 K is observed to produce smooth, monatomically stepped films. However, annealing to 710 K causes the films to break up into large 3-D islands resting on a base monolayer. The base monolayer is found for the first time to form a 7×14 superstructure arising due to the lattice misfit between the W(110) surface and the hexagonal Gd monolayer. The dimensions of the Gd islands produced by 710 K annealing are used to calculate the in-plane demagnetization factor and Curie temperature for 11 ML



thick films. These results are compared to previous magnetic ac-susceptibility ( $\chi_{ac}$ ) measurements. Our calculations accurately predict the 97% decrease observed in the  $\chi_{ac}$  signal between the 530 and 710 K annealed films as well as the increase in the Curie temperature from 247 to 284 K, respectively.

## SURFACE SCIENCE

Room A201 – Session SS2-WeA

### Solid Liquid Interfaces

Moderator: E. M. Stuve, University of Washington.

2:00 pm **SS2-WeA1 Surface Reconstruction at the Metal-Electrolyte Interface**, D. M. Kolb, Dept. of Electrochemistry, University of Ulm, D-89069 Ulm.

The low-index faces of gold and platinum are well-known to reconstruct when annealed under ultra-high vacuum (UHV) conditions. We have shown in the past that reconstructed gold surfaces are also stable in an electrochemical environment, if certain precautions are taken [1, 2]. At positive potentials specific adsorption of anions usually removes the reconstruction, while by applying negative surface charges the reconstruction is readily restored. The transitions between reconstructed and unreconstructed phase have been studied for Au(100) by in-situ STM which has led to an atomistic view on the dynamics of the potential-induced reconstruction and its anion-induced lifting. It will be shown that the transitions always start at surface defects such as monoatomic steps and therefore, the overall kinetics of these processes depends markedly on the step density. The corresponding current transients point to a nucleation-and-growth process which, however, cannot satisfactorily be described by the standard models of instantaneous or progressive nucleation. For many adsorption processes on gold the potential-induced reconstruction has to be taken into account, because depending on the potential region the reaction may take place on a surface structure vastly different from the one expected for the unreconstructed case. This is demonstrated for pyridine on Au(100) where the molecule adsorbs flat on the reconstructed surface, but assumes a vertical position on Au(100)-(1×1). A reorientation of the molecule occurs concomitantly with the lifting of the reconstruction.

INVITED

[1] D. M. Kolb and J. Schneider, *Electrochim. Acta* 31 (1986) 929.

[2] D. M. Kolb, in: *Structure of Electrified Interfaces*, eds. J. Lipkowski and P. N. Ross, VCH, New York, 1993, chap. 3.

2:40 pm **SS2-WeA3 Underpotential Deposition of Silver on the Au(111) Single Crystal Electrode in Sulfate Media. Ex Situ and In Situ Comparison**, P. Mrozek, Y-E. Sung, A. Wieckowski, and C-h. Chen, A. A. Gewirth, Department of Chemistry, University of Illinois, 600 S. Mathews Ave., Urbana, IL 61801.

The interactions of sulfate anions in sulfuric acid solutions with the Au(111) and Ag/Au(111) surfaces were studied using Auger Electron Spectroscopy (AES), Low Energy Electron Diffraction (LEED), Atomic Force Microscopy (AFM), Core Electron Energy Loss Spectroscopy (CEELS) and electrochemistry. At electrode potentials more positive than those within the silver deposition range sulfate adsorbate forms an ordered Au(111)/( $\sqrt{3} \times \sqrt{3}$ )R30° adlattice, and gives rise to a corresponding LEED pattern. Following extensive rinsing, silver forms two well-ordered structures: Au(111)p(3×3) and Au(111)p(5×5). However, AFM images reveal a clear p(3×3)-4Ag structure, which condenses to a close packed p(1×1)-Ag overlayer at more negative potentials. Distinctive S(LMM) Auger electron transitions and the S(L<sub>2,3</sub>) core electron energy loss of surface sulfate show a characteristic S<sup>6+</sup> sulfur valency, giving evidence that the sulfur oxidation state is not altered in the UHV environment. The downshift in the electron loss energy at the S(L<sub>2,3</sub>) level is indicative of increased electron density on sulfur with increasing sulfate-surface bonding. This increased sulfate-surface interaction arises, most probably, from back-donation into empty Rydberg states in the outer-potential wall. These data suggest that metal conduction electrons participate in the anion chemisorption. We conclude that the techniques used are complementary and together provide considerable insight into the Ag upd process.

3:00 pm **SS2-WeA4 Characterization of Carbon and Sulfur Covered Pt(111) and Their Influence on CO Adsorption and Electrooxidation**, D. E. Sauer, R. L. Borup and E. M. Stuve, Dept. of Chem. Eng., BF-10, University of Washington, Seattle, WA 98195.

The electrochemical and vacuum behavior of carbon and sulfur adlayers (formed by dehydrogenating ethylene or H<sub>2</sub>S) were studied with LEED, Auger spectroscopy, work function measurements, and cyclic voltammetry. The carbon adlayers were graphitic, as measured by Auger spectroscopy and LEED, and sulfur formed ordered adlayers, e.g. p(2×2) at 0.25 ML.

Cyclic voltammetry of carbon-covered Pt shows that the well known butterfly peak of clean Pt(111), often interpreted as a measure of surface order, remains for coverages as high as 1.0 ML of carbon, where ML refers to the C:Pt surface atom ratio. (A full carbon adlayer has a C:Pt ratio of 2.57.) Increasing the carbon coverage above 1.3 ML results in a broadened peak that eventually disappears at higher coverages, an effect attributed to interactions between graphitic islands on the surface. In contrast, the hydrogen adsorption/desorption behavior remains largely unchanged in extent and energetics up to carbon coverages of 3.3 ML. A sulfur coverage of 0.05 ML eliminates the sharp butterfly peak, and higher sulfur coverages cause both hydrogen adsorption and the butterfly peak to disappear completely.

For carbon coverages <2.57 ML electrooxidation of CO dosed from either solution or UHV occurs in a broader peak that is shifted 40 mV negative in potential relative to the clean surface. A carbon coverage of 2.8 ML completely blocks CO adsorption in vacuum, yet electrooxidation of solution dosed CO occurs at a potential 100 mV more positive than that of the clean surface.

3:20 pm **SS2-WeA5 Structure and Phase Behavior of Electrode Surfaces**, B. M. Ocko, J. Wang, G. M. Watson, O. M. Magnussen, and R. Adzic, Brookhaven National Laboratory, Upton, NY 11973-5000.

With the advent of synchrotron radiation, surface x-ray scattering has emerged as an important new probe of the structure and phase behavior of electrode surfaces. The low-index faces of Au, Pt, and Ag have been investigated in a variety of electrolytes. These studies reveal that well-ordered monolayers of electrodeposited anions (I, Br, and Cl) and metals (Cu, Pb, Bi, and Ti) can be formed at the electrode surface. The structure of these monolayers, and of the underlying substrate, can be studied with great precision using surface x-ray scattering. These studies show that commensurate, uniaxial-incommensurate, and biaxial-incommensurate adlayer structures may form and that transitions between these structures can be induced via the applied potential. For adsorbed anions, all three structure types have been observed and the incommensurate structures always electrocompress in the incommensurate phases. Coadsorbed phases, composed of anions and cations, may exist over a range of potential. An overview of x-ray scattering from electrode surfaces will be presented, and a comparison with vacuum studies will be provided. **INVITED**

This work was supported by the Department of Energy, Materials Sciences Division under Contract No. DE-AC02-74CH00016.

4:00 pm **SS2-WeA7 In Situ EXAFS of Cu on Pt Under Electrochemical Control\***, L. Wang and T. E. Furtak, Colorado School of Mines, Golden, CO 80401, L. B. Lurio, J. Pant, and T. M. Hayes, Rensselaer Polytechnic Institute, Troy, NY 12180.

The Cu atomic-scale environment, in a layer of Cu deposited electrochemically on a large Pt electrode, has been studied *in situ* using grazing-incidence, fluorescence-detection x-ray absorption fine structure spectroscopy. The size of the sample made it possible to acquire data of unusually high quality for an electrochemical x-ray absorption experiment. Measurements were performed on the same deposit using x-rays polarized with both s- and p-orientations. This is essential for a clear determination of the number of near-neighbor atoms of a given type. The results show that O, Cu, and Pt neighbors are located at distances consistent with a strongly bound structure with a fairly open geometry.

\*This research was supported by the Office of Naval Research, contract Nos. N00014-90-J-1326 and N00014-90-J-1332. The measurements were performed at the National Synchrotron Light Source on beamline X9B, built and operated by the National Biostructures Research Resource.

4:20 pm **SS2-WeA8 Model Electrochemical Interfaces in Ultrahigh Vacuum: Ionic and Surface Solvation Probed by Infrared Spectroscopy**, M. J. Weaver, N. Kizhakevariam, and I. Villegas, Department of Chemistry, Purdue University, West Lafayette, Indiana 47907, USA.

The last few years have witnessed notable advances in our ability to acquire atomic- and molecular-level structural information for in-situ metal-solution interfaces. The emergence of such spectroscopic and microscopic methods, applicable at metal-vacuum and metal-solution interfaces, is also enhancing the significance of systematic electrochemical modeling studies utilizing the former interfacial environment. This talk will focus on the use of one such method, infrared reflection-absorption spectroscopy, along with work-function measurements (i.e. surface potential) to yield information regarding ionic and surface solvation for model electrochemical interfaces ("synthetic double layers") in u.h.v. Specifically considered will be aqueous and non-aqueous solvation on Pt(111) surfaces in the presence of potassium ions and carbon monoxide. Although this type of information is still largely unobtainable for in-situ systems, the use of a common technique enables the intercomparison, and possibly enrichment, of the information obtained in both metal-liquid and metal-vacuum environments.

4:40 pm **SS2-WeA9 Thermal and Photon-stimulated Interactions of Oxygen and Water Coadsorbed with Potassium on Graphite**, D. Chakarav, L. Osterlund, B. Kasemo, Department of Applied Physics, Chalmers University of Technology and University of Gothenburg, 412 96 Göteborg, Sweden.

Interactions of O<sub>2</sub> and H<sub>2</sub>O with clean and potassium covered graphite constitute interesting model systems of both purely scientific and technological relevance. We have investigated these adsorbate and coadsorbate systems on graphite (0001) using Temperature Programmed Desorption (TPD), Photo Induced Desorption (PID), and High Resolution Electron Energy Loss spectroscopy (HREELS) at temperatures 85–1000 K. The clean graphite surface is non-reactive toward molecular oxygen or water: at 85 K O<sub>2</sub> sticking is below the detection limit, while H<sub>2</sub>O condenses to form hydrogen-bonded ice aggregates that sublime at ~150 K. In contrast, O<sub>2</sub> readily adsorbs on the K-covered surface to form K-O complexes with stoichiometry depending on the concentrations of the coadsorbates and on temperature. Water coadsorption with K, at low  $\theta_K$ , results in substantial structural changes of the H<sub>2</sub>O layer without dissociation. Above a critical coverage of K, H<sub>2</sub>O dissociates and reacts with K, to form KOH and KH. During subsequent annealing a number of surface reactions and transformations occur, including formation of potassium oxides and CO<sub>2</sub>. Photon irradiation causes desorption from the pure K-adlayer but does not desorb pure H<sub>2</sub>O. It induces a variety of transformations in coadsorbed H<sub>2</sub>O + K layers including formation of CO<sub>2</sub>.

5:00 pm **SS2-WeA10 Adsorption, Desorption, and Phase Transformation Kinetics of Multilayer D<sub>2</sub>O and H<sub>2</sub>O on Au(111) and Ru(0001)**, C. Huang, E. K. L. Wong, R. Scott Smith, and Bruce D. Kay, Molecular Science Research Center, Pacific Northwest Laboratory\*, Richland, WA 99352.

Molecular beam scattering and programmed desorption (both TPD and isothermal) are used to study the adsorption, desorption, and phase transition kinetics of H<sub>2</sub>O and D<sub>2</sub>O on multilayer ice surfaces. Two substrates, Au(111) and Ru(0001), are used as templates for the multilayer (5–200) water film growth. Water does not wet Au(111) but is known to form an ice-like bilayer structure on Ru(0001). Below 130K the adsorption probability is unity for both surfaces. Above 130K the desorption rate becomes comparable to the incident beam flux and, as such, the net condensation rate decreases rapidly with increasing temperature. On both substrates water films grown below 130K are initially amorphous in nature but undergo an irreversible phase transformation to a crystalline phase at a rate that is both strongly temperature and thickness dependent. Accompanying this phase transformation the multilayer shows complete isotopic scrambling over a thickness range exceeding 60 layers. The desorption kinetics from both phases are markedly non-zero order and substrate dependent. The desorption kinetics can be quantitatively described by a universality scaled rate law. The non-zero order kinetics and the attendant universality class are attributed to the morphology of the multilayer ice films. The experimental results, a quantitative kinetic model, and their implications concerning the structure of thin multilayer films will be discussed.

\*Pacific Northwest Laboratory is operated for the U.S. Department of Energy by Battelle Memorial Institute under contract DE-AC06-76RLO 1830.

# NANO 3/NANOMETER-SCALE SCIENCE AND TECHNOLOGY/BIOMATERIAL INTERFACES

Room A209 - Session NSBI-WeA

## Biology at the Nanoscale: I

**Moderator:** L. Bottomley, Georgia Institute of Technology.

2:00 pm **NSBI-WeA1 Non-contact Scanning Force Microscopy of F-actin**, David Braunstein, and James A. Spudis, Dept. of Biochemistry, Stanford University, Stanford CA 94305.

Filamentous actin or F-actin, a ubiquitous cytoskeletal protein, consists of 5 nm monomers assembled into a helical structure of 36 nm pitch, and 7 nm in diameter. F-actin is one of the best characterized cytoskeletal proteins, and serves as a good sample for testing the limits of resolution of non-contact scanning force microscopy (NCSFM). Unlike contact SFM, NCSFM probes the surface topography of a sample without direct physical contact of the sample with the cantilever tip, hence avoids the type of tip inflicted sample damage that one encounters with contact SFM. Rhodamine-Phalloidin-stabilized F-actin was deposited on sapphire substrates, which provide a flat, reusable surface, that upon submersion to an aqueous environment at pH 7 exhibits a positive surface charge that complements the negative surface charge of F-actin. The F-actin is sufficiently immobilized on the surface to withstand subsequent rinsing with distilled H<sub>2</sub>O and drying with dry N<sub>2</sub> gas. NCSFM images of F-actin clearly show filamentous structures, an ~40 nm periodicity, an apparent thickness of ~20 nm, and ~3 nm high, the reduced height probably the result of sample shrinkage. Although tip artifacts are apparent, such as the larger apparent diameter of the filaments, they are much less pronounced than that seen in contact images of the same samples. Contact SFM images, although showing the filamentous structure of the F-actin, display less of the periodic structure of the filaments over shorter stretches of the filaments, probably as a result the changes in orientation of the tip relative to the filament on the surface. The use of NCSFM in combination with the sapphire substrates should make it possible to image the ultrastructure of other cytoskeletal proteins.

This work is supported by NIH fellowship PHS AR08202-02.

2:20 pm **NSBI-WeA2 Atomic Force Microscopy of Collagen Monomers, Fibrils and Fibrillar Complexes**, E. A. G. Chernoff, Dept. of Biology, IUPUI, Indianapolis, IN 46202, and D. A. Chernoff, Advanced Surface Microscopy, Inc., 6009 Knyghton Rd., Indianapolis, IN 46220.

We are studying how the extracellular matrix is built up from individual molecules of collagen and associated polymers. We used a TappingMode™ AFM (NanoScope III) to image Type I collagen monomers, fibrils and complexes of collagen with the proteoglycan decorin. Collagen monomers (obtained from pepsinized bovine skin) appeared as flexible rods of variable length. Knob-like structures may be non-helical regions produced as a result of enzymatic digestion. We also found some oligomers in these preparations. Reconstituted collagen fibrils showed well-defined D-banding, with a period of 68 nm, as well as sub-bands at intervals as small as 20 nm. Asymmetry in these sub-bands was sufficiently distinct to indicate the direction of the carboxyl termini within the polymerized fibrils. The sub-band height contrast was increased by using TappingMode in a dry He atmosphere, suggesting that dehydration is a factor in visualizing the sub-bands. On fibrils reconstituted from a collagen-decorin mixture, decorin was visualized as an orderly pattern of bumps in the gap region. This is the first report of stable imaging of collagen monomers by AFM at room temperature. It is also the first report of direct visualization of collagen-bound decorin without using antibodies or other labels.

We thank Kathryn Vogel for providing the decorin and Helen Hansma and Magdalena Bezanilla for AFM work in dry He.

2:40 pm **NSBI-WeA3 Imaging Biological Systems with Near-Field Scanning Optical Microscopy**, Jeeseong Hwang\*, Eric Betzig\*, and Michael Edidin\*, The Johns Hopkins University, Baltimore, MD 21209, \*AT&T Bell Laboratories, Murray Hill, NJ 07974.

The Near-Field Scanning Optical Microscope (NSOM) exploits the near-field optical interaction between a sharp probe and a sample of interest to image surfaces at a resolution ( $< \lambda/50$ ) inaccessible by

traditional far-field microscopy. In addition to the resolution enhancement, many of the advantages in the conventional optical microscopy such as noninvasiveness, contrast mechanisms and reliability are retained as well in the NSOM technique. Here, the application of the NSOM will be discussed in imaging a variety of biological systems, including phospholipid domains and HLA-I proteins in the membranes of human skin fibroblasts and dynamic features of the model membrane systems during phase transition.

INVITED

3:20 pm **NSBI-WeA5 Imaging Individual Protein Molecules by Scanning Probe Microscopy**, S. L. Tang and A. J. McGhie, DuPont Central Research and Development, Wilmington, DE 19880-0356.

Scanning tunneling microscopy (STM) and atomic force microscopy (AFM) have been used to study the tertiary structures of protein molecules such as Chaperonin (Gro-EL) and Immunoglobulin (IgG). We have obtained nanometer-scale STM images of individual, randomly-spaced molecules deposited on thin films of sputter-deposited Au (111) on mica in ultrahigh vacuum. The many well-defined defects such as steps and kinks among the atomically flat (111) terraces act as physical "traps" for anchoring the molecules for imaging. The two-layered, ring-like structure of Chaperonin agree well with that deduced from transmission electron microscopy. The seven domains in the ring are not distinct. In addition, a structure attributable to a complex of Gro-EL and Gro-ES was also observed. The IgG molecule was observed to be lying flat on the surface. The well-known "Y"-shaped structure derived from x-ray crystallography of the IgG was readily observed. Although the dimensions of both molecules in the plane of the gold surface agree well with the known dimensions of the molecules, the vertical dimension of the Chaperonin molecules is severely compressed from over 10 nm to ~2 nm, whereas the vertical height of the IgG molecules was compressed much less severely from ~3 nm to ~2 nm. Possible mechanisms for imaging these molecules with the STM will be discussed. The STM results will also be compared to those obtained with the atomic force microscope (AFM).

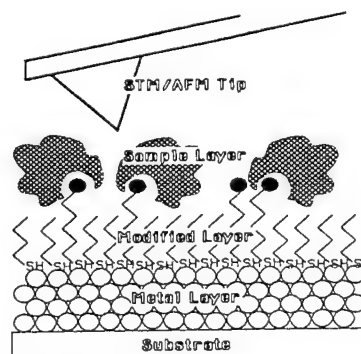
3:40 pm **NSBI-WeA6 Nanometer-scale Modification of Biological Membranes by Field Emission Scanning Tunneling Microscopy**, J. Tamayo and R. García, Centro Nacional de Microelectrónica, Madrid, Spain.

Manipulation and modification at atomic and nanometerscales of some semiconductor and metallic surfaces has been demonstrated by using one or a combination of the interactions present in Scanning Tunneling Microscopy. This has stimulated a variety of methods for fabrication of nanometer-scale structures and devices. The poor electronic conductivity of biological molecules has prevented the extension of those methods to them. Here, it is described how a low current Scanning Tunneling Microscope (STM) operated in the field emission regime allows to do, reproducible imaging and selective modification of biological membranes. A method is presented (i) to visualize at high resolution hydrated purple membrane sheets, (ii) to produce nanometerscale marks on them and (iii) to image the altered membranes.

These experiments pose the problem of electron transport through 5-10 nm thick insulating materials. We propose a model where the contrast mechanism is controlled by two factors, the electric field at the interface and the transmission through empty states in the membrane.

4:00 pm **NSBI-WeA7 SPM Studies of Supramolecular Architecture at Biological Interfaces**, M. Hara and W. Knoll, Frontier Research Program, RIKEN, Wako, Saitama 351-01, Japan.

Supramolecular architecture, which is composed of base substrate, single-crystal metal layer, modified layer and biological macromolecules, has been studied by scanning probe microscopy (SPM) to design



and build up novel artificial layered structures with well-controlled inorganic-organic interfaces. In order to fabricate such heterogeneous interfaces, we have combined self-assembly (SA) and LKB wet processes with dry MBE technique in one system.

Single-crystal metal layer, Au(111) was prepared by metal MBE with *in situ* RHEED monitoring under UHV condition. The substrate was transferred into an aqueous solution of SA materials such as thiol derivatives, and then biological macromolecules were introduced onto the modified Au(111) surface by SA and/or LKB.

STM/AFM imaging has been carried out in air and solution at room temperature. The images showed homogeneous domains and dislocations of protein monolayers immobilized and superimposed in the well-defined array of the modified Au(111) surfaces with high reproducibility.

This is the first step toward realizing novel material structures with well-controlled biological interfaces, which will provide an outstanding capability to identify specific sites and reveal nanoscopic aspects of supramolecular structures at individual molecular level.

**4:20 pm NSBI-WeA8 Control of the Adsorption of the Photoactive Biological Purple Membrane to Surfaces Using Self-Assembled Monolayers, R. A. Brizzolara, NSWC-White Oak, Code R34, Silver Spring, MD 20903.**

Bacteriorhodopsin is a photoactive protein found in the purple membrane of the *Halobacterium Halobium*. Bacteriorhodopsin is of interest for applications which utilize its photovoltaic properties, for example in devices for next-generation computational architectures. Potential benefits over semiconductor-based implementations include reduced device size and power consumption. In order to realize the goal of microfabricating devices based on purple membrane, a method is needed which allows the site-selected attachment of the purple membrane to a surface with a controlled orientation. Self-assembled monolayers (SAMs) are being investigated as a means to accomplish this. By patterning SAM terminal groups which inhibit and promote purple membrane adsorption, attachment sites for the purple membrane can be defined on a substrate. This talk will present results on the affinity of various SAM terminal groups for the purple membrane. Silane-based SAMs on glass were characterized by angle-resolved x-ray photoelectron spectroscopy (XPS) and contact-angle measurements. Purple membrane films on these SAMs were characterized by XPS and fluorescence microscopy. SAM terminal groups which promote and inhibit purple membrane adsorption have been identified. By using this information together with one of the SAM patterning approaches described in the literature, PM adsorption sites may be formed on a substrate. Other approaches which may allow the attachment of different genetic variants or other functional biomolecules to adjacent sites on a surface will also be discussed.

**4:40 pm NSBI-WeA9 Force Modulation Imaging of Protein Membranes, Hirofumi Yamada, Yoshiki Hirata\* and Jun Miyake\*, Joint Research Center for Atom Technology, 1-1-4 Higashi, Tsukuba 305, Japan, \*National Institute for Bioscience and Human-technology, 1-1-4 Higashi, Tsukuba 305, Japan.**

Force modulation (FM) technique in atomic force microscopy (AFM) provides new information about the local, mechanical properties of samples using the modulation of the applied load through vertical vibration of the sample at a frequency exceeding the feedback bandwidth of the AFM. This technique is expected to detect the difference in composition and/or conformation of organic molecular films. Using the FM technique, we have investigated Langmuir-Blodgett films of the photosynthetic protein membranes, chromatophores, obtained from photosynthetic bacteria *Rhodospseudomonas viridis* deposited on glass substrates. Chromatophores with various sizes from 50 nm to 1  $\mu$ m are composed of lipids and transmembrane proteins, photoreaction units (PRUs). The modulation frequency used here was 30–40 kHz and the amplitude was about 0.5 nm. The FM images show a remarkable contrast between the glass substrate and the membrane. The hexagonally packed structure of PRUs with the average spacing of 10 nm can be clearly observed in the FM images even when the corresponding structure cannot be found in the normal topography images taken simultaneously. In addition, the FM images reveal that some membranes do not contain PRUs while the topography data show no difference between these membranes and the others.

**5:00 pm NSBI-WeA10 LB Films of Disintegrated Purple Membranes: Photo-Electrical Properties and STM Investigation, E. A. Fedorov, V. V. Kislov, V. V. Panov, A. A. Kononenko, E. P. Lukashev, D. S. Chernavskii.**

The purple membranes (PM) fragments obtained by ultrasonic dis-

integration were used as a material for preparing monolayer LB films. The procedures of sample preparation, photo-electrical and STM methods of their study are described. As shown, the LB technique for a buildup of thin PM fragment films gives preparations in which the native optical and photo-induced electrical properties of bacteriorhodopsin (bR) are completely retained. The method of STM (under normal conditions in the absence of any conducting coatings and/or replicas) makes it possible to obtain stable contrast images of membrane surface which have a regular quasicrystalline structure of bR trimers with parameters in the range of (6.19–6.31) nm. The optimum conditions to obtain contrast images are found to be namely modulation regime, initial bias voltages about (150–300) mV, negative potential at probing tip and rather deep modulation  $U_m = 100$  mV at the frequency of 2.4 kHz. The problems of anomalous high conductivity, space resolution, nature of a noise character in STM experiments with biological objects are discussed. The analysis is accomplished of the possibility of electron conductivity and conductivity closely related to protein hydration state, where charge transfer occurs through network of collective surface hydrogen bonds coordinated by polar hydration centers.

## NANOMETER-SCALE SCIENCE AND TECHNOLOGY

**Room A207 – Session NS2-WeA**

### Optical Properties of Silicon Nanostructures

**Moderator: O. J. Glemboki, Naval Research Laboratory.**

**2:00 pm NS2-WeA1 Light from Silicon, F. Koch, Physics Department, Technical University Munich, 85747 Garching, Germany.**

In searching for ways to employ Si in light-emitting sources for optoelectronic applications, a great deal of progress has been made recently in the understanding of the fundamental processes involved. We review the various emissions between 0.8 and 2.7 eV that can be observed for bulk, crystalline Si (band gap 1.1 eV) by appropriate electrical and optical excitation. Particular interest attaches to the luminescence of Si which is finely divided in nanometer-sized crystalline grains in porous Si or colloidal suspensions. This is quite efficient and persists at room temperature. We show how the physics of quantum confinement and the chemistry of realistic surfaces combine to account for the observed luminescence. **INVITED**

**2:40 pm NS2-WeA3 Visible Luminescence from Plasma Deposited Nanocrystalline Silicon Thin Films, R. E. Hollingsworth, M. Estes\*, C. DeHart and P. K. Bhat, Materials Research Group, Inc., Wheat Ridge, CO 80033, \*Optoelectronic Computing Systems Center, University of Colorado, Boulder, CO 80309.**

We report on efficient visible luminescence from nanocrystalline silicon thin films deposited by plasma enhanced chemical vapor deposition using hydrogen diluted silane source gas mixtures and 110 MHz high frequency plasmas. This technique produces thin films consisting of silicon grains <100 nm in size in an amorphous silicon matrix. The grain size was controlled by varying the hydrogen dilution and substrate temperature. Films have been deposited on glass, ITO coated glass, Cr coated glass, metal foils and silicon wafer substrates. Stain etching with HF:HNO<sub>3</sub>:H<sub>2</sub>O solutions yielded films with orange-red photoluminescence at room temperature with efficiencies close to anodically etched porous silicon films on wafer substrates. Temperature dependent photoluminescence measurements were performed on as-deposited and etched films. The luminescence from as-deposited nanocrystalline films was virtually identical to the luminescence from hydrogenated amorphous silicon films deposited from pure silane plasmas with a single PL peak at 1.5 eV. After stain etching, a visible luminescence peak at 1.7–1.8 eV developed while the amorphous silicon peak intensity decreased considerably. Variations in the luminescence with deposition conditions, including doping with boron, phosphorus, or carbon, will be presented. The implications of these results on the explanation of the origin of visible luminescence in nanocrystalline silicon thin films produced by various methods will be discussed.

**3:00 pm NS2-WeA4 The Mechanism of Room Temperature Red Light Emission in Porous Silicon and Fabricated Silicon Nanostructures, S. M. Prokes, W. E. Carlos and O. J. Glemboki, Naval Research Laboratory, Washington, D.C. 20375.**



Raman spectroscopy, photoluminescence (PL), and electron spin resonance (ESR) experiments have been performed on as made and atmospherically oxidized porous silicon. Results indicate the presence of oxygen shallow donors of binding energy of about 0.1 eV, which show a distinct correlation with the intensity of the red room temperature PL observed. It is suggested that the shallow donors become paramagnetic by photo-induced capture of carriers created by light absorption into the silicon crystallites. Annealing studies have shown a correlation between the PL intensity and the paramagnetic shallow donor signal strength. In view of these results, a model is suggested linking the presence of the shallow donors to the presence of non-bridging oxygen hole centers, which are thought to be responsible for the intense red PL reported in porous silicon. In addition, lithographically fabricated silicon nanostructures have also been formed, and they have been examined using micro-photoluminescence and micro Raman spectroscopy. Their light emission and structural properties will be discussed in view of the above suggested model.

**3:20 pm NS2-WeA5 Properties of Ultrathin Films of Porous Silicon,\* J. von Behren,<sup>1</sup> Y. Kostoulas,<sup>2</sup> L. Tsybeskov, Ju. V. Vandyshv,<sup>3</sup> and P. M. Fauchet,** Department of Electrical Engineering, University of Rochester, NY 14627.

We have produced films of light-emitting porous silicon (LEPSi) as thin as  $\sim 1 \mu\text{m}$ , lifted them off the silicon wafer by an electropolishing step, and deposited them onto sapphire windows where they remain attached by Vanderwaals or electrostatic forces. Although others have previously obtained free-standing LEPSi films, our films are one order of magnitude thinner, luminesce strongly and have excellent mechanical properties because of the sapphire substrate. The important steps in this procedure will be discussed in some detail and the structural, chemical and optical properties of these films as measured using a variety of probes will be reported. These films are semi-transparent in the visible and thus make several new optical measurements possible. We will report the results of photoinduced absorption measurements performed with 100 femtosecond time resolution which reveal the first step in the carrier dynamics, namely the trapping of carriers in surface states.

<sup>1</sup>also at the Technical University of Munich, Garching, Germany.

<sup>2</sup>also with the Department of Physics & Astronomy.

<sup>3</sup>also with Moscow State University, Moscow, Russia.

\*Work supported in part by grants from the New York State Energy Research & Development Authority and Rochester Gas & Electric.

**3:40 pm NS2-WeA6 Luminescent Porous Silicon Layers Fabricated by Anodisation and Supercritical Drying, L. T. Canham and T. I. Cox,** Defence Research Agency, St. Andrew's Road, Great Malvern, Worcestershire, WR14 3PS, United Kingdom.

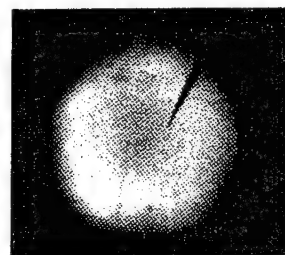
There is currently enormous interest in the optoelectronic properties of luminescent porous silicon. We have recently demonstrated that ultrahigh porosity layers ('aerocrystals') can be realized by removing the electrolyte from the pores with supercritical  $\text{CO}_2$  (1). We show here that a wide range of porous silicon structures, not previously attainable, may be fabricated with good structural integrity using supercritical drying. In many high porosity layers, much of the inhomogeneity reported to date is shown to arise from the capillary force induced collapse of the silicon network during normal ambient drying. Supercritical drying enables us to reveal clearly the large porosity gradients that can result from the electrochemical etching process itself. Oxidation of complete layers gives rise to films of high porosity silica which have subsequently been impregnated with laser dyes to give very bright photoluminescent films. Cross-sectional PL spectroscopy data of the structures described above is presented revealing the depth dependent luminescent properties of such layers. The importance of porosity gradients in elucidating optoelectronic properties will also be discussed.

1. L. T. Canham, A. G. Cullis, C. Pickering, O. Dosser, T. I. Cox, T. P. Lynch, *Nature* 368, 177 (1994).

**4:00 pm NS2-WeA7 Visible Electroluminescence from Ultrathin Stain-Etched Porous Silicon Films, J. Xu and A. J. Steckl,** Nano-electronics Laboratory, Department of Electrical and Computer Engineering, University of Cincinnati, Cincinnati, OH 45221.

While porous Si(PoSi) produced by stain-etch in  $\text{HF:HNO}_3$ -based solutions exhibits similar photoluminescence (PL) to that of prepared by anodization in HF-based electrolytes, stain-etching process possess some unique advantages over anodization in addition to its significant

simplicity. This includes sub-micron PoSi pattern formation and poly-PoSi thin films on glass. We report for the first time visible electroluminescence (EL) from *stain-etched* ultrathin PoSi films. Uniform PoSi films of  $\sim 200 \text{ nm}$  were obtained by stain etching (100) p-Si substrates of  $6\text{--}16 \Omega\text{-cm}$  in  $\text{HF:HNO}_3:\text{H}_2\text{O}$  (1:3:5) for several minutes. An Al film was deposited onto the back side of the wafer to provide an ohmic contact before PoSi formation. Indium tin oxide (ITO) thin films of  $\sim 2000 \text{ \AA}$  were deposited onto PoSi samples through a shadow mask resulting in Schottky diodes with a strong rectifying I-V characteristics. The diodes have a leakage current of 43 nA at a reverse bias of 10V and a rectifying ratio of  $>10^4$  from 1–15V, better than any reported value for PoSi LED's. Red-orange EL was easily observable to the naked eye in dark for a forward bias of  $\geq 10\text{V}$ . The light output (brightness) increases with increasing diode current. The EL spectrum, with a peak at 640 nm, is very similar to that of the PL, indicating both EL and PL have common luminescent centers. This result represents the first LED from stain-etched PoSi with ultrathin film layer. At the current stage the EL intensity is much lower than that of the PL. Quantitative measurement of the EL external quantum efficiency (EQE) and techniques to improve the device performance are currently being pursued.



EL topography at a forward bias of  $40 \text{ mA/cm}^2$

**4:20 pm NS2-WeA8 Properties of Partially Oxidized Porous Silicon,\* L. Tsybeskov and P. M. Fauchet,** Department of Electrical Engineering, University of Rochester, Rochester, NY 14627, USA.

We report the preparation and characterization of partially oxidized porous silicon layers obtained for example by anodization of p-type silicon wafers in an HF solution with light assistance. In these samples, FTIR measurements detect a significant amount of  $\text{O}_n\text{-Si-H}_m$  bonds and the photoluminescence (PL) is stable, peaks between 600 and 570 nm, and has a temperature dependence that can be fitted by an activation energy of only 10 meV. Light-emitting diodes have been made in this type of porous silicon and their very promising electrical and optoelectronic properties have been fully characterized. We find that the electroluminescence (EL) occurs at 760 nm (and not at 600 nm) and is stable (no degradation after 100 hours of operation). In addition, the EL intensity increases linearly with current up to  $\sim 1 \text{ A/cm}^2$ . The origin of the PL and EL and the prospects for commercial devices will be discussed.

\*Work supported in part by grants from the New York State Energy Research & Development Authority and Rochester Gas & Electric.

**4:40 pm NS2-WeA9 Enhancement and Suppression of the Formation of Porous Silicon,\* S. P. Duttagupta, C. Peng and P. M. Fauchet,** Department of Electrical Engineering, University of Rochester, Rochester, NY 14627, S. K. Kurinec, Department of Microelectronic Engineering, Rochester Institute of Technology, Rochester, NY 14623; T. Blanton, Eastman Kodak Co., Kodak Park, Rochester, NY 14652.

We present the results of an investigation of various means to enhance or suppress the formation of porous silicon. Our results demonstrate that porous silicon LEDs and silicon electronic devices can coexist in close proximity (within  $1 \mu\text{m}$  or less) on the same chip. The first method uses a trilayer photolithographic process together with silicon nitride to produce light-emitting porous silicon (LEPSi) lines as narrow as  $\sim 2 \mu\text{m}$  adjacent to fully protected silicon regions. The second method consists of amorphizing regions of the wafer prior to anodization with high energy/high dose ions (ion implantation) such as Si, B or P, followed by anodization and annealing. In this method, LEPSi is produced on the unimplanted regions only. The crystallinity



and electrical properties of the implanted region have been fully characterized after annealing. Using focussed ion-beam implantation, 50 nm patterns have been obtained. The third method consists of low energy/low dose bombardment (ion milling/reactive ion etching) with argon ions prior to anodization. Under appropriate conditions, we have observed a strong enhancement of the formation rate of LEPSi where bombardment took place, possibly due to the generation of a large number of defects on the wafer surface.

\*Work supported in part by grants from the New York State Energy Research & Development Authority and Rochester Gas & Electric.

## APPLIED SURFACE SCIENCE Room A101 - Session AS-WeA

### Depth Profiling

**Moderator:** A. L. Testoni, Digital Equipment Corporation.

2:00 pm **AS-WeA1 Fundamental Limits to Sputter Depth Profiling: Atomic Force Microscopy of Ion Beam-Induced Topography,** Eun-Hee Cirlin, Hughes Research Laboratories, Malibu, CA 90265.

Sputter-induced surface topography, atomic mixing, and the statistical nature of the sputtering process contribute to degradation of the depth resolution and changes in secondary ion yields of sputter depth profiles. Hence accurate sputter depth profiling of atomically abrupt interfaces of modern layered structures poses stringent requirements for the understanding of the energy transport of ions in matter, and the physics and chemistry of ion-target interaction at the surface and interface. In this talk, first, recent advances in understanding of the mechanism of the ion bombardment-induced roughening and smoothing of surfaces caused by various factors—sputtering, redeposition, implantation of primary ion, ion-target interaction, surface diffusion, and segregation—will be reviewed. Sputter-induced roughening has long been attributed primarily to variations in secondary ion yield with angle of incidence and surface temperature for a given primary ion specie. To illustrate, an exciting video involving AFM investigation of ripple nucleation, formation, evolution on a GaAs surface during 3 keV  $O_2^+$  bombardment at  $\theta = 45^\circ$  will be shown. In addition, recent insights gained on the fundamental limits to sputter depth profiling from the studies of SIMS and AFM of delta-doped layers and superlattices will be discussed. Next, using AFM measurements together with SIMS depth profiles of Si delta-doped GaAs, with and without sample rotation, various contributing components of the depth resolution including sputter-induced roughness, atomic mixing, statistical sputtering, and inhomogeneity of the ion beam current density will be quantified. Also, the Gaussian resolution functions of  $2\sigma = \Delta z$  before and after ripple formation will be examined. Finally, recent international SIMS round robin studies of the depth resolution of Si delta-doped GaAs from 25 laboratories will be discussed.

### INVITED

2:40 pm **AS-WeA3 Determination of the Electron Attenuation Length from High Resolution AES Depth Profiles,** S. Hofmann, Max-Planck-Institut für Metallforschung, Institut für Werkstoffwissenschaft, Seestr. 92, D-70174 Stuttgart, Germany.

AES depth profiles of well defined interfaces in bilayers or in sandwich structures can be used to determine the attenuation length of the respective Auger electrons. The precision of the value obtained is strongly dependent on the absolute magnitude of the depth resolution  $\Delta z$ , which has to be optimized by minimizing all the distortional contributions to  $\Delta z$  like ion induced atomic mixing and surface roughening. Appropriate are values of  $\Delta z$  of 2-3 nm which are obtained in high resolution depth profiling of GaAs/AlAs superlattice structures with 10 nm single layer thickness. The shapes of the profiles are used to extract the attenuation length of Al (LVV, 68 eV) and of Al (KLL, 1396 eV) Auger electrons which are found to be 0.55 and 2.3 nm, respectively, and which are in reasonable agreement with recent calculations of the inelastic mean free path by Tanuma et al. /1/. The accuracy of the experimental values is correlated with the knowledge of the exact layer thickness (e.g. from cross section TEM images) and with the absence of strongly detrimental effects in profiling such as

preferential sputtering, segregation or radiation enhanced diffusion. The presented example shows that an accuracy of better than  $\pm 20\%$  can be obtained in favorable cases.

/1/ S. Tanuma, C. J. Powell and D. R. Penn, S.I.A. 17 (1991) 927.

3:00 pm **AS-WeA4 Resolution in Sputter Depth Profiling Assessed by AlAs/GaAs Superlattices,** K. Kajiwara<sup>1</sup> and R. Shimizu<sup>2</sup>, <sup>1</sup>Sony Corp. Research Center, Yokohama, 240, <sup>2</sup>Osaka University, Suita, 565 Japan.

AlAs/GaAs superlattices are proposed as a potential reference material for sputter depth profiling since, at present,  $Al_xGa_{1-x}As$ /GaAs superlattices are grown in a defect-free single crystalline state with atomically flat and abrupt interfaces by metalorganic chemical vapor deposition. It is possible to determine accurately the depth resolution of AES, XPS and SIMS depth profiles using AlAs/GaAs superlattices. A preliminary round robin test was performed by the ISO/TC201 Depth Profiling WG in Japan.

As a result, it is clear that in all the AES and SIMS data, the depth resolution is constant having no relation to the sputtered depth. On the contrary, in the XPS data, which have a larger probing area, a degradation of depth resolution occurs with increased sputtered depth. It is estimated that the depth resolution is correlative with the probing area owing to the crater edge effect. In addition, in the SIMS data, the resolution of the leading and trailing edges depends strongly on primary reactive ion species ( $O_2^+$ ,  $Cs^+$ ). This is in contrast to AES and XPS data using inert ions (e.g.  $Ar^+$ ). It was confirmed that AlAs/GaAs superlattices as a reference material are very useful for accurate evaluation of the resolution in sputter depth profiling.

3:20 pm **AS-WeA5 The Effects of Misorientation of the GaAs(100) Surface on the Secondary Ion Yield during  $O_2^+$  or  $Cs^+$  Ion Sputtering,** J. W. Lee, S. H. Kim, W. J. Choi, C. Y. Kim and S. T. Kim, GoldStar Central Research Laboratory, 16 Woomyeon-Dong, Seocho-Gu, Seoul, 137-140 Korea.

The effects of misorientation on the ion yield during SIMS sputter depth profiling have been studied for the GaAs(100) surfaces miscut by  $0^\circ$ ,  $2^\circ$ ,  $5^\circ$  and  $7^\circ$ . The MOCVD grown samples with the structure of  $AlGaInP/GaAs/GaAs$  (Si doped substrate) were sputtered with 5 keV  $O_2^+$  or  $Cs^+$  primary ion beam at an incident angle of  $60^\circ$  from the surface normal. The relative secondary ion yields of Al and In were measured. In case of  $Cs^+$  primary ion beam, there was no detectable change in the secondary ion yield with the surface misorientations. On the contrary, the analysis with  $O_2^+$  primary ion beam showed a correlation between the change of secondary ion yield and the degree of misorientation of the surface. The relative secondary ion yield increased with increasing the degree of misorientation. In order to investigate this dependence from the topographical point of view, the crater bottoms after sputter erosion were scanned by AFM. The AFM results revealed a close resemblance to the observed correlation between the change of ion yield and the degree of misorientation. The relationship among the degree of misorientation, the secondary ion yield and the topographical change will be discussed.

3:40 pm **AS-WeA6 Sputtering Effects in SIMS Depth Profiles of Multicomponent Glasses,** V. J. Bojan, T. E. Paulson, C. G. Pantano, The Pennsylvania State University, Materials Characterization Laboratory, University Park, PA 16802.

The high sensitivity of SIMS makes it a desirable technique to quantitatively study the compositional gradients produced in glass surfaces due to manufacturing and secondary processing conditions. Earlier studies of commercial soda-lime silicate glass, done in a Cameca IMS-3F using negative primary beam bombardment, showed unexpected gradients in the sodium, silicon and calcium concentrations within 100 nm of a fracture surface of this glass. A series of similar sodium-silicate and soda-lime glasses has been prepared and analyzed to study these unexpected gradients. Both the magnitude and depth of the gradients observed in the silicon profile show a strong dependence on the presence of calcium in the glass. The sodium profiles in all the glasses show an apparent surface enrichment, however the in-depth behavior of the sodium profile varies with the glass composition. This result, coupled with the difficulty in reproducing the measured Na/Si signal ratios suggest that sodium may be mobile during the analysis, despite stable surface charge compensation. The calcium profiles in all the glasses show an apparent surface depletion, and the approach to steady state signal levels is not effected much by the glass composition. These gradients are not expected on fracture surfaces, there-

fore their presence on manufactured or processed surfaces does not necessarily indicate true compositional changes. Methods to correct for these gradients will be discussed.

**4:00 pm AS-WeA7 The Effect of Tilt Angle on As Implants in Si, J. M. Anthony, and J. A. Keenan, Texas Instruments, Dallas, TX 75265.**

Arsenic implantation is often used to dope the walls of trench capacitors in high density DRAM structures. In order to investigate As incorporation during angled implantation, Si wafers have been implanted with As ions (100 keV,  $1.25 \times 10^{15}$  at/cm<sup>2</sup>) at a variety of tilt angles from 0–80 degrees. BF<sub>2</sub> ions (80 keV,  $5 \times 10^{14}$  at/cm<sup>2</sup>) were also implanted at 0 degrees in each wafer to establish a consistent depth marker during SIMS analysis. Range and peak concentration have been extracted from the SIMS data and are compared to predictions from simulation programs. Dose measurements for the steeply angled implants are difficult with SIMS due to surface ion yield transients, so absolute dose measurements have been made using RBS and neutron activation analysis. At high tilt angles (similar to the geometries used for trench implants) backscattering of the As ions greatly reduces the implanted fraction, and this is also compared with computer simulations.

**4:20 pm AS-WeA8 Nondestructive and Quantitative Depth Profiling Analysis of Ion Bombarded Surfaces by Medium Energy Ion Scattering Spectroscopy, J. C. Lee, H. J. Kang, H. K. Kim, D. W. Moon, Korea Research Institute of Standards and Science, Yousoung P.O. 102, Taejeon, Korea 305-606.**

Ion beam sputtering has been widely used for sputtering depth profiling with XPS and AES. However the problem of the surface compositional change due to ion bombardment has remained to be understood and solved. In this work, the altered surface layer of amorphous Ta<sub>2</sub>O<sub>5</sub> thin films due to Ar<sup>+</sup> ion bombardment was depth profiled nondestructively and quantitatively, for the first time by Medium Energy Ion Scattering Spectroscopy as a function of the ion incidence angle, the ion energy, and the ion dose with the depth resolution of better than 1 nm. The MEIS spectrum showed that the oxygen depleted depth is 30 Å under normal incident 3 keV Ar<sup>+</sup> ion bombardment and it decreases continuously with the incidence angle to 15 Å under the 80° glancing incidence angle. The increased Ta concentration at the surface due to preferential sputtering of oxygen atoms was about 47% under normal incident 3 keV Ar<sup>+</sup> ion bombardment and about 20% under 80° glancing incidence. The altered zone was saturated in the ion dose of  $3 \times 10^{16}$  ions/cm<sup>2</sup>. With the increase of the ion energy from 3 keV to 5 keV, the depth of oxygen depleted zone increased slightly from 30 Å to 40 Å. The above experimental results are compared with XPS results and the Monte Carlo Simulations.

**4:40 pm AS-WeA9 Nondestructive EPMA Depth Profiling of Buried Oxide Layers in Silicon, A. P. Alexeyev, Research Centre for Surface and Vacuum Investigation, 2 Andreyevskaya nab. Moscow 117334 Russia.**

The application of electron probe X-ray microanalysis (in wavelength dispersive mode) to obtain the depth profiles of buried oxide layers in silicon is discussed.

If the electron beam of energy  $E_p$  falls onto the surface of the analyzed specimen, the characteristic X-ray intensity of oxygen atoms will be proportional to the convolution of two functions: the depth profile  $W(Z)$  of oxygen atoms and the depth distribution of X-ray production for the characteristic X-rays of oxygen atoms  $\Phi(Z, E_p)$ . One needs to take into account the absorption of X-rays in the analyzed specimen. One can obtain  $m$  coupled equations with respect to  $W(Z)$  by measuring the oxygen intensities at  $m$  values of  $E_p$ . In this case one can find the input parameters ( $m$  no more) for this unknown profile which will provide the coincidence between the calculated and measured X-ray intensities. 4–5 parameter fitting of  $W(Z)$  curve was developed to characterize the buried near-surface oxide layers created by high dose ion implantation ( $2.6 \times 10^{17}$  cm<sup>-2</sup>). This approach requires an accurate knowledge of  $\Phi(Z, E_p)$  functions. The set of "polysilicon/SiO<sub>2</sub>/bulk Si" sandwich structures having the polysilicon and SiO<sub>2</sub> layers of different thickness was prepared. The measurements of O-Ka intensities on these structures made possible to find the  $\Phi(Z, E_p)$  curves that were used for  $W(Z)$  determination.

The results, obtained, show good agreement with depth profiles measured by Auger electron spectroscopy. It was shown that EPMA measurements at 2–8 keV  $E_p$  range make it possible to determine the oxygen distribution in depth up to 0.4 μm.

**5:00 pm AS-WeA10 Real Time Monitoring of Depth Profiling, L. A. Vasilyev, A. V. Naumkin, V. I. Rakhovsky, Research Center for Surface and Vacuum Investigations, 6, bld. 1, Kazarmenny per., 109028 Moscow, Russia.**

Depth profiling (DP) is a widespread procedure in XPS, AES and SIMS. Ion sputtering is very convenient for DP. Usually DP experiment takes a lot of time and destroys a sample. If the region of interest has been passed one has to get another sample and to repeat an experiment. Ion sputtering can modify the sample composition and affect DP results (broad the interfaces, alter the composition of the inhomogeneities and the interfaces, etc.) So it is a good idea to change the sputtering conditions when the region of interest is at the depth of 100–200 Å under the surface sputtered. In our investigation we studied the ion induced true secondary electron peak (ITSEP) sensitivity to monitor the interfaces and inhomogeneities appearance. The results show that with samples consisting of the insulating film on the conducting substrate (SiO<sub>2</sub> at Si-like) it is possible to detect the interface at the depth of 100–300 Å under the surface sputtered.

## PLASMA SCIENCE

### Room A109 – Session PS—WeA

#### Plasma-Induced Charging and Contamination Effects

**Moderator: M. G. Blain, Sandia National Laboratories.**

**2:00 pm PS-WeA1 Effect of Plasma Overetch of Polysilicon on Gate Oxide Damage, J. P. McVittie and C. T. Gabriel\*, Stanford University, Stanford, CA 94305-4070, \*VLSI Technology, San Jose, CA 95131.**

Modeling and previous experiments have indicated that charging damage during polysilicon etching occurs just before endpoint when the last of the exposed polysilicon can collect excess plasma currents which cause damage by flowing through the gate oxides. During overetch, this damage mechanism is suppressed by the poor collection efficiency of the exposed polysilicon edges, and as such damage from this mechanism is expected to remain constant during this period. Although there is an additional edge damage mode where damage can increase during overetch, we here report results showing a decrease in damage with overetch time. The experiment consisted of two lots of fully processed CMOS wafers where the polysilicon overetch percentage was varied from 0 to 90%. The etch tool was a triode system which showed antenna dependent charging damage. The test structures were large area capacitors with a 10.5 nm thin oxide whose breakdown statistics were measured after the full process including anneals. Both the n-channel and p-channel devices showed damage which decreased with overetch time. The damage was significantly worse for the n-channel devices—the mean n-channel gate oxide breakdown voltage was 3 V at endpoint and increased to 11.5 V after 90% overetch. The effect was repeatable in that both lots showed the same results.

The results indicate an apparent annealing during overetch. In the past, rf annealing has been reported for e-beam damage with a proposed mechanism involving rf heating and carrier motion. We consider this unlikely and suspect that low plasma currents collected by the gate edge could be being playing a role in this annealing; however, etching of the exposed gate oxide during overetch may also be important. The n and p channel differences can be explained by a voltage drop across the n-well which reduces the tunnel current through the p-channel gate oxides.

**2:20 pm PS-WeA2 Plasma-Induced Gate Oxide Charging Issues for sub-0.5 μm CMOS Technologies, A. K. Stamper, J. B. Lasky, and J. W. Adkisson, IBM Microelectronics, Essex Junction, Vermont 05452.**

Gate oxide charging issues which occurred during the development of IBM's 200mm wafer sub-0.5 μm 16-Mb DRAM and logic processes are discussed. We show that gate oxide degradation is caused by a constant electron current, but it can be modulated by systematically changing the plasma properties. Gate oxide charging can occur during reactive ion etching (RIE) and plasma-enhanced chemical vapor deposition (PECVD) processes. Using poly-conductor (PC) antenna structures and fully integrated PC test sites, we investigated three RIE processes: metal etch (BCL<sub>3</sub>/CF<sub>4</sub>/N<sub>2</sub>), oxide etch (CHF<sub>3</sub>/CF<sub>4</sub>/Ar), and polysilicon etch (HCl/O<sub>2</sub>/He); Ar sputter processes; and TEOS and SiH<sub>4</sub>-based PECVD processes. Charging increased when the PC was

exposed during the etch and decreased when the PC was coated with photoresist. Oxide RIE and Ar sputter were the most charge-sensitive etch processes; TEOS oxide was the most charge sensitive PECVD process. I-V measurements on PC antenna structures showed that the degradation can be separated into two components: gate oxide trap creation and catastrophic gate oxide defects. The gate oxide traps result in a transient current during I-V testing and can be passivated (or activated) by a 400°C H<sub>2</sub> (N<sub>2</sub>) anneal. Significant charging can occur during TEOS oxide depositions. In general, charging decreased as TEOS partial pressure decreased, as phosphorus doping decreased, as rf power decreased, and as overall pressure increased. By measuring the optical emission, rf current, and rf voltage during the film depositions, we concluded that charging decreased as rf voltage and optical emission of the plasma decreased, indicating that gate oxide charging is a strong function of electron energy and density in the plasma.

**2:40 pm PS-WeA3 Gate Oxide Damage due to Local Charging Caused by Electron Shading, Koichi Hashimoto, Fujitsu Limited, C832, 1015, Kamikodanaka Nakahara-ku, Kawasaki 211, Japan.**

Degraded gate oxide breakdown voltages have been observed after exposing antennas (10,000:1 area ratio) to an electron cyclotron resonance (ECR) plasma when the antennas were covered with resist patterns having high-aspect-ratio openings. Similar antenna structures appear near the endpoint of ordinary metal etching transiently, because of microloading effect, and also appear in via hole etching inherently. In contrast to the well-studied damage caused by charge-up voltage difference across the wafer, the damage reported here was observed even when the test wafer was cut into small (5 mm square) chips where the wafer-scale voltage difference, if existed, could not affect any longer. In addition, higher aspect ratio of the resist patterns raised the gate oxide failure frequency. These results indicated that the structure itself induced a local differential charging; and they led the author to "electron shading" model: the resist patterns above antenna metal shaded it from oblique-incidence electrons, resulting in an excessive positive current from ions impinging normally. This effect was observed in various plasmas, such as parallel plate and ECR plasmas, for metal etching and via hole etching. Moreover, the damaging current appeared to increase by a factor of more than ten with a decrease in gate oxide thickness from 8 nm to 6 nm, and hence serious damage could be expected for future ULSIs. This dependence on gate oxide thickness can be explained with a somewhat complicated model taking into account the electric field building up in between and around the resist patterns.

**INVITED**

**3:20 pm PS-WeA5 Plasma-Induced-Damage of GaAs During Etching of Refractory Metal Contacts, R. J. Shul, M. L. Lovejoy, A. G. Baca, J. C. Zolper, C. I. H. Ashby, D. J. Rieger, M. J. Hafich, and J. F. Klem, Sandia National Laboratories, Albuquerque, NM 87185.**

Refractory metal thin films for non-alloyed ohmic and Schottky contacts are finding wide application in the fabrication of high-speed GaAs FETs and HBTs. Although reactive ion etch (RIE) and electron cyclotron resonance (ECR) etches have been reported to yield sub-micron dimensions and anisotropic profiles, plasma-induced-damage to the GaAs active layers has not been reported.

We have studied the effect of plasma-induced-damage on the majority carrier transport properties of GaAs by monitoring changes in sheet resistance of thin film conducting layers under etch conditions for refractory metal contacts. Sheet resistance ( $R_s$ ) determined from transmission line measurements are used to evaluate the depth of plasma-induced-damage for ECR and RIE etch conditions by varying the thickness of active epitaxial layers. At high dc-bias ECR conditions (300 V), damage extends throughout the conduction layer yielding infinite  $R_s$  for 1E18 cm<sup>-3</sup> and 3E17 cm<sup>-3</sup> material at thickness of 900 Å and 1800 Å, respectively. Under RIE conditions at 490 V dc-bias, only the 1E18 cm<sup>-3</sup> material was completely depleted. This data suggests the bulk of the damage occurs within 1000 Å of the surface, however increasing the dc-bias can significantly extend this depth. For low dc-bias conditions in the ECR and RIE plasmas (70 and 190 V, respectively), the  $R_s$  were lower in the RIE (by approximately a factor of 2) indicative of less plasma-induced-damage. This observation may be attributed to significantly higher ion densities in the ECR which will be investigated as a function of microwave power.

**3:40 pm PS-WeA6 2-D Visualization of Powder Formation and Trapping Dynamics in Silane Plasmas, J.-L. Dorier, Ch. Hollenstein, A. A. Howling, C. Courteille, L. Sansonnens, CRPP/EPFL, 21 Av. des Bains CH-1007 Lausanne, Switzerland.**

Particulate studies in deposition plasmas are motivated by the need

to reduce contamination in the plasma and films. Models for the forces acting upon particles in rf discharges suffer from a lack of quantitative experimental data for comparison in the case of silane-containing plasmas. In this work, a cross-section of the parallel-plate capacitor discharge is illuminated with a polarized beam-expanded laser and global spatio-temporal scattered light and extinction are recorded by CCD cameras. This method allows a self-consistent estimation of the particle size and number density throughout the discharge volume. Spatially regular Mie interference fringes are visible over large regions in the electrode gap, which unambiguously demonstrates the uniform monodisperse nature of the early stage of particle growth. Later, the boundaries between powder-free plasma, monodisperse growing particulates, and zones of mixed sizes are sharply delineated. Finally, a spatial size segregation of successive particle generations occurs. The effect of on/off power modulation frequency on particulate location and agglomeration is also presented. The plasmas investigated are pure silane, argon-diluted silane or pure argon containing particles. In the latter case, comparison is made with a 2-D self-consistent fluid model. In conclusion, this global diagnostic improves understanding of particle dynamics in silane rf discharges and provides experimental input for testing the validity of models.

**Acknowledgments:** This work was funded by Swiss Federal Research Grant EF-REN(93)035 and BBW93.0136 for BRITE-EURAM project BE-7328.

**4:00 pm PS-WeA7 The Role of Electrode Characteristics in Particulate Trapping in RF Discharges, J. E. Daugherty and D. B. Graves, University of California at Berkeley, Chemical Engineering, 201 Gilman Hall #1462, Berkeley, CA 94720-1462.**

The control of plasma-induced particulate contamination is a matter of increasing concern in the microelectronics industry. It has been observed that particles are often "trapped" in dome and ring shaped clouds.<sup>1,2</sup> Since these clouds are usually located in close proximity to the wafer, they pose a considerable contamination threat. It has been suggested that topographical features on the electrode surface (e.g., the wafer) may cause weak electric field nonuniformities that result in cloud formation.<sup>3</sup> However, electrode topography could also cause thermal nonuniformities as well as disruptions in the gas flow and ion motion in the vicinity of the topography. Consequently, it is not certain that the electrostatic force is the dominant force trapping the particles. We present the results of a series of experiments with a specially designed aluminum electrode. This electrode has an electrically and thermally isolated aluminum ring imbedded in its surface. The temperature, electrical bias, and local geometry of the ring may be controlled independently from the rest of the electrode. In addition, the aluminum ring may be replaced by an alumina (electrically insulating) ring. In this way we examine the relative importance of thermal, electrical, topographical, and materials properties in forming particle traps. The particle traps are analyzed in terms of the fundamental forces that act on the particles.

<sup>1</sup>G. S. Selwyn, J. Vac. Sci. Technol. B 9, 3487 (1991).

<sup>2</sup>G. M. Jellum, J. E. Daugherty, and D. B. Graves, J. Appl. Phys. 69, 6923 (1991).

<sup>3</sup>R. N. Carlile, S. Geha, J. F. O'Hanlon and J. C. Stewart, Appl. Phys. Lett. 59, 1167 (1991).

**4:20 pm PS-WeA8 Strategies for Controlling Dust Particle Transport in Inductively Coupled Plasmas<sup>1</sup>, Helen H. Hwang, Michael Grapperhaus and Mark J. Kushner, University of Illinois, Dept. Electrical and Computer Engineering, Urbana, IL 61801.**

Dust particle transport and contamination of wafers in plasma etching and deposition tools depend on the relative importance of fluid drag, ion drag, electrostatic, thermophoretic and gravitational forces on the particles. Previous work has shown that electrode topography (i.e., grooves) in conventional RIE tools can influence dust particle transport by perturbing the sheath edge at which particles accumulate. Similar strategies are less successful in high plasma density etching tools since the sheath voltages are lower and ion fluxes (producing ion drag forces) are larger. We have developed set of computer models to investigate the transport of dust particles (0.1—many microns) in inductively coupled plasma (ICP) reactors. A 2-dimensional plasma equipment model is used to produce ion fluxes, electric fields and advective gas flow fields. A dust particle tracking model uses these quantities to formulate the forces on the dust particles and resolve their trajectories. Results from those models will be discussed with regard to the trapping of dust particles and contamination of wafers.

The dominance of ion drag forces results in most particles produced in the volume being swept out of the plasma to surfaces. However, particles do accumulate in the periphery of the reactor where ion fluxes are low. These particles may then be redistributed when the power is lowered, and ion drag forces decrease.

<sup>1</sup>Work supported by NSF, SRC, Sandia/Sematech and Univ. of Wisconsin ERC for Plasma Aided Manufacturing.

4:40 pm **PS-WeA9 The Dynamics of Particulates in the Afterglow of an RF Excited Plasma**, C. K. Yeon, J. H. Kim, K. W. Whang, Department of Electrical Engineering, Seoul National University, Seoul, Korea.

The formation of the particulate cloud was examined by the laser light scattering method with the DLC film deposited wafer in an RF excited Ar plasma. The particulates suspended around the plasma-sheath boundary above the substrate and continued to grow during the discharge. The absolute value of the negative self-bias voltage and the plasma potential decreased when the particulates agglomerated around the plasma-sheath boundary. We used the laser sheet and the medium speed camera to obtain the time-resolved images of the moving particulates and observed the particulates showing directional motions in the afterglow. When the RF power was turned off, the direction and the characteristic time of the particulate density decay were highly dependent on the experimental conditions such as the electrode temperature, the gas flow rate and the pressure. In some experimental conditions, most of the particulates were observed to drift onto the wafer surface in a few tens of milliseconds. The afterglow particulate behavior was highly influenced by the DC bias voltage which was applied to the electrode and it indicates that the particulates have residual negative charges. The dependence of the afterglow particulate behavior on the experimental conditions suggests some modified plasma turn-off process which can reduce the particulate contamination of the substrate surface.

5:00 pm **PS-WeA10 Post-Plasma Particle Dynamics in a Gaseous Electronics Conference Standard Cell**, S. M. Collins, J. F. O'Hanlon and R. N. Carlile, Dept. of Electrical and Computer Engineering, University of Arizona, Tucson, AZ 85721; D. A. Brown, Org. 1332, Sandia National Laboratories, Albuquerque, NM 87185.

Particle contamination in plasma tools used for the manufacture of VLSI semiconductor devices on silicon wafers is a major cause of yield loss. Understanding the dynamics of particle movement in the post-plasma regime is important to explain the process of their transport to the wafer. The movement of particle contamination in a Gaseous Electronics Conference Standard Cell in the post-plasma regime was investigated using a novel technique. Particle clouds were observed using laser light scattering together with an image intensifier and a monochromator. This technique allows particle clouds of low density to be seen which cannot otherwise be detected. Video analysis of the particles showed movement of the cloud front in the first few milliseconds after the plasma is turned off. The particle cloud is destroyed in the first 10 to 20 milliseconds of the post plasma. The role of the thermophoretic force on particles during the post plasma is investigated. Values for this force are obtained from the video analysis of particle movement for various electrode temperatures and are compared with theoretical values.

## SURFACE SCIENCE/ELECTRONIC MATERIALS Room A102 - Session SSEM-WeA

### Semiconductor Reactions II

**Moderator:** T. W. Engel, University of Washington.

2:00 pm **SSEM-WeA1 Thermal Stability of Hydroxyl Species on the SiO<sub>2</sub> Surface**, Ofer Sneh and Steven M. George, Department of Chemistry and Biochemistry, University of Colorado, Boulder, CO 80309.

Many semiconductor device processing steps occur on the SiO<sub>2</sub> surface. The main functional group on the SiO<sub>2</sub> surface is the hydroxyl (SiOH) species. The chemical properties of the SiO<sub>2</sub> surface depend on the hydroxyl coverage and the stability of the SiOH species versus temperature. In this study, the thermal stability of SiOH species was investigated on SiO<sub>2</sub> films deposited by chemical vapor deposition on

Si(100) substrates. The hydroxyl coverage was determined using two monolayer-sensitive methods in ultrahigh vacuum. In one set of experiments, methanol (CH<sub>3</sub>OH) was used to "titrate" the hydroxyl species because CH<sub>3</sub>OH forms hydrogen bonds to SiOH species. The methanol coverage hydrogen-bonded to SiOH species was measured by CH<sub>3</sub>OH temperature programmed desorption (TPD) using a mass spectrometer. Additional experiments measured the hydroxyl coverage by desorbing the SiOH species as H<sub>2</sub>O (SiOH + SiOH → H<sub>2</sub>O + Si-O-Si) using laser induced thermal desorption (LITD) techniques. Both the CH<sub>3</sub>OH TPD and H<sub>2</sub>O LITD experiments monitored the progressive and nearly linearly decrease of the hydroxyl coverage versus thermal annealing from 300-900 K. The declining hydroxyl coverage versus annealing temperature is attributed to the thermal dehydroxylation of the SiO<sub>2</sub> surface, i.e., SiOH + SiOH → H<sub>2</sub>O + Si-O-Si. The results on these well-defined SiO<sub>2</sub> surfaces are consistent with earlier infrared and nuclear magnetic resonance measurements of hydroxyl species versus thermal annealing on high surface area silica powders. Implications of these measurements for semiconductor device processing of SiO<sub>2</sub> surfaces will be discussed.

2:20 pm **SSEM-WeA2 Correlation of Surface Core Levels and Structural Building Blocks Through High Resolution Core Level Spectroscopy: Si(111)-(7 × 7)**, J. J. Paggel, W. Theis, K. Horn, Fritz-Haber-Institut der MPG, D-14195 Berlin, Germany, Ch. Jung, C. Hellwig, and H. Petersen, BESSY GmbH, D-14195 Berlin, Germany.

The Si(111)-7 × 7 reconstruction is among the most frequently studied semiconductor surface, and in view of its complexity it is particularly important to understand the relationship between the geometric and electronic structure of its building blocks. Surface core level shifts. It is hence surprising that the origin of the SCL shifts is still a subject of controversy. Here we demonstrate by high resolution core level photoemission, using one of the new generation of plane grating synchrotron radiation monochromators, that apart from the two surface lines that were previously found, additional core level shifts exist. In agreement with a previous study<sup>1</sup> is found that, due to diffraction effects, the intensities of the surface components exhibit large variations with photon energy, such that an analysis of SCL intensities at fixed photon energies, and its use in assignment on the basis of electron mean free paths and relative numbers of contributing atoms may be subject to error. We arrive at a consistent assignment of the SCL peaks to the different structural building blocks of the (7 × 7) structure by comparing our low temperature data with spectra recorded above the temperature of the (7 × 7) - (1 × 1) phase transition at 1100 K, and through an evaluation of SCL intensities over a range of photon energies. These data yield new insight into the influence of different bonding environments on photoemission core level line shifts.

1. J. Carlisle, M. T. Sieger, T. Miller, T.-C. Chiang, Phys. Rev. Lett. **71**, 2955 (1993).

2:40 pm **SSEM-WeA3 Abstraction of H from Group IV Surfaces by Atomic Hydrogen**, D. D. Koleske\* and S. M. Gates, IBM T.J. Watson Research Center, Yorktown Heights, NY 10598, and B. Jackson, Dept. of Chem., U. of Mass., Amherst, MA 01003-0035.

Real time studies of abstraction of surface H and D by atomic D and H (D<sub>at</sub> and H<sub>at</sub>) from polycrystalline diamond, and single crystal Si and Ge surfaces are presented. Time-of-flight detection of low energy H<sup>+</sup> and D<sup>+</sup> ions enables real time kinetic measurements of the surface H and D coverages (θ<sub>H</sub> and θ<sub>D</sub>) [1,2]. On all surfaces the abstraction rates are linear in D<sub>at</sub> or H<sub>at</sub> flux, 1st order in θ<sub>H</sub> or θ<sub>D</sub>, and independent of the initial θ<sub>H</sub> or θ<sub>D</sub>. The "apparent" activation energy for the abstraction reactions ranges from 0.3-1.0 Kcal/mole. The apparent "activation" energy is due to enhanced abstraction rates from v = 1 vibrational states of the adsorbed H-C, H-Si [1,2], and H-Ge bond. The ratio of the abstraction rate of H by D<sub>at</sub> to the absorption rate of D<sub>at</sub> on the clean surfaces is 0.03, 0.36, and 0.41 for diamond, Si, and Ge surfaces, respectively. Using these ratios, we find that the abstraction barriers are approx. 4-5 Kcal/mole on Si and Ge and are approx. 16 Kcal/mole on diamond. The origin of the abstraction barrier on Group IV surfaces appears to depend on the change in π-bonding between the clean and H terminated surfaces. All observations are consistent with a generalized Eley-Rideal abstraction mechanism.

\*currently at: Naval Research Lab, Code 6177, Washington D.C. 20375.

1. D. D. Koleske, S. M. Gates, and J. A. Schultz, J. Chem. Phys. **99**, 5619 (1993).

2. D. D. Koleske, S. M. Gates, and B. Jackson, J. Chem. Phys., in press.



3:00 pm **SSEM-WeA4 Local Adsorbate Structures of F<sub>2</sub> Chemisorbed onto the Si(111)-7×7 Surface: A Molecular Beam/STM Study**, J. A. Jensen, C. Yan, A. C. Kummel, U.C. San Diego Chemistry, La Jolla, CA 92093.

The chemisorption of a mono-energetic molecular beam of F<sub>2</sub> onto a room temperature Si(111)-7×7 surface is examined using scanning tunneling microscopy and the resulting adsorbate structures are studied as a function of translational energy/chemisorption mechanism. For F<sub>2</sub> chemisorption on Si(111)-7×7, there is no intrinsic physisorption state and therefore no island formation at low incident translational energy, E<sub>trans</sub>. Instead at low E<sub>trans</sub> (0.03eV), we observe that the dominant adsorption sites are single reacted adatoms (Si-F), while at higher E<sub>trans</sub> (0.27eV) dimers/pairs of reacted adatoms are commonly observed. From previous work by the Ceyer and Carter groups, it is known that at low E<sub>trans</sub>, F<sub>2</sub> can adsorb via abstraction (F<sub>2</sub> collides, one F atom chemisorbs, the other is ejected into the gas phase), while at higher E<sub>trans</sub>, dissociative chemisorption becomes the predominant adsorption mechanism. Our STM experiments, in conjunction with a simple Monte Carlo model, show that at low E<sub>trans</sub>, the abstraction mechanism accounts for nearly all chemisorption because nearly all adsorption sites are single reacted adatoms. At higher E<sub>trans</sub>, the dissociative chemisorption mechanism becomes important and the predominance for single site adsorption is greatly reduced while the occurrence of dimers/pairs of reacted adatoms is increased. Comparisons are made to the high E<sub>trans</sub> chemisorption of Cl<sub>2</sub> onto the Si(111)-7×7 surface which produces almost exclusively reacted dimers/pairs of adjacent adatoms.

3:20 pm **SSEM-WeA5 First-Principles Study of Structures and Reactions on Si/SiO<sub>2</sub> Surfaces**, Krishnan Raghavachari, AT&T Bell Laboratories, Murray Hill, NJ 07974.

In this work, we have used first-principles quantum chemical techniques to understand the nature of the structural species and microscopic reaction mechanisms on Si/SiO<sub>2</sub> surfaces. We use the "cluster approach" where the surface is represented by clusters of atoms designed to model the important aspects of the local interactions. Examples will be given on detailed structural assignments based on correlations between the local structures and the experimentally observed vibrational frequencies of hydrogen terminated silicon surfaces. Additional studies investigating microscopic reaction mechanisms for processes such as etching reactions of HF and H<sub>2</sub>O on Si/SiO<sub>2</sub> surfaces are also reported. Kinetic considerations are found to be extremely important and an understanding of the relevant energy barriers is critical to provide a proper description of such surface reactions.

INVITED

4:00 pm **SSEM-WeA7 Translational-Energy-Induced Etching of n<sup>+</sup>Si(100) by Hyperthermal Cl<sub>2</sub> Molecular Beams**, Y. Teraoka, I. Nishiyama, Microelectronics Research Laboratories, NEC Corporation, 34 Miyukigaoka, Tsukuba, Ibaraki 305, Japan.

The reactivity of Cl<sub>2</sub> molecules with n<sup>+</sup>Si(100) in hyperthermal translational energy region was investigated using a seeded molecular beam technique with a high temperature nozzle. The translational energy threshold had been already found to be 2.1eV and anisotropic etching profiles had been also achieved owing to the stimulated etching [1]. In order to understand the role of translational energy, the etch rates were measured as a function of substrate temperature as well as translational energy. The two kinds of thermal desorption processes were found by the resulting Arrhenius plots of etch rates. The activation energies, correspondent to each desorption process, are 2.7eV and 1.2eV, respectively. The former is the same as those of a conventional gas etching and the latter governs the translational-energy-induced etching. The small activation energy implies that a new type of chlorinated Si structure is formed on the surface. In addition, the small activation energy was not changed by the translational energy up to 3.0eV. Even though the impinging Cl<sub>2</sub> molecules have translational energies over the small activation energy, the etching is driven by the thermal desorption of the chlorinated structure. The translational energy over 2.1eV may be necessary for overcoming an energy barrier to produce such new chlorinated structure.

[1] Y. Teraoka and I. Nishiyama: Appl. Phys. Lett. 63, 3355 (1993).

4:20 pm **SSEM-WeA8 Vacancy-Mediated and Ion-Enhanced Surface Diffusion on Semiconductors**, C. E. Allen and E. G. Seebauer, Dept. of Chem. Eng., Univ. of Illinois, Urbana, IL 61801, and I. I. Suni, Dept. of Chem. Eng., Clarkson Univ., Potsdam, NY 13699.

Surface diffusion of adsorbates has been notoriously difficult to

measure on semiconductors, and the effects of techniques intended to speed diffusion have been even more difficult to quantify. However, an understanding and quantification of such effects are needed to develop improved processes for chemical vapor deposition and molecular beam epitaxy. We have been employing second harmonic microscopy (SHM) for this purpose. In SHM, the decay of a step concentration profile is measured directly. Recent experiments on Si have confirmed the results obtained previously in our laboratory for several adsorbates on Ge. That is, under processing temperatures surface diffusion occurs by a vacancy mechanism with an extraordinarily high activation energy and prefactor. For example, for Sb on Si(111) the activation energy is 54 kcal/mol and the prefactor is  $1.5 \times 10^2$  cm<sup>2</sup>/s. Molecular dynamics simulations give insight into this mechanism. The diffusion rate may be enhanced substantially by bombardment with low-energy (50 eV) argon ions. Enhancements of pure diffusive motion by factors of 100 have been quantified. The enhancement appears to be a momentum transfer effect, because electron bombardment even at high energies provides no measurable enhancement. When the ion bombardment is near glancing evidence, there is evidence that a net convective motion of adsorbate is induced as well. That is, adsorbate atoms are actually "blown" across the surface. These results are important for processing applications because the ion energies are so low that little surface damage results.

4:40 pm **SSEM-WeA9 Thermal and Photochemical Reactions of HN<sub>3</sub> on Ge(100): A Lower Temperature Route to Germanium Nitride**, Craig Tindall, John C. Hemminger, Department of Chemistry and the Institute for Surface and Interface Science, University of California Irvine, Irvine, CA 92717.

Because of the reactivity of its thermally grown native oxide, an optimal process for passivating the germanium surface has yet to be found. Ge<sub>3</sub>N<sub>4</sub> and GeO<sub>x</sub>N<sub>1-x</sub> compounds have been found to be promising candidates. However, the most commonly used nitrogen precursor, NH<sub>3</sub>, requires a relatively high temperature in order to thermally grow Ge<sub>3</sub>N<sub>4</sub>. For this reason, alternative precursors for growing Ge<sub>3</sub>N<sub>4</sub> are desirable. We describe here the first use of HN<sub>3</sub> as a nitrogen precursor for forming Ge<sub>3</sub>N<sub>4</sub>. We have studied the chemistry of HN<sub>3</sub> with Ge(100) using HREELS, TDS, LEED, and AES. HN<sub>3</sub> adsorbs molecularly below 25C. It begins to decompose around 100C, desorbing N<sub>2</sub> and leaving N-H groups on the surface. At 300C the N-H is dehydrogenated and germanium nitride is formed. We have found that HN<sub>3</sub> facilitates the formation of Ge<sub>3</sub>N<sub>4</sub> at a substantially lower temperature (350C) than that required previously when using NH<sub>3</sub> (700C). In addition, HN<sub>3</sub> adsorbed on Ge(100) is photosensitive. Visible light decomposes HN<sub>3</sub> on the germanium surface, again desorbing N<sub>2</sub> and leaving N-H groups on the surface.

5:00 pm **SSEM-WeA10 Surface Phase Transformations in the Ni/Si(111) system: Real-Time Observations using LEEM and STM**, P. A. Bennett, M. Y. Lee, S. A. Parikh, Physics Dept., Arizona State University, Tempe, AZ 85287-1504, K. Worm, Phys. Inst. Tech. U. Clausthal, D-3392 Clausthal-Zellerfeld, Germany and R. J. Phaneuf, Physics Dept U. Maryland, College Park, MD 20742-4111.

Using STM we find that quench cooling a Ni/Si(111) surface results in a 1×1 lattice gas of "ring-clusters" (RCs) plus small 2×2 patches of Si adatoms on T<sub>4</sub> sites, similar to the Co/Si case. [1] LEEM observations show that the 1×1 structure forms preferentially on wide terraces, decorating steps with a denuded zone of clean 7×7 whose width decreases with cumulative Ni dose and quench rate. As coverage is increased above 0.16ML a √19 structure forms followed by islands of NiSi<sub>2</sub>. At 700C the 1×1 structure dissolves without change of domain shape, leaving clean 7×7. This shows that the RCs do not diffuse across the surface. For warm deposition (reactive epitaxy), islands of NiSi<sub>2</sub> form in a matrix of 7×7 with no RCs. The island size distribution is narrowly peaked at 100nm, suggesting coherent, strained islands, similar to the Ge/Si(100) system. These dissolve at 700C, leaving clean 7×7. Implications for silicide processing are described.

[1] P. A. Bennett, M. Copel, D. Cahill, J. Falta and R. M. Tromp, Phys. Rev. Lett. 69 (1992) 1224.





## THIN FILM

Room A105 - Session TF-WeA

### Deposition and Characterization Techniques of Nanostructures in Thin Films

Moderator: R. Sargent, OCLI:

2:00 pm **TF-WeA1 Deposition and Characterization Techniques for Nanostructures in Thin Films**, *J. C. Bilello and S. M. Yalisove*, Department of Materials Science and Engineering, University of Michigan, Ann Arbor, MI 48109.

Traditional methods of characterizing the magnitude of the internal stresses in thin film nanostructures involves measuring the physical curvature of the film-substrate couple. These common procedures, which include laser scanning and optical interferometry; measure only the average stress throughout the film thickness and are sensitive to surface conditions. Two new x-ray diffraction techniques will be discussed in the present paper. The first, double crystal diffraction topography (DCDT) allows an assessment of the strains of the crystal lattice planes and is hence inherently less sensitive to the state of the sample termination surface. Rough surfaces, as well as studies of buried layers, are possible by this method. It is feasible to obtain a complete map of the strain tensor field over the entire area of a large wafer using DCDT. The second characterization technique, which will be described, uses grazing angle incidence x-ray scattering (GIXS) measurements of the strain distributions through out the depth of a thin film, i.e. depth strain profiling. On a microscopic level, the details of the strain distribution as a function of depth through the thickness of the film can have important consequences in governing film quality and the ultimate morphology of the microstructure. The information obtained from GIXS observations allows one to determine the depth dependence of the principal strains for polycrystalline thin films of virtually any composition. In practice, for very thin films, the GIXS technique requires using a synchrotron to have sufficient intensity in the scattered x-rays to make measurements practical. The application of these techniques will be reported for a variety of refractory metal films, including Mo, W, and Ta on Si substrates. The implications with respect to controlling the internal stress in thin films and their concomitant microstructure will be discussed. **INVITED**

Research supported by the USARO and ARPA under contract DAAL03-91-0235 and at SSRL, funded by the USDoE, Office of Basic Sciences.

2:40 pm **TF-WeA3 Crystallographic Relations in Zirconia-Alumina Multilayer Nanolaminates**, *M. Gajdardziska-Josifovska and C. R. Aita*, Laboratory for Surface Studies, U. Wisconsin-Milwaukee, P.O. Box 784, Milwaukee, WI 53201.

Nanoscale multilayer films of polycrystalline zirconia and amorphous alumina were characterized by high resolution electron microscopy. Previous results (1) show that the layer spacing can be scaled to insure the growth of metastable tetragonal (t) zirconia, the desired phase for good film mechanical behavior. Here, we report the crystallographic relations between tetragonal zirconia and adjacent regions that have transformed to monoclinic zirconia (m), the STP phase. The growth orientation of the parent phase is  $t\{111\}$  parallel to the growth interface.  $t - \{111\}$  transforms to  $m - (111)$ , resulting in a displacement of  $\sim 9^\circ$  vicinal to the growth interface.  $m - (200)/t - (200, 020)$  planes are invariant under transformation. Twinning in the monoclinic phase is the dominant mode by which strain is accommodated. Monoclinic unit cell distortions and the implications for transformation toughening behavior of these nanolaminates are discussed.

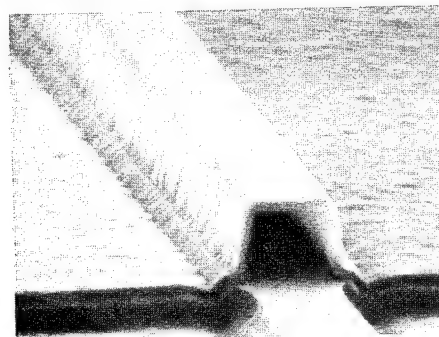
1. C. M. Scanlan, et al., Appl. Phys. Lett. 64, (1994), in press; Proc. MRS 343, (1994) in press.  
Research supported under ARO Grant No. DAAH0493G0238 and NSF Grant No. DMR9115680.

3:00 pm **TF-WeA4 A Novel Technique for Characterizing the Surface Coverage of CVD Films in Ultra-High-Aspect Ratio Microstructures**, *R. J. Soave\*, G. W. Tasker\*, J. W. Mayer† and Y. Shacham-Diamand\**, \*Galileo Electro-Optics Corp., Sturbridge, MA, †Cornell University, Ithaca, NY., ‡Arizona State University, Tempe, AZ.

Nanostructure fabrication often requires the conformal deposition of thin films in trenches, vias, and other high-aspect-ratio structures. Characterizing the surface coverage of thin films deposited in such

structures usually requires cross-sectional SEM, which can be difficult. To study more easily the conformality of nanometer-scale thin films deposited in high-aspect-ratio structures, we have developed a process for producing a planar array of silicon micro-capillary structures on a silicon wafer. Capillaries with cross sections as small as  $1 \mu\text{m} \times 2 \mu\text{m}$  and lengths as long as  $400 \mu\text{m}$  have been fabricated using conventional microfabrication processes. After fabrication, silicon oxide or silicon nitride films are deposited on the inner and outer surfaces of the capillaries by LPCVD. After deposition, the capillary "roof" is removed via selective etching and/or mechanical techniques. This exposes the oxide or nitride deposited on the silicon capillary "floor". The film thickness as a function of distance down the capillary can be accurately measured on the capillary floor by interferometry. We will present surface coverage measurements for several LPCVD dielectric thin film processes in structures with aspect ratios from 10:1 to 200:1 or greater.

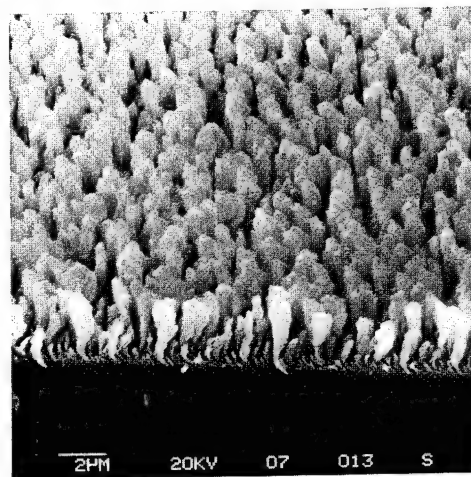
This technique of optically measuring thin films deposited inside micro-capillaries is useful for studying the surface coverage, kinetics and transport characteristics of deposition processes in ultra-high-aspect-ratio structures.



$2 \mu\text{m} \times 2 \mu\text{m} \times 400 \mu\text{m}$   
Silicon Micro-Capillary

3:20 pm **TF-WeA5 Fabrication of Thin Films with Highly Porous Microstructures**, *K. Robbie, S. K. Dew, T. Smy\* and M. J. Brett*, Univ. of Alberta, Edmonton, Canada and \*Carleton University, Ottawa, Canada.

Metal and insulator thin films of densities less than 50% of bulk and with very high surface area to volume ratios have been deposited by an evaporation technique. Multiple evaporation sources were used to provide a symmetrical but very oblique ( $> 80^\circ$ ) flux incident on the substrate. Extreme self-shadowing produced vertical columnar microstructures consisting of isolated and evenly spaced columns. Significant columnar anisotropy may be produced in the plane of the substrate by variations of the deposition geometry. For metal films, this anisotropy gives rise to a directional conductivity variation exceeding 20% between two axes parallel to the substrate surface. The growth of these structures has been simulated by a model incorporating ballistic deposition and minimization of chemical potential in order to better understand and optimize their formation. Applications of these films as catalytic surfaces for gas sensors, thermal insulators, and polarizers will be discussed.



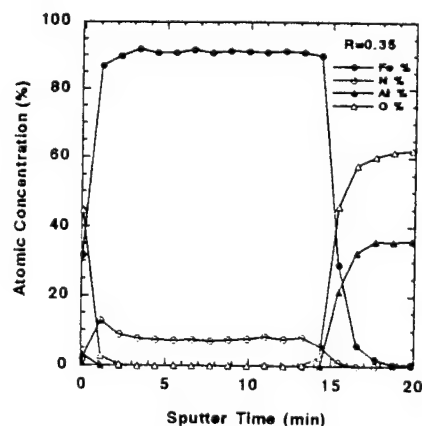
Highly Porous  $\text{MgF}_2$  Film

3:40 pm **TF-WeA6 Heteroepitaxial Growth of C<sub>70</sub> Films on MoS<sub>2</sub> and their Characterization by LEED, XPS, and UPS, B. Y. Han, K. Hevesi, L. M. Yu, G. Gensterblum, J.-J. Pireaux, P. A. Thiry, R. Caudano, Laboratoire Interdisciplinaire de Spectroscopie Electronique, Institute for Studies in Interface Sciences, Facultés Universitaires Notre-Dame de la Paix, B-5000 Namur, Belgium.**

UHV sublimation has been used to deposit C<sub>70</sub> fullerite on in-situ cleaved lamellar substrate MoS<sub>2</sub>(0001). The van der Waals epitaxy is evidenced by the observation of the hexagonal LEED pattern characteristic of the close-packed C<sub>70</sub> structure with an intermolecular spacing of ~10.9 Å. At low coverage, the simultaneous observation of LEED spots corresponding to the substrate and the C<sub>70</sub> overlayer allows to specify the geometry of the epitaxy. The intensity curve of C1s photoemission line as a function of the C<sub>70</sub> dose indicates a layer by layer (Franck-van der Merwe) growth mode. A detailed analysis of the photoemission lines of the substrate and the C<sub>70</sub> core levels recorded at submonolayer and multilayer coverage indicates a small electron transfer ( $\leq 0.02$  electron per C<sub>70</sub> molecule) from the substrate to the first C<sub>70</sub> layer. A C1s line shift of ~100meV to higher binding energy, for emission from a multilayer film with respect to a submonolayer, is observed and interpreted as reflecting a solid state effect. The valence band probed by UPS ( $h\nu = 21.21$  eV) at various coverages shows only a weak hybridization between energy bands of the substrate and those of C<sub>70</sub>, notwithstanding a work function decrease of ~1eV upon C<sub>70</sub> deposition.

4:00 pm **TF-WeA7 Compositional and Microstructural Characterization of Fe-N Thin Films for Recording Sensor Applications, Y. K. Kim and P. B. Narayan, Rocky Mountain Magnetics, Inc., 2270 South 88th St., Louisville, CO 80303-8188.**

Polycrystalline Fe-N thin films with typical thicknesses less than 100 nm have been characterized. Fe-N films are promising for recording sensor applications due to good magnetic properties and materials reliability. Films were fabricated reactively on Al-oxide precoated Si wafers by a dc magnetron sputtering system under Ar and N<sub>2</sub> environment. Magnetic properties measurements indicate that the control of N is critical to achieve desired magnetic softness. The purpose of this study is to understand processing, properties, and microstructure relationship as a function of N content in the film. Characterization of compositional and microstructural evolution will, therefore, provide valuable insights to uncover the magnetic behavior of Fe-N films. Figure shown on the right represents the XPS composition-depth profile of an Fe-N film prepared at R = 0.35 where soft magnetic properties were achieved. R is defined as a ratio between N<sub>2</sub> and Ar flow rate. TEM studies showed that when R = 0.0, the film has an average grain size of 50 nm with many grain clusters. As R increased, the grain size became as small as 10 nm with nanocrystalline selected area diffraction pattern. Annealing at 150°C for two hours did not produce any noticeable change in the microstructure.



4:20 pm **TF-WeA8 Positron Annihilation Studies of Diamond-Like Nanocomposite (DLN) Films, P. Asoka-Kumar, Brookhaven National Laboratory, Upton, New York 11973, B. F. Dorfman, M. G. Abravzov, IIMT, Polytechnic University, Brooklyn, New York, Don Yan, F. H. Pollak, Dept. of Physics, Brooklyn College of CUNY, Brooklyn, NY 11210.**

Positron Annihilation Spectroscopy (PAS) as a nondestructive, depth-sensitive probe was applied to study dielectric strength of Diamond-Like Nanocomposite (DLN) films. DLN films were deposited from a plasma discharge (plasma current 1-4 A, DC voltage 150V) of

polyphenylmethylsiloxane on RF (1.76 MHz) biased p-type Si(100) substrate. The voltage applied to the substrate was varied from U<sub>RF</sub>=0 to 1000 V. The IV characteristics of the DLN films were independently measured using contacts made with Al, Cu, or silver paste in the temperature range 20-200°C. The electric breakdown voltage increased with increases in U<sub>RF</sub>. The highest breakdown voltage (up to 700-800V for a film thickness of 30-40 nm) was observed on DLN grown under simultaneous Ar bombardment at U<sub>RF</sub>=1000V. PAS results are in good agreement with I-V characteristics of the films. Ellipsometric measurements and Raman scattering results from films grown under different RF voltage also will be presented.

4:40 pm **TF-WeA9 Microhardness Characterization of Substrates and Films, Richard C. Bradt, Mackay School of Mines, University of Nevada-Reno, Reno, NV 89557-0136 USA.**

The use of indentation microhardness as a technique for the characterization of substrates and also for films deposited on substrates is addressed. Single crystal microhardness is initially considered from the viewpoint of its anisotropy and the significant role on the measured microhardness. This naturally leads into the indentation size effect and its role on the apparent microhardness values. The critical importance of obtaining data over an extended range of indentation test loads and thus for indentation depths and sizes is emphasized. Finally the major effects of superimposing different thickness films on the substrate are considered. The indentation depth relative to the film thickness is considered and the many problems that are associated with the cracking of the film, the underlying substrate and the interface between the two are next addressed. Properties of the substrate and the films are also considered, including relative hardness and their "plasticities". Uses for characterization vs. the measurement of "true" microhardness are considered. **INVITED**

## ELECTRONIC MATERIALS Room A108 - Session EM-WeA

### Wide-bandgap Nitrides

**Moderator: P. D. Holloway, University of Florida, Gainesville.**

2:00 pm **EM-WeA1 Low Carrier Concentration GaN Grown by MOCVD at Low Temperature (720°C), J. C. Chen, Bing Yang, F. Semendy\*, and N. Bambha\*, Dept. of Electrical Engineering, Univ. of Maryland Baltimore County, Baltimore, MD 21228; \*IR Optics Technology OFC, Army Research Lab., Ft. Belvoir, VA 22060.**

Gallium nitride (GaN) based materials are wide-band-gap III-V compound semiconductors ideally suited for devices in the visible-to-ultraviolet region of the spectrum. Successful growths of GaN have been reported by several groups. However the growth of device-quality GaN films is still a difficult task. Problems such as high growth temperatures, difficulty in achieving low n-type background concentration and difficulty in achieving p-type material make it difficult to fabricate GaN-based devices.

In this study, we have carried out a series of experiments in the growth of GaN/AlGaN by MOCVD. The typical growth was conducted at atmospheric pressure. Sapphire with (0001) orientation, one inch diameter, was used as a substrate. TMGa, TMAI, NH<sub>3</sub> and H<sub>2</sub> were used as Ga, Al, N and carrier, respectively. The GaN films was characterized by C-V, PL and double crystal x-ray diffraction methods. The preliminary results indicates that we are able to get the crystalline GaN (confirmed by double crystal x-ray measurement). The FWHM of GaN (002) peak is around 220 arc seconds which is comparable to the result grown at high temperatures (> 1000°C). The background n-type concentration as low as  $2 \times 10^{16}/\text{cc}$  (measured by C-V method) was achieved by using normal growth conditions at low temperature (720°C). In addition, a special purification method was employed to purify source materials. After using this purification method, the background concentration becomes very low (less than  $5 \times 10^{15}/\text{cc}$ , estimated) and it is too low to be measured by CV method.

2:20 pm **EM-WeA2 Ohmic Contacts to Intrinsic N-Type GaN,\* S. Miller, P. H. Holloway, Department of Materials Science and Engineering, University of Florida, P.O. Box 116400, Gainesville, FL 32611, J. Pankove, Department of Electrical Engineering, University of Colorado at Boulder, Box 425, Boulder, Colorado 80309-0425.**

Ohmic contacts by In, Ti, Ti/Au, and Ti/Si/Au were made to intrinsically n-type CVD grown GaN ( $n = 2 \times 10^{18}/\text{cm}^3$ ) films 2  $\mu\text{m}$  thick. The contacts were deposited by thermal evaporation or planar magnetron sputter deposition. Contact properties were investigated by current-voltage analysis, scanning Auger microscopy, scanning electron microscopy, and secondary ion mass spectroscopy. It was found that as deposited In formed an ohmic contact with a resistance of 0.5  $\Omega\text{cm}^2$ . No interfacial compounds were found after heat treatments of up to 200 C for 30 minutes. Ohmic behavior will be explained by an analysis of the Fermi level and the band alignment between In and GaN. The Ti/Au contacts, annealed for 15 seconds in  $\text{N}_2$  gas at 900 C, formed an excellent ohmic contact. Thermodynamic data suggest that formation of a TiN layer at the interface is the mechanism for the ohmic behavior. This will be further explained by an examination of the Fermi levels and band alignments. The best ohmic contacts have been observed for the previously unreported metallization scheme of Ti/Si/Au after annealing for 15 seconds in  $\text{N}_2$  gas at 900 C. The superior performance will be explained on the basis an interfacial reaction and diffusion, supported by SIMS and Auger data.

\*This work supported by ONR/ARPA Grant N00014-92-J-1895.

2:40 pm **EM-WeA3 InGaN/AlGaN Blue-Light-Emitting Diodes**, *Shuji Nakamura*, Department of Research and Development, Nichia Chemical Industries, Ltd., P.O. Box 6, Anan, Tokushima 774, Japan.

Much research has been done on high-brightness blue light-emitting diodes (LEDs) for the use of full-color display or full-color indicators with the characteristics of high-reliability and high-speed. However, it has been impossible to obtain high brightness blue LEDs with the luminous intensity over 1 cd. Recently, we have succeeded in commercializing InGaN/AlGaN double heterostructure (DH) blue LEDs with the luminous intensity over 1 cd for the first time. In this report, the characteristics of the InGaN/AlGaN DH blue LEDs is described. Figure 1 shows the structure of the InGaN/AlGaN DH LEDs. The peak wavelength of the electroluminescence is 450 nm and the FWHM of the peak emission is 70 nm. The typical output power of the InGaN/AlGaN DH LEDs is 1.5 mW at 20 mA. The external quantum efficiency is 2.7% at 20 mA. A typical on-axis luminous intensity is 1.2 cd at 20 mA. The forward voltage is 3.6 V at 20 mA. **INVITED**

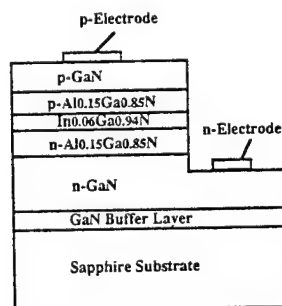


Fig.1 InGaN/AlGaN DH LEDs.

3:20 pm **EM-WeA5 Atomic Layer Deposition of Aluminum Nitride at Lower Temperatures Using Dimethylethylamine:alane and Ammonia**, *J. N. Kidder, Jr., J. W. Rogers, Jr., T. P. Pearsall, Jason Kuo\*, Heng Lui\*, and Audunn Ludviksson\**, Department of Materials Science and Engineering and \*Department of Chemical Engineering, University of Washington, Seattle, WA 98195.

We have studied an atomic layer growth process using amine-alane adducts as precursors for depositing aluminum nitride thin films at temperatures between 300–700 K. Adsorption and decomposition of these precursors were studied in UHV using Auger electron spectroscopy, temperature programmed desorption and Fourier transform infrared spectroscopy. The atomic layer deposition process was carried out in a horizontal MOCVD reactor at atmospheric pressure using  $\text{H}_2$  as a carrier gas. Dimethylethylamine:alane ( $\text{Me}_2\text{EtN:AlH}_3$ ) and ammonia ( $\text{NH}_3$ ) were used to deposit AlN thin films at temperatures as low as  $T = 610\text{K}$ . The source gases were sequentially flowed into the reactor with hydrogen flush steps between each source gas step. Thin films were deposited onto Si(100) and  $\text{Al}_2\text{O}_3(0001)$  substrates that were heated on a susceptor by rf-induction. Analysis by x-ray photoelectron spectroscopy and electron microscopy reveals the deposition of AlN at a temperature of 610 K. A high resolution scan of the N(1s) region

shows a peak component at a binding energy 396.8 eV corresponding to AlN; the spectrum contains a second component at 398.3 eV which is associated with surface  $\text{NH}_2$  species. Processing at a lower temperature ( $T = 510\text{K}$ ) results in no detectable AlN deposition. Processing at higher temperature ( $T = 723\text{K}$ ) results in nitridation of the Si surface to  $\text{Si}_3\text{N}_4$  but no detectable AlN deposition.

3:40 pm **EM-WeA6 Growth of Epitaxial Aluminum Nitride Films on Hydrogen Terminated Si(111) Surfaces**, *F. Ahmad, T. Lenane, G. Auner*, Department of Electrical and Computer Engineering and *R. Naik*, Department of Physics, Wayne State University, Detroit, Michigan 48202.

Thin films of Aluminum nitride (AlN) were grown using the technique of plasma source molecular beam epitaxy (PSMBE). The deposition method uses a magnetically enhanced hollow cathode lined with aluminum as the target material. The films were grown on hydrogen terminated Si(111) substrate. Epitaxy was achieved at substrate temperatures ranging from 400°C to 600°C. Several bias settings ranging from 0 to -20V were used to control the energy of the depositing ions and the flux. Structural characterization of the films were performed by x-ray diffraction (XRD) and high resolution electron microscopy (HREM). The XRD pattern shows only AlN (0002) reflection peak. The absence of other reflections indicate complete film texture with  $\text{AlN}[0001] \parallel \text{Si}[111]$ . Cross-sectional transmission electron micrograph reveals epitaxy of AlN on Si(111) with orientation relationships of  $\text{AlN}[2110] \parallel \text{Si}[011]$ . Furthermore HREM micrograph of AlN/Si(111) interface shows parallel lattice fringes of Si(111) and AlN(0001) extending up to the interface, indicating sharpness and the absence of interfacial diffusion. Although it is commonly believed that below 600°C polycrystalline growth occurs, our observations clearly indicate epitaxial growth in the temperature range of 400°C to 600°C. Low temperature epitaxial growth of AlN probably occurs due to a combination of the controlled kinetic energy of the depositing species from the PSMBE source and the change in surface energy of the hydrogen terminated silicon substrate.

4:00 pm **EM-WeA7 Growth of  $\text{In}_x\text{Al}_{1-x}\text{N}$  and  $\text{In}_x\text{Ga}_{1-x}\text{N}$  by Metalorganic Molecular Beam Epitaxy**, *C. R. Abernathy, S. J. Pearton, J. D. MacKenzie, S. Bharatan, and K. S. Jones*, Department of Materials Science and Engineering, University of Florida, Gainesville, FL 32611.

III-N devices such as heterostructure lasers or heterojunction bipolar transistors require development of the ternary materials. To date, most attention has been focused on the binary compounds GaN, AlN and InN. In this work, growth of the In-containing ternaries,  $\text{In}_x\text{Al}_{1-x}\text{N}$  and  $\text{In}_x\text{Ga}_{1-x}\text{N}$ , on GaAs (100) substrates by metalorganic molecular beam epitaxy (MOMBE) has been investigated. In order to suppress the desorption of In from the surface, the growth temperature was kept below 540°C. As the In mole fraction,  $X_{\text{In}}$ , is increased in either material, the polytype changes from cubic to a mixture of cubic and hexagonal and becomes increasingly defective. Electrically, the carrier concentration decreases with decreasing In content from  $n \sim 10^{20}\text{cm}^{-3}$  in the InN to semi-insulating in the GaN and AlN. The decline is more rapid for  $\text{In}_x\text{Al}_{1-x}\text{N}$  than for  $\text{In}_x\text{Ga}_{1-x}\text{N}$ , probably due to the larger bandgap of the  $\text{In}_x\text{Al}_{1-x}\text{N}$ . The rate of the drop with  $X_{\text{In}}$  in either material system is increased if hydrogen is used as the carrier gas rather than He. Presumably this effect is due to passivation of the native defect or impurity responsible for the electron concentration. TEM, XRD, growth rate and morphology as a function of material composition will be given. Material grown on sapphire substrates will also be discussed for comparison.

4:20 pm **EM-WeA8 Outdiffusion of Deuterium from GaN, AlN and InN**, *R. G. Wilson<sup>1</sup>, S. J. Pearton<sup>2</sup>, C. R. Abernathy<sup>2</sup> and J. M. Zavada<sup>3</sup>*, <sup>1</sup>Hughes Research Laboratories, Malibu, CA 90265, <sup>2</sup>Department of Materials Science and Engineering, University of Florida, Gainesville, FL 32611, <sup>3</sup>U.S. Army Research Office, Research Triangle Park, NC 27709.

Blue lasers in the III-N materials system require achievement of high p-type doping levels. It is found that hydrogen passivation occurring during MOCVD growth of GaN and related alloys limits the acceptor concentrations in as-grown samples and that post-growth annealing at  $\geq 550^\circ\text{C}$  is necessary to reactivate the dopants. We have quantified the outdiffusion using  $^2\text{H}$  plasma treated (250° or 400°C, 30 min) of  $^2\text{H}^+$  implanted GaN, AlN and InN annealed from 300°–900°C, and SIMS profiling to measure the resultant redistribution. In plasma treated samples two populations of  $^2\text{H}$  are found—(i) a high-concentration ( $> 10^{20}\text{cm}^{-3}$ ) near-surface ( $< 0.2\mu\text{m}$ ) region probably due to the formation of platelet defects and (ii) a lower concentration ( $\sim 10^{18}$

cm<sup>-3</sup>) plateau region extending throughout the film thickness (1  $\mu$ m), most likely due to <sup>2</sup>H-point defect pairing. Deuterium in region (i) begins outdiffusion at 300°C in GaN, but in region (ii) does not commence until >800°C. In implanted samples the 2H redistribution occurs with the same characteristics as the bulk population in plasma-treated material. The thermal stability of the deuterium profiles is much higher than in GaAs. Implications for device structure growth, and comparisons with other semiconductor systems will be discussed.

5:00 pm **EM-WeA10 Dry Etching of GaN and AlGaIn, I. Adesida and A. T. Ping**, Center for Compound Semiconductor Microelectronics and Department of Electrical and Computer Engineering, University of Illinois at Urbana-Champaign, Urbana, IL 61801; **M. Asif Khan, D. T. Olson, and J. N. Kuznia**, APA Optics, Inc., Minneapolis, MN 55434.

Gallium Nitride (GaN) and Aluminum Gallium Nitride (AlGaIn) are wide, direct bandgap materials with high potential for novel electronic and optical devices. To date, the progress in the growth and characterization of these materials has not been matched by advances in processing both in terms of etching, ohmic contacts, and metallization. In particular, it is known that GaN and AlGaIn are not easily etched using wet chemistry. Initial progress in etching of GaN has been recorded using reactive ion etching (RIE) techniques. More work needs to be done in the processing of these materials in order to realize their application potential.

In this paper, we present our results on the dry etching properties of GaN and AlGaIn. Both reactive ion etching and chemically assisted ion beam etching (CAIBE) methods have been investigated. Etch rate and etch profile results for RIE in Cl<sub>2</sub>-based and HBr mixtures with H<sub>2</sub> and Ar will be presented. Also, results using CAIBE with Ar beam bombardment in an ambient of Cl<sub>2</sub> will be presented. The effect of temperature on the CAIBE etch rates and profiles will be discussed. High etch rates and anisotropic profiles have been obtained for the various methods. For AlGaIn, etch rates do slow down significantly at high temperatures if there is any trace of water vapor in the etching chamber. Auger electron spectroscopy (AES) and X-ray photoelectron spectroscopy (XPS) are used to study etching-induced changes on etched surfaces.

## MANUFACTURING SCIENCE AND TECHNOLOGY

Room A110 - Session MS-WeA

### Diagnostics, Sensors, and Control

**Moderator:** L. M. Cecchi, Sandia National Laboratories.

2:00 pm **MS-WeA1 Process Control in Semiconductor Manufacturing, S. W. Butler**, Semiconductor Process and Device Center, Texas Instruments, Dallas, TX 75025.

The goal of this presentation is to propose what level of process control in semiconductor manufacturing is required for current device technology and future device technology. The current level of process control implemented in the industry will be highlighted and areas requiring further development will be suggested. Some of the benefits of process control that Texas Instruments has already experienced will be related. The major concepts of process control will be discussed. The technical need for process control, such as machine aging, will be presented, along with the appropriate control implementation schemes. The basic requirements for control to be possible will also be introduced. The role of metrology, specifically *in situ* vs. *ex situ*, as pertaining to process control methods will be presented. Examples of process control applications in semiconductor manufacturing will assist in explaining the concepts introduced during this presentation. The various control methods will be linked to facilities doing research and development of process control.

2:40 pm **MS-WeA3 A Production Demonstration of Wafer-to-Wafer Plasma Gate Etch Control by Adaptive Real-Time Computation of the Over-Etch Time From In-Situ Process Signals, E. A. Rietman, \*S. H. Patel**, AT&T Bell Labs., Murray Hill, NJ 07974 and \*AT&T Microelectronics, Orlando, FLA 32819.

We describe an adaptive nonlinear controller for wafer-to-wafer plasma gate etch for 0.9 micron CMOS technology. The typical process

requires constant human intervention to estimate the over-etch time. The algorithm uses *in situ* process signatures and information from a historical database to compute, in real time, the ideal over-etch time for the current wafer etching within the reactor. Our adaptive process gives a comparable standard deviation (about 10 Angstroms) for the remaining gate oxide without human intervention. Since humans have effectively been removed from the feedback loop the process throughput has improved. The production worthy controller is being installed on two reactors in our MOS line in Orlando, Florida.

3:00 pm **MS-WeA4 Real-Time Process Control Method Using Ellipsometry Applied to Gate Etching, J. T. C. Lee, N. Blayo, A. Grevoz, H. L. Maynard, and D. E. Ibbotson**, AT&T Bell Laboratories, Murray Hill, NJ 07974.

Current trends toward single wafer processing using advanced low pressure, high density plasma sources require rapid etching rates that place ever higher demands on the accuracy of process control algorithms and diagnostic techniques. In particular, etching of multilayer gate stacks for ULSI applications requires an extremely anisotropic and rapid process that exhibits unprecedented selectivity to the gate oxide. The high cost of wafers precludes extensive use of time consuming, destructive post-process diagnostics for process development. Optically based diagnostic techniques such as interferometry, optical emission and ellipsometry offer non-invasive and non-destructive means for obtaining real-time information during etching.

We have discovered that with judicious selection of the probing wavelength, ellipsometry signals remain highly sensitive over patterned features, and thus can be used for real-time control of manufacturing processes. The ability to use ellipsometry over patterned structures was unexpected. In this paper, we present the real-time traces obtained at energies from 1.5 to 4.0 eV during the gate etching step of sub 0.35  $\mu$ m CMOS devices using a helicon plasma source. We quantify the effect of mask patterns and underlying topography on the effective band of "useful" wavelengths, i.e., wavelengths that provide characteristic signatures of the endpoints of the various films being etched.

3:20 pm **MS-WeA5 The Application of Real-Time Optical Monitors to Semiconductor Manufacturing, James A. O'Neill**, IBM Microelectronics, Semiconductor Research and Development Center, Hopewell Junction, NY, 12533.

The manufacture of advanced microelectronic devices is testing the limits of dry processing technology. Emerging technologies such as high density etching plasmas and high pressure chemical vapor deposition systems are being developed to meet the fabrication demands of advanced devices. Also, the utility of conventional processing tools is being extended to reduce development and manufacturing costs. In both efforts, optical sensors have received increased attention as a means to characterize novel technologies and to improve the productivity of existing tools. Optical technologies are particularly appropriate for semiconductor manufacturing applications since they provide a sensitive, non-perturbing means to monitor and control dry processes in real-time. This talk discusses the novel application of two optical sensing techniques to semiconductor device fabrication equipment. First, an infrared-based sensor is employed to control the delivery of condensable feedgases to CVD reactors used to deposit dielectric films. This sensor continuously monitors the flow of reactants to the chamber and reduces the need for test wafers typically used to verify film thickness and dopant concentration. Second, an ultraviolet absorption technique is employed to monitor reactants in a high density plasma reactor used for the selective etching of SiO<sub>2</sub> films. This sensor aids process development by identifying reactor parameters which affect the concentration of species which control etch selectivity.

INVITED

4:00 pm **MS-WeA7 Real-Time Process and Product Diagnostics in RTCVD Using In-Situ Mass Spectroscopic Sampling, L. L. Tedder<sup>1</sup>, G. W. Rubloff<sup>2</sup>, I. Shareef<sup>2</sup>, M. Anderle<sup>2</sup>, D.-H. Kim<sup>2</sup>, and G. N. Parsons<sup>1</sup>**, <sup>1</sup>North Carolina State Univ., Raleigh, NC 27695, <sup>2</sup>IBM Research, Yorktown Heights, NY 10598.

Reactive chemical processes play a critical role in semiconductor manufacturing, but concentrations of reactive gas species are rarely monitored during the process, nor used for process control. Mass spectroscopy, already in use as residual gas analysis for contamination control in manufacturing, has been exploited here for rapid real-time sensing of both reactant and product species in single-wafer CVD reactions, including RTCVD polySi from SiH<sub>4</sub> and LPCVD SiO<sub>2</sub> from TEOS. Active mass spectrometric sampling at pressures to 5 Torr is achieved using two-stage differential pumping of a sampling aperture in the exhaust gas stream, permitting response times as short as ~5



sec to concentration and pressure changes in the reactor. In addition to reactant species, gaseous reaction products have been identified and distinguished from cracking fragments of the reactant through relative intensities of mass fragments as a function of wafer temperature (i.e., reaction rate). For rapid thermal polySi CVD from  $\text{SiH}_4$ , carried out in  $\sim 30$  sec in the range 500–800°C at 5 Torr in 10% $\text{SiH}_4$ /Ar, mass spectra reveal not only the time dependence of reactant (monitored by  $\text{SiH}_2$ , 30 amu), but also—at higher temperatures—reactant depletion and product generation (from  $\text{H}_2$ , 2 amu). These results demonstrate a basis for using mass spectroscopy in real-time process and product diagnostics for control.

**4:20 pm MS-WeA8 Mass Spectrometric *in situ* Process Monitoring Applied to Silicon Dioxide Electron Cyclotron Resonance Chemical Vapor Deposition.** L. M. Williams, Lam Research Corp., Fremont, CA 94538, L. C. Frees, T. Vo, Leybold Inficon Inc., East Syracuse, NY 13057.

Conventional residual gas analyzer systems are not adequate for *in situ* monitoring of processes such as chemical vapor deposition (CVD) which involve reactive species. A closed ion source mass spectrometer (MS) system was installed on an electron cyclotron resonance (ECR) CVD tool for  $\text{SiO}_2$  films. A mixture of  $\text{SiH}_4$ ,  $\text{O}_2$  and Ar at a total pressure of 0.4 Pa was used for the film deposition. The tool was plasma etch cleaned with  $\text{NF}_3$  at 400 Pa. The data collected during deposition suggested that the primary pathway involved the reaction  $\text{SiH}_4$  with  $\text{O}_2$  to form  $\text{SiO}_2$  and  $\text{H}_2$ , although a lesser amount of  $\text{H}_2\text{O}$  was also observed. Flourine containing residues were detected in the tool after the etch clean. Baking of the MS after sampling an etch clean eliminated the major contribution of MS system flourine residuals to HF and  $\text{SiF}_4$  levels detected during  $\text{SiO}_2$  deposition. The ability to rapidly and conveniently change the MS ionizer electron energy from the normal 70 eV to 35 eV prevented  $\text{Ar}^{2+}$  from interfering with  $\text{HF}^+$ . Monitoring  $\text{F}^+$  is not a satisfactory way to track HF levels because of the many potential sources of  $\text{F}^+$ .

**4:40 pm MS-WeA9 Microsensors for Process Control and Monitoring.** Robert C. Hughes and James J. Wiczer, Microsensor Dept., Sandia National Labs, Albuquerque, NM 87185.

The Microsensor Dept. at Sandia National Labs is performing Research, Development and Application of microsensor technologies using microelectronic and opto-electronic platforms. The goal is to provide real-time, *in-situ*, inexpensive, multipoint environmental and process control monitoring. Several examples will be described including a new microelectronic hydrogen sensor that accurately measures the partial pressure over 12 decades, from  $10^{-9}$  Torr to 100%  $\text{H}_2$ , surface acoustic wave devices as gas sensors and a fiber optic micromirror for measuring a variety of gas phase species. A multifiber version is being built for NASA/Russian Mars mission to test soil reactivity. Multipoint hydrogen sensors are looking for liquid  $\text{H}_2$  leaks at both NASA Stennis and NASA Kennedy. A fully portable system based on the acoustic wave vapor sensor has been fielded as a downhole well monitor. Acoustic wave devices are also finding use in contamination free microelectronics manufacturing. Both regulatory requirements and a desire for cost saving in processing is driving the development and application of microsensor technologies.

INVITED

This work was supported by the US Dept. of Energy under contract DE-AC04-94AL85000.

## VACUUM METALLURGY

### Room A106 – Session VM-WeA

#### Thin Film Microstructure Evolution

**Moderator:** L. Hultman, Linköping University, Sweden.

**2:00 pm VM-WeA1 Effects of High Flux Low Energy ( $\sim 20$  eV) Ion Irradiation During Growth on the Microstructure and Preferred Orientation in TiN Films Deposited by Magnetron Sputtering.** I. Petrov and J. E. Greene, Department of Materials Science, University of Illinois, Urbana, IL 61801, and L. Hultman, and J.-E. Sundgren, Department of Physics, Linköping University, S-581 83 Linköping, Sweden.

The effects of incident ion/metal flux ratio  $J_i/J_{Ti}$  on the microstructure and texture of TiN films produced by ultra-high vacuum reactive magnetron sputtering have been investigated using x-ray diffraction and cross-sectional transmission electron microscopy (XTEM) including high-resolution XTEM. The films, typically 1.0  $\mu\text{m}$  thick, were deposited at a pressure of 20 mTorr in  $\text{N}_2$  on thermally oxidized  $\text{SiO}_2$  substrates at 350°C. The flux ratio  $J_i/J_{Ti}$  at the substrate was controlled between 1 and 15 by means of a variable axial magnetic field superimposed on the permanent field of the magnetron. The potential difference accelerating the ions to the floating substrates remained relatively constant ( $\sim 20$  V) as the ion flux (primarily  $\text{N}_2^+$ ) was varied. Films deposited at  $J_i/J_{Ti} = 1$  nucleated with a mixed texture, but subsequent film growth resulted in a porous columnar structure in which the preferred orientation evolved to complete (111) texture at film thickness above 0.2  $\mu\text{m}$ . In contrast, films deposited at  $J_i/J_{Ti} = 14$  nucleated with a complete (002) texture which was retained during growth to yield a dense columnar structure. Once film texture fully evolves, however, changing ion flux has little further effect on preferred orientation, as pseudomorphic forces dominate, but still controls intercolumn porosity.

**2:20 pm VM-WeA2 The Effect of 20-95 eV Ar Ion Bombardment on Molecular Beam Epitaxy of GaAs(100).** J. Mirecki Millunchick and S. A. Barnett, Department of Material Science and Engineering and the Materials Research Center, Northwestern University, Evanston, Illinois, 60208, L. Hultman, Physics Department, Linköping University, Linköping, S-581 83, Sweden.

Low-energy ion-assisted molecular beam epitaxy (IAMBE) is useful for suppressing three-dimensional island nucleation and phase separation in III-V semiconductor alloys. However, little is known about ion damage in this energy range. Defect generation in GaAs(100) has been studied *in situ* by Reflection High Energy Electron Diffraction (RHEED) and *ex situ* by cross-sectional Transmission Electron Microscopy (XTEM).  $\text{Ar}^+$  bombardment was performed at energies  $E = 20$  to 95 eV and current densities  $J = 0.1$  to 0.75  $\text{mA}/\text{cm}^2$  both on static surfaces and during homoepitaxy. RHEED patterns exhibited  $2 \times 4$  reconstruction and strong Kikuchi lines at all times, indicative of flat and ordered surfaces. XTEM showed that subsurface dislocation loops and stacking faults were generated when  $E > 50$  eV. For example, during bombardment of a static surface at  $E = 75$  eV and  $J = 0.5$   $\text{mA}/\text{cm}^2$ , the density of the defects was on the order of  $5 \times 10^{10} \text{ cm}^{-2}$ . Films grown under  $20 < E < 50$  eV and  $0.25 < J < 0.75$   $\text{mA}/\text{cm}^2$  ion irradiation did not exhibit any defects. While there was no measurable ion etching for  $E < 50$  eV, the deposition rate of films grown at  $E = 50$  eV and  $J = 0.5$   $\text{mA}/\text{cm}^2$ , for example, was decreased by 0.16 nm/s. These results show that the beneficial effects of IAMBE can be achieved without causing ion damage or sputtering for  $20 < E < 50$  eV.

**2:40 pm VM-WeA3 Theoretical Considerations on Stress Effects on Thin Film Microstructure.** David J. Srolovitz, Dept. of Materials Science & Eng., University of Michigan, Ann Arbor, MI 48109-2136 USA.

Stresses affect the microstructure of thin films in several ways. These include texture effects, island formation, film morphology, and the nature of defects (such as grain boundaries) that make up the microstructure. The microstructure can also play a key role in determining the magnitude of the stresses in a thin film by controlling stress relaxation mechanisms. This talk will review several important areas of stress/microstructure interaction and will focus primarily on how stresses modify texture, grain size, grain boundaries and other planar defects in thin films.

INVITED

**3:20 pm VM-WeA5 Surface Thermodynamics Effects on Thin Film Microstructure.** R. C. Cammarata, Department of Materials Science and Engineering, The Johns Hopkins University, Baltimore, MD 21218.

Associated with every surface (interface) are surface thermodynamic quantities referred to as surface (interfacial) tension and stress. It is well known how surface tension influences such processes as normal grain growth in thin films. However, there are several other less well known mechanisms of microstructural development where surface thermodynamic properties play a central role.

Surface and interfacial tensions and stresses will first be defined and related to thin film systems. This will be followed by a discussion of how these quantities can affect processes involving texture development, epitaxial growth, surface structure, and internal stresses. In particular, the work of Thompson et al. on surface tension effects on



texture development by abnormal grain growth as well as recent developments concerning the influence of surface and interface stresses on film growth be presented.

INVITED

4:00 pm **VM-WeA7 A Molecular Dynamics Study of Transient Processes During Deposition on (001) FCC Metal Surfaces**, C. M. Gilmore<sup>1,2</sup> and J. A. Sprague<sup>2</sup> (1) School of Engineering and Applied Science, The George Washington University, Washington, D.C. 20052, (2) Surface Modification Branch, U.S. Naval Research Laboratory, Washington, D.C. 20375-5345.

Strong RHEED oscillations have been observed during growth of Cu onto (001) Ag substrates at 77 K.<sup>(1)</sup> This result indicates layer by layer film growth and surface mobility of the deposited atoms. This unexpected result was explained by proposing a "transient mobility" to account for the atom mobility normally required for layer by layer growth. We have utilized molecular dynamics simulations with the embedded atom method to study transient processes that occur over hundreds of ps. Transient processes were observed that promoted the formation of clusters, and other processes were observed that resulted in spreading atoms across the surface.

1. W. F. Egelhoff and I. Jacob, Phys. Rev. Lett., 62(8) 921 (1989).

4:20 pm **VM-WeA8 Synthesis of Epitaxial  $\text{Sn}_x\text{Ge}_{1-x}$  Alloy Films by Ion Assisted Molecular Beam Epitaxy and Pulsed Laser Deposition**, Gang He, Maggie E. Taylor, Harry A. Atwater, California Institute of Technology, Pasadena, CA 91125.

The metastable  $\text{Sn}_x\text{Ge}_{1-x}$  alloy system is an interesting group IV semiconductor material with potential applications in the fabrication of Si-based high performance heterojunction devices and long wavelength infrared optoelectronic devices. Band structure calculations have suggested that the  $\text{Sn}_x\text{Ge}_{1-x}$  alloys may have direct energy gaps continuously tunable from 0.55 eV to 0 eV for compositions  $x$  from 0.2 to 0.6 with very low electron effective masses and hence high mobilities. However, syntheses of  $\text{Sn}_x\text{Ge}_{1-x}$  alloy films in this composition range by conventional epitaxial or polycrystalline film growth techniques have not been successful due to the severe surface segregation of Sn during the film growth. In this work, we report the synthesis of epitaxial  $\text{Sn}_x\text{Ge}_{1-x}\text{Ge}(001)/\text{Si}(001)$  with compositions up to  $x = 0.35$  by ion assisted molecular beam epitaxy with 20–40 eV  $\text{Ar}^+$  ions produced by an electron cyclotron resonance ionization source with ion to atom flux ratios of the order of unity in the substrate temperature range of 140 to 170°C. High flux low energy ion beam irradiation greatly inhibits Sn segregation without interrupting epitaxy. *In situ* reflection high energy electron diffraction during the film growth indicated that the  $\text{Sn}_x\text{Ge}_{1-x}$  films were epitaxial up to a thickness of 10–20 nm and subsequently undergo a gradual epitaxial to polycrystalline transformation. Rutherford backscattering spectra confirmed the  $\text{Sn}_x\text{Ge}_{1-x}$  alloy compositions and indicated an absence of Sn segregation. Comparison of ion assisted molecular beam epitaxy and pulsed laser dep-

osition in the same chamber, as well as ion channeling, x-ray diffraction, transmission electron microscopy, and optical absorption studies will be discussed.

4:40 pm **VM-WeA9 Scanning Tunneling Microscopy Studies of the Effect of Annealing on Gold Films**, D. Porath, E. Bar-Sadeh, M. Wolovelsky, A. Grayevsky, Y. Goldstein and O. Millo, Racah Institute of Physics, The Hebrew University of Jerusalem, Israel.

We have studied systematically thermal annealing effects on the surface morphology of 800 Å thick gold films, using a scanning tunneling microscope (STM). The gold films were thermally evaporated onto glass and mica substrates, and were then measured with the STM at room temperature before and after annealing. The annealing treatments were done at temperatures between 200 to 500°C and for times from 3 to 60 hours. The topographic images were analyzed using various statistical methods and image processing techniques. We present data showing the evolution of the surface-grain size distribution and roughness amplitude of the gold films as a function of annealing temperature and duration. The typical grain size was found to increase with time for all annealing temperatures, whereas the roughness amplitude shows a more complex dependence on the annealing parameters. We are now developing a theoretical model to describe quantitatively the surface processes taking place during annealing. Computer simulations based on our model will be performed and compared with experiment. The possible fractal nature of the film surfaces and its change upon annealing will also be discussed.

5:00 pm **VM-WeA10 Structure-Property Relationships in Compositionally Modulated Titanium-Aluminum Thin Films**, Rajiv Ahuja and Harnish L. Fraser, Department of Materials Science and Engineering, The Ohio State University, 116 W 19th Ave., Columbus, OH 43210.

In a previous study by the authors, on compositionally modulated Ti-Al thin films, evidence was presented for a series of structural transitions that occur as a function of the bilayer thickness of the multilayer. There is evidence which indicates the occurrence of a titanium based *fcc* structure in these films, at a bilayer thickness of 9.8 nm. Upon reducing the bilayer thickness further to 5.2 nm, both the Ti and Al layers adopt the *hcp* structure and are coherent with each other. This paper aims at examining the influence of crystallographic structure, bilayer thickness and growth morphology on the electrical resistivity and some of the mechanical properties of Ti-Al multilayers. The resistivity is essentially determined by interface scattering and to some extent by grain boundary scattering in the multilayers with small bilayer thicknesses. There is no evidence of the 'supermodulus effect' in these multilayers, but there is a significant increase in the multilayer hardness, as a function of the bilayer thickness. There appears to be a Hall-Petch type of relationship between the hardness and the bilayer thickness, indicative of the fact that the mode of plastic deformation in these multilayers appears to be influenced not only by the presence of interfaces, but by their nature too.

## SURFACE SCIENCE

### Room BR4 - Session SS-WeP

#### Aspects of Surface Science

**Moderator:** J. C. Hemminger, University of California, Irvine.

**SS-WeP1 Elevated Temperature Structures of the Ag on Si(111) System at Submonolayer Coverages, G. Navrotsky and J. M. Blakely,** Cornell University, MS&E, Ithaca, N.Y. 14853-1501.

Adsorption of Ag on the Si(111) surface has been studied by almost every available surface science technique over the last 27 years, yet its structure remains an enigma. We study here the effects of three experimental variables on the atomic positions in the Ag/Si(111) ( $\sqrt{3} \times \sqrt{3}$ )R30° Ag and ( $3 \times 1$ ) Ag phases at temperatures up to 560°C. The average location of Ag atoms for each phase and the magnitude of the Si surface contraction are determined by combining the results of two complementary synchrotron x-ray techniques; the X-ray Standing Wave (XSW) technique and the polarization dependent Surface Extended X-ray Absorption Fine Structure (SEXAFS) technique, supplemented by Rutherford Backscattering (RBS)- and AES/LEED. We find that with sub-monolayer levels of carbon, the distance of the Ag (in the  $\sqrt{3}$  phase) along the surface normal is increased by about 0.36d<sub>(111)</sub> and is more narrowly confined. Carbon apparently occupies sites normally taken by Ag in the  $3 \times 1$  phase. At C coverages of greater than 1/3 monolayer, all of the  $3 \times 1$  adsorption sites are occupied and the adsorbed Ag in the  $\sqrt{3}$  phase moves outward from the surface to  $(0.68 \pm 0.016)d_{(111)}$  with a Ag-Si nearest neighbor bond length of  $(2.5 \pm 0.05)$  Å. We find there is no measurable effect from incidental surface contamination by boron introduced during wet chemical sample preparation. At low coverages on clean surfaces, we infer that Ag in the  $3 \times 1$  phase adsorbs at a different site from that in the  $\sqrt{3}$  Ag; this makes Ag multi-positional when grown at temperatures below 400°C. Clean Si(111) binds the  $\sqrt{3}$  Ag phase at  $(0.33 \pm 0.020)d_{(111)}$  above the surface with a Ag-Si nearest neighbor bond length of  $(1.6 \pm 0.05)$  Å.

**SS-WeP2 Surface Morphology Induced by Ga and Sn Overlayers on Si(100) and Si(311) Surfaces, L. Li, Y. Wei and I. S. T. Tsong,** Arizona State University, Tempe, AZ 85287.

The evolution of surface reconstructions and facets on Si(100) and Si(311) as a function of Ga and Sn coverages  $\geq 1$  monolayer (ML) is presented. The changes in surface morphology with annealing temperature were followed by scanning tunneling microscopy (STM). When the Ga coverage on Si(100) exceeded 1 ML, square depressions shaped like inverted pyramids were formed on the Si(100)-(4 × 8)Ga surface. The inverted pyramid walls were (311) facets. Deposition of Sn on Si(100) at coverages exceeding 2 ML also produced (311) facets, but they formed faces of long orthogonal prisms, giving rise to a large scale maze structure on the surface. As expected, deposition of Sn on Si(311) did not produce facets. Layer-by-layer of epitaxial (1 × 1)Sn growth was observed on the Si(311) surface up to 2 ML. On the other hand, deposition of Ga on Si(311) produced highly ordered (211) and (611) facets at coverages above 1 ML.

**SS-WeP3 STM Studies of Benzene Adsorption on Both Clean and O-preadsorbed Ni(110), L. Ruan\*, I. Stensgaard, F. Besenbacher, and E. Lægsgaard,** Institute of Physics, Aarhus University, DK-8000, Aarhus C, Denmark.

Interaction between benzene and both clean and O-preadsorbed Ni(110) has been investigated using STM in ultra-high vacuum. The benzene adsorption on clean Ni(110) at room temperature and low temperature produces disordered and short-range ordered structure, respectively. Most of the molecules are observed as flat rings lying on the substrate and this result is consistent with other studies. The rest observed as tilted rings are ascribed to the benzene molecules losing one hydrogen. On O-preadsorbed Ni(110) the benzene adsorption results in a structural transformation from p( $3 \times 1$ ) to p( $2 \times 1$ ) by compressing the -Ni-O- chains.

\*Present address: Department of Chemistry and Department of Engineering, University of Western Ontario, London, Ontario, Canada.

**SS-WeP4 Determination of the Reconstruction of Pt(100) Surface on Atomic Scale by Scanning Tunneling Microscope\*, C. S. Chang, W. B. Su, and T. T. Tsong,** Institute of Physics, Academia Sinica, Taiwan, ROC.

Two rotational phases of the stable reconstruction for the clean Pt(100) surface have been identified on an atomic scale by the scanning tunneling microscope. The slightly rotated buckled hexagonal close-packed model is strongly substantiated by our STM results. Our data also provide information about the atom positions in the top hexagonal layer with respect to the square substrate via the determination of the registry. These data can be useful for the further theoretical study of the nature of the distortion waves originated from a high order commensurate hexagonal layer over a square substrate.

\*Supported by the National Science Council of ROC under grant No. NSC83-0208-M001-038 and the special surface science project of Academia Sinica.

**SS-WeP5 Multiple Tunneling Gap Resistance Imaging for Surface Structure Determination with the STM, J. C. Dunphy, P. Sautet\*, D. F. Ogletree, and M. Salmeron,** Material Science Division, Lawrence Berkeley Laboratory, Berkeley, CA 94720 USA, \*Institut de Recherche sur la Catalyse, Villeurbanne, France and Laboratoire de Chimie Théorique, ENS, Lyon, France.

We have used Electron Scattering Quantum Chemistry (ESQC) STM theory for surface structure determination of adsorbates on metal surfaces from STM images. The theory indicates that the contrast in STM images is sensitive to changes of order 0.1 Å in surface, adsorbate, and tip geometry. Additionally, the decay of the tunneling current with tip-surface separation was found to be non-uniform across the unit cell. This causes the image contrast to change with the gap-resistance. Therefore, we have implemented an image acquisition mode where images are acquired at up to eight different tunneling gap resistance. To overcome the experimental problems of thermal-drift, piezo hysteresis, and unknown tip changes, each scan line of an image is acquired at a range of gap resistances before proceeding to the next scan line. We have applied this technique to determine the structure of adsorbate on metal systems (S and C on Mo and Cu) using Pt, oxygen treated W, and clean W tips.

**SS-WeP6 Cu Deposition on Ru(0001) by Low Energy Li<sup>+</sup> Ion Scattering, Y. G. Shen<sup>1</sup>, D. J. O'Connor<sup>1</sup>, J. Yao<sup>1</sup>, R. J. MacDonald<sup>1</sup>, H. van Zee<sup>2</sup>, R. H. Roberts<sup>1</sup> and K. Wandelt<sup>3</sup>,** <sup>1</sup>Department of Physics, University of Newcastle, New South Wales 2308, Australia, <sup>2</sup>Department of Physics, Eindhoven University of Technology, 5600 MB Eindhoven, The Netherlands, <sup>3</sup>Institut für Physikalische und Theoretische Chemie der Universität Bonn, Wegelerstrasse 12, D-5300 Bonn 1, Germany.

The surface structure of Cu thin films on Ru(0001) has been studied by low energy Li<sup>+</sup> ion scattering, AES and LEED. It was found that Cu formed pseudomorphic layers for the first two layers. Experimental results obtained by analyzing the incident angle dependence associated with shadowing of Ru by Cu confirmed that the first layer Cu atoms were in a normal Ru registry position, i.e. there was a continuation of the hcp stacking sequence. The second layer Cu atoms have also been determined to be at the fcc sites by analyzing the shadowing critical angles for the second layer Cu focusing onto the first layer Cu atoms in the [1010] azimuth. The structure of the Cu thin films up to 6 ML have also been probed by measuring the incident and azimuthal angle dependences. The results were consistent with an epitaxial Cu(111) structure by comparing with the results of standard Cu(111) structure.

**SS-WeP7 Morphological Effects of Ultrathin Metal Films on Mo(111)\*, Jie Guan, Robert A. Campbell and Theodore E. Madey,** Departments of Physics and Chemistry and Laboratory for Surface Modification, Rutgers, The State University of New Jersey, Piscataway, NJ 08855.

The interaction of Pd, Rh, Pt, Au, Ti, Mn, Fe, Co, Ni, Cu, Ag and Gd ultrathin films with a Mo(111) substrate has been investigated by means of Auger electron spectroscopy (AES), low energy electron diffraction (LEED) and temperature programmed desorption (TPD). The deposition of >1.0 ML of Pt, Au, Pd and Rh results in the Mo(111) surface reconstructing to form pyramidal facets with {211} orientation upon sample annealing. Average facet dimensions are

~10 Å. The remaining metals are not effective in inducing the morphological reconstruction. An analysis of the electronic, physical and chemical properties of the metal overlayers strongly suggests that the electronic structure plays a dominant role in causing surface instability on Mo(111). Metals with a Pauling electronegativity of >2.0 are effective for inducing faceting. These results are consistent with the previous investigation of the W(111) surface.

\*Supported by DOE, Office of Basic Energy Sciences.

**SS-WeP8 Highly Angular Resolved Patterns of Photo- and Auger-Electron Diffraction from MgO(001),** *Y. Nihei, H. Ishii, M. Owari and Y. Ichinohe*, Inst. of Ind. Sci., University of Tokyo, Roppongi 7-22-1, Minato-ku, Tokyo 106, Japan.

In an aim to understand the nature of photoelectron and Auger electron diffraction from a single crystal, the two dimensional diffraction patterns of the emitted electrons from a cleavage MgO(001) were precisely measured with high angular resolutions. In the electron diffraction patterns with the angular resolution of  $0.6^\circ$  (an angular step size was  $0.5^\circ$ ), several interesting features were clearly observed: bands, lines, bright spots and "dark" spots at the crossing points of those lines, and circular diffraction patterns. The band and line structures were closely related to the low-index crystallographic planes. However, to our knowledge, this is the first observation of these types of spots in photoelectron and Auger electron diffraction. With a highly angular resolved measurement, these fine structures described above were clearly observed.

**SS-WeP9 Structural Surface Phase Transitions During Segregation Competition,** *M. Militzer<sup>1</sup> and S. Hoffmann<sup>2</sup>*, <sup>1</sup>The Centre for Metallurgical Process Engineering, The University of British Columbia, Vancouver, B.C., Canada V6T 1Z4, <sup>2</sup>Max-Planck-Institut für Metallforschung, D-70174 Stuttgart, Germany.

The kinetics of surface segregation competition, when the segregants form different saturation structures, is investigated for three cases: S-P at the (110) surface in Cu, S-Si and Sn-S at the (100) surface in Fe-6at%Si. In these cases the weaker segregant (P, Si) first forms a  $C(2 \times 2)$  structure before being replaced by the stronger segregant (S, Sn) with a  $p(1 \times 1)$  saturation structure. The surface phase transition,  $c(2 \times 2) \Rightarrow p(1 \times 1)$ , indicates complex site competition mechanisms; these are described with phenomenological models. Further, enrichment by bulk as well as pipe diffusion is taken into account. The changes in the enrichment rates associated with the surface phase transition can be explained within the proposed approach. The S segregation rate is markedly reduced by the phase transition since the contribution from pipe diffusion vanishes when the new surface phase nucleates at the pipes. For Sn, on the other hand, the surface phase transition provides a higher driving force for segregation by removing the retardation effect of Si, allowing the Sn segregation rate to increase. The models are in good agreement with results from AES measurements.

**SS-WeP10 Direct Determination of Adsorbate Positions with Energy-Dependent and Angle-Resolved Photoelectron Diffraction,** *Huasheng Wu and G. J. Iapeyre*, Physics Department, Montana State University, Bozeman, MT 51717.

While we successfully implemented a method to directly determine the adsorbate position using energy-dependent and angle-resolved photoelectron diffraction for the  $\text{Si}(111)\sqrt{3} \times \sqrt{3}\text{-Al}$ , we also found large artifacts in the atomic image. To reduce the artifacts, the angular behavior of the effective scattering factor was examined. The result suggests that the artifacts are from the large variation in factor's phase in the case where the emission directions are far from the emitter-scatterer direction. As a consequence, we proposed a new transform scheme—the small cone method where the cone size is from the data. To calculate the image function intensity at a given position vector in real space, we now use only those diffraction curves with their emission directions within a small cone, the axis of which is opposite to the given position vector. The small cone method dramatically reduces the artifacts and interesting results are obtained from all measured structures. In  $\text{Si}(111)\sqrt{3} \times \sqrt{3}\text{-Ga}$ , the image reveals that the Ga atoms occupy the  $T_4$  site. The image for the  $\text{Si}(111)1 \times 1\text{-As}$  structure shows that the As atoms substitute the top layer Si atoms. The result for the more complicated two-inequivalent-site structure  $\text{Si}(100)2 \times 1\text{-As}$  clearly shows an adatom dimer: the first case for a two site image. The atomic position values obtained with the small-cone method are in good agreement with other values where they exist.

Research and SRC supported by NSF.

**SS-WeP11 Magneto-Optical Kerr Effect of Exchange Coupling in Co/Cr/Co Films on Pd(111) and Pd(100) Substrates,** *J. D. McKinley, C. Rau*, Department of Physics and Rice Quantum Institute, Rice University, Houston, TX 77251-1892, USA.

Oscillatory exchange coupling between Fe or Co layers through variable thickness transition/noble metal spacer layers (Cr, Au, Cu) may induce spin polarization in the spacer layers. Previous studies only examine exchange coupling between in-plane magnetized layers. Films of Co on Pd(111) are known to be magnetized out of plane, in contrast to the in plane magnetization of Co films on Pd(100). Co/Cr/Co films grown on Pd(111) constitute a model system for exchange coupling between out of plane magnetized layers through a spacer layer. Identical Co/Cr/Co films are grown on Pd(100) for comparison to in-plane exchange coupling. Results are reported for polar and longitudinal magneto-optical Kerr effect (MOKE) of Co/Cr/Co/Pd(111) and Co/Cr/Co/Pd(100) films.

\*Supported by the National Science Foundation, the Welch Foundation, and the Texas Higher Education Coordinating Board.

**SS-WeP12 Thickness- and Temperature-Dependent Spin Reorientation Transition of Epitaxial Ni Films on Single Crystal Cu Surfaces,** *S. Z. Wu, G. J. Mankey, and R. F. Willis*, Department of Physics, The Pennsylvania State University, University Park, PA 16802.

We have studied the ferromagnetism of Ni films deposited on Cu(100), Cu(110) and Cu(111) surfaces *in situ* using the surface magneto-optic Kerr effect (SMOKE). For ultrathin Ni films grown on Cu(100) and Cu(110), the easy axis of magnetization lies in the plane of the films. Above a switching thickness, the easy axis of magnetization is perpendicular to the film. In addition, the magnetization increases dramatically by about an order of magnitude. This behavior is opposite to the conventional spin reorientation transition where ultrathin films exhibit perpendicular magnetization and thicker films exhibit in-plane magnetization above the switching thickness. We will report SMOKE measurements of the magnetic anisotropy as functions of both film thickness and temperature. The switching occurs at 8 ML film thickness for Ni on Cu(100) and at 16 ML for Ni on Cu(110). For Ni on Cu(111) no switching is observed. These results are discussed in terms of competing interfacial, volume and surface anisotropy energy terms in a complex Hamiltonian.

**SS-WeP13 Experimental Fermi Surface of Magnetic Multilayers,** *C. Casado, J. Avila, A. Vjatkin, F. Soria\*, M. C. Asensio*, LURE, bât. 209D, Université Paris-Sud, 91405 Orsay cedex, FRANCE, Fax (34)164464148. \*Instituto de Ciencia de Materiales de Madrid, CSIC, c/Serrano 144, (28006) Madrid, SPAIN.

The behavior of the Fermi Surface (FS) has a decisive influence on the understanding of a wide variety of phenomena such as magnetic thin film multilayers and high  $T_c$  superconductors. Traditional methods of FS measurements demand strong restrictions on the crystalline quality, therefore they can be hardly suited by low-dimensional systems. In these cases, Angle-resolved Photoelectron Spectroscopy (ARUPS) is one of the most convenient tools to determine FS contours. In ARUPS, the momentum parallel to the surface and the energy are rigorously conserved, such as the Fermi-level crossing by the bands of systems localized at a few layers can be easily sampled.

In this contribution, we present the evolution of the FS of the Co/Cu(100) interface as a function of Co coverage. The FS 2-D images show the Co transition from a thin two-dimensional metallic layer to a three-dimensional one with a FCC structure. The FS of sandwich structures as Cu/Co/Cu and Cu/Fe/Cu were also investigated as a function of the non-magnetic metal coverage. In order to perform the full mapping of the FS,  $2\pi$  angular distributions of density of states at the Fermi level were recorded along all directions of the Brillouin Zone. Typical energy and full angular resolution were less than 100 meV and  $1^\circ$ , respectively.

In addition, ARUPS was combined with a synchrotron radiation source in order to obtain well defined cuts through the three-dimensional FS at different  $k_\perp$  values. Polarized and unpolarized radiation with photon energy of 21.2, 33, 50 and 55 eV were employed to study the symmetry of the states sampled.

**SS-WeP14 Combined XPD, STM, and LEED Study of Iron Oxide Films on Pt(111),** *Y. J. Kim<sup>a,b</sup>, C. Westphal<sup>a,c</sup>, R. X. Ynzunza<sup>a,d</sup>, H. Xiao<sup>a,d</sup>, Z. Wang<sup>a,d</sup>, H. C. Galloway<sup>a,e</sup>, M. Salmeron<sup>a</sup>, M. A. Van Hove<sup>a</sup>, and C. S. Fadley<sup>a,d</sup>*, <sup>a</sup>Lawrence Berkeley Laboratory, Berkeley, CA 94720, <sup>b</sup>Dept. of Chem., University of Hawaii, Honolulu, HI 96822, <sup>c</sup>Dept. of Phys., University-GHS-Essen, 45141 Essen, Ger-

many, <sup>a</sup>Dept. of Phys., Univ. of California-Davis, Davis, CA 95616, <sup>b</sup>Dept. of Phys., University of California-Berkeley, Berkeley, CA 94720.

For the first time, three complementary surface structure probes, x-ray photoelectron diffraction (XPD), scanning tunneling microscopy (STM), and low-energy electron diffraction (LEED) have been combined in a single system. This system has been utilized to study the structure of iron oxide films grown on Pt(111). XPD is a near-surface structure probe of the short-range order in the first 3–5 shells of neighbors around each emitter. STM probes both short- and long-range order of the top-most surface layer(s). LEED is primarily sensitive to long-range two-dimensional order. XPD is atom-specific, while STM and LEED are not. For ~1 ML of FeO grown on Pt(111), XPD shows a topmost oxygen layer relaxed inward by ~0.6 Å compared to bulk FeO(111), while STM and LEED show an incommensurate oxide film with short- and long-range periodicities of ~3.1 Å and ~26.0 Å. The dependence on oxide layer thickness of both short- and long-range structures of FeO<sub>x</sub> grown on Pt(111) will be discussed.

**SS-WeP15 Surface-Specific Magnetic Order Transitions for Ising Ferromagnets and Antiferromagnets: Implications for Spin-Polarized Photoelectron Diffraction**, F. Zhang<sup>a,\*</sup>, S. Thevuthasan<sup>a</sup>, R. Scalettar<sup>a</sup>, R. Singh<sup>a</sup>, and C. S. Fadley<sup>a,b</sup>, <sup>a</sup>Physics Dept., U.C. Davis, Davis, CA 95616; <sup>b</sup>MSD, Lawrence Berkeley Laboratory, Berkeley, CA 94720, <sup>c</sup>MSRC, Pacific Northwest Laboratory, Richland, WA 99352.

We have used Monte Carlo simulations on simple cubic Ising lattices with modified surface interaction parameters to model phenomenologically the temperature dependence of magnetic order near ferromagnetic and antiferromagnetic surfaces. These results are also discussed in connection with previous experiments suggesting surface-specific magnetic transition temperatures for semi-infinite systems, with special emphasis on spin-polarized photoelectron diffraction as a probe of short-range magnetic order. The calculated spin-spin correlation functions show no evidence of a high-temperature transition in short-range magnetic order. However, over a plausible range of choices for the surface interaction parameters, these correlation functions do show distinct surface transitions in long-range magnetic order that can be well above  $T_{C,bulk}$  for ferromagnets and well above  $T_{N,bulk}$  for antiferromagnets (both frustrated and non-frustrated). Thus, prior spin-polarized photoelectron data from antiferromagnetic KMnF<sub>3</sub> [1] and MnO [2] could in fact have been observing such surface-specific magnetic order transitions at  $T_{N,surf}$  of 2.7 and 4.5 times  $T_{N,bulk}$  respectively.

- [1] B. Sinkovic et al., Phys. Rev. Lett. 55, 1227 (1985).  
[2] B. Hermsmeier et al., Phys. Rev. Lett. 62, 478 (1989).

**SS-WeP16 Imaging Short-Range Magnetic Order by Spin-Polarized Photoelectron Holography**, Z. Wang<sup>a,b</sup>, A. P. Kaduwela<sup>b</sup>, S. Thevuthasan<sup>c</sup>, M. A. Van Hove<sup>a</sup>, and C. S. Fadley<sup>a,b</sup>, <sup>a</sup>Department of Physics, University of California, Davis, CA 95616, <sup>b</sup>MSD, Lawrence Berkeley Laboratory, Berkeley, CA 94720, <sup>c</sup>MSRC, Pacific Northwest Laboratories, Richland, WA 99352, USA.

We propose extending spin-polarized photoelectron diffraction (SPPD) [1, 2] to the direct holographic imaging of magnetic spin configurations. If a spin-polarized photoelectron is somehow emitted from a core level (e.g., as resolved in a final-state multiplet splitting), it can then undergo spin-dependent scattering from neighboring magnetic atoms to produce SPPE effects. Measuring such SPPE patterns over a large solid angle and/or over several energies should yield a data set of sufficient size to be analyzed using holographic Fourier-transform inversion methods. We discuss the potential of this approach based on multiple-scattering simulations of SPPE patterns for small clusters of Mn<sup>2+</sup> ions and of Mn<sup>2+</sup> and O<sup>2-</sup> ions, with the latter simulating the MnO lattice. Two spin-sensitive holographic image functions  $\Delta$  and  $\Delta'$  are considered, with both suppressing the effects of non-magnetic scatterers,  $\Delta'$  providing information on the locations of magnetic scatterers, and  $\Delta$  being sensitive to both the position and orientation of magnetic scatterers. Although some image artifacts and distortions are seen, multienergy holographic imaging appears capable of determining magnetic spin configurations near surfaces.

- [1] B. Sinkovic et al., J. of Magnetism and Magnetic Materials 92 (1991).  
[2] B. D. Hermsmeier et al. Phys. Rev. B48, 12425 (1993).

**SS-WeP17 Magnetic Circular and Linear Dichroism in Angular Resolved Fe 3p Core Level Photoemission**, E. Tamura, G. D. Waddill, J. G. Tobin and P. A. Sterne, Lawrence Livermore National Laboratory.

The Fe 3p angle-resolved soft x-ray photoemission spectra reveal a large magnetic dichroism for both linearly and circularly polarized light incidence which can be quantitatively explained within a single-particle picture. The obtained spin-orbit and exchange splittings (1.0–1.2 eV and 0.9–1.0 eV), via comparison between the theory and experiment, are 50–100% larger than those hitherto reported [1, 2]. We also predict numerically three independent spin-polarizations, which are induced only by exchange, by spin-orbit and by their interference effects in the case where the magnetic moment vector, the electric field vector of p-polarized light and the wave vector of photoelectrons lie simultaneously in a crystallographic symmetry plane. Comparison will be made between theoretical predictions and an extensive magnetic x-ray circular dichroism photoemission data set from Fe/Cu(001). Work performed under the auspices of the U.S. Department of Energy by the Lawrence Livermore National Laboratory under contract No. W-7405-ENG-48.

- 1) Ch. Roth, F. U. Hillebrecht, H. B. Rose and E. Kisker, Phys. Rev. Lett. 70 (1993) 3479.  
2) Ch. Roth, H. B. Rose, F. U. Hillebrecht and E. Kisker, Solid State Commun. 86 (1993) 647.

**SS-WeP18 Investigation of the Curie Temperature of Iron Bilayer Components of Fe(110)/Ag(111) Multilayers Grown by Molecular Beam Epitaxy**, D. F. Storm, D. J. Keavney, J. W. Freeland, I. Grigorov, and J. C. Walker, Dept. of Physics and Astronomy, Johns Hopkins University, Baltimore, MD 21218.

The temperature dependence of the magnetization of ultrathin films, surfaces, and multilayers is well-documented for a variety of systems when the temperature  $T$  is well below the Curie point. Due to the metastability of these structures, however, almost no reliable measurements have been made at temperatures significantly above room temperature. Hence  $T_c$  for ultrathin films is still a matter of great uncertainty. We have used fast-passage zero-velocity Mossbauer spectroscopy in the transmission geometry to investigate the behavior of the magnetic ordering of ultrathin Fe bilayers in <sup>57</sup>Fe<sub>x</sub>(110)/Ag(111) multilayered systems, where  $x = 3, 4$ , or 5 monolayers (ML). The Ag thickness in each multilayer is 50 ML. We have observed reversible behavior, and our results are indicative of a discrete set of Curie temperatures for each sample and not a continuous distribution. The behavior we observe is consistent with computer simulations we have made of a magnetically-ordered Fe film composed of multiple domains, each with its own  $T_c$ , critical exponent, and temperature-dependent isomer shift. The multilayers exhibit no measurable oxidation, even after exposure to temperatures as high as bulk  $T_c$  (1043 K), although there is evidence of an annealing transition, particularly during the initial heating ramp. However, Mossbauer spectroscopy before and after heating suggests that annealing improves the film quality rather than degrades it. We have used X-ray diffractometry to confirm the structural integrity of the as-grown multilayers and after two temperature ramps.

**SS-WeP19 Reaction of HN<sub>3</sub> with Al(111): Growth of an AlN Film**, J. N. Russell, Jr., Chemistry Division, Naval Research Laboratory, Washington, DC 20375-5342.

Wide energy bandgap III-V semiconductors, such as AlN, have received increased attention due to their optical and electronic properties. Hydrazoic acid, HN<sub>3</sub>, is a potential precursor for low temperature nitridation of aluminum. The chemistry of HN<sub>3</sub> on an Al(111) surface was investigated between 100 and 780 K under ultrahigh vacuum with temperature programmed desorption (TPD), low energy electron diffraction (LEED), Auger electron spectroscopy (AES) and electron energy loss spectroscopy (ELS). Molecular HN<sub>3</sub> desorption was observed at 125 K from multilayer coverages of HN<sub>3</sub>. A broad N<sub>2</sub> desorption feature was peaked at 295 K. H<sub>2</sub> desorption had a peak maximum at 615 K, well above the temperature for H<sub>2</sub> desorption from the hydrogen covered surface. These observations imply the presence of an NH surface reaction intermediate. The Al LVV Auger lineshape was monitored after exposing the 300 K Al(111) surface to HN<sub>3</sub> and annealing at 780K. A series of exposure/anneal cycles revealed the sequential conversion of the metallic Al AES feature at 68eV into a feature at 58 eV which is representative of an AlN film. A new N<sub>2</sub> desorption state at 580 K appeared as the surface became more nitrated. The nitridation mechanism is discussed.



**SS-WeP20 Tailoring Sensing Film Selectivity and Sensitivity Using Principles from the Hard/Soft Lewis Acid-Base (HSAB) Paradigm, V. Thomas, J. W. Schwank, J. L. Gland\***, University of Michigan, Department of Chemistry\*, Department of Chemical Engineering, Ann Arbor, MI 48109-2136.

There are two primary factors restricting the further advancement of gas sensor technology today, sensing film selectivity and sensitivity. The sensing event is a manifestation of the interaction between the gaseous species to be detected and the sensing film. A fundamental and directive approach that addresses these issues is needed. In this research, HSAB principles are used to tailor platinum sensing films to selectively chemisorb aromatic cyclic hydrocarbons amongst other cyclic hydrocarbons. The HSAB Paradigm is a predictive approach that can be used to tailor sensing films for selective chemisorption. This research illustrates the effective use of these principles to understand adsorbate-adsorbent chemical interaction occurring during a sensing event.

A prototypical polycrystalline platinum sensing film, deposited on a 1 cm<sup>2</sup> piece of silicon wafer equipped with a tantalum heater on its backside, is used. Chemical species coadsorption and thermal treatment are used to tailor the sensing film for selective aromatic cyclic hydrocarbon chemisorption. The effect of prescribed modification protocols on the sensing film is studied by characterizing the sensing film, before and after modification, using temperature programmed desorption, work function measurements and both exsitu X-ray diffraction and X-ray photoelectron spectroscopy. Correlations between particle size and both particle and electron distributions are discussed from the perspective of the HSAB paradigm.

**SS-WeP21 Differential-Conversion Temperature Programmed Desorption: A New Method for Obtaining Bimolecular Surface Rate Constants, R. P. Southwell and E. G. Seebauer**, Department of Chemical Engineering, University of Illinois, Urbana, IL 61801.

For bimolecular surface reactions of the form  $A + B \rightarrow AB$ , temperature programmed desorption (TPD) cannot be used efficiently to detect AB if either of the reactants desorbs before AB. A modification of TPD (differential-conversion TPD, or DCTPD) that circumvents this problem is described in this poster. The reactant desorbing at high temperature is first adsorbed as in normal TPD. The surface is then exposed to a continuous flux of the other reactant, and the rate of product AB desorption is monitored at the same time. The flux is kept so low that the coverage of the reactant adsorbed initially scarcely changes. The rate constant is then determined using this measured coverage and that calculated for the impinging species from its previously-determined adsorption/desorption kinetics. Application of DCTPD is demonstrated in the particular case of HCl production from SiH<sub>4</sub> and TiCl<sub>4</sub> on TiSi<sub>2</sub>.

**SS-WeP22 Effect of Fluorination on the Reaction Kinetics of the Phenyl Coupling Reaction on Cu(111), Jerry M. Meyers**, University of Illinois, Urbana, IL 61801 and **Andrew J. Gellman**, Carnegie Mellon University, Pittsburgh, PA 15213.

Understanding surface reaction kinetics and the transition states which determine their kinetics is of fundamental importance in numerous fields of science and technology. The amount of charge separation in the transition state can be determined by comparing activation energies of reactions of fluorinated and hydrogenated molecules. Fluorination has been shown to have a significant effect on the activation energies of reactions in which there is charge separation in the transition state. Fluorination of the iodobenzenes at the *ortho*, *meta* and *para* positions (*o*, *m*, *p* F-C<sub>6</sub>H<sub>4</sub>I) has been used to study transition states of the phenyl coupling reaction. On the Cu(111) surface, iodobenzene (C<sub>6</sub>H<sub>5</sub>I) dissociates into adsorbed phenyl groups (C<sub>6</sub>H<sub>5</sub>(<sub>ads</sub>)) and adsorbed iodine (I(<sub>ads</sub>)) atoms at approximately 175 K. Upon heating, the phenyl groups couple to form biphenyl (C<sub>6</sub>H<sub>5</sub>-C<sub>6</sub>H<sub>5</sub>), which desorbs molecularly at 400 K. Temperature Programmed Desorption (TPD) has been used to determine the activation energies and Fourier-Transform Infrared Reflection-Absorption Spectroscopy (FT-IRAS) has been used to determine the geometry of the adsorbed molecules. The evidence shows that there is little charge separation in the transition state for phenyl coupling.

**SS-WeP23 Thermal and Electron-Induced Chemistry of CF<sub>3</sub>I on Ni(100), M. B. Jensen and P. A. Thiel**, Department of Chemistry and Ames Laboratory, Iowa State University, Ames, IA 50011.

We have used thermal desorption spectroscopy (TDS) to study the reactions of CF<sub>3</sub>I following adsorption at 100 K on Ni(100). At lowest exposures no molecular CF<sub>3</sub>I or CF<sub>n</sub> species are observed, although atomic iodine is visible at 1100 K, indicating C-I bond cleavage. At

higher exposures molecular CF<sub>3</sub>I is observed at 200 K, along with etched Ni desorbing as NiF<sub>2</sub> in a peak at 900 K. This is followed by a small amount of CF<sub>3</sub>, and finally multilayer CF<sub>3</sub>I, with increasing exposure.

The interaction of low-energy electrons ( $E < 60$  eV) with CF<sub>3</sub>I multilayers shows very interesting chemistry. Electron-induced dissociation of the parent molecule occurs with a cross-section of approximately  $1 \times 10^{-16}$  cm<sup>2</sup>. Atomic fluorine is the major product detected during irradiation. TDS of electron-irradiated multilayers shows CF<sub>2</sub>I, CFI, and CF<sub>3</sub>, as well as carbon-carbon bond formation. Multiple-carbon species (as high as C<sub>4</sub>F<sub>n</sub>) desorb in a peak centered at 400 K. This process may be analogous to the electron-induced cross-linking of polytetrafluoroethylene.

**SS-WeP24 Thermally Stimulated Desorption of Neutral CF<sub>3</sub> from CF<sub>3</sub>I on Ag(111), K. H. Junker, Z.-J. Sun, T. B. Scoggins, and J. M. White**, Department of Chemistry and Biochemistry, University of Texas at Austin, Austin, TX 78712.

The low temperature thermal chemistry of CF<sub>3</sub>I on Ag(111) presents an example of competing catalytic reaction pathways: molecular desorption versus desorption of radical CF<sub>3</sub>. Temperature programmed desorption and angle resolved temperature programmed desorption, complemented with Auger electron spectroscopy and low energy electron diffraction, were used to discern the mechanism of the CF<sub>3</sub> radical desorption channel. Isothermal scans, desorption yields, and angular distributions at several coverages are presented. Initially, CF<sub>3</sub>I dissociatively adsorbs to the metal, breaking the C-I bond. The CF<sub>3</sub> thermally desorbs as a radical at high temperatures (~350 K) and saturates at a coverage of ~0.5 ML. As the coverage increases, CF<sub>3</sub>I adsorbs molecularly with the iodine toward the surface. Over a narrow range of coverages (~0.6-0.9 ML), a low temperature (120-160 K) radical desorption channel appears. Results indicate that low temperature CF<sub>3</sub> thermal desorption occurs via direct dissociation of molecular CF<sub>3</sub>I, yielding radical CF<sub>3</sub> and adsorbed iodine.

**SS-WeP25 Cyclopropyl on Cu(111): Area Selective Preparation and Vibrational Analysis Using a Dispersion-Compensation HREELS Spectrometer, R. Martel, A. P. Rochefort and P. H. McBreen**, Département de chimie, Université Laval, Québec, G1K-7P4, Canada.

The preparation of a chemisorbed cyclopropyl species localized on a small area of the Cu(111) surface at 90K and the subsequent vibrational analysis has been carried out using a high throughput Dispersion-Compensation (DC) HREELS spectrometer. We describe the application of this novel approach to excite physisorbed alkanes on a small area of the surface using low energy electron impact produced by the DC-HREELS monochromator. The activation and the vibrational analysis were achieved in two different operating modes of the spectrometer and hence it is not a simple autoscopic experiment. Energy dependent excitations of physisorbed cyclopropane showed a resonance centered at around 10 eV and yielded the cyclopropyl on Cu(111) with a cross section of  $\approx 1 \times 10^{-17}$  cm<sup>2</sup>. A careful energy and angular dependent vibrational analysis of the physisorbed cyclopropane at 90K did not indicate a vibrational enhancement due to the resonance state at 10 eV. The chemistry of the cyclopropyl species on Cu(111) has also been studied using vibrational measurements. A CH bond activation by the metal at around 250K has been observed just before a desorption at around 320K.

**SS-WeP26 Electron Induced Dissociation of Methanol Multilayers on Mo(110), T. D. Harris, D. H. Lee, M. Q. Blumberg, C. R. Arumainayagam**, Department of Chemistry, Wellesley College, Wellesley, MA 02181.

Studying the interaction of electrons with surfaces and adsorbates will offer better understanding of electron beam lithography, photochemistry on surfaces, and electron damage to adsorbates. Temperature programmed reaction spectroscopy (TPRS) has been used successfully to probe the molecular fragmentation of methanol multilayers adsorbed on a Mo(110) single crystal caused by low energy electrons (~55 eV) under ultrahigh vacuum (UHV) conditions. Electron induced dissociation (EID) of methanol in the multilayers followed by heating of the Mo(110) single crystal results in the formation of CH<sub>2</sub> species on the surface. These CH<sub>2</sub> (a) species recombine at ~350 K to yield ethene which desorbs immediately upon formation. No evidence was found for the desorption of ethane, formaldehyde or dimethyl ether. Isotopically labeled experiments reveal that the carbon atoms of the ethene originate exclusively in the methanol multilayers upon electron irradiation. The cross section for EID of methanol in the multilayers is  $4 \times 10^{-15}$  cm<sup>2</sup> at an electron energy of ~55 eV. The above value for the cross section is higher than typical values



measured previously for EID of monolayer adsorbates. The higher cross section in the multilayers is attributed to the diminished role of the surface in quenching electronic excitations occurring in the multilayers. This novel phenomenon offers the possibility of synthesizing catalytically interesting surface intermediates in significant quantities.

**SS-WeP27 Kinetics of Propene Desorption from Pd(111), N. A. Thornburg, I. M. Abdelrehim, C. M. Gerth, E. A. Picciotto, D. P. Land,** Department of Chemistry, UC Davis, Davis, CA 95616.

A new surface science instrument which incorporates several techniques, including Fourier transform mass spectrometry (FTMS), thermal desorption spectroscopy (TDS), laser-induced thermal desorption (LITD), low energy electron diffraction and Auger electron spectroscopy has been built at UC Davis to study surface processes. In particular, the interaction of propene with Pd(111) has been investigated to model palladium catalysis. Thermal desorption spectroscopy was used to determine exposure versus coverage dependence for propene adsorbed to Pd(111). TDS showed that propene did not react or decompose at a mono-layer coverage; propene desorbed intact from the Pd(111) surface. A near monolayer coverage (0.26 L) of propene was chosen for the initial kinetics studies.

LITD/FTMS was used to ascertain kinetic parameters, such as activation energies and pre-exponential factors, for desorption. Briefly, LITD/FTMS operates as follows: a Nd:YAG laser pulse desorbs neutral molecules from the sample surface; the neutrals effuse into the mass spectrometer cell where they are ionized by electron ionization and are detected by FTMS. Each laser shot yielded a complete mass spectrum. Ion intensities for propene and fragments were plotted as a function of time from a sequence of spectra taken at a set temperature. Data was acquired at temperatures between 260 K and 350 K—propene's desorption temperature range. Rate constants were extracted from the data and an Arrhenius plot yielded kinetic parameters ( $E_s$  and  $A$ ):  $E_s = 75 \pm 5$  kJ/mol and  $A = 1 \times 10^{10 \pm 0.9}$ /s. The dependence of the kinetic parameters on propene coverage will be presented.

**SS-WeP28 Adsorption and Film Growth of BTA on the Clean and Oxygen Adsorbed Cu(110) Surfaces, K. Cho\*, J. Kishimoto, T. Hashizume, H. W. Pickering\* and T. Sakurai,** Institute for Materials Research (IMR), Tohoku University, Sendai 980-77, Japan, \*Department of Materials Science and Engineering, The Pennsylvania State University, University Park, PA 16802, USA.

The benzotriazole (BTA) is widely used as a corrosion inhibitor of the Cu surface. We have performed the detailed experiment of adsorption, film growth and polymerization of the BTA on the clean,  $2 \times 1$ -O and  $c(6 \times 2)$ -O surfaces of Cu(110) in situ of the UHV FI-STM (field-ion scanning tunneling microscope).

The BTA molecules adsorbed on the clean Cu(110) surface are mobile at the initial stage adsorption, segregate to the steps, and form the  $c(4 \times 2)$  phase. Another type of the  $c(4 \times 2)$  phase growth at brightly imaged double line structures of BTA molecules are also observed, which may be related to the polymerization of BTA at the surface Cu defects. After completion of the first layer of the  $c(4 \times 2)$  phase, double string shaped second layer forms.

On the oxygen adsorbed Cu(110) surfaces, BTA molecules bond to the surface strongly from the initial stage, resulting in random adsorption and clustering. By the further deposition of BTA, the surface is covered by the amorphous-like three dimensional islands. The electronic structures of BTA studied by photoemission spectroscopy will be discussed.

\*Present address: Korea Institute of Science & Technology, P.O. Box 131, Cheong Ryang, Seoul 130-650, Korea.

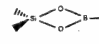
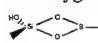
**SS-WeP29 Thermal Stability of Silver in Ion Exchanged Soda Lime Glasses, Paul W. Wang, and Tao Fan,** Department of Physics and Materials Research Institute, The University of Texas at El Paso, El Paso, Texas 79968.

The refractive index of sodium silicate glass can be easily modified by ion exchange technique. Silver is commonly used to replace sodium in order to fabricate the planar waveguide. However, the thermal stability of silver in glass is a major concern of the performance of the device. The X-ray Photoelectron Spectroscopy was used in attempt to study the thermal stability of silver in sodium calcium silicate glass during heat treatment in ultra-high vacuum. Surface diffusion and segregation of silver were observed. The three-step thermal diffusion of silver, slower at temperature below 100°C, faster between 100 to 300°C, and slower again at temperature above 300°C, was seen. The lower binding energy of silver and higher binding energy of oxygen after sample annealing show that the chemical structure of the sample

surface has been changed. Silvers form metallic clusters and oxygens originally bonded to silvers reconnect to silicon atoms. The surface relaxation of the stress introduced by the exchange process is the possible reason to explain the surface diffusion and segregation of silver under heating. The estimated activation energy of the silver surface diffusion is 0.23 eV.

**SS-WeP30 First IR Spectroscopic Evidence of Strained Cyclic Reaction Sites on the Borosilicate Glass (BSG) Surface, Laura L. Tedder<sup>(a)</sup> and John E. Crowell,** Dept. of Chemistry, UC, San Diego, La Jolla, CA 92093-0314, Kevin J. Uram, CVD Division, Lam Research Corp., 49026 Milmont Drive, Fremont, CA 94538-7301.

Understanding potential reaction sites present on dielectric surfaces is an important consideration for the control of further deposition or passivation. Transmission Fourier transform infrared (FTIR) vibrational spectroscopy was used to identify previously undetected reaction sites on the borosilicate glass (BSG) surface by monitoring the dissociative chemisorption of ethanol on BSG pre-treated at 1000K. Low temperature (450K) low pressure (0.5–10 torr) ethanol exposure results in the consumption of Si(OH) and B(OH) and the production of (mono)ethoxide groups bound to both Si and B sites. Highly strained, highly reactive surface sites, analogous to the edge-sharing cyclic disiloxane [(SiO)<sub>2</sub>] and [(SiO)<sub>2</sub>(OH)] species, were observed. The reaction

of C<sub>2</sub>H<sub>5</sub>OH with  results in a silanol hydrogen-bonded with the oxygen atom of the neighboring ethyl borate, and reaction with  produces geminal silanols (Si(OH)<sub>2</sub>) and ethyl borate. These

results are distinct from ethanol chemisorption on SiO<sub>2</sub>. Neither partial nor saturation ethanol exposures on SiO<sub>2</sub> pre-treated at 1000K result in the production of H-bonded or Si(OH)<sub>2</sub> groups. However, the unique geometry of the B-incorporated surface sites gives rise to the observation of H-bonded and Si(OH)<sub>2</sub> groups, providing the first spectroscopic evidence of important reaction sites on the BSG surface.

<sup>(a)</sup>Present Address: NSF Engineering Research Center for Advanced Electronic Materials Processing, NCSU, Box 7920, Raleigh, NC 27695.

## NANOMETER-SCALE SCIENCE AND TECHNOLOGY

Room BR4 – Session NS-WeP

### Nanometer-Scale Science and Technology

**Moderator:** R. C. Colton, Naval Research Laboratory.

**NS-WeP1 The Nanometer-Scale Structure of Isocyanide Functionalized Polyaniline Thin Films, T. L. Porter, A. G. Sykes, Y. Shi, G. Caple,** Northern Arizona University, Flagstaff, AZ 86011.

The functionalization of conductive polymers allows one to tailor the chemical and electronic properties of these synthetic metals for a wide range of needs. Isocyanide functionalized polyaniline may show promise as a material that can bind to metal ions, with many possible uses in a variety of important catalytic reactions. The electronic and chemical properties of films of isocyanide functionalized polyaniline are determined in large part by the nanometer-scale film structures. Other polyaniline films have displayed a rich nanometer-scale domain structure which inhibits the overall macroscopic conductivity of these materials. We have used the techniques of contact and non-contact scanning probe microscopy (SPM) to study the surface nanometer-scale structure of new poly-isocyananiline thin films. We have also investigated the structural changes that occur within these films upon exposure to Ir<sup>+</sup> cations in solution. We will discuss these nanostructures and their changes as they apply to conduction, catalysis and sensing applications for this material.

**NS-WeP2 Structural Characteristics of a Uniquely Nanostructured Organic Thin Film, M. K. Debe and A. R. Drube,** Sci. Res. Lab., 3M Co., St. Paul, MN 55144.

The red pigment N,N-Di(3,5-xylyl)perylene-3,4:9,10 bis(dicarboximide) is easily vacuum deposited and when subsequently vacuum annealed, a 1500 Å film transforms to an extremely dense (~50/μm<sup>2</sup>, random array of crystalline whiskers, (~50 nm × 2 μm)

uniformly oriented with their long axes normal to the substrate. We have previously reported on growth kinetics of the whiskers by surface diffusion to screw dislocations. Here we present a structural characterization of the whiskers and a minority platelet phase, using TEM and selected area electron diffraction. The whiskers' dimensions, size distributions, specific surface area and lattice structure are determined. Surprisingly, the lattice is determined to be bcc with a 14.5 (5) Å lattice constant. The growth tips are in the  $[-211]$  direction, bounded by  $(-111)$  and  $(01-1)$  side planes. The latter side plane surfaces are decorated with steps lying parallel to the long axis, and spaced  $\sim 44$  Å apart. The pigment whiskers can be readily sputter or vapor coated over large areas to provide conformally coated nanostructure sized features with numerous novel chemical and physical properties.

**NS-WeP3 Nucleation and Growth Kinetics of Monolayer Organic Films Studied with Graphite Etch Pits and STM, Victor J. Cee, David L. Patrick, and Thomas P. Beebe, Jr.,** Department of Chemistry, The University of Utah, Salt Lake City, UT 84112.

Etch pits on the (0001) surface of highly oriented pyrolytic graphite (HOPG) were used to study the nucleation kinetics of self-assembled monolayer organic films. High temperature oxidation of HOPG creates circular, monolayer-deep pits in the basal layer. These etch pits function as small "nanosamples" which are semi-independent from the surrounding terrace. Nucleation rates for self-assembly can be calculated for thin films of molecules on graphite by measuring the changing distribution of pits containing ordered molecules vs. those containing disordered molecules with time. By varying the pit size, the relative influence of pit edges and pit area on nucleation and growth can be determined. Self-assembled films of the liquid crystal 4'-octyl-4-cyanobiphenyl nucleate and grow from open terrace sites rather than edge sites, in contrast to the growth modes exhibited by most adsorbate-surface systems. The temperature dependence of nucleation rates can also be measured using etch pits, yielding values for nucleation activation energies.

**NS-WeP4 Scanning Force Microscopy of Quasi-single Crystalline Polyethylene and Nylon 6 Produced by Channel Dye Compression, C. Wang, R.-E. Riemann, M. Drechsler, H.-J. Cantow,** Freiburg Materials Research Center F·M·F, Albert-Ludwigs University, Stefan-Meier-Str.21, 79104 Freiburg, Germany.

Oriented semicrystalline polymers form a class of advanced materials with high tensile strength in the direction of orientation. Such materials are available by different processes, which are accompanied by morphological changes. Thus, the study of relationships between structure, morphology and properties of those polymers is of significant interest.

In our studies, PE and Nylon 6 were oriented in a channel die from initially spherulitic structure into a quasi-single crystalline perfection. SFM in the lateral mode was employed to examine the morphology of the oriented polymers at three perpendicular surfaces, compression, constraint and flow direction. The images show that nano-fibrils are the main structural elements. The visualized long periods of alternating lamellar crystals and amorphous layers are completely identical with those derived by SAXS. Tie molecules can be distinguished between the fibrils. Molecular resolution images of PE show interchain distances of 4.6 Å and 7.3 Å, which agrees fairly well with the  $d_{010}$  and  $d_{100}$  interchain distances in orthorhombic PE. With 8.7 Å the interchain distance by STM approach the crystal parameter  $a = 9.42$  Å of  $\alpha$ -monoclinic Nylon 6.

It is evident that, at the first time, SFM permits a direct visualization of nano-scale morphological elements in oriented polymer structures, PE and Nylon 6, which are inaccessible by electron microscopic methods. This leads to a deeper understanding of plastic deformation mechanisms.

**NS-WeP5 Nanoclusters of Polymethylene at Au(111) Surfaces, K. Seshadri, S. Atre, Y. T. Tao\* and D. L. Allara,** Departments of Chemistry and Materials Science, Pennsylvania State University, University Park, PA 16802; and Academia Sinica, Taipei, Taiwan, ROC. Nanometer scale clusters of polymethylene have been formed on evaporated gold surfaces of high (111) texture by the decomposition of diazomethane. Atomic force microscopy shows that the clusters form in grain boundary regions. Characteristic crystal field splitting of vibrational modes as seen by infrared spectroscopy shows the polymethylene to be crystalline. Further interpretation of the infrared spectra shows that the polymer chains run parallel to the gold surface plane. Thermal annealing of the clusters improves the crystallinity and the melting point of the material appears similar to that of the bulk

form. The polymethylene is highly hydrophobic and can serve to protect the grain boundary regions while chemical manipulation of the remaining gold surface takes place.

**NS-WeP6 Amorphous and Ordered Layers of Oligothiophenes: A Combined AFM-, UPS-, HREELS-, and Conductivity Study, Oliver Böhme, Dietmar Oeter, Christiane Ziegler, and Wolfgang Göpel,** Institute of Physical Chemistry, University of Tübingen, Morgenstelle 8, D-72076 Tübingen, FRG.

Amorphous layers of oligothiophenes with chain lengths between 4 and 8 monomeric units ( $\alpha 4T$ - $\alpha 8T$ ) were deposited and characterized under UHV conditions. With increasing chain length the development of the  $\pi$ -band was studied by means of high resolution electron energy loss spectroscopy (HREELS). This makes it possible to determine the ideal band-gap (2.1 eV) of an infinitely long and defect-free polythiophene. Because of the resulting low conductivities, oligothiophenes (and polythiophene) have to be doped for future applications as semiconducting molecular material. A new method of cosublimation of the dopant (here:  $FeCl_3$ ) was developed in this context, which allows for an ultrapure UHV-preparation of doped thin films. The success of the p-type doping process of  $\alpha 5T$ ,  $\alpha 6T$ , and  $\alpha 7T$  was checked by UV-photoemission spectroscopy (UPS) and HREELS. The DC-conductivity of  $\alpha 6T$  at room temperature could be increased upon doping from less than  $10^{-10}$  S/cm to  $10^{-1}$  S/cm (four-point measurement).

For  $\alpha 5T$  two coherent and intact monolayers could be prepared under UHV-conditions on  $SiO_2$  and  $SiO$  substrates. In these layers the molecules are oriented with their long axis perpendicular to the substrate surface.

**NS-WeP7 Substrate Effects on Two-Dimensional Ordering of Self-Assembled Layers on TMDs by STM, David L. Sampson, and Bruce A. Parkinson,** Department of Chemistry, Colorado State University, Fort Collins, CO 80523.

A large body of research has centered on the imaging of self-ordered films by scanning tunneling microscopy. The majority of this work has been done with graphite as a substrate. We have studied the ordering of various liquid crystals, alkanes and hydrogen bonded systems on a series of transition metal dichalcogenide (TMD) compounds. TMDs offer the cleavability of graphite but with lattice constants varying from 3.16 Å for  $MoS_2$  to 3.80 Å for  $SnSe_2$ . As the lattice changes, the interfacial order must adjust to maintain commensuration with the substrate while maximizing surface coverage. We have observed a wide variety of structures including several structures never before reported.

**NS-WeP8 Scanning Force Microscopy of Stearic Acid LB Film Deposited on Mica, Jing Li, Wang Yan Shiquan Xi Erkang Wang\*,** The Laboratory of Electroanalytical Chemistry, Changchun Institute of Applied Chemistry, Chinese Academy of Sciences, Changchun, 130022, CHINA.

In this paper, the surface morphology of monolayer stearic acid LB film and their intrinsic defect structures as well as the modifications of these films induced by the image process were investigated using SFM(TMX 2000 mode SPM, Santa Clara, CA, USA). Especially the interaction between the tip and the stearic acid molecules was discussed in detail. Nanowriting on the LB film can be performed through controlling SFM force sensor. But the interaction between the tip and the surface molecules is so small that it is impossible to write some letters on the fresh mica and aging LB film/mica. Some letters can be only written on the fresh LB film/mica. If the LB film has stored for two and three months, many pinholes occurred on the LB film surface due to aging. When the nanowriting was performed, where did those molecules go? We first proposed a theoretical model of LB film to explain it was dependent on the experimental results. High resolution SFM images showed that stearic acid molecules freshly deposited on the mica was basically perpendicular to the substrate surface to form order stains, which width corresponds to the molecular size in 0.4 nm. When a relative stronger force exerted on the molecules to scan along TV letters, the orientation of these molecules were really changed. After that, you could see the TV traces due to the different height of molecules when you enlarged the original range to scan. This is very significant for fabrication of biosensor and micro machining of single molecules.

**NS-WeP9 Atomic Force Microscopy Investigation of the Structure and Orientation Ordering in  $C_{70}$  Single Crystal, L. Jiang, L. A. Nagahara, J. Li<sup>1</sup>, N. Kino<sup>1</sup>, T. Iyoda, K. Hashimoto, K. Kitazawa<sup>1</sup>, and A. Fujishima,** Department of Synthetic Chemistry and <sup>1</sup>Department

of Industrial Chemistry, Faculty of Engineering, University of Tokyo, Hongo, Bunkyo-ku, Tokyo 113, Japan.

C<sub>70</sub> single crystals which are free from solvent contamination were grown via vapor phase transport. Large C<sub>70</sub> crystals, typically 1.5 × 1 × 1 mm<sup>3</sup> in size, can be grown with this technique. The (0001) face of the crystal was imaged using atomic force microscopy (AFM) under ambient conditions. For a freshly made crystal, low resolution images revealed well-ordered faceted regions with multiply terraces extending for several hundred square nanometers. At higher resolution, individual C<sub>70</sub> molecules packed in a hcp structure could be resolved with an average diameter of 11 Å. After the crystal was kept for about one month at room condition, the molecules rearranged into a mixed phase of both hcp and fcc packing. Molecular images of the phase transformed surface was directly observed with the AFM.

**NS-WeP10 Force Microscopic Studies of Langmuir-Blodgett Film of Complex TTF<sub>3</sub>C<sub>60</sub>Br<sub>2</sub>, P.-C. Zhang, C. Bai, D. Zhu, M. Han, Y. Xu, Y. Liu, Institute of Chemistry, Chinese Academy of Sciences, Beijing 100080, CHINA.**

By reaction of tetrathiafulvalene(TTF) with C<sub>60</sub>Br<sub>2</sub> a donor-acceptor complex of TTF<sub>3</sub>C<sub>60</sub>Br<sub>2</sub> was synthesized. The preparation of LB film containing the complex was performed in a computer-controlled KSV instrument at room temperature. The multi-layer LB films were transferred to a slide substrate at a constant pressure with a suitable dipping speed. The topographic and the frictional properties of the LB films were studied with atomic force microscope (AFM) and lateral force microscope (LFM) in the contact mode in air at ambient temperature. Furthermore, the LB films were imaged with the AFM in the tapping mode and magnetic force microscope (MFM) in the lift mode. The MFM images of this TTF<sub>3</sub>C<sub>60</sub>Br<sub>2</sub> LB films show characteristic magnetic domains in many regions. This magnetic properties are consistent to the results of ferromagnetic measurements of the bulk. This is the first report on the magnetic behavior on the C<sub>60</sub> complex LB film. Structural and magnetic features of the LB films are discussed. **INVITED**

**NS-WeP11 Structure and Electrical Property of C<sub>60</sub>, Ag Ultrafine Particle-Polymer Thin Films, H. J. Gao, Z. Q. Xue, and Q. D. Wu, Dept. of Radio Electronics, Peking University, Beijing 100871, P.R. China, S. Pang, Beijing Laboratory of Vacuum Physics, Academia Sinica, Beijing 100080, P.R. China.**

The electrical conductance of ICB fabricated C<sub>60</sub>, Ag-NM thin films is presented, therein the NM is a newly synthesized conducting polymer which shows the very strong third non-linear optic properties. The thin films are characterized by transmission electron microscopy, STM/AFM and electronic spectroscopy. The TEM results indicate that the thin films contain ultrafine Ag and C<sub>60</sub> particles which may play an important role in the conductance of the films. The thin films possess a relatively uniform surface structure and the periodic arrangement of the molecules at the surface of the films is also reported. Moreover the electronic spectroscopic results evidenced the formation of the charge transfer in the films. The thickness of the film is of ~100 nm. The possible mechanism of the electrical bistability of the films is discussed in the paper.

**NS-WeP12 The AFM as a Tool for Metal Surface Modification, H. Göbel, P. v. Blanckenhagen and W. Schommers, Kernforschungszentrum Karlsruhe, Institut für Materialforschung I, Postfach 3640, 76021 Karlsruhe, Germany.**

The AFM has been widely used as a tool for surface imaging and more recently also for surface machining [1]. We have applied an AFM for structurization of polycrystalline metal surfaces (Au, Cu). Programmed periodic and none periodic structures with a typical depth of 10–30 nm were produced using a cantilever with a sufficient high spring constant. By analyzing surface profiles as a function of time surface diffusion constants have been determined. The applicability of the AFM for nano-hardness measurements will be discussed.

[1] T. A. Jung et al. Ultramicroscopy 42–44, 1446 (1992)

**NS-WeP13 Nanometer Scale Modifications of Gold Surfaces by STM, A. Ohi, W. Mizutani\*, H. Tokumoto\*, JRCAT-ATP, \*JRCAT-NAIR, Higashi 1-1-4, Tsukuba 305, JAPAN.**

It has been shown that one can modify surfaces in nanometer scale by using local probe methods like scanning tunneling microscopy (STM) and atomic force microscopy (AFM). Depositing gold from gold tips by applying voltage pulses was demonstrated and the mechanism of field evaporation was proposed by Mamin et al. [1]. Recently Pascual et al. [2] showed the neck formation during the process. We have

investigated the field-induced surface modification under various conditions in UHV.

By applying negative pulses to the tip, a hole or a mound was produced on the sample surface. With a tunneling resistance of about 20GΩ where the separation between the tip and the surface is sufficiently large, a hole of typical size <15nm and depth <2.5nm was produced without the tip contact, indicating that the positive gold ions are transferred from the surface to the tip. On the other hand, as the resistance was decreased down to about 0.2GΩ, the mound was created. According to the observed current during applying pulses, it seems that the tip contacted to the modified surface when the mounds appeared. The threshold voltage for the modification indicates the critical field of about 5V/nm, comparable to 4V/nm by Mamin et al. [1]. In the case of positive pulses, sizes of created mounds varied widely from several hundreds nm to tens nm.

We have concluded that the mechanism of gold surface modification is due to the field evaporation of positive Au ions and the formation of mound in the case of negative pulses is a result of necking due to the tip contact.

[1] H. J. Mamin et al., Phys. Rev. Lett. **65**, 2418 (1990).

[2] J. I. Pascual et al., Phys. Rev. Lett. **71**, 1582 (1993).

**NS-WeP14 Nano-scale Layer Removal of Metal Surfaces by SPM Scratching, T. Sumomogi<sup>1</sup>, T. Endo<sup>1</sup>, K. Kuwahara<sup>1</sup> and R. Kaneko<sup>2</sup>**  
<sup>1</sup>Hiroshima-Denki Institute of Technology, Nakano 6-20-1, Aki-ku, Hiroshima 739-03, Japan, <sup>2</sup>NTT Interdisciplinary Research Laboratories, Midori-cho 3-9-11, Musashino-shi, Tokyo 180, Japan.

This paper describes micromachining of metal surfaces in air by a scanning probe microscope (SPM) which has a very sharp diamond tip mounted on the end of a cantilever beam. The sample surface of metals, such as Ni, Cu, Ti and W, was prepared by mechanical polishing from commercially available pure metal bulks. The sample surface was scanning-scratched by a diamond tip with a scan width of 2–3μm and a loading force of 500–1000nN, and topographies of the scratched area were observed by the same SPM with a loading force of less than 100nN.

In the case of Ni, flat square hollows of nanometer-scale depth were obtained. The scratched depth was increased with increasing loading force and repetition numbers of scratching. The effects of x direction scan rate, y direction feed, and scan width on the scratched depth were also revealed. Scratched surface of other materials was discussed comparing with the case of Ni.

Results obtained indicate that the nano-scale thickness material removal can be controlled and that the method presented here will be applied for micromachining of various materials.

**NS-WeP15 Nanofabrication of Gold Surface with Scanning Tunneling Microscope by Combination of Mechanical and Electrical Method, Yoshihisa Ishikawa, Norihiro Umeda, and Atsuo Takayanagi, Faculty of Technology, Tokyo University of Agriculture and Technology, Tokyo, 184 JAPAN.**

Scanning Tunneling Microscope (STM) is known as an instrument for producing an image of surface structure with atomic scale. Recently, it has proven to be a powerful tool for nanoscale fabrication technique. This paper describes a mechanical and electrical fabrication technique by using the STM in air environment. In mechanical technique, an indentation to gold surface with the STM tip is performed. It is shown that the nano-indentation was caused at some threshold value of indent displacement of the tip. In electrical technique, the electrical pulse voltage is applied to surface structure after indentation. In contrast of applying a pulse voltage only, the nanoscale pit with good shape is formed by the pulse voltage after indentation. Finally, the damage of tip apex by the fabrication is evaluated by the SEM micrograph.

**NS-WeP16 Ordered Nanostructures Prepared by Oxidizing Treatment of Graphite Surface: STM and Angle-Resolved XPS Study, M. O. Bashkin, S. D. Dubrovensky, A. V. Emelyanov, A. A. Malkov, A. A. Malygin, S. M. Portnov, A. V. Schukarev and A. V. Zimin, Zelenograd Research Institute of Physical Problems, Moscow 103460, Russia.**

To determine the possible mechanisms of ordering, nanostructures prepared by the graphite surface treatment with oxidizing agents (vanadium (V) and phosphorus (V) oxichlorides) were studied with STM and angle-resolved XPS. It was shown that two types of the ordered structures with the periods near 0.32 nm and 0.42 nm appeared after the treatment with vanadium oxichloride depending on the synthesis conditions. Their formation is explained in terms of direct oxidation

of the substrate or the reagent interaction with the oxygen-contained surface species. Mixing of vanadium oxichloride with oxygen stimulated an increase of vanadium concentration at the surface and resulted in appearance of the graphitic-like layer over the vanadium-contained layer. The latter fact can be attributed to intercalation process. The graphite surface treatment with phosphorus oxichloride did not cause any ordering. However, after combined treatment with the both oxichlorides, the nanostructures were formed which could change easily the surface relief after the pulse increase of the tunnel voltage. Crystallochemical models of the nanostructures observed were proposed. Possibilities of application of the ordered nanostructures on graphite are discussed.

**NS-WeP17 Nanostructure of Cleaved Surface of Bi Crystal, A. M. Troianovskii and V. S. Edelman\***, Institute for High Pressure Physics, \*Institute for Physical Problems, Academy of Science of Russia, Moscow.

We investigated by STM the cleaved surface of a Bi-crystal. The crystal was placed in a sample holder of a STM and was cleaved 'in situ' at a working pressure low than  $10^{-9}$  torr. The sample holder with a sample can be heated up to melting point of Bi. On the STM images of Bi surface with atomic resolution there were clearly seen atomically smooth terraces with dimensions of a few hundred nm and 'islands' with dimensions  $\sim 1 + 10$  nm and atomic height  $\approx 3.9$  Å. We found that boundaries of such 'nanoislands' which coincides with the directions of the atomic rows are stable. But other boundaries can move randomly on  $2 + 3$  interatomic distance around equilibrium position. The amplitude of these movements increases with increasing of a temperature and can reach several nm at  $\approx 520 + 530$  K. Moreover we observed the drifting of 'nanoislands' from one place of the terrace to the other on a distance  $\approx 50$  Å without visible changing of their size. The velocity of drifting was  $\approx 0.04$  Å/s. Formation of the observed 'nanoislands' can not be connected with impurities, because the density of impurities was 3 orders smaller than density of 'nanoislands'. We can suppose that they are formed due to dynamically deformations while cleaving the sample. After annealing of the sample at  $\approx 530$  K they were formed on the sample wide atomically smooth terraces without any small details.

**NS-WeP18 Scanning Tunneling Microscopy of Transition-Metal Clusters on Nonmagnetic Surfaces, P. E. Quesenberry, T. A. Hann, and P. N. First**, Georgia Institute of Technology, Atlanta, GA 30332-0430.

A great deal of previous research has addressed the question of how to grow uniform thin films of magnetic materials. Whether for fundamental studies of low-dimensional magnetism or for technological applications, this goal is often quite difficult to achieve, since it involves details of both the energetics of the film/substrate couple and the growth kinetics. Thus the initial stages of transition-metal film growth often involve the formation of monolayer islands or 3-D clusters of the magnetic metal. This initial growth influences both the ultimate film morphology and the magnetic properties of the film. Recognizing that the clusters are often superparamagnetic, this presentation will describe a technique by which the STM might be used to determine magnetic properties of superparamagnetic clusters, up to the thin-film limit. The measurements rely upon spin-polarized tunneling from a ferromagnetic tip. Initial results will be presented from transition metal clusters grown by vapor deposition on Au(111).

Supported by ONR N00014-93-1-0475 and by NSF DMR-9223684.

**NS-WeP19 Lateral Anisotropic Anodization Property of Silicon, In-sik Yu\*\*\*, Ki-Yeul Park\*, Jun-Hwan Sim\*, Jang-Kyoo Shin\*, Jung-Hee Lee\*, Jong-Hyun Lee\***, \*Dept. of Electronics, Kyungpook National University, Taegu, Korea, \*\*Kyungdong Junior College, Taegu, Korea.

Porous silicon has recently become an important optoelectronic material. We have for the first time observed lateral directionality of anodization for Si during porous silicon formation. The starting material was (100)  $n/n^+/n$  silicon wafers doped with phosphorous. The dopant concentrations of top  $n$ -type silicon layer,  $n^+$  middle layer, and  $n$ -type substrate were  $10^{17}/\text{cm}^3$ ,  $10^{19}/\text{cm}^3$ , and  $10^{15}/\text{cm}^3$ , respectively. The thicknesses of the top  $n$ -type silicon layer and the  $n^+$  middle layer were  $4\mu\text{m}$  and  $20\mu\text{m}$ , respectively. After the top  $n$ -silicon window layer was etched in a 147  $\text{HNO}_3$ : 3 HF solution, anodization was carried out in a 20% HF solution. Only the  $n^+$  middle layer was anodized to become porous silicon. The porous silicon layer was removed in a 5% NaOH solution and the size of the resulting silicon

cavity was approximately  $150\mu\text{m} \times 150\mu\text{m}$ . Even though the shapes of top silicon windows were different, the shapes of reacted porous silicon area under the top silicon layer were all roughly square and the sizes were almost identical. The ratio of the horizontally anodized distance for [100] direction to that for [110] direction was about 1.2. This means that the porous silicon layer is formed anisotropically. This result is contrary to the conventional concept that porous silicon formation is isotropic. A model explaining this behavior will be presented in this paper.

**NS-WeP20 Doping and Photoeffects in Layered Semiconductors Studied with Scanning Tunneling Microscopy, D. R. Louder and B. A. Parkinson**, Department of Chemistry, Colorado State University, Ft. Collins, CO 80523.

The scanning tunneling microscope (STM) has become a valuable tool in studying not only the topography of a sample, but also its electronic properties. Layered dichalcogenides, such as  $\text{WSe}_2$  and  $\text{MoS}_2$ , exhibit spots on their surfaces when viewed with the STM. These features can have the appearance of hills or depressions on the sample surface depending on the sample bias. It was concluded that the spots were electronic effects because the number of spots seen in a certain area relates to the bulk doping density of the sample, and they are not seen in atomic force microscope images of the same samples. Dopants on layers below the top layer can also be seen.

The STM has also been used to image layered materials using photo-induced tunneling current (PTC). This tunneling current is separated from the normal tunneling current by using a lock-in technique. PTC can be used to measure the effect of defects, such as steps, on charge carriers just as electron beam induced current (EBIC) is used in scanning electron microscopy. Islands of another semiconductor grown on  $\text{MoS}_2$ , such as  $\text{SnS}_2$ , can be distinguished by the absence of PTC due to  $\text{SnS}_2$ 's higher bandgap. This method surpasses EBIC in resolution, is nondestructive and can be done in atmosphere with no sample preparation.

**NS-WeP21 X-SFM, XPS, and SIMS Study of Cobalt Catalysts on Silica, K. A. Pischow, <sup>a</sup>E. O. Ristolainen, <sup>b</sup>M. K. Niemelä, and <sup>b</sup>K. O. Krause**, Laboratory of Processing and Heat Treatment of Materials, <sup>a</sup>Center for Chemical Analysis, <sup>b</sup>Laboratory of Industrial Chemistry, Helsinki University of Technology, FIN-02150 Espoo, FINLAND.

Cross sectional scanning force microscopy (X-SFM) and secondary ion mass spectrometry (SIMS) was used to find study Mg-Co/SiO<sub>2</sub> and Co-Mg/SiO<sub>2</sub> catalysts prepared from acetate and nitrate precursors on silica. It was shown that the SFM scanning altered markedly some surface structure of the catalyst prepared from nitride precursor. On the contrary, the scanning seemed to have no effect on the surface structure of the catalysts prepared from the acetate precursors. The reasons for this fact and the possible structural changes occurring on the catalyst surface activated by the SFM scan will be discussed and compared with the XRD and XPS measurements. In addition, the cross sectional sample preparation method used will be discussed in details.

INVITED

**NS-WeP22 Observation of Atomic Ordering in GaInP<sub>2</sub> by Scanning Probe Microscopy, Y. Leng, Y. J. Huang, and C. C. Williams**, Dept. of Physics, L. C. Su and G. B. Stringfellow, Dept. of Material Science, Univ. of Utah, Salt Lake City, Utah 84112 USA.

Under certain growth conditions, GaInP<sub>2</sub> spontaneously orders on the group III sublattice with gallium and indium atoms occupying alternating {111} planes. The atomic ordering of GaInP<sub>2</sub> has been established and studied by a variety of methods, including transmission electron diffraction (TED), cathodoluminescence (CL), and photoluminescence (PL). In this work, Kelvin Probe Force Microscopy (KPFM) and Scanning Capacitance Microscopy (SCM) have been employed to image several GaInP<sub>2</sub> samples previously characterized by the established techniques mentioned above. Images have been performed both on as grown GaInP<sub>2</sub> surfaces and cleaved cross sectional surfaces. KPFM and SCM images of epitaxially grown GaInP<sub>2</sub> layers on grooved substrates (multiple samples) have been directly correlated with TED and CL images to establish their sensitivity to ordering in GaInP<sub>2</sub>. The results of our study clearly show that KPFM and SCM are capable of distinguishing between ordered and disordered regions in GaInP<sub>2</sub>. Local electronic spectroscopies, such as capacitance vs. voltage, reveal that atomic ordering influence the measured surface potential, surface pinning, and band bending. The mechanism of image contrast by KPFM and SCM and the influence of ordering on electronic property of surface will be discussed.



**NS-WeP23 Structural Analysis of Domain Boundaries on Si(111)7 × 7 Surfaces by STM, Q. J. Gu, Z. L. Ma, N. Liu, X. Ge, W. B. Zhao, X. Chu, Z. Q. Xue, S. Pang,** Beijing Laboratory of Vacuum Physics, Academia Sinica, Beijing 100080, P.R. China.

We have observed several well-formed domain boundaries on Si(111)7 × 7 surfaces, which always appear regular structures, in many cases even show periodic structures. In order to describe and classify the domain boundaries, we introduce an adatom registry shift (ARS) vector  $S$  and boundary running direction index  $D$ . According to  $S$  vector, we classify 36 kinds of domain boundaries into 3 categories, based on  $D$  index, we have systematically investigated the domain boundaries on Si(111)7 × 7 surfaces. Combining with the DAS model, we propose a model to construct the configuration of probably existing domain boundaries on Si(111)7 × 7 surfaces. With this model, we analyse several well-formed domain boundaries on Si(111)7 × 7 surfaces in details, the structure model is well consistent with the experiment. Based on our knowledge about the domain boundaries, we also explain which structures are stable and which structures can't exist in manipulation.

**NS-WeP24 Atomically Resolved Image of Cleaved Surface of Compound Semiconductors Observed with an Ultrahigh Vacuum Atomic Force Microscope, M. Ohta, Y. Sugawara, M. Suzuki\*, S. Mishima\*\*, T. Okada\*\*, S. Morita,** Department of Physics, Faculty of Science, Hiroshima University, Higashi-Hiroshima, 724, Japan, \*NTT Interdisciplinary Research Laboratories, Atsugi, Kanagawa, 243-01, Japan, \*\*Research Department, Olympus Optical Co., Ltd., Hachioji, Tokyo, 192, Japan.

By using an atomic force microscope (AFM), there are many reports for achieving the atomic resolution for layered materials and ionic crystals. On the other hand, there are few reports on atomic resolution of a clean semiconductor surface. So observation for a clean semiconductor surface with atomic resolution by using a contact-mode AFM was considered to be difficult due to the adhesion between tip and sample. In order to investigate the imaging capability of an AFM on atomic resolution for a clean semiconductor surface, we observed the compound semiconductors surfaces by using an ultrahigh vacuum atomic force microscope (UHV-AFM) with a sample cleaving mechanism. As a result, for the first time, atomic resolution imaging of GaAs(110) and InP(110) surfaces was performed. On the GaAs(110) surface, the zigzag rows of atomic protrusions were observed. These zigzag rows might be interpreted as quasi-one-dimensional zigzag chains consisting of alternating Ga and As atoms. Furthermore, the rectangular lattice of the surface was atomically destroyed by the sequential scanning. This atomic destruction might be induced by the overload due to the force by probing tip. These results have demonstrated the feasibility of using the UHV-AFM to investigate clean semiconductor surfaces on an atomic scale.

**NS-WeP25 Studies of Ecalle Deposition of CDSE on the Low Index Planes of Gold, T. E. Lister, R. D. Herrick II, and J. L. Stickney,** Department of Chemistry, University of Georgia, Athens, Georgia 30602.

Electrochemical atomic layer epitaxy is a method designed to facilitate the growth of ordered compound semiconductor thin films. Growth is controlled on the atomic level by underpotential deposition (UPD). Films are formed by alternately depositing UPD layers of each element using separate solutions for each element. Studies are reported of the initial CdSe layer(s) on the low index planes of gold. Techniques such as cyclic voltammetry, coulometry, low energy electron diffraction (LEED), Auger electron spectroscopy and x-ray photoelectron spectroscopy (XPS) provide structure and composition. The information is needed to construct a growth cycle which will be used to form thicker deposits in an automated flow cell.

**NS-WeP26 Effects of Current Stimulated Adsorption in STM Investigation of Si Surface in Ambient Air, A. A. Bukharaev, E. A. Samarsky, V. M. Junduganov, N. V. Berdunov, P. G. Antonov,** Kazan Physical Technical Institute Russian Academy of Science, Sibirsky Tract 10/7, Kazan, 420029, Russian Federation.

Scanning tunneling microscopy (STM) and related techniques offer the rare opportunity of the Si surface investigation and modification for the tasks of nanotechnology in different environment including ambient air. It is of great interest to develop these methods to test and form adsorbed films which are in equilibrium with gases on high pressure. We used the current-distance dependencies and experimental evaluations of the tip-sample separation along with the traditional scanning tunneling spectroscopy methods to reveal and test the adsorbate films in STM contact on HF-treated Si surfaces in air. Our

experimental research and theoretical analysis of current-voltage characteristics and current-distance dependencies have shown that adsorbed films can be formed by the current of STM operated in ambient air. These current-induced adsorbed films can cover both W tip and Si surface under the tip causing the transitions of the conductivity process from direct tunneling to Schottky emission. It appears as extremely large gap distances and low potential barrier heights in STM experiments on HF-treated Si surfaces in air. To our mind hydrocarbons and water are most likely candidates to form these mobile (fluid-like) films.

## PLASMA SCIENCE

### Room BR4 - Session PS-WeP

#### Plasma Etching and Inertial Confinement Fusion

##### Targets

**Moderator:** J. L. Cecchi, University of New Mexico.

**PS-WeP1 Extraction of Oxygen from CO<sub>2</sub> Using Glow-Discharge and Permeation Techniques, D. Wu, R. A. Outlaw, R. L. Ash,** Old Dominion University, Norfolk, Virginia 23508.

A promising method to extract oxygen from CO<sub>2</sub>, which constitutes more than 95% of the Mars atmosphere, is by using glow-discharge dissociation of CO<sub>2</sub> combined with the permeation of the generated oxygen through a silver membrane. A quadrupole mass spectrometer on the downstream side of an ultra-high vacuum permeation system was used to measure the oxygen flux through a 0.34 mm thick silver separation membrane. On the upstream side of the membrane, with 400 V, 5 mA dc glow-discharge, it was found that as much as 70 percent of the CO<sub>2</sub> was dissociated to form CO and O (which recombined to form O<sub>2</sub>). The downstream oxygen flux as a function of upstream CO<sub>2</sub> pressure, discharge current, discharge probe to membrane distance, and membrane temperature was also studied. It was found that a small amount of atomic oxygen, generated by the glow-discharge, bypassed the dissociative adsorption step and produced much higher flux through the membrane than with molecular oxygen. An estimation of the atomic oxygen sticking coefficient is also presented and suggests that the value approaches 1 at a membrane temperature of 300 K. The total oxygen flux through the membrane with a 5 torr CO<sub>2</sub> glow-discharge and a membrane temperature of 450°C was found to be greater than 10<sup>14</sup> cm<sup>-2</sup>s<sup>-1</sup>. Since the oxygen permeation flux varies inversely with membrane thickness, a membrane of 1 μm is being developed which will increase the flux by two orders of magnitude. This method can be used to continuously and efficiently supply oxygen to astronauts in a future manned mission to Mars.

**PS-WeP2 Temperature Dependent Reaction Kinetics for the Si/XeF<sub>2</sub> System, M. J. M. Vugts, M. F. A. Eurlings, G. L. J. Verschuieren, L. J. F. Hermans and H. C. W. Beijerinck,** Eindhoven University of Technology, Department of Physics, P.O. Box 513, 5600 MB Eindhoven, The Netherlands.

In a UHV beam surface experiment (J. Vac. Sci. Techn. A, 12 1994 in press) we studied the interaction of XeF<sub>2</sub> molecules with the Si(100) surface in a quantitative manner. Although this system has been studied frequently in the past as a model for plasma etch interactions, most data are qualitative and a consistent model has not yet been developed. The question addressed in this study is the temperature dependence of the steady state reaction kinetics. The reaction of XeF<sub>2</sub> and the production of SiF<sub>x</sub> species were measured using XeF<sub>2</sub> fluxes from 0.1 to 5.0 ML/s and for sample temperatures ranging from 100 to 1000 K. At room temperature 20% of the XeF<sub>2</sub> reacts with the silicon; this increases to 50% at 900 K. At 300 K SiF<sub>4</sub> is the dominant etch product. For higher temperatures it is gradually replaced by SiF<sub>2</sub> up to 90% of the total production at 900 K. In the regime studied the reaction coefficient and product distribution are independent of XeF<sub>2</sub> flux, the reaction is limited by the XeF<sub>2</sub> flux. For temperatures below room temperature we also observe an increase in the XeF<sub>2</sub> reaction and corresponding SiF<sub>x</sub> production. This is due to an increasing XeF<sub>2</sub> precursor concentration. At 150 K this even leads to the formation of a XeF<sub>2</sub> overlayer which blocks the reaction. By TDS-analysis of this layer the adsorption energy of the precursor could be determined. Combining this with the high temperature data we were able to model the reaction kinetics of the Si/XeF<sub>2</sub> system as a function of temperature.



**PS-WeP3 Reactive Ion Etching-Induced Damages in GaAs/AlGaAs Quantum Well Structures and Recovery by Rapid Thermal Annealing and Hydrogen Passivation, Byung-Su Yoo, Seong-Ju Park, and Kyung-Ho Park,** Electronics and Telecommunications Research Institute, Yusong Post Office, P.O. Box 106, Taejeon, 305-600, Korea.

In this study, we have investigated the spatial distribution of RIE-induced damages using low temperature photoluminescence (PL) of a GaAs/AlGaAs quantum well structure. We have also studied the recovery of defects by rapid thermal annealing (RTA) and passivation of defects in a hydrogen plasma. A typical sample structure consisted of four quantum wells of widths 2, 4, 6, and 10 nm with barriers of 30 nm thickness. A mixture of He and  $\text{CCl}_2\text{F}_2$  gases were used in RIE experiments. The PL intensities from quantum wells in etched samples decreased uniformly across the depth of 150 nm without any line shift or broadening of PL spectrum. This indicates that the damages are created in quantum wells by penetration of energetic ions into substrate during the reactive ion etching process. The results obtained under the various etching conditions suggest also that the physical sputtering induces more damages in the quantum wells and reduces selective etching ratio of GaAs over AlGaAs than the chemical etching process. Furthermore, the RIE-etched quantum well structures were annealed by rapid thermal annealing or passivated in a hydrogen plasma to understand the nature of defects. For both cases, the PL intensities from quantum wells situated at the deep region from surface were drastically recovered. These results suggest that the origins of defects created by energetic ions in the deep region are quite different from those in the near surface region. Moreover, the results indicate also that the damages in deep region are closely related to the vacancies of sublattice, particularly when light He ions are involved in the etching process.

**PS-WeP4 Characterization of ECR Plasmas with a Quadrupole Mass Spectrometer and Cylindrical Mirror Energy Analyzer, S. Bederka\*, I. Bello, H. Ibrahim, and W. M. Lau,** Department of Materials Engineering, University of Western Ontario, London, Ontario, Canada N6A 5B9.

The composition and energy distributions of both ions and neutrals from electron cyclotron resonance (ECR) plasmas were studied by a quadrupole mass spectrometer and cylindrical mirror energy analyzer. These characteristics were found to be very sensitive to the plasma parameters including the power input, magnetic field strength, and gas pressure for plasmas such as the hydrogen, nitrogen, ammonia, water, and methane systems. It was also found that the energy spread of ion beams extracted from such ECR plasmas could be controlled to about 2 eV. We believe that this is the lowest energy spread ever shown for ECR ion beams. With such a low energy spread, the measurements of energy distributions as a function of the plasma parameters were found to be informative about the plasma reactions. The implications of these and the beam energy control on ECR plasma induced etching/deposition will be discussed.

\*Permanent address: Microelectronics Department, Slovak Technical University, Ilkovicova 3, 812 19 Bratislava, Slovakia.

**PS-WeP5 High Voltage Sheath Evolution in the Presence of Negative Ions,\* J. T. Scheuer, T. B. Mitchell, M. Tuszewski, J. A. Tobin, K. P. Kremeyer and A. Williams,** Los Alamos National Laboratory, Los Alamos, NM 87545.

An understanding of sheath evolution and ion current incident on the target in the presence of negative ions is important for the development of a tool for semiconductor thin film growth based on the plasma immersion ion implantation technique. This compact, inexpensive, high throughput implanter allows separate control of dose rate, ion energy and substrate temperature while mitigating charging effects. The time variation of sheath position around a high voltage (1–10 kV) pulse biased electrode in an oxygen plasma ( $\sim 10^{10} \text{ cm}^{-3}$ ) has been measured using Langmuir and capacitive probes. The presheath existing prior to the pulsed bias was measured using an emissive probe. Sheath evolution and collected current has been measured for both positive and negative pulse biases, while varying the fraction of negative ions present in the oxygen plasma as measured with an ion mass spectrometer.

\*Work supported by U.S. Department of Energy.

**PS-WeP6 Power Versus Time in Pulsed, Parallel Plate rf Discharges, Lawrence J. Overzet,** University of Texas at Dallas, Plasma Applications Laboratory, PO Box 830688, Richardson, TX 75083-0688.

While it is now easy to make measurements of the power delivered to a steady state discharge as a function of frequency; it is more difficult to measure the power delivered to the discharge as a function of both frequency and time during the transient turn on and turn off of the discharge. We have now measured the power transients to pulsed rf discharges in the Gaseous Electronics Conference Reference Reactor on a microsecond time scale. There are large swings in the power delivered to the cell as a function of time during the first 10 microseconds of the transient turn on and turn off. These power swings are in large part caused by the passive circuitry between the current-voltage probes and the electrode assembly of the cell and have been modeled using an equivalent network with reasonable accuracy. This circuitry can store rf energy and release it both to the plasma and to the rf generator at plasma turn off. The power delivered to a 500 mTorr argon discharge does not reach steady state until approximately 500 microseconds after the discharge turn on even though the initial power swings end within the first 10 microseconds. This second power variation appears to be related to a contraction of the electrode sheath as well as an electron density increase during this time. The method used in making time resolved rf power measurements will be presented along with results obtained from a 500 mTorr argon discharge.

**PS-WeP7 Electron Temperature Measurement in Magnetrons by Optical Emission Spectroscopy and Langmuir Probes, K. F. Lai, and W. Tsai,** Ginzton Research Center, Varian Associates, Palo Alto, CA 94304.

Langmuir probes (LP) have been widely used in characterizing the properties of sputtering magnetron plasmas. Due to probe interferences and coating problems, however, LP were limited to low power discharges and not suitable for high power commercial magnetrons. On the other hand, optical emission spectroscopy (OES) which was also used in the study of magnetrons was more suitable for the monitor and control of the discharge in manufacturing applications. The major drawback of OES is the difficulty in extracting plasma parameters from the measured light intensities. We have developed an analytic model to describe light emission in a magnetron discharge. In this model, the amount of emitted light can be related to the maximum electron excitation cross section and the excitation energy of the argon species. By measuring the light emissions of argon neutrals at selected wavelengths, the electron temperature in a magnetron plasma can be deduced. With this technique a real time electron temperature monitor for argon plasmas can be developed. The accuracy of this method has been verified using LP at low discharge power. The electron temperature was found to vary inversely with pressure and increased from 5 eV at 2 millitorr to as high as 15 eV at 0.1 millitorr in a commercial sputtering magnetron. The dependence of electron temperature with distance from cathode surface, and discharge power have also been determined using this diagnostics. The aspect of extending this technique to other species like argon ions and sputtered neutrals will be discussed.

**PS-WeP8 Ion and Neutral Ar Temperatures in MW ECR Plasmas by Doppler Broadened Emission Spectroscopy, David V. Tsu, R. T. Young, S. R. Ovshinsky,** Energy Conversion Devices, Troy, MI 48084, C. C. Klepper, L. A. Berry, ORNL, P.O. Box 2009, Oak Ridge, TN 37831.

Plasma excitation using microwave electron cyclotron resonance (MW ECR) has been used extensively not only in plasma ion assisted etching, but also in thin film chemical vapor deposition. The gas (both ion and neutral) temperatures ( $T_g$ ) are crucial parameters in determining etching and thin film qualities.

In this paper, we evaluate a widely used technique for obtaining the  $T_g$ 's; measuring the thermal Doppler broadening of emission lines. Here, we focus on Ar lines from MW ECR plasmas. In particular, we are interested in the most relevant factors in achieving the greatest accuracy and precision in the determination of  $T_g$ . We emphasize using the same technique for both ion and neutral species. We identify three important factors that contribute to obtaining reasonable temperatures: (1) knowing the correct instrument response or width ( $\Gamma_i$ ) for each ion and neutral line; (2) understanding all the factors that lead to variations in the measured widths, i.e., the noise; and (3) knowing how the magnetic field affects the spectra (Zeeman processes). Ion temperatures cannot be directly obtained from their measured widths ( $\Gamma_m$ ) unless  $\Gamma_i$  at the same spectral position is known. Also, because  $\Gamma_i$  is greater than the Doppler width ( $\Gamma_D$ ), knowing  $\Gamma_m$  accurately, i.e., reducing the noise  $\delta\Gamma_m$ , is critical. An analytical expression for  $\delta\Gamma_m$  is derived consisting of two sources, the signal counting and a constant instrument noise related to mechanical aspects of the spectrograph. These sources fully account for the size of  $\delta\Gamma_m$ . With proper signal averaging, we estimate that changes in  $T_g$  of  $\sim 100$  K are detectable.

**PS-WeP9 Ion Chemistry Effects on SiO<sub>2</sub> to Si Selectivity in a High Density Fluorocarbon Plasma**, K. H. R. Kirmse, A. E. Wendt, R. A. Breun, S. Y. Perez-Montero, J. A. Meyer, N. Hershkowitz, Engineering Research Center for Plasma-Aided Manufacturing, University of Wisconsin-Madison, Madison, WI 53706.

SiO<sub>2</sub> to Si selectivity is an important control parameter in etching process. The goal of this study was to determine how changes in the chemistry at the wafer influence the SiO<sub>2</sub> to Si selectivity in high density fluorocarbon plasmas. To do this, Si and SiO<sub>2</sub> etch rates in an ECR source were measured with an *in-situ* HeNe interferometer under a variety of etching conditions. The source gas chemistry for these experiments included CHF<sub>3</sub> and C<sub>2</sub>H<sub>2</sub>F<sub>4</sub>. The microwave power, RF bias, pressure, and chemical composition were varied to determine a parameter space producing significant changes in the SiO<sub>2</sub> to Si selectivity. These data were correlated with ion chemistry data taken over the same parameter space which was obtained using an in line, differentially pumped quadrupole mass spectrometer. The spectrometer orifice was mounted directly beneath a substrate holder with a sampling hole that admits some of the ions and neutrals incident at the substrate surface into the spectrometer. The effects of chemical species present at the wafer surface on selectivity control in high density plasmas will be discussed.

This work is supported by the National Science Foundation under Grant #ECD-8721545.

**PS-WeP10 Determining the Neutral Radical Composition of Plasma Environments: Pulsed, Supersonic, Plasma Sampling Mass Spectrometry**, Hongbin Zhu and Rik Blumenthal, Department of Chemistry, Auburn University, Auburn, AL 36849.

Over the past decade, the use of plasmas in materials processing has become almost commonplace. However, a chemical understanding of these plasma processes has lagged far behind their application in both thin film etching and deposition, as a result of the difficulty in obtaining direct experimental information from the energetic and hostile environment of the plasma. In this talk, a new mass spectrometric technique will be introduced in which neutral radical species are extracted from the plasma by a supersonically expanding pulse of noble gas atoms. By limiting the interactions of the "plasma-borne" radical species to collisions with the noble gas atoms of the cooling pulse, the radical species are removed from the plasma with virtually no likelihood of reactions with walls or other chemical species. Experimental results relating to the deposition of diamond films and growth of the III-V Nitrides will be presented.

**PS-WeP11 Fluid Simulations of Particle Contamination in Afterglow of Plasma Processes**, Mary P. Garrity and Thomas Peterson, Department of Chemical Engineering, Lisa Garrett and John F. O'Hanlon, Department of Electrical and Computer Engineering, University of Arizona, Tucson, AZ 85721.

Particles are problematic in plasma. Once generated, either by gas phase processes or by fragmentation from chamber surfaces, particles acquire a negative charge and are trapped at the plasma sheath interface. In the absence of the electric field at the sheath upon rf extinction, the trajectories of the particles depend on their mass and the local gas velocity and pressure.

Using FIDAP, a commercially available finite element code, we have simulated fluid flow patterns and particle trajectories in the afterglow of a single wafer, parallel plate reactor. Particle trajectories are calculated using a Lagrangian technique and the viscous drag on the particle has been modified to account for noncontinuum effects at low pressures. Two dimensional axi-symmetric simulations as a function of pressure, flow rate, initial particle location, and reactor configuration are presented.

**PS-WeP12 Simulations of Damage Profiles Due to Reactive Ion Etching and Ion-Assisted Etching**, R. J. Davis and P. Jha, Microelectronics Sciences Laboratory, Columbia Univ., 1001 Schapiro Research Center, 530 W. 120th Street, New York, NY 10027.

Dry etching of surfaces with low-energy ions is important to the fabrication of electronic and optoelectronic devices, yet these techniques can cause severe damage to semiconductors. There still is debate regarding the separate contributions of ion channeling and damage diffusion to the anomalously deep damage which is observed after dry etching. Recently, we have theoretically modeled steady-state damage profiles, and shown that such profiles are quite sensitive to etch rate and etch yield effects, regardless of the contributions of channeling and diffusion. The parameter  $D/\alpha\epsilon$ , where  $D$  is the damage diffusivity,

and  $\epsilon$  the etch rate is an important parameter in determining the relative contribution of diffusion and range (channeling) effects to the final damage profile. In this work, we simulate the evolution of dry etching damage profiles from inception to steady-state, and establish characteristic settling times for realistic dry etching situations. We also simulate profiles using Gaussian and more realistic damage distribution functions, and examine the validity of theoretical predictions and guidelines to more complex and realistic dry etching damage situations.

**PS-WeP13 Identification of Plasma Induced Failure Modes in the Development of a BiCMOS ASIC Process**, M. J. Dion, J. J. Hackenberg, D. F. Hemmenway, L. G. Pearce, J. W. Werner, Harris Semiconductor, Melbourne, FL 32902.

Development of a BiCMOS ASIC process encountered MOS device failure behaviors that were traced to a single processing plasma source. Despite the fact that the process employed relatively thick 500 Å MOS gate oxides and was made in a manufacturing line that also produces CMOS product with gates below 200 Å, significant plasma damage effects were identified. Four distinct failure signatures were observed: shorted NMOS gates, leaky NMOS gates with functioning channels, parasitic depletion mode conduction at the ends of the enhancement NMOS device channel, and PMOS threshold shift as observed in a differential amplifier input offset. Test devices based on work originating at SEMATECH and specifically designed to monitor plasma damage through various gate antenna configurations and device protection fuses were employed to identifying the cause of the failures as electrical damage induced during the backend of wafer processing. Although the methodology was successful, the experience points toward significant improvements that can be made and will be employed in future development and characterization efforts on a routine basis. Sequential characterization of device performance from first metal out quickly identified the PECVD tool used for final passivation deposition as the primary contributor to the plasma damage. Subsequent process flow changes did eliminate this source of plasma damage, and continuing efforts center on correcting the basic tool problem.

**PS-WeP14 Modeling of Wafer Charging and Damage in High Plasma Density Etching Tools<sup>1</sup>**, Michael Grapperhaus, and Mark J. Kushner, University of Illinois, Dept. Electrical and Computer Engineering, Urbana, IL 61801.

Wafer charging and nonuniform fluxes of ions to the wafer have been identified as damage mechanisms to thin oxide layers in conventional RIE and magnetically enhanced RIE etching systems. The propensity for ion impact damage in high plasma density tools [inductively coupled plasmas (ICP), electron cyclotron resonance (ECR)] is less than in RIE tools due to the lower substrate biases. However the higher plasma densities of ICP tools and the uniformity of their ion fluxes still leave open questions regarding damage caused by charging and oxide tunneling currents. We have developed a computer model of ICP reactors, oxide charging and current transport through simple MOS devices with the goal of assessing plasma induced damage. The integrated tunneling current through oxide layers during etching has been correlated with low breakdown voltages, and is our measure of plasma damage. The ICP reactor model is a 2-dimensional hybrid model which produces spatially resolved electron and ion fluxes. A second integrated microscopic model examines the charging of thin oxide layers while accounting for device conduction and tunneling currents in MOS structures. We will discuss the differences in oxide charging and oxide tunneling currents caused by nonuniform ion fluxes in typical ICP reactors.

<sup>1</sup>Work supported by NSF, SRC, Sandia/Sematech and Univ. of Wisconsin ERC for Plasma Aided Manufacturing.

**PS-WeP15 Plasma Parameter Dependence of Thin-Oxide Damage from Wafer Charging During Electron-Cyclotron-Resonance Plasma Processing**, J. B. Friedmann,\* S.-M. Ma,<sup>†</sup> J. P. McVittie,<sup>‡</sup> and J. L. Shohet,\* \*Engineering Research Center for Plasma-Aided Manufacturing, University of Wisconsin—Madison, Madison, WI 53706, and <sup>†</sup>Center for Integrated Systems, Stanford University, Stanford, CA 94305.

The main objective of these studies is to determine the relationship between plasma parameters and charging damage to polysilicon-gate metal-oxide-semiconductor (MOS) capacitor test structures upon exposure to electron-cyclotron-resonance (ECR) plasmas. The test structures are designed as "antennas" with a gate-oxide thickness of 10 nm and antenna ratios of from 16 to 11,000. After plasma exposure,

the damage is quantified using a number of damage-sensitive electrical measurements, including ramp-voltage oxide breakdown. Langmuir and emissive probe measurements of  $O_2$  plasmas in the ECR system have been made as a function of microwave input power, neutral pressure, magnetic field configuration, and radial position above the wafer stage. Contour plots of the plasma parameters (plasma potential, electron temperature, plasma density, etc.) have been generated from this data. We have concentrated on determining the effects of plasma potential uniformity and exposure time on the ramp-voltage oxide breakdown of the MOS capacitors. Results show that early breakdown of the antenna structures at below 5 volts increases as the antenna area increases, indicating that charging is the primary damage mechanism. Experiments in a plasma with a uniform plasma potential across the wafer revealed that processing time did not have a significant effect on the early breakdown distributions, indicating that damage induced during either plasma ignition or turn-off may be the dominant damage mechanism. Results of the role of plasma-induced damage in non-uniform plasmas will be presented.

This work was supported by the National Science Foundation under grant no. ECD-8721545, the Semiconductor Research Corporation under grant no. 93-M6-106, and ARPA.

**PS-WeP16 Impact of High-Z Limiters on Ion Fluxes in the Plasma Edge of the Textor Tokamak.** *M. Rubel<sup>1</sup>, B. Emmoth<sup>1</sup>, L. Könen<sup>2</sup>, V. Philipps<sup>2</sup>, A. Pospieszczyk<sup>2</sup>, J. von Seggern, T. Tanabe<sup>3</sup>, Y. Ueda<sup>3</sup> and P. Weinhold<sup>2</sup>.* <sup>1</sup>Physics Department—Frescati, Royal Institute of Technology, Association EURATOM—NFR, 24, S-104 05 Stockholm, Sweden, <sup>2</sup>Institute of Plasma Physics, KFA, D-52425 Jülich, Germany, <sup>3</sup>Department of Nuclear Engineering, Osaka University, Japan.

Heavy metals of high melting point are reconsidered as plasma facing materials in controlled fusion devices. Recently, extensive tests of molybdenum and tungsten limiters were performed in the TEXTOR tokamak. It was important to recognize the erosion of the limiters and its impact on the transfer of heavy metals to the plasma and scrape-off layer (SOL). Among many diagnostic techniques active during the experiment, the surface collector probe measurements were also done in order to trace ionic fluxes in the SOL. Probe exposures were made under different conditions (density, position of limiters, neon edge cooling) during ohmic and NBI heated discharges. The species deposited on the probes' surfaces were qualitatively and quantitatively determined by means of high energy ion beam techniques. The operation with the high-Z limiters did not increase the fluxes of other impurity atoms (B, Si, Ni) when compared to the operation without those limiters in the boronized or siliconized TEXTOR. The results of the collector probe measurements for the fluxes in the SOL are compared with the spectroscopic observations of impurity atoms in the plasma.

**PS-WeP17 Mass Spectrometric Analysis of the Gas Phase Coating Environment in Plasma Polymerization.** *S. Letts and R. Brusasco,* Lawrence Livermore National Laboratory, Livermore, CA 94550.

Plasma polymerization is used to prepare highly crosslinked organic polymer layers on shells used as targets in Inertial Confinement Fusion experiments. Optimization of the plasma polymerization process is desirable to make the coating process more reliable and to produce smoother coatings at higher deposition rates. To begin investigating the gas phase and surface chemical reactions and their kinetics, it is necessary to identify the gas phase species impinging on the substrate. A novel, close-coupled coating chamber combining a quadrupole mass spectrometer with a helical resonator that allows one to identify the gas phase species formed in the plasma has been built. The mass spectrometer shows that gas phase oligomerization occurs to create organic species of molecular weight greater than the  $C_4$  starting material. The co-axial design of the reaction chamber allows one to probe the ions in the gas phase as well as neutral species. The gas phase at the point of contact with the substrate is rich in hydrogen ions but ionic hydrocarbon species concentrations are very low. It is possible to alter the distribution of gas phase species present by blending precursor gases. Work to correlate the effects of the gas phase composition on coating properties is ongoing and will be discussed in terms of residual coating stress and surface roughness.

Work performed under the auspices of the U.S. Department of Energy by Lawrence Livermore National Laboratory under Contract W-7405-ENG-48.

**PS-WeP18 Argon Permeation through Polyvinyl Alcohol (PVA) Coatings,\*** *D. A. Steinman, M. L. Hoppe,* General Atomics, San Diego, CA 92186-9784.

Polyvinyl alcohol (PVA) is used as a gas-barrier to hold deuterium and diagnostic gases (such as argon) inside the hollow, spherical shells used as laser fusion targets. A PVA layer several microns thick will, at room temperature, hold on the order of 50 atmospheres of deuterium in the shells for several hours, a time sufficient for laser experiments. However, this thickness of PVA permanently entraps the argon. Normally, the argon is entrapped when the PVA coating is applied. We have developed a procedure whereby argon is permeated through the PVA layer of completed shells to fill them to specified fill pressures (typically 0.1 to 1.0 atm). The shells are placed in a sealed fill tube pressurized with the desired amount of argon. The tube is then heated to approximately 100°C and kept at temperature until the argon pressure in the shell reaches equilibrium. An X-Ray Fluorescence (XRF) system is used to measure the argon content of the shells so that permeation coefficients can be calculated. We have found that half-millimeter shells coated with 3  $\mu\text{m}$  of PVA can be filled with argon in approximately ten days. This procedure offers the prospect of argon fills in excess of 1 atmosphere, uniform shell-to-shell argon content, removal of residual gases (*i.e.*, air and water vapor) from the shells, and calibration standards for XRF measurement of shell argon content.

\*Work supported by the U.S. Department of Energy under Contract No. DE-AC03-91SF18601.

**PS-WeP19 Preparation of Germanium Doped Plasma Polymerized Coatings as ICF Target Ablators,** *R. Brusasco, M. Saculla and R. Cook,* Lawrence Livermore National Laboratory, Livermore, CA 94550.

Targets for Inertial Confinement Fusion (ICF) experiments at Lawrence Livermore National Laboratory (LLNL) utilize an organic (CH) ablator coating prepared by plasma polymerization. Some of these experiments require a mid-Z dopant in the ablator coating to modify the opacity of the shell. Bromine had been used in the past, but the surface finish of brominated CH degrades rapidly with time upon exposure to air. This paper describes the preparation and characterization of plasma polymerized layers containing germanium as a dopant at concentrations of between 0.9–1.8 atom percent. The coatings are stable in air and have an rms surface roughness of 30 to 75 nm which is similar to that obtained with undoped coatings. High levels of dopant result in cracking of the inner mandrel during target assembly. Possible explanations for the observed cracking behavior will be discussed.

Work performed under the auspices of the U.S. Department of Energy by Lawrence Livermore National Laboratory under Contract W-7405-ENG-48.

**PS-WeP20 Liquid Hydrogen Layering Dynamics in Large Plastic Capsules,** *\*\*T. Bernat, \*D. Bittner, \*\*G. W. Collins, \*\*E. R. Mapoles, \*\*J. Sanchez, \*J. Sater, \*W. J. Schafer Associates,* 303 Lindbergh Avenue, Livermore, CA 94550, \*\*Lawrence Livermore National Laboratory, P.O. Box 808, Livermore, CA 94550.

Advanced inertial confinement fusion targets require uniform condensed cryogenic hydrogen fuel layers with inner surface smoothness as low as 1000 Å rms for some designs. For a liquid layer stabilized against gravity, surface tension would provide this surface smoothness. Liquid layers less than 10  $\mu\text{m}$  thick have been created by a thermal gradient layering technique in glass shells with a few hundred micron diameters<sup>1</sup>. Advanced targets have diameters of 1-to-2 mm, with fuel layers up to 100  $\mu\text{m}$  thick. Current experiments are being conducted in this size range. Liquid oscillations as well as stable liquid surface configurations have been observed. We will report on our progress towards creating stable uniform liquid layers.

Work performed under the auspices of the U.S. Department of Energy by Lawrence Livermore National Laboratory under Contract W-7405-ENG-48 and by W. J. Schafer Associates under Contract DE-AC03-91SF18601.

1. K. Kim et al., J. Vac. Sci. Technol. **A3**, 1196 (1985).

**PS-WeP21 Hollow Foam Microshells for Liquid-Layered Cryogenic ICF Targets,** *George E. Overturf III, Robert Cook, Bob Reibold,* Lawrence Livermore National Laboratory, Livermore, CA 94550, *Diana Schroen-Carey,* WJ Schafer Associates, Livermore, CA 94550.

Foam shell targets are being considered as a liquid-layered cryogenic target for the Omega Upgrade and the National Ignition Facility. For

Omega Upgrade the target consists of a 1 mm diameter and 100 mm thick spherical, 50 mg/cm<sup>3</sup> foam shell surrounding a central void. The foam is overcoated with a full density polymer fuel barrier which must be topologically smooth. The foam will be slightly overfilled with liquid D<sub>2</sub> or DT, the overfilled excess being symmetrically distributed on the inside of the shell using thermal gradient techniques. The technology for producing this style of foam shell involves microencapsulation techniques that have been developed at Osaka University's Institute for Laser Engineering. Our goal has been to adapt this technology to meet US ICF objectives. We will report on our progress in accomplishing this goal.

Work performed under the auspices of the U.S. Department of Energy by Lawrence Livermore National Laboratory under Contract W-7405-ENG-48.

**PS-WeP22 Determination of the Wall Thickness and Uniformity of Inertial-Fusion Capsules Using the Self-Interference Fringes Produced with Narrow-Bandwidth Illumination, Mark D. Wittman, Hyo-gun Kim, and Albert S. Chow,**<sup>(a)</sup> Laboratory for Laser Energetics, University of Rochester, 250 East River Road, Rochester, NY 14623-1299.

Direct-drive inertial-fusion capsules must possess a high degree of spherical symmetry including concentricity of the inner and outer wall surfaces. When viewed with a compound microscope using transmitted narrow-bandwidth light, such as that produced with a thin-film interference filter, self-interference fringes appear within the image of a capsule that are localized to its equatorial plane. The fringes are distinct and concentric when the capsule is uniform, whereas faint, distorted, or discontinuous rings indicate nonuniformity. We have formulated a model that predicts this self-interference pattern as a function of capsule parameters, and it agrees well with actual measurements from the image of a well-characterized capsule. The wavefront directly transmitted through the capsule and wavefronts that are multiply reflected within its walls interfere to produce these rings. These wavefronts are constructed by tracing a single paraxial ray through the capsule and including reflections and third-order spherical aberration. The diameters of the rings are predicted from the intersection of the wavefronts. Changes in wall thickness as small as 10 nm affect the self-interference rings' diameters by several micrometers, whereas the ring diameters are independent of both the internal gas-fill pressure and the angle that rays impinge on the capsule.

<sup>(a)</sup>Participant in LLE's 1990 High School Summer Research Program from Webster High School, Webster, NY 14580. This work was supported by the U.S. Department of Energy Office of Inertial Confinement Fusion under Cooperative Agreement No. DE-FC03-92SF19460, the University of Rochester, and the New York State Energy Research and Development Authority. The support of DOE does not constitute an endorsement by DOE of the views expressed in this article.

## THIN FILM

### Room BR4 - Session TF-WeP

#### Aspects of Thin Films

**Moderator:** F. Sequeda, Conner Peripherals.

**TF-WeP1 A Novel Approach to the Calculation of ITO Films' Figures of Merit, S. A. Knickerbocker, A. K. Kulkarni,** Michigan Technological University, Houghton, MI 49931.

As flat panel display devices gain in popularity, the need for highly conductive transparent films will increase. Indium tin oxide (ITO) is just such a film and it presently exhibits some of the most impressive qualities with regards to electrical conductivity and optical transparency. These qualities have competing mechanisms which give rise to the need for a compromise between the transmission and conductivity. To allow films with various properties to be compared, several figures of merit have been developed to relate the transmission (T) and electrical sheet resistivity (R<sub>s</sub>) of ITO thin films. Of these figures of merit, two are based on ratios of the transmission and the sheet resistivity and these are thickness dependent quantities. The other two are based on the product of the parameters and yield thickness independent formulas.

In order to optimize the conductivity and the transmission as a

function of doping, it is necessary to determine the figure of merit as a function of the carrier concentration. We have compared different figures of merit as a function of carrier concentration on the basis of basic theoretical concepts instead of experimental values of conductivity and transmission. Estimates of the refractive index (n) and the extinction coefficient (k) are made and used to predict the optical transmission as a function of the carrier concentration in the films. These values are then used in four separate figures of merit F<sub>FC</sub>, F<sub>H</sub>, F<sub>IS</sub> and F<sub>JK</sub>. From these plots it appears there is an optimum value of doping in ITO thin films.

$$* -F_{FC} = \frac{T}{R_{\square}}, \quad F_H = \frac{T^x}{R_{\square}}, \quad F_{IS} = R_{\square}(1 - T) \text{ and } F_{JK} = -R_{\square} \ln(T).$$

**TF-WeP2 Protecting Silver Polymer Mirrors with Oxide Coatings for Solar Applications, C. E. Kennedy,** National Renewable Energy Laboratory, Golden, CO 80401.

Large mirrors are used to concentrate sunlight for renewable power generation for the solar thermal technologies. The reflector materials must be low in cost and maintain high specular reflectance for extended lifetimes under severe outdoor environments. Compatibility with mass production techniques is necessary to meet the low-cost requirements. Currently the best candidate materials for solar mirrors are silver-coated low-iron glass and silvered polymer films. Polymer reflectors are lighter in weight, offer greater system design flexibility, and have the potential for lower cost than glass mirrors. A promising low-cost construction uses an inexpensive polymer substrate, a silver reflective layer, and an optically clear protective top coat. Test samples were fabricated by magnetron sputtering. SiO<sub>2</sub>, Al<sub>2</sub>O<sub>3</sub>, and Si<sub>3</sub>N<sub>4</sub> were used as the protective layer. The samples were characterized by optical and surface analysis. The optical durability of the reflector materials was evaluated by accelerated weathering in controlled laboratory environments and real time exposure at outdoor test sites.

**TF-WeP3 UHV E-Beam Deposition of Pt and Ti on Single Crystal Si and SiO<sub>2</sub> Substrates for the Preparation of Pb(Zr, Ti)O<sub>3</sub> Thin Films by Laser Ablation, M. Dubey, W. Wilber, L. Casas, R. Lareau, K. A. Jones,** Army Research Lab, EPSCD, Fort Monmouth, NJ 07703.

The use of PZT, Pb(Zr, Ti)O<sub>3</sub> films in electronic applications requires the preparation of PZT on a conducting substrate. In this experiment, the Pt or/and Ti (100-200 nm) were deposited at a rate of 1-2 Å and at different temperatures (100-650°C) on Si (100), (111) and silicon oxide (50-200 nm) surfaces using UHV (10<sup>-9</sup>-10<sup>-10</sup> Torr) E-Beam evaporation. The PZT films were deposited by laser ablation onto the metallized substrate at a temperature of approximately 600°C under 100 mTorr oxygen atmosphere. The substrate-metal interface reactions, grain size, orientation and structure of Pt, Ti, Pt/Ti, and the PZT films grown on them, with and without oxide on silicon substrates, were analyzed by X-ray, STM, SIMS and AES. The PZT films were analyzed electrically for resistivity and hysteresis.

**TF-WeP5 Microstructure and Characterization of Electron-Trapping Stimulable Phosphor SrS:Eu,Sm Thin Films on Glass, T. J. Hsieh<sup>1</sup>, R. Revay<sup>1</sup>, D. Brower<sup>1</sup>, P. H. Chi<sup>2</sup>, D. S. Simons<sup>2</sup>, D. E. Newbury<sup>2</sup>, S. W. Robey<sup>2</sup>,**<sup>1</sup>Optex Communications Corporation, 2 Research Court, Rockville, MD 20850, <sup>2</sup>National Institute of Standards and Technology, Gaithersburg, MD 20899.

Strontium sulfide doped with europium and samarium is a stimulable phosphor that is being investigated as the active layer of a photonic data storage disk. Lithium and fluorine are added to the SrS:Eu,Sm in order to fully activate the photonic properties of the material. Thin films are grown on glass substrates above 650 K by ion-assisted e-beam evaporation and RF magnetron sputtering. The resulting films may have a preferred orientation which is dependent on substrate temperature. To obtain high performance films, care must be taken to assure sufficient crystallite size, minimize structural defects within crystal grains, and maintain a uniform chemistry throughout the thickness of the films. We present results on film performance in which we show the relationship to these latter properties employing X-ray diffraction (XRD), transmission electron microscopy (TEM), and secondary ion mass spectrometry (SIMS). Structural defects within grains have a major impact on film performance. The relative influence of the difference in the coefficients of the thermal expansion and deposition-induced defects will be discussed.

**TF-WeP6 The Structure and Magneto-Optical Properties of Ta/Fe and Ta/Co Bilayers, E. E. Shaligina, L. V. Kozlovsky,** University of Daugavpils, Daugavpils, Latvia, LV-5407.



Magnetic films have received much attention in recent years. The purpose of the present study is to investigate the influence of non-magnetic layer between substrate and magnetic film on crystallographic structure and magneto-optical properties of the film.

The films were prepared by sputtering in Penning discharge at Xe pressure of  $7 \times 10^{-4}$  Torr and substrate temperature near to room temperature. Before each run the chamber was evacuated to  $5 \times 10^{-9}$  Torr. 40 nm Ta films were deposited on glass substrates. The thickness of Fe and Co films was varied between 0.5 and 200 nm. The X-ray measurements were performed on a X-ray diffractometer. The magnetic measurements were performed on the magneto-optical micro-magnetometer and the spectral technique by means of transverse Kerr effect (TKE).

40 nm Ta films could be characterized as a mixture of  $\alpha$  and  $\beta$ -Ta crystalline phases and were textured. Fe and Co films had preferred orientation of {110} and {001} lattice planes respectively parallel to the surface. The degree of crystallographic texture of Fe and Co films on textured Ta layers was much higher than that in the case of these films on glass substrates.

It is discovered that the magnetic films with the thickness varying between 2 and 20 nm have an in-plane easy axis. The magnitude of coercivity  $H_C$  decreases with reducing magnetic film thickness. The coercivity of the samples with Ta layer was 2-3 times more than  $H_C$  of ones without non-magnetic layer. The investigations of dispersion dependencies of TKE were performed over the spectral range 2-4.5 eV. TKE was absent for the samples with magnetic film thickness smaller than 1 nm.

**TF-WeP7 Surface Compositions of Chemically Treated CdTe Thin Films for Photovoltaic Applications: an XPS and AES Study, D. W. Niles, X. Li, P. Sheldon,** National Renewable Energy Laboratory, 1617 Cole Boulevard, Golden, CO 80401.

We use x-ray photoelectron spectroscopy and Auger electron spectroscopy to investigate chemical treatments used to form back contacts in CdTe-based photovoltaic devices. We produce photovoltaic grade thin film CdTe by closed space sublimation (CSS). Because CSS CdTe is highly resistive and not amenable to low resistance back contact formation, one must treat the CdTe to form a highly p-type conductive layer on which to make the back contact. We etch our CSS CdTe in  $H_3PO_4 + HNO_3$  in an effort to form Te rich, p-type CdTe surfaces, and show that chemically etching the CdTe thin films leaves a highly conductive, pure Te layer. Auger depth profiles show a Te-rich region extending up to a depth of 1000 nm for CSS grown CdTe. In comparison, the same etch applied to single crystal CdTe leaves a 50 nm Te layer, implying enhanced etching along grain boundaries for CSS CdTe. The Te layers oxidize in air at a rate of 0.3 at. % per minute, and saturate at  $TeO_2/(Te + TeO_2) = 60\%$  after an overnight exposure. We will discuss compositional analyses of CdTe after  $H_3PO_4 + HNO_3$  etches and KOH treatments, the implications in forming shunt paths that inhibit efficient photovoltaic performance, and the formation of low resistance back contacts to CdTe.

**TF-WeP8 Plasma-Deposition of Low Stress Electret Films for Electroacoustic and Solar Cell Applications, P. Günther, R. Schellin, G. Sessler, C. Thielemann,** Institute for Telecommunications and Electroacoustics, Technical University of Darmstadt, Germany, and J. E. Klemberg-Sapieha, L. Martinu, M. R. Wertheimer, Engineering Physics Department, Ecole Polytechnique, Montreal, Canada.

Low energy ion bombardment during the plasma enhanced chemical vapor deposition (PECVD) process can be used effectively to control the film microstructure-related properties such as density, internal stress and surface charge retention. In the present work we study the characteristics of silicon-compound films (silicon nitride, oxide and oxynitrides) prepared from  $SiH_4/NH_3/N_2O$  mixtures in a dual-mode microwave/radiofrequency plasma system at a low substrate temperature ( $\sim 30^\circ C$ ). We have found that a tensile stress ( $\sim +0.1$  GPa) develops at very low ion energies ( $E_i \sim 5-30$  eV), that it changes into an elevated compressive stress ( $\sim -0.5$  GPa) at higher  $E_i$  values ( $E_i \geq 200$  eV), and that the lowest stress values occur for  $E_i$  between 80 and 100 eV. However, the best electret properties (the longest charge retention times on the order of years) have been observed for the case of very dense films grown at high ion energies ( $\geq 200$  eV). We investigate the possibilities to obtain low stress electret films by evaluating the performance of single layer, multilayer and graded-density structures, and of the effects of postdeposition treatment (annealing, gas adsorption). These materials have been successfully applied for electret-enhanced MIS-IL solar cells, and are very promising for micro-machined membranes in electret microphones.

**TF-WeP9 Low Temperature Formation of Textured ZnO Transparent Electrodes by Magnetron Sputtering, T. Minami, H. Sonohara, S. Takata and I. Fukuda,** Kanazawa Institute of Technology, 7-1 Ohgigaoka, Nonoichi, Ishikawa 921, Japan.

Milky transparent conducting ZnO films with a textured surface have attracted attention as low-cost transparent electrodes for thin-film solar cells such as a-Si and CuInSe<sub>2</sub>. Although these applications require film deposition at temperatures below about  $250^\circ C$ , large-area film coatings produced by magnetron sputtering normally involve high-temperature treatments to obtain a low resistivity. In this paper, we demonstrate a dc magnetron sputtering technique that results in highly conductive ZnO films with a textured surface prepared on substrates at a temperature of  $200^\circ C$ . Large-area transparent conducting impurity-doped ZnO films with textured surface have been prepared at a sputter pressure of 60 to 80 Pa and temperature above  $200^\circ C$  by conventional dc magnetron sputtering using sintered ZnO powder doped with impurity as the target. A resistivity of  $4.6 \times 10^{-4} \Omega \cdot cm$  and a total transmittance of 84% were obtained for textured ZnO:Al films prepared at a temperature of  $200^\circ C$ . Textured ZnO:Al transparent electrodes with a sheet resistance of  $4\Omega/sq$  and a haze ratio of 54% at a wavelength of 550 nm were formed with large-area  $1.3\text{-}\mu m$ -thick ZnO:Al films.

**TF-WeP10 Vacuum Deposition Parameters for Thin Film Shape Memory Alloys, A. Peter Jardine and Rand Dannenberg,** Dept. of Materials Science and Engineering, SUNY at Stony Brook, Stony Brook, NY 11794-2275.

Thin film Shape Memory Alloys are an interesting new material, both from fundamental physical properties and from technological interest. When in their highly twinned, low temperature martensitic state, these alloys are ductile due to the easy motion of twin boundaries. The high temperature austenitic state does not possess these properties and so the internal stress of the thin film changes dramatically with state. Technological interest is due to their comparatively high energies for actuation, making them interesting as linear drive elements for Micro-Electro-Mechanical Machines, for example.

There has yet to be a definitive study on deposition parameters for these alloys. In particular, there is a need for better determination of vacuum processing parameters for thin film SME materials. In particular, the effect of base pressure, gas cleanliness, target to sample distance, substrate material and post-processing of the material all affect the transformation properties of the alloy. Using a UHV deposition chamber with in-situ heating and two DC sputter deposition sources, thin film TiNi and CuAlNi were deposited onto Si and ceramic substrates. In this paper, we correlate the transformation properties using Resistance-temperature profiles and the microstructural properties of thin film TiNi using XRD and SEM with these mentioned deposition parameters.

**TF-WeP11 Low-Temperature Synthesis of High-Quality SiO<sub>2</sub> Thin Films from Low Energy Ion Beams, S. S. Todorov, D. Marton, K. J. Boyd, A. H. Al-Bayati, and J. W. Rabalais,** Department of Chemistry, University of Houston, Houston, Texas 77204-5641.

Low-temperature processing is essential for the fabrication of semiconductor devices of decreasing dimensions and increasing complexity. The energy necessary for the oxidation reaction to proceed can be supplied without heating the substrate by using low energy ions. A two-step process using deposition from low-energy ion beams produces dense SiO<sub>2</sub> films of any desired thickness. The experiments are performed at the unique dual-source, fast-switching, mass-selected low-energy ion beam system at the University of Houston. First, ion beam oxidation of the Si substrate is carried out, forming the SiO<sub>2</sub>/Si interface below the original Si surface. This is followed by deposition of silicon dioxide using alternating Si<sup>+</sup> and O<sup>+</sup> ion beams. The films are deposited at temperatures between 20 and  $350^\circ C$  using ions with energies between 5 and 50 eV. The first step of the process leads to self-limiting oxide film growth with a steady-state thickness determined by the substrate temperature and, to a lesser extent, by the O<sup>+</sup> energy. The composition of the films is studied by *in situ* Auger electron spectroscopy (AES) and *ex situ* X-ray photoelectron spectroscopy (XPS). The films are stoichiometric and show no traces of suboxides as indicated by analysis of the Si 2p XPS peaks of, e.g., a film grown at  $350^\circ C$  by 25 eV O<sup>+</sup> ion beam oxidation. This instrument provides individual control over the experimental parameters which in essence allows modelling and possibly optimization of commercially viable batch-scale plasma processing.



**TF-WeP12 A Compact Negative Metal Ion Beam Source for Low Energy Thin Film Deposition,** *S. I. Kim, Y. O. Ahn*, SKION Corporation, Hoboken, NJ 07030.

A compact negative metal ion beam source for various direct low energy ion beam depositions in high vacuum environment, has been developed. The ion source is based on the state-of-the-art solid state cesium ion technology. The negative ion beams are very effectively produced by cesium ion bombardment (negative sputter ion yield varies in 0.2-0.5 for various metals). The ion source produces negative metal ion currents of up to 0.5 mA/cm<sup>2</sup> for the beam diameter of 1". The ion beam energy can be independently controllable in the range of 10-2000 eV. The ion source is very compact, stable, and easy to use. Due to the complete solid state ion technology, 10<sup>-10</sup> Torr of chamber pressure can be maintained while operating the source. The source can be used for various species of metals such as C, Au, Ag, Pt, Al, W, Ta, Mo etc. The source has been successfully used for the deposition of the amorphous diamond carbon and carbon nitride films.

**TF-WeP13 Bias Sputter Deposition of Dense Yttria-Stabilized Zirconia Films on Porous Substrates,** *T. Tsai and S. A. Barnett*, Department of Materials Science and Engineering, Northwestern University, Evanston, Illinois, 60208.

In thin-film solid oxide fuel cells (SOFC), yttria-stabilized zirconia (YSZ) electrolyte thin films deposited on porous substrate/electrodes must be electrically isolating and gas impermeable. In this paper, we describe YSZ film deposition by reactive magnetron sputtering of Zr-Y targets in Ar-O<sub>2</sub> mixtures onto porous substrates, typically La<sub>0.8</sub>Sr<sub>0.2</sub>MnO<sub>3</sub> (LSM) with pore size <0.5 μm. Without substrate bias, SEM images of the films showed rough surfaces with evidence of nodular growth and porous structure; these films were dense enough for SOFC applications only for thicknesses >20 μm. SEM fracture cross-section images showed that a negative DC substrate bias V<sub>s</sub> of 150V produced an apparently dense structure with columnar features, while V<sub>s</sub> = 300V produced a dense featureless morphology. Residual surface roughness was still present, showing dune-like morphologies. Both -150V and -300V biased samples have same peak to valley roughness values, ~0.5 μm, but different lateral period, ~1 μm for V<sub>s</sub> = 150V and ~5 μm for V<sub>s</sub> = 300V. The stress field in the films increased with increasing bias. Cracking was observed for highly biased samples. Using optimal conditions, dense and leak-tight YSZ films were obtained at a thickness of only 3 μm, with measured SOFC open circuit voltages within 15% of theoretical values.

**TF-WeP14 Modeling and Experimental Studies of Multi-Phase Formation in Reactive Sputtering,** *C. Nender, T. Nyberg and S. Berg*, Inst. of Technology, Uppsala University, Box 534, S-751 21 Uppsala, Sweden, *K. O. Legg, M. Graham, P. J. Rudnik, M. S. Wong and W. D. Sproul*, BIRL, Northwestern University, 1801 Maple Ave., Evanston, IL 60201-3135, USA.

Reactive sputtering is a complex thin film deposition technique. Several material properties (mechanical, electrical and optical) of the deposited film are highly dependent on the process conditions. Due to instabilities (hysteresis effects) it may be necessary to use a real time advanced feedback control loop in order to produce compounds with correct properties. In the following paper it is experimentally verified for a number of materials that different phases of the reactively sputtered compound can be formed at different reactive gas pressures. Since the deposition rate varies with reactive gas pressure, one phase may be deposited at a much higher rate, which may be of high importance for the cost of industrial processes. In order to better understand the process behavior of reactive sputtering and to be able to better predict the deposited film properties, computer models are becoming an important tool. This enables a much faster process development. An extended reactive sputtering model for the deposition of two compound phases is presented. The model enables predictions of the compositional changes of the deposited compound and the relative deposition rates versus the reactive gas pressure. A comparison with experimental result is also presented.

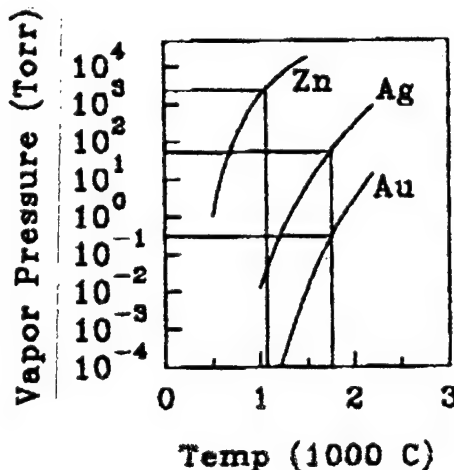
**TF-WeP15 Ionized Magnetron Sputtering of Carbon Nitride Thin Films,** *D. Li\*, Y. W. Chung\*, S. Lopez\*\*, M. S. Wong\*\*, and W. D. Sproul\*\**, \*Department of Materials Science, Northwestern University, \*\*BIRL Industrial Research Laboratory, 1801 Maple Ave., Northwestern University.

Carbon nitride thin films were prepared using an ionized magnetron sputtering system. An inductively coupled rf plasma was generated in the region between the sputtering source (high purity graphite) and the substrate table. An argon and nitrogen mixture was used as the sputtering gas. Sputtered atoms which pass through the high density

plasma may be ionized, and the degree of ionization depends on several processing variables, such as the gas total pressure, reactive gas partial pressure, and applied rf power. Pulsed dc bias voltage, applied to the substrates, was varied up to -500V. The chemical bonding, composition, and microstructure of the deposited films were studied by infrared analysis, Raman spectroscopy, Auger electron microscopy, and analytical transmission electron microscope. Optical properties were evaluated using ellipsometry. An ultra-micro indentation system was used to measure the hardness. The preliminary results showed that nitrogen is bonded to carbon in various configurations, that the nitrogen to carbon ratio in the films can be up to 0.8, and that the optical band gap is as high as 1.7 eV.

**TF-WeP16 Developments in the Ionized Cluster Beam Deposition Technique,** *M. F. Tabet, S. Feng, A. J. Cox, and F. K. Urban*, Electrical and Computer Engineering, Florida International University, Miami, Florida 33199.

Ionized cluster beam deposition uses a beam of ionized, accelerated atom clusters to grow thin films. Late in 1991, following nearly 20 years of development, synthesis of large clusters of zinc by homogeneous nucleation was achieved through significant changes in two source parameters. Crucible pressure was increased from 2 Torr to over 1000 Torr and the nozzle was changed from cylindrical (1 × 1 mm) to converging-diverging (18 mm long and 0.4 mm in diameter at the throat). Such high vapor pressure is presently impractical for materials of industrial interest such as gold, silver, copper, and aluminum. The vapor pressure of Zn, Au, and Ag as a function of temperature are shown below. Recent results using gold with the converging-diverging nozzle at a pressure of just under 1 Torr showed no significant synthesis of large clusters. The work presented here describes results using silver at an intermediate pressure of around 100 Torr. The deposition rate was intermediate (1.7 nm s<sup>-1</sup>) between gold (0.02 nm s<sup>-1</sup>) and zinc (4.3 nm s<sup>-1</sup>). Silver purity influenced the appearance of the beam. X-ray analysis of deposited films will be presented. Ongoing work in real time, in-situ cluster size measurement will be reported. Preliminary results of ICB for trench filling will also be shown.



**TF-WeP17 Development of Vacuum Arc Metal Ion Sources and Techniques TAMEK for Material Surface Modification,** *Alexander M. Tolopa*, Appl. Phys. Inst., Ukraine Acad. Sci., P.O. Box 561. 244024, Sumy, Ukraine, and Pan TAMEK, 13 Partizansky prospect, Vladivostok, 690002, Russia.

Review summarizes the development of vacuum arc ion sources from the first version made in 1984 which generated any metal ion beams of 20 cm diameter with current up to 1 A at an accelerating voltage up to 130 kV, pulse duration of 300 μs and repetition rate up to 50 Hz, for doing high dose implantation (HDI), to the ciation of the Technological Accelerator of Metal ions and Electron Kit—TAMEK source which can produce, without switching of the source, the regimes HDI, ion deposition, ion beam mixing, and ion beam assisted deposition of the same metal ions, as well as electron beam generation. Ion beam (S = 300 cm<sup>2</sup>, Ei < 100 keV) sources with vacuum arc current of several amperes (Iarc > 2 A, Ii > 0.1 A) and milliseconds duration, and with arc current up to 100 kA (Ii = 1 to 10 kA) and microseconds duration, are described. Application of these sources for improving

the properties of surface layers of tools, construction materials, electrical contacts and electrodes, biomaterials, optical, dielectric, glass are discussed.

1. A. M. Tolopa, Rev. Sci. Instrum., 65(4) 1994.
2. A. D. Pogrebnjak and A. M. Tolopa, Nucl. Instr. & Methods., B52, 25 (1990).
3. S. M. Duvanov, A. P. Kobzev and A. M. Tolopa, Nucl. Instrum. & Methods, B85, 264 (1994).

**TF-WeP18 Synthesis and Properties of Polycrystalline CrN/TiN Superlattices, P. Yashar\*, X. Chu\*, M. S. Wong\*\*, W. Sproul\*\*, S. A. Barnett\***, \*Department of Materials Science and Engineering, Northwestern University, Evanston, Illinois 60201, \*\*BIRL, Industrial Research Laboratory, Northwestern University, Evanston, Illinois, 60201.

One of the primary factors believed to determine the hardness enhancement in superlattice (multi-layered) coatings, is the difference in layer shear moduli. The CrN/TiN superlattice system, with a larger modulus difference than previous nitride superlattices, was investigated in order to determine whether the modulus difference is the main factor determining the hardness. Polycrystalline CrN/TiN superlattices were deposited on M1 tool steel in an opposed-cathode unbalanced magnetron sputtering system with a rotating substrate holder. In initial experiments, the individual layers (CrN and TiN) of the superlattice were made of equal thickness. During reactive sputtering cubic CrN requires a  $N_2$  partial pressure that is about one order of magnitude more than that required to form cubic TiN. In order to deposit both CrN and TiN in the cubic phase in the same deposition chamber, we attempted to produce a nitrogen pressure gradient. Semi-quantitative analysis of Auger electron spectroscopy data from CrN<sub>x</sub> coated samples was used to estimate this pressure gradient, as well as to study the stoichiometry of the CrN and TiN films. The superlattice structure was characterized by X-ray diffraction which showed first order satellite peaks around the (111) Bragg peak of the material. The superlattice periods were varied from 1.8 nm to 16 nm. For 2  $\mu$ m CrN/TiN coated samples, the results of the UMIS 2000 Ultra-Micro indentation hardness testing showed an increase in hardness of more than 1000 kgf/mm<sup>2</sup> over the rule of mixtures for CrN and TiN, and the scratch testing showed critical loads that exceeded 6 kgf.

**TF-WeP19 Neutralized Beam Assisted Evaporation of Cubic Boron Nitride on Si(100), Ming Lu, A. Bousetta, and A. Bensaoula, SVEC, University of Houston, TX 77204 and K. Waters, A. Schultz Ionwerks.**

We report the growth of cubic boron nitride (CBN) films on Si(100) substrates using electron beam evaporation of boron and a neutralized nitrogen beam. The beam neutralizer was adapted to 3 cm Kaufman-type ion source. The films were grown at substrate temperatures in the 400–500°C range and a boron evaporation rate of 2–3 nm/sec. Using this new approach, we show that highly stoichiometric BN films can be obtained with up to 80% cubic phase. We will present data from a variety of thin film characteristic techniques including FTIR, RBS, EPMA and TEM.

Supported by NASA NAGW-977, ARP under grant #93-00365-2224, and Ionwerks under SDIO Grant #L0391C0045.

**TF-WeP20 An X-ray Diffraction Study of Epitaxial Nitride Superlattices, A. Madan, Department of Physics and Astronomy, Northwestern University, Evanston, IL 60208, M. Shinn and S. A. Barnett, Department of Materials Science and Engineering, Northwestern University, Evanston, IL 60208.**

Thin film superlattices generally exhibit substantial strength and/or hardness enhancements relative to the corresponding homogeneous materials. For example, epitaxial TiN/NbN superlattices exhibit a maximum Vickers microhardness value of 4900 kg/mm<sup>2</sup> at a superlattice period  $\Lambda = 4.6$  nm, compared with  $\approx 2000$  kg/mm<sup>2</sup> for TiNbN alloys. Recent calculations suggest that there is a strong dependence of the strength and hardness enhancements on interface widths and concentration gradients. X-ray diffraction measurements and simulations were thus carried out to determine the nature of the superlattice composition modulation. A trapezoidal form of the composition wave was assumed. Layer thickness fluctuations and random d-spacing variations were included to explain the broadening of the diffraction peaks. For cases where the layer materials were miscible, the composition within each layer and the interface widths was varied. Best fits to the experimental data for nitride superlattices showed that considerable interdiffusion was present. In TiN/NbN, for example, the layers contained up to 20 at% of the other metal constituent and

the interface widths were found to be  $\approx 1$  nm. This latter value, when used in calculations of TiN/NbN hardness, provides reasonable agreement with the measured hardness values.

**TF-WeP21 Defect Structure of Low Energy Ion Modified Diamond(100) Surfaces, B. W. Sun, L. J. Huang, I. Bello, W. M. Lau, Department of Materials Engineering, University of Western Ontario, London, Ontario N6A 5B9 Canada; S.-T. Lee, Analytical Laboratory, Eastman Kodak Company, Rochester, New York 14650-2132, P. A. Stevens, B. D. DeVries, Exxon Research and Engineering Company, Annandale, New Jersey 08801.**

The surface defect structures on diamond (100) surfaces induced by 500 eV neon ion bombardment and by subsequent annealing were studied *in situ* with x-ray absorption near-edge structure (XANES) spectroscopy using 250 to 800 eV synchrotron radiation and with low energy electron diffraction. *Ex situ* x-ray photoemission spectroscopy (XPS) was also used to characterize the defective layer. Significant changes in the XANES spectra were identified for the defects induced by ion bombardment and subsequent annealing. The diamond discrete exciton absorption at 289.0 eV was clearly suppressed even at the lowest ion fluence used in this study, i.e.  $3 \times 10^{14}$ /cm<sup>2</sup>, and no such exciton could be observed at  $7 \times 10^{14}$ /cm<sup>2</sup>. However, the changes in the multi-maxima shape-resonance absorption structure in the range of 290–310 eV indicated that amorphization of the diamond surface required a fluence of  $1 \times 10^{15}$ /cm<sup>2</sup>. The structural changes were also manifested by the transformation of gap state absorption typical of clean ( $2 \times 1$ ) surfaces to the  $\pi^*$  absorption typical of amorphous carbon. Calculations from the XPS data showed that the defective layer was about 2 nm thick. Both the XANES and XPS data also indicated that the defects were stable upon annealing up to a temperature of 1100°C with no phase transformation to graphite.

**TF-WeP22 The Effect of the Physical Vapor Deposition Techniques of Sputtering and Evaporation of Ti on the Formation and Transformation of C49 to C54 TiSi<sub>2</sub>, C. Cabral, Jr., R. A. Roy, L. A. Clevenger and K. L. Saenger, IBM T. J. Watson Research Center, P.O. Box 218, Yorktown Heights, NY 10598.**

It has been demonstrated that sputtered Ti thin films on polycrystalline Si substrates undergo the C49 to C54 TiSi<sub>2</sub> phase transformation at lower temperatures than evaporated films. In particular sputtered Ti films deposited at room temperature in the presence of 10 mTorr of Ar undergo the C49 to C54 phase transformation at a lower temperature than those deposited using alternate deposition conditions. High substrate bias and sputter deposition pressure cause the C49 to C54 transformation to be delayed by as much as 80°C and 30°C respectively. Sputtered and evaporated Ti films, 45 to 63 nm thick, were deposited on polycrystalline Si substrates. The sputtering parameters of temperature, pressure and substrate bias were varied. The films were annealed in He either in a furnace or rapid thermal annealing system while *in-situ* resistivity and/or stress as a function of temperature were monitored. To confirm TiSi<sub>2</sub> phase formation isothermally annealed films were analyzed using x-ray diffraction (XRD).

**TF-WeP23 Residual Stress in Ion Implanted Titanium Nitride Films by Parallel Beam Glancing Incidence X-ray Diffraction, Anthony J. Perry and James R. Treglio, ISM Technologies Inc., 9965 Carroll Canyon, San Diego, CA 92131; Daniel E. Geist, Martin Marietta, Mail Stop 9683, P.O. Box 179, Denver, CO 80201.**

It has long been thought that the improvements in the wear behavior of titanium nitride TiN after ion implantation with gas or metal ions is due to an increase in the compressive residual stress. Previous work using Seemann-Bohlin glancing angle focusing x-ray geometry [1] has shown that implanting TiN with argon or krypton ions has a negligible effect on the residual stress. In the present study, the work is extended to implants with ions of practical importance, namely nitrogen or a nickel-titanium dual implant in coatings made by both chemical and physical vapor deposition, CVD and PVD respectively, technologies. The coatings are in a state of low and high compressive residual stress respectively. Parallel beam glancing angle x-ray diffraction at incident angles in the range 0.5–10° is used to study the state of stress at depths of penetration in the range 0.1–1.6  $\mu$ m, before and after implantation. The effect of nitrogen implantation or the nickel-titanium dual implantation is discussed in this work. Further, the effect on the resulting data of using the x-ray elastic constants for titanium nitride in place of the bulk values is discussed.

[1] A. J. Perry, V. Valvoda, D. Rafaja, D. L. Williamson and B. D. Sartwell, Surf. Coat. Technol., 54/55 (1992) 180.

## VACUUM TECHNOLOGY

### Room BR4 - Session NP-WeP

#### New Products

**Moderator:** W. Weed, Sandia National Laboratories.

**NP-WeP2 Latest Developments on Valve Seat-Seal Assembly,** *R. De Villepoix, M. Lefrançois, J. Montuclard, C. Rouaud*, Carbone Lorraine/Céfilac-Etanchéité & Helicoflex Saint-Etienne, FRANCE/Columbia, SC USA.

The Helicoflex® metallic seal initially designed for static assemblies is presently used as a valve primary seal for some specific applications where the elastomeric seal commonly used in such configuration becomes totally unsuitable due to low resistance to radiation and high temperature, and incompatibility with ultra-high vacuum conditions.

The hydrogen injection quick valves on JET fusion reactor, as well as the aluminum ultra-high vacuum valves on TRISTAN accelerator already operate using this technique over a rather narrow range of working conditions.

In order to widen the field of applications and establish the basic principles of the sealing function applied to a valve seat-seal assembly, tests were carried out in the Sealing Techniques Laboratory of the French Atomic Energy Commission (CEA).

Seat configuration and seal holding device have been reconsidered. Seals have been tested using different grades of sealing lining material i.e. successively aluminum, silver and copper. In that respect, such assembly configuration was found in full compliance with the requirements of the new types of valve, those which are being considered for applications where ultra-high vacuum is combined with a leak rate requirement of  $1.10 \cdot 10^{-10} \text{ Pa} \cdot \text{m}^3 \cdot \text{s}^{-1}$  and a high bake-out temperature.

**NP-WeP3 Reliable In-Situ Gas Analysis for Aggressive Gas Processes,** *W. Eisinger*, Leybold Inficon Inc.

The Transceptor® AGM is a mass spectrometer designed for process monitoring of aggressive and reactive gas environments. It employs a patented gas shield sampling method (the Virtual Valve), minimizing the exposure of the sampling system and gas analyzer to reactive gases and particulates in the process vessel. The Virtual Valve uses a small stream of the process' carrier gas (typically 10 sccm) to shield the sampling orifice. A laminar flow of this gas creates a barrier in front of the sampling orifice, essentially stopping the flow of particulates and process gases into the mass spectrometer. To begin analysis the diverted flow of the gas is stopped.

Applications include CVD processes between .1 and 100 torr. Specifically, the Transceptor® AGM has been used to monitor impurities such as water and oxygen during a thermally activated LPCVD blanket tungsten process run of several wafers over 10 minutes at 40 torr. The process used tungsten hexafluoride (WF<sub>6</sub>) as the precursor, hydrogen (H<sub>2</sub>) as the primary reducing agent, silane (SiH<sub>4</sub>) as an initiator and argon (Ar) as a dilutant (also used as the shield gas).

The Transceptor AGM has demonstrated extended life in an extremely hostile environment, fast time response to follow rapid events (due to its close coupling to the process and absence of mechanical parts in the Virtual Valve), and detection limits for impurities in the ppb range; all of which contribute to reliable sampling in aggressive gas environments relative to conventional sampling techniques.

**NP-WeP4 Non-Reclosing Pressure Relief Device for Vacuum Systems,** *W. A. Swansiger*, Sandia National Laboratories, Livermore, CA 94550.

Many vacuum systems have components which cannot withstand pressures greater than 1 or 2 psig. Relief valves do not have the leak-

tightness required for high vacuum applications and existing rupture discs do not relieve at sufficiently low pressures. Sandia National Laboratories was recently granted a patent for a non-reclosing pressure relief device for vacuum systems that is UHV-compatible and relieves at precisely settable pressures ranging from 0.5 psig to 2 psig. The device consists of a welded metal bellows with conventional vacuum flanges on both ends. One end is attached to the vacuum system in a vertical position; the other end is closed by a thin metal membrane. A four-bladed cutter is positioned so that the extending bellows will drive the membrane into the cutter blade when the system reaches the desired relief pressure. Relief pressures above 0.5 psig can be set by adding weight to the bellows. This has the effect of increasing the reference pressure (normally atmospheric) and allows one bellows to be used for a range of pressures. The rupture element (a 0.001" thick stainless steel disc brazed to a copper Mini-Conflat™ gasket) can be easily and cheaply replaced without removing the device from the vacuum system and without altering the relief pressure of the device.

**NP-WeP5 New Compact Total Pressure Gauges,** *A. Schmid, R. Stocker*, BALZERS Limited, Vacuum Technology Instruments, FL-9496 Balzers, Liechtenstein.

The design criteria and applications of the new gauges are discussed. The new unique FullRange™ gauge is the combination of Pirani and cold cathode ionisation gauge with on-board electronic, giving lin/log voltage to pressure response with overrange, underrange and failure indication. This new compact gauge combines two gauges in one housing and provides significant advantages compared to conventional gauges:

- The salient feature is a linear voltage output as a function of the logarithmic pressure over the very large pressure range of 1000 to  $10^{-9}$  mbar without discontinuities.
- The user just needs one formula to easily convert from voltage to pressure in any desired unit.
- The rugged, space-saving compact design makes these intelligent gauges ideally suited for cost-saving integration into any computer-controlled vacuum system with no separate gauge controller required.
- The extremely low power consumption of max. 2 VA and the power range from 15 to 30 VDC without stabilisation allows multiple use in existing vacuum system with their own power supply.

The output includes in addition to the pressure readout an overrange, underrange and failure indication.

The gauge head design will be presented and the properties, such as the large measuring range, accuracy, up time, ultra small size and fail-safe construction will be discussed.

**NP-WeP7 Combination Valve Enables In-Situ Zeroing and Calibration of Capacitance Manometers,** *Jonathan Skuba*, HPS Division of MKS Instruments, Boulder, CO, *John Dunn*, MKS Instruments, Santa Clara, CA.

Thin film process repeatability involves the predictable control of a variety of parameters, including pressure measurement. As with most process and gauge technologies, proper use of capacitance manometers requires periodic verification to ensure calibration integrity. The In-Situ Diagnostics Access Valve (I.D.A. Valve™) from HPS Division of MKS Instruments is a compact, high conductance combination gauge isolation valve with a secondary, manually valved port for calibration and diagnostic access. The I.D.A. Valve™ fulfills the following: It functions as a gauge isolation valve. While isolated from the process chamber, the gauge may be zeroed or calibrated without its removal from the system, eliminating system dependent variables. With both valves open, leak check and system related diagnostics can be performed. Used regularly, the I.D.A. Valve™ reduces labor time requirements and enhances system uptime and availability.

## SURFACE SCIENCE

Room A205 - Session SS1-ThM

### Nanoscale Measurements

**Moderator:** J. E. Reutt-Robey, University of Maryland.

8:20 am **SS1-ThM1 Nanostructuring of Surfaces by Diffusion Controlled Growth**, *Klaus Kern*, Institut de Physique Expérimentale, EPF Lausanne, CH-1015 Lausanne, Switzerland.

We demonstrate a novel technique for the synthesis of densely packed planar nanostructures: diffusion controlled aggregation on surfaces. By exploiting the dependence of the mobility of adsorbed atoms on substrate crystal face and temperature, we are able to grow linear, two-dimensional compact or tenuous fractal aggregates of nanometer dimensions. The high number density ( $10^{11}$ – $10^{14}$  cm $^{-2}$ ) of these structures means that their physical and chemical properties can be easily measured with conventional surface spectroscopies. The underlying kinetic surface processes, like diffusion, nucleation and aggregation are discussed and their implication for selforganized two-dimensional growth is outlined.

INVITED

9:00 am **SS1-ThM3 Observation of Quantum Size Effects at Room Temperature on Metal Surfaces with the STM**, *Ph. Avouris, I.-W. Lyo and Y. Hasegawa\**, IBM Research Division, T. J. Watson Research Center, Yorktown Heights, NY 10598.

The study of the physics of electrons confined in low-dimensional structures, such as the two-dimensional electron gas (2DEG) systems provided by semiconductor heterostructure interfaces, is a very active area of research, the results of which have an important impact on basic science and technology.

A different, higher density 2DEG system is provided by electrons in Shockley metal surface states. Surface steps and adsorbates act as potential energy barriers reflecting the electron de Broglie waves. We use this property to confine the metal surface electrons in low-dimensional structures which, because of their size and stability, show quantum-size effects even at room temperature. The structures involve narrow terraces or single-atom-high islands and are formed by the deposition and annealing of metal films. A variety of different size and shape structures which are stable over a wide range of temperatures can be produced. Scanning tunneling spectroscopy is used to image the probability distributions of the confined states and determine their energies. The results allow us to estimate the confining barriers and provide evidence for the existence of 1D step-edge states. Steps and point defects are also found to mix surface and bulk states and lead to the scattering of surface electrons to bulk states, limiting the extent of confinement.

The charge-density distributions and field-gradients of the confined states formed during film growth are different from those at an extended terrace. These factors are likely to influence surface processes that depend on them, such as the sticking, diffusion and spatial distribution of adatoms and the growth of islands.

\*Present address: Mesoscopic Materials Center, Kyoto University, Kyoto 606-01, Japan.

9:20 am **SS1-ThM4 STM of Thin Film MgO Grown on Mo(001)**, *M. C. Gallagher, M. Fyfield, James P. Cowin, and S. A. Joyce*, Molecular Science Research Center, Pacific Northwest Laboratory,\* Richland, WA 99352.

Recently the surface properties of metal oxides have attracted a great deal of attention. The rocksalt crystal structure and the single valence of the Mg ion makes MgO an attractive model system. Although Scanning Tunneling Microscopy is a powerful probe of surfaces, the technique is restricted to conducting samples. One approach to extend STM to insulating materials is to study well defined thin films on metal substrates. To this end we have used *in-situ* STM to investigate the growth and electronic properties of MgO thin films deposited on Mo(001). The films were grown by evaporating Mg metal in a background pressure of oxygen.<sup>1</sup> Correct stoichiometry of the films was ensured using Auger electron spectroscopy. To date we have successfully studied films as thick as 25 Å clearly demonstrating the feasibility of this method. Growth temperatures from room temper-

ature to 750°C have been studied. Drastic changes in film morphology were observed. Films grown at 750°C exhibited a higher degree of microscopic roughness than those grown at room temperature. Post growth annealing reduced the overall roughness. Quantitative results for films grown under a range of growth conditions will be presented.

1. M.-C. Wu, J.-S. Corneille, C. A. Estrada, J.-W. He, & D. W. Goodman, *Chem. Phys. Lett.* 182, 472 (1991).

\* Pacific Northwest Laboratory is operated for the U.S. Department of Energy by Battelle Memorial Institute under contract DE-AC06-76RLO 1830.

9:40 am **SS1-ThM5 Nanosphere Lithography**, *John C. Hulteen and Richard P. Van Duyne*, Department of Chemistry, Northwestern University, Evanston, IL 60208.

The fabrication of nanoparticles with diameters,  $d_p < 100$  nm, is usually carried out by e-beam and/or x-ray lithography. In this presentation, we discuss the implementation of an inherently parallel nanofabrication technique based on the self-assembly of polymer colloid nanospheres. This process is termed nanosphere lithography (NSL). Using NSL, periodic particle arrays (PPAs) of Ag and Au on freshly cleaved mica substrates have been fabricated with particle diameter,  $20 \text{ nm} < d_p < 200 \text{ nm}$  and interparticle spacing,  $d_{ip} \sim 6d_p$ . PPAs with tunable structural characteristics  $d_p$ ,  $d_{ip}$ , and particle height,  $h$ , can be fabricated by: (i) varying nanosphere diameter,  $D_{sp}$ ; (ii) angle,  $\theta$ , between collimated vapor deposition beam and the nanosphere mask surface normal; and (iii) mass thickness,  $D_m$ , of particle material,  $M$ . The structural characteristics of NSL-derived PPAs are determined by atomic force microscopy (AFM). It will be shown that the standard deviations of  $d_p$  and  $d_{ip}$  histograms are entirely determined by the original size distribution of  $D_{sp}$  (viz.,  $\leq 2\text{--}3\%$ ). NSL processing is essentially independent of the choice of  $M$  and substrate material,  $S$ . Any  $M$  capable of gas phase introduction and any  $S$  on which nanospheres will coherently self-assemble may be used. Preliminary optical property vs. particle size investigations have been carried out using UV-VIS absorption spectroscopy and surface-enhanced Raman excitation spectroscopy (SERES) demonstrating that these properties are extremely sensitive to  $d_p$ ,  $d_{ip}$ ,  $h$ , and particle shape.

INVITED

10:00 am **SS1-ThM6 Nanofabrication on Electron Beam Resist Using Scanning Tunneling Microscopy**, *M. H. Nayfeh, A. Archer, J. M. Hetrick, and I. Adesida*, University of Illinois at Urbana-Champaign, Urbana, Illinois 61801.

Recently, techniques have been developed which use a scanning tunneling microscope (STM) as a tool to fabricate nanometer-scale structures. Using electron beam resist in the nanometer-scale fabrication of structures has the potential for pattern transfer, since resists exposed to electrons can be developed and used as masks for further processing. Standard electron beam lithography on resist at energies of approximately 50 KeV has already been used for the fabrication of structures in the nanometer range, yielding line widths of approximately 95 nm. Investigations of STM fabrication on electron beam resist by Marrian et al. have already shown that this technique has potential in both the achievable resolution and the dimensions of the fabricated structures. We report here the results of nanofabrication using a scanning tunneling microscope on silicon coated with SAL 601 electron beam resist. The resist was exposed to an electron beam with a range of energies between 1 and 50 eV approximately. The results of this exposure were found to be complex, switching over from producing structures that appear as mounds to structures that appear as grooves as the biasing voltage drops below 6 V. Mound-like structures of width as small as 18 nm with a 2 nm corrugation, and structures like grooves as small as 15 nm in width and 0.5 nm in depth were fabricated. Somewhat narrower but shallower structures can be produced in the resist, but we believe that these results are reaching the practical limit of fabrication. If pattern transfer can be achieved, STM-based techniques will be able to compete and even surpass the capabilities of more conventional approaches.

INVITED.

10:20 am **SS1-ThM7 Nanometer-Scale STM Electrochemical Syntheses of Electronic Materials**, *W. Li, J. Zoval, J. A. Virtanen, and R. M. Penner*, ISIS, Dept. of Chemistry, University of California, Irvine, 92717-2025.

Metals (e.g., Ag, Cu, Cd), semiconductors (e.g., CdSe), and organic



conductors (e.g. TTF-Br) have been synthesized in single nanoscopic batches on the van der Waals surfaces of graphite and the semiconductor MoS<sub>2</sub> using the scanning tunneling microscope (STM). The synthesis reaction is localized at a shallow, circular pit approximately 100 Å in diameter which is induced by the application of a 4–6 V bias pulse—applied between the STM tip and the surface while tunneling—with a duration of  $\approx 2$   $\mu$ sec. This pulse can be extended to longer times (from 3–50  $\mu$ sec), generally at a lower amplitude ( $\approx 300$  mV–3V), to effect the electrochemical synthesis reaction of interest which then occurs selectively in the freshly formed pit. The dimensions of the synthesized products are typically 100–500 Å in diameter and 20–100 Å in height. The characterization of the deposited materials is accomplished using TEM e<sup>−</sup>-diffraction, scanning Auger microprobe elemental analysis, and laser-induced fluorescence (for semiconductor nanostructures) in addition to STM. *In-situ* STM investigations of nanostructure reactivity and chemical passivation will be reported.

INVITED.

11:00 am **SS1-ThM9 Self-Assembled Monolayers of Pendant Monomers: A Basis for Fabrication with the Scanning Tunneling Microscope**, R. J. Willicut and R. L. McCarley, Department of Chemistry, Louisiana State University, Baton Rouge, Louisiana 70803.

We are interested in nanofabrication with the STM using well-defined electrochemical reactions on surfaces. Our approach is to attach monomeric species onto smooth surfaces and polymerize them using the STM. We describe here the synthesis and characterization of a series of electropolymerizable monomers which are covalently attached to electrode surfaces via self-assembly. We have taken advantage of the well-known interaction of organothiols with Au and Pt surfaces in order to form monolayers of N-( $\omega$ -mercaptoalkylthiol)pyrroles on solid electrodes. The voltammetry of the surface-confined pyrroles in various electrolyte systems will be presented in order to establish whether or not electrolyte penetration into the monolayer occurs and what effects monolayer disordering have on possible coupling reactions between neighboring pyrrole sites. Investigations of orientational and chain length effects will also be presented. The adhesion of poly(pyrrole) films to the electrode surface has been increased dramatically by use of the monomer monolayers. We will also present SEM and  $\mu$ m images of poly(pyrrole) films deposited on the monolayers.

INVITED

11:20 am **SS1-ThM10 STM-Induced Etching of Ultra-thin Organic Resists: Structure, Mechanism, and Post-etching Elaboration**, J. K. Schoer and R. M. Crooks, Department of Chemistry, Texas A&M University, College Station, TX 77843-3255; T. Corbit and M. J. Hampden-Smith, Department of Chemistry, University of New Mexico, Albuquerque, NM 87131.

We have prepared ultra-thin organic resists by spontaneous adsorption of organomeraptan molecules onto Au (111) substrates. The resists can be patterned by scanning tunneling microscopy (STM). To better understand the resist etching mechanism, we varied the tip bias, tunneling current, resist composition, duration of exposure, scan rate, and the environmental conditions. The results indicate that organomeraptan monolayers form excellent STM resist materials. However, we found a strong dependence of etching efficiency on the applied tip bias. For example, we observed a distinct bias threshold below which etching did not occur. The tunneling current, resist composition, and other variables also affect the pattern formation, but less dramatically. In addition to fabrication and characterization of patterns as small as 10 nm, we have also recently shown that patterned surfaces can be further elaborated by subsequent selective Cu chemical vapor deposition. Results of these studies will also be discussed.

11:40 am **SS1-ThM11 NEXAFS Spectroscopy, A Tool for Studying Metal-Organic Molecule Interfaces**, G. Tourillon, LURE-Bât. 209D, 91405 Orsay, France.

The interaction of unsaturated molecules with a metallic surface is of great interest both from a theoretical point of view (charge-transfer mechanisms between the substrate and the compound, modifications of the molecular orbital distribution) and from a practical point of view (surface chemistry, catalysis). A considerable amount of work has thus been devoted to the adsorption of benzene, pyridine, CO or ethylene on various substrates. However questions regarding i) the nature of the interaction and/or the chemical bond between the organic compound and the metal and ii) the organization of the monolayer on the surface need a better knowledge. Near edge X-ray absorption fine structure spectroscopy (NEXAFS) is well adapted to probe these parameters, since it allows the determination of the unoccupied density

of states, the bond lengths and the orientation of the organic molecule. Our aim here is to get a better understanding of the chemical structure influence of ethylenic derivatives on the interactions modes with platinum, particularly when a hydrogen atom is replaced by an acidic, ester or aldehyde function (acrylic acid: CH<sub>2</sub>=CH-COOH), acrolein (CH<sub>2</sub>=CH-CHO) and methylmetacrylate (CH<sub>2</sub>=C(CH<sub>3</sub>)-COOCH<sub>3</sub>). When a monolayer of acrylic acid is adsorbed on Pt(111) at 95K, the C K edge NEXAFS spectra reveal that i) the molecule is flat on the surface and ii) interacts strongly with a di- $\sigma$  configuration (hybridization effects between the  $\pi$  orbital and the Pt d band, formation of Pt-C bond). Similar results are obtained with methylmetacrylate. On the contrary acrolein in physisorbed on Pt (111) at 95K, the molecule lying parallel to the surface. These differences in the interactions modes must be linked to a more or less important delocalization of the C=C  $\pi$  orbital with the chemical group which induces molecular levels able or not to hybridize with the Pt d band. XPS, UPS and theoretical multiple scattering calculations will be presented to support the NEXAFS results.

## SURFACE SCIENCE

### Room A201 - Session SS2-ThM

#### Surface Interactions

**Moderator:** D. N. Belton, General Motors Research and Development Center.

8:20 am **SS2-ThM1 Coadsorption of Alkalis and Hydrogen on W(100)**, W. Hago\* and P. J. Estrup, Department of Chemistry, Brown University, Providence, Rhode Island 02912.

Substrate reconstruction is known to be essential to understanding the structure and desorption features of H/W(100) and H/Mo(100), as well as the effective repulsion of coadsorbed H and O on W(100) and Mo(100). Similar effects are expected for other coadsorbates on these surfaces. In the present study we have investigated the effect of substrate distortions on the interactions between alkalis (Li, Na and K) and hydrogen on W(100). We have examined the desorption, work function and LEED behavior of the coadsorbed systems Li + H/W(100), Na + H/W(100), and K + H/W(100). We find that the desorption energy of the most strongly bound state of hydrogen is raised by 500, 100 and 0 meV in the presence of Li, Na and K, respectively. We deduce from the work function behavior that alkalis significantly reduce the effective dipole moment of hydrogen on the surface. LEED observations reveal that alkalis strongly affect the surface phases of H/W(100), except in the case of Na. For the systems Li + H/W(100) and Na + H/W(100), the substrate does not significantly alter the adatom interactions. For K + H/W(100), a strong effect is seen. Contrary to expectations, for all three coadsorbed systems, we find evidence of attractive interactions between the alkalis and hydrogen at early coverages.

\*Present Address: Department of Chemical Engineering, University of California, Santa Barbara, California 93106.

8:40 am **SS2-ThM2 Comparative HREELS Study of H and CO on Pt(335)**, Hong Wang<sup>a</sup>, R. G. Tobin<sup>a</sup>, David K. Lambert<sup>b</sup>, Galen B. Fisher<sup>c</sup>, and Craig L. DiMaggio<sup>c</sup>, <sup>a</sup>Dept. of Physics and Astronomy and CFMR, Michigan State University, East Lansing, MI 48824-1116, <sup>b</sup>Physics Department, <sup>c</sup>Physical Chemistry Department, General Motors R&D Center, Warren, MI 48090-9055.

The interactions of CO and H on Pt surfaces affect the operation of catalytic converters, exhaust gas sensors and fuel cells. We studied the coadsorption of CO and H on Pt(335) [Pt(s)[4(111) × (100)]] by high resolution electron energy loss spectroscopy and temperature programmed desorption. Both CO and H adsorb preferentially at edge sites. Along the edge, islands of mixed H and CO coexist with regions of pure CO, in sharp contrast with the complete segregation found on the structurally similar Pt(112) surface. These results suggest a dependence of the CO-H indirect interaction on terrace width. Within the mixed islands coadsorbed H locally shifts atop CO to bridge sites; at saturation H coverage the shift is almost complete. On the terrace, however, the intensity and frequency of the atop CO vibration are unaffected by coadsorbed H. The EELS cross sections of bridge and



atop CO on the step edge are equal, whereas on Pt(111) atop CO's cross section is 1.8 times larger than that of bridge CO.

Supported in part by the Petroleum Research Fund and NSF Grant No. DMR-9201077.

9:00 am **SS2-ThM3 The Adsorption of Hydrogen to the NiAl(110) Surface**, *Aubrey T. Hanbicki*, Univ. of Pennsylvania, *E. W. Plummer*, Univ. of Tennessee and Oak Ridge National Laboratory,<sup>†</sup> and *A. P. Baddorf*, Oak Ridge National Laboratory.<sup>†</sup>

Dissociative adsorption of molecular hydrogen at a metal surfaces requires d-holes.<sup>1</sup> The (110) surface of the bimetallic alloy NiAl, a rippled surface terminated with 50% Ni and 50% Al, provides a rigorous test for this theory as its d-bands are filled while those of elemental Ni are not. Although molecular hydrogen dissociatively adsorbs on Ni, this is not the case for NiAl(110) above 110 K, indicating that an activation barrier for dissociation is present. Predissociated hydrogen will adsorb on this surface and desorbs as H<sub>2</sub> between 280 K to 300 K, lower than from either Ni or Al, with desorption occurring through second order kinetics. At higher coverages, a low frequency vibration, seen with electron energy loss spectroscopy, is assigned to a hydrogen mode. This assignment is corroborated by an isotopic shift with deuterium. The low frequency of this mode indicates a high coordination site, probably involving both surface species. Hydrogen also modifies the substrate vibrations, inducing the surface optical phonon to shift up in energy from the center to the top of the bulk band gap, and increasing the surface resonance cross section. A  $c(2 \times 2)$  periodicity is seen with LEED with weak fractional order spots suggesting a hydrogen superstructure. Coverage measurements using nuclear reaction analysis, and a structural analysis using x-ray diffraction are intended.

<sup>†</sup>Managed by Martin Marietta Energy Systems, Inc. under U.S. Department of Energy contract DE-AC05-84OR21400.

<sup>1</sup>J. Harris and S. Andersson, *Phys. Rev. Lett.* 55 (1985) 1583.

9:20 am **SS2-ThM4 Thermal Desorption Studies of High-Coverage Hydrogen Overlayers Created with Gas-Phase Atomic Hydrogen on Ru(001)\***, *T. A. Jachimowski*, *B. Meng*, *D. F. Johnson*, and *W. H. Weinberg*, Department of Chemical Engineering, University of California, Santa Barbara, CA 93106.

The adsorption and desorption of high-coverage hydrogen overlayers on Ru(001), created at 100 K using gas-phase atomic hydrogen, has been investigated using thermal desorption mass spectrometry. Hydrogen surface coverages up to 1.42 hydrogen adatoms per primitive Ru(001) unit cell have been obtained, in excess of the saturation coverage of unity obtained by dissociative chemisorption of molecular hydrogen. Furthermore the desorption spectra are characterized by a peak, previously present for dissociative adsorption of molecular hydrogen, which increases in area but does not change in peak temperature (320 K) for coverages greater than unity. Impinging gas-phase atomic hydrogen (deuterium) was also found react with chemisorbed deuterium (hydrogen) and desorb molecularly. The abstraction of surface hydrogen by gas-phase atomic hydrogen occurs at more than 150 K below the associative thermal desorption temperature of hydrogen from this surface. The ratio of the cross section for abstraction to the cross section for adsorption was found to be 0.4. These experimental results suggest that the abstraction reaction is occurring via an Eley-Rideal mechanism.

\*Work supported by the National Science Foundation (grant CHE-930020).

9:40 am **SS2-ThM5 The Adsorption of Hydrogen on the Mo<sub>0.75</sub>Re<sub>0.25</sub> (100), (110), and (111) Surfaces**, *M. Okada*, The University of Tennessee, Knoxville, TN, and *D. B. Poker* and *D. M. Zehner*, Oak Ridge National Laboratory,\* Oak Ridge, TN 37831-6057 USA.

From low-energy electron diffraction (LEED), low-energy ion scattering, and surface core-level photoemission results, it is known that the relative distribution of Mo and Re in the outermost layers of the (100), (110), and (111) surfaces of the random alloy Mo<sub>0.75</sub>Re<sub>0.25</sub> is orientation dependent. As a consequence, there is a distribution of inhomogeneous arrangements of both species that participate in any adsorption process. The adsorption of hydrogen (deuterium) has been studied with LEED, thermal desorption spectroscopy (TDS), and nuclear reaction analysis to investigate this distribution. Following ex-

posure to H<sub>2</sub>, only (1 × 1) patterns are observed with LEED for all coverages, indicating no adsorbate-induced reconstruction. Using deuterium and the D(<sup>3</sup>He,p)<sup>4</sup>He reaction, the saturation coverages for the (100), (110), and (111) surfaces were determined to be 2.0, 1.0, and 2.9 respectively. A coverage of 2.0 for the (100) surface is in excellent agreement with a model determined with a LEED-IV analysis in which all bridge sites on the predominantly Mo terminated surface are occupied at saturation coverage. The TDS spectra from the saturated (110) and (111) surfaces show two peaks, whose relative intensities are different. These may correspond to desorption from inhomogeneous rich Mo and Re regions respectively, providing additional evidence for excess Re in the outermost layer of the (110) surface. Exposure of the clean surfaces to atomic deuterium results in the same set of observations with no indication of absorption into the bulk.

\*This work is supported by the U.S. Department of Energy, under contract DE-AC05-84OR21400 with Martin Marietta Energy Systems, Inc.

10:00 am **SS2-ThM6 Separating Ensemble and Electronic Effects on Bimetallic and Alloy Surfaces**, *Chen Xu* and *Bruce E. Koel*, Department of Chemistry, University of Southern California, Los Angeles, CA 90089-0482.

We have recently compared the chemistry of ordered surface alloys formed by Sn on Pt(111) and Ni(111) surfaces. CO adsorption is strongly suppressed on the  $(\sqrt{3} \times \sqrt{3})R30^\circ$  Sn/Ni(111) surface alloy, with  $\Theta_{\text{Sn}} = 0.33$ . Only 0.04 ML CO is adsorbed at 110 K, exclusively at atop sites with a binding energy of only 15 kcal/mol. These results are in sharp contrast to those for CO adsorption on the  $(\sqrt{3} \times \sqrt{3})R30^\circ$  Sn/Pt(111) surface alloy, where a similar saturation coverage, adsorption site population, and adsorption energy to that on Pt(111) was observed. These Ni-Sn and Pt-Sn alloys are isostructural in two dimensions, but have different buckling distances for the Sn atoms with respect to the surface plane. We attribute the dramatic differences in the chemistry of these similar surfaces to the vertical position of the Sn in the surface layer. The balance between direct interactions of Sn with adsorbed molecules and the interactions of the transition metal atoms with adsorbed molecules controls the effectiveness of Sn as a site-blocking surface modifier, and this balance is affected by the vertical position of the Sn. These results reveal new insight into the influence of surface modifiers on chemical reactions at surfaces and force us to reevaluate simple concepts of site-blocking and ensemble sizes on alloy surfaces.

10:20 am **SS2-ThM7 Adsorption of Sulfur on Bimetallic Surfaces\***, *M. Kuhn* and *J. A. Rodriguez*, Chemistry Department, Brookhaven National Laboratory, Upton, NY 11973.

The coadsorption of S and a noble metal (Cu, Ag or Au) on Ru(001) has been investigated using LEED, TDS, XPS and XAES. The Au<sub>a</sub> ↔ S<sub>a</sub> and Ag<sub>a</sub> ↔ S<sub>a</sub> interactions are repulsive. In the Au/S/Ru(001) system, the Ru-noble metal bond is stronger than the Ru-S bond, and the presence of Au leads to a significant change in the kinetics of sulfur desorption. On Ru(001) sulfur desorbs in a flat feature between 1100 and 1500 K, whereas on Au/Re(001) a sharp desorption peak is seen at 1100 K. The Au atoms compress S into 2D islands, keeping the local coverage of S large. In the Ag/S/Ru(001) system, the Ru-S bond is stronger than the Ru-noble metal bond, and the presence of S reduces the desorption temperature of Ag from Ru(001) by almost 150 K. Results of XPS and XAES indicate that sulfur and copper atoms coadsorbed on top of Ru(001) react to form a sulfide. The Cu atoms in this compound exhibit as CO-desorption temperature smaller than those of Cu/Ru(001) or pure Cu.

\*This work was supported by the US Department of Energy (DE-AC02-76CH00016).

10:40 am **SS2-ThM8 'Nanocatalysis' by the Tip of a Scanning Tunneling Microscope Operating Inside a Reactor Cell**, *B. J. McIntyre*,<sup>1</sup> *Uwe Schröder*,<sup>2</sup> *M. Salmeron*,<sup>1</sup> and *G. A. Somorjai*,<sup>1,11</sup> Lawrence Berkeley Laboratory and Department of Chemistry, University of California, Berkeley, CA 94720, USA, <sup>2</sup>Institut für Physikalische Chemie der Universität Bonn, Wegelerstr. 12, 53115 Bonn, Germany.

The platinum tip of a Scanning Tunneling Microscope that operates inside an atmospheric pressure chemical reactor cell, has been used to locally rehydrogenate carbonaceous fragments deposited on the surface of Pt(111). The Pt tip acted as a catalyst after activation by short voltage pulses when in atmospheric pressures of hydrogen. In this active state the clusters in the area scanned by the tip were reacted

away with nanometer spatial resolution. This effect did not occur when using gold tips, or in CO environments. The tip catalysis was observed to be strongly dependent upon tip proximity to the surface, extent of hydrocarbon decomposition, reactant gas composition and reactant gas pressure.

11:00 am **SS2-ThM9 SPA-RHEED—Spot Profile Analysis for *in situ* Characterization**, B. Müller and M. Henzler, University of Hannover, Appelstr. 2, D-30167 Hannover, Germany.

The morphology of the surface dominates the quality of the epitaxial growth. In order to tailor low dimensional artificial structures the surface must be characterized during growth. One of the most powerful methods for *in situ* studies is RHEED. The quantitative analysis on island sizes and step distributions, however, is mainly performed by LEED because of the more complicated geometry of RHEED and the influence of inelastic scattering. To overcome these difficulties, a novel RHEED instrument with extremely high angular resolution (0.1 mrad) and energy resolution of about 2 eV is developed. For the first time the SPA-RHEED instrument points out the important contribution of inelastic processes to the intensity distribution of the spot profiles. Electronic losses due to plasmons and band transitions are clearly detected and quantitatively described by the dipole scattering theory. A meaningful evaluation of the profiles with respect to defects is only possible with a good energy resolution. For well prepared Si(111) with various island sizes in different azimuths the elastic and inelastic scattering is investigated throughout several Brillouin zones. Mean terrace sizes between 50 and 5000 Å are detected. Characteristic structures are correlated with the scattering vectors and are separated into surface and bulk related phenomena because of the refraction effect. The extremely high angular resolution of SPA-RHEED enables determination of island size up into the micrometer range and lattice constants with an accuracy <0.1%. Surface damage is reduced due to the extremely low current. Therefore the features of the SPA-RHEED instrument offer new applications for RHEED.

11:20 am **SS-ThM10 Experimental and Numerical Investigation of Ignition Conditions of H<sub>2</sub>/O<sub>2</sub> Mixtures on Pt**, M. Rinnemo,<sup>1</sup> O. Deutschmann,<sup>2</sup> P. Ahlström,<sup>1</sup> F. Behrendt,<sup>1,2</sup> and B. Kasemo,<sup>1</sup>  
<sup>1</sup>Department of Applied Physics, Chalmers University of Technology and University of Göteborg, S-41296 Göteborg, Sweden, <sup>2</sup>Universität Stuttgart, Institut für Technische Verbrennung, Pfaffenwaldring 12, D-70569 Stuttgart, Germany.

Catalytic ignition is the sudden transition in a catalytic reaction from kinetic control to mass transport control. Its description requires a detailed knowledge of both the elementary reactions steps on the surface as well of the transport processes between surface and gas phase.

In the experiment mixtures of hydrogen and oxygen, diluted with nitrogen and flowing slowly at atmospheric pressure, were ignited by a resistively heated platinum wire. Temperature vs. time traces were recorded for a wide range of compositions. Such data have been used [1] to verify the Frank-Kamenetskii [2] criterion for ignition, which states that at this point the derivatives of the dissipated chemical power and of the heat loss, respectively, become equal. In this work we have investigated further the ignition condition, and in addition the transient behaviour after ignition until a new equilibrium is established.

The experimental results are compared with detailed numerical simulations. For this purpose a code simulating laminar reactive flows above catalytically active surfaces is applied to the experimental conditions. The chemical reactions in the gas phase as well as on the surface are described using a mechanism consisting of elementary reaction steps. Experimentally found ignition behaviours are compared with numerical results. Additionally, the evolution of surface coverages and gas phase gradients with time is discussed. The comparison elucidates the complex interaction between surface and gas phase kinetics.

[1] M. Rinnemo, M. Fassihi, and B. Kasemo, Chem. Phys. Lett. 211, 60–64 (1993).

[2] D. A. Frank-Kamenetskii: "Diffusion and Heat Transfers in Chemical Kinetics, 2nd edition, Plenum Press, New York (1969)."

11:40 am **SS2-ThM11 The Synthesis of Ammonia on Ru(0001)**, P. A. Taylor and E. Törnqvist, Haldor Topsøe Research Laboratories, DK-2800 Lyngby, Denmark.

Ruthenium based catalysts have been subject to several studies as an alternative to the traditional iron ammonia catalyst [1]. In this work the synthesis of ammonia over Ru(0001) has been studied in a combined high pressure/ultrahigh vacuum (UHV) system. The Ru(0001) crystal

was cleaned and characterized in UHV using conventional surface science techniques. Once clean, the crystal was placed into a high pressure cell (HPC) contained within the UHV chamber, where the design pressure of the HPC is 10 bar. A controlled leak from the HPC to a quadrupole mass spectrometer made it possible to monitor the gas composition during synthesis. The concentration of ammonia was measured as a function of crystal temperature and total pressure, both under static and flow conditions. In the temperature range of 573–673 K (at 9 different temperatures), the overall activation energy for ammonia synthesis was measured to be 128 kJ mol<sup>-1</sup> in a stoichiometric (N<sub>2</sub>/3H<sub>2</sub>) gas-mixture at 2 bar. After synthesis, the only detectable adsorbed species was nitrogen. The presence of low concentrations of water during ammonia synthesis had no measurable effect on the measured rates. Adsorbed sulfur, however, acts as a poison blocking approximately 6 active surface sites. The promotional effects of adsorbed potassium will also be reported. The results provide essential information needed to construct a micro-kinetic model for the synthesis of ammonia over ruthenium.

[1] A. Ozaki and K. Aika, in: Catalysis, Science and Technology, (Eds. J. R. Anderson and M. Boudart), Springer-Verlag, New York (1981) pp. 87–158.

## NANO 3/NANOMETER-SCALE SCIENCE AND TECHNOLOGY/BIOMATERIAL INTERFACES Room A209 – Session NSBI-ThM

### Biology at the Nanoscale: II

Moderator: S. Lindsay, Arizona State University.

8:20 am **NSBI-ThM1 Molecular Recognition Between DNA Base Pairs by AFM**, B. D. Ratner, T. Boland, Department of Chemical Engineering and Center for Bioengineering, University of Washington, Seattle, WA 98195.

Small, planar aromatic molecules such as purines and pyrimidines are systems that exhibit spontaneous self-assembly on gold surfaces. The self-assembly processes have been investigated by STM, AFM, ESCA, Static SIMS, and TPD characterizations of the organic systems corroborate the observations. At equilibrium, ordered monolayers of molecules in an edge on conformation were observed for most systems. A lone nitrogen pair is chemisorbed to the surface, and molecules are interacting through mutual  $\pi$ -base stacking to yield lateral stability. To probe if these biological monolayers exhibit similar molecular recognition capabilities as in living organisms, the four DNA bases were self-assembled onto gold coated AFM tips and flat gold surfaces that were then allowed to interact. Only when complementary bases are assembled on tip and surface, the AFM detects additional forces that are absent for bare gold samples or assemblies of noncomplementary bases. This additional, attractive force is attributed to hydrogen bonding, and can be used as a qualitative indicator of molecular recognition. Force curves and recognition AFM images will be shown. Quantitative statistical analysis of the measured forces will be presented. Finally, a strategy for patterning surfaces with DNA bases and subsequently recognizing the pattern and its relevance to DNA sequencing and biological sensors will be discussed.

8:40 am **NSBI-ThM2 Direct Measurement of the Interaction Forces Between Complementary Strands of DNA with the Atomic Force Microscope**, G. U. Lee, L. A. Chrisey,<sup>#</sup> and R. J. Colton, Chemistry Division, Code 6177 and <sup>#</sup>Center for Bio/Molecular Science and Engineering, Code 6900, Naval Research Laboratory, Washington, DC 20375-5342 USA.

We have used an Atomic Force Microscope (AFM) to measure directly the binding interaction associated with Watson-Crick base pairing between single strands of DNA that have been immobilized on the surfaces of the AFM probe and substrate. The binding interaction is measured by first bringing the two surfaces together, allowing the molecules to interact, and then separating them. The measurements are conducted in solution to maintain bioactivity of the molecules and reduce nonspecific surface forces. Two different experiments are performed: a direct assay in which oligonucleotides are immobilized on opposing surfaces and a sandwich assay in which a homopolynucleotide is placed between opposing surfaces that are covered with its complement. The first experiment revealed strong adhesive forces (~1.6

nN) only when the base sequences of the oligonucleotides are complementary. The magnitude and distribution of the rupture forces are consistent with single molecule interactions. In fact, a direct correlation is observed between rupture force and the number of base pairs in the double-helix. The addition of the homopolymer did not change the magnitude of the adhesive force but increased the distance (up to 400 nm) between the surfaces at which the bond rupture occurs. As the surfaces are separated an exponentially increasing force is required to elongate the molecule resulting in the measure of the molecule's elasticity. These results demonstrate that the AFM can measure inter- as well as intra-molecular forces in complex macromolecular systems.

**9:00 am NSBI-ThM3 Scanning Probe Microscopic Visualization of Electrostatically Immobilized Intercalating Drug-Nucleic Acid Complexes, L. A. Bottomley, J. E. Coury, G. Gardner, E. A. Handley and L. D. Williams, School of Chemistry & Biochemistry, Georgia Institute of Technology, Atlanta, GA 30332-0400 USA.**

DNA intercalators are small molecules which insert between the base pairs of the DNA double helix. Intercalation into DNA necessarily results in radical changes in DNA conformation, separating base pairs along the helical axis. Thus, intercalators are of great importance as probes of nucleic acid structure and as interferents or inhibitors of DNA replication, transcription and/or topoisomerase activities. Relationships between structures of intercalators and conformations of intercalated DNA complexes are subtle and unresolved. Intercalating drug molecules have been synthesized incorporating markers easily distinguishable by STM and AFM. Specifically designed psoralen and methidium bromide derivatives have been intercalated into DNA. Scanning tunneling and atomic force micrographs were obtained following electrostatic immobilization of the complexes onto chemically modified gold or mica surfaces. To facilitate recognition of the point of intercalation, the psoralen and methidium derivatives were covalently linked to biotin and then exposed to streptavidin-coated colloidal gold beads. The effects of intercalation on the tertiary structure of DNA will be presented. Comparisons will be made between the structures determined by AFM and STM to those determined crystallography.

**INVITED**

**9:40 am NSBI-ThM5 Sequence Effects in the Images and Bonding of Single Stranded DNA on Au(111) Observed by Electrochemical STM, Y. Lyubchenko, Dima Rekes, T. W. Jing and S. M. Lindsay, Department of Physics and Astronomy, Arizona State University, Tempe, AZ 85287.**

STM images of the adsorption process of the complementary nucleic acid oligomers 5'-CCCCCTTTTCCCCCTTTT and 5'-AAAAAGGGGGAAAAAGGGGGG on Au(111) show that it is strongly dependent on sequence. The polypyrimidine adsorbs readily without potential control, even onto electrodes that are slightly negative of the potential for zero charge. The adsorption process for the polypurine is similar to what we have found for random sequence DNA, requiring a positive charge on the electrode and co-adsorption of a small anion.

The images of the spontaneously adsorbed polypyrimidine and the electrochemically adsorbed polypurine are very different, but when the polypyrimidines are electrochemically adsorbed, their STM images are similar to those of the polypurines adsorbed in the same conditions. The images of both polymers are fitted by a base-stacked helix with a pitch of 3 to 4 nm. In contrast, the polypyrimidines adsorbed near the potential for zero charge give images that are fitted by an elongated helix with a pitch of 6 to 9 nm. This interpretation is confirmed by images which show a single molecule transforming from the elongated phase to the compacted phase. The transformation is followed by an azimuthal rotation of the molecule so that its alignment on the substrate is identical to that of its neighbors. These transitions may be a consequence of the changes in screening of the phosphate backbone as the effective ionic strength at the electrode surface is changed by altering the electrode potential.

This work was supported by grants 1R21 HG00818-01A1 from the National Institutes of Health and N00014-90-J-1455 from the Office of Naval Research.

**10:00 am NSBI-ThM6 Imaging Polyten Chromosomes with the Atomic Force Microscope, Daniel M. Jondle, Linda Ambrosio, James Vesenska & Eric Henderson, Department of Zoology and Genetics, Iowa State University, Ames, IA 50011.**

Polytene chromosomes from the salivary glands of *Drosophila melanogaster* have been examined under a combined inverted fluorescence/atomic force microscope (AFM). This study revealed a

correlation between the banding pattern apparent by fluorescence microscopy and topographic features resolved by the atomic force microscope (Fig. 1). Since the banding pattern correlates with the distribution of genes on the chromosome, the AFM can be used to identify genetic loci. The AFM resolved chromosomal sub-structure down to the limits of the tip sharpness, about 300 Å, far greater than the resolution limit of conventional optical microscopes. Attempts to improve resolution of chromosomes in the AFM using electron beam deposited tips with high aspect ratios are ongoing. High resolution AFM images of chromosomes can be obtained under physiologically relevant buffered media, suggesting that dynamics of chromosome condensation or decondensation may be observed. Previously unseen furrows within the compacted banded regions of chromosomes have been imaged and may correlate to delineations of specific genes. The utility of the AFM as a precise dissection tool on unfixed specimens will be discussed.

**10:20 am NSBI-ThM7 The Topology of Supercoiled DNA by SFM Imaging, Bruno Samori, Carmelo Nigro, Innocenzo Muzzalupo, Giampaolo Zuccheri, Carla Quagliariello, University of Calabria, Arcavacata di Rende, 87030 Italy.**

Agarose gel electrophoresis provides a means for separating single topoisomers from a population of supercoiled pBR322 DNA molecules. The DNA electroeluted from a single electrophoretic band is constituted of molecules with the same linking deficit ( $\Delta Lk$ ). Molecules with relatively high and low linking deficits are obtained from electrophoresis of native supercoiled and topoisomerase relaxed pBR322 molecules.

We image single topoisomers with known  $\Delta Lk$ . The analysis of the topologically equivalent molecules extracted from the gel gives insight on the equilibria in which supercoiled DNA is involved in solution.

$\Delta Lk$  is the purely topological parameter commonly used to describe supercoiling. SFM makes it possible to characterize the supercoiling of a single molecule of the sample by a more complete parameter which describes each conformation possible, the writing number (Wr). We already reported the calculation of Wr from a SFM topography.

On this basis we can determine the partition of  $\Delta Lk$  between the changes in the supercoiling state (Wr) and the change in the twist of the DNA strand (Tw).

The procedure of DNA deposition on mica has been tailored in order to consider the effects of both phase transition (B to A) and high salt concentration on the original supercoiling of the DNA under investigation.

**10:40 am NSBI-ThM8 Scanning Probe Microscopy Studies of Macromolecular Interactions, S. J. B. Tendler, C. J. Roberts, P. M. Williams, M. C. Davies and D. E. Jackson, Laboratory of Biophysics and Surface Analysis, Department of Pharmaceutical Sciences, The University of Nottingham, Nottingham, NG7 2RD, UK.**

The scanning probe microscope (SPM) offers the ability to obtain high resolution structural information on a range of biological molecules including proteins, carbohydrates and nucleic acids. In order to obtain this data, a number of sample preparation methods have been developed, including coating the sample with a metallic layer, the use of immobilizing self-assembled monolayers and streptavidin-biotin binding systems.

We have been utilizing the above techniques in order to investigate biomolecular interactions with the scanning tunnelling microscope (STM) and the atomic force microscope (AFM). The process of self-association of short synthetic peptides to produce protein-like macromolecules has been studied in detail. STM and AFM images of protein self-assembly have been obtained at various stages of assembly, and the data has been correlated with that obtained using electron microscopy.

The SPM allows the study of this self-assembly process and provides information on structural features of the molecular systems that are not normally observed using more conventional microscopy techniques.

**11:00 am NSBI-ThM9 DNA Surface Attachment Schemes for Scanning Probe Microscopy, Lisa A. Wenzler and Thomas P. Beebe, Jr., Department of Chemistry, University of Utah, Salt Lake City, UT 84112.**

Using the thiol-gold adsorption system, we are developing reproducible methods for depositing, immobilizing and imaging deoxyribonucleic acid (DNA) on a supporting gold substrate for scanning tunneling microscopy (STM) and atomic force microscopy (AFM). These methods involve chemical modifications which can be made to a DNA oligonucleotide that will cause the DNA to adsorb to a suitable

surface. In addition, chemical schemes involving the modification of the surface as opposed to the DNA will be presented. This involves the use of self-assembled monolayers that contain groups at the outer interface which are known to interact with DNA. Additional surface-sensitive methods such as X-ray Photoelectron Spectroscopy (XPS) and reflection-FTIR will be presented for independent structural information, verification and quantification of the amount of DNA adsorbed. The strength of this project is the correlation between STM/AFM results and other spatially averaged traditional surface analytical techniques.

11:20 am **NSBI-ThM10 Studying the Dynamics of Polymer Surface Degradation by Scanning Force Microscopy**, *K. M. Shakesheff, M. C. Davies, A. Domb<sup>†</sup>, C. J. Roberts, A. Shard, S. J. B. Tendler and P. M. Williams*, Laboratory of Biophysics and Surface Analysis, Department of Pharmaceutical Sciences, The University of Nottingham, Nottingham, NG7 2RD, U.K., <sup>†</sup>The Hebrew University of Jerusalem, School of Pharmacy, Jerusalem, Israel 91120.

The controlled release of drug molecules from surface eroding biodegradable polymer devices is an area of active research which promises many clinical and economic opportunities. Drug release from these devices occurs only as a result of polymer chain scission at the polymer-aqueous interface. In the design of these novel devices, it is vital to understand the dynamics of polymer degradation at the interface with the body. The study of these dynamics has been advanced by the development of *in situ* scanning force microscopy (SFM) which enables the polymer surface degradation to be visualized within an aqueous environment.

For the semi-crystalline polyanhydride, poly(sebacic acid) (PSA), we have visualized the preferential loss of amorphous material resulting in the exposure of crystalline fibres and spherulites at the polymer-aqueous interface and the pH dependence of the kinetics of surface morphological changes has been recorded.

Phase separations at the surface of incompatible polymer blends composed of PSA and poly(lactic acid) (PLA) have been imaged and the differential rates of degradation of these two polymers has been visualized by SFM. These differential degradation rates result in the exposure of slowly degrading PLA regions at the surface.

The successful implementation of *in situ* SFM in the study of surface degradation dynamics of biodegradable polymers has generated a new powerful approach to advance our understanding of erosion processes which can assist the rational design of novel degradable biomedical materials and devices.

11:40 am **NSBI-ThM11 In-situ Observation of the Protonation of Cytosine on Au(111) by Electrochemical STM**, *D. Lampner, T. W. Jing, J. Pan and S. M. Lindsay*, Department of Physics and Astronomy, Arizona State University, Tempe, AZ 85287.

We have studied the adsorption of cytosine molecules onto an Au(111)  $23\sqrt{3}$  surface in  $\text{NaClO}_4$  (which does not adsorb to gold). Spontaneous adsorption on an uncontrolled electrode only occurs when the rest potential is slightly positive of the potential for zero charge. At least two phases are commonly seen, coexisting in adjacent domains. One corresponds to the cytosines stacked on edge ('edge-on' phase) and the order to the cytosines lying flat ('flat' phase). When the substrate potential is controlled and raised to larger positive values, the edge on phase is largely transformed into the flat phase. Furthermore, systematic variations in brightness across the unit cell that were present at low potential disappear at the higher potentials.

Because the electrolyte is unbuffered, these changes could reflect changes in protonation of the cytosines at the N3 position. Chronocoulometry measurements indicate that charge regulation may be occurring. We confirm that the changes in the form and contrast of the images are owing to protonation by examining the same area of adlayer (at molecular resolution) as the pH is lowered through addition of  $\text{HClO}_4$ . We find that images characteristic of low electrode potentials in neutral, unbuffered electrolyte are found at low pH, and images characteristic of positive electrode potentials in neutral, unbuffered electrolyte are observed at higher pH. These results indicate that the protonation of a single molecule can be followed by contrast changes in the STM image.

This work was supported by grants 1R21 HG00818-01A1 from the National Institutes of Health and N00014-90-J-1455 from the Office of Naval Research.

## NANO 3/NANOMETER-SCALE SCIENCE AND TECHNOLOGY

Room A207 – Session NS2-ThM

### Proximal Probe Based Fabrication

**Moderator:** H. G. Craighead, Cornell University.

8:20 am **NS2-ThM1 Electrical and Mechanical Properties of Metallic Nanowires: Conductance Quantization and Localization**, *J. I. Pascual, J. Méndez, J. Gómez-Herrero, A. M. Baró, N. García*, Universidad Autónoma de Madrid and C.S.I.C., 28049 Madrid, Spain, and *U. Landman, W. D. Luedtke, E. N. Bogachev, H. P. Cheng*, Georgia Institute of Technology, Atlanta, GA 30332.

Measurement of electrical and mechanical properties of nano-scale junctions and wires is of extreme relevance in the area of integrated nanocircuitry and related technology. It has been shown recently [1] that it is possible to fabricate small nanowires using a scanning tunneling microscope (STM). Furthermore, atomic scale processes underlying the formation of intermetallic nano-contacts have been revealed via molecular dynamics (MD) simulations [2]. In this work, we present results for two regimes of nanowires produced by STM. For short gold wires (50 Å) we show clear evidence at room temperature of conductance quantization, with additional fine structure correlating with the order-disorder states of layers of atoms in the wire, predicted by MD simulations [2]. The resistance of long wires, as long as 400 Å, demonstrates the transition to a localization regime. Current versus voltage characteristics indicates gradual loss of metallic character as the wire narrows.

[1] J. I. Pascual et al, Phys. Rev. Lett. 71, 1852 (1993) and J. I. Pascual et al, (1994) to be published.

[2] U. Landman et al, Science 248, 454 (1990).

8:40 am **NS2-ThM2 Quantized Conductance in an Atom-Sized Point Contact**, *F. Besenbacher, L. Olesen, E. Laegsgaard, and I. Stensgaard*, Center for Atomic-Scale Materials Physics and Institute of Physics and Astronomy, Aarhus University, DK 8000 Aarhus C. Denmark.

Point-contact experiments are carried out at room temperature on single-crystal Cu, Ni, and Pt surfaces with an STM. The preamplifier is modified such that both the current and the voltage in the tip-surface junction are measured simultaneously during tip indentation and retreat from the surface. During the indentation, the tip suddenly snaps into point contact with the surface, causing a jump in the conductance. A point-contact neck is formed, and when the tip is withdrawn, the contact neck stretches. During this stretching, it is observed that for all the three metals, the conductance is quantized in units of one or two times  $2e^2/h$  (77.5  $\mu\text{S}$ ) even at room temperature. A typical length per quantum step is  $\sim 1$  Å. Exactly which quanta of  $2e^2/h$  are observed differ from one indentation to the other. Recently, we have [1] combined these experiments with atomistic simulations of the contact and model calculations of the conductance based on a Landauer-Büttiger type theory. We show that the jumps in the conductance is a direct consequence of the transverse electron motion in the contact consisting of one to ten atoms only rather than of a quantization of the cross-sectional area as the contact is stretched. Experiments are in progress to use these thin wires to study stick and slip motion on clean and chemically modified surfaces.

[1] L. Olesen, E. Laegsgaard, I. Stensgaard, F. Besenbacher, J. Schiøtz, P. Stoltze, K. W. Jacobsen, and J. K. Nørskov, Phys. Rev. Lett. 35, 2251 (1994).

9:00 am **NS2-ThM3 Nanoscale Mechanical and Chemical Processing of Surfaces: Molecular Dynamics Simulations**, <sup>1</sup>*Susan B. Sinnott*, <sup>2</sup>*Richard J. Colton, Carter T. White and Donald W. Brenner*, <sup>3</sup>US Naval Research Laboratory, Surface Science Branch, Code 6170, Washington, DC 20375-5342.

Atomic force and related microscopies are powerful techniques, not just for imaging, but also for the engineering and processing of matter on the nanometer scale. Computer simulations can provide important insight into the mechanisms at work in these processes. We have been using molecular dynamics simulations to study the interaction of nanometer-scale diamond tips and asperities with surfaces. Specifically, we are interested in atomic-scale indentation and scraping of diamond and metal surfaces with diamond tips. Such simulations provide in-



formation on the stability of the tip compared to the surface as a function of the size of the tip and the nature of the surface. In addition, we have modelled the selective alteration of a diamond surface by using a chemically reactive tip to abstract a surface atom. This creates an active site on the surface where controlled chemistry can take place. We propose a novel tip design to perform the abstraction without inadvertently damaging the surface or tip.

<sup>1</sup>Supported by ONR.

<sup>2</sup>NRC Postdoctoral Associate.

<sup>3</sup>Address after August 1, 1994: Dept. of Materials Science and Engineering, North Carolina State, Raleigh, NC.

9:20 am **NS2-ThM4 Electrical Measurements on STM Patterned Silicon MOSFETs**, Ty Fayfield and T. K. Higman, Department of Electrical Engineering, University of Minnesota, Minneapolis, MN 55455.

Periodic surface potential gratings have been created in the active area of a silicon MOSFET with a scanning tunneling microscope (STM). Gratings running both parallel and perpendicular to the direction of electron flow in the channel were produced. Electrical measurements were made to determine the effect of the potential grating on MOSFET transport. The STM writing was accomplished through a selective field enhanced oxidation process on the bare silicon channel. The devices were then cleaned with a modified RCA process and subsequently gate oxidized. Atomic force microscope images confirm that the gratings translate through the cleaning and gate oxide steps to provide a modulation of the gate oxide thickness. Because the thickness modulation can be made as large as 100 Å, macroscopic threshold voltage shifts exist between areas that are STM modified and those that are unmodified. A device with a grating parallel to the electron flow has a continuous conductive path from source to drain at the unmodified threshold voltage. A perpendicular grating forms pools of electrons which are electrically disconnected from the source and drain. The contrast in these electrical properties can be measured at or slightly above the unmodified threshold voltage. Data will be presented which show these effects.

9:40 am **NS2-ThM5 Nanolithographic Patterning of Metal Films with the STM**, C. Van Haesendonck, L. Stockman, G. Neuttiens, C. Strunk, Y. Bruynseraede, Laboratorium voor Vaste-Stoffysika en Magnetisme, Katholieke Universiteit Leuven, B-3001 Leuven (Belgium).

We have developed a new and reliable lithographic method to pattern this evaporated gold films by locally exposing a Langmuir-Blodgett layer of an electron beam resist with the STM. The resist layer consists of only 4 monolayers of omega-tricosenoic acid. For the exposure the STM operates in a dry nitrogen atmosphere at a voltage difference of about -10 V between the electrochemically etched Pt-Ir tip and the gold layer on top of which the very thin resist layer has been deposited. The omega-tricosenoic acid acts as a negative resist, where, after development in ethanol, the unexposed areas can be removed via argon ion milling.

We have written several fine-line structures with a linewidth down to 15 nm. The lines interconnect larger predefined contact pads, which can be used for ultrasonic wire bonding. We will present the results of our detailed study of the dependence of the fine-line quality on the exposure parameters (tunneling voltage and current, exposure dose, Pt-Ir tip quality, ...). Low-temperature magnetoresistance measurements confirm the electrical quality of the narrow gold lines.

While the possibility to use the STM lithography for technological applications is still unclear, our lithographic patterning technique certainly provides an inexpensive and flexible tool for the preparation of mesoscopic samples. As a nice application of our technique, gold contacts have been attached to small bundles (diameter of about 50 nm) of carbon nanotubes, enabling to measure their resistance as a function of temperature and magnetic field.

INVITED

10:20 am **NS2-ThM7 Spectroscopic Investigation of PEDA, an Ultrathin Resist for STM Lithography**, F. K. Perkins,\* E. A. Dobisz, M.-S. Chen, J. M. Calvert, C. R. K. Marrian, Naval Research Laboratory, Washington, DC, \*NRC/NRL Cooperative Research Associate.

Self-assembled monolayers are of great interest as resist materials for STM-based lithography. We have investigated the STM interaction with phenylethylenediamine (PEDA) on Si. The molecule consists of a silane group attached to a ligating amine group. PEDAs differs from Langmuir-Blodgett film forming molecules in that the silane group

chemisorbs to the native oxide of Si forming a densely packed film. Low energy electron exposure inhibits the ligating action of the PEDAs. A Ni film will then selectively form from an electroless plating solution in the unexposed regions. STM lithography on PEDAs was performed in vacuum with currents between 3 pA and 1 nA, tip-sample voltages between -8 and -100 V, and tip speed of 0.2-2 μm/sec. We have examined the exposure threshold bias, dose and tip-sample bias behavior, and IV characteristics of the tip-resist-Si system. We find a threshold voltage between -8 and -10 V. This threshold depends on the condition of the tip. The changes brought about by STM exposure are visible in subsequent STM imaging under below-threshold bias conditions. We have observed that the width of exposed lines (in nm) in the latent resist image is on the order of the bias voltage (in V). The tip-sample I-V curves showed that, for negative tip bias, tip sample conductivity is sensitive to the exposure history of the PEDAs. The I-V curves in both directions are in good agreement with a field emission model of tunnelling through a barrier.

10:40 am **NS2-ThM8 Scanning Probe Lithography of Novel Langmuir-Schaeffer Films: Electrochemical Applications**, U. Demir, K. K. Balasubramanian, V. Cammarata, and C. Shannon, Department of Chemistry, Auburn University, Auburn, AL 36849 USA.

Langmuir-Schaeffer films composed of novel rigid rod molecules have been studied as potential resist materials for use in SPM lithography. These materials are ideally suited for electrochemical applications for two reasons: first, the blocking ability of the films can be easily controlled by the number of layers transferred to the substrate; second, the fidelity of the tip induced features is high due to the mechanical properties of the film. We have used the tip of a STM to define features with lateral dimensions ranging from 10 nm to 3 μm. The depth and overall morphology of the features depend on the lithography conditions. We have studied the electrochemical deposition of Cu into the lithographically defined domains. We find that for resists consisting of a single LS monolayer, deposition of Cu occurs over the entire surface of the electrode; however, for two or more LS layers, deposition occurs selectively at the lithographically defined features. Furthermore we find that material deposits first at the perimeter of the holes followed by deposition into the hole itself. In addition it appears that larger holes fill before smaller ones. Other electrochemical applications of these systems will be briefly discussed.

11:00 am **NS2-ThM9 Cyanide Etching of n-Alkanethiol-Modified Au(111) Surfaces Studied by Electrochemical Scanning Tunneling Microscopy**, Y. Q. Li, O. Chailapakul, R. M. Crooks, Department of Chemistry, Texas A&M University, College Station, TX 77843-3255.

A systematic *in-situ* electrochemical scanning tunneling microscopy (ECSTM) study of the electrochemical dissolution of Au(111) in dilute cyanide solutions has been carried out. Atomic resolution and large-scale images showing the  $\sqrt{3} \times \sqrt{3}$  reconstruction stripes were routinely obtained to insure the quality of the Au(111) surfaces. At ca. 300 mV negative of the substrate rest potential, surface diffusion is activated and surface adatoms become highly mobile. Under these conditions it was possible to use STM tips to induce surface changes such as pitting, island growth, and step edge movement. The bare Au(111) surface was found to dissolve in KF, Na<sub>2</sub>HPO<sub>4</sub>, and KOH solutions containing 1 mM KCN at electrode potentials above -530 mV vs. SCE. However, the Au(111) surface is stable in CN<sup>-</sup> solutions when the surface potential is held below -530 mV. When the surface was modified with a single monolayer of HS(CH<sub>2</sub>)<sub>15</sub>CH<sub>3</sub> the Au surface was passivated and no etching was observed even at high positive potentials. The Au(111) surface can be selectively etched in CN<sup>-</sup> solution when it is coated with a highly defective monolayer, which can be achieved by immersing the substrate in the organomercaptan solution for a very short time (< 1 minute). When a monolayer of iodide is adsorbed onto Au(111), dissolution is initiated at defect sites in the I<sup>-</sup> adlayer, but the covered areas are largely passivated. Various mechanisms of the dissolution processes will be discussed.

11:20 am **NS2-ThM10 Nanometer Structure Fabrication on Insulator and Magnetic Material using Scanning Probe Microscope**, S. Hosaka, H. Hajime, A. Kikukawa, M. Miyamoto, T. Shintani, K. Nakamura, J. Brugger and R. Imura, Advanced Research Laboratory, Hitachi, Ltd., 1-280, Higashi-Koigakubo, Kokubunji, Tokyo 185 Japan.

Field evaporation and current induced point heating using scanning probe microscope (SPM) for fabrication of nanometer structure on an insulator and a magnetic material are presented. We have studied them using an atomic force microscope (AFM) and a scanning tunneling microscope (STM). In AFM experiment, applying the pulsed



voltage to the gold-thin-film covered AFM tip has made nanometer-sized gold dots of around 10 nm in diameter on a SiO<sub>2</sub>/Si as an insulator/conducting substrate in the case of negative tip bias. On the other hand, positive tip bias has made small hills to evaporate and remove the silicon dioxide. The former is due to field evaporation of gold atoms on the insulator. This is because the bias means that negative gold ions are contributed in field evaporation and the threshold field is about  $-1.6 \text{ V/\AA}$ , which agree well with theoretical results. The latter is due to current induced heating of surface. The silicon appears in bottom of the hill after the voltage application. This means that the current heating makes temperature in the local area rise up to higher than 1000 C. Furthermore, we applied the current heating to make nanometer-sized magnetic domain structures in magneto-optical material by STM. Using a current imaging tunneling spectroscopy technique, small magnetic domains with around 100 nm in diameter were made in PtCo multilayer at the voltage of less than 2V for 1 ms. It is considered that the temperature in local area rise up to over Curie point of about 400 C.

These results indicate that SPM has a potential to achieve an ultrahigh density recording and to fabricate nanometer-sized electron device patterns.

**11:40 am NS2-ThM11 Field-induced Atom Transfer of Gold and Platinum Systems in the Scanning Tunneling Microscope Configuration,** C. S. Chang, H. N. Lin, W. B. Su, and T. T. Tsong, Institute of Physics, Academia Sinica, Taiwan, ROC.

We study the effects of the polarity and the height of applied voltage pulses as well as the atmospheric environments on the process of atom transfer between the tip and the sample of STM. In vacuum, mounds of gold atoms of size less than 200 Å in diameter and pits of width less than 50 Å can be produced on a gold surface with nearly equal probabilities by applying negative voltage pulses to a gold tip. In air, most frequently created features for the gold system are mounds, independent of the polarity of applied field. For the platinum system in air, the transfer direction of atoms is uniquely from the positive electrode to the negative. Our results are in accordance with the model calculations extended from a theoretical model of field evaporation for the FIM. The study of the Pt system in vacuum is currently under way and a new approach is employed in trying to clarify the mechanism of the atom transfer process under high field.

\* Supported by the National Science Council of R.O.C. under grant No. NSC83-0208-M001-038.

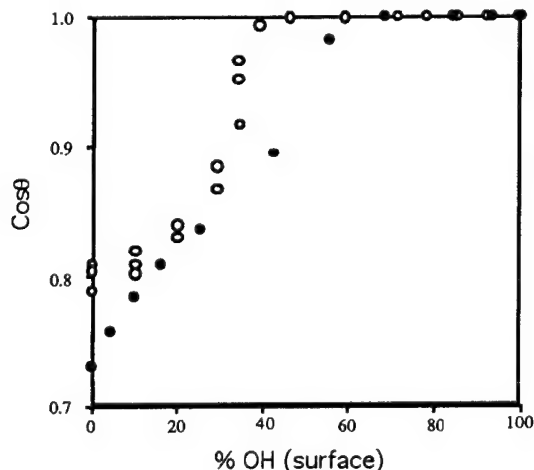
## APPLIED SURFACE SCIENCE

### Room A101 - Session AS-ThM

#### Self-Assembled Monolayers

**Moderator:** A. W. Czanderna, National Renewable Energy Laboratory.

**8:20 am AS-ThM1 Surface Engineering Using Mixed Alkanethiolate Monolayers on Gold,** Abraham Ulman, Department of Chemistry, Polytechnic University, Brooklyn, NY 11201.



Self-assembled monolayers (SAMs) of thiolates on gold open exciting new possibilities of engineering smooth surfaces with their chemical properties fine-tuned at the molecular level. This leads to new avenues of control of physico-chemical properties of surfaces. Wettability studies of mixed monolayers containing hydrophobic (CH<sub>3</sub>) and hydrophilic (OH) terminal groups are discussed. Cosθ of hexadecane for HO(CH<sub>2</sub>)<sub>11</sub>SH:CH<sub>3</sub>(CH<sub>2</sub>)<sub>11</sub>SH (○), and for HO(CH<sub>2</sub>)<sub>11</sub>SH:CH<sub>3</sub>(CH<sub>2</sub>)<sub>11</sub>SH (●) mixed alkanethiolate monolayers on gold, as a function of the surface OH-concentration.

#### INVITED

**9:00 am AS-ThM3 Probing the Phase Transition in Alkyl Thiol Assemblies on Gold Surfaces,** F. Bensebaa,<sup>1</sup> T. Ellis,<sup>1</sup> A. Badia<sup>2</sup> and B. Lennox,<sup>2</sup> <sup>1</sup>Dept of Chimie, Univ. de Montréal, Montréal, H3C 3J7, <sup>2</sup>Dept. of Chimie, Univ. de McGill, Montréal, H3A 2K6.

In spite of the numerous experimental and theoretical investigations on self-assembled monolayers (SAM) of n-alkyl thiol, CH<sub>3</sub>-(CH<sub>2</sub>)<sub>n</sub>SH, on gold surfaces, there is some uncertainty about the nature of the phase transition. Whether the disordering, believed to be the origin of the phase transition, is due to gauche defects<sup>1</sup> or to random chain tilt<sup>2</sup> is the main focus of our work. Thiols, with chain length varying from n = 10 to n = 22, were adsorbed on evaporated gold films and investigated by infrared reflexion absorption spectroscopy (IRAS), with and without polarization modulation, in the temperature range 140–150 K. The spectral deconvolution was performed with commercial software and the temperature dependence of the linewidth, peak frequency and integrated intensity were extracted. We will discuss our results within existing models. Relevance of IR studies on bulk n-alkanes is also discussed.

1. L. H. Dubois and R. G. Nuzzo, *Annu. Rev. Phys. Chem.*, 43 (1992) 437.
2. P. Fenter, P. Eisenberger and K. S. Liang, *Phys. Rev. Lett.*, 70 (1993) 2447.

**9:20 am AS-ThM4 A NEXAFS—Investigation of the Adsorption of Pyromellitic Dianhydride (PMDA) on Pt(111),** C. Thümmel, T. Strunskus, A. Schertel, C. W. Hutchings, H. Wegner, Ch. Wöll and M. Grunze, Angewandte Physikalische Chemie, Im Neuenheimer Feld 253, W-69120 Heidelberg, F.R.G.

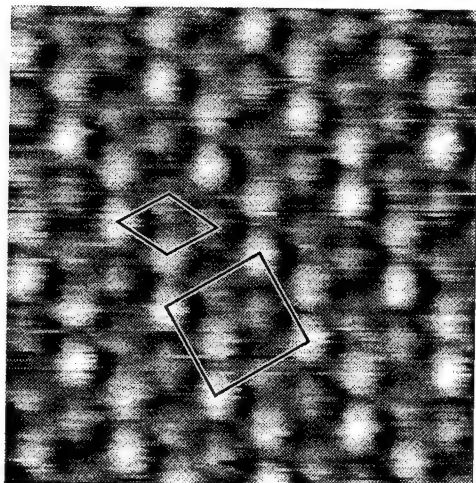
In order to determine the molecular orientation of PMDA on Pt(111) NEXAFS-spectra were measured at the C1s and O1s-absorption edge. For the multilayer the absence of angular variation in the resonances indicates that the PMDA molecules are oriented randomly. For the monolayer the observed strong angular variation of the π\*-resonance intensities reveals an orientation of the PMDA molecules with their ring-plane parallel to the Pt surface. Further support for this planar arrangement is provided by the substantial broadening and shift of the π\*-resonances indicating a strong interaction between the monolayer and the substrate. If all molecules in the well oriented monolayer were adsorbed in a planar arrangement, the NEXAFS spectra taken at normal incidence should show no intensity in the energy range of the π\*-resonances. In our experiments, however, a finite transition intensity of about 20% of the edge jump is observed. A careful analysis of our NEXAFS data suggests the presence of excitations into empty hybrid substrate-molecule orbitals for photon energies above the XPS-binding energy. Such transitions are expected for strongly chemisorbed molecules and have been discussed previously for benzene on Ag(110) [1]. This explanation is supported by the observation of a considerably strongly angular variation for an epitaxially grown triple layer.

[1] J. Stöhr, NEXAFS Spectroscopy, Springer Verlag, 1991.

**9:40 am AS-ThM5 Structure and Dynamics of Alkanethiol Self-Assembled Monolayers on Au(111) Characterized by Scanning Tunneling Microscopy,** G. E. Poirier, M. J. Tarlov and H. E. Rushmeier, National Institute of Standards and Technology, Gaithersburg, MD 20899.

We report the results of an ultrahigh vacuum scanning tunneling microscope (STM) study of n-alkanethiol [CH<sub>3</sub>(CH<sub>2</sub>)<sub>n-1</sub>SH] (C<sub>n</sub>) monolayers self-assembled on Au(111) single-crystal surfaces. The STM images show that the saturation coverage self-assembled monolayer (SAM) unit cell measures 0.86 × 1.0 nm and contains four thiolate molecules (see graphic). The observed unit cell is consistent with results from recent x-ray, and helium diffraction studies. This unit cell corresponds to a c(4 × 2) superlattice of a basic (√3 × √3)R30 dense-packed monolayer. The domain size ranges from 5.0 to 15 nm with domains separated by molecular-width rotational boundaries, anti-phase

boundaries and stacking faults. SAMs composed of longer chain thiols (C8 and C10) were stable in vacuum for over 40 days. Short-chain homologues (C4 and C6) exhibited a 2-D liquid phase at room temperature. Facile mass transport of surface gold atoms was observed in the presence of the liquid phase using time-lapse STM movies. Nucleation and growth of ordered domains having a unit cell of  $\sqrt{3} \times \sqrt{3}$  (p = 8–10) were observed for the short-chain liquid-phase SAM.



10:00 am **AS-ThM6 Metal Overlayers on Self-Assembled Monolayers: 6. XPS of Cr/COOH on Mercaptohexadecanoic Acid,\* D. R. Jung and A. W. Czanderna**, National Renewable Energy Laboratory, Golden, CO 80401.

We present a study by XPS of the chemical and physical interactions of Cr with the COOH groups of a self-assembled monolayer (SAM) of  $\text{HS}(\text{CH}_2)_{15}\text{COOH}$  on gold. For each overlayer thickness, a new SAM was exposed to the evaporative deposition of Cr at  $\leq 1 \times 10^{-8}$  torr and then transferred immediately in-situ to a surface analysis chamber held at  $\leq 5 \times 10^{-10}$  torr. Metallic Cr can be produced in this way as evidenced by a Cr 2p  $3/2-1/2$  splitting of 9.2 eV for 10 Å Cr films on Au. The C 1s and O 1s binding energies and intensities for the initial COOH-terminated SAM are consistent with the presence of the O=C-OH end group at the surface. For Cr overlayers of 0.4–10 Å average thickness, we identify Cr-COOH reactions primarily by changes in the O 1s level, and by comparison with the O 1s spectra for Cr/CH<sub>3</sub> and Cr/Au films in UHV and after exposure to oxygen. For 0.4 Å Cr/COOH, the O 1s peak at 532.7 eV is narrowed and located between the original C-O (533.9 eV) and C=O (532.5 eV) components, indicating a Cr/COOH reaction. In comparison, an oxidized 30 Å Cr film on Au yields large peak at 530.3 eV consistent with Cr<sub>2</sub>O<sub>3</sub>, as well as a smaller peak at 532.1 eV that we attribute to surface-bound oxygen species. For 0.7–10 Å Cr/COOH, a growing second O 1s component is found at 531.1–530.6 eV that may be attributed either to an adsorbed oxygen species on the Cr surface (although it is 3 times greater in intensity than for Cr/CH<sub>3</sub>) or to a second, more highly oxidized form of Cr/COOH bonding.

\* This work was supported by the U.S. Department of Energy under Contract DE-AC02-83CH10093.

10:20 am **AS-ThM7 An Unexpected Packing of Fluorinated n-Alkane Thiols on Au(111): An Atomic Force Microscopy Study, G. Liu,<sup>1</sup> C. E. D. Chidsey,<sup>2</sup> D. F. Ogletree and M. Salmeron**, Material Science Division, Lawrence Berkeley Laboratory and Department of Chemistry,<sup>1</sup> University of California, Berkeley, CA 94720; <sup>2</sup>Department of Chemistry, Stanford University, Stanford, CA 94305.

Using atomic force microscopy (AFM), we have conducted a comprehensive study of the structure of  $\text{CF}_3(\text{CF}_2)_n(\text{CH}_2)_2\text{SH}$  (n = 11, 7 and 5) on a Au(111) surface. Surprisingly, although the nearest neighbor fluorinated alkane thiol distance is very close to the lattice constant of a commensurate  $\sqrt{2} \times \sqrt{2}$  structure, the close-packed rows of molecules are rotated  $\sim 30^\circ$  with respect to the underlying gold lattice. This packing is incommensurate or at most only close to a high-order commensurate  $c(7 \times 7)$  structure. Our finding is in excellent agreement with the observation of an independent x-ray diffraction experiment. The relative orientation of the organic monolayer and the Au(111) substrate has been determined unambiguously because AFM tips can

reversibly displace the thiol molecules under high loads. In addition, the issues of defects and domain boundaries within these fluorinated monolayers will also be discussed.

10:40 am **AS-ThM8 The Surface Chemistry of Self-Assembled and Vapor Deposited Perfluorinated n-Alkanoic Acid Monolayers on Native Aluminum-oxide, Robert M. Wallace, Steven A. Henck, Peijun Chen, and Douglas A. Webb**, Texas Instruments Incorporated, Dallas, TX 75265.

Perfluorinated monolayers, typically in the form of long-chain perfluorinated polyethers, have found wide application in tribology for boundary layer lubrication. We have examined the surface chemistry of a homologous series of alternative boundary layer lubricants consisting of perfluorinated n-Alkanoic (n = 10, 12, 14, 16, 18) acid monolayers on the smooth, native oxide surfaces of MBE-grown aluminum using monochromatic x-ray photoelectron spectroscopy, *ex-situ* grazing-incidence infrared absorption reflection spectroscopy, and ellipsometry. We present results of studies of the adsorption kinetics of the self-assembled monolayer formation and compare these results to films produced by thermal CVD methods. We find evidence for chemical interaction between the perfluorinated backbone of the acid and the aluminum-oxide surface for monolayer films produced by either method. The interaction results in the formation of aluminum oxy-fluoride surface species even at room temperature.

11:00 am **AS-ThM9 Quantitative Analysis of Monolayer Molecular Films Using 'Molecule Corrals' and STM, David L. Patrick, Victor J. Cee, and Thomas P. Beebe, Jr.**, Department of Chemistry, University of Utah, Salt Lake City, UT 84112.

Nanometer-diameter etch pits on the basal plane of highly oriented pyrolytic graphite (HOPG) are used as 'molecule corrals' to study self-assembled monolayer films of organic molecules. The corrals are produced during high temperature oxidation by a method that allows precise control over their size, and are uniformly circular and one graphite layer (3.4 Å) deep. Molecular self-assembly along the bottom of pits occurs semi-independently from that on the surrounding terrace, allowing a statistical approach to the analysis of information in STM images. Rates of molecular self-assembly, active nucleation sites (step edge vs. open terrace sites), as well as the relative configurational free energies of different monolayer structures can all be determined as a function of corral size. Variable-temperature STM experiments allow measurement of nucleation activation energies and other film characteristics dependent on thermal conditions. We also present a general method for the extraction of orientational interaction energies between nearby two-dimensional crystalline domains of molecules directly from STM images of self-assembled films in etch pits.

11:20 am **AS-ThM10 In Situ AFM/STM Study of Nucleation, Growth and Electron Transfer Reactions of Purines at the Graphite-Water Interface, N. J. Tao and Z. Shi**, Department of Physics, Florida International University, University Park Campus, Miami, FL 33199.

We have studied xanthine and guanine at the graphite-water interface with AFM and STM. The molecules were found to condense spontaneously into monolayer films at the interface. The nucleation and growth processes were studied by AFM in real-time as a function of the surface potential. The molecular packing structures were determined from the molecular resolution AFM images. Although the STM images of the molecules were obtained with submolecular resolution, they are less straight forward to interpret because the mixed states of the molecules and the underlying graphite were imaged. At low potentials the monolayers dissolved into the bulk solution, while at high potentials oxidations took place. The kinetics of the oxidations was studied in real-time with AFM. The reactions were observed to start preferentially from defect sites, and the reaction rates were determined from the images. Both AFM and STM images of the reaction product of xanthine were obtained with molecular resolution which allowed us to extract the molecular packing structure of the product molecules. However the oxidation product of guanine dissolved into the bulk solution which made it difficult to examine with AFM/STM. From the total amount of charge transfer and the number of reacted molecules, the numbers of electrons per molecule involved in the reactions were directly determined to be two for guanine and four for xanthine.

\* This work was supported by Research Corporation and the Petroleum Research Fund of the American Chemical Society.

11:40 am **AS-ThM11 Multi-Step Assembly of Polymeric Monolayers, D. W. Grainger, G. Mao, and F. Sun**, Colorado State University and D. G. Castner, Univ. of Washington, Seattle, WA.

Self-assembly of organic silanes provides a promising method of preparing materials with well-defined surface chemistries for solid lubricants, photoresists, biosensors, biomaterials, protective coatings, etc. This study examines a three-step process that combines the benefits of monomeric and polymeric self-assembly. First 7-oct-1-enyltri-chlorosilane (OETS) is self assembled onto a Si wafer. Then siloxane polymers were coupled to the bound OETS olefins by hydrosilylation of Si-H groups or photo-initiated side chain thiol radicals. Finally the attached siloxane polymers were derivatized with ethylene glycol allyl ether oligomers (PEG) or a perfluoroalkyl allyl ether (FC). An alternative two-step method of directly coupling a PEG or FC derivatized siloxane polymer to the OETS monolayer was also examined. XPS, contact angle, ellipsometry, and FTIR were used to characterize the film structure at each step of the processes and to determine the efficiency of each assembly step. Both processes produced monolayers that were surface enriched in either PEG or FC groups. The attachment of the PEG oligomers was more facile than the attachment of the FC chains. The amount of PEG attached depended on the degree of siloxane polymer attachment to the OETS surface and the molecular weight of the PEG oligomer. The three-step method produced films with higher PEG concentrations than the two-step method. The results from these experiments will also be compared to our previous results for multifunctional polymeric monolayers on Au.

## PLASMA SCIENCE

### Room A109 - Session PS-ThM

#### Charge Free Processing

**Moderator:** K. L. Maxwell, SEMATECH.

8:20 am **PS-ThM1 Overview of Charge-Free Processing—Mechanisms and Applications**, *H. H. Sawin*, Massachusetts Institute of Technology, Cambridge, MA 02139.

Charge-free processing of microelectronics is currently being considered to augment conventional plasma processes in order to eliminate damage of the devices being processed and skewing of the etching directionality caused by the deflection of ion bombardment. Many experimental means, e.g. neutral beams and atom sources, are under investigation to replace reactive ion etches and wet cleans. The first success of neutral processes is likely to be realized in cleaning applications since the rate of directional neutral etching processes is typically an order of magnitude slower than that of plasma processes. The fundamental barriers associated with pumping and surface mechanisms encountered in designing directional neutral beams with etching rates comparable to plasmas will be discussed. The rate of etching and pumping dictates a minimum process pressure of order 0.1 mTorr. However, at these pressures neutral beam processes with surface etching probabilities of order 1, could have etching rates comparable to plasma processes.

The cleaning of surfaces represents a different set of challenges as less material must be removed, but that processes which are non-selective must be developed to clean the damaged/contaminated surfaces left by reactive ion etching. All cleaning products must be volatile at reasonable temperatures. The roughening of surfaces by dry cleaning and selectivities of these processes will be discussed. It is likely that multi-step dry processes will be necessary for cleaning. Proposed processes involving sacrificial oxide layers will be discussed.

9:00 am **PS-ThM3 Charge Measurements and Damage Effects in the Reaction Chamber of a Remote Plasma Etcher**, *D. J. Bonser, P. K. Aum, T. Ta, SEMATECH, Austin, TX 78741, M. G. Blain, T. L. Meisenheimer*, Sandia National Laboratories, Albuquerque, NM 87185, *W. M. Holber*, ASTeX, Inc., Woburn, MA 01801.

Remote plasma etching is thought to produce a charge free environment in which etching is due to reactive neutral species. We have measured the charge present in an etching chamber that is approximately one meter removed from a microwave plasma discharge. In contrast to the notion that etching is accomplished in a charge free environment, both electronically excited and ionized species were detected near the wafer surface. We present results of high sensitivity, direct current measurements using both single and double probes as well as a.c. measurements in a remote etching chamber for various inert and process plasma conditions. Charge measurements are compared with damage induced in gate oxide integrity test structures. The

species responsible for the charge are investigated by Fourier transform infrared spectroscopy, optical emission spectroscopy, and quadrupole mass spectrometry.

9:20 am **PS-ThM4 In situ Diagnostic Measurements of the Gas Phase Process Chemistry in the Reaction Chamber of a Remote Plasma Etcher**, *M. G. Blain, T. L. Meisenheimer*, Sandia National Laboratories, Albuquerque, NM 87185, *J. A. O'Neill*, IBM Microelectronics, Hopewell Junction, NY 12533, *D. J. Bonser, P. K. Aum, T. Ta, SEMATECH, Austin, TX 78741*.

Remote plasma etching is generating interest as an alternative to conventional close-coupled plasma technology in an effort to reduce wafer charge damage. Despite the potential of remote plasma etching, little is known about the chemistry of the processes used in these reactors. We report the gas phase species in an etch chamber that is approximately one meter removed from a microwave discharge region for three different gas mixtures;  $\text{NF}_3$ ,  $\text{CF}_4/\text{O}_2/\text{N}_2$ , and  $\text{CF}_4/\text{O}_2/\text{N}_2/\text{Cl}_2$ . Fourier transform infrared spectroscopy, optical emission spectroscopy, and quadrupole mass spectrometry were used to detect etch reactants and products while etching  $\text{Si}_3\text{N}_4$  and polycrystalline silicon. Sensitive charge measurement techniques were employed to measure charge in the etch chamber. All gas mixtures produced highly dissociated reactants as measured in the etch chamber. In contrast to the notion that etching is accomplished in a charge free environment, both electronically excited and ionized species were detected near the wafer surface. These *in situ* gas measurements are directly compared to measured etch rates and the species responsible for etching are inferred.

9:40 am **PS-ThM5 Effects of Reactor Wall on Downstream Stripping**, *Moritaka Nakamura, Kiyoko Nishikawa, and Keisuke Shinagawa*, c851, Process Dev. Div., Fujitsu Limited, 1015 Kamikodanaka, Nakahara-ku, Kawasaki, 211 Japan.

High stripping rate is required in downstream resist stripping, even though it has the advantage of less processing damage to devices in charging and metallic or alkaline contamination. Metallic shielding plate between plasma and wafer is required to prevent charged particles from reaching the wafer surface. Stainless steel or heavy metals cause metallic contamination. So, aluminum is used as a shielding plate. Aluminum surface, however, causes recombination of radical species and reduces the stripping rate. We studied the transportation of O and OH radicals using ESR (Electron Spin Resonance) with different wall surface conditions in  $\text{O}_2 + \text{H}_2\text{O}$  downstream. Radical recombination was enhanced on aluminum surface, especially after long time  $\text{O}_2$  plasma exposure. On the contrary, recombination was significantly small on quartz surface. Thus, high stripping rate was obtained with quartz covering of aluminum shielding plate. Moreover quartz covering prevented the surface oxidation of aluminum, and high stripping rate was maintained for long time in production usage of stripping equipments. Temperature control of aluminum surface is also important. More radicals recombined with higher wall temperature. We believe that build up of water molecules on the surfaces prevented sticking and recombination of radicals at low temperature. We also discuss the effects of residual charged particles or radiation on the wafer surface.

10:00 am **PS-ThM6 UV-Stimulated Dry Stripping of Silicon Nitride Films**, *David C. Gray, Jeffery W. Butterbaugh, C. Fred Hiatt*, FSI International, Chaska, MN 55318.

UV light-stimulated processes have been developed for rapidly stripping films of silicon nitride, silicon oxy-nitride, silicon, and composite films thereof in a dry reaction environment, free of plasma or plasma effluents. These processes are carried out in vacuum reactor which allows simultaneous exposure of a substrate wafer to a polyatomic halogen gas and UV radiation. Silicon nitride stripping rates in excess of 1000 Å/min have been demonstrated for UV-stimulated fluorine-based processes, while maintaining the bulk wafer temperature below 250°C. It has been shown that the mechanism for UV-stimulated silicon nitride etching requires direct photon exposure of the etching surface. Selectivities between silicon nitride, silicon oxide, and silicon films are controlled through UV lamp exposure, substrate temperature, and additions of oxygen, nitrogen, and various halogen-containing gases. Selectivities for silicon nitride-to-silicon oxide etching of greater than 30 can be achieved for the stripping of silicon nitride LOCOS masks layers in the presence of field oxide and pad oxide layers. These processes address many of the limitations of plasma-downstream etch tools for dry silicon nitride stripping, including complete elimination of charged particles and sputtered contaminants associated with plasma effluents.

10:20 am **PS-ThM7 Neutral-Beam-Assisted Etching**, *T. Yunogami, K. Yokogawa, and T. Mizutani*, Central Research Laboratory, Hitachi Ltd., Kokubunji, Tokyo 185, Japan.

For future ULSI process, low damage etching is required. Current plasma etching, however, has serious disadvantages that charged particles cause various radiation damages.

In order to avoid charge-related damage, we have pursued "neutral-beam-assisted etching." In this etching, low-energy neutral beam and neutral radicals are simultaneously supplied to the specimen, and the etching reactions are enhanced by the kinetic energy of the neutral beam.

We have applied this method to the SiO<sub>2</sub> etching. Ar neutral beam with 500eV is generated from Ar ion beam by charge-exchange reactions. Neutral radicals are generated in CHF<sub>3</sub> plasma. The SiO<sub>2</sub> is exposed only to these neutral particles by eliminating charged particles with retarding grids. We achieved quartermicron pattern delineation without dielectric breakdown. The typical etch rate is 60 nm/min.

The neutral beam energy distribution and the beam divergence are critical issues for precise etching. Increasing the etch rate and the etch diameter are also important for practical use. Key points of these problems are how to supply high density, large diameter, and uniform neutral beam and neutral radicals. These problems will be reviewed with recent experimental results using a newly designed neutral-beam-assisted etching machine.

**INVITED**

11:00 am **PS-ThM9 Hyperthermal Neutral Beam Etching**, *K. P. Giapis and T. A. Moore*, Division of Chemistry and Chemical Engineering, and *T. K. Minton*, Jet Propulsion Laboratory, California Institute of Technology, Pasadena, California 91125.

Fast neutral beams of highly reactive species have been suggested as an inherently better means for the anisotropic etching of semiconductors due to minimization of bombardment-induced damage and complete elimination of charge damage. However, difficulties associated with the generation of high fluxes of neutral reactive species with hyperthermal ( $\geq 2$  eV) kinetic energies have hindered progress towards assessing their potential for etching. We report here on the generation of beams of neutral fluorine atoms with translational energies between 2–10 eV and their use in the anisotropic etching of silicon. The fluorine atoms are produced by laser-induced detonation of SF<sub>6</sub> in a nozzle, then collimated and brought onto the etched wafer. For room temperature etching of Si, we measured 7:1 anisotropy ratio and 30:1 selectivity to SiO<sub>2</sub> while the photoresist mask underwent no erosion whatsoever.

The ability to control the translational energy of the incident beam in the hyperthermal range (2–10 eV) facilitated the investigation of the dynamics of fluorine atom scattering from the fluorinated Si surface during steady-state etching. A rotatable quadrupole mass spectrometer was used in a Time-Of-Flight mode of operation to angularly resolve the flux and energy distribution of fluorine atoms after the collision with the etched surface. A low ( $3.2 \text{ eV} \pm 0.4 \text{ eV}$ ) and a high ( $6.4 \text{ eV} \pm 1 \text{ eV}$ ) incident translational energy have been employed. It is found that, for both energies, the flux-weighted angular distribution of inelastically scattered fluorine atoms does not follow a cosine law but it rather peaks near the specular direction. More remarkably, for wide incident angles, the unreacted fluorine atoms scattering in the specular direction may retain up to 60% of the incident energy. This wide-angle scattering mechanism dramatically affects profile evolution and explains phenomena such as microtrenching and reverse micro-loading.

11:20 am **PS-ThM10 A Thermalized Neutral Radical Source for Charge-Free Processing**, *L. Chen, Q. Yang, D. R. Wright, K. L. Maxwell*, Interconnect Division, SEMATECH, Austin, TX 78741.

We have designed and characterized a thermalized neutral radical source suitable for use in effusive neutral beam processing and Chemical Downstream Etching (CDE). A single grounded neutralizer screen with high aspect-ratio (10:1) above-Debye holes is used for the neutralization of the primary heated plasma. The primary plasma is heated by a water-submerged radio-frequency (RF) induction antenna through a ceramic window. An axial magnetic field near the neutralizer screen enhances the plasma discharge; an electrostatic quadrupole downstream removes residual charges. Characterization of the source for species content, flux and energy distribution, is performed by both time-of-flight and neutral energy analyzer. The source provides an effusive neutral beam with translational energies in the range from 80 meV to 300 meV. The source can be used with a wide range of gases, and is scalable to larger sizes. Preliminary results from silicon etching show a promising technology for charge-free processing.

11:40 am **PS-ThM11 Hyperthermal Neutral Beam Anisotropic Etching for Submicron Patterning of Electronic Materials**, *J. B. Cross and M. A. Hoffbauer*, Los Alamos National Laboratory, Los Alamos, NM 87545.

The anisotropic etching of electronic materials presently relies upon charged particle bombardment to produce damage sites that react with suitable adsorbed chemical reactants. This technique of reactive ion etching has gained widespread acceptance for the mass production of large scale integrated circuits and is routinely used in the manufacture of memory and microprocessor chip having feature sizes down to 0.5  $\mu\text{m}$ . The desire to put more functionality onto a chip requires that feature sizes smaller than 0.5  $\mu\text{m}$  be manufactured with high reliability and yield. This drive for smaller feature size requires that process induced damage be minimized in order to maximize production yield. The use of fast neutral beams as the anisotropic agent eliminates essentially all of damage mechanisms associated with ions. We have performed some preliminary atomic oxygen etching studies that show striking differences between ion and neutral beam processes. Feature size of 0.3  $\mu\text{m}$  has been etched in photoresist polymers using high kinetic energy atomic oxygen with an etch rate of  $\approx 1800 \text{ \AA/minute}$  at an incident O-atom flux of  $10^{17} \text{ AO/s-cm}^2$ . Our results in etching photoresists and other polymers shows that the reaction of the fast O atoms is direct. At a translational energy of 5 eV, roughly 10% of the incident flux reacts to form the volatile products water, carbon monoxide, and nitrogen oxides. Reaction rates for various polymers are independent of the polymer structure if the polymer only contains carbon, hydrogen, oxygen, and nitrogen. The reaction rate depends strongly on the incident energy of the O atoms, and thermal O atoms react at a negligible rate (approximately  $10^{-4}$  that of 5 eV atoms). This direct reaction of fast O atoms with the polymer is unprecedented and is the key to fast neutral anisotropic etching. Extension of these concepts to anisotropic etching of silicon, GaAs, and other materials is presently being investigated and will be discussed.

## **ELECTRONIC MATERIALS/SURFACE SCIENCE** **Room A102 – Session EMSS-ThM**

### **Semiconductor Surface Reactions III**

**Moderator:** J. R. Engstrom, Cornell University.

8:20 am **EMSS-ThM1 Sputtering of GaAs(110) Studied with Scanning Tunneling Microscopy**, *R. J. Pechman, X.-S. Wang, and J. H. Weaver*, University of Minnesota, Department of Materials Science and Chemical Engineering, Minneapolis, MN 55455.

Ion bombardment is a common surface processing technique that is important in sputtering and ion-assisted etching applications. Scanning tunneling microscopy (STM) provides an atomic-scale view of the result of such bombardment. We have used STM to investigate material removal from GaAs(110) via Ar<sup>+</sup> and Xe<sup>+</sup> bombardment, spanning the range from initial impact on a pristine cleaved surface through multilayer roughening. Low energy ions (300–3000 eV) create defects that are largely confined to one or two unit cells. Diffusion of the vacancies created in this way produces two-dimensional single-layer-deep pits in a manner analogous to island formation during growth. Temperature-dependent studies of vacancy island nucleation yields the activation energy for diffusion. Continued sputtering results in temperature-dependent roughening that relates to interlayer diffusion. Finally, sputter yields have been determined as a function of ion energy and incident direction.

8:40 am **EMSS-ThM2 Atomically-Resolved Decomposition of Phosphine and Formation of P-terminated Layers on Si(001)**, *R. J. Hamers and Y. Wang*, Dept. of Chemistry, University of Wisconsin, Madison, WI 53706.

We have investigated the thermal decomposition of phosphine and the formation of phosphorous-terminated layers on Si(001) using scanning tunneling microscopy (STM) and tunneling spectroscopy. While at room temperature PH<sub>3</sub> adsorbs molecularly, at elevated temperatures PH<sub>3</sub> decomposes to P and H atoms. The phosphorus atoms are readily incorporated into the outermost layer of silicon, ejecting silicon atoms onto the terrace and allowing the P atoms to mix with Si in the outermost dimerized layer. The resulting surface is an alloy of Si-Si, Si-P, and P-P dimers. Surprisingly, a statistical analysis of the images reveals that Si-P heterodimers are found more often than expected on the basis of random mixing, despite the fact that Si-P heterodimers



have a "dangling bond." At higher coverages where P-P dimers predominate the surface reveals strain-induced defects. The role of lattice strain and Si-P chemistry in determining the chemistry and morphology of the surface will be discussed.

This work is supported in part by the U.S. Office of Naval Research and by the National Science Foundation.

9:00 am **EMSS-ThM3 Semiconductor Etching with Halogens: Scanning Tunneling Microscopy Investigations**, *J. H. Weaver*, Department of Materials Science and Chemical Engineering, University of Minnesota, Minneapolis, MN 55455 USA.

This talk will review recent progress made in understanding surface etching of Si(100)-2 × 1 and GaAs(110), particularly as offered through *in situ* scanning tunneling microscopy investigations. These studies have involved exposure of the surface to controlled fluxes and fluences of Br<sub>2</sub> and Cl<sub>2</sub> as a function of temperature, with surface imaging at room temperature. The results show that ordered removal of surface layers can be achieved under suitable conditions. They make it possible to compare phenomena related to material removal (etching) to those associated with overlayer formation (growth) and offer insights into surface chemical pathways and the dynamics of etching.

INVITED

9:40 am **EMSS-ThM5 Analysis of Nanometer-Scale Surface Roughness with Reflection Inelastic Electron Scattering from Silicon Surfaces**, *H. N. Frase, H. A. Atwater, S. S. Wong, and C. C. Ahn*, California Institute of Technology, Pasadena, CA 91125.

In this paper, we demonstrate how inelastic electron scattering measurements can be used to complement reflection high energy electron diffraction (RHEED) to obtain information about nanometer-scale surface roughness. Reflection electron energy loss spectroscopy (REELS) at 25 keV has been employed to investigate nanometer-scale roughness via low-loss (0–80 eV) inelastic electron scattering from silicon (001) surfaces. Surfaces with roughness length scales from the atomic scale to microns were produced by microfabrication and epitaxial growth. Roughness was quantified from scanning electron and atomic force microscope images. REELS measurements in the low-loss region, which are dominated by surface and bulk plasmon scattering, were performed as a function of incidence angle and surface roughness was correlated with the extent of multiple inelastic scattering. While the inelastic scattering spectra are complicated functions of roughness and incidence angle, several conclusions can be made about roughness based on trends apparent in the relative bulk and surface plasmon intensities. First, very smooth surfaces with only atomic-scale roughness exhibit considerable multiple plasmon scattering and significant surface plasmon contributions at typical RHEED incidence angles. Second, as-polished silicon surfaces, and surfaces intentionally roughened by microfabrication exhibit reduced multiple inelastic scattering as compared with very smooth surfaces. A method for fitting experimental inelastic intensity distributions, and correlations with roughness, will be discussed.

10:00 am **EMSS-ThM6 Sub-surface Diffusion of Ni on Si(100) and (111)**, *M. Y. Lee and P. A. Bennett*, Box 871504, Physics Dept., Arizona State University, Tempe, AZ 85287-1504.

We directly compare the rates of surface vs. bulk diffusion for Ni on/in Si by depositing a laterally confined dot of Ni on one side of a double-polished and UHV cleaned Si wafer and measuring the lateral Auger profile on the reverse side following annealing. Ni reaches the far side of the wafer at temperatures as low as 500°C via bulk diffusion with no measurable contribution from surface paths. This is attributed to the relatively high product of solubility and diffusivity for Ni in bulk Si. In related experiments with a uniform lateral dose of Ni, we find that surface phases (a 1 × 1 "ring-cluster" structure and an ordered √19 structure) disappear by solution of Ni into bulk silicon. For low initial coverages, the 7 × 7 structure can even be recovered. Virtually all the metal so dissolved can be restored to the surface (both top and bottom) by quench cooling, driven by the vertical temperature gradient. The role of these diffusion and segregation phenomena in silicide reactions is described.

10:20 am **EMSS-ThM7 Chemical Vapor Deposition of TiSi<sub>2</sub> using SiH<sub>4</sub> and TiCl<sub>4</sub>**, *M. A. Mendicino, R. P. Southwell, and E. G. Seebauer*, Department of Chemical Engineering, University of Illinois, Urbana, IL 61801.

TiSi<sub>2</sub> has been the object of considerable study because of its low resistivity among the transition metal silicides and its compatibility

with existing ULSI technology. However, CVD of TiSi<sub>2</sub> from gas phase SiH<sub>4</sub> and TiCl<sub>4</sub> is accompanied by a competing reaction which consumes intolerable amounts of the Si substrate. The reaction mechanism for TiSi<sub>2</sub> growth is poorly understood, and some disagreement even exists about the reaction stoichiometry. The combined CVD/UHV approach we have developed fills many gaps in the current understanding of TiSi<sub>2</sub> CVD. Our approach is unique in that it attempts to predict optimal processing conditions from surface reactivity measurements under well-characterized ultrahigh vacuum conditions. These predictions are then tested directly in a CVD chamber, connected to the ultrahigh vacuum system, that operates at normal processing temperatures and pressures. Special effort centers on understanding and controlling the first stages of TiSi<sub>2</sub> film growth on the silicon surface. In addition to tackling these problems in the particular case of TiSi<sub>2</sub> growth, we are developing a framework of chemical reasoning that will be widely applicable in deposition technology.

10:40 am **EMSS-ThM8 FTIR Study of Intrinsic TEOS Surface Reaction Kinetics on SiO<sub>2</sub> at CVD Process Temperatures and Pressures**, *M. E. Bartram and H. K. Moffat*, Sandia National Laboratories, Albuquerque, NM 87185.

Tetraethoxysilane (TEOS) is used in numerous microelectronics processes for the deposition of conformal SiO<sub>2</sub> films. Good conformality is achieved only if the surface chemistry is controlled by the appropriate rate-limiting step during deposition. Therefore, to provide process reliability and improved methods for TEOS-based SiO<sub>2</sub> CVD, it is essential to understand the rate-limiting step and its dependence on process conditions.

To improve the molecular-level understanding of both the overall rate-determining step for SiO<sub>2</sub> deposition and the transition state for initial chemisorption, we have used FTIR and isotopically labeled silanols to measure the intrinsic kinetics of the TEOS reaction on SiO<sub>2</sub>. Importantly, we performed these measurements in a cold-wall research reactor under carefully controlled conditions that pertain to TEOS-based CVD processes (10 to 100 mTorr TEOS at 765 to 1200 K).

We have determined that the *E<sub>a</sub>* for the initial chemisorption step is only 6 kcal/mol between 900 and 1200 K. Nevertheless, the initial chemisorption probability is 3 × 10<sup>-3</sup> and decreases to lower values as the reaction proceeds. In addition, there is a continuous build-up of ethoxy groups on the surface. This suggests that the rate of ethoxy decomposition to SiO<sub>2</sub> and silanols may be insufficient to keep up with the rate of TEOS chemisorption under steady-state CVD conditions. If the ethoxy build-up is responsible for the observed decrease in the TEOS chemisorption probability, this may indicate that ethoxy decomposition is the overall rate-limiting step in SiO<sub>2</sub> CVD. Our results also show that silanols are consumed by TEOS surface reactions at CVD temperatures and yet their steady-state concentration remains constant as a result of ethoxy decomposition. Although surface silanols are consumed during chemisorption, TEOS reacts with Si-OH and Si-OD with equal rates at 765K. This suggests that proton transfer is not the rate-limiting step in the chemisorption transition state.

This work was performed at Sandia National Laboratories under DOE contract DE-AC04-76DP00789.

11:00 am **EMSS-ThM9 Investigation of the Chemical Mechanisms of Ta/Ta-oxide Halogen Etch Selectivity**, *L. A. DeLouise*, Xerox Corporation, 800 Phillips Road, 114-41D, Webster, NY 14580.

XPS and LEED techniques are used to investigate the interaction of a Cl<sub>2</sub> supersonic molecular beam with a Ta(110) surface as a function of temperature. The starting surface is an ordered submonolayer oxide with ~1/3 monolayer coverage. Surface oxygen originates from a bulk contamination. Low and high O 1s binding energy components are found and associated with Ta<sup>+1</sup> and Ta<sup>+2</sup> oxidation states, respectively. The oxide states are unequally populated and studies show they also exhibit an inequivalent reactivity toward chlorine. Three temperature regimes were distinguished in terms of the reactivity of the surface towards chlorine. At room temperature chlorine readily adsorbs on the Ta(110)-suboxide surface causing further oxidation of Ta sites. Between room temperature and 300°C a chemical state selective etching reaction involving only oxygen bonded in Ta<sup>+2</sup> sites occurs. LEED studies show the initial Ta-suboxide overlayer is slightly disordered along the <100> direction and that etching preferentially depletes oxygen bonded in Ta<sup>+2</sup> disordered domains. Between 300°C and 650°C surface sites are passivated by Cl overlayer domains of p(4 × 1) orientation in which a slight disordering along the <110> site stacking direction is observed. Above 650°C chlorine is thermally depleted and surface segregation of bulk oxygen contamination occurs. Oxygen segregation occurs at 400°C in the absence of Cl. At room



temperature chlorine adatoms initially bond to both Ta and Ta-O sites but at higher temperatures chlorine adatoms complex with Ta-O sites. The propensity for Cl to react at Ta-O sites has important consequences in understanding the overwhelming etch selectivity of Ta metal to Ta-oxide in halogen-based plasmas used for microelectronic device fabrication which is discussed.

11:20 am **EMSS-ThM10 Scanning Tunneling Microscopy and Spectroscopy of the Reaction of  $\text{NH}_3$  with GaAs(110)**, *G. Brown and M. Weimer*, Department of Physics, Texas A&M University, College Station, TX 77843-4242.

It is known that the reaction of gaseous ammonia with the (110) surfaces of GaAs and InP produces non-dissociative chemisorption, but important details concerning the adsorption geometry and local electronic structure, as well as the extent of surface etching, are not well understood. These issues are relevant to such complex processes as the Atomic Layer Epitaxy of nitride compounds (e.g., GaN), and to continuing efforts to grow suitable insulating nitride layers for compound semiconductor device applications.

We have examined the adsorption of submonolayer amounts of ammonia on the (110) surface of *p*-type GaAs with scanning tunneling microscopy (STM) and spectroscopy (STS), and find two chemisorption-related features whose structure is attributed to the perturbations in substrate surface atoms rather than to molecular orbitals of the adsorbate.

The first structure appears as two symmetrically raised in-chain arsenic atoms whose mutual gallium neighbor is either depressed or enhanced depending on the nature of the probe tip. This structure is accompanied by asymmetric screening similar to that expected for a tilted dipole above a dielectric surface. Simple chemical arguments, symmetry, and the dipole moment of  $\text{NH}_3$  suggest that these structures reflect ammonia bonded to gallium atoms. The second structure appears as an arsenic vacancy along with ammonia adsorption at one or both of the adjoining gallium sites. Since these defects occur with greater frequency than the native vacancies on clean GaAs(110), they imply that surface etching of arsenic atoms can occur along with adsorption.

Preliminary spectroscopic measurements indicate that ammonia adsorption is also associated with a shift of the surface Fermi-level from below the valance band edge (on degenerate material) into the band gap, and the relationship of this observation to chemisorption-induced charge transfer and surface states will be addressed.

11:40 am **EMSS-ThM11 MBE Growth of  $\text{SnS}_2$  and  $\text{SnSe}_2$  on Cleaved Mica, Single Crystal  $\text{SnS}_2$ ,  $\text{WSe}_2$ , and Other Layered Semiconductors—RHEED, LEED, Photoemission and STM Characterization**, *R. Schlaf* (‡), *D. Louder* (†), *O. Lang* (‡), *C. Pettenkofer* (‡), *W. Jaegermann* (‡), *K. Nebesny* (\*), *P. Lee* (\*), *B. A. Parkinson* (†) and *N. R. Armstrong* (\*)-(‡) = Hahn Meitner Institute, Berlin, Germany; (†) = Department of Chemistry, Colorado State University, Ft. Collins, Colorado; (\*) = Department of Chemistry, University of Arizona, Tucson, Arizona 85721.

Both of the layered semiconductors,  $\text{SnS}_2$  and  $\text{SnSe}_2$  are possible materials for photovoltaic solar energy conversion. In window-absorber structures  $\text{SnSe}_2$  (bandgap: 1.1 eV) could be used as the absorber whereas  $\text{SnS}_2$  (bandgap: 2.2 eV) is promising for use as a window material. The growth of heterojunctions of these materials by straight-forward MBE techniques is therefore quite attractive. In this paper we describe the epitaxial deposition of  $\text{SnS}_2$  and  $\text{SnSe}_2$  on several other layered semiconducting substrates. RHEED and LEED were used to demonstrate ordered layer growth of these materials, and XPS/UPS studies were used to confirm stoichiometry, sharpness of the interfaces formed, and band edge positions at the interface. STM investigations of these materials suggest that, although the electron diffraction techniques indicate layer-by-layer growth, the actual surface layers formed vary considerably in their long range order, and in the mechanism of film growth.



## THIN FILM/VACUUM METALLURGY Room A105 - Session TFVM-ThM

### Energetic Condensation: Processes, Properties and Products

**Moderator:** D. A. Glocker, Eastman Kodak Research Laboratories.

8:20 am **TFVM-ThM1 Energetic Condensation: Processes, Properties and Products**, *J. S. Colligon*, Research Institute for Design, Manufacture and Marketing, University of Salford, Salford, M5 4WT, England, UK.

When film deposition is accompanied by bombardment by low (less than a few 100 eV) particles the resulting film nucleation, growth, stress content, adhesion, density, composition, morphology and crystal structure may be significantly altered. Latest methods for providing the energy-assisted environments for film growth are described and recent selected results demonstrating all the above features presented. Selected applications of the novel materials that can now be created on various substrates to improve friction, wear, corrosion resistant and optical qualities are given. The review concludes with a discussion of the fundamental requirements for systems producing these new coatings and the latest developments to extend the work to allow larger objects and complex-shaped components to be treated.

### INVITED

9:00 am **TFVM-ThM3 Primary-Ion Deposition of Al on a-C and Ge on Si(001): Role of Low-Energy Ion/Surface Interactions**, *Y.-W. Kim*, *I. Petrov*, *H. Ito*, and *J. E. Greene*, Dept. of Materials Science, University of Illinois, 1101 W. Springfield, Urbana, IL 61801.

High-flux, low-energy, UHV-compatible Kaufman-type ion sources have been developed for primary ion deposition (PID) of relatively low vapor pressure materials such as Al and Ge. The source can deliver up to  $200 \mu\text{A cm}^{-2}$   $\text{Al}^+$  and  $\text{Ge}^+$ , at a distance of 25 cm, with energies as low as 15 eV. A magnetic fiber separates the ion and neutral components to provide a pure ion beam. The nucleation and coalescence kinetics of Al, deposited at room temperature from thermal, 35 eV, and 75 eV beams, on amorphous C substrates were studied using transmission electron microscopy (TEM). The results showed an increasingly larger average island size  $\langle d \rangle$ , for a given average film thickness  $t$  (accounting for loss by sputtering), with increasing ion energy  $E_{\text{Al}}$ :  $\langle d \rangle = 18, 53$ , and  $102 \text{ nm}$  with  $E_{\text{Al}} = \text{thermal}, 35 \text{ eV}$ , and  $75 \text{ eV}$  for  $t = 5 \text{ nm}$ . This led to larger average grain sizes and smaller grain size distributions in thick layers grown by PID. The islands, as well as continuous films, also exhibited increasingly strong (111) preferred orientation with increasing  $E_{\text{Al}}$ . An analysis of island size distributions and growth kinetics shows that the primary mechanism for island coarsening is the collisional dissociation of small incipient islands into still smaller clusters and adatoms with higher surface mobilities which diffuse to feed stoichiastically-formed larger stable islands. Partially ionized (50%) 40 eV  $\text{Ge}^+$  beams were used to grow 100-nm-thick epitaxial buffer layers at  $300^\circ\text{C}$  on Si(001) prior to the growth of thick Ge overlayers by MBE. The PID buffer layers, which were epitaxial with periodic discontinuous lenticular-shaped amorphous regions perpendicular to the growth direction, were shown to be extremely effective in relieving interfacial misfit strain and reducing the dislocation density in the Ge overlayer by more than an order of magnitude. In this case,  $E_{\text{Ge}}$  and  $T_s$  were chosen such that the ion-induced damage was not fully annealed during growth.

9:20 am **TFVM-ThM4 Topography and Structure of Homoepitaxial Si Films Grown by Mass Selected Ion Beam Deposition**, *A. H. Al-Bayati*, *S. S. Todorov*, *D. Marton*, *K. J. Boyd*, and *J. W. Rabalais*, Department of Chemistry, University of Houston, Houston, TX 77204-5641, *Y. Lifshitz*, Applied Physics & Mathematics, Nuclear Research Center Soreq, Yavne 70600, Israel.

Analyses of the topography and structure of films deposited from low energy ions as a function of ion energy and substrate temperature provide insight into the ion/surface interactions and the effects of ion energy on the mechanisms of film growth. Atomic force microscopy (AFM), reflection high energy electron diffraction (RHEED) and Rutherford backscattering spectrometry (RBS) have been utilized to study the topography and morphology of silicon films deposited on Si(001) using  $^{28}\text{Si}^+$  beams of energy  $< 100 \text{ eV}$  in the temperature range of  $50$  to  $600^\circ\text{C}$ . Preliminary results using ion energy of  $15 \text{ eV}$  showed that film growth at  $350^\circ\text{C}$  and above was proceeding epitaxially, layer-by-layer. At temperatures  $200^\circ\text{C}$  and below, 2D epitaxial growth was

inhibited and evidence for formation of 3D islands in the early stage of growth followed by transition to an amorphous phase was observed. However, AFM results of films of 200 Å thick showed that the surface of films deposited at 200°C and below is smooth and featureless. On the other hand, the surface of films deposited at 350°C and above is characterized by islands of typical height and diameter equal to 2.5 and 100 nm, respectively, and the density of these features increases with temperature. The effects of substrate temperature, contamination, and surface damage on the growth mechanisms are discussed.

**9:40 am TFVM-ThM5 Formation of Thin C-N Films by Ion Beam Deposition, K. J. Boyd, D. Marton, S. S. Todorov, A. H. Al-Bayati, J. Kulik, and J. W. Rabalais, Department of Chemistry, University of Houston, Houston, Texas 77204-5641.**

Thin carbon-nitrogen films have been deposited by direct impingement of 5–50 eV  $C^+$  and  $N^+$  or  $N_2^+$  ions on surfaces, using the dual-source ion beam deposition system at the University of Houston. The influences of ion energy, N and C arrival rates, and substrate have been studied. The deposited films are essentially amorphous, with some graphitic regions on a scale of 1–2 nm. The films are analyzed by *in situ* Auger electron spectroscopy (AES) and *ex situ* X-ray photoelectron spectroscopy (XPS). Both AES and XPS show two distinct types of C-N bonding: one assigned to a graphitelike local structure (C-N  $\pi$  bonding), with stoichiometry varying from  $C_3N$  to  $C_2N$ , and one attributed to a  $C_3N_4$ -like local structure (C-N  $\sigma$  bonding), with stoichiometry very near  $C_3N_4$ . Overall nitrogen fractions of up to 0.47 are obtained. No phase evolution with increasing ion fluence is observed, although the stoichiometry of the graphite-like phase does increase with ion fluence up to an energy dependent steady-state value. Initial growth proceeds through a mixed nitride-carbonitride layer. Film growth can be described by a subplantation model, with little or no interconversion between the two phases. The merits of IBD as a model for other film growth techniques utilizing energetic species are discussed, and implications of this work for C-N film growth by other methods are mentioned.

**10:00 am TFVM-ThM6 Energetic Condensation Using Filtered Arc Evaporation, P. J. Martin, A. Bendavid, T. J. Kinder, X. Wang, CSIRO Division of Applied Physics, Lindfield, NSW 2070, Australia.**

The cathodic arc is an intense source of low energy particles which may be separated from the associated microdroplets of cathode material by a simple magnetic plasma duct. The resulting filtered energetic particle beam may then be deposited onto a substrate to produce smooth, dense films. Oxide and nitride films are formed by condensation of metal ions in the presence of reactive gases. High quality oxide films are readily deposited at ambient temperature with good optical properties and when deposited at oblique angles, with significant optical angular selectivity. Such coatings have practical application in thermal control of solar radiation. Hard, smooth and adherent coatings of TiN are deposited onto heated substrates. The stress and hardness of the deposited layers is determined by the degree of negative bias applied to the substrate which in turn controls the energy of the depositing ions. The properties of the depositing films can be influenced further by concurrent bombardment with low energy (0.5–1 keV) inert or reactive ions. Ion assisted arc deposition (IAAD) enables the deposition of hard materials such as amorphous diamond-like carbon, carbon nitride and TiN onto unheated substrates. TiN may be synthesized by nitrogen bombardment of condensing Ti ions or Ar or Xe ion bombardment of Ti in a nitrogen background. IAAD provides a controllable method of modifying the stress in the growing films without the requirement of raising the substrate temperature significantly. TiN films prepared by IAAD show a strong (220) orientation and have hardnesses up to 3700 Hv. Films deposited onto Si show a stress reduction from around 9 GPa to 5 GPa by IAAD.

**INVITED**

**10:40 am TFVM-Th8 The Deposition of AlCu and TiN Films for Microelectronic Applications using Ionized Magnetron Sputter Deposition, S. M. Rossnagel, IBM Research, PO 218, Yorktown Heights, NY 10598 and Y.-W. Kim, I. Petrov, J. Moser and J. E. Greene, Coordinated Science Lab and Materials Research Dept., University of Illinois, Urbana, IL 61801.**

Ionized Magnetron Sputter Deposition (IMSD) has been developed as a means of depositing metal and compound films from highly ionized metal discharges. The technique uses post-ionization of the metal atoms sputtered from a conventional magnetron cathode in an RF-Inductively-coupled (RFI) discharge situated in the region between the cathode and the sample. Metal ions are then accelerated across a sample sheath by means of a DC potential on the sample. The primary

advantages of this deposition technique are the high level of control of the depositing metal kinetic energy, the controlled directionality of the deposit, and the ability to drive various surface reactions (e.g. Ti-TiN) at low temperature. The technique has been used successfully for microelectronics applications to deposit diffusion barriers (liners) as well as fully filled trenches and vias of moderate aspect ratio at sub-0.5 micron dimensions. The deposited films have been examined using plain view and cross-sectional TEM, X-ray diffraction and RBS and compared to films deposited with Collimated Magnetron Sputter Deposition (CMSD) and conventional sputtering. The IMSD AlCu films are more highly oriented than the CMSD films, with virtually no Ar contamination. The stress was slightly tensile for the IMSD films and weakly compressive for CMSD films. Ti-nitride films were also measured.

**INVITED**

**11:20 am TFVM-ThM10 Further Perspectives on Stresses in Sputter-Deposited Thin Films, D. W. Hoffman, Advanced Modular Power Systems, 4667 Freedom Dr., Ann Arbor, MI 48108.**

In a recent review the author gave a perspective on the principal findings of John Thornton and himself in their survey of stresses and properties of magnetron sputtered thin films. The present talk picks up where the previous review left off by describing some of the more novel and significant spin-offs that evolved from that central body of work. Among the topics of interest, special attention is given to a novel device for in-situ measurement of film stresses, which appears to solve the problems of previous in-situ stress instruments and offers the possibility of a work-a-day film stress monitor that could be employed in much the same way as, and perhaps in tandem with, a quartz crystal thickness monitor.

**INVITED**

## **ELECTRONIC MATERIALS**

### **Room A108 – Session EM-ThM**

#### **Optical Diagnostics for Materials Processing**

**Moderator: P. Herman, Columbia University.**

**8:20 am EM-ThM1 Ellipsometry for III-V Epitaxial Growth Diagnostics, G. N. Maracas, C. H. Kuo, S. Anand and R. Droopad, Dept. of Electrical Engineering, Arizona State University, Tempe, AZ 85287-6206, G. R. L. Sohie, General Electric Corporate Research Lab, Building KW Room C603, Schenectady, NY 12301.**

Spectroscopic ellipsometry's (SE) strength as an in-situ semiconductor crystal growth process diagnostic lies in the fact that the materials' dielectric properties (pseudodielectric functions) are dependent upon temperature and alloy composition. These dependencies can be exploited to monitor and control epitaxial growth in real time. This paper reviews several aspects of growth and control of III-V semiconductors grown by molecular beam epitaxy (MBE) and gas source MBE (GSMBE) using SE.

Chamber and manipulator design considerations for implementing SE on an MBE and GSMBE with substrate rotation will first be discussed. A commercially available "ellipsometer-ready" MBE system will be discussed.

It will then be shown that an MBE process can be established without conventional analysis tools such as RHEED. Measurement and control of substrate temperature by SE will be shown. This is possible by using the temperature-dependent pseudodielectric functions for GaAs and AlGaAs which we have measured. Calibration of MBE growth will be discussed including in-situ measurement of oxide desorption, V/III flux ratio, growth rate and alloy composition measurements. Tracking the growth of the epitaxial layer provides information on thickness, alloy composition and surface roughness. Algorithms for deconvoluting these effects from the data will be discussed.

Finally, examples of structures used in optoelectronic devices will be presented including quantum well thickness control and microcavity laser device growth.

**INVITED**

**9:00 am EM-ThM3 Real-Time Monitoring of Resonant Tunneling Diode Growth Using Spectroscopic Ellipsometry,\* F. G. Celii, Y.-C. Kao, W. M. Duncan, T. S. Moise and A. J. Katz, Corporate Research & Development, M/S 147, Texas Instruments, P.O. Box 655936, Dallas, TX 75265.**

Sensor-based growth control appears to be necessary to insure manufacturability of quantum devices, such as resonant-tunneling diodes (RTDs), due to the inherent sensitivity of the devices to monolayer

changes in layer thickness. We are applying spectroscopic ellipsometry (SE) to the MBE growth of AlAs/InGaAs RTDs, with the eventual goal of SE-based control. SE provides a versatile and sensitive method to monitor wafer-state properties, such as layer thickness and composition, in real-time.

We acquired SE data from rotating wafers during MBE growth of single and multiple RTDs. The active regions consisted of 50 Å wells, including a 20 Å compressive-strained InAs notch, between 20 Å tensile-strained AlAs barriers. Layer thicknesses were derived from real-time model fits to the SE spectra using growth-temperature optical constants (determined in the same MBE/SE system). Effusion cell flux and surface roughness data were obtained independently by reflection mass spectrometry and laser light scattering, respectively. Correlations between electrical I-V curves of the processed devices and the *in situ* sensor data will be presented. We have found that the effects of strained layer (AlAs or InAs) relaxation on the I-V curves depended on the (tensile or compressive) nature of the strain, and can be distinguished with *in situ* monitoring. Prospects for SE-based real-time control of RTD growth will be addressed.

\*Partially supported by ARPA under contract MDA972-93-H-0005.

9:20 am **EM-ThM4 Real-Time Spectroscopic Ellipsometry (RTSE) Monitoring of  $\text{Si}_{1-x}\text{Ge}_x/\text{Si}$  Epitaxial Growth**, C. Pickering, D. A. O. Hope, R. T. Carline, D. J. Robbins, Defence Research Agency, Malvern, Worcs, UK.

$\text{Si}_{1-x}\text{Ge}_x$  heterostructures and multi-quantum wells are being studied for applications as heterojunction bipolar transistors (HBT) and far-IR detectors. For the growth of these structures to a tight specification, *in-situ* optical monitoring and control is required. This paper reports the first results of RTSE obtained during  $\text{Si}_{1-x}\text{Ge}_x/\text{Si}$  vapour-phase epitaxial growth. Spectra were obtained using a SOPRA RTSE system which uses an optical multi-channel analyzer to provide typically  $\tan \Psi$ ,  $\cos \Delta$  spectra at 256 energies over the range 1.5–4.7 eV in 1 sec.

RTSE has been used to study all stages of HBT growth: surface oxide desorption at  $\sim 900^\circ\text{C}$ , B-doped  $\text{Si}_{0.85}\text{Ge}_{0.15}$  (p-base) growth at  $610^\circ\text{C}$ , As-doped Si (n-emitter) growth at  $700^\circ\text{C}$ . Spectra have been obtained as a function of temperature for the substrate initially covered by 10 Å oxide and after desorption, which was clearly observed at  $\sim 850^\circ\text{C}$ .

The  $\epsilon_1$  spectra of  $\text{Si}_{0.85}\text{Ge}_{0.15}$  and Si at  $610^\circ\text{C}$  are dominated by  $E_1$  peaks near 2.95 eV and 3.1 eV, respectively. In this region the alloy layers become optically thick after  $\sim 300$  Å deposition. Below this thickness the observed spectra are a convolution of layer and substrate spectra, and the peak shifts to higher magnitudes and to energies below 2.9 eV before approaching the bulk alloy value. Multilayer modelling shows this behaviour to be consistent with growth of a uniform alloy layer. Si-rich regions with thicknesses of a few monolayers have been detected at hetero-interfaces and in alloy layers grown with growth interrupts. Beyond these initial regions growth rates are uniform for undoped and B-doped  $\text{Si}_{0.85}\text{Ge}_{0.15}$  and for undoped Si, but for As-doped Si decrease with time due to As surface accumulation.

9:40 am **EM-ThM5 Real Time Investigation of Nucleation and Growth of Si on  $\text{SiO}_2$  Using Silane and Disilane in a Rapid Thermal Processing System**, Y. Z. Hu, D. Diehl, C. Y. Zhao, Q. Liu and E. A. Irene, Department of Chemistry, University of North Carolina, Chapel Hill, NC 27599, K. N. Christensen and D. M. Maher, Department of Materials Science and Engineering, North Carolina State University, Raleigh, NC 27695.

Systematic studies of the nucleation and film growth of Si on amorphous  $\text{SiO}_2$  covered Si using rapid thermal chemical vapor deposition from  $\text{SiH}_4$  and  $\text{Si}_2\text{H}_6$  were performed at temperatures between 600 and  $850^\circ\text{C}$  and reactant gas (5% in He) pressures between 20 and 500 mTorr. Quantitative assessment of the nucleation parameters (incubation time, mean nuclei density, growth rate and coalescence) have been determined by a numerical analysis of *in situ* real time single wavelength ellipsometry measurements. Optical properties of polysilicon films have been investigated using *in situ* spectroscopic ellipsometry in the 2.5–5.0 photon energy range. A Bruggeman effective-medium approximation for the ellipsometric data reveals that the rough-surface overlayer and microstructure of the deposited films depend significantly on the substrate temperature, reactant gases and their partial pressures. Atomic Force Microscopy was used *ex-situ* to observe the initial stage of nucleation and the roughness of the films. The structure of the deposited Si films were characterized by cross-sectional transmission electron microscopy.

10:00 am **EM-ThM6 Real Time Monitoring of the Electron Cyclotron Resonance Etching of Semiconductors by In-situ Spectroscopic Ellipsometry**, N. J. Ianno, P. G. Snyder, S. Ahmer, Center for Microelectronic and Optical Materials Research, Dept. of Elec. Eng., University of Nebraska, 209N WSEC, Lincoln, NE 68588-0511, S. Pittal, B. Johs, and J. A. Woollam, J. A. Woollam Co., 650 J Street, Suite 39, Lincoln, NE 68508.

Processing of III-V materials by high density plasmas has been extensively studied in the electron cyclotron resonance (ECR) tool, where a  $\text{CH}_4/\text{H}_2/\text{Ar}$  gas mixture has been shown to etch GaAs, AlGaAs, InP, AlInAs, and InGaAs. Accurate endpoint detection, overall process monitoring and control of the etching of multilayer stacks are essential to reproducible fabrication of devices. Spectroscopic ellipsometry is a nondestructive optical technique that can determine thicknesses and compositions in multilayer stacks of III-V materials. Recent advances in ellipsometric data acquisition and processing enable us to acquire accurate ellipsometric data at 44 wavelengths simultaneously in real time. A rapid analysis algorithm extracts the top layer film thickness and allows process monitoring.

*In-situ* ellipsometry was employed to monitor the ECR etching of diamond-like carbon, AlGaAs/GaAs structures, and bulk GaAs in real time. Since the film thickness in real time is determined, a wide range of etch parameters can be investigated without changing samples. This allows rapid optimization of the etch rate, and provides endpoint detection to within a nanometer, in the face of a time dependent etch rate.

10:20 am **EM-ThM7 Bulk Ordering and Optical Anisotropy of  $\text{In}_x\text{Ga}_{1-x}\text{As}/\text{InP}$** , D. E. Aspnes,<sup>a\*</sup> K. Hingerl, I. Kamiya, L. T. Florez, B. Phillips,<sup>b\*</sup> S. Mahajan,<sup>b\*</sup> and J. P. Harbison, Red Bank: <sup>a</sup>Physics Dept., NCSU, Raleigh, NC; <sup>b</sup>Materials Science Dept., CMU, Pittsburgh, PA.

We report the first real-time observation of atomic ordering during epitaxial growth, specifically of  $\text{In}_x\text{Ga}_{1-x}\text{As}$  lattice-matched to InP. Reflectance-difference (RD) spectra of thick layers of  $\text{In}_x\text{Ga}_{1-x}\text{As}$  grown at  $335^\circ\text{C}$  show extra derivative-like structure in the vicinity of the  $E_1$ ,  $E_1 + \Delta_1$  transitions near 2.5 eV relative to RD spectra for  $\text{In}_x\text{Ga}_{1-x}\text{As}$  grown at  $450^\circ\text{C}$ . For the lower-temperature material, both RHEED patterns during growth and TEM micrographs after growth exhibit threefold periodicity, consistent with results recently reported for  $\text{Al}_x\text{In}_{1-x}\text{As}$  by Gomyo et al. (Phys. Rev. Lett. **72**, 673 (1994)). If the ordered phase is grown on the disordered phase or vice versa, the 2.5 eV RD signal exhibits interference oscillations with increasing thickness, thereby unequivocally relating the extra structure to bulk anisotropy. Post-growth ellipsometric spectra of ordered material show that this extra structure is due primarily to an increased broadening of the dielectric response for polarization along  $\langle 110 \rangle$ . This is consistent with a simple model where the increased broadening is attributed to fluctuations in the  $E_1$  and  $E_1 + \Delta_1$  absorption edges that result from intraband coupling (zone folding) driven by the superperiodicity. These fluctuations occur whether or not the ordering is complete. The results show how, and under what conditions, ordering in the bulk can be assessed by optical measurements during growth.

\*Work supported by the Office of Naval Research.

10:40 am **EM-ThM8 Monitoring of Deposition and Dry Etching of Si/SiGe Multiple Stacks**, B. Tillack, G. Ritter, H. H. Richter, A. Wolff, G. Morgenstern, C. Eggs\*, Institut für Halbleiterphysik Frankfurt (Oder), Walter-Korsing-Straße 2, D-15230 Frankfurt (Oder), Germany, \*Universität Greifswald, Domstraße 10a, D-17489 Greifswald, Germany.

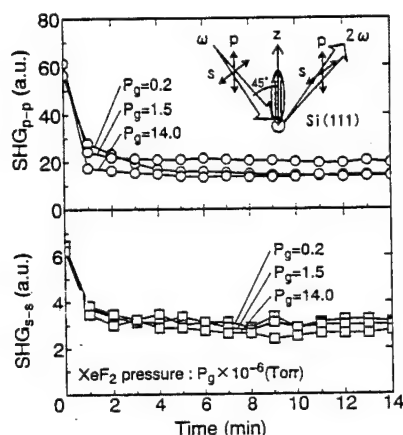
Reflection supported interferometry (PYRITTE) has been used for the *in situ* observation of deposition of  $\text{Si}_{(1-x)}\text{Ge}_x/\text{Si}$  multiple stacks by Rapid Thermal Chemical Vapor Deposition (RTCVD). The thickness and optical parameters of each of the thin films of the stack have been evaluated during the deposition process. During patterning of the so prepared  $\text{Si}_{(1-x)}\text{Ge}_x/\text{Si}$  stacks by reactive ion etching (RIE) the nonselectivity of the etching process has been eluded by optical emission spectroscopy (OES). The monitoring of the 265.1 nm Ge line provides a sensitive and accurate indicator which allows an etch stop within any of the thin films of the stack.

TEM has been used to analyse the structure and thickness of the  $\text{Si}_{(1-x)}\text{Ge}_x/\text{Si}$  multiple stacks after deposition. The composition of the surface layer formed as a result of RIE was examined using X-ray photoelectron spectroscopy (XPS).

The results demonstrate for the first time an opportunity for *in situ* investigation and control of deposition and patterning of  $\text{Si}_{(1-x)}\text{Ge}_x/\text{Si}$  multiple stacks.

11:00 am **EM-ThM9 Observation of Etching Reaction Using Second Harmonic Generation**, *S. Haraichi, F. Sasaki, S. Kobayashi, M. Komuro, T. Tani*, Electrotechnical Laboratory, Tsukuba-shi, Ibaraki 305, JAPAN.

The understanding of atomic scale mechanism in dry etching process is very important for the next microfabrication technology. We have investigated the basic characteristics of surface second harmonic generation (SHG) in the Si etching to pursue the possibility of time-resolved observation of etching reaction. A Nd:YAG laser at 1.064  $\mu\text{m}$  was used as the fundamental incident light which was focused on the sample at 45° incident angle. The surface SHG output was detected by a photo-multiplier and a gated integrator. Figure shows SHG<sub>p-p</sub> and SHG<sub>s-s</sub> intensity decay curves during the spontaneous etching for Si/XeF<sub>2</sub> system. The suffix of SHG indicates the combination of input-output polarization and the p- and the s-polarization mainly reflect dangling-bond and back-bond dipoles respectively. Both SHG<sub>p-p</sub> and SHG<sub>s-s</sub> signals quickly decay with the etching because of the formation of SiF<sub>x</sub> layer and approach to the values independent of XeF<sub>2</sub> pressure. Fluorine atom probably does not attack only dangling-bonds but also back-bonds in the time duration observed here and the thickness of SiF<sub>x</sub> layer is independent of XeF<sub>2</sub> flux in the steady-state of the etching.



SHG intensity decay curves for Si/XeF<sub>2</sub> etching.

11:20 am **EM-ThM10 Hydrogen Annealing Effect on SHG from SiO<sub>2</sub>/Si(111) Interfaces**, *Hirokyu Hirayama, Fuminori Ito and Kohji Watanabe*, Microelectronics Research Laboratories, NEC Corporation, 34 Miyukigaoka, Tsukuba 305, Japan.

Due to the importance of SiO<sub>2</sub>/Si interfaces on MOS devices, many efforts have been reported on the interfacial character. However, SiO<sub>2</sub>/Si interfaces are still not fully understood because of the difficulty to probe the interface. With this respect, optical second harmonic generation (SHG) is recently paid attention due to its sensitivity to the interface. But, it is not clear what kind of information on the interfacial character is obtained from SHG. To clarify the origin of the interfacial SHG, especially the effect of interfacial dangling bond, we studied the hydrogen annealing effect on SHG from SiO<sub>2</sub>/Si(111) interfaces.

In this study, SHG was excited by a 45° incident, s-polarized Nd:YAG laser beam ( $\lambda = 1064 \text{ nm}$ ). P-polarized SHG from 500Å thermally oxidized SiO<sub>2</sub>/Si(111) interfaces was measured as a function of the azimuthal rotation, after hydrogen- and nitrogen-annealing. Annealing temperature was 430°C in both cases. By fitting the azimuthal rotation dependence of the SHG with a theoretical equation, we obtained nonlinear susceptibility  $\chi_{xx}$  and  $\chi_{xxx}$  for the interfacial SHG. Here, z and x indicate direction along the interface normal and parallel, respectively. We found that  $\chi$  is decreased only for the hydrogen-annealing. Moreover, the decrease of  $\chi_{xxx}$  is much larger than that of  $\chi_{xx}$ . On the other hand, in our C-V measurement, density of interfacial dangling bond state was found to be decreased only for the hydrogen-annealing. This means that the passivation of the interfacial dangling bond is reflected to the interfacial SHG. The large decrease of  $\chi_{xxx}$  is caused by the dominance of the interfacial dangling bond along the interface normal direction.

11:40 am **EM-ThM11 Single Photon Ionization Time-of-Flight Mass Spectrometric Probing of III-V Semiconductor Growth**, *S. M. Casey,† A. L. Alstrin, A. K. Kunz, and S. R. Leone,†* Joint Institute for Laboratory Astrophysics, National Institute of Standards and Technology and University of Colorado, Boulder, CO 80309-0440.

Epitaxial growth of III-V semiconductor materials is probed *in situ* in a molecular beam epitaxy reactor by single photon ionization of the gaseous fluxes using vacuum ultraviolet (VUV) laser radiation. The ninth harmonic of the Nd:YAG laser is used to ionize the species of interest. This radiation is produced by frequency tripling the Nd:YAG laser output to 355 nm and then to 118 nm in a Xe/Ar mixture. Coupled with time-of-flight mass spectrometry, this radiation selectively probes the gaseous fluxes of Ga, As<sub>2</sub>, and As<sub>4</sub> during molecular beam epitaxy of III-V materials. The essential aspects of the method and details of calibration procedures to obtain relative fluxes are described. Cracking of the arsenic species does not occur in the laser/mass spectrometer, making relative species concentration measurements very reliable. Rapid data acquisition provides real time measurements of the incident and scattered fluxes and of materials desorbed during growth. Recent work to correlate the flux determinations with Reflection High Energy Electron Diffraction (RHEED) oscillations during GaAs epitaxial growth will be discussed.

†Staff Members, Quantum Physics Division, National Institute of Standards and Technology.

## MANUFACTURING SCIENCE AND TECHNOLOGY

Room A110 - Session MS-ThM

### Micro-Contamination and Defects

Moderator: A. C. Diebold, SEMATECH.

### MS-ThM1 ABSTRACT NOT AVAILABLE

9:00 am **MS-ThM3 An *in situ* XPS Study of Metal Surface Recontamination and Hollow Cathode Plasma Cleaning**, *H. Li, A. Belkand, Z. Orban*, BOC Group Technical Center, Murray Hill, NJ 07974, and *F. Jansen*, Airco Coating Technology, Concord, CA 94524.

Adhesion of coatings depends on the substrate surface condition poor to the coating deposition. Pre-cleaning of metal substrates has been known to improve the coating adhesion; however, little has been published on the quantitative effect of *in situ* plasma cleaning and metal surface recontamination upon exposure to the air.

Using *in situ* XPS, we have studied the recontamination of previously plasma cleaned metal surfaces by exposure to controlled amounts of air. It was found that the initial formation of a thin metal oxide film was followed by the continuing growth of hydrocarbon film as well as hydroxides and moisture from the air. The main source of hydrocarbon is believed to be due to the backstreaming of vacuum pumps. We have evaluated the suitability of a reactive hollow cathode plasma for the removal of the surface contamination. The quantitative reduction of hydrocarbon, moisture, hydroxides and metal oxide films is discussed. A linear plasma source, based on the hollow cathode principle, used for in-line cleaning of metal coil is shown.

9:20 am **MS-ThM4 Generation of Standard Test Wafers for Cleaning Efficiency Evaluations in Semiconductor Manufacturing**, *M. Liehr, S. L. Cohen, R. Tsai, K. Pope, B. Furman, R. Purtell*, IBM T. J. Watson Research Center, P.O. Box 218, Yorktown Heights, NY 10598, *K. Albaugh, S. Basiliere, S. Estes, M. J. Fleming, R. Gaylord, C. Gow, W. Syverson*, IBM Microelectronic Division, Essex Junction, VT.

Wet cleaning processes are ubiquitous in silicon integrated circuit manufacturing. Due to the large consumables cost and potential surface roughening effects there is great interest in evaluation of new and dilute chemical cleans. Thus, it is desirable to use well defined contaminant test wafers so as to enable quantitative comparison of cleaning processes prior to costly evaluations on product wafers. In this study, particle (Si<sub>3</sub>N<sub>4</sub> and SiO<sub>2</sub>), metal (Fe, Cu, Ni), and hydrocarbon (hexamethyl-di-silazane) standards were prepared and analyzed for use as test wafers for wet cleaning process development. These standard wafers are representative of typical line contamination and at concentrations which are high enough to be a 'worst case' situation. They were designed such that high cleaning efficiency is obtained with a 'good' clean, while for example, water rinsing alone is ineffective for removal. The test wafer preparation and analysis is reproducible cost effective and readily accessible. Using a design of experiments package (BestDesign) which minimizes the number of runs and simultaneously



optimizes multiple responses, it is possible to use this approach for process optimization on manufacturing tools. Requirements for successful implementation of these methods and details of the test wafer preparation/analysis will be described.

9:40 am **MS-ThM5 Rapid Yield Learning**, *D. M. H. Walker*, Dept. of Computer Science, Texas A&M University, College Station, TX 77843-3112.

Yield is a dominant economic consideration in semiconductor manufacturing. The yield ramp must occur quickly to maximize profits. *Rapid yield learning* is the set of activities directed at increasing the slope of the yield ramp and maintaining high yields once they are achieved.

The basic yield learning cycle is: process a wafer, measure the result, diagnose problems when they occur, and take corrective action. Measurements can be either direct (e.g. optical inspection of a test structure), or indirect (e.g. electrical test of a product chip). Direct measurements can accurately diagnose problems, but are high in cost and low in throughput. They are most useful early in process development, but later become a bottleneck. Indirect measurements are relatively cheap and fast, and are ideal for use during the yield ramp, but require models relating process disturbances to test failures. This has limited their use in the past.

We have developed models relating process disturbances to failures, simulators that implement these models and methods for using them in rapid yield learning. The models must traverse the domains from equipment to process to device to circuit to gate to test. We have used existing and new technology CAD and EDA tools to develop compact, computationally-efficient models that span the domains, providing the defect to failure relationship.

These models have been successfully applied at several companies for diagnosis of parametric and catastrophic defects. Some of these techniques have been commercialized in the *pdFab* simulator from PDF Solutions, Inc. Two challenges have been rapid model characterization and the cultural problems in the use of simulation models in semiconductor manufacturing and test.

**INVITED**

10:20 am **MS-ThM7 New Ashing Technology with Multi-plasma-mode Reactor**, *R. L. Bersin, M. Kikuchi, I. Nakayama*, ULVAC Technologies, Inc., Andover, MA 01810.

Photoresist has been employed in all aspects of wafer processing, such as etching, deposition, and ion implantation etc., to protect a surface from damage caused by highly reactive, or heavily damaging chemical environments to which the wafer is exposed. During the processing, the photoresist mask is subjected to physical and chemical erosion, high temperatures, impregnation with assorted chemical species, surface coating with all sorts of contaminant films and polymers. Considering all of the possible individual processes, and the variety of different chemistries they involve, any manufacturing tool purported to be a stripper of photoresist faces a severe test of flexibility. Historically, photoresist dry stripping equipment has concentrated on the simple chemistry of oxygen plasma, which quite effectively handles the virgin organic resist material. However, this approach ignores completely the complexity of the chemistry associated with the residue problems. It has been the practice of the industry to leave that problem up to the device manufacturer, to develop the necessary complex wet chemical process steps. We have developed a new process methodology, that combines microwave downstream free-radical chemistry and low-bias ion chemistry in one reactor, and in appropriate processing-step sequences to remove bulk photoresist, leaving behind most residuals converted to a water-soluble state. This suggests that DI Rinser-Dryers could replace most of acid and solvent wet stations. Processes have been developed for all significant masking steps. Questions of substrate loss and damage, undercutting of multiple layers, gate-oxide damage, are all being carefully considered. In this paper we discuss about the reactor concept, and present examples of process results and its advantages.

10:40 am **MS-ThM8 Vapor Phase SiO<sub>2</sub> Etching and Pre-gate Oxide Cleaning in an Integrated Cluster System**, *Y. Ma, M. L. Green, D. March\*, K. Hanson, J. Sapjeta and D. Brasen*, AT&T Bell Laboratories, Murray Hill, NJ 07974, \*Submicron System, Inc., Allentown, PA 18106.

Silicon dioxide etching and pre-gate oxide Si surface cleaning with vapor phase processing has been studied in a high vacuum, integrated cluster system. The system contains cleaning/etching and rapid thermal oxidation chambers. The integration enables us to process (pre-gate cleaning and oxide growth) an entire cassette without interruption. The SiO<sub>2</sub> etch rate fluctuates from wafer to wafer. The standard

deviation is less than 10% for a 25 wafer lot etched at a rate of 70 Å/min. The on-wafer uniformity is controlled by the IR lamp configuration with higher non-uniformity at higher process temperature. The non-uniformity of etching across a 5 inch wafer is less than 1% with lamps turned off (i.e. room temperature). Both the non-uniformity and the etch rate fluctuation from wafer to wafer can be compensated by an over-etch process since AFM measurement reveals no added roughness to the Si surface. Particles (>0.2 µm) generation during the process is in the range of 20 per wafer after about 100 Å oxide has been etched off. However, the particles counts can be reduced if the etching is carried out at a higher temperature. We are currently engaged in electrical device characterization studies.

11:00 am **MS-ThM9 Detection and Analysis of Ultra-Small Particles on 8" Unpatterned Si Wafers**, *C. R. Brundle, C. R. Brundle and Associates, San Jose, CA 95125, and Y. Uritsky*, Applied Materials, Santa Clara, CA 95054.

As the line-widths of IC's get smaller, the allowed size of "adder" particles deposited on Si wafers by the manufacturing tool/process also decreases. Currently it is 0.16 µm as detected by laser scanners which allow process engineers to determine the number of "adder" particles on an unpatterned test wafer and establish whether the process/tool is out of spec.

The laser scanner-generated particle map then becomes the reference co-ordinate system for our subsequent attempts to identify the nature of the particles and, therefore, their origin. Particle identification is usually performed using SEM/EDX (morphology information and elemental composition). Problems with this approach increase as particle size decreases, especially since some "particles" turn out to be thin film and organic/polymeric like. This paper reviews these problems and describes approaches for improved characterization capability. The problems are: the difficulty of relocating very small particles in an SEM on 8" unpatterned wafers (a co-ordinate transfer accuracy and an SEM contrast problem); the inability of EDX to effectively separate particle signal from substrate signal; and the fact that morphology and elemental composition are not always sufficient for a positive ID. The improved approaches described are: improved 8" wafer reference origin description and co-ordinate transform algorithms; improved EDX capability; and evaluation of Auger, SIMS, and FIB as "add-ons" to an SEM/EDX system.

11:20 am **MS-ThM10 The Nature of Copper Precipitation From Dilute HF Solutions on to Si Surfaces**, *T. S. Sriram, R. Sampson, J. Shyu, W. C. Harris, D. Liu and S. Bill*, Digital Equipment Corporation, 77 Reed Road, Hudson, MA 01749.

It is well known that the presence of Cu and other transition metals on the Si surface prior to oxidation can lead to increased junction leakage and possible loss of gate-oxide integrity<sup>1</sup>. This contribution examines the effect of Cu contamination of the HF used in HF-last cleaning processes prior to gate oxidation in deep sub-micron Si CMOS processes. We examined P-type (20-40 Ω-cm) Si [100] wafers exposed to a dilute HF solution which was quantitatively contaminated with Cu. Two concentrations of Cu, 1 ppm and 0.1 ppm were used in this study. The surface of the wafers was examined using TXRF and AFM. It was found that the Cu distribution on the wafer surfaces was non-uniform on both large and small scales. AFM imaging showed that the copper deposited in the form of small circular precipitates on the surface. Some areas of the sample exposed to the higher Cu concentration solution showed the aggregation of smaller precipitates in to large platelets. Subsequent Cu deposition on these platelets appears to occur in a layer-by-layer fashion. The surfaces of these platelets were very smooth (~0.1 nm RMS). No aggregation of platelets was seen in the sample exposed to 0.1 ppm Cu in HF. Diffraction analysis of planar samples from these wafers in the TEM revealed that the precipitates were composed of metallic copper.

1. E. Hsu, H. G. Parks, R. Craigin, S. Tomooka, J. S. Ramberg and R. K. Lowry, "Deposition Characteristics of Transition Metal Contaminants from HF-based Solutions on to Wafer Surfaces," Proc. 2nd Intl. Symp. on Cleaning Technology in Semiconductor Device Manufacturing, Phoenix, AZ, 14-18 Oct. 1992, pp. 170-178.





## VACUUM METALLURGY

### Room A106 - Session VM-ThM

#### Pulsed Laser and Pulsed Ion Technology for Film Deposition and Surface Modification

**Moderator:** B. Sartwell, Naval Research Laboratory.

8:20 am **VM-ThM1 Dual Laser Ablation of Particulate Free Optical Films**, *S. Witanachchi, K. Ahmed, P. Sakthivel and P. Mukherjee*, Department of Physics, University of South Florida, Tampa, FL 33620.

The excimer laser ablation of a poorly absorbing ceramic target has been shown to produce high density of particulates that render the films grown by this method inappropriate for optical applications. We report here the results of a dual laser process, where a pulsed CO<sub>2</sub> laser and an excimer laser were spatially overlapped on a Er doped Y<sub>2</sub>O<sub>3</sub> target, that produced defect free films that are suitable for waveguide laser fabrication. The delay between the two lasers was seen to significantly affect the particulate density in the deposited films. The particulate ejection was observed to be minimum when, temporally, the excimer pulse arrives at the target during the rising time of the CO<sub>2</sub> pulse. The optical emission of the plume has been studied for different delays between the lasers, and indicate a significant enhancement on the plume excitation. The role of the two lasers and the results leading to the optimization of this process will be discussed.

8:40 am **VM-ThM2 Nanostructured Films and Particles Produced by Femtosecond Pulsed-Laser Ablation**, *S. L. Rohde, A. Lateef, B. Robertson, T. Voiles, D. Doerr, and D. R. Alexander*, University of Nebraska-Lincoln, Lincoln, NE 68588.

Investigations of thin film formation and particle generation have been carried out using ultrafast femtosecond laser ablation of pure metals onto a variety of substrates. Both particles and thin films of Au and other metals have been deposited using femtosecond laser producing 20  $\mu$ J pulses with a pulse-width of 100 femtoseconds, focused into a 5  $\mu$ m spot-size. Particles produced and collected on carbon grids were examined using TEM and shown to have particles sizes down to a few nm in diameter; similar grainsizes were observed for very thin films of Au as well. Comparisons are presented for particles deposited in air, low vacuum, and moderate vacuum environments. Other parameters investigated include location of the substrates relative to the incident laser, target-to-substrate distance, and various laser pulse parameters. Comparisons are drawn between the films and particles produced in this work and those results found in the literature for pulse durations of several nanoseconds and longer. These initial results indicate that use of femtosecond pulsed-lasers may provide a means of producing ultrafine particles and nanostructured thin films with unique properties.

9:00 am **VM-ThM3 Large-Area Pulsed Laser Deposition: Techniques and Applications**, *J. A. Greer and M. D. Tabat*, Raytheon Company-Research Division, Lexington, MA 02173.

Due to its unique ability to quickly produce high quality films of complex chemical compounds, Pulsed-Laser Deposition (PLD) is currently being used to grow an estimated 200 different materials in laboratories world-wide. Most of the effort involving PLD has been geared toward obtaining high-quality films for electronic and optical applications. Also, significant research has been conducted on obtaining an understanding of the laser-target interaction and the laser-induced plume dynamics. However, relatively little work has been conducted on scaling-up this process to substrate sizes compatible with most device and process line requirements. Clearly, techniques for scaling the process will be needed in order for PLD to become more than a unique laboratory tool. This talk will focus on several large-area techniques which have been used to scale the PLD process to substrate sizes from 50 mm to 150 mm in diameter. The uniformity of a variety of film properties produced by PLD using these large-area PLD techniques will be presented, and the advantages and disadvantages of each approach will be discussed. A variety of properties and applications of large-area PLD films will be presented throughout the talk including subjects such as high-temperature superconductors, thin-film phosphors, and optical AR coatings. Finally, potential techniques and future equipment requirements to scale the process to substrates sizes of at least 200 mm in diameter will be examined.

INVITED

9:40 am **VM-ThM5 Laser Induced Fluorescence Studies of Atomic and Molecular Species in Laser Generated Plumes**, *Terry L. Thiem*, Dept. of Chemistry, USAF Academy, CO 80840, and *Paul J. Wolf*, F. J. Seiler Research Laboratory, USAF Academy, CO 80840.

Thin film growth by laser ablation deposition depends on both the nature and the energy of the material in the plume. The state of this material can be modified through interactions with a reactive ambient gas as in the case of oxide and high T<sub>c</sub> superconducting film formation in the presence of O<sub>2</sub> which is required for correct film oxidation. In addition, an understanding of the interaction of the plume species with a background gas and the substrate is needed to delineate the relative importance of gas phase or surface reactions in stoichiometric thin film formation.

As an initial measure of the relative importance of the film growth mechanisms mentioned above, we tracked ground state Ge and GeO using laser induced fluorescence in a plume generated by ablating a GeO<sub>2</sub> target at various pressures of O<sub>2</sub>, Ar and N<sub>2</sub>. Time of flight (TOF) profiles and the intensity behavior were mapped in time resolved experiments. The Ge TOF profiles in O<sub>2</sub> revealed a bi-modal behavior suggesting plume-ambient interactions which affected the Ge distributions. This behavior was absent in both the Ge distributions with other ambient gases and the GeO distributions. The most probable velocity was determined by fitting the TOF distributions to an isentropic expansion expression. Typical values ranged from 6  $\times$  10<sup>5</sup> cm/s to 1  $\times$  10<sup>5</sup> cm/s for Ge in vacuum and 100 mTorr of O<sub>2</sub>, respectively. The population of the ground state species decreased with increasing pressures for all ambient gases which indicated that gas phase chemical reactions were not kinetically important. These results will be detailed and subsequently correlated to mechanisms for thin film growth.

10:00 am **VM-ThM6 GeO<sub>2</sub> Films Prepared by Pulsed Laser Deposition**, *B. M. Patterson, P. J. Wolf*, F. J. Seiler Research Laboratory, USAF Academy, CO 80840; *M. Scott*, Dept. of Physics, USAF Academy, CO 80840; *T. Christensen*, University of Colorado, Colorado Springs, CO 80918.

In recent years pulsed laser deposition (PLD) has been used to prepare thin films of several materials having applications in integrated optical systems. Our group, in particular, has used the PLD technique to fabricate thin films of amorphous germanium dioxide (GeO<sub>2</sub>), as a preliminary step towards preparing GeO<sub>2</sub>-doped silica films for optical waveguiding and nonlinear optical applications. Our goal in the present work is to assess the suitability of PLD for preparing the flat and uniform films required for waveguiding.

The GeO<sub>2</sub> films were prepared on heated quartz substrates by ablating a rotating GeO<sub>2</sub> target in the presence of an oxygen plasma. In order to improve the thickness uniformity of the films, the target was inclined with respect to its rotation axis, thereby scanning the ablation plume over the substrate surface as the target rotated. X-ray diffraction measurements confirmed that the films were amorphous. The oxygen/germanium ratio (x) at various film locations was inferred from Fourier transform infrared spectroscopy measurements; the films were generally uniform in composition and near-stoichiometric (x > 1.9). Ellipsometry measurements were carried out on selected samples; these measurements indicated that the thickness variation was  $\leq$  1% over a 2.5 cm length across the film surface, although the index varied by up to 4%. In prism-coupling experiments ( $\lambda$  = 676 nm), 3-5 TM modes were typically observed in 2-3  $\mu$ m thick films, although no visual indication of guided light was observed. We detail these results and discuss the applicability of PLD for building waveguiding films.

10:20 am **VM-ThM7 High Energy, High Flux, Pulsed Ion Beams for Rapid Thermal Surface Treatment**, *D. C. McIntyre, R. W. Stinnett, R. G. Buchheit*, Sandia National Laboratories-New Mexico\*, *D. J. Rej and R. Muenchausen*, Los Alamos National Laboratory, *J. Greenly and M. Thompson*, Cornell University, and *G. Johnston*, University of New Mexico-Albuquerque.

There is an increasing interest in the use of ion-beams as broad-area sources for modifying surfaces using rapid thermal excursions. Recent developments in pulsed power technology have enabled the production of high average power (5-250 kW), repetitively pulsed (= 100 ns pulse duration) ion beams with beam diameters of 10-20 cm and with energies up to 2 MeV. The ion beams efficiently deposit energy in a thin surface layer (top 2-20 micrometers) of the surface of materials. Deposition of small energy doses of less than 10J/cm<sup>2</sup> is typically sufficient to melt the surface of metals and ceramics. Following melting, the surface layer rapidly cools at rates of approximately 10<sup>8</sup>-10<sup>10</sup> K/sec. These cooling rates are sufficient to produce amorphous, nanocrystalline, and/or supersaturated solid solutions in the treated layer. The resultant unique phases can, in turn, enhance the hardness and wear resistance of tool steels, the corrosion resistance

of engineering alloys, and the density of ceramic surfaces. This talk will review the effects of using ion beam surface treatment to enhance the properties of ferrous, nonferrous, and ceramic materials.

#### INVITED

\*This work was performed at Sandia National Laboratories, supported by the US Department of Energy under contract #DE-AC04-94AL85000.

11:00 am **VM-ThM9 Carbon and Nitrogen Implantation in a Large-Scale PSII Experiment\***, *B. P. Wood, J. T. Scheuer, D. J. Rej, I. Henins, W. A. Reass, R. J. Faehl, K. C. Walter, and M. A. Nastasi*, Los Alamos National Laboratory, Los Alamos, NM 87545.

In Plasma Source Ion Implantation (PSII), a target to be implanted is immersed in a weakly ionized plasma and pulsed to a high negative voltage. Ions in the plasma are accelerated toward the target and implanted in its surface, thereby modifying the properties of the surface. A large-scale PSII experiment is operating at Los Alamos, in which implantation of targets with surface areas of several  $m^2$  is performed in an  $8 m^3$  vacuum chamber using a 100 kV modulator supplying 20  $\mu s$  pulses at 2 kHz, with a peak current of 50 A. Our goal is to demonstrate that PSII can be scaled-up to an industrially useful process. In this talk I will describe the operational problems encountered and the results obtained in the implantation of carbon from methane, ethane, and acetylene plasmas, nitrogen implantation of large chrome-plated industrial parts, and nitrogen implantation of tool steels at elevated temperature.

\*Work supported by U.S. Department of Energy.

11:20 am **VM-ThM10 Film Deposition and Surface Modification Using Intense Pulsed Ion Beams**, *C. A. Meli, K. S. Grabowski, D. D. Hinshelwood, S. J. Stephanakis*, Naval Research Laboratory, Washington, DC 20375; *D. J. Rej, W. J. Waganaar*, Los Alamos National Laboratory, Los Alamos, NM 87545; *Michael O. Thompson*, Cornell University, Ithaca, NY 14853.

High-power pulsed ion beams have been used to ablate material for ultra-high-rate film deposition, and to modify the surface properties of alloys. Pulsed ion beams were provided by the Anaconda facility at LANL ( $\sim 500$  keV H, C, and O ions,  $\sim 1:1:1$  ratio,  $\sim 400$  ns

duration,  $E \sim 30 J/cm^2$ ) and the Gamble II facility at NRL ( $\sim 1.2$  MeV H and C ions,  $\sim 9:1$  ratio,  $\sim 100$  ns duration,  $E \leq 100 J/cm^2$ ). Instantaneous film deposition rates produced by ablation reached up to  $\sim 0.1$  cm/s, at the maximum available fluences. Films of pure Al, pure Ta, and a nickel-zinc ferrite compound were deposited on glass and single crystal substrates, in some cases heated. The film deposition process was studied with framing photography, a bolometer, and other diagnostics to gain an understanding of the ablation, transport, and deposition steps. These diagnostics provided guidelines for the production of desirable films. Smooth films, and oriented ferrite films have now been produced. Beams with a lower fluence ( $\sim 5 J/cm^2$ ) were used to investigate rapid thermal processing of metal surfaces for the enhancement of corrosion resistance. Bare steel surfaces were treated to smoothen surface features and dissolve precipitates, and thin metallic films on aluminum were treated to produce supersaturated surface alloys. Recent results in these two areas of effort will be presented.

11:40 am **VM-ThM11 Reactive DC Magnetron Sputtering of Oxide Coatings**, *W. D. Sproul\*, M. E. Graham\*, M. S. Wong\*, and R. A. Scholl\*\**, \*BIRL, Northwestern University, 1801 Maple Avenue, Evanston, IL 60201 and \*\*Advanced Energy Industries, Inc., 1600 Prospect Parkway, Fort Collins, CO 80525.

Conventional DC magnetron sputtering of nonconducting oxide films via reactive sputtering is extremely difficult. Without good separation of the oxygen from the target, the surface of the target rapidly becomes covered with an oxide film or "poisoned" when there is a high enough partial pressure of the reactive gas to form the desired film composition on the substrate. Breakdown of the oxide film on the target surface leads to arcing, which can damage the power supply and which can also eject droplets into the growing film. Depending on the application, these droplets can degrade performance of the oxide film. Recent advances in power supply technology with the introduction of pulsed DC power has overcome many of the problems in using DC power for the reactive sputtering of oxide films. The DC power is switched rapidly, at a rate up to 20 kHz, between the normal negative target potential and a positive potential, and during the positive pulse any charging on the target surface is discharged, which prevents the formation of an arc. It is now possible to reactively DC sputter such previously difficult materials as aluminum oxide with pulsed power. Details of these pulsing sources, the reactive sputtering process, and the properties of the resulting films will be discussed.

## SURFACE SCIENCE

Room A205 - Session SS1-ThA

### Oxidation and Adsorption

**Moderator:** J. W. Rogers, University of Washington.

2:00 pm **SS1-ThA1 Molecular Beam Homoepitaxial Growth and Surface Characterization of MgO(001)**, *T. T. Tran, T. A. Hileman, and S. A. Chambers*, Pacific Northwest Laboratory\*, Richland, WA 99352.

Homoepitaxial growth of thin MgO(001) films was accomplished by evaporating magnesium in a high-flux, low-energy beam of oxygen ions produced by an electron cyclotron resonance plasma source. Growths at different substrate temperatures in the 450–750°C range were attempted with improved film topography, as determined by ex-situ atomic force microscopy (AFM), obtained at the most elevated temperature. During growth, film composition was monitored by Auger electron spectroscopy and long-range crystallographic order was determined by reflection high energy electron diffraction. Post-growth analysis include low-energy electron diffraction and x-ray photoelectron diffraction data, providing long- and short-range crystallographic order information, respectively. Auger Mg KLL/O KLL intensity ratios obtained during growth were calibrated against Mg 2p/O 1s photoemission intensity ratios which had been previously normalized with data from a cleaved MgO(001) reference surface. Reproducible stoichiometry in the MgO films was obtained. Excellent short- and long-range crystallographic order in the films grown at 750°C, as observed with diffraction probes, along with AFM data suggest that a step-flow growth mechanism is operative in this temperature range.

\*Pacific Northwest Laboratory is operated for the U.S. Department of Energy by Battelle Memorial Institute under contract DE-AC06-76RLO1830.

2:20 pm **SS1-ThA2 Step Fluctuation Kinetics and the Formation of  $(n \times 1)\text{-O}/\text{Ag}(110)$** , *W. W. Pai, M. R. Peng, N. C. Bartelt, and J. E. Reutt-Robey*, University of Maryland, College Park, MD 20742.

We will present strong experimental evidence that  $(n \times 1)\text{-O}/\text{Ag}(110)$  adopts an "added-row" structure similar to  $(2 \times 1)\text{-O}/\text{Cu}(110)$ <sup>1</sup>. Despite the structural similarities between these two systems, we show that the formation mechanism for O/Ag(110) is different from that of O/Cu(110) because of differences in mass transfer from step edges.

STM images of the oxygen chains indicate that the O atoms are situated in the short 2-fold bridge sites with respect to the original Ag(110) substrate. The apparent contradiction to oxygen's observed preference for long 2-fold bridge sites is resolved by incorporating extra Ag adatoms to form a Ag-O-Ag chain-like structure. Additional evidence for this added row structure is provided by the 100 Å-scale displacements of 'isolated' steps upon oxygen adsorption, revealing that Ag atoms detach from the step edges to create the added rows. With infrared vibrational spectroscopy and LEED, we observe the atomic oxygen stretching frequency shifts continuously from 310 cm<sup>-1</sup> to 330 cm<sup>-1</sup> as the  $(7 \times 1)$  phase is compressed into the  $(3 \times 1)$  phase. This shift is consistent with a first principles calculation based on an optimized added-row structure.<sup>2</sup>

Details of the mass transport are obtained through analysis of step fluctuations on the clean surface at room temperature. From the autocorrelation in the position of the step edge, thermal step fluctuations appear dominated by adatom exchange processes at the step edge. The mean time between attachment/detachment is of the order of 100 ms. This rapid exchange indicates the presence of mobile silver adatoms on the terraces and that the rate of overlayer formation is not limited by step detachment kinetics. We suggest that the formation of Ag-O-Ag nuclei on terraces is the rate limiting step, in contrast to the step-atoms-supply limited process for O/Cu(110).

<sup>1</sup>D. J. Coulman, J. Wintterlin, R. J. Behm and G. Ertl, Phys. Rev. Lett., 64, 1761 (1990).

<sup>2</sup>T. Shimizu and M. Tsukada, Surf. Sci., 295, L1017 (1993).

2:40 pm **SS1-ThA3 Oxidation Behavior of the (100) and (110) FeAl Surfaces**, *H. Graupner, L. Hammer, and K. Müller*, Univ. of Erlg.-Nbg., Erlangen, Germany,\* and *D. M. Zehner*, Oak Ridge National Laboratory, Oak Ridge, TN 37831-6057 USA\*\*.

The initial stages of oxidation of the (100) and (110) surfaces of FeAl have been examined with XPS, AES, and LEED. Exposure to oxygen at sample temperatures up to 500°C leads to the formation of an amorphous Al<sub>2</sub>O<sub>3</sub> film on both surfaces. At higher temperatures, ordered oxide phases are observed. A  $(6 \times 6)$  superstructure is formed on the (100) surface at an oxidation temperature of 700°C, which is probably caused by an oxide film with a structure similar to  $\gamma\text{-Al}_2\text{O}_3$ . The thickness of this film has been determined to be  $4 \pm 1$  Å, which corresponds to two Al-O bilayers in  $\gamma\text{-Al}_2\text{O}_3$ . Apart from the chemically shifted Al 2p line associated with the oxide film, a second component is observed in the XPS spectra, which can be attributed to Al atoms in the substrate-oxide interface. Oxidation at 850°C leads to the development of a streaky  $(2 \times 1)$  diffraction pattern similar to that reported for the NiAl(100) surface. For the (100) surface, the initial rate of oxygen uptake is significantly higher compared with that of the (110) surface at all temperatures. The composition and thickness of the oxide film on the (110) surface is dependent on the initial oxidation rate. Low rates, as in normal ultrahigh vacuum experiments, lead to the formation of thin Al<sub>2</sub>O<sub>3</sub> films ( $\sim 6$  Å), while at higher rates thicker films are grown (8–15 Å) which contain iron oxide as well. Exposure to oxygen at a sample temperature of 850°C leads to the formation of a well-ordered oxide overlayer of  $6 \pm 1$  Å thickness and a large, nearly rectangular unit cell. The structure of this film is probably related to  $\delta\text{-Al}_2\text{O}_3$ . A film with identical unit cell parameters is present on NiAl(110). All observed oxide films are stable up to temperatures of 900°C.

This work is supported by \*Univ. of Erlg.-Nbg., FRG and DAAD, and \*\*U.S. Department of Energy, under contract DE-AC05-84OR21400 with Martin Marietta Energy Systems, Inc.

3:00 pm **SS1-ThA4 Electron Stimulated Oxidation of Metals at Low Temperature: Ni(111) at 120 K**, *Wei Li, M. J. Stirniman and S. J. Sibener*, The James Franck Institute and Department of Chemistry, The University of Chicago, 5640 S. Ellis Ave., Chicago, IL 60637.

Oxygen adsorption and oxide growth on Ni(111) has been investigated at 120 K. We have found that electrons stimulate nickel oxide growth at all energies examined, spanning the range from 5 eV to 2 keV. These electron stimulated effects occur under conditions which would otherwise lead to oxygen chemisorption in the absence of electron irradiation. Moreover, we find that electron induced oxidation can be achieved by two different procedures: one with the electron beam and oxygen exposure occurring simultaneously; the other with the electron beam and oxygen exposure alternating during the course of oxidation. These results differ from previous work, which concluded that appreciable oxide formation would occur upon exposure of low temperature Ni(111) to molecular oxygen—a result which we now attribute to synergistic effects involving electrons. We propose a model for the observed effect in which electrons create oxide nucleation centers on the Ni(111) surface in the presence of chemisorbed oxygen. This model allows us to quantitatively account for the data, including extraction of the relevant cross sections. These findings are of fundamental importance in the areas of metallic oxidation and corrosion, and may find application in electron beam lithography. Measurements are now continuing with a new seeded supersonic oxygen beam, allowing us to probe even finer details of the energetics and mechanism for this process.

\*Supported by the Air Force Office of Scientific Research and by the NSF Materials Research Laboratory at the University of Chicago.

3:20 pm **SS1-ThA5 Cesium/Oxide Interactions for Ultrathin Films on an  $\alpha\text{-Al}_2\text{O}_3(0001)$  Surface**, *K. R. Zavadil*, Sandia National Laboratories, Albuquerque, NM 87185, *Judith L. Ing*, AEA Technology, Albuquerque, NM 87106.

The nature of alkali metal/oxide surface interactions is important for predicting the stability and surface electronic properties of insulators in thermionic systems as well as understanding the chemical activity of promoters in catalytic systems. The chemical nature of the Cs-sapphire ( $\alpha\text{-Al}_2\text{O}_3$ ) interaction along with the growth of ultrathin Cs films has been studied using electron spectroscopy (XPS/AES),

electron diffraction (LEED) and mass spectrometry (RMS/TDMS). Reflection mass spectrometry (RMS) demonstrates facile adsorption of Cs, with an initial sticking coefficient of 0.9, on the unreconstructed (0001) surface at 300 K. This initial, energetic interaction is evident in the thermal desorption of Cs at temperatures in excess of 1000 K. Core level spectroscopic data show no formal oxidation of Cs despite this initial high affinity between the adsorbate and the surface. A critical coverage of Cs is reached at  $1.5 \times 10^{14}$  atoms  $\text{cm}^{-2}$  after which the sticking coefficient decays exponentially to a value less than 0.1. LEED results show only increased background intensities indicative of limited long-range order in the film. Comparison of TDMS and XPS/AES data indicate that cluster formation occurs with increased Cs exposure. The absence of an oxidized Cs signal coupled with cluster formation suggests selective interaction of Cs with coordinatively unsaturated O sites on the surface. Selective Cs-O interaction is further supported by comparison of the sticking coefficient versus exposure data for the  $(3\sqrt{3} \times 3\sqrt{3})\text{R}30$  and the  $(\sqrt{31} \times \sqrt{31})\text{R} \pm 9^\circ$  reconstructions of the (0001) surface. These surfaces show a decrease in sticking coefficient consistent with their reported oxygen deficient structure. The impact of adsorbed C on the Cs/substrate interaction will also be discussed.

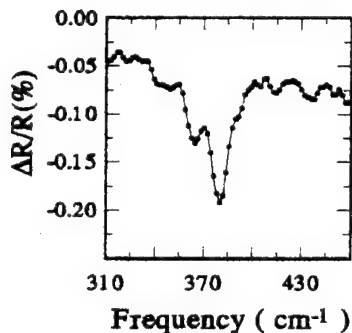
\*Funded by Ballistic Missile Defense Organization and supported by the U.S. Department of Energy under Contract No. DE-AC04-94AL85000.

**3:40 pm SS1-ThA6 Infrared Spectroscopy of Oxygen and Formate on Cu(100): Broadband Reflectance and Low-Frequency Vibrations,** K. C. Lin and R. G. Tobin, Dept. of Physics and Astronomy and CFMR, Michigan State University, East Lansing, MI 48824-1116 and P. Dumas, LURE, France.

We have studied the adsorption of oxygen and formate on a Cu(100) surface using synchrotron-based IR spectroscopy, from 100 to 2000  $\text{cm}^{-1}$ . Oxygen adsorption induces a frequency-dependent broadband reflectance change. Our measurements provide the first independent test of a model based on conduction electron scattering that incorporates nonlocal electrodynamics. Excellent agreement is found for low O coverage. Some discrepancies with theory remain, in the high-coverage behavior and the value of the rolloff frequency.

Exposure of the O-predosed surface to formic acid removes the oxygen and leaves a formate layer. The broadband reflectance returns to its clean-surface value. Two low-frequency vibrational modes are observed, at 360 and 380  $\text{cm}^{-1}$ , as shown in the figure. Previous EELS investigations could not resolve these modes. The observation of two modes presumably due to Cu-O vibrations suggests that more than one adsorption site may be occupied.

Supported by NSF Grant Nos. DMR-8815616 and DMR-9201077 and NSF/CNRS Int'l. Collaborative Award No. INT-9016771.



**4:00 pm SS1-ThA7 Atomically Resolved STM Study of the Interaction of Boron with Si(001),** Yajun Wang and Robert J. Hamers, Department of Chemistry, University of Wisconsin, Madison, WI 53706, USA.

The interaction of boron with Si(001) is very important for semiconductor processing. STM, tunneling spectroscopy and surface photovoltage measurement have been used to study the geometric and electronic structures of boron-induced reconstructions produced by thermal decomposition of diborane on Si(001). At  $T > 675$  K, boron atoms organize into ordered structures on the surface. STM images reveal a number of boron-induced reconstructions which arise from the arrangements of three structural subunits. Boron atoms bond at

substitutional sites and form a delta-doped layer. These boron-induced structures are chemically inactive, but electrically active. Over 1075K, most boron atoms diffuse into bulk and it also produces surface faceting. This is the first atomic-scale study of boron-induced reconstructions on Si(001) and it will provide a deeper understanding of semiconductor doping. The formation process of new structures and their effects on further silicon film growth will be discussed. This work is supported by the U.S. Office of Naval Research.

**4:20 pm SS1-ThA8 The Structure and Stability of Methyl Thiolate on Ni(111),** D. R. Huntley, D. R. Mullins, S. H. Overbury, Oak Ridge National Laboratory, Oak Ridge, TN 37871-6201 and H. Yang, North Carolina State University, Raleigh, NC 27695-8204.

The production of methane from the reaction of either methanethiol or dimethyldisulfide on the Ni(111) surface involves at least two intermediate species at high coverage which are readily discernable by high resolution XPS. One of these intermediates is formed upon adsorption at temperatures less than 100 K and is identified as methyl thiolate, based on the HREEL spectra. A second intermediate is formed upon heating the surface, and is stable between 200 and 275 K. HREEL spectra measured both on and off specular scattering conditions as a function of both annealing time and temperature exhibit no new modes due to the activated formation of this species, indicating that it is also a methyl thiolate fragment. However, changes in the relative intensities of the methyl deformation and stretching modes suggest a difference in orientation of the methyl group. The thiolate formed at low temperature is proposed to reside in a low coordination site such as a two-fold bridge site and have the C-S bond tilted toward the surface. The thiolate formed at higher temperature occupies a three-fold hollow site and has the C-S bond nearly perpendicular to the surface. Recent calculations using the many electron embedding theory support this conclusion, indicating nearly equal adsorption energies for these two configurations.

Research Sponsored by Division of Chemical Sciences, Office of Basic Energy Sciences, U.S. Department of Energy.

**4:40 pm SS1-ThA9 A Comparative Study of  $\text{P}(\text{CH}_3)_3$  and  $\text{PH}_3$  Decomposition on Ru(0001),** H.-S. Tao and T. E. Madey, Dept. of Physics & Astron. and Lab. for Surface Modification, Rutgers, The State U. of NJ, Piscataway, NJ 08855-0849, U. Diebold, Dept. of Physics, Tulane U., New Orleans, LA 70118-5698 and N. D. Shinn, Sandia Nat. Labs., MS-0344, Albuquerque, NM 87185-0344.

The decomposition mechanisms for precursors on surfaces are important in determining the efficiency of CVD processes. As a model system, the decomposition of  $\text{P}(\text{CH}_3)_3$  and  $\text{PH}_3$  on Ru(0001) has been studied by soft X-ray photoelectron spectroscopy using synchrotron radiation. By mean of the chemical shifts in the  $\text{P}(2p)$  core-levels, we are able to identify stable phosphorus containing surface reaction intermediates and elucidate the overall reaction mechanism.  $\text{P}(\text{CH}_3)_3$  undergoes a step-wise demethylation, i.e.,  $\text{P}(\text{CH}_3)_3 \rightarrow \text{P}(\text{CH}_3)_2 \rightarrow \text{P}(\text{CH}_3) \rightarrow \text{P}$ , which is complete at  $\sim 450\text{K}$ . In contrast,  $\text{PH}_3$  decomposition involves a single stable intermediate of undetermined stoichiometry,  $\text{PH}_3 \rightarrow \text{PH}_x \rightarrow \text{P}$ , and is complete at  $\sim 190\text{K}$ . The subsequent conversion of chemisorbed phosphorus to ruthenium phosphide by annealing is complete at  $\sim 700\text{K}$ . Molecular adsorption and decomposition energetics are estimated using the bond order conservation Morse potential (BOCMP) method, and are found to agree semi-quantitatively with the experimental data. These mechanistic and energetic insights are useful in designing future phosphorus-containing molecular precursors for low-temperature, selective deposition of phosphorus in materials growth technologies.

Experiments performed at the National Synchrotron Light Source and supported, in part, by DOE-BES (DE-AC04-94AL85000).

**5:00 pm SS1-ThA10 Long Range Periodicity and Local Order in Complex Molecule Chemisorption,** B. G. Frederick, F. M. Leibsle, S. Dhesi, M. B. Lee, K. Kitching and N. V. Richardson, IRC in Surface Science, University of Liverpool L69 3BX, U.K.

For a fundamental understanding of organic film growth it is critical to understand and control the orientation and chemistry of the initial layer. The periodicity and orientation in complex molecule adsorption involves a balance between intermolecular interactions and local site requirements of the substrate; such a competition is evident in the chemisorption of benzoic acid on Cu(110). At saturation coverage, the surface benzoate species forms an ordered  $c(8 \times 2)$  structure and STM images suggest that the benzene rings are aligned along the close



packed rows. This configuration is consistent with the ring coplanar with the carboxylate group, which is expected to bond in the short bridge site by analogy to formate/Cu(110). Because the barrier to rotation about the carboxylate-ring bond is known to be small ( $\sim 4$  kcal/mol), dynamic near-neighbor repulsion will be important in restricting torsional motion at 300 K. With electron irradiation in LEED and STM, the long-range periodicity is lost but considerable local order is evident in STM measurements. The local order appears to be constrained by adsorption in well-defined sites and may be driven by the preferred interaction between rings at nearly perpendicular angles as found for solid benzene. With annealing, the surface returns to the  $c(8 \times 2)$  structure. We compare the kinetics of disordering in LEED with microscopic evidence that disordering initiates at domain boundaries and above a bias threshold of  $\sim 3$  V. Evidence from other spectroscopic probes (HREELS, NEXAFS, RA) of azimuthal orientation is also discussed in relation to the dynamics of the electron-induced disordering and thermal re-ordering processes.

## SURFACE SCIENCE

### Room A201 - Session SS2-ThA

#### Surface and Adsorbate Structure

**Moderator:** P. Avouris, IBM T. J. Watson Research Center.

2:00 pm **SS2-ThA1 Br/Si(211)2 $\times$ 1 Structure Investigated by X-Ray Standing Waves**, V. Eteläniemi, E. G. Michel, and G. Materlik, HASYLAB at DESY, 22603 Hamburg, Germany.

The interaction of halogens with silicon surfaces has been a subject of interest in recent years since it represents the first step of the etching process. We have studied the system Br/Si(211)2 $\times$ 1 by using the x-ray standing wave (XSW) technique, which allows a precise determination of the adsorption geometry of an interface. A clean, non-faceted Si(211)2 $\times$ 1 surface was prepared by annealing in vacuum a chemically etched crystal. The ideal Si(211) surface is formed by [111] terraces and [100] steps, and thus it is an ideal model surface to investigate the interaction between both types of sites. After Br adsorption, the surface reconstruction reverts to 1 $\times$ 1 (as is typical of several other silicon surfaces). The adsorption sites of Br were investigated as a function of Br coverage and annealing temperature in order to characterize the competition between step and terrace sites at the surface. Three different substrate reflections ([422], [111], and [220]) were employed to locate Br atoms independently of the silicon surface geometry. Our results indicate that both atop (on terraces) and step sites (with Br atoms along empty dangling bond directions) co-exist at the surface at room temperature. After annealing, the step sites are relaxed in such a way that the Br-Br interatomic distance is maximized. The change in bond angles estimated from our analysis fits well within the limits fixed by current models for the elasticity of silicon bonds. Annealing to higher temperatures favors the occupation of terrace sites only.

2:20 pm **SS2-ThA2 The Structural Characterization of Ga on Si(112)**, J. E. Yater\*, A. Shih, Y. Idzerda, Naval Research Laboratory, Washington, DC 20375.

The structure of gallium overlayers on the Si(112) surface has been investigated using the technique of angle-resolved Auger electron spectroscopy (ARAES). This system is of scientific interest because previous studies suggest that the Ga atoms form well-ordered chains along the stepped Si(112) surface. The fabrication of quantum well wire arrays has much significance in solid state device applications, as does the growth of III-V materials on silicon substrates. However, no studies to date have determined the exact gallium atomic site locations relative to the Si(112) substrate lattice. In this study, angle-resolved AES data is used to distinguish between a host of possible overlayer/lattice structures based on a comparison with single scattering cluster (SSC) calculations. These calculations show that low energy AES data is very surface sensitive and therefore appropriate for overlayer structural studies. A well-ordered gallium overlayer is grown on a clean (1 $\times$ 2) reconstructed Si(112) surface such that a (6 $\times$ 1) LEED pattern is observed. The angular dependence of the Auger electron intensity is measured for two low energy gallium peaks along the [110] and [111] directions. The theta scans are taken in .5° incremental steps, and modulations are observed in the intensity patterns which correspond

to scattering minima and maxima along the forward direction of the overlayer structure and reflect the symmetry of the overlayer structure along the scan direction. These measurements are the first ARAES data from such chain-like overlayer structures. A comparison with cluster calculations can be used to determine the gallium atomic site locations and the resulting Si(112) surface structure.

\*NRC Postdoctoral Fellow.

2:40 pm **SS2-ThA3 Transition Metal Induced Ring-Cluster Structures on Si(111) Studied by STM**, S. A. Parikh, M. Y. Lee and P. A. Bennet, Physics Dept., ASU, Tempe, AZ 85287-1504.

We characterize a "ring-cluster" (RC) structure produced by high temperature annealing of transition metals (TMs) on Si(111). Originally discovered for Co,<sup>1</sup> this structure consists of a single metal atom on a substitutional site in the top layer of Si(111) plus an overlying ring of 6 Si adatoms with an unusual bridge-bonded topology. The same structure occurs for all near noble metals (Co, Ni, Pd, Pt, Ir) but not for earlier TMs (Fe, Ti and Ta) or noble metals (Cu). The RCs first form at 700C and at higher temperatures will phase separate from clean Si(111)-7 $\times$ 7 into large triangular patches containing a 1 $\times$ 1 lattice gas of RCs plus small 2 $\times$ 2 patches of Si adatoms on T4 sites. The metal coverage in the 1 $\times$ 1 phase ranges from a minimum of .02 ML to a maximum of .14 ML at which point the RCs are close-packed and can order into a  $\sqrt{7}$  superlattice. In the case of Ni, a second ring-like structure forms simultaneously with the RCs and orders into a  $\sqrt{19}$  superlattice at a minimum coverage of .16ML. These rings are centered on T4 sites of Si(111). A unit cell structure with 3 sub-surface Ni atoms is presented.

<sup>1</sup>P.A. Bennett, M. Copel, D. Cahill, J. Falta and R. M. Tromp, Phys. Rev. Lett. 69 (1992) 1224.

3:00 pm **SS2-ThA4 Surface Geometry of S-Passivated InP(100)-(1 $\times$ 1)**, O. L. Warren, G. W. Anderson, M. C. Hanf, and P. R. Norton, University of Western Ontario, London, Ontario, Canada.

Surface cleaning/passivation is a key step in semiconductor manufacturing processes. In the case of InP(100), the surface is passivated effectively by S after dipping in an aqueous solution of (NH<sub>4</sub>)<sub>2</sub>S at 65°C. Upon transfer to UHV, the surface exhibits a coherent (1 $\times$ 1) LEED pattern without further treatment. In order to ascertain the role of S in surface passivation, we have determined the geometric structure of S-passivated InP(100)-(1 $\times$ 1) by dynamical LEED analysis. Sulfur atoms occupy the expected surface bridge sites which continue the zincblende structure of the substrate, the bond only to In atoms in the next layer. Other structural models, such as S bonded to sp<sup>2</sup>-hybridized In, can be clearly ruled out. Investigation of random vacancies in the S layer favors nearly a full monolayer coverage. The distance between the S layer and the In plane directly beneath is 1.45 Å, and all interlayer spacings of the substrate remain at the bulk value of 1.47 Å; therefore, the In-S-In bond angle is nearly exactly tetrahedral. The quality of fit between experiment and theory is good, as indicated by a minimum Pendry r factor of 0.26. The bonding configuration determined in the analysis is consistent with the idea that S passivates the surface by saturating the dangling bonds. These results are in general agreement with those obtained previously by XANES, although the details differ on a quantitative level.

3:20 pm **SS2-ThA5 Structural Determination of Methyl Halides on GaAs(110): Analysis by NEXAFS and TOF Measurements of Photodissociation**, P. J. Lasky, P. H. Lu, Q. Y. Yang, and R. M. Osgood, Jr., Columbia Radiation Laboratory, Columbia University, NY, NY 10027.

The structure of methyl halides physisorbed on GaAs(110) has been investigated by NEXAFS and correlated with angular resolved time of flight (TOF) measurements of methyl radicals ejected from the photoinduced dissociation of the adsorbed molecules. The photo-induced dissociation is due to electron attachment to the adsorbate molecules from electron-hole pairs created in the GaAs substrate. The results from both experiments show that the methyl halide molecules in the first monolayer are oriented so as to tilt away from the surface normal in the [01] direction. These results indicate that the dissociation process takes place on a time scale faster than reorientation of the CH<sub>3</sub>X<sup>-</sup> ion intermediate and demonstrates clearly the ability to use angle-resolved TOF measurements of fragments generated from photo-induced dissociation by low energy electron attachment as a probe of the structure of adsorbed molecular layer. In addition, the results show that the molecules in the second layer are oriented differently from



those in the first and have also been investigated with NEXAFS and TOF. The correlation of results from NEXAFS and TOF measurements, along with insights gained from the modeling of temperature programmed desorption (TPD) data has elucidated the structure of methyl halides on the GaAs(110) surface. This structural information provides insight into the interactions of small, dipolar molecules with the corrugated GaAs(110) surface. Preliminary computations indicate that the molecular tilt is in agreement with electrostatic interactions between the adsorbate molecule and the surface fields.

**3:40 pm SS2-ThA6 Structure of Sulfided Ultra-Thin Ni Films on W(001), S. H. Overbury, Oak Ridge National Laboratory, Oak Ridge, TN 37831-6201.**

Low energy alkali ion scattering, LEED and AES have been used to determine the interaction and structures of co-adsorbed S and Ni on the W(001) surface. This work follows previous research to characterize the structures obtained for Ni/W(001) and of S/W(001), and provides structural details on a model system study of sulfidation of ultra-thin metal films. Ni alloys with W(001) to form a single mixed layer at sub-monolayer coverages, but at 1 ML it remains at the surface and forms a relatively pure, pseudomorphic overlayer. Pseudomorphic growth continues into the second layer. It is found for annealing temperatures of around 900 K that S adsorbs as an overlayer on Ni films of thicknesses of 1 to 2 ML without inducing separation of Ni into islands of Ni or of Ni sulfide. A  $c(2 \times 2)$  pattern is obtained for S coverages near 0.5 ML on W(001) and on the thin Ni films. Ion scattering demonstrates that this pattern is due to ordering of S atoms adsorbed on four-fold sites on the W or pseudomorphic Ni. This structure can also be obtained by reversing the order of deposition, due to thermally induced place exchange of Ni and S atoms. Surface bonding distances can be determined from the location of shadowing edges observed in angular scans of Ni and W single scattering. A ML of Ni allows S adatoms to be slightly closer to underlying second layer W atoms than on Ni-free W(001). Sorbed S causes outward relaxation of the Ni layer. As S coverage increases above 0.5 ML, the  $(1/3, 2/3)$  beam of the  $c(2 \times 2)$  pattern is replaced by diffuse features. LEIS indicates that S continues to fill four-fold Ni hollow sites.

Research sponsored by Division of Chemical Sciences, Office of Basic Energy Sciences, U.S. Department of Energy.

**4:00 pm SS2-ThA7 Morphology and Mobility of Steps on a Metallic Surface Cu(1,1,1), Influence of Sulphur Adsorption, L. Masson, L. Barbier, J. Cousty, and B. Salanon, SRSIM CE Saclay C.E.A., 91191 Gif sur Yvette Cedex, France.**

Growth on semiconductor or metal vicinal surfaces exhibits some interesting features: The miscut allows to perform good quality thick layer heteroepitaxy by compensating lattice mismatch. Moreover selective adsorption along the steps may be interesting for applications (reactivity or quantum wire structures). Such systems set some fundamental questions: What are the conditions for a step adsorption, what is the mutual influence between the adsorbate and the steps...?

In order to answer some of these questions we have performed an adsorption study with sulphur (by a  $H_2S$  exposure) on a vicinal surface of copper namely Cu(1,1,1). The S adsorption is studied in the low coverage range (lower than 5% S at/Cu at.). The coverage rate is stable without intermixing below 875 K. The results for the bare surface and the adsorbate covered one obtained by Hc diffraction (TEAS) and Scanning Tunneling Microscopy (STM) are compared.

The TEAS study allows to conclude to a random deposition at room temperature. On the Cu surface the broadening of out of phase (relatively to the step displacement) diffraction peaks measures the step disorder. Upon adsorption the peak broadening increases with the coverage and the step disorder accordingly. STM pictures at room temperature confirm these results and provide detailed information on the adsorption sites and morphology of the steps. The S adsorption is clearly random on the terraces. A statistical analysis of the Cu and S/Cu pictures gives a reduced Cu mobility along the steps (unit length  $a_0$ ) and an increase of the kink density upon adsorption: The diffusivity  $b^2$  for the bare surface and the surface covered by 2% S are respectively 0.017 and 0.036  $kink^2/a_0$ . After annealing (675 K) the kink density further increases ( $b^2=0.093$ ) and sulphur adsorbed along the steps becomes pinned at kinks. Correlatively the step mobility vanishes. The correlation function (along the steps) of the step position, altered at short distances ( $<40 a_0$ ) remains unmodified at large distances ( $>40 a_0$ ) as compared to the clean surface.

**4:20 pm SS2-ThA8 Second Harmonic Generation from Alkali Metal Overlayers on Al(111) Surface, Jian Wang, Z. C. Ying, University of Pennsylvania, Philadelphia, PA 19104; E. W. Plummer, University of Tennessee, Knoxville, TN 37996.**

In order to fully explore the potentials of the optical second harmonic generation (SHG) as a useful surface probe, it is necessary to understand the microscopic mechanism of the surface nonlinear optical process. Surface SHG from metal surfaces is paid special attention since such system is theoretically tractable by first-principle calculations. Using a mode-locked Nd:YAG laser at 1064 nm ( $\hbar\omega=1.17$  eV) and 532 nm ( $\hbar\omega=2.34$  eV), we were able to measure the SHG from clean Al(111) surface as well as from alkali metals (Na, K, Rb) adsorbed on Al(111) surface as functions of azimuthal angle, coverage and temperature. The SHG from clean Al(111) and (Na, K, Rb)/Al(111) exhibits both isotropic and anisotropic responses with respect to the rotation of the crystal azimuthal angle. For isotropic components, the enhancement of SHG from alkali metal overlayers adsorbed on Al(111) over that of the clean Al(111) surface agrees well with the recent time dependent local density calculations (TDLDA).<sup>1</sup> This agreement confirms that the induced second-order current normal to the surface is the dominating component in SHG from metal surfaces and alkali metal overlayers on metal surfaces. Yet, the strong anisotropic SHG from our experiment suggests that there is still a need to extend our current physical picture as embedded in the TDLDA calculations beyond the free-electron models, even for the simplest metal surfaces.

<sup>1</sup>A. Liebsch, Phys. Rev. B 40, 3421 (1989).

**4:40 pm SS2-ThA9 Depolarization and Phase Behavior in a Model for Alkali Adsorption on Simple Metals,\* L. D. Roelofs and Daniel Fromowitz, Physics Dept., Haverford College, Haverford, PA 19041 USA.**

Alkali adsorption on metallic surfaces results in complex phase behavior due to the interplay between the charge-transfer-based bonding behavior and adatom interactions. Observed phenomenon<sup>1</sup> include phase transitions involving depolarization,<sup>2</sup> coverage-driven changes in binding site and substrate reconstruction. We have developed a model for these systems based on dipole-dipole adatom interactions with moment strengths determined (self-consistently) by the competition between bonding-induced moment formation and depolarization based on adatom proximity. The model also incorporates multiple binding sites. We report simulation results obtained from this model including: the nonlinear work-function variation (with coverage) characteristic of these systems; low-coverage ordered phases; and the novel coverage-driven depolarization transitions proposed in ref. 2. Some parameter variation is also presented in order to point toward consistency with experimental systems.

\*Supported by NSF grant DMR-9106804.

<sup>1</sup>J. N. Andersen, E. Lundren, R. Nyholm and M. Qvarford, Surface Sci. 289, 307 (1993).

<sup>2</sup>J. Neugebauer and M. Scheffler, Phys. Rev. Lett 71, 577 (1993).

**5:00 pm SS2-ThA10 The Structures of CO and O on the Rh(110) Surface as Determined by Tensor LEED, J. D. Batteas, A. Barbieri, E. K. Starkey, M. A. Van Hove, and G. A. Somorjai, Materials Sciences Division, Center for Advanced Materials, Lawrence Berkeley Laboratory, and Department of Chemistry, University of California, Berkeley, CA 94720.**

The structure and bonding of atoms and molecules on defect sites such as steps and kinks are of particular interest since these are proposed "active sites" of surface reactions. Rh(110) is a densely stepped surface with rows of (111) microfacets. Both CO and O form ordered  $p2mg(2 \times 1)$  surface phases at 1 monolayer coverage on the Rh(110)-(1  $\times$  1) surface. The detailed structures of these phases have been determined by an automated tensor LEED intensity analysis.

In the Rh(110)- $p2mg(2 \times 1)$ -2Co structure, the clean surface relaxations are removed with the top interlayer spacing expanded by 0.15 Å with respect to the clean surface. The CO molecules are bonded near the short bridge sites with Rh-C bond lengths of 1.97 Å, a C-O bond length of 1.13 Å, and the molecular axis tilted by  $\sim 24^\circ$  from the surface normal. In the Rh(110)- $p2mg(2 \times 1)$ -2O structure, a cluster-like bonding for the O is found. The clean surface relaxations are removed and the oxygen atoms are bonded asymmetrically in the 3-fold hollow-site. Two Rh-O bonds are formed with the top metal layer with bond lengths of 1.86 Å and a third Rh-O bond is formed with the second metal layer of 2.07 Å. The second metal layer Rh atoms

are found to shift away from their clean surface positions, towards the oxygen positions, introducing a zig-zag lateral "splitting" of the layer by  $\sim 0.10 \text{ \AA}$ .

## **NANO 3/NANOMETER-SCALE SCIENCE AND TECHNOLOGY/ BIOMATERIAL INTERFACES Room A209 - Session NSBI-ThA**

### **Micro-Instrumentation and Sensors**

**Moderator:** M. H. Hecht, Jet Propulsion Laboratory.

2:00 pm **NSBI-ThA1 Micromachined Neural Interface Technology**, Gregory T. A. Kovacs, Stanford University.

Direct interfaces between living neural tissue and electronic circuits have long been desired, both as research and rehabilitation tools. Recent developments in the micromachining of silicon and other materials has led to the ability to fabricate arrays of microelectrodes that offer great promise in this area. Currently, research is underway to fabricate three types of neural interface: penetrating cortical probes, regeneration electrode arrays for peripheral and selected cranial nerve applications, and "electric Petri dishes" for in vitro preparations. Work at Stanford's Center for Integrated Systems in each of these areas will be reviewed. Issues of microfabrication and the potential integration of signal processing circuitry will be discussed, as well as future research directions. **INVITED**

2:40 pm **NSBI-ThA3 Fabrication and Characterization of a Nanosensor for Admittance Spectroscopy of Biomolecules**, L. Montelius, J. T. Tegenfeldt and T. Ling, Lund University, Dept. of Solid State Physics and The Nanometer Structure Consortium, Box 118, S-221 00 Lund, Sweden.

We have fabricated nanometer-sized interdigitated electrode patterns using electron beam lithography and lift-off techniques. The silicon dioxide surface was before patterning treated with APTS in order to promote selective adsorption of biomolecules in between the electrodes. The aim of the investigation was to find out whether the dimensions (i.e., the electrode separations) of the pattern would affect the admittance signal of the biomolecules in between the electrodes. The biomolecule we chose to study was horseradish peroxidase. Since the admittance signal scales with the geometrical factor  $A/d$ , where  $A$  is the electrode area and  $d$  is the separation, we chose to keep  $A/d$  constant when changing the electrode separation in order to eliminate this trivial effect on the admittance signal. Our findings suggest that a much more sensitive "biosensor" is possible to fabricate with nanometer technology than the present "biosensors" having dimensions on the micron scale. We also found that the biosensor in the nanometer regime—the nanosensor—actually is not only more sensitive but also more biospecific than a larger micro-sensor would be.

3:00 pm **NSBI-ThA4 Interfacial Aspects of Acoustic Plate Mode (APM) Biosensor Response**, J. Renken, R. Dahint, F. Josse\*, M. Grunze, Universität Heidelberg, Lehrstuhl für Angewandte Physikalische Chemie, Im Neuenheimer Feld 253, 69120 Heidelberg, Germany, \*Department of Electrical and Computer Engineering, Marquette University, Milwaukee, WI 53233, USA.

Recently, preliminary results on a mass-sensitive 150-MHz APM biosensor on  $\text{Zr-LiNbO}_3$  have been reported. It has been shown that the adsorption of non-labeled antigens can be monitored in real-time at the nanogram scale. However, interfacial effects of the antibody film have not yet been taken into account. Therefore, films of different chemical structure were used for the coupling of antibodies to the crystal surface. An aminosilane, a dextran, and a new polyether-polyurea based immunosorbent were prepared and their antigen binding capacities determined by a modified ELISA test. The results show that the antigen binding capacities for the dextran and the polyether-polyurea films are enhanced by a factor of 4.5 and 2.7, respectively, compared to the aminosilane film. Sensor experiments, however, reveal that an increased antigen binding capacity does not necessarily result in a higher dynamic range of the acoustic device. No significant enhancement is observed neither for the dextran film nor for the polyurea film. This deviation is discussed in terms of the viscoelastic properties of the different films.

3:20 pm **NSBI-ThA5 Fast Temperature Modulation for Selective Gas Sensor Operation**, R. E. Cavicchi, J. S. Suehle, P. Chaparala\*, K. G. Kreider, and M. Gaitan, National Institute of Standards and Technology, Gaithersburg, MD 20899.

Many solid state gas sensors use the electrical conductance change of a semiconducting oxide as the sensing principle. These devices, usually fabricated as discrete single sensors, typically use elevated temperatures in the range  $200^\circ\text{C}$ – $500^\circ\text{C}$  to effect the surface reactions required for sensing. A key drawback of this class of sensors is that many different reducing gases will cause a conductance change. Partial selectivity is attempted through the use of catalytic additives to the semiconducting oxide. There is now considerable interest in the application of thin film technology to produce arrays of sensors with different additives to create a selective sensing instrument on a chip. Here we describe an approach which takes advantage of the fast thermal response of micro-machined "hotplates," fabricated on a silicon wafer using CMOS technology. Micro-hotplates have a wide range of temperature control, from  $20^\circ\text{C}$ – $550^\circ\text{C}$  or  $1000^\circ\text{C}$ , depending on design materials, and a fast thermal response of about 1 ms. They may be fabricated in arrays with electrical circuitry on the same chip. We demonstrate operating modes in which ramped sequences of temperature pulses are applied to a micro-hotplate, while monitoring the conductance of a  $\text{SnO}_2$  film grown over contact pads on the micro-hotplate. The kinetics for adsorption, desorption, and reaction on the sensing surface are thereby controlled by the sensing instrument. A smart sensor would use on-chip pattern recognition techniques to analyze incoming data, and adjust the temperature-pulse sequence to refine composition analysis. Response differences between the vapors of ethanol, methanol, and other gases are demonstrated.

\*Dept. of Materials and Nuclear Engineering, Univ. of Maryland at College Park.

3:40 pm **NSBI-ThA6 New Techniques of Thermal Imaging Using the Atomic Force Microscope**, M. Chandrachood, O. Nakabeppu, Y. Wu, J. Lai, and A. Majumdar, Department of Mechanical Engineering, University of California, Santa Barbara, CA 93106.

Trends in VLSI technology suggest that when semiconductor devices are fabricated in the deep sub-micron range, power dissipation can be a critical factor in chip design and operation. With the goal of developing a temperature measuring technique in the nanometer range to understand the thermal behavior of sub-micron devices, this paper presents two new techniques of thermal imaging using the atomic force microscope (AFM). The first uses the mismatch in thermal expansion coefficients of a metal, such as aluminum or gold, and silicon nitride. When an aluminum film is deposited on a regular silicon nitride AFM cantilever, a temperature change results in cantilever bending. By sensing the temperature-induced deflections while scanning the probe, the temperature of a surface can be measured. An AC heating method is used to separate deflections due to topography and temperature. The second technique uses a microfabricated thin film thermocouple on a regular silicon nitride AFM probe. By scanning the thin-film thermocouple tip on the surface, the surface temperature can be mapped. For both techniques, experiments done in air and in vacuum suggest that due to the small tip-sample contact area, heat conduction through air dominates over that through the tip-sample point contact and could be the limiting factor in the spatial resolution. Thermal images of sub-micron metal lines and semiconductor devices will be presented.

4:00 pm **NSBI-ThA7 Initial Tests of a Micromachined SEM**, D. A. Crewe, A. D. Feinerman, University of Illinois at Chicago, Chicago, IL 60680.

A Micromachined Scanning Electron Microscope (MSEM) consisting of square-cm sized silicon die aligned and separated by optical fibers has been built and is in the initial stages of experimental testing. Each die contains a set of four orthogonal anisotropically etched v-grooves and a small ( $5\text{--}200 \mu\text{m}$ ) aperture. Short ( $5 \text{ mm}$ ) lengths of precision  $300 \mu\text{m}$  diameter Pyrex fibers are placed in the grooves and a die with a matching v-groove pattern is placed on top of the fibers. The two die are then anodically bonded together. In its final form the MSEM will consist of 6 silicon die aligned, stacked, and insulated from one another in this manner. One die will contain a field emission electron source, 4 die function as electrostatic electrodes for extraction, focusing, and deflection of the beam, and a final die for detection of secondary electrons. The entire structure measures less than one cubic cm. Arrays of MSEM can also be fabricated for applications in high throughput e-beam lithography.

Our goal is to provide a small, inexpensive low voltage SEM that performs as well as commercially available instruments. Because of

the advantages inherent in size reduction and batch processing the cost of the MSEM is dramatically lower than that of conventional machines. The MSEM operating at 2.2 kV with a working distance of 0.5 mm has a theoretical performance limit of 3.8 nm.<sup>1</sup> In its current form the MSEM being tested utilizes a micromachined 3 electrode electrostatic lens, a commercial ZrO<sub>2</sub> TFE electron source, and conventionally machined electrostatic parallel plate deflectors. Initial line scan experimental data and early images will be presented along with results of resolution experiments.

<sup>[1]</sup> Microfabrication of Arrays of Scanning Electron Microscopes, A. D. Feinerman, and D. A. Crewe, J. Vac. Sci. Technol. B (submitted).

4:20 pm **NSBI-ThA8 Localized Photodiode for Near-Field Photodetection Optical Microscopy**, R. C. Davis, C. C. Williams, Dept. of Physics, University of Utah, SLC, UT 84112.

In Near-Field Scanning Optical Microscopy (NSOM) an optical fiber with a small aperture at the end is the light collector. In contrast Near-Field Photodetection Optical Microscopy (NPOM) employ a small photodetector placed directly in the near-field as the light collector. We have fabricated a Schottky photodiode localized to the end of a silicon tip for use as the photodetector in NPOM.

A silicon tip has been cleaved to create a sharp tip. We have developed a novel approach for constructing a very small device at the end of a silicon tip without the use of lithography. Using this approach we have fabricated a small Al-Si Schottky diode. The diode contact area is approximately 1 micron square with a sub-micrometer tip curvature. We have electrically characterized the diode by I-V and have measured the optical sensitivity as a function of position on the diode using a micrometer size focused laser spot.

4:40 pm **NSBI-ThA9 Production and Characterization of High Aspect Ratio Probes for Resonance-Mode Atomic Force Microscopy**, K. F. Jarausch, K. M. Edenfeld, C. B. Mooney, D. P. Griffiths, G. M. Shedd, and P. E. Russell, Precision Engineering Center, North Carolina State University, Box 7918, Raleigh, NC 27695.

Nano-metrology applications of atomic force microscopy (AFM) have led to the development of special-purpose, high-aspect-ratio probes. The probe radius and aspect ratio are the primary determinants of the congruence of the acquired AFM image to the true profile of the sample. Unfortunately, batch fabricated silicon probe geometry (radius, symmetry, roughness and aspect ratio) varies from sensor to sensor. Controlled geometry AFM probes have been developed. High aspect ratio AFM probes of  $\leq 100$  nm shaft diameter and microns in length are created by electron-beam induced growth. Focused ion beams have also been used to sharpen conventional probes. This paper extends the application of these techniques to the creation of probes for resonance-mode AFM, and characterizes the performance of the resulting probes.

Combining the advantages of high aspect ratio probes with the reduced lateral and contact forces of resonance-mode AFM provides an improved ability to measure different samples. This has been demonstrated with recently developed tip characterization structures. The advantages of regular tip shape for crystal grain metrology have also been shown. The lower lateral forces of resonance mode scanning significantly reduce artifacts associated with tip flexing that are often observed during contact mode imaging with e-beam grown microtips. A discussion of the probe-forming techniques, and an experimental evaluation of the imaging capabilities will be presented.

5:00 pm **NSBI-ThA10 Tunnel Sensors for High Spatial Resolution and Sensitivity Force Sensors**, R. C. White and J. C. Jiang, Columbia University, New York, NY 10027 USA.

A microscale force transducer for implementation in arrayed force sensors has been fabricated and evaluated for performance and reliability. The mechanism of operation is based on cold field emission from a Si emitter which can be fabricated individually or in field emitter arrays. The performance of the vacuum diode device is dependent on a nanometer scale radius of curvature at the emitter surface for field enhancement and tunneling current which is exponentially dependent on distance between emitter and anode. Initial devices exhibited stable emission current of greater than 1 mA at bias voltages less than 10V. This result, although stable and reliable for sensor applications, was inconsistent with the physics of cold field emission for these structures, described by the Fowler-Nordheim model. Investigation of individual tip performance has been carried out using an "STM-like" setup where radius of curvature of the anode could be controlled, as well as anode-

cathode spacing, and vacuum environment. Results indicate an unstable operating region for the devices, which can result in breakdown of the emitting material if the bias voltage is increased. Such breakdown results in large emission currents, and physical damage to the nanometer scale emitter. Surface modification of the "as-prepared" Si emitters has been performed which allows for better control of the device near the unstable point. This modification is the simple addition of an ultra-thin ( $< 100$  Å) metal overlayer. Modeling indicates that the modification creates a resonant tunnel enhancement at the emitter surface.

## NANO 3/NANOMETER-SCALE SCIENCE AND TECHNOLOGY

Room A207 - NS2-ThA

### Nanomechanics and Nanotribology: II

Moderator: N. A. Burnham, École Polytechnique Fédérale de Lausanne.

2:00 pm **NS2-ThA1 Observation of Superlubricity by Using Scanning Tunneling Microscope Method**, Motohisa Hirano, NTT Interdisciplinary Res. Labs., Musashino, Tokyo 180, Japan; Kazumasa Shinjo, ATR Optical and Radio Communications Res. Labs.; Reizo Kaneko, NTT Interdisciplinary Research Labs.; Yoshitada Murata, The University of Tokyo.

This study aims to observe the state of vanishing friction, called superlubricity, by examining sliding between atomically-clean surfaces. Theoretical study prior to experiments found that the case occurs in which frictional forces exactly vanish even in realistic systems such as metals when incommensurately contacting crystal surfaces slide against each other [1]. The measured frictional forces between mica surfaces under very dry atmosphere decrease when the contacting surfaces approach being incommensurate [2]. In this experiment, Si(001) (n-type, 0.01  $\Omega$ -cm) is one-dimensionally scanned against a W tip in UHV by using STM method, and the W tip-deflection caused by the friction appearing between the scanned Si(001) and the W(110) on the polycrystalline W tip is measured. This STM method achieves the sliding with the elastic contact of the surfaces as in the attractive-mode of AFM operation. The commensurate contact is obtained by aligning the lattice orientation of the contacting surfaces in such a way that [111] of W(110) corresponds to [100] of Si(001) since the inter-atomic distances are almost identical to each other along these directions. The lattice orientation of W(110) is determined by field emission microscope and that of Si(001) by low-energy electron diffraction. Typical scanning amplitude is 100 nm and the scanning rate is 0.5 Hz. We have observed friction of magnitude  $10^{-7}$  N, which is comparable to the calculated value, when the contact is commensurate. However, when the contact is incommensurate, friction is not observed in this measurement which can resolve the frictional forces of  $10^{-8}$  N. It is thus concluded that the observed frictional anisotropy stemming from the differences in the commensurability of the contacting surfaces implies the existence of superlubricity.

[1] M. Hirano and K. Shinjo, PRB 47, 11837 (1990).

[2] M. Hirano, K. Shinjo, R. Kaneko, and Y. Murata, PRL 67, 2642 (1991).

2:20 pm **NS2-ThA3 Influence of Water Vapor on Nanotribology Studied by Friction Force Microscopy**, M. Binggeli, Centre Suisse d'Electronique et de Microtechnique (CSEM), CH-2007 Neuchâtel, Switzerland; C. M. Mate, IBM Research Division, Almaden Research Center, San Jose, California 95120 USA.

It has long been known that presence of water vapor can dramatically influence the friction and wear properties of materials. In order to simulate the nanotribological effects of adsorbed water molecules and the capillary condensation of water around contacting asperities, we have studied the friction and adhesive forces acting on the tip of an atomic force microscope in contact with a flat surface as function of humidity. On a hydrophilic surface such as silicon oxide, water films grow to tens of nanometers in thickness at high relative humidity, and strong capillary formation occurs around the tip. In contrast, on hydrophobic surfaces such as amorphous carbon films or lubricated silicon oxide, only a few layers of water molecules condense, and the water capillary formation around the tip is greatly suppressed. Friction

and adhesive forces during sliding of the tip across the sample surfaces decrease substantially with increasing relative humidity, implying that the surfaces are lubricated by the condensed water.

**2:40 pm NS2-ThA4 AFM Studies of Corrosive Tribological Wear: Single Crystal  $\text{NaNO}_3$  Exposed to Moist Air,\* S. Nakahara, J. T. Dickinson, and S. C. Langford,** Washington State University, Pullman, WA 99164-2814.

In a number of mechanical wear situations, a surface experiences simultaneous tribological loading and chemical exposure; the combination can greatly increase wear rates. We have modified our air AFM to permit measured variations in relative humidity during scanning. The relative humidity can be varied from less than 10% up to 95% at 23°C. Scanning is performed using  $\text{Si}_3\text{N}_4$  tips with nominal tip radii of 40 nm, normal loads ( $F_N$ ) from 1 to 30 nN, and tip velocities from 1 to 200  $\mu\text{m/s}$ . The surface of interest is cleaved single crystal  $\text{NaNO}_3$ , a hygroscopic salt with rhombohedral calcite structure. Initial scans (dry) exhibit numerous long, sharp 6 Å steps, corresponding to two unit cells, exhibiting high stability. In high humidity, infrequent scans at low  $F_N$  show clear uniform step dissolution at typical velocities of 100 nm/s. With frequent scanning at  $F_N = 10$  nN at high humidity, dramatic mechanically stimulated corrosive attack is observed at the steps, producing 3 Å staircases, oriented grooves, and possible formation of carbonate from reaction with  $\text{CO}_2$  in the air. We present the influence of  $F_N$ , tip velocity, and relative humidity on the rates of corrosive wear and possible mechanochemistry.

**3:00 pm NS2-ThA5 Nanotribology in Electrochemically Controlled Environment, M. Bingeli, J. Burger and R. Christoph,** Centre Suisse d'Electronique et de Microtechnique S.A., 2007 Neuchâtel, Switzerland.

In order to achieve information about nano-mechanical properties of materials and to complement classical tribological research with nanometer scale investigations, friction force microscopy has become a well established tool over the last few years. Simulation of a single asperity contact of a real tribosystem with an FFM tip has proven to be a promising approach towards a more detailed understanding of tribological processes. As the surface conditions of two sliding materials determine their friction behavior, rigorous control of these conditions is crucial. Therefore, a standalone bidirectional force microscope, the atomic scale tribometer, has been combined with an electrochemical environment, which enables to control the cleanliness and thermodynamics of the sample (and tip) surface. The standalone design allows for scanning the probe (not the sample) and therefore no restrictions to the electrolyte cell design and weight apply. Sliding experiments carried out on graphite in 0.1 M  $\text{NaClO}_4$  electrolyte evidenced the potential of this method. Lateral forces on the tip during the scanning process (conventionally: friction) show a clear dependence upon the applied electrochemical potential and therefore the chemical state of the surface. Friction force microscopy in electrolytic environment is thus the first tool capable of detecting local electric double-layer properties, thereby contributing analytical information for the modelling of this strongly disputed subject.

**3:20 pm NS2-ThA6 Friction and Adhesion Properties of Hard Carbon Surfaces Measured by Atomic Force Microscopy, Scott S. Perry and Gabor A. Somorjai,** Lawrence Berkeley Laboratory and Department of Chemistry, University of California, Berkeley, CA 94720, C. Mathew Mate, IBM Almaden Research Center, 650 Harry Road, San Jose, CA 95120.

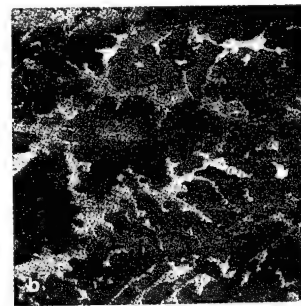
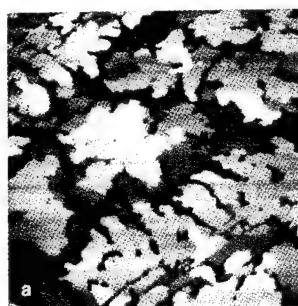
The friction and adhesion properties of amorphous carbon films have been studied on the nanometer scale by atomic force microscopy (AFM). Sputtered hard carbon films are used as protective coatings in many applications including computer disk drives. Interaction forces between a sharp tungsten tip and the surface of the carbon films have been measured as a function of chemical composition and structure. Normalization of adhesive forces at different surfaces has been accomplished by estimating radii of curvature through electrostatic measurements. Variations of hydrogen content within the films, surface oxidation and the presence of lubricant films all influence the tip-surface adhesion. Friction forces between a sliding tungsten tip and carbon surface have been measured simultaneous to load forces allowing the calculation of coefficients of friction. Friction forces are seen to vary with both the chemical and topographic structure of the films. The relevance of atomic force measurements to industrial tribological applications will be discussed.

**3:40 pm NS2-ThA7 Orientational Ordering of Polymers with A.F.M. in Contact Mode: An Application to Conjugated Polymers, Z. Elkaakour, J. P. Aimé, T. Bouhacina, C. Odin, T. Masuda\*, L.C.P.C. Université Bordeaux I, 351 Cours de la Libération 33405, Talence cedex, France, \*Department of Polymer Chemistry, Kyoto University, Kyoto 606-01, Japan.**

Among near field microscope, the atomic force microscope appears as a powerful and versatile tool allowing to investigate local viscoelastic properties, friction coefficient and adhesiveness. In addition, we can take advantage of the tip sample interaction, in part due to the adhesion, to perturb and, in turn, modify the surface of soft samples. Here we report an attempt to modify the structure of a substituted polyacetylene film spread on a surface. Regular patterns are obtained, and we show that scan frequency and applied load are the pertinent parameters that control the period. These results allow us to describe the bundle formation with a peeling process. In this way, we are able to predict, thus to prepare structure with a chosen period. Because of the drastic changes of conjugated polymer properties when chain alignment is performed, the creation of controlled periodic arrangement should be of great interest.

**4:00 pm NS2-ThA8 Nanotribological Investigations of Epitaxial  $\text{C}_{60}$  Films on  $\text{GeS(001)}$  by Lateral Force Microscopy and Force Spectroscopy, W. Allers, U. D. Schwarz, G. Gensterblum\* and R. Wiesendanger,** University of Hamburg, D-20355 Hamburg, Germany; \*Facultés Universitaires Notre-Dame de la Paix, B-500D Namur, Belgium.

The spherical shape of  $\text{C}_{60}$  molecules as well as their rotational motion at room temperature have led to speculations about possible unique nanotribological properties of thin  $\text{C}_{60}$  films. We have applied lateral force microscopy and force spectroscopy to study the variation of the local frictional coefficient on submonolayer  $\text{C}_{60}$  films epitaxially grown on  $\text{GeS(001)}$  substrates under ultra-high vacuum conditions. The local frictional coefficient derived for the  $\text{C}_{60}$  islands was found to be significantly smaller than on the layered  $\text{GeS(001)}$  substrate (see figure). This demonstrates that well-ordered  $\text{C}_{60}$  films can indeed lower the frictional force even compared with a layered substrate. On the other hand, graphite was found to exhibit significantly better lubricating properties compared with the  $\text{C}_{60}$  films.



**4:20 pm NS2-ThA9 UHV Boundary Lubrication of the  $\text{Cu(111)/Cu(111)}$  Interface by Submonolayer Coverages of Trifluoroethanol, Christopher F. McFadden,** University of Illinois at Urbana-Champaign, Urbana, IL 61801; Andrew J. Gellman, Department of Chemical Engineering, Carnegie Mellon University, Pittsburgh, PA 15213.

The ability of adsorbed films of molecular thickness to lubricate solid-solid interfaces is of critical importance to many areas of technology and engineering. An ultrahigh vacuum (UHV) tribometer has been used to study the friction behavior of  $\text{Cu(111)}$  surfaces separated by adsorbed films of 2,2,2-trifluoroethanol ranging from  $\sim 0.05$  monolayers (ML) to  $\sim 10$  ML thickness. The instrument is designed such that both samples may be prepared and characterized under UHV conditions and then brought into contact and sheared relative to one another without exposure to atmosphere. Shear and normal forces are measured independently and simultaneously during sliding. The friction behavior of clean  $\text{Cu(111)}$  surfaces is characterized by high, erratic friction forces with static friction coefficients in the range 3-8. The friction coefficient is reduced to approximately 0.87 by as little as 0.05 ML of trifluoroethanol and remains constant at coverages up to 1 ML. This represents the first demonstration of boundary lubrication of metals by submonolayer films and challenges the classical view that a close-packed monolayer film is prerequisite for effective boundary lubrication.



4:40 pm **NS2-ThA10 Interfacial Friction of Physisorbed Rare-Gas Films on Metal Surfaces,\*** C. Daly and J. Krim, Northeastern University, Boston, MA 02115.

We have employed a quartz crystal microbalance (QCM) technique [1] to measure sliding friction levels of rare-gas monolayers adsorbed on various (111) metal surfaces. We have studied the effects of substrate corrugation and film-substrate incommensurability on the sliding of the adsorbed film, as well as the absolute strength of the film-substrate interaction potential. Several metals with differing lattice spacings and corrugations were deposited on the QCM, which was then exposed to Ar, Kr, and Xe. The interfacial friction is observed to progressively increase as the gas is varied from Ar to Xe on account of the increasing interaction strength. Substrates with relatively high corrugation decrease the slippage of the adsorbed layers. The results are interpreted within the context of current theories of atomic-scale friction.

[1] J. Krim, D. H. Solina, and R. Chiarello, *Phys. Rev. Lett.*, **66**, 181 (1991).

\* Work supported by NSF#DMR9204022.

## APPLIED SURFACE SCIENCE

### Room A101 - Session AS-ThA

#### Polymer/Organic Surfaces

**Moderator:** A. B. Ulman, Eastman Kodak Company.

2:00 pm **AS-ThA1 Polymer Surface Damage by X-ray Photoelectron Spectroscopy,** W. F. Stickle, P. E. Sobol, H. Iwai, Physical Electronics Laboratories, 6509 Flying Cloud Drive, Eden Prairie, MN 55344.

X-ray photoelectron spectroscopy is often regarded as not damaging to surface chemistry. Polymer surfaces can show degradation during analysis, especially with non-monochromatic x-ray sources because of thermal effects, exposure to Bremsstrahlung radiation, or interaction with low energy electrons. With the common use of modern monochromatic XPS, damage to a polymer surface during analysis is minimized or eliminated, except in the cases of many halogenated polymers. While some damage to polymer surfaces can still occur, the resolution and sensitivity of modern spectrometers makes it possible to more closely examine the effect of monochromatic radiation damage to a polymer surface. Using high by focused x-ray sources and focused electron optics for analyzers, changes in surface chemistry can be especially important for polymers as well as other materials. Chlorinated and fluorinated polymers have been studied using different analytical conditions. Experiments were conducted by varying the x-ray flux density by using focused and broad beam monochromatic radiation combined with analysis from different size areas. From these experiments a methodology for examining polymer degradation will be discussed by contrasting the different analysis conditions.

2:20 pm **AS-ThA2 Surface Vibrational Characterization of Thick Polymer Films Using High Resolution Electron Energy Loss Spectroscopy,** G. Apai, W. P. McKenna, L. Gerenser, and C. A. Fleischer, Eastman Kodak Company, Rochester, NY 14650.

We demonstrate that high-resolution electron energy loss spectroscopy (HREELS) can be used to elucidate the surface vibrational structure of both thin (<300 Å) and thick (>1 micron) polymers. The effects that charge neutralization may have on vibrational selection rules will be addressed. Experimental conditions necessary to achieve a unique vibrational identification of the polymer surface will be discussed. Examples include end-group terminations in polyethylene and polycarbonate, surface reorganization of end-functionalized polystyrenes, surface chemical reactivity of oligomeric vinylidene chloride, and plasma/corona modification of polyethylene terephthalate.

2:40 pm **AS-ThA3 Surface Studies of Filled Silicone Elastomers,** B. D. Ratner, D. Leach-Scampavia, W. Ciridon, C. D. Tidwell, T. Boland, P. Yang,\* University of Washington, Seattle, WA 98195 and Mentor, Inc.,\* Santa Barbara, CA.

In medical grade silicone (poly(dimethyl siloxane)(PDMS)) elastomers, silica filler is added to improve mechanical properties. This study asks a question important to the performance of silicone medical devices: can the filler be observed at the surface? Silicone elastomer

surfaces were studied by ESCA, SSIMS, SEM, and AFM. Specimens were challenged by abrasion, enzymatic, and peroxide treatments.

Standard materials were analyzed to establish that SiO<sub>2</sub> and PDMS could be distinguished. A complex curve envelope associated with adventitious carbon contamination was present in the ESCA C1s spectrum for all silica standards. Although the high resolution Si 2p envelope will fit with one peak, with a binding energy (BE) consistent with SiO<sub>2</sub> (104.0 eV), a low BE shoulder was present in all spectra. This may be indicative of sample charging or a low level of a -(CH<sub>3</sub>)<sub>2</sub>SiO-(102.4 eV) contaminant.

The elemental composition for "silica-free" silicone was near the expected theoretical values for PDMS. The BE's were consistent with C-C (285.0 eV), -(CH<sub>3</sub>)<sub>2</sub>SiO- (532.6 eV) and Si-O (102.4 eV). SIMS spectra for an SiO<sub>2</sub> standard were consistent with the negative ion spectra for silica with peaks at 60 m/z and 76 m/z. Although there appears to be a small 76 m/z feature in the negative ion mass spectra for some of the silicone materials, there is no enhancement of the 60 m/z mass fragment one would expect if silica were present. The SIMS negative ion mass fragments for biomedical silicone elastomers do not indicate silica is present in the top 15 Å of the samples. Negative ion peaks at 59, 60, 75 and 149 m/z, as well as, positive ion mass peaks at 73 and 147 m/z are consistent with PDMS. Thus, on all silicone biomedical elastomers, by ESCA or SIMS, only PDMS was found in the outermost 10-80 Å.

The possibility of silica coming to the surface upon hydration of the elastomer was also investigated. No silica was observed by ESCA of a frozen-hydrated specimen following a 24 hour soak in water.

3:00 pm **AS-ThA4 High Resolution XPS and ToFSIMS Studies of Polyamidoamines,** A. G. Shard, M. C. Davies, S. J. B. Tendler, G. Beamson,<sup>†</sup> A. J. Paul, L. Sartore\* and P. Ferruti\*, Laboratory of Biophysics and Surface Analysis, Department of Pharmaceutical Sciences, The University of Nottingham, Nottingham, NG7 2RD, UK, <sup>†</sup>SERC, Daresbury Laboratory, <sup>‡</sup>CSMA Ltd., \*Universita di Brescia.

The surface analysis of polymers containing amine groups is an area which has not received a great deal of attention. In this work we describe for the first time high resolution X-Ray Photoelectron Spectroscopy (XPS) and Time of Flight Secondary Ion Mass Spectroscopy (ToFSIMS) analysis of a novel series of polyamidoamines, polymers which are of interest to the biomedical community.

The Scienta ESCA300, which attains an instrumental resolution of well below 1 eV was employed for XPS analysis. Following the deconvolution of C<sub>1s</sub>, O<sub>1s</sub> and N<sub>1s</sub> regions the component peaks within each spectra revealed detailed information concerning the chemical environments of each element. In addition, degradation of some of the polymers under X-Ray irradiation was investigated and valence band spectra recorded. Polymers with closely related compositions could be readily distinguished in the ToFSIMS spectra. High resolution of ToFSIMS work allows accurate ion assignments to be made. Secondary ions are interpreted as being derived from intact polymer structural units, which implies the occurrence of specific fragmentation mechanisms. A good understanding of polyamidoamine surface chemistry has been achieved which will prove invaluable in future studies of similar materials.

3:20 pm **AS-ThA5 Mass Spectra of Low-Molecular-Weight Materials on Corona-Treated Polypropylene,** O. Kornienko, J. A. Burroughs, L. Hanley, University of Illinois at Chicago, Chicago, IL 60607-7061.

Corona discharge treatment is widely used in the industrial processing of polymeric films, particularly to improve wetting and adhesive properties. Corona discharge treatment in air leads to the formation of a complex low-molecular-weight oxidized material (LMWOM) which has been only partially characterized by standard surface analysis methods. We utilize in these experiments laser desorption ion trap mass spectrometry to analyze LMWOM which has been solvent extracted from the surface of corona-treated polypropylene. Molecular weight distributions are determined as a function of total discharge energy and relative humidity of the ambient air. A comparison of mass spectrometric data with prior ESCA, IR, and contact angle measurements permit at least partial elucidation of the chemical composition of the LMWOM. These results indicate the general feasibility of using ion trap mass spectrometers for the analysis of complex organic surfaces.

3:40 pm **AS-ThA6 Addition of a Single Chemical Functional Group to a Polymer Surface with a Mass-Separated Low Energy Ion Beam,** P. Nowak and N. S. McIntyre, Surface Science Western and Department of Chemistry, University of Western Ontario, London, On-



tario, Canada N6A 5B7; I. Bello and W. M. Lau, Department of Materials Engineering, University of Western Ontario, London, Ontario, Canada N6A 5B9.

A mass-separated low energy ion beam system was used to deliver pure  $\text{OH}^+$  and  $\text{NH}^+$  to 15nm thick polystyrene films on silicon in ultrahigh vacuum for the study of polymer surface modifications yielding specific surface chemical functional groups. X-ray photoelectron spectroscopy showed that when the bombardment energy of  $\text{OH}^+$  exceeded 10 eV or dose was higher than  $1 \times 10^{16}/\text{cm}^2$ , the introduction of a mixture of C-OH, C-C=O, and C-COOH, together with a severe damage of the aromatic rings, was observed. However, for bombardment at 10 eV with a dose at  $1 \times 10^{16}/\text{cm}^2$ , only C-OH (or COR) was found. Similarly, bombardment with  $\text{NH}^+$  at 10 eV and a dose of  $1 \times 10^{16}/\text{cm}^2$  induced nitrogen incorporation with a symmetrical N 1s peak, which suggests the absence of vastly different surface functionalities. The C 1s data on such surfaces indicated the major surface functionality being C-NH<sub>2</sub> (or C-NHR) with a minor component of C-(NH<sub>2</sub>)<sub>2</sub>. Hence, surface functionality can indeed be controlled by controlling the molecular nature, energy, and dose of the bombardment species.

4:00 pm **AS-ThA7 Polyfluoroether Lubricant Analysis by TOF-SIMS**, P. Kasai, A. M. Spool, IBM Storage Systems Division, San Jose, CA 95193.

Perfluoro-poly(ethers) (PFPE) produce rich and intense SIMS spectra. This study represents an attempt to further understand how to interpret these spectra. We compare and contrast TOF-SIMS analyses of demnum, krytox, perfluoro-poly(dioxolane), and Z fomblins. For all of these compounds, the negative ion spectra have intense regular peak patterns that persist up to high masses approaching the mean MW for the polymer. In contrast, the positive ion spectra are much more complex, with a less persistent repeat pattern at higher masses. The results suggest differences in ion formation/decay mechanisms between positive and negative ions. The demnum molecule, with its symmetric monomeric unit, produces two identical patterns in the negative ion spectrum that differ by the weight difference of the 2 end groups. The other compounds studied here have asymmetric monomers and produce spectra indicative of asymmetric cleavage. The negative ion fragmentation patterns of the Z fomblins can be modelled with a random distribution of the 2 monomers that comprise these polymers, and with symmetric fragmentation of the polymer. The addition of functionalized endgroups of these molecules has surprising effects on the TOF-SIMS spectra. The endgroups affect either ion formation probabilities or ion lifetimes.

4:20 pm **AS-ThA8 Time of Flight-Secondary Ion Mass Spectrometry Analysis of Langmuir-Blodgett Films of Isotactic, Syndiotactic, and Atactic Poly(methyl methacrylate)**, Richard W. Nowak, Joseph A. Gardella Jr., Paul A. Zimmerman and David A. Hercules.

Well ordered Langmuir-Blodgett monolayers of Poly(methyl methacrylate) have been studied with ToF-SIMS. The high mass range from 1000 to 3500 Da. is investigated in the present study.

Samples of different tacticities were prepared at two different surface pressures on a Langmuir-Blodgett trough. The surface coverage was confirmed by an ESCA study.

A Reflectance-Absorption FT-IR study of the samples provides information of the configuration of the polymers on a silver substrate. Previous work by Brinkhaus was compared to confirm the results.<sup>1</sup> The ToF-SIMS results of L-B films of polymers with different tacticities have been analyzed following previous published approaches based on statistical chain breaking to form radical ions.<sup>2</sup> Clearly, different ion formation patterns result from different structures (e.g., atactic, isotactic, syndiotactic) leading to the conclusion that polymeric tertiary structures may lead to different ions. This will lead to a better understanding of the effects of polymer ion formation in ToF-SIMS.

(1) Brinkhuis, R. H. G., Schouten, A. J., *Macromol.* 24, 1496-504, 1991.

(2) Zimmerman, P. A., Hercules, D. A., Benninghoven, A., *Anal. Chem.* 65, 983-91, 1993.

4:40 pm **AS-ThA9 Probing the Interfacial Properties of Poly(vinyl acetate-ethylene) Copolymers and Poly(vinyl chloride) Laminations by Time-of-Flight Secondary Ion Mass Spectrometry**, Paula A. Cornelio Clark, Sharon A. Gardner, and David Horwat, Air Products and Chemicals, Inc., 7201 Hamilton Blvd., Allentown, PA 18195-1501.

A better understanding of polymer interfaces is being driven by the need to develop new materials for coating and adhesive applications.

Time-of-Flight Secondary Ion Mass Spectrometry (ToF-SIMS) is emerging as a powerful analytical probe for unambiguously identifying surface species that can impact a material's performance. Here, we report on our efforts to elucidate the interfacial properties of poly(vinyl acetate-ethylene) copolymer (VA-E) based adhesives bonded to poly(vinyl chloride) (PVC) substrates. We find surface segregation of plasticizers, found within certain grades of PVC, contributes to the delamination of the VA-E adhesive from the PVC substrate. In addition, ToF-SIMS provides valuable information on the spatial distribution of components which contribute to adhesive failure.

5:00 pm **AS-ThA10 Morphological and Nanomechanics Investigations of Surface Modified Poly(tetrafluoroethylene)**, A. J. Howard, R. R. Rye, P. Tangyonyong, and J. E. Houston, Sandia National Laboratories, Albuquerque, NM 87185.

Using both atomic and interfacial force microscopies (AFM and IFM), we have studied the surface morphology and nanomechanical properties of surface modified and virgin poly(tetrafluoroethylene) (PTFE). The modified surfaces of PTFE were prepared by exposure to electron-beam irradiation, wet chemical etching in a sodium naphthalenide solution, and a combination thereof. These surface treatments are used in our laboratory in combination with conventional integrated-circuit processing techniques to pattern adherent conductors directly on low dielectric constant PTFE substrates for high frequency device applications. AFM images (performed in tapping-mode since contact-mode AFM on this soft material yielded images dominated by tip-induced artifacts) show that stress dependent crazing resulting from chemical etching is necessary for strong metal adhesion to etched PTFE. IFM force versus displacement curves and creep experiments are used to probe the changes in mechanical properties of PTFE resulting from electron-beam irradiation. This information will be used to discuss why poor metal adhesion to irradiated and etched PTFE surfaces is observed. These nanomechanics results, as well as our AFM and SEM (for comparison) morphological data will be presented.

This work was performed at Sandia National Laboratories and supported by the U.S. Dept. of Energy under contract DE-AC04-94AL85000.

## PLASMA SCIENCE

### Room A109 - Session PS1-ThA

#### Plasma Surface Interactions

Moderator: M. Nakamura, Fujitsu Ltd., Japan.

2:00 pm **PS1-ThA1 Chemical Topography of Masked Poly-Si Films Etched in Cl<sub>2</sub> and HBr-Containing, High-Density Plasmas**, V. M. Donnelly, C. C. Cheng, K. V. Guinn, and I. P. Herman<sup>(a)</sup>, AT&T Bell Laboratories, Murray Hill, NJ 07974.

The spatially-resolved adsorbate composition, or "chemical topography", of small features (polycrystalline Si masked with photoresist or SiO<sub>2</sub> stripes) etched in Cl<sub>2</sub>, or HBr-containing plasmas has been quantitatively determined by angle-resolved x-ray photoelectron spectroscopy (XPS), using shadowing of photoelectrons by adjacent features and geometric modeling. The plasma reactor consisted of a helical resonator source and a radio-frequency-biased substrate stage. Samples with equal line and space width features (0.5-2  $\mu\text{m}$ ) were etched and then transferred under high-vacuum to the XPS chamber. Real-time, laser-induced thermal desorption showed that the Si-halide layer formed during etching was stable during the sample transfer period. For resist-masked samples etched in Cl<sub>2</sub> plasmas,  $\sim 1 \times 10^{15}$  Cl-atoms/cm<sup>2</sup> cover vertical and horizontal surfaces of poly-Si and resist. Little or no C or O was found on the poly-Si, and a trace amount of Si was found on the side (but not top) of the resist. Analogous results were found with pure HBr plasmas, with slightly less Br covering all surfaces. Adding O<sub>2</sub> to either Cl<sub>2</sub> or HBr plasmas increases O coverage on the poly-Si sidewall, and leads to formation of a relatively thick SiO<sub>x</sub>X<sub>y</sub> (X = Cl or Br) layer on the side of the resist. **INVITED**

<sup>(a)</sup>Also at Columbia Univ., New York, NY.

2:40 pm **PS1-ThA3 Reactivity of Plasma Radicals with the Surface of Depositing Films**, N. F. Dalleska and Ellen R. Fisher, Department of Chemistry, Colorado State University, Fort Collins, CO 80523.

Understanding the interactions of molecules with surfaces is important for development of thin-film materials processing technologies, although few direct reactivity studies have been made during deposition. Direct measurements of radical reactivities are thus vital to acquiring knowledge of the complex chemistry of chemical vapor deposition (CVD) and plasma enhanced CVD processes. The presentation will center on a relatively new technique, IRIS (Imaging of Radicals Interacting with Surfaces), which combines spatially resolved laser-induced fluorescence (LIF) and molecular beam methods to measure the reactivity of radicals with the surface of depositing films. The technique also employs a state-of-the-art gated and intensified charge coupled device array detector. The radicals studied are observed in materials-processing systems and may be important to such processes as plasma deposition of Si, SiO<sub>2</sub>, Si<sub>3</sub>N<sub>4</sub> and diamond thin films. Indeed, many proposed mechanisms indicate that small molecules such as SiH, SiO, CH, CF, and CF<sub>2</sub> play significant roles in these deposition processes. Previous results show major differences in radical reactivities, indicating that additional results for a large number of molecules are needed. Preliminary reactivity results on some of these radical species using a newly constructed IRIS apparatus at Colorado State University will be presented.

3:00 pm **PS1-ThA4 Molecular Dynamics Simulation of Atomic Layer Etching of Si(100)**, *Satish D. Athavale and Demetre J. Economou*, Plasma Processing Laboratory, Department of Chemical Engineering, University of Houston, Houston, TX 77204-4792.

Atomic Layer Etching (ALET) is a technique capable of etching a crystalline solid with monolayer accuracy. ALET is a cyclic process consisting of: (1) adsorption of a monolayer of gas onto the solid surface, (2) evacuation of excess gas, (3) exposure of the surface to energetic particles (ions, electrons, photons) to induce reaction, and (4) pump out of the reaction products. These steps are repeated in a cyclic manner so that a monolayer of material is removed in each cycle. To achieve monolayer etching, it is necessary to limit reaction to the topmost layer.

We have used molecular dynamics (MD) simulations to study the effect of Ar ion bombardment on the chemistry of a Si(100) surface covered with a monolayer of Cl atoms. In contrast to other studies, the surface is exposed to ions only, without simultaneous neutral bombardment. MD results elucidate the effect of ion energy (<100 eV) and flux on the surface reaction, product distribution, and the extend of lattice damage and surface roughness. The goal is to determine the range of ion energy and flux to achieve ALET. Simulation results are used to guide an experimental ALET system.

3:20 pm **PS1-ThA5 Generation of Ionic Radicals by a Fragmentation Process on Surface**, *Y. Mitsuoka<sup>a,b</sup>, S. Takahashi<sup>a</sup>, H. Toyoda<sup>a</sup>, S. Mukainakano<sup>b</sup>, T. Hattori<sup>b</sup>, H. Sugai<sup>a</sup>*, <sup>a</sup> Nagoya University, Nagoya 464-01, Japan; <sup>b</sup> Research Laboratories, Nippondenso Co., Ltd., Nissin-cho, Aichi-ken 470-01, Japan.

There has been a great need to understand ion-surface interactions in plasma-assisted deposition and etching. In this paper, we describe observation of ionic radicals generated by fragmentation, i.e., dissociative scattering on surfaces: a polyatomic ion breaks up on solid surface into smaller ionic fragments (radicals). First of all, an ionic species CH<sub>4</sub><sup>+</sup> ( $x = 2-4$ ) is extracted through a mass filter from a methane plasma and irradiated on an aluminum target. The dependence of production rate of each fragment ion on the primary ion energy is measured, together with the branching ratio. In the case of CH<sub>4</sub><sup>+</sup> incidence, two types of dissociation processes are clearly found, depending on the incident energy  $E$ . One is the dissociation into CH<sub>3</sub><sup>+</sup> and CH<sub>2</sub><sup>+</sup> for  $E < 30$  eV, and the other is the fragmentation into CH<sup>+</sup> and C<sup>+</sup> for  $E > 100$  eV. Tentatively, the former is explained by dissociation of the molecule excited electronically with charge neutralization on the metal surface, and the latter by dissociation of the molecule excited vibrationally due to high translational energies. Further details will be presented, together with another experiment on fragmentation of fluorocarbon ion, a key radical CF<sub>x</sub><sup>+</sup> ( $x = 1-3$ ) in reactive ion etching.

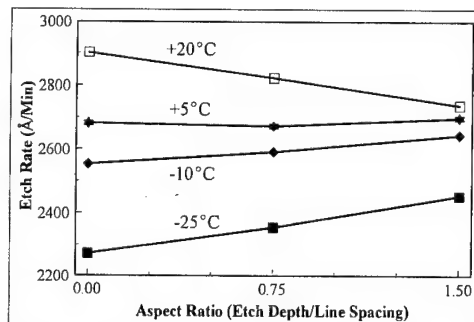
3:40 pm **PS1-ThA6 Aspect Ratio Dependent Etching of Polysilicon**, *T. J. Dalton, and H. H. Sawin*, Massachusetts Institute of Technology, Cambridge, MA 02139.

Aspect ratio dependent etching (ARDE) phenomena (e.g., RIE Lag) were measured for polysilicon etching in an HBr/Cl<sub>2</sub> chemistry on an Applied Materials Precision 5000 plasma etcher using a CCD camera to measure etch rate *in situ* by spatially resolved optical emission interferometry. A test mask containing gratings of various dimensions was used. We were able to measure variations of etch rate with aspect

ratio of only a few percent. Such measurements are very difficult to make by measuring film thicknesses from SEM photographs for a partial etch.

ARDE was found to be a function of residence time (gas flowrate), pressure, magnetic field strength, temperature, feed gas composition, and the seasoning/history of the etcher. At high gas flow rates, no ARDE was seen; decreasing the flow rate resulted in RIE Lag (smaller features etched slower than large features). Increasing pressure resulted in increased RIE Lag due to ion shadowing caused by the increase in off-normal ion bombardment, while increased magnetic field strength decreased ARDE. Decreasing the cathode temperature below 0°C resulted in inverse RIE Lag (see figure). Etch rate decreased more rapidly in large features/open areas due to unimpeded deposition. Narrow features experienced a slower decrease in etch rate due to the sticking of depositing species on the sidewalls.

Work supported by SEMATECH, under contract 93-MC-503, and by a NSF Graduate Student Fellowship.



4:00 pm **PS1-ThA7 Real-Time Investigation of DC Bias Effects on Ultra Thin Silicon Oxide Growth in an Oxygen Plasma**, *M. Kitajima, I. Kamioka, and K. G. Nakamura*, National Research Institute for Metals, 1-2-1 Sengen, Tsukuba, Ibaraki 305, Japan.

We have studied positive and negative bias effects on the plasma oxidation of silicon using real-time ellipsometry, to understand the oxidation kinetics in the ultra thin film region. The oxidation experiments were performed in UHV chamber having a background pressure of 10<sup>-7</sup> Pa. A dry oxygen plasma was generated by a radio frequency (rf) discharge (frequency of 13.56 MHz, and power of 300W) with 2.0 Pa O<sub>2</sub>. The sample used was p-Si (111) wafer, and the distance from the rf coil to the sample was 1 m. Applied biases to the sample were -60V, -30V, -15V, +15V, +30V, +45V, and +60V. The oxide film growth was monitored with a time resolution of 1 s by using a PEM-type ellipsometer. We found that the plasma oxidation rate was strongly affected by the sample biases, and the bias effect depends on oxidation stage (oxide film thickness). For longer time oxidation (thicker oxide film), the oxidation rate increases as positive bias increases, but little effect was observed for negative bias. This shows that the dominant oxidizing species are negative ions. For initial oxidation stage immediately after starting the plasma ignition (thinner oxide film), the negative bias also enhanced the plasma oxidation rate; the oxidation rate increases as both the positive and negative biases increase with showing a minimum at +15V. This suggests that both positive and negative ions contribute in the initial oxidation process to the plasma oxidation of silicon surface. Results of XPS measurements will be also described.

4:20 pm **PS1-ThA8 Defect Production and Recombination During Low-Energy Ion Processing**, *Bruce K. Kellerman\*, J. A. Floro, E. Chason, D. K. Brice, S. T. Picraux*, Sandia National Laboratories, Albuquerque, NM 87185, and *J. M. White\*\**, Science and Technology Center at the University of Texas at Austin, Austin, TX 78712.

Plasma processing produces damaged, micro-roughened semiconductor surfaces due to low-energy ion bombardment. We have quantified ion-induced point defect production experimentally on the Ge(001) surface in real time using *in situ* Reflection High Energy Electron Diffraction. We have developed Monte Carlo simulations of defect diffusion to model defect recombination in the bulk and on the surface, as well as to predict distribution profiles of defects percolating to the surface. Defect production statistics generated by our binary collision simulator, TRIMRC, coupled with our simulation of bulk defect diffusion, predict the number of ion-induced defects that reach the surface and suggest that TRIMRC may overestimate the depth

distribution of the defects. The experimental defect yield decreases as the substrate temperature increases from 175 to 475 K. Our Monte Carlo simulations of surface diffusion (applicable to any crystalline surface) support a defect annealing mechanism that involves surface recombination of defects generated within a single cascade (at low ion fluxes).

This work was performed at Sandia National Laboratories and supported by the U.S. Dept. of Energy under Contract DE-AC04-94AL85000.

\*AWU-DOE Fellow, U. of Texas, dissertation work performed at SNL.

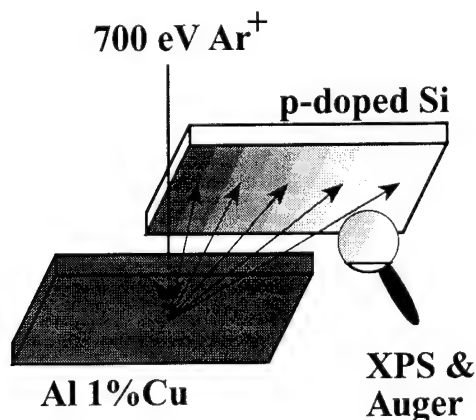
\*\*Supported by NSF grant CHE 8920120.

4:40 pm **PS1-ThA9 Characterization of Ion Directionality in Plasma Enhanced Chemical Vapor Deposition of Silicon Dioxide**, *Junling Li, Calvin Chang, James P. McVittie, and Krishna C. Saraswat*, Center for Integrated Systems, Stanford University, CA 94305.

Plasma Enhanced Chemical Vapor Deposition has emerged in recent years as an important technique for the deposition of interlevel dielectric (ILD) and intermetal dielectric (IMD) materials in modern multi-level ULSI technology, especially when the device dimension decreases to sub-micron level. The main concern here is the filling of high-aspect-ratio structures. The step-coverage ability of a PECVD process is directly related to the spatial angular distributions of the incoming species (probably ions) but this has never been carefully studied. The ion angular distribution depends on the initial ion temperature, bias power, and the sheath transport kinetics, and is, however, very difficult to be experimentally characterized due to the complexity of real processes. In this work a profile simulator and an experimental overhang test structure have been used to study the contribution of directional fluxes in different PECVD systems. Detailed comparison between experimental results and simulation shows that for conventional PECVD processes (several Torr), both a directional (sticking coefficient of 1) component and an isotropic (probably thermal CVD) component are observed, whereas for low pressure ECR CVD system the directional component dominates. It is found that this directional component is consistent with the kinetics model of ion transport. In general, the ion directionality plays a major role in determining the conformality of PECVD processes and the characteristic shape of this directionality can be extracted from test structure results. This work will help to clarify the mechanism of ion induced deposition and makes it possible to provide a useful design tool to help optimize the PECVD processes.

5:00 pm **PS1-ThA10 An Auger and XPS Study of Ar<sup>+</sup> Sputtering Yield and Angular Distribution of Al**, *P. C. Smith, R. B. Turkot, J. P. Kelly, D. N. Ruzic*, University of Illinois, 103 S. Goodwin, Urbana, IL 61801.

Sputtering due to low energy ions occurs in many applications including plasma processing and magnetically confined plasma devices. A surface collector technique for the measurement of low energy sputtering has been investigated. A sample taken from an Al 1% Cu magnetron sputtering target has been exposed to 700 eV Ar<sup>+</sup> beam. The sputtered material was collected on a p-doped silicon wafer that was subsequently analyzed with angularly resolved XPS and Auger surface analysis techniques to determine the density distribution of Al across the collector. This data was analyzed and compared to a reference wafer to determine the total sputtering yield and the angular distribution function of the sputtered material. In addition, the sput-



tered Al target was analyzed to determine the changes in its topology and to look for indications of resputtering. This experimental setup has also been modeled and compared to the vectorized fractal TRIM code for both reflection and sputtering. Results indicate the expected aluminum distribution in lower concentrations than predicted by computer models.

## PLASMA SCIENCE

### Room A102 - Session PS2-ThA

#### Target Fabrication For Inertial Confinement Fusion Moderator: H. G. Kim, University of Rochester.

2:00 pm **PS2-ThA1 Target Area Design Basis and System Performance for the National Ignition Facility**, *Michael T. Tobin, V. Karpenko, K. Hagans, A. Anderson*, Lawrence Livermore National Laboratory, P.O. Box 808, Livermore, CA 94550, and *R. Wavrik, and R. Garcia*, Sandia National Laboratories, P.O. Box 5800, Albuquerque, NM 87185.

The Department of Energy is proposing to construct the National Ignition Facility (NIF) to achieve ignition and modest gain in the laboratory early in the next century. The NIF will consist of a 1.8 MJ, 0.35  $\mu\text{m}$  laser with  $\sim 200$  beams. This is a 50-fold increase in laser energy over the Nova laser at LLNL. Target experiments will be positioned and contained in a 5-m radius, 10-cm thick sphere. Diagnostics are positioned around the equator of the sphere to collect data. NIF is expected to make major contributions to the evaluation of Inertial Fusion as an energy source, to defense sciences national security needs, and to basic science research. The specific requirements of each user community for the NIF Target Area is currently under evaluation and will be considered in the design process.

The NIF Target Area is designed to safely contain an annual yield of 385 MJ distributed among monthly  $\sim 20$  MJ shots, weekly  $\sim 5$  MJ shots, and  $\sim 100$  kJ shot on a daily basis, a total of 145 shots that produce significant D-T neutron yield. In addition, another 500-1000 non-yield shots will also be conducted. The environments created by this range of performance introduce unique design issues.

Solutions to these issues required development of new predictive capabilities and validation of existing capabilities in assessing the in-chamber material responses to multiple exposures of unconverted laser light, x-rays, debris, and neutrons, and the consequences to the overall system of those responses. Confidence in overall system performance was developed by evaluating the ability of the various target area systems, once designed to meet their individual design requirements, to interact safely, affordably, and with low risk to meet the required shot rate.

**INVITED**

2:40 pm **PS2-ThA3 Precision Shell Characterization Using Radial Averaging of X-ray Images**, *R. B. Stephens*, General Atomics, P.O. Box 85608, San Diego, CA 92186-9784.

Measurement of shell dimensions from X-radiograph plates are normally limited by film graininess and camera resolution. We have taken advantage of the circular symmetry of microsphere X-ray images to substantially improve the resolution with which surfaces can be detected, and to detect interfaces between layers with only slight differences in X-ray absorption. This capability has been created with a desktop computer and slight modification to a freeware image processing program.

The digitized image of a shell is analyzed in three steps. 1) A radial averaging routine finds the image center to sub-pixel accuracy by maximizing the amplitude of the peaks in the 360° averaged radial intensity profile. 2) The 2<sup>nd</sup> derivative of the radial intensity profile is displayed as a rectangular plot of distance vs. radial angle. 3) The 2<sup>nd</sup> derivative of the 360° average of the radial intensity profile is plotted.

Peaks occur in the 2<sup>nd</sup> derivative plots at interfaces between materials of differing X-ray absorption strength. Therefore the rectangular plot shows a bright line indicating the radius of the shell surfaces and interfaces as a function of angle; fluctuations in radius  $\leq 1 \mu\text{m}$  can be detected. The peak location can be located with a reproducibility of 0.25  $\mu\text{m}$  off the graph of 2<sup>nd</sup> derivative of 360° averaged radial intensity profile.

Such precision requires minimization of vibrations in the exposure and distortions during digitization.

\*Work supported by the U.S. Department of Energy under Contract No. DE-AC03-91SF18601.

3:00 pm **PS2-ThA4 High Yield Fabrication of Uniform, Large Diameter Foam Shells for Laser Fusion Targets Using Polymerization by Photo Initiation with UV Light**, *M. Takagi, Y. Kobayashi, T. Norimatsu, Y. Izawa and S. Nakai*, ILE Osaka University, Yamada-oka, Suita, Osaka, 565, Japan.

In ignition experiments, one (1)-mm-diameter foam shells with 100- $\mu$ m uniform walls will be used as liquid fuel sustainers for a laser with output power of several hundred kilo joules. The low density, uniform foam layer is saturated with liquid deuterium and tritium fuel to make a uniform hollow fuel layer and covered with a membrane to prevent the evaporation of the fuel.

In a previous work [1], we heated hollow water/oil/water emulsions to start polymerization. This temperature change, however, induced density mis-matching and breaks of the hollow emulsions resulting very low yield for uniform foam shells.

Recently we have developed a new technique to make such foam shells using polymerization of trimethylolpropane trimethacrylate (TMPT) initiated by UV light. The TMPT and polymerization initiator were dissolved in a mixture of diethyl phthalate and di-n-butyl phthalate (oil phase). The oil solution was injected into a water bath using a dual orifice droplet generator to make a cylindrical oil column that broke into hollow water/oil/water emulsions with constant diameter and wall thickness. The emulsions were irradiated at room temperature using a high pressure UV lamp to gel the oil phase. After several rinse processes, the wet foam shells were dried in a critical point drying vessel using carbon dioxide as the drying fluid.

Since there is no temperature change in the process from formation of hollow emulsions through gelation of the oil phase, the yield for uniform hollow foam shells was greatly improved.

[1] T. Norimatsu et al. PS2-TuM5, 40th Nation. Symp. AVS. Nov. 15-19, 1993, Orlando, USA.

3:20 pm **PS2-ThA5 The Historical Development of the Microencapsulation Technique Used to Fabricate ICF Capsules**, *U. Kubo, H. Nakano, and H. Tsubakihara*, Kinki Univ., Dept. of Electrical Eng., Higashiosaka, Osaka 577, JAPAN.

The historical aspects regarding the development of the microencapsulation technique used to fabricate polymer capsules are presented. Initially, the production of paraffin capsules was attempted using this technique, which proved to be unsuccessful. However, polystyrene capsules were easily fabricated using microencapsulation at ambient temperatures. Recently, similar techniques have been used to fabricate foam capsules and polymer-layer-overcoated foam capsules. Foam capsules and their derivatives may make it possible to prepare cryogenic targets for ignition and ignition-scale experiments. The microencapsulation technique has been extended to fabricate polyvinyl alcohol (PVA) capsules overcoated with a polystyrene layer. These capsules retain fuel for a prolonged periods of time, and the polystyrene layer protects the hygroscopic PVA layer from degrading due to airborne water vapor. The microencapsulation technique produces capsules with diameters ranging from 50 to 1000  $\mu$ m, PVA layer thicknesses of 6-10  $\mu$ m, and 10-20- $\mu$ m-thick polystyrene layers.

**INVITED**

4:00 pm **PS2-ThA7 Vapor Deposited Solid Hydrogen Crystals: Size, Structure, and Roughening**, *Gilbert Collins, Evan Mapoles, Walt Unites and Tom Bernat*, Lawrence Livermore National Laboratory, Livermore, CA 94550.

Grown slowly from the liquid phase, solid hydrogen crystals can easily be made very large, and at temperatures above 4 K have an HCP crystal structure. This tendency to form large crystals (several millimeters in extent) with flat crystal facets presents a problem when forming smooth, spherical hydrogen shells for ICF targets. We report the crystal size and crystal structure of solid hydrogen deposited from the gas phase from the triple point temperature down to 3 K. Hydrogen and deuterium crystals, deposited below half their respective triple point temperatures are microcrystalline with a mixed HCP + FCC crystal phase. This mixed phase transforms into an HCP phase continuously and irreversibly as the temperature increases through half the triple point temperature. During this crystal structure transformation the crystallite size increases.

As the deposition temperature approaches the triple point, single

crystals of millimeter extent are easily formed. We report the roughening transition temperature from these crystals for two specific crystallographic orientations of the HCP lattice. Finally, above the roughening transition temperature, the equilibrium facet curvature is still larger than the curvature needed for NIF targets.

Work performed under the auspices of the U.S. Department of Energy by Lawrence Livermore National Laboratory under Contract W-7405-ENG-48.

4:20 pm **PS2-ThA8 The Design, Performance, and Application of an Atomic-Force Microscope-Based Profilometer**, *R. L. McEachern, C. E. Moore, and R. J. Wallace*, Lawrence Livermore National Laboratory, Livermore, CA 94550.

Rayleigh-Taylor instabilities during implosions of inertially confined fusion (ICF) capsules effect capsule performance. During acceleration, surface imperfections grow and can, if large enough, lead to an asymmetric implosion or even shell breakup. For this reason, characterizing the topography of target capsules is extremely important. We have developed a profilometer based on an atomic force microscope combined with a precision rotary air bearing. Averaged 1D surface height power spectra obtained with this instrument are converted to 2D mode spectra, which are used as input to LASNEX simulations. We describe the design of the system and its performance in terms of runout and repeatability. We will also discuss the simulation of these measurements and the statistics involved in averaging 1D power spectra. Finally, we will show the application of this measurement technique to capsules that have been laser-ablated, resulting in a well-defined surface topography. This special case provides an excellent test for the system, since the expected results are exactly calculable.

Work performed under the auspices of the U.S. Department of Energy by Lawrence Livermore National Laboratory under Contract W-7405-ENG-48.

4:40 pm **PS2-ThA9 Cryogenically Resealable Vacuum Seals**,\* *N. B. Alexander*, General Atomics, P.O. Box 85608, San Diego, CA 92186-9784.

General Atomics is developing a transfer cryostat that will permit gas cooled inertial confinement fusion (ICF) targets to be transferred cryogenically ( $T < 20$  K) from a cryostat where they are filled to a cryostat where they will be layered and inserted into the target tank of the OMEGA Upgrade ICF facility at the University of Rochester's Laboratory for Laser Energetics. The transfer cryostat's bottom sections will be resealed inside of the fill cryostat and vacuum reestablished between the sections. Vacuum seals have been developed that allow resealing while at cryogenic temperatures. A number of designs and materials were investigated. The best design material combination had a median leak rate of  $2 \times 10^{-9}$  mbar 1/sec for differential helium pressure of 100 torr and temperature 15 K. The median leak rate was computed from data gathered from a seal continuously kept at 15 K while being unsealed and resealed. During one test run, a seal was successfully resealed 11 times before the test was demonstrated.

The seal developed easily allows for the vacuum spaces of the transfer cryostat to be evacuated with a modest pump, once the bottom sections have been resealed.

\*Work supported by the U.S. Department of Energy under Contract No. DE-AC03-91SF18601.

5:00 pm **PS2-ThA10 Estimation for Heating Uniformity on a Solid Fuel Layer by a Glow Discharge Plasma in Plasma Layering Technique to Make a Uniform Cryogenic Fuel Layer Inside an ICF Target**, *T. Norimatsu, M. Ishihara, M. Takagi, Y. Izawa and S. Nakai*, ILE Osaka University, Yamada-oka, Suita, Osaka, 565, Japan.

Recent interests in fabrication of laser fusion targets include a cryogenic target with a uniform solid or liquid fuel layer inside a spherical hollow capsule. We proposed plasma layering technique to redistribute a nonuniform solid fuel layer into uniform one with adds of glow discharge plasma initiated in the void of the capsule located in a strong microwave field (1). Higher surface temperature at the thicker solid fuel layer induces sublimation of fuel at the thicker area and condensation of the vapour at the thinner area. Through this sublimation and deposition cycle, the nonuniform solid fuel layer turns to be uniform after lapse of time.

The key points in this method are uniform heating of the solid layer by the plasma and uniform cooling of the capsule. Last year we es-



timated the heating uniformity by the plasma under one dimensional electric field using data obtained by a simulation experiment at room temperature. The heat transfer by thermal radiation, however, was not included in the data analysis. This year we improved infrared imaging technique to measure the surface temperature. The heat transfer by thermal radiation inside the capsule was included in the estimation.

Resultant heating uniformity was worse than the previous estimations without radiation heat transfer but still sufficient to obtain a solid layer with uniformity >99% in an abnormal glow discharge regain.

Another interest of this method is a practical time scale to obtain a uniform solid hydrogen layer, which is currently supposed to depend on the cooling rate of the shell. We are going to demonstrate this technique using a quartz shell filled with deuterium gas cooled by liquid helium. The preliminary experimental results will be reported.

(1) C. M. Chen, et al., JVST, A11(3) 509 (1993).

## THIN FILM

### Room A105 - Session TF-ThA

#### Thin Films for Energy Conversion and Efficiency/ Active Films

**Moderator:** B. P. Hichwa, Optical Coating  
Laboratory Inc.

2:00 pm **TF-ThA1 Thin-Film Rechargeable Lithium Batteries,\***  
**J. B. Bates**, Solid State Division, Oak Ridge National Laboratory,  
P.O. Box 2008, Oak Ridge, Tennessee 37831-6030.

Miniaturization of batteries has not kept pace with the reduction in size and power requirements of electronic devices. A lower limit on the dimensions of conventional batteries such as mm-sized coin cells is dictated by bulk materials processing methods and by the battery container, which is typically a metal can. Recently, solid state batteries that are less than 10- $\mu$ m thick have been developed. These batteries, which can be fabricated in a variety of shapes and sizes on virtually any type of substrate, consist of a lithium metal anode and an inorganic insertion cathode that are separated by a lithium phosphorus oxynitride electrolyte. The cathode films, which include  $V_2O_5$ ,  $LiMn_2O_4$ , and  $LiCoO_2$ , are deposited by reactive magnetron sputtering and evaporation. Processing conditions such as working gas composition and pressure, substrate temperature, and post deposition treatment have important effects on the physical and chemical properties of the cathode films and therefore have a major impact on the performance of thin-film batteries. Because they have high energies per unit of volume and mass and because they can be recharged thousands of times, thin-film lithium batteries have potentially many applications as small power supplies for electronic devices. **INVITED**

\*This research was sponsored by the Divisions of Materials Sciences and Chemical Sciences, U.S. Department of Energy, under contract DE-AC05-84OR21400 with Martin Marietta Energy Systems, Inc.

2:40 pm **TF-ThA3 Sputter Deposition of Cermet Fuel Electrodes for Solid Oxide Fuel Cells, T. Tsai and S. A. Barnett**, Department of Materials Science and Engineering, Northwestern University, Evanston, IL 60208.

Electrodes for medium-temperature (600–800°C) solid oxide fuel cells (SOFC) should exhibit both low resistivity and low interfacial reaction resistance  $R_i$  with the electrolyte. In order to achieve this, common fuel electrode materials, such as  $Ni-(Y_2O_3)_x(ZrO_2)_y(Ni-YSZ)$  cermets, must have both significant porosity and small Ni particle size to achieve high three-phase contact area between Ni, YSZ, and the fuel gas. In this talk, the use of DC magnetron reactive sputtering of  $Ni-Zr-Y$  (68.8 wt% Ni, 26.6 wt% Zr, 4.52 wt% Y) targets in  $Ar-O_2$  mixtures to deposit porous Ni-YSZ films is described. The films contained 50 vol% Ni, were deposited with 0.6 mTorr  $O_2$  at a rate of  $\approx 3 \mu m/h$ , and exhibited resistivities of  $\approx 0.005 \Omega cm$ .  $R_i$  values between Ni-YSZ films and YSZ electrolytes were measured in  $H_2/H_2O$  fuel gases by impedance spectroscopy. The spectra showed two arcs, attributed to electrochemical reactions and gas diffusion. Films sputtered at 20 mTorr total pressure gave the lowest  $R_i$  values, with SEM images

showing cracks due to tensile stress at higher pressures and insufficient porosity at lower pressures. The initial YSZ substrate morphology also played an important role, with the lowest  $R_i$  values obtained for YSZ substrates roughened by polishing with 25  $\mu m$  particles. The roughened surfaces presumably provided higher contact area and increased film porosity. The best  $R_i$  values of  $0.15 \Omega cm^2$  at 750°C were much lower than bulk Ni-YSZ and low enough for high-power-density SOFC operation.

3:00 pm **TF-ThA4 Morphology of Precursors and  $CuIn_{1-x}Ga_xSe_2$  Thin Films Prepared by Two-Stage Selenization Process, N. G. Dhere, S. Kuttath, Florida Solar Energy Center, 300 State Rd. 401, Cape Canaveral, FL 32020-4099, H. R. Moutinho, National Renewable Energy Laboratory, 1617 Cole Blvd., Golden, CO 80401.**

A novel two-stage, *nontoxic* selenization process consisting of sputter-deposition and homogenization of Cu-rich Cu-In-Ga precursor, first selenization, deposition of In-rich Cu-In-Ga precursor, and second selenization has been developed for the preparation of  $CuIn_{1-x}Ga_xSe_2$  thin films. Morphology of precursors and  $CuIn_{1-x}Ga_xSe_2$  thin films was studied because of their effect on photovoltaic (PV) properties of solar cells. Very small sub-grain features were studied for the first time by atomic force microscopy (AFM), and quantitative data on rms roughness and 3-d images were obtained. Morphology of precursors was found to change from initial very smooth layers with 200–300 Å size features and a rms surface roughness of <10 Å, to 3-d  $\sim 9000$  Å size islands, coalescing grains with a fine sub-grain structure, and finally to compact, well-faceted, large-grain  $CuIn_{1-x}Ga_xSe_2$  thin films with rms roughness in the range 950–1500 Å. Improvement of the morphology of completed  $CuIn_{1-x}Ga_xSe_2$  thin films with the complete elimination of the sub-grain structure, substantial increase in the grain-size, more homogeneous distribution of the grain-size, and development of well-faceted grains was achieved by *in situ* homogenization of Cu-rich precursors prior to the first selenization and by employment of a maximum temperature of 550°C during the selenization so as to benefit from the fluxing action of copper selenide. Efficient PV solar cells were fabricated using 500 Å thick conformal CdS heterojunction partner layers even though rms roughness of completed  $CuIn_{1-x}Ga_xSe_2$  thin films was  $\sim 1400$  Å.

3:20 pm **TF-ThA5 Structure, Morphology, and Properties of  $CuIn_{1-x}Ga_xSe_2$  Epitaxial Layers on GaAs, G. Berry, D. Schroeder, L-Chung Yang, H. Z. Xiao, and A. Rockett**, Coordinated Science Laboratory and Materials Research Laboratory, University of Illinois, 1101 W. Springfield Ave., Urbana, IL 61801.

Single crystal epitaxial layers of  $Cu(In_{1-x}Ga_x)Se_2$  (CIGS) have been grown on (111) and (001) GaAs substrates by a hybrid sputtering and evaporation method. Results are presented showing the relationship of composition to film surface morphology, density and type of lattice defects, phases present, and optoelectronic properties. Films containing moderate amounts of Ga (<10%) are shown to have structures and surface morphologies consistent with those of pure  $CuInSe_2$  epitaxial layers. At higher Ga contents (>20%) the surface becomes faceted and roughened and significantly increased bulk defect densities were observed. Second phases are also observed in the high-Ga content alloys. In-rich films having a composition  $CuIn_3Se_5$  have also been examined and found to include an ordered array of point defects. The In-rich films have increased energy gaps and show evidence of extended subgap absorption consistent with the presence of extended band tails (Urbach edges). Interdiffusion between the layers and the GaAs substrates was higher when the Ga flux used to grow the epitaxial layer was lower. The use of these materials in photovoltaic applications is discussed and preliminary results of solar cell performances are described.

3:40 pm **TF-ThA6 Growth of Chalcopyrite  $Cu(Ga, In)Se_2/CuIn_3Se_5$  Absorbers by r.f. Sputtering, J. L. Hernández-Rojas, I. Martíl, G. González-Díaz, J. Santamaría, and F. Sánchez-Quesada**, Dpto. Física Aplicada III, Facultad de Ciencias Físicas, Universidad Complutense, 28040 Madrid, (SPAIN).

Recently several groups have shown that high efficiency multinary chalcopyrite thin film solar cells have a copper-poor surface layer which induces the formation of a buried homojunction. In the case of  $CuInSe_2$  this Cu-poor phase is  $CuIn_3Se_5$  (OVC). In this communication we have a two-fold motivation: On one hand we want to characterize OVC films r.f. sputtered from a single target, on the other hand we have fabricated absorbers by sequential deposition of  $Cu(Ga, In)Se_2$  and  $CuIn_3Se_5$  by r.f. sputtering. We find that films grown at growth temperatures ( $T_g$ ) below 400°C are homogeneous with a composition close to the target, no secondary phases are detected. These films have a



bandgap of 1.25 eV and a much stronger 112 orientation than CGIS thin films. For  $T_g$  above 400°C film composition in a ternary phase diagram approaches the line that joins  $\text{CuInSe}_2$  and  $\text{InSe}$ . X-ray diffraction shows the presence of  $\text{InSe}$ , and optical properties a bandgap of 1.0 eV with a high sub-bandgap absorption. We conclude that in the Cu-poor side of the phase diagram film formation takes place from the selenide binaries analogously to CGIS. Nevertheless, for high  $T_g$   $\text{Cu}_2\text{Se}$  and  $\text{In}_2\text{Se}_3$  do not react completely leaving unreacted  $\text{In}_2\text{Se}_3$  that decomposes in  $\text{InSe(s)} + \text{Se}_2(\text{g})$ . Absorbers grown by the sequential growth of high  $T_g$  Cu-rich CGIS and OVC films show a complete intermix of the element, and an improved performance with respect to devices r.f. sputtered from a single target.

4:00 pm **TF-ThA7 Attaining a Solar Energy Economy with Active Thin Film Structures**, *R. B. Goldner*, Electro-Optics Technology Center, Tufts University, Medford, MA 02155.

Quantitative arguments are presented which support the conclusion that the probability is high for the U.S. to attain a solar energy economy in the relatively near future. The basis of the arguments is the use of four active thin film structures: (i) electrochromic "smart" windows for energy conservation; (ii) thin film photovoltaic cells for energy conversion; (iii) & (iv) thin film batteries & fuel cells for portable energy storage and delivery. The paper focuses on the pivotal role of thin film deposition processes. Particular attention is paid to some of the deposition challenges presented by electrochromic smart windows and the thin film batteries.

**INVITED**

4:40 pm **TF-ThA9 Low Temperature, High Rate Deposition of Electrochromic Materials/Devices with MetaMode®**, *Nada A. O'Brien, J. Gordon, H. Mathew, and Bryant P. Hichwa*, Optical Coating Laboratory, Inc., 2789 Northpoint Parkway, Santa Rosa, California 95407-7397.

MetaMode® reactive sputtering [1] is used to manufacture uniform multilayer anti-reflection coatings and transparent conductive films. Recently, we have deposited electrochromic (EC) materials and devices with the MetaMode® process. MetaMode® offers the advantage of low temperature deposition and relatively high deposition rates compared to conventional reactive sputtering. Moreover, we have reproducibly fabricated complete monolithic EC devices at manufacturable rates with the MetaMode®. For example, a  $25 \text{ cm}^2$  transmissive device shows a photopic transmission change  $\geq 50\%$  and coloring/bleaching time  $\leq 20$  seconds. In this paper, a description of the MetaMode® process and its capabilities will be given. In addition, we will compare the behavior of MetaMode®-prepared  $\text{WO}_3$  EC films with other more conventional EC deposition techniques: We will report on electrochromic properties, i.e., coloring efficiency, optical density, switching time and current-voltage characteristics.

1. M. A. Scobey, R. I. Seddon, J. W. Seeser, R. R. Austin, P. M. LeFebvre, and B. W. Manley, US Patent #4,851,095, July 25, 1989.

5:00 pm **TF-ThA10 Properties of Transparent Conducting Zinc-Stannate Films Prepared by RF Magnetron Sputtering**, *T. Minami, S. Takata, H. Sato and H. Sonohara*, Kanazawa Institute of Technology, 7-1 Ohgigaoka, Nonoichi, Ishikawa 921, Japan.

The preparation of newly developed transparent conducting oxide films by rf magnetron sputtering is demonstrated. The  $\text{SnO}_2$ -ZnO films were prepared on glass substrates using  $\text{SnO}_2$  targets with a ZnO content of 0 to 35wt%. The resistivity of the deposited films markedly decreased as the Zn/Sn + Zn atomic ratio introduced into the films was increased. The minimum resistivity was obtained for films with a Zn/Sn + Zn atomic ratio of about 0.2. It was found that the composition of the deposited films is  $\text{ZnSnO}_3$  rather than  $\text{Zn}_2\text{SnO}_4$ . The electrical and optical properties of films deposited using Ar- $\text{O}_2$  mixture sputter gases were strongly dependent on the  $\text{O}_2$  partial pressure as well as the substrate temperature. Resistivities as low as  $4 \times 10^{-3} \Omega\cdot\text{cm}$  and an average transmittance above 80% in the visible range were obtained for undoped zinc-stannate films prepared with substrate temperatures of RT to 300°C by controlling the  $\text{O}_2$  partial pressure. Especially for the zinc-stannate films, thermal stability in a hydrogen environment was improved over that of  $\text{SnO}_2$  films and chemical stability in acidic and basic atmospheres was improved over that of ZnO films.

## ELECTRONIC MATERIALS

Room A108 - Session EM-ThA

### Materials for Nanostructures

**Moderator:** H. P. Gillis, Georgia Institute of Technology.

2:00 pm **EM-ThA1 Magnetotransport in Semiconductor Nanostructures**, *K. P. Martin*, Georgia Institute of Technology, Atlanta, GA, 30332.

Semiconductor nanostructures have important device applications and present opportunities to investigate fundamental issues in condensed matter physics. This talk will discuss the use of magnetotransport as a tool to study of these systems. Quite generally, the magnetic field allows the experimentalist to introduce an external scale for length, time, and energy through (respectively) the cyclotron radius, frequency, and energy. In turn, these B-induced quantities can be used to probe the material and transport properties related to phase coherent tunneling, elastic and inelastic scattering, charge buildup, and band-structure. In some instances, magnetotransport can be used to evaluate properties related to growth (interface roughness) and processing (etch-induced damage) of these nanostructures. Supported by NSF grants DMR-92022879, ECS-8922512, and ECS-9111866.

**INVITED**

2:40 pm **EM-ThA3 Nanoscale Structures in III-V Semiconductors Using Sidewall Masking and High Ion Density Dry Etching**, *F. Ren<sup>1</sup>, S. J. Pearton<sup>2</sup>, C. R. Abernathy<sup>2</sup> and J. R. Lothian<sup>1</sup>*, <sup>1</sup>AT&T Bell Laboratories, Murray Hill, NJ 07974, <sup>2</sup>Department of Materials Science and Engineering, University of Florida, Gainesville, FL 32611.

The optical and electrical properties of nanostructures in III-V semiconductors are of interest from both a fundamental viewpoint and for technological applications in quantum confined lasers or wires and dots for low power photonic and electronic device arrays. We have developed a simple deposition and etch-back technique to form narrow ( $\sim 300 \text{ \AA}$ ) masks for subsequent pattern transfer into the semiconductors. High ion density ( $5 \times 10^{11} \text{ cm}^{-3}$ ) ECR  $\text{CH}_4/\text{H}_2/\text{Ar}$  (for In-containing materials) or  $\text{BCl}_3/\text{Ar}$  (for Ga-containing materials) are used to give anisotropic low-damage etching. After initial resist patterning using conventional stepper lithography, conformal PECVD or reactive sputtering of a metal (W,  $\text{WSi}_x$ ) or a low temperature dielectric ( $\text{SiN}_x$ ,  $\text{SiO}_2$ ) is followed by an anisotropic etch-back to leave a thin sidewall on the resist feature. The resist is then removed by dry etching, leaving the sidewall which can be used as a mask for pattern transfer into the semiconductor. Examples of optically-pumped quantum wire laser structures fabricated in GaN and InP-InGaAsP systems will be shown. The nano-laser structures can be integrated with microdisk lasers using combined dry etching and selective wet chemical etching. Low ion energies ( $\leq 100 \text{ eV}$ ) are required to avoid sputtering of the mask material and changes in the near-surface stoichiometry of the semiconductor.

3:00 pm **EM-ThA4 Optical Evaluation and Surface Passivation of Quantum Structures Fabricated by Neutral Atom Etching at Cryogenic Temperatures**, *M. B. Freiler, M. C. Shih, S. Kim, M. Levy, R. Scar-mozzino, I. P. Herman, and R. M. Osgood, Jr.*, Columbia Radiation Laboratory, Columbia University, New York, NY 10027.

We report the photoluminescence spectroscopy of etch-defined quantum box- and wire-like structures fabricated in  $\text{GaAs}/\text{Al}_{0.3}\text{Ga}_{0.7}\text{As}$  quantum wells by a novel form of excimer-laser-excited neutral Cl atom etching. Our etching technique is suitable for the fabrication of these structures because it enables high resolution, noncrystallographic, dry etching, using neutral atom reactions. Such low-energy atom chemistry is not expected to damage the feature sidewalls, as is often the case for other high resolution, ion-based etch techniques. This damage has often been cited as a primary cause of the limited luminescence efficiency of etch-defined quantum wire- and box-like structures. In fact, comparison of our results with the luminescence of wet-etched samples shows little or no etch-induced damage to the feature sidewalls. In this connection, we have conducted a series of photoluminescence measurements at 10 K which show strong luminescence from our smallest features. As a result we have measured the photoluminescence efficiency and spectrum shape as a function of the feature lateral dimension from several micrometers to less than  $0.25 \mu\text{m}$ . For smaller features, the chemical state of the surface is crucial for the luminescence efficiency, and so different surface chemical treatments, such as H-ECR passivation, have been used to enhance the luminescence efficiency to near that of the unprocessed material.

Our results will be explained in terms of standard models of carrier recombination. This work has been funded by JSEP, ARPA, and AFOSR.

**3:20 pm EM-ThA5 Room Temperature Photoluminescence and Electroluminescence from Ge Nanocrystals in SiO<sub>2</sub> Formed by Ion Implantation and Precipitation, C. M. Yang, K. V. Shcheglov, S. S. Wong, H. A. Atwater, California Institute of Technology, Pasadena, CA 91125.**

There is a growing interest in the luminescent properties of group IV semiconductor nanocrystals driven by a need for optoelectronic devices compatible with current VLSI Si-based manufacturing technology. Ion implantation and thermal annealing, standard Si processing methods, have been used to fabricate Ge nanocrystals in SiO<sub>2</sub> matrix. This configuration has an advantage over porous silicon in that it is mechanically robust and insensitive to environmental influences. It was found that by varying annealing conditions for the sample implanted with 6 atomic percent Ge, narrow size distributions can be obtained with mean size ranging from 3 nm for the 600°C anneal to 10 nm for the 1200°C anneal. Visible photoluminescence at room temperature has been observed from the above samples with peaks between 500 nm and 700 nm, depending on annealing conditions. Lastly, an electroluminescent device has been fabricated in a PIN configuration, the 'intrinsic' layer being Ge nanocrystal-containing SiO<sub>2</sub>, with similar photoluminescence and electroluminescence spectra peaked at 700 nm. Comparison of photoluminescence and electroluminescence for this device with the particle-size distribution will be presented, as well as a systematic correlation of particle-size distributions with photoluminescence spectra for the above samples.

**3:40 pm EM-ThA6 Direct Characterization of a 2 Dimensional Electron Gas in Heterostructure FETs with Scanning Tunneling Microscopy,†, S. L. Skala, W. Wu, J. R. Tucker, K.-Y. Cheng, and J. W. Lyding, Department of Electrical and Computer Engineering, Beckman Institute and Microelectronics Laboratory, University of Illinois at Urbana-Champaign, Urbana, IL 61801.**

Cross-Sectional Scanning Tunneling Microscopy (XSTM) has been used to directly image a 2 DEG in cleaved HFET devices. Variation in electron concentration within the 2 DEG can be measured as well as the location of the maximum of the first electron subband. We explore the uniformity of the 2 DEG as a function of material parameters such as barrier-channel interface quality and alloy fluctuations within a tertiary channel. Additionally, agreement between theoretically predicted characteristics of 2 DEG and direct measurements for a variety of device structures is determined.

†Supported by NSF under contract NSF EDC 89-43166 and by JSEP under contract N00014-90-J-1270.

**4:00 pm EM-ThA7 Temporal Evolution of Nanoscale Interfacial Phases Between GaAs and Metal Films, Tae-Jin Kim, Paul H. Holloway, Dept. of Materials Science and Engineering, University of Florida, Gainesville, FL 32611.**

The electrical, thermal and mechanical properties of metal thin films on semiconductors depend on interfacial reactions. In the case of GaAs, multilayer films such as Au-Ge-Ni produce binary (AuGa, NiGa, NiAs etc.) and ternary (Ni<sub>3</sub>GaAs) phases. Very often the phases extend irregularly into the semiconductors over distances on the order of 5–50 nm, leading to degradation of interfacial properties. To achieve regular nanoscale structures with desired properties, precise dimensional control based on a theory is essential. A "regrowth" model will be suggested to explain variation of the properties associated with the interfaces. It will be shown that Ga and As from the binary or ternary phases "regrow" into GaAs as a result of temporal evolution of the interfacial phases. It will be shown that the electrical and the other properties of the interfaces can be controlled by the regrowth.

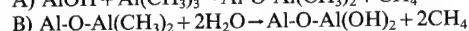
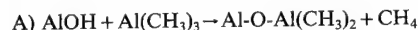
**4:20 pm EM-ThA8 Selective Chemical Vapor Deposition of Copper on Pd-Activated Self-Assembled Films, Stephen J. Potochnik<sup>1,2</sup>, David S. Y. Hsu<sup>1</sup>, Jeffrey M. Calvert<sup>2</sup>, and Pehr E. Pehrsson<sup>1</sup>, 1. Chemistry Division, 2. Center for Bio/Molecular Science and Engineering, Naval Research Laboratory, Washington, DC.**

A process has been developed for selective chemical vapor deposition (CVD) of conductive, adherent copper films using self-assembled organosilane films to tailor substrate surface chemistry. Selective copper CVD was achieved on single-crystal diamond substrates at 423–453 K in a low-pressure, cold-walled reactor using hexafluoroacetylacetonate-Cu<sup>1</sup>-trimethyl-vinylsilane (hfac-Cu<sup>1</sup>-tmvs) in H<sub>2</sub> (1:1). Diamond

was activated for copper deposition by covalent attachment of a ligating aminosilane film and a Pd-based catalyst; only isolated copper particles formed on unmodified diamond surfaces. Copper deposition on growth and nongrowth surfaces was characterized by Auger electron spectroscopy (AES), x-ray photoelectron spectroscopy (XPS), x-ray fluorescence (XRF), and scanning electron microscopy (SEM). Patterned copper features were formed on diamond substrates by exposing photosensitive aminosilane films to patterned ultraviolet (193 nm) radiation prior to Pd-catalyst addition and copper CVD.

**4:40 pm EM-ThA9 Surface Chemistry of Al<sub>2</sub>O<sub>3</sub> Deposition Using Al(CH<sub>3</sub>)<sub>3</sub> and H<sub>2</sub>O in a Binary Reaction Sequence, A. W. Ott, A. C. Dillon and S. M. George, Dept. of Chem. and Biochem., University of Colo., Boulder, CO 80309, J. D. Way, Dept. of Chem. Engin. and Petroleum Refining, Colo. School of Mines, Golden, CO 80401.**

Sequential surface chemical reactions for the atomic layer controlled deposition of Al<sub>2</sub>O<sub>3</sub> were studied using transmission Fourier transform infrared spectroscopy (FTIR) and atomic force microscopy (AFM). A binary reaction for Al<sub>2</sub>O<sub>3</sub> chemical vapor deposition (2Al(CH<sub>3</sub>)<sub>3</sub> + 3H<sub>2</sub>O → Al<sub>2</sub>O<sub>3</sub> + 6CH<sub>4</sub>) was separated into two half-reactions:



The trimethylaluminum [Al(CH<sub>3</sub>)<sub>3</sub>] (TMA) and H<sub>2</sub>O reactants were employed alternately in an ABAB... binary reaction sequence to achieve atomic layer controlled Al<sub>2</sub>O<sub>3</sub> deposition. FTIR analysis of these surface reactions was performed *in situ* in an ultrahigh vacuum (UHV) chamber using high surface area alumina membranes. The AlOH and AlCH<sub>3</sub> surface species were monitored by the infrared absorbance of the AlO-H stretching vibration between 3800–2600 cm<sup>-1</sup> and the AlC-H<sub>3</sub> stretching vibrations between 2942–2838 cm<sup>-1</sup>. The optimal conditions for controlled Al<sub>2</sub>O<sub>3</sub> growth were observed using TMA and H<sub>2</sub>O exposures at 0.3 Torr on substrates at 500 K. The spectra revealed that both the A and B reactions were self-limiting and complete. The atomic layer controlled deposition of amorphous Al<sub>2</sub>O<sub>3</sub> thin films was demonstrated on Si(100) and sapphire using the ABAB... binary reaction sequence. Atomic force microscopy was employed to determine deposition rates versus temperature as well as examine the film conformality. A growth rate of 3 Å/AB binary reaction cycle was observed for the optimal Al<sub>2</sub>O<sub>3</sub> growth conditions.

**5:00 pm EM-ThA10 Study of Polycrystalline CdTe Thin Films by Atomic Force Microscopy, H. R. Moutinho, F. A. Hasoon, F. Abul-fotuh and L. L. Kazmerski, National Renewable Energy Laboratory, Golden, CO 80401.**

Polycrystalline CdTe thin films grown by different methods, including physical vapor deposition, sputtering, closed space sublimation, and MOCVD have been studied by atomic force microscopy (AFM). The results are compared with scanning electron microscopy (SEM) investigations. The films have been analyzed as-deposited and after heat and chemical treatments with CdCl<sub>2</sub>, processing used to realize high-efficient thin-film (>15%) photovoltaic devices. It was found that the results for the AFM and SEM agree well up to the resolution of the later. At higher spatial resolutions (beyond the limit of the SEM) new structures have been observed for the first time in these films. For samples deposited by sputtering, AFM analysis showed that the micron-size features (observed also with the SEM) are actually formed by smaller grains, having few hundred of angstroms cross-sectional dimensions. These films, when treated with CdCl<sub>2</sub> at different temperatures show the nanograin structure coalescing, with complete recrystallization at temperatures of approximately 400°C. The nanograin structure has also been observed in some films grown by physical vapor deposition. A post-deposition heat-treatment of these films also changed this structure. The existence of the nanograins is a function not only of the deposition method, but also of the substrate on with the film is grown, and of the post-deposition heat-treatment. These nanoscale studies provide the first direct evidence linking the processing of the films to the change in nanostructure and the resulting efficiency improvement of the photovoltaic cells.



**MANUFACTURING SCIENCE AND  
TECHNOLOGY/VACUUM TECHNOLOGY**  
**Room A110 - Session MSVT-ThA**

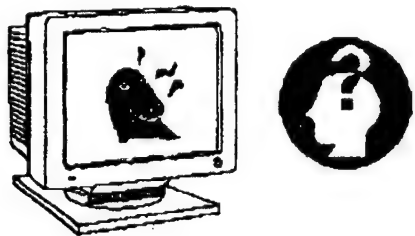
**Vacuum Process Control for Manufacturing**

**Moderator:** W. Weed, Sandia National  
Laboratories.

**2:00 pm MSVT-ThA1 Top Ten List of User-Hostile Interface Design,** *Dwight P. Miller*, Sandia National Laboratories, MS 1045, Albuquerque, New Mexico 87185.

This paper describes ten of the most frequent ergonomic problems found in computer-based user-system interfaces (USIs) used in sophisticated industrial machines. In contrast with being "user friendly," many of these machines are considered "user-hostile" by the author. The historical lack of consistent application of ergonomic principles in computer-based USIs has led to a breed of very complex industrial equipment that few people can operate safely and efficiently without extensive orientation, training, and experience. This design oversight has created the need for extensive training programs and help documentation, unnecessary "human" errors and incidents, machine downtime, and reduced productivity resulting from operator stress and confusion. The ten issues are treated in a problem-solution format with real-world graphic examples of good and poor design. Intended for a diverse audience, the paper avoids technical jargon, and is appropriate reading for those involved in software, product engineering, marketing, and management.

**INVITED**



**2:40 pm MSVT-ThA3 Advanced Control Methodologies Into the Future,** *Richard W. McMahon*, Techware Systems Corporation, 100-12051 Horseshoe Way, Richmond, BC, V7A 4V4, Canada.

Along with other aspects of vacuum deposition and etch, control system methodologies and practices are undergoing a process of maturation. During the 1980s exciting research was conducted into the use of exotic techniques such as real-time expert systems, artificial neural networks, and fuzzy logic, with the aim of modeling and closing control loops on poorly understood plasma based processes. Currently, researchers are exploring a variety of sensor technologies and a more classical approach to multivariate control, while systems developers direct their efforts towards quality, usability and interoperability issues, reflecting the maturing needs of the deposition and etch industry. A great deal of collaborative work is going into the creation of designs and standards for connecting equipment controls into factory networks and, in the case of cluster tools, to each other. Standards are also evolving for human interfaces, sensor buses, and electronic document retrieval. Software quality improvements such as the separation of applications (customization) code from systems (standard platform) software modules, self diagnostics, version control, and qualification tests are beginning to appear. By selectively drawing upon software technologies available in a wider range of processing industries, vacuum control systems of the future will have improved friendliness, reliability, and integration with other computer systems used throughout the user's facility.

**INVITED**

**3:20 pm MSVT-ThA5 Adaptive Extensions to a Multi-branch Run-to-Run Controller for Plasma Etching,** *James R. Moyne, Nauman Chaudhry, and Roland Telfeyan*, Univ. of Michigan, DTM Center, Ann Arbor, MI 48109-2108.

Fuzzy logic and database learning mechanisms have been incorporated into a generic plasma etching run-to-run controller, resulting in a very dynamic, adaptable and robust system. The system features an Applied 8300 RIE controlled by a Techware II equipment controller. A TCP/IP connection links this equipment controller to the run-to-run controller residing on a SUN. The run-to-run control environment

is generic in that the basic control framework and controller development results are applicable to VLSI manufacturing in general. The controller is multibranch as it utilizes multiple algorithms in complementary fashion to achieve process optimization and control. The current implementation utilizes three branches: (1) a linear approximation control algorithm, (2) an optimization algorithm that utilizes (real-time) data collected in-situ to determine optimal run-to-run process parameter settings, and (3) a statistical optimization algorithm that utilizes run-to-run data. The controller has been extended to incorporate an automated branch selection process that utilizes fuzzy logic to incorporate process engineer as well as optimization and control algorithmic knowledge. The controller has also been extended to adapt to unforeseen events through utilization of a learning mechanism; this mechanism detects these unforeseen events, intelligently queries the process engineer, guides the engineer through the development of an event servicing scheme, and incorporates this new knowledge into its control knowledge base so that the event may be serviced automatically in the future. Implementation results of the controller (in the control of the etcher) confirm the robust control capabilities in the face of process shift and drift, and recipe change.

**3:40 pm MSVT-ThA6 Real-Time Feedback for Sidewall Profile Control,** *Brian Rashap, Jim Freudenberg and Michael Elta*, University of Michigan.

Real-time feedback control is being applied to the Reactive Ion Etching process as part of a strategy to control sidewall profile. As with a number of etch characteristics, it is not possible to measure sidewall profile in-situ and in real-time. Therefore, an indirect method of controlling these characteristics is necessary. In previous work, we have shown that it is possible to stabilize etch rate by using feedback control to regulate various plasma characteristics.

Currently, we are investigating sidewall profile control, again using feedback to manipulate plasma properties. The sidewall shape produced by an etch is determined by the isotropic and anisotropic etch rate components. Free radicals diffusing to the surface determine isotropic etch rate. Anisotropic etching is caused by an enhanced etch rate in areas exposed to ion bombardment and a reduced rate in areas where a passivation layer is present. This paper reports on the first step in the development of a strategy for controlling sidewall profile. Using a real-time controller for the plasma generation process in a CF<sub>4</sub>/O<sub>2</sub> chemistry, a response surface from plasma characteristics (self-bias voltage, pressure, and fluorine concentration) to vertical and horizontal etch rates is developed. A string model simulation, optimized to match scanning electron microscope images of the etch profile, is used to calculate etch rate components. This response surface will then be used to develop trajectories for the plasma environment that produce desired sidewall profiles. Finally, the real-time controller will be employed to actuate these trajectories.

**4:00 pm MSVT-ThA7 Process Monitoring with Residual Gas Analyzers,** *Charles R. Tilford*, National Institute of Standards and Technology, Gaithersburg, MD 20899.

Residual Gas Analyzers (RGAs), most commonly mass spectrometers of the quadrupole type, have long been used for qualitative vacuum-system diagnostics. Increasingly, they are also being used for quantitative process monitoring and control, often involving highly reactive contaminant and process gases. RGAs are complicated instruments and their performance is affected by a number of instrument and vacuum-environment variables, so that even "calibrated" instruments can behave significantly different than expected. The magnitude of the performance anomalies varies for different instruments, but can reach orders of magnitude in extreme cases. This talk will review the important factors affecting instrument performance (including ion-source and quadrupole-filter parameters, total pressure, and exposure to active gases), illustrate the magnitude of observed effects for different instruments, recommend instrument test and calibration procedures, and suggest operating parameters and procedures that can minimize anomalies.

**4:20 pm MSVT-ThA8 An Improved Method of Non-Intrusive Deposition Rate Monitoring by Atomic Absorption Spectroscopy for PVD Processes,** *C. Lu and Y. Guan*, Intelligent Sensor Technology, Inc., 1012A Linda Vista Avenue, Mountain View, CA 94043.

Deposition rate is a critical parameter that needs to be precisely controlled in all PVD processes. Atomic absorption spectroscopy (AAS) is a well established technique for determining the atomic density in vapor phase, and it has been tested for non-intrusive monitoring of deposition rate in PVD processes. However, previous AAS based monitors encountered serious problems during typical deposition processes

due to changes in optical signal levels caused by viewport coating and temperature-induced movements in optical alignment, resulting in poor accuracy for long-term operation. We have developed a novel optical scheme named COPACT (Common Optical Path for Automatic Correction of Transmission) which significantly improves the long-term stability of AAS deposition rate monitors. The emission from a broadband light source, with its central wavelength and bandwidth properly defined by a wavelength selection device, is utilized to compensate the overall optical system transmission change in real-time. This method enables us to fully realize the advantages of AAS for deposition rate monitoring, which include absolute material specificity, high sensitivity, extended vapor sampling region, no background pressure limitation, uninterrupted operation and non-intrusive optical probing. Experimental results are presented to show that it is possible to accurately control very low deposition rates, on the order of one monolayer per minute, over an extended time period.

4:40 pm **MSVT-ThA9 A Model Based Technique for Estimation of Fluorine in a CF<sub>4</sub>/Ar Plasma**, *P. D. Hanish, Jessy W. Grizzle, and M. D. Giles*, University of Michigan, Ann Arbor, MI 48109.

A technique for quantitative interpretation of actinometric data to deduce bulk plasma fluorine concentration in a CF<sub>4</sub>/Ar plasma has been developed and tested on an RIE. This static, in situ measurement is useful for monitoring fluorine in a manufacturing environment and, in particular, for application of real time feedback control to plasma etching. Based upon a model of CF<sub>4</sub> chemistry reaction pathways and products, it improves upon current fluorine estimation techniques by accounting for varying levels of argon dilution resulting from CF<sub>4</sub> dissociation. A simple experiment was also developed in order to obtain an estimate of the actinometric scaling factor without an independent measurement of fluorine. Performance of this fluorine estimation technique was compared to that of a standard technique by using time resolved etch rate measurements as an independent indicator of fluorine concentration, while a feedback control scheme decoupled the effects of physical etching by stabilizing the induced dc bias. The model based estimator reduced perturbations in the etch rate by more than 50% compared to those seen when using the standard estimator.

5:00 pm **MSVT-ThA10 Role of Inert Carrier Gases in Modeling, Design and Operation of a Single Wafer APCVD Reactor for Manufacturing**, *Prasad N. Gadgil*, Department of Physics, Queen's University, Kingston, Ontario, K7L 3N6, CANADA.

Atmospheric Pressure Chemical Vapor Deposition (APCVD) with inert carrier gases can offer several potential advantages in microelectronic device manufacturing. In a simple stagnation point flow configuration, lower viscosity of inert gases such as Argon and Nitrogen results in a lower pressure drop across the gas distributor and a smaller magnitude of undesirable entrance effects as compared to Hydrogen. In addition, lower thermal conductivity of N<sub>2</sub> leads to the development of isotherms with a higher temperature gradient adjacent to the susceptor surface that are highly desirable to suppress homogeneous gas phase reactions. A hydrodynamic model of a single wafer stagnation point flow reactor is developed. An inverted APCVD stagnation point flow reactor with a novel flow distributor, optimized by flow visualization and fluid flow modeling is designed. The results of its operation with inert carrier gases are described. The suitability of mixing of inert gases with reactive gases such as H<sub>2</sub>, NH<sub>3</sub> and O<sub>2</sub> is evaluated for process chemistry of various microelectronic materials. Also, additional economic advantages in the back end of a CVD system in exhaust processing are outlined.

## VACUUM METALLURGY

### Room A106 - Session VM-ThA

#### Manufacturing Technology for Coatings

**Moderator:** D. C. Carmichael, Vacuum Technology Inc.

2:00 pm **VM-ThA1 Environmentally Compatible Coating Technology**<sup>†</sup>, *Keith O. Legg, A. Adamski, C. West, P. Rudnick, F. Rastagar\*, J. Schell\*\*, A. Gonzales†, B. Sartwell††*, BIRL Industrial Research Lab., Northwestern University, Evanston, IL; \*Cummins Piston Ring Division; \*\*GE Aircraft Engines; †Corpus Christi Army Depot; ††Naval Research Lab.

This paper will discuss what is involved in replacing electrolytic hard chrome with modern, clean alternatives. We shall illustrate the discussion with the results thus far of a program designed to evaluate various modern coating technologies as alternatives to hard chrome electroplate on military components. The primary uses of hard chrome in DoD are to hard-coat new components and to rebuild worn parts that come in a wide variety of shapes, sizes, and materials. Any chrome alternative must fit into the total life cycle of the part, which usually includes tear-down, inspection, and recoating several times during its service life.

We shall discuss the uses, capabilities, and performance of thermal spray, laser deposition methods, thin PVD coatings, and plasma nitriding for creating low-wear surfaces at the initial fabrication stage, and for building up worn parts in both military and commercial applications.

INVITED

<sup>†</sup>Supported by ARPA Grant #MDA972-93-1-0006.

2:40 pm **VM-ThA3 Development of a Manufacturing Process to Sputter AlN Barrier Layers on MO Recording Disks**, *David A. Glocker*, Eastman Kodak Company, Rochester, NY 14650-2022.

This paper describes the development of an in-line reactive sputtering process to deposit AlN films on polycarbonate disks as barrier layers for magneto-optical recording media. Manufacturing requirements were for an equivalent static deposition rate of at least 2 nm/s and a temperature rise of less than 40°C for the free-standing substrates. The 100 nm thick films had to have low absorption and an index of refraction close to 2.00, as well as be able to provide corrosion protection for the active TbFeCo layer. A dc rather than rf process was chosen in order to achieve the rates and low substrate temperatures needed. Factorial experiments were done to study the dependence of power, total pressure, and the Ar/N<sub>2</sub> partial pressure ratio on the deposition process and film properties. Differences in substrate heating were found that were related to the nature of the dc supply used. Methods of arc suppression were also studied. A dark-space shield that confined the plasma to the racetrack region significantly reduced the number of arcs. However, we concluded that any arcing was unacceptable because it would eventually lead to a loss of control. In order to eliminate arcs completely, we used a 40 kHz power supply driving two cathodes out of phase with one-another. Several methods of process control were compared. Two of them—either operating the target at constant power and using the target voltage to control the reactive gas flow or using an RGA to control the partial pressure of the reactive gas—produced adequate results as demonstrated by control charts of the thickness and optical properties. The effects of target wear on process drift were measured as well.

INVITED

3:20 pm **VM-ThA5 Simultaneous Deposition and Lamination Process in Vacuum**, *A. W. Freeland, J. R. Germundson, R. L. Swisher, K. Barnes and C. T. Wan*, Sheldahl Inc., Northfield, MN 55057.

Laminating a protective layer onto a freshly deposited film on a web in situ in a vacuum chamber is very useful in many applications where the deposited film must be protected from scratches or reacting with the atmosphere when it is removed from the vacuum chamber. There are materials that will oxidize in the atmosphere very quickly resulting in undesirable changes in the film's properties. When the laminated protective coverlay is used, the material can be protected until it is further processed or put in final use. The process combining the deposition and lamination in one pump-down involves the evaporation of highly reactive material such as bismuth onto a polycarbonate substrate on a roll-to-roll system. Immediately following the deposition, the coated substrate moves to a section of the vacuum chamber where a heat sealable coverlay film is bonded to the coated substrate and then rewound onto a take-up roll. A description of such a process and equipment will be presented. A comparison of the film properties with and without the in situ lamination will be presented.

3:40 pm **VM-ThA6 Anode Effects in Magnetron Sputtering**, *A. Belkind, F. Jansen, Z. Orban, and J. Vossen*, The BOC Group Technical Center, Murray Hill, NJ 07974.

The anode size and their spatial distribution affect the magnetron discharge characteristics and the deposition rate distribution. Reducing the anode size requires an increased voltage to maintain the same cathode current. Although the magnetron plasma is confined in the race track area, changing the position of small anodes redistributes the plasma density and changes the deposition rate distribution. Applying additional voltage between multiple small anodes allows one to vary the deposition rate distribution in a desired way. The potential



distribution in a magnetron plasma with small anodes and a floating power supply is discussed. Electron escape from the race track plasma of a rectangular planar magnetron in prevailing directions is shown.

**4:00 pm VM-ThA7 Recent Technology Advancements in Optical Thin Film Manufacturing**, *Paul M. LeFebvre, Bryant P. Hichwa, Robert W. Adair*, Optical Coating Laboratory Inc., Santa Rosa, California 95407.

The optical thin film industry faces numerous challenges in today's marketplace. Films must be optically clear and pass stringent specifications for spectral performance, environmental resistance, and durability including abrasion resistance.  $\text{SiO}_2$  is one of the few durable, low index of refraction materials, available for the design and manufacture of optical thin film interference coatings. In recent years, several critical technological advancements in the field of DC magnetron sputtering have led to reliable manufacturing systems for the high rate, arc free, sputter deposition of  $\text{SiO}_2$ . For high throughput, price sensitive products, cylindrical magnetrons, such as the Airco C-MAG<sup>®</sup>, and dual planar magnetrons, such as the Leybold TwinMag<sup>™</sup>, allow  $\text{SiO}_2$  to be reliably and cost effectively deposited in "in-line" sputter coaters. In addition, novel machine geometries, such as the OCLI MetaMode<sup>®</sup> system, have led to the production of complex, high layer count, interference coatings on glass and plastic substrates. Currently, pulse modulated DC magnetron sputter deposition has further improved the rate and quality of  $\text{SiO}_2$  films. In this paper, we compare these technology advances in  $\text{SiO}_2$  sputter deposition and

include examples of multilayer optical interference coatings such as anti reflection, enhanced high reflectance, hot mirror and narrow band pass coatings.

**4:40 pm VM-ThA9 Sputter Deposition of Indium Tin Oxide (ITO) from a Cylindrical Ceramic Target**, *Kevin P. Gibbons, Tami Van Skike and C. K. Carniglia*, Airco Coating Technology, 4020 Pike Lane, Concord, CA 94520.

ITO is usually sputtered from planar ceramic targets. The uptime of such planar targets is severely limited by the growth of "cones" in the racetrack area. In this paper we report on the sputter deposition of ITO from cylindrical rotating magnetrons. The use of rotary magnetron technology has significant process advantages. When a rotary ceramic target is used, the growth of target nodules or cones is significantly delayed. Using a 3 inch diameter by 15 inch long cylindrical target, ITO was sputtered for over 74 hours with no measurable decrease in rate or film conductivity. This result extrapolates to at least 6 days of running in a production size system before nodules or cones affect deposition rate. An ITO coating optimized for the CRT anti-static, antireflection market was developed. The effects of oxygen pressure, deposition temperature and deposition power on film properties are presented and discussed. Optical modelling was carried out using a three parameter fit to the refractive index in the visible spectral region. As expected, the films with the lowest resistivity and lowest visible absorption were produced at the highest deposition temperature.



## NANO 3/NANOMETER-SCALE SCIENCE AND TECHNOLOGY

Room BR4 - Session NS-ThP

### Nanoelectronics and Nanofabrication

**Moderator:** J. D. Dagata, National Institute of Standards and Technology.

**NS-ThP1 Voltage Controlled Nanometer Scale Oxidation of Si(100) Surface by STM, F. Pérez-Murano, G. Abadal, N. Barniol and X. Aymerich,** Dept. of Física Electrònica, Universitat Autònoma Barcelona, E-08913-Bellaterra, Spain.

In a previous paper we have presented a new technique to produce a local modification on Si(100) surface by STM in air (F. Pérez-Murano et al., J. Vac. Sci. Technol. B 11, 651 (1993)), consisting on locally oxidize the surface by controlling the electrical field between tip and sample. In order to improve the resolution of the technique and also to improve the velocity at which the modification can be produced, we have revised the technique. As it has been shown by other authors (E.S. Snow et al., Appl. Phys. Lett. 63, 749 (1993)), when the n-type silicon sample is polarized at positive bias, the surface becomes quickly oxidized, being possible to produce local modifications, but the surface quality is degraded. In this communication, we show how the modification can be better controlled if positive voltage pulses are applied to the sample while scanning. As the feedback condition is fixed by the negative voltage applied to the sample, both the tip and surface quality are preserved. Moreover, adjusting the value of the positive voltage and the time duration of the pulse, the resolution is improved and the modification can be performed at selected points of the sample. Finally, we will show that this technique can be used not only for n-type silicon samples but also for p-type silicon sample if the surface is kept under illumination.

**NS-ThP2 Local Electrical Switching Effects in CuTCNQ Films Studied by Surface Modification with STM, L. Wang, C. W. Yuan, J. W. Liang, H. Chen, and Y. Wei,** National Laboratory of Molecular Electronics, Southeast University, Nanjing 210018, People's Republic of China.

Local threshold electrical switching phenomena and reversing process of CuTCNQ films have been investigated by electronic beam etching and mechanical lithography with STM. A 5 nm thick highly polycrystalline organometallic semiconducting CuTCNQ film was grown directly on a copper plate by reacting neutral TCNQ in acetonitrile solution with the copper metal. When triggered by a 20 ms wide, 3 V electrical pulse 10 times in 5 minutes with STM tip, a convex of 10 nm diameter and 5 nm high appeared on the STM images. By continuously observation, we found, for the first time, this protuberance was spontaneously diminishing and disappeared at last in ca. 5 minutes. The STS analyses showed the protuberance was due to the conductivity increase at the triggered portion of the film. It is revealed that the local high-conductivity state on the CuTCNQ film can automatically restored to the low-conductivity state after electrical pulse was removed. Through the mechanical etching by STM, a concave of ca. 50 nm in diameter and 20 nm high was formed on the film and it could not be remedied. The hole is probably due to the local destruction in structure on the film surface rather than the change of conductivity.

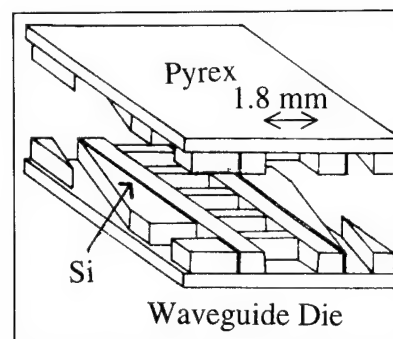
**NS-ThP3 Deep-Etch Silicon MM-Waveguide Structure for the Relativistic Acceleration of Electrons, T. L. Willke and A. D. Feinerman,** EECS Department (M/C 154), University of Illinois at Chicago, Chicago, IL 60607-4348.

A UHV compatible planar corrugated waveguide structure possessing bi-fold symmetry and a beam aperture has been simulated with MAFIA software, micromachined, and initially characterized. The waveguide was fabricated for use at 120 GHz ( $\lambda = 2.5$  mm) with  $2\pi/3$  phase advance operation [1]. In order to provide a semi-closed conducting surface to serve as the waveguide and free-space aperture, two opposed composite Si/Pyrex metallized substrates patterned with the waveguide's corrugated geometry (see figure) were vertically stacked with Pyrex fibers to an accuracy of  $\sim 1$   $\mu$ m. Feinerman et al. has shown that precision-drawn optical fibers can be anodically bonded to Si substrates to provide fixed orientation of two or more object planes [2].

The structures upper- and lower topographies consist of rectangular anisotropically etched Si muffin-tin patterns and are electrically conductive to a few skin depths. The most critical aspects are the muffin-tin dimensions and the upper-to-lower die orientation error. The alignment mechanism keeps the two periodic structures in phase spatially while maintaining a 600  $\mu$ m uniform gap (which determines the impedance and efficiency of the waveguide) to the accuracy that the corrugated geometry meets.

Eventually each two-surface waveguide section will be horizontally arrayed to form a structure 4.95 meters in length. Results of RF bead-pull testing a 70 GHz microfabricated waveguide section will be presented and compared with modeling data.

- [1] A. Nassiri et al., 1993 IEDM, Washington, D.C., Dec. 1993.
- [2] A. D. Feinerman et al., J. Vac. Sci. Tech. A4, 10 (1992).



**NS-ThP4 Measurement of the Piezoelectricity of Thin Films with STM, R. Winters, M. Reinermann, C. Enss, G. Weiss\*,** Institut für Angewandte Physik, Universität Heidelberg, Albert-Ueberle-Str. 3-5, 69120 Heidelberg, Germany, \*present address: Physikalisches Institut, Universität Karlsruhe Engesserstr. 7, 76131 Karlsruhe, Germany.

With its extraordinary vertical and lateral spatial resolution the scanning tunnelling microscope (STM) is preeminently apt for measurements of the piezoelectric constant of thin films, especially if high lateral resolution is required, e.g. for the imaging of domains. For STM measurements the surface of the piezoelectric film has to be metallized. A variation in thickness due to an electric field applied across the film causes a vertical displacement of the surface relative to the tunnelling tip: Therefore the piezoelectric effect can directly be monitored by the STM. With its vertical resolution of less than 1 Å even weak piezo-effects can be studied. Test measurements with X-cut quartz in air at room temperature show qualitatively correct behavior, but surprisingly the measured value of the piezoelectric constant varied both temporally and spatially. These fluctuations originate from the non-ideal characteristics of the tunnelling contact, the physical properties of which are not well understood hitherto. Our experiment clearly shows that this is a principal problem of STM-measurements under ambient conditions. To investigate piezoelectric films we circumvented this difficulty using a novel bridge technique, where the unknown piezoelectric is mounted on a X-cut quartz. We present measurements of polymer layers and sputtered ZnO-films that show the ability of measuring value and sign of piezo constants and the potential of imaging domains. As an additional benefit this technique allows the in-situ calibration of the z scale of the STM.

**NS-ThP5 Chemically Assisted Micromachining of Diamond with a Focused Ion Beam, G. M. Shedd, T. J. Stark, D. P. Griffis, and P. E. Russell,** Analytical Instrumentation Facility, North Carolina State University, Box 7916, Raleigh, NC 27695.

A focused ion beam (FIB) can sputter submicron features directly into a substrate, without the need for masks or lithography. However, the amount of material that can be removed in this way is limited. When an etch-enhancing gas is introduced at the surface being sputtered (e.g., Cl<sub>2</sub> at a GaAs surface<sup>1</sup>), the material removal rate can increase by an order of magnitude or more. An etch-enhancing gas speeds the removal process by increasing the formation of gaseous byproducts. The point of this work is to explore the utility of several candidate etch-enhancers for diamond, which is a technologically important material for precision edge tools, and, conceivably, for future

electronic materials applications. FIB sputtering in the presence of a halogen gas (commonly used to assist in the removal of Si) produced no significant increase in etch rate relative to that observed when no gas was present. However, preliminary results indicate a factor of 3–4 improvement in the etch rate of diamond when using H<sub>2</sub>O as the gaseous species. Given the positive results observed with H<sub>2</sub>O, other gases chosen for this investigation include the constituents of H<sub>2</sub>O, O<sub>2</sub> and H<sub>2</sub>. Oxygen ion beams have already been observed to etch diamond (100) at  $\approx 10$  times the rate of Ar ion beams,<sup>2</sup> so O<sub>2</sub> seems a likely candidate for a diamond etch-enhancer. Hydrogen is of interest as it may encourage the production of volatile hydrocarbon compounds as byproducts of FIB-induced reactions of H<sub>2</sub> gas with the diamond substrate.

1. Y. Ochiai, K. Gamo, and S. Namba, *J. Vac. Sci. Technol. B* 3, 67 (1985).

2. I. Miyamoto and S. Kiyohara, *Proc. of the 8th Annual Meeting of the American Society for Precision Engineering (Seattle, 1993)*, p. 301.

**NS-ThP6 Nanometer-Scale Definition of Conductors on Insulators Using the AFM**, M. Falvo, D. Glick and R. Superfine, University of North Carolina, Chapel Hill, NC 27599 USA.

While many studies have explored the modification of surfaces using an STM or AFM, few have focused on the modification of thin films with the intent of creating isolated metallic features on insulating substrates. We present our results on defining nanometer scale conducting regions and devices in gold films deposited on insulating substrates (mica, SiO<sub>2</sub>) using the AFM. Our results demonstrate the utility of the AFM for conveniently creating structures for research purposes that would otherwise involve the extensive processing and hardware requirements of e-beam lithography. These results also bear on the eventual use of the AFM as a nanometer scale machining tool. We have successfully created isolated wires 70 nm wide by 1  $\mu$ m by machining 15 nm evaporated gold films using Si cantilevers with nominal force constants of 30 N/m. These cantilevers allow nondestructive contact force and "tapping mode" imaging, while also providing the large forces (>100 nN) necessary for nanometer scale plastic deformation. We have defined holes, isolation trenches and cleared areas and determined their parameters as a function of applied force, tip velocity, machining technique, tip orientation and substrate compliance. We will present our progress in AFM/STM imaging of these structures and electrical measurements on the fabricated wires and tunnel junctions.

**NS-ThP7 Electrochemical Nanoscale Patterning of Surfaces with Electrically Conductive Polymers**, X. Y. Zheng, Y. Ding, C. Tong, L. A. Bottomley, J. Kowalik and L. M. Tolbert, School of Chemistry & Biochemistry, Georgia Institute of Technology, Atlanta, GA 30332-0400 USA.

The ultimate goal of our research is the nanometer-scale patterning of electrically conductive polymeric fibers on the surface of insulators, semiconductors and metals. Our approach involves the use of electrochemistry, scanning probe microscopy and chemical synthesis. We have synthesized a series of monomers which possess surface active substituents. We have shown that monolayer films of covalently attached monomers can be prepared and electrochemically polymerized *in situ*. We have demonstrated that the growth rate and direction of the polymer can be electrochemically controlled. Using this methodology, polymer-based patterns and the three-dimensional interconnection of conductive polymers has also been developed. The growth mechanism and properties of the corresponding electrically conductive polymeric features on various substrates has been elucidated.

**NS-ThP8 Local Fusion of Metallic Surfaces and Dots Formation Using STM**, L. Libioulle and J.-M. Gilles, Institute for Studies in Interface Sciences, Facult s Notre-Dame de la Paix, 61 rue de Bruxelles, B-5000 Namur, Belgium.

The formation of nanometer-scale structures is become an important application of the Scanning Tunneling Microscope. Recently, it has been shown that gold tips can be used to produce stable nano hillocks on gold (111) terraces. In our work we have studied the dot formation on gold and platinum surfaces using well-defined gold and platinum tips with known geometry. During the applied bias pulses, the tunnel current is also measured to deduce the contact resistance. This induced contact between the tip and the sample leads to the local fusion of the sample or the tip depending on the fusion temperature of used materials.

**NS-ThP9 Nanometer-Size Features Produced by Highly Charged Ions**, Daniel C. Parks,\* Martin P. St ckli,\* Robert W. Schmieder,† and Robert J. Bastasz,† \*Department of Physics, Kansas State University, Manhattan, KS 66506, †Sandia National Laboratories, Livermore, CA 94551-0969.

The interaction of highly charged ions with surfaces provides a way to study the behavior of surfaces exposed to ion generated high electric fields, ion neutralization processes, and material response to local charge depletion. We study the surfaces of insulating materials that were irradiated with 5–500 keV Xenon ions produced in an Electron Beam Ion Source. Surfaces are then imaged by Atomic Force Microscopy. We observe individual ion impact sites. These sites are typically conical protrusions with a diameter of 20 nm and a height of 0.3 nm. The changes in these features as a function of impinging ion kinetic energy, charge state, and potential energy are discussed. Target material sensitivities are also explored.

**NS-ThP10 The Self-Assembled Ordered Structures for Nanoelectronics: Stability and Local Modification**, A. V. Emelyanov, V. V. Protasenko, V. N. Ryabakon, Zelenograd Research Institute of Physical Problems, Moscow, 103460, Russia.

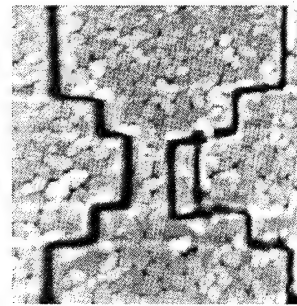
Solution stability and accuracy problems in manufacturing nanoelectronic elements (NE) has been proposed by the use of self-assembled ordered structures (SAOS), because they permit to form NE with atomic accuracy. The work on simulation of formation processes on molecular level local nonuniformity of atomic scale with application pointed probe has been carried out. It makes possible to extract from necessary characteristics received on base modified SAOS nanostructures and to put forward the definite requirements to SAOS parameters and influencing tool. Particularly, using the activation model of the processes of local modification on atomic scale for SAOS has been considered, their cells contain the adsorbed fragments, teared off with help of STM probe for account of polarization interaction. This model, for example, in case of consideration of storage medium of large density, permits to connect the reliability and definite quantity of reading cycles, storage time, resolution and so on with parameters of SAOS and influencing tool.

**NS-ThP11 Mechanical Nanofabrication Based on Scanning Force Methods**, S. Lukas, M. L hndorf, C. Hahn, U. D. Schwarz and R. Wiesendanger, University of Hamburg, D-20355 Hamburg, Germany.

Nanofabrication based on the mechanical interaction between a sharp tip and a substrate offers a reliable and well controllable method to obtain nanometer-scale devices. We have used a scanning force microscope (SFM) to pattern a variety of different thin film substrates, including polycarbonate films, high-T<sub>c</sub> superconducting and metallic thin films (see figure). This has been achieved by using a dynamic mode of SFM operation at high loading forces. To address the problem of connecting the nanoscopic to the macroscopic world, we have combined photolithographic techniques with SFM nanofabrication. This allowed to perform transport measurements at low temperatures on some of the nanofabricated devices.



High-T<sub>c</sub> superconducting thin film microbridge



Gold thin film

**NS-ThP12 New Design of STM-CVD Nanofabrication**, S. Rubel, X.-D. Wang, and A.L. de Lozanne, Department of Physics, University of Texas, Austin, TX 78712-1081, USA.

For the past few years we have made transport measurements of pure nickel wires made by decomposing nickel carbonyl with the electrons from an STM, which is a form of chemical vapor deposition (CVD). The need to align the tip with four micron-size contact pads resulted in a design incorporating a non-UHV SEM, and a concomitant

low throughput of samples. To improve throughput and reliability, we have finished a novel design that utilizes a high power optical microscope instead of an SEM. Two key features of this design are a custom window welded directly on the side of the chamber and a very compact x-y positioner. The 2-inch sapphire window, which protrudes into the vacuum chamber, makes it possible to have the tip as close as 6 mm from the atmosphere side. This gives an excellent view of the whole STM and allows us to use a 40x (or 20x) objective lens with 14 mm working distance (or 19 mm). The extra distance on the outside is useful to be able to have different viewing angles with the objective. This, together with the technique of Rapid Field Emission Imaging which we have demonstrated earlier (J. Vac. Sci. Technol. B, May/June 1994, to appear), will make it possible to locate any desired feature on the surface. The x-y positioner is built into a standard fine-screw tripod. It provides 200–300  $\mu\text{m}$  of orthogonal motion by tilting a 0.25-inch ball bearing that holds a 0.125-inch ball bearing in an off-center position. We will present results from both STMs.

**NS-ThP13 Submicron Pattern Transfer in HgCdTe and GaAs by Reactive-Ion Etching Through Nanochannel Glass Lithographic Masks,** C. R. Eddy, Jr. and R. J. Tonucci, Naval Research Laboratory, Washington, D.C. 20375.

A new technique has been developed for parallel patterning of submicron high definition features on HgCdTe and GaAs substrates. The technique utilizes reactive ion etching through nanochannel glass (NCG) array structures. Nanochannel glass materials contain a uniform array of submicron parallel channels or capillaries arranged in a 2-dimensional hexagonal closed packed configuration. Thin wafers of the glass are placed on the surface of the substrate forming the basis for a contact lithographic mask. A low pressure plasma of methane and hydrogen is used to reactive-ion etch HgCdTe substrates biased from 50 to 200 volts and held at room temperature. The addition of argon to this mixture is used to pattern GaAs. Both positive and negative feature replication of the NCG pattern has been demonstrated by this parallel processing technique. The relevance of channel glass aspect ratios to plasma processing parameters, especially pressure and ion energy anisotropy, on the definition of patterned structures will be discussed.

**NS-ThP14 The Technological Aspects of Cluster Film Application in Nanoelectronics with Use of ETM,** P. N. Luskovich, E. E. Gutman and I. A. Ryzhikov, "Delte" R&D Institute, Stchelkovekoje shosse. 2, 107122 Moscow, Russia, Karpov Institute of Physical Chemistry, 10 Obukha ul., Moscow 103464, Russia.

We describe the investigations on the reversible processes of stable potential-relief features by the way of the local electrical influence on the surface of the cluster conducting films with the help of STM. In particular we discuss the results of investigation of the films which have the property of selective sensor in respect of various gases ( $\text{CO}$ ,  $\text{N}$  and so on). The investigations are made on condition of the low pressure and the controlled medium. It's shown that the stable features of potential relief with character size of several nanometers are achieved. The variants of application of such technological method are offered.

**NS-ThP15 Nanoscale STM Patterning of Silicon Dioxide Thin Films by Catalyzed HF Vapor Etching,** J. Allgair, M. N. Kozicki, H. J. Song and T. K. Whidden, Center for Solid State Electronics Research, Arizona State University, Tempe, AZ 85287-6202.

Previously, we have reported on the addition and electron beam exposure of various forms of carbon on silicon dioxide surfaces. We observe localized rate enhancements in the HF vapor oxide etching process where such exposure has occurred and have shown this route (Carbon Enhanced Vapor Etching, CEVE) to be a viable alternative approach for fine pattern delineation in silicon dioxide. This work is a continuation of this study in which we examine carbon-containing coatings as a means of generating nanoscale features on silicon dioxide using a scanning tunneling microscope (STM) as an electron beam source. A Digital Instruments Nanoscope III was used to expose oxide films of ca. 5 nm thickness (insulator coatings > 10 nm inhibit tunneling), with tip voltages and currents varied between 4 to 10 V and 0.1 to 1 nA respectively and ambient hydrocarbons used as the carbon source. Careful selection of voltage and current settings allowed the controllable production of oxide trenches of widths 10 to 75 nm following HF vapor etching. Evidence eliminating STM oxidation of the underlying silicon as the trench forming mechanism will be presented. Additional work on the use of controlled ambients as a means of further reducing trench width and possible reaction pathways for the rate catalysis will be discussed.

**NS-ThP16 Ambient Dependence of Nanometer Scale Writing on Silicon (100) Surfaces by an Atomic Force Microscope,\*** L. Tsau, Dawen Wang, and K. L. Wang, Department of Electrical Engineering, University of California at Los Angeles, Los Angeles, CA 90024-1594 USA.

Nanometer scale writing has been performed on Si(100) surfaces by using an atomic force microscope. The writing work was firstly demonstrated in a regular atmospheric environment. By biasing a p-type heavily doped silicon AFM tip negatively above  $\sim 3$  V, patterns as small as  $\sim 10$  nm could be generated. There were evidences showing that local oxidation takes place within a few atomic layers below the silicon surface during the AFM writing process. It was also found that no pattern could be generated for positive bias voltages up to 10 V. In order to investigate the mechanism of the tip-surface reaction during writing, similar work was performed in a controlled ambient environment in a plexiglass dry box. Firstly, it was found that, in a dry nitrogen or dry oxygen environment, it was difficult to generate patterns for bias voltages up to  $-10$  V. Further, the writing efficiency for each bias voltage (ranging from  $-3$  V to  $-10$  V) was examined by introducing water vapor into the box at various flow rates. The experimental results indicate that the moisture content plays an important role in the tip-surface reaction. A strong dependence of the writing speed upon the humidity was observed.

\*This work was in part supported by JSEP and AFOSR.

**NS-ThP17 The Formation of Nanometer-Scale Molecular Memory by STM,** K. Matsushige and S. Taki,\* Dept. of Electronics, Fac. of Eng., Kyoto Univ., Kyoto 606-01 Japan, and \*Dept of Appl. Sci., Fac. of Eng., Kyushu Univ., Fukuoka 812, Japan.

A scanning tunneling microscope (STM) was utilized to form a nanometer-scale molecular memory. First, n-alkane molecules ( $\text{n-C}_{33}\text{H}_{68}$ ) were adsorbed on a highly oriented pyrolytic graphite (HOPG), and then electric pulses with various pulse heights and duration times were applied through the STM tip to the molecular layers. After many trials, it was first revealed that some pulses, for example 2.0 V in height and 0.3  $\mu\text{s}$  in duration, can cause the morphological changes of nanometer sizes to the organic layer, as depicted schematically in the figure. The diameter of the column created by such the electric treatment was very small in the range of a half nanometer. Since this kind of molecular column may be utilized to get on/off or 1/0 signals, a present result proves the possibility for the creation of a novel and an extremely high density molecular memory with about  $10^{14}$  bits/ $\text{cm}^2$ , which is about  $10^6$  times higher than a conventional CD.

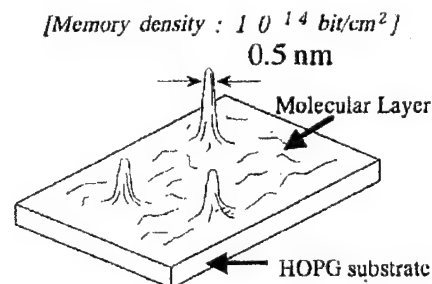


Fig. Schematic illustration for the nm-scale memory unit formed by applying electric pulses to a molecular layer using a STM tip.

**NS-ThP18 Using of Scanning Tunnelling Microscopy for Control and Revision of Strong Rifle Surfaces of Plane Carbon Field Emitters Modified by Ion Beams,** A. L. Suvorov, V. V. Protasenko, V. G. Stolyarova, E. P. Sheshin, Institute of Theoretical and Experimental Physics, B. Cheremushkinskaya 25, Moscow, Russia.

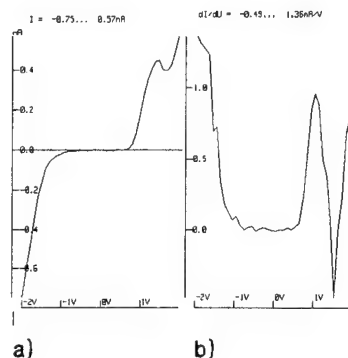
Here is offered and realized method of preparing plane carbon field emission cathodes with  $10^5$  [ $\text{cm} \cdot \text{cm}$ ] density of emission centres. At first stage this method include modification of initial plane surface of monolithic carbon half-finished products. In this work,  $\text{La}^+$ ,  $\text{Ar}^+$  tested, found and optimized energy of ions ( $E_n = 35$  keV), at an angle of 45 deg, irradiation intensity is  $5 \cdot 10^{14}$  [ions/( $\text{cm} \cdot \text{cm} \cdot \text{s}$ )] and a flux is about from  $10^{17}$  to  $10^{18}$  [ions/( $\text{cm} \cdot \text{cm}$ )].

The quality control of obtained field cathodes surfaces is carried out with using of air STM (original construction). This instrument (air STM) used for the final precision processing of surface formed by ion beams. Volt-Amper and other emission characteristics of prepared field cathodes is carried out.

Using of this method is useful for realizing of such basic goal of vacuum microelectronics as creation of plano display screens and effective light sources (on the base of field electron emission of carbon materials).

**NS-ThP19 Negative-Differential Conductivity Observed on a Germanium Layer on Si(001),** H.-J. Müssig, D. Krüger, S. Hinrich, Institut für Halbleiterphysik, Walter-Korsing-Str. 2, D-15230 Frankfurt (O), Germany, and P. O. Hansson, Max-Planck-Institut für Festkörperforschung, Heisenbergstr. 1, D-70569 Stuttgart, Germany.

During the last years there has been a great interest in  $\text{Si}_{1-x}\text{Ge}_x/\text{Si}$  layered heterostructures, considering both basic material issues and applications in high performance devices. The morphology and the surface electronic structure of heteroepitaxial germanium layers grown pseudo-morphically by solution epitaxy on Si(001) has been investigated by scanning tunneling microscopy (STM) and -spectroscopy (STS). The Ge layer thickness has been estimated to be 4 to 5 monolayers by Auger electron spectroscopy. This thickness is near the critical thickness of strain relaxation by coherent island nucleation. By means of STS the tunneling current is measured as a function of sample voltage at a constant distance between tip and the sample on certain surface atom positions. A significant decrease of tunneling current at a sample voltage of 1.5 V is observed in areas of 0.5 nm diameter between dimer rows. This decrease is due to a negative-differential conductivity at a tunnel diode configuration consisting of a surface defect structure of the germanium layer and the STM tungsten tip. A negative-differential conductivity is a characteristic of quantum-well type structures. The same effect is utilized in the Esaki tunnel diode which is widely used in high-speed electronics applications.



**NS-ThP21 Manipulation of Nanometer Scale Structures in Langmuir-Blodgett Film Using Atomic Force Microscopy,** J. Garnæs,<sup>1</sup> N. B. Larsen,<sup>2</sup> T. Bjørnholm,<sup>2</sup> <sup>1</sup>Danish Institute of Fundamental Metrology, Build. 307, Lundtoftevej 100, DK-2800, Lyngby, Denmark, <sup>2</sup>Centre for Interdisciplinary Studies of Molecular Interactions, Chemistry Department, University of Copenhagen, Fruebjergvej 3, DK-2100 Copenhagen, Denmark.

By increasing the force when scanning with an atomic force microscope (AFM), it is possible to scratch holes in a Langmuir-Blodgett (LB) monolayer of behenic acid, and "write" lines with a width of 50 to 90 nm. A molecular electron acceptor<sup>1</sup> and a molecular donor have been synthesized and investigated as monolayers by synchrotron x-ray diffraction and as multilayer LB-films by AFM. The number of defects and the degree of order show that these functionalized molecules may be suitable for application relying on the potential defect-free periodic structure of LB-films. In this talk it is shown that nanometer scale structures of 100 nm to 500 nm, and stable over at least 24 hours, can be written on these functionalized molecules. Progress on forming more narrow lines and defect free areas suitable for electrical contact, using very sharp tips, will be reported. The prospect of this technique to form proto type functionalized electronic devices using alternating layer of molecular electron donors and acceptors will be discussed.

<sup>1</sup>J. Garnæs, N. R. Larsen, T. Bjørnholm et al. Science (in press).

**NS-ThP22 Experimental Design for Determining the Duration of Quantum Tunneling with Laser-Illuminated Field Emission,** M. J. Hagmann, Florida International University, Miami, FL 33199 USA.

Previous experiments with heterostructures and Josephson junctions suggest that tunneling has a specific duration. However, the many procedures used to calculate tunneling times do not agree and there

has been no definitive measurement. We have used two different methods to simulate laser-illuminated field emission with the Fowler-Nordheim model for the static potential and the distribution of energies in a free-electron metal. Our calculations suggest that the laser-induced increase in the emitted current is greatest for illumination at long wavelengths (period  $\gg$  traversal time) but decreases to zero at shorter wavelengths. Thus, it appears possible to determine the duration of quantum tunneling by measuring the emitted current with several different lasers from 1 to 10  $\mu\text{m}$ . We will make laser/FEM measurements rather than laser/STM in order to 1) increase the interaction of tunneling electrons with optical fields by increasing the barrier length, 2) facilitate illuminating the tip, 3) avoid photovoltaic and thermal effects in the sample, and 4) avoid errors due to drift in the tip-sample separation. It is necessary to use relatively large values of power flux density ( $\sim 10^{10}\text{W/m}^2$ ) so other phenomena due to heating are significant. We will chop or switch the laser and make synchronous measurements in order to distinguish the modeled effects ( $\tau_{\text{rise}} < \text{ps}$ ) from thermal phenomena ( $\tau_{\text{rise}} \approx 1 \text{ ms}$ ). The value of the applied static field must be optimized because the laser-induced effects vary inversely with the strength of the static field, but the current must not be too small due to limitations from noise with the bandwidth required for pulsed measurements.

This work is supported by NSF grant ECS-9303397.

**NS-ThP23 Cross-Sectional Characterization of Thin Film Transistors with Transmission Electron Microscopy,** S. Tsuji, M. Tanaka, H. Iwama, N. Tsutsui, K. Kuroda, and H. Saka, Yamato Laboratory, IBM Japan, Ltd., Shimotsuruma, Yamato-shi, Kanagawa-ken 242, Japan.

Hydrogenated amorphous silicon thin film transistors (a-Si:H TFTs) are now widely used as elements for active matrix liquid crystal displays (AMLCDs). It is important to recognize the mechanisms by which TFTs can fail in service and also to consider how defects can be introduced during fabrication of the TFTs. TFTs can consist of more than ten layers of different materials and it is necessary to obtain discrete layer structure through all these layers. This paper describes how an array can be characterized electrically by using a TFT array tester<sup>1</sup> that can detect, accurately locate, and identify pixel faults. A transmission electron microscope (TEM) is used to investigate the discrete layer construction of a faulty TFT. Cross-sectional results for various faulty TFTs were obtained. The observed contamination composed of silicon oxide had a thickness of 10–30 nm. This led to identification of the fault and analysis of its cause, which in turn led to a marked yield improvement. The observed electron irradiation damage for a-Si layer is also discussed.

<sup>1</sup>S. Kimura, Y. Ichioka, K. Suzuki, and R. Polastre, SID 92 Digest, 33.4, 628 (1992).

**NS-ThP24 Single Crystal Epitaxial Ge Based Ohmic Contacts to III-V Nanoelectronic and Mesoscopic Devices,** M. Dubey, K. A. Jones, L. M. Casas, Army Research Lab, EPSC, Fort Monmouth, NJ 07703.

The single crystal epitaxial layer ohmic contacts are very promising in the fabrication of shallow junction nanoelectronic and mesoscopic devices based on III-V compounds. Several metals and semiconductor epitaxial layers (e.g. Au, Ge or Pd, Ge) are deposited at a temperature range of 300–450°C on GaAs or InGaP using an Ultra High Vacuum ( $10^{-9}$ – $10^{-10}$  Torr) Electron Beam (UHV E-Beam) deposition system. The interface between the metal and semiconductor is almost atomically abrupt, smooth and oxide free, and there is a minimum of disruption of the underlying layers. The in-situ cleaning of the III-V substrate at a temperature range of 500–650°C is achieved without any As or P over pressure which is a very common practice in a molecular beam epitaxial (MBE) deposition system. A detailed analysis of interface quality, crystal structure and defect propagation in GaAs/Ge/Au, GaAs/Ge/Pd, InGaP/Ge structures are presented. High resolution Transmission Electron Microscope (HRTEM), Double Crystal X-ray Diffraction (DXRD), and Auger Electron Spectroscopy (AES) are used to characterize the materials.

**NS-ThP25 Nanoscale Lithography and Pattern Transfer on Si(100) with a UHV Scanning Tunneling Microscope,** G. C. Abeln, T.-C. Shen, C. Wang, J. R. Tucker, and J. W. Lyding, Department of Electrical and Computer Engineering and Beckman Institute, University of Illinois, Urbana.

We demonstrate nanoscale patterning of the hydrogen passivated Si(100) surface using a UHV STM, with linewidths as low as 1 nm



being achieved. H atoms saturating the Si dangling bonds are desorbed by low energy electrons from the tunneling probe—it is shown that depassivation occurs when the classical electron energy exceeds the Si-H bond energy (3.5–3.8 eV). Oxidation of the patterned areas is also demonstrated. The effect of  $\text{NH}_3$  exposure on the oxidation of the patterned areas will also be discussed.

<sup>†</sup>Supported by the ONR URI under contract N00014-92-J-1519.

## ELECTRONIC MATERIALS Room BR4 – Session EM-ThP

### Aspects of Electronic Materials and Processing II Moderator: A. Rockett, University of Illinois, Urbana.

**EM-ThP1 Study of Damage Cause by W Etchback and Effect of Subsequent AlCu Deposition, L. R. Allen and J. M. Grant, Sharp Microelectronics Technology, Inc., Camas, WA 98607.**

The use of W plugs for interconnect has become a widely used technology. There are several different process flows which can be used to achieve W plugs coupled with Al interconnect. To reduce the number of processing steps the TiN adhesion layer for the CVD W can be left intact after W etch for use as the barrier layer for the Al. Previous workers have found that this process scheme can affect the EM lifetime of the interconnect.<sup>1</sup> They determined that the crystal structure of the Al was affected by damage to the underlying TiN layer during etch. We extended that work by looking at the damage systematically and quantitatively as a function of the process parameters and at the effect the extent of the damage has the subsequent AlCu sputter deposition.

The surface roughness due to etch damage of the TiN adhesion layer was studied using AFM. This roughness was compared to the structures of the as-deposited TiN and W films. We find that the roughness of the TiN film is influenced by the etch process and is not due only to the transfer of the W roughness into the TiN film during etchback.

The roughness of the AlCu film was also studied by AFM. We determined that there were significant differences in the roughness and grain size of the AlCu film as a result of the structure of the TiN film. These differences are discussed in light of the roughness of the TiN film and related to the etchback process parameters.

<sup>1</sup>“Improving EM Lifetime of AlCu/TiN Lines and W-Plug Metal System by Controlling Crystal Structure of AlCu,” H. Horikoshi, et al, VMIC June 1993.

**EM-ThP2 Low-Resistivity Ohmic Contacts to Moderately Doped n-GaAs with Low Temperature Processing, Michael L. Lovejoy, Arnold J. Howard, Peter A. Barnes,<sup>1</sup> Dennis J. Rieger, Kevin R. Zavadil, Randy J. Shul and John C. Zolper, Sandia National Laboratories, Albuquerque, NM 87185, <sup>1</sup>Auburn University, Department of Physics, Auburn, AL.**

Low temperature ohmic contact processing is required for a variety of novel material systems such as II-VI materials that are grown at temperatures as low as 300°C which limits processing temperatures. In addition, for some photonic device applications where free carrier absorption degrades device performance, low-to-moderately doped substrates are desirable. PdGe contacts which are formed by solid phase epitaxy have shown excellent specific contact resistance on n<sup>+</sup>-GaAs; most work on this metallization scheme has focused on improving thermal properties to make the contact suitable for subsequent high-temperature processing. In this paper we report a complementary study of PdGe ohmic contacts to moderately-doped n-GaAs with the lowest possible anneal temperature and time.

The mechanism believed to be responsible for the excellent ohmic property is doping of the GaAs surface by Ge that diffuses through the Pd. During the Ge-diffusion PdGe is formed and the film is highly non-uniform and resistivity is high. Variation in composition is characterized by Auger and XPS. Surface morphology is mapped out with AFM and is compared to common Au/Ge alloyed contacts which suffer from non-uniformity and surface roughness which makes interconnect metallization difficult. The Cox and Strack method is used to measure the contact resistivity. For 30 minute anneals, a minimum specific contact resistance of  $\sim 2 \mu\Omega\text{-cm}^2$  is obtained at 250°C which

is 75°C lower than previous investigations considered at this doping level. To investigate the implication of incomplete PdGe formation on electrical properties, we measured and report the average sheet resistance of the PdGe contact metal as a function of anneal temperatures from 200–400°C. The degree of PdGe formation determined by spectroscopy is correlated to the sheet resistance properties.

**EM-ThP3 Excimer Laser Induced Deposition of Tungsten on GaAs from  $\text{WF}_6$  and  $\text{SiH}_4$ , Maleck Tabbal, Michel Meunier, Ricardo Izquierdo and Arthur Yelon, Groupe des Couches Minces and Département de Génie Physique, École Polytechnique de Montréal, Québec, Canada, H3C 3A7.**

The excimer laser direct projection patterning of W Schottky contacts on GaAs to form, in one step, self-aligned gates for MESFETs could prove to be an advantageous process compared to the conventional sputtering, patterning and etching process now used in the industry. We present recent results on large area excimer laser induced deposition of tungsten using  $\text{WF}_6$ . Silane gas is used as the reductant, permitting the deposition of W at a temperature as low as 200°C and thus limiting the thermal budget on the fragile GaAs substrates. Typical operating pressures were  $\sim 14$  torr for a mixture of  $\text{WF}_6$ ,  $\text{SiH}_4$ ,  $\text{H}_2$  and Ar, having flow rates of 1, 3, 50 and 140 sccm, respectively. Using a KrF excimer laser (248 nm) at 25 mJ/cm<sup>2</sup>, metallic W films, as determined by XPS, are deposited with an average growth rate of 1 Å/pulse. The tungsten layers have an island structure, as evidenced by SEM. Auger Electron Spectroscopy profiling shows that no impurities (such as F, C and O) are detected above the noise level ( $\sim 1$  at%). The absence of Si suggests that the  $\text{SiH}_4$  reduction is complete. X-ray diffraction spectra show that the pure and stable  $\alpha$ -W is deposited and that very little  $\beta$ -W is present. Resistivities are 20  $\mu\Omega\text{-cm}$ , in agreement with the observed predominance of  $\alpha$ -W. Possible deposition mechanisms are discussed in terms of gas phase chemistry and surface reactions.

**EM-ThP4 The Effect of Chemical Etchants on Back Contact Formation to CdTe-Based Solar Cells, Xiaonan Li, Dave Niles, Falah Hasoon, and Peter Sheldon, National Renewable Energy Laboratory, 1617 Cole Boulevard, Golden, CO 80401.**

CdTe is an important material for a variety of thin film electro-optical applications. For example, CdS/CdTe photovoltaic devices have reached conversion efficiencies of up to 15.8%. Forming a low resistance ohmic contact to CdTe thin films is critical to the success of this technology. Pre-surface treatments are used to modify the surface chemistry to facilitate ohmic contact formation. In this study, CdTe thin films, deposited by close spaced sublimation (CSS), are characterized using cathodoluminescence (CL), and light and dark I-V measurements both before and after chemically etching in a  $\text{H}_3\text{PO}_4\text{:HNO}_3\text{:H}_2\text{O}$  solution. CL measurements of CdTe films etched for 1 minute had a  $\sim 2 \mu\text{m}$  thick low emission layer. This low emission layer was found to result from conversion of the near surface region from stoichiometric CdTe to a Te-rich layer. The Te-rich layer is thought to improve the series resistance, however, light and dark I-V measurements show that the conductive Te-rich layer introduces shunt paths into the CdS/CdTe device. These shunt paths are found to significantly degrade device performance. We demonstrate that shunting can be reduced by varying the surface treatment. Finally, devices etched in bromine methanol, prior to contact application, are made for comparison.

**EM-ThP5 STM Observations of Sub-Surface Donor and Acceptors in GaAs, Jun-Fei Zheng, D. Frank Ogletree, Eicke Weber and Miquel Salmeron, Materials Sciences Division, Lawrence Berkeley Laboratory, and Materials Science Department, University of California, Berkeley, California 94720.**

The scanning electron microscope has been widely used to study the structure and electronic properties of semiconductor surfaces. Recently we have used this technique to investigate the *bulk* electronic properties of point defects in GaAs. When cleaved, GaAs(110) shows minimal reconstruction and no new states are created in the gap. As a result perturbations in the STM tunneling current due to *sub-surface* features can be observed. We have investigated Si doped n-type and Zn doped p-type GaAs. Sub-surface donor and acceptor sites can be identified in the top six layers of the crystal. Unlike dopant atoms at the surface, which induce localized states in the gap, the sub-surface dopant atoms appear in the STM images as delocalized protrusions a few nm wide superimposed on the normal atomic lattice of the surface. Both donors and acceptors produce positive protrusions in filled and empty state images, circular for Si and Zn in filled state images and triangular for Zn in empty state images. The protrusions decrease in height as the



STM bias voltage moves away from the band edge and for dopants further below the surface. Imaging mechanisms, and evidence for sub-surface vacancies will be discussed.

**EM-ThP6 Microscopic-Scale Lateral Inhomogeneities of Heterostructure Energy Barriers, F. Gozzo, H. Berger, I. R. Collins, and G. Margaritondo,** Ecole Polytechnique Fédérale de Lausanne, CH-1015 Lausanne, Switzerland, W. Ng, A. K. Ray-Chaudhuri, S. Singh, and F. Cerrina, Center for X-Ray Lithography, University of Wisconsin-Madison, USA.

Most measurement techniques of Schottky barrier heights and heterojunction band discontinuities are based on an inherent assumption of homogeneity. The recent development of new microscopic-scale experimental techniques enabled us to reveal strong lateral variation of these interface parameters.

In particular, our scanning photoemission spectromicroscopy data revealed substantial inhomogeneities in the band lineup of the interface between the two semi-conductors GaSe and Ge. These inhomogeneities lead to valence band discontinuity changes from place to place, whose magnitude is at least of 0.4 eV.

**EM-ThP7 Interface Electronic Structure in the Ceramic-ZnO/Bi System: Evidence for the Varistor Effect, K. O. Magnusson,** Dept. of Natural Science, University of Karlstad, and ABB HV Switchgear AB, Sweden, S. Wiklund, Dept. of Synchrotron Radiation Research, University of Lund, Sweden.

The evolution of the interface between Bi and polycrystalline, ceramic ZnO has been studied *in situ* with photoelectron spectroscopy (PES) under ultra-high-vacuum conditions. This system is a model varistor (variable resistor) compound. Evaporation of Bi on highly n-doped (Al) sintered ZnO bodies, fractured *in situ* and held at room-temperature, results in a considerable upward bandbending. After evaporation of 10 Å of Bi (3 monolayers), a Bi-induced bandbending of 0.43 eV, can be observed from the energy-shift of the Bi 5d emission in PES. Valenceband and bandgap studies using ultraviolet PES, directly reveals the states responsible for the observed bandbending: Bi induces states in the ZnO bandgap at 0.9 eV above the valenceband maximum. The filling of this high density of bandgap states yields a pinning of the surface Fermi-level which makes the bandbending proportional to the Bi coverage, with a rapid increase during the formation of the first monolayer and a markedly slower thereafter. These results clearly show the importance of Bi in the formation of the varistor Schottky barriers.

**EM-ThP8 Internal Photoemission of Adjustable Band-offset Heterojunctions, G. Mensing, R. Albridge, A. Barnes, J. McKinley, N. Tolk,** Dept. of Physics and Astronomy, Vanderbilt University, J. Davidson, T. Stultz, Dept. of Electrical Engineering, Vanderbilt University, B. McCombe, A. Petrou, Dept. of Physics and Astronomy, State University of New York, Buffalo.

We report internal photoemission measurements of the low temperature band-offset of diluted magnetic semiconductor (DMS) heterojunctions as a function of magnetic field (0-2 Tesla). Two photon sources were used covering the wavelength range from 4 nm to 10 μm: the Vanderbilt University Free Electron Laser which produces intense 2-10 μm infrared and a monochromatized quartz halogen lamp covering the visible to 3 μm range. The optical nature of the measurements allows us to determine the photoconductivity threshold associated with the band-offset to an accuracy of better than 5 meV. Tunnel effects have been corrected by varying the bias voltage. The light was brought to the interface at grazing incidence so that both s and p polarizations could be used to determine the k-space dependence of the band-offset. Other interfaces to be discussed include diamond Schottky barriers and GaAs homojunctions with Si δ-layers.

**EM-ThP9 Interface Exciton Luminescence: Indication of Interface Inhomogeneities in Single GaAs/GaAlAs Heterostructures, V. N. Bes-solov, V. V. Evstropov, M. V. Lebedev, V. V. Rossin, A. F. Ioffe** Physics-Technical Institute, St. Petersburg, 194021, Russia.

A specific luminescence band originating from heterointerface (H-band) has been observed in the photoluminescence spectrum (at 4.2 K) of a single GaAs/GaAlAs heterostructure. Threshold effect of interface formation conditions (epitaxial temperature and growth rate) on interface luminescence has been found. The H-band is observed if growth temperatures are above some critical value and is absent if those temperatures are below. The threshold emergence of the H-band is interpreted as consequence of the GaAs surface roughening transition observed earlier only for homoepitaxial growth. Inhomogeneities on interface critically depend on growth temperature, drastically de-

creasing above critical temperature. The model has been proposed which attributes interface luminescence to annihilation of interface exciton which is composed from 2D-electron (2D-hole) in the notch at the interface and 3D-hole (3D-electron) in GaAs bulk region near interface. In the case of large inhomogeneities the interface potential fluctuations prevent formation of such exciton and corresponding H-band is not observed in spectrum. Thus, interface exciton luminescence can be used for characterization of the interface inhomogeneity.

**EM-ThP10 The Nature of Ambient (100) GaAs Surfaces, O. J. Glembocki, J. A. Tushman, K. K. Ko,\* S. W. Pang,\* J. A. Dagata,\*\* R. Kaplan and C. E. Stutz,\*\*** U.S. Naval Research Laboratory, Washington, DC 20375, USA.

Photoreflectance (PR) spectroscopy has been used to study the Fermi-level pinning position of chemically modified (100) GaAs surfaces. The stoichiometry of the GaAs/oxide interface was obtained by Auger electron spectroscopy and time of flight SIMS. PR shows that there are two pinning positions for the unmodified (100) GaAs surface. For n-GaAs, the Fermi level pins near midgap, while for p-GaAs the Fermi level pins near the valence band. An Ar/Cl<sub>2</sub> plasma generated by an electron-cyclotron resonance (ECR) source and a P<sub>2</sub>S<sub>5</sub> chemical passivation treatment were used to change the stoichiometry of the surface. ECR etching resulted in an As rich GaAs/oxide interface, while P<sub>2</sub>S<sub>5</sub> passivation produced a thin Ga rich oxide. The Fermi-level pinning position for the As rich oxide is shown to be near midgap while for the Ga rich oxide it is near the valence band. These results allow us to relate the Fermi-level pinning position to the stoichiometry of the GaAs/oxide interface and to test various models for the Fermi-level pinning position of ambient (100) GaAs surfaces.

\* The University of Michigan, EE Dept., Ann Arbor, MI 48109.

\*\* National Institute of Standards and Technology, Gaithersburg, MD 20899.

\*\*\* Wright Patterson Laboratories, Dayton, OH 45433.

**EM-ThP11 Surface Studies of MBE Grown GaAs(111)A by HREELS, XPS, UPS and LEED, J. Wu and G. J. Lapeyre,** Physics Department, Montana State University, Bozeman, MT 59715.

P-type GaAs(111)A (2×2), grown by molecular-beam-epitaxy (MBE) method, has been studied by high-resolution electron energy-loss spectroscopy (HREELS), X-ray and ultra-violet photoelectron spectroscopy (XPS and UPS), and low-energy electron diffraction (LEED). During atomic hydrogen exposure, XPS spectra of Ga 3d (~126.5eV) and As 3d (~106.5eV) revealed no significant changes of surface stoichiometry, and the band bending ranges from 0.4eV to 0.6eV from the UPS data. At 300L hydrogen exposure, (1×1) LEED pattern with very high background develops due to the surface disorder. The HREELS results from the clean surface shows the Fuchs-Keller surface optical phonon energy (~35meV) with large a broad background, which is caused by small hole mobility and the dependence on the incident electron energy. With increasing hydrogen exposure, characteristic changes in the intensities of surface optical phonon and the hole plasmon excitation, features strong Ga-H stretching mode (~233meV) is observed. At 2000L hydrogen exposure, double surface optical phonon show up. Those are interpreted by the changes in the space charge regime and GaAs(111)A vacancy buckling model.

Research supported by NSF.

**EM-ThP12 Geometric and Electronic Structure of Ni Silicide on Si(100), Y.-H. Khang, D. Jeon\* and Young Kuk,** Department of Physics, Seoul National University, Seoul 151-742, Korea, \*Department of Physics, Myong-ji University, Kyunggi-do 449-728, Korea.

It is now understood that NiSi<sub>2</sub>/Si(111) is a model system in which the Schottky barrier heights are determined by the atomic structure of the interfaces. In NiSi<sub>2</sub>/Si(100) system, it was reported that the measured Schottky barrier heights varies with samples having different dopant concentrations, annealing times and temperatures.

We have studied this system by scanning tunneling microscope/spectroscopy and tunneling electron interferometry. Besides the previously reported the (1×1)-NiSi<sub>2</sub> phase in TEM and STM studies, phases such as the (2×1)-NiSi<sub>2</sub>, (√2×√2)-R45° and (111) facet growth have been observed under various growing conditions. We propose a model for the (1×1) phase structure, in which the inverse-pyramidal patch structure with stacking fault is considered. The lower interface energy along the <111> direction causes the pyramidal shape, resulting in uniformly spaced antiphase boundaries. The observed multiple phases are due to several local minima in the interfacial phase diagram

as suggested by a theoretical calculation. By measuring the differential conductivity in a Fowler-Nordheim regime, the structure of Ni/Si interface was imaged together with the surface topography. The observed interfacial structure will be compared with the results by BEEM.

**EM-ThP13 Electronic Band Structure of Epitaxial  $\gamma$ -FeSi<sub>2</sub>(111)2×2,** J. Alvarez, C. Limones, E. G. Michel, R. Miranda, M. E. Davila, and J. Martin-Gago, Univ. Autonoma de Madrid, Spain.

Epitaxial iron silicides have been actively investigated in recent years due to their possible applications and their interesting phenomenology. Out of the many existing phases,  $\beta$ -FeSi<sub>2</sub> is the only bulk stable, semiconducting phase. It presents an orthorhombic structure. When epitaxially grown on Si(111), a metastable phase (called  $\gamma$ -FeSi<sub>2</sub>) can be obtained under suitable conditions.  $\gamma$ -FeSi<sub>2</sub> crystallizes in the fluorite structure, and is metallic. It has been proposed that it might be spin polarized. On the other hand, a 2×2 surface reconstruction is observed when this phase is grown on Si(111). Two important issues remained to be clarified concerning the electronic structure of  $\gamma$ -FeSi<sub>2</sub>: nature of the states giving rise to the Fermi edge; nature of the electronic states associated to the 2×2 reconstruction (which depends on its detailed geometric structure). We have answered both questions by performing a detailed angle-resolved photoemission-spectroscopy study. We have mapped the band structure of  $\gamma$ -FeSi<sub>2</sub> along the  $\Gamma$ L direction, and the dispersion of the surface states along the high-symmetry directions of the surface unit cell. The symmetry of the states was determined by taking polarization-sensitive measurements. The results were compared to existing theoretical calculations. We have measured the dispersion of bulk states, in particular for the band crossing the Fermi level, whose shape significantly differs from theoretical predictions. The dispersion of the observed surface states supports an adatom-based model for the 2×2 reconstruction.

**EM-ThP14 Sensor for Measuring the Atomic Fraction in Highly Dissociated Hydrogen,\*** W. L. Gardner, Oak Ridge National Laboratory, Oak Ridge, TN 37831-8071.

Atomic hydrogen is a very important constituent for processes ranging from amorphous silicon and diamond deposition to the cleaning of silicon wafers. Because measurement of the actual atomic species fraction in highly dissociated hydrogen is very challenging, a specially designed catalytic sensor was developed. The sensor is simple and inexpensive to fabricate. It also inhibits thermal runaway, which occurs when atomic species density is high enough to impart enough recombination energy to a non-catalytic surface to substantially raise its temperature. While recombination coefficients for such surfaces are very low near room temperature, they increase nearly exponentially with temperature unless actively cooled. The sensor comprises a cooled quartz diffusion tube that is open at one end to sample the highly dissociated gas. The other end is terminated by a catalytic surface of nickel. This surface is actually one end of a nickel rod that is thermally anchored at its other end. Temperature is measured at two points along the rod to determine power deposited by recombining hydrogen on the rod tip. This is employed with the known recombination coefficient of nickel to determine atomic species fraction. With the use of a straightforward calibration scheme to determine the nonlinear variation in species fraction along the tube, the atomic species fraction at the tube opening is then determined. For example, the atomic hydrogen species fraction at the output of a flow tube operating at a flow of 100 sccm, pressure of 400 mTorr, and rf input power of 200W was measured to be 0.8 decreasing to 0.5 when pressure was increased to 1.0 Torr. Details of sensor design, calibration, and application will be discussed.

\*Research sponsored by the U.S. Department of Energy, under contract DE-AC05-84OR21400 with Martin Marietta Energy Systems, Inc.

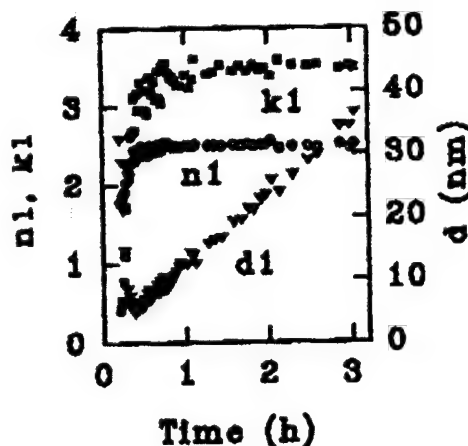
**EM-ThP15 Spectroscopic Ellipsometry Studies of a-Si<sub>1-x</sub>C<sub>x</sub>:H Film Growth by Reactive Magnetron Sputtering,** Y. H. Yang, M. Katiyar and J. R. Abelson, Coordinated Science Lab. and Materials Science Department, U. Illinois, Urbana, IL 61801.

Hydrogenated amorphous silicon carbide (a-Si<sub>1-x</sub>C<sub>x</sub>:H) films with  $x \geq 0.3$  are suitable for use as the active layer in visible-light-emitting diodes, as the dielectric in metal-insulator-semiconductor devices, and as mechanically hard coatings. We deposit a-Si<sub>1-x</sub>C<sub>x</sub>:H films by dc reactive magnetron sputtering of a Si target in a mixture of Ar+CH<sub>4</sub>+H<sub>2</sub>. This process produces dense and homogeneous material. We demonstrate that real-time, in-situ spectroscopic ellipsometry (2.0–4.5 eV) provides information on the structure of films and interfaces. Films are deposited at temperatures of 100–400°C with 0.2 mTorr CH<sub>4</sub> on native-oxide-covered crystal silicon substrates. Be-

low 170°C, a layer with high refractive index is formed between the substrate and film; the thickness of this layer diminishes at higher temperatures. The dielectric functions of the films deposited above 230°C have the same values for the imaginary part, while the real part values increase with temperature. This indicates that the films are denser at higher temperatures. Ex-situ IR measurements show an increased absorption around 780 cm<sup>-1</sup>, corresponding to SiC stretching mode. Study of the films deposited under different CH<sub>4</sub> or H<sub>2</sub> pressures is underway.

**EM-ThP16 Numerical Ellipsometry; Applications of a New Algorithm for Real Time, in-situ Film Growth Monitoring,** John Craig Comfort and Frank K. Urban III, School of Computer Science and Department of Electrical Engineering, Florida International University, Miami, FL 33199.

The equations associated with the popular models of film deposition of a material on a substrate tend not to be invertible in practical situations. Thus development of numerical techniques for obtaining approximate solutions to these equations has become necessary. At present, real time, in-situ thin film growth ellipsometry data is limited to a single angle of incidence due to the deposition system windows. The 2C algorithm, developed by the authors, represents a new approach to solve this problem. This algorithm is fast enough for reliable real time solutions without requiring either accurate initial estimates or any off line processing. Algorithm 2C employs the techniques of dynamic step adjustment, overrelaxation, and reduction in dimension, as well as curve following and curve intersection location techniques developed by the authors. In this paper, the algorithm has been extended to solve the equations for silver, silicon, and gold depositions on BK7 glass. An example of the results generated by the algorithm is shown at the right for nickel deposited on BK7 glass.



**EM-ThP17 ARXPS-Studies of Oxidation of 6H SiC Single Crystal (001) Si- and (001) C-Surfaces,** B. Hornetz, University of Karlsruhe, 76131 Karlsruhe; H.-J. Michel, J. Halbritter, KfK, IMF I, Postfach 3640, 76021 Karlsruhe, Fed. Repl. Germany.

The main puzzle in oxidation of hexagonal SiC is the slower rate of the Si-terminated surface as compared to the C-terminated surface, which is blamed on an unknown interface compound. ARXPS is a unique method to identify minor amounts of interface compounds, especially for smooth surfaces. Our ARXPS analysis of oxidized Si-(001) and C-(001) surfaces of 6 H SiC reveals the interface oxide Si<sub>4</sub>C<sub>4-x</sub>O<sub>2</sub> ( $x < 2$ ), likely a reaction product of a peroxidic O<sub>2</sub>-bond to a SiC double layer. Si<sub>4</sub>C<sub>4-x</sub>O<sub>2</sub> occurs in larger thickness ( $\approx 1$  nm) at the slowly oxidizing Si-(001) surface, whereas the C-(001) surface shows smaller amounts, only, diminishing fast with oxidation above 700°C. Evidence is presented that with increasing amount of Si<sub>4</sub>C<sub>4-x</sub>O<sub>2</sub>, the oxidation of SiC to SiO<sub>2</sub> is reduced. ARXPS is consistent with a layer of SiO<sub>2</sub> containing less than 3% Si<sub>4</sub>C<sub>4</sub>O<sub>4</sub> being an oxidation product of Si<sub>4</sub>C<sub>4-x</sub>O<sub>2</sub>. At the surface of SiO<sub>2</sub>, graphite and some Si<sub>4</sub>C<sub>4</sub>O<sub>4</sub> exist, aside from standard adsorbates.

**EM-ThP18 Adsorption and Co-adsorption of Boron and Oxygen on Ordered  $\alpha$ -SiC Surfaces,** V. M. Bermudez, Naval Research Laboratory, Washington, DC 20375.

Boron layers have been grown (by thermal decomposition of B<sub>10</sub>H<sub>14</sub>) on ordered Si- and C-terminated surfaces of  $\alpha$ -SiC and studied using AES, ELS, and LEED. Adsorption of O<sub>2</sub> on the clean and B-adsorbed surfaces has also been studied. Cleaning the Si-face by annealing in

a flux of Si vapor yields a  $(3 \times 3)$  structure due to a layer of chemisorbed Si. Annealing the  $(3 \times 3)$  in UHV produces Si vacancies, giving a  $(\sqrt{3} \times \sqrt{3})R30^\circ$  structure. A  $(1 \times 1)$  structure is seen for the C-face. Boron interacts only weakly with the  $(3 \times 3)$  Si- and  $(1 \times 1)$  C-faces. On the  $(\sqrt{3} \times \sqrt{3})R30^\circ$  Si-face, structure in the Si  $L_{2,3}VV$  and B KLL lineshapes suggests compound formation, and an incommensurate  $(1 \times 1)$  overlayer appears in LEED. On B-free surfaces, room-temperature chemisorption of  $O_2$  is slower on the  $(1 \times 1)$  C-face than on the  $(3 \times 3)$  Si-face, but the rates of O uptake become comparable as coverage increases and chemisorption gives way to oxidation. On the  $(\sqrt{3} \times \sqrt{3})R30^\circ$  Si-face, chemisorption is rapid but oxidation slow. Pre-adsorbed B suppresses  $O_2$  chemisorption on all surfaces but has little or no effect on oxidation. The implications of this work for "δ-doping" of α-SiC will be discussed.

**EM-Thp19 Oxide Layer Growth on Gallium Arsenide Using High Kinetic Energy Neutral Atomic Oxygen.** *M. A. Hoffbauer and J. B. Cross*, Los Alamos National Laboratory, Los Alamos, NM 87545 and *J. C. Gregory*, Univ. of Alabama, Huntsville, AL 38899.

Traditionally hot atoms can be used to overcome many problems translationally associated with processing, passivation, and oxide layer growth on compound semiconductor materials. The unprecedented growth of thick, uniform, and extremely high-quality oxide layers on (100) and (110) GaAs wafers has been demonstrated by exposing the substrate ( $T_s < 250^\circ\text{C}$ ) to a high kinetic energy ( $\sim 2.5$  eV) beam of neutral atomic oxygen at flux levels of  $\sim 50$  monolayers/second. Oxide layer characterization was performed using x-ray photoemission spectroscopy (with  $Ar^+$  ion sputter profiling), Raman spectroscopy, XPS, infrared spectroscopy, x-ray diffraction, and photoluminescence. ATRP shows the oxide layer to be  $>200$  Å thick and uniform in composition, with the Ga and As species formed in their highest oxidation states (implying the formation of either  $Ga_2O_3$  and  $As_2O_3$  or  $GaAsO_4$ ). Raman spectroscopy indicates that there is no metallic As (amorphous or crystalline) in the oxide or at the interface between the oxide and substrate and that there is no appreciable oxidation induced disorder of the substrate as is seen in high temperature thermal and plasma oxidation processes. Photoluminescence measurements also show no degradation of the oxide/substrate interface and are used to evaluate oxide quality. The effects of GaAs substrate temperature and beam exposure time on the oxide layer growth kinetics will be discussed. GaAs samples flown on the Space Shuttle and exposed to ambient atomic-O will be compared to results from our laboratory. Applications of this new non-thermal materials synthesis technology to semiconductor processing will also be discussed, and results for other semiconductor materials will be presented.

**EM-Thp20 Oxidation-Induced Roughening and Oxide Nucleation on Si(001)- $2 \times 1$  Surfaces: An STM Study.** *J. P. Pelz and J. V. Seiple*, The Ohio State University, Department of Physics, Columbus, OH 43210.

Room temperature STM measurements were used to study surface roughening on Si(001)- $2 \times 1$  samples exposed to  $O_2$  to pressures from  $1 \times 10^{-8}$  to  $5 \times 10^{-6}$  torr and temperatures from 500 to  $700^\circ\text{C}$ . At  $T \geq 600^\circ\text{C}$  and  $P_{O_2} < 1 \times 10^{-7}$  torr preferred B-type step retraction is observed, but single A-domain formation is prevented due to step pinning. This pinning roughens the surface via step "fingering" and the formation of multi-level Si islands. The strong dependence of pinning density with oxidation pressure and the characteristic nature of the pinning defects indicate that the pinning sites are nucleated oxide clusters. These pinning sites were counted over large areas to estimate an oxide nucleation rate,  $J_{ox}$ . This nucleation rate was found to scale with the oxidation pressure as  $J_{ox} \propto P_{O_2}^m$ , with  $m \geq 2$ . This dependence is consistent with a simple model in which two diffusing oxygen species are required to nucleate a stable oxide cluster. The critical  $O_2$  pressure (at a dose of 63L) for the transition between the etching dominated regime and oxide growth dominated regime is about  $1 \times 10^{-7}$  torr at  $600^\circ\text{C}$  and  $4 \times 10^{-6}$  torr at  $700^\circ\text{C}$ , but is sensitively dependent on the starting defect density of the surface. Preliminary results regarding the temperature dependence of  $J_{ox}$  will also be reported.

**EM-Thp21 Growth of Layered Semiconductors by Molecular Beam Epitaxy: Formation and Characterization of GaSe, and MoSe<sub>2</sub> Layers on Sulfur Passivated GaP(111) and GaAs(111).** *C. Hammond*(\*), *M. Lawrence*(†), *K. Nebesny*(\*), *P. Lee*(\*), *R. Schlaf*(‡), and *N. R. Armstrong*(\*)—(\*)=Department of Chemistry, University of Arizona, Tucson, Arizona 85721; (†)=Department of Chemistry, Concordia University, Montreal, Canada; (‡)=Hahn Meitner Institute, Berlin, Germany.

Layered compound semiconductors are attractive for the growth of heterojunctions and multilayers with molecularly sharp interfaces, which are "tailored" to optimize their electronic and photonic device properties. Weak interactions between adjacent layers may permit the formation of ordered heterojunctions from materials with a large lattice mismatch. In this first of two papers, we discuss the MBE growth and characterization of ordered layers of GaSe and MoSe<sub>2</sub> and related semiconductors, on sulfur-passivated GaP(111) and GaAs(111). Simple solution passivation procedures allow formation of a III-V semiconductor surface which will readily support the growth of highly ordered layers of GaSe ( $E_{\text{bandgap}} = 2.0\text{eV}$ ). These thin layers then permit the further growth of ordered layers of a semiconductor like MoSe<sub>2</sub> ( $E_{\text{bandgap}} = 1.0\text{eV}$ ). RHEED and angle resolved XPS data confirm the molecularly sharp nature of the heterojunctions formed and complement the spectroscopic characterization of ordered GaSe/MoSe<sub>2</sub> ("quantum-well-like") multilayers.

**EM-Thp22 An Atomically-Resolved STM Study of the Interaction of Trimethyl Gallium with Si(001).** *M. J. Bronikowski and R. J. Hamers*, Dept. of Chemistry, University of Wisconsin, Madison, WI 53706.

Using Scanning Tunneling Microscopy (STM) and tunneling spectroscopy, we have studied the interaction of trimethyl gallium with Si(001). At room temperature we observe the formation of gallium-induced reconstruction, indicating that at least some of the TMG molecules completely dissociate. We also observe a corresponding number of fragments which we identify as adsorbed  $CH_3$  fragments as well as some larger fragments attributed to partially-dissociated  $Ga(CH_3)_x$  molecules. By studying the images at successively higher decomposition temperatures we have identified the sequential decomposition of  $CH_3$  species on the surface. A statistical analysis of the number and types of fragments produced as a function of temperature provides insight into the mechanism of TMG decomposition.

This work is supported by the National Science Foundation and by the U.S. Office of Naval Research.

**EM-Thp23 Reactions of Tetraethoxysilane (TEOS) Vapor on Titanium Dioxide Surfaces.** *T. A. Jurgens*<sup>1,2</sup>, *G. S. Herman*<sup>1</sup>, *T. T. Tran*<sup>2</sup>, *S. A. Chambers*<sup>2</sup>, *C. H. F. Peden*<sup>2</sup>, and *J. W. Rogers, Jr.*<sup>1</sup>, <sup>1</sup>University of Washington, Seattle, WA 98195 and <sup>2</sup>Pacific Northwest Laboratory,\* Richland, WA 99352.

The reactions of tetraethoxysilane (TEOS) vapor on different  $TiO_2$  surfaces were studied using Fourier transform infrared spectroscopy (FTIR), temperature programmed desorption (TPD), Auger electron spectroscopy (AES), x-ray photoelectron spectroscopy (XPS) and x-ray photoelectron diffraction (XPD). Adsorption of TEOS on dehydroxylated or water pre-dosed polycrystalline  $TiO_2$  produces a monoethoxy silyl ligand and ethoxide species, which decompose in the range 450 to 650 K as gas phase ethanol and ethylene and yield surface bound  $SiO_2$ . On the water pre-dosed surface, FTIR shows vibrations characteristic of a hydroxylated silica species. FTIR, TPD, XPS, and AES were used to characterize the reactions of TEOS on model  $TiO_2$  films deposited on a W(110) substrate. The intermediate silyl ligand formed by dissociative adsorption of TEOS on a water- and hydroxyl-free  $TiO_2$ (110) single crystal surface was examined by XPD.

\*Pacific Northwest Laboratory is operated for the U.S. Department of Energy by Battelle Memorial Institute under contract DE-AC006-76RLO1830.

**EM-Thp24 Synchrotron Radiation Induced Decomposition of closo-1,2-dicabado-decaborane.** *Dongjin Byun*<sup>1,2</sup>, *Seong-don Hwang*<sup>1,2</sup>, *Jiandi Zhang*<sup>1</sup>, *Hong Zeng*<sup>2</sup>, *F. Keith Perkins*<sup>3</sup>, *G. Vidali*<sup>2</sup> and *P. A. Dowben*<sup>1</sup>, 1) Center for Materials Research and Analysis, University of Nebraska, Lincoln, NE 68588-0111, 2) Solid State Science and Technology Program and Dept. of Physics, Syracuse University, Syracuse, N.Y. 13244-1130, 3) Electronic Science Technology Division, Code 6864, Naval Research Laboratory 4555 Overlook Ave., SW, Washington, D.C. 20375-5320.

We have observed that molecular films of closo-1,2-dicabado-decaborane ( $C_2B_{10}H_{12}$ ) decompose to form a heterogeneous intermediate phase between associative molecular fragments and solid, thin film boron-carbide. This heterogeneous phase has an observed electronic structure that is an admixture of the electronic structure observed for molecularly condensed orthocarborane and the electronic structure anticipated for rhombohedral boron-carbide (based on the  $B_{12}$  icosahedral "building block"). With the synchrotron radiation ex-

posure at room temperature there is dissociative adsorption of this icosahedral molecule and the growth of boron-carbide film is enhanced. The composition of the growing film changes for very thin films on Si(111), as determined by the boron to carbon ratio. The boron concentration of the film increases with increasing film thickness until the boron to carbon ratio reaches 5 at the point when the film thickness is approximately 12 Å. After about 12 Å of film growth the composition is constant, i.e., B<sub>5</sub>C. As a result of synchrotron radiation induced decomposition of *closo*-1,2-dicabadodecaborane on Si(111), the p-n junction was formed and shows the diode I-V characteristics. This result clearly shows that the film formed was p-type and this technique can be used for device fabrication.

**EM-ThP25 Interaction of Tungsten Hexafluoride with W(100),** *Wei Chen and Jeffrey T. Roberts*, Department of Chemistry, University of Minnesota, Minneapolis, MN 55455.

Tungsten hexafluoride (WF<sub>6</sub>) is a precursor for the selective chemical vapor deposition (CVD) of tungsten, an important material for ultra-large-scale integrated circuit (ULSI) applications. Deposition occurs on conducting and semiconducting substrates, but not on insulating substrates. To gain insight into the basis of the selectivity, it is crucial to investigate the initial nucleation, surface reactions, and formation of surface subfluorides of WF<sub>6</sub> on model growth surfaces. We have studied the interaction of tungsten hexafluoride with W(100) using temperature programmed reaction spectroscopy (TPRS), Auger electron spectroscopy (AES), and x-ray photoelectron spectroscopy (XPS). A multilayer of WF<sub>6</sub> condenses on W(100) at 100 K. Upon heating to 700 K, WF<sub>6</sub> is the sole gaseous product. Besides sublimation of the multilayer, two more thermal desorption features, attributed to the reactions of surface subfluorides (WF<sub>x</sub>, 0 < x < 6) are observed between 200 and 430 K. The formation of the subfluorides begins below 200 K, and is evidenced by XPS as shifts of the F(1s) and W(4f) binding energies. One of the subfluorides is probably tungsten pentafluoride. The fluorides dissociate to atomically adsorbed fluorine around 700 K. Remaining fluorine can be removed by the electron bombardment heating.

**EM-ThP26 Chemisorption and Thermally Activated Etching of Iodine on Si(100)-2 × 1,** *D. Rioux, F. Stepniak, R. J. Pechman, and J. H. Weaver*, University of Minnesota, Department of Materials Science and Chemical Engineering, Minneapolis, MN 55455.

Halogen-semiconductor systems are of interest as models of surface-adsorbate interactions, and a systematic study of adsorption and etching across the halogen family reveals the influence of electronegativity and size. These simple systems also yield insight into the complex plasma etching processes commonly used in device manufacturing. Scanning tunneling microscopy (STM) and photoemission spectroscopy were used to investigate the adsorption and thermally activated etching of I<sub>2</sub> on Si(100)-2 × 1. STM indicates that room temperature adsorption was dissociative on dimer dangling bonds without disruption of the dimers. Steric hindrance influenced the surface structures so that 4 × 2 domains were created where alternating dimers were iodine-terminated. Photoemission spectra revealed the presence of SiI<sub>x</sub> species where x = 1 was the majority species, in support of the STM-derived adsorption model. Exposure at temperatures in the range 600 to 900 K resulted in etching. Single-layer etch pits formed on terraces and step edges were roughened. Regrowth structures on the terraces were characterized by 2D islands and dimer chains. Etching at 900 K resulted in iodine-free areas where dimer vacancy interactions yielded a network of line defects perpendicular to the dimer row direction. At 800 K, etching produced 4 × 2 domains of iodine-terminated dimers, whereas mixed 2 × n domains dominated at lower temperatures. Etching resulted in layer-by-layer removal at the temperatures investigated here.

## THIN FILM

### Room BR4 - Session TF-ThP

#### Thin Film Characterization and Sensors Applications

**Moderator:** A. C. Wall, IBM Corporation.

**TF-ThP1 Auger Electron Spectroscopy as a Real-Time Probe of Film Composition During MBE Growth,** *S. A. Chambers and T. T. Tran*, Pacific Northwest Laboratory,\* Richland, WA 99352.

We have incorporated a commercially available, high-speed Auger electron spectrometer into an MBE system for the purpose of obtaining real-time compositional information on evolving epitaxial films. We have used the same primary electron beam as is used to generate RHEED patterns. The range of detected electron emission angles is such that Auger electron attenuation lengths are less than or equal to the penetration depth of the primary beam. We have used the system to explore incident-beam diffraction and its effect on measured Auger intensities, and to monitor composition during the epitaxial growth of MgO/MgO(001) and Al<sub>x</sub>Mg<sub>1-x</sub>O/MgO(001). By using well-defined standard specimens and cross calibrating with x-ray photoemission measurements, we have been able to obtain spectral intensities at the rate of ~10 seconds per Auger transition, leading to composition determinations that are accurate to within ~±2%. Incident beam diffraction effects are dramatic, producing Auger intensity enhancements of up to ~50% when the primary beam is aligned with the [100] and [110] low-index directions in the MgO(001) surface. These enhancements are due to strong elastic scattering and constructive interference (forward focussing) that occurs when the primary beam is aligned with chains of atoms in the surface plane. The Auger ratio varies by ~10% with incident angle, making primary beam alignment critical in generating reproducible intensities.

\*Pacific Northwest Laboratory is operated for the U.S. Department of Energy by Battelle Memorial Institute under contract DE-AC06-76RLO1830.

**TF-ThP2 B-Doped Si(001) Grown by Gas-Source Molecular-Beam Epitaxy from Si<sub>2</sub>H<sub>6</sub> and B<sub>2</sub>H<sub>6</sub>: B Incorporation and Electrical Properties,** *Q. Lu, T. R. Bramblett, N.-E. Lee, M.-A. Hasan, T. Karasawa, and J. E. Greene*, University of Illinois, 1101 West Springfield, Urbana, IL 61801.

B-doped Si(001)2 × 1 films were grown on Si(001) substrates by gas-source molecular beam epitaxy (GS-MBE) using Si<sub>2</sub>H<sub>6</sub> and B<sub>2</sub>H<sub>6</sub>. B concentrations C<sub>B</sub> (5 × 10<sup>16</sup>–5 × 10<sup>19</sup> cm<sup>-3</sup>) were found to increase linearly with increasing flux ratio J<sub>B<sub>2</sub>H<sub>6</sub></sub>/J<sub>Si<sub>2</sub>H<sub>6</sub></sub> (9.3 × 10<sup>-5</sup>–2.5 × 10<sup>-2</sup>) at constant film growth temperature T<sub>s</sub> (600–950°C) and to decrease exponentially with 1/T<sub>s</sub> at constant J<sub>B<sub>2</sub>H<sub>6</sub></sub>/J<sub>Si<sub>2</sub>H<sub>6</sub></sub> ratio. The B<sub>2</sub>H<sub>6</sub> reactive sticking probability ranged from 6.4 × 10<sup>-4</sup> at T<sub>s</sub> = 600°C to 1.4 × 10<sup>-3</sup> at 950°C. The difference in the overall activation energies for B and Si incorporation at T<sub>s</sub> = 600–950°C is 0.34 eV. A comparison of quantitative secondary-ion mass spectrometry (SIMS) and temperature-dependent Hall-effect measurements showed that B was incorporated into substitutional electrically-active sites over the entire B concentration range investigated. SIMS B depth-profiles from modulation-doped samples were abrupt with no indication of surface segregation to within the instrumental resolution limit and initial δ-doping experiments were carried out. Structural analysis by *in-situ* reflection high energy electron diffraction combined with post-deposition plan-view and high-resolution cross-sectional transmission electron microscopy showed that all films were high-quality single crystals with no evidence of dislocations or other extended defects. Temperature-dependent (20–300 K) hole carrier mobilities were equal to the best reported bulk Si:B values and in good agreement with theoretical maximum values.

**TF-ThP3 Mass Spectroscopy of Recoiled Ions(MSRI) as a Tool Both for Surface Analysis of Boron Nitride Thin Films During Deposition and Exsitu,** *Laura Woolverton, J. Albert Schultz, Ketti Eipers-Smith, and Kelly Waters*, IONWERKS, 2472 Bolsover Suite 255, Houston, TX 77005.

MSRI is performed by impinging a pulsed keV ion beam onto a surface at grazing incidence and mass analyzing the subsequently produced forward recoiled keV ionized surface atoms by time of flight. The ionized recoils are collected in specially shaped electrostatic analyzers which provide time focusing so that moderate resolution can be obtained (400 at mass 238). The spectra are entirely free of molecular interferences because of the violence of the binary collision and the speed with which the recoils leave the surface.

Recent developments in instrumentation will be illustrated in our study of boron nitride surface chemistry. The dependence of the recoiled ion intensity upon the chemical state of the boron and upon the ambient pressure of the growth reactor will be discussed. We report a 15/1 relative sensitivity of boron/nitrogen. This relative sensitivity is good when compared to that obtained by SIMS of 10<sup>5</sup>/1. It will be also shown that in addition to nitrogen, MSRI is also good for several other elements which are poorly detected by SIMS.



**TF-ThP4 Deposition of Polysilicon by ECRCVD and RTCVD,** P. Müller, E. Conrad, Hahn-Meitner-Institut, Berlin, FRG and T. R. Omstead, CVC Products, Inc., Rochester, NY 14603.

At present there is great interest in preparing polysilicon layers at lowest possible temperatures or with limited thermal budget for quite different applications (thin film displays, solar cells etc.). These layers should exhibit good thickness homogeneity and morphology as well as controllable grain size. In order to meet these requirements we deposited polysilicon by using ECRCVD (electron cyclotron resonance chemical vapor deposition) and RTCVD (low pressure CVD in a rapid thermal process unit) with  $\text{SiH}_4$  as precursor diluted in different amounts of  $\text{H}_2$  and/or Ar. Both process chambers are part of a newly developed Cluster Tool which allows deposition onto wafers up to 6" or 10 cm  $\times$  10 cm substrates. In first experiments layers with smooth surfaces were grown on crystalline and non-crystalline substrates with rates up to 0.3  $\mu\text{m}/\text{min}$  and thicknesses up to 1.5  $\mu\text{m}$ . Layer characterization took place by morphological (REM) and microstructural (AES, EDX) investigation as well as optical (FTIR, VIS, UV) and electrical (IV, CV) measurements. The two deposition methods will be compared with respect to grain size, defect density and maximum layer thickness. Moreover the effect of in-situ doping by  $\text{PH}_3$  and  $\text{B}_2\text{H}_6$  to the growth conditions will be considered.

**TF-ThP5 Oxygen Content of Indium Tin Oxide Films Fabricated by Reactive Sputtering,** S. Honda, A. Tsujimoto, M. Watamori, K. Oura, Dept. of Electronic Eng. Fac. of Eng., Osaka Univ., 2-1 Yamadaoka, Suita, Osaka 565, Japan, F. Shoji, Dept. of Electric Eng. Fac. of Eng., Kyushu Kyoritsu Univ., Yahata-nishi, Kitakyushu 807, Japan.

Indium tin-oxide (ITO) films, which are transparent conductive films, have been widely used in optoelectronic applications. Recently, it has been recognized that a high quality film with correct stoichiometric composition is essential to make a flat panel display.

However, it is difficult to estimate the absolute oxygen concentration. There have been few studies of oxygen depth profiling for ITO films. We investigated the relationship between the oxygen content of ITO films and the electrical properties under various deposition conditions. Absolute oxygen content has been determined by  $^{16}\text{O}(\alpha, \alpha')^{16}\text{O}$  resonant back scattering.

It has been found that there is a correction between a depth profile of oxygen concentration of ITO films and the films properties. In the case of the ITO film fabricated at RT., the large deficiency of oxygen can be seen at the surface of the film. When the film was formed at 400°C, no deficiency of oxygen at the film surface was observed. The observed oxygen concentration will be discussed in terms of the electrical and optical properties of the films.

**TF-ThP6 Thin-Film and Buried Interface Characterization Using High Brightness Synchrotron Radiation,** J. J. Jia, T. A. Callcott, U. Tennessee, Knoxville, TN 37996, F. J. Himpsel and H. Akatsu, IBM T. J. Watson Research Center, POB 218, Yorktown Heights, NY 10598, M. G. Samant, J. Stohr, IBM Almaden Res. Center, 650 Harry Rd., San Jose, CA 95120-6099, D. L. Ederer, Tulane University, New Orleans, LA 70118, J. A. Carlisle, E. A. Hudson, and L. J. Terminello, Lawrence Livermore National Laboratory, Livermore, CA 94550, R. C. C. Perera and D. K. Shuh, Lawrence Berkeley Laboratory, Berkeley, CA 94720.

We have used one of the first high-brightness, third generation synchrotron radiation sources that use undulators to boost the spectral brilliance to characterize the structure, morphology, and thickness of several variety of thin-films and buried heterointerfaces. The systems characterized include higher fullerenes, conductive polymers, oxynitride growth on silicon, and buried heterointerface. We present the first photoabsorption, soft-X-ray fluorescence, and photoemission data obtained from the IBM/U. of Tennessee/Tulane U./LLNL/LBL beam line at the Advanced Light Source, Lawrence Berkeley Laboratory. The spectral range of 70–1200 eV covers the sharpest core levels of all elements with optimum surface sensitivity and resolution. The high brightness of this new facility has made possible the probing of thin and buried layers that were previously undetectable. In particular, a resonant soft-X-ray fluorescence measurement of a buried BN heterojunction was performed and we were able to detect the buried 3 Å layer of BN under 50 Å of amorphous carbon. The morphology of this buried BN layer was determined to be  $\text{sp}^2$ -like owing to the sen-

sitivity of the resonant fluorescence. These experiments and prospects for other high brightness experiments will be discussed.

This work was supported by the Director, Office of Energy Research, Office of Basic Energy Sciences, Materials Science Division, of the U.S. Department of Energy under Contract No. DE-AC03-76SF00098 for the Advanced Light Source, Lawrence Berkeley Laboratory and under Contract No. W-7405-ENG-48 for the Lawrence Livermore National Laboratory.

**TF-ThP7 Structure and Composition of Hydrogenated  $\text{Ti}_x\text{C}_y$  Thin Films Prepared by Reactive Sputtering,** M. P. Delplancke, V. Vassileris and R. Winand, Université Libre de Bruxelles, Faculté des Sciences Appliquées, Métallurgie-Electrochimie, 1050 Brussels.

Thin films of hydrogenated titanium carbide are prepared by reactive magnetron d.c. sputtering in mixed atmosphere of argon and methane or argon and acetylene. The deposition process is followed by optical emission spectroscopy (OES). The films are characterized by various techniques: scanning electron microscopy, transmission electron diffraction and microscopy (high resolution), atomic force microscopy, X-ray diffraction, Auger electron spectroscopy, X-ray photoelectron spectroscopy, and Fourier transform infrared spectroscopy.

The influence of the total and partial pressures, the current density and voltage on the structure and composition of the films is examined. The morphology and crystallinity of the deposits are strongly dependent on the carbon content in the films. The presence of amorphous carbon phase results in a decrease of the  $\text{TiC}$  grain size. The proportion of  $\text{Ti-C}$  bonds in the films is correlated to the decomposition of the carbon precursor in the discharge as shown by optical emission spectrometry. This is especially strong in the case of  $\text{C}_2\text{H}_2$ -Ar mixture.

**TF-ThP8 Ion Beam-Induced SiC Crystallization of Carbon Implanted Layers in Si(100) Studied by Electron Spectroscopy,** H. J. Steffen, V. Heera, R. Koegler, W. Skorupa, Research Center Rossendorf Inc., Institute for Ion Beam Physics and Materials Research, P.O.B. 510119, D-01314 Dresden, Germany.

Ion beam-induced crystallization of SiC in Si(100) was investigated by valence band Auger electron spectroscopy and electron energy loss spectroscopy in combination with sputter depth profiling. After pre-amorphization by 200 keV  $\text{Ge}^+$  ion bombardment and 25 keV  $\text{C}^+$  ion implantation at room temperature and various doses, recrystallization of the amorphous silicon-carbon layer was induced by a subsequent 300 keV  $\text{Si}^+$  ion bombardment at 700 K. The depth dependent composition, the different chemical states and the crystal order were obtained by a thorough analysis of the plasmon losses and the Auger line shape with Factor Analysis and least-squares fitting. This study discloses the migration of the recrystallization front from the underlying amorphous silicon substrate into the carbon-rich layer in dependence on the  $\text{Si}^+$  ion dose.

**TF-ThP9 Interfacial Properties of FCC-Iron Grown on Diamond,** R. Swineford, Feng Yue, D. P. Pappas, Physics Dept., Virginia Commonwealth University, Richmond, VA 23284-2000.

The growth of 1 to 4 monolayers of iron on the (100) face of single crystal, synthetic diamond substrates has been studied with low energy electron diffraction (LEED) and angle resolved Auger electron spectroscopy (ARAES). The film thickness was measured using an *in-situ* fluorescence flux monitor which was calibrated against a quartz crystal monitor and an *ex-situ* x-ray fluorescence thickness monitor. The 4 monolayer films are shown to be in the metastable fcc phase, which is stabilized by the lattice match to the diamond substrate ( $a = 3.59$  Å, extrapolated from the high temperature fcc-phase of Fe, as compared to 3.57 Å for diamond). This is expected to put a compressive in-plane strain on the epitaxial fcc-Fe films. A single scattering simulation of the ARAES data was performed using a 216 atom cluster, and it is found that the films have a tetragonal distortion which is due to an  $\approx 3\%$  expansion of the lattice perpendicular to the plane of the film, in agreement with previous estimates [1]. The LEED patterns of these films have been measured, and the reconstructions observed are compared to those observed from metastable fcc-Fe films grown on a Cu(100) substrate ( $a = 3.61$  Å). Finally, the adsorption site of the first monolayer of Fe onto the diamond lattice has been determined by modeling the carbon ARAES data.

[1] D. P. Pappas, J. W. Glesener, V. G. Harris, J. J. Krebs, Y. U. Idzerda, G. A. Prinz, Appl. Phys. Lett., 64, 28 (1994).



**TF-ThP10 Study of Adsorption and Desorption of 1,5-Cyclooctadiene on Cu(111) Surface, Q. Cheng, K. Griffiths, S. Serghini, Z. Yan, P. R. Norton,\* and R. J. Puddephatt,** Department of Chemistry, The University of Western Ontario, London, Ontario N6A 5B7, Canada.

The adsorption and desorption of 1,5-cyclooctadiene (COD) on the Cu(111) surface have been studied under ultra-high vacuum (UHV). Although the Cu(111) surface does not appear to exert a strong catalytic effect on the molecule, it does influence the surface adsorption of COD. Temperature programmed desorption (TPD) shows that both chemisorption and physisorption occur on the Cu(111) surface. It also indicates that most of the desorption from the surface occurs as parent ions and the peak desorption temperatures are at  $\sim 175\text{K}$  and  $\sim 240\text{K}$ , from the chemisorbed layer and the physisorbed layers respectively. FTIR spectra indicates a parallel orientation of the C=C double bonds via the absence of  $1650\text{ cm}^{-1}$  vibration feature in the chemisorbed layer and its presence in multi-layer. The AES spectrum shows no contamination from the adsorbed molecule on the surface after the desorption.

**TF-ThP11 Spatial Grating Formation in Amorphous Chalcogenide Thin Films,\* E. López-Cruz, J. González-Hernández, F. Ruiz,\*\* C. Vázquez-López, and E. Haro-Poniatowski,\*\*** Programa Multidisciplinario de Materiales Avanzados, CINVESTAV-Salttillo, Salttillo Coahuila, México, \*\*On leave from Universidad Autónoma de San Luis Potosí, \*\*\*Universidad Autónoma Metropolitana-Iztapalapa, México-DF.

During the measurements of the phase conjugation via degenerate four wave mixing in amorphous Se, laser induced gratings were formed. We used Scanning Force Microscopy (SFM) to characterize the gratings. It is found that the periodicity of the grating is a film-thickness-dependent parameter. Several possible mechanisms which may result in atomic displacement, including bond-softening due to electronic effects, are discussed. It will be reported the dependence of grating formation on several parameters such as film thickness and laser power.

\* Work partially supported by CONACyT-Mexico.

**TF-ThP12 Synchrotron Radiation Photoelectron Emission Microscopy of Natural and Chemical Vapor Deposited Diamond Surfaces, J. D. Shovlin, M. E. Kordesch,** Ohio University, Athens, OH 45701, **D. Dunham, B. P. Tonner,** Synchrotron Radiation Center and University of Wisconsin-Milwaukee, Milwaukee, WI 53201, and **W. Engel, Fritz Haber Institute, Faradayweg 4-6, Berlin, Germany, D-14195.**

Natural and chemical vapor deposited diamond surfaces have been imaged using a photoelectron emission microscope and synchrotron radiation in the 4–18 eV and 250–350 eV ranges. Both images and spatially resolved electron yield spectra could be acquired simultaneously. Near-edge spectra at the carbon 1s edge show a resonance due to graphite; extended fine-structure due to diamond was also observed. The image intensity varies above and below the C 1s edge. Contrast variations between individual crystallites are very sensitive to the alignment of the diamond surfaces to the microscope axis. In the 4–18 eV range, no photoemission threshold was observed in the electron yield spectra on any of the specimens. The image contrast was not strongly dependent on the illumination energy. Natural type IIa diamond showed severe charging effects.

An applied electric field of 20 kV/cm was present during observation. No spectroscopic or image related evidence for field emission from the surfaces tested was found.

Work supported by NATO and ONR-BMDO Grant #N00014-5-91-1596.

**TF-ThP13 Surface Spectroscopic Studies of the Deposition of TiN Thin Films From Tetrakis(dimethylamido)-titanium and Ammonia, P. J. Chen, C. M. Truong, J. S. Corneille, W. S. Oh and D. W. Goodman,** Department of Chemistry, Texas A&M University, College Station, TX 77845-3255.

The transamination reaction of  $\text{Ti}[(\text{CH}_3)_2\text{N}]$  (TDMAT) in excess  $\text{NH}_3$  has been shown to produce carbon-free TiN thin films. However, due to the rapid reaction in the gas-phase, it remains a challenge to simultaneously achieve good film conformality and film purity. The results of this investigation indicate that pure TiN thin films can still be deposited via a growth mechanism which is completely surface-mediated. At the low pressure threshold ( $< 10^{-3}$  Torr) where the direct reaction between TDMAT and  $\text{NH}_3$  in the gas-phase becomes negligible, and film growth is controlled by the surface reactions between

adsorbed TDMAT and  $\text{NH}_x$  species. In this work, X-ray photoelectron (XPS) and Auger spectroscopic (AES) analyses show that TiN thin films possessing low carbon-contents can be deposited at pressures below  $10^{-4}$  Torr. In order to detail the basic surface chemistry which is relevant to the deposition process, the adsorption and reaction of TDMAT on Ti and  $\text{TiN}_x$  surfaces were also examined using XPS, infrared reflection absorption (IRAS) and thermal desorption (TDS) spectroscopy.

**TF-ThP14 Phase Stability and Al Solubility in Epitaxial  $\text{Nb}_{1-x}\text{Al}_x\text{N}$  Films Grown on MgO (001) by Reactive Sputtering, T. I. Selinder, D. J. Miller, K. E. Gray, L. Hultman,\* and M. R. Sardela, Jr.,\*** Argonne National Laboratory, MSD-223, 9700 S. Cass Ave., Argonne, IL 60539, \*Thin Film Division, Linköping University, S-581 83 Linköping, Sweden.

Ternary Nb-Al-N films were grown on single-crystal MgO (001) substrates by reactive triode sputtering in  $\text{Ar} + \text{N}_2$  gas mixtures. A phase spread deposition technique was employed to fabricate films with a composition gradient. For a substrate temperature of  $500^\circ\text{C}$ , x-ray diffraction (XRD) showed that the compound films had cubic B1 structure for Al fractions in the range from 0 to 0.62. The lattice parameter decreased with increasing x, from  $4.40\text{Å}$  at  $x=0$  to approximately  $4.27\text{Å}$  for  $x=0.62$ . Moreover, determination of elastic strain, crystallographic tilt and microstructural quality was performed by high resolution XRD mapping. The films were found to exhibit pseudomorphic growth up to at least  $x=0.50$ , for  $x>0.56$  the films were two-phase, and finally, pure AlN had the Wurtzite structure. The growth modes and phase decomposition paths of the metastable B1 films at  $x=0.50$ – $0.62$  were assessed by planar and cross sectional transmission electron microscopy (TEM). The results are discussed in the light of results from previous work on the related transition-metal nitride based system  $\text{Ti}_{1-x}\text{Al}_x\text{N}$  which exhibits similarities in Al solubility and formation regime of the metastable B1 structure.

This work was supported by the U.S. Department of Energy, Basic Energy Sciences-Materials Sciences, under contract #W-31-109-ENG-38. L.H. and M.R.S. acknowledge support from the Swedish National Research Council (NFR).

**TF-ThP15 Growth and Structure of Silicon Oxide Thin Films on Polymers by AFM and XPS, H. Li, S. Krommenhoek and E. Ezell,** BOC Group Technical Center, Murray Hill, NJ 07974, and **F. Jansen,** Airco Coating Technology, Concord, CA 94524.

The structure and chemistry of silicon oxide films were studied by Atomic Force Microscopy and X-ray Photoelectron Spectroscopy. Films were deposited at room temperature on plastics, like, poly(ethylene terephthalate), by plasma enhanced chemical vapor deposition from hexamethyldisiloxane and oxygen gas. At low oxygen flow rate, the film consists of silicon sub-oxide as well as a significant amount of carbon. With increasing oxygen flow rate, the film structure becomes more like silicon dioxide. Increasing oxygen flow rate also leads to a denser film; for example, clusters of the silicon oxides are more closely packed and more uniformly distributed. The gas barrier quality of the film is shown to be directly related to the film chemistry as well as morphology. The influence of the plastics substrate roughness on the growth and structure of the films is also discussed.

**TF-ThP16 Characterization of Aluminum Based Oxide Layers Formed by Microwave Plasma, Z. Katz,** Dept. of Mater. Eng., Ben-Gurion-University, A. Raveh, NRC-Negev, P.O.B. 9001, Beer-Sheva, Israel.

Intensive efforts have been invested in solid state surface modifications by various techniques. These, intensify the requirements for appropriate layer assessments. In this context, microwave plasma oxidation has been applied to polycrystalline commercially pure aluminum 1100 and 7075-Al alloy, at relatively low temperature ( $400 \pm 50^\circ\text{C}$ ) under non-equilibrium low pressure (0.3–2.5 mbar) plasma. Chemical composition and the oxygen profile were established by Auger electron spectroscopy (AES), X-ray photoelectron spectroscopy (XPS) and Fourier Transform Infrared (FTIR) spectroscopy. In the 1100-Al, typical oxide layers thickness of  $1\text{ }\mu\text{m}$  in scale were obtained. Here, the AES/XPS spectra revealed that the layer was composed from aluminum oxide and aluminum metal. The FTIR spectra showed sharp and strong absorption bands at  $940$ – $960\text{ cm}^{-1}$  due to stoichiometric composition with high crystallinity of the  $\gamma\text{-Al}_2\text{O}_3$  with peaks at  $1345\text{ cm}^{-1}$  and  $732\text{ cm}^{-1}$  indicating Al=O and Al-O stretch bands, respectively. In contrast, in the 7075-Al under similar oxidation conditions,  $\text{Al}_2\text{O}_3$  was absent while sharp and intense peak at  $732\text{ cm}^{-1}$ , as well as broad absorption bands at  $870\text{ cm}^{-1}$  and  $1100\text{ cm}^{-1}$  were

observed. Thus, magnesium segregation and the formation of MgO thin layer in the uppermost oxidation layer was here manifested. However, the inner layer was composed from Al-O and Al metal due to oxygen penetration into aluminum under ion bombardment. Atomic Force Microscope (AFM) was supplemented for fine scale surface topography features in different processing conditions. The role of micro-alloying effects and plasma dominant parameters are considered in order to provide some rationale to the current findings.

**TF-ThP17 Investigation of Pyroelectric Characteristics of Lead Titanate Thin Films for Microsensor Applications, K. K. Deb, Army Research Laboratory, Ft. Belvoir, VA 22060, K. W. Bennett, and P. S. Brody, Army Research Laboratory, Adelphi, MD 20899.**

Pyroelectric  $\text{PbTiO}_3$  thin films deposited on Si(100) substrates (Pt/Ti/SiO<sub>2</sub>/Si) by sol-gel processing have been characterized in some detail to determine the usefulness of these films for uncooled detector applications. The films have been deposited without substrate heating. The amorphous films were then annealed in the range of 600–750°C in the oxygen atmosphere. X-ray diffraction patterns taken on these films showed single phase tetragonal structure with a slight c-axis preference. The grain size was in the range of 0.2–0.4 micron. The D-E hysteresis loop characteristics at room temperature, as well as measurements of the dielectric and pyroelectric properties versus temperature and frequency, were performed. The influence of poling treatment on the dielectric and pyroelectric properties was also investigated. The results of measurements show that  $\text{PbTiO}_3$  thin films exhibit a relatively high pyroelectric coefficient relative to the dielectric permittivity contributing to a very high figure of merit for voltage responsivity that is competitive with  $\text{PbTiO}_3$  single crystal and PZT ceramics.

**TF-ThP18 ReSi<sub>2</sub> Thin Film Infrared Detectors, James P. Becker and John E. Mahan, Department of Electrical Engineering, Colorado State University, Fort Collins CO 80523; Robert G. Long, Hewlett-Packard Co., Fort Collins, CO 80525.**

For the first time, infrared sensing devices have been demonstrated using the narrow bandgap semiconductor,  $\text{ReSi}_2$  ( $E_g \approx 0.1$  eV). They are the  $\text{ReSi}_2$ /n-Si heterojunction internal photoemission (HIP) detector, and the  $\text{ReSi}_2$  thin film photoconductive detector. Both devices were characterized with monochromatized infrared radiation using phase-sensitive detection. The HIP detector's spectral response was found to obey the Fowler law with a long wavelength cutoff of  $\sim 2.3$   $\mu\text{m}$  (0.55 eV) at room temperature. Considering the energy band diagram of the HIP structure, this behavior suggests that the detection mechanism is free carrier absorption leading to internal photoemission of hot electrons from the silicide into the substrate. The HIP detector's cutoff wavelength falls well short of the theoretical limit,  $\sim 12\mu\text{m}$ , for a  $\text{ReSi}_2$ -based photonic detector. In hopes of approaching this ultimate limit, the photoconductive device was used to explore a second mechanism of detection, the photogeneration of excess free carriers in  $\text{ReSi}_2$  as manifested by intrinsic band-to-band photoconductivity. It was found that the spectral response of the  $\text{ReSi}_2$  photoconductor (normalized to photon flux and measured at 10 K) extends to 6  $\mu\text{m}$  (0.21 eV, the present limit of our measurement equipment) with no indication of a detection cutoff. In conclusion, these first-ever demonstrations of infrared detection with  $\text{ReSi}_2$ , using unoptimized devices, suggest that this narrow bandgap semiconductor may lend itself to practical applications as a silicon-integrated detector element for long wavelength infrared radiation. (This research was supported by the National Science Foundation through Grant No. DMR-9021507.)

**TF-ThP19 Detection of Chlorinated Hydrocarbon Vapors Using 1,3-bis-(1-pyrene)propane in a Poly(vinyl alcohol) Film, Susan L. Rose-Pehrsson, John Krech, Naval Research Laboratory, Washington, DC 20375.**

Development of remote sensors for hazardous materials is an important part of the Navy's Environmentally-Sound Ships program. 1,3-bis-(1-pyrene)propane (bpp) has been incorporated into a thin film of cross-linked poly(vinyl alcohol) (PVA) on a glass slide and used to detect chlorinated hydrocarbon molecules in the vapor phase. The changes in the fluorescence emission from bpp in the film have been followed upon exposure to dichloromethane, chloroform, or carbon tetrachloride vapors. The spectra contains emissions from pyrene monomer (377, 382, 388 and 397 nm) and excimer (480 nm) units. The intensity ratios  $I_{377\text{nm}}/I_{388\text{nm}}$  and  $I_{\text{excimer}}/I_{\text{monomer}}$  can be used to examine the polarity and micro-viscosity of the bpp's local environment, respectively. As the more non-polar vapors diffuse into the film, their better solvation properties destroy the excimers and change the polarity of the bpp's local environment. For each vapor, these spectral parameters are sufficiently different to distinguish them. Of the polymer

matrices that have been investigated, poly(epichlorohydrin), poly(ethylene oxide), OV-1 and others, PVA has given the best results. It is felt that the porous network and the polar environment of the hydrogel contribute to the initial ease of excimer formation and the subsequent interactions of bpp with the vapors. The PVA/bpp film is presently being investigated for chlorinated hydrocarbon detection in an aqueous environment.

**TF-ThP20 Electrochemical and Surface Properties of a Unique Electro-Ceramic Sensor for Selective Detection of Chlorinated Organics, J. Vetrone, J. R. Stetter, W. R. Penrose, and W. R. Buttner, Transducer Research, Inc., 999 Chicago Ave., Naperville, IL 60540.**

Despite tremendous environmental interest in monitoring chlorinated organic (R-Cl) solvents such as trichloroethylene (TCE) in contaminated ground water and hazardous waste sites, there does not exist until now an inexpensive, portable R-Cl detector. We have synthesized a sodium-based silicate compound whose conductance at elevated temperatures is sensitive to ppm levels of R-Cl vapors, but not to elemental chlorine or hydrocarbons. Gas sensing mechanisms were investigated by studying the material's conductance during gas exposures while heated inside a tube furnace. Temperature studies indicate an activation energy of about 0.2 eV for common R-Cl vapors. Current-voltage scans follow non-ohmic behavior with significant hysteresis. Both capacitive and "inductive" components were measured by a.c. impedance spectroscopy, suggesting the material is a mixed conductor. X-ray diffraction patterns of gas tested material demonstrate R-Cl exposure transforms the bulk structure into a pyrosilicate, while electron micrographs clearly show NaCl crystal growth on the outer surface. Chemical analysis of the exhaust gas from the tube furnace shows no  $\text{Cl}_2$  molecules, indicating the gas sensing reaction involves chlorine atoms or radicals. We discuss the electronic and chemical nature of this novel material and its potential as an R-Cl sensor.

**TF-ThP21 Surface Characterization of Ultra-Thin Metallic Sensing Films, H. Liu, J. L. Gland, J. W. Schwank\*, K. Wise, Department of Chemistry, Department of Chemical Engineering\*, The University of Michigan, Ann Arbor, Michigan 48109.**

Various pretreatment protocols for ultra-thin Pt/Ti and Pt/Al films used for oxygen sensing have been investigated. The pretreatments are meant to obtain a stabilized film structure that is capable of interacting with certain types of gases. The sensing films are evaporated onto a silica substrate. They are studied as a 1  $\text{cm}^2$  macroscopic model of the sensing element in an ultra-thin film conductivity-type gas sensor.

Adsorption and desorption of gases such as oxygen and hydrogen from such thin films at different temperatures have been studied using TPD. Results from characterization by ex situ ESCA and STM will also be presented. These results give us a better understanding of the chemical compositions and structures of the films. Results from these studies will also be combined with the electrical responses from the gas sensors to determine the influences of different pretreatment protocols on the sensing performance of such gas sensors and find effective windows for real time gas detection.

**TF-ThP22 Electron Spectroscopy (XPS, UPS, HREELS) Study of the Cu/SrTiO<sub>3</sub>(100) Interface, T. Conard, A.-C. Rousseau, R. L. Sporken, J. Ghijsen, R. Caudano, Facultés Universitaires Notre Dame de la Paix, Laboratoire Interdisciplinaire de Spectroscopie Electronique, 5000 Namur, Belgium.**

The copper on oxide interface is of general interest in many different domains including catalysis and microelectronics. It is also relevant as a model for the copper/superconductors oxides interfaces formations. We investigate here the formation of the interface between copper on two different surface preparation of  $\text{SrTiO}_3$ , namely a reduced form prepared by high temperature heating under vacuum (1000°C) and an stoichiometric form obtained after re-oxidation of the reduced form.

Using simple growth model to calculate the intensity evolution of the XPS of Sr, Ti, O and Cu core level lines, we were able to show that copper grows on  $\text{SrTiO}_3$  with the simultaneous formation of several monolayers followed by the formation of island on the surface. It was also shown that the growth mode is similar for both forms of  $\text{SrTiO}_3$  but that the number of monolayers formed is higher for the reduced form, which is explained by the higher number of defects on the surface. UPS and Auger parameter studies of the interface formation showed a strong interaction between copper and the substrate, bringing copper in a  $\text{Cu}_2\text{O}$ -like electronic configuration.

HREELS studies confirmed the growth model developed for the XPS intensities. In addition, we were able to show the importance of

the impact interaction mode in the HREELS spectra obtained for the metal/oxide interface.

**TF-ThP23** **AlN Thin Film Structure Development and Quality During Magnetron Sputter Deposition on Si(100) and Si(111), Studied by XRD, AES, and FE SEM, Barbara Ladna, Marc Chason, Steve Voight, Motorola, IL02/Rm 1014, 1301 E. Algonquin, Schaumburg, IL 60196.**

AlN is a material of great interest for its properties as a piezoelectric, a wide band-gap semiconductor, and a protective thin film. The development of the AlN thin film structure, during sputter deposition on the Si substrate, was investigated to understand the structure-properties relationship. XRD was used to determine the film crystallinity and orientation. AES was used to analyze the film surface composition and the elemental concentration changes within the film. SEM was used to analyze the film grain structure, thickness and uniformity. It was found that AlN films as thin as 200 Å can have oriented, columnar grain structure. The grains grow in diameter as well as in height during the film deposition while the film density increases. The AlN/Si interface was found to be clean and well defined and it didn't change with the film growth. The AlN (0002) XRD peak intensity, representative of the degree of the oriented grain structure, increased with the film thickness and the grain structure quality.

**TF-ThP24** **Microstructural Characterization of Pd/InP and Ag/InGaAs Films Grown at Room Temperature and 77K, M. E. Hawley, Q. X. Jia, Los Alamos National Laboratory, Los Alamos, NM 87545, J. Palmer, H. J. Lee, and W. Anderson, SUNY at Buffalo, Center for Electronic and Electro-optic Materials, Depart. of Electrical and Computer Engineering, Amherst, NY 14260, and D. Hoelzer, Alfred U., NYS College of Ceramics, Alfred, NY 14802.**

Atomic force and scanning tunneling microscopes have been used to characterize the microstructure of metal films grown on wide-band semiconducting substrates at 300K and at a cryogenic temperature. Previous work has shown a significant increase in the barrier heights of resulting Schottky Diodes as the deposition temperature was decreased. Because of the importance of the structure-property relationship, structural differences were expected to shed some light on the factors responsible for this increase in barrier height.

Pd and Ag were thermally evaporated on onto InP and InGaAs, respectively, at RT and 77K. The films were grown to thicknesses of 14 and 85 nm. Grain size surface roughness were measured with the scanning probes. Not surprisingly, thicker films have larger average grain size and RMS roughness. The low temperature Pd films were found to possess significant cracking while both all Ag films were characterized by varying densities of holes.

## SURFACE SCIENCE

Room A205 - Session SS1-FrM

### Surface Electronic Structure

**Moderator:** R. Hwang, Sandia National Laboratories.

8:20 am **SS1-FrM1 Theory of Clean and H-Covered Be(0001), Roland Stumpf and Peter J. Feibelman,<sup>†</sup>** Sandia National Labs, Albuquerque, NM 87185-0344.

Be is a "marginal metal." The stable phase, hcp-Be, has a low Fermi-level density of states and very anisotropic structural and elastic properties, similar to a semiconductor's. At the Be(0001) surface, surface states drastically increase the Fermi-level density of states. The different nature of bonding in bulk-Be and at the Be(0001) surface explains the large outward relaxation (ca. 3% according to our LDA-total energy calculations) in the presence of a large tensile stress ( $0.2 \text{ eV}/\text{\AA}^2$ ).

We have calculated the energy of H/Be(0001) at different coverages and various geometries. For coverages  $< 1/2 \text{ ML}$ , H atoms sit in 3-fold hcp sites which are separated by a barrier of  $\leq 0.2 \text{ eV}$ . The low T phase will therefore be disordered at 300 K, which explains the experimentally observed  $1 \times 1$  surface state dispersion. At higher H-coverages the dilute phase will coexist with two condensed phases of novel adsorption geometry: H-atoms sit on tilted bridge sites, next to Be vacancies. At  $2/3 \text{ ML}$ , H adopts a  $1 \times 3$  structure, in which every third row of Be surface atoms is missing. At  $1 \text{ ML}$  the stable structure has a  $\sqrt{3} \times \sqrt{3} R30^\circ$  unit cell with the Be surface atoms forming a honeycomb lattice. In both H-induced vacancy structures the H atoms are particularly close to the surface so that the H-H repulsion is especially low. Additionally the Fermi-level density of states at the surface is efficiently quenched, i.e., the near covalent bonding of bulk Be is recovered for the H-covered surface. We discuss the energetics of the H-induced vacancy structures in terms of the vacancy formation energy of the clean surface.

<sup>†</sup>Work supported in part by US-DOE under contract DE-AC04-94AL85.

8:40 am **SS1-FrM2 Core-Level Spectroscopy of Metal Monolayers and Interfaces, N. D. Shinn<sup>1</sup>, B. Kim<sup>2</sup>, K. J. Kim<sup>3</sup>, T.-H. Kang<sup>2</sup>, and J. L. Erskine<sup>4</sup>,** (1) Sandia National Labs., Albuquerque, NM 87185-0344; (2) Pohang Univ. of Science and Technol., Pohang 790-784, Korea; (3) Dept. of Physics, Kon-Kuk Univ., Seoul 133-701, Korea; (4) Dept. of Physics, Univ. of Texas, Austin, TX 78712.

The electronic, chemical and mechanical properties of ultra-thin-film and metal-multilayer structures are largely determined by the electronic structure at the heterogeneous interface. For epitaxial interfaces, substrate atoms in the bulk and at the interface have geometrically equivalent coordination spheres; hence the interface-atom core-level shifts are a measure of only the local bonding between the dissimilar metals, mediated by final state screening effects of the photoemission process itself. Using monochromatized soft X-ray synchrotron radiation, we have obtained high-resolution  $W(4f_{7/2})$  photoemission spectra ( $\Delta E = 100 \text{ meV}$ ) from M/W(110) interfaces, where M = Fe, Ni, Pd, Pt, Cu, Ag, and Au. By rigorous Doniach-Sunjic lineshape deconvolution methods, we can determine and compare the  $W(4f_{7/2})$  binding energy shifts for the single layer of interface tungsten atoms at these isostructural interfaces. Systematic  $W(4f_{7/2})$  core-level shifts are found that, in many cases, follow expectations based upon bulk electronegativities, i.e., there is no anomalous "charge transfer" between metals as proposed by others [1]. However, we show that for other bi-metallic interfaces this correlation with electronegativities breaks down, thereby invalidating a simple "charge-transfer" interpretation of core-level shifts at bi-metallic interfaces.

[1] J. A. Rodriguez and D. W. Goodman, *Science* **257**, 897 (1992). Work performed at the NSLS and supported by DOE-BES under contract DE-AC04-94AL85000 with Sandia, the NSF under contract DMR93-03091 with U. Texas, and by the user program of the Pohang Light Source.

9:00 am **SS1-FrM3 Core Level Shifts in Trimetallic Systems, Darrell R. Rainer, Jason S. Corneille, and D. Wayne Goodman,** Department of Chemistry, Texas A&M University, College Station, Texas 77843-3255.

Recent XPS and CO chemisorptive studies of metal overlayers vapor deposited on metal single crystal surfaces to form bimetallic systems have indicated a correlation between observed electronic and chemical properties. Trimetallic surfaces consisting of various combinations of Cu, Pd, Ag, and Au supported on a Mo(110) single crystal, prepared in the above manner, have been studied using X-ray photoelectron spectroscopy (XPS) and ion scattering spectroscopy (ISS). Because the dissimilar second layer can be resolved from the bulk substrate with XPS, this approach allows the core level shifts (CLS) for the first and second layers in the trimetallic system to be measured. With its superb surface sensitivity, ISS was employed to measure the relative surface composition of the sample in order to determine the degree, if any, to which the deposited metals mixed. This revealed, for example, that upon sequential adsorption of monolayers of Pd and Cu followed by annealing, Pd segregated to the surface, even though it binds more strongly to the Mo(110) substrate than does Cu. For the Pd(1.0 ML)/Cu(1.0 ML)/Mo(110) system, the observed CLS's for Pd and Cu were consistent with the simple charge transfer model previously advanced regarding electron donor-electron acceptor interactions in bimetallic surfaces. Similar studies were performed on Ag/Cu, Au/Cu, Au/Pd, and Ag/Au overlayers deposited on Mo(110).

9:20 am **SS1-FrM4 Substrate Core-Level Response to Nucleation and Growth of Ultra-Thin Ni Films on W(001), S. H. Overbury, D. R. Mullins, P. F. Lyman,** Oak Ridge National Laboratory, Oak Ridge, TN 37831-6201, **N. D. Shinn,** Sandia National Laboratories, Albuquerque, NM 87185-0344.

Core level binding energies are sensitive to electronic changes associated with intermetallic bonding and alloying at bi-metallic interfaces. By combining  $W 4f_{7/2}$  photoemission and alkali ion scattering studies of Ni overlayer growth on W(001), we have tested the sensitivity of core-level binding energies to known structural and compositional changes at the interface. Deposition and annealing of sub-monolayer coverages of Ni yields a rippled, alloyed layer pseudomorphic to the W(001) substrate. At  $1 \text{ ML}$  coverage, a pure, stable Ni layer is formed. The Ni-W interplanar spacing is less than that of bulk W(001). A second pseudomorphic layer of pure Ni grows upon the first, but 3-D Ni islands are nucleated at higher coverages in Stranski-Krastanov growth. High resolution, surface sensitive  $W 4f_{7/2}$  spectra were obtained at the NSLS following deposition at 300 K, and after annealing to elevated temperatures. Instrumentally broadened Doniach-Sunjic lineshapes were fit to the measured spectra. These components are associated with surface, sub-surface, bulk and interface W atoms. Specific binding energies are found for W atoms at the Ni interface in the  $1\text{--}2 \text{ ML}$  regime and for W atoms beneath the 3-D islands at higher coverages.

Research sponsored by DOE-BES Chemical Sciences, (DE-AC05-84OR21400) and DOE-BES Materials, Sciences (DE-AC04-94AL8500).

9:40 am **SS1-FrM5 Nature of the 4s-Derived States of Adsorbed K Studied by X-Ray Absorption Spectroscopy and the Core Hole Clock Method, A. Sandrell, A. Nilsson, P. A. Brühwiler, and N. Mårtensson,** Department of Physics, Uppsala University, Box 530, S-751 21 Uppsala, Sweden.

The local properties of the K 4s-substrate bonding in the low coverage limit has been studied for a number of substrates. Using the fact that the final state of a core excited Ar-atom is similar to K (the  $Z+1$  approximation), core excitation and decay spectra of adsorbed Ar provide information of the nature of the empty states in adsorbed K. X-ray absorption gives the energy position of the 4s resonance whereas a measure of the alkali-substrate hybridization strength is obtained by the core hole clock method. We find large variations depending on the choice of substrate. For K/graphite, the 4s resonance is situated clearly above  $E_F$ , showing weaker hybridization in the 4s-substrate bonding than for the metallic substrates. This is taken as evidence for a more ionic bonding. In the presence of a neighboring K-atom, the 4s level moved to a position just below  $E_F$  as expected. On metallic substrates (Pt(111), Au(110), Cu(100) and Ag(110)) there is a clear tendency for increased covalency of the K 4s-metal bonding as the substrate work function decreases, which is in accordance with the



Gurney-model. The increased covalency is characterized by a shift of the 4s resonance towards  $E_F$ , a distortion of its lineshape and a steady increase in the charge transfer rate. The K 4s-substrate bonding is, however, still considered to be primarily ionic for all the studied systems, since the main part of the 4s resonance is situated above  $E_F$ .

10:00 am **SS1-FrM6 Photoemission Study of Alkali Metal Adsorption on the Passivated Si(111)1 × 1-As Surface**, *M. C. Håkansson, M. Johansson, and L. S. O. Johansson*, Department of Synchrotron Radiation Research, Institute of Physics, University of Lund, Sölvegatan 14, S-223 62 Lund, Sweden.

We have studied potassium adsorption on the Si(111)1 × 1-As surface with angle-resolved photoemission and core-level spectroscopy. The As-terminated Si(111) surface is well known for its ideal bulklike termination of the Si lattice, as well as for its passivated nature. The electronic structure of the surface is dominated by the filled lone-pair state near the valence band edge and an empty state close to the conduction band edge, with no electronic states in the fundamental bandgap.

Deposition of small amounts of K on the surface led to an abrupt shift in the Fermi level position and to the occupation of the minimum of the empty state. This state showed up as a sharp peak at the Fermi level near the surface Brillouin zone boundary at the  $\bar{M}$  point, as expected from quasiparticle band structure calculations. This allowed us to determine the surface band gap to 1.7 eV, in good agreement with calculations.

In the core-level spectra from the surface after K deposition, large K-induced shifts were observed. In the As 3d spectra a new component at 1.1 eV lower binding energy emerged, whereas in the Si 2p spectra a K-induced peak was found at higher binding energy. This indicates significant charge rearrangements in the surface layer as a result of the K adsorption.

These results are very different from previous core-level studies of alkali adsorption on clean Si surfaces, where generally only small shifts in the Si 2p level have been seen.

10:20 am **SS1-FrM7 Spectroscopic Characterization of Unique Electronic and Catalytic Properties of Vanadium Carbide Films on V(110)**, *J. G. Chen, B. Frühberger and B. D. DeVries*, Corporate Research Laboratories, Exxon Research and Engineering Co., Annandale, NJ 08801.

One of the most intriguing aspects of early transition-metal carbides is that they often show electronic and catalytic properties similar to those of platinum-group metals. In an attempt to understand the fundamental correlation between the electronic and catalytic properties of this important class of materials, we have chosen vanadium carbide films on a vanadium (110) surface as model systems for our experimental investigations. By using HREELS and NEXAFS, we determine that the electronic properties of vanadium, especially the characteristics of the d-orbitals, are substantially modified by the formation of carbides. We detect a charge transfer from vanadium to carbon, with approximately 1.3 electrons/per vanadium, as a result of C-V bond formation. Such an electronic modification in turn gives rise to unique catalytic properties. For example, by using carbon monoxide and ethylene as probing molecules, we observe a strong similarity between the surface reactivities of carbide-modified V(110) and platinum-group metals. These results can be explained by a narrowing of the d-orbitals in vanadium carbide and therefore a less d- $\pi^*$  interaction. More interestingly, we observe that the formation of carbide has opposite effects on the selective activation of C=C and C-H bonds, based on a comparative study of reactivities of several saturated and unsaturated C<sub>4</sub> molecules with clean and carbide-modified V(110) surfaces. Our results indicate that, although the formation of carbide reduces the decomposition probabilities of C=C bonds, it selectively enhances the activation of C-H bonds. These observations will be explained by comparing the different roles of  $\sigma$ - and  $\pi$ -type orbitals in the decomposition of C-H and C=C bonds on transition metal surfaces. These results represent the first experimental study of hydrocarbon chemistry on clean and carbide-modified vanadium surfaces.

10:40 am **SS1-FrM8 Electronic Transitions and Excitations in Solid C<sub>70</sub> Studied by HREELS and XPS C1s Shakeup Structures**, *B. Y. Han, L. M. Yu, K. Hevesi, G. Gensterblum, P. Rudolf, J.-J. Pireaux, P. A. Thiry, R. Caudano*, Laboratoire Interdisciplinaire de Spectroscopie Electronique, Institute for Studies in Interface Sciences, Facultés Universitaires Notre-Dame de la Paix, B-5000 Namur, Belgium.

The electronic transition and excitation properties of highly ordered C<sub>70</sub> films grown on lamellar substrates MoS<sub>2</sub>(0001) and GeS(001) have been studied by means of High Resolution Electron Energy Loss Spec-

trospectroscopy and XPS C1s shakeup structures. From the HREELS study, a total of eleven features were observed in the energy loss range 1–30 eV. These include the lowest electronic excitation ever observed in C<sub>70</sub> fullerite, a peak at 1.53 eV loss energy, assigned to a Frenkel-type molecular exciton; the double peak at 5.1 eV and 5.9 eV corresponding to the two split levels of the  $\pi$ -plasmon of C<sub>70</sub> induced by its lower symmetry compared to C<sub>60</sub>. Other features reflect  $\pi$ - $\pi^*$  or  $\sigma$ - $\sigma^*$  transitions. A broad hump at ~28 eV corresponds to the  $\sigma$ -plasmon. In XPS ( $h\nu$  = 1486.6 eV, instrumental resolution 0.3 eV) C1s shakeup structures, several features (out of a total of seven within 30 eV from main C1s line) find their counterparts in the HREELS spectra. A prominent peak at ~2.5 eV, present in both spectra, appears to reveal the fundamental gap (exempt of the off-site correlation effect) in C<sub>70</sub> fullerite. Two plasmon peaks, at ~6 eV and ~27 eV, are also present. A few weak features were resolved for the first time, thanks to the high energy resolution of our SCIENTA ESCA-300 instrument.

11:00 am **SS1-FrM9 Inverse Photoemission Study of CO Chemisorption on Metallic Quantum Wells**, *F. G. Curti, R. A. Bartynski*, Rutgers University, Department of Physics and Astronomy and Laboratory for Surface Modifications, Rutgers, The State University of New Jersey, Piscataway, NJ 08855.

We have used isochromat inverse photoemission spectroscopy to study the chemisorption of CO on Cu/fccCo/Cu(100) and fccCo/Cu(100) layered structures. Under optimal growth conditions, these systems exhibit metallic quantum well (MQW) states in the region of the Fermi level.<sup>1</sup> Upon chemisorption of CO at 140 K a c(2 × 2) LEED pattern forms on all Cu/fccCo/Cu(100) structures studied. A modification in the first MQW state takes place on adsorption of 1 ML of CO and it is no longer observed in inverse photoemission. A shift to lower energies of the CO derived peaks also occurs. The chemisorption behavior of the Cu overlayers, a weak chemisorption system, will be contrasted with that of the more strongly interacting Co overlayers. The change in the density of states in the region of the Fermi level will be related to changes in both the electronic interaction and thermal desorption properties of the CO/metallic quantum well systems.

<sup>1</sup>J. E. Ortega and F. J. Himpsel, Phys. Rev. Lett. 69, 844 (1992).

11:20 am **SS1-FrM10 A Core Level Spectroscopy Study of Different Adsorption States of Ethylene on Pt(111)**, *B. Hernnäs, A. Nilsson, O. Karis, C. Puglia, A. Sandell and N. Mårtensson*, Dept. of Physics, Uppsala University, Box 530, S-751 21 Uppsala, Sweden.

We have studied the C<sub>2</sub>H<sub>4</sub>/Pt(111) system by means of core level spectroscopies, such as x-ray photoelectron spectroscopy (XPS), x-ray absorption spectroscopy (XAS) and deexcitation electron spectroscopy (DES also denoted resonant Auger). Three different temperature phases were studied; monolayer at 30 K, monolayer at 90 K and the high temperature phase at 300 K where a 2 × 2 ethylidyne phase forms. In the 90 K state, XPS intensities of C1s and the Pt 4f surface core level shifted components a bridge adsorption site can be derived i.e. as denoted di- $\sigma$  configuration. This is consistent with a strong modification of the  $\pi$  intensity in XAS. The 30 K monolayer phase, that earlier has been suggested to contain only  $\pi$  bonded molecules, has shown to be a mixture of two differently adsorbed ethylene species. One with the earlier proposed  $\pi$  bonding configuration, and the second, which is weakly adsorbed with a standing up configuration. The latter one clearly shows that an intact  $\pi^*$  orbital, i.e. this orbital does not participate in the bond to the surface. It is a higher lying orbital that hybridizes with the surface and thereby creates the chemisorption bond. Also the ethylidyne species that is created on this surface has been studied, and we present a new way of interpreting the XAS spectra for this species. Furthermore, coverage measurements using the C1s and Pt 4f core level lines suggest domains of 2 × 1 structure with a coverage of 0.41 ± 0.05.

11:40 am **SS1-FrM11 The Auger Relaxation of <sup>37</sup>Cl following Electron Capture Decay of <sup>37</sup>Ar\***, *L. Zhu, R. Avci, G. J. Lapeyre*, Montana State University, *M. M. Hindi, R. L. Kozub, S. J. Robinson*, Tennessee Technological University.

We developed an experimental system to study the Auger relaxation process following the <sup>37</sup>Ar → <sup>37</sup>Cl +  $\nu$  electron capture (EC) decay. A mixture of 5 × 10<sup>-5</sup> parts <sup>37</sup>Ar and one part <sup>36</sup>Ar is physisorbed on a flat cold substrate kept at 16 K under UHV conditions. Using time of flight and coincidence technique we, for the first time, measured the energy dependence of the probability distribution for one of the two electrons emitted as a result of double Auger process. The two electrons share the total energy with one of the electrons prefers to have the most of the energy, which agrees with the theoretical prediction<sup>1</sup>. Using



a cylindrical mirror analyzer (CMA), we also measured the kinetic energy distribution of the regular LMM Auger electrons following the EC decay. We observed a sharp Auger peak at  $\sim 193$  eV which does not appear in any known Ar or Cl Auger data. We believe that this extra feature is due to the particular initial state configuration with one hole in the K-shell produced by the EC decay process.

\*Work supported by USDOE Grant No. DE-FG05-87ER40314 (TTU) and by NSF Grant No. DMR 91-07854 (MSU).

<sup>†</sup>M. Ya. Amusia, I. S. Lee, and V. A. Kilin, Phys. Rev. A **45**, 4576, (1992).

## SURFACE SCIENCE

### Room A201 - Session SS2-FrM

#### Group IV Semiconductor Surface Structure

**Moderator:** R. Hamers, University of Wisconsin.

8:20 am **SS2-FrM1 New Method for Empirically Determining Surface Electronic Species from Multiple-Bias STM Images: A Multivariate Classification Approach**, A. M. Bouchard, G. C. Osbourn, and B. S. Swartzentruber, Sandia National Laboratories, Albuquerque, NM 87185-0350.

We introduce the use of multivariate image classification techniques in determining surface electronic structure from multiple-bias scanning tunneling microscope (STM) images. Multiple measurements at each site are used to distinguish and categorize inequivalent electronic or atomic species on the surface via a computerized classification algorithm. Then, comparison with theory or other suitably chosen experimental data enables the identification of each class. We demonstrate the technique by analyzing dual-polarity constant-current topographs of the Ge(111) surface. Utilizing no prior knowledge of the atomic structure of the surface, we find that the two measurements, negative- and positive-bias topography height, enable pixels to be separated into seven different classes. In order to assess the validity of our classifications and determine the identity of each class, we compare the results with the atomic structure of the  $c(2 \times 8)$  reconstruction of Ge(111). If we label four of the classes as adatoms, first-layer atoms, and two inequivalent rest-atom sites ( $R_3$  and  $R_4$ ), we find that our results are in very good agreement with the  $c(2 \times 8)$  structure. The remaining classes are associated with structural defects and contaminants. This work represents the first step towards developing a general electronic/chemical classification and identification tool for multispectral scanning probe microscopy imagery.

This work was supported by the U.S. Department of Energy under contract DE-AC04-94AL85000.

8:40 am **SS2-FrM2 High Resolution TEM Determination of the  $(5 \times 2)$  Au/Si(111) Structure**, R. Plass and L. D. Marks, Dept. of Mat. Sci. and Eng., Northwestern Univ., 2225 North Campus Drive, Evanston, IL 60208.

Among the numerous unsolved metal semiconductor interfaces the submonolayer gold on silicon (111) system is of interest as it displays a linear  $5 \times 2$  surface structure between .1 and .5 monolayers of metal coverage. Recent x-ray diffraction and high resolution STM studies have yielded new information about this structure, yet the placement of the gold atoms remains unclear [1, 2]. We present here a solution for this structure found using off-axis plan view high resolution transmission electron microscopy and digital image restoration.

Si(111) TEM samples were prepared by ion sputter cleaning and electron beam annealing cycles in ultrahigh vacuum conditions to obtain fairly flat  $7 \times 7$  reconstructed surfaces. Approximately .4 ml of gold was evaporated onto the top surface of the sample followed by annealing to produce the  $5 \times 2$  structure. A ten member 250kV off zone high resolution through focal series was taken, digitized, and analyzed using Wien and Schiske filters and a Chi-squared form of the Schiske filter to obtain the atomic potential map.

The proper analysis of the HREM data requires the  $1 \times 1$  and bulk spacings, omitted in the x-ray diffraction study, be included and gives a simple result: two gold atoms have a spacing near-coincident with the silicon  $1 \times 1$  spacing. This interpretation is supported by diffraction patterns which show that in near kinematical diffraction conditions

the  $1 \times 1$  and bulk diffraction spots are always the strongest set of spots in the pattern. Further details of atomic structure will be presented.

1. C. H. Schamper et al, Phys. Rev. B **43** (1991) 12310.

2. J. D. O'Mahoney et al, Surf. Sci. Lett. **277** (1992) L51.

9:00 am **SS2-FrM3 FT-IRAS of Adsorbed Alkoxides: Methoxide and Ethoxides on Cu(111)**, Shane C. Street, University of Illinois Urbana-Champaign 61801, and Andrew J. Gellman, Carnegie Mellon University, Pittsburgh, PA 15213.

The surface chemistry and structure of methoxide and ethoxide adsorbed on Cu(111) has been studied by FT-IRAS and TPD. The structure of methoxy on Cu(111) has been a matter of debate. Previous IRAS results were interpreted to show that the  $C_{3v}$  axis of methoxy at saturation coverage lies perpendicular to the surface. Subsequent X-ray diffraction and backscattering photoelectron diffraction experiments support this orientation. However recent work with methoxy cluster compounds has led to the proposal that at low coverages methoxy is tilted, and that steric crowding reorients the molecular axis towards the surface normal at saturation. We present high resolution spectra for methoxy at a range of coverages. For the more complex ethoxy adsorbate we present the FT-IRAS spectra for a set of seven deuterated and isotopically ( $^{13}C$ ) labelled ethoxides. This is by far the most detailed labelling study to assign vibrational modes of an adsorbate. The  $C_{3v}$  axis of the methyl group of ethoxy is found to lie roughly parallel with the surface.

9:20 am **SS2-FrM4 Boron Induced Structures on the Si(111) Surface**, C. Wang, T. C. Shen, J. W. Lyding and J. R. Tucker, University of Illinois at Urbana-Champaign, Urbana, IL 61801.

It has been known that B-saturated Si(111) surface will be  $(\sqrt{3} \times \sqrt{3})R30^\circ$  reconstructed. It is not clear, however, how the transition from the B-free  $7 \times 7$  surface to the B-rich  $\sqrt{3}$  surface occurs. We have used STM to study the boron-doped Si(111) surface as a function of annealing times and temperatures. The surface structure is found to be determined by the concentration of B. When the substitutional B concentration is less than 1% of the top  $1 \times 1$  bi-layer atoms, the surface is largely  $7 \times 7$  but surrounded by adatom-covered  $1 \times 1$  regions (which have higher B concentration). When the B concentration is more than 3%, the whole surface will be adatom-covered  $1 \times 1$  including  $\sqrt{3}$  structures. The  $\sqrt{3}$  domains will increase with the B concentration. The effect of the surface B on  $7 \times 7$  growth is hence deduced. Rows of the  $7 \times 7$  domain preferentially grow along the 3 equivalent  $[112]$  directions. The adatom-covered  $1 \times 1$  regions are bounded by faulted halves of the  $7 \times 7$  domains. The domain size of  $7 \times 7$  or  $9 \times 9$  can be as small as a faulted half of a unit cell. The energy relations and the transition temperatures between the  $2 \times 2$ ,  $c(4 \times 2)$ ,  $7 \times 7$  and  $9 \times 9$  reconstructions are discussed. The dark sites of  $7 \times 7$  are observed and counted. They are further interpreted in terms of a B substitution model. The pattern of bright and dark atoms in  $\sqrt{3}$  domains is analyzed and a criterion for a B stabilized Si- $\sqrt{3}$  structure is obtained.

Supported by the Office of Naval Research URI:N00014-92-J-1519.

9:40 am **SS2-FrM5 Surface-Induced Optical Anisotropies of Single-Domain  $(2 \times 1)$ -Reconstructed (001) Si and Ge Surfaces**, L. Mantese, T. Yasuda, and D. E. Aspnes, North Carolina State University, Raleigh.

Above-bandgap surface-induced optical anisotropy (SIOA) is becoming increasingly important in elucidating the electronic structure of non-uhv surfaces and interfaces, yet the accurate theoretical calculation of SIOA spectra remains a difficult challenge. To provide an opportunity for critically testing theoretical approaches, we have performed SIOA measurements on clean and oxygen-exposed single-domain  $(2 \times 1)$  reconstructions of (001) Si and Ge from 1.5 to 5.5 eV using reflectance-difference spectroscopy (RDS). Single-domain surfaces were obtained by heating chemically cleaned vicinal wafers cut  $4^\circ$  off [001] toward [110] in uhv, and were assessed by in situ Auger and LEED. The clean  $(2 \times 1)$  Ge surface exhibits two broad peaks at 1.8 and 3.1 eV, while the Si surface shows a relatively sharp peak at 3.4 eV and broader features at higher energy. By exposing the surface to oxygen and analyzing the resulting LEED patterns, we separate the individual SIOA contributions from dimers and steps. Only dimers contribute to the Ge spectra, whereas both dimers and steps contribute to Si. The  $(2 \times 1)$  Si spectrum disagrees with published calculations

not only in lineshape but also by nearly an order of magnitude in amplitude, suggesting the importance of these results in critically testing theoretical models.

\*Supported by ONR Contract N-00014-93-1-0255.

**10:00 am SS2-FrM6 High-Temperature Structural Phases of the Si(111) Surface Studied with High-Resolution Energy-Resolved Helium Atom Scattering, C. A. Meli, Naval Research Laboratory, Washington, DC 20375 (USA); G. Lange and J. P. Toennies, Max-Planck-Institut für Strömungsforschung, 37073 Göttingen (Germany).**

The structure of the Si(111) surface in the temperature range 900–1550 K has been investigated using high-resolution thermal-energy helium atom scattering with energy resolution. The well-known  $7 \times 7$  to  $1 \times 1$  transition near 1140 K was confirmed by the loss of all fractional-order diffraction peaks, as well as sharp changes in the intensity of all integral-order diffraction peaks. An additional order-disorder transition occurring near 1410 K was unequivocally confirmed by the loss of all integral-order diffraction peaks above this temperature. Measurements of the thermal attenuation of diffraction peaks, hysteresis of peaks through the phase transition region, relative disorder, and inelastic scattering over the entire high-temperature range were performed. These results will be discussed in light of possible models of the Si(111) structure above 900 K, and in relation to the high-temperature behavior of related surfaces.

**10:20 am SS2-FrM7 Two-Dimensional Surface Interactions and Dynamics of Benzene on Cu{111}, M. M. Kamna, S. J. Stranick, and P. S. Weiss, Department of Chemistry, The Pennsylvania State University, University Park, PA 16802.**

We seek to understand the interactions that determine the chemistry, structure, and dynamics of surface adsorbates. We have used ultrahigh vacuum scanning tunneling microscopy to study the low temperature behavior of benzene adsorbed on Cu{111}. Electron standing waves are apparent in STM images of Cu{111} at low temperature due to scattering of surface states from step edges, defects, and benzene molecules. The resulting charge density modulations influence the binding of the benzene molecules. We find that at low coverage, adsorbed benzene binds along Cu step edges and at other high charge density sites. The molecules form a tightly bound 2-D solid at the step edges while benzene molecules on terraces move across the surface as a 2-D molecular gas. At the interface between the solid and gas we observe 2-D adsorption and desorption in real time. We discuss the relative strengths of the interactions at various step and terrace sites due to these nanometer scale variations in the surface electronic structure.

This work was supported by BRDC, NSF, and ONR.

**10:40 am SS2-FrM8 Strain-induced Surface Morphology on Si(111)- $(7 \times 7)$ , Y. Wei, L. Li and I. S. T. Tsong, Arizona State University, Tempe, AZ 85287.**

A special strain stage was designed for a scanning tunneling microscope (STM) to apply an isotropic tensile stress on a Si(111) surface at elevated temperatures. After straining, the surface was allowed to cool to room temperature and STM images of the strained surface were taken. Glide steps along  $\langle 110 \rangle$  directions with single atomic layer height of  $3.1 \text{ \AA}$  were observed. These steps could be easily distinguished from the normal wandering single-steps on the (111) surface by their linearity over large distances and their alignment with the  $\langle 110 \rangle$  directions. At some of the intersections between a glide step and a normal step, or between two glide steps, "kissing" sites were formed. The glide steps were determined to be caused by slips of {111} planes intersecting the (111) surface. Despite the application of  $\sim 1\%$  isotropic strain, the anticipated  $(5 \times 5) \rightarrow (7 \times 7)$  phase transition was not observed on the Si(111) surface because the strain was taken up by the slippage of {111} planes occurring in the bulk.

**11:00 am SS2-FrM9 A Novel Facet Reconstruction of Si(112) Revealed by STM, A. A. Baski and L. J. Whitman, Naval Research Laboratory, Code 6177 Washington, DC 20375.**

Si(112) has attracted attention as a potential substrate for electronic devices due to its large vicinality. [It is a (111) surface "miscut" by  $19.5^\circ$ .] The ideally terminated surface would consist of short (111) terraces separated by monoatomic-height steps running along the  $[1\bar{1}0]$  direction (unit cell =  $9.4 \text{ \AA}$   $[111] \times 3.84 \text{ \AA}$   $[1\bar{1}0]$ ). In contrast, our STM images reveal that the surface has a sawtooth-like morphology,

with upward-sloping, 50–100  $\text{\AA}$ -wide terraces oriented  $4\text{--}5^\circ$  steeper than the (112) plane and downward-sloping, relatively short regions. The dominant, upward terraces consist of a periodic arrangement of bright rows oriented along  $[1\bar{1}0]$  with an inter-row spacing of  $\sim 16 \text{ \AA}$  along  $[111]$ . To maintain the net sample orientation, the upward terraces are broken up by a variety of downward-sloping structures, including short reconstructed (111) terraces, disordered multiple step bunches and other types of terrace reconstructions oriented toward the (111) plane. A quantitative analysis of the STM images indicates that the upward faceted terraces are  $(337)$  planes: a plane tilted  $23.5^\circ$  away from the (111) surface with a  $[111]$  unit cell length of  $15.7 \text{ \AA}$ .

We have also investigated the atomic-scale structure of this surface by acquiring high-resolution images. Atomic corrugations occur along the bright rows with a  $1a$  ( $3.84 \text{ \AA}$ ) periodicity in the  $[1\bar{1}0]$  direction. Other surface features include dim rows located adjacent to the dominant bright rows and bright protrusions ( $\sim 10 \text{ \AA}$  dia.) located between the periodic row structures. Models of this surface incorporating both the observed atomic-scale structures and the facet reconstruction will be discussed.

**11:20 am SS2-FrM10 Structural Determination of the Dimerized Si(100) Surface, Y. Olan, M. J. Bedzyk, G. E. Franklin, S. Tang and A. J. Freeman, Argonne National Lab and Northwestern University, Argonne, IL 60439.**

The atomic structure of Ga chemisorbed on the Si(100)  $2 \times 1$  surface at low coverage has been studied by a combination of X-ray standing wave (XSW) measurements and molecular cluster total energy calculation. For various Ga coverages below  $1/2 \text{ ML}$ , the Ga ad-dimer is found to be  $1.03 \pm 0.01 \text{ \AA}$  above the Si(400) diffraction plane. The measured Ga ad-dimer bond length is  $2.50 \pm 0.06 \text{ \AA}$ , which matches the covalent bond length of gallium. By comparing experimental results with the theoretical calculation, we conclude that the Ga ad-dimers are oriented parallel to the underlying Si dimers, which is consistent with a previous total-energy calculation. This parallel dimer geometry is in contrast to the orthogonal dimer model proposed by previous LEED, AES, and STM studies. Our measurement is the first experimental confirmation of this parallel Ga ad-dimer model.

This work was sponsored by the U.S. Department of Energy, Office of Basic Energy Sciences, Division of Materials Sciences, under contract W-31-109-ENG-38.

**11:40 am SS2-FrM11 Fluctuations of Monatomic Steps on Si(001), H. J. W. Zandvliet and B. Poelsema, Faculty of Applied Physics, University of Twente, P.O. Box 217, 7500 AE Enschede, The Netherlands; H. B. Elswijk, Philips Research Laboratories, P.O. Box 80.000, 5600 JA Eindhoven, The Netherlands.**

The motion of monatomic steps on Si(001) is studied on an atomic scale at elevated temperatures with scanning tunneling microscopy. The kinks in the step edges move in units of 2 dimers alongside the monatomic A-type step edge and perpendicular to the monatomic B-type step edges. The overall time dependencies of the equilibrium step fluctuations of A- and B-type step edges were found to be both proportional to the square root of time but with different prefactors for the different steps. The fluctuations of long kinks in the B-type step edge are however much larger and exhibit initially a more t-like dependence, i.e. one-dimensional random walk behavior. Both time dependencies can be understood in terms of the Langevin equation.

## NANO 3/NANOMETER-SCALE SCIENCE AND TECHNOLOGY

**Room A209 – Session NS1-FrM**

### Novel Materials and Methods for Nanofabrication

**Moderator:** Y. Kuk, Seoul National University, Korea.

**8:20 am NS1-FrM1 Chemistry and Applications of Self-Assembled Films, Jeffrey M. Calvert, Center for Bio/Molecular Science & Engineering (Code 6900), Naval Research Lab, Washington, DC 20375-5348.**

Precise positional control of surface chemical functionalities and physical properties such as wetting can be obtained by direct patterning of organosilane self-assembled (SA) monolayer films with lithographic

exposure tools. A variety of transformations have been investigated for film irradiated with deep UV photons, x-rays, ions, and low energy electrons. Patterned SA film surfaces have been used as a template of reactivity for selective deposition, attachment, and orientation of a wide variety of materials to surfaces including catalysts, electroless and CVD metal films, proteins, cells, nucleic acids, and liquid crystals. Selectively metallized, patterned SA films have been produced with linewidths to 20 nm using STM lithography, and high resolution metal patterns have also been used to fabricate functioning electronic test structures. The utility of patterned SA films for microelectronics, sensors, displays, and other applications will be discussed.

#### INVITED

9:00 am **NS1-FrM3 Preparation and Characterization of Highly Organized Self-Assembled Monolayers as Substrates for Nanoelectronics**, C. W. Sheen, A. N. Parikh and D. L. Allara, Department of Materials Science, Pennsylvania State University, University Park, PA 16802; M. J. Lercel and H. G. Craighead, School of Applied and Engineering Physics, Cornell University, Ithaca, NY 14853.

Self-assembled monolayers have been prepared on a variety of substrates for the purpose of ultrahigh resolution electron-beam lithography and etching of features in the substrate. The major emphasis has been on maximizing the density of the films in order to maximize the etch resistance. Film stability has been designed by utilizing both direct chemical bonding to the substrate and film crosslinking. For GaAs(100), film formation was accomplished by reactions with octadecanethiol. X-ray photoemission data show that an oxide-free, S-GaAs interface is formed. For  $\text{TiO}_2$  and  $\text{SiO}_2$ , films were formed using octadecyltrichlorosilane and the highest degree of organization was obtained by decoupling the film from the substrates by ultrathin water films. In these cases the high stability is due to intermolecular crosslinking. Characterization of the molecular structure using infrared spectroscopy and ellipsometry show that the molecules are highly oriented and densely packed and thus quite suitable as etch resists.

This work was sponsored by the Advanced Research Projects Agency ULTRA program.

9:20 am **NS1-FrM4 Nanometer Resolution Near-field Optical Lithography**, M. Rudman, A. Shchemelinin, K. Lieberman and A. Lewis, Hebrew University of Jerusalem, Department of Applied Physics, Givat Ram Campus, 91904 Jerusalem, Israel.

In this work we develop and present results on a new method of optical lithography which can write structures with a resolution that is normally associated with electron beam techniques. This method is based on near-field optics, which involves illuminating a substrate with a subwavelength aperture that is maintained above the surface at a height of a few hundred Angstroms. The spot of light thus created corresponds to the dimension of the aperture rather than the wavelength of the light. In this paper we combine the methods of near-field optics with the capability of an argon fluoride (ArF) excimer laser to ablate materials without heating. Specifically, our method involves passing the deep ultraviolet wavelength of the 193 nm ArF excimer laser through a hollow glass micropipette that can be readily drawn with heat to an aperture at the tip as small as a few nanometers. We describe an instrument which incorporates lateral atomic force feedback to track such a micropipette over an arbitrary surface with nanometer accuracy. We present results of patterns that have been produced on photoresists and other substrates with linewidths that are as small as 50–70 nm. By investigating the dimensionality of the structures drawn on the photoresist and on the substrate on which the photoresist was deposited, it appears that nonlinear characteristics of the ablation process may allow the near-field dimensionalities to be maintained at distances that are relatively remote from the tip of the pipette aperture.

9:40 am **NS1-FrM5 Fabrication of 10nm Holes on a 20nm Hexagonal Lattice in Si(100)**, T. A. Winningham,\* J. T. Moore,\* S. D. Williams,\* K. Douglas,\* D. Choutov,<sup>†</sup> J. D. Piper,<sup>†</sup> K. P. Martin,<sup>†</sup> H. P. Gillis,<sup>†</sup> \*Department of Physics, University of Colorado, Boulder, CO 80309-0390, <sup>†</sup>School of Chemistry and Microelectronics Research Center, Georgia Institute of Technology, Atlanta, GA 30332-0400.

Using a biological template and Low Energy Electron Enhanced Etching (LEEEE), we have fabricated a nanometer-scale hexagonal array of holes in Si(100). The holes are 10nm in diameter with a lattice constant of 20nm, and have been etched to depths approaching 10nm.

The biological template (S-layer) is fixed on the Si substrate with an organosilane adhesion promoter and metal-shadowed with 12 Å of

Ti, which oxidizes to 35 Å of  $\text{TiO}_2$ . Ion milling transfers the pattern of the template into the  $\text{TiO}_2$  overlayer, exposing the Si only at the holes of the template.<sup>1</sup> The  $\text{TiO}_2$  pattern is then transferred into the Si substrate by LEEEE in an  $\text{H}_2/\text{He}$  DC plasma, which inflicts minimal damage on the substrate.<sup>2</sup> In previous attempts at fabrication, ion milling and reactive ion etching (RIE) have either destroyed the ultrathin mask or shown low selectivity between mask and substrate. LEEEE leaves the mask intact while transferring the pattern to the substrate.

To evaluate the extent of etching, the samples have been examined with atomic force microscopy (AFM) before and after LEEEE. The etch rate, anisotropy, and quality of the Si surface will be described as functions of current density and gas composition. During etching, the  $\text{TiO}_2$  mask is chemically modified, and becomes difficult to image after etching. The implications of surface chemical modifications on AFM imaging will be discussed.

1 K. Douglas, G. Devaud, and N. A. Clark, *Science* **257**, 642 (1992).

2 H. P. Gillis, J. L. Clemons, and J. P. Chamberlain, *J. Vac. Sci. Technol. B* **10**, 2729 (1992).

10:00 am **NS1-FrM6 New Compound Quantum Dot Materials Produced by Electron-Beam Induced Deposition**, M. Weber, H. W. P. Koops\*, M. Rudolph, J. Kretz, and G. Schmidt\*\*, Institut für Angewandte Physik, Technische Hochschule Darmstadt, Schlossgartenstr. 7, D-64289 Darmstadt, Germany, \*Deutsche Bundespost Telekom, FTZ, Am Kavalleriesand 3, D-64295 Darmstadt, Germany, \*\*Institut für Anorganische Chemie, Universität Hamburg, Martin-Luther-King-Platz 6, D-20146 Hamburg, Germany.

Electron-beam induced deposition represents a new technology for production of nanoscale structures. Three-dimensional shapes can be obtained with nanometer accuracy, which may have impact on many applications in scanning probe microscopy or in vacuum microelectronics. The properties of the deposited material are determined by the precursor material as well as the deposition parameters. At certain conditions, the deposits of very different organometallic precursor molecules show similar morphologies. The metal content of those deposits is strongly dependent on the beam current and the energy of the primary electrons. Using high beam currents and a power density of about  $50 \text{ MW cm}^{-2}$  for deposition a polycrystalline material is built up, consisting of single crystallites with diameters of 1–4 nm embedded in an amorphous carbon containing matrix. The distance between the metallic crystallites is in the Ångström range. Thus electrical conductivity of the material is accomplished by tunneling between the nanocrystallites. Wires built up from these materials are able to carry current densities up to  $2 \text{ MA cm}^{-2}$ . Several materials have been characterized by TEM, EDX, and electrical measurements.

10:20 am **NS1-FrM7 Synthesis of Polymers at Highly Ordered Pyrolytic Graphite Templates via Flow Injection Scanning Tunneling Microscopy**, M. L. Myrick, P. G. Van Patten, and J. D. Noll, Department of Chemistry and Biochemistry, University of South Carolina, Columbia, SC 29208 USA.

Highly Ordered Pyrolytic Graphite (HOPG) has step defects that are formed during the manufacturing process of the HOPG monochromator. If we derivatize these steps with functional groups that will react with the polymer, we can use the HOPG monochromator as a template to initiate the growth of a polymer at the nanometer scale. Recently, we have developed a method that will allow us to flow a solution over a surface while scanning with the Scanning Tunneling Microscope (STM). We can inject a reactant into an injector and watch the reactant hit the surface. The reactant flows out of the cell, and we can capture images of the surface before, during, and after the reaction. This Flow Injection Scanning Tunneling Microscopy (FISTM) technique allows us to inject the polymer and watch the polymer initiate and grow along the step of the HOPG. We show the initiation and growth of conducting polymers onto HOPG step defects.

10:40 am **NS1-FrM8 Nanoarchitectures of Poly(di-n-alkylsil-ylene)s**, S. Sheiko, H. Frey and M. Möller, Organische Chemie III/Makromolekulare Chemie, Universität Ulm, D-89069 Germany.

As a conceptual intermediate between linear hydrocarbons and bulk silicon, catena Si polysilylenes (PSi) demonstrate strong electro-optical activity with a possibility to tune the physical properties chemically. Due to encapsulating of a Si backbone in a shell of hydrocarbon side chains, the molecular properties of those polymers are strongly anisotropic. This forms a basis for well defined nanoarchitectures with electro-optical functions. In this report, novel techniques to fabricate

fibres and films of poly(di-n-alkylsilylene)s with controlled nanostructure will be demonstrated.

Fibres carrying highly oriented nanometer size domains of PSi were prepared by polyethylene gel crystallization and subsequent ultra-drawing. The resulting fibres exhibit linear optical activity and anisotropy of the radiation induced conductivity. Orientation in a polymer host enables to combine the one-dimensional photo- and semiconducting properties of PSi with good stability and processability of the polyethylene.

Submicrometer thick films of different PSi showing a high degree of order were obtained by crystallization on a special substrate. Well defined  $50 \times 500 \times 5000 \text{ nm}^3$  crystals of extended and uniaxially oriented PSi molecules were grown on 50 nm in diameter polytetrafluoroethylene fibres. Morphology and growth of these "hetero-shish-kebab" structures were examined by scanning force microscopy. Microlithography on the prepared films was performed to realize conductivity measurements.

1. G. P. van der Laan, M. P. de Haas, et al. *Macromolecules*, 1994, 27, 1897.

2. M. Möller, H. Frey, S. Sheiko, *Coll. & Polym. Sci.*, 1993, 271, 554.

3. H. Frey, S. Sheiko, M. Möller, et al., *Adv. Mater.*, 1993, 5, 917.

11:00 am **NS1-FrM9 Carbon Nanotubes, Sumio Iijima**, NEC R&D Group, 34 Miyukigaoka Tsukuba, Ibaraki 305, Japan.

Carbon nanotubes are expected to show unusual electronic properties like a semiconductor according to the theoretical calculations. The properties depends on a tubule diameter and helicity, and the tubule diameters are required to be around 1 nm. We have successfully synthesized such nanotubes of a single-wall graphitic shell (Iijima et al. *Nature* 361, 603(1993)). In order to refine the tubules specimens we continued to study the mechanisms of the tubule growth. In particular we examined a structural relationship between single wall nanotubes and "single wall balloons" which are considered as giant fullerenes. The latter structures often coexist with the nanotubes in our specimens. Their growth behaviors seem to be controlled by catalytic carbide particles (FeC<sub>3</sub>) which are used in our synthesis.

Other topics on nanotubes include TEM observations on atomic-scale mechanical deformation where individual tubules show a characteristic sharp bent figure, single-shell nanotubes enclosing nearly a single atom chain (or filament) of carbon atoms inside their central hollows, and an abnormally large separation (c-spacing) in double-shelled tubules in comparison with conventional graphite crystals.

INVITED

11:40 am **NS1-FrM11 C<sub>60</sub> on Silicon: Self-organization, Film Growth, and SiC Formation, D. Sarid and D. Chen**, Optical Sciences Center, University of Arizona, Tucson, AZ 85721, USA.

We report on studies of UHV-prepared submonolayers, monolayers and multilayers of C<sub>60</sub> molecules on silicon surfaces with the following results: (1) UHV-STM reveals that a single monolayer of C<sub>60</sub> molecules, adsorbed on a Si(111)- $7 \times 7$  surface, will self-organize in two ordered structural phases having different orientations on the Si surface. (2) UHV-STM and ambient AFM reveal the growth of crystalline C<sub>60</sub> films on Si(111) and Si(100) surfaces that exhibit partially ordered layers and crystalline islands that differ in their morphologies. Annealing the samples to 600°C causes the C<sub>60</sub> islands to evaporate, leaving a full layer of C<sub>60</sub> molecules capped on the substrate. (3) UHV-STM reveals the interaction of deposited silicon atoms with C<sub>60</sub> molecules already adsorbed on a Si(111)-( $7 \times 7$ ) surface. It is found that the interaction of the deposited silicon atoms with the adsorbed C<sub>60</sub> molecules is rather weak. Also, the silicon atoms, when deposited on top of a monolayer of C<sub>60</sub> adsorbates, form 3-dimensional clusters rather than wet the underlying surface. These results indicate that the adsorption of a C<sub>60</sub> molecule on a Si surface reduces its reactivity with additional Si atoms. (4) Ambient AFM, SEM, and infrared spectroscopy were used to characterize thick SiC films, fabricated on Si(100) wafers held at 900°C, using C<sub>60</sub> molecules as a carbon source.



## NANO 3/NANOMETER-SCALE SCIENCE AND TECHNOLOGY

Room A207 - Session NS2-FrM

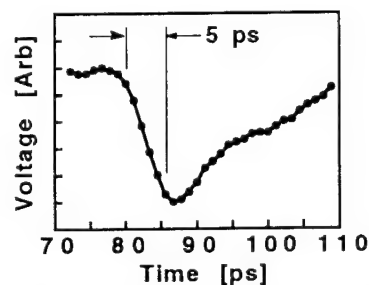
### Novel Probes

**Moderator:** D. Rugar, IBM Almaden Research Center.

8:20 am **NS2-FrM1 Applications of an AFM Probe with Ultrafast Time Resolution, B. A. Nechay, F. Ho, A. S. Hou, and D. M. Bloom**, Ginzton Laboratory, Stanford University, Stanford, CA 94305, USA.

We have developed a new measurement tool for probing ultrafast voltage waveforms on the nanometer length scale. This technique is based on mixing due to the nonlinear electrical force interaction between an atomic force microscope (AFM) tip and the sample-under-test. We have used this AFM probe for non-contact, electrical testing of internal nodes on VLSI and microwave circuits, demonstrating submicron spatial resolution and temporal resolution below 5 picoseconds. The probe also has the exciting capability for studying the transient physics within nanoelectronic devices.

In developing the ultrafast AFM probe, we microfabricated cantilevers on gallium arsenide with integrated microwave transmission lines, which allow picosecond sampling signals to propagate to the tip. The sampling signals are generated using nonlinear transmission line technology which produces voltage steps with sub-picosecond fall times. The result is a compact all-electronic system with measurement bandwidths beyond tens of gigahertz. In our presentation, we will discuss advances in instrumentation and our current research into the high-speed characterization of nanostructures.



Measurement of an electrical waveform with 5 ps fall time.

8:40 am **NS2-FrM2 Measurement of Ultra Fast Optoelectronic Phenomena in Organic Molecular Assembly by Scanning Maxwell Stress Microscopy, Takahito Inoue and Hiroshi Yokoyama**, Molecular Physics Section, Electrotechnical Laboratory, 1-1-4 Umezono, Tsukuba-shi, Ibaraki 305, JAPAN.

The scanning Maxwell stress microscope (SMM) is an electric force microscope, designed to simultaneously image topography, dielectric constant, surface charge and potential, based only on harmonic analysis of oscillations of the cantilever driven at nonresonant frequencies [1]. In the SMM the nonlinear dependence of the Maxwell stress on the field strength can be utilized to image high frequency voltages running on the sample by the heterodyne force detection technique [2]. In the measurement of ultra fast optoelectronic phenomena, the high frequency voltages associated with sample irradiation by periodically modulated light are detected by heterodyne force detection. By changing the modulation frequency, furthermore, this technique allows observations of temporal responses of photovoltaic and photoconductive substances.

In the present paper we report observations of ultra fast optoelectronic phenomena, i.e. photoconduction and photoisomerization, in organic molecular assemblies by use of the SMM equipped with the heterodyne force detection system.

1. H. Yokoyama and T. Inoue, *Thin Solid Films*, 242 (1994) 33.

2. H. Yokoyama, M. J. Jeffery and T. Inoue, *Jpn. J. Appl. Phys.*, 32 (1993) L1845.



9:00 am **NS2-FrM3 High Frequency Pattern Extraction in Digital Integrated Circuits Using Scanning Electrostatic Force Microscopy**, G. E. Bridges, R. A. Said, M. Mittal, D. J. Thomson, Department of Electrical and Computer Engineering, University of Manitoba, Winnipeg, R3T 2N2, Canada.

The ability to perform logic analysis at the internal points of integrated circuits is crucial in the design and test of advanced microelectronics. As density and speed increases, conventional direct electrical contact probing methods are no longer adequate due to low spatial resolution and disturbance of the circuit's operation due to parasitic loading. We present a non-contact scanned probe technique for extracting the high-frequency digital patterns at internal points of an integrated circuit. The digital waveforms are determined by sensing the localized electrostatic force between a small probe and point on the circuit being measured. The force is monitored by detecting the deflection of the probe using a fiber-optic interferometer. High spatial resolutions can be achieved if the interaction is localized and the probe can be scanned over the circuit with high precision. The temporal bandwidth of force measurements made using proximal probes are typically limited by the mechanical frequency response of the probe. In the presented instrument high frequency measurements are enabled by using a heterodyne technique. In conjunction with a nulling approach, the technique is capable of accurate measurements without complex calibration or probe positioning, and can be performed over passivated structures. Using a probe with a kHz resonant frequency, Mb/s patterns have been measured and digital logic levels with a voltage resolution less than 100 mV has been demonstrated.

9:20 am **NS2-FrM4 Room Temperature Quantum Mechanical Capacitance Measured With the Ultrafast Scanning Probe Microscope**, D. Botkin, S. Weiss, D. F. Ogletree, M. Salmeron and D. S. Chemla, Department of Physics, University of California at Berkeley, CA 94720, USA.

Recently, we proposed and demonstrated a general technique to wed ultrafast laser spectroscopy and Scanning Probe Microscopies to obtain simultaneous picosecond time and atomic space resolution. One of the most exciting prospects for this technique is the potential to create movies of surface dynamics on atomic scale, with atomic (ultrafast) time resolution. To this end, understanding the dynamic response of the quantum point contact formed between the STM tip and the sample surface is essential. Our measurements suggest that a large portion of the tunneling signal comes from a capacitive-like response. The tunneling gap height dependence of this response is very different from the one expected for the geometrical capacitance of the junction. In fact, the geometrical capacitance of the tip assembly contributes negligibly to the signal. These observations, which have been reconfirmed many times, suggest that "quantum mechanical capacitance", associated with the tunneling process itself, is responsible for the time resolved tunnel current data. The existence of an intrinsic capacitance associated with the tunneling process itself (quantum susceptance) has been discussed for instance in the context of the hotly disputed problem of "tunneling time" and in the context of photon assisted tunneling in SIS tunnel junctions. In both cases, quantum susceptance is the result of time lag between excitation and the tunnel current itself. A detailed study of the nature and the origin of the tunnel-gap capacitance is currently under way. Our current efforts are directed at comparing the predictions of the existing theories for quantum susceptance with our experimental results.

9:40 am **NS2-FrM5 Continuous Observation of the Motion of Single Adsorbed Atoms and Molecules with Picosecond and Sub-nanometer Resolution**, G. M. McClelland, F. Watanabe, and H. Heinzelmann, IBM Research Division, Almaden Research Center, San Jose, CA 95120, USA.

We have developed a new instrument, the femtosecond field emission camera (FFEC), which can follow continuously the motion of single adsorbed atoms and molecules adsorbed on a sharp metal tip. To detect motion through its effect on the field emission rate, the emitted electrons are tightly focussed into a beam which is electrostatically swept across a detection screen. Very fast time resolution is possible, because the tip is an ideal point source, and the strong field near the tip minimizes the time-of-flight spread of the field emitted electrons. To observe the hopping of a Cs atom between sites, field ion microscopy methods are used to form a sharp W(111) tip on which the field emission is confined to a region  $\approx 1$  nm across. A Cs atom is deposited onto a 90 K tip, and a field emission image is recorded. The tip is then pulsed negatively for 2 ns while the focussed emission beam is swept across the screen. The increased field emission excites the Cs, which hops to a nearby site. After the sweep, the new position of the

Cs atom is observed in the field emission image. When a copper phthalocyanine molecule is adsorbed on the tip,  $10^{11}$  Hz oscillations in the field emission intensity are frequently observed. These are believed to result from the slow overall vibration of this heavy molecule with respect to the tip.

**INVITED**

10:20 am **NS2-FrM7 Magnetic Resonance Detection and Imaging Using Force Microscope Techniques**, O. Zueger, S. Hoen, C. S. Yannoni and D. Rugar, IBM Almaden Research Center, 650 Harry Rd., San Jose, CA 95120.

Electron spin resonance (ESR) and nuclear magnetic resonance (NMR) were detected via the magnetic force acting between the spins of the sample and a ferromagnetic particle. An oscillatory magnetic force was generated by polarizing the spins in a strong magnetic field and then modulating the sample magnetization using magnetic resonance techniques. The resulting femtonewton magnetic force was detected by sensing the angstrom-scale vibration of a micromechanical cantilever on which the sample was mounted. Detection of both ESR and NMR was demonstrated with nanogram sensitivity. Magnetic resonance imaging was performed with micrometer-scale spatial resolution by scanning the ferromagnetic particle with respect to the sample.

10:40 am **NS2-FrM8 Parallel Imaging with an Atomic Force Microscope**, S. C. Minne, Ph. Flueckiger, H. Soh, C. F. Quate, Applied Physics, Stanford University, Stanford, CA 94305-4090.

If the atomic force microscope (AFM) is to become an effective production tool, its scan size and image acquisition rate must be improved. The current scan size is generally limited to about  $100 \mu\text{m}$  by  $100 \mu\text{m}$  because, at large sizes, the piezoelectric tube scanner becomes nonlinear. AFMs operate with a single probe and thus the entire image must be obtained serially by measuring each pixel in sequence. This is quite time consuming, even for scans smaller than the  $100 \mu\text{m}$  by  $100 \mu\text{m}$  limit. To address these problems of size and speed, we have fabricated and operated AFMs incorporating multiple probes formed by parallel arrays of piezoresistive cantilevers. We have obtained  $400 \mu\text{m}$  by  $100 \mu\text{m}$  images by operating four probes simultaneously. Thus, either the acquisition time is decreased or the scan size is increased by a factor equal to the number of probes acting in parallel. We anticipate that there will be many areas where parallel imaging will be highly beneficial; one that we are currently investigating is its incorporation into an AFM lithography system.

11:00 am **NS2-FrM9 Detection of Sub-Femtonewton Forces**, S. Hoen, O. Züger, C. S. Yannoni, H. J. Mamin, K. Wago, and D. Rugar, IBM Research Division, Almaden Research Center, San Jose, CA 95120.

We have developed micromechanical cantilevers capable of detecting sub-femtonewton forces. These cantilevers have been used to detect nuclear magnetic resonance (NMR) signals from microscopic samples, inaugurating a technique which is several orders of magnitude more sensitive than conventional NMR schemes. The cantilevers are fabricated from low stress silicon nitride grown on  $\langle 110 \rangle$  oriented silicon using low-pressure chemical vapor deposition. After an anisotropic wet etch, the fixed end of the cantilever is determined by a vertical slow-etching  $\langle 111 \rangle$  plane, eliminating the need for backside alignment or anodic bonding. The release process is completed by a critical point drying step which is necessary to protect these delicate structures from meniscus forces. Using this process, we have fashioned  $200 \text{ \AA}$  thick silicon nitride cantilevers with thickness to length ratios of 1:2500 and spring constants of  $\sim 10^{-5}$  N/m. Their thermally limited force sensitivity is  $2.4 \times 10^{-17}$  N/ $\sqrt{\text{Hz}}$  at room temperature. Damping measurements have been made as a function of temperature for  $600 \text{ \AA}$  thick nitride cantilevers. These cantilevers may provide enough sensitivity for the detection of single electron spins and move this NMR technique significantly closer to the ultimate goal of detecting single nuclear spins.

11:20 am **NS2-FrM10 Atomic Force Microscope Tip Modification with Self-Assembled Monolayer Molecules**, Taejoon Han, John Williams, T. P. Beebe, Jr., Department of Chemistry, University of Utah, Salt Lake City, UT 84112.

Atomic force microscopy (AFM) generates precise topographical information for both conductive and non-conductive materials. AFM is not without limitations however, and foremost among them is its lack of chemical specificity. Since the tip material most commonly used in AFM is  $\text{Si}_3\text{N}_4$ , AFM tips do not have much chemical variability without some international modifications. We discuss a method to modify AFM tips with self-assembled monolayers (SAM) of organic molecules in order to give the tip well defined chemical characteristics.



Alkanethiols on gold are used as the SAM system. Since both the surface and the tip can be chemically modified and have well known characteristics, several experiments and measurements are possible under this scheme. In this study, we discuss the artifacts arising in scanning probe microscopy measurements caused by the structural interaction of a finite-sized tip and small hollow surface structures ("pits" in the SAM). The analysis of SAM-modified surfaces with several spatially-averaging UHV techniques is also presented. We develop a statistical method which produces information about individual chemical bond forces and present evidence for detection of individual bond force changes which can be attributed to hydrophilic forces. Furthermore, it is possible to detect changes in the interaction force by varying the chemical environment without assuming which chemical bonds are involved.

11:40 am **NS2-FrM11 Photon Channeling: A New Approach to Photoelectron Microscopy**, J. E. Rowe, R. A. Malic, E. E. Chaban and N. V. Smith<sup>(a)</sup>, AT&T Bell Laboratories, Murray Hill, New Jersey 07974.

We report a new type of focusing of far ultraviolet light,  $\lambda < 1000 \text{ \AA}$ , using tapered capillary tubes similar to those first developed for the near-field scanning optical microscope (NSOM) which we call photon channeling. Silica tubes with taper-half-angles of  $\sim 0.5^\circ$  to  $6^\circ$  have been tested. An array of capillaries mounted on a rotatable drum is placed in front of a collimated photon source obtained from a rare-gas discharge lamp, successive capillaries can be brought into alignment, and the photoemission detected by a channeltron-grid detector. The straight capillary intensity shows no significant light guide effect; it simply decreases as the area of the capillary. However, the tapered capillaries show an enhanced transmission (or photon channeling effect). In quantitative agreement with simple numerical estimates [1] we find that the transmission enhancement factor varies from  $\sim 10$ –500 times the collimated transmission of a pinhole aperture of the same dimensions with an approximately linear dependence of channeling factor on inverse of the half angle. Useful intensity suitable for photoelectron energy analysis with capillary openings of  $\sim 0.7 \mu$  has been demonstrated. The expected spatial resolution is comparable to that obtained with more complex lithographically formed Fresnel zone plates and has the important advantage that the image probe size is independent of photon wavelength. A scanning stage has been developed to form spectral energy-resolved images and requires a tip approach feedback control different from that of NSOM to operate in high vacuum. Preliminary calibration measurements and scanning tests will be presented.

<sup>(a)</sup>Present address: Advanced Light Source, Lawrence Berkeley Laboratory, Berkeley, CA 94720.

[1] N. V. Smith, W. A. Royer and J. E. Rowe, Rev. Sci. Instr. 65, (1994) in press.

## APPLIED SURFACE SCIENCE Room A101 – Session AS-FrM

### Adhesion and Adhesive Bonding

**Moderator:** C. R. Anderson, Martin Marietta Laboratories.

8:20 am **AS-FrM1 Plasma Polymerized Primers for Adhesive Bonding of Aluminum**, I. Segall, C. E. Taylor, F. J. Boerio, and W. J. van Ooij, University of Cincinnati, Cincinnati, Ohio 45221-0012, R. A. Dickie, Ford Motor Company, Dearborn, MI 48121-2053, D. J. Ondrus, Ford Motor Company, Detroit, MI 48239.

Plasma polymerized films of monomers such as hexamethyldisiloxane (HMDS) and trimethylsilane (TMS) were deposited on aluminum substrates and evaluated as primers for adhesive bonding of aluminum. As-deposited films were characterized by a variety of techniques including X-ray photoelectron spectroscopy (XPS), ellipsometry, secondary ion mass spectrometry (SIMS), atomic force microscopy (AFM), and scanning electron microscopy (SEM). The results showed that the molecular structure of the films depended strongly on the nature of the carrier gas. When argon was used as the carrier, films having siloxane-like structures were obtained but when oxygen was used as the carrier, silica-like films were obtained. The films were composed of spherically shaped particles whose growth seemed to be nucleated

by the oxidized aluminum surface. The properties of the films as primers for adhesive bonding of aluminum were evaluated by preparing lap joints from coated aluminum substrates, applying a load to the joints, and measuring the time required for failure to occur during exposure to a corrosive environment. It was found that the silica-like films were excellent primers.

8:40 am **AS-FrM2 Plasma Sprayed Coatings as Surface Treatments of Aluminum Adherends**, G. D. Davis, D. K. Shaffer, P. L. Whisnant, and G. B. Groff, Martin Marietta Laboratories, Baltimore, MD 21227 and J. D. Venables, Venables and Associates, Baltimore, MD 21204.

Conventional surface treatments for aluminum adherends commonly involve chromates and almost always involve strong acids or bases and significant quantities of waste water. Environmentally safe means to dispose of the wastes are costly and will become more expensive in the future. Plasma spray coatings can potentially reduce or eliminate much of the disposal and cleanup costs associated with chemical treatments. We have characterized and evaluated several different plasma spray coatings as surface treatments of aluminum adherends. In wedge tests, the various aluminum-rich aluminum/polyester and aluminum/PEEK coatings give better results than either constituent by itself. The best durability performances are better than that of FPL-treated bonds and equivalent to that of PAA-treated bonds for some adhesives. In blended coatings, the polymer is believed to toughen the coatings and provide moisture-resistant chemical bonds to enhance durability. The aluminum in the coating provides coating strength and adherence to the substrate.

This work was supported by Wright Laboratory Materials Directorate under contract F33615-93-C-5324.

9:00 am **AS-FrM3 Characterization of the Interphase Formed on Adhesion of Polymers to Metal Oxides**, J. P. Wightman, Virginia Tech, Blacksburg, VA 24061.

The interphase region at polymer/metal oxide interfaces may be critical in determining the strength and durability of adhesive bonds. Methods to investigate these regions are limited however and this research has focused on the complementary techniques of infrared spectroscopy (IRS) and x-ray photoelectron spectroscopy (XPS) to investigate the molecular structure of the interphase. Dielectric thermal analysis was used in earlier work to probe the properties of thin polysulfone films on pretreated aluminum surfaces. A significant increase in the activation energy associated with segmental motion in the backbone of polysulfone occurred for films between 1–2  $\mu\text{m}$  thick deposited on an acid-etched aluminum substrate. A new technique, variable temperature reflection absorption infrared spectroscopy, was developed recently as a method to investigate the reorganization of ultra-thin polyphenylene sulfide (PPS) films on a variety of substrates. PPS films on copper showed a loss in crystallizability in contrast to results observed for chromium and aluminum. Loss of cuprous oxide film underlying the PPS film was also observed. Bonded PPS/copper laminates showed that the particular surface chemistry was critical in determining the peel strength observed. For example, after a simple thermal oxidation pretreatment for copper foil, an order of magnitude increase in peel strength was observed in agreement with XPS and IRS results.

INVITED

9:40 am **AS-FrM5 Practical Multi-Technique Analysis of Metal Surfaces for Adhesive Bonding Applications**, A. P. Diwanji, A. R. Madura, R. Martin, LORD Corporation, Erie, PA 16514.

Metal components used in adhesive bonding applications are often subjected to machining and forming processes. These processes leave residue to contamination on the bonding surface. Contamination is one of the most insidious factors affecting adhesive bond performance and reliability in metal-to-rubber, structural bonding and coating applications. Contamination is generally removed by cleaning treatments to yield a clean surface. A clean surface is one that contains no significant amount of undesired material. The nature and composition of these undesired materials can vary depending on bonding applications.

Metal production and cleaning treatments are continuously changing with new applications, developments in materials technology and regulatory requirements. This necessitates ongoing characterization of both contaminated and cleaned surfaces to assess the nature of the contamination and the effectiveness of current cleaning treatments.

In this study, processed metal alloys were cleaned by methods including acid pickling, alkaline cleaning and vapor degreasing. Multi-technique surface investigations including ISS, SIMS and XPS were used to characterize the effectiveness of the treatments and determine

the composition and chemistry of the bonding surfaces. These results are compared to results from methods such as wettability determination and evaporative rate analysis that are used within the production environment to assess the extent of surface cleanliness. Data from these techniques correlate well with each other and reveal the presence of both organic and inorganic surface contaminants that may be significant to bond performance.

**10:00 am AS-FrM6 Strained Siloxane Rings in the Surface of Silica: their Reaction with Organosiloxanes, Organosilanes, and Water\*, A. Grabbe, T. A. Michalske, and W. L. Smith, Sandia National Laboratories, Dept. 1114, Albuquerque, NM 87185.**

The glass network on the surface of highly dehydroxylated silica contains strained siloxane defects. The SiO dimer defects are edge shared tetrahedra, some of which have lessened reactivity due to an attached hydroxyl. Using Infrared spectrometry we show that dimer defects react with organosiloxanes or with water at rates that can be comparable, depending on the structure of the organosiloxane. A polar bond component is a necessary condition for a rapid reaction with dimer defects, since non-polar organosilanes react orders of magnitude slower than do water or organosiloxanes. The important features of the reacting bond that control the rapidity of the reaction are its polarity, steric accessibility, and bond strain. The reactions require 6 orders of magnitude of gas exposure to go from one to ninety-nine percent completion, showing that the surface is highly heterogeneous. We have applied a simple model of the surface's heterogeneity to our data, incorporating a linearly distributed activation energy in the defect population. A fit using this model indicates that the spread in activation energy is approximately 40 kJ/mole in all cases. The organosiloxane reaction with dimer defects produces hydrolytically stable coupling points for adhesion to polymers, which cannot be readily synthesized by conventional silane chemistry.

\*Work supported by D.O.E. contract DE-AC04-94AL8500 and AT&T Bell Laboratories.

**10:20 am AS-FrM7 A New Probe of Plastic Deformation Accompanying Metal-Ceramic Interfacial Failure,\* J. T. Dickinson, S. Nakahara, S. C. Langford, and L. C. Jensen, Washington State University, Pullman, WA 99164-2814.**

The ability of a metal-ceramic bond to resist fracture is a function of the interfacial adhesion and toughening mechanisms due to metal plasticity. We have developed a sensitive method of detecting and quantifying the extent of metal plasticity on the atomic scale produced at such interfaces during fracture. It involves the detection of emitted electrons whose intensity is directly related to the number of metal atoms exposed during fracture. Plastic deformation greatly increases this number due to surface roughening, which to first order is proportional to the extent of slip. A description of the experimental arrangement, absolute calibration of the electron emission intensities vs. surface area, and results from a series of interfacial failure experiments will be presented. Comparisons with post-fracture AFM measurements performed on the metal surface will be made; limitations of the AFM results are discussed. Our model systems are 1  $\mu$ m, thick Mg and Ti films detached from soda-lime glass in a chevron notch geometry. We have established a linear relationship between electron emission intensity and fracture toughness.

\*This work supported by AFOSR and NSF-DMR.

**10:40 am AS-FrM8 Improved Adhesion at the Copper/Polyimide Interface Using an Organometallic Additive, D. Coulman, The DuPont Company, Central Research and Development, Wilmington, DE 19880-0326.**

Polyimide Kapton® films containing an organo-tin additive have been found to improve adhesion of direct metallized copper-polyimide clads. The peel strength of the polyimide films which contain the organo-tin additive, after 500 hours at 85% RH and 85°C, are substantially higher 4-7 lb./in compared to 2-3 lb./in for the comparable films without the additive. More importantly the normally marked decrease in peel strength after temperature humidity aging is not observed with the organo-tin additive. Changes in the surface chemistry and structure of these films has been investigated using XPS, RBS, and TOF SIMS analysis. RBS analysis clearly indicates the segregation of the tin additive to the near surface region of the polyimide film. Atomic force microscopy (AFM) has been used to study the surface morphology of the Kapton® films. A factor of two improvement in peel strength has been observed even with no surface pretreatment.

The effect of plasma etching on the peel strength will also be presented. These results on copper-Kapton® film laminates will be correlated with ultra high vacuum studies of copper deposition on the organometallic containing film.

**11:00 am AS-FrM9 Observing Bond Orientation and Chemistry at the Buried Metal/Benzocyclobutene (BCB) Polymer Interface with Near Edge X-ray Absorption Fine Structure (NEXAFS), B. M. DeKoven<sup>1</sup>, D. A. Fischer<sup>2</sup>, S. J. Babinec<sup>1</sup>, J. J. Curphy<sup>1</sup>, J. L. Gland<sup>3</sup>, G. E. Mitchell<sup>1</sup>, D. H. Parker<sup>1</sup>, C. A. Wedelstaedt<sup>1</sup>, (1) The Dow Chemical Company, Midland, MI 48674, (2) National Institute of Standards and Technology, Gaithersburg, MD 20899, (3) Department of Chemistry, University of Michigan, Ann Arbor, MI 48109.**

Benzocyclobutene (BCB) polymers are used for dielectric layers in new generation multilayer interconnect devices (multichip modules). In this metal/polymer application it is important to understand the nature of the bonding and complexing which occurs at the metal/polymer interface in order to optimize adhesion. We have observed the relative orientation and chemistry of polymer functional groups in several buried metal [Al, Ti, Cu, and Au (10-100 nm thick)]/BCB polymer interfaces using the bond specific polarization anisotropy of carbon K fluorescence yield NEXAFS.

The depth sensitivity (about 200 nm) and the non destructive nature of our fluorescence yield NEXAFS technique are particularly useful in studying the buried metal/BCB interface. The aromatic ring of BCB appears to undergo a dramatic enhancement in orientation after the formation of the metal polymer interface for the Al and Au overlayers compared to free standing BCB surfaces. These preliminary results highlight the use of fluorescence yield NEXAFS as a probe of chemical structure at buried interfaces.

**11:20 am AS-FrM10 Adhesive Bonding between Self-Assembling Monolayer Films Measured by Interfacial Microscopy, R. C. Thomas<sup>1</sup>, R. M. Crooks<sup>1,2</sup>, Taisun Kim<sup>2</sup>, J. E. Houston<sup>3</sup>, and T. A. Michalske<sup>3</sup>, <sup>1</sup>Department of Chemistry, University of New Mexico, Albuquerque, NM 87131; <sup>2</sup>Department of Chemistry, Texas A&M University, College Station, TX 77843-3255; <sup>3</sup>Surface and Interface Sciences Department, Sandia National Laboratories, Albuquerque, NM 87185-0710.**

We have used the interfacial force microscope (IFM) to study adhesive bonding between n-alkanethiol monolayer films that are strongly adsorbed to both a Au probe and a Au sample. Our results demonstrate that force-versus-displacement curves can be used as "fingerprints" to identify specific bonding mechanisms between monolayers having either the same or different endgroups. For example, we have measured the magnitude of the van der Waals interactions between two methyl-terminated, surface-confined monolayer films over the entire range of interfacial separation. Moreover, the force curves are continuous (e.g., no jump-to-contact) and show no hysteresis between loading and unloading. By measuring the adhesive pull-off force and using DMT theory, we calculate surface energies that are in excellent agreement with literature values for these low-energy hydrocarbon films. We will contrast these results to IFM studies between surface-confined monolayer films modified with the chemically reactive end groups, COOH and NH<sub>2</sub>, which have additional adhesive contributions arising from acid-based and hydrogen-bonding interactions. The force curves for these data are also continuous, but show a distinct hysteresis between loading and unloading. We have found that it is possible to calculate bond energies for specific types of chemical interactions by integrating the area under the unloading curves and estimating the contact area at zero load. We will compare our results to those recently obtained using both the surface forces apparatus and the atomic force microscope.

**11:40 am AS-FrM11 Micromachining Induced Adhesion Enhancement Between High Performance Polymer and Silicon Dioxide Substrate, Hyo-Soo Jeong, Institute for Advanced Engineering, C.P.O. Box 2849, Seoul, Korea, and Jack Jiang, Thomas Electronics, Inc., Wayne, NJ 07470.**

It is well known that polymers do not adhere to silicon dioxide (SiO<sub>2</sub>). Surface modification is required for adhesion enhancement. The surfaces of thermally grown silicon oxide films have been fabricated by silicon micromachining technology in order to enhance adhesion between polyimide and SiO<sub>2</sub> substrate. An artificial interphase is thus formed between the two materials. The microfabricated mushroom structure (on the order of 100 Å) act as mechanical hooks between those interfaces, contributing to enhanced bonding strength via mechanical interlocking mechanism between the two materials.

Our results show that the fracture energy (G<sub>c</sub>) of the microfabricated

structures measured by the blister test is many orders of magnitude larger than that of the untreated plain structures. Since the enhanced bonding mechanism is purely mechanical, it can be employed in applications where chemical resistance and/or biological compatibility are paramount.

## THIN FILM

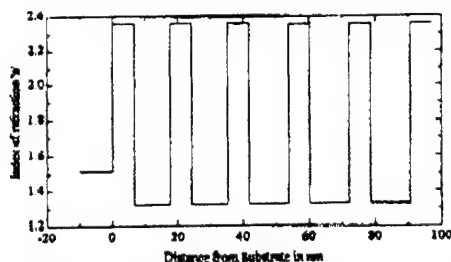
### Room A105 - Session TF-FrM

#### In Situ Thin Film Characterization

**Moderator:** C. R. Aita, University of Wisconsin, Milwaukee.

8:20 am **TF-FrM1 In-situ Ellipsometric Monitoring and Post-Deposition Characterization of Dielectric Optical Multilayers**, P. He, S. Pittal, B. Johs, J. A. Woollam, J. A. Woollam Co., Inc., Lincoln, NE 68508, J. H. Kim, CVI Laser Corp., Albuquerque, NM 87192.

A multi-wavelength *in-situ* ellipsometer has been developed for *in-situ* thin film deposition monitoring and control. This instrument acquires ellipsometric data  $\psi$  and  $\Delta$  at 44 different wavelengths simultaneously in spectral range from about 410 to 750 nm. Typical data acquisition rate is about 1 measurement per second with maximum rate of 25 measurements per second. The *in-situ* ellipsometer was mounted at a 70° angle of incidence on a deposition. The typical chamber vacuum was about  $10^{-5}$  Torr. A multilayer stack of quarter-wave ZnS and Cryolite was thermally evaporated onto BK7 glass substrate. Quarter-wave thicknesses were determined by reading transmitted light intensity maxima or minima recorded using a photomultiplier tube. The *in-situ* ellipsometer acquired data during the deposition in real-time without interaction with the deposition process. The ellipsometric data were analyzed after the deposition. *Ex-situ* ellipsometric measurement, spectral transmission measurement, and XRD were also performed for post-deposition analysis and characterization. Thicknesses of each layer and optical constants of ZnS and Cryolite were obtained. Optical constants were found to have changed after the sample was exposed to air.



Depth profile of the ZnS/Cryolite high-low stack at 600nm.

8:40 am **TF-FrM2 Real Time Monitoring of the Deposition and Growth of Thin Organic Films by In situ Ellipsometry**, J. F. Wall, E. Claiberg, R. W. Murray, E. A. Irene, University of North Carolina, Chapel Hill, NC 27599-3290.

Polyphenylene oxide (PPO) films have been electrochemically deposited onto gold substrates, yielding ultrathin films on the order of 10 nm. The deposition is monitored by *in situ* ellipsometry in real time in order to follow the growth mechanism. The films are subsequently characterized by *ex situ* spectroscopic ellipsometry to confirm the final film thickness and growth rate. This data, combined with the optical properties of PPO films previously established in our laboratory, allow for theoretical calculations of the growth mechanism. These calculations are compared to the real time *in situ* measurements. This comparison, combined with atomic force microscopy observations made in the early and final stages of film formation, leads to judgement as to whether deposition is by a layer by layer or an island formation mechanism.

9:00 am **TF-FrM3 Surface Analysis at Low to Ultra-High Vacuum by Ion Beam Recoil Spectroscopy**, M. S. Hammond, SI Diamond Technology Inc., Houston, TX 77098, J. A. Schultz, Ionwerks Inc., Houston, TX 77005.

An overview of widely used *ex situ* ion beam surface analysis techniques will be given. These techniques will be compared to the recently developed ion beam recoil spectroscopies which are capable of *in situ* surface analysis at pressures ranging from tens of milliTorr to UHV. Ion beam recoil techniques, by using forward scattering in the keV range, enhance surface selectivity and enable the beam and the detected constituents to be detected at vacuum levels far higher than ordinary surface spectroscopy techniques. In addition, the energy range used results in higher detector efficiencies, thereby relaxing constraints imposed by ion scattering cross sections. Time of flight detection is used to provide both energy and mass information from the scattered constituents. Two variations of this technique exist. Direct Recoil Spectroscopy (DRS) uses line of sight detection and detects both neutrals and ions, resulting in high detection efficiencies. DRS has the added advantage of being able to detect H, C, O, and N surface stoichiometries at pressures up to 100 mTorr per cm of pathlength. Mass Spectroscopy of Recoiled Ions (MSRI) uses a mass and charge filtering scheme to detect only ions and is applicable to a wide variety of elements and isotopes. The higher resolution afforded by the use of mass and charge filtering enables the use of isotopic labeling techniques during adsorption experiments. Examples of data taken during the CVD growth of diamond, high  $T_c$  superconductors and Group III-nitrides will be presented, along with H-D exchange experiments on silicon and diamond.

INVITED

9:40 am **TF-FrM5 Deposition and Characterization of Transition-Metal Nitride Superlattices**, Scott A. Barnett, Northwestern University, Evanston, IL 60208.

In this talk, the role of *in situ* monitoring and control as well as *ex situ* characterization is described for the case of epitaxial and polycrystalline nitride superlattice thin films that exhibit extremely high hardnesses. The use of *in situ* Auger electron spectroscopy for determining nucleation mechanisms during epitaxial growth of various nitride layers is described, particularly the effect of lattice mismatch. The use of *in situ* nitrogen gas pressure monitoring during superlattice deposition for maintaining high-rate reactive sputtering conditions and for obtaining the desired stoichiometry of both layer materials is described. Post-deposition characterization is also critical for determining both the nature of the layers and the properties. The use of x-ray diffraction combined with simulations of the resulting scans yields information on crystal structure, interface widths, and layer coherency strains; factors that are critical for determining properties. Cross-sectional and plan-view TEM provide critical information that is largely complementary to the x-ray results, including direct observation of dislocation relaxation of coherency strains, porosity, and layer morphology. Finally, the results of Vickers microhardness and nanoindenter measurements are described and compared with models of superlattice properties.

INVITED

10:20 am **TF-FrM7 Spectroscopic Ellipsometry of Thin Films on Transparent Substrates: A Formalism for Data Interpretation**, Y. H. Yang and J. R. Abelson, Coordinated Science Lab. and Materials Science Department, U. Illinois, Urbana, IL 61801.

Real time, *in-situ* spectroscopic ellipsometry is a powerful tool for characterizing thin film growth or surface modification, and thus providing process control. Virtually all studies to date have examined thin layers on a semi-infinite substrate, i.e., the transmitted beam is completely absorbed (as in crystalline silicon) or scattered at the back of the substrate (as with roughened glass). This situation is required since the coherent optic formulae are used in modeling. However, the requirement for a special substrate has limited spectroscopic ellipsometry to experimental conditions which are not typical for industrial device-making.

Here, we propose an explicit analytical formalism for rotating analyzer ellipsometry which permits the analysis of spectroscopic ellipsometry data for thin films on transparent substrates such as glass, where the transmitted beam becomes phase-incoherent and reflects back toward the sample surface. We show that the incoherent optical limit can be incorporated into the first-level data reduction routine. As an example, we present data and analysis for hydrogenated amorphous silicon growth on transparent conductive oxides, and show that film nucleation and coalescence, and chemical reduction of the oxide can reliably be determined.

10:40 am **TF-FrM8 Optical Emission Spectroscopy of Plasmas for Diamond Growth**, R. Manukonda, R. Dillon, Electrical Engineering Department and Center for Microelectronic and Optical Materials Research, University of Nebraska, Lincoln, NE 68588 and T. Furtak, Physics Department, Colorado School of Mines, Golden, CO 80401.

Our radio frequency chemical vapor deposition system has been used to deposit diamond films with water-alcohol and the traditional hydrogen-carbon-oxygen source gases. The water-alcohol source gases yield high atomic hydrogen and electron densities. Optical emission spectroscopy (OES) was performed with both source gases with a 1/2 meter monochromator in the spectral range from 200 to 800 nm. OES is only sensitive to emitting species and therefore does not provide fundamental information on diamond growth. However, a low ratio of CH to atomic H peaks has been found by ourselves and others to be an empirical indicator of faceted diamond growth for the traditional source gases. Thus, OES has excellent potential as an inexpensive and non-intrusive diagnostic for quality control in diamond growth. In this paper, we compare the OES spectra for diamond growth from the water-alcohol and the traditional hydrogen-carbon-oxygen source gas and discuss correlations between the spectra and film characteristics such as growth rate and Raman spectra.

11:00 am **TF-FrM9 Optical Second Harmonic Generation (SHG) as an in Situ Technique to Monitor the Growth and to Analyse the Structure of Thin Films**, M. Buck, Ch. Dressler, M. Grunze, F. Träger\*, Angewandte Physikalische Chemie der Universität Heidelberg, Im Neuenheimer Feld 253, 69120 Heidelberg, Germany, \*Fachbereich Physik der Universität Kassel, Heinrich-Plett-Str. 40, 34132 Kassel, Germany.

To analyse thin films and their interface to the substrate a nondestructive characterization is desirable. Ellipsometry and infrared spectroscopy are two examples of linear optical techniques that are widely used for thin film investigation. SHG as a nonlinear technique well established for interface analysis has also been applied recently to study thin film growth.

Polyamic acid films on metal substrates have been investigated. Pyromellitic dianhydride (PMDA) and various diamines were used as constituents of the polymer. The shape of the thickness dependent SH-signal is found to vary with the monomers. A theoretical model shows that the phase sensitive superposition of contributions generated in the film and in the substrate strongly affects the shape of the SH-signal. Most importantly, the thickness dependent SH-signal bears information about the orientation of the molecules and therefore can serve to infer on the structure of the films.

11:20 am **TF-FrM10 Real Time Infrared Spectroscopy of Chemical Bonding During Thin Film Growth and Surface Modification: A Review of Techniques**, M. Katiyar, Y. H. Yang and J. R. Abelson, Coordinated Science Lab. and the Materials Science Dept., University of Illinois, Urbana, IL 61801.

Infrared spectroscopy is ideally suited for real time studies of chemical bonding on thin film surfaces during processing in gas ambients, eg., chemical vapor deposition, reactive etching, or surface modification. The vibrational spectra reveal the identity, configuration, and local environment of bonds, both on the physical surface and in the bulk.

Since infrared absorption is relatively weak, optical enhancement is necessary to observe the signals from a surface layer or very thin film in real time. Here, we critically review five techniques which permit analyses during processing. Optical enhancement in a reflection-mode geometry can be obtained using (i) metal substrates, (ii) a thin dielectric layer on a metal substrate, (iii) multiple internal reflection substrates, (iv) infrared ellipsometry, or (v) multilayer optical cavity substrates (the latter pioneered by our group). The choice of technique depends on the material system, IR modes of interest, and experimental constraints. We calculate the electric fields in each structure and the quantity that is measured, normally the change in reflectance. We consider the effect of experimental variables on the measured signal, e.g., substrate material, incident angle, polarization and wavelength of light, dielectric constants of the film, and thickness of the film. Examples are drawn from systems of current interest, eg., H on and in Si. For future practitioners, we compare these techniques in terms of their ability to identify bonds on the physical surface vs. the bulk, flexibility in measurement conditions, and ease of data analysis.

11:40 am **TF-FrM11 In Situ Analysis of Thin Film Deposition Processes Using Time-of-Flight (TOF) Ion Beam Analysis Methods\***, Y. Lin<sup>1,2</sup>, A. R. Kruass<sup>1</sup>, O. Auciello<sup>3</sup>, D. M. Gruen<sup>1</sup> and R. P. H. Chang<sup>2</sup>, <sup>1</sup>Argonne National Laboratory, Materials Science & Chem-

istry Divisions, Argonne, IL 60439; <sup>2</sup>Materials Science & Engineering Dept., Northwestern University, Evanston, IL 60208; <sup>3</sup>MCNC Microelectronics Center of N. Carolina, Research Triangle Park, NC 27709.

The use of comprehensive, non-destructive, in situ methods for the characterization of thin film growth phenomena is key to obtaining both a better understanding of thin film growth processes and to developing more reliable deposition procedures, especially for complex layered structures involving multi-phase materials. However, surface characterization methods that utilize either electrons (e.g. AES or XPS) or low energy ions (e.g. SIMS) for the signal require an UHV environment and utilize instrumentation which obstructs line-of-sight access to the substrate. These methods are therefore incompatible with thin film deposition processes which introduce gas, either for the deposition process or the production of the desired phase such as an oxide, and require line-of-sight deposition. We have developed a means of differentially pumping both the ion beam source and detectors of a TOF ion beam surface analysis spectrometer that does not interfere with the deposition process and permits compositional and structural analysis of the growing film at pressures up to several tens of mTorr. In order to quantify the sensitivity of Ion Scattering Spectroscopy (ISS), Direct Recoil Spectroscopy (DRS) and Mass Spectroscopy of Recoiled Ions (MSRI) we have measured the signal intensity for stabilized clean metal and well-characterized oxide surfaces in a variety of gas environments as a function of the ambient gas species and pressure, and ion beam species and kinetic energy. The results are interpreted in terms of collisional cross sections which are compared with known gas phase scattering data, and provide an *a priori* basis for the evaluation of the method for various industrial processing environments which involve both inert and reactive gases at pressures up to several hundred mTorr.

\*Work supported by the Department of Energy Division of Basic Energy Sciences under contract W-31-109-ENG-38.

## ELECTRONIC MATERIALS Room A108 - Session EM-FrM

### Interface Characterization

**Moderator:** S. A. Chambers, Pacific Northwest Laboratory.

8:20 am **EM-FrM1 High Resolution X-ray Reflectivity Characterization of Interface Roughness and Correlation**, R. L. Headrick, Cornell High Energy Synchrotron Source, Cornell University, Ithaca, NY 14853.

X-ray specular reflectivity has become a standard tool for analysis of interface abruptness in thin film microstructures. However, low resolution specular reflectivity scans only yield information about the average density profile. High-Resolution X-ray Reflectivity allows measurement of diffuse scattering that contains additional information about the amplitude and lateral wavelength of the roughness and its evolution from interface to interface.

We have performed High Resolution X-ray Reflectivity on Si/Ge short-period and Si/Ge<sub>x</sub>Si<sub>1-x</sub> long period superlattices. Roughness from at least two different physical origins can be observed. The first is an interface corrugation with an upper limit on the lateral wavelength of 1.2 microns. The corrugation is asymmetric and oriented along the direction of miscut and is highly periodic, producing characteristic peaks in reflectivity rocking scans. A second roughness exists on a much shorter length scale, and exhibits a strong dependence on growth temperature. The amplitude of this roughness is highest for very low (250°C), and very high growth temperatures (>650°C).

The degree of vertical correlation can also be analyzed with this technique. Very low and intermediate growth temperatures produce highly correlated roughness, while growth at temperatures above 650°C produces only partially correlated roughness. This suggests that random noise is introduced in the growth front at higher temperatures causing a fluctuation of the roughness from interface to interface.

Other techniques such as cross-sectional electron microscopy and double crystal x-ray diffraction have been performed on the same long and short period superlattices for comparison.

**INVITED**



9:00 am **EM-FrM3 Buffer Layer-Superlattice Interactions in the AlAs/GaAs Superlattice System**, J. G. Pellegrino, \*S. B. Qadri, <sup>†</sup>B. Roushani, <sup>‡</sup>C. A. Richter, D. Chandler-Horowitz, N. V. Nguyen, P. M. Amiritharaj, NIST Semiconductor Electronics Division, Gaithersburg, Maryland 20899, \*Naval Research Lab, <sup>†</sup>GMI Engineering and Management Institute, <sup>‡</sup>NRC Research Associate.

An issue of crucial materials concern in producing high quality reproducible layered semiconductor devices is whether roughness originates at the substrate and propagates up the layer versus growth-induced roughness. We present results which clearly indicate that the thickness of the buffer layer affects the roughness observed in a subsequently grown (AlAs)<sub>m</sub>/(GaAs)<sub>n</sub> superlattice test structure where  $m = n = 3$  and  $p = 18$ . A comprehensive set of samples grown on both (001) and (111) substrates were examined. Growth rates of 0.1  $\mu\text{m/hr}$  and 0.2  $\mu\text{m/hr}$  were used for the AlAs and GaAs sublattices. High resolution x-ray reflectivity was used to examine the interfacial structural properties for typical scans  $Q = (0.7-1.7) \text{ \AA}^{-1}$ . These results were correlated with optical properties obtained by Raman, photo-reflectance, and ellipsometric measurements. Results indicate that roughening is promoted by thin GaAs buffer layers (10-100 nm). Smoother interfaces were observed in samples with buffer layer thicknesses 250 nm and greater. The analysis of roughness in the (AlAs)<sub>3</sub>/(GaAs)<sub>3</sub> system is of interest because the sublattices are sufficiently thin such that a strict step-flow growth mode cannot be assumed. The implications of these results on electron transport properties were investigated in a series of modulation doped heterostructures.

9:20 am **EM-FrM4 Interfacial Properties of Metal-Insulator Semiconductor Capacitors on GaAs(110)**, L. J. Huang, R. Krishnamurthy, W. M. Lau, Department of Materials Engineering, University of Western Ontario, London, Ontario N6A 5B9 Canada; S. Ingre, Bell Northern Research, P.O. Box 3511, Station C, Ottawa, Ontario K1Y 4H7 Canada; D. Landheer, and J.-P. Noël, Institute for Microstructural Sciences, National Research Council of Canada, Ottawa, Ontario K1A 0R6 Canada.

Metal-insulator-semiconductor capacitors were fabricated on cleaved *n*-GaAs (110) facets and on *n*-GaAs(110) wafers using remote plasma deposited silicon nitride as gate insulator. The interface properties of the capacitors made on this surface were analyzed by capacitance-voltage (CV) measurements. X-ray absorption near-edge structure (XANES) spectroscopy and x-ray photoemission spectroscopy were also used to investigate the structures of the buried interface. Prior to the insulator deposition, the cleaved facets were processed with different surface treatments including HF-etch of native oxide, passivation with an ammonium sulfide solution, passivation with hydrogen polysulfide, and passivation with a silicon interface control layer. It was found that while the passivation procedures with the sulfur compounds did improve the CV data when compared with the HF oxide etch, the silicon interface control layer technique led to the best CV results. By comparing the quasi-static and high frequency (1 MHz) CV data, we found that the minimum interface state density of the fabricated capacitors was about  $10^{12} \text{ eV}^{-1} \text{ cm}^{-2}$ . The results were compared with those obtained from GaAs(100) and the difference was addressed with respect to the surface geometry and the electronic structures.

9:40 am **EM-FrM5 Growth Kinetics and Interface Chemistry: Site-Specific Diffraction and Spectroscopy of Ultra-Thin Insulators**, <sup>†</sup>Marjorie A. Olmstead, Department of Physics, University of Washington, FM-15, Seattle, WA 98195.

During the heteroepitaxy of strongly dissimilar materials, the complex growth kinetics and interface reactions of the first few molecular layers can control the structures and morphology of the next several hundred layers. Within these first few layers, the atomic and electronic structure continuously evolves as the bare substrate reacts to form a new interface compound, which in turn serves as the substrate for the nucleation and coalescence of subsequent layers. The interface structure may also change as it is covered. Using the powerful in-situ combination of X-ray photoelectron spectroscopy and diffraction, we have monitored this evolution of the atomic and electronic structure when the insulator  $\text{CaF}_2$  is deposited on Si. We observe and explain different photoemission and auger emission energies for 8 different atomic layers, and exploit energy-resolved diffraction to separately determine their local structure. We also determine the extent of interface reaction and average film morphology as a function of growth kinetic conditions, and have successfully modelled the results. We have

also observed changes in the buried interface structure when the reacted layer is covered by additional fluoride or when the surface of the film is modified by oxidation or by deposition of Si. **INVITED**

<sup>†</sup>Work in collaboration with U. Hessinger, M. Leskovar, J. Denlinger and E. Rotenberg; supported by the U.S. Dept. of Energy.

10:20 am **EM-FrM7 Modified Surface Charge Spectroscopy for the Characterization of Insulator-Semiconductor Structures**, W. M. Lau and L. J. Huang, Department of Materials Engineering, University of Western Ontario, London, Ontario, Canada N6A 5B9; and R. W. M. Kwok and G. Jin, Department of Chemistry, Chinese University of Hong Kong, Shatin, Hong Kong.

The operation of all thin-gate-insulator/semiconductor structures relies on two basic properties, charge maintenance by the insulator and the response of the semiconductor surface potential to the insulator charging potential. In surface charge spectroscopy (SCS), external negative/positive charge is put on the insulator surface in vacuum. The breakdown and leakage characteristics as well as the relationship between the semiconductor surface potential and insulator charging potential are then measured using an x-ray photoelectron spectrometer. Once the relationship between the semiconductor and insulator surface potential is determined, the interface state distributions are calculated using a typical space-charge analysis model. Hitherto, SCS has only been applied with low energy electron flooding for negative surface charging, and thus no data corresponding to positive gate-insulator voltages have been shown. The present study shows that by collecting secondary electrons emitted from the sample surface, positive charging of the insulator could be obtained and controlled. The modified SCS, which covers both negative and positive charging, has been successfully applied to the studies of  $\text{SiO}_2/\text{Si}$  and  $\text{SiN}_x/\text{InP}$ . The interface state density data were found to be consistent with those from the conventional capacitance-voltage analyses of the equivalent metal-insulator-semiconductor structures.

10:40 am **Em-FrM8 Buried Contaminant Structure Determination with Component-Resolved X-Ray Photoelectron Diffraction in  $\text{CaF}_2/\text{O}/\text{Si}(111)$  Heterostructures**, <sup>†</sup>M. Leskovar, U. Hessinger, and Marjorie A. Olmstead, Dept. of Physics, Univ. of Washington, Seattle, WA 98195.

Contamination during heteroepitaxial growth or subsequent processing may alter the chemical and structural properties of buried interfaces and other subsurface structures. The technique of component-resolved X-ray photoelectron diffraction (CR-XPD) enables simultaneous, *in situ* determination of both the chemical identity and the local structure of buried contaminants through the energies and diffraction intensities, respectively, of the photo-emitted electrons. We used CR-XPD to investigate ultrathin  $\text{CaF}_2/\text{Si}(111)$  heterostructures exposed both to residual gases in an UHV environment and to atmosphere. While a stoichiometric  $\text{CaF}_2$  surface should be stable under these conditions, in both cases at least two oxygen species were incorporated in the  $\text{CaF}_2$  layer at room temperature. This room temperature incorporation dramatically reduces the energy splitting between Ca emission from interface and bulk layers, indicating structural changes well below the surface. Subsurface incorporation of oxygen is confirmed by the presence of O 1s XPD modulations. These results may explain the differences reported between *in situ* and *ex situ* measurements of  $\text{CaF}_2/\text{Si}(111)$  interface properties.

<sup>†</sup>Work supported by the U.S. Dept. of Energy.

11:00 am **EM-FrM9 A Study of Thermal Oxidation of Rough Silicon Surfaces**, Q. Liu, L. Spanos, and E. A. Irene, Department of Chemistry, University of North Carolina, Chapel Hill, NC 27599.

As the thickness of the gate oxide is projected to be of the order of 5 nm, the magnitude of interface roughness at the nm scale becomes a large fraction of the device dimensions. Therefore it is crucial to control the atomic scale structure of an interface. We studied the oxidation of rough silicon surfaces by Spectroscopic Immersion Ellipsometry (SIE) and Atomic Force Microscopy (AFM). Essentially, SIE uses liquids that refractive index match to the films, thereby optically removing the films and consequently increase the sensitivity to the interface. We found that as the thickness of the thermally grown  $\text{SiO}_2$  overlayer increases, the average radius of the crystalline silicon protrusions (roughness) at the interface decreases as measured using both SIE and AFM. A fractal analysis which characterizes the irregularity and complexity of a surface is concordant and furthermore shown a simpler surface resulting from oxidation. The frequency spec-



tra of AFM images give important information about how the interface roughness changes with oxidation, and these results are in agreement with the Kelvin equation which predicts that small features are more reactive.

**11:20 am EM-FrM10 Interfacial and Microstructural Study of Epitaxial Aluminum Nitride Films Using Atomic Force Microscopy and Transmission Electron Microscopy, T. D. Lenane, F. Ahmad, and G. W. Auner, Department of Electrical and Computer Engineering, and R. Naik, Department of Physics, Wayne State University, Detroit, MI 48202.**

Interfacial studies and growth initiation studies are necessary to help predict the morphology and structure of the resulting epilayer and to determine under which conditions heteroepitaxial growth is favored. In this study we investigate the evolution of the growth morphology of AlN thin films on sapphire substrates. The growth initiation and interface structure are correlated with the surface morphology of the AlN film. Thin films of aluminum nitride (AlN) were grown on sapphire (0001) and sapphire (1102) substrates by plasma source molecular beam epitaxy (PSMBE). AlN film quality is correlated with substrate temperature and bias effects. The substrate temperature was varied between 400°C and 800°C. The acceleration bias was varied between 0 V and -20 V dc. Interface reconstruction and growth kinetics of thin overlayers are investigated using transmission electron microscopy (TEM). Periodic measurements during the growth stages of AlN were performed by high resolution atomic force microscopy (AFM) by transferring under vacuum to an AFM analysis chamber. Local structure at the interface is correlated with growth mode. Our current AFM and TEM studies on c-plane and a-plane AlN films grown at 600°C indicate that the growth mode is a 3-D mechanism. Layer-by-layer (2D) growth is highly desirable and favored at lower substrate temperatures (400°C) under bias conditions of approximately -10 V dc. AFM and TEM studies of the temperature and bias effects on interfacial growth will be presented.

## VACUUM METALLURGY

### Room A106 - Session VM-FrM

#### Surface Engineering for Wear and Corrosion Protection

**Moderator:** C. R. Parent, The Gillette Company.

**8:20 am VM-FrM1 Friction and Wear of Gas Lubricated SiC/Mo Couples in Sliding Contact, I. L. Singer<sup>1</sup>, Th. le Mogne<sup>2</sup>, Ch. Donner<sup>2</sup> and J. M. Martin<sup>2</sup>, <sup>1</sup>U.S. Naval Research Laboratory, Washington, DC, USA and <sup>2</sup>Ecole Centrale de Lyon, Ecully, France.**

Friction test were performed in a UHV chamber with a SiC pin against a Mo flat exposed to various gases. At  $p = 13 \text{ Pa}$  ( $10^{-1}$  Torr), friction coefficients were between 0.1 and 0.2 with  $\text{SO}_2$  and  $\text{O}_2$  gas and less than 0.01 with  $\text{H}_2\text{S}$  gas. Tests performed at  $p < 10^{-3} \text{ Pa}$  ( $< 10^{-7}$  Torr) after  $\text{H}_2\text{S}$  exposure gave friction coefficients of 1. *In-situ* XPS analysis indicated the gas reacted layers on Mo were less than 1 nm thick. *In-situ* Auger analysis of Mo wear tracks showed tribo-reacted surface films of Mo oxysulfide, Mo oxide and Mo sulfide for the three gases, respectively, and transfer films of Si oxide for  $\text{SO}_2$  and  $\text{O}_2$  exposures. In SiC wear tracks, transfer films of Mo oxide were seen after sliding in  $\text{SO}_2$  and  $\text{O}_2$ ; in addition, Si oxide and Si sulfide were detected. Microscopy of wear tracks showed more wear debris in the  $\text{SO}_2$  and  $\text{O}_2$  tests than in the  $\text{H}_2\text{S}$  tests; EDX and TEM identified the debris as metallic Mo. Gas/solid reactions and lubrication processes responsible for up to three orders of magnitude reduction in the friction coefficient will be discussed.

**8:40 am VM-FrM2 Microstructural Effects on Tribological Properties of Electron Enhanced Magnetron Sputtered Coatings, J. M. Schneider, A. A. Voevodin, C. Reholz and A. Matthews, The Research Centre in Surface Engineering, The University of Hull, Hull, HU67RX, UK, D. B. Lewis, Materials Research Institute, Sheffield Hallam University, Sheffield S1 1WB, UK.**

X-ray diffraction measurements on tungsten carbo-nitride and titanium carbo-nitride coatings produced in an electron enhanced unbalanced magnetron system were performed. The films were deposited onto steel substrates with an Argon background pressure in the range of  $3 \times 10^{-3}$  mbar and introducing a gas mixture of nitrogen and

acetylene in different ratios, which alters the carbon to nitrogen ratio in the coating. The chemical composition of the film was analysed by means of GDOS. The peak positions, integral breadth and shape parameters were determined by X-ray diffraction. The tribological performance under adhesive and abrasive wear have been determined and correlated to micro structure and phase composition.

**9:00 am VM-FrM3 Coatings Defects on Corrosion Behavior of Hard Nitride Coatings on Steel, Y. B. Wang, M. S. Wong, R. Krueger, W. D. Sproul, and T. J. Barlo, BIRL Industrial Research Laboratory, Northwestern University, Evanston, IL 60201.**

The corrosion behavior of reactively sputtered niobium nitride (NbN) on 1018 carbon steel was investigated in a deaerated solution of sulfuric acid and sodium chloride using electrochemical corrosion tests. In general, NbN coatings, similar to other hard nitride coatings such as TiN and ZrN, exhibited high corrosion resistance and reduced the corrosion rate of the base metal by a factor of 1000. The defects in the coatings have a dominant effect on the corrosion behavior of the coated samples. By studying the variation of the corrosion potentials and corrosion current densities of coated samples with time, the influence of the coating defects on the corrosion behavior became evident. The results showed that the corrosion process consisted of three stages related to the initial interaction and nucleation and growth of corrosion pits. All of the observed corrosion pits on the tested coated samples corresponded to the positions of the preexisting defects on the coating surfaces before the test. The effects of several types of defects were studied.

**9:20 am VM-FrM4 Thermo-Mechanical and Chemical Properties of SiC-C Functionally Gradient Coatings on C/C Composites, M. R. Richards, A. C. Richards, M. Taya\*, and F. S. Ohuchi, Department of Materials Science and Engineering, and \*Department of Mechanical Engineering, University of Washington, Seattle, WA 98195.**

Functionally Gradient Coatings (FGC) represent a new class of composite materials in which the material composition and/or structure has been intentionally graded to overcome interfacial discontinuities. When depositing FGCs for applications requiring a homogeneous coating over the entire surface of the material, conventional CVD techniques produce gaps which compromise the coating integrity. We have developed an innovative cold-wall Chemical Vapor Deposition (CVD) apparatus specifically designed to overcome these problems. A key feature of the design is to employ electromagnetic fields to simultaneously heat and levitate the substrate. This technique has been applied to the fabrication SiC-C functionally gradient coatings on graphite and C/C composites. By controlling the flow rate of the reactant gases,  $\text{SiCl}_4$ ,  $\text{C}_3\text{H}_8$  and  $\text{H}_2$  a gradient layer can be grown with any compositional profile, to any desired thickness. Thermo-mechanical, chemical, and oxidation properties of the SiC-C FGCs are then characterized in order to assess the coating reliability for use in high temperature oxidizing environments.

**9:40 am VM-FrM5 Plasma-based Surface Engineering Processes for Wear and Corrosion Protection, A. Matthews, A. Leyland, B. Dorn, P. R. Stevenson, M. Bin-Sudin, C. Reholz, A. Voevodin, J. Schneider, Research Centre in Surface Engineering, University of Hull, Hull, HU6 7RX, UK.**

In a study of wear and corrosion coatings usage in an industrial economy (Ref. 1) it was shown that the advanced plasma- or ion-assisted PVD and CVD methods account for less than 0.5% of the market by value. This is surprising, given the widely reported benefits of these new coating methods. The lack of market penetration by these processes is due to several factors, amongst which is their perceived unsuitability for cheaper substrate materials such as low alloy steels, and their relatively higher cost. This paper discusses how recent developments in plasma-based processing are beginning to extend these processes into new applications sectors. These developments include hybrid methods, in which two or more processes are combined (e.g. PVD plus plasma diffusion treatment or PVD plus electroless nickel coating), or the development of new tougher PVD or CVD coatings which can be applied to relatively soft substrates (e.g. thick Ti/TiN multilayer coatings or multilayer ceramic/DLC coatings). Wear and corrosion data obtained with these coatings is reported, and new application sectors identified.

**INVITED**

1. The UK Engineering Coatings Industry in 2005, A. Matthews, R. Artley, P. Stevenson and P. Holiday, Hull University, 1992.

10:20 am **VM-FrM7 Vacuum Technology for Coating TiCN-Based Cermets**, *Igor Yu. Konyashin*, Hardmetal Technologies, Zelyony Prospekt, 67-1-117, Moscow 111558, Russia.

Conventional CVD and PVD processes for deposition of wear-resistant coatings have been shown not to be highly effective for improvement of service life of TiC or TiCN based cermets with a Ni-Mo binder. A new technology for deposition of multilayer wear-resistant coatings onto cermets of the TiCN-Ni-Mo or TiCN-WC-Ni-Mo systems is developed. The technology is based on an interaction between the cermets and chromium vapors carried out under a special regime in vacuum. The coatings deposited by use of the process are composed of an upper hard carbide layer and an intermediate thin metal layer. The carbide layer is composed of a mixture of (Cr, Ni) 7C3 and (Cr, Ni) 23C6 and provides improved wear-resistance of coated cermet cutting inserts. The interlayer is composed of Ni-based solid solution and serves as a barrier for penetration of a crack from the carbide layer into the cermet substrate; it also reduces a level of residual stresses in the carbide layer and eliminates surface defects. Because of formation of a large diffusional zone between the coating and the substrate the coating has extremely high adhesion and cannot be removed from the substrate without failure of the coating itself. Substantial improvement in tool life of cermet indexable cutting inserts coupled with maintenance or even slight increase of transverse rupture strength, toughness and performance strength of the TiCN-based cermets is achieved by use of the technology developed. The coated cermets have more than an order of magnitude higher corrosion resistance and far better high-temperature oxidation resistance compared with the uncoated ones. The new technology has been introduced in

industry on a large scale and the coated cermet cutting inserts have up to 3 times higher tool life being tested under real operation conditions.

10:40 am **VM-FrM8 Fluoroplastic Coating of Cold Drying—"TETRON"**, *V. Ju. Demin, V. I. Rakhovsky*.

The new type of protection coating has been developed. It possesses all the advantages of ordinary fluoroplastic coatings, but it has better adhesion and does not require any thermal treatment. "TETRON" is a composition based on organosoluble fluorocopolymers with specific modifiers—adhesion promoters. The coating is applied on cleaned metal surface (iron, carbon steel, aluminum) by dipping, spraying or brush and dried at room temperature.

**Mechanical properties:**

adhesion strength	200 KG/sm,
ultimate tensile strength of free film	350 KG/sm,

**Chemical stability:** testing for adhesion strength and stability were conducted in hydrochloric (3–36% concentration), nitric (6–56%), hydrofluoric (10–40%) and sulphuric (10–40%) acids at temperatures of 20–70°C. The duration of testing until the emergence of corrosion damage is more than 4 years.

The main field of application—long-term (several years) protection against corrosion of chambers, pipelines and exhausting fans of chemical and radiochemical industry. The coating could be used as protective and/or decorative for metal surfaces working in a sea, fertiliser solutions and other aggressive media. The coating is easy to clean and does not exude toxic substances.

# EXHIBITORS PROGRAM

**41st  
NATIONAL  
SYMPOSIUM  
of the  
AMERICAN VACUUM SOCIETY**

**COLORADO CONVENTION CENTER**

**Denver, Colorado**

**Tues., October 25 – 11 a.m. to 6 p.m.**

**Wed., October 26 – 10 a.m. to 5 p.m.**

**Thurs., October 27 – 10 a.m. to 3 p.m.**

## **A & N CORPORATION**

P.O. Box 878  
Inglis, FL 34449  
Contact: Daniel Vaudreuil  
Tel: 904-447-2411  
Fax: 904-447-2322

**#707**

## **ADVANCED ENERGY INDUSTRIES**

1600 Prospect Parkway  
Fort Collins, CO 80525  
Contact: Barbara Bremer  
Tel: 303-221-4670  
Fax: 303-221-5583

**#417, 419**

A manufacturer of high vacuum components since 1965. Our product lines include: ISO-KF (QF) flanges, ISO-MF (LF) flanges, UHV (CF) flanges, ASA flanges, vacuum couplings, feedthroughs, and vacuum ball valves. We maintain extensive inventories of all catalogued items, and routinely ship products on a same or next day basis.

The next generation of AE Plasma-processing products will be on display for you to see. Our technical staff will be there to explain the product features. These new products measure greater numbers of parameters with more control than ever before. Cutting-edge technology provides tighter control, greater stability, and outstanding repeatability. AC, dc, or a combination. On display will be: MDXII dc magnetron drives, Sparc-Le, RFXII/RFG 13.56-MHz generator, mid frequency generator, impedance probe and RF measurement equipment.

## **ACADEMIC PRESS**

525 B Street  
Suite 1900  
San Diego, CA 92101-4495  
Contact: Elizabeth Bellanger  
Tel: 619-699-6390  
Fax: 619-699-6580

**#943**

## **AJA INTERNATIONAL**

P.O. Box 246  
809 Country Way  
N. Scituate, MA 02060  
Contact: William Hale  
Tel: 617-545-7365  
Fax: 617-545-4105

**#608**

Will display among its new and best selling books: Ohring's *Material Science & Thin Films*; Tsao's *Materials Fundamentals of Molecular Beam Epitaxy*; Berman's *Vacuum Engineering Calculations*; Israelachvili's *Intermolecular and Surface Forces*; d'Agostino's *Plasma Deposition, Treatment and Etching of Polymers*; Bube's *Electrons in Solids, 3rd ed.*; Guiochon's *Fundamentals of Preparative and Nonlinear Chromatography*.

Circular and rectangular magnetron sputtering sources and targets, ATC R&D sputtering systems, vacuum components, microwave power supplies and components, ECR sources electrostatic chucks and LN2 cooled electrodes, diamond film equipment, electron beam sources and systems.

## **ADVANCED CERAMICS CORP.**

11907 Madison Ave.  
Cleveland, OH 44107  
Contact: Larry Mann  
Tel: 216-529-3959  
Fax: 216-529-3975

**#450**

## **ALBERTA MICROELECTRONIC CENTRE**

11315-87 Av, #318  
Edmonton, AB T6G 2TG  
Canada  
Contact: Thomas Janacek  
Tel: 403-492-3914  
Fax: 403-492-1643

**#509**

Non-oxide ceramics and coatings for semi-conductor and super-conductor processing, hydrogen and ultra-high vacuum environments. Products include BoralloyR pyrolytic boron nitride, pyrolytic graphite (PG), BoralectricR and SiC heaters. New product introductions include "high thermal conductivity PG" and flash evaporators.

SIMBAD™ Monte Carlo thin film process simulator incorporating surface diffusion, geometrical shadowing. Predicts microstructure, density, coverage of metal film over ULSI topography. SIMBAD™ can simulate PVD processes-bias sputtering, alloy co-sputtering, collimation; evaporation; ion etching; CVD of refractory metals. All features were experimentally tested.

**ALCATEL VACUUM PRODUCTS #204,205,206,207**

67 Sharp Street  
Hingham, MA 02043  
Contact: Gail Williams  
Tel: 408-947-7000  
Fax: 408-280-7847

Exhibiting its complete and comprehensive oil-free products which include dry roughing pumps/systems, dry leak detectors, maglev turbomolecular pumps, Drytel product line, and the unique inverted seal turbomolecular pump. A demonstration of the patented leak testing method for long tubes or conductance limited lines will be performed during the exhibition.

**ALTA GROUP #219**

RR2 Box 710  
Marion School Road  
Fombell, PA 16123-9403  
Contact: Edward F. Cawley  
Tel: 412-452-1300  
Fax: 412-452-7701

Provides specialty target materials for thin film deposition. Metals and alloys are available or are made to order. Titanium 99.999% pure, nickel 99.99%, cobalt 99.95%, chrome 99.99% and others.

**AMERICAN BOA, INC. #549**

1420 Redi Road  
P.O. Box 1301  
Cumming, GA 30130  
Contact: Michael Nappi  
Tel: 404-889-9400  
Fax: 404-889-0661

Designer and manufacturer of flexible metal hoses, bellows and expansion joints for high vacuum and cryogenic piping systems. Services include design and stress analysis for piping systems and fabrication of custom components. Products offer superior flexibility, long cycle life to ISO standards, low spring forces, compact size and design reliability.

**AMERICAN INDUSTRIAL MICROWAVE #1016**  
(See Manitou Systems)**AMERICAN INSTITUTE OF PHYSICS #641, 643**

500 Sunnyside Blvd.  
Woodbury, NY 11797  
Contact: William Phillips  
Tel: 516-576-2484  
Fax: 516-576-2481

Visit the AIP booth. Examine new and best selling titles from AIP PRESS, including: *Molecular Beam Epitaxy*, *Reversible Crystal Plasticity*, *The Handbook of Electron Spin Resonance*, *The AIP Handbook of Modern Sensors*, and new paper edition of *Measurement Errors*, and the AVS Classic Series. While in the booth, take a moment to see a demonstration of our growing list of electronic products, including PINET, AIP's Online physics information network, APL Online, the searchable electronic version of *Applied Physics Letters*, and the CD-ROM version of *JVST*. Also on display will be AIP and AIP Member Society journals, including *CHAOS* and *Computers in Physics*.

**AMETEK/DYCOR #331, 333**

150 Freeport Road  
Pittsburgh, PA 15238  
Contact: Richard Shehab  
Tel: 412-828-9040  
Fax: 412-826-0399

Exhibiting the New Dycor System 1000 and our PC-Based DyCard System 1000 Quadrupole Mass Spectrometers. These analyzers offer the most versatile software and control capabilities available in industry today. Also, exhibiting the Model 303B Moisture Monitor and Model 5700 Trace Moisture Analyzer for process gas monitoring.

**AMPLIFIER RESEARCH #716**

160 School House Road  
Souderton, PA 18964  
Contact: Gail Supplee  
Tel: 215-723-8181  
Fax: 215-723-5688

RF power amplifiers for plasma etching/deposition, RF heating, ultrasonics, laser research, NMR/MRI and many other research applications. Output power varies from 1 watt to 10 kilowatts with frequency coverage from 1 kHz to 1 GHz. Full bandwidth instantly available without need for tuning or bandswitching, plus total immunity to load mismatch.

**ANGSTROM SCIENCES #808**

1200 Lebanon Road  
West Mifflin, PA 15122  
Contact: Vincent E. Kostelnik  
Tel: 412-462-2777  
Fax: 412-462-2780

Dedicated to the advancement of magnetron sputtering technology. Our Onyx™ line of sputtering sources are exceptional tools for research and production applications. The Onyx™ sources are standard in (1", 2", 4", 6", 8") and Linear. Also offering a complete array of sputtering targets, evaporation materials, backing plates and target bonding.

**APD CRYOGENICS**

#704, 706

1833 Vultee Street  
Allentown, PA 18103  
Contact: Robyn H. Gross  
Tel: 610-791-6700  
Fax: 610-791-0440

A company devoted solely to the design and development of both standard and customized cryogenic equipment for use in semiconductor manufacturing, laboratory research, military surveillance/guidance systems, and medical diagnostics. NEW AT AVS: 1) Optical exchange cryostat with interchangeable tailpieces, 2) LHe Cryostat for UHV manipulators - fully rotatable under vacuum, 3) 6.5 K Displex 4) MARATHON™ Cryopumps-Low Profile and 250mm.

**APPLIED AUTOMATIONHARTMANN & BRAUN #347**

P.O. Box 9999  
Bartlesville, OK 74005  
Contact: Marianne Keith  
Tel: 918-662-7343  
Fax: 918-662-7358

Exhibiting the MB series of FTIR spectrometers. The MB's versatile, rugged design dramatically facilitates ease of integration to vacuum chamber ports. Instrument stability allows for extended acquisition times (upwards of 5 hours) and long delays between reference and acquisition. Advanced purge features minimize problems due to water vapor lines as exhibited in self-assembled monolayer studies.

**APPLIED SCIENCE & TECHNOLOGY**

#545

35 Cabot Road  
Woburn, MA 01801  
Contact: Michele M. Meagher  
Tel: 617-937-5121  
Fax: 617-933-0750

Manufactures a wide range of microwave power supplies, plasma sources, and plasma deposition systems for materials processing. Applications include CVD (diamond, GaN, SiC, cBN, a-Si, and other coatings), production of ions and radicals, etching, and ashing. ASTeX also offers a low-cost Raman spectrometer for materials analysis.

**APPLIED SURFACE TECHNOLOGIES**

#522

15 Hawthorne Drive  
New Providence, NJ 07974  
Contact: Robert Sherman  
Tel: 908-464-6675  
Fax: 908-464-7475

The carbon dioxide snow cleaning jet will be demonstrated. This surface cleaning process can remove particulates of all sizes (even submicron), remove hydrocarbon based contamination and reduce the background surface carbon concentration - all nondestructively and residue-free. New large-area cleaning units and automated cleaning stations will be shown.

**ATI INSTRUMENTS N.A.**

#642

1001 Fourier Drive  
Madison, WI 53717  
Contact: Mary Postweiler  
Tel: 608-831-5155  
Fax: 608-831-2093

Will exhibit the Research Series FTIR spectrometer and new real-time PM-FTIR system for analysis of surface adsorbates. Research Series FTIR provides the highest sensitivity and stability available in FTIR. PM-FTIR eliminates the need for a reference background in surface analysis by FTIR. Only surface adsorbed species are detected, enhancing the range of applications for FTIR in surface analysis.

**AUSTIN SCIENTIFIC CO.**

#924

4114 Todd Lane  
P.O. Box 18863  
Austin, TX 78760  
Contact: L.F. Templeton  
Tel: 512-441-6893  
Fax: 512-443-6665

A manufacturer of after-market replacement parts and accessories for CTI cryopumps and compressors and has specialized in the repair and exchange of cryopump equipment for 15 years. Based on this extensive experience, we now also manufacture complete cryopumps and compressors that are "CTI compatible".

**BALZERS**

#517 - 523 &amp; 616 - 622

8 Sagamore Park Road  
Hudson, NH 03051  
Contact: Julie Coutu  
Tel: 603-889-6888  
Fax: 603-889-8573

Breakthroughs in vacuum equipment provide high performance vacuum pumping, measurement and control. New wide-range turbopumps for standard and corrosive gases let you use a backing pump 100 times smaller. New gas analyzer has high sensitivity and stability for process gas analysis and quality control. New Full Range™ compact gauge measures from atmosphere to UHV with or without a separate controller. New laboratory coater starts at just \$36,000. Also representing Bal-Tec Products for EM sample preparations.

**BERTAN HIGH VOLTAGE**

#827

121 New South Road  
Hicksville, NY 11801  
Contact: Jim Donley  
Tel: 516-433-3110  
Fax: 516-935-1766

Precision high voltage power supplies for detectors, electrophoresis, electron and ion beams, X-ray sources, spectroscopy. Power supply outputs range from 500V to 100kV, from several watts to 1kW. Supplies are available in modular,



rack-mount, bench-top and NIM configurations. Standard and custom supplies are offered. UL, CSA, VDE approval on some models.

**BI-BRAZE® DIV. of ALTEC INT'L.**

**#747**

2191 Ward Avenue  
La Crosse, WI 54601  
Contact: George W. Snapp  
Tel: 608-787-2266  
Fax: 608-787-2266

Manufactures metallurgically bonded transitions consisting of cylindrical sections of aluminum and stainless steel bonded together to form vacuum/pressure tight couplings, the ends of which are welded to similar metals in systems operating at cryogenic temperatures as low as 1.5 Kelvin and high vacuum/elevated pressure.

**BROOKS INSTRUMENTS**

**#922**

407 W. Vine Street  
Hatfield, PA 19440  
Contact: David W. Dedman  
Tel: 215-362-3617  
Fax: 215-362-3745

Will exhibit its line of Mass Flow Controllers, pressure regulators and controllers, and flow meters for gas and liquids. All support instrumentation and electronics also available. Brooks services the vacuum/semi industry with a network of service/sales centers around the world.

**BURLEIGH INSTRUMENTS**

**#933**

Burleigh Park  
P.O. Box E  
Fishers, NY 14453-0755  
Contact: Patricia Payne  
Tel: 716-924-9355  
Fax: 716-924-9072

New affordable personal AFM, STM, UHV/STM 3-D measuring microscopes are designed for routine imaging of fine surface topography with precise 3-D quantitation. Instructional STM microscopes use atomic resolution to improve teaching about atoms. Linear positioning stages and UHV motors for submicron and nanometer applications.

**CAMBRIDGE MILL PRODUCTS**

**#916**

6005 Alliance Road N.W.  
Malvern, OH 44644  
Contact: Charles E. LeBeau III  
Tel: 216-863-1121  
Fax: 216-863-2043

Will display our complete line of vacuum pump oils and reclamation services. New Products will include pump parts for Stokes piston pumps. Information will also be available on our repair services for vane pumps, piston pumps and vacuum blowers.

**CAMECA INSTRUMENTS**

**#846,848,850**

2001 West Main Street  
Stamford, CT 06902  
Contact: Florence Pindrys  
Tel: 203-348-5252  
Fax: 203-348-5516

Displaying our new Cameca TOF SIMS IV -- a most advanced Time-of-Flight Secondary Ion Mass Spectrometer. This no-compromise, fully-digital static SIMS offers the best in high-resolution imaging and mass spectroscopy thanks to our new, patented "Burst-Mode" Gallium source. Also available for viewing, Cameca IMS 6f/1270 interactive software.

**CAPITOL RESEARCH EQUIPMENT**

**#345**

13897 Willard Road  
Chantilly, VA 22021  
Contact: Joseph Cannon  
Tel: 703-631-3933  
Fax: 703-631-3936

Sales of Shimadzu Magnetic-Levitated Compound and Standard Turbo pumps for use in semi-conductor and research application. Specializes in the remanufacture of all makes of Turbo Molecular, Cryogenic and Mechanical vacuum pumps with emphasis on turn-around time and reliability. Manufacturers representatives in the Washington D.C. area for all lines of vacuum systems and component needs.

**CARFAX PUBLISHING CO.**

**#748**

P.O. Box 25  
Abingdon,  
Oxfordshire, OX 14 3UE  
UNITED KINGDOM  
Contact: John Wilson  
Tel: 44 235 555335  
Fax: 44 235 553559

A leading UK journal publisher for 22 years. We have recently acquired a US base in Cambridge, MA. The AVS Conference provides a launch platform for their new premier quarterly journal *Probe Microscopy*. This will consolidate the significant position of Carfax, current publishers of *Nanobiology*, in the field of nanoscale science.

**CERAC, INC.**

**#928**

407 N. 13th Street  
P.O. Box 1178  
Milwaukee, WI 53201-1178  
Contact: Nora Bauer  
Tel: 414-289-9800  
Fax: 414-289-9805

Manufacturer of a full line of thin-film materials, vacuum deposition chemicals, sputtering targets, hearth liners, and high purity and specialty inorganic chemicals, organometallics and metals. Custom preparations, sizes, shapes and compositions readily available in both R&D and production quantities.

**CERAMASEAL**

#544,546

P.O. Box 260  
New Lebanon, NY 12125  
Contact: Lenore Laier  
Tel: 518-794-7800  
Fax: 518-794-8080

Exhibit will feature new Type D connector, crystal quartz viewports and quartz rod assemblies. Has over 40 years experience designing and manufacturing ceramic-metal components, including vacuum feedthroughs, connectors, thermocouples, cables, viewports and related hardware. Products meet demanding applications including UHV, high temperature, cryogenics, pressure extremes, and high voltage/current ratings.

**CHA INDUSTRIES**

#322

4201 Business Center Dr.  
Fremont, CA 94538  
Contact: Shannon Pimentelli  
Tel: 510-683-8554

A manufacturer and OEM supplier of standard and custom High Vacuum systems. Systems include Evaporation; Thermal and Electron Beam, Sputtering; Magnetron and Ion Beam, Ion Beam etch, and combinations. Systems are complemented by CHA's full line of Fixturing and other components.

**COMDEL INC.**

#844

126 Sohler Road  
Beverly, MA 01915  
Contact: Theodore E. Johnson Jr.  
Tel: 508-927-3144  
Fax: 508-922-8205

Offers highly Stable and Reliable RF Power delivery. CPS series: 4 to 60 Mhz from 250 to 5K W solid state. CLF series: 20Khz to 2 Mhz up to 5K W solid state. New - CMS series: 200 and 400 watts at 915 Mhz solid state. New - CHS series: 10,15,25 KW at 13.56 Mhz. New - CX series microprocessor controlled 4 to 60 Mhz. New - CD series: Dual frequency power in one supply. New Matchpro series automatic matching networks. RPM-1: Measures and controls delivered power at the plasma load - assures process repeatability. New - RPM - 2 Dual frequency capability.

**COMMONWEALTH SCIENTIFIC**

#405

500 Pendleton Street  
Alexandria, VA 22314  
Contact: Claire Moss  
Tel: 703-548-0800  
Fax: 703-548-7405

Will be displaying its complete line of ion beam sources and systems. Applications include Ion-Assisted Deposition,

Sample Precleaning, Ion Beam Etching, and Reactive Ion beam etching. CSC's gridded sources range from 3 to 38cm in size to accommodate any application. New products to be displayed this year include the Cathodic Arc Source and the 1 Meter Linear Gridless Ion Source.

**COOKE VACUUM PRODUCTS**

#902

13 Merritt Street  
S. Norwalk, CT 06854  
Contact: Jerry P. Santucci  
Tel: 203-853-9500  
Fax: 203-838-9553

Displayed this year will be Model CV301, a Thermal Evaporation System, high vacuum valves, traps, feedthroughs and other associated vacuum components.

**CTI-CRYOGENICS**

#603, 605

Nine Hampshire Street  
Mansfield, MA 02048  
Contact: Susan Pieroni  
Tel: 508-337-5104  
Fax: 508-337-5169

The On-Board® vacuum control system expands upon traditional ideas about vacuum management. Its unique, total integration of microprocessor-controlled pump operations with the overall vacuum system, significantly improves performance and economics. Real-time pump monitoring and control maximizes process repeatability and uptime, reduces regeneration time significantly, and provides predictive diagnostics, for single and multiple pumps. Modularity supports easy upgrade and process-specific applications flexibility for cryopumps, water-vapor pumps, and turbopumps.

**CVC PRODUCTS**

#416

525 Lee Road  
P.O. Box 1886  
Rochester, NY 14603-1886  
Contact: Tim Sladden  
Tel: 716-458-2550  
Fax: 716-458-0424

Supplier of MESC cluster tools for integrated thin film processes. Also offers systems for physical vapor deposition (PVD), plasma enhanced chemical vapor deposition (PECVD), rapid thermal processing (RTP). CVC offers the Connexion™ a fully MESC compliant modular cluster tool for VLSI fabrication. Founded in 1934, CVC continues to serve the world semiconductor and data storage markets from our base in Rochester, NY, and regional technical centers in Fremont, CA, Leuven, Belgium, Hong Kong and Osaka, Japan.

**CVI INC.****#526, 528**

P.O. Box 2138  
Columbus, OH 43216  
Contact: Kenneth F. Wilson  
Tel: 614-876-7381  
Fax: 614-876-5648

A designer and manufacturer of vacuum and cryogenic systems and components. Included are cryopumps (6" to 48" diameter), Mini-refrigerators, vacuum jacketed cryogenic piping and valves, high pressure cryogenic pumps and LNG fuel systems. We also include turnkey thermal vacuum test facilities, helium refrigerator/liquefiers and miscellaneous systems.

**DANIELSON ASSOCIATES****#817, 819**

1989A University Lane  
Lisle, IL 60532  
Contact: Antonio Garza  
Tel: 708-960-0086  
Fax: 708-960-0546

Manufactures innovative products for the high vacuum industry, designed to solve common vacuum technology problems in an uncommon way. Products include 27 models of oil-free Tribodyn, Barodyn, Spiradyn, and Cyclodyn vacuum pumps, six models of the high and ultrahigh vacuum Sorbodyn bulk getter pumps, two models of the ultrahigh vacuum Sorbion bulk getter pump, Omnibar portable leak sensor, and the patented Phototron device.

**DENTON VACUUM, INC.****#837, 839**

1259 N. Church Street  
Moorestown, NJ 08057  
Contact: Sharron Williams  
Tel: 609-439-9100  
Fax: 609-439-9111

Proudly featuring its full line of thin film coating systems, from its laboratory line of economical evaporation and sputtering systems to its powerful, flexible and fully automated load-lock systems and production coating systems. On display will be a broad array of subsystems such as the CC-102R cold cathode ion source, the SD-10 optical monitor, as well as an exciting assortment of electrical and mechanical feedthroughs. Stop by and peruse valuable technical literature and brand new brochures.

**DIGITAL INSTRUMENTS****#511, 513**

520 E. Montecito Street  
Santa Barbara, CA 93103  
Contact: Terry Mehr  
Tel: 805-899-3380  
Fax: 805-899-3392

Manufactures a complete line of NanoScope® scanning probe microscopes (SPMs). The Dimension™ 3000 Atomic Force

Microscope (AFM) offers the complete range of AFM techniques for small or large samples and analyzes samples up to 8" in diameter in air or liquid with manual and automated stepping for scanning multiple areas of your sample. Its new TrakScan™ scanning system makes setup simple and provides superior images for the full range of scanning techniques including Tapping Mode™ magnetic force, lateral force, electrochemistry and others. The MultiMode™ AFM is a high resolution scanning probe microscope. It supports both AFM and scanning tunneling microscopy (STM) in conventional and electrochemical operation. Samples can be imaged in different modes including contact, non-contact, lateral force, LiftMode™, magnetic force and Tapping Mode™.

**DUNIWAY STOCKROOM****#524**

1600 N. Shoreline Blvd.  
Mountain View, CA 94043  
Contact: Bob Friedrich  
Tel: 415-969-8811  
Fax: 415-965-0764

Replacement parts, both new and rebuilt, for pumps, leak detectors and systems. Silver-plated bolts - no extra cost. Bakeable leak valve, sapphire seat type - in stock. Ion pumps new and rebuilt, also rebuilding service. Catalog available. The last 6 pages show surplus equipment, rebuilt equal to new, including prices.

**DYNAVAC****#927**

30 Woodrock Road  
Weymouth, MA 02189  
Contact: Liz Claflin  
Tel: 617-337-4111  
Fax: 617-337-5145

Designs and manufactures systems for a wide range of process requirements. Our major product line includes systems for space simulation, optical coating, metallizing, sputtering, evaporation and medical labware processing. Retrofitting services are also offered to refurbish existing systems or upgrade process capabilities with our supervisory control system.

**EBARA TECHNOLOGIES****#1020, 1022**

3560 Bassett Street  
Santa Clara, CA 95054  
Contact: Kathy Baro  
Tel: 408-496-2825  
Fax: 408-496-2801

Manufacturer of clean, dry vacuum products including dry roughing pumps for CVD, etch, and load lock applications and Dry Gas Scrubbers. Cryopumps for Sputter, Ion Implant, MBE, and general vacuum applications. Magnetically levitated turbos and CryTurbos™ with high water pumping. Data acquisition and diagnostics for all products.

**EDWARDS HIGH VACUUM INT'L.****#700, 702**

301 Ballardvale Street  
Wilmington, MA 01887  
Contact: Lisa Doody  
Tel: 508-658-5410  
Fax: 508-658-7969

Displaying its full line of RV Mechanical Vacuum Pumps, Scroll Drypump, Active Vacuum Gauges, EXT Turbopumps, STP Turbopumps, Barocel Pressure Transducers, Leak Detectors, Vacuum Coating Systems, and a complete array of Vacuum Hardware and Accessories.

**ELNIK SYSTEMS****#617, 619**

3 Edison Place  
Fairfield, NJ 07004  
Contact: Claus J. Joens  
Tel: 201-882-8033  
Fax: 201-882-8037

Will exhibit: 100% Oil Free Roots Pump Stations that contain Diaphragm Pumps with pumping speeds from 6 to 30 CFM and ultimate vacuums from 10<sup>-2</sup> and 10<sup>-4</sup> Torr. 100% Oil Free Diaphragm Pumps with pump speeds from 1.4 to 4.6 CFM and ultimate vacuum ranges of 1.5 Torr. These pumps are available in Aluminum/Vitron or chemically resistant PTFE versions. High Temperature/High Vacuum Furnaces with ultimate vacuum capability of 10<sup>-9</sup> Torr and fully integrated computer operating system.

**ELSEVIER SCIENCE INC.****#648**

655 Avenue of the Americas  
New York, NY 10010  
Contact: Sandra Pierre-Lys  
Tel: 212-633-3758  
Fax: 212-633-3764

Will exhibit journals and books dealing with physics and chemistry of surface and analytical tool, vacuum processing of materials and surface technology. Free sample copies are available of journals including Surface Science, Applied Surface Science, Surface Science Reports, Progress in Surface Science and Vacuum. Detailed information about the alerting service in Condensed Matter Science called CoDAS, will be available.

**ENGELHARD CORPORATION****#842**

101 Wood Avenue  
Iselin, NJ 08830-0770  
Contact: D.A. Toenshoff  
Tel: 908-205-5772  
Fax: 908-205-7476

Specialists in precious metal sputter targets for all segments of science and industry. Worldwide producers and suppliers of precious metals. Provides full service capability from refining, reclamation, working, and financing. Introducing a newly expanded sputter coating capability for the production of

enhanced precious metal coatings on wire, ribbon, and foil. This capability brings to all industries an opportunity to benefit from the unique characteristics of precious metal with tailor-made physical properties associated with base metals.

**ENI****#547**

100 Highpower Road  
Rochester, NY 14623  
Contact: Philip A. LaTulipe  
Tel: 716-292-7437  
Fax: 716-427-7839

Will display a DC plasma generator designed for high-power sputtering of hard disks and flat panel displays. Also ideal for semiconductor wafer sputtering and deposition, the DCG-100 features major industry advances in repeatability, and arc control. Also on display: 13.56MHz RF generators for plasma etching, sputtering and deposition.

**E.T. SYSTEMS/ELECTROTECH****#1023**

3350 Scott Blvd., Bldg. 8  
Santa Clara, CA 95054  
Contact: Lynn Tocci  
Tel: 408-727-5501  
Fax: 408-988-6385

300 Series, Multiplex Cluster Plasma Systems will be displayed. These systems provide plasma processing solutions for R&D, pilot production, and fullscale production. Available in PECVD, RIE, and PVD.

**EVAC INTERNATIONAL****#918**

215 River Vale Road  
River Vale, NJ 07675  
Contact: Ruth Tschudin  
Tel: 201-666-8558  
Fax: 201-666-8470

Exhibiting our chain clamps, flanges, fittings and seals for high vacuum and UHV. Our chain clamps are designed to provide high, even clamping force with time-saving one- and two-bolt convenience. They are especially suitable for metal seals, i.e. aluminum knife-edge seals, bakeable to 150-degrees C. New product: glass components NW 10...125.

**EVEY ENGINEERING CO.****#305**

154 Center Street  
Groveland, MA 01834  
Contact: Robert A. Saldarini  
Tel: 508-372-5511  
Fax: 508-521-1631

Buys and sells all types of vacuum related equipment as well as all types of related oils. We sell and service leak detectors and equipment utilized in glass and semiconductor manufacturing. Please call us for a free catalogue.

**EXTREL MASS SPECTROMETRY #1002,1004,1006**

575 Epsilon Drive  
Pittsburgh, PA 15238  
Contact: Rita M. Smith  
Tel: 412-967-5763  
Fax: 412-963-6578

Featuring quadrupole mass spectrometers and systems including: quadrupole power supplies with mass ranges up to 4000 amu; quadrupole mass filters - 9.5 mm, 16 mm and 19 mm diameter quadrupole rods; Electron impact ionizers - axial crossbeam and direct inlet; and the electronics of quadrupole mass spectrometers. All are used in applications such as: thermal desorption, surface analysis, molecular beam and cluster chemistry. Also exhibiting the MS-250™ - high performance gas analyzer. This high performance quadrupole mass spectrometer is designed for general purpose analytical requirements.

**FEI CO.****#430, 432**

7451 NE Evergreen Pkwy.  
Hillsboro, OR 97124  
Contact: Andree Kraker  
Tel: 503-640-7500  
Fax: 503-640-7502

Introduces a new line of high brightness, compact, Schottky field emission focusing columns. These components complement FEI's existing line of focused ion beam columns featuring reliable UHV construction and a modular design philosophy. Also featured are LaB<sub>6</sub>/CeB<sub>6</sub>, Schottky and LMI sources, as well as FEI's line of focused ion beam and DualBeam™ workstations.

**FERRAN SCIENTIFIC****#1017,1019**

11558 Sorrento Valley Road  
Suite 2  
San Diego, CA 92121  
Contact: Brian Sutherland  
Tel: 619-792-2332  
Fax: 619-792-0065

"Micropole™ sensor (MPA): Miniature quadrupole gas analyzer, featuring 10 mTorr maximum operating pressure, 2-200 AMU range, occupies < 5cc in vacuum, low cost (<\$3000). "Gas Sampling system: 30psia to 10torr operating pressure, includes differentially pumped MPA, <1 ppm detection, portable. "MPA logic controller: New production process monitor enhanced Micropole™ Sensor System."

**FERROFLUIDICS****#849,851,948,950**

40 Simon Street  
Nashua, NH 03061  
Contact: Kim Campbell  
Tel: 603-598-7329  
Fax: 603-883-2308

The world leader in magnetic fluid sealing technology manufactures hundreds of standard and custom rotary feedthrough designs and continues to develop next-generation HV and UHV sealing and valve solutions. Other products are automated crystal growing systems, electron beam evaporation sources, bearings for high performance optical scanners, ferrofluids for audio speakers.

**FIL-TECH, INC.****#744**

6 Pinckney Street  
Boston, MA 02114  
Contact: Paula L. Becker  
Tel: 617-227-1133  
Fax: 617-742-0686

Offers savings, with new, lowered pricing, on the following vacuum system supply items: Quartz crystals, single and dual sensor heads with shutters, electron beam gun replacement parts, FT704 and DC704 diffusion pump fluids, Du Pont Krytox and other mechanical pump fluids, ionization gauge tubes, and thermocouple gauge tubes.

**FISONS INSTRUMENTS****#500,501,502,503,504,505**

55 Cherry Hill Drive  
Beverly, MA 01915  
Contact: Jacky Kieras  
Tel: 508-524-1000  
Fax: 508-524-1019

Manufacturer of equipment designed to meet applications from research to quality control: includes surface analysis spectrometers for ESCA, Auger, SIMS and complete MBE systems.

**FUJI SEIKI INC.****#900**

B-6 Scotty Hollow Drive  
N. Chelmsford, MA 01863  
Contact: Eckhard Bez  
Tel: 508-251-1365  
Fax: 508-251-1365

Total Dry oil-free vacuum pumps are designed to replace small oil-sealed vacuum pumps. Their double sealed design, guarantees that no gases can leak into or out of the pumps, even when not operating. Gases can be pumped or circulated without contamination from oil, air, or nitrogen. They are suitable for leak detectors, mass spectrometers, electron microscopes, instruments, load-locks, and general vacuum systems.

**GELLER MICROANALYTICAL****#806**

One Intercontinental Way  
Peabody, MA 01960-3885  
Contact: Joseph D. Geller  
Tel: 508-535-5595  
Fax: 508-535-7653



Offers products and analytical services to the technical community. Products include NIST and NPL traceable magnification reference standards for atomic force, optical and scanning electron microscopy; and reference materials for surface analysis and microprobe techniques; high vacuum dessicators; and metallographic equipment. Analytical services include Auger electron spectroscopy, SEM, X-ray, Electron Microprobe, profilometry and metallography.

**GFE GES. FÜR ELEKTROMETALLURGIE**

**#446**

45 Hoefener Str.  
Nuernberg D-90431  
GERMANY  
Contact: Kalb Werner  
Tel: 49 911 9315 311  
Fax: 49 911 314 980

As an integrated producer of high purity metals, alloys, ceramics and cermets GfE offers a wide variety of coating materials for thin film technology. The targets, cathodes, slugs and granules are used in electronics, optics, flat glass coating and for wear and decorative applications.

**GNB CORPORATION**

**#320**

29393 Pacific Street  
Hayward, CA 94544  
Contact: Marsha Braaten  
Tel: 510-537-4722  
Fax: 510-537-4729

Designs and fabricates application-specific and standard vacuum equipment: Chambers -- Custom and Semi-custom, round, square, in-line and cluster. Valves -- Custom and standard, 0.5" to 144" free aperture, slit, gate and poppet. Components -- Bellows, viewports, spools, baseplates, and manifolds. Integrated Components -- Load-locks with valves, valves with traps.

**GRANVILLE-PHILLIPS**

**#720,721,722,723**

5675 Arapahoe Avenue  
Boulder, CO 80303  
Contact: Lisa Whitten  
Tel: 303-443-7660  
Fax: 303-443-2546

Featuring the new STABIL-ION® Vacuum Measurement System, which helps remove significant waste in vacuum processing caused by widely used Bayard-Alpert and inverted magnetron type ionization gauges. The STABIL-ION® gauge provides stability of calibration approximately ten times better than older technology gauges—giving dependable process repeatability and reduced defects.

**HAUZER VAC-TEC**

**#1025**

5400 Spine Road  
Boulder, CO 80301  
Contact: Robert S. Clarke  
Tel: 303-530-0144  
Fax: 303-530-0262

Manufactures a full range of PVD production coating systems. Representing Hauzer Techno Coating Europe, B.V. of The Netherlands, Hauzer Vac-Tec addresses both wear-resistant and decorative coating markets. Hauzer's proprietary Arc Bond Sputtering™ (ABStm) unit combines cathodic arc and unbalanced magnetron processes to enhance both adhesion and finish quality.

**HELICOFLEX CO.**

**#431**

P.O. Box 9889  
Columbia, SC 29290  
Contact: Ryan McCall  
Tel: 803-783-1880  
Fax: 803-783-4279

Specializes in high performance sealing systems for Ultra-High Vacuum and high purity chemicals. The Helicoflex Delta® Seal is an all metal, low load spring energized seal that provides Helium sealing at  $1 \times 10^{-12}$  cc/sec from -272°C to 700°C. The seal fits standard ISO flanges and is available in custom shapes and sizes. Applications include: quartz windows, cryogenics, radioactive environments and high power RF joints. The Helicoflex Quick Disconnect System: QDS™ is available for ISO KF fittings.

**HIDEN ANALYTICAL LTD.**

**#400, 402**

231 Europa Blvd.  
Warrington, WA5 5TN  
United Kingdom  
Contact: Peter Hatton  
Tel: 44 925 445225  
Fax: 44 925 416518

Manufactures quadrupole mass spectrometers for Vacuum, Gas, Surface and Plasma analysis. Hiden's exhibit includes the EQP plasma analyser, the new auto-analysis Langmuir probe, live RGA demonstrations and details of a new range of quadrupoles for the scientific user. U.S.A. distribution and service by AVC, Inc. headquarter in Pittsburgh, PA.

**HIGH VACUUM APPARATUS MFG.**

**#919, 921**

1763 Sabre Street  
Hayward, CA 94545  
Contact: Mary Osborne  
Tel: 510-785-2744  
Fax: 510-732-9853

Will feature a variety of UHV gate valves, including our 3-position gate valve. Also displaying our stainless rectangular valve line, and featuring our latest product "The quick coupling bonnet valve". Also displaying a variety of flanges and fittings.

**HUNTINGTON MECHANICAL LAB.****#201,203**

1040 L'Avenida  
Mountain View, CA 94043  
Contact: Bruce Harley  
Tel: 415-964-3323  
Fax: 415-964-6153

An integrated supplier of UHV components hardware including valves, roughing components and viewports as well as positioners, feedthroughs and custom chambers. Also offering prototype and high volume production support services for custom or standard UHV requirements including engineering design assistance.

**IBM ANALYTICAL SERVICES****#825**

1580 Route 52  
Hopewell Junction, NY 12533  
Contact: Kevin Hutchings  
Tel: 914-892-4556  
Fax: 914-892-2003

A world-leading technological resource now available to analyze, evaluate, and help improve your company's products or industrial processes. Our professionals have the first-hand knowledge it takes to understand your needs, solve your problems, and work with you as technical peers. For your general analytical requirements, we perform: chemical, structural, and surface analysis; metallography and microscopy. Stop by and see us at booth #825 to discuss your needs.

**INLAND VACUUM****#841**

35 Howard Avenue  
P.O. Box 373  
Churchville, NY 14428  
Contact: Nancy Silivestro  
Tel: 716-293-3330  
Fax: 716-293-3093

For over two decades, we have offered its customers a complete line of quality cost effective vacuum pump fluids. Through a combination of superior customer service, technical support, competitive pricing and just-in time delivery, Inland has become the leader in the industry.

**INNOTECH GROUP INC.****#307**

61 W. Moreland Road  
Simi Valley, CA 93065  
Contact: William T. Read  
Tel: 805-522-9040  
Fax: 805-522-6017

Introduces their new ILS-28C vertical in-line sputtering system. The ILS-28C is primarily designed for the manufacture of flat panel displays. It can process substrate areas up to 28" X 28" and includes features such as cassette to cassette robotic

substrate load and un-load, dual substrate pallets with a centrally located substrate heater for dual sided deposition, buffer chambers to maximize substrate throughput and target utilization and a pallet return system which allows a through-the-wall installation. Process chambers can be installed with options such as RF and DC cathodes, RF etching, RF and DC bias and ion beam cleaning.

**INTEGRATED VACUUM TECHNOLOGY****#647**

505 Violet Street  
Golden, CO 80401  
Contact: William L. Goldsworth  
Tel: 303-278-7271  
Fax: 303-278-4922

Designs, and manufactures cathodes for sputter deposition, they produce custom cathodes, their standard cathodes, or sub-contract manufacture other designs. They own and use sputtering cathode technology which was formerly that of Vac-Tec systems. Offering proven cathodes for sputtering in RF and DC and magnetic materials.

**ION TECH INC.****#829, 831**

2330 East Prospect  
Fort Collins, CO 80525  
Contact: Gerald Isaacson  
Tel: 303-221-1807  
Fax: 303-493-1439

Available equipment ranges from linear, round DC and filamentless RF ion beam sources, which can be fitted to existing systems; to complete optical deposition or DLC systems. Systems can be designed to meet any specific customer requirements in producing various high quality thin films.

**JEOL USA, INC.****#311**

11 Dearborn Road  
Peabody, MA 01960  
Contact: Mike Kersker  
Tel: 508-535-5900  
Fax: 508-536-2205

Manufactures a full line of surface analysis instrumentation including UHV-STMs featuring a high temperature sample heating stage, Scanning Auger Microprobes with ESCA attachments and ultra high resolution, low voltage, field emission SEMs.

**JOHN CRANE BELFAB****#507**

305 Fentress Blvd.  
Daytona Beach, FL 32114  
Contact: John Egbert  
Tel: 904-257-0131  
Fax: 904-257-0122

High precision edge-welded bellows products used for vacuum seals, feedthroughs, manipulators, stem seals, etc. Where cleanliness, reliability, performance, and lead time are paramount. Winner of Industry Week's "America's Best Plants" award as well as The Governor's Sterling award for quality and customer service. Offers custom engineered Sealing Solutions.

#### **KDF ELECTRONIC & VACUUM SVCS.**

**#1013**

70 South Greenbush Road  
Orangeburg, NY 10962  
Contact: Tom Stensgard  
Tel: 914-398-2000  
Fax: 914-398-2222

We remanufacture, rebuild, reengineer and reautomate your sputter tool or one from our inventory. Our factory trained technical staff provide uptime enhancements not offered by the manufacturer. Hard to find parts are available from our stock, at significant savings.

#### **KEY HIGH VACUUM PRODUCTS**

**#638**

36 Southern Blvd.  
Nesconset, NY 11767  
Contact: A. J. Kozyski  
Tel: 516-360-3970  
Fax: 516-360-3973

Manufacturers of high vacuum equipment and components. Standard catalog items include: portable pumping stations, valve controllers, foreline traps, ASA, CF, NW, ISO flanges. Featuring a wide selection of valves, the stainless steel family 3/8" thru 2" having a mtbf of 500,000 cycles on stem seal. Custom chambers, manifolds and systems quoted to customer specifications.

#### **KIMBALL PHYSICS**

**#810, 812**

311 Kimball Hill Road  
Wilton, NH 03086  
Contact: Faye M. Bigarel  
Tel: 603-878-1616  
Fax: 603-878-3700

UHV electron sources, ion sources, Systems: 5 eV to 100 keV. 10-15 A to 1 A;  $\mu$ m to m diameters. Applications: surface physics, RHEED, ESD, MBE, heating, space physics, semiconductor processing, microscopy, etc. UHV components: cathodes, cathode mounts, Wehnelts, and cartridges; Faraday cups, multi-CF fittings, phosphor screens, eV parts, insulators, materials.

#### **KRATOS ANALYTICAL**

**#ISLAND B**

535 East Crescent Avenue  
Ramsey, NJ 07446  
Contact: David Surman  
Tel: 201-825-7500  
Fax: 201-825-8659

Developer and supplier of surface analysis instrumentation. On display will be the latest in high performance, small area x-ray photoelectron and Auger electron spectroscopy equipment. Also on display will be the Vision Data System for instrument control and data processing.

#### **L.D.S. VACUUM PRODUCTS**

**#429**

980T Sunshine Lane  
Altamonte Springs, FL 32714  
Contact: A. Greer  
Tel: 407-862-4643  
Fax: 407-862-8723

Introducing the 911AM Industrial helium leak detector. This rugged leak detector is designed to test products in continuous production for both gross and fine leaks during a single test. See our line of calibrated leaks including our exclusive Cal-Link data tracking program. A complete line of vacuum components is featured.

#### **LARSON ELECTRONIC GLASS**

**#410**

2840 Bay Road  
P.O. Box 371  
Redwood City, CA 94064  
Contact: Chuck Craft  
Tel: 415-369-6734  
Fax: 415-369-0728

Manufacturer of viewports, glass-to-metal tubular seals, double-ended or domed adaptors, stainless steel bellows-to-glass, and fiberoptic and electrical feedthrus, usable in vacuum systems and bakable to 400°C. Flanges, accessories and viewport repairs offered. Custom glass-to-metal seal requests welcome.

#### **KURT J. LESKER CO.**

**#708 - 713**

1515 Worthington Avenue  
Clairton, PA 15025  
Contact: Bill Zinn  
Tel: 412-233-4200  
Fax: 412-233-4275

USA agents for Vacuum Generators' high precision, UHV manipulators; VG Microtech's excellent surface science components (XPS, AES, UPS, ARUPS, LEED & RHEED); and VG Quadrupoles' complete line of quadrupoles. Additional displays include: sputter systems, sources and materials; electrical and motion feedthroughs; flanges and hardware; multi-sensor vacuum gauges and Inficon deposition monitors.

#### **LEYBOLD INFICON INC.**

**#737,739,741,743**

Two Technology Place  
East Syracuse, NY 13057  
Contact: Betty Ann Kram  
Tel: 315-434-1126  
Fax: 315-437-3803

Transpector® AGM (Aggressive Gas Monitor) offers dependable process monitoring for aggressive gas environments. It provides valid data from in-situ gas analysis for improved process control, increased yield, higher quality, and reduced downtime. Designed specifically for chemical vapor deposition (CVD) processes, the Transpector AGM uses a patented sampling method the Virtual Value™.

#### **LEYBOLD TECHNOLOGIES**

**#740, 742**

120 Post Road  
Enfield, CT 06082  
Contact: Tim Day  
Tel: 203-741-2267  
Fax: 203-741-0267

Manufacturer of vacuum coating systems employing EBPVD, sputtering, evaporation, PECVD, for applications including microelectronics, decorative and functional coatings, optics, architectural and automotive glass, data storage media and thin film heads, web coating, CD mastering, metallizers, and replication lines, and the deposition of active matrix LCD's.

#### **LEYBOLD VACUUM PRODUCTS**

**#736, 738**

5700 Mellon Road  
Export, PA 15632-8900  
Contact: Eugene Fuselier  
Tel: 412-327-5700  
Fax: 412-733-5960

New product Sogevac SV25 Single Stage pump vacuum. Other products include ceramic ball bearing and magnetic bearing TMP's and TMP pumping systems for instruments and research, rotary vane pumps for standard and corrosive applications, Cluster tool video demonstrates vacuum technology capabilities. Ask about worldwide service.

#### **LK TECHNOLOGIES**

**#904**

3910 Roll Avenue  
Bloomington, IN 47403  
Contact: Greg Hepfer  
Tel: 812-332-4449  
Fax: 812-332-4493

High Resolution Electron Energy Loss Spectrometers (HREE-LS): New Model ELS3000 based on the KFA, Julich design at 1 meV resolution and LK2000 at 3 meV resolution. Also exhibiting our line of ion guns, Auger spectrometers and scanning tunneling microscopes.

#### **LUXTRON CORPORATION**

**#328**

2775 Northwestern Parkway  
Santa Clara, CA 95051-0941  
Contact: William Kolbeck  
Tel: 408-727-1600  
Fax: 408-727-1677

Optical fiber temperature measurement and control instrumentation. Offers non-contact temperature measurement from -200 to 4,000°C with resolution to 0.01°C.

#### **MAGNETIC BEARING TECHNOLOGIES**

**#1011**

4030 Braker Lane W.  
Suite 300  
Austin, TX 78759  
Contact: Bryan Plater  
Tel: 512-346-6576  
Fax: 512-346-9949

Is a leading innovator in the field of magnetic bearings for turbomachinery. MBT was the first company in the world to demonstrate a room-temperature five-axis magnetic bearing without the use of active electronic components.

#### **MANITOU SYSTEMS**

**#1016**

12 Lower South Street  
Danbury, CT 06810  
Contact: Steven M. Simons  
Tel: 203-792-8797  
Fax: 203-792-7097

Will be exhibiting it's line of RF and microwave power systems and components. Our display will include the Series PS-3 & PB-3 low cost RF plasma power systems, the Series AT automatic impedance matching networks, the Delta Glow™ high energy plasma source and, the American Industrial Microwave™ line of 915 MHz/2.45 GHz microwave power generators, tuners, and components.

#### **MASS-VAC, INC.**

**#823**

247 Rangeway Road  
N. Billerica, MA 01862-0359  
Contact: Herb Gatti  
Tel: 508-667-2393  
Fax: 508-671-0014

MV products manufactures a complete line of vacuum inlet traps, oil mist eliminators, oil filtration systems, degassing systems and central source vacuum systems. A variety of filter and trapping elements are available for laboratory and production applications.

#### **MAT-VAC TECHNOLOGY**

**#920**

411 S. Central Ave.  
Flagler Beach, FL 32136  
Contact: Mary Sales  
Tel: 904-439-7003  
Fax: 904-439-7004

Offers a complete line of vacuum related products including: sputtering targets, evaporation sources, target bonding, backing plates, ETERNA™ 2", 4" & 8" planar magnetron sputtering cathodes for conventional and self-sustaining sputtering. New AC/DC magnetron power supply will be introduced. Sputtering cathode upgrades/retrofits. Sputtering process optimization.

**MATERIALS RESEARCH GROUP**

**#1009**

12441 West 49th Avenue, Suite 2  
Wheat Ridge, CO 80033-1927  
Contact: Pawan K. Bhat  
Tel: 303-425-6688  
Fax: 303-425-6562

A thin film technology company, MRG specializes in the design and fabrication of UHV systems for various processing applications with guaranteed materials performance. MRG's products include PECVD and sputtering cluster tool systems, PV lamination, large area light sputtering, PV production plant design and integration, custom coatings, and product specific research.

**MATERIALS SCIENCE INC.**

**#329**

1010 Turquoise St., 302  
San Diego, CA 92109  
Contact: John R. Miller  
Tel: 619-488-8200  
Fax: 619-488-0924

The patented design of SunSource™ Planar Magnetron Cathodes provides: 40-60% target utilization (25-30% for magnetic materials); highest possible rates (power densities up to 500 watts/in<sup>2</sup>); nearly constant voltage/current throughout target lifetime; low 10-4 torr operation; broad, stable plasma discharge across target surface.

**R.D. MATHIS CO.**

**#836**

2840 Gundry Avenue  
P.O. Box 6187  
Long Beach, CA 90806  
Contact: Barbara Bennett  
Tel: 310-426-7049  
Fax: 310-595-0907

Will display a variety of vacuum evaporation sources. Also offers an inert gas purifier; and a low voltage high current AC power supply.

**MAXTEK, INC.**

**#326**

2908 Oregon Court G-3  
Torrance, CA 90503  
Contact: Ferne Hildebrand  
Tel: 310-320-6604  
Fax: 310-320-6609

The new MDC-360 Film Deposition Controller, powerful and low cost. Release 2.0 of the DCM-100, deposition control management software which includes support for data logging on a display of system temperatures and pressures. The ASF-140 Adjustable Sensor/Feedthrough combination. No internal coaxial cable. New crystal and carousel packaging.

**MCALLISTER TECHNICAL SERVICES**

**#833**

West 280 Prairie Avenue  
Coeur d'Alene, ID 83814  
Contact: Robert McAllister  
Tel: 208-772-9527  
Fax: 208-772-3384

Will exhibit various UHV analyzers including the new Kelvin Probe KP-5000, scanning tunneling microscope and electron energy loss spectrometer. Full range of custom UHV devices such as bellows-sealed instrument positioners, XYZ manipulators, quick-entry load lock system and linear motion feedthrough.

**MDC VACUUM PRODUCTS**

**#600,602,604,606**

23842 Cabot Blvd.  
Hayward, CA 94539  
Contact: Mike Weiss  
Tel: 510-887-6100  
Fax: 510-887-0626

Complete line of UHV components including: flanges and fittings, valves, roughing components, instrumentation, electrical feedthroughs, XYZ manipulators, rotary and linear feedthroughs, fast entry load-lock systems, all-metal sealed right angle valves and M.E.S.A. compatible rectangular gate valves. A complete line of electron beam evaporation sources in single pocket and multi-pocket configuration with matching 6kW, 10kW and 15kW solid state switching power supplies.

**MEIVAC, INC.**

**#343**

6292-A San Ignacio Avenue  
San Jose, CA 95119  
Contact: Richard A. Meidinger  
Tel: 408-362-1000  
Fax: 408-362-1010

Offers a unique line of vacuum throttle valves in standard or cryocooled versions. These patented high conductivity valves are either pneumatically actuated or motor driven with flange configurations including ASA, ISO, JIS or Conflat. Working diameters range from 6" to 35". Also offered are thermocouple gauge tubes, controllers and monitors.

**METROLINE INDUSTRIES**

**#929**

251 Corporate Terrace  
Corona, CA 91719  
Contact: Tom Frantz  
Tel: 909-371-2500  
Fax: 909-371-9792



Vacuum pump remanufacturing for all brands and all types of vacuum pumps including rotary vane, roots, turbomolecular, cryogenic, and dry pumps. We carry hydrocarbon, P.F.P.E., silicon plus other synthetic fluids. Central vacuum and degassing systems are available in many configurations. New pumps of all types can be provided to you along with hardware from inventory.

#### **MKS INSTRUMENTS**

6 Shattuck Road  
Andover, MA 01810  
Contact: Amanda Singer  
Tel: 508-975-2350  
Fax: 508-975-0093

**#ISLAND A**

Will exhibit its latest generation Baratron® capacitance manometers; Mass-Flo® meters and controllers; SensaVac® vacuum gauging; VacuComp™ fittings, flanges and valves; CalStand™ calibration systems; and the PPT Series of residual gas analyzers.

#### **MVAK TECHNOLOGIES**

29 Cook Street  
Billerica, MA 01821  
Contact: John C. Welch Jr.  
Tel: 508-671-0070  
Fax: 508-671-0838

**#750**

Remanufacturer of high vacuum pumps, valves, & systems. Sales of high vacuum pumping fluids, greases & filters. Applications engineering & field service - our specialty. Why buy new high vacuum equipment when it can be rebuilt by MVAK!

#### **NIST/STANDARD REFERENCE DATA**

Bldg. 221  
Room A320  
Gaithersburg, MD 20899  
Contact: Cheryl Williams  
Tel: 301-975-2209  
Fax: 301-926-0416

**#931**

Provides reliable reference data for use in technical problem solving, research, and development in the form of a wide array of comprehensive, easy-to-use databases that include sophisticated software. These databases help the analytical chemist identify materials and characterize substances. SRD databases cover a wide range of analytical techniques, including mass spectrometry, x-ray spectrometry, surface analysis, single crystal and electron diffraction.

#### **NOR-CAL PRODUCTS**

P.O. Box 518  
1967 South Oregon St.  
Yreka, CA 96097  
Contact: Tom Deany  
Tel: 916-842-4457  
Fax: 916-842-9130

**#701, 703**

The SureSeal ISO-KF clamp guarantees 28% O-ring compression for maximum seal performance. Other fixed geometry clamps provide 12%. This reduces permeability by lengthening the path the gas must travel, while reducing the area available for gas entry. O-ring recovery directly effects its longevity. According to the Parker O-ring Handbook, "...a 30% squeeze is often beneficial because recovery is more complete in this range". SureSeal clamps have a lever which locks over center when closed, and come with a locking pin to prevent accidental openings. The pin has a bright red ring, making it easy to inspect connections of large vacuum installations. Rings are available in an assortment of colors on request for color coding.

#### **NORDIKO USA, INC.**

P.O. 8270  
Webster, NY 14580  
Contact: Tamela Nelson  
Tel: 716-671-3570  
Fax: 716-671-3579

**#300, 302**

Offers an advanced line of automated Sputtering Systems, including Cluster and multi-chamber configurations for advanced development and production applications; Ion Beam Deposition and Etching systems for reactive and non-reactive processes; and a complete range of RF excited filamentless multi-polar sources, which are impervious to oxygen and resistant to reactive gases.

#### **NOYES PUBLICATIONS**

120 Mill Road  
Park Ridge, NJ 07656  
Contact: George Narita  
Tel: 201-391-2805  
Fax: 201-391-6833

**#1005**

Displaying new and important books in the Materials science; process technology; Vacuum technology; Thin films; Multilevel metallization; and Semiconductor safety, Industrial hygiene, contamination and defect control, and wafer cleaning technology.

#### **NUVAC INNOVATIONS**

P.O. Box 1468  
22 Ponderosa Court  
Montrose, CO 81401  
Contact: Jim Bernard  
Tel: 303-249-0233  
Fax: 303-249-0607

**#551, 650**

Introducing pumps with a pumping range from atmosphere to 5 x 10<sup>-5</sup> Torr! These pumps use a revolutionary scroll pumping technique with our patent pending dynamic orbital vacuum seal to continuously trap gas and deliver high performance contamination free vacuum for a wide range of industrial applications.

**OCI VACUUM MICROENGINEERING**

#427

993 Thistledown Way  
London, Ontario N6G 4L6  
Contact: Joseph G. Ociepa  
Tel: 519-472-9421  
Fax: 519-471-9913

Will be exhibiting its new High Energy Resolution INTEGRALEED Spectrometer with variable electron beam size in two model sizes. We also manufacture the miniature precision electron guns, low pressure compact ion sputtering guns, custom high resolution and sensitivity energy analyzers and control electronics.

**OMICRON ASSOCIATES**

#516, 518, 520

1738 N. Highland Road  
Suite G101  
Pittsburgh, PA 15241  
Contact: Peter H. Sales  
Tel: 412-831-2262  
Fax: 412-831-9828

Offers surface science and material research laboratories a complete range of analytical equipment including a comprehensive range of UHV/variable temperature scanning probe microscopes. One of our key objectives is to offer complete solutions to major materials research groups who require multi-technique systems, with guaranteed performance, to allow the presentation of results in the fastest practical time.

**ORYX TECHNOLOGY**

#221

47341 Bayside Parkway  
Fremont, CA 94538  
Contact: Richard F. Hough  
Tel: 510-249-1144  
Fax: 510-249-1150

Introducing a new SIMS, the TTS-1000. This sector double focusing instrument is transportable to the production line, weighing only about 250 pounds. It produces spectra in less than 10 minutes, and features simplicity of operation, Windows software control, and excellent mass resolution. It is ideal for rapid characterization of surfaces in metals, semiconductors, thin-films, ceramics, and polymers.

**OSAKA VACUUM LTD.**

#422, 424

911 Bern Court  
Suite 140  
San Jose, CA 95112  
Contact: Jackson Leung  
Tel: 408-441-7658  
Fax: 408-441-7660

Offers turbo molecular pump, compound molecular pump, magnetic suspended turbo molecular pump, magnetic suspended compound molecular pump, helical grooved pump, pump station. 50 1/s to 20,000 1/s nitrogen pumping speed.

**OXFORD INSTRUMENTS**

#336

130A Baker Avenue Ext.  
Concord, MA 01742  
Contact: Kerry Horahan  
Tel: 508-369-9933  
Fax: 508-371-7595

The Plasmalab System 100 modular cluster tool is the latest in Oxford Plasma Technology's Plasmalab range, of which there are over 1000 systems installed worldwide. This system facilitates the integration of R&D activities into a production environment through compliance with the MESC mechanical standard. As research projects develop and grow the modular design offers flexibility of configuration and assures future upgrade capability with minimum on-site disruption. One of the new process modules for the system is exhibited on the booth.

**PARK SCIENTIFIC INSTRUMENTS**

#649, 651

1171 Borregas Avenue  
Sunnyvale, CA 94089  
Contact: Lindsey Mitobe  
Tel: 408-747-1600  
Fax: 408-747-1601

Award-winning UHV AFM/STM from the SPM technology leader. AutoProbe VP images conducting and nonconducting samples in a contamination-free environment. Compact microscopes require no optics or alignment, and tips/cantilevers can be interchanged in situ. Easy-to-use non-contact AFM, and demonstrated atomic resolution in AFM/STM.

**PHELPS ELECTRONICS**

#838

P.O. Box 6566  
Santa Barbara, CA 93160  
Contact: John D. Phelps  
Tel: 805-964-4224  
Fax: 805-683-2994

Specializes in the manufacturing of AT-Cut quartz crystals for all rate and thickness controllers and monitors, offering high quality crystals with gold and silver electrodes. Other products and services are universal sensor heads, feedthroughs, coaxial cables and quartz crystal recycling.

**PHILIPS SEMICONDUCTORS**

#403

Materials Analysis Group  
M565, 811 E. Arques Ave.  
Sunnyvale, CA 94088  
Contact: Alan Morgan  
Tel: 408-991-4868  
Fax: 408-991-4801

Analytical services laboratory offering SIMS, TOF-SIMS, FIB, Auger, ESCA, RBS, AFM/STM, TEM, FESEM, EDX, XRF, XRD, Raman, FTIR, UV/Vis, GC/MS/IR, GPC, ICP, AA, IC, TGA/TMA/DSC, and acoustic microscopy for sur-

face, interface, particle, thin film and bulk material characterization. Trace element detection, high-resolution imaging and depth profiling, and precision cross-sectioning.

**PHYSICAL ELECTRONICS, INC. #436-441 & 536-541**

6509 Flying Cloud Drive  
Eden Prairie, MN 55344  
Contact: Robert Jaynes  
Tel: 612-828-6156  
Fax: 612-828-6322

A leader in surface analysis will present the latest in ESCA technology. Software demonstrations will be available for Auger, TOF-SIMS/SALI and PHI-MATLAB applications. Graphics and literature will also be available on our latest components, subsystems, XPS Research System and UHV equipment.

**PLASMARC™**

**#444**

50 Sims Avenue  
Providence, RI 02909  
Contact: Darlene M. Reza  
Tel: 401-456-0800  
Fax: 401-421-2419

Is a fully integrated manufacturer of ITO (Indium Tin Oxide) and ITM (Indium Tin Metal), accommodating all equipment requirements, including planar, disc, rotatable and enhanced design sputtering targets. Also offers custom manufactured silicon rotatable targets and related materials for the display industry. Localized bonding is offered in Providence, RI (USA); Brussels, Belgium, (Europe); and Hong Kong (Far East).

**PLASMATRON COATING SYSTEMS**

**#1018**

102 Executive Drive #4  
Moorestown, NJ 08057  
Contact: William M. Egler  
Tel: 609-439-0991  
Fax: 609-439-9288

Offers a complete range of high and ultra-high vacuum thin film coating systems. All systems are custom-engineering to address the specific requirements of each application and can include a variety of deposition equipment, including: magnetron sputtering, thermal and electron beam evaporation, cathodic arc, ion beam sputtering, laser ablation and chemical vapor deposition.

**PLASMA-THERM, INC.**

**#640**

9509 International Court  
St. Petersburg, FL 33716  
Contact: Frank Lowry  
Tel: 813-577-4999  
Fax: 813-577-7035

Supplier of plasma processing systems for RIE, PECVD, ECR, ICP and sputtering for many applications. Systems include the Batchtop, tabletop RIE system, Series 790 Modular process system for single or dual chamber operation and our Model SLR 700 loadlocked single and dual chamber reactor.

**PLASMAQUEST, INC.**

**#718**

850 N. Dorothy Drive  
Suite 504  
Richardson, TX 75081  
Contact: John Spencer  
Tel: 214-680-1811  
Fax: 214-680-1539

Has developed dry etching applications for advanced device structures using the ferroelectric materials PZT and BST (combined with Pt electrodes). Combining the high current ion beam of the ECR source with an RF biased chuck, PlasmaQuest has developed a reactive sputter etch technology which etches the complex metal and dielectric multilayer structures required by these devices.

**PLASMATERIALS, INC.**

**#404**

3223 Crow Canyon Road  
Suite 290  
San Ramon, CA 94583  
Contact: Don Sarrach  
Tel: 510-277-0440  
Fax: 510-277-0469

Offers a complete line of physical vapor deposition materials. These include sputtering targets and evaporation materials. Materials include nearly every element on the periodic table (plus their alloys and compounds). Fabrication methods utilize hot pressing, sintering, and HIP'ing of powders as well as vacuum casting and melting of metals. Also offers backing plates and all metal bonding services.

**POLYCOLD SYSTEMS**

**#306**

67 Mark Drive  
San Rafael, CA 94903  
Contact: Patrick Mahoney  
Tel: 415-479-0577  
Fax: 415-499-0927

Offering cryogenic refrigeration systems for use with vacuum deposition systems. High speed fast cycle water vapor cryopumps for use in combination with all high vacuum pumps. Total regeneration times of 6.5 minutes or less. Cooling capacities from 5 watts at -160°C to greater than 3,600 watts at -90°C. All systems utilize safe CFC-free refrigerants.

**PRECISION FERRITE & CERAMICS INC.**

#751

5576 Corporate Drive  
Cypress, CA 90630  
Contact: Ji Soo Lee  
Tel: 714-828-9061  
Fax: 714-828-0408

Fabrication of high precision ceramic parts. Serving major manufactures of microwave tubes, vacuum tubes, semi-conductor equipments, lasers, aerospaces, medicals, nuclear systems.

**PROCESS PHYSICS, INC.**

#1007

385 Reed Street  
Santa Clara, CA 95050  
Contact: Peter Dusza  
Tel: 408-988-8161  
Fax: 408-988-2206

Oil free vacuum pump packages, iris type throttle valves, vacuum components and fittings, low cost vacuum box chambers, DataQuad II residual gas analyzers, cylindrical magnetron sputtering cathodes.

**PRECISION PLUS VACUUM PARTS**

#942

30 Troy Road  
Whippany, NJ 07981  
Contact: A.E. Maskrey  
Tel: 201-887-8630  
Fax: 201-887-0749

In our continuing effort to help those of you involved in vacuum pump maintenance reduced costs, we will be introducing our growing line of newly manufactured cast iron pump components. On display will be rotors, front, intermediate and rear flanges and plates as well as stators for Alcatel, Edwards, and Leybold vane pumps.

**PROCESS SYSTEMS INT'L.**

#941

20 Walkup Drive  
Westborough, MA 01581  
Contact: Joseph J. Sgambato  
Tel: 508-898-0209  
Fax: 508-898-0308

Designs and manufactures custom vacuum systems and components for a wide range of applications. On exhibit will be photographs and brochures depicting a cross-section of the products we manufacture including: Inline Coating Systems, Thermal Vacuum Systems, Optical Coaters and General Vacuum Process Systems.

**PRINCETON RESEARCH INSTRUMENTS**

#543

P.O. Box 1174  
Princeton, NJ 08542  
Contact: Charles A. Crider  
Tel: 609-924-0570  
Fax: 609-924-4970

We are exhibiting a full range of Reverse View LEED optics now including 5 RVL models (1 moveable, 2 standard, & 2 with shutter) and the new CVL 8-120 conventional/convertible LEED optics which can subsequently be upgraded to reverse view. All optics operate with the PRI 11-020 LEED Electronics. The PRI RHEED system and the complete offering of in-vacuum stepper motors, translation stages, drive electronics and accessories will be shown.

**PROCESS VACUUM SERVICES**

#1001,1003

2369 Bering Drive  
San Jose, CA 95131  
Contact: Gerald Catalano  
Tel: 408-955-1900  
Fax: 408-955-0229

A new concept in dry pump technology, the new Busch line of Cobra dry vacuum pumps. These pumps use a unique pumping principal utilizing two horizontal screws. This single stage design achieves base pressures better than 10 millitorr without the use of a booster. Pump packages are available in sizes ranging from 46 cfm to over 600 cfm and can be interfaced to most types of semiconductor equipment. The simple, efficient screw design provides a very short gas path and is ideally suited to CVD nitride applications. Will also display it's capabilities in vacuum equipment services ranging from complete dry pump rebuilds to custom modifications and upgrades.

**PRINCETON SCIENTIFIC CORP.**

#323,325

Magtron GmbH  
P.O. Box 143  
Princeton, NJ 08542  
Contact: Hank D. Gerwers  
Tel: 609-924-3011  
Fax: 609-924-3018

Will display: all metal valves, fast closing valves, vacuum scopes as replacement for regular viewing ports, pulsed power supplies for deposition systems, offering numerous advantages over conventional power supplies. Also showing: metal - and metal oxide single crystals and particle beam line diagnostics equipment.

**PURE TECH INC.**

#433

P.O. Box 1319  
Commerce Drive  
Carmel, NY 10512  
Contact: Earle R. Ellefsen  
Tel: 914-878-4499  
Fax: 914-878-4727

An ISO 9002 Certified American manufacturer of high purity materials for sputtering and evaporation. Produces both stan-

standard and custom materials for research and development as well as production. In-house capabilities include vacuum melting, hot pressing, metal and ceramic machining, custom backing plates and target bonding.

#### **QUANTAR TECHNOLOGY**

**#330**

3004 Mission Street  
Santa Cruz, CA 95060  
Contact: Mike Mellon  
Tel: 408-429-5227  
Fax: 408-429-5131

Detectors for multichannel spectroscopy and 2D scientific imaging. Pulse-counting, position-sensitive MCP detectors for electron, ion, positron and soft and hard X-ray detection; EUV, visible and NIR photons. New low-noise scientific CCD camera. New Multi-Parameter MCA Data System simultaneously acquires up to 8 parameters for TOF, gamma-ray coincidence, time-resolved spectroscopy and other applications.

#### **QUESANT INSTRUMENT CO.**

**#448**

28038 Dorothy Drive  
Suite 2  
Agoura Hills, CA 91301  
Contact: George McMurtry  
Tel: 818-597-0311  
Fax: 818-991-5490

Designs and produces superior, industry standard, scanning probe microscopes for a wide variety of applications. Proprietary improvements include: AnaLoop™, our analog feedback loop with digital input, the Isotopic Focal System™ which allows the laser to track the rastering probe and Modulite™ non-contact mode. Prices range from \$25,495 up.

#### **REES INSTRUMENTS**

**#406**

1900 Lake Park Drive  
Suite 315  
Contact: Robert Angus  
Tel: 404-433-9991  
Fax: 404-433-9994

Will display their range of computer controlled optical spectrum analyzer systems. These units are based on our unique fast scanning monochromator and feature our menu-driven easy to use software package for data collection and processing. Typical applications include plasma monitoring, end point detection in coating chambers, and reflection/transmission measurement.

#### **RESEARCH & PVD MATERIALS**

**#412**

P.O. Box 4796  
Wayne, NJ 07474  
Contact: Melvin J. Hollander  
Tel: 201-575-4245  
Fax: 201-227-2530

The Materials Servicer, providing a comprehensive offering of highly characterized specialty and exotic materials for the diverse and sophisticated requirements of the semiconductor, electronics, electro optic and related research communities. Metals, alloys, and ceramics, manufactured by this single quality source include but are not limited to: sputtering targets, evaporation materials and custom "one off" fabrications.

#### **RF POWER PRODUCTS**

**#745**

502 Gibbsboro - Marlton Rd.  
Voorhees, NJ 08043  
Contact: Michael Lagarde  
Tel: 609-751-0033  
Fax: 609-751-1673

Manufacturer of solid state microprocessor controlled RF generators with frequency available from 50 kHz to 60 MHz and power output levels of 500 watts to 25,000 watts. We also manufacture automatic matching networks and accessories. Visit our booth to see our newest products, the LF30 and RF20M.

#### **RF SERVICES**

**#821**

1293 Old Mountain View  
Alviso Road  
Sunnyvale, CA 94089  
Contact: John Simmons  
Tel: 408-734-5191  
Fax: 408-734-3710

Offers a complete line of services to those customers who utilize or are contemplating having RF applied to their systems. We sell a full range of Automatic Matching Networks, as well as RF power supplies up to 1KW presently. We also provide service, repair and training for most RF systems produced for the vacuum industry.

#### **RHK TECHNOLOGY**

**#301, 303**

1750 West Hamlin Road  
Rochester Hills, MI 48309  
Contact: John M. Green  
Tel: 810-656-3116  
Fax: 810-656-8347

Our exhibit will feature our NEW Model UHV 300, UHV-STN along with our line of high performance SPM control and software solutions. Silicon Graphics and PC based scanning probe microscopy control systems will be on display and our STMCPs and STiMage software will be demonstrated throughout the show. SPM control accessories including the IWC 100 Inchworm Motor Controller and AFM 100 Interface Module will also be on display.



**RIGAKU/USA**

199 Rosewood Drive  
Danvers, MA 01923  
Contact: Walter Helgeland  
Tel: 508-777-2446  
Fax: 508-777-3594

#304

Producer of instrumentation for electron spectroscopy. Our high performance XPS instruments ESCA 310 and ESCA 200, as well as our UPS instrument SES 200, achieve the best resolution among instruments on the market today, both in terms of energy and spatial resolution".

"Magnaseal" rotary motion feethroughs by Rigaku offers premium sealing solutions at very competitive prices. We stock a wide range of catalog products for immediate delivery, including direct replacement products for units made by Ferrofluidics. Custom-designed units are available for OEM applications. All Magnaseal products employ the unique, patented multi-magnet/multi-pole design which distinguishes this product line from all others. Join the growing number of OEM and end-user customers who now enjoy the benefits of working with us. Application engineering assistance is available directly or through our local sales representative.

**SEIKO SEIKI CO., LTD.**

#339, 341

1130 Ringwood Court  
San Jose, CA 95131  
Contact: Takenori Hori  
Tel: 408-922-5932  
Fax: 408-922-1959

Manufacturer of magnetic levitation type turbomolecular pumps. Exhibiting magnetic levitated turbomolecular pumps (300 l/s to 2000 l/s) which achieves hydrocarbon-free, extremely low level of vibration and noise, free mounting position, easy operation and full safety function.

**RUSHMORE TECHNOLOGY INC.**

#940

P.O. Box 817  
Watertown, SD 57201  
Contact: Daryl Bittner  
Tel: 605-886-3218  
Fax: 605-886-7412

Contamination Reduction System (CRS). The CRS is a flow control device that eliminates turbulence during the venting and pumpdown of vacuum chambers. The device is micro-processor controlled with a user definable opening profile for custom applications.

**SENIOR FLEXONICS, INC.**

#930

Metal Bellows Div.  
1075 Providence Highway  
Sharon, MA 02067  
Contact: John R. Barrett  
Tel: 617-784-1400  
Fax: 617-784-1405

Edge welded metal bellows and component assemblies for flawless performance in high vacuum and ultra high vacuum equipment. Hermetically sealed to provide total vacuum integrity, manufactured from non-corrosive stainless steel and other special materials, reliable-normal life span of several million cycles, variety of off-the-shelf sizes or designed to specific requirements.

**SAES GETTERS U.S.A.**

#340, 342

1122 E. Cheyenne Mtn. Blvd.  
Colorado Springs, CO 80906  
Contact: Leigh Westin  
Tel: 719-576-3200  
Fax: 719-576-5025

Introducing a new generation of spinning rotor gauge with free-positioning head which permits vacuum pressure measurements at any angle, from atmospheric pressure down to below  $10^{-6}$  torr. Also displayed will be the CapaciTorr high-capacity getter pump for high- and ultrahigh-vacuum applications and the Physical Electronics-SAES Getters getter-ion pump.

**SERVICE PHYSICS**

#428

101 First Street  
Suite 474  
Los Altos, CA 94022  
Contact: Ruth Ann Chaney  
Tel: 415-948-6142  
Fax: 415-948-6143

Provides maintenance service for Surface Science Instruments and HP ESCA Instrumentation. We carry an extensive stock of spare parts, provide hourly service, annual service contracts and conduct on-site User training courses in ESCA operation. SPI will be showing new accessories and upgrades developed for the X-Probe and M-Probe ESCA systems.

**SC TECHNOLOGY: See TELEMAR****SCIENTA INSTRUMENT AB**

#332

Seminariegtan 33H  
25228 Uppsala  
Sweden  
Contact: Lars Hauildahl  
Tel: 46 18 500160  
Fax: 46 18 543638

**L.M. SIMARD, INC.**

#445

61535 S. Hwy. 97  
Suite 9-505  
Bend, OR 97702  
Contact: Paul R. Fournier  
Tel: 503-389-8408  
Fax: 503-388-8199

Specializing in high-rate sputtering devices, from R&D to production applications. Two product lines are available - the TRI-MAG Series and the ULTIMAG Series, along with feedthroughs and power. Customized designs to match the application, either UHV or O-ring.

#### **SMC CORPORATION**

**#548, 550**

1437 Caminito Halago  
La Jolla, CA 92037  
Contact: Frank K. Koide  
Tel: 619-456-9084  
Fax: 619-456-1926

Products that exploit the outstanding advantages of aluminum for high vacuum and high purity applications will be exhibited. SMC aluminum CF flanges provide the most convenient way of putting metal seals on aluminum chambers and are nearly as hard and durable as stainless steel flanges. Information will also be available on the latest techniques in aluminum surface preparation, fabrication, sealing, sealing and degassing. The consistently high performance now possible is driving industry-wide acceptance.

#### **SOLERAS LTD.**

**#425**

81 Landry Street  
P.O. Box BC  
Biddeford, ME 04005  
Contact: Traci Langevin  
Tel: 207-282-5699  
Fax: 207-284-6118

Is a manufacturer of sputter targets, metallic bonding, original and enhanced backing plates and vacuum related spare parts. Has R & D design, reverse engineering, failure analysis, CAD/CAM and full traceability of materials with archival data on products, design material, composition and characteristics. Also has full documentation on product design, material composition, reverse engineering, failure analysis and CAD/CAM programs. All targets are serialized or lot numbered and materials are traceable, with physical samples archived.

#### **SPECS GMBH**

**#610,611,612,613**

Voltastr. 5  
13355 Berlin  
Germany  
Contact: Stefan Plateel  
Tel: 49 30 4633031  
Fax: 49 30 4642083

A major vendor of surface analysis components and systems. Components manufactured are: electron energy spectrometer, mass spectrometer, ion guns, electron guns, UV-sources, X-Ray sources. Systems are compiled up to customer need for XPS, AES, ISS, SIMS, SNMS. Product displayed is full automatic ESCA machine for routine analysis with CIM capability.

#### **SPECTRA INSTRUMENTS**

**#800,802,804**

700A East Dunne Avenue  
Morgan Hill, CA 95037  
Contact: Russ Carr  
Tel: 408-778-6060  
Fax: 408-776-8575

Residual Gas Analyzers for all applications. New easy but powerful windows software and systems provide RGA dynamic data exchange (DDE) with process computers and other windows programs. Closed ion source gives PPM/PPB sensitivity for contaminants in different processes. Sensitivity, automation and process security for any process or experiment.

#### **SPECTRAVAC INC.**

**#840**

5045 N. 30th Street  
Colorado Springs, CO 80919  
Contact: David J. Hilton  
Tel: 719-531-7711  
Fax: 719-531-7714

Provides service and computerized testing on a full range of high vacuum pumps. These include blowers, mechanical, dry, cryo and turbo pumps. By utilizing state of the art facilities, repair and testing methods. Provides leading edge technology in vacuum pump service.

#### **STAIB INSTRUMENTE**

**#317**

Obere Hauptstrasse 45  
Freising 85354  
Germany  
Contact: Ute Staib  
Tel: 49 8161 7740  
Fax: 49 8161 7709

Featuring 35 kV, 20 kV, 12 kV RHEED-SYSTEMS usable over a wide range of operating pressures; RHEED-VISION a powerful digital Imaging Processing System; PEEM - Photo Emission electron Microscope - a new technic for dynamic studies of surface potential and work function distribution at submicron spatial resolution. AUGER spectrometer with highest sensitivity.

#### **STEPHENS ANALYTICAL**

**#309**

P.O. Box 1126  
Champlain, NY 12919-1126  
Contact: Stan Conquest  
Tel: 514-332-1230  
Fax: 514-335-6566

M.C.M. Trace Moisture Analyzers for air and non corrosive gases, feature accuracy, reliability and rapid response from saturation to 0.5 ppm(v) in 15 seconds. These instruments incorporate a silicon based sensor that renders all other technologies obsolete. Sensors can operate in static or dynamic flows as well as in a vacuum and at pressures up to 4000 psi.

**STOKES VACUUM INC.**

#936, 938

5500 Tabor Road  
Philadelphia, PA 19120  
Contact: Bart Hebble  
Tel: 215-831-5400  
Fax: 215-831-5420

Featuring the new Stokes Stealth Pump - an 88 CFM dry pump. Its compact design delivers more oil-free CFM with greater volumetric efficiency. Also available, a wide variety of vane pumps, the 2000 CFM bypass blower and information on the latest in blower lobe coatings for handling corrosive gases.

**SUPER CONDUCTOR MATERIALS**

#401

128 Orange Avenue  
Suffern, NY 10901  
Contact: Aftab Dar  
Tel: 914-368-0240  
Fax: 914-368-0250

Small woman owned American company producing high purity sputtering targets and evaporation materials since 1987. (High density ITO and Zinc Oxide is one of the specialties. S.C.M. is one stop for thin film requirement: targets, evaporation materials, E-beam guns and their spare parts, emitter assemblies, crucible liners, backing plates bonding, ion implantor sources, ceramics, vacuum and pressure fittings.

**SURFACE/INTERFACE**

#820, 822

110 Pioneer Way  
Suite D  
Mountain View, CA 94041  
Contact: Judy Ackeret  
Tel: 415-965-8205  
Fax: 415-965-8207

Provides innovative product solutions to meet the needs of ultrahigh vacuum, semiconductor manufacturing, and surface analysis customers. Surface/Interface specializes in "ultra-clean" components for vacuum and manufacturing applications, analytical systems and software for surface analysis and highly pure, characterized reference materials for materials characterization and failure analysis laboratories. S/I also offers custom products and consulting services to industry and the materials science community.

**SURFACE SCIENCE SPECTRA**

#746

150 West Iowa Avenue  
Suite 104  
Sunnyvale, CA 94086  
Contact: Melissa Beers  
Tel: 408-737-0285  
Fax: 408-737-9529

An official journal of the AVS published by the American Institute of Physics, is devoted to archiving XPS, AES, and SIMS spectra of technological and scientific interest. Published in both a hard copy journal and in a digitized data format on disk, the journal is an evolving database of standardized, peer-reviewed spectra and related sample and instrument data.

**SWAGELOK CO.**

#944

31400 Aurora Road  
Solon, OH 44139  
Contact: John Burton  
Tel: 216-349-5934  
Fax: 216-349-5843

Tube fittings, valves, quick connects, flexible hoses and fluids & gas system components rated from ultra-high vacuum to 10,000 p.s.i. Temperatures from cryogenic to 1,200°F.

**SYCON INSTRUMENTS**

#426

6757 Kinne Street  
East Syracuse, NY 13057  
Contact: Gwen Stell  
Tel: 315-463-5297  
Fax: 315-463-5298

Displaying its complete line of Thin Film Deposition Monitors and Controllers utilizing the quartz crystal sensing techniques. A complete line of HV and UHV sensors and shutters for these products will also be displayed. A new deposition monitor based on the principle of Atomic Absorption will also be displayed for continuous monitoring of film deposition. A multi-pocket E-Beam Source Indexer for the control of 4 x 6 pocket E-Beam Guns will also be displayed.

**T-M VACUUM PRODUCTS INC.**

#925

630 S. Warrington Ave.  
Cinnaminson, NJ 08077  
Contact: John Strada  
Tel: 609-829-2000  
Fax: 609-829-0990

Presents equipment available from thin film deposition (sputter, E-beam, etc.) and from the vacuum oven and furnace systems line including inert gas glove box/purification systems. Controls and new advancements can be seen and discussed along with custom and modified standard systems.

**TARGET MATERIALS, INC.**

#621

1145 Chesapeake Avenue  
Columbus, OH 43212  
Contact: J.R. Gaines  
Tel: 614-486-0261  
Fax: 614-486-0912

Manufactures high quality sputtering targets including indium/tin oxide, aluminum, tantalum, niobium, zirconium, zinc oxide and high temperature superconductors. We also provide bonding, backing plates and toll deposition services. Visit our booth to pick-up our new price list and display magnets featuring our "800" numbers, or call 1-800-292-8639.

#### **TECHNICAL INSTRUMENT CO.**

**#1000**

348 Sixth Street  
San Francisco, CA 94103  
Contact: Francis E. Lundy  
Tel: 415-431-8231  
Fax: 415-431-6491

The Rasterscope™ from DME is an ultra-high vacuum scanning tunneling microscope for the fundamental study of both static and dynamic structures. The Rasterscope UHV-STM was developed in collaboration with leading scientists, and is designed to be flexible and uncomplicated in a compact rigid system. It is extremely insensitive to vibration, and has a simple damping system. Typically, images are recorded in two to ten seconds.

#### **TECHNOTRADE INTERNATIONAL**

**#447,449,451**

P.O. Box 543  
Londonderry, NH 03053-0543  
Contact: Albrecht Auwaerter  
Tel: 603-437-2991  
Fax: 603-437-3091

Introduces the MECO® Chain, an innovative chain clamp for fast, reliable and economical connection of pipes, and Pink GmbH, a German vacuum engineering firm, with products ranging from standard vacuum components to the management and implementation of special projects according to customer specification, and Wolf feedthroughs for Sub-D connections.

#### **TECHWARE SYSTEMS**

**#319, 321**

#100-12051 Horseshoe Way  
Richmond, BC V7A 4V4  
Canada  
Contact: Mark Hanna  
Tel: 604-271-2000  
Fax: 604-275-8572

Showing their latest hardware and software products for advanced equipment control of thin film process applications. Cluster tool controls, and updated graphical user interface, PC-based process programming and networking capabilities will be featured. Our controls are designed for single chamber, multi-chamber and in-line systems applications.

#### **TELEDYNE BROWN ENGINEERING**

**#607, 609**

804 Newcombe Avenue  
Hampton, VA 23669  
Contact: James F. Pouchot  
Tel: 804-723-6531  
Fax: 804-723-3925

Displaying the newly introduced miniaturized silicon based thermal vacuum sensor and gauge which covers the range of 760 Torr to  $1 \times 10^{-4}$  Torr with a linear output signal and digital readout. This sensor can be mounted in any orientation, is very rugged and possesses a very fast response to pressure variations. In addition, our complete line of mass flow meters and controllers will be available.

#### **TELEMARK**

**#923**

51 Whitney Place  
Fremont, CA 94531  
Contact: Gerald Henderson  
Tel: 510-770-8700  
Fax: 510-770-8879

Produces electron beam guns, power supplies and other pvd components. New products include low cost 3kw sources, 6kW UHV sources and related power supplies. An affiliate, SC Technology, produces multi-wavelength insitu monitors that measure and control film thickness and develop rate of photoresist at multiple locations on track coaters; insitu film thickness measurement systems for cd's, FPD's; full spectral OES diagnostic systems that characterize and identify spectral signatures of plasmas and light sources.

#### **TELEVAC**

**#324**

2400 Philmont Avenue  
Huntingdon Valley, PA 19006  
Contact: Richard Glazewski  
Tel: 215-938-4444  
Fax: 215-947-7464

Will the introduction of their new line of Intelevac™ active gauges, continues its tradition of dependable innovation. The Intelevac™ Extended Range Cold Cathode Gauge operates over the  $10_{-2}$  to  $10_{-11}$  Torr range. The Televac Convection Gauge covers the  $10_{-3}$  to  $10_{+3}$  Torr vacuum range.

#### **TEMESCAL**

**#408**

2700 Maxwell Way  
P.O. Box 2529  
Fairfield, CA 94558  
Contact: Brian J. Kaemmer  
Tel: 707-423-2620  
Fax: 707-425-1706

Manufactures high quality thin film components and deposition systems. They will be introducing and exhibiting several

new products this year including: SuperSource2 Modular Electron Beam Source; TRC-3460, Turret Electron Beam Source Rotation Controller; VSW-1090, Variable Wave Form Sweep Controller; Temescal's Patent High Performance Electron Beam Emitter Assembly.

#### **TENCOR INSTRUMENTS**

**#316**

2400 Charleston Road  
Mountain View, CA 94043  
Contact: Gail Nishimura  
Tel: 415-988-4313  
Fax: 415-968-9482

Surface profiling systems for a variety of applications and budgets providing comprehensive surface analysis on even very soft films. Guaranteed repeatability ensures highly accurate measurements. Large sample profiler for flat panel displays. Thin film stress measurement systems for analysis at temperatures from -65 to 900°C and automated film stress measurement system with radial stress mapping.

#### **TERRANOVA SCIENTIFIC**

**#705**

5841 Bell Road  
Auburn, CA 95602  
Contact: Ron Paitich  
Tel: 916-889-1100  
Fax: 916-269-2877

High-performance, low-cost vacuum gauge controllers include: new Model 934 and 934-UHV Vacuum Gauge Controller with three digital displays, for ion gauge and two CONVECTRON™ gauges; covering 10-11 torr to 1000 torr. Also showing are Model 935 Ion/TC Gauge Controller, Model 914A digital TC gauge, measuring 10-3 torr to 1000 torr and Model 916 CONVECTRON™ Gauge Controller. CONVECTRON™ is a trademark of Granville-Phillips Company.

#### **TFS TECHNOLOGIES**

**#318**

3700 Osuna NE  
Suite 605  
Albuquerque, NM 87109  
Contact: John Hornkohl  
Tel: 505-344-3979  
Fax: 505-344-1976

Carries a large inventory of used and rebuilt vacuum equipment in New Mexico. We service, rebuild, and sell evaporation systems, sputtering systems, turbo pumps, cryopumps, vacuum valves, baffles, bell jars, collars, fittings, ion gauges, TC gauges, and leak detectors. Large coating chambers, mechanical pumps, from 1-7000 cfm.

#### **THERMIONICS LAB.**

**#637, 639**

22815 Sutro Street  
P.O. Box 3711  
Hayward, CA 94540  
Contact: John Brooks  
Tel: 510-538-3304  
Fax: 510-538-2889

Vacuum systems, components and hardware with a 5 year guarantee. UHV manipulators; sample introduction, handling, and transfer, with heating and cooling, differentially pumped rotary seals and mechanical feed throughs. MBE systems, components for PLD, MBE and PLD/MBE combined processes. R-HEED (15-50 KeV), new CCD based R-HEED imaging and analysis system. Hanks HMe e-guns, 3-20kW, evaporation systems, power supplies, ion pumps and systems. PyraFlat flanges, gate valves, all-metal valves, T.C. gauges and digital/analog controllers.

#### **TOPOMETRIX**

**#421, 423**

5403 Betsy Ross Drive  
Santa Clara, CA 95054  
Contact: Tim Van Slambrouck  
Tel: 408-982-9700  
Fax: 408-982-9751

Manufactures and distributes worldwide a complete line of scanning probe microscopes, including the Aurora Near-Field Scanning Optical Microscope, the Explorer LifeSciences SPM (for integration with an inverted optical microscope) and the Voyager Semiconductor Wafer Analyzer. These complete research workstations feature TopoMetrix' Windows based SPMLab acquisition and analysis software.

#### **TYLAN GENERAL**

**#801, 803, 805**

9577 Chesapeake Drive  
San Diego, CA 92123  
Contact: Leslie Helsel  
Tel: 619-571-1222  
Fax: 619-576-1703

Produces precision gas flow & pressure measurement and control instrumentation. Displaying capacitance diaphragm gauges, adaptive pressure control systems, motorized throttling valves, mass flow controllers and meters, and ultra clean gas distribution systems.

#### **U-C COMPONENTS, INC.**

**#932**

410 Logue Avenue  
Mountain View, CA 94043-4019  
Contact: Ron Anderson  
Tel: 415-964-3827  
Fax: 415-964-0216

All vented and non-vented fasteners are 300 series stainless steel and chemically cleaned for high vacuum use. We offer



stainless, MoS<sub>2</sub>, Ws<sub>2</sub>, and graphite coatings, as well as nickel and silver platings. Over 5,000 different items in stock. Special orders are available upon request. Fully illustrated, free catalog available.

#### **ULVAC TECHNOLOGIES**

**#843, 845**

6 Riverside Drive  
Andover, MA 01810  
Contact: Karen Blandford-Anderson  
Tel: 508-686-7550  
Fax: 508-689-6300

Will be displaying the company's new 8" RIE and downstream microwave asher technology used in the Phoenix which renders residuals on the wafer surface DI water soluble. Also exhibiting will be information on the Z-1000 Multi-chamber sputtering system, which has been designed for advanced VLSI and ULSI production applications. In addition, Ulvac's patented DI water treatment technology and Materials including; sputter targets, evaporation sources and ultra-fine powders will be promoted.

#### **US THIN FILM PRODUCTS**

**#939**

1999 S. Bascom Avenue  
Suite 405  
Campbell, CA 95008  
Contact: Blair D. Kott  
Tel: 408-371-6900  
Fax: 408-559-1739

Manufacturer of 1" through 4" diameter planar magnetron sputtering sources; also provides special sources and multiple source systems on a common flange. High temperature (950°C) resistive substrate heater for use in UHV to O<sub>2</sub> atmosphere. Gen-A-Torr, a cryopump regeneration gas purge monitor.

#### **UTI INSTRUMENTS**

**#418, 420**

2030 Fortune Drive  
Suite C  
San Jose, CA 95131  
Contact: Glynis Finsterbusch  
Tel: 408-428-9400  
Fax: 408-428-0823

Quadrupole mass analysis systems from UHV to atmospheric pressure for equipment monitoring, process monitoring, process control, process development, and cylinder/house gas analysis. Featuring QualiTorr Remote™ for simultaneous monitoring of multiple stations/process systems at any combination of pressures analyzed. Key feature: Parallel operation of multiple analyzer stations, independent data output style (rate of rise, baseline, calibration, leak check, selected peak monitoring, etc.) at each display station, any combination of open or closed ion-source analyzers, and remote 486 computer control.

#### **VACUUM ENGINEERING & MATERIALS**

**#338**

P.O. Box 4480  
Santa Clara, CA 95056  
Contact: Jack Kavanaugh  
Tel: 408-986-8900  
Fax: 408-986-8980

Manufactures sputtering targets, evaporation materials, evaporation cones, hearth liners and backing plates. We furnish a large selection of high purity metals, intermetallics, dielectrics and cermets. Sputtering targets are manufactured to customers exact specifications to size and purity. Purities are available from 99 to 99.999% upon request.

#### **VACUUM INC.**

**#1027**

5541 Central Avenue  
Boulder, CO 80301  
Contact: Ted Van Vorous  
Tel: 303-444-8750  
Fax: 303-444-0104

Introduce a number of new products for 1994 including Random Arc Sources, the Ohmega-10 Barrel Coater, added cathodes in the Micro-PM//3 line of magnetrons; revised UHV cathodes for R/D, the Ohmega-SM Surface mount Resistor Coater and a line of throttle plates.

#### **VACUUM RESEARCH CORP.**

**#200, 202**

2401 Smallman Street  
Pittsburgh, PA 15222  
Contact: John F. Hartnett  
Tel: 412-261-7630  
Fax: 412-261-7220

Small size, low cost Dry Roughing Pumps. 5 to 32 CFM, 20 mTorr ultimate pressure. Bellows sealed aluminum gate valves with metal bonnet seal, Viton gate and Con Flatr ports up to 10 inch. diaphragm, Pirani and thermocouple gauges from 10<sup>-5</sup> to 1500 Torr digital display, analog output. Explosion proof gauge tubes.

#### **VACUUM TECHNOLOGY**

**#636**

1003 Alvin Weinberg Drive  
Oak Ridge, TN 37830  
Contact: George Solomon  
Tel: 615-481-3342  
Fax: 615-481-3788

Manufactures the AERO VAC 1000TM, an innovative and rugged mass spectrometer/RGA featuring our AERO SCANTM system for true computer control and data acquisition/analysis using either a PC or Mac. AERO SCANTM provides all the functions you want, including storage, recall, true calibration, library, and spectral interpretation. Our new AERO SCAN 1200 and 1600 systems with all these functions plus process-parameter controls, turn the UTI, Extrel, VG and other quadrupoles into versatile PC or Mac controlled RGA's.

**VARIAN ASSOCIATES**

#901,903,905,907

121 Hartwell Ave.  
Lexington, MA 02173  
Contact: Ron Stanton  
Tel: 800-882-7426  
Fax: 617-860-5437

Will exhibit maintenance free, ceramic bearing turbo pumps in a wide range of models. Varian's UHV products will include ion pumps and controllers, valves and other hardware. A complete line of vacuum instrumentation is on display measuring pressure from two atmospheres down to  $5 \times 10^{-12}$  Torr. Also on display will be a host of leak detectors including dry portables and cabinet models as well as the ultra-portable helium sniffer, Helitest®.

**VAT, INC.**

#530, 532

600 West Cummings Park  
Woburn, MA 01801  
Contact: John Freeman  
Tel: 617-935-1446  
Fax: 617-935-3940

Will display vacuum valves for pump-isolation, load-locks, throttling, soft-starts and other applications from atmosphere to extreme UHV. Included are aluminum and stainless steel gate valves, angle valves, and valves for fast cycling, 2 million cycles, low-vibration, or particle sensitive applications.

**VEECO INSTRUMENTS**

#717, 719

Terminal Drive  
Plainview, NY 11803  
Contact: Fran Brennan  
Tel: 516-349-8300  
Fax: 516-349-8321

Featuring surface measurement and precision ion etching for microelectronic and industrial applications. Worldwide sales/service offices are located in the United States, Europe and Asia Pacific.

**VSI VACUUM SCIENCE INSTRUMENTS GMBH #818**

Auguste-Viktoria-Straße 16  
Wiesbaden 65185  
Contact: Karin Neukirchen  
Tel: 49 611 990450  
Fax: 49 611 376145

Will be exhibiting our reverse view ErLEED optics with digital controlled power supply for highest performance in LEED and AES applications, the real time image processing system for quantitative LEED measurements. AIDA-PC and the ErEELS 31 toroidal electron loss spectrometer (resolution <2meV at 8pA guaranteed) with rotatable analyser and large scattering chamber.

**VSW LIMITED**

#1021

Graeme House, Chorlton  
Manchester M21 1AQ  
ENGLAND  
Contact: Mike Brayford  
Tel: 44 61 881 6213  
Fax: 44 61 881 4624

Will be featuring their wide range of surface science components. These will include the well established CLASS range of hemispherical analysers, the HIB1000 EELS system, ARIES components for photoemission studies and excitation sources. As well as the existing components the latest developments in surface science systems, detectors, and software will be shown.

**WELCH VACUUM TECHNOLOGY**

#349

7300 N. Linder Avenue  
Skokie, IL 60077  
Contact: Joseph A. Saxe  
Tel: 708-676-8800  
Fax: 708-677-8606

Vacuum pumps for instruments and laboratory applications. Introducing Chemstar™ vacuum pump for pumping corrosive gases such as HCl, Cl<sub>2</sub>, HNO<sub>3</sub>, etc. in laboratory applications. Also featuring a complete line of belt and direct-drive vacuum pumps and accessories.

**JOHN WILEY & SONS, INC.**

#645

605 Third Avenue  
New York, NY 10158  
Contact: Sally Sanford  
Tel: 212-850-6000  
Fax: 212-850-6799

Publishers since 1807, offers a diverse selection of professional & reference books & journals. Stop by our booth to browse through our latest vacuum science publications.

**WILLIAMS ADVANCED MATERIALS**

#327

2978 Main Street  
Buffalo, NY 14214  
Contact: Richard Sager  
Tel: 716-837-1000  
Fax: 716-833-2926

Fully integrated manufacturer specializing in high purity precious metal sputtering and evaporation materials. The company has full analytical capabilities including: Mass Spec, ICP, SEM, Atomic Absorber and modern chemical laboratory. A complete on site chemical refining facility supports quick turnaround and customer material recycling programs.

**WILLSON SCIENTIFIC GLASS**

#926

528 E. Fig Street  
Monrovia, CA 91016  
Contact: Robert C. Willson  
Tel: 818-303-1656  
Fax: 818-303-0559

Specializing in Ametek/Dupont helium leak detectors - new, used, upgrades & components. Stainless steel vacuum chambers - custom, to your specifications. Glass/stainless steel bell jars, new, repair, or recalibration of your helium leak standards, technical glassblowing, vacuum bake-out, heliarc welding, helium leak testing.

**WORLD SCIENTIFIC PUBL.**

#646

1060 Main Street  
River Edge, NJ 07601  
Contact: Jo Anne Dingler  
Tel: 201-487-9655  
Fax: 201-487-9656

A selection of new books on display include: *Monte Carlo Methods in AB Initio Quantum Chemistry* (Hammond), *Physical Chemistry of Solids* (Franzen), and *Microwave Properties of Magnetic Films* (Vittoria). Sample copies of our new journal *Surface Review and Letters* (SRL) will be available. World Scientific will discount all conference book orders.

**J.A. WOOLLAM CO.**

#917

650 J Street  
Suite 39  
Lincoln, NE 68508  
Contact: Kevin Lilly  
Tel: 402-477-7501  
Fax: 402-477-8214

Multilayer and multi-constituent materials analysis by spectroscopic ellipsometry. In situ real-time data acquisition and analysis, as well as research grade ex situ variable angle spectroscopic ellipsometry (vase). Both fully automated, computer controlled, 250 nm to 1700 nm spectral range. Measure film thickness, optical constants, alloy fractions, surface and interfacial roundness.

**YEAGLE TECHNOLOGY**

#816

P.O. Box 217  
Ashford, CT 06278  
Contact: Edward W. Yeagle  
Tel: 203-429-1908  
Fax: 203-429-7176

Displaying vacuum equipment support instruments, such as electron beam sweep controls, analog vacuum gauge controls, and microprocessor based valve controller electronics. Also showing electron beam guns, expendable items for electron beam guns, crystal monitors and other vacuum equipment.

# AUTHORS INDEX

Author		Prog. Abst. Pg. # Pg. #		Prog. Abst. Pg. # Pg. #		Prog. Abst. Pg. # Pg. #		
ABADAL, G.	NS-ThP1	104 304	ALLEN, C.E.	SSEM-WeA8	83 243	AUMANN, C.E.	NS-TuP5	67 203
ABBOTT, P.J.	VT-MoM3	38 122	ALLEN, L.H.	EM-MoM5	39 124	AUNER, G.	EM-WeA6	84 246
ABBOTT, P.J.	VT-MoM4	38 122	ALLEN, L.R.	EM-ThP1	105 308	AUNER, G.W.	EM-FrM10	111 329
ABDELREHIM, I.M.	SS1-MoM5	36 114	ALLEN, R.E.	NS1-TuA7	61 186	AVCI, R.	SS1-FrM11	108 318
ABDELREHIM, I.M.	SS-WeP27	86 254	ALLEN, R.E.	NS2-TuA3	61 187	VERY, A.R.	SS-TuP23	66 201
ABELES, B.	NS1-MoA2	43 129	ALLEN, T.H.	TF-WeM4	75 228	AVILA, J.	SS-WeP13	86 251
ABELN, G.	SS2-TuM8	52 166	ALLERS, W.	NS2-ThA8	99 292	AVOURIS, PH.	SS1-ThM3	90 267
ABELN, G.C.	NS-ThP25	104 307	ALLGAIR, J.	NS-ThP15	104 306	AYDIL, E.S.	PS-WeM1	74 225
ABELSON, J.R.	TF-FrM10	110 327	ALLRED, R.E.	TF-TuM3	55 175	AYDIL, E.S.	PS-MoA3	44 134
ABELSON, J.R.	TF-FrM7	110 326	ALPERSON, B.	NS1-MoA1	43 129	AYMERICH, X.	NS-ThP1	104 304
ABELSON, J.R.	EM-ThP15	105 310	ALSTRIN, A.L.	EM-ThM11	94 282	BABINEC, S.J.	AS-FrM9	110 325
ABERNATHY, C.R.	EM-WeA8	84 246	ALSTRUP, I.	SS2-WeM7	72 220	BACA, A.G.	PS-WeA5	82 241
ABERNATHY, C.R.	EM-ThA3	102 299	ALVAREZ, J.	EM-ThP13	105 310	BACHMANN, K.J.	EM-WeM7	76 230
ABERNATHY, C.R.	PS-MoP15	50 156	ALVAREZ, M.M.	NS1-TuM7	53 167	BACHRACH, R.Z.	MS-TuA1	64 195
ABERNATHY, C.R.	EM-WeA7	84 246	ALVESTEFFER, W.J.	VT-MoM8	38 123	BADDORF, A.P.	SS2-MoM3	36 116
ABERNATHY, C.R.	EM-TuP16	69 214	AMBROSIO, L.	NSBI-ThM6	91 271	BADDORF, A.P.	SS2-ThM3	90 269
ABRAIZOV, M.G.	TF-WeA8	83 245	AMEEN, M.	MS-TuM11	56 179	BADIA, A.	AS-ThM3	92 274
ABULFOTUH, F.	EM-ThA10	102 300	AMIRTHARAJ, P.M.	EM-FrM3	111 328	BAER, D.R.	MS-TuP9	70 217
ADA, E.	SS-MoP9	48 145	AMME, R.C.	AS-TuP24	68 210	BAER, D.R.	ASSS-TuA7	62 189
ADACHI, H.	SS1-MoA8	42 127	ANAND, S.	MS-TuP5	70 216	BAI, C.	NS-WeP10	87 256
ADAIR, R.W.	VM-ThA7	103 303	ANAND, S.	EM-ThM1	94 280	BAINBRIDGE, R.C.	SS1-MoM9	36 114
ADAMS, D.L.	SS2-MoM4	36 116	ANCONA, M.G.	NS2-TuM4	53 169	BAIR, A.E.	EM-TuP15	69 213
ADAMS, D.P.	SS-TuP11	66 199	ANDEREGG, J.W.	BI-MoP6	51 160	BAKER, J.	SS-MoP26	48 147
ADAMS, D.P.	SS-TuP12	66 200	ANDERLE, M.	MS-TuA10	64 196	BAKER, M.A.	TFVM-TuA3	63 193
ADAMS, D.P.	SS2-MoA5	42 128	ANDERLE, M.	MS-WeA7	84 247	BAKHTIZIN, R.Z.	NS-TuP19	67 206
ADAMS, E.	EM-TuP4	69 211	ANDERSEN, J.N.	SS2-MoM4	36 116	BALASUBRAMANIAN, K.K.	NS2-ThM8	91 273
ADAMSKI, A.	VM-ThA1	103 302	ANDERSON, A.	PS2-ThA1	101 296	BALLENTINE, P.H.	MS-TuA5	64 195
ADEM, E.H.	NS2-MoA9	43 132	ANDERSON, C.R.	AS-TuM7	54 171	BALTES, H.	VT-MoM7	38 122
ADEM, E.H.	EM-MoM4	39 124	ANDERSON, G.W.	EMMS-TuM10	56 178	BAMBHA, N.	EM-WeA1	84 245
ADESIDA, I.	SS1-ThM6	90 267	ANDERSON, G.W.	SS2-ThA4	98 288	BANDIS, C.	SS-MoP39	48 149
ADESIDA, I.	EM-WeA10	84 247	ANDERSON, T.J.	NS-TuP8	67 204	BANDIS, C.	EM-TuP24	69 215
ADKISSON, J.W.	PS-WeA2	82 240	ANDERSON, T.J.	PS-TuA8	62 191	BANDO, H.	NS1-TuA8	61 186
ADKISSON, J.W.	MS-WeM1	76 230	ANDERSON, W.	TF-ThP24	106 316	BANERJEE, S.	SS-TuP28	66 202
ADZIC, R.	SS2-WeA5	80 235	ANTHONY, J.M.	AS-WeA7	82 240	BANG, D.S.	MS-MoA7	46 141
AFFENTAUSCHEGG, C.M.	SS-MoP16	48 146	ANTONOV, P.G.	NS-WeP26	87 258	BANSENAUER, B.A.	SS-MoP29	48 148
AGARWAL, A.	VT-MoM1	38 122	AOKI, R.	MS-WeM2	76 230	BAR-SADEH, E.	VM-WeA9	85 249
AHLSTRÖM, P.	SS2-ThM10	90 270	AONO, M.	NS1-MoA5	43 130	BAR-SADEH, E.	NS1-MoA2	43 129
AHMAD, F.	EM-WeA6	84 246	APAI, G.R.	AS-ThA2	100 293	BARANAUSKAS, V.	NS-MoP6	49 150
AHMAD, F.	EM-FrM10	111 329	APEN, E.	SS-TuP24	66 202	BARBIER, L.	SS2-ThA7	98 289
AHMAD, M.	SS-MoP17	48 146	ARCHER, A.	SS1-ThM6	90 267	BARBIERI, A.	SS2-ThA10	98 289
AHMED, H.	NS1-MoA3	43 129	ARCHIBALD, D.D.	BI-TuM10	57 180	BARBIERI, A.B.	SS2-MoM6	36 116
AHMED, K.	VM-ThM1	95 284	ARLINGHAUS, H.F.	AS-TuP17	68 209	BARBOUR, J.C.	EM-TuP6	69 212
AHMED, K.	EM-TuP4	69 211	ARMSTRONG, N.R.	AS-TuP2	68 206	BARBOUR, J.C.	PS-MoA6	44 135
AHMER, S.	EM-ThM6	94 281	ARMSTRONG, N.R.	EMSS-ThM11	93 279	BARIBEAU, J.-M.	EM-TuP13	69 213
AHN, C.C.	EMSS-ThM5	93 278	ARMSTRONG, N.R.	EM-ThP21	105 311	BARKER, J.L.	BINS-WeM0	77 231
AHN, Y.O.	TF-WeP12	89 264	ARNOLD, J.C.	PS-MoP17	50 156	BARKER, J.L.	BI-MoP12	51 162
AHUJA, R.	VM-WeA10	85 249	ARONSSON, B.-O.	BI-TuM9	57 180	BARKSHIRE, I.R.	AS-MoA2	44 133
AILEY, K.S.	TFVM-TuA1	63 193	ARUMAINAYAGAM, C.R.	SS-WeP26	86 253	BARLO, T.J.	VM-FrM3	111 329
AIMÉ, J.P.	NS2-ThA7	99 292	ASADA, M.	EM-MoA9	46 140	BARNES, A.	EM-ThP8	105 309
AITA, C.R.	TF-WeA3	83 244	ASAKURA, S.	NS-MoP12	49 151	BARNES, A.V.	NS-TuP7	67 204
AIURA, Y.	NS1-TuA8	61 186	ASANO, K.	VT-MoP5	51 158	BARNES, K.	VM-ThA5	103 302
AJITO, K.	AS-MoM11	37 119	ASCHERO, G.	BI-MoP11	51 161	BARNES, P.A.	EM-ThP2	105 308
AJJI, Z.	TFVM-MoA4	45 137	ASENSIO, M.C.	SS-WeP13	86 251	BARNETT, S.A.	TF-WeP18	89 265
AKAISHI, K.	VT-MoP9	51 159	ASH, R.L.	PS-WeP1	88 258	BARNETT, S.A.	TFVM-TuA7	63 194
AKAISHI, K.	VT-MoP13	51 159	ASHBY, C.I.H.	PS-WeA5	82 241	BARNETT, S.A.	TF-WeP20	89 265
AKATSU, H.	TF-ThP6	106 313	ASHBY, C.I.H.	EM-TuP6	69 212	BARNETT, S.A.	TF-WeP13	89 264
AKBULUT, M.	SS-TuP2	66 198	ASHIDA, S.	PS-MoP22	50 157	BARNETT, S.A.	VM-WeA2	85 248
ÅKERLUND, C.	SS1-TuA3	60 182	ASIF KHAN, M.	EM-WeA10	84 247	BARNETT, S.A.	EM-TuP10	69 213
AL-BAYATI, A.H.	TFVM-ThM4	93 279	ASKELAND, P.A.	SS1-MoA7	42 126	BARNETT, S.A.	TF-ThA3	101 298
AL-BAYATI, A.H.	TFVM-ThM5	93 280	ASOKA-KUMAR, P.	TF-WeA8	83 245	BARNETT, S.A.	TF-FrM5	110 326
AL-BAYATI, A.H.	TF-WeP11	89 263	ASPNES, D.E.	EM-ThM7	94 281	BARNIOL, N.	NS-ThP1	104 304
AL-SHAREEF, H.N.	TF-WeM5	75 228	ASPNES, D.E.	SS2-MoA7	42 128	BARÓ, A.M.	NS2-ThM1	91 272
ALBAUGH, K.	MS-ThM4	94 282	ASPNES, D.E.	SS2-FrM5	108 319	BARONE, M.E.	PS-TuM11	54 173
ALBERAS, D.J.	SS1-MoM7	36 114	ASTHANA, A.	PS-TuA4	62 190	BARR, T.L.	AS-MoA9	44 134
ALBRIDGE, R.	EM-ThP8	105 309	ATHAVALE, S.D.	PS1-ThA4	100 295	BARR, T.L.	AS-TuM10	54 171
ALBRIDGE, R.G.	NS-TuP7	67 204	ATHAVALE, S.D.	PS-MoA8	44 135	BARTEL, T.J.	MS-MoA5	46 141
ALEXANDER, D.R.	VM-ThM2	95 284	ATLURI, V.	EMMS-TuM7	56 177	BARTEL, T.J.	PS-TuM5	54 172
ALEXANDER, J.	NS-MoP19	49 152	ATRE, S.	NS-WeP5	87 255	BARTELT, M.C.	SS2-TuA5	60 184
ALEXANDER, N.B.	PS2-ThA9	101 297	ATRE, S.V.	BI-MoP13	51 162	BARTELT, N.C.	SS1-ThA2	98 286
ALEXANDER, W.B.	TFVM-MoA3	45 137	ATWATER, H.A.	MS-TuP1	70 215	BARTH, J.V.	SS1-WeA3	80 233
ALEXEYEV, A.P.	AS-WeA9	82 240	ATWATER, H.A.	EMSS-ThM5	93 278	BARTRAM, M.E.	EMSS-ThM8	93 278
ALFEEV, V.N.	NS2-TuM11	53 170	ATWATER, H.A.	EM-ThA5	102 300	BARTYNSKI, R.A.	SS1-FrM9	108 318
ALFORD, T.	EM-TuP14	69 213	ATWATER, H.A.	VM-WeA8	85 249	BASHKIN, M.O.	NS-WeP16	87 256
ALFORD, T.	EM-TuP15	69 213	ATZMON, Z.	EM-TuP15	69 213	BASILIERE, S.	EMMS-TuM8	56 177
ALIVISATOS, A.P.	NS1-TuM6	53 167	AUCIELLO, O.	TF-FrM11	110 327	BASILIERE, S.	MS-ThM4	94 282
ALLARA, D.	BI-MoP13	51 162	AUCIELLO, O.	TF-WeM5	75 228	BASKI, A.A.	SS2-FrM9	108 320
ALLARA, D.L.	NS2-TuM8	53 169	AUERBACH, D.J.	SS1-TuA1	60 182	BASKI, A.A.	SS-TuP30	66 203
ALLARA, D.L.	NS1-FrM3	109 321	AUM, P.K.	PS-ThM3	92 276	BASS, A.H.	VT-MoM1	38 122
ALLARA, D.L.	NS-WeP5	87 255	AUM, P.K.	PS-ThM4	92 276	BASS, J.	VT-MoM1	38 122

Author		Prog. Abst.				Prog. Abst.					Prog. Abst.			
		Pg. #	Pg. #			Pg. #	Pg. #				Pg. #	Pg. #		
BASTASZ, R.	SS1-MoA6	42	126	BHAT, I.	MS-TuP5	70	216	BREUN, R.	PS-MoP12	50	155			
BASTASZ, R.J.	NS-ThP9	104	305	BHAT, P.K.	NS2-WeA3	81	237	BREUN, R.A.	PS-WeP9	88	260			
BATES, J.B.	TF-ThA1	101	298	BHUSHAN, B.	NS-MoP2	49	150	BRICE, D.K.	PS1-ThA8	100	295			
BATTEAS, J.D.	SS2-ThA10	98	289	BIERSACK, J.P.	AS-MoA6	44	133	BRIDGES, G.E.	NS2-FrM3	109	323			
BAUER, A.	EM-MoA5	46	139	BIHAM, O.	SS1-TuM7	52	164	BRIGGMAN, K.A.	AS-TuP25	68	210			
BAUER, E.	SS1-WeM2	72	218	BILLELO, J.C.	TF-WeA1	83	244	BRIGGMAN, K.A.	SS2-TuM10	52	166			
BEAMSON, G.	AS-ThA4	100	293	BILL, S.	MS-ThM10	94	283	BRIGGS, D.	AS-MoM3	37	118			
BEAN, J.C.	NS1-MoA8	43	130	BIN-SUDIN, M.	VM-FrM5	111	329	BRIGHT, F.V.	BI-MoA10	47	143			
BEARD, B.C.	AS-WeM1	74	223	BINGGELI, M.	NS2-ThA3	99	291	BRILLSON, L.J.	EM-WeM4	76	229			
BECK, D.D.	SS2-WeM5	72	220	BINGGELI, M.	NS2-ThA5	99	292	BRITLAND, S.	BINS-WeM2	77	231			
BECK, W.	BI-TuA9	65	197	BINGGELI, M.	NSMS-WeM0	73	221	BRIZZOLARA, R.A.	NSBI-WeA8	81	237			
BECKER, J.P.	TF-ThP18	106	315	BIRCHFIELD, B.	NS1-TuA5	61	185	BRIZZOLARA, R.A.	AS-WeM1	74	223			
BEDERKA, S.	VT-MoM10	38	123	BIRK, H.	NS2-WeM5	73	223	BRODY, P.S.	TF-ThP17	106	315			
BEDERKA, S.	PS-WeP4	88	259	BISHOP, G.G.	SS-MoP26	48	147	BRONGERSMA, H.H.	AS-TuM8	54	171			
BEDROSSIAN, P.J.	SS2-TuA2	60	183	BITTNER, D.	PS-WeP20	88	261	BRONIKOWSKI, M.J.	EM-ThP22	105	311			
BEDZYK, M.J.	SS2-FrM10	108	320	BJÖRNHOLM, T.	NS-ThP21	104	307	BROWER, D.	TF-WeP5	89	262			
BEEBE, JR., T.P.	AS-ThM9	92	275	BLAIN, M.G.	PS-ThM3	92	276	BROWN, D.A.	PS-WeA10	82	242			
BEEBE, JR., T.P.	NS2-FrM10	109	323	BLAIN, M.G.	PS-ThM4	92	276	BROWN, D.E.	SS-TuP7	66	199			
BEEBE, JR., T.P.	NSBI-ThM9	91	271	BLAKELY, J.M.	SS-WeP1	86	250	BROWN, G.	NS-TuP6	67	203			
BEEBE, JR., T.P.	AS-WeM5	74	224	BLANALT, P.	NS2-MoA8	43	132	BROWN, G.	EMSS-ThM10	93	279			
BEEBE, JR., T.P.	NS-WeP3	87	255	BLANTON, T.	NS2-WeA9	81	238	BROWN, R.	PS-TuA3	62	190			
BEHM, R.J.	EMMS-TuM3	56	177	BLAYO, N.	PS-TuA2	62	190	BROWN, R.	PS-MoP12	50	155			
BEHM, R.J.	NS2-WeM6	73	223	BLAYO, N.	MS-WeA4	84	247	BROWNSON, N.E.	BI-MoA3	47	142			
BEHRENDT, F.	SS1-MoM11	36	115	BLAYO, N.	PS-WeM3	74	225	BRUGGER, J.	NS2-ThM10	91	273			
BEHRENDT, F.	SS2-ThM10	90	270	BLOOM, D.M.	NS2-FrM1	109	322	BRÜHWILER, P.A.	SS1-FrM5	108	317			
BEHRENDT, F.	SS2-WeM8	72	220	BLÜGEL, S.	SS1-WeA7	80	233	BRUNDE, C.R.	MS-ThM9	94	283			
BEHRINGER, E.R.	SS-MoP27	48	147	BLUMBERG, M.Q.	SS-WeP26	86	253	BRUNFELDT, K.	NS1-TuM2	53	167			
BEIJERINCK, H.C.W.	PS-WeP2	88	258	BLUMENTHAL, R.	PS-WeP10	88	260	BRUNMEIER, B.	PS-TuA5	62	190			
BEKOS, E.	BI-TuM11	57	181	BOCK, D.	BI-MoP14	51	162	BRUSASCO, R.	PS-WeP19	88	261			
BEKOS, E.J.	BI-MoA10	47	143	BOECKMANN, M.D.	VT-MoA3	45	136	BRUSASCO, R.	PS-WeP17	88	261			
BELKAND, A.	MS-ThM3	94	282	BOERIO, F.J.	AS-FrM1	110	324	BRUYNSERAEDE, Y.	NS2-ThM5	91	273			
BELKIND, A.	VM-ThA6	103	302	BOGACHEK, E.N.	NS2-ThM1	91	272	BRYAN, S.R.	AS-MoM3	37	118			
BELLINA, JR., J.J.	AS-TuP25	68	210	BOGART, K.H.A.	PS-MoP3	50	154	BU, H.	SS2-MoM9	36	116			
BELLO, I.	TF-WeP21	89	265	BOHLAND, J.F.	NS-MoP14	49	152	BUATIER DE MONGEOT, F.	SS1-TuA2	60	182			
BELLO, I.	VT-MoM10	38	123	BOHLING, D.A.	EM-TuP16	69	214	BUCHHEIT, R.G.	VM-ThM7	95	284			
BELLO, I.	PS-WeP4	88	259	BÖHME, O.	NS-WeP6	87	255	BUCK, M.	TF-FrM9	110	327			
BELLO, I.	AS-ThA6	100	294	BOJAN, V.J.	AS-WeA6	82	239	BUCK, M.	TFVM-MoA4	45	137			
BELTON, D.N.	SS2-WeM0	72	219	BOJAN, V.J.	AS-TuM11	54	171	BUKHARAEV, A.A.	NS-WeP26	87	258			
BELTON, D.N.	SS-MoP15	48	146	BOL, C.W.J.	SS-MoP20	48	146	BUKOWSKI, J.D.	PS-MoP21	50	157			
BELTON, D.N.	AS-TuP22	68	209	BOLAND, T.	AS-ThA3	100	293	BURCHHARDT, J.	SS2-MoM4	36	116			
BELTON, D.N.	SS2-WeM2	72	219	BOLAND, T.	NSBI-ThM1	91	270	BURGER, A.	NS-TuP1	67	203			
BENDAVID, A.	TFVM-ThM6	93	280	BONNELL, D.	NS1-TuA10	61	186	BURGER, A.	NS-TuP15	67	205			
BENESCH, J.	VT-TuM6	55	174	BONSER, D.J.	PS-ThM3	92	276	BURGER, A.	AS-TuM9	54	171			
BENNETT, K.W.	TF-ThP17	106	315	BONSER, D.J.	PS-ThM4	92	276	BURGER, J.	NS2-ThA5	99	292			
BENNETT, P.A.	SSEM-WeA10	83	243	BONSER, D.J.	SS-TuP26	66	202	BURGER, J.	NSMS-WeM0	73	221			
BENNETT, P.A.	SS2-ThA3	98	288	BORG, H.J.	SS-MoP13	48	145	BURNETT, D.S.	AS-WeM8	74	225			
BENNETT, P.A.	EMSS-ThM6	93	278	BORG, H.J.	SS2-WeM1	72	219	BURNHAM, N.A.	NS2-TuA4	61	187			
BENNETT, P.A.	EM-MoA7	46	140	BORKHOLDER, D.	BI-TuA3	65	196	BURNS, A.R.	SS2-TuM7	52	165			
BENNICH, P.	SS-MoP18	48	146	BORUP, R.L.	SS2-WeA4	80	235	BURROUGHS, J.A.	SS-MoP9	48	145			
BENNINGHOVEN, A.	BI-MoP9	51	161	BOSWELL, R.	PS-MoA5	44	134	BURROUGHS, J.A.	SS-MoP38	48	149			
BENNINGHOVEN, A.	AS-TuM4	54	170	BOITCHKAREV, A.E.	SS2-MoA9	42	129	BURROUGHS, J.A.	AS-ThA5	100	293			
BENNINGHOVEN, A.	AS-MoM4	37	118	BOTHA, S.	EM-MoM3	39	123	BUSCH, D.G.	SS2-TuM2	52	165			
BENNINGHOVEN, A.	AS-TuP5	68	207	BOTKIN, D.	NS2-FrM4	109	323	BUTLER, J.E.	SS-TuP27	66	202			
BENNINGHOVEN, A.	AS-WeM7	74	224	BOTTOMLEY, L.A.	NS1-TuM10	53	168	BUTLER, J.E.	SS-MoP25	48	147			
BENNINGHOVEN, A.	AS-TuP8	68	207	BOTTOMLEY, L.A.	NS-ThP7	104	305	BUTLER, S.W.	MS-WeA1	84	247			
BENSAOULA, A.	TF-WeP19	89	265	BOTTOMLEY, L.A.	NSBI-ThM3	91	271	BUTTERBAUGH, J.W.	PS-ThM6	92	276			
BENSAOULA, A.	TFVM-TuA4	63	193	BOUCHARD, A.M.	SS2-FrM1	108	319	BUTTNER, W.R.	TF-ThP20	106	315			
BENSEBAA, F.	AS-ThM3	92	274	BOUHACINA, T.	NS2-ThA7	99	292	BUURON, A.J.M.	PS-MoP1	50	153			
BERDUNOV, N.V.	NS-WeP26	87	258	BOUSETTA, A.	TF-WeP19	89	265	BYUN, D.	EM-ThP24	105	311			
BERG, S.	PS-MoP8	50	155	BOUSETTA, A.	TFVM-TuA4	63	193	BYUN, D.	NS-TuP16	67	205			
BERG, S.	TF-WeP14	89	264	BOWEN KATARI, J.E.	NS1-TuM6	53	167	CABRAL, JR., C.	TF-WeP22	89	265			
BERGER, H.	EM-ThP6	105	309	BOWERS, W.J.	TFVM-TuA5	63	193	CABRERA, C.R.	NS-TuP4	67	203			
BERGGREN, B.P.	NS-TuP17	67	205	BOWMAN, T.	MS-TuA3	64	195	CAHILL, D.G.	SS2-MoA9	42	129			
BERGMANS, R.H.	AS-TuM8	54	171	BOYD, K.J.	TFVM-ThM4	93	279	CAHILL, D.G.	SS1-TuM4	52	163			
BERGQUIST, L.	VT-MoA6	45	136	BOYD, K.J.	TFVM-ThM5	93	280	CAHILL, D.G.	TF-WeM4	75	228			
BERGSTROM, D.B.	EM-MoM5	39	124	BOZLER, C.	TF-WeP11	89	263	CALABRESE, G.S.	NS-MoP14	49	152			
BERMUDEZ, V.M.	EM-ThP18	105	310	BRADT, R.	NS1-TuA10	61	186	CALAWAY, W.F.	AS-WeM8	74	224			
BERNARD, J.F.	EM-MoM4	39	124	BRADY, M.J.	TF-WeA9	83	245	CALDERON, M.	VT-TuA8	63	192			
BERNAT, T.	PS-WeP20	88	261	BRAIDE, M.	EM-MoM11	39	125	CALDWELL, T.E.	SS1-MoM5	36	114			
BERNAT, T.	PS2-ThA7	101	297	BRAMBLETT, T.R.	BI-MoA8	47	143	CALE, T.S.	EM-TuP25	69	215			
BERNEY, B.	MS-MoA5	46	141	BRAND, O.	TF-ThP2	106	312	CALE, T.S.	EM-MoM7	39	124			
BERNSTEIN, G.H.	NS2-TuM6	53	169	BRANDOW, S.L.	VT-MoM7	38	122	CALE, T.S.	MS-MoA1	46	140			
BERRY, G.A.	TF-ThA5	101	298	BRANDOW, S.L.	BINS-WeM8	77	232	CALE, T.S.	PS-MoA4	44	134			
BERRY, L.A.	PS-WeP8	88	259	BRANDOW, S.L.	NS1-TuA9	61	186	CALE, T.S.	MS-MoA10	46	141			
BERRY, L.A.	PS-MoM8	38	121	BRASEN, D.	NS2-TuM7	53	169	CALLCOTT, T.A.	TF-ThP6	106	313			
BERSIN, R.L.	MS-ThM7	94	283	BRATINA, G.	MS-ThM8	94	283	CALVERT, J.M.	NS1-TuA9	61	186			
BESENBACHER, F.	SS2-TuA8	60	184	BRAUNSTEIN, D.	EM-WeM4	76	229	CALVERT, J.M.	NS1-FrM1	109	320			
BESENBACHER, F.	NS2-ThM2	91	272	BRENNAN, S.	NSBI-WeA1	81	236	CALVERT, J.M.	EM-ThA8	102	300			
BESENBACHER, F.	SS-WeP3	86	250	BRENNER, D.W.	SS2-MoA7	42	128	CALVERT, J.M.	BI-MoP3	51	160			
BESSOLOV, V.N.	EM-ThP9	105	309	BRETT, M.J.	NS2-ThM3	91	272	CALVERT, J.M.	NS-MoP14	49	152			
BETZIG, E.	NSBI-WeA3	81	236	BRETTSCHNEIDER, E.	TF-WeA5	83	244	CALVERT, J.M.	NS2-TuM7	53	169			
BEY, JR., P.P.	BI-TuA3	65	196	BREUN, R.	NS-TuP8	67	204	CALVERT, J.M.	NS2-ThM7	91	273			
BHARATAN, S.	EM-WeA7	84	246		PS-TuA3	62	190	CAMMARATA, R.C.	VM-WeA5	85	248			



Author		Prog. Abst.		Prog. Abst.		Prog. Abst.		Prog. Abst.
		Pg. # Pg. #		Pg. # Pg. #		Pg. # Pg. #		Pg. # Pg. #
CAMMARATA, V.	NS2-ThM8	91 273	CHEN, J.R.	VT-TuA4	63 192	COLTON, R.J.	NS-MoP4	49 150
CAMPBELL, A.A.	BI-TuM1	57 179	CHEN, K.-T.	NS-TuP1	67 203	COLTON, R.J.	NS2-TuA7	61 187
CAMPBELL, B.	NS2-TuM6	53 169	CHEN, L.	SS-TuP29	66 202	COLTON, R.J.	NSBI-ThM2	91 270
CAMPBELL, R.A.	SS-WeP7	86 250	CHEN, L.	PS-ThM10	92 277	COLTON, R.J.	NS2-ThM3	91 272
CANHAM, L.T.	NS2-WeA6	81 238	CHEN, L.	MS-WeM3	76 230	COLVIN, V.L.	NS1-TuM6	53 167
CANTELL, M.C.	MS-WeM1	76 230	CHEN, M.-S.	NS2-ThM7	91 273	COMFORT, J.C.	EM-ThP16	105 310
CANTOW, H.-J.	NS-WeP4	87 255	CHEN, M.S.	NS-MoP14	49 152	COMSA, G.	SS2-TuA2	60 183
CAO, J.L.	NS-MoP7	49 151	CHEN, P.	SS2-WeM6	72 220	CONARD, T.	TF-ThP22	106 315
CAPLE, G.	NS-WeP1	87 254	CHEN, P.	AS-ThM8	92 275	CONRAD, D.W.	BI-TuA5	65 197
CARLILE, R.N.	MS-WeM8	76 231	CHEN, P.J.	TF-ThP13	106 314	CONRAD, E.	TF-ThP4	106 313
CARLILE, R.N.	PS-WeA10	82 242	CHEN, S.-Y.	AS-TuP2	68 206	COOK, R.	PS-WeP21	88 261
CARLINE, R.T.	EM-ThM4	94 281	CHEN, W.	EM-ThP25	105 312	COOK, R.	PS-WeP19	88 261
CARLISLE, J.A.	TF-ThP6	106 313	CHEN, X.	SS1-TuM6	52 163	COOPER, B.H.	SS-TuP17	66 201
CARLOS, W.E.	NS2-WeA4	81 237	CHENG, C.C.	PS-WeM0	74 225	COOPER, B.H.	SS2-TuA1	60 183
CARNES, J.	NS-MoP5	49 150	CHENG, C.C.	PS1-ThA1	100 294	COOPER, J.M.	BI-MoA4	47 142
CARNIGLIA, C.K.	VM-THA9	103 303	CHENG, H.	EM-WeM5	76 230	COOPER, J.M.	BI-TuA4	65 197
CARPICK, R.	SS2-MoM8	36 116	CHENG, H.P.	NS2-ThM1	91 272	CORBIT, T.	SS1-ThM10	90 268
CARPINELLI, J.M.	NS-TuP16	67 205	CHENG, K.-Y.	EM-MoA1	46 139	CORNEILLE, J.S.	TF-ThP13	106 314
CARTER, R.N.	SS-MoP3	48 144	CHENG, K.-Y.	EM-ThA6	102 300	CORNEILLE, J.S.	SS1-FrM3	108 317
CASADO, C.	SS-WeP13	86 251	CHENG, Q.	TF-ThP10	106 314	CORNELIO CLARK, P.A.	AS-ThA9	100 294
CASAS, L.	TF-WeP3	89 262	CHERNAVSKII, D.S.	NSBI-WeA10	81 237	CORNELISON, D.M.	AS-TuP1	67 206
CASAS, L.M.	NS-ThP24	104 307	CHERNOFF, D.A.	NSBI-WeA2	81 236	COTTE, J.	MS-TuA10	64 196
CASERI, W.R.	AS-TuP11	68 208	CHERNOFF, D.A.	NS-MoP17	49 152	COUCH, R.E.	AS-WeM4	74 224
CASEY, S.M.	EM-ThM11	94 282	CHERNOFF, E.A.G.	NSBI-WeA2	81 236	COULMAN, D.	AS-FrM8	110 325
CASTLEBERRY, H.	EM-WeM7	76 230	CHEW, A.D.	VT-MoP2	51 157	COULTER, K.	SS-MoP23	48 147
CASTNER, D.G.	BI-MoP9	51 161	CHEW, K.H.	PS-MoP2	50 153	COURTEILLE, C.	PS-WeA6	82 241
CASTNER, D.G.	AS-ThM11	92 275	CHEY, S.J.	SS2-MoA9	42 129	COURY, J.E.	NS1-TuM10	53 168
CASTNER, D.G.	AS-MoM5	37 118	CHEY, S.J.	SS1-TuM4	52 163	COURY, J.E.	NSBI-ThM3	91 271
CAUDANO, R.	SS1-FrM8	108 318	CHI, P.H.	TF-WeP5	89 262	COUSTY, J.	SS2-ThA7	98 289
CAUDANO, R.	TF-ThP22	106 315	CHIA, W.-J.	ASSS-TuA2	62 188	COWIN, J.P.	SS1-ThM4	90 267
CAUDANO, R.	TF-WeA6	83 245	CHIANG, C.-M.	SS-MoP4	48 144	COX, A.J.	TF-WeP16	89 264
CAUGHMAN, J.B.O.	PS-MoP5	50 154	CHIANG, S.	SS1-WeM2	72 218	COX, T.I.	NS2-WeA6	81 238
CAVICCHI, R.E.	NSBI-ThA5	99 290	CHIDSEY, C.E.D.	AS-ThM7	92 275	CRAIGHEAD, H.G.	NS2-TuM8	53 169
CAVICCHI, R.E.	SS1-MoA3	42 126	CHILDS, R.A.	VT-TuM11	55 175	CRAIGHEAD, H.G.	NS1-FrM3	109 321
CECCHI, J.L.	PS-TuA1	62 190	CHILKOTI, A.	BI-TuM1	57 179	CRAIGHEAD, H.G.	MS-TuP8	70 217
CEE, V.J.	AS-ThM9	92 275	CHIN, W.-B.	SS2-MoM7	36 116	CRAMER, H.-G.	AS-TuM4	54 170
CEE, V.J.	NS-WeP3	87 255	CHIU, T.H.	EM-TuP12	69 213	CREIGHTON, J.R.	SS-MoP29	48 148
CELII, F.G.	EM-ThM3	94 280	CHO, K.	SS-WeP28	86 254	CREIGHTON, J.R.	SSEM-WeM0	75 226
CELIO, H.	SS1-MoM8	36 115	CHO, S.T.	VT-MoM5	38 122	CREWE, D.A.	NSBI-ThA7	99 290
CELOTTA, R.J.	NS2-WeM7	73 223	CHOI, W.J.	AS-WeA5	82 239	CROOKS, R.M.	TF-TuM3	55 175
CELOTTA, R.J.	SS1-WeM0	72 218	CHORKENDORFF, I.	SS1-MoM10	36 115	CROOKS, R.M.	NS2-TuA8	61 187
CERRINA, F.	EM-ThP6	105 309	CHOUTOV, D.	NS1-FrM5	109 321	CROOKS, R.M.	NS2-ThM9	91 273
CHABAL, Y.J.	SSEM-WeM6	75 227	CHOW, A.	TF-WeM5	75 228	CROOKS, R.M.	SS1-ThM10	90 268
CHABAN, E.E.	NS2-FrM11	109 324	CHOW, A.S.	PS-WeP22	88 262	CROOKS, R.M.	AS-FrM10	110 325
CHABAN, E.E.	SS-MoP4	48 144	CHOW, G.M.	NS1-TuA9	61 186	CROSS, J.B.	PS-ThM11	92 277
CHAILAPAKUL, O.	NS2-ThM9	91 273	CHRISEY, D.B.	BI-MoP3	51 160	CROSS, J.B.	EM-ThP19	105 311
CHAKAROV, D.	SS2-WeA9	80 235	CHRISEY, L.A.	NSBI-ThM2	91 270	CROWELL, J.E.	SS-MoP16	48 146
CHAMBERLAN, S.L.	AS-WeM4	74 224	CHRISEY, L.A.	BI-MoP3	51 160	CROWELL, J.E.	SS-TuP27	66 202
CHAMBERS, A.	VT-MoP2	51 157	CHRISTENSEN, K.N.	EM-ThM5	94 281	CROWELL, J.E.	SS-WeP30	86 254
CHAMBERS, S.A.	SS1-ThA1	98 286	CHRISTENSEN, T.	VM-ThM6	95 284	CSERNY, E.	SS1-MoA8	42 127
CHAMBERS, S.A.	TF-ThP1	106 312	CHRISTOPH, R.	NSMS-WeM0	73 221	CULBERTSON, R.J.	EM-TuP14	69 213
CHAMBERS, S.A.	EM-ThP23	105 311	CHRISTOPH, R.	NS2-ThA5	99 292	CULBERTSON, R.J.	EM-TuP15	69 213
CHAMBLISS, D.D.	SS2-TuA9	60 184	CHU, W.-K.	PS-MoA8	44 135	CULBERTSON, R.J.	EMMS-TuM7	56 177
CHAN, K.K.	EM-MoM11	39 125	CHU, X.	TF-WeP18	89 265	CUMPSON, P.J.	AS-WeM0	74 223
CHANDLER-HOROWITZ, D.	EM-FrM3	111 328	CHU, X.	TFVM-TuA7	63 194	CUNNICK, J.E.	BI-MoP6	51 160
CHANDRACHOOD, M.	NSBI-ThA6	99 290	CHU, X.	NS2-WeM2	73 222	CURCIC, T.	SS-TuP17	66 201
CHANG, C.	BINS-WeM8	77 232	CHU, X.	NS-WeP23	87 258	CURPHY, J.J.	AS-FrM9	110 325
CHANG, C.	PS1-ThA9	100 296	CHUNG, Y.-W.	ASSS-TuA2	62 188	CURTI, F.G.	SS1-FrM9	108 318
CHANG, C.S.	NS2-ThM11	91 274	CHUNG, Y.W.	TF-WeP15	89 264	CURTIS, A.S.G.	BINS-WeM2	77 231
CHANG, C.S.	SS-WeP4	86 250	CIRIDON, W.	AS-ThA3	100 293	CURTIS, R.	SS1-TuM1	52 163
CHANG, M.	EM-MoM6	39 124	CIRLIN, E.-H.	AS-WeA1	82 239	CUSTER, J.S.	PS-MoA6	44 135
CHANG, R.P.H.	TF-FrM11	110 327	CIRLIN, E.-H.	AS-TuP16	68 208	CYGAN, M.T.	SS-TuP16	66 200
CHANG, S.-L.	SS2-MoM7	36 116	CLARK, R.	NS-MoP11	49 151	CZANDERNA, A.W.	AS-ThM6	92 275
CHANG, T.H.P.	NS-MoP24	49 153	CLARK, R.	BI-TuM1	57 179	CZANDERNA, A.W.	AS-TuP3	68 207
CHANG, T.H.P.	NS2-MoA6	43 132	CLARYSSE, T.	NSMS-WeM3	73 221	D'AMATO, C.	AS-MoM10	37 119
CHANG SHIH, M.	EMMS-TuM9	56 178	CLAUBERG, E.	TF-FrM2	110 326	DABIRAN, A.M.	SS2-MoA10	42 129
CHAPARALA, P.	NSBI-ThA5	99 290	CLAUSTHAL, T.U.	SS1-WeM2	72 218	DAGATA, J.A.	EM-ThP10	105 309
CHARLES, P.T.	BI-TuA5	65 197	CLEAVER, J.R.A.	NS1-TuM5	53 167	DAGATA, J.A.	NSMS-WeM4	73 221
CHARYCH, D.H.	BI-TuA7	65 197	CLEVENGER, L.A.	TF-WeP22	89 265	DAHINT, R.	NSBI-ThA4	99 290
CHASON, E.	PS1-ThA8	100 295	COHEN, P.I.	SS2-MoA10	42 129	DAI, Q.	SS2-MoM8	36 116
CHASON, M.	TF-ThP23	106 316	COHEN, S.L.	EMMS-TuM8	56 177	DAKSHINA MURTHY, S.	MS-TuP5	70 216
CHAU, L.-K.	AS-TuP2	68 206	COHEN, S.L.	MS-ThM4	94 282	DALEY, K.	EM-TuP14	69 213
CHAUDHRY, N.	MSVT-ThA5	102 301	COHEN, S.R.	NS1-MoA1	43 129	DALEY, K.	EM-TuP15	69 213
CHAUDHURI, J.	EM-TuP23	69 215	COLLIGON, J.S.	TFVM-ThM1	93 279	DALLESKA, N.F.	PS1-ThA3	100 294
CHEMLA, D.S.	NS2-FrM4	109 323	COLLINS, G.J.	PS-TuA6	62 190	DALTON, T.J.	PS1-ThA6	100 295
CHEN, C.-H.	SS2-WeA3	80 234	COLLINS, G.W.	PS-WeP20	88 261	DALVIE, M.	MS-WeM5	76 231
CHEN, D.	NS1-FrM11	109 322	COLLINS, G.W.	PS2-ThA7	101 297	DALVIE, M.	MS-MoA6	46 141
CHEN, F.F.	PS-MoP14	50 156	COLLINS, I.R.	EM-ThP6	105 309	DALVIE, M.	MS-WeM7	76 231
CHEN, H.	NS-ThP2	104 304	COLLINS, R.W.	TFVM-MoA7	45 138	DALY, C.	NS2-ThA10	99 293
CHEN, J.	PS-MoP2	50 153	COLLINS, S.M.	PS-WeA10	82 242	DANE, D.	PS-TuA10	62 191
CHEN, J.C.	EM-WeA1	84 245	COLLINS, W.E.	NS-TuP1	67 203	DANNENBERG, R.	TF-WeP10	89 263
CHEN, J.G.	SS1-FrM7	108 318	COLLINS, W.E.	AS-TuM9	54 171	DAUGHERTY, J.D.	PS-WeA7	82 241
CHEN, J.R.	VT-MoP7	51 158	COLTON, R.J.	NS-MoP3	49 150	DAVIDSON, J.	EM-ThP8	105 309

Author		Prog. Abst.		Prog. Abst.		Prog. Abst.		Prog. Abst.
		Pg. # Pg. #		Pg. # Pg. #		Pg. # Pg. #		Pg. # Pg. #
DAVIDSON, M.R.	AS-TuM5	54 170	DOWBEN, P.A.	EM-ThP24	105 311	ESTES, S.	EMMS-TuM8	56 178
DAVIES, J.E.	BI-MoA1	47 142	DOWBEN, P.A.	SS1-WeA9	80 234	ESTES, S.	MS-ThM4	94 282
DAVIES, M.C.	NSBI-ThM10	91 272	DOWBEN, P.A.	NS-TuP16	67 205	ESTRUP, P.J.	SS2-ThM1	90 268
DAVIES, M.C.	AS-ThA4	100 293	DRAPER, C.F.	NS-MoP4	49 150	ETELÄNIEMI, V.	SS2-ThA1	98 288
DAVIES, M.C.	BI-TuM4	57 180	DRAPER, C.F.	NS2-TuA7	61 187	EURLINGS, M.F.A.	PS-WeP2	88 258
DAVIES, M.C.	NSBI-ThM8	91 271	DRAWL, W.	TFVM-MoA7	45 138	EVANS, D.A.	EM-TuP17	69 214
DAVIES, M.C.	NS2-MoA4	43 131	DRECHSLER, M.	NS-WeP4	87 255	EVANS, J.W.	SS2-TuA5	60 184
DAVILA, M.E.	EM-ThP13	105 310	DRESSICK, W.	BI-MoP3	51 160	EVANS, P.	AS-TuM10	54 171
DAVIS, G.D.	AS-FrM2	110 324	DRESSICK, W.J.	NS1-TuA9	61 186	EVSTROPOV, V.V.	EM-ThP9	105 309
DAVIS, R.C.	NSBI-ThA8	99 291	DRESSICK, W.J.	NS-MoP14	49 152	EZELL, E.	TF-ThP15	106 314
DAVIS, R.F.	TFVM-TuA1	63 193	DRESSLER, CH.	TF-FrM9	110 327	FADLEY, C.S.	SS-WeP16	86 252
DAVIS, R.J.	PS-WeP12	88 260	DROBNY, G.	BI-TuM1	57 179	FADLEY, C.S.	SS1-WeM7	72 219
DAVYDOV, A.	NS-TuP8	67 204	DROOPAD, R.	MS-TuP5	70 216	FADLEY, C.S.	SS-WeP15	86 252
DAWSON, D.H.	SS1-MoA2	42 126	DROOPAD, R.	EM-ThM1	94 280	FADLEY, C.S.	AS-WeM4	74 224
DE HOOG, F.J.	PS-WeM7	74 226	DRUBE, A.R.	NS-WeP2	87 254	FADLEY, C.S.	SS-WeP14	86 251
DE LOZANNE, A.L.	NS-ThP12	104 305	DU, W.	SS-TuP29	66 202	FADLEY, C.S.	SS1-WeA10	80 234
DE SIMON, M.	VT-TuM8	55 174	DU, Y.-Z.	AS-TuP4	68 207	FAEHL, R.J.	VM-ThM9	95 285
DE VILLEPOIX, R.	NP-WeP2	89 266	DUBASH, J.H.	PS-MoP17	50 156	FAHY, M.R.	SS-TuP23	66 201
DE WOLF, P.	NSMS-WeM3	73 221	DUBEY, M.	NS-ThP24	104 307	FAIN, JR., S.C.	SS-MoP36	48 149
DEB, K.K.	TF-ThP17	106 315	DUBEY, M.	TF-WeP3	89 262	FAIRBROTHER, D.H.	SS2-TuM10	52 166
DEBE, M.K.	NS-WeP2	87 254	DUBROVENSKY, S.D.	NS-WeP16	87 256	FALVO, M.	NS-ThP6	104 305
DEHART, C.	NS2-WeA3	81 237	DUDEN, T.	SS1-WeM2	72 218	FAN, L.S.	NSMS-WeM5	73 221
DEIMEL, M.	AS-MoM4	37 118	DUFFIN, R.	MS-TuA6	64 196	FAN, T.	SS-WeP29	86 254
DEIMEL, M.	AS-TuP5	68 207	DUKE, C.B.	SS2-MoM10	36 117	FANG, C.C.	SS-MoA2	46 140
DEIMEL, M.	AS-WeM7	74 224	DULCEY, C.S.	NS1-TuA9	61 186	FAUCHET, P.M.	NS2-WeA9	81 238
DEIMEL, M.	AS-TuP8	68 207	DULCEY, C.S.	BI-MoP3	51 160	FAUCHET, P.M.	NS2-WeA8	81 238
DEKOVEN, B.M.	AS-FrM9	110 325	DULCEY, C.S.	NS-MoP14	49 152	FAUCHET, P.M.	NS2-WeA5	81 238
DELGADO, E.	SS1-MoM5	36 114	DUMAS, P.	SS1-ThA6	98 287	FAVIA, P.	BI-MoP10	51 161
DELOUISE, L.A.	EMSS-ThM9	93 278	DUNCAN, W.M.	EM-ThM3	94 280	FAYFIELD, T.	NS2-ThM4	91 273
DELPLANCKE, M.P.	TF-ThP7	106 313	DUNHAM, D.	TF-ThP12	106 314	FEDERLIN, P.	MS-WeM3	76 230
DEMIN, V.J.	VM-FrM8	111 330	DUNN, J.	NP-WeP7	89 266	FEDOROV, E.A.	NSBI-WeA10	81 237
DENG, U.	NS2-ThM8	91 273	DUNPHY, J.C.	SS-WeP5	86 250	FEIBELMAN, P.	NS1-TuM1	53 166
DENG, H.	NS1-MoA2	43 129	DURANDET, A.	PS-MoA5	44 134	FEIBELMAN, P.J.	SS2-TuA6	60 184
DENIER VAN DER GON, A.W.	AS-TuM8	54 171	DÜRR, H.	SS-TuP15	66 200	FEIBELMAN, P.J.	SS1-FrM1	108 317
DENLINGER, J.	AS-MoM7	37 119	DUTTAGUPTA, S.P.	NS2-WeA9	81 238	FEIJOO, D.	SSEM-WeM6	75 227
DENLINGER, J.	EM-FrM5	111 328	DWYER, D.J.	SS1-MoA1	42 126	FEIL, H.	PS-TuM9	54 173
DEPRISTO, A.E.	SS1-TuM8	52 164	DYLLA, H.F.	VT-TuM2	55 173	FEINERMAN, A.D.	NSBI-ThA7	99 290
DEPUYDT, J.M.	EM-WeM5	76 230	DYLLA, H.F.	VT-TuA5	63 192	FEINERMAN, A.D.	NS-ThP3	104 304
DESHMUKH, S.C.	PS-MoA3	44 134	DYLLA, H.F.	VT-TuM6	55 174	FELTER, T.E.	NS-MoP23	49 153
DEUTSCHMANN, O.	SS1-MoM11	36 115	DYSON, C.S.	TF-TuM11	55 176	FELTON, R.H.	NS1-TuM10	53 168
DEUTSCHMANN, O.	SS2-ThM10	90 270	EAGLESHAM, D.J.	SS-TuP11	66 199	FENG, S.	TF-WeP16	89 264
DEVINE, D.J.	NS-MoP23	49 153	EBERT, PH.	SSEM-WeM4	75 227	FERENCZ, A.	AS-TuP2	68 206
DEVRIES, B.D.	SS1-FrM7	108 318	ECONOMOU, D.	PS-TuM5	54 172	FERGUSON, J.F.	EM-TuP12	69 213
DEVRIES, B.D.	TF-WeP21	89 265	ECONOMOU, D.J.	PS1-ThA4	100 295	FERNANDEZ, M.	PS-MoP6	50 154
DEW, S.K.	TF-WeA5	83 244	ECONOMOU, D.J.	PS-MoA8	44 135	FERRIS, J.H.	SS-TuP16	66 200
DHERE, N.G.	TF-ThA4	101 298	EDDY, JR., C.R.	NS-ThP13	104 306	FERRUTI, P.	AS-ThA4	100 293
DHESI, S.	SS1-ThA10	98 287	EDELMAN, V.S.	NS-WeP17	87 257	FIJOL, J.J.	EM-TuP19	69 214
DICKIE, R.A.	AS-FrM1	110 324	EDELSTEIN, D.C.	EM-MoM1	39 123	FIJOL, J.J.	EM-WeM3	76 229
DICKINSON, J.T.	AS-FrM7	110 325	EDENFELD, K.M.	NSBI-ThA9	99 291	FILES, L.A.	NS2-MoA3	43 131
DICKINSON, J.T.	NS2-ThA4	99 292	EDERER, D.L.	TF-ThP6	106 313	FILIPPELLI, A.R.	VT-MoM4	38 122
DICKINSON, J.T.	SS2-TuM6	52 165	EDIDIN, M.	NSBI-WeA3	81 236	FINE, H.A.	VT-MoA7	45 136
DIEBOLD, U.	SS1-ThA9	98 287	EGGS, C.	EM-ThM8	94 281	FINGER, K.	VT-TuM6	55 174
DIEHL, D.	EM-ThM5	94 281	EHRICH, G.	SS2-TuA10	60 185	FIRST, P.N.	NS-WeP18	87 257
DIETZ, N.	EM-WeM7	76 230	EIGLER, D.M.	NS1-MoM9	37 117	FISCHER, D.A.	AS-FrM9	110 325
DILLINGHAM, T.R.	AS-TuP1	68 206	EIPERS-SMITH, K.	TF-ThP3	106 312	FISHER, E.R.	PS1-ThA3	100 294
DILLON, A.C.	EM-ThA9	102 300	EISINGER, W.	NP-WeP3	89 266	FISHER, E.R.	PS-MoP3	50 154
DILLON, R.	TF-FrM8	110 327	EIZENBERG, M.	EM-MoM6	39 124	FISHER, E.R.	PS-MoP4	50 154
DIMAGGIO, C.L.	SS2-WeM5	72 220	EKERDT, J.G.	SS-TuP25	66 202	FISHER, G.B.	SS2-ThM2	90 268
DIMAGGIO, C.L.	SS2-ThM2	90 268	EKERDT, J.G.	NS-TuP28	66 202	FLAUM, H.C.	SS-MoP27	48 147
DING, Y.	NS-ThP7	104 305	ELKAAKOUR, Z.	SS2-ThA7	99 292	FLECHTER, S.	EM-WeM7	76 230
DINWIDDIE, R.B.	NS-MoP10	49 151	ELLIS, T.	AS-ThM3	92 274	FLEISCHER, C.A.	AS-ThA2	100 293
DION, M.J.	PS-WeP13	88 260	ELLIS, W.P.	SS1-MoA6	42 126	FLEMING, M.J.	EMMS-TuM8	56 178
DIPESO, G.	PS-MoP20	50 157	ELSLWIJ, H.B.	SS2-FrM11	108 320	FLEMING, M.J.	MS-ThM4	94 282
DIPESO, G.	PS-MoP24	50 157	ELTA, M.	MSVT-ThA6	102 301	FLOREZ, L.T.	EM-ThM7	94 281
DIRUBIO, C.A.	BI-MoP7	51 161	ELTSOV, K.N.	NS-MoP20	49 152	FLORO, J.A.	PS1-ThA8	100 295
DITTMANN, S.	VT-MoM4	38 122	EMELIANOV, A.V.	NS-WeP16	87 256	FLUECKIGER, PH.	NS2-FrM8	109 323
DIWANJI, A.P.	AS-FrM5	110 324	EMELIANOV, A.V.	NS-ThP10	104 305	FOERSTER, C.L.	VT-TuA8	63 192
DOBISZ, E.A.	NS2-TuM7	53 169	EMMOTH, B.	PS-WeP16	88 261	FOLLSTAEDT, D.M.	PS-MoA6	44 135
DOBISZ, E.A.	NS2-ThM7	91 273	ENDO, T.	NS-WeP14	87 256	FONG, S.	EM-MoM4	39 124
DOERING, P.	TFVM-MoA3	45 137	ENG, P.J.	EM-MoA7	46 140	FONTAINE, N.H.	AS-TuP18	68 209
DOERR, D.	VM-ThM2	95 284	ENGEL, T.	SS1-TuM9	52 164	FORBES, K.	MS-WeM3	76 230
DOI, T.	EM-TuA1	64 194	ENGEL, W.	TF-ThP12	106 314	FORSYTH, N.M.	AS-MoM9	37 119
DOMB, A.	NSBI-ThM10	91 272	ENGELHARD, M.H.	ASSS-TuA7	62 189	FOSTER, K.E.	BINS-WeM0	77 231
DONNELLY, V.M.	PS-WeM0	74 225	ENGEMANN, J.	PS-MoP13	50 155	FOSTER, K.E.	BI-MoP12	51 162
DONNELLY, V.M.	PS1-ThA1	100 294	ENGEMANN, J.	PS-TuA7	62 190	FOSTER, K.E.	BI-TuA3	65 196
DONNET, CH.	VM-FrM1	111 329	ENGSTROM, J.R.	SSEM-WeM1	75 227	FOSTER, K.E.	BI-MoA3	47 142
DORAISWAMY, N.	SS2-MoA1	42 127	ENSS, C.	NS-ThP4	104 304	FOWLDER, D.E.	SS1-WeA3	80 233
DORFMAN, B.F.	TF-WeA8	83 245	EO, Y.P.	PS-MoA10	44 135	FRANCIOSI, A.	EM-WeM4	76 229
DORHOUT, P.K.	NS-TuP3	67 203	EPPELL, S.J.	BI-TuM5	57 180	FRANCIS, G.M.	NS1-TuM5	53 167
DORIER, J.-L.	PS-WeA6	82 241	ERCOLI, A.	TF-WeM3	75 228	FRANCIS, T.	AS-TuM1	54 170
DORN, B.	VM-FrM5	111 329	ERKLINE, J.L.	SS1-FrM2	108 317	FRANKEL, D.J.	TF-TuM6	55 175
DOTY, R.E.	AS-TuP16	68 208	ESPADAS-TORRE, C.	BI-TuA1	65 196	FRANKLIN, G.E.	SS2-FrM10	108 320
DOUGLAS, K.	NS1-FrM5	109 321	ESTES, M.	NS2-WeA3	81 237	FRASE, H.N.	EMSS-ThM5	93 278

Author		Prog. Abst.			Prog. Abst.			Prog. Abst.			
		Pg. #	Pg. #		Pg. #	Pg. #		Pg. #	Pg. #		
FRASER, H.L.	VM-WeA10	85	249	GARRETT, L.	PS-WeP11	88	260	GOODMAN, D.W.	TF-ThP13	106	314
FRAUSTO, P.	PS-MoP7	50	154	GARRITY, M.P.	PS-WeP11	88	260	GOODMAN, D.W.	SS1-FrM3	108	317
FREDERICK, B.G.	SS1-ThA10	98	287	GATES, S.M.	SSEM-WeA3	83	242	GOODMAN, D.W.	SS2-WeM4	72	220
FREELAND, A.W.	VM-ThA5	103	302	GAY, D.H.	NS2-TuA1	61	186	GOODMAN, D.W.	SS2-WeM6	72	220
FREELAND, J.W.	SS1-WeA5	80	233	GAYLORD, R.	EMMS-TuM8	56	178	GÖPEL, W.	NS1-MoM3	37	117
FREELAND, J.W.	SS-WeP18	86	252	GAYLORD, R.	MS-ThM4	94	282	GÖPEL, W.	BI-TuA9	65	197
FREEMAN, A.J.	SS2-FrM10	108	320	GE, M.	ASSS-TuA9	62	189	GÖPEL, W.	NS-WeP6	87	255
FREES, L.C.	MS-WeA8	84	248	GE, X.	NS-WeP23	87	258	GORBATKIN, S.M.	PS-MoM8	38	121
FREILER, M.B.	EM-ThA4	102	299	GEE, P.E.	SSEM-WeM8	75	227	GORDON, J.	TF-ThA9	101	299
FREUDENBERG, J.	MSVT-ThA6	102	301	GEIST, D.E.	TF-WeP23	89	265	GORDON, R.	EM-MoM7	39	124
FREY, H.	NS1-FrM8	109	321	GELLMAN, A.J.	SS-WeP22	86	253	GOTOH, N.	VT-MoM2	38	122
FRIEDMAN, R.M.	AS-TuP9	68	207	GELLMAN, A.J.	NS2-ThA9	99	292	GOTTSCHO, R.A.	PS-MoM1	38	120
FRIEDMANN, J.B.	PS-WeP15	88	260	GELLMAN, A.J.	SS-MoP12	48	145	GOTTSCHO, R.A.	PS-WeM1	74	225
FRIEND, C.M.	SS-MoP10	48	145	GELLMAN, A.J.	SS2-FrM3	108	319	GOW, C.	EMMS-TuM8	56	178
FRIEND, C.M.	SS-MoP20	48	146	GENSTERBLUM, G.	SS1-FrM8	108	318	GOW, C.	MS-ThM4	94	282
FROHN, J.	SS1-TuM9	52	164	GENSTERBLUM, G.	TF-WeA6	83	245	GOZZO, F.	EM-ThP6	105	309
FROMMER, J.E.	NS1-TuA3	61	185	GENSTERBLUM, G.	NS2-ThA8	99	292	GRABBE, A.	AS-FrM6	110	325
FROMWITZ, D.	SS2-ThA9	98	289	GEORGE, M.A.	NS-TuP1	67	203	GRABOWSKI, K.S.	VM-ThM10	95	285
FRUHBERGER, B.	SS1-FrM7	108	318	GEORGE, M.A.	NS-TuP15	67	205	GRAHAM, G.W.	SS-MoP17	48	146
FRÜHBERGER, B.	SS1-MoA1	42	126	GEORGE, M.A.	AS-TuM9	54	171	GRAHAM, J.D.	SS-TuP4	66	198
FUCHS, H.	NSMS-WeM1	73	221	GEORGE, S.M.	EM-ThA9	102	300	GRAHAM, M.	TF-WeP14	89	264
FUJII, T.	NS-MoP18	49	152	GEORGE, S.M.	SS-MoP28	48	148	GRAHAM, M.E.	VM-ThM11	95	285
FUJII, T.	NS2-MoA7	43	132	GEORGE, S.M.	SSEM-WeA1	83	242	GRAHAM, M.J.	EMMS-TuM10	56	178
FUJII, T.	NS-MoP8	49	151	GEORGE, S.M.	SS-TuP7	66	199	GRAINGER, D.W.	AS-ThM11	92	275
FUJIMAKI, S.	TFVM-TuA10	63	194	GERENSR, L.	AS-ThA2	100	293	GRAINGER, D.W.	AS-MoM5	37	118
FUJISAWA, S.	NS-MoP1	49	150	GERMAN, K.A.H.	SS-MoP30	48	148	GRANT, J.M.	EM-ThP1	105	308
FUJISHIMA, A.	NS-TuP4	67	203	GERMAN, K.A.H.	SS-MoP35	48	149	GRAPPERHAUS, M.	PS-WeA8	82	241
FUJISHIMA, A.	ASSS-TuA10	62	189	GERMUNDSON, J.R.	VM-ThA5	103	302	GRAPPERHAUS, M.	PS-TuM1	54	171
FUJISHIMA, A.	NS-WeP9	87	255	GEROGER, JR., J.H.	NS-MoP14	49	152	GRAPPERHAUS, M.	PS-WeP14	88	260
FUJISHIMA, A.	AS-MoM11	37	119	GERTH, C.M.	SS1-MoM5	36	114	GRAUPNER, H.	SS1-ThA3	98	286
FUJII, T.	NS-MoP18	49	152	GERTH, C.M.	SS-WeP27	86	254	GRAVES, D.B.	PS-TuM8	54	173
FUJIWARA, N.	PS-MoM7	38	120	GEWIRTH, A.A.	ASSS-TuA9	62	189	GRAVES, D.B.	PS-TuM11	54	173
FUKANO, Y.	NS1-MoA6	43	130	GEWIRTH, A.A.	SS2-WeA3	80	234	GRAVES, D.B.	PS-MoP19	50	156
FUKATSU, S.	EM-TuA9	64	195	GHANAHEIM, S.	EM-MoM6	39	124	GRAVES, D.B.	PS-MoP21	50	157
FUKAZAWA, T.	PS-MoM5	38	120	GHISEN, J.	TF-ThP22	106	315	GRAVES, D.B.	PS-WeA7	82	241
FUKUDA, I.	TF-WeP9	89	263	GHOTS, S.S.	NS-TuP19	67	206	GRAY, D.C.	PS-ThM6	92	276
FUKUDA, K.	NS-MoP12	49	151	GIAPIS, K.P.	PS-ThM9	92	277	GRAY, K.E.	TF-ThP14	106	314
FULGHUM, J.E.	AS-MoM8	37	119	GIBBONS, K.P.	VM-ThA9	103	303	GRAY, M.	VT-MoP12	51	159
FULGHUM, J.E.	AS-WeM6	74	224	GIBSON, A.	SS2-TuM6	52	165	GRAYEVSKY, A.	VM-WeA9	85	249
FULGHUM, J.E.	AS-TuP20	68	209	GIELEN, J.W.A.	PS-MoP1	50	153	GREEN, M.L.	MS-ThM8	94	283
FUNATO, Y.	VT-MoP9	51	159	GIESEN-SEIBERT, M.	SS-TuP8	66	199	GREENE, J.E.	SS1-TuM4	52	163
FUNATO, Y.	VT-MoP13	51	159	GILES, M.D.	MSVT-ThA9	102	302	GREENE, J.E.	EM-TuP21	69	214
FUOSS, P.H.	SS2-MoA7	42	128	GILL, W.	MS-TuA10	64	196	GREENE, J.E.	TF-ThP2	106	312
FURMAN, B.	MS-ThM4	94	282	GILLAND, J.	PS-TuA3	62	190	GREENE, J.E.	EM-MoM5	39	124
FURMAN, B.K.	EMMS-TuM8	56	177	GILLAND, J.	PS-MoP12	50	155	GREENE, J.E.	TFVM-ThM3	93	279
FURTA, T.	TF-FrM8	110	327	GILLEN, G.	TFVM-TuA5	63	193	GREENE, J.E.	VM-WeA1	85	248
FURTA, T.E.	AS-TuP18	68	209	GILLES, D.C.	NS-TuP1	67	203	GREENE, J.E.	TFVM-ThM8	93	280
FURTA, T.E.	SS2-WeA7	80	235	GILLES, J.-M.	NS-ThP8	104	305	GREENLIEF, C.M.	SS-TuP29	66	202
FYFIELD, M.	SS1-ThM4	90	267	GILLIS, H.P.	NS1-FrM5	109	321	GREENLY, J.	VM-ThM7	95	284
GAARENSTROOM, S.W.	AS-TuP29	68	210	GILLMAN, E.S.	SS-MoP26	48	147	GREER, J.A.	VM-ThM3	95	284
GABER, B.P.	BI-TuM10	57	180	GILMORE, C.M.	VM-WeA7	85	249	GREGORY, J.C.	BI-MoP8	51	161
GABRIEL, C.T.	PS-WeA1	82	240	GISSLER, W.	TFVM-TuA3	63	193	GREGORY, J.C.	EM-ThP19	105	311
GADGIL, P.K.	PS-TuA4	62	190	GIZDULICH, P.	BI-MoP11	51	161	GREGUS, J.A.	PS-WeM1	74	225
GADGIL, P.N.	MSVT-ThA10	102	302	GLAND, J.L.	TF-TuM8	55	176	GREMAUD, G.	NS2-TuA4	61	187
GAITAN, M.	NSBI-ThA5	99	290	GLAND, J.L.	SS-MoP11	48	145	GREVOZ, A.	MS-WeA4	84	247
GAITAN, M.	SS1-MoA3	42	126	GLAND, J.L.	SS-WeP20	86	253	GREVOZ, A.	PS-WeM3	74	225
GAJDARDZISKA-JOSIFOVSKA, M.	TF-WeA3	83	244	GLAND, J.L.	SS1-MoA5	42	126	GRIES, W.H.	AS-MoA6	44	133
GALLAGHER, M.C.	SS1-ThM4	90	267	GLAND, J.L.	TF-ThP21	106	315	GRIES, W.H.	AS-WeM2	74	224
GALLIGAN, J.M.	ASSS-TuA3	62	188	GLAND, J.L.	SS-TuP24	66	202	GRIFFIS, D.P.	NSBI-ThA9	99	291
GALLOWAY, H.C.	SS-WeP14	86	251	GLAND, J.L.	AS-FrM9	110	325	GRIFFIS, D.P.	NS-ThP5	104	304
GANZ, E.	SS1-TuM1	52	163	GLASBEY, T.O.	NS2-MoA4	43	131	GRIFFITH, J.E.	NS2-MoA1	43	131
GAO, H.J.	NS-WeP11	87	256	GLEMBOCKI, O.J.	NS2-WeA4	81	237	GRIFFITHS, A.	BI-MoA4	47	142
GAO, Y.	AS-MoM1	37	118	GLEMBOCKI, O.J.	EM-ThP10	105	309	GRIFFITHS, K.	TF-ThP10	106	314
GARCIA, A.	SS-MoP1	48	144	GLICK, D.	NS-ThP6	104	305	GRIGOROV, I.	SS-WeP18	86	252
GARCÍA, N.	NS2-ThM1	91	272	GLOCKER, D.A.	VM-ThA3	103	302	GRIGOROV, I.L.	SS1-WeA5	80	233
GARCÍA, R.	NSBI-WeA6	81	236	GNADE, B.E.	EM-MoM9	39	125	GRILLO, D.C.	EM-WeM0	76	229
GARCIA, R.	EM-TuP14	69	213	GÖBEL, H.	SS-MoP24	48	147	GRIZZLE, J.W.	MSVT-ThA9	102	302
GARCIA, R.	PS2-ThA1	101	296	GÖBEL, H.	NS-WeP12	87	256	GROBE, J.	AS-TuP8	68	207
GARCIA, S.	PS-MoP6	50	154	GOEDBLOED, M.	SS-MoP6	48	144	GROFF, G.B.	AS-FrM2	110	324
GARDELLA, JR., J.A.	AS-ThA8	100	294	GOH, M.C.	NS-MoP15	49	152	GROSSMAN, E.	TFVM-TuA8	63	194
GARDELLA, JR., J.A.	BI-MoA10	47	143	GOLD, J.	BI-MoA7	47	142	GROTJOHN, T.A.	PS-TuM3	54	172
GARDELLA, JR., J.A.	AS-TuP4	68	207	GOLDNER, R.B.	TF-ThA7	101	299	GRUEN, D.M.	TFVM-MoA10	45	138
GARDELLA, JR., J.A.	BI-TuM11	57	181	GOLDSTEIN, Y.	VM-WeA9	85	249	GRUEN, D.M.	AS-WeM8	74	225
GARDNER, D.S.	MS-TuP1	70	215	GOLDSTEIN, Y.	NS1-MoA2	43	129	GRUEN, D.M.	TF-FrM11	110	327
GARDNER, G.	NSBI-ThM3	91	271	GÓMEZ-HERRERO, J.	NS2-ThM1	91	272	GRUNZE, M.	TF-FrM9	110	327
GARDNER, S.A.	AS-ThA9	100	294	GONG, L.S.	BI-MoP1	51	160	GRUNZE, M.	AS-ThM4	92	274
GARDNER, W.L.	EM-ThP14	105	310	GONG, W.S.	BI-MoP1	51	160	GRUNZE, M.	NSBI-ThA4	99	290
GARFUNKEL, E.	EM-MoA3	46	139	GONZALES, A.	VM-ThA1	103	302	GRUVERMAN, A.	NS1-MoA10	43	131
GARFUNKEL, E.	EMMS-TuM4	56	177	GONZÁLEZ-DIAZ, G.	TF-ThA6	101	298	GRYKO, J.	NS1-TuA7	61	186
GARFUNKEL, E.	SS1-MoA10	42	127	GONZÁLEZ-DIAZ, G.	PS-MoP6	50	154	GRZELAKOWSKI, K.	SS1-WeM2	72	218
GARFUNKEL, E.	SS-MoP8	48	145	GONZÁLEZ-HERNÁNDEZ, J.	TF-ThP11	106	314	GU, Q.J.	NS2-WeM2	73	222
GARNAES, J.	NS-ThP21	104	307	GONZÁLEZ-HERNÁNDEZ, J.	NS-TuP11	67	204	GU, Q.J.	NS-WeP23	87	258
				GOODHUE, W.	NS1-TuA10	61	186	GUAN, J.	SS-WeP7	86	250

Author	Prog. Abst.			Prog. Abst.			Prog. Abst.	
	Pg. #	Pg. #		Pg. #	Pg. #		Pg. #	Pg. #
GUAN, Y.	MSVT-ThA8	102 301	HARRIOTT, L.	PS-WeM1	74 225	HERR, D.J.C.	MS-TuM9	56 179
GUARNIERI, C.R.	MS-WeM5	76 231	HARRIS, T.D.	SS-WeP26	86 253	HERRICK III, R.D.	NS-WeP25	87 258
GUARNIERI, C.R.	MS-MoA6	46 141	HARRIS, W.C.	MS-ThM10	94 283	HERSHKOWITZ, N.	PS-WeP9	88 260
GUARNIERI, C.R.	MS-WeM7	76 231	HARTMANN, A.	BI-MoP14	51 162	HERSHKOWITZ, N.	PS-TuA3	62 190
GUDMUNDSON, F.	SS2-WeM8	72 220	HARUYAMA, Y.	NS1-TuA8	61 186	HERSHKOWITZ, N.	PS-MoP12	50 155
GUHA, S.	EM-WeM5	76 230	HARVATH, L.	BI-MoA3	47 142	HESS, S.T.	TF-TuM6	55 175
GUINN, K.V.	PS-WeM0	74 225	HASAN, M.-A.	SS1-TuM4	52 163	HESSINGER, U.	SS2-MoA4	42 128
GUINN, K.V.	PS-TuA2	62 190	HASAN, M.-A.	TF-ThP2	106 312	HESSINGER, U.	EM-FrM8	111 328
GUINN, K.V.	PS1-ThA1	100 294	HASEGAWA, M.	AS-MoM6	37 118	HESSINGER, U.	EM-FrM5	111 328
GUNSHOR, R.L.	EM-WeM0	76 229	HASEGAWA, Y.	SS1-ThM3	90 267	HETRICK, J.M.	SS1-ThM6	90 267
GUNTER, P.L.J.	AS-TuP19	68 209	HASHIMOTO, K.	ASSS-TuA10	62 189	HEVESI, K.	SS1-FrM8	108 318
GÜNTHER, P.	TF-WeP8	89 263	HASHIMOTO, K.	NS-WeP9	87 255	HEVESI, K.	TF-WeA6	83 245
GUO, X.	SS1-WeM8	72 219	HASHIMOTO, K.	PS-WeA3	82 241	HEWETT, D.W.	PS-MoP20	50 157
GUO, X.-C.	SS1-MoM2	36 114	HASHIMOTO, K.	AS-MoM11	37 119	HEWETT, D.W.	PS-MoP24	50 157
GUPTA, R.	NS2-WeM7	73 223	HASHIZUME, T.	SS2-MoA6	42 128	HIATT, C.F.	PS-ThM6	92 276
GUSEV, E.P.	EM-MoA3	46 139	HASHIZUME, T.	SS-WeP28	86 254	HICHWA, B.P.	TF-ThA9	101 299
GUSEV, E.P.	EMMS-TuM4	56 177	HASHIZUME, T.	SS-MoP7	48 145	HICHWA, B.P.	VM-ThA7	103 303
GUSTAFSSON, T.	EM-MoA3	46 139	HASHIZUME, T.	SS2-MoM11	36 117	HICKMAN, J.J.	BINS-WeM0	77 231
GUSTAFSSON, T.	EMMS-TuM4	56 177	HASOON, F.	EM-ThP4	105 308	HICKMAN, J.J.	BI-MoP12	51 162
GUSTAFSSON, T.	SS-MoP8	48 145	HASOON, F.A.	EM-ThA10	102 300	HICKMAN, J.J.	BI-TuA3	65 196
GUTMAN, E.E.	NS-ThP14	104 306	HATANO, J.	NS1-MoA10	43 131	HICKMAN, J.J.	BI-MoA3	47 142
HA, J.S.	EM-TuP7	69 212	HATTORI, T.	PS1-ThA5	100 295	HICKS, R.F.	SSEM-WeM8	75 227
HAASE, J.	SS2-MoM4	36 116	HAUPT, J.	TFVM-TuA3	63 193	HIGMAN, T.K.	NS2-ThM4	91 273
HAASE, M.A.	EM-WeM5	76 230	HAWK, R.M.	TF-TuM7	55 176	HIGUCHI, T.	NS2-MoA8	43 132
HACKENBERG, J.J.	PS-WeP13	88 260	HAWLEY, M.E.	TF-ThP24	106 316	HIGUCHI, T.	NS-MoP8	49 151
HAFICH, M.J.	PS-WeA5	82 241	HAWORTH, L.	VT-MoP10	38 123	HIKOSAKA, Y.	PS-WeM5	74 226
HAFICH, M.J.	EM-TuP6	69 212	HAYASAKA, N.	MS-WeM2	76 230	HILEMAN, T.A.	SS1-ThA1	98 286
HAGANS, K.	PS2-ThA1	101 296	HAYASAKA, N.	VT-MoP10	51 159	HILLIS, D.L.	VT-TuM5	55 174
HAGENHOFF, B.	BI-MoP9	51 161	HAYASHI, H.	MS-TuP2	70 216	HIMPSEL, F.J.	TF-ThP6	106 313
HAGENHOFF, B.	AS-TuM4	54 170	HAYES, J.P.	EM-TuP11	69 213	HINDI, M.M.	SS1-FrM11	108 318
HAGENHOFF, B.	AS-MoM4	37 118	HAYES, T.M.	SS2-WeA7	80 235	HINES, M.A.	SSEM-WeM6	75 227
HAGENHOFF, B.	AS-TuP5	68 207	HE, G.	VM-WeA8	85 249	HINGERL, K.	EM-ThM7	94 281
HAGENHOFF, B.	AS-WeM7	74 224	HE, H.	AS-TuM10	54 171	HINKLE, L.D.	VT-MoA5	45 136
HAGENHOFF, B.	AS-TuP8	68 207	HE, P.	MS-TuP5	70 216	HINRICH, S.	NS-ThP19	104 307
HAGGERTY, D.	SS-MoP39	48 149	HE, P.	TF-FrM1	110 326	HINSBERG, W.D.	SS1-TuA7	60 182
HAGGERTY, D.	EM-TuP24	69 215	HE, Y.L.	SS1-WeM6	72 218	HINSHELWOOD, D.D.	VM-ThM10	95 285
HAGMANN, M.J.	NS-ThP22	104 307	HEADRICK, R.L.	EM-FrM1	111 327	HIRANO, M.	NS2-ThA1	99 291
HAGO, W.	SS-MoP40	48 149	HEALEY, F.	SS-MoP3	48 144	HIRANO, N.	VT-TuA9	63 193
HAGO, W.	SS2-ThM1	90 268	HEARNE, S.	EM-TuP1	69 211	HIRATA, Y.	NSBI-WeA9	81 237
HAHN, C.	NS-ThP11	104 305	HEARNE, S.	EM-TuP2	69 211	HIRAYAMA, H.	EM-ThM10	94 282
HÄHNER, G.	AS-TuP11	68 208	HEERA, V.	TF-ThP8	106 313	HIRAYAMA, S.	NS-TuP18	67 205
HAIJME, H.	NS2-ThM10	91 273	HEIDUSCHKA, P.	BI-TuA9	65 197	HIROSE, K.	NS2-WeM0	73 222
HÄKANSSON, M.C.	SS1-FrM6	108 318	HEINRICH, M.	SSEM-WeM4	75 227	HIROSE, M.	EM-TuA1	64 194
HALBRITTER, J.	ASSS-TuA4	62 188	HEINZ, T.F.	SS2-TuM1	52 164	HIROTA, Y.	EMMS-TuM11	56 178
HALBRITTER, J.	EM-ThP17	105 310	HEINZELMANN, H.	NS2-FrM5	109 323	HISAMATSU, H.	VT-MoM2	38 122
HALLEY, J.W.	SS-TuP1	66 198	HEITZINGER, J.M.	SS-TuP25	66 202	HITCHCOCK, A.P.	EM-TuP13	69 213
HAMADA, S.	VT-TuA10	63 193	HEITZINGER, J.M.	SS-TuP26	66 202	HO, F.	NS2-FrM1	109 322
HAMAGUCHI, S.	PS-MoM10	38 121	HELLEMANS, L.	NSMS-WeM3	73 221	HO, W.	SS2-TuM2	52 165
HAMERS, R.J.	SS-TuP9	66 199	HELLMOLDT, D.H.	SS-MoP16	48 146	HO, W.	SS-MoP37	48 149
HAMERS, R.J.	EM-ThP22	105 311	HELLWIG, C.	SSEM-WeA2	83 242	HO, W.	AS-TuP28	68 210
HAMERS, R.J.	EMSS-ThM2	93 277	HELMER, J.C.	VT-MoA1	45 135	HOBSON, J.P.	VT-TuM1	55 173
HAMERS, R.J.	SS1-ThA7	98 287	HEMMENWAY, D.F.	PS-WeP13	88 260	HOBSON, W.S.	EM-TuP5	69 212
HAMMER, L.	SS1-ThA3	98 286	HEMMINGER, J.C.	SS1-MoM1	36 114	HODES, G.	NS1-MoA1	43 129
HAMMOND, C.	EM-ThP21	105 311	HEMMINGER, J.C.	SSEM-WeA9	83 243	HODGSON, A.	SS-MoP3	48 144
HAMMOND, M.S.	TF-FrM3	110 326	HEMMINGSSON, J.	BI-MoP16	51 162	HOEKSTRA, R.J.	PS-TuM4	54 172
HAMPDEN-SMITH, M.J.	SS1-ThM10	90 268	HENCK, S.A.	AS-ThM8	92 275	HOELZER, D.	TF-ThP24	106 316
HAMPIKIAN, J.M.	NS1-TuM7	53 167	HENDERSON, D.O.	NS-TuP15	67 205	HOEN, S.	NS2-FrM9	109 323
HAN, B.Y.	SS1-FrM8	108 318	HENDERSON, D.O.	AS-TuM9	54 171	HOEN, S.	NS2-FrM7	109 323
HAN, B.Y.	TF-WeA6	83 245	HENDERSON, E.	NSBI-ThM6	91 271	HOEN, S.	NSMS-WeM5	73 221
HAN, J.	EM-WeM0	76 229	HENDERSON, E.	NS-MoP5	49 150	HOFFBAUER, M.A.	PS-ThM11	92 277
HAN, J.S.	MS-TuP4	70 216	HENDERSON, E.	BI-MoP4	51 160	HOFFBAUER, M.A.	EM-ThP19	105 311
HAN, M.	NS-WeP10	87 256	HENGELHOLD, R.	EM-TuP3	69 211	HOFFMAN, D.M.	PS-MoA8	44 135
HAN, T.	NS2-FrM10	109 323	HENINS, I.	VM-ThM9	95 285	HOFFMAN, D.W.	TFVM-ThM10	93 280
HANBICKI, A.T.	SS2-MoM3	36 116	HENRY, C.H.	EM-TuA3	64 195	HOFFMANN, S.	AS-TuP15	68 208
HANBICKI, A.T.	SS2-ThM3	90 269	HENSHAW, G.S.	SS1-MoA2	42 126	HOFLER, G.E.	EM-WeM5	76 230
HANDLEY, E.A.	NSBI-ThM3	91 271	HENZLER, M.	SS-TuP6	66 198	HOFMANN, S.	SS-WeP9	86 251
HANF, M.C.	EMMS-TuM10	56 178	HENZLER, M.	SS2-ThM9	90 270	HOFMANN, S.	AS-WeA3	82 239
HANF, M.C.	SS2-ThA4	98 288	HERBOTS, N.	EM-TuP1	69 211	HOGGATT, C.	EM-TuP18	69 214
HANISH, P.D.	MSVT-ThA9	102 302	HERBOTS, N.	EM-TuP2	69 211	HOLBER, W.M.	PS-ThM3	92 276
HANLEY, L.	SS-MoP9	48 145	HERBOTS, N.	EM-TuP15	69 213	HOLLENSTEIN, CH.	PS-WeA6	82 241
HANLEY, L.	SS-MoP38	48 149	HERBOTS, N.	EMMS-TuM7	56 177	HOLLINGSWORTH, R.E.	NS2-WeA3	81 237
HANLEY, L.	AS-ThA5	100 293	HERCULES, D.A.	AS-ThA8	100 294	HOLLOWAY, P.H.	EM-WeA2	84 245
HANN, T.A.	NS-WeP18	87 257	HERDT, G.C.	AS-TuP3	68 207	HOLLOWAY, P.H.	EM-TuP19	69 214
HANSON, K.	MS-ThM8	94 283	HERMAN, G.S.	SS1-MoA9	42 127	HOLLOWAY, P.H.	EM-WeM3	76 229
HANSSON, P.O.	NS-ThP19	104 307	HERMAN, G.S.	EM-ThP23	105 311	HOLLOWAY, P.H.	TFVM-MoA3	45 137
HAQ, S.	SS1-MoM9	36 115	HERMAN, I.P.	PS-WeM0	74 225	HOLLOWAY, P.H.	EM-ThA7	102 300
HARA, M.	NSBI-WeA7	81 236	HERMAN, I.P.	EM-ThA4	102 299	HOLMES, D.M.	SS-TuP23	66 201
HARAICHI, S.	EM-ThM9	94 282	HERMAN, I.P.	PS1-ThA1	100 294	HOLMES, S.J.	MS-WeM1	76 230
HARBISON, J.P.	EM-ThM7	94 281	HERMANS, L.J.F.	PS-WeP2	88 258	HONDA, M.	TFVM-TuA9	63 194
HARDCASTLE, S.	AS-TuM10	54 171	HERMSMEIER, B.	MS-ThM1	94	HONDA, S.	TF-ThP5	106 313
HÄRING, P.	ASSS-TuA5	62 189	HERNÁNDEZ-ROJAS, J.L.	TF-ThA6	101 298	HONEA, E.C.	AS-TuP13	68 208
HARO-PONIATOWSKI, E.	TF-ThP11	106 314	HERNNÄS, B.	SS1-FrM10	108 318	HONG, B.	TFVM-MoA7	45 138
HARRELL, S.	MS-TuM7	56 179	HERNNÄS, B.	SS-MoP18	48 146	HONG, Y.	SS-MoP31	48 148

Author		Prog. Abst.		Prog. Abst.		Prog. Abst.		
		Pg. # Pg. #		Pg. # Pg. #		Pg. # Pg. #		
HÖÖK, F.	BI-TuA10	65 197	IBBOTSON, D.E.	MS-WeA4	84 247	JIANG, L.	AS-MoM11	37 119
HOPE, D.A.O.	EM-ThM4	94 281	IBBOTSON, D.E.	PS-WeM3	74 225	JIANG, L.	NS-WeP9	87 255
HOPPE, M.L.	PS-WeP18	88 261	IBRAHIM, H.	PS-WeP4	88 259	JIANG, W.S.	VT-MoP11	51 159
HOPSTER, H.	SS1-WeA1	80 233	ICHIMIYA, A.	SS2-MoA6	42 128	JIN, G.	EM-TuP9	69 212
HORI, Y.	VT-TuA9	63 193	ICHIMURA, S.	VT-MoP3	51 158	JIN, G.	EM-FrM7	111 328
HORIUE, Y.	PS-MoM5	38 120	ICHIMURA, S.	VT-MoM11	38 123	JIN, T.	NS-TuP12	67 204
HORIOKA, K.	MS-TuP2	70 216	ICHINOHE, Y.	SS-WeP8	86 251	JING, T.W.	NS2-TuA9	61 188
HORIOKA, K.	MS-TuP3	70 216	IDZERDA, Y.	SS2-ThA2	98 288	JING, T.W.	NSBI-ThM5	91 271
HORN, K.	SSEM-WeA2	83 242	IJIMA, S.	NS1-FrM9	109 322	JING, T.W.	NSBI-ThM11	91 272
HORN, K.	EM-TuP17	69 214	IKEDA, M.	EM-WeM1	76 229	JING, T.W.	NS1-TuA1	61 185
HORNETZ, B.	EM-ThP17	105 310	IKEDA, S.	MS-TuP3	70 216	JING, Z.	EM-MoA2	46 139
HORNYAK, G.L.	NS-TuP17	67 205	IKEDA, Y.	VT-TuA3	63 191	JOHANSSON, L.S.O.	SS1-FrM6	108 318
HORWAT, D.	AS-ThA9	100 294	IMBIHL, R.	SS2-WeM3	72 220	JOHANSSON, M.	SS1-FrM6	108 318
HOSAKA, S.	NS2-ThM10	91 273	IMURA, R.	NS2-ThM10	91 273	JOHNSON, D.F.	SS2-ThM4	90 269
HOSHI, T.	AS-TuP6	68 207	INAYOSHI, S.	VT-TuA3	63 191	JOHNSON, K.E.	SS2-TuA9	60 184
HOU, A.S.	NS2-FrM1	109 322	INAZAWA, K.	MS-TuP2	70 216	JOHNSON, JR., R.W.	AS-TuP4	68 207
HOUBERTZ, R.	ASSS-TuA6	62 189	INAZAWA, K.	MS-TuP3	70 216	JOHNSTON, E.E.	BI-TuM7	57 180
HOULE, F.A.	SS1-TuA7	60 182	ING, J.L.	SS1-ThA5	98 286	JOHNSTON, G.	VM-ThM7	95 284
HOUSTON, J.E.	NS2-TuA8	61 187	INGREY, S.	EM-FrM4	111 328	JOHS, B.	MS-TuP5	70 216
HOUSTON, J.E.	BI-MoP7	51 161	INOUE, T.	NS2-FrM2	109 322	JOHS, B.	EM-ThM6	94 281
HOUSTON, J.E.	SS1-TuM2	52 163	IOFFE, I.	VT-MoP12	51 159	JOHS, B.	TF-FrM1	110 326
HOUSTON, J.E.	AS-ThA10	100 294	IRENE, E.A.	EM-ThM5	94 281	JONDLE, D.M.	NSBI-ThM6	91 271
HOUSTON, J.E.	AS-FrM10	110 325	IRENE, E.A.	EM-FrM9	111 328	JONES, F.	MS-MoA2	46 140
HOUSTON, P.L.	SS-MoP37	48 149	IRENE, E.A.	TF-FrM2	110 326	JONES, G.	AS-MoM9	37 119
HOWARD, A.J.	EM-MoM8	39 124	ISAACSON, M.S.	MS-TuP7	70 217	JONES, K.	EM-WeM3	76 229
HOWARD, A.J.	AS-ThA10	100 294	ISHAUG, B.E.	SS2-MoA10	42 129	JONES, K.A.	NS-ThP24	104 307
HOWARD, A.J.	EM-ThP2	105 308	ISHIBASHI, A.	EM-WeM1	76 229	JONES, K.A.	TF-WeP3	89 262
HOWARD, J.K.	TF-TuM9	55 176	ISHIHARA, M.	PS2-ThA10	101 297	JONES, K.S.	EM-WeA7	84 246
HOWARD, T.R.	MS-TuP9	70 217	ISHII, H.	SS-WeP8	86 251	JONES, K.S.	NS-TuP8	67 204
HOWLING, A.A.	PS-WeA6	82 241	ISHIKAWA, Y.	MS-TuP2	70 216	JONES, L.A.	NS-TuP10	67 204
HRBEK, J.	SS-MoP21	48 147	ISHIKAWA, Y.	NS-WeP15	87 256	JONES, P.	PS-TuM7	54 172
HSEUH, H.C.	VT-MoP11	51 159	ISHIMARU, H.	VT-MoA9	45 136	JONES, T.S.	SS-TuP23	66 201
HSIAO, K.M.	VT-MoP7	51 158	ISHIMARU, H.	VT-MoM2	38 122	JOO, S.J.	PS-MoA10	44 135
HSIAU, K.	MS-MoA7	46 141	ISHIMARU, H.	VT-MoP8	51 158	JORDAN, B.C.	MS-TuM3	56 178
HSIEH, J.J.	MS-MoA2	46 140	ISHIMARU, H.	VT-MoP5	51 158	JORRITSMA, J.	NS2-WeM5	73 223
HSIEH, T.J.	TF-WeP5	89 262	ITO, F.	EM-ThM10	94 282	JORRITSMA, L.	SS2-TuA2	60 183
HSIUNG, G.Y.	VT-MoP7	51 158	ITO, H.	TFVM-ThM3	93 279	JOSHI, R.V.	MS-MoA2	46 140
HSIUNG, G.Y.	VT-TuA4	63 192	ITO, Y.	VT-MoP14	51 159	JOSSE, F.	NSBI-ThA4	99 290
HSU, C.C.	EM-TuP9	69 212	IVANOV, G.K.	NS-TuP20	67 206	JOYCE, B.A.	SS-TuP23	66 201
HSU, D.S.Y.	EM-ThA8	102 300	IVANOVA, O.P.	AS-TuP21	68 209	JOYCE, S.A.	SS1-ThM4	90 267
HSU, S.N.	VT-MoP7	51 158	IVES, L.K.	TFVM-TuA5	63 193	JOYNER, C.F.	AS-TuP17	68 209
HU, J.	AS-TuP12	68 208	IWAI, H.	AS-ThA1	100 293	JUAN, W.H.	PS-MoP9	50 155
HU, J.	NS2-TuA5	61 187	IWAMA, H.	NS-ThP23	104 307	JULIANO, D.R.	PS-MoP7	50 154
HU, Y.Z.	EM-ThM5	94 281	IYODA, T.	NS-WeP9	87 255	JUNG, CH.	SSEM-WeA2	83 242
HU, Z.	NS-TuP1	67 203	IZAWA, Y.	PS2-ThA4	101 297	JUNG, D.R.	AS-ThM6	92 275
HUA, G.C.	EM-WeM0	76 229	IZAWA, Y.	PS2-ThA10	101 297	JUNG, G.	BI-TuA9	65 197
HUANG, C.	SS-TuP3	66 198	IZQUIERDO, R.	EM-ThP3	105 308	JUNG, S.K.	TFVM-MoA6	45 138
HUANG, C.	SS2-WeA10	80 235	JACHIMOWSKI, T.A.	SS2-ThM4	90 269	JUNKER, K.H.	SS-WeP24	86 253
HUANG, J.R.	VT-MoP7	51 158	JACKMAN, T.E.	EM-TuP13	69 213	JURGENSEN, T.A.	EM-ThP23	105 311
HUANG, L.	EM-TuP9	69 212	JACKSON, B.	SSEM-WeA3	83 242	JURGENSEN, C.W.	PS-MoP16	50 156
HUANG, L.J.	TF-WeP21	89 265	JACKSON, D.E.	BI-TuM4	57 180	KADOKURA, Y.	MS-WeM0	76 230
HUANG, L.J.	EM-FrM7	111 328	JACKSON, D.E.	NSBI-ThM8	91 271	KADUWELA, A.P.	SS-WeP16	86 252
HUANG, L.J.	EM-FrM4	111 328	JACKSON, D.E.	NS2-MoA4	43 131	KADUWELA, A.P.	SS1-WeM7	72 219
HUANG, X.	NS2-TuM6	53 169	JACKSON, H.E.	TFVM-MoA5	45 138	KADUWELA, A.P.	AS-WeM4	74 224
HUANG, Y.	NSMS-WeM7	73 221	JACOBS, D.C.	VT-MoM8	38 123	KADUWELA, A.P.	SS1-WeA10	80 234
HUANG, Y.J.	NS-WeP22	87 257	JACOBS, D.C.	SS2-TuM3	52 165	KAHN, A.	SS2-MoM10	36 117
HUANG, Z.	NS-TuP8	67 204	JAEGERMANN, W.	EMSS-ThM11	93 279	KAJIWARA, K.	AS-WeA4	82 239
HUDSON, E.A.	TF-ThP6	106 313	JANDUGANOV, V.M.	NS-WeP26	87 258	KALAMARIDES, A.	SS2-TuM1	52 164
HUES, S.M.	NS-MoP4	49 150	JANKOWSKI, A.F.	EM-TuP11	69 213	KAMENSKY, Y.	BI-MoP2	51 160
HUES, S.M.	NS-MoP3	49 150	JANSEN, F.	VM-ThA6	103 302	KAMIOKA, I.	PS1-ThA7	100 295
HUES, S.M.	NS2-TuA7	61 187	JANSEN, F.	TF-ThP15	106 314	KAMIYA, I.	SS2-MoA7	42 128
HUGHES, R.C.	SS1-MoA6	42 126	JANSEN, F.	MS-ThM3	94 282	KAMIYA, J.	EM-ThM7	94 281
HUGHES, R.C.	MS-WeA9	84 248	JARAUSCH, K.F.	NSBI-ThA9	99 291	KAMNA, M.M.	SS-MoP14	48 146
HULTEEN, J.C.	SS1-ThM5	90 267	JARDINE, A.P.	TF-WeP10	89 263	KAMNA, M.M.	SS-TuP16	66 200
HULTMAN, L.	TF-ThP14	106 314	JARDINE, A.P.	TF-WeM7	75 228	KAMNA, M.M.	SS2-FrM7	108 320
HULTMAN, L.	VM-WeA1	85 248	JAYARAM, G.	SS2-MoA1	42 127	KAN, H.-C.	SS1-TuM5	52 163
HULTMAN, L.	VM-WeA2	85 248	JENKS, C.J.	SS2-MoM7	36 116	KANEKO, R.	NS2-ThA1	99 291
HULTMAN, L.	EM-TuP10	69 212	JENNISON, D.R.	SS2-TuM7	52 165	KANEKO, R.	NS-WeP14	87 256
HUNTLEY, D.R.	SS1-ThA8	98 287	JENNISON, D.R.	NS1-TuM1	53 166	KANG, H.J.	AS-WeA8	82 240
HUSSEY, B.W.	NS2-MoA6	43 132	JENSEN, J.A.	SSEM-WeA4	83 243	KANG, T.-H.	SS1-FrM2	108 317
HUTCHINGS, C.W.	AS-ThM4	92 274	JENSEN, J.A.	SS-MoP32	48 148	KAO, Y.-C.	EM-ThM3	94 280
HWANG, C.-Y.	EM-TuP22	69 215	JENSEN, L.C.	AS-FrM7	110 325	KAPLAN, R.	EM-ThP10	105 309
HWANG, H.H.	PS-WeA8	82 241	JENSEN, M.B.	SS-WeP23	86 253	KARASAWA, T.	TF-ThP2	106 312
HWANG, J.	NSBI-WeA3	81 236	JENTZ, D.	SS1-MoM8	36 115	KARIMI, M.	SS1-TuM7	52 164
HWANG, K.H.	PS-MoA10	44 135	JEON, D.	EM-ThP12	105 309	KARIS, K.O.	SS-MoP18	48 146
HWANG, R.Q.	SS2-TuA7	60 184	JEON, H.	EM-WeM0	76 229	KARIS, O.	SS1-FrM10	108 318
HWANG, S.-D.	EM-ThP24	105 311	JEONG, H.-S.	AS-FrM11	110 325	KARLSSON, C.	BI-MoA8	47 143
HWANG, S.H.	PS-MoA10	44 135	JERVIS, T.R.	NS1-TuM11	53 168	KARPENKO, O.P.	SS2-MoA5	42 128
HYLAND, R.W.	VT-MoM9	38 123	JHA, P.	PS-WeP12	88 260	KARPENKO, V.	PS2-ThA1	101 296
IANNO, N.J.	EM-ThM6	94 281	JIA, J.J.	TF-ThP6	106 313	KARPENKO, V.P.	VT-TuM9	55 174
IBACH, H.	SS-TuP8	66 199	JIA, Q.X.	TF-ThP24	106 316	KASAI, P.	AS-ThA7	100 294
IBBOTSON, D.E.	PS-MoP16	50 156	JIANG, J.	AS-FrM11	110 325	KASEMO, B.	BI-TuA10	65 197
IBBOTSON, D.E.	PS-TuA2	62 190	JIANG, J.C.	NSBI-ThA10	99 291	KASEMO, B.	SS2-WeA9	80 235



Author		Prog. Abst. Pg. # Pg. #			Prog. Abst. Pg. # Pg. #			Prog. Abst. Pg. # Pg. #
KASEMO, B.	BI-MoA7	47 142	KINOSHITA, H.	TFVM-TuA9	63 194	KOZICKI, M.N.	BINS-WeM7	77 232
KASEMO, B.	SS1-TuA3	60 182	KIRMSE, K.H.R.	PS-WeP9	88 260	KOZICKI, M.N.	NS-ThP15	104 306
KASEMO, B.	BI-MoP5	51 160	KISHI, E.	NS-MoP1	49 150	KOZLOVSKY, L.V.	TF-WeP6	89 262
KASEMO, B.	SS2-ThM10	90 270	KISHIMOTO, J.	SS-WeP28	86 254	KOZUB, R.L.	SS1-FrM11	108 318
KASEMO, B.	SS2-WeM8	72 220	KISHIMOTO, J.	SS-MoP7	48 145	KRAFT, J.	SS2-MoA2	42 127
KASEMO, B.	BI-TuM9	57 180	KISKER, D.K.	SS2-MoA7	42 128	KRAMER, N.	NS2-WeM5	73 223
KASHIMOTO, Y.	MS-WeM0	76 230	KISLOV, V.V.	NSBI-WeA10	81 237	KRASNOPOLER, A.	ASSS-TuA1	62 188
KASPER, E.	NS1-MoA8	43 130	KITAGAWA, A.	VT-MoP8	51 158	KRATSCHEMER, E.	NS-MoP24	49 153
KATANE, M.	VT-TuA9	63 193	KITAJIMA, M.	PS1-ThA7	100 295	KRAUSE, K.O.	NS-WeP21	87 257
KATARDJIEV, I.V.	PS-MoP8	50 155	KITAJIMA, M.	SS-MoP33	48 148	KRAUSS, A.R.	TFVM-MoA10	45 138
KATAYAMA, I.	SS-TuP13	66 200	KITAZAWA, K.	NS-WeP9	87 255	KRAUSS, A.R.	TF-FrM11	110 327
KATIYAR, M.	TF-FrM10	110 327	KITCHING, K.	SS1-ThA10	98 287	KRECH, J.	TF-ThP19	106 315
KATIYAR, M.	EM-ThP15	105 310	KITOH, M.	TFVM-TuA10	63 194	KREIDER, K.G.	TFVM-TuA5	63 193
KATO, S.	PS-TuA9	62 191	KIYOTA, T.	MS-WeM0	76 230	KREIDER, K.G.	NSBI-ThA5	99 290
KATZ, A.J.	EM-ThM3	94 280	KIZHKEVARIAM, N.	SS2-WeA8	80 235	KREIFELS, T.	EM-TuP3	69 211
KATZ, Z.	TF-ThP16	106 314	KLEBANOFF, L.E.	SS1-WeM4	72 218	KREMEYER, K.P.	PS-WeP5	88 259
KAWAHARA, D.	BI-MoP8	51 161	KLEM, J.F.	PS-WeA5	82 241	KRETZ, J.	NS1-FrM6	109 321
KAWAKATSU, H.	NS2-MoA8	43 132	KLEMBERG-SAPIEHA, J.E.	TF-WeP8	89 263	KRIM, J.	NS2-ThA10	99 293
KAWAKATSU, H.	NS-MoP8	49 151	KLEMENS, F.P.	PS-MoP16	50 156	KRISHNAMURTHY, R.	EM-FrM4	111 328
KAY, B.D.	SS-TuP3	66 198	KLEMENS, F.P.	PS-TuA2	62 190	KRIVOKAPIC, Z.	MS-MoA7	46 141
KAY, B.D.	SS2-WeA10	80 235	KLEPPER, C.C.	PS-WeP8	88 259	KROESEN, G.M.W.	PS-WeM7	74 226
KAZMERSKI, L.L.	EM-ThA10	102 300	KLIESE, R.	SS-MoP31	48 148	KROM, K.R.	SS-TuP16	66 200
KAZUTA, M.	SS1-MoM10	36 115	KLIMOV, A.N.	NS-MoP20	49 152	KROMMENHOEK, S.	TF-ThP15	106 314
KEAVNEY, D.J.	SS1-WeA5	80 233	KLINOWSKI, J.	AS-TuM10	54 171	KROZER, A.	BI-MoP5	51 160
KEAVNEY, D.J.	SS-WeP18	86 252	KLITSNER, T.	NS1-TuM1	53 166	KRUEGER, R.	VM-FrM3	111 329
KEAVNEY, D.J.	SS-TuP29	66 202	KLUMB, L.	BI-TuM1	57 179	KRÜGER, D.	NS-ThP19	104 307
KEELING, L.A.	AS-WeA7	82 240	KNEISEL, P.	VT-TuM7	55 174	KUBO, U.	PS2-ThA5	101 297
KEENAN, J.A.	NS2-MoA3	43 131	KNEISEL, P.	VT-TuM6	55 174	KUBOTA, K.	PS-MoM5	38 120
KELLER, D.	PS1-ThA8	100 295	KNICKERBOCKER, S.A.	TF-WeP1	89 262	KUBOTA, Y.	VT-MoP9	51 159
KELLERMAN, B.K.	SS-TuP28	66 202	KNOLL, W.	NSBI-WeA7	81 236	KUBOTA, Y.	VT-MoP13	51 159
KELLERMAN, B.K.	EM-WeM7	76 230	KNOLL, W.	BI-TuM3	57 179	KUDO, M.	AS-TuP6	68 207
KELLIHER, J.T.	SS1-TuM10	52 164	KNOLL, W.	BINS-WeM1	77 231	KUHN, M.	SS2-ThM7	90 269
KELLOGG, G.L.	SS-MoP40	48 149	KNOTTS, T.A.	MS-WeM1	76 230	KUIPERS, E.W.	SS-MoP6	48 144
KELLY, D.	PS1-ThA10	100 296	KO, K.K.	PS-WeM8	74 226	KUK, Y.	EM-ThP12	105 309
KELLY, J.P.	SS1-TuM2	52 163	KO, K.K.	EM-ThP10	105 309	KUK, Y.	NS1-MoA7	43 130
KENDALL, D.L.	TF-WeP2	89 262	KOBARI, T.	VT-TuA9	63 193	KULGINOV, D.	SS1-TuA3	60 182
KENNEDY, C.E.	SS1-TuM7	52 164	KOBAYASHI, M.	VT-TuA9	63 193	KULIK, A.J.	NS2-TuA4	61 187
KENNETT-FOX, R.	BI-TuM8	57 180	KOBAYASHI, S.	EM-ThM9	94 282	KULIK, J.	TFVM-TuA8	63 194
KERBER, S.J.	MS-TuM5	56 179	KOBAYASHI, Y.	PS2-ThA4	101 297	KULIK, J.	TFVM-ThM5	93 280
KERBY, H.R.	SS1-ThM1	90 267	KOCH, F.	NS2-WeA1	81 237	KULIK, J.	TF-WeP1	89 262
KERN, K.	BINS-WeM7	77 232	KOEGLER, R.	TF-ThP8	106 313	KULKARNI, A.K.	SS-MoP27	48 147
KERSEY, S.E.	TFVM-TuA1	63 193	KOEL, B.E.	SS2-ThM6	90 269	KUMMEL, A.C.	SSEM-WeA4	83 243
KESTER, D.J.	AS-MoM7	37 119	KOHO, Y.	EM-MoA9	46 140	KUMMEL, A.C.	SS2-TuM9	52 166
KEVAN, S.	SS1-TuA9	60 183	KOIDL, P.	TFVM-MoA1	45 137	KUMMEL, A.C.	SS-MoP32	48 148
KEVAN, S.D.	EM-ThP12	105 309	KOINKAR, V.N.	NS-MoP2	49 150	KUMMEL, A.C.	NS1-TuM11	53 168
KHANG, Y.	NS1-MoA7	43 130	KOKAKU, Y.	TFVM-TuA10	63 194	KUNG, H.	EM-ThM11	94 282
KHANG, Y.-H.	EM-WeA5	84 246	KOKUBUN, K.	VT-MoM11	38 123	KUNZ, A.K.	MS-TuP5	70 216
KIDDER, JR., J.N.	MS-ThM7	94 283	KOLASINSKI, K.W.	SS1-TuA4	60 182	KUO, C.H.	EM-ThM1	94 280
KIKUCHI, M.	NS2-ThM10	91 273	KOLB, D.M.	SS2-WeA1	80 234	KUO, C.H.	EM-WeA5	84 246
KIKUKAWA, A.	PS-MoP19	50 156	KOLESAR, E.S.	TF-TuM11	55 176	KUO, J.	NS-MoP12	49 151
KILGORE, M.D.	SS1-FrM2	108 317	KOLESKE, D.D.	SSEM-WeA3	83 242	KURAYA, E.	NS2-WeA9	81 238
KIM, B.	AS-WeA5	82 239	KOLOSKE, D.D.	BI-TuA5	65 197	KURINEC, S.K.	NS-ThP23	104 307
KIM, C.Y.	MS-TuA10	64 196	KOLOSKE, D.D.	NS2-TuM7	53 169	KURODA, K.	EM-TuA1	64 194
KIM, D.-H.	MS-WeA7	84 247	KOLOSKE, D.D.	NS1-MoA10	43 131	KURODA, K.	PS-WeA8	82 241
KIM, D.-H.	PS-WeP22	88 262	KOLOSOV, O.	VT-MoP8	51 158	KUSHNER, M.J.	PS-TuM1	54 171
KIM, H.-G.	NS-MoP24	49 153	KOMURA, A.	EM-ThM9	94 282	KUSHNER, M.J.	PS-TuM4	54 172
KIM, H.-S.	NS2-MoA6	43 132	KOMURO, M.	PS-WeP16	88 261	KUSHNER, M.J.	PS-WeP14	88 260
KIM, H.K.	AS-WeA8	82 240	KÖNEN, L.	NSBI-WeA10	81 237	KUSHNER, M.J.	TF-ThA4	101 298
KIM, H.K.	EM-WeM3	76 229	KONONENKO, A.A.	VM-FrM7	111 330	KUTTATH, S.	NS-WeP14	87 256
KIM, J.	TF-WeM2	75 228	KONYASHIN, I.Y.	NS1-FrM6	109 321	KUWAHARA, K.	VT-TuA6	63 192
KIM, J.	PS-WeA9	82 242	KOOPS, H.W.P.	SS1-TuA5	60 182	KUZAY, T.M.	VT-TuA7	63 192
KIM, J.H.	TF-FrM1	110 326	KORDESCH, M.E.	TF-ThP12	106 314	KUZAY, T.M.	BI-TuA7	65 197
KIM, J.H.	SS1-FrM2	108 317	KORDESCH, M.E.	SS-MoP1	48 144	KUZIEMKO, G.	EM-WeA10	84 247
KIM, K.J.	EM-ThA4	102 299	KORDESCH, M.E.	AS-ThA5	100 293	KUZNIA, J.N.	EM-TuP9	69 212
KIM, S.	EM-TuP7	69 212	KORNIENKO, O.	PS-MoP13	50 155	KWOK, R.W.M.	AS-WeM3	74 224
KIM, S.-B.	TFVM-MoA6	45 138	KORZEC, D.	PS-TuA7	62 190	KWOK, R.W.M.	EM-FrM7	111 328
KIM, S.H.	AS-WeA5	82 239	KORZEC, D.	VT-MoP12	51 159	KWOK, R.W.M.	VT-TuM3	55 174
KIM, S.H.	TF-WeP12	89 264	KOSS, V.	NS2-WeA5	81 238	LA MARCHE, P.H.	EM-TuP10	69 212
KIM, S.I.	AS-WeA5	82 239	KOSTOULAS, Y.	ASSS-TuA5	62 189	LABANDA, J.G.C.	EM-MoA8	46 140
KIM, S.T.	AS-FrM10	110 325	KÖTZ, R.	NS2-MoA8	43 132	LABELLA, V.	MS-MoA8	46 141
KIM, T.	EM-ThA7	102 300	KOUGAMI, H.	NS-MoP8	49 151	LABUN, A.H.	PS-MoP17	50 156
KIM, T.-J.	BI-TuM11	57 181	KOUGAMI, H.	BI-TuA3	65 196	LABUN, A.H.	TF-TuM6	55 175
KIM, Y.	TFVM-ThM3	93 279	KOVACS, G.T.	NSBI-ThA1	99 290	LAD, R.J.	EM-TuP4	69 211
KIM, Y.-W.	TFVM-ThM8	93 280	KOVACS, G.T.A.	SS1-MoA8	42 127	LADIPO, F.	TF-ThP23	106 316
KIM, Y.-W.	SS-WeP14	86 251	KOVÁCS, ZS.	SS1-MoM7	36 114	LADNA, B.	SS2-TuA8	60 184
KIM, Y.J.	TF-WeA7	83 245	KOVAR, M.	BI-TuM11	57 181	LÆGSGAARD, E.	NS2-ThM2	91 272
KIM, Y.K.	EM-TuA7	64 195	KOVATICH, S.	SS1-MoA8	42 127	LÆGSGAARD, E.	SS-WeP3	86 250
KIMERLING, L.C.	SS2-TuM5	52 165	KÖVÉR, L.	NS-ThP7	104 305	LÆGSGAARD, E.	SS-TuP20	66 201
KIMMEL, G.A.	TFVM-ThM6	93 280	KOWALIK, J.	SS1-TuA8	60 183	LAFEMINA, J.P.	SS2-TuM6	52 165
KINDER, T.J.	SS-MoP34	48 148	KOWALSKI, D.V.	BI-TuA3	65 196	LAFEMINA, J.P.	SSEM-WeM4	75 227
KING, B.V.	AS-TuM6	54 170	KOWTHA, V.C.	EM-TuA1	64 194	LAGALLY, M.G.	NS1-MoA8	43 130
KING, D.E.	TF-WeM5	75 228	KOYANAGI, M.	EM-TuA5	64 195	LAGALLY, M.G.	SS1-TuM6	52 163
KINGON, A.I.	NS-WeP9	87 255	KOYANAGI, M.	NS-TuP20	67 206	LAGALLY, M.G.	SS1-TuM3	52 163
KINO, N.			KOZHUSHNER, M.A.					

Author		Prog. Abst.			Prog. Abst.			Prog. Abst.			
		Pg. #	Pg. #		Pg. #	Pg. #		Pg. #	Pg. #		
LAGALLY, M.G.	NS2-WeM1	73	222	LEE, R.N.	AS-TuP30	68	211	LINDAHL, J.	NS-TuP9	67	204
LAGRAFF, J.R.	ASSS-TuA9	62	189	LEE, S.-M.	TF-WeM4	75	228	LINDSAY, S.M.	NS2-TuA9	61	188
LAI, C.	PS-TuA5	62	190	LEE, S.-T.	TF-WeP21	89	265	LINDSAY, S.M.	NSBI-ThM5	91	271
LAI, J.	NSBI-ThA6	99	290	LEE, W.H.	VT-TuA4	63	192	LINDSAY, S.M.	NSBI-ThM11	91	272
LAI, K.F.	PS-WeP7	88	259	LEE, Y.H.	EM-MoM11	39	125	LINDSAY, S.M.	NS1-TuA1	61	185
LAMBERT, D.K.	SS2-ThM2	90	268	LEFEBVRE, P.M.	VM-ThA7	103	303	LING, T.	NSBI-ThA3	99	290
LAMONT SCHNOES, M.	EM-TuP5	69	212	LEFRANCOIS, M.	NP-WeP2	89	266	LINTON, R.W.	AS-TuP9	68	207
LAMONTAGNE, B.	SS2-MoA3	42	128	LEGG, K.O.	TF-WeP14	89	264	LINTON, R.W.	AS-MoA3	44	133
LAMPNER, D.	NS2-TuA9	61	188	LEGG, K.O.	VM-ThA1	103	302	LIPKIN, N.N.	SS2-TuA2	60	183
LAMPNER, D.	NSBI-ThM11	91	272	LEHOCZKY, S.L.	NS-TuP1	67	203	LISTER, T.E.	NS-WeP25	87	258
LAMPNER, D.	NS1-TuA1	61	185	LEIBSLE, F.M.	SS1-ThA10	98	287	LITTAU, K.	EM-MoM6	39	124
LAND, D.P.	SS1-MoM5	36	114	LEIJALA, A.	NSMS-WeM0	73	221	LIU, C.	VT-TuA6	63	192
LAND, D.P.	SS-WeP27	86	254	LEKSONO, M.W.	EM-TuP18	69	214	LIU, C.	VT-TuA7	63	192
LANDHEER, D.	EM-FrM4	111	328	LEMNOS, Z.J.	MS-MoA3	46	141	LIU, D.	MS-ThM10	94	283
LANDMAN, U.	NS2-ThM1	91	272	LEMPERT, G.D.	TFVM-TuA8	63	194	LIU, G.	AS-ThM7	92	275
LANE, B.	PS-MoP23	50	157	LENANE, T.	EM-WeA6	84	246	LIU, H.	EM-TuP22	69	215
LANG, O.	EMSS-ThM11	93	279	LENANE, T.D.	EM-FrM10	111	329	LIU, H.	TF-ThP21	106	315
LANGE, G.	SS2-FrM6	108	320	LENG, Y.	NS-WeP22	87	257	LIU, J.-R.	PS-MoA8	44	135
LANGFORD, S.C.	AS-FrM7	110	325	LENGEL, G.	NS1-TuA7	61	186	LIU, N.	NS2-WeM2	73	222
LANGFORD, S.C.	NS2-ThA4	99	292	LENGGENHAGER, R.	VT-MoM7	38	122	LIU, N.	NS-WeP23	87	258
LANNI, C.	VT-TuA8	63	192	LENNOX, B.	AS-ThM3	92	274	LIU, Q.	EM-ThM5	94	281
LANZENDORF, E.J.	SS-MoP27	48	147	LENT, C.S.	NS2-TuM3	53	168	LIU, Q.	EM-FrM9	111	328
LANZENDORF, E.J.	SS2-TuM9	52	166	LEONE, S.R.	EM-ThM11	94	282	LIU, Y.	NS-WeP10	87	256
LAPEYRE, G.J.	SS-WeP10	86	251	LERCEL, J.	NS2-TuM8	53	169	LIU, Y.C.	VT-MoP7	51	158
LAPEYRE, G.J.	SS1-FrM11	108	318	LERCEL, M.J.	NS1-FrM3	109	321	LIU, Y.C.	VT-TuA4	63	192
LAPEYRE, G.J.	EM-ThP11	105	309	LESKOVAR, M.	SS2-MoA4	42	128	LIVESEY, R.G.	VT-MoP12	51	159
LAREAU, R.	TF-WeP3	89	262	LESKOVAR, M.	EM-FrM8	111	328	LO, C.W.	MS-TuP8	70	217
LARSEN, J.	NS2-TuA9	61	188	LESKOVAR, M.	EM-FrM5	111	328	LO, W.K.	MS-TuP7	70	217
LARSEN, N.B.	NS-ThP21	104	307	LETTIS, S.	PS-WeP17	88	261	LOBODA, M.J.	EM-TuP23	69	215
LARSON, D.D.	BI-MoP4	51	160	LEVEDAKIS, D.A.	EM-TuP25	69	215	LOCHER, R.	TFVM-MoA1	45	137
LASKY, J.B.	PS-WeA2	82	240	LEVI, G.	VT-MoA1	45	135	LOCKWOOD, D.J.	EM-TuP13	69	213
LASKY, P.	EMMS-TuM9	56	178	LEVY, M.	EM-ThA4	102	299	LÖFGREN, P.	BI-MoP5	51	160
LASKY, P.J.	SS2-TuM11	52	166	LEWIS, A.	NS1-FrM4	109	321	LÖHNDORF, M.	NS-ThP11	104	305
LASKY, P.J.	SS2-ThA5	98	288	LEWIS, D.B.	VM-FrM2	111	329	LONG, C.L.	BI-TuM1	57	179
LASTRAS-MARTÍNEZ, A.	EM-TuP21	69	214	LEWIS, J.P.	NS1-TuA1	61	185	LONG, R.G.	TF-ThP18	106	315
LATEEF, A.	VM-ThM2	95	284	LEYLAND, A.	VM-FrM5	111	329	LOONEY, J.P.	VT-MoM3	38	122
LAU, W.M.	EM-TuP9	69	212	LI, D.	SS1-WeA9	80	234	LOONEY, J.P.	VT-MoM4	38	122
LAU, W.M.	TF-WeP21	89	265	LI, D.	TF-WeP15	89	264	LOONEY, J.P.	VT-MoM9	38	123
LAU, W.M.	PS-WeP4	88	259	LI, H.	TF-ThP15	106	314	LOONEY, J.P.	VT-MoA2	45	136
LAU, W.M.	AS-ThA6	100	294	LI, H.	MS-ThM3	94	282	LOONEY, J.P.	VT-TuA1	63	191
LAU, W.M.	EM-FrM7	111	328	LI, J.	NS-WeP9	87	255	LOPEZ, S.	TFVM-TuA6	63	193
LAU, W.M.	EM-FrM4	111	328	LI, J.	NS-WeP8	87	255	LOPEZ, S.	TF-WeP15	89	264
LAUGHON, G.J.	VT-TuM5	55	174	LI, J.	PS1-ThA9	100	296	LÓPEZ-CRUZ, E.	TF-ThP11	106	314
LAUSMAA, J.	BI-MoP5	51	160	LI, L.	SS-WeP2	86	250	LÓPEZ-CRUZ, E.	NS-TuP11	67	204
LAUSMAA, J.	BI-TuM9	57	180	LI, L.	SS2-FrM8	108	320	LOTHIAN, J.R.	EM-ThA3	102	299
LAVOIE, M.A.	EM-TuP4	69	211	LI, M.	VT-TuA5	63	192	LOUDER, D.	EMSS-ThM11	93	279
LAWING, A.S.	EM-TuP8	69	212	LI, W.	SS1-ThM7	90	267	LOUDER, D.R.	NS-WeP20	87	257
LAWING, A.S.	EMMS-TuM6	56	177	LI, W.	SS1-ThA4	98	286	LOVEJOY, M.L.	PS-WeA5	82	241
LAWRENCE, M.	EM-ThP21	105	311	LI, X.	TF-WeP7	89	263	LOVEJOY, M.L.	EM-MoM8	39	124
LAZARIDES, A.	SS2-MoM10	36	117	LI, X.	EM-ThP4	105	308	LOVEJOY, M.L.	EM-ThP2	105	308
LE MOGNE, TH.	VM-FrM1	111	329	LI, Y.	VT-TuA6	63	192	LOZANO, M.L.	SS1-TuA10	60	183
LEA, A.S.	ASSS-TuA7	62	189	LI, Y.	VT-TuA7	63	192	LOZZI, L.	TF-WeM3	75	228
LEACH-SCAMPAVIA, D.	AS-ThA3	100	293	LI, Y.	SS1-TuM8	52	164	LU, C.	MSVT-ThA8	102	301
LEACH-SCAMPAVIA, D.	BI-TuM10	57	180	LI, Y.P.	NS-TuP12	67	204	LU, H.C.	EM-MoA3	46	139
LEBEDEV, M.V.	EM-ThP9	105	309	LI, Y.Q.	NS2-TuA9	61	188	LU, H.C.	EMMS-TuM4	56	177
LEDFOORD, J.S.	TF-TuM5	55	175	LI, Y.Q.	NS2-ThM9	91	273	LU, M.	TF-WeP19	89	265
LEDFOORD, J.S.	SS1-MoA7	42	126	LI, Y.S.	NS1-TuM1	53	166	LU, M.	TFVM-TuA4	63	193
LEE, C.	PS-TuM8	54	173	LIANG, J.W.	NS-ThP2	104	304	LU, P.H.	SS2-TuM11	52	166
LEE, C.	PS-MoP22	50	157	LIANG, Y.	ASSS-TuA7	62	189	LU, P.H.	SS2-ThA5	98	288
LEE, D.H.	SS-WeP26	86	253	LIANG, Y.	NS1-TuA10	61	186	LU, Q.	TF-ThP2	106	312
LEE, D.R.	EMMS-TuM5	56	177	LIAO, H.	EM-TuP25	69	215	LU, Q.B.	SS-MoP34	48	148
LEE, E.-H.	EM-TuP7	69	212	LIAO, H.	EM-MoM7	39	124	LU, Y.	EM-TuP22	69	215
LEE, G.U.	NSBI-ThM2	91	270	LIAO, H.	MS-MoA10	46	141	LU, Z.	EM-MoA4	46	139
LEE, H.J.	TF-ThP24	106	316	LIBIOULLE, L.	NS-ThP8	104	305	LU, Z.H.	EMMS-TuM10	56	178
LEE, J.	SS1-TuA1	60	182	LICHTENWALNER, D.J.	TF-WeM5	75	228	LU, Z.H.	EM-TuP13	69	213
LEE, J.-H.	NS-WeP19	87	257	LIEBERMAN, K.	NS1-FrM4	109	321	LUCAKS, J.	AS-WeM6	74	224
LEE, J.-H.	NS-WeP19	87	257	LIEBERMAN, M.A.	PS-TuM8	54	173	LUCAS, L.C.	BI-MoP8	51	161
LEE, J.-W.	TFVM-MoA6	45	138	LIEBERMAN, M.A.	PS-MoP22	50	157	LUCOVSKY, G.	EM-MoA2	46	139
LEE, J.C.	AS-WeA8	82	240	LIEBERMAN, M.A.	PS-MoP24	50	157	LUCOVSKY, G.	EMMS-TuM5	56	177
LEE, J.T.C.	PS-MoP16	50	156	LIEHR, M.	EMMS-TuM8	56	177	LUCOVSKY, G.	EM-MoA4	46	139
LEE, J.T.C.	PS-TuA2	62	190	LIEHR, M.	MS-ThM4	94	282	LUDEKE, R.	EM-MoA5	46	139
LEE, J.T.C.	MS-WeA4	84	247	LIFSHTITZ, Y.	TFVM-TuA8	63	194	LUDVIKSSON, A.	EM-WeA5	84	246
LEE, J.T.C.	PS-WeM3	74	225	LIFSHTITZ, Y.	TFVM-ThM4	93	279	LUEDTKE, W.D.	NS2-ThM1	91	272
LEE, J.W.	AS-WeA5	82	239	LIGLER, F.S.	BI-TuA5	65	197	LUI, H.	EM-WeA5	84	246
LEE, K.Y.	NS-MoP24	49	153	LIMANSKAYA, O.	BI-MoP2	51	160	LUKANC, T.	EM-MoM4	39	124
LEE, M.B.	SS1-ThA10	98	287	LIMANSKY, A.	BI-MoP2	51	160	LUKAS, S.	NS-ThP11	104	305
LEE, M.Y.	SSEM-WeA10	83	243	LIMONES, C.	EM-ThP13	105	310	LUKASHEV, E.P.	NSBI-WeA10	81	237
LEE, M.Y.	SS2-ThA3	98	288	LIN, H.N.	NS2-ThM11	91	274	LUNDGREN, E.	SS2-MoM4	36	116
LEE, M.Y.	EMSS-ThM6	93	278	LIN, K.C.	SS1-ThA6	98	287	LUO, Y.	EMMS-TuM9	56	178
LEE, M.Y.	EM-MoA7	46	140	LIN, M.	EM-MoM4	39	124	LURIO, L.B.	SS2-WeA7	80	235
LEE, N.-E.	TF-ThP2	106	312	LIN, Y.	TF-FrM11	110	327	LUSKINOVICH, P.N.	NS-ThP14	104	306
LEE, P.	EMSS-ThM11	93	279	LIN, Z.	MS-MoA1	46	140	LYDING, J.W.	SS2-TuM8	52	166
LEE, P.	EM-ThP21	105	311	LINARES, R.	TFVM-MoA3	45	137	LYDING, J.W.	EM-MoA1	46	139

Author		Prog. Abst.				Prog. Abst.					Prog. Abst.				
		Pg. #	Pg. #			Pg. #	Pg. #				Pg. #	Pg. #			
LYDING, J.W.	NS-ThP25	104	307	MÅRTENSSON, N.	SS1-FrM10	108	318	MCVITTIE, J.P.	PS1-ThA9	100	296				
LYDING, J.W.	NS2-WeM3	73	222	MÅRTENSSON, N.	SS-MoP18	48	146	MCVITTIE, J.P.	MS-TuP4	70	216				
LYDING, J.W.	EM-ThA6	102	300	MÅRTENSSON, N.	SS1-FrM5	108	317	MCVITTIE, J.P.	PS-MoP18	50	156				
LYDING, J.W.	SS2-FrM4	108	319	MARTIL, I.	TF-ThA6	101	298	MCVITTIE, J.P.	MS-MoA7	46	141				
LYMAN, P.F.	SS1-FrM4	108	317	MARTIL, I.	PS-MoP6	50	154	MCWAID, T.	NS-MoP19	49	152				
LYO, I.-W.	SS1-ThM3	90	267	MARTIN, C.R.	NS-TuP17	67	205	MEEKS, E.	PS-TuM7	54	172				
LYUBCHENKO, Y.	NSBI-ThM5	91	271	MARTIN, C.R.	BI-MoP15	51	162	MEEUSEN, G.J.	PS-MoA9	44	135				
MA, S.-M.	PS-WeP15	88	260	MARTIN, C.R.	NS-TuP22	67	206	MEIS-HAUGEN, G.	EM-WeM5	76	230				
MA, Y.	MS-ThM8	94	283	MARTIN, J.A.	NS-TuP5	67	203	MEISENHEIMER, T.L.	PS-ThM4	92	276				
MA, Y.Y.	NS-MoP7	49	151	MARTIN, J.M.	PS-MoP6	50	154	MEISENHEIMER, T.L.	PS-ThM3	92	276				
MA, Z.L.	NS2-WeM2	73	222	MARTIN, J.M.	VM-FrM1	111	329	MELI, C.A.	SS2-FrM6	108	320				
MA, Z.L.	NS-WeP23	87	258	MARTIN, K.P.	EM-ThA1	102	299	MELI, C.A.	VM-ThM10	95	285				
MACDONALD, R.J.	SS-WeP6	86	250	MARTIN, K.P.	NS1-FrM5	109	321	MEMMERT, U.	EMMS-TuM3	56	177				
MACDONALD, R.J.	SS-MoP34	48	148	MARTIN, L.D.	BI-MoP4	51	160	MEMMERT, U.	ASSS-TuA6	62	189				
MACKAY, S.G.	AS-MoA5	44	133	MARTIN, P.J.	TFVM-ThM6	93	280	MEMMERT, U.	NS2-WeM6	73	223				
MACKENZIE, J.D.	EM-WeA7	84	246	MARTIN, R.	AS-FrM5	110	324	MÉNDEZ, J.	NS2-ThM1	91	272				
MACKAY, B.L.	SS-TuP27	66	202	MARTIN-GAGO, J.	EM-ThP13	105	310	MENDICINO, M.A.	EMSS-ThM7	93	278				
MACKIE, N.	PS-MoP4	50	154	MARTINU, L.	TF-WeP8	89	263	MENG, B.	SS2-ThM4	90	269				
MACLEOD, H.A.	TF-WeM0	75	228	MARTON, D.	TFVM-ThM4	93	279	MENON, M.M.	VT-TuM5	55	174				
MADAN, A.	TF-WeP20	89	265	MARTON, D.	TFVM-ThM5	93	280	MENON, V.P.	NS-TuP22	67	206				
MADEY, T.E.	SS1-MoA10	42	127	MARTON, D.	TF-WeP11	89	263	MENSING, G.	EM-ThP8	105	309				
MADEY, T.E.	SS-TuP2	66	198	MARUSKA, H.P.	NS-TuP8	67	204	MERCADO, P.G.	TF-WeM7	75	228				
MADEY, T.E.	SS1-ThA9	98	287	MARUYAMA, T.	PS-MoM7	38	120	MERCER, B.S.	PS-MoP10	50	155				
MADEY, T.E.	SS-WeP7	86	250	MASLOVA, N.	NS-TuP21	67	206	MERCHANT, R.M.	SS1-MoA5	42	126				
MADIX, R.J.	SS1-MoM2	36	114	MASSON, D.	SS-MoP27	48	147	MERTZ, F.F.	PS-MoA7	44	135				
MADIX, R.J.	SS-TuP10	66	199	MASSON, D.P.	SS2-TuM9	52	166	MESSIER, R.	TFVM-MoA7	45	138				
MADURA, A.R.	AS-FrM5	110	324	MASSON, L.	SS2-ThA7	98	289	MEUNIER, M.	EM-ThP3	105	308				
MAEDA, Y.	EM-MoM6	39	124	MASUDA, T.	NS2-ThA7	99	292	MEYER, J.A.	PS-WeP9	88	260				
MAGNUSSSEN, O.M.	SS2-WeA5	80	235	MATE, C.M.	NS2-ThA3	99	291	MEYER, K.	AS-WeM7	74	224				
MAGNUSSON, K.O.	EM-ThP7	105	309	MATE, C.M.	NS2-ThA6	99	292	MEYERHOFF, M.E.	BI-TuA1	65	196				
MAGNUSSON, K.O.	EM-TuP17	69	214	MATERER, N.	SS2-MoM6	36	116	MEYERS, J.M.	SS-WeP22	86	253				
MAGRUDER III, R.H.	NS-TuP15	67	205	MATERLIK, G.	SS2-ThA1	98	288	MICHALSKE, T.A.	NS2-TuA8	61	187				
MAGRUDER III, R.H.	AS-TuM9	54	171	MATHEW, J.G.H.	TF-ThA9	101	299	MICHALSKE, T.A.	BI-MoP7	51	161				
MAHAJAN, A.	SS-TuP28	66	202	MATSUDA, T.	BINS-WeM3	77	232	MICHALSKE, T.A.	AS-FrM6	110	325				
MAHAJAN, A.	EM-ThM7	94	281	MATSUMOTO, D.	EM-MoM4	39	124	MICHALSKE, T.A.	AS-FrM10	110	325				
MAHAN, J.E.	TF-ThP18	106	315	MATSUMOTO, H.	TFVM-TuA10	63	194	MICHEL, E.G.	EM-ThP13	105	310				
MAHDAVI, M.A.	VT-TuM5	55	174	MATSUO, S.	PS-MoM9	38	121	MICHEL, E.G.	SS2-ThA1	98	288				
MAHER, D.M.	EM-ThM5	94	281	MATSUSHIGE, K.	NS-ThP17	104	306	MICHEL, H.-J.	EM-ThP17	105	310				
MAINGI, R.	VT-TuM5	55	174	MATSUZAKI, M.	VT-TuA9	63	193	MICHEL, J.	EM-TuA7	64	195				
MAJOO, S.	TF-TuM8	55	176	MATTHEWS, A.	VM-FrM5	111	329	MIETHE, K.	AS-MoA6	44	133				
MAJUMDAR, A.	NSBI-ThA6	99	290	MATTHEWS, A.	VM-FrM2	111	329	MIGEON, H.-N.	AS-MoM1	37	118				
MAK, A.	EM-MoM6	39	124	MATUMOTO, M.	VT-TuA9	63	193	MIKHAILOV, A.	SS2-WeM3	72	220				
MALIC, R.A.	NS2-FrM11	109	324	MATZKE, C.M.	SS1-TuM2	52	163	MIKI, M.	VT-MoA9	45	136				
MALIC, R.A.	SS-MoP4	48	144	MAVRIKAKIS, M.	SS-MoP11	48	145	MILITZER, M.	SS-WeP9	86	251				
MALIK, I.	SS-MoP21	48	147	MAWN, M.P.	AS-TuP9	68	207	MILLER, D.J.	TF-ThP14	106	314				
MALKOV, A.A.	NS-WeP16	87	256	MAXWELL, K.L.	PS-ThM10	92	277	MILLER, D.P.	MSVT-ThA1	102	301				
MALLETTE, R.P.	MS-WeM1	76	230	MAYER, C.	SS-MoP24	48	147	MILLER, R.	NS-MoP5	49	150				
MALYGIN, A.A.	NS-WeP16	87	256	MAYER, J.W.	TF-WeA4	83	244	MILLER, R.	BI-MoP4	51	160				
MAMIN, H.J.	NS2-FrM9	109	323	MAYER, T.M.	SS-TuP12	66	200	MILLER, S.J.	EM-WeA2	84	245				
MAMIN, H.J.	NSMS-WeM5	73	221	MAYNARD, H.L.	MS-WeA4	84	247	MILLO, O.	VM-WeA9	85	249				
MAMMOSSER, J.	VT-TuM6	55	174	MAYO, W.E.	EM-TuP22	69	215	MILLO, O.	NS1-MoA2	43	129				
MANGO, F.	BI-MoP11	51	161	MCBREEN, P.H.	SS-WeP25	86	253	MINABE, T.	AS-MoM11	37	119				
MANIVANNAN, A.	NS-TuP4	67	203	MCCARLEY, R.L.	SS1-ThM9	90	268	MINATO, M.	VT-MoP14	51	159				
MANKEY, G.J.	SS-WeP12	86	251	MCCELLELAND, G.M.	NS2-FrM5	109	323	MINER, G.A.	AS-TuM5	54	170				
MANKEY, G.J.	SS1-WeM5	72	218	MCCELLELAND, J.	NS2-WeM7	73	223	MINIAMI, T.	TF-WeP9	89	263				
MANOS, D.M.	PS-TuM2	54	172	MCCOMAS, A.	EM-MoM4	39	124	MINIAMI, T.	TF-ThA10	101	299				
MANNING, B.	PS-MoP7	50	154	MCCOMBE, B.	EM-ThP8	105	309	MINNE, S.C.	NS2-FrM8	109	323				
MANTEI, T.D.	PS-TuA10	62	191	MCCORMACK, K.	MS-TuA6	64	196	MINTMIRE, J.W.	NS2-TuA2	61	187				
MANTEI, T.D.	PS-MoA1	44	134	MCCOY, J.M.	SS-TuP20	66	201	MINTON, T.K.	PS-ThM9	92	277				
MANTEI, T.D.	TFVM-MoA5	45	138	MCCURDY, P.R.	PS-MoP4	50	154	MIRANDA, R.	EM-ThP13	105	310				
MANTESE, L.	SS2-MoA7	42	128	MCEACHERN, R.L.	PS2-ThA8	101	297	MIRECKI MILLUNCHICK, J.	VM-WeA2	85	248				
MANTESE, L.	SS2-FrM5	108	319	MCEACHERN, R.L.	AS-TuP13	68	208	MISEWICH, J.A.	SS2-TuM1	52	164				
MANUDONDA, R.	TF-FrM8	110	327	MCELLISTREM, M.	SS-TuP26	66	202	MISHIMA, S.	NS-WeP24	87	258				
MAO, G.	AS-ThM11	92	275	MCELLISTREM, M.T.	SS-TuP21	66	201	MISHRA, S.	AS-TuP10	68	208				
MAPES, M.	VT-MoP11	51	159	MCFADDEN, C.F.	NS2-ThA9	99	292	MITCHELL, G.E.	AS-FrM9	110	325				
MAPOLES, E.	PS2-ThA7	101	297	MCGHIE, A.J.	NSBI-WeA5	81	236	MITCHELL, M.A.	EM-MoM8	39	124				
MAPOLES, E.R.	PS-WeP20	88	261	MCINTYRE, B.J.	SS2-ThM8	90	269	MITCHELL, T.B.	PS-WeP5	88	259				
MARACAS, G.N.	MS-TuP5	70	216	MCINTYRE, D.C.	VM-ThM7	95	284	MITCHELL, T.E.	NS1-TuM11	53	168				
MARACAS, G.N.	EM-ThM1	94	280	MCINTYRE, N.S.	AS-ThA6	100	293	MITSUOKA, Y.	PS1-ThA5	100	295				
MARCH, D.	MS-ThM8	94	283	MCKENNA, W.P.	AS-ThA2	100	293	MITTAL, M.	NS2-FrM3	109	323				
MARCHANT, R.E.	BI-TuM5	57	180	MCKEOWN, P.J.	AS-MoM5	37	118	MIYAJIMA, H.	MS-WeM2	76	230				
MARCHMAN, H.M.	NS2-MoA10	43	132	MCKEOWN, P.J.	AS-MoA5	44	133	MIYAKE, J.	NSBI-WeA9	81	237				
MARGARITONDO, G.	EM-ThP6	105	309	MCKINLEY, J.	EM-ThP8	105	309	MIYAKE, K.	EM-TuA1	64	194				
MARGARITONDO, G.	NS-TuP7	67	204	MCKINLEY, J.D.	SS-WeP11	86	251	MIYAMOTO, M.	NS2-ThM10	91	273				
MARGARITONDO, G.	SS1-MoA8	42	127	MCKINLEY, J.T.	NS-TuP7	67	204	MIYAMOTO, T.	EM-TuA1	64	194				
MARINENKO, R.	TFVM-TuA5	63	193	MCKRELL, T.J.	ASSS-TuA3	62	188	MIYAZAKI, S.	EM-TuA1	64	194				
MARKIEWICZ, P.C.	NS-MoP15	49	152	MCLEAN, J.G.	SS-TuP17	66	201	MIYOSHI, M.	VT-MoP13	51	159				
MARKS, L.D.	SS2-MoA1	42	127	MCLEAN, J.G.	SS2-TuA1	60	183	MIZUTANI, T.	PS-ThM7	92	277				
MARKS, L.D.	SS2-FrM2	108	319	MCMAHON, R.W.	MSVT-ThA3	102	301	MIZUTANI, T.	NS2-TuA10	61	188				
MARRIAN, C.R.K.	NS1-TuA9	61	186	MCMILLIN, B.K.	PS-WeM4	74	226	MIZUTANI, W.	NS-WeP13	87	256				
MARRIAN, C.R.K.	NS2-TuM7	53	169	MCNEVIN, S.C.	PS-MoM4	38	120	MOFFAT, H.K.	EMSS-ThM8	93	278				
MARRIAN, C.R.K.	NS2-ThM7	91	273	MCVITTIE, J.P.	PS-WeA1	82	240	MOHIDEEN, U.	EM-TuP5	69	212				
MARTEL, R.	SS-WeP25	86	253	MCVITTIE, J.P.	PS-WeP15	88	260	MOISE, T.S.	EM-ThM3	94	280				

Author		Prog. Abst.		Prog. Abst.		Prog. Abst.	
		Pg. # Pg. #		Pg. # Pg. #		Pg. # Pg. #	
MOISEEV, Y.N.	NS-TuP21	67 206	NAKAMICHI, E.	NS-TuP10	67 204	NORTHOVER, P.	AS-MoM10 37 119
MÖLLER, M.	NS1-TuM9	53 167	NAKAMURA, K.	PS-WeM5	74 226	NORTON, P.R.	EMMS-TuM10 56 178
MÖLLER, M.	NS1-FrM8	109 321	NAKAMURA, K.	NS2-ThM10	91 273	NORTON, P.R.	TF-ThP10 106 314
MÖLLERS, R.	AS-TuM4	54 170	NAKAMURA, K.G.	PS1-ThA7	100 295	NORTON, P.R.	SS2-ThA4 98 288
MOMOSE, T.	VT-MoP5	51 158	NAKAMURA, K.G.	SS-MoP33	48 148	NOVAK, D.	SS-MoP8 48 145
MONROE, D.R.	AS-TuP22	68 209	NAKAMURA, M.	PS-WeM5	74 226	NOWAK, P.	AS-ThA6 100 293
MONTELIUS, L.	NSBI-ThA3	99 290	NAKAMURA, M.	BI-MoP8	51 161	NOWAK, R.W.	AS-ThA8 100 294
MONTELIUS, L.	NS-TuP9	67 204	NAKAMURA, M.	PS-ThM5	92 276	NULTY, J.E.	PS-MoM3 38 120
MONTUCLARD, J.	NP-WeP2	89 266	NAKAMURA, S.	EM-WeA3	84 246	NUNES, N.L.	SS1-WeM3 72 218
MOON, D.W.	AS-WeA8	82 240	NAKAMURA, T.	AS-TuP23	68 210	NURMIKKO, A.V.	EM-WeM0 76 229
MOONEY, C.B.	NSBI-ThA9	99 291	NAKAMURA, Y.	NS-TuP18	67 205	NXUMALO, J.N.	NSMS-WeM8 73 222
MOORE, B.C.	VT-MoP15	51 159	NAKANO, H.	PS2-ThA5	101 297	NYBERG, T.	TF-WeP14 89 264
MOORE, C.E.	PS2-ThA8	101 297	NAKASAKI, Y.	MS-WeM2	76 230	NYFFENEGGER, R.	ASSS-TuA5 62 189
MOORE, J.T.	NS1-FrM5	109 321	NAKASAKI, I.	MS-WeM0	76 230	NYGREN, H.	BI-MoA8 47 143
MOORE, T.A.	PS-ThM9	92 277	NAKAYAMA, I.	MS-ThM7	94 283	O'BRIEN, D.F.	AS-TuP2 68 206
MORANT, C.	NS2-TuA5	61 187	NAMBA, T.	EM-TuA1	64 194	O'BRIEN, N.A.	TF-ThA9 101 299
MORELAND, J.	NS-MoP9	49 151	NAMBA, Y.	NS-MoP7	49 151	O'BRIEN, W.L.	SS1-WeA6 80 233
MORELAND, J.	NS-MoP21	49 153	NARAYAN, P.B.	TF-WeA7	83 245	O'CONNOR, D.J.	SS-WeP6 86 250
MORELAND, J.	NS-MoP22	49 153	NARAYANASWAMY, A.	TF-TuM7	55 176	O'CONNOR, D.J.	SS-TuP19 66 201
MORETTI, G.	SS1-MoA8	42 127	NASTASI, M.	NS-TuM11	53 168	O'CONNOR, D.J.	SS-MoP34 48 148
MORETTO, L.	AS-MoM10	37 119	NASTASI, M.A.	VM-ThM9	95 285	O'FERRALL, C.E.	BI-MoP3 51 160
MOREY, I.	PS-TuA4	62 190	NATHANSON, G.M.	SS1-TuA8	60 183	O'HANLON, J.F.	PS-WeA10 82 242
MORGAN, H.	BI-MoA4	47 142	NAUKA, K.	PS-MoA7	44 135	O'HANLON, J.F.	PS-WeP11 88 260
MORGAN, H.	BI-TuA4	65 197	NAUMKIN, A.V.	AS-WeA10	82 240	O'NEILL, J.	MS-WeA5 84 247
MORGAN, S.H.	NS-TuP15	67 205	NAUMKIN, A.V.	AS-TuP21	68 209	O'NEILL, J.A.	PS-ThM4 92 276
MORGAN, S.H.	AS-TuM9	54 171	NAVARRO-CONTRERAS, H.	EM-TuP21	69 214	OASA, T.	NS1-MoA6 43 130
MORGENSTERN, G.	EM-ThM8	94 281	NAVROTSKI, G.	SS-WeP1	86 250	OCKO, B.M.	SS2-WeA5 80 235
MORITA, S.	NS1-MoA6	43 130	NAYFEH, M.H.	SS1-ThM6	90 267	ODAKA, K.	VT-MoP6 51 158
MORITA, S.	NS-MoP1	49 150	NEBESNY, K.	EMSS-ThM11	93 279	ODIN, C.	NS2-ThA7 99 292
MORITA, S.	NS-WeP24	87 258	NEBESNY, K.	EM-ThP21	105 311	OEPEN, H.P.	SS1-WeM3 72 218
MORKOC, H.	SS2-MoA9	42 129	NECHAY, B.A.	NS2-FrM1	109 322	OETER, D.	NS-WeP6 87 255
MOSER, J.	TFVM-ThM8	93 280	NEDDERMEYER, H.	SS-MoP31	48 148	OFFENHAUSSER, A.	BINS-WeM1 77 231
MOSLEHI, M.	MS-TuA5	64 195	NEE, C.C.	VT-TuA4	63 192	OGASAWARA, M.	MS-TuP2 70 216
MOTEGI, N.	MS-WeM0	76 230	NEJOH, N.	NS1-MoA5	43 130	OGASAWARA, M.	MS-TuP3 70 216
MOTOJIMA, O.	VT-MoP9	51 159	NELSON, C.E.	SS-MoP29	48 148	OGINO, T.	EMMS-TuM11 56 178
MOTOMATSU, M.	NS2-TuA10	61 188	NELSON, J.T.	SS-TuP7	66 199	OGLETREE, D.F.	AS-TuP12 68 208
MOUNTAIN, R.D.	VT-MoA2	45 136	NENDER, C.	TF-WeP14	89 264	OGLETREE, D.F.	AS-ThM7 92 275
MOUTINHO, H.R.	TF-ThA4	101 298	NETZER, F.P.	SS2-MoA2	42 127	OGLETREE, D.F.	SS2-MoM8 36 116
MOUTINHO, H.R.	EM-ThA10	102 300	NEUGROSCHL, D.A.	EMMS-TuM8	56 177	OGLETREE, D.F.	NS2-FrM4 109 323
MOYNE, J.R.	MSVT-ThA5	102 301	NEUHOLD, G.	EM-TuP17	69 214	OGLETREE, D.F.	SS-WeP5 86 250
MROZEK, P.	SS2-WeA3	80 234	NEUHTIENS, G.	NS2-ThM5	91 273	OGLETREE, D.F.	SS2-TuA5 61 187
MU, R.	NS-TuP15	67 205	NEUWALD, U.	EMMS-TuM3	56 177	OGLETREE, D.F.	EM-ThP5 105 308
MU, R.	AS-TuM9	54 171	NEW, R.M.H.	NS1-MoA9	43 130	OGURE, N.	VT-MoP10 51 159
MUENCHHAUSEN, R.	VM-ThM7	95 284	NEWBURY, D.E.	TF-WeP5	89 262	OH, W.S.	TF-ThP13 106 314
MUHR, G.T.	EM-TuP16	69 214	NG, W.	EM-ThP6	105 309	OHARA, K.	PS-TuA9 62 191
MUIJSERS, J.C.	SS-MoP6	48 144	NGUYEN, N.V.	EM-FrM3	111 328	OHBA, Y.	SS-TuP13 66 200
MUIRHEAD, D.A.	VT-TuM9	55 174	NICHOLS, C.A.	PS-TuM2	54 172	OH, A.	NS-WeP13 87 256
MUKAINAKANO, S.	PS1-ThA5	100 295	NICO, J.	MS-TuM11	56 179	OHMI, T.	EMMS-TuM1 56 176
MUKHERJEE, P.	VM-ThM1	95 284	NIE, H.-Y.	NS2-TuA10	61 188	OHNISHI, H.	SS-TuP13 66 200
MÜLLER, B.	SS-TuP6	66 198	NIEHUIS, E.	AS-TuM4	54 170	OHTA, M.	NS-WeP24 87 258
MÜLLER, B.	SS2-ThM9	90 270	NIEHUS, H.	SS2-MoM1	36 115	OHUCHI, F.S.	VM-FrM4 111 329
MÜLLER, K.	SS1-ThA3	98 286	NIELSEN, M.M.	SS2-MoM4	36 116	OHUCHI, F.S.	SS2-MoA8 42 128
MÜLLER, P.	TF-ThP4	106 313	NIELSEN, R.	VT-TuA6	63 192	OKADA, L.A.	SS-MoP28 48 148
MULLINS, D.R.	SS1-FrM4	108 317	NIELSEN, R.W.	VT-TuA7	63 192	OKADA, M.	SS2-ThM5 90 269
MULLINS, D.R.	SS1-ThA8	98 287	NIEMANTSVERDRIET, J.W.	SS-MoP13	48 145	OKADA, T.	NS-WeP24 87 258
MUNN, J.R.	MS-TuP9	70 217	NIEMANTSVERDRIET, J.W.	AS-TuP19	68 209	OKANO, H.	MS-TuP2 70 216
MURATA, Y.	NS2-ThA1	99 291	NIEMANTSVERDRIET, J.W.	SS-MoP6	48 144	OKANO, H.	MS-TuP3 70 216
MURPHY, D.B.	BINS-WeM8	77 232	NIEMANTSVERDRIET, J.W.	SS2-WeM1	72 219	OKANO, H.	MS-WeM2 76 230
MURRAY, R.W.	TF-FrM2	110 326	NIEMELÄ, M.K.	NS-WeP21	87 257	OKANO, H.	VT-MoP10 51 159
MURTHY, S.	NS1-TuM7	53 167	NIGRO, C.	NSBI-ThM7	91 271	OKRONGLY, D.A.	BI-MoA5 47 142
MUSCAT, A.J.	EM-TuP8	69 212	NIHEI, Y.	SS-WeP8	86 251	OKUMURA, K.	MS-TuA7 64 196
MUSCAT, A.J.	EMMS-TuM6	56 177	NIKANOROV, V.	NS-TuP21	67 206	OKUMURA, K.	VT-MoP10 51 159
MUSHIAKI, M.	VT-MoP9	51 159	NILES, D.	EM-ThP4	105 308	OKUSAKO, T.	NS1-MoA6 43 130
MUSHIAKI, M.	VT-MoP13	51 159	NILES, D.W.	TF-WeP7	89 263	OLCINIK, I. I.	NS-TuP20 67 206
MÜSSIG, H.-J.	NS-ThP19	104 307	NILSSON, A.	SS1-FrM10	108 318	OLESEN, L.	NS2-ThM2 91 272
MUZZALUPO, I.	NSBI-ThM7	91 271	NILSSON, A.	SS-MoP18	48 146	OLMSTEAD, M.A.	SS2-MoA4 42 128
MYERS, F.R.	PS-MoA4	44 134	NILSSON, A.	SS1-FrM5	108 317	OLMSTEAD, M.A.	EM-FrM8 111 328
MYRICK, M.L.	NS-MoP13	49 151	NILSSON, B.	BI-MoA7	47 142	OLMSTEAD, M.A.	EM-FrM5 111 328
MYRICK, M.L.	NS1-FrM7	109 321	NINGEL, K.-P.	PS-MoP13	50 155	OLSON, D.T.	EM-WeA10 84 247
NAGAHARA, L.A.	AS-MoM11	37 119	NINOMIYA, K.	AS-MoM6	37 118	OLTHOFF, J.K.	MS-TuP6 70 216
NAGAHARA, L.A.	ASSS-TuA10	62 189	NISHIHARA, T.	AS-TuP6	68 207	OMSTEAD, T.	MS-TuA5 64 195
NAGAHARA, L.A.	NS-WeP9	87 255	NISHIHARA, Y.	NS1-TuA8	61 186	OMSTEAD, T.R.	TF-ThP4 106 313
NAGAI, M.	VT-TuA9	63 193	NISHIKAWA, K.	PS-ThM5	92 276	ONDRUS, D.J.	AS-FrM1 110 324
NAGATA, T.	EM-TuA1	64 194	NISHIMURA, H.	PS-MoM9	38 121	ONELLION, M.	SS1-WeA9 80 234
NAGY, J.	BI-TuA7	65 197	NISHIYAMA, I.	SSEM-WeA7	83 243	ONG, J.L.	BI-MoP8 51 161
NAIK, R.	EM-WeA6	84 246	NISHIYAMA, Y.	MS-WeM2	76 230	ONO, K.	VT-MoP10 51 159
NAIK, R.	EM-FrM10	111 329	NOËL, J.-P.	EM-FrM4	111 328	ONO, R.H.	NS-MoP21 49 153
NAKABEPPU, O.	NSBI-ThA6	99 290	NOLL, J.D.	NS-MoP13	49 151	ONO, T.	PS-MoM9 38 121
NAKAGAWA, H.	NS-MoP12	49 151	NOLL, J.D.	NS1-FrM7	109 321	OPRISON, R.C.	BINS-WeM0 77 231
NAKAGAWA, S.	AS-FrM7	110 325	NOMURA, S.	TFVM-TuA9	63 194	ORBAN, Z.	VM-ThA6 103 302
NAKAHARA, S.	NS2-ThA4	99 292	NOONAN, G.O.	TF-TuM5	55 175	ORBAN, Z.	MS-ThM3 94 282
NAKAI, S.	PS2-ThA4	101 297	NORIMATSU, T.	PS2-ThA4	101 297	ORLANDO, T.M.	SS2-TuM5 52 165
NAKAI, S.	PS2-ThA10	101 297	NORIMATSU, T.	PS2-ThA10	101 297	OSBOURN, G.C.	SS2-FrM1 108 319

Author	Prog. Abst.		Author	Prog. Abst.		Author	Prog. Abst.	
	Pg. #	Pg. #		Pg. #	Pg. #		Pg. #	Pg. #
OSBURN, E.	AS-TuP2	68 206	PEARCE, L.G.	PS-WeP13	88 260	POELSEMA, B.	SS2-TuA2	60 183
OSGOOD, JR., R.M.	EMMS-TuM9	56 178	PEARSALL, T.P.	EM-WeA5	84 246	POIRIER, G.E.	SS1-MoA3	42 126
OSGOOD, JR., R.M.	SS2-TuM11	52 166	PEARSON, C.	SS1-TuM1	52 163	POIRIER, G.E.	AS-ThM5	92 274
OSGOOD, JR., R.M.	SS2-ThA5	98 288	PEARTON, S.J.	EM-WeA8	84 246	POKER, D.B.	SS2-ThM5	90 269
OSGOOD, JR., R.M.	EM-ThA4	102 299	PEARTON, S.J.	EM-ThA3	102 299	POKER, D.B.	EM-TuP14	69 213
OSHIMA, M.	EMMS-TuM11	56 178	PEARTON, S.J.	PS-MoP15	50 156	POKER, D.B.	PS-MoP10	50 155
ÖSTERLUND, L.	SS2-WeA9	80 235	PEARTON, S.J.	EM-WeA7	84 246	POLLAK, F.H.	TF-WeA8	83 245
OTSUBO, T.	PS-TuA9	62 191	PEARTON, S.J.	EM-TuP5	69 212	POOLE, J.	PS-MoP7	50 154
OTT, A.W.	EM-ThA9	102 300	PEASE, R.F.W.	NS1-MoA9	43 130	POPE, K.	EMMS-TuM8	56 177
OURA, K.	AS-TuP23	68 210	PECHMAN, R.J.	EMSS-ThM1	93 277	POPE, K.	MS-ThM4	94 282
OURA, K.	SS-TuP13	66 200	PECHMAN, R.J.	EM-ThP26	105 312	POPPA, H.	SS1-WeM2	72 218
OURA, K.	TF-ThP5	106 313	PECKERAR, M.	NS2-TuM9	53 170	PORATH, D.	VM-WeA9	85 249
OUTLAW, R.A.	AS-TuM5	54 170	PEDEN, C.H.F.	SS2-WeM0	72 219	PORATH, D.	NS1-MoA2	43 129
OUTLAW, R.A.	PS-WeP1	88 258	PEDEN, C.H.F.	SS1-MoA9	42 127	POROD, W.	NS2-TuM3	53 168
OVERBURY, S.H.	SS1-FrM4	108 317	PEEK, B.M.	EM-ThP23	105 311	PORTER, T.L.	AS-TuP14	68 208
OVERBURY, S.H.	SS2-ThA6	98 289	PEHRSSON, P.E.	BI-TuM10	57 180	PORTER, T.L.	NS-WeP1	87 254
OVERBURY, S.H.	SS1-ThA8	98 287	PELLEGRINO, J.G.	EM-ThA8	102 300	PORTNOV, S.M.	NS-WeP16	87 256
OVERTURF, III, G.E.	PS-WeP21	88 261	PELLIN, M.J.	EM-FrM3	111 328	POSADOWSKI, W.M.	PS-MoM11	38 121
OVERZET, L.J.	PS-WeP6	88 259	PELZ, J.P.	AS-WeM8	74 225	POSPIESZCZYK, A.	PS-WeP16	88 261
OVSHINSKY, S.R.	PS-WeP8	88 259	PENG, C.	EM-ThP20	105 311	POTOCHNIK, S.J.	EM-ThA8	102 300
OWARI, M.	SS-WeP8	86 251	PENG, C.	NS2-WeA9	81 238	POTTER, B.G.	PS-MoA6	44 135
PAFFETT, M.T.	SS1-MoM6	36 114	PENNER, R.M.	SS1-ThA2	98 286	POWELL, C.J.	AS-MoA8	44 133
PAGGEL, J.J.	SSEM-WeA2	83 242	PENROSE, W.R.	SS1-ThM7	90 267	POWELL, R.C.	EM-TuP21	69 214
PAI, W.W.	SS1-ThA2	98 286	PERERA, R.C.C.	TF-ThP20	106 315	PRASAD, V.	MS-MoA2	46 140
PAITICH, R.	VT-MoM2	38 122	PÉREZ-LUNA, V.H.	TF-ThP6	106 313	PRATER, C.	NS-MoP21	49 153
PALEUDIS, L.	AS-MoM8	37 119	PÉREZ-MONTERO, S.Y.	BI-MoP10	51 161	PRITCHARD, D.J.	BI-TuA4	65 197
PALEUDIS, L.	AS-WeM6	74 224	PÉREZ-MURANO, E.	PS-WeP9	88 260	PROKES, S.M.	NS2-WeA4	81 237
PÁLINKÁS, J.	SS1-MoA8	42 127	PERKINS, C.	NS-ThP1	104 304	PROKHOROV, A.M.	NS-MoP20	49 152
PALMER, J.	TF-ThP24	106 316	PERKINS, F.K.	VT-TuA8	63 192	PROTASENKO, V.V.	NS-ThP10	104 306
PALMER, R.E.	NS1-TuM5	53 167	PERKINS, F.K.	EM-ThP24	105 311	PROTASENKO, V.V.	NS-ThP10	104 305
PALMIERI, A.	AS-MoM10	37 119	PERKINS, F.K.	NS1-TuA9	61 186	PRUTTON, M.	AS-MoA2	44 133
PAN, J.	NSBI-ThM11	91 272	PERKINS, F.K.	NS2-TuM7	53 169	PUDDEPHATT, R.J.	TF-ThP10	106 314
PAN, J.	NS1-TuA1	61 185	PERMANA, H.	NS2-ThM7	91 273	PUGLIA, C.	SS1-FrM10	108 318
PANG, S.	NS2-WeM2	73 222	PERMANA, H.	SS-MoP15	48 146	PUGLIA, C.	SS-MoP18	48 146
PANG, S.	NS-WeP11	87 256	PERMANA, H.	SS2-WeM2	72 219	PURTELL, R.	MS-ThM4	94 282
PANG, S.	NS-WeP23	87 258	PERNG, S.Y.	VT-MoP7	51 158	PYLKKI, R.J.	NS-MoP10	49 151
PANG, S.W.	PS-MoP9	50 155	PERRY, A.J.	TF-WeP23	89 265	QADRI, S.B.	EM-FrM3	111 328
PANG, S.W.	PS-WeM8	74 226	PERRY, S.S.	NS2-ThA6	99 292	QI, H.	SSEM-WeM8	75 227
PANG, S.W.	EM-ThP10	105 309	PERRSON, M.	SS1-TuA3	60 182	QIAN, Y.	SS2-FrM10	108 320
PANG, S.W.	EM-WeA2	84 245	PETERS, M.W.	PS-MoA4	44 134	QIU, C.H.	EM-TuP18	69 214
PANKOVE, J.	EM-TuP18	69 214	PETERSEN, H.	SSEM-WeA2	83 242	QIU, J.	EM-WeM5	76 230
PANKOVE, J.I.	NS-TuP21	67 206	PETERSON, T.	PS-WeP11	88 260	QUAGLIARIELLO, C.	NSBI-ThM7	91 271
PANOV, V.	NSBI-WeA10	81 237	PETICOLAS, L.J.	NS1-MoA8	43 130	QUATE, C.F.	NS2-FrM8	109 323
PANOV, V.V.	SS1-MoM1	36 114	PETROU, A.	EM-ThP8	105 309	QUESENBERRY, P.E.	NS-WeP18	87 257
PANSOY-HJELVIK, M.E.	SS2-WeA7	80 235	PETROV, I.	EM-MoM5	39 124	QUINIOU, B.	PS-WeM1	74 225
PANT, J.	AS-WeA6	82 239	PETROV, I.	TFVM-ThM3	93 279	RA, Y.	PS-TuM7	54 172
PANTANO, C.G.	AS-TuM11	54 171	PETROV, I.	VM-WeA1	85 248	RABALAIS, J.W.	TFVM-TuA8	63 194
PANTANO, C.G.	SS2-TuA3	60 183	PETROV, I.	TFVM-ThM8	93 280	RABALAIS, J.W.	TFVM-ThM4	93 279
PAPAGEORGIOPOULOS, C.	AS-MoM10	37 119	PETTENKOFER, C.	EMSS-ThM11	93 279	RABALAIS, J.W.	TFVM-ThM5	93 280
PAPARAZZO, E.	TF-ThP9	106 313	PFANNKUCHEN, B.	PS-MoP13	50 155	RABALAIS, J.W.	TF-WeP11	89 263
PAPPAS, D.P.	NS2-TuM8	53 169	PHANEUF, R.J.	SSEM-WeA10	83 243	RABALAIS, J.W.	SS2-MoM9	36 116
PARDO, F.D.	NS2-TuM8	53 169	PHANEUF, R.J.	SS1-TuM5	52 163	RABALAIS, J.W.	AS-MoM4	37 118
PARIKH, A.N.	NS1-FrM3	109 321	PHANG, Y.H.	NS1-MoA8	43 130	RADING, D.	AS-WeM7	74 224
PARIKH, A.N.	SSEM-WeA10	83 243	PHANG, Y.H.	SS1-TuM3	52 163	RADING, D.	AS-TuP8	68 207
PARIKH, S.A.	SS2-ThA3	98 288	PHILLIPS, V.	PS-WeP16	88 261	RADING, D.	PS-MoM11	38 121
PARIKH, S.A.	PS-WeP3	88 259	PICCOLI, B.	EM-ThM7	94 281	RADZIMSKI, Z.J.	SSEM-WeA5	83 243
PARK, K.-H.	NS-WeP19	87 257	PICCHOTTO, E.A.	SS-WeP27	86 254	RAGHAVACHARI, K.	NS2-MoA9	43 132
PARK, K.-Y.	EM-TuP7	69 212	PICKERING, C.	EM-ThM4	94 281	RAHEEM, A.R.	EM-MoM4	39 124
PARK, S.-J.	PS-WeP3	88 259	PICKERING, H.W.	SS-WeP28	86 254	RAHEEM, A.R.	BI-MoP8	51 161
PARK, S.-J.	PS-MoA10	44 135	PICKERING, H.W.	SS-MoP7	48 145	RAIKAR, G.N.	SS1-FrM3	108 317
PARK, S.J.	TFVM-MoA6	45 138	PICOZZI, P.	TF-WeM3	75 228	RAINER, D.R.	EM-WeM4	76 229
PARKER, D.H.	AS-FrM9	110 325	PICRAUX, S.T.	PS1-ThA8	100 295	RAISANEN, A.D.	VT-MoA10	45 137
PARKINSON, B.A.	NS-WeP20	87 257	PIERCE, D.T.	SS1-TuM11	52 164	RAKHOVSKY, V.I.	VM-FrM8	111 330
PARKINSON, B.A.	NS-WeP7	87 255	PIERCE, D.T.	SS1-WeM0	72 218	RAKHOVSKY, V.I.	AS-WeA10	82 240
PARKINSON, B.A.	EMSS-ThM11	93 279	PING, A.T.	EM-WeA10	84 247	RAKHOVSKY, V.I.	AS-TuP21	68 209
PARKS, D.C.	NS-ThP9	104 305	PIPER, J.D.	NS1-FrM5	109 321	RAMAN, S.N.	AS-TuP7	68 207
PARSONS, G.N.	MS-WeA7	84 247	PIREAU, J.-J.	SS1-FrM8	108 318	RAMASWAMY, G.	EM-MoA8	46 140
PARTHASARATHY, R.V.	BI-MoP15	51 162	PIREAU, J.-J.	TF-WeA6	83 245	RAMÍREZ-FLORES, G.	EM-TuP21	69 214
PASCUAL, J.I.	NS2-ThM1	91 272	PISCCEVIC, D.	BI-TuM3	57 179	RANDALL, J.N.	NS2-MoA3	43 131
PASSACANTANDO, M.	TF-WeM3	75 228	PISCHOW, K.A.	AS-TuP15	68 208	RANDALL, J.N.	NS2-TuM1	53 168
PATE, B.B.	SS-MoP39	48 149	PISCHOW, K.A.	NS-WeP21	87 257	RANGARAJAN, S.P.	PS-MoA8	44 135
PATE, B.B.	EM-TuP24	69 215	PISTOL, M.-E.	NS-TuP9	67 204	RAO, B.U.M.	SS-MoP17	48 146
PATEL, S.H.	MS-WeA3	84 247	PITTAL, S.	MS-TuP5	70 216	RAO, M.G.	VT-MoP4	51 158
PATHANGEY, B.	NS-TuP8	67 204	PITTAL, S.	EM-ThM6	94 281	RAO, M.G.	VT-TuM2	55 173
PATON, A.	SS2-MoM10	36 117	PITTAL, S.	TF-FrM1	110 326	RAO, M.G.	VT-TuM7	55 174
PATRICK, D.L.	AS-ThM9	92 275	PITTS, E.C.	NS1-TuM10	53 168	RAO, M.G.	VT-TuM6	55 174
PATRICK, D.L.	NS-WeP3	87 255	PITTS, G.E.	MS-TuM1	56 178	RASHAP, B.	MSVT-ThA6	102 301
PATTERSON, B.M.	VM-ThM6	95 284	PLASS, R.	SS2-FrM2	108 319	RASMUSSEN, P.B.	SS1-MoM10	36 115
PAUL, A.J.	AS-ThA4	100 293	PLETH NIELSEN, L.	SS2-TuA8	60 184	RASTAGAR, F.	VM-ThA1	103 302
PAUL, O.	VT-MoM7	38 122	PLUMMER, E.W.	NS-TuP16	67 205	RATHMAN, D.	NS1-TuA2	61 186
PAULSON, T.E.	AS-WeA6	82 239	PLUMMER, E.W.	SS2-ThM3	90 269	RATNER, B.D.	AS-ThA3	100 293
PAULSON, T.E.	AS-TuM11	54 171	PLUMMER, E.W.	SS2-ThA8	98 289	RATNER, B.D.	BI-MoP13	51 162
PEALE, D.R.	SS2-TuA1	60 183	POELSEMA, B.	SS2-FrM11	108 320	RATNER, B.D.	BI-MoP10	51 161



Author		Prog. Abst.			Prog. Abst.			Prog. Abst.			
		Pg. #	Pg. #		Pg. #	Pg. #		Pg. #	Pg. #		
RATNER, B.D.	BI-TuM7	57	180	RODAHL, M.	BI-TuM9	57	180	SAKURAI, T.	SS2-MoA6	42	128
RATNER, B.D.	BI-MoP9	51	161	RODRIGUEZ, J.A.	SS2-ThM7	90	269	SAKURAI, T.	SS-WeP28	86	254
RATNER, B.D.	NSBI-ThM1	91	270	ROELOFS, L.D.	SS2-ThA9	98	289	SAKURAI, T.	SS-MoP7	48	145
RATNER, C.D.	BI-MoA9	47	143	ROESCHER, A.	NS1-TuM9	53	167	SAKURAI, T.	SS2-MoM11	36	117
RAU, C.	SS1-WeM3	72	218	ROGERS, J.L.	EM-TuP4	69	211	SALANON, B.	SS2-ThA7	98	289
RAU, C.	SS1-WeA4	80	233	ROGERS, JR., J.W.	EM-ThP23	105	311	SALDI, F.	AS-MoM1	37	118
RAU, C.	SS-WeP11	86	251	ROGERS, JR., J.W.	EM-WeA5	84	246	SALEH, A.A.	SS-TuP18	66	201
RAUPP, G.B.	EM-TuP25	69	215	ROGNLIEN, T.D.	PS-MoP20	50	157	SALLING, C.T.	NS2-WeM1	73	222
RAUPP, G.B.	MS-TuM11	56	179	ROHDE, S.L.	VM-ThM2	95	284	SALMERON, M.	AS-TuP12	68	208
RAUSCHER, H.	NS2-WeM6	73	223	ROHL, A.L.	NS-TuP14	67	205	SALMERON, M.	SS2-ThM8	90	269
RAVEH, A.	TF-ThP16	106	314	ROHL, A.L.	NS2-TuA1	61	186	SALMERON, M.	SS2-MoM8	36	116
RAY-CHAUDHURI, A.K.	EM-ThP6	105	309	RONK, W.R.	SS1-TuA8	60	183	SALMERON, M.	NS2-FrM4	109	323
REASS, W.A.	VM-ThM9	95	285	ROOKE, M.A.	AS-TuP27	68	210	SALMERON, M.	SS-WeP5	86	250
REBHOLZ, C.	VM-FrM5	111	329	ROOKS, M.	NS2-TuM8	53	169	SALMERON, M.	NS2-TuA5	61	187
REBHOLZ, C.	VM-FrM2	111	329	ROOKS, M.J.	MS-TuP8	70	217	SALMERON, M.	EM-ThP5	105	308
REDINBO, G.F.	NS2-TuM8	53	169	ROOS, K.	SS2-TuA3	60	183	SALMERON, M.	SS-WeP14	86	251
REIBOLD, B.	PS-WeP21	88	261	ROSE-PEHRSSON, S.L.	TF-ThP19	106	315	SALMERON, M.B.	AS-ThM7	92	275
REICHERT, A.	BI-TuA7	65	197	ROSÉN, A.	SS2-WeM8	72	220	SALOKATVE, A.	EM-WeM0	76	229
REICHLMAIER, S.	AS-MoM3	37	118	ROSENBERG, R.A.	VT-TuA6	63	192	SAMANT, M.G.	TF-ThP6	106	313
REINERMANN, M.	NS-ThP4	104	304	ROSENFELD, G.	SS2-TuA2	60	183	SAMARSKY, E.A.	NS-WeP26	87	258
REINHOUDT, D.N.	NS1-MoM3	37	117	ROSOLEN, G.	NS-MoP11	49	151	SAMORI, B.	NSBI-ThM7	91	271
REJ, D.J.	VM-ThM10	95	285	ROSSIN, V.V.	EM-ThP9	105	309	SAMPSON, D.L.	NS-WeP7	87	255
REJ, D.J.	VM-ThM9	95	285	ROSSNAGEL, S.M.	PS-MoM10	38	121	SAMPSON, R.	MS-ThM10	94	283
REJ, D.J.	VM-ThM7	95	284	ROSSNAGEL, S.M.	TFVM-ThM8	93	280	SAMUELSON, L.	NS-TuP9	67	204
REKESH, D.	NSBI-ThM5	91	271	ROSSNAGEL, S.M.	PS-MoM8	38	121	SANCHEZ, J.	PS-WeP20	88	261
REN, F.	EM-ThA3	102	299	ROTENBERG, E.	AS-MoM7	37	119	SÁNCHEZ-QUESADA, F.	TF-ThA6	101	298
REN, F.	PS-MoP15	50	156	ROTENBERG, E.	EM-FrM5	111	328	SANDELL, A.	SS1-FrM10	108	318
REN, F.	EM-TuP5	69	212	ROTH, W.C.	MS-WeM8	76	231	SANDELL, A.	SS1-FrM5	108	317
RENDELL, R.W.	NS2-TuM4	53	169	RÖTTGER, B.	SS-MoP31	48	148	SANDLER, N.P.	MS-TuA9	64	196
RENKEN, J.	BINS-WeM5	77	232	ROUAUD, C.	NP-WeP2	89	266	SANJINÉS, R.	SS1-MoA8	42	127
RENKEN, J.	NSBI-ThA4	99	290	ROUGHANI, B.	EM-FrM3	111	328	SANKEY, O.F.	NS1-TuA1	61	185
REPPHUN, G.	ASSS-TuA4	62	188	ROUSSEAU, A.-C.	TF-ThP22	106	315	SANSONNENS, L.	PS-WeA6	82	241
RETTNER, C.T.	SS1-TuA1	60	182	ROWE, J.E.	NS2-FrM11	109	324	SANTAMARIA, J.	TF-ThA6	101	298
REUTT-ROBEY, J.E.	SS1-ThA2	98	286	ROWE, J.E.	SS-MoP4	48	144	SANTOS, P.F.	EM-MoA4	46	139
REVAY, R.	TF-WeP5	89	262	ROY, D.	SS2-MoA3	42	128	SANTUCCI, S.	TF-WeM3	75	228
REYNOLDS, J.	SS1-TuM9	52	164	ROY, R.A.	TF-WeP22	89	265	SAPIETA, J.	MS-ThM8	94	283
RHOADES, R.L.	PS-MoP10	50	155	RUAN, L.	SS-WeP3	86	250	SAPROO, A.	PS-TuA10	62	191
RHOADES, R.L.	PS-MoM8	38	121	RUBEL, M.	PS-WeP16	88	261	SARASWAT, K.C.	PS1-ThA9	100	296
RICCO, A.J.	TF-TuM3	55	175	RUBEL, S.	NS-ThP12	104	305	SARASWAT, K.C.	MS-MoA7	46	141
RICCO, A.J.	EM-MoM8	39	124	RUBINSTEIN, I.	NS1-MoA1	43	129	SARDELA, JR., M.R.	TF-ThP14	106	314
RICE, J.E.	VT-TuM11	55	175	RUBLOFF, G.W.	MS-TuA10	64	196	SARID, D.	NS1-FrM11	109	322
RICE, P.	NS-MoP9	49	151	RUBLOFF, G.W.	MS-WeA7	84	247	SARTORE, L.	AS-ThA4	100	293
RICHARDS, A.C.	VM-FrM4	111	329	RUDMAN, M.	NS1-FrM4	109	321	SARTWELL, B.	VM-ThA1	103	302
RICHARDS, M.R.	VM-FrM4	111	329	RUDNICK, P.	VM-ThA1	103	302	SASAKI, F.	EM-ThM9	94	282
RICHARDSON, N.V.	SS1-ThA10	98	287	RUDNIK, P.J.	TF-WeP14	89	264	SASAKI, I.	PS-TuA9	62	191
RICHARDSON, N.V.	SS1-MoM9	36	115	RUDOLF, P.	SS1-FrM8	108	318	SASAKI, Y.T.	VT-MoA6	45	136
RICHTER, C.A.	EM-FrM3	111	328	RUDOLPH, F.	VT-MoA5	45	136	SATER, J.	PS-WeP20	88	261
RICHTER, H.H.	EM-ThM8	94	281	RUDOLPH, M.	NS1-FrM6	109	321	SATO, H.	TF-ThA10	101	299
RICKERT, J.	BI-TuA9	65	197	RUEBUSH, S.D.	AS-WeM4	74	224	SATOH, T.	TF-WeM8	75	229
RIEGER, D.J.	PS-WeA5	82	241	RUGAR, D.	NS2-FrM9	109	323	SAUER, D.E.	SS2-WeA4	80	235
RIEGER, D.J.	EM-MoM8	39	124	RUGAR, D.	NS2-FrM7	109	323	SAULT, A.G.	AS-TuM3	54	170
RIEGER, D.J.	EM-ThP2	105	308	RUGAR, D.	NSMS-WeM5	73	221	SAULT, A.G.	SS-MoP23	48	147
RIEMANN, R.-E.	NS-WeP4	87	255	RUHE, J.	BINS-WeM1	77	231	SAUTET, P.	SS-WeP5	86	250
RIETMAN, E.A.	MS-WeA3	84	247	RUIZ, F.	TF-ThP11	106	314	SAVINOV, S.	NS-TuP21	67	206
RING, Z.	TFVM-MoA5	45	138	RUIZ, F.	NS-TuP11	67	204	SAWIN, H.H.	PS1-ThA6	100	295
RINGLE, M.D.	EM-WeM0	76	229	RULLE, H.	AS-TuM4	54	170	SAWIN, H.H.	PS-MoP17	50	156
RINNEMO, M.	SS2-ThM10	90	270	RUMANER, L.E.	SS2-MoA8	42	128	SAWIN, H.H.	EM-TuP8	69	212
RIOUX, D.	EM-ThP26	105	312	RUSHMEIER, H.E.	AS-ThM5	92	274	SAWIN, H.H.	EMMS-TuM6	56	177
RISHTON, S.A.	NS-MoP24	49	153	RUSSELL, N.	SS-TuP28	66	202	SAWIN, H.H.	PS-ThM1	92	276
RISTOLAINEN, E.O.	NS-WeP21	87	257	RUSSELL, P.E.	NSBI-ThA9	99	291	SCALETAR, R.	SS-WeP15	86	252
RITTER, G.	EM-ThM8	94	281	RUSSELL, P.E.	NS-ThP5	104	304	SCARMOZZINO, R.	EM-ThA4	102	299
RITTER, M.	SS2-MoM6	36	116	RUSSELL, JR., J.N.	SS-TuP27	66	202	SCHAEFER, D.M.	NS-MoP3	49	150
ROBBIE, K.	TF-WeA5	83	244	RUSSELL, JR., J.N.	SS-WeP19	86	252	SCHAEFER, D.M.	NS-MoP4	49	150
ROBBINS, D.J.	EM-ThM4	94	281	RUZIC, D.N.	PS-WeM2	74	225	SCHAEFER, D.M.	NS2-TuA7	61	187
ROBERSON, R.W.	BINS-WeM7	77	232	RUZIC, D.N.	PS1-ThA10	100	296	SCHAEFER, H.-E.	NS1-TuM3	53	167
ROBERTS, C.J.	NSBI-ThM10	91	272	RUZIC, D.N.	PS-MoP7	50	154	SCHAFF, J.E.	SS-TuP5	66	198
ROBERTS, C.J.	BI-TuM4	57	180	RYABAKON, V.N.	NS-ThP10	104	305	SCHATZ, K.D.	PS-WeM2	74	225
ROBERTS, C.J.	NSBI-ThM8	91	271	RYDING, D.	VT-TuA6	63	192	SCHAUMBURG, K.	NS1-TuM2	53	167
ROBERTS, C.J.	NS2-MoA4	43	131	RYDING, D.	VT-TuA7	63	192	SCHIEFFLER, M.	SS2-MoM4	36	116
ROBERTS, J.T.	EM-ThP25	105	312	RYE, R.R.	EM-MoM8	39	124	SHELL, J.	VM-ThA1	103	302
ROBERTS, J.T.	SS-TuP4	66	198	RYE, R.R.	AS-ThA10	100	294	SHELLIN, R.	TF-WeP8	89	263
ROBERTS, J.T.	SS-TuP5	66	198	RYZHIKOV, I.A.	NS-ThP14	104	306	SCHERTEL, A.	AS-ThM4	92	274
ROBERTS, P.M.	BI-MoP3	51	160	SACK, N.J.	SS-TuP2	66	198	SCHUEUR, J.T.	PS-MoP11	50	155
ROBERTS, R.H.	SS-WeP6	86	250	SACULLA, M.	PS-WeP19	88	261	SCHUEUR, J.T.	PS-WeP5	88	259
ROBERTSON, B.	VM-ThM2	95	284	SAENGER, K.L.	TF-WeP22	89	265	SCHUEUR, J.T.	VM-ThM9	95	285
ROBEY, S.W.	TF-WeP5	89	262	SAFRON, S.A.	SS-MoP26	48	147	SCHIERBAUM, K. D.	NS1-MoM3	37	117
ROBINS, L.H.	TFVM-TuA5	63	193	SAID, R.A.	NS2-FrM3	109	323	SCHLAF, R.	EMSS-ThM11	93	279
ROBINSON, I.K.	EM-MoA7	46	140	SAITOH, K.	VT-TuA3	63	191	SCHLAF, R.	EM-ThP21	105	311
ROBINSON, S.J.	SS1-FrM11	108	318	SAKA, H.	NS-ThP23	104	307	SCHMALZ, A.	SS2-MoM4	36	116
ROCCA, M.	SS1-TuA2	60	182	SAKAI, I.	MS-TuP3	70	216	SCHMID, A.	NP-WeP5	89	266
ROCHEFORT, A.P.	SS-WeP25	86	253	SAKATA, T.	SS2-MoM11	36	117	SCHMIDT, G.	NS1-FrM6	109	321
ROCKETT, A.	TF-ThA5	101	298	SAKTHIVEL, P.	VM-ThM1	95	284	SCHMIEDER, R.W.	NS-ThP9	104	305
RODAHL, M.	BI-TuA10	65	197	SAKUMOTO, K.	NS-MoP12	49	151	SCHMIEG, S.J.	SS2-WeM0	72	219

Author		Prog. Abst.		Prog. Abst.		Prog. Abst.		Prog. Abst.
		Pg. # Pg. #		Pg. # Pg. #		Pg. # Pg. #		Pg. # Pg. #
SCHMIEG, S.J.	SS-MoP15	48 146	SHAKESHEFF, K.M.	BI-TuM4	57 180	SIMONS, D.S.	TF-WeP5	89 262
SCHMIEG, S.J.	AS-TuP22	68 209	SHAKESHEFF, K.M.	NS2-MoA4	43 131	SIMPSON, P.	NS2-TuM8	53 169
SCHMIEG, S.J.	SS2-WeM2	72 219	SHALIGINA, E.E.	TF-WeP6	89 262	SIMPSON, W.C.	SSEM-WeM3	75 227
SCHMITZ, F.	SS-TuP8	66 199	SHANNON, C.	NS2-ThM8	91 273	SINCLAIR, M.B.	PS-MoA6	44 135
SCHNABEL, P.	SS1-MoM1	36 114	SHARD, A.	NSBI-ThM10	91 272	SINGER, I.L.	VM-FrM1	111 329
SCHNEIDER, J.	VM-FrM5	111 329	SHARD, A.G.	AS-ThA4	100 293	SINGH, R.	SS-WeP15	86 252
SCHNEIDER, J.M.	VM-FrM2	111 329	SHAREEF, I.	MS-TuA10	64 196	SINGH, S.	EM-ThP6	105 309
SCHNEIDER, W.	VT-TuM6	55 174	SHAREEF, I.	MS-WeA7	84 247	SINHA, A.K.	EM-MoM6	39 124
SCHNEIR, J.	NS-MoP19	49 152	SHAW, D.M.	PS-TuA6	62 190	SINNOTT, S.B.	NS2-ThM3	91 272
SCHOER, J.K.	SS1-ThM10	90 268	SHCHEGLOV, K.V.	EM-ThA5	102 300	SITZ, G.O.	SS-MoP2	48 144
SCHOLL, R.A.	VM-ThM11	95 285	SHCHEMELININ, A.	NS1-FrM4	109 321	SKALA, S.L.	EM-MoA1	46 139
SCHOLTEN, R.E.	NS2-WeM7	73 223	SHEDD, G.M.	NSBI-ThA9	99 291	SKALA, S.L.	EM-ThA6	102 300
SCHOMMERS, W.	SS-MoP24	48 147	SHEDD, G.M.	NS-ThP5	104 304	SKELTON, D.C.	SS1-TuA9	60 183
SCHOMMERS, W.	NS-WeP12	87 256	SHEEN, C.W.	NS2-TuM8	53 169	SKOFRONICK, G.L.	NS-TuP5	67 203
SCHÖNNENBERGER, C.	NS2-WeM5	73 223	SHEEN, C.W.	NS1-FrM3	109 321	SKOFRONICK, J.G.	SS-MoP26	48 147
SCHOTT, M.	PS-MoP13	50 155	SHEIKO, S.	NS1-FrM8	109 321	SKORUPA, W.	TF-ThP8	106 313
SCHOTT, M.	PS-TuA7	62 190	SHELDON, P.	TF-WeP7	89 263	SKUBA, J.	NP-WeP7	89 266
SCHOWALTER, L.J.	EM-MoA8	46 140	SHELDON, P.	EM-ThP4	105 308	SKVARLA, M.	MS-TuP7	70 217
SCHRAM, D.C.	PS-MoA9	44 135	SHEN, T.-C.	SS2-TuM8	52 166	SLINKMAN, J.	NSMS-WeM7	73 221
SCHRAM, D.C.	PS-MoP1	50 153	SHEN, T.-C.	NS-ThP25	104 307	SLOAN, D.	SS-TuP22	66 201
SCHRÖDER, U.	SS2-ThM8	90 269	SHEN, T.C.	SS2-FrM4	108 319	SLOAN, D.	SS-TuP21	66 201
SCHROEDER, D.	TF-ThA5	101 298	SHEN, Y.G.	SS-WeP6	86 250	SLOAN, D.W.	SSEM-WeM5	75 227
SCHROEN-CAREY, D.	PS-WeP21	88 261	SHEN, Y.G.	SS-TuP19	66 201	SLOAN, J.T.	SS1-MoM5	36 114
SCHUKAREV, A.V.	NS-WeP16	87 256	SHEN, Y.G.	SS-MoP34	48 148	SLOAN, L.R.	EM-MoM8	39 124
SCHULMAN, E.N.	NS1-TuA5	61 185	SHERWOOD, P.M.A.	AS-TuP27	68 210	SLUSHER, R.E.	EM-TuP5	69 212
SCHULTZ, A.	TF-WeP19	89 265	SHESHIN, E.P.	NS-ThP18	104 306	SMITH, A.R.	NS1-TuA6	61 186
SCHULTZ, J.A.	TF-ThP3	106 312	SHEVLYUGA, V.M.	NS-MoP20	49 152	SMITH, B.B.	SS-TuP1	66 198
SCHULTZ, J.A.	TF-FrM3	110 326	SHI, J.	NS-TuP13	67 205	SMITH, J.A.	VT-MoP4	51 158
SCHULTZ, P.A.	NS1-TuM1	53 166	SHI, X.	SS1-TuM1	52 163	SMITH, N.V.	NS2-FrM11	109 324
SCHWANER, A.	SS-TuP22	66 201	SHI, Y.	NS-WeP1	87 254	SMITH, P.C.	PS1-ThA10	100 296
SCHWANER, A.L.	SS1-MoM7	36 114	SHI, Z.	AS-ThM10	92 275	SMITH, R.J.	SS-TuP18	66 201
SCHWANK, J.W.	TF-TuM8	55 176	SHIBAEV, P.V.	NS1-TuM2	53 167	SMITH, R.S.	SS-TuP3	66 198
SCHWANK, J.W.	SS-WeP20	86 253	SHIBATA, A.	VT-MoP10	51 159	SMITH, R.S.	SS2-WeA10	80 235
SCHWANK, J.W.	SS1-MoA5	42 126	SHIH, A.	SS2-ThA2	98 288	SMITH, W.L.	AS-FrM6	110 325
SCHWANK, J.W.	TF-ThP21	106 315	SHIH, C.K.	NS1-TuA6	61 186	SMOLINSKI, C.C.	MS-WeM1	76 230
SCHWARZ, U.D.	NS2-ThA8	99 292	SHIH, M.C.	EM-ThA4	102 299	SMY, T.	TF-WeA5	83 244
SCHWARZ, U.D.	NS-ThP11	104 305	SHIH, Y.C.	NS1-TuA6	61 186	SNAUWAERT, J.	NSMS-WeM3	73 221
SCHWENK, H.	TFVM-MoA4	45 137	SHIMADA, M.	PS-MoM9	38 121	SNEH, O.	SSEM-WeA1	83 242
SCOGGINS, T.B.	SS-WeP24	86 253	SHIMIZU, D.	NSMS-WeM8	73 222	SNIJKERS, R.J.M.M.	PS-WeM7	74 226
SCOTT, M.	VM-ThM6	95 284	SHIMIZU, R.	AS-WeA4	82 239	SNITKA, V.	NS-MoP6	49 150
SEABAUGH, A.	EM-MoA1	46 139	SHIN, J.-K.	NS-WeP19	87 257	SNOW, K.	TF-TuM6	55 175
SEAH, M.P.	AS-MoA1	44 132	SHINAGAWA, K.	PS-ThM5	92 276	SNYDER, P.G.	EM-ThM6	94 281
SEAL, S.	AS-MoA9	44 134	SHINJO, K.	NS2-ThA1	99 291	SOAVE, R.J.	TF-WeA4	83 244
SEAL, S.	AS-TuM10	54 171	SHINN, M.	TF-WeP20	89 265	SOBOL, P.E.	AS-ThA1	100 293
SEARS, M.P.	NS1-TuM1	53 166	SHINN, N.D.	SS1-FrM4	108 317	SOBOLEWSKI, M.A.	MS-TuP6	70 216
SEAWARD, K.L.	PS-MoA7	44 135	SHINN, N.D.	SS1-FrM2	108 317	SOH, H.	NS2-FrM8	109 323
SEE, A.K.	SS1-WeM4	72 218	SHINN, N.D.	SS1-ThA9	98 287	SOHE, G.R.L.	EM-ThM1	94 280
SEEBAUER, E.G.	EMSS-ThM7	93 278	SHINOHARA, H.	SS-MoP7	48 145	SOKOLOV, I.Y.	NS-MoP16	49 152
SEEBAUER, E.G.	SS-WeP21	86 253	SHINTANI, T.	NS2-ThM10	91 273	SOLOMON, G.M.	VT-MoA3	45 136
SEEBAUER, E.G.	SSEM-WeA8	83 243	SHIOZAWA, K.	PS-MoM7	38 120	SOMMA, F.	TF-WeM3	75 228
SEEGER, S.	BI-MoP14	51 162	SHIRAKI, Y.	EM-TuA9	64 195	SOMORJAI, G.A.	SS2-ThM8	90 269
SEEGER, S.	BINS-WeM5	77 232	SHIU, S.H.	EM-TuP14	69 213	SOMORJAI, G.A.	SS2-MoM6	36 116
SEGALL, I.	AS-FrM1	110 324	SHIU, S.H.	EM-TuP15	69 213	SOMORJAI, G.A.	SS2-ThA10	98 289
SEGO, S.	EM-TuP14	69 213	SHLUGER, A.L.	NS-TuP14	67 205	SOMORJAI, G.A.	NS2-ThA6	99 292
SEGO, S.	EM-TuP15	69 213	SHLUGER, A.L.	NS2-TuA1	61 186	SON, G.-A.	SS-MoP11	48 145
SEIPLE, J.V.	EM-ThP20	105 311	SHOHET, J.L.	PS-MoP2	50 153	SONG, H.J.	NS-ThP15	104 306
SEKINE, M.	MS-TuP3	70 216	SHOHET, J.L.	PS-WeP15	88 260	SONG, X.	SS2-MoA10	42 129
SEKINE, S.	VT-MoP3	51 158	SHOJI, F.	TF-ThP5	106 313	SONOHARA, H.	TF-WeP9	89 263
SEKINE, S.	VT-MoM11	38 123	SHON, J.W.	PS-TuM7	54 172	SONOHARA, H.	TF-ThA10	101 299
SELINDER, T.I.	TF-ThP14	106 314	SHORROSH, R.	NS1-TuM10	53 168	SORBA, L.	EM-WeM4	76 229
SELWYN, G.S.	MS-WeM5	76 231	SHOVLIN, J.D.	TF-ThP12	106 314	SORIA, F.	SS-WeP13	86 251
SELWYN, G.S.	MS-MoA6	46 141	SHRIVER-LAKE, L.C.	BI-TuA5	65 197	SOUTHWELL, R.P.	EMSS-ThM7	93 278
SELWYN, G.S.	MS-WeM7	76 231	SHU, D.	VT-TuA6	63 192	SOUTHWELL, R.P.	SS-WeP21	86 253
SEMANCIK, S.	SS1-MoA3	42 126	SHUFFLEBOTHAM, P.K.	MS-MoA5	46 141	SOWA, M.J.	PS-TuA1	62 190
SEMENDY, F.	EM-WeA1	84 245	SHUGRUE, J.K.	MS-TuA9	64 196	SPAGNOL, M.	VT-TuM8	55 174
SEMOND, F.	SS2-MoA3	42 128	SHUH, D.K.	TF-ThP6	106 313	SPANOS, L.	EM-FrM9	111 328
SENFT, D. COWELL	SS2-TuA10	60 185	SHUL, R.J.	PS-WeA5	82 241	SPATZ, J.P.	NS1-TuM9	53 167
SERGHINI, S.	TF-ThP10	106 314	SHUL, R.J.	EM-ThP2	105 308	SPENCER, N.D.	AS-TuP11	68 208
SESHADRI, K.	NS-WeP5	87 255	SHUL, R.J.	EM-TuP6	69 212	SPOOL, A.M.	AS-ThA7	100 294
SESSLER, G.	TF-WeP8	89 263	SHUTTHANANDAN, V.	SS-TuP18	66 201	SPORKEN, R.L.	TF-ThP22	106 315
SEUTTER, S.M.	SS2-MoA10	42 129	SHYU, J.	MS-ThM10	94 283	SPRAGUE, J.A.	VM-WeA7	85 249
SEVERENS, R.J.	PS-MoA9	44 135	SHYY, J.G.	VT-MoP7	51 158	SPROUL, W.	TF-WeP18	89 265
SEVERIN, K.G.	TF-TuM5	55 175	SIBENER, S.J.	SS1-ThA4	98 286	SPROUL, W.D.	TFVM-TuA6	63 193
SEVERINI, E.	AS-MoM10	37 119	SICHTERMANN, W.	AS-WeM7	74 224	SPROUL, W.D.	VM-FrM3	111 329
SHA, Y.-G.	NS-TuP1	67 203	SIDERS, J.L.W.	SS-MoP2	48 144	SPROUL, W.D.	TF-WeP15	89 264
SHABALOVSKAYA, S.A.	BI-MoP6	51 160	SIEDLECKI, C.	BI-TuM5	57 180	SPROUL, W.D.	TFVM-TuA7	63 194
SHACHAM-DIAMAND, Y.	TF-WeA4	83 244	SIEGENTHALER, H.	ASSS-TuA5	62 189	SPROUL, W.D.	TF-WeP14	89 264
SHAFAI, C.	NSMS-WeM8	73 222	SILVER, R.M.	NSMS-WeM4	73 221	SPUDICH, J.A.	NSBI-WeA1	81 236
SHAFFER, D.K.	AS-FrM2	110 324	SIM, J.-H.	NS-WeP19	87 227	SRIRAM, T.S.	MS-ThM10	94 283
SHAFFNER, A.E.	BINS-WeM0	77 231	SIMON, M.	SSEM-WeM4	75 227	SROLOVITZ, D.J.	VM-WeA3	85 248
SHAFFNER, A.E.	BI-MoP12	51 162	SIMON NG, K.Y.	SS-MoP15	48 146	STAIR, P.C.	SS2-TuM10	52 166
SHAH, S.I.	TFVM-MoA9	45 138	SIMON NG, K.Y.	SS2-WeM2	72 219	STAMPER, A.K.	PS-WeA2	82 240
SHAKESHEFF, K.M.	NSBI-ThM10	91 272	SIMONS, D.S.	AS-MoA7	44 133			

Author		Prog. Abst.		Prog. Abst.		Prog. Abst.		
		Pg. # Pg. #		Pg. # Pg. #		Pg. # Pg. #		
STAMPFL, C.	SS2-MoM4	36 116	SULLIVAN, D.J.D.	SS-MoP27	48 147	TEDDER, L.L.	MS-WeA7	84 247
STANBERRY, B.J.	PS-TuA8	62 191	SUMETSKII, M.	NS2-TuM5	53 169	TEDDER, L.L.	SS-WeP30	86 254
STANLEY, K.	SS2-TuA3	60 183	SUMOMOGI, T.	NS-WeP14	87 256	TEGENFELDT, J.T.	NSBI-ThA3	99 290
STARK, T.J.	NS-ThP5	104 304	SUN, B.W.	TF-WeP21	89 265	TEICHERT, C.	NS1-MoA8	43 130
STARKE, U.	SS2-MoM6	36 116	SUN, F.	AS-ThM11	92 275	TELFEYAN, R.	MSVT-ThA5	102 301
STARKEY, E.K.	SS2-ThA10	98 289	SUN, Y.-M.	SSEM-WeM5	75 227	TENDLER, S.J.B.	NSBI-ThM10	91 272
STAYTON, P.S.	BI-TuM1	57 179	SUN, Y.-M.	SS-TuP22	66 201	TENDLER, S.J.B.	AS-ThA4	100 293
STECHEL, E.B.	SS2-TuM7	52 165	SUN, Z.-J.	SS-WeP24	86 253	TENDLER, S.J.B.	BI-TuM4	57 180
STECKL, A.J.	NS2-WeA7	81 238	SUNDGREN, J.-E.	VM-WeA1	85 248	TENDLER, S.J.B.	NSBI-ThM8	91 271
STECKL, A.J.	EM-TuP23	69 215	SUNG, M.M.	SS2-MoM9	36 116	TENDLER, S.J.B.	NS2-MoA4	43 131
STECKL, A.J.	EM-TuP20	69 214	SUNG, Y.-E.	SS2-WeA3	80 234	TENGVAL, P.	BI-MoP16	51 162
STEFFEN, H.J.	TF-ThP8	106 313	SUNI, I.I.	SSEM-WeA8	83 243	TEPERMEISTER, I.	PS-TuA2	62 190
STEIERL, G.	SS1-WeM3	72 218	SUPERFINE, R.	NS-ThP6	104 305	TERAOKA, Y.	SSEM-WeA7	83 243
STEIERL, G.	SS1-WeA4	80 233	SURENDRA, M.	MS-WeM5	76 231	TERMINELLO, L.J.	TF-ThP6	106 313
STEINER, A.	TFVM-TuA3	63 193	SURENDRA, M.	MS-MoA6	46 141	TERRIS, B.	NSMS-WeM5	73 221
STEINER, P.A.	SS-TuP26	66 202	SURENDRA, M.	MS-WeM7	76 231	TERSOFF, J.D.	SS1-TuM3	52 163
STEINMAN, D.A.	PS-WeP18	88 261	SURMAN, D.J.	AS-MoM8	37 119	THEIS, W.	SSEM-WeA2	83 242
STENGER, D.A.	BINS-WeM0	77 231	SURMAN, D.J.	AS-WeM6	74 224	THEVUTHASAN, S.	MS-TuP9	70 217
STENGER, D.A.	BI-MoP12	51 162	SURNEV, S.	SS2-MoA2	42 127	THEVUTHASAN, S.	SS-WeP16	86 252
STENGER, D.A.	BI-TuA3	65 196	SUVOROV, A.L.	NS-ThP18	104 306	THEVUTHASAN, S.	SS-WeP15	86 252
STENSGAARD, I.	SS2-TuA8	60 184	SUZUKI, M.	NS-WeP24	87 258	THEVUTHASAN, S.	AS-WeM4	74 224
STENSGAARD, I.	NS2-ThM2	91 272	SUZUKI, M.	NS-MoP18	49 152	THIEL, P.A.	SS2-MoM5	36 116
STENSGAARD, I.	SS-WeP3	86 250	SUZUKI, M.	NS2-MoA7	43 132	THIEL, P.A.	SS-WeP23	86 253
STEPHANAKIS, S.J.	VM-ThM10	95 285	SUZUKI, M.	NS-MoP8	49 151	THIEL, P.A.	SS2-MoM7	36 116
STEPHEN, T.M.	AS-TuP24	68 210	SWAN, A.K.	SS2-TuA4	60 184	THIELEMANN, C.	TF-WeP8	89 263
STEPHENS, R.B.	PS2-ThA3	101 296	SWANSIGER, W.A.	NP-WeP4	89 266	THIEM, T.L.	VM-ThM5	95 284
STEPHENSON, G.B.	SS2-MoA7	42 128	SWARTZENTRUBER, B.S.	SS-TuP12	66 200	THIRY, P.A.	SS1-FrM8	108 318
STEPNIAK, F.	EM-ThP26	105 312	SWARTZENTRUBER, B.S.	SS1-TuM2	52 163	THIRY, P.A.	TF-WeA6	83 245
STERNE, P.A.	SS-WeP17	86 252	SWARTZENTRUBER, B.S.	SS2-FrM1	108 319	THOKALA, R.	EM-TuP23	69 215
STETTER, J.R.	TF-ThP20	106 315	SWINEFORD, R.	TF-ThP9	106 313	THOMAS, D.F.	NS-TuP10	67 204
STEVENS, J.E.	PS-TuA1	62 190	SWISHER, R.L.	VM-ThA5	103 302	THOMAS, R.C.	NS2-TuA8	61 187
STEVENS, J.L.	SS2-TuA7	60 184	SYKES, A.G.	AS-TuP14	68 208	THOMAS, R.C.	AS-FrM10	110 325
STEVENS, P.A.	TF-WeP21	89 265	SYKES, A.G.	NS-WeP1	87 254	THOMAS, V.	SS-WeP20	86 253
STEVENS, R.	BI-TuA7	65 197	SYKES, A.G.	AS-TuP1	68 206	THOMAS III, S.	PS-WeM8	74 226
STEVENSON, P.R.	VM-FrM5	111 329	SYVERSON, W.	EMMS-TuM8	56 178	THOMPSON, M.	VM-ThM7	95 284
STEWART, R.A.	PS-MoP21	50 157	SYVERSON, W.	MS-ThM4	94 282	THOMPSON, M.O.	VM-ThM10	95 285
STICKLE, W.F.	AS-ThA1	100 293	SZANYI, J.	SS1-MoM6	36 114	THOMPSON, P.E.	EM-TuP3	69 211
STICKNEY, J.L.	NS-WeP25	87 258	TA, T.	PS-ThM3	92 276	THOMS, B.D.	SS-MoP25	48 147
STINNETT, J.A.	SS-TuP10	66 199	TA, T.	PS-ThM4	92 276	THOMSON, D.J.	NSMS-WeM8	73 222
STINNETT, R.W.	VM-ThM7	95 284	TABAT, M.D.	VM-ThM3	95 284	THOMSON, D.J.	NS2-FrM3	109 323
STIRNIMAN, M.J.	SS1-ThA4	98 286	TABATA, K.	TF-WeM8	75 229	THOMSON, M.G.R.	NS-MoP24	49 153
STOCKER, R.	NP-WeP5	89 266	TABBAL, M.	EM-ThP3	105 308	THOMSON, R.E.	NS-MoP21	49 153
STÖCKLI, M.P.	NS-ThP9	104 305	TABET, M.F.	TF-WeP16	89 264	THOMSON, R.E.	NS-MoP22	49 153
STOCKMAN, L.	NS2-ThM5	91 273	TAE, H.S.	PS-MoA10	44 135	THORNBURG, N.A.	SS1-MoM5	36 114
STOHR, J.	TF-ThP6	106 313	TAGA, Y.	TF-TuM1	55 175	THORNBURG, N.A.	SS-WeP27	86 254
STOLYAROVA, V.G.	NS-ThP18	104 306	TAHARA, Y.	MS-TuP2	70 216	THÜMMER, C.	AS-ThM4	92 274
STORM, D.F.	SS1-WeA5	80 233	TAHARA, Y.	MS-TuP3	70 216	TIBERIO, R.C.	NS2-TuM8	53 169
STORM, D.F.	SS-WeP18	86 252	TAKAGI, M.	PS2-ThA4	101 297	TIDWELL, C.D.	AS-ThA3	100 293
STORZ, F.G.	EM-TuP12	69 213	TAKAGI, M.	PS2-ThA10	101 297	TIDWELL, C.D.	BI-MoA9	47 143
STRANICK, S.J.	SS-MoP14	48 146	TAKAHASHI, K.	NS1-MoA10	43 131	TIELSCH, B.J.	AS-WeM6	74 224
STRANICK, S.J.	SS-TuP16	66 200	TAKAHASHI, S.	PS1-ThA5	100 295	TIELSCH, B.J.	AS-TuP20	68 209
STRANICK, S.J.	SS2-FrM7	108 320	TAKAMA, T.	VT-MoP8	51 158	TILFORD, C.R.	MSVT-ThA7	102 301
STREET, S.C.	SS-MoP12	48 145	TAKATA, S.	TF-WeP9	89 263	TILFORD, C.R.	VT-MoM4	38 122
STREET, S.C.	SS2-FrM3	108 319	TAKATA, S.	TF-ThA10	101 299	TILLACK, B.	EM-ThM8	94 281
STREETMAN, B.G.	NS1-TuA6	61 186	TAKAYANAGI, A.	NS-WeP15	87 256	TINDALL, C.	SSEM-WeA9	83 243
STREITZ, F.H.	NS2-TuA2	61 187	TAKI, S.	NS-ThP17	104 306	TISON, S.A.	VT-TuA1	63 191
STRINGFELLOW, G.B.	NS-WeP22	87 257	TALIN, A.A.	NS-MoP23	49 153	TLALI, S.	TFVM-MoA5	45 138
STROSCIO, J.A.	SS1-TuM11	52 164	TAMAYO, J.	NSBI-WeA6	81 236	TOBER, E.D.	SS1-WeA10	80 234
STRUNK, C.	NS2-ThM5	91 273	TAMURA, E.	SS-WeP17	86 252	TOBIN, J.A.	PS-MoP11	50 155
STRUNSKUS, T.	AS-ThM4	92 274	TAMURA, H.	PS-TuA9	62 191	TOBIN, J.A.	PS-WeP5	88 259
STRUSNY, H.	AS-MoA6	44 133	TANABE, T.	PS-WeP16	88 261	TOBIN, J.G.	SS1-WeM8	72 219
STULTZ, T.	EM-ThP8	105 309	TANAKA, M.	NS-MoP12	49 151	TOBIN, J.G.	SS-WeP17	86 252
STUMPF, R.	SS1-FrM1	108 317	TANAKA, M.	NS-ThP23	104 307	TOBIN, M.T.	PS2-ThA1	101 296
STUTZ, C.E.	EM-ThP10	105 309	TANG, S.	SS2-FrM10	108 320	TOBIN, R.G.	SS2-ThM2	90 268
STUVE, E.M.	ASSS-TuA1	61 188	TANG, S.L.	NSBI-WeA5	81 236	TOBIN, R.G.	SS1-ThA6	98 287
STUVE, E.M.	SS2-WeA4	80 235	TANGYUNYONG, P.	NS2-TuA8	61 187	TODOROV, S.S.	TFVM-ThM4	93 279
SU, C.-H.	NS-TuP1	67 203	TANGYUNYONG, P.	BI-MoP7	51 161	TODOROV, S.S.	TFVM-ThM5	93 280
SU, J.N.	EM-TuP20	69 214	TANGYUNYONG, P.	AS-ThA10	100 294	TODOROV, S.S.	TF-WeP11	89 263
SU, L.C.	NS-WeP22	87 257	TANI, T.	EM-ThM9	94 282	TOENNIES, J.P.	SS2-FrM6	108 320
SU, W.B.	NS2-ThM11	91 274	TAO, H.-S.	SS1-ThA9	98 287	TOKUMOTO, H.	NS2-TuA10	61 188
SU, W.B.	SS-WeP4	86 250	TAO, N.J.	NS2-TuA9	61 188	TOKUMOTO, H.	NS1-MoA10	43 131
SUDHARSANAN, R.	NS-TuP8	67 204	TAO, N.J.	AS-ThM10	92 275	TOKUMOTO, H.	NS-WeP13	87 256
SUDIT, I.D.	PS-MoP14	50 156	TAO, Y.T.	NS-WeP5	87 255	TOLBERT, L.M.	NS-ThP7	104 305
SUEHLE, J.S.	NSBI-ThA5	99 290	TARLOV, M.	BI-TuM3	57 179	TOLK, N.	EM-ThP8	105 309
SUEHLE, J.S.	SS1-MoA3	42 126	TARLOV, M.J.	TFVM-TuA5	63 193	TOLK, N.H.	NS-TuP7	67 204
SUEMASU, T.	EM-MoA9	46 140	TARLOV, M.J.	AS-ThM5	92 274	TOLOPA, A.M.	TF-WeP17	89 264
SUGAI, H.	PS1-ThA5	100 295	TASCH, A.	SS-TuP28	66 202	TONAMI, K.	ASSS-TuA10	62 189
SUGAI, H.	PS-WeM5	74 226	TASKER, G.W.	TF-WeA4	83 244	TONG, C.	NS-ThP7	104 305
SUGAWARA, Y.	NS1-MoA6	43 130	TAYA, M.	VM-FrM4	111 329	TONG, S.Y.	SS1-WeM8	72 219
SUGAWARA, Y.	NS-MoP1	49 150	TAYLOR, C.E.	AS-FrM1	110 324	TONKYN, R.G.	SS2-TuM5	52 165
SUGAWARA, Y.	NS-WeP24	87 258	TAYLOR, M.E.	VM-WeA8	85 249	TONNER, B.P.	TF-ThP12	106 314
SUGIYAMA, Y.	NS1-MoM6	37 117	TAYLOR, P.A.	SS2-ThM11	90 270	TONNER, B.P.	AS-MoM7	37 119
SUKAMTO, J.P.H.	AS-MoM11	37 119	TEDDER, L.L.	SS-TuP12	66 200	TONNER, B.P.	SS1-WeA6	80 233

Author		Prog. Abst.				Prog. Abst.					Prog. Abst.				
		Pg. #	Pg. #			Pg. #	Pg. #				Pg. #	Pg. #			
TONUCCI, R.J.	NS-ThP13	104	306	VAN DUYN, R.P.	SS1-ThM5	90	267	WALLACE, R.M.	AS-ThM8	92	275				
TOPRAC, A.	EM-MoM7	39	124	VAN HAESSENDONCK, C.	NS2-ThM5	91	273	WALTER, K.C.	VM-ThM9	95	285				
TÖRNQVIST, E.	SS2-ThM11	90	270	VAN HARDEVELD, R.M.	SS-MoP6	48	144	WAMBACH, J.	SS1-MoM10	36	115				
TORR, D.	TF-WeM2	75	228	VAN HOVE, M.A.	SS2-MoM6	36	116	WAN, C.T.	VM-ThA5	103	302				
TORRES-DELGADO, G.	NS-TuP11	67	204	VAN HOVE, M.A.	SS2-ThA10	98	289	WANDELT, K.	SS-WeP6	86	250				
TOUGAW, P.D.	NS2-TuM3	53	168	VAN HOVE, M.A.	SS-WeP16	86	252	WANG, C.	NS-WeP4	87	255				
TOWNSEND, S.	AS-TuP1	68	206	VAN HOVE, M.A.	SS1-WeM7	72	219	WANG, C.	SS2-TuM8	52	166				
TOYODA, H.	PS1-ThA5	100	295	VAN HOVE, M.A.	AS-WeM4	74	224	WANG, C.	NS-ThP25	104	307				
TRÄGER, F.	TF-FrM9	110	327	VAN HOVE, M.A.	SS-WeP14	86	251	WANG, C.	SS2-FrM4	108	319				
TRAMMEL, P.S.	PS-MoM3	38	120	VAN IJENDOORN, L.J.	SS-MoP6	48	144	WANG, C.S.	NS-TuP12	67	204				
TRAN, T.T.	SS1-ThA1	98	286	VAN NOSTRAND, J.E.	SS2-MoA9	42	129	WANG, D.	NS-ThP16	104	306				
TRAN, T.T.	TF-ThP1	106	312	VAN NOSTRAND, J.E.	SS1-TuM4	52	163	WANG, D.J.	VT-MoP7	51	158				
TRAN, T.T.	EM-ThP23	105	311	VAN OOI, W.J.	AS-FrM1	110	324	WANG, E.	NS-WeP8	87	255				
TREGLIO, J.R.	TF-WeP23	89	265	VAN PATTEN, P.G.	NS-MoP13	49	151	WANG, H.	SS2-ThM2	90	268				
TRENARY, M.	SS1-MoM8	36	115	VAN PATTEN, P.G.	NS1-FrM7	109	321	WANG, J.	SS2-WeA5	80	235				
TREXLER, J.	EM-WeM3	76	229	VAN SANTEN, R.A.	SS-MoP13	48	145	WANG, J.	SS2-ThA8	98	289				
TREXLER, J.T.	EM-TuP19	69	214	VAN SANTEN, R.A.	SS2-WeM1	72	219	WANG, K.L.	NS-ThP16	104	306				
TRINGIDES, M.C.	SS1-TuA10	60	183	VAN SKIKE, T.	VM-ThA9	103	303	WANG, L.	NS-ThP2	104	304				
TRINGIDES, M.C.	SS2-TuA3	60	183	VAN ZEE, H.	SS-WeP6	86	250	WANG, L.	SS2-WeA7	80	235				
TROIANOVSKII, A.M.	NS-WeP17	87	257	VAN ZYL, B.	AS-TuP24	68	210	WANG, L.-Q.	ASSS-TuA7	62	189				
TROUP, A.P.	VT-MoP2	51	157	VANDERVORST, W.	NSMS-WeM3	73	221	WANG, P.W.	SS-WeP29	86	254				
TROWBRIDGE, T.	EM-MoM3	39	123	VANDYSHEV, J.V.	NS2-WeA5	81	238	WANG, X.	TFVM-ThM6	93	280				
TRUONG, C.M.	TF-ThP13	106	314	VANHOMMERIG, M.J.H.	AS-TuM8	54	171	WANG, X.-D.	SS-MoP7	48	145				
TSAL, R.	EMMS-TuM8	56	177	VANZETTI, L.	EM-WeM4	76	229	WANG, X.-D.	NS-ThP12	104	305				
TSAL, R.	MS-ThM4	94	282	VAREKAMP, P.R.	SSEM-WeM3	75	227	WANG, X.-S.	EMSS-ThM1	93	277				
TSAL, T.	TF-WeP13	89	264	VARGHESE, R.	MS-TuM11	56	179	WANG, Y.	SS-TuP9	66	199				
TSAL, T.	TF-ThA3	101	298	VARGO, T.G.	BINS-WeM6	77	232	WANG, Y.	EMSS-ThM2	93	277				
TSAL, W.	PS-WeP7	88	259	VARHUE, W.J.	EM-TuP4	69	211	WANG, Y.	SS1-ThA7	98	287				
TSAL, L.	NS-ThP16	104	306	VASILYEV, L.A.	AS-WeA10	82	240	WANG, Y.B.	VM-FrM3	111	329				
TSANG, W.	NSMS-WeM4	73	221	VASILYEV, L.A.	AS-TuP21	68	209	WANG, Y.C.	AS-TuP28	68	210				
TSONG, I.S.T.	SS-MoP31	48	148	VASSILERIS, V.	TF-ThP7	106	313	WANG, Z.	SS-WeP14	86	251				
TSONG, I.S.T.	SS-WeP2	86	250	VAUGHT, A.	NS1-TuA1	61	185	WANG, Z.	SS-WeP16	86	252				
TSONG, I.S.T.	SS2-FrM8	108	320	VÁZQUEZ-LÓPEZ, C.	TF-ThP11	106	314	WARKENTIN, P.	BI-MoP16	51	162				
TSONG, T.T.	NS2-ThM11	91	274	VÁZQUEZ-LÓPEZ, C.	NS-TuP11	67	204	WARNATZ, J.	SS1-MoM11	36	115				
TSONG, T.T.	SS-WeP4	86	250	VENABLES, J.D.	AS-FrM2	110	324	WARREN, O.L.	SS2-MoM5	36	116				
TSU, D.V.	PS-WeP8	88	259	VENDER, D.	PS-WeM7	74	226	WARREN, O.L.	NS2-TuA8	61	187				
TSUBAKIHARA, H.	PS2-ThA5	101	297	VENTRICE, JR., C.A.	EM-MoA8	46	140	WARREN, O.L.	BI-MoP7	51	161				
TSUJI, S.	NS-ThP23	104	307	VENTZKE, P.L.G.	PS-TuM1	54	171	WARREN, O.L.	SS2-ThA4	98	288				
TSUJIMOTO, A.	TF-ThP5	106	313	VERSCHUEREN, G.L.J.	PS-WeP2	88	258	WARWICK, A.	AS-MoM7	37	119				
TSUKADA, M.	NS2-WeM0	73	222	VESECKY, S.M.	SS2-WeM6	72	220	WASA, K.	TF-WeM8	75	229				
TSUKADA, M.	NS1-MoA5	43	130	VESENKA, J.	NSBI-ThM6	91	271	WATAMORI, M.	AS-TuP23	68	210				
TSUKAHARA, S.	VT-TuA3	63	191	VESENKA, J.	NS-MoP5	49	150	WATAMORI, M.	TF-ThP5	106	313				
TSUTSUI, N.	NS-ThP23	104	307	VESEK, G.	BI-MoP4	51	160	WATANABE, F.	NS2-FrM5	109	323				
TSUYUGUCHI, T.	NS1-MoA6	43	130	VETELINO, J.F.	SS2-WeM3	72	220	WATANABE, K.	EM-ThM10	94	282				
TSYBESKOV, L.	NS2-WeA8	81	238	VETRONE, J.	TF-TuM6	55	175	WATANABE, M.	EM-MoA9	46	140				
TSYBESKOV, L.	NS2-WeA5	81	238	VIDALI, G.	TF-ThP20	106	315	WATANABE, S.	NS-MoP18	49	152				
TUCHMAN, J.A.	EM-ThP10	105	309	VIDALI, G.	EM-ThP24	105	311	WATANABE, Y.	NS-TuP18	67	205				
TUCKER, J.R.	SS2-TuM8	52	166	VIDALI, G.	SS1-TuM7	52	164	WATANABE, Y.	EMMS-TuM11	56	178				
TUCKER, J.R.	EM-MoA1	46	139	VIDALI, G.	SS-TuP14	66	200	WATERS, K.	TF-ThP3	106	312				
TUCKER, J.R.	NS-ThP25	104	307	VILLARRUBIA, J.S.	NS2-MoA5	43	131	WATERS, K.	TF-WeP19	89	265				
TUCKER, J.R.	EM-ThA6	102	300	VILLEGAS, I.	SS2-WeA8	80	235	WATSON, G.M.	SS2-WeA5	80	235				
TUCKER, J.R.	SS2-FrM4	108	319	VILLEGAS, I.	NS1-TuA2	61	185	WAVRIK, R.	PS2-ThA1	101	296				
TULLY, J.C.	SS-TuP10	66	199	VIRTANEN, J.A.	SS1-ThM7	90	267	WAVRIK, R.W.	VT-TuM9	55	174				
TURKOT, R.B.	PS1-ThA10	100	296	VITTELLO, P.	PS-MoP21	50	157	WAY, J.D.	EM-ThA9	102	300				
TURNER, D.C.	BINS-WeM8	77	232	VITTERA, M.	AS-TuP1	68	206	WEARE, C.B.	SS-MoP30	48	148				
TURNER, D.C.	BI-TuM10	57	180	VJATKIN, A.	SS-WeP13	86	251	WEARE, C.B.	SS-MoP35	48	149				
TURNER, W.	VT-TuM2	55	173	VO, T.	MS-WeA8	84	248	WEAVER, J.H.	EMSS-ThM1	93	277				
TUSZEWSKI, M.	PS-MoP11	50	155	VOEVODIN, A.	VM-FrM5	111	329	WEAVER, J.H.	EMSS-ThM3	93	278				
TUSZEWSKI, M.	PS-WeP5	88	259	VOEVODIN, A.A.	VM-FrM2	111	329	WEAVER, J.H.	EM-ThP26	105	312				
TYLISZCZAK, T.	EM-TuP13	69	213	VOIGHT, S.	TF-ThP23	106	316	WEAVER, M.J.	SS2-WeA8	80	235				
TZENG, H.S.	VT-MoP7	51	158	VOILES, T.	VM-ThM2	95	284	WEBB, D.A.	NS1-TuA2	61	185				
UCHIHASHI, T.	NS1-MoA6	43	130	VOLLMER, R.	SS2-MoM8	36	116	WEBER, E.	AS-ThM8	92	275				
UEDA, S.	VT-MoP6	51	158	VON BEHREN, J.	NS2-WeA5	81	238	WEBER, M.	EM-ThP5	105	308				
UEDA, Y.	PS-WeP16	88	261	VON BLANCKENHAGEN, P.	SS-MoP24	48	147	WEBER, M.	NS1-FrM6	109	321				
ULMAN, A.	AS-ThM1	92	274	VON BLANCKENHAGEN, P.	NS-WeP12	87	256	WEDELSTAEDT, C.A.	AS-FrM9	110	325				
UMEDA, N.	NS-WeP15	87	256	VON SEGGERN, J.	PS-WeP16	88	261	WEGNER, G.	AS-TuP2	68	206				
UNITES, W.	PS2-ThA7	101	297	VOSSER, J.	VM-ThA6	103	302	WEGNER, H.	AS-ThM4	92	274				
URAM, K.J.	SS-WeP30	86	254	VUGTS, M.J.M.	PS-WeP2	88	258	WEI, D.-H.	SS1-TuA9	60	183				
URAM, K.J.	MS-TuA9	64	196	WADDILL, G.D.	SS1-WeM8	72	219	WEI, Y.	NS-ThP2	104	304				
URBAN, F.K.	TF-WeP16	89	264	WADDILL, G.D.	SS-WeP17	86	252	WEI, Y.	SS-MoP31	48	148				
URBAN, K.	SSEM-WeM4	75	227	WADE, M.R.	VT-TuM5	55	174	WEI, Y.	SS-WeP2	86	250				
URBAN III, F.K.	EM-ThP16	105	310	WAGANAAR, W.J.	VM-ThM10	95	285	WEI, Y.	SS2-FrM8	108	320				
URITSKY, Y.	MS-ThM9	94	283	WAGO, K.	NS2-FrM9	109	323	WEI, Y.	ASSS-TuA10	62	189				
UVDAL, K.D.	BI-MoP13	51	162	WAINHAUS, S.B.	SS-MoP9	48	145	WEIGAND, P.	SS2-TuM1	52	164				
UVDAL, P.U.	SS-MoP10	48	145	WAINHAUS, S.B.	SS-MoP38	48	149	WEIMER, J.J.	TF-WeM2	75	228				
VAHEDI, V.	PS-MoP20	50	157	WAITE, M.M.	TFVM-MoA9	45	138	WEIMER, J.J.	AS-TuP10	68	208				
VAHEDI, V.	PS-MoP24	50	157	WALIVAARA, B.	BI-MoP16	51	162	WEIMER, M.	NS-TuP6	67	203				
VAJO, J.J.	AS-TuP16	68	208	WALKER, A.R.	AS-WeM6	74	224	WEIMER, M.	EMSS-ThM10	93	279				
VALBUSA, U.	SS1-TuA2	60	182	WALKER, D.M.H.	MS-ThM5	94	283	WEIMER, M.	NS1-TuA7	61	186				
VAN CAMPEN, D.	SS-MoP21	48	147	WALKER, J.C.	SS1-WeA5	80	233	WEINBERG, W.H.	SS-MoP40	48	149				
VAN DE SANDEN, M.C.M.	PS-MoA9	44	135	WALKER, J.C.	SS-WeP18	86	252	WEINBERG, W.H.	SS2-ThM4	90	269				
VAN DE SANDEN, M.C.M.	PS-MoP1	50	153	WALL, J.F.	TF-FrM2	110	326	WEISS, G.	NS-ThP4	104	304				
VAN DE VEN, E.	MS-TuA3	64	195	WALLACE, R.J.	PS2-ThA8	101	297	WEISS, P.S.	SS-MoP14	48	146				

Author		Prog. Abst.			Prog. Abst.			Prog. Abst.			
		Pg. #	Pg. #		Pg. #	Pg. #		Pg. #	Pg. #		
WEISS, P.S.	SS-TuP16	66	200	WILSON, R.M.	NS2-TuA1	61	187	YALISOVE, S.M.	TF-WeA1	83	244
WEISS, P.S.	SS2-FrM7	108	320	WINAND, R.	TF-ThP7	106	313	YAMADA, H.	NSBI-WeA9	81	237
WEISS, S.	NS2-FrM4	109	323	WINNINGHAM, T.A.	NS1-FrM5	109	321	YAMADA, N.	VT-MoP5	51	158
WEISS, T.	NS1-MoM3	37	117	WINTERS, R.	NS-ThP4	104	304	YAMAGUCHI, M.	NS2-MoA7	43	132
WEISS, W.	SS2-MoM6	36	116	WISE, K.	TF-ThP21	106	315	YAMAGUCHI, Y.	PS-TuA9	62	191
WEITZ, E.	SS2-TuM10	52	166	WISE, K.D.	TF-TuM8	55	176	YAMAMOTO, Y.	SS-TuP13	66	200
WELDON, M.K.	SS-MoP10	48	145	WISE, K.D.	SS1-MoA5	42	126	YAMANISHI, Y.	NS1-MoA6	43	130
WENDELKEN, J.F.	SS2-TuA4	60	184	WISE, M.L.	SS-MoP28	48	148	YAMAZAKI, S.	SS-MoP7	48	145
WENDELKEN, J.F.	SS-TuP15	66	200	WISEMAN, M.	VT-TuM6	55	174	YAN, C.	SSEM-WeA4	83	243
WENDT, A.E.	PS-WeP9	88	260	WITANACHCHI, S.	VM-ThM1	95	284	YAN, C.	SS-MoP32	48	148
WENZLER, L.A.	NSBI-ThM9	91	271	WITTMAN, E.L.	TF-TuM6	55	175	YAN, D.	TF-WeA8	83	245
WERNER, F.	PS-TuA7	62	190	WITTMAN, M.D.	PS-WeP22	88	262	YAN, W.	NS-WeP8	87	255
WERNER, J.W.	PS-WeP13	88	260	WOLF, P.J.	VM-ThM5	95	284	YAN, Z.	TF-ThP10	106	314
WERTHEIMER, M.R.	TF-WeP8	89	263	WOLF, P.J.	VM-ThM6	95	284	YANG, B.	EM-WeA1	84	245
WERTZ, T.E.	BI-TuM10	57	180	WOLFF, A.	EM-ThM8	94	281	YANG, C.M.	EM-ThA5	102	300
WEST, C.	VM-ThA1	103	302	WÖLL, CH.	TFVM-MoA4	45	137	YANG, H.	SS1-ThA8	98	287
WEST, P.E.	NS-MoP10	49	151	WÖLL, CH.	AS-ThM4	92	274	YANG, L.-C.	TF-ThA5	101	298
WESTERHEIM, A.C.	PS-MoP17	50	156	WOLOVELSKY, M.	VM-WeA9	85	249	YANG, P.	EM-MoA7	46	140
WESTPHAL, C.	SS-WeP14	86	251	WOLOVELSKY, M.	NS1-MoA2	43	129	YANG, P.	AS-ThA3	100	293
WEY, W.D.	VT-MoP7	51	158	WOLSTENHOLME, J.	AS-MoM9	37	119	YANG, Q.	PS-ThM10	92	277
WHANG, K.W.	PS-WeA9	82	242	WONG, E.K.L.	SS-TuP3	66	198	YANG, Q.Y.	SS2-TuM11	52	166
WHANG, K.W.	PS-MoA10	44	135	WONG, E.K.L.	SS2-WeA10	80	235	YANG, Q.Y.	SS2-ThA5	98	288
WHETTEN, R.L.	NS1-TuM7	53	167	WONG, K.W.	AS-WeM3	74	224	YANG, X.	NS-TuP7	67	204
WHIDDEN, T.K.	BINS-WeM7	77	232	WONG, M.S.	TFVM-TuA6	63	193	YANG, X.	ASSS-TuA10	62	189
WHIDDEN, T.K.	NS-ThP15	104	306	WONG, M.S.	TF-WeP18	89	265	YANG, Y.	VT-TuA3	63	191
WHISNANT, P.L.	AS-FrM2	110	324	WONG, M.S.	VM-FrM3	111	329	YANG, Y.H.	TF-FrM10	110	327
WHITAKER, T.J.	AS-TuP17	68	209	WONG, M.S.	TF-WeP15	89	264	YANG, Y.H.	TF-FrM7	110	326
WHITE, C.T.	NS2-ThM3	91	272	WONG, M.S.	TFVM-TuA7	63	194	YANG, Y.H.	EM-ThP15	105	310
WHITE, C.W.	NS-TuP15	67	205	WONG, M.S.	TF-WeP14	89	264	YANNONI, C.S.	NS2-FrM9	109	323
WHITE, C.W.	AS-TuM9	54	171	WONG, M.S.	VM-ThM11	95	285	YANNONI, C.S.	NS2-FrM7	109	323
WHITE, J.M.	SSEM-WeM5	75	227	WONG, S.S.	EM-ThA5	102	300	YAO, J.	SS-WeP6	86	250
WHITE, J.M.	SS-TuP22	66	201	WONG, S.S.	EMSS-ThM5	93	278	YAO, J.	SS-TuP19	66	201
WHITE, J.M.	PS1-ThA8	100	295	WOOD, B.P.	VM-ThM9	95	285	YARMOFF, J.A.	SS-MoP30	48	148
WHITE, J.M.	SS1-MoM7	36	114	WOOD, G.	EM-WeM7	76	230	YARMOFF, J.A.	SS-MoP35	48	149
WHITE, J.M.	SS-WeP24	86	253	WOODS, J.P.	SS1-WeM6	72	218	YARMOFF, J.A.	SSEM-WeM3	75	227
WHITE, J.M.	SS-TuP28	66	202	WOODS, R.C.	PS-TuA5	62	190	YASHAR, P.	TF-WeP18	89	265
WHITE, J.M.	SS-TuP26	66	202	WOODS, R.C.	PS-MoP2	50	153	YASUDA, T.	SS2-FrM5	108	319
WHITE, J.M.	SS-TuP21	66	201	WOOLLAM, J.A.	MS-TuP5	70	216	YATER, J.E.	SS2-ThA2	98	288
WHITE, R.C.	NS1-TuA5	61	185	WOOLLAM, J.A.	EM-ThM6	94	281	YATES, JR., J.T.	SS1-MoM3	36	114
WHITE, R.C.	NSBI-ThA10	99	291	WOOLLAM, J.A.	TF-FrM1	110	326	YE, P.	EM-TuP1	69	211
WHITE, R.L.	NS1-MoA9	43	130	WOOLVERTON, L.	TF-ThP3	106	312	YE, P.	EM-TuP2	69	211
WHITMAN, L.J.	SS2-FrM9	108	320	WORM, K.	SSEM-WeA10	83	243	YE, P.	EM-TuP15	69	213
WHITMAN, L.J.	SS-TuP30	66	203	WORTHINGTON, J.N.	MS-TuP9	70	217	YE, P.	EMMS-TuM7	56	177
WHITTEN, J.L.	EM-MoA2	46	139	WRIGHT, D.R.	PS-ThM10	92	277	YELON, A.	EM-ThP3	105	308
WICHTERMAN, B.M.	AS-TuM11	54	171	WRIGHT, D.R.	MS-WeM3	76	230	YEO, Y.K.	EM-TuP3	69	211
WICZER, J.J.	MS-WeA9	84	248	WU, B.J.	EM-WeM5	76	230	YEON, C.K.	PS-WeA9	82	242
WIECKOWSKI, A.	SS2-WeA3	80	234	WU, D.	PS-WeP1	88	258	YING, Z.C.	SS2-ThA8	98	289
WIENHOLD, P.	PS-WeP16	88	261	WU, H.	SS-WeP10	86	251	YNZUNZA, R.X.	SS-WeP14	86	251
WIENS, R.C.	AS-WeM8	74	224	WU, J.	EM-ThP11	105	309	YNZUNZA, R.X.	AS-WeM4	74	224
WIESENDANGER, R.	NS2-ThA8	99	292	WU, J.H.	BI-MoP1	51	160	YNZUNZA, R.X.	SS1-WeA10	80	234
WIESENDANGER, R.	NS-ThP11	104	305	WU, M.-C.	SS2-WeM4	72	220	YOKOGAWA, K.	PS-ThM7	92	277
WIGHTMAN, J.P.	AS-FrM3	110	324	WU, Q.D.	NS-WeP11	87	256	YOKOYAMA, H.	NS2-FrM2	109	322
WIKLUND, S.	EM-ThP7	105	309	WU, S.Z.	SS-WeP12	86	251	YOKOYAMA, S.	EM-TuA1	64	194
WILBER, W.	TF-WeP3	89	262	WU, S.Z.	SS1-WeM5	72	218	YONEDA, M.	PS-MoM7	38	120
WILD, C.	TFVM-MoA1	45	137	WU, W.	EM-MoA1	46	139	YOO, B.-S.	PS-WeP3	88	259
WILDER-SMITH, P.	BI-MoP7	51	161	WU, W.	EM-ThA6	102	300	YOON, E.	PS-MoA10	44	135
WILFLEY, B.	NS-MoP19	49	152	WU, Y.	NSBI-ThA6	99	290	YOSHIDA, Y.	MS-TuP2	70	216
WILPITTYA, D.	SS1-WeM6	72	218	WU, Y.	SS1-MoA10	42	127	YOSHIDA, Y.	MS-TuP3	70	216
WILKINS, R.	NS1-TuA7	61	186	WURM, K.	SS-MoP31	48	148	YOSHIHARA, K.	AS-TuP26	68	210
WILKINSON, C.D.W.	BINS-WeM2	77	231	XI, S.	NS-WeP8	87	255	YOSHIKAWA			
WILLIAMS, A.	PS-WeP5	88	259	XIA, B.	SS-MoP36	48	149	YOUNGQUIST, M.G.	SS-TuP16	66	200
WILLIAMS, C.C.	NSMS-WeM7	73	221	XIA, S.D.	NS-TuP12	67	204	YOSHITAKE, M.	AS-TuP26	68	210
WILLIAMS, C.C.	NS-WeP22	87	257	XIANG, J.	EM-TuP1	69	211	YOUNG, R.T.	PS-WeP8	88	259
WILLIAMS, C.C.	NSBI-ThA8	99	291	XIANG, J.	EM-TuP2	69	211	YU, I.	NS-WeP19	87	257
WILLIAMS, D.E.	SS1-MoA2	42	126	XIAO, H.	SS-WeP14	86	251	YU, J.	NS-MoP7	49	151
WILLIAMS, E.D.	SS1-TuM5	52	163	XIAO, H.	SS1-WeM7	72	219	YU, J.E.	NS-TuP8	67	204
WILLIAMS, J.	NS2-FrM10	109	323	XIAO, H.Z.	TF-ThA5	101	298	YU, L.M.	SS1-FrM8	108	318
WILLIAMS, J.M.	AS-WeM5	74	224	XIAO, X.	AS-TuP12	68	208	YU, L.M.	TF-WeA6	83	245
WILLIAMS, L.D.	NSBI-ThM3	91	271	XIAO, X.-D.	NS2-TuA5	61	187	YU, M.L.	NS2-MoA6	43	132
WILLIAMS, L.M.	MS-WeA8	84	248	XU, C.	TF-TuM3	55	175	YU, M.L.	NS-MoP24	49	153
WILLIAMS, M.D.	EM-TuP12	69	213	XU, C.	SS2-ThM6	90	269	YU, N.	NS1-TuM11	53	168
WILLIAMS, M.J.	EM-MoA4	46	139	XU, H.	EM-TuP8	69	212	YU, Z.	PS-TuA6	62	190
WILLIAMS, P.M.	NSBI-ThM10	91	272	XU, H.	EMMS-TuM6	56	177	YU-WANG, V.	PS-MoP17	50	156
WILLIAMS, P.M.	BI-TuM4	57	180	XU, J.	NS2-WeA7	81	238	YUAN, C.	EM-TuP23	69	215
WILLIAMS, P.M.	NSBI-ThM8	91	271	XU, X.	SS2-WeM6	72	220	YUAN, C.W.	NS-ThP2	104	304
WILLIAMS, P.M.	NS2-MoA4	43	131	XU, Y.	NS-WeP10	87	256	YUE, F.	TF-ThP9	106	313
WILLIAMS, R.T.	NS2-TuA1	61	187	XUE, Q.K.	SS2-MoA6	42	128	YUNOGAMI, T.	PS-ThM7	92	277
WILLIAMS, S.D.	NS1-FrM5	109	321	XUE, Q.K.	SS2-MoM11	36	117	YUROV, V.	SS-MoP7	48	145
WILLICUT, R.J.	SS1-ThM9	90	268	XUE, Z.Q.	NS2-WeM2	73	222	YUROV, V.Y.	NS-MoP20	49	152
WILLIS, R.F.	SS-WeP12	86	251	XUE, Z.Q.	NS-WeP11	87	256	YUSUPOV, R.	NS-TuP21	67	206
WILLIS, R.F.	SS1-WeM5	72	218	XUE, Z.Q.	NS-WeP23	87	258	ZACHARIAH, M.R.	PS-WeM4	74	226
WILLKE, T.L.	NS-ThP3	104	304	YALISOVE, S.M.	SS-TuP11	66	199	ZAJCHOWSKI, L.	NS-TuP10	67	204
WILSON, R.G.	EM-WeA8	84	246	YALISOVE, S.M.	SS2-MoA5	42	128	ZALAR, A.	AS-TuP15	68	208



Author		Prog. Abst.				Prog. Abst.				Prog. Abst.			
		Pg. #	Pg. #			Pg. #	Pg. #			Pg. #	Pg. #		
ZANDVLIET, H.J.W.	SS2-FrM11	108	320	ZHANG, Y.	NS-TuP1	67	203	ZIEGLER, C.	NS-WeP6	87	255		
ZAVADA, J.M.	EM-WeA8	84	246	ZHANG, Z.	SS1-TuM3	52	163	ZIMIN, A.V.	NS-WeP16	87	256		
ZAVADIL, K.R.	EM-ThP2	105	308	ZHANG, Z.G.	SS1-TuM6	52	163	ZIMMERMAN, F.M.	SS-MoP37	48	149		
ZAVADIL, K.R.	EM-TuP6	69	212	ZHANG, Z.H.	EM-TuP18	69	214	ZIMMERMAN, P.A.	AS-ThA8	100	294		
ZAVADIL, K.R.	SS1-ThA5	98	286	ZHAO, C.Y.	EM-ThM5	94	281	ZOLPER, J.C.	PS-WeA5	82	241		
ZEHNER, D.M.	SS1-ThA3	98	286	ZHAO, W.B.	NS2-WeM2	73	222	ZOLPER, J.C.	EM-ThP2	105	308		
ZEHNER, D.M.	SS2-ThM5	90	269	ZHAO, W.B.	NS-WeP23	87	258	ZORIC, I.	SS1-TuA3	60	182		
ZEHNPFFENNING, J.	AS-TuM4	54	170	ZHENG, J.	MS-TuP4	70	216	ZOVAL, J.	SS1-ThM7	90	267		
ZELENSKI, C.M.	NS-TuP3	67	203	ZHENG, J.	PS-MoP18	50	156	ZUCCHERI, G.	NSBI-ThM7	91	271		
ZENG, H.	EM-ThP24	105	311	ZHENG, J.-F.	EM-ThP5	105	308	ZUEGER, O.	NS2-FrM7	109	323		
ZENG, H.	SS1-TuM7	52	164	ZHENG, X.Y.	NS-ThP7	104	305	ZÜGER, O.	NS2-FrM9	109	323		
ZENG, H.	SS-TuP14	66	200	ZHENG, Z.	PS-MoA8	44	135	ZUHR, R.A.	NS-TuP15	67	205		
ZHANG, C.-M.	SS2-MoM7	36	116	ZHOU, H.J.	AS-TuP28	68	210	ZUHR, R.A.	AS-TuM9	54	171		
ZHANG, F.	SS-WeP15	86	252	ZHOU, J.	SS2-MoA6	42	128	ZUIKER, C.D.	TFVM-MoA10	45	138		
ZHANG, H.F.	NS-TuP12	67	204	ZHOU, J.	SS2-MoM11	36	117	ZUKIC, M.	TF-WeM2	75	228		
ZHANG, J.	EM-ThP24	104	311	ZHU, D.	NS-WeP10	87	256	ZUO, J.-K.	SS-TuP15	66	200		
ZHANG, J.	SS1-WeA9	80	234	ZHU, D.-M.	NS-TuP13	67	205	ZUPP, T.A.	AS-MoM8	37	119		
ZHANG, P.-C.	NS-WeP10	87	256	ZHU, H.	PS-WeP10	88	260	ZUPP, T.A.	AS-WeM6	74	224		
ZHANG, Q.	NS1-MoA2	43	129	ZHU, L.	SS1-FrM11	108	318						

# NOTES

## NOTES

## **FUTURE SYMPOSIUM LOCATIONS**

- |      |   |
|------|---|
| 1995 | October 16–20<br>Minneapolis Convention Center<br>Minneapolis, MN   |
| 1996 | October 14–18<br>Philadelphia Convention Center<br>Philadelphia, PA |
| 1997 | October 20–24, 1997<br>San Jose Convention Center<br>San Jose, CA   |
| 1998 | November 2–6<br>Baltimore Convention Center<br>Baltimore, MD        |

*Use of video recording equipment, cameras, or audio equipment at any American Vacuum Society National Symposium, Short Course or Topical Conference is prohibited without prior written approval of the Society. The Society reserves the right to reproduce, by any means selected, any or all of these presentations and materials.*

# 1994 TECHNICAL PROGRAM

ROOM/ DAY	A101	A102	A105	A106	A108	A109
<b>MoM</b>	<b>AS</b> Imaging and Small Area Analysis	<b>VT</b> Total Pressure Gauging			<b>EM</b> Materials for Device Integration	<b>PS</b> Plasma Etching & Deposition
<b>MoA</b>	<b>AS</b> Data Processing and Reference Methods	<b>VT</b> Partial Pressure Analysis, and Leak Detection	<b>TFVM</b> Cubic Boron Nitride and Other Ultra-Hard Films I	<b>BI</b> Cell-Solid Surface Interactions	<b>EM</b> Thin Film Heterostructures	<b>PS</b> Plasma Deposition
<b>MoP</b>						
<b>TuM</b>	<b>AS</b> Surface Chemistry and Contamination	<b>VT</b> Vacuum Systems for Accelerators and Fusion	<b>TF</b> Thin Films for Sensors	<b>BI</b> Protein-Solid Surface Interactions	<b>EMMS</b> Surface Preparation and Passivation	<b>PS</b> Plasma Process & Reactor Modeling
<b>TuA</b>	<b>ASSS</b> Electrochemistry and Liquid/Solid Interfaces	<b>VT</b> Vacuum System Outgassing and Cleaning	<b>TFVM</b> Diamond, Cubic Boron Nitride and Other Ultra-Hard Films II	<b>BI</b> The Biosensor- Biology Interface	<b>EM</b> Silicon-based Optoelectronics	<b>PS</b> Advanced Plasma Reactors
<b>TuP</b>						
<b>WeM</b>	<b>AS</b> Quantitative Analysis, Em- phasizing Angle- Resolved XPS	<b>SSEM</b> Semiconductor Surface Reactions I	<b>TF</b> Optical, Piezoelectric and Ferroelectric Films	<b>BINS</b> Artificial Cellular Assemblies	<b>EM</b> Heterostructures for Optoelectronics	<b>PS</b> Plasma Diagnostics
<b>WeA</b>	<b>AS</b> Depth Profiling	<b>SSEM</b> Semiconductor Reactions II	<b>TF</b> Deposition & Char- acterization Techni- ques of Nanostruc- tures in Thin Films	<b>VM</b> Thin Film Microstructure Evolution	<b>EM</b> Wide-bandgap Nitrides	<b>PS</b> Plasma-Induced Charging and Contamination Effects
<b>WeP</b>						
<b>ThM</b>	<b>AS</b> Self-Assembled Monolayers	<b>EMSS</b> Semiconductor Surface Reactions III	<b>TFVM</b> Energic Condensa- tion: Processes, Properties and Products	<b>VM</b> Pulsed Laser & Pul- sed Ion Tech. for Film Deposition & Surface Modification	<b>EM</b> Optical Diagnostics for Materials Processing	<b>PS</b> Charge Free Processing
<b>ThA</b>	<b>AS</b> Polymer/Organic Surfaces	<b>PS2</b> Target Fabrication for Inertial Confinement Fusion	<b>TF</b> Thin Films for Energy Conversion and Efficiency/ Active Films	<b>VM</b> Manufacturing Technology for Coatings	<b>EM</b> Materials for Nanostructures	<b>PS1</b> Plasma Surface Interactions
<b>ThP</b>						
<b>FrM</b>	<b>AS</b> Adhesion and Adhesive Bonding		<b>TF</b> In Situ Thin Film Characterization	<b>VM</b> Surface Engineering for Wear and Corrosion Protection	<b>EM</b> Interface Characterization	

 Si-Based Optoelectronics

 Sensors, In-Situ Diagnostics, Process Control



# AT A GLANCE

A110	A201	A205	A207	A209	BR1	BR4
	<b>SS2</b> Alloy and Compound Surface Structure	<b>SS1</b> Reactions on Metals: Hydrocarbons			<b>NS1</b> NANO 3 Plenary Session	
<b>MS</b> Process and Equipment Modeling	<b>SS2</b> Nucleation and Growth: Semiconductors	<b>SS1</b> Surface Mechanisms and Materials for Chemical Sensors	<b>NS2</b> Nanometrology	<b>NS1</b> Nanostructure Properties: Structural and Electronic		
						<b>POSTER SESSIONS</b>
<b>MS</b> Manufacturing Overview and Environmental Issues	<b>SS2</b> Non-Thermal Surface Dynamics	<b>SS1</b> Nucleation and Growth: Homoepitaxy	<b>NS2</b> Nanoelectronics	<b>NS1</b> Nanostructured Materials		
<b>MS</b> Advanced Manufacturing Equipment - A	<b>SS2</b> Nucleation and Growth: Metals	<b>SS1</b> Dynamics and Kinetics of Surface Processes	<b>NS2</b> Nanomechanics and Nanotribology: I	<b>NS1</b> Nanostructure Properties: Chemical and Electrochemical		
						<b>POSTER SESSIONS</b>
<b>MS</b> Advanced Manufacturing Equipment - B	<b>SS2</b> Reactions on Metals: Diatomics	<b>SS1</b> Surface Magnetism I	<b>NS2</b> Atomic Manipulation	<b>NSMS</b> Industrial Applications of Scanned Probes		
<b>MS</b> Diagnostics, Sensors, and Control	<b>SS2</b> Solid Liquid Interfaces	<b>SS1</b> Surface Magnetism II	<b>NS2</b> Optical Properties of Silicon Nanostructures	<b>NSBI</b> Biology at the Nanoscale: I		
						<b>POSTER SESSIONS</b>
<b>MS</b> Micro- Contamination and Defects	<b>SS2</b> Surface Interactions	<b>SS1</b> Nanoscale Measurements	<b>NS2</b> Proximal Probe Based Fabrication	<b>NSBI</b> Biology at the Nanoscale: II		
<b>MSVT</b> Vacuum Process Control for Manufacturing	<b>SS2</b> Surface and Adsorbate Structure	<b>SS1</b> Oxidation and Adsorption	<b>NS2</b> Nanomechanics and Nanotribology: II	<b>NSBI</b> Micro- Instrumentation and Sensors		
						<b>POSTER SESSIONS</b>
	<b>SS2</b> Group IV Semiconductor Surface Structure	<b>SS1</b> Surface Electronic Structure	<b>NS2</b> Novel Probes	<b>NS1</b> Novel Materials and Methods for Nanofabrication		

 Surface and Contamination Control

 Nanostructure Fabrication and Atomic Scale Manipulation of Surfaces



*The American Vacuum Society is pleased to welcome you as a participant in the 41st Annual Symposium. We hope that you will be satisfied by the content of the meeting whether your main interest lies in the technical sessions, which contain over 1,000 papers, the short courses, the equipment exhibit, the companions' program or the special events and functions which are scheduled throughout the week. The Board of Directors of the Society, through the Program and Local Arrangements Committees, strives to make the National Symposium meet the needs of the community which utilizes all aspects of vacuum science and technology. To assist the Board in meeting this objective, suggestions for improvement in any aspect should be directed to Patricia Thiel, Iowa State University, Department of Chemistry, Ames, IA 50011, 515/294-8985, or Harry Meyer, Martin Marietta Energy Systems Inc., PO Box 2009, Oak Ridge, TN 38831, 615/576-3866 who are respectively chairs of the Program and Local Arrangements Committees for the*

**42nd NATIONAL SYMPOSIUM**  
to be held at the  
**MINNEAPOLIS CONVENTION CENTER**  
**MINNEAPOLIS, MN**  
**OCTOBER 16-20, 1995**

**AMERICAN VACUUM SOCIETY**  
**120 WALL STREET, 32ND FLOOR**  
**NEW YORK, NY 10005**  
**212/248-0200**



*Minneapolis Convention Center (Courtesy of M.C.C.)*